

2



THIS DOCUMENT IS BEST QUALITY PRACTICABLE.
THE COPY FURNISHED TO DDC CONTAINED A
SIGNIFICANT NUMBER OF PAGES WHICH DO NOT
REPRODUCE LEGIBLY.

Product Assurance

OPERATIONAL QUALITY ASSURANCE

WIDEBAND RADIO ANALYSIS

DTIC
ELECTE
JUN 18 1982
S D
D

20 MAY 1976

DISTRIBUTION STATEMENT

Approved for public release. Distribution
unlimited

DTIC FILE COPY

VOICE OF THE ARMY

AD A115765

**HEADQUARTERS
U. S. ARMY COMMUNICATIONS COMMAND
FORT HUACHUCA, ARIZONA 85613**

82 06 16 052

DISCLAIMER NOTICE

THIS DOCUMENT IS BEST QUALITY PRACTICABLE. THE COPY FURNISHED TO DTIC CONTAINED A SIGNIFICANT NUMBER OF PAGES WHICH DO NOT REPRODUCE LEGIBLY.

Accession For	
NTIS GRA&I	<input checked="" type="checkbox"/>
DTIC TAB	<input type="checkbox"/>
Unannounced	<input type="checkbox"/>
Justification	
By _____	
Distribution/ _____	
Avail _____	
Date _____	
Spec _____	
A	



CCP 702-1

Department of the Army
 Headquarters, US Army Communications Command
 Fort Huachuca, Arizona 85613

USACC Pamphlet
 CCP 702-1

20 May 1976

Product Assurance
 OPERATIONAL QUALITY ASSURANCE
 WIDEBAND RADIO ANALYSIS

	Paragraph	Page
LIST OF FIGURES		iii
LIST OF TABLES		v
CHAPTER 1. INTRODUCTION		
Purpose	1-1	1-1
Scope	1-2	1-1
Acknowledgments and References	1-3	1-2
Comments on Publication	1-4	1-3
CHAPTER 2. PROGRAM CONCEPTS AND REQUIREMENTS		
General	2-1	2-1
Program Objectives and Background	2-2	2-1
Operations	2-3	2-2
Responsibilities	2-4	2-2
Administrative Requirements	2-5	2-6
Logistical Support	2-6	2-6
CHAPTER 3. REPORT PROCESSING AND SUBMISSION		
General	3-1	3-1
Link Performance Characteristics	3-2	3-2
Required Tests	3-3	3-3
Data Submission	3-4	3-5

	Paragraph	Page
APPENDIX A. SAMPLE TEP REPORT		A-1
B. PREDICTED PERFORMANCE LEVELS		
Section I. Instructions		B-1
Section II. Tables and Figures		B-25
C. DATA ANALYSIS		
Section I. Instructions		C-1
Section II. Figures		C-65
Section III. Noise Calculations		C-93
Section IV. Minimum Noise Capability		C-99
Section V. Fault Isolation		C-103
D. FINAL ANALYSIS OF THE TEST DATA		
Section I. Instructions		D-1
Section II. Figures		D-5
Section III. Notes on Tests and Forms		D-15
E. TABLES, FIGURES, AND SPECIFICATIONS		
Section I. Multiplex Equipment		E-1
Section II. Radio Equipment		E-37
F. MISCELLANEOUS DATA		
Section I. Formulas and Equations		F-1
Section II. Symbols and Definitions		F-7
Section III. Station Ground Measurement		F-11
Section IV. Noise Figure Primer		F-19
Section V. Microwave System Engineering Using Large Passive Reflectors		F-27
Section VI. Radiation Patterns and the Passive Repeater		F-35
Section VII. National Bureau of Standards Technical Note 101, Transmission Loss Predictions for Tropospheric Communication Circuits, Vol I ...		F-69
Section VIII. National Bureau of Standards Technical Note 101, Transmission Loss Predictions for Tropospheric Communication Circuits, Vol II		F-269
Section IX. Phase Jitter Measurement		F-479

LIST OF FIGURES

Figure	Title	Page
B-1	Typical Profile Plot	B-29
B-2	Line of Sight Worksheet	B-30
B-3	Troposcatter Transmission Loss Worksheet	B-31
B-4	Rough Earth Diffraction Worksheet	B-35
B-5	Forward Scatter Multipath Coupling Loss Worksheet..	B-40
B-6	Echo Distortion Worksheet	B-41
B-7	Multipath Distortion Worksheet	B-44
B-8	Multipath Distortion Worksheet	B-48
B-9	Link Noise Performance Worksheet	B-49
B-10	Smooth Earth Diffraction Worksheet	B-51
B-11	Knife Edge Diffraction Worksheet	B-53
B-12	Optimum Noise Graph	B-55
B-13	REL Pre-Emphasis Curve	B-56
B-14	CCIR Pre-Emphasis Graph	B-57
B-15	FM Noise Quieting Curve	B-58
B-16	FM Noise Quieting Worksheet	B-59
B-17	Return Loss vs VSWR	B-60
C-1	Peak/RMS Measurement	C-65
C-2	Peak to Average Values	C-65
C-3	White Noise Loading--NLR	C-66
C-4	NPR Test	C-67
C-5	Basic Noise Ratio--BNR	C-68
C-6	Bandwidth Ratio--BWR	C-68
C-7	Slot Bandwidth, NPR and S/N	C-69
C-8	NPR Test Results	C-69
C-9	NPR Curves	C-70
C-10	NPR Curve Analysis	C-70
C-11	NPR And Channel S/N	C-71
C-12	Channel S/N for Various Baseband Levels	C-72
C-13	Optimum Loading Point System Optimization Deviation	C-73
C-14	Basic Noise vs IM Noise	C-74
C-15	Noise Quieting Curve (Typical)	C-75
C-16 through C-20	Family of NPR Curves	C-76-- C-78
C-21	RSL and 20 dB Quieting	C-79
C-22	20-dB Quieting as a Function of RF/IF Bandwidth ...	C-80
C-23	IF Bandpass and Discriminator Characteristics	C-81
C-24	IF Bandpass and Discriminator Characteristics	C-82
C-25	DC Control Voltage as a Function of RSL	C-83

Figure	Title	Page
C-26	Channel Frequency Response Worksheet	C-84
C-27	Channel Frequency Response Graph	C-85
C-28	Channel Delay Distortion Worksheet	C-86
C-29	Channel Delay Distortion Graph	C-87
C-30	Typical Stroke Chart for RSL Recording	C-88
C-31	Typical Graph of Median RSL	C-89
C-32	Typical Graph of Median Baseband Loading	C-90
C-33	Typical Graph of Median ICN	C-91
C-34	Composite Noise Contribution Quieting Curve	C-101
C-35	Power Supply Ripple Influence on Noise Readings Graph	C-109
C-36	Test Data Factors for Consideration Graph	C-105
D-1	Receive Signal Level	D-5
D-2	Radio Thermal Noise	D-6
D-3	Loopback BNR vs Quieting Data	D-8
D-4	Link BNR vs Quieting Data	D-9
D-5	Combined Thermal Noise	D-10
D-6	Loopback Radio Intermodulation Noise	D-11
D-7	Link Combined Intermodulation Noise	D-17
D-8	Multiplex Noise	D-13
D-9	Radio Link vs Baseband Loading Worksheet	D-20
E-1	Typical Block and Level Diagram, AN/FCC-55	E-21
E-2	Typical Block and Level Diagram, MX-106	E-22
E-3	Typical Block and Level Drawing, AN/UCC-4	E-23
E-4	Typical Block and Level Drawing, AN/FCC-18	E-24
E-5	Frequency Allocations and Modulation Plan for the AN/FCC-17 Family of Multiplexers	E-25
E-6	Typical Block and Level Diagram, AN/FCC-17.....	E-26
E-7	Trans-Isthmian Microwave System (TIMS) Multiplex Plan	E-27
E-8	Typical Block and Level Drawing, AN/FCC-18	E-28
E-9	Siemens VZ12 Transmit	E-29
E-10	Siemens VZ12 Receive	E-30
E-11	Siemens VZ60 Transmit	E-31
E-12	Siemens VZ60 Receive	E-32
E-13	Typical Block and Level Drawing, AN/TRC-90B	E-38
E-14	Typical Block and Level Drawing, AN/TRC-90	E-39
E-15	Typical Block and Level Drawing, LRC-3	E-40
E-16	Typical Quieting Curve, LRC-3	E-41
E-17	Typical NPR Curve, LRC-3 (To Be Published)	E-42
E-18	Typical Block Diagram, LC-4E (AN/FRC-154)	E-43
E-19	Typical Block Diagram (Receiver) LC4-E (AN/FRC-154.	E-44
E-20	Typical Quieting Curve, LC-4E (AN/FRC-154)	E-45

Figure	Title	Page
E-21	Typical NPR Curve, LC-4E (AN/FRC-154)	E-46
E-22	Typical Block and Level Diagram, AN/FRC-109	E-47
E-23	Typical AN/FRC-109 Block and Level Diagram, AN/ FRC-109	E-48
E-24	AN/FRC-109 Block and Level Drawing Multiplex Interface	E-49
E-25	Typical Quieting Curve, AN/FRC-109	E-50
E-26	Typical NPR Curve, AN/FRC-109	E-51
E-27	Typical Block and Level Diagram, AN/FRC-80(V)1	E-52
E-28	Typical Block and Level Diagram, AN/FRC-80(V)2-3 ..	E-53
E-29	Typical Quieting Curve, AN/FRC-80	E-54
E-30	Typical NPR Curve, AN/FRC-80 (To be published)	E-55
E-31	Simplified Block Diagram AN/FRC-159(V) Radio	E-56
E-32	Trans-Isthmian Microwave System (TIMS)	E-57
E-33	Typical Block and Level Drawing, AN/FCC-18	E-58
E-34	78F2 Microwave Radio - White Sands	E-59
E-35	Siemens FM/8000 Transmitter	E-60
E-36	Siemens FM/8000 Receiver	E-61
E-37	Typical NPR vs RSL, Siemens FM 120/8000	E-62
E-38	Typical NPR vs BBL, Siemens FM 120/8000	E-63
E-39	Typical AGC and FM Quieting Curve FM 120/8000	E-64
E-40	Simplified Block Diagram, 2600-Series Exciter	E-65
E-41	Simplified Block Diagram, 2600-Series Receiver	E-66
E-42	Typical NPR vs RSL for the REL 2600 Radio	E-67
E-43	Typical NPR vs Baseband Loading	E-68
E-44	Typical AGC and FM Quieting Curve REL-2600	E-69
E-45	AN/GRC-66 Transmitter	E-70
E-46	AN/GRC-66 Simplified Block Diagram, Receiver	E-71
E-47	Typical NPR vs RSL for the AN/GRC-66 Radio	E-72
E-48	Typical Equipment NPR vs Baseband Loading	E-73
E-49	Typical AGC and FM Quieting Curve AN/GRC-66	E-74

LIST OF TABLES

Table	Title	Page
B-1	Parameters Required for Path Calculations	B-25
B-2	Baseband Test Frequencies for Modulator Deviation..	B-27
E-1	Multiplex Equipment - Pacific	E-1
E-2	Multiplex Equipment - CONUS	E-1
E-3	Multiplex Equipment - Europe	E-1
E-4	Nominal Multiplex Noise Contribution	E-2
E-5	Impedance Conversion	E-3
E-6	Frequency Translation in the Multiplex	E-5

Table	Title	Page
E-7	DCS Technical Schedules	E-10
E-8	DCS Circuit Parameters and Schedules	E-14
E-9	Manufacturer's Multiplex Specifications	E-33
E-10	Radio Equipment - Pacific	E-37
E-11	Radio Equipment - CONUS	E-37
E-12	Radio Equipment - Europe	E-37
E-13	Manufacturer's Radio Specifications	E-75

CHAPTER 1. INTRODUCTION

1-1. PURPOSE. The purpose of this document is to provide the test teams with information of a general and technical nature which may be useful during their evaluation of wideband communications systems. It is basically a compendium of instructional notes and technical papers developed, or compiled, by the 6th Signal Command TEP Detachment.

1-2. SCOPE. Chapter 2 of this handbook covers the general administrative and logistical information on the conduct of the tests, care and protection of assigned equipment and the basic responsibilities of the test personnel. Chapter 3 covers report processing and submission, and contains instructional information.

Appendix A is a sample TEP report.

Appendix B provides information and procedures for preparing predicted performance levels on which to compare the data measured by the field test teams. Transmitter deviation, receiver quieting curves and bandwidth calculations are discussed in this section. This calculated data along with the path performance calculations provides a base of theoretical data that can be compared with measured results to determine the performance quality of a system. An attempt has been made to cover the basic analysis procedures necessary to arrive at an intelligent conclusion as to system performance. It should not, however be considered the answer to all problems that may be encountered by the field test teams. It is anticipated that this document will be updated as additional information and improved test procedures are developed by evaluation personnel.

Appendix C contains detailed information on the analysis of the measured test results and the correlating of this information into a meaningful analysis of system performance. In this appendix the major test results are examined with respect to system performance, and with application to trouble shooting and equipment improvement.

Appendix D provides a method of summarizing the test results and comparing the results to the calculated performance values. This will provide the team chief with a final look at the collected data and aid in the preparation of Volume 1 of the final test report.

Appendix E contains typical noise performance specifications for various multiplex equipments, and block and level diagrams of selected equipment. It also provides a listing of microwave and troposcatter equipment employed within each subordinate command, and includes typical block and level drawings, noise power ratio curves and receiver quieting curves based on the manufacturer's specifications or empirical data collected by the test teams. The manufacturer's specification for each test compared to the design objectives contained in the applicable MILSTD's are also included for use in comparing measured results to expected performance.

CCP 702-1

Appendix F contains extracts of technical literature obtained from commercial sources that will aid in the calculation of system performance.

As stated previously, this document is not the answer to all problems or anomalies that may be encountered by the test teams. The teams will find that in many cases extensive research will be required in order to arrive at a logical conclusion to a problem area, and when this research results in new information that will be of value to other Team Chiefs, they are encouraged to provide the information for inclusion into this CCP.

1-3. **ACKNOWLEDGEMENTS AND REFERENCES.** The US Army Communications Command expresses its appreciation to the following for material used directly, or indirectly, in this CCP:

Telecommunications Technology, Inc. "Taking The Mystery Out of Phase Jitter Measurement", by Elton Cookson and Charles Volkland, Telephony Magazine, September 1972.

James G. Biddle Co. "Getting Down To Earth", Booklet 25T, 1970.

Hewlett-Packard Co. "Noise Figure Primer", HP Application Note 57, January 1965.

Microflect Co., Inc. "Radiation Patterns And The Passive Repeater", 1971.

The Lenkurt Demodulator. "Take The Mystery Out of Microwave Literature", July 1962.

The Bell System Technical Journal. "Intermodulation In Tropospheric Radio Systems", January 1963.

IRE Transactions On Communications Systems. "Microwave System Engineering Using Large Passive Reflectors", April 1962.

Carlson, Bruce A. "Communications Systems: On Introduction To Signals And Noise In Electrical Communications"; Chapter 6, McGraw-Hill Book Co., 1968.

Panter, P.F. "Communications System Design"; McGraw-Hill Book Co., 1972.

National Bureau Of Standards. "Transmission Loss Predictions For Tropospheric Communications Circuits"; Technical Note 101, Volumes I and II, January 1967.

HQ, Air Force Communications Service. AFCS 100-35 and 100-61.

1-4. COMMENTS ON PUBLICATION. Users of this publication are encouraged to submit recommended changes or comments to improve the publication. Comments should be keyed to the specific page, paragraph, and line of the text in which the change is recommended. Rationale should be provided for each comment to insure understanding and complete evaluation. Comments should be prepared using DA Form 2028 (Recommended Changes to Publications) and submitted directly to "Commanding General, US Army Communications Command, ATTN: CC-OPS-0X, Fort Huachuca, Arizona 85613".

CHAPTER 2. PROGRAM CONCEPTS AND REQUIREMENTS

2-1. GENERAL. This chapter provides general administrative procedures to the test team for accomplishing the program directives as outlined in DCAC 310-70-57.

2-2. PROGRAM OBJECTIVES AND BACKGROUND.

a. The USACC Technical Evaluation Program was established in 1970 to provide for regularly scheduled technical evaluations of the DCS wideband facilities operated and maintained by USACC worldwide. The results of these evaluations are to be used to identify those systems requiring replacement or upgrade, standardization and improvement of on-site operating, maintenance, and logistical procedures; establishment of a baseline of equipment and system performance; and to develop a data base of equipment and system performance characteristics to be used for cost effective time phased modernization of the DCS facilities.

b. The initial evaluation program established by DCAC 300-195-4 provided for the evaluation of wideband systems only. This program has since been expanded by DCAC 310-70-57 to include; the evaluation of AUTOSEVOCOM, SATELLITE and AUTOVON subsystems of the DCS. It is anticipated that additional subsystems of the DCS and eventually the non-DCS facilities will be incorporated into the program. This CCP is designed primarily around the evaluation of wideband line of sight (LOS) and tropospheric scatter systems, however, some of the data contained herein may be applicable to types of other subsystems.

c. With the installation of the World Wide Technical Control Improvement Program (WWTCIP) and automation equipment under the Automated Technical Control Program (ATEC), it is anticipated that the role of the evaluation teams will change during the late 1970's. Currently, the test teams are deployed on a scheduled cyclic basis with an objective of evaluating all systems a minimum of every two years, or more often if required. The completion of the Automated Technical Control Program (ATEC) should result in the test teams assuming a more positive role in the overall Quality Assurance Program. It is anticipated that the data obtained from the automation techniques will provide for more efficient scheduling of the resources. These teams would provide a nucleus of highly trained and experienced personnel that could be deployed on short notice to restore a system to an operational condition and to improve system performance when analysis of the data provided by ATEC reveals the system is approaching a threshold condition. It must be recognized that not all stations will be equipped with ATEC and these must still be scheduled for a routine evaluation. Further, the test teams will still be required for the foreseeable future in order to establish or revise the threshold parameters for ATEC.

CCP 702-1

2-3 OPERATIONS.

a. The wideband evaluation test teams have been provided to accomplish the objectives outlined in DCAC 310-70-57. These teams will not normally be diverted to other missions except when an emergency situation arises which necessitates a temporary diversion from their primary mission.

b. The test teams will be deployed based on the master test schedule and the period of deployment will vary depending on the complexity of the facility to be evaluated, transportation problems and the amount of effort required to optimize the equipment and link parameters. As a general rule an objective of three wideband links will be successively scheduled for each test team. It is anticipated that the three link tests should not exceed 60 days in duration (with an objective of 45 days), at which time the test teams would return to their parent station.

c. During the time that the test teams are not on TDY performing an evaluation of wideband systems in accordance with the master test schedule, they will analyze the raw test data, review test procedures, develop revised and/or new procedures, and prepare detailed maintenance and operations procedures for the communications equipment employed within USACC. Additionally, the systems located in the proximity of the test teams base will be scheduled for a cyclic evaluation during the times that the teams are not on TDY to other geographical areas.

2-4. RESPONSIBILITIES.

a. TEAM CHIEF (7750/7601/0856)

(1) Supervising the test team activities and insuring all data is collected and analyzed on a daily basis and that required reports are prepared as outlined in Chapter 3.

(2) Implementing deviations to test procedures as may be required and/or approved to insure the collected data is complete and valid.

(3) Assisting the test technicians in monitoring, setting up of test configurations and data collection.

(4) Coordinating test activities with the command point of contact, other test teams and personnel as required.

(5) Insuring that all test equipment is accounted for, properly maintained, and protected from loss.

(6) Coordinating system downtime as may be required and maintaining a historical journal of all activities while on site.

(7) Formulating test procedures when the procedures contained in DCAC 310-70-57 are incomplete or are not adaptable to the particular equipment being evaluated. Authorizing minor deviations to the established procedures, fully documenting the change and insuring the data elements remain essentially unchanged.

(8) Directing system adjustments to improve the performance and the validity of the test data being collected.

(9) Reviewing the test procedures contained in DCAC 310-70-57 and providing recommended changes or additions that may be required to improve the program.

(10) Insuring that the completed data package and summary of the test results are forwarded to the TEP detachment within five days of test completion.

(11) Notifying the in-country coordinator of the desired date and time recommended for the out briefing. Notification should be given at least four working days prior to the date scheduled for the briefing.

(12) Providing the operating unit, site personnel, O&M Commander and the local DCA representative with an out briefing at the conclusion of the evaluation.

(13) Providing the O&M Command in writing, a list of on-going corrective actions required to improve the system performance.

(14) Directing sufficient diagnostic testing to isolate a problem or potential problem and providing positive recommendations to correct any noted anomalies.

(15) Providing the in-country coordinator a telephonic report on a daily basis as to the status of testing, problems encountered or other areas that may be of interest to the TEP detachment headquarters.

(16) Advising the in-country coordinator of TMDE that has become non-operational on a daily basis.

(17) Performing a detailed inventory of all equipment in conjunction with the replacement team chief or in-country coordinator.

(18) Advising the detachment headquarters directly of any problems encountered which would influence the test results or cause an alteration of the test schedule.

(19) Insuring that the final test data is representative of the system capability.

CCP 702-1

(20) Maintaining a journal throughout the period of testing to reflect all significant items occurring during the evaluation. As a minimum the journal will include:

(a) Start and stop time for all testing.

(b) Acquisition of systems or circuits for testing and release to the user or time of notification to the technical controller or site personnel that the test sequence has been completed.

(c) Arrival and departure times of test personnel.

(d) Difficulties encountered in technical, logistical or administrative areas.

(21) Assuming responsibility for the health, welfare, morale and conduct of assigned team members when in a test status.

(22) Reviewing and submitting team travel vouchers as a single package to the Commander, TED within 3 working days upon return to detachment headquarters.

(23) Assuring adherence of all team members to locally published dress standards within the command being evaluated.

(24) Other duties as assigned.

b. SENIOR MICROWAVE TECHNICIANS

(1) Conducting the test and measurements in accordance with DCAC 310-70-57 and CCP Regulation 105-4.

(2) Completing the required data elements for all test data collected and insuring the data is valid, legible and is representative of the system potential.

(3) Initiating corrective adjustment, maintenance and/or alignment of the radio and multiplex equipment in coordination with site personnel.

(4) Insuring the test equipment is performing properly, testing techniques are correct and the data being collected is accurate.

(5) Performing organizational maintenance on all assigned equipment.

(6) Other duties as assigned.

c. IN-COUNTRY COORDINATOR.

(1) Providing a centralized point of contact for all test activities within the geographical area being evaluated.

(2) Remaining cognizant of daily testing activities and maintaining a journal of these activities. A copy of the journal will be turned into the detachment for review, and action as required, on a monthly basis.

(3) Initiating requests for authorized outage as may be required and initiating follow-up action as necessary in monitoring the progress of the request. The request will be provided the O&M Command in writing approximately 30 days in advance of the requested outage.

(4) Coordinating with the team chiefs and the O&M Command to establish a mutually agreeable date and time for briefing the O&M Command on the condition of each link evaluated. Notification of the date and time for the briefing will be in writing and will also be provided to the appropriate in-country DCA representative.

(5) Receiving defective or non-operational test equipment from the test teams and replacing the equipment from the Operational Readiness Float (ORF) insofar as possible.

(6) Insuring that non-operational test equipment is turned into the appropriate maintenance activity on an expedited basis. In-country repair facilities will be used to the maximum extent possible; however, equipment may be evacuated to the detachment when deemed appropriate. Equipment evacuated to the detachment must be adequately packed for protection in transit and insured where applicable. The U.S. Mail Service will be used for evacuating defective equipment to the detachment whenever possible.

(7) Maintaining adequate records to reflect the status of all detachment test equipment located in the geographical area being evaluated.

(8) Arranging for movement of test equipment between test teams when necessary to insure that the required on site tests are completed.

(9) Planning in-country transportation requirements for personnel and equipment and insuring that the O&M Commands are provided the requirements in writing far enough in advance to preclude changes to the test schedule. An objective of not less than 10 days prior notice is established for this purpose.

(10) Controlling, issuing, shipping, accounting for, and turn-in of ORF equipment.

(11) Performing periodic inventories of all detachment assets located in the area being evaluated.

(12) Inventorying, securing and maintaining operational control over all vans and equipment not on hand receipt to a team chief. On completing the inventory, the receiving party will receipt for and be responsible for the equipment.

CCP 702-3

(13) Arranging for billeting, messing, and transportation for test personnel prior to their arrival in-country. To accomplish this, it may be necessary for the coordinator to visit the sites to be evaluated. Results of the visit or coordination on the availability of transportation, quarters, messing and related information will be provided the detachment headquarters by electrical transmission after coordinating with the O&M Command.

(14) Providing arriving test personnel with an in-briefing on local customs, regulations, policies, and restrictions that may influence their activities.

(15) Other duties as assigned and as delineated by the Detachment Commander.

2-5. ADMINISTRATIVE REQUIREMENTS.

a. WEARING THE UNIFORM. All personnel are required to comply with the uniform standards outlined in Department of Army Regulations. Additionally, personnel are required to review and comply with the local command policies on wearing the uniform pertaining to the geographical TDY area. The appropriate uniform will be worn during normal duty hours unless the wearing of civilian clothing is encouraged by the host command.

b. TDY ORDERS. All TDY Orders will be prepared and processed by the detachment in sufficient time to permit orderly planning by affected personnel. The orders will normally require that personnel utilize, to the maximum extent possible, government quarters, mess and transportation to include MAC Facilities. When it is impracticable to use these facilities or their use would adversely affect the test teams mission, or they are not available, the orders will be appropriately annotated. In the event quarters and rations are available in a particular area and the team chief determines that the use of such facilities would adversely affect the mission, he will prepare and submit a written certification so that an appropriate amendment to the original orders can be initiated.

2-6. LOGISTICAL SUPPORT.

USACC Subordinate Commanders have been assigned responsibility for logistical support of the TEP. This support includes, but is not limited to; transportation, billeting and messing. Prior to arrival of the test teams in the test area, the Commander, TED will insure that adequate coordination has been effected with the supporting USACC Commander. To this end, team chiefs will be responsible for insuring that their personnel comply with any and all support agreements.

CHAPTER 3. REPORT PROCESSING AND SUBMISSION

3-1. GENERAL.

a. The TEP raw test data is to be analyzed and reduced to the format shown in Appendix A. The data entered in this report will be based on the final test data, after all preliminary tests, adjustments and/or repairs have been accomplished.

b. The TEP report will consist of three volumes for each link and will be assembled as follows:

(1) Volume I: Results of the data reduction and analysis of the final test data for both ends of the link. The required content and format for this volume is shown in Appendix A.

(2) Volume II: Copies of the final raw test data for Station A (less chart recordings, which are to be retained by the TEP activity until the link is reevaluated).

(3) Volume III: Copies of the final raw test data for Station B (less chart recordings, which are to be retained by the TEP activity until the link is reevaluated).

c. Entries on the raw test data forms included in Volumes II and III are to be typed or printed to assure they are legible. Further, the data entries should be checked for completeness, accuracy, neatness and validity (Reproduced copies must be fully legible).

d. An index of the report contents will be inserted in the front of each volume similar to the format contained in Appendix A.

e. The data used for completing Volume I, and the raw test data provided in Volumes II and III will be the final test data, taken after all possible maintenance and/or adjustments have been accomplished by the TEP teams and/or site personnel. Preliminary test data will not be included in these reports, however, it may be used by the TEP team in preparing the team chief's comments.

f. The team chief will maintain a journal throughout the test period. The journal should be used as a historical record of events during the time that test personnel are on site, and as a source of information for out-briefing the O&M commander. The journal will contain information such as the following:

(1) Start and stop times of all tests.

(2) Problems encountered with on-site equipment or equipment organic to the AN/TSM-125 test set.

(3) Transportation, billeting, mess, and related support facilities.

(4) Acquisition time for any system outage and the time that the system was turned back for operations to the local personnel.

3-2 LINK PERFORMANCE CHARACTERISTICS (VOLUME I). This volume of the test report contains the evaluation of the performance characteristics and tabulation of pertinent data on the DCS link or subsystem tested. The required content and format for this report is shown in Appendix A. A brief description of the contents to be contained in each paragraph of the report is shown below. Paragraphs below correspond to those listed in Appendix A, and are therefore keyed to the format of Appendix A.

1.0 General: This paragraph contains a short description of the reports content including such information as the test period, O&M element, test team composition, key personnel contacted and selected link and equipment parameters as shown in Tables I and II of Appendix A. Details should also be included in this paragraph on any denial of requests for AO to perform the required tests.

2.0 Include information on the design number of channels on which path performance calculations and equipment NPR loading tests were based and a tabulation of median noise as shown in Tables III and IV of Appendix A.

2.1 thru 2.XXX These paragraphs contain interpretive discussion of the test results, any anomalies, discrepancies or deviations from expected results (path calculations, design standards, manufacturer's specifications and test and acceptance data) must be included in the discussion. Deficiencies attributed to the O&M element which were not corrected by the test teams or site personnel prior to collecting the final test data must be discussed in detail with supporting documentation. Deficiencies which are corrected by either the test team or site personnel prior to recording of the final test data will be documented in the team chief's comments of the applicable data sheets.

3.0 This paragraph of the report will be used to list the graphical presentation of the performance characteristics of the major equipment on the link. As a minimum the following will be included in the report for each station tested:

- a. Equipment NPR vs Baseband Loading.
- b. Receiver AGC & FM Quieting vs RSL.

The figure numbers outlined in Appendix A will be expanded within the same numerical designation (link or loopback) as may be required to include all combinations tested.

4.0 This paragraph of the report will be used to list the graphical presentation of the link's transmission quality as determined at each end of the link. These transmission quality indicator graphs will be obtained

primarily from the strip chart recordings. As a minimum, the graphs listed in Appendix A will be included in the report. The figure numbers may be expanded within the same numerical designation as required to cover additional tests or for clarification of the test data.

5.0 Omitted and Incomplete Tests: A listing in tabular form of all tests which were omitted, incomplete or which provided invalid data will be contained in Table V. As shown in Appendix A, a concise statement will be entered in the remarks column to explain the reason for the incomplete or invalid test data.

6.0 Conclusions: This paragraph should contain the conclusions reached as a result of the evaluation of the reduced data and test results.

7.0 Technical Recommendations: The recommendations should provide a reasonable solution for correcting any problems or deficiencies which could not be corrected on site. Recommendations must be in sufficient detail to insure that timely corrective actions can be accomplished.

8.0 Link Data Tabulation: The contents of this paragraph will include those elements listed in Appendix A. All elements will be listed and NA will be entered for elements not applicable to a particular station. DNA will be entered where the required data was not available. Separate data sheets for troposcatter and microwave links are inclosed.

9.0 Station Data Tabulation: The required data elements are shown in Appendix A. All elements will be listed and NA will be entered for elements not applicable to a particular station. DNA will be entered where the required data was not available. Separate data sheets for troposcatter and microwave links are inclosed.

10.0 Miscellaneous Station Information: The information required in this paragraph is listed in Appendix A and is self-explanatory.

3-3. REQUIRED TESTS. The tests listed below are the minimum required to be performed at each end of the link in order to provide a complete and comprehensive test report. Test procedures used and documentation of test results will be in accordance with DCAC 310-70-57. All audio series tests are to be performed at the equal level board on a minimum of three channels per group unless noted otherwise.

a. Audio Series Tests

- (1) In-Service Customer Levels (T-3)
- (2) 1 kHz Test Tone Level (T-4)
- (3) Idle Channel Noise (T-8)
- (4) Impulse Noise (T-9). Record the impulse noise on three

channels per group for a minimum of 15 minutes per channel. After completing the initial 15 minute impulse noise count test, establish a long term impulse measurement on a minimum of three channels from those previously tested. The long term impulse count will be a minimum of eight (8) hours duration and should be conducted during a period of heavy traffic loading.

(5) Voice Channel Frequency Response (T-10 or T-11)

(6) Voice Channel Delay Distortion (T-12 or T-13)

(7) Voice Channel Harmonic Distortion (T-14)

(8) Voice Channel Frequency Translation (T-15)

(9) Voice Channel Phase Jitter (T-16 or T-17)

(10) Voice Channel Crosstalk (T-18)

(11) Voice Channel Bit Error Rate (T-19). A minimum of one channel per link at each station will be evaluated. The measurements will be time correlated with other recorded parameters as listed under the recording tests. The tests will be for a minimum of eight hours on each channel tested and the results will be graphically depicted in paragraph 4 of the report.

b. Radio Series Tests

(1) Radio Equipment Noise Power Ratio vs Baseband Loading, RF and/or IF Loopback (T-22).

(2) Link Noise Power Ratio vs Baseband Loading (T-23)

(3) Baseband Level and Frequency Response (T-24)

(4) RF/IF Spurious Emissions (T-25)

(5) Transmitter Carrier Frequency Accuracy (T-27)

(6) Transmitter Modulator Frequency Deviation (T-29)

(7) Transmitter Output Power and VSWR (T-30)

(8) RF Exciter and Power Amplifier Bandwidth (T-31)

(9) Receiver RSL vs AGC, IF and FM Quieting (T-34)

(10) RF Receiver Pre-amplifier Gain and Bandwidth (T-35)

(11) Total Receiver Noise Figure (T-36)

(12) Pre-amplifier and Preselector Bandwidth, Gain and Noise
Figure (T-35)

(13) Receiver Local Oscillator Accuracy (T-37)

(14) Receiver IF Bandpass, FM Discriminator Characteristics (T-39)

(15) Transmit and Receive Baseband Sweep: This test consists of examining the baseband spectrum with the Sierra 128 and display unit with particular attention to carrier leak, low level interference or other extraneous signals. All extraneous signals in excess of -70 dBm0 will be identified and reported in the test data summary of Volume 1 of the report.

c. Multiplex Tests (T-40)

(1) Noise Power Ratio and Basic Noise Ratio of the Multiplex (Back-to-Back): Prior to performing this test the multiplex must be completely aligned and adjusted.

(2) Pilot Levels and Alarm Activation (Link Basis) (T-41)

d. Recording Tests

(1) The following data are to be recorded and used to prepare the graphs listed in Paragraph 4.0 of Appendix A.

(a) Received signal level (microwave - both receivers)
(tropo - at least 3 receivers)

(b) Idle channel noise "C" message.

(c) Phase jitter and phase impulses (when jitter meters become available).

(d) Test tone stability.

(e) Received baseband level.

(2) The RSL of all active receivers, baseband loading and idle channel noise should be recorded throughout the test period. However, a minimum of three days (72 hours) will be recorded after all maintenance and/or adjustments have been accomplished. This is considered the minimum recording period for completing the information outlined in Paragraph 4.0 of Appendix A.

e. Additional tests may be performed at the option of the team chief.

3-4. DATA SUBMISSION. The completed test report in draft will be forwarded to the analysis section within five days after the evaluation has been concluded.

CCP 702-1

APPENDIX A
Sample TEP Report

TECHNICAL EVALUATION PROGRAM

RCS: DCA (AR) A070-1

SUBSYSTEM PERFORMANCE CHARACTERISTICS

FOR

DCS LINK M-0000

STATION A

TO

STATION B

DEPARTMENT OF THE ARMY
6TH SIGNAL COMMAND
TECHNICAL EVALUATION DETACHMENT
BOX 3, APO SF 96263

1.0 GENERAL

The performance of DCS Link M-0000 between Station A and Station B was evaluated in accordance with DCAC 310-70-57. The performance of this link and its capability are reflected in this summary of test results. The link and equipment parameters are shown in Tables I and III, respectively; the raw test data for each station is contained in Volumes II and III. Omitted tests, and reasons for omission, are given in Table V.

1.1 PERIOD OF EVALUATION: 21 APRIL to 1 MAY 1975.

1.2 O&M AGENCY AND MAILING ADDRESS

Headquarters

USACC - (Organization/Country)

ATTN: (Office Symbol)

APO SF 96824

1.3 6TH (or 5TH or 7TH) SIGNAL COMMAND TECHNICAL EVALUATION TEST TEAM COMPOSITION.

1.3.1 STATION A

<u>Name</u>	<u>Rank</u>	<u>Position</u>
Smith, R.L.	Cpt	Team Chief
Brown, R. Q.	SFC	NCOIC
Green, J. R.	SSG	Technician

1.3.2 STATION B

Hartman, G. L.	1 LT	Team Chief
Charles, B. G.	SFC	NCOIC
Richmond, T. R.	SSG	Technician

1.4 KEY PERSONNEL CONTACTED

<u>Name</u>	<u>Grade</u>	<u>Organization</u>	<u>Position</u>
Cartwright, B.A.	Col	CCPXX-CO	Commander
Hoss, C. B.	Maj	CCPXX-OP	C, Ops Div.
Little, J.	Civ	ITT-FEC	Site Tech Supervisor (Station A)
Spock, S. O.	Civ	ITT-FEC	Site Tech Supervisor (Station B)
Kirk, J. T.	Cpt	CCPXX-LOG	Logistics Officer

2.0 SUMMARY OF TEST RESULTS2.1 MEDIAN NOISE (T-1)

This link is currently configured for transmission of 12 voice channels; however, path performance calculations and the evaluation in this report are based on the 300 channel design capacity. A summary of measured and potential median noise performance for Station A and Station B are given in Tables III and IV, respectively. Analysis of the idle channel noise recordings at Station B indicated a median of 19.4 dBmCO for the performance of the Station C to Station B system. A problem in the ink flow system in the chart recorder precluded any long-term recordings; however, no significant variations in recordings were observed during this period. A composite average of short-term measurements taken at Station C and Station B was 17.5 dBmCO, disregarding the one noisy channel (SG2 GP4 CH2) at Station C. At the current low loading level, this appears to be a more realistic representation of system performance.

2.2 MEDIAN RECEIVE SIGNAL LEVEL (RSL) (T-1)

Analysis of the recorded data taken at Station A revealed considerable variation in the receive signal level. Similar variations were also noted on the Station C to Station A link during a previous evaluation. These variations are attributed to instability of the antenna structure at Station A which results in excursions of as much as 5 dB whenever the antenna is subjected to

only moderate winds. There is a possibility that during high winds the antenna alignment would be sufficiently altered so as to result in major communications outage. To preclude this, action should be taken to install stabilizing bars or guys on the antenna system. Considering the signal level variations discussed above, a median of -39.4 dBm was obtained at Station A, which is approximately 4.3 dB lower than the predicted level. This is primarily attributed to the low output power of the transmitter at Station B as outlined in Paragraph 2.17 of this report.

Recordings at Station B were suspended after several hours due to a defective chart recorder. An interpolated median for the short recording period, however, provided a favorable reverse path correlation.

2.3 1 kHz TEST TONE LEVEL CHECK (T-4)

The internal multiplex levels deviated considerably from the required level at both sites with the worst case being the receive group distribution point at Station B. Reviewing the block and level diagram [KHAOS drawing 15872-G1-676(1.45 (B))] reveals that the 0 dBm level at the group receive is -8 dBm; however, the measured levels at this point were 15.6 to 17.5 dB higher than the required level. An attempt was made to adjust the group modules to the correct output level, but to no avail. Consideration was given to installing attenuators at the group to reduce the output level and bring the equipment within specifications; however, the

CCP 702-1

majority of the channel modems did not have sufficient gain to compensate for the level discrepancies. The high levels are a potential source of crosstalk and intermodulation, and action should be taken to properly align the multiplex and ascertain the specific cause of the high levels. At Station C the group levels varied from 5 to 7 dB from the required level, while the levels at the HF distribution were within specifications. The multiplex on this end of the line should also be completely aligned to insure that it is within specifications at the various test points.

2.4 IDLE CHANNEL NOISE (T-8)

None of the channels tested at Station C or Station B exceeded the DCA standard of 27 dBrnC0 as contained in DCAC 300-175-9. This was to be expected due to the extremely light loading on the system. A significant difference exists at both ends of the link when measuring in C-message weighting as opposed to flat weighting. This is primarily attributed to the 60 Hz components and various harmonics that are passed by the 3 kHz flat filter but are not within the bandpass of the C-message filter. The installation of an effective station ground at both stations and reducing the rectifier ripple voltage at Station C should result in a corresponding improvement in flat weighted measurements.

2.5 IDLE CHANNEL IMPULSE NOISE (T-9)

The channels evaluated at both ends of the link met the specification of 15 counts per fifteen minutes at 72 dBrnC0. The

cumulative long-term results were also well within the prescribed tolerance.

2.6 VOICE CHANNEL FREQUENCY RESPONSE (T-11)

Only one channel (SG2 GP4 CH11) at Station B met the specification as outlined in Paragraph 5.3.2.3.1 of MIL-STD 188-300, while at Station C all of the channels evaluated failed to meet this requirement. The majority of channels, however, did meet the less stringent manufacturer's design objective.

2.7 ENVELOPE DELAY DISTORTION (T-12)

All of the channels failed to meet the standards as specified in MIL-STD 188-300. The fact that the channels do not meet these objectives is not considered a serious limitation since external equalization equipment would normally be used to condition those circuits carrying data traffic. The unusual characteristic noted at Station C is apparently attributed to the test equipment and not the channel modem.

2.8 VOICE CHANNEL HARMONIC DISTORTION (T-14)

Of the channels tested at Station C, only one channel met the 1% specification, while at Station B all channels were within specifications. A manual sweep of the channels displaying high distortion levels revealed that the second harmonic of the 700 Hz fundamental tone was prevalent in the channels. A signal appearing outside the normal channel bandpass characteristics was also detected at the VF patch board.

2.9 VOICE CHANNEL FREQUENCY TRANSLATION (T-15)

No frequency translation was observed on any of the channels tested. These were short-term measurements, however, and would not necessarily reflect an accurate portrayal over an extended period of time.

2.10 VOICE CHANNEL PHASE JITTER (T-17)

The phase jitter measurements were performed using the oscilloscope method. Therefore, the accuracy of the test results are subject to interpretation. Considering this, the measured phase variations were approximately 5.7° at Station B and 1.25° or less at Station C. These measurements are substantially lower than the maximum allowable variation of 15° as contained in DCAC 300-175-9. A more accurate and precise measurement of this parameter will be possible when the test teams are equipped with a phase jitter meter.

2.11 VOICE CHANNEL CROSSTALK (T-18)

Both near and far end crosstalk measurements on all of the channel tested met the specification outlined in Paragraph 5.2.1.6 of MIL-STD 188-300. At Station C it was found that the -10 dBm0 test tone on channel 12 increased idle channel noise measurements taken on channel 11. The test team noted a difference of about 1 dB additional noise with the tone on as opposed to tone off condition. Moreover, ICN's appeared to follow a periodic sinusoidal response of 1 cycle per minute.

2.12

RADIO LINK NOISE POWER RATIO (T-23)

The radio link noise power ratio (NPR) was measured for a maximum of 240 channels, although the equipment was designed for 300 channel CCIR loading. The test equipment contained in the AN/TSM-125 test set does not provide the capability for evaluating equipment beyond 240 channel loading. A review of the test data indicates that the overall NPR performance for this link is extremely poor in comparison to the generally accepted standard of 55 dB. Also the data indicates that the equipment is operating below the manufacturer's performance specification as stated in TM 11-5820-684-15.

The NPR curves plotted from the data taken at Station A peak at typical NPR values but occur below the CCIR or DCA recommended loading levels. At Station B the NPR's were extremely poor in all slots and configurations tested even at current traffic loading levels. Although the NPR's were poor, BNR values were typical. Therefore, the low NPR's appear to be attributed to poor klystron linearization and receiver equalization.

2.13

RADIO LINK BASEBAND LEVEL AND FREQUENCY RESPONSE (T-24)

During pre-liminary testing it was found that the transmitters were incorrectly strapped resulting in the baseband being double terminated. The test teams corrected the strapping in the "B" transmitters and also installed appropriate pads in the baseband filter units to insure that the proper level was being provided

the modulators. Final test results showed that all transmitter-receiver combinations were within the ± 0.5 dB requirement except for those taken with the "B" transmitter at Station B which reflected abnormal frequency characteristics below 100 kHz. Further investigation of this problem should be accomplished by the O&M Command.

2.14 SPURIOUS EMISSIONS (T-25)

Examinations of the RF and IF spectrums revealed that all discernable emissions were well below the DCA specifications at both stations.

2.15 TRANSMITTER CARRIER FREQUENCY ACCURACY (T-27)

Only the "A" transmitter at Station A and the "B" transmitter at Station B met the DCA objective of ± 150 kHz from the assigned frequency. All transmitters, however, were well within the manufacturer's specification of 0.02%.

2.16 TRANSMITTER MODULATOR FREQUENCY DEVIATION (T-29)

At Station A the initial setting of modulator deviation was measured to be 214.3 kHz RMS and 229.6 kHz RMS for the "A" and "B" transmitters respectively. At Station B deviation was found to be 178 kHz RMS and 176 kHz RMS for the "A" and "B" transmitters respectively. Deviation was adjusted by the test teams to the required level of 200 kHz RMS. Modulator linearity checks were accomplished on all transmitters using the carrier drop out method. Minor deviations were noted between the measured versus calculated

values at both sites.

17 TRANSMITTER OUTPUT POWER & VSWR (T-30)

Neither the "A" nor the "B" transmitter at Station B met the manufacturer's minimum requirement of 0.562 watts. The "A" transmitter, being the lower of the two with an output power of only 0.372 watts, should be replaced immediately, while the "B" transmitter can be programmed for replacement during the next maintenance period. At Station A the measured output power was 0.776 watts and 1.349 watts for the "A" and "B" transmitters respectively. VSWR measurements of the waveguide system at both ends reflected realistic test results for this equipment, although not meeting the DCA standards of 1.05:1.

18 RF RECEIVER INPUT POWER VERSUS AGC AND FM QUIETING CHARACTERISTICS (T-34)

Receiver quieting characteristics at Station A were typical for this type of equipment, with FM thresholds slightly better than the normal value of -81 dBm on both receivers. The quieting curves taken at Station B show considerable amount of residual noise in the 70 kHz slot at RF input levels above -75 dBm. From previous experience it was determined that the Alfred 650 RF generator contained high intrinsic noise components which drastically affect the low slot with less serious effect on the mid and high slots at input signal levels above -45 dBm as shown by the graphs. Test results, however, are still considered valid below RF input signal

levels of -75 dBm. FM thresholds of -81 dBm and -82 dBm were extrapolated from the quieting curves for the "A" and "B" receivers respectively, using the mid slot as a reference. A review of the quieting data also indicates that the "B" receiver at Station B has a slightly lower IF gain than normal.

2.19 RF RECEIVER LOCAL OSCILLATOR FREQUENCY ACCURACY (T-37)

An indirect approach to determine the local oscillator frequency accuracy was attempted at Station A by inserting the assigned signal into the front end of the receiver and measuring the resultant IF frequency at the IF monitor point. Measurements taken with the AFC circuitry disabled compared closely with those taken with the AFC circuitry activated. The calculated results, however, indicated that the local oscillator frequency accuracy exceeded the DCA requirements of 0.02%. The AN/FRC-109 LO cannot be measured directly and, therefore, the method used provides only a relative indication of the LO frequency.

2.20 RECEIVER IF BANDPASS AND DISCRIMINATOR CHARACTERISTICS (T-39)

The IF bandpass test was not attempted at either station due to the lack of appropriate subminiature connectors used to interface the IF amplifier output to the instrumentation. The discriminator characteristics for both receivers at Station A appear to be linear over the required bandwidth. The zero crossover frequency was detected at 70 MHz and 71 MHz for the "A" and "B" receivers respectively. The discriminator for both receivers at

Station B tends to indicate minor non-linearities; however, the data was taken with an HP 410C voltmeter which does not provide sufficient accuracy. Additional measurements should be accomplished by the O&M Command with a microwave link analyzer similar to the HP 3701 to verify and/or correct any non-linearities in the equipment.

2.21 MISCELLANEOUS OBSERVATIONS

- a. Group pilot equipment is not installed at Station B.
- b. It was observed that the TA-182 signalling converters introduced noise in the baseband whenever the ringers were activated.
- c. The waveguide system at Station B contains excessive amounts of flexible waveguide which could result in unnecessary signal attenuation.
- d. The waveguide pressurization system at Station B and Station A consists of a reserve air tank and a hand pump.
- e. There are no audible alarms installed on either the multiplex or radio equipment. This could result in unnecessarily extended outages since a failure could go unnoticed for a period of time.
- f. The radio orderwire between the two sites does not provide for a ringdown capability or other convenient means of signalling other than the "shutdown" method.
- g. On-site test equipment is not available to perform the

test required by DCAC 310-70-1, DCAC 310-70-57, and USACC-PAC Regulation 105-4.

h. No provision is made for monitoring voice circuits at the VF patch bays. Both jacks on the VF patch strip are "break" type jacks.

EQUIPMENT PERFORMANCE INDICATORS

Using the data obtained during the evaluation, the performance of the major radio equipment are contained in the figures listed below. (Actual figures not part of this sample)

<u>FIGURE</u>	<u>DESCRIPTION</u>
1	Receiver AGC & FM Quieting Characteristics, "A" Receiver at Station A
1a	Receiver AGC & FM Quieting Characteristics, "B" Receiver at Station A
2	Receiver AGC & FM Quieting Characteristics, "A" Receiver at Station B
2a	Receiver AGC & FM Quieting Characteristics, "B" Receiver at Station B
3	Typical Quieting Characteristics of the AN/FRC-109 Based on the Manufacturer's Data

4.0 TRANSMISSION QUALITY INDICATORS

From the reduced test data, transmission quality as determined from each end of the link is reflected in the figures listed below (Actual figures not part of this sample)

- 4 Distribution of Median Received Signal Level (RSL), Station A
- 5. Distribution of Median Idle Channel Noise (ICN), Station B

<u>FIGURE</u>	<u>DESCRIPTION</u>
6	NPR vs Baseband Loading, "A" Transmitter at Station B to "A" Receiver at Station A
6a	NPR vs Baseband Loading, "A" Transmitter at Station B to "B" Receiver at Station A
6b	NPR vs Baseband Loading, "A" Transmitter at Station B to Receiver Combined at Station A
6c	NPR vs Baseband Loading, "B" Transmitter at Station B to "A" Receiver at Station A
6d	NPR vs Baseband Loading, "B" Transmitter at Station B to Receiver at Station A
6e	NPR vs Baseband Loading, "B" Transmitter at Station B to Receiver Combined at Station A
7	NPR vs Baseband Loading, "A" Transmitter at Station A to "A" Receiver at Station B
7a	NPR vs Baseband Loading, "A" Transmitter at Station A to "B" Receiver at Station B
7b	NPR vs Baseband Loading, "A" Transmitter at Station A to Receiver Combined at Station B
7c	NPR vs Baseband Loading, "B" Transmitter at Station A to "A" Receiver at Station B
7d	NPR vs Baseband Loading, "B" Transmitter at Station A to "B" Receiver at Station B
7e	NPR vs Baseband Loading, "B" Transmitter at Station A to Receiver Combined at Station B

5.0 OMITTED AND/OR INCOMPLETE TESTS

The tests listed in Table V of this report were either not performed at all or were performed in such a way as to yield incomplete or invalid data.

6.0 CONCLUSIONS

Considerable on-site maintenance, adjustments, and alignment are required to bring the system up to its peak performance capability.

7.0 TECHNICAL RECOMMENDATIONS

a. The recommended standard for idle channel noise under the performance monitoring program for the Station A - Station B - Station C system is 18 dBmC0. The recommended standard for receive signal level for the Station A - Station B link is -34.5 dBm. The recommended standard at current loading levels for baseband loading for this system is +1 dBm0.

b. The antenna support structure at Station A should be reinforced to stabilize the antenna.

c. A routine quality assurance program should be established at both sites to insure that channel levels are being maintained within the required tolerance. This program should include the measurement and adjustment of the channel output, group, supergroup, and baseband level on a periodic basis using a 1 kHz test tone referenced to the engineered level.

d. Further investigation of the hot levels at the group distribution point at Station B should be accomplished and the levels adjusted to -8 dBm.

e. The 60 Hz components which are affecting the flat weighting measurements should be investigated and eliminated. This investigation should include a survey and measurement of the

station ground, potential between equipments, bonding, shielding, and proper termination of the distribution cables.

f. The DC rectifier at Station C should be replaced with a DC power distribution system that is DCA compliant. The power system currently being installed at a number of locations in this geographical area should be considered for all sites that do not have a power distribution system that meets DCA requirements.

g. A complete realignment of the multiplex equipment is necessary at both sites, and this should reduce the inter-modulation, crosstalk, and harmonic distortion so that the equipment meets the manufacturer's specifications.

h. The radio equipment at both ends of the link should be optimized and procedures established to insure that the equipment is maintained to specifications. To optimize the radio equipment and to obtain the best possible noise power ratio performance, a delay and linearity test set similar to the HP 3710 will be required.

i. Further investigation of the "B" transmitter at Station B should be accomplished to determine the specific problem that is limiting the frequency response below 100 kHz. From previous testing of the AN/FRC-109 radio equipment in this area, there is a possibility that the "B" transmitter has not been properly strapped for hot standby operation.

j. The modulator linearity should be verified at both sites

with a link analyzer.

k. The transmit klystrons for both radios at Station B should be replaced. The O&M Command should establish a record at each site that will show the date the klystron was installed and that output power measurements and klystron activity checks were accomplished. This record should be reviewed to insure that the manufacturer's recommendations for klystron life-cycle is being observed.

l. The output power on the "A" transmitter at Station A should be measured periodically and the klystron replaced when it can no longer meet the manufacturer's minimum specifications.

m. The "B" receiver at Station B should be examined using a link analyzer to ascertain the reason for the low IF gain.

n. The local oscillator on all receivers should be tuned to the correct crossover frequency using a link analyzer with internal adjustments of the IF amplifiers as required.

o. A master multiplex synchronizing plan should be developed and implemented as soon as possible. This plan should include all existing and proposed DCS links.

p. Future installations of radio equipment should include provisions and be configured to facilitate measurements such as receiver noise figure, VSMR, output power, equipment NPR's, etc., without disassembly of the waveguide.

q. The TA-182 signalling converters should be replaced with a modern solid-state unit similar to the CV-1548. If not replaced, action should be taken to insure the output tone does not exceed -10 dBm0. Further, a contingency plan should be developed to insure uninterrupted service to the subscriber in the event of failure of the primary power to these units.

r. The waveguide system at Station B should be reengineered to reduce the amount of flexible waveguide and to provide a transmission line that is in accordance with good engineering practices.

s. The waveguide pressurization system at Station B and Station B should be replaced with one that will automatically maintain pressure to the transmission line.

t. Audible alarms should be installed at both sites to alert personnel of equipment or system failure.

u. The orderwire should be reengineered at both sites to provide a better method for coordinating system alignment, maintenance, and/or system restoral.

v. The sites should be provided as-built drawings, required technical publications, operational standards, and test and acceptance data.

w. The patch and test facilities at both sites should be engineered to provide standardization throughout the system in accordance with MIL-STD 188-310.

CCP 702-1

x. The sites should be provided the test equipment required to perform the test outlined in DCAC 310-70-1 and 6th Signal Command Regulation 105-4.

LINK PARAMETERS (TABLE 1)		LINK NO.	DATE (DAY, MONTH, YEAR)				
Station Tested	Link Length (mi/km)	Propagation Mode	Scatter Angle	Transmitter Frequency (MHz)	Type Terminal	Diversity	
						Order	Type
STATION A	32.87/52.9	LOS	NA	/182.5	Repeater/Mux	N/A	
STATION B							MUX
REMARKS							
The radio equipment is configured for hot standby transmission.							

LINK EQUIPMENT TESTED (TABLE II)							DATE (day, month, year)			
STATION TESTED	RADIO TYPE	OUTPUT POWER	MUX TYPE	CHAN CAPACITY	CHAN INSTALLED	ANTENNA TYPE AND SIZE				
STATION A	AN/FRC-109	Normal 1 watt	AN/FCC-55	300	See comments	PARABOLIC _____ FT	NEAR FIELD PASSIVE _____ FT	FAR FIELD PASSIVE _____ FT		
STATION B	AN/FRC-109	Normal 1 watt	AN/FCC-55	300	12	PARABOLIC _____ FT	NEAR FIELD PASSIVE _____ FT	FAR FIELD PASSIVE _____ FT		
RF PREAMPLIFIER TYPE (Identify station and type if installed)							None			
COMMENTS CONCERNING ANTENNA PARAMETERS NOT LISTED:										
OTHER COMMENTS:										
The 12 channels from Station B are thru - grouped at Station A and breakout at Station C.										

TABLE III

SUMMARY OF LINK PERFORMANCE		DATE <u>day, month, year</u> _____	
STATION UNDER TEST		PAGE _____ OF _____ PAGES	
STATION A		DCS LINK NO. <u>M-0000</u>	
PARAMETER	MEASURED		POTENTIAL
RECEIVE SIGNAL LEVEL	dbm		dbm
A PATH:	<u>-39.3</u>		
B PATH:	<u>NA</u>		<u>-34.5</u>
RADIO LINK NOISE	NPR db	BNR db	NPR / PWCO
A PATH LOW <u>70</u> KHz	<u>49</u>	<u>71</u>	
MID <u>534</u> KHz	<u>45.5</u>	<u>69</u>	
HIGH <u>1002</u> KHz	<u>45.5</u>	<u>71</u>	<u>54.2 / 204.8</u>
B PATH LOW <u>70</u> KHz	<u>43</u>	<u>72</u>	
MID <u>534</u> KHz	<u>47</u>	<u>71</u>	
HIGH <u>1002</u> KHz	<u>50</u>	<u>71</u>	<u>54.2 / 204.8</u>
COMBINED LOW <u>70</u> KHz	<u>48.5</u>	<u>72</u>	
MID <u>534</u> KHz	<u>45</u>	<u>67</u>	
HIGH <u>1002</u> KHz	<u>48</u>	<u>72</u>	<u>54.2 / 204.8</u>
MULTIPLEX NOISE	NPR db	BNR db	dbmCO pwcO
LOW _____ KHz	<u>NA</u>	<u>NA</u>	<u>DNA</u> <u>DNA</u>
MID _____ KHz	<u>NA</u>	<u>NA</u>	<u>DNA</u> <u>DNA</u>
HIGH _____ KHz	<u>NA</u>	<u>NA</u>	<u>25.3</u> <u>338.3</u>
RADIO AND MULTIPLEX NOISE	dbmCO	pwcO	dbmCO pwcO
LOADED	<u>NA</u>	<u>NA</u>	<u>27.3</u> <u>543.1</u>
TRAFFIC LOADED (MEDIAN)	<u>NA</u>	<u>NA</u>	
DCA OPERATIONAL STANDARD (DCAC 300-175-9)	<u>27</u> dbmCO		pwcO <u>501</u>
RECOMMENDED STANDARD	<u>18**</u> dbmCO		pwcO <u>63</u>

* NPR/BNR measurements are shown at +14.8 dbmO loading.
 ** Applicable for the Station B thru Station A to Station C system.

TABLE IV

SUMMARY OF LINK PERFORMANCE		DATE <small>day, month, year</small> _____	
		PAGE _____ OF _____ PAGES	
STATION UNDER TEST		DCS LINK NO.	
Station B		M-0000	
PARAMETER	MEASURED		POTENTIAL
RECEIVE SIGNAL LEVEL	dbm		dbm
A PATH:	<u>39.5*</u>		<u>-34.5</u>
B PATH:	<u>NA</u>		
RADIO LINK NOISE **	NPR db	BNR db	NPR / PWCO
A PATH LOW <u>70</u> KHz	<u>DNA</u>	<u>68</u>	
MID <u>534</u> KHz	<u>DNA</u>	<u>66</u>	
HIGH <u>1002</u> KHz	<u>DNA</u>	<u>61</u>	<u>54.2 / 204.8</u>
B PATH LOW <u>70</u> KHz	<u>DNA</u>	<u>68</u>	
MID <u>534</u> KHz	<u>28</u>	<u>69</u>	
HIGH <u>1002</u> KHz	<u>DNA</u>	<u>64</u>	<u>54.2 / 204.8</u>
COMBINED LOW <u>70</u> KHz	<u>DNA</u>	<u>69</u>	
MID <u>534</u> KHz	<u>31</u>	<u>68</u>	
HIGH <u>1002</u> KHz	<u>DNA</u>	<u>65</u>	<u>54.2 / 204.8</u>
MULTIPLEX NOISE	NPR db	BNR db	dbmCO pwcO
LOW _____ KHz	<u>DNA</u>	<u>DNA</u>	<u>DNA</u> <u>DNA</u>
MID _____ KHz	<u>DNA</u>	<u>DNA</u>	<u>DNA</u> <u>DNA</u>
HIGH _____ KHz	<u>DNA</u>	<u>DNA</u>	<u>25.3</u> <u>338.1</u>
RADIO AND MULTIPLEX NOISE	dbmCO	pwcO	dbmCO pwcO
LOADED	<u>DNA</u>	<u>DNA</u>	<u>27.3</u> <u>543.1</u>
TRAFFIC LOADED (MEDIAN)	<u>18.7*</u>	<u>74.1</u>	
DCA OPERATIONAL STANDARD (OCAC 300-175-9)	<u>27</u> dbmCO		pwcO <u>501</u>
RECOMMENDED STANDARD	<u>18***</u> dbmCO		pwcO <u>63</u>

* Short term recordings.

** NPR/BNR measurements are shown at +14.8 dBmO loading.

***Applicable for the Station B thru Station A to Station C system.

OMITTED AND/OR INCOMPLETE TESTS - TABLE V

STATION	TEST DESCRIPTION	REMARKS
Both	Radio Equipment Noise Power Ratio (NPR) Test (T-22)	No test points to permit for RF or IF loopback configuration.
Both	Total RF Receiver Noise Figure (T-36)	Proper band noise source not available.
Both	RF Receiver IF Bandpass Characteristics (T-39)	Not performed due to lack of subminiature connectors.

8.0	LINK DATA TABULATION - LOS	FROM	STATION	TO
8.1	DCS Link Number	()
8.2	DCA Area			
8.3	TEP Testing MILDEP			
8.4	Test Period			
8.5	Operating MILDEP			
8.6	Path Length (smi/km/nm)	()
8.7	Diversity:			
	a. Order			
	b. Type			
8.8	Transmitter Output Power (watts)			
8.9	Path Antenna Gain (dB)	()
8.10	Transmission Line & Miscellaneous Loss (dB)			
8.11	Path Transmission Loss (dB)	()
8.12	Calculated Median RSL (dBm)	()
8.13	Measured Receive Signal Level (dBm):			
	a. Receiver #1			
	(1) Exceeded 10% of Time			
	(2) Exceeded 50% of Time			
	(3) Exceeded 90% of Time			

LINK DATA TABULATION LOS (CONT'D)

FROM STATION TO

b. Receiver #2

(1) Exceeded 10% of Time

(2) Exceeded 50% of Time

(3) Exceeded 90% of Time

c. Recommended PMP Level
(Suppl 4, DCAC 310-70-57)8.14 Fade Margin (Difference between Median
RSL and RSL at FM Improvement Threshold
(dB):a. Value from Path Loss Calculation
(dB)

b. Measured:

(1) Receiver #1

(2) Receiver #2

8.15 Link NPR/BNR (dB) at ____ dBm0 Loading:

a. Measured (TX No ____ RX No ____):

(1) Low ____ (kHz)

(2) Mid ____ (kHz)

(3) High ____ (kHz)

(4) Median RSL During Test
(dBm)

b. Measured (TX No ____ RX No ____):

LINK DATA TABULATION LOS (CONT'D)

FROM STATION TO

- (1) Low _____ (kHz)
- (2) Mid _____ (kHz)
- (3) High _____ (kHz)
- (4) Median RSL During Test
(dBm)

c. Combined:

- (1) Low _____ (kHz)
- (2) Mid _____ (kHz)
- (3) High _____ (kHz)
- (4) Median RSL During Test
(dBm) (Best Receiver)

8.16 Voice Channel Noise (dBrnC0):

- a. DCA Standard ()
- b. Measured (from recorded data):
 - (1) Exceeded 10% of Time
 - (2) Exceeded 50% of Time
 - (3) Exceeded 90% of Time

8.17 Impulse Noise (for 8 - hour period)
(counts):

- a. Measured (CH _____ GP _____ SG _____):
 - (1) Low _____ dBrnC0

LINK DATA TABULATION LOS (CONT'D)

FROM STATION TO

(2) Mid _____ dBrnC0

(3) High _____ dBrnC0

b. Measured (CH___ GP___ SG___):

(1) Low _____ dBrnC0

(2) Mid _____ dBrnC0

(3) High _____ dBrnC0

c. Measured (CH___ GP___ SG___):

(1) Low _____ dBrnC0

(2) Mid _____ dBrnC0

(3) High _____ dBrnC0

8.18 Baseband Loading:

a. Calculated (see Suppl 4, DCAC 310-70-57)

b. Exceeded 10% of Time

c. Exceeded 50% of Time (median) ..

d. Recommended PVP Level

9.0	STATION DATA TABULATION - LOS	FROM	STATION	TO
9.1	Type Terminal			
9.2	VF Channel Data:			
	a. Design Capacity			
	b. Number of Channels Installed ...			
	c. Number of Channels in Use			
	d. Number of VF Channels			
	e. Number of Data Channels			
	f. Number of Thru Groups			
	g. Number of Thru Supergroups			
9.3	Multiplex Equipment Type			
9.4	Radio Equipment Type			
9.5	Antenna System:			
	a. Antenna Size (ft):			
	(1) Parabolic			
	(2) Near Field Passive			
	(3) Far Field Passive			
	b. Antenna Gain (dB):			
	(1) Parabolic			
	(2) Parabolic and Passive			

STATION DATA TABULATION-LOS (CONT'D)

FROM STATION
TO

(3) Far Field Passive

c. Transmission Line:

(1) Type (RG/WR, etc)

(2) Length (meters)

(3) Loss (dB)

9.6 VSWR:

a. DCA Standard ()

b. Measured:

(1) Transmission Line #1

(2) Transmission Line #2

9.7 Transmitter Frequency Assignment (GHz):

a. Transmitter #1

b. Transmitter #2

9.8 Transmitter Frequency Accuracy (%):

a. DCA Standard ()

b. Manufacturer's Specifications ..

c. Measured:

(1) Transmitter #1

(2) Transmitter #2

STATION DATA TABULATION-LOS (CONT'D)		FROM	STATION	TO
9.9	Transmitter Power (watts):			
	a. Manufacturer's Specifications ..			
	b. Measured:			
	(1) Transmitter #1			
	(2) Transmitter #2			
9.10	Transmitter Deviation (kHz RMS):			
	a. Manufacturer's Specifications ..			
	b. Measured/Adjusted to:			
	(1) Transmitter #1			
	(2) Transmitter #2			
9.11	Transmitter Spurious Emissions (dBm/GHz):			
	a. DCA Standard	()
	b. Manufacturer's Specifications ..			
	c. Measured:			
	(1) Transmitter #1			
	(2) Transmitter #2			
9.12	RF Pre-Amplifier Gain & Noise Figure (dB/dB):			
	a. DCA Standard	()
	b. Manufacturer's Specifications ..			

STATION DATA TABULATION-LOS (CONT'D)

FROM STATION TO

- c. Measured:
 - (1) Receiver #1
 - (2) Receiver #2
- 9.13 Total Receiver Noise Figure (dB):
 - a. DCA Standard ()
 - b. Manufacturer's Specifications ..
 - c. Measured:
 - (1) Receiver #1
 - (2) Receiver #2
- 9.14 Receiver LO Frequency Accuracy (%):
 - a. DCA Standard ()
 - b. Manufacturer's Specifications ..
 - c. Measured:
 - (1) Receiver #1
 - (2) Receiver #2
- 9.15 Receiver FM Threshold (dBm):
 - a. Manufacturer's Specifications ..
 - b. Measured:
 - (1) Receiver #1

STATION DATA TABULATION-LOS (CONT'D)

FROM STATION TO

(2) Receiver #2

9.16 Threshold Extension Improvement (dB):

a. DCA Standard ()

b. Manufacturer's Specifications ..

c. Measured:

(1) Receiver #1

(2) Receiver #2

9.17 Receiver IF Bandwidth (MHz):

a. Manufacturer's Specifications ..

b. Measured:

(1) Receiver #1

(2) Receiver #2

9.18 IF Frequency at Zero Discriminator Output (MHz):

a. Manufacturer's Specifications ..

b. Measured:

(1) Receiver #1

(2) Receiver #2

9.19 Receiver Discriminator Characteristics (% of Non-Linearity):

STATION DATA TABULATION-LOS (CONT'D)

FROM STATION TO

- a. DCS Standard ()
- b. Manufacturer's Specifications ..
- c. Measured:
 - (1) Receiver #1
 - (2) Receiver #2

9.20 Radio Equipment NPR/BNR (dB) for RF _____
or IF _____ Loop at _____ dBm Loading:

- a. DCA Standard ()
- b. Manufacturer's Specifications ..
- c. Measured (TX No _____ RX No _____):
 - (1) Low _____ (kHz)
 - (2) Mid _____ (kHz)
 - (3) High _____ (kHz)
 - (4) RSL During Test (dBm)
- a. Measured (TX No _____ RX No _____):
 - (1) Low _____ (kHz)
 - (2) Mid _____ (kHz)
 - (3) High _____ (kHz)
 - (4) RSL During Test (dBm)

STATION DATA TABULATION-LOS (CONT'D)

FROM STATION TO

9.21 Multiplex Equipment Loop -NPR/BNR (dB)
for dBm0 Loading:

a. Manufacturer's Specifications ..

b. Measured:

(1) Low _____ (kHz)

(2) Mid _____ (kHz)

(3) High _____ (kHz)

8.0	LINK DATA TABULATION - TROPO	FROM	STATION	TO
8.1	DCS Link Number	()
8.2	DCA Area			
8.3	TEP Testing MILDEP			
8.4	Test Period			
8.5	Operating MILDEP			
8.6	Path Length (smi/km/mm)	()
8.7	Scatter Angle (mr)			
8.8	Diversity:			
	a. Order	()
	b. Type	()
8.9	Transmitter Output Power (watts) Design.	()
8.10	Path Antenna Gain (dB)	()
8.11	Transmission Line & Miscellaneous Loss (dB)			
8.12	Path Transmission Loss (dB)	()
8.13	Calculated Median RSL (dBm)	()
8.14	Measured Receive Signal Level (dBm):			
	a. Receiver #1			
	(1) Exceeded 10% of Time			
	(2) Exceeded 50% of Time			
	(3) Exceeded 90% of Time			

LINK DATA TABULATION-TROPO (CONT'D)

STATION
FROM TO

b. Receiver #2

- (1) Exceeded 10% of Time
- (2) Exceeded 50% of Time
- (3) Exceeded 90% of Time

c. Receiver #3

- (1) Exceeded 10% of Time
- (2) Exceeded 50% of Time
- (3) Exceeded 90% of Time

d. Receiver #4

- (1) Exceeded 10% of Time
- (2) Exceeded 50% of Time
- (3) Exceeded 90% of Time

e. Recommended PMP Level
(Suppl 4, DCA 310-70-57)

8.15 Fade Margin (Difference between Median
RSL and RSL at FM Improvement Threshold
(dB):

- a. Value from Path Loss Calculation
(dB)
- b. Measured:
 - (1) Receiver #1
 - (2) Receiver #2

LINK DATA TABULATION-TROPO (CONT'D)

FROM STATION TO

(3) Receiver #3

(4) Receiver #4

8.16 Link NPR/BNR (dB) at ____ dBm0 Loading:

a. Measured (TX No ____ RX No ____):

(1) Low ____ (kHz)

(2) Mid ____ (kHz)

(3) High ____ (kHz)

(4) Median RSL During Test
(dBm)

b. Measured (TX No ____ RX No ____):

(1) Low ____ (kHz)

(2) Mid ____ (kHz)

(3) High ____ (kHz)

(4) Median RSL During Test
(dBm)

c. Measured (TX No ____ RX No ____):

(1) Low ____ (kHz)

(2) Mid ____ (kHz)

(3) High ____ (kHz)

(4) Median RSL During Test
(dBm)

LINK DATA TABULATION-TROPO (CONT'D)

FROM STATION TO

d. Measured (TX No _____ RX No _____):

- (1) Low _____ (kHz)
- (2) Mid _____ (kHz)
- (3) High _____ (kHz)
- (4) Median RSL During Test (dBm)

e. Combined:

- (1) Low _____ (kHz)
- (2) Mid _____ (kHz)
- (3) High _____ (kHz)
- (4) Combined (or average) RSL During Test

f. Combined:

- (1) Low _____ (kHz)
- (2) Mid _____ (kHz)
- (3) High _____ (kHz)
- (4) Combined (or average) RSL During Test

8.17 Voice Channel Noise (dBrnC0):

- a. DCA Standard ()
- b. Measured (from recorded data):
 - (1) Exceeded 10% of Time

LINK DATA TABULATION-TROPO (CONT'D)

STATION
FROM TO

(2) Exceeded 50% of Time

(3) Exceeded 90% of Time

8.18 Impulse Noise (for 8-hour period)
(counts):

a. Measured (CH ___ GP ___ SG ___):

(1) Low _____ dBrnC0

(2) Mid _____ dBrnC0

(3) High _____ dBrnC0

b. Measured (CH ___ GP ___ SG ___):

(1) Low _____ dBrnC0

(2) Mid _____ dBrnC0

(3) High _____ dBrnC0

c. Measured (CH ___ GP ___ SG ___):

(1) Low _____ dBrnC0

(2) Mid _____ dBrnC0

(3) High _____ dBrnC0

8.19 Baseband Loading:

a. Calculated (see Suppl 4,
DCAC 310-70-57)

b. Exceeded 10% of Time

c. Exceeded 50% of Time (median) ..

d. Recommended PMP Level

9.0	STATION DATA TABULATION - TROPO	FROM STA .ON TO
9.1	Type Terminal	
9.2	VF Channel Data:	
	a. Design Capacity	
	b. Number of Channels Installed ...	
	c. Number of Channels in Use	
	d. Number of VF Channels	
	e. Number of Data Channels	
	f. Number of Thru Groups	
	g. Number of Thru Supergroups	
9.3	Multiplex Equipment Type	
9.4	Radio Equipment Type	
9.5	Antenna System:	
	a. Antenna Size (ft):	
	(1) Parabolic	
	(2) Near Field Passive	
	(3) Far Field Passive	
	b. Antenna Gain (dB):	
	(1) Parabolic	
	(2) Parabolic and Passive	
	(3) Far Field Passive	

STATION DATA TABULATION-TROPO (CONT'D)

FROM STATION TO

c. Transmission Line:

- (1) Number # ____ .
 - (a) Type (RG, WR, etc) ..
 - (b) Length (meters)
 - (c) Loss (dB)
- (2) Number # ____ .
 - (a) Type (RG, WR, etc) ..
 - (b) Length (meters)
 - (c) Loss (dB)
- (3) Number # ____ .
 - (a) Type (RG, WR, etc) ..
 - (b) Length (meters)
 - (c) Loss (dB)
- (4) Number # ____ .
 - (a) Type (RG, WR, etc) ..
 - (b) Length (meters)
 - (c) Loss (dB)

9.6 VSWR:

- a. DCA Standard ()
- b. Measured:

STATION DATA TABULATION-TROPO (CONT'D)

FROM STATION TO

- (1) Transmission Line #1
- (2) Transmission Line #2
- (3) Transmission Line #3
- (4) Transmission Line #4

- 9.7 Transmitter Frequency Assignment (GHz):
 - a. Transmitter #1
 - b. Transmitter #2

- 9.8 Transmitter Frequency Accuracy (%):
 - a. DCA Standard
 - b. Manufacturer's Specifications ..
 - c. Measured:
 - (1) Transmitter #1
 - (2) Transmitter #2

- 9.9 Transmitter Power (watts):
 - a. Manufacturer's Specifications ..
 - b. Measured:
 - (1) Transmitter #1
 - (2) Transmitter #2

- 9.10 Transmitter Deviation (kHz RMS):
 - a. Manufacturer's Specifications ..
 - b. Measured/Adjusted to:

STATION DATA TABULATION-TROPO (CONT'D)

FROM STATION TO

(1) Transmitter #1

(2) Transmitter #2

9.11 Transmitter Spurious Emissions (dBm/GHz):

a. DCA Standard ()

b. Manufacturer's Specifications ..

c. Measured:

(1) Transmitter #1

(2) Transmitter #2

9.12 RF Pre-Amplifier Gain:

a. Manufacturer's Specifications .. ()

b. Measured:

(1) Receiver #1

(2) Receiver #2

(3) Receiver #3

(4) Receiver #4

9.13 RF Pre-Amplifier Noise Figure:

a. DCA Standard

b. Manufacturer's Specifications ..

c. Measured :

(1) Receiver #1

(2) Receiver #2

STATION DATA TABULATION-TROPO (CONT'D)

STATION
FROM TO

(3) Receiver #3

(4) Receiver #4

R Pre-Amplifier Bandwidth:

a. Manufacturer's Specifications .. ()

b. Measured:

(1) Receiver #1

(2) Receiver #2

(3) Receiver #3

(4) Receiver #4

Total Receiver Noise Figure (dB):

a. DCA Standard .. ()

b. Manufacturer's Specifications ..

c. Measured:

(1) Receiver #1

(2) Receiver #2

(3) Receiver #3

(4) Receiver #4

Receiver LO Frequency Accuracy (%):

a. DCA Standard .. ()

b. Manufacturer's Specifications ..

c. Measured:

STATION DATA TABULATION-TROPO (CONT'D)

FROM STATION TO

- (1) Receiver #1
- (2) Receiver #2
- (3) Receiver #3
- (4) Receiver #4

9.17 Receiver FM Threshold (dBm):

a. Manufacturer's Specifications ..

b. Measured:

- (1) Receiver #1
- (2) Receiver #2
- (3) Receiver #3
- (4) Receiver #4

9.18 Threshold Extension Improvement (dB):

a. DCA Standard ()

b. Manufacturer's Specifications ..

c. Measured:

- (1) Receiver #1
- (2) Receiver #2
- (3) Receiver #3
- (4) Receiver #4

9.19 Receiver IF Bandwidth (MHz):

DATA TABULATION-TROPO (CONT'D)

STATION
FROM TO

a. Manufacturer's Specifications ..

b. Measured:

(1) Receiver #1

(2) Receiver #2

(3) Receiver #3

(4) Receiver #4

c. Frequency at Zero Discriminator
Output (MHz):

a. Manufacturer's Specifications ...

b. Measured:

(1) Receiver #1

(2) Receiver #2

(3) Receiver #3

(4) Receiver #4

d. Discriminator Characteristics
(% of Non-linearity):

a. ICS Standard ()

b. Manufacturer's Specifications ...

c. Measured:

(1) Receiver #1 ()

(2) Receiver #2

(3) Receiver #3

(4) Receiver #4

9 22 Radio Equipment NPR/BNR (dB) for RF Loop
at _____ dBmO Loading:

a. DCA Standard

b. Manufacturer's Specifications ...

c. Measured (TX No. _____ RX No. _____):

(1) Low _____ (kHz)

(2) Mid _____ (kHz)

(3) High _____ (kHz)

(4) RSL During Test (dBm)

d. Measured (TX No. _____ RX No. _____):

(1) Low _____ (kHz)

(2) Mid _____ (kHz)

(3) High _____ (kHz)

(4) RSL During Test (dBm)

e. Measured (TX No. _____ RX No. _____):

(1) Low _____ (kHz)

(2) Mid _____ (kHz)

(3) High _____ (kHz)

(4) RSL During Test (dBm)

STATION DATA TABULATION-TROPO (CONT'D)

FROM STATION TO

f. Measured (TX No _____ RX No _____):

(1) Low _____ (kHz)

(2) Mid _____ (kHz)

(3) High _____ (kHz)

(4) RSL During Test (dBm)

23 Radio Equipment NPR/BNR (dB) for IF Loop at _____ dBm0 Loading:

a. DCA Standard

b. Manufacturer's Specifications ...

c. Measured (TX No _____ RX No _____):

(1) Low _____ (kHz)

(2) Mid _____ (kHz)

(3) High _____ (kHz)

(4) RSL During Test (dBm)

d. Measured (TX No _____ RX No _____):

(1) Low _____ (kHz)

(2) Mid _____ (kHz)

(3) High _____ (kHz)

(4) RSL During Test (dBm)

e. Measured (TX No _____ RX No _____):

(1) Low _____ (kHz)

STATION DATA TABULATION-TROPIC (CONT'D)

FROM STATION TO

- (2) Mid _____ (kHz)
- (3) High _____ (kHz)
- (4) RSL During Test (dBm)

f. Measured (TX No _____ RX No _____):

- (1) Low _____ (kHz)
- (2) Mid _____ (kHz)
- (3) High _____ (kHz)
- (4) RSL During Test (dBm)

9.24 Multiplex Equipment Loop NPR/BNR (dB) for _____ dBm Loading:

- a. Manufacturer's Specifications
- b. Measured:
 - (1) Low _____ (kHz)
 - (2) Mid _____ (kHz)
 - (3) High _____ (kHz)

Predicted Performance Levels

Section I - Instructions

B-1

GENERAL:

- a. Prior to each wideband evaluation, certain calculations must be performed so that a prediction of the key system parameters (RSL, Receive Threshold, ICN, etc.) can be obtained. These predictions will be used on arrival at the site to be evaluated as a basis for fault isolation and determining equipment performance under specified conditions. In order that valid predictions can be made, certain parameters and specifications are essential. Generally, these can be obtained from the equipment technical manuals, engineering design plans or site records. Table B-1 contains a list of parameters that are necessary to perform the required calculations.
- b. The test teams must also review the CREDATA, PMP, and other data available within the detachment prior to departing for an evaluation. Pertinent data such as; on hand TMDE, site coordinates, and etc., will be extracted from the CREDATA and verified while on site. The PMP data will provide some indication of the quality of the system and can be used to isolate and correct problem areas while on site. This data along with the preliminary testing should also provide information on additional diagnostic test routines that must be completed before the final data collection is initiated.

PATH PROFILES

- a. The first step in obtaining accurate system predictions is the preparation of a path profile for the link to be evaluated. The profiles are used to obtain detailed information about the terrain between the transmitting and receiving antenna. Therefore, accuracy is of utmost importance in their preparation. Detailed instructions on preparing the path profile can be found in CCTM 105-50 and AFCS 100-61.
- b. The path profile is to be prepared by the test teams and entered on the data sheet shown at Figure B-1. Entries on this form must be legible and of sufficient quality to permit reproduction without loss or degradation of the information.

PATH CALCULATIONS

- a. Once the path profile has been completed, path predictions can be performed. Detailed instructions for the calculation of LOS, tropospheric scatter, and transhorizon path parameters can be found in CCTM 105-50, AFCS 100-61, and NBS Technical Note 101. The most important parameters derived from these calculations are:
 - (1) Predicted Receive Signal Level.
 - (2) Fade Margin.
 - (3) RSL at FM Threshold.
 - (4) System outage probability.
 - (5) Predicted Receiver Thermal Noise.

(6) Total Radio Noise.

(7) Total Link Noise.

A typical list of required parameters are shown in Table B-1.

- b. The measured values of the preceding parameters must be compared to the predicted values to determine what problems, if any, exist in the equipment. The Team Chiefs are required to perform the necessary calculations and complete the data elements shown in Figure B-2 through B-11, as applicable for each system to be evaluated. The predicted performance levels can be accomplished while the test teams are at the evaluated station, however, it is recommended that they be completed prior to departing their home station. The calculations shown in Figures B-2 through B-11 are typical of links that have been evaluated.

B-4

TRANSMITTER DEVIATION (FIRST CARRIER DROPOUT METHOD)

- a. The proper amount of carrier deviation to be used on any particular FM radio system is established during system design, and depends upon the balance between thermal noise and intermodulation distortion to be permitted in the system. Before proceeding further, it is necessary to remember that in FM systems, noise of thermal origin appearing in the baseband after frequency demodulation is inversely proportional to the received RF carrier level and the square of carrier deviation; similarly, baseband noise appearing as intermodulation products increases

CCP 702-1

with the square of deviation. The absolute value of these intermodulation products depends upon equipment linearity, feeder echo distortion, and in the case of tropospheric scatter, frequency selective fast fading due to multipath propagation. All this means is that for any specific carrier level (RSL), equipment configuration, and path geometry, thermal noise decreases with increasing deviation, and intermodulation products increase with increasing deviation. This would suggest that some optimum deviation exists at which the sum total of thermal and intermodulation noise is minimum. It is a proven fact that for second order terms, the sum of thermal and intermodulation noise is minimized when they are equal to each other (see Figure B-12). Thus to achieve the minimum amount of noise for the maximum period of time, it is the usual practice of FM system designers to calculate the test tone deviation which results in equal contribution of thermal and intermodulation noise in the presence of some specified RF signal level, usually the expected or median value. When a specific optimum carrier deviation has been established, it is a problem for the technician to set and periodically check that the deviation is of the proper value; remembering that all test tone power levels in the system are proportional to the square of deviation, it should be apparent that all system levels (and consequently channel noise) are critically dependent upon carrier deviation.

- b. The method used by the TEP test teams to set deviation is the first carrier dropout method. It is characteristic of all frequency or phase modulated radio systems that for certain frequencies of modulation tones, the carrier (in the modulated signal) will disappear. This disappearance is due to phase cancellation of certain components produced during modulation and always occurs with mathematical precision. The mathematical relationships describing this phenomenon are termed "Bessel Functions." Specifically of interest here is the relationship:

$$M = \frac{D_p}{f_t}$$

This defines the modulation index and indicates the modulation index equals the ratio of peak per channel carrier deviation to the frequency of the tone used to produce it. When the modulation index (this ratio of carrier deviation to test tone modulation frequency) equals 2.41, the carrier will disappear. Knowing the carrier disappears when the modulating index equals 2.41, the desired "Optimum" deviation D_p can be substituted and the above equation solved for f_t , the so-called, Bessel drop-out test tone frequency. This frequency at a level of 0 dBm0 will produce the required deviation if the system does not have pre-emphasis. However, a number of the systems encountered by the TEP teams during an evaluation will have pre-emphasis networks. The problem can be summarized as follows: If modulator

deviation is adjusted using the test tone (f_t) above with a level of 0 dBm0 in a pre-emphasized system, the actual baseband traffic will not be represented. The amount of pre-emphasis (and consequently, deviation) will be different for other baseband frequencies because of the pre-emphasis. Therefore, some baseband frequency must be found at which the net pre-emphasis effect is zero. This frequency is called the pivot frequency, or in some references, mean baseband frequency. Below this frequency, the modulator input level is less and above this frequency, the input level is greater. A formal definition of pivot frequency would be that frequency in the baseband for which the RMS deviation in an emphasized system with white noise loading is equal to that of a flat system when the RMS power input (modulating white noise level) to the modulator is the same in both cases.

The problem now becomes one of determining the pivot frequency and the test tone level that must be used to set deviation in an emphasized system. The first step in solving this problem is to determine the type of pre-emphasis in the system. There are basically three types of pre-emphasis that may be encountered in the field. These three types are discussed in the succeeding paragraphs.

REL Pre-emphasis: REL type pre-emphasis provides a 12 dB boost to the top baseband frequency. The characteristic curve for

REL pre-emphasis is shown in Figure B-13. Figure B-13 is plotted for any baseband configuration. The abscissa is the normalized frequency (f/f_{\max}) where f is the baseband frequency of interest and f_{\max} is the maximum baseband frequency. The following equation is used to derive this curve:

$$I_p = 10 \log [1 + 15 (f/f_{\max})^2]$$

where: I_p = Pre-emphasis improvement for the frequency of interest

f = The baseband frequency of interest

f_{\max} = Maximum baseband frequency

The pivot frequency for this type of pre-emphasis can be found by using the following relationship:

$$\text{Pre-emphasis improvement } (I_p) \text{ at pivot frequency} = 10 \log \left[\frac{\int_{R_1}^{R_2} (I_p \text{ linear}) dR}{\int_{R_1}^{R_2} dR} \right]$$

where: $I_p \text{ linear}$ = the linear portion of the pre-emphasis equation

$$1 + 15 (f/f_{\max})^2$$

$R_1 = f/f_{\max}$ = Lowest baseband frequency divided by the maximum baseband frequency

$R_2 = f_{\max}/f_{\max}$ = Maximum baseband frequency divided by the maximum baseband frequency = 1

As an example let's assume a 24 channel system with a baseband of 12 kHz - 108 kHz.

$$\begin{aligned}
 I_p &= 10 \log \left[\frac{\int_{R_1}^{R_2} (I_p \text{ linear}) dR}{\int_{R_1}^{R_2} dR} \right] \\
 &= 10 \log \left[\frac{\int_{R_1}^{R_2} (1 + 15R^2) dR}{\int_{R_1}^{R_2} dR} \right] \quad \text{where } R = f/f_{\max} \\
 &= 10 \log \left[\frac{\int_{R_1}^{R_2} dR + 15 \int_{R_1}^{R_2} R^2 dR}{\int_{R_1}^{R_2} dR} \right] \\
 &= 10 \log \left[\frac{R \Big|_{R_1}^{R_2} + 15 \frac{R^3}{3} \Big|_{R_1}^{R_2}}{R \Big|_{R_1}^{R_2}} \right] \\
 &= 10 \log \left[\frac{(R_2 - R_1) + 5 (R_2^3 - R_1^3)}{R_2 - R_1} \right]
 \end{aligned}$$

but

$$R_1 = 12 \times 10^3 / 108 \times 10^3 = 0.11$$

$$R_2 = 108 \times 10^3 / 108 \times 10^3 = 1.0$$

$$\begin{aligned}
 I_p &= 10 \log \left[\frac{1.00 - 0.11 + 5 \{ (1)^3 - (0.11)^3 \}}{1.00 - 0.11} \right] \\
 &= 10 \log \left[\frac{0.98 + 5 (0.998669)}{0.89} \right]
 \end{aligned}$$

$$= 10 \log [6.61]$$

= 8.2 dB = pre-emphasis improvement at the pivot frequency

In every case where REL pre-emphasis is used, this integration will yield approximately 8 dB. Therefore, the pivot frequency for any baseband can be found from the pre-emphasis curve by finding the frequency corresponding to 8 dB.

Now that the pivot frequency is known, the level used to set deviation can be found. The RMS (or peak) deviation per channel can usually be found in the Equipment Technical Manual or Manufacturer's Specifications. This value is stated for the pivot frequency. With this per channel RMS deviation value and the pivot frequency obtained from the above calculations, the test tone level can be determined from the following equation:

$$L_n(\text{dBmO}) = 20 \log \left[\frac{2.4 f_p}{\sqrt{2} D_{\text{RMS}}} \right]$$

where:

$L_n(\text{dBmO})$ = required test tone level

f_p = modulating (pivot) frequency

D_{RMS} = RMS per channel deviation desired

Using the pivot frequency at the test tone level calculated above, the correct deviation can be set on a modulator with REL pre-emphasis.

- d. CCIR Pre-emphasis: Probably the most common type of pre-emphasis is that recommended by CCIR. The characteristic curve for CCIR pre-emphasis is shown in Figure B-14. Once again the pre-emphasis improvement is plotted versus f/f_{\max} . The CCIR pre-emphasis curve is defined by:

$$I_p = 5 - 10 \log \left[1 + \frac{6.9}{1 + \left(\frac{5.25}{(f_r/f - f/f_r)^2} \right)} \right]$$

where:

f_r = circuit resonant frequency = $1.25 f_{\max}$

f_{\max} = the highest baseband frequency

f = the frequency of interest

The pivot frequency is once again found by the integration method used on the REL curve. In the case of CCIR pre-emphasis,

I_p - linear would be:

$$I_p \text{ linear} = \left[1 + \frac{6.9}{1 + \left(\frac{5.25}{(f_r/f - f/f_r)^2} \right)} \right]$$

If the integration is performed in the same manner as with REL pre-emphasis, the results would be that the pivot frequency occurs at the frequency corresponding to 0 dB on the curve.

As in the REL case, the test tone level is found using the formula:

$$L_n(\text{dBm}) = 20 \log \left[\frac{2.4 f_p}{\sqrt{2} D_{\text{RMS}}} \right]$$

Using the pivot frequency and the level calculated by the formula above, the deviation can be set correctly on systems utilizing pre-emphasis networks recommended by CCIR.

- e. Systems Defined by a Time Constant: Sometimes a system will have a time constant that differs from that recommended by REL. If this is the case, the REL pre-emphasis curve will not accurately define the pre-emphasis effects. Therefore, a method is needed to plot a pre-emphasis curve, if only the pre-emphasis circuit time constant is known. If this is the case, the following relationship can be used:

$$I_p = 10 \log (1 + 39.5 f^2 \tau^2)$$

where:

f = Any baseband frequency in Hz

τ = Pre-emphasis circuit time constant

The pre-emphasis improvement at the pivot frequency can be found by the same integration method that was used for the REL curve. I_p linear in this case would be:

$$I_p \text{ linear} = 1 + 39.5 f^2 \tau^2$$

If the results of this integration is equated to $I_p = 10 \log (1 + 39.5 f^2 \tau^2)$ a general formula can be derived to find the pivot frequency. This formula is:

$$f_p = \sqrt{\frac{f_{\max}^3 - f_0^3}{3(f_{\max} - f_0)}}$$

where:

f_p = pivot frequency

f_{\max} = maximum baseband frequency

f_0 = lowest baseband frequency

The test tone level can be calculated in the same manner as it was for CCIR and REL pre-emphasis.

- f. It should be made clear that sometimes a technical manual will prescribe a frequency and level other than the pivot frequency at the appropriate level. There is nothing wrong with this as long as the difference in pre-emphasis between the pivot frequency and the new frequency is taken into account in the new level. This is exactly what is done in the case of the AM/FRC-84. On the NEC equipment, the pre-emphasis is removed and replaced with a 5 dB pad and the deviation is set using a 200 kHz tone ($f_p = 810$ kHz for this system). It is clear that the equipment technical specifications should be consulted to determine if special techniques are used to set deviation. Table B-2 presents the pivot frequencies for different baseband configurations for both REL and CCIR.

B-5

QUIETING CURVE CALCULATIONS

- a. Probably the most informative radio data obtained during an

evaluation is the quieting data. Since the results of this test are dependent upon IF bandwidth, receiver noise figure, RSL, and frequency deviation, it can be used as a check of the results obtained during other tests. It is essential that the data and plots be as accurate as possible. Slight variations can result in large errors when the other parameters are calculated.

- b. Referring to Figure B-15, there are four distinct regions on the quieting curve defining output idle noise as a function of increasing RF carrier input. At minimum inputs, the output noise has a constant value which does not vary with small changes of input carrier. This portion may be considered the first region. In well designed FM receivers, gain is sufficient to cause limiter saturation by this noise. When this is the case, increasing carrier input to the receiver results in the output noise decreasing sharply. This may be considered the second region. It represents capture of the limiters by the carrier. At the end of this region is a transition point, the threshold of limiter-capture curvature. This is also known as FM threshold. Beyond this threshold, noise output intensity decreases linearly with carrier intensity. This is the third region of the curve. In this region S/N increases 1 dB with every 1 dB increase in RSL. Eventually, a final plateau of asymptotic quieting is reached due to saturation of the IF

amplifier by the carrier. The noise in this region represents a fully quieted receiver. In this fourth region, further increases in RSL will cause no change in the noise output, and the noise output should be the same as would exist if the receiver stages prior to the limiter were removed. Asymptotic quieting usually occurs in the region of -75 to -85 dBm0 noise power. Back-to-back equipment performance loop tests should be performed in this region so that parameters such as intermodulation and test tone levels can be examined with minimum masking effects from thermal noise.

- c. Prior to each evaluation, calculations can be performed to determine the signal to noise (S/N) for RSLs falling in the linear portion of the quieting curves. These calculated values can then be used as a "Quick check" of data as it is being measured.

The first step of this process is determination of the approximate extent of the linear portion of the quieting curve. The following equation can be used to determine FM threshold:

$$\text{FM Threshold} = 10 \log kT + 10 \log Bw + NF + 10 \text{ dB}$$

where:

$$k = \text{Boltzmann's constant} = 1.38 \times 10^{-23} \frac{\text{w} \cdot \text{sec}}{\text{ok}}$$

$$T = 290 \text{ degrees (Kelvin)}$$

$$NF = \text{Noise Figure}$$

B_w = IF Bandwidth (3 dB points) in Hz

NOTE: $10 \log kTB$ equals power in watts. This is converted to M_w by subtracting 30 dB from $10 \log kTB$

Substituting values for k and T gives:

$$\text{FM Threshold} = -164 + 10 \log B_w + \text{NF}$$

The quieting curves can be assumed linear at RSLs above the value obtained for the FM threshold. The limit of linearity occurs at the asymptotic quieting (Region IV) portion of the curve.

Knowing the possible extent of the linear portion, the S/N for a signal receiver at any RSL in the region can be calculated from the following equation:

$$S/N = \text{RSL} - 10 \log kT - \text{NF} + 20 \log \frac{D_p}{f_m} + I_p - 10 \log 2b$$

where:

S/N = Signal to thermal noise ratio (dB)

RSL = Receive Signal Level

k = Boltzmann's constant = $1.38 \times 10^{-23} \frac{\text{w} \cdot \text{sec}}{\text{°k}}$

f_m = Frequency of interest (usually the top frequency slot)

T = 290° Kelvin

NF = Noise Figure

D_p = The per channel peak deviation at zero pre-emphasis

I_p = Pre-emphasis improvement for the slot involved (from equation or pre-emphasis curve)

b = Channel bandwidth, Hz

Since we know the values of k and T the above equation can be simplified to the following relationship:

$$S/N = RSL + 174 - NF + 20 \log \frac{D_p}{f_m} + I_p - 10 \log 2b$$

- d. At this point, several of the factors in the above equation should be discussed since their meaning may not be obvious to the engineer performing the analysis.
- (1) D_p -this factor is the per channel peak deviation at the point of zero pre-emphasis. It is most important that this term be calculated for systems using REL pre-emphasis. In the discussion on pivot frequency it was pointed out that the RMS (or peak) per channel deviation given in the Technical Manual or Equipment Literature is stated for the pivot frequency. It should also be remembered that the pivot frequency occurs at a pre-emphasis improvement of approximately 8 dB for REL pre-emphasis. Since pre-emphasis improvement (I_p) is included in the equation, the per channel RMS deviation has to be translated back to 0 dB pre-emphasis so that the equation accurately defines the curve. The following procedures are used to calculate D_p :
- a. From the equipment specification determine the per channel RMS deviation.
 - b. From the deviation test (or Technical Manual) find the

test tone frequency and level required to produce first carrier dropout.

c. From the pre-emphasis curve (or appropriate equation) find the pre-emphasis improvement for the above test tone frequency.

d. Apply the above values to the following relationship:

$$D_p = \frac{2.4 f_p}{\text{Antilog} \left[\frac{L_n(0 \text{ dBm0}) + I_p}{20} \right]}$$

where:

f_p = Test tone pivot frequency required for first carrier dropout

$L_n(0 \text{ dBm0})$ = The level of the test tone used for first carrier dropout

I_p = Pre-emphasis improvement at the test tone frequency

The value calculated from the above equation is to be used in the quieting curve equations for any slot of interest. This allows for the pre-emphasis improvement for the slot of interest to be taken directly from the pre-emphasis curve or calculated from the appropriate equation. It should be pointed out that D_p only has to be calculated for systems using REL pre-emphasis or systems where pre-emphasis is defined by a time constant. Transmitters with CCIR pre-emphasis don't require the calculation of D_p since the pivot frequency occurs at 0 dB pre-emphasis.

As a point of interest, the per channel RMS deviation for any frequency in an emphasized baseband can be computed using the following formula:

$$D'_{RMS} = \left(\frac{D_p}{\sqrt{2}} \right) \text{Antilog} (I'_p/20)$$

where:

D'_{RMS} = Per channel RMS frequency deviation for any frequency in the baseband

I'_p = Pre-emphasis improvement for the desired frequency

- (2) Pre-emphasis improvement (I_p): The value of I_p is determined directly from the pre-emphasis curve or with the appropriate equation at the frequency of interest. However, for systems utilizing REL type pre-emphasis, D_p must be calculated and used in the S/N equation as previously discussed to obtain accurate results.
- (3) Channel bandwidth: This refers to the test channels bandwidth. In most cases the Sierra 128A frequency selective voltmeter or equivalent is used for measuring the quieting data. The bandwidth is 3.1 kHz, however, if other instruments are used, the bandwidth of the test slot should be noted on the quieting data sheet.

Applying the above information, assume a radio is to be evaluated with the following specifications:

NF = 4 dB

IF B_w = 6 MHz at the 3 dB points

Per channel RMS deviation = 100 kHz

Number of channels = 120

Baseband = 60 - 552 kHz

Type of pre-emphasis = REL (1.2) usec

The first step is to calculate a theoretical FM threshold:

$$\begin{aligned} \text{FM Threshold} &= -164 + 10 \log B_w + \text{NF} \\ &= -164 + 10 \log (6 \times 10^6) + 4 \\ &= -92.2 \text{ dBm} \end{aligned}$$

Next, the S/N at any RSL on the linear portion of the curve can be calculated. Before applying the S/N equation it should be noted that the specifications call for REL pre-emphasis, thus requiring that D_p be calculated.

$$D_p = \frac{2.4 f_p}{\text{Antilog} \left(\frac{L (0 \text{ dBm}) + I_p}{20} \right)}$$

From the pre-emphasis curve we find:

$$f_p = 337 \text{ kHz (equation shown on Page 2-12).}$$

$$I_p \text{ 337 kHz} = 10 \log \left[1 + 15 \left(\frac{337}{552} \right)^2 \right] = 8.19 \text{ dB}$$

$$L (0 \text{ dBm}) = 20 \log \left(\frac{2.4 (337)}{\sqrt{2} (100)} \right) = +15.1 \text{ dBm}$$

$$D_p = \frac{(2.4) (337)}{\text{Antilog} \left[\frac{(15.1 + 8.2)}{20} \right]}$$

$$= 55 \text{ kHz}$$

CCP 702-1

Assume an RSL of -80 dBm and a 3.1 kHz channel:

$$\text{For 80 kHz slot } I_p = 10 \log \left[1 + 15 \left(\frac{80}{552} \right)^2 \right] = 1.2 \text{ dB}$$

$$\begin{aligned} S/N &= \text{RSL} + 174 - \text{NF} + 20 \log \frac{D_p}{f_m} + I_p - 10 \log 2b \\ &= -80 + 174 - 4 + 20 \log \frac{55}{80} + 1.2 - 37.9 \end{aligned}$$

$$= 50.1 \text{ dB}$$

$$\text{For 270 kHz slot } I_p = 10 \log \left[1 + 15 \left(\frac{270}{252} \right)^2 \right] = 6.6 \text{ dB}$$

$$S/N = -80 + 174 - 4 + 20 \log \left(\frac{55}{270} \right) + 6.6 - 37.9$$

$$= 44.9 \text{ dB}$$

$$\text{For 550 kHz slot } I_p = 10 \log \left[1 + 15 \left(\frac{550}{552} \right)^2 \right] = 12.0 \text{ dB}$$

$$S/N = -80 + 174 - 4 + 20 \log \frac{55}{550} + 12 - 37.9$$

$$= 44.1 \text{ dB}$$

- (4) The value obtained for FM Threshold and S/N should be listed on a form such as the one illustrated in Figure B-16 and given to the radio technicians prior to the mission. The values measured in the field can be compared to the calculated values for a quick check of system performance while the test is being conducted. It should be noted at this point that the calculated value for the low slot may not always agree with the calculated data. The accuracy will depend on the residual modulation of the signal generator used to perform the test.

An important point that should be apparent from this discussion is that S/N at RSLs above FM Threshold is not affected by the IF bandwidth. Only FM Threshold is determined by the IF bandwidth.

- (5) One other factor that may be used to determine the quality of FM quieting data is the degree of S/N improvement at threshold. This is the noise reduction between noise saturation and FM threshold. This can be calculated as follows:

$$\text{S/N Improvement factor} = 20 \log \frac{D'_p}{f_m} + 10 \log \frac{B_w}{2b}$$

where:

D'_p = Per channel peak deviation for the modulating frequency with the effects of pre-emphasis included (kHz)

$$= D_p \text{ Antilog } \frac{I'_p}{20}$$

I'_p = Pre-emphasis for the slot being investigated

f_m = Baseband frequency, (kHz)

B_w = IF bandwidth in Hz

b = Channel bandwidth in Hz

To illustrate the use of this relationship, consider the receiver with the characteristics of the one used in the preceding example. The IF bandwidth was 6 MHz and D_p was found to be 55 kHz. Therefore:

$$D'_p = D_p \text{ Antilog } \frac{I'_p}{20}$$

CCP 702-1

For the 270 kHz slot:

$$D'_p = (55) \left(\text{Antilog } \frac{6.6}{20} \right)$$

$$= 117.6 \text{ kHz}$$

$$\text{FM Improvement} = 20 \log \frac{117.6 \text{ (kHz)}}{270} + 10 \log \left(\frac{6 \times 10^6}{6.2 \times 10^3} \right)$$

$$= 22.6 \text{ dB for the 270 kHz slot}$$

The value calculated above should equal the difference in S/N between noise saturation and FM Threshold on the quieting curves.

- (6) With the calculations of S/N, FM Threshold, and FM Improvement at threshold, the validity of the quieting data can easily be checked in the field. If the calculated values do not agree with the measured values, a problem exists which would require further investigation.

B-6

EMISSION BANDWIDTH

The emission bandwidth required for different channel configurations varies according to the highest frequency in the baseband and the desired per channel RMS deviation. The required bandwidth for different channel configurations can be calculated using the following relationships:

$$B_w = 2 f_{\max} + 2 D_s K$$

where:

$$B_w = \text{Required bandwidth in kHz}$$

$$f_{\max} = \text{Maximum modulating frequency}$$

D_s = Peak system deviation in kHz

$$D_s = \left[4.47 D_{RMS} \cdot \text{Log}^{-1} \left(\frac{-1 + 4 \log N}{20} \right) \right]$$

D_{RMS} = RMS per channel deviation desired

K = A numerical factor depending upon allowable distortion. The value commonly used is 0.9

N = Number of channels

The above relationship provides accurate results as long as the deviation ratio (M) is less than 2. The deviation ratio is defined as maximum carrier deviation/maximum modulating frequency. If $2 \leq M \leq 10$ the following relationship should be used to find emission bandwidth:

$$B_w = 4 f_{\max} + 2 D_s K$$

The above formulas allow emission bandwidth (3 dB points) to be calculated if the number of channels (N) is less than 240. If the number of channels (N) is equal to or greater than 240 channels, $-1 + 4 \log N$ must be replaced with $-15 + 10 \log N$. For DCA loading use $-10 + 10 \log N$ for all channel capacities.

B-7

SUMMARY

The preliminary analysis procedures are designed to provide the test teams with a general idea of what to expect from the systems during an evaluation. Many factors will cause deviations from the predicted values, however, the predicted values provide a basis for fault detection and correction. One important consideration when evaluating the quieting data is

CCP 702-1

that of test equipment capability. The accuracy of lower slot data is limited by the residual noise of the signal generator and this fact should be kept in mind during the data analysis. The quieting data can, however, provide much insight into the receiver faults if properly evaluated.

TABLE B-1

LIST OF PARAMETERS REQUIRED FOR PATH CALCULATIONS

a. Type Diversity	_____	
b. Transmit Power	_____	dBm
c. Transmit Antenna Gain	_____	dB
d. Receive Antenna Gain	_____	dB
e. Receive Frequencies	_____	MHz
f. Line and Miscellaneous Losses:		
1. Interface losses	_____	dB
2. Insertion losses	_____	dB
3. Waveguide losses	_____	dB
4. Total transmit losses	_____	dB
5. Total receive losses	_____	dB
g. IF Bandwidth (3 dB points)	_____	MHz
h. Receiver Noise Figure	_____	dB
i. FM Threshold	_____	dBm
j. Per Channel RMS Deviation	_____	kHz
k. Peak Deviation	_____	kHz
m. Modulation Index	_____	
n. Baseband Bandwidth	_____	kHz
o. Maximum Modulating Frequency	_____	kHz
p. Type of Pre-emphasis (from TM or equip specs)	_____	sec
q. Pre-emphasis Network Time Constant (REL only)	_____	dB
r. Noise Power Ratio (high slot)	_____	dB

TABLE B-1

LIST OF PARAMETERS REQUIRED FOR PATH CALCULATIONS

a. Type Diversity	_____
b. Transmit Power	_____ dBm
c. Transmit Antenna Gain	_____ dB
d. Receive Antenna Gain	_____ dB
e. Receive Frequencies	_____ MHz
f. Line and Miscellaneous Losses:	
1. Interface losses	_____ dB
2. Insertion losses	_____ dB
3. Waveguide losses	_____ dB
4. Total transmit losses	_____ dB
5. Total receive losses	_____ dB
g. IF Bandwidth (3 dB points)	_____ MHz
h. Receiver Noise Figure	_____ dB
i. FM Threshold	_____ dBm
j. Per Channel RMS Deviation	_____ kHz
k. Peak Deviation	_____ kHz
m. Modulation Index	_____
n. Baseband Bandwidth	_____ kHz
o. Maximum Modulating Frequency	_____ kHz
p. Type of Pre-emphasis (from TM or equip specs)	_____ sec
q. Pre-emphasis Network Time Constant (REL only)	_____ dB
r. Noise Power Ratio (high slot)	_____ dB

CGP 702-1

TABLE B-1 (Cont'd)

s. Multiplex Noise Loaded	_____	dBa0 or pwCO
t. VSWR	_____	
u. Antenna Diameter	_____	ft
v. Type of Waveguide and/or Coaxial Cable	_____	
w. Length of Transmit Waveguide and/or Coaxial Cable Run	_____	ft/M
Length of Receive Waveguide and/or Coaxial Cable Run	_____	ft/M
z. Inside Diameter of Waveguide	_____	in/cm
aa. Path Length	_____	Km/smi
ab. Theoretical Asymptotic Quieting	_____	dB

TABLE B-2

BASEBAND TEST FREQUENCIES FOR MODULATOR DEVIATION

Type of Pre-emphasis

<u>NO. CHANNELS</u>	<u>REL (kHz)</u>	<u>CCIR (kHz)</u>	<u>BASEBAND SPECTRUM</u>
12	38.6	40.1	12-60
12	85.1	89.5	60-108
24	66.2	68.9	12-108
24	111.0	114	60-156
36	93.7	97.8	12-156
36	138	142	60-204
48	121	127	12-204
48	166	171	60-252
60	149	157	12-252
60	193	200	60-300
72	177	185	12-300
72	211	222	12-360
72	277	235	60-360
120	322	337	12-552
120	337	352	60-552
180	482	504	60-804
240	625	654	60-1052
252	611	643	12-1052
300	770	810	60-1300
312	756	792	12-1300
360	896	945	12-1548

CCP 702-1

TABLE B-2 (Continued)

<u>NO. CHANNELS</u>	<u>REL (kHz)</u>	<u>CCIR (kHz)</u>	<u>BASEBAND. SPECTRUM</u>
372	896	945	12-1548
420	1055	1105	60-1796
432	1040	1090	12-1796
480	1205	1258	60-2044
492	1189	1245	12-2044
540	1340	1410	60-2292
552	1327	1395	12-2292
600	1489	1555	60-2540
612	1475	1550	12-2540

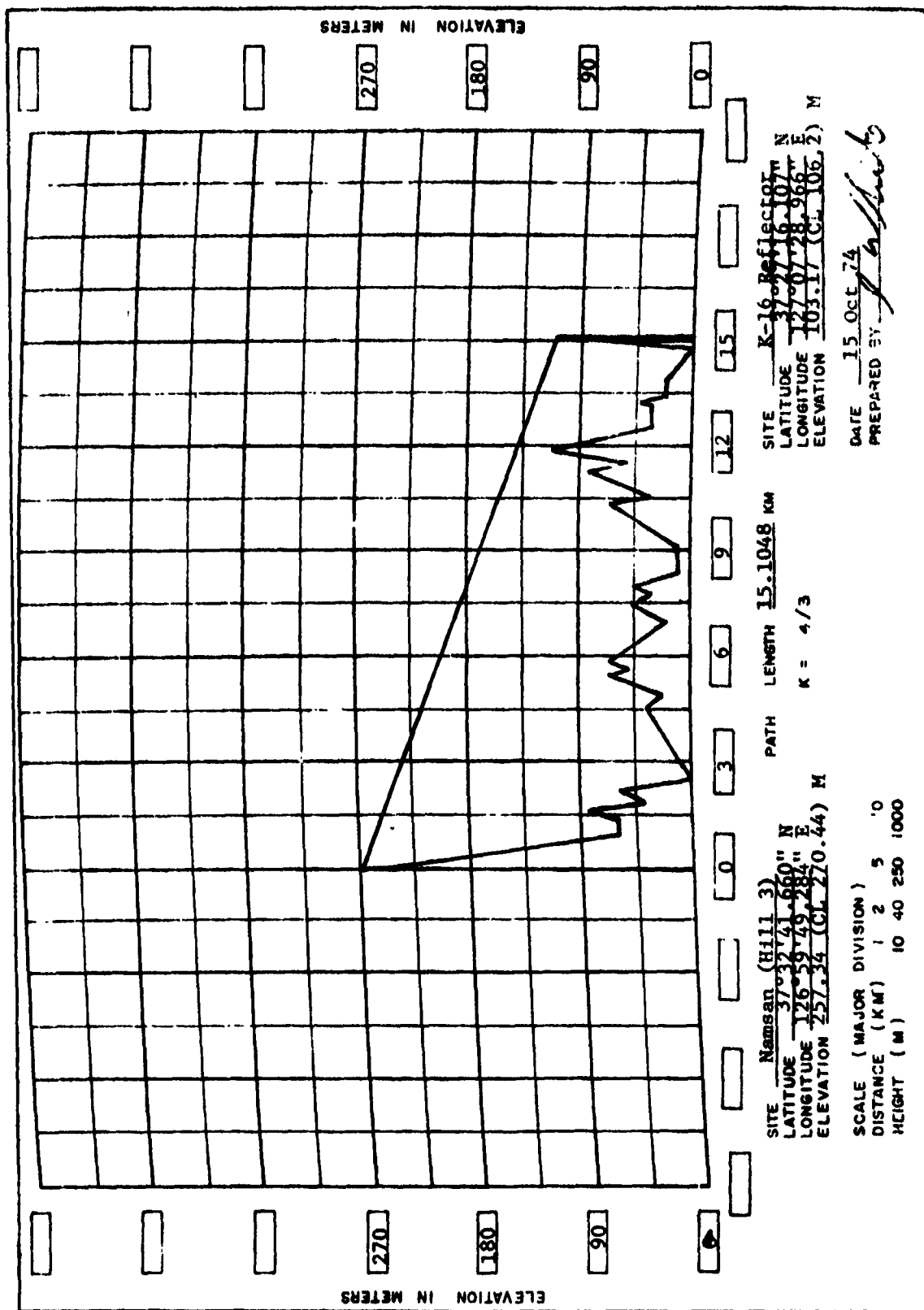


Figure B-1

LINE OF SIGHT WORKSHEET		TEST ENGINEERS SIGNATURE	
DCS LINK NO.	STATIONS UNDER TEST		
M2089	NAMSAN (Hill 3)	TO	BEASCOM
DEFINITION	SYMBOL	VALUE	REFERENCE / EQUATION
Path distance	d	<u>48.96 km</u>	
Height of transmit antenna above sea level	h_{ts}	<u>.2575 km</u>	(257.34 m* + 50 ft.) * = 3rd order geodatic survey
Height of receive antenna above sea level	h_{rs}	<u>1.161 km</u>	(1147.98 m + 43 ft.)
Surface refractivity reduced to sea level	N_o	<u>305</u>	Figure 4.1 (page 4-3)
Average value of N at the earth surface	N_s	<u>296.8</u>	Page 4-1
Effective earth radius	a	<u>8428 km</u>	Equation 4.4 or Figure 4.2
Effective height of transmit antenna above ground	h_1	<u>.166 km</u>	Page 5-8
Effective height of receive antenna above ground	h_2	<u>.315 km</u>	Page 5-8
Carrier frequency	f	<u>7347.5MHz</u>	
Loss relative to free space	A	<u>0 dB</u>	Section 5
Atmospheric absorption	A_a	<u>0.5 dB</u>	Section 3 and Figure 3.5
Basic median transmission loss	L_b	<u>144.1dB</u>	$20 \log d + 20 \log f + 32.45 + A + A_a$
Effective distance	d_e	<u>43.8 km</u>	Page 10-8
Type climate (continental temperate/polar)		<u>1 #</u>	Page 10-6 and 10-7
Correction factor	$V(0.5, d_e)$	<u>0 dB</u>	Figure 10.13 (page 10-26)
Predicted median long term transmission loss	$L_n(0.5)$	<u>144.1dB</u>	$L_b - V(0.5, d_e)$
Long term variability for 99.99% of all hours	$Y(0.9999)$	<u>4.3 dB</u>	Section 10 and III.7
Transmission loss not exceeded for 99.99% of all hours	$L_n(q)$	<u>148.4 dB</u>	$L_n(0.5) - Y(0.9999)$

TROPOSCATTER TRANSMISSION LOSS WORKSHEET (REFERENCE: NBS TECH NOTE 101)		TEST ENGINEER'S SIGNATURE	
DCS LINK NO	STATIONS UNDER TEST		
T-1609	TAKHLI TO PHITSANULOKE (PSL-03)		
DEFINITION	SYMBOL	VALUE	REFERENCE/EQUATION
Path distance	d	170.22 km	170.216878
Distance from transmit antenna to horizon	d_{Lt}	29.29 km	18.2 mi = 29.3 km
Distance from receive antenna to horizon	d_{Lr}	10.46 km	6.5 mi = 10.5 km
Height of transmit antenna above sea level	h_{ts}	.2786 km	859' + 55'
Height of receive antenna above sea level	h_{rs}	.0680 km	143' + 80'
Height of transmit horizon obstacle above sea level	h_{Lt}	.1853 km	608' = .1853 km
Height of receive horizon obstacle above sea level	h_{Lr}	.0613 km	201' = .0613 km
Effective height of transmit antenna above ground	h_{te}	.2149 km	Page 6-4 750' = .2149 km
Effective height of receive antenna above ground	h_{re}	.0244 km	Page 6-4 80' = .0244 km
Surface refractivity reduced to sea level	N_0	362	Figure 4.1 (page 4-3)
Average value of N at the earth surface	N_s	360	Equation 4.3
Effective earth radius	a	9770 km	Equation 4.4
Horizon elevation angle at transmit antenna	θ_{et}	-.00468 rad	$(h_{Lt} - h_{ts})/d_{Lt} - d_{Lt}/2a$
Horizon elevation angle at receive antenna	θ_{er}	-.00118 rad	$(h_{Lr} - h_{rs})/d_{Lr} - d_{Lr}/2a$
Angular distance (scatter angle)	θ	.01156 rad	$d/a + \theta_{et} + \theta_{er}$, valid for θd less than 2
Angle between line joining antennas and transmit horizon ray	α_{oo}	.00527 rad	$d/2a + \theta_{et} + (h_{ts} - h_{rs})/d$

CONTINUATION: TROPOSCATTER TRANSMISSION LOSS WORKSHEET -2 TKL-02/PSL-03 T-1609			
DEFINITION	SYMBOL	VALUE	REFERENCE/EQUATION
Angle between line joining antennas and receive horizon ray	β_{00}	$\frac{.00629}{\text{rad}}$	$d/2a + \theta_{er} + (h_{rs} - h_{ts})/d$
Distance angle assuming straight rays for radius a	α_{00}	$\frac{.01156}{\text{rad}}$	$\alpha_{00} + \beta_{00}$
Angular elevation of transmit horizon ray at transmit horizon	θ_{ot}	$\frac{-.00168}{\text{rad}}$	$\theta_{et} + d_{Lt}/a$
Angular elevation of receive horizon ray at receive horizon	θ_{or}	$\frac{-.00011}{\text{rad}}$	$\theta_{er} + d_{Lr}/a$
Distance transmit horizon to horizon ray crossover	d_{st}	$\frac{63.3}{\text{km}}$	$d \beta_{00}/\alpha_{00} - d_{Lt}$
Distance receive horizon to horizon ray crossover	d_{sr}	$\frac{67.1}{\text{km}}$	$d \alpha_{00}/\beta_{00} - d_{Lr}$
Distance between horizon obstacles	D_o	$\frac{130.5}{\text{km}}$	$d_{st} + d_{sr}$ or $d - d_{Lt} - d_{Lr}$
Correction angle for exponential atmosphere (transmit)	$\Delta\alpha_o$	NA rad	Pages 6-6 and 6-7
Correction angle for exponential atmosphere (receive)	$\Delta\beta_o$	NA rad	Pages 6-6 and 6-7
Corrected α_{00}	α_o	$\frac{.00527}{\text{rad}}$	$\alpha_{00} + \Delta\alpha_o$
Corrected β_{00}	β_o	$\frac{.00629}{\text{rad}}$	$\beta_{00} + \Delta\beta_o$
Angular distance (scatter angle)	θ	$\frac{.01156}{\text{rad}}$	$\alpha_o + \beta_o$, valid for all values of θd
Path asymmetry factor	s	$\frac{.8378}{\text{rad}}$	α_o/β_o
Attenuation function for scatter paths	$F(\theta d)$	$\frac{139.7}{\text{db}}$	VOL I, Page 9.12; VOL II, Pages III.11, III.12, III.13, III.14, and III.24.
Product of scatter angle and path distance	θd	$\frac{1.9677}{\text{rad}}$	

Figure B-3 (Cont'd)

CONTINUATION: TROPOSCATTER TRANSMISSION LOSS WORKSHEET - 3 T-1609
 TKL-02/PSL-03

DEFINITION	SYMBOL	VALUE	REFERENCE/EQUATION
Height horizon ray crossover above line connecting antennas	h_0	<u>.4881 km</u>	$s\theta d / (1+s)^2$
Function of h_0 and N_s	n_s	<u>.25873</u>	Equation 9.3a
Carrier frequency	f	<u>1802.5MHz</u>	Mean
Parameter for computing H_0 (transmit)	r_1	<u>187.697</u>	$41.92 \theta f h_{t_e}$
Parameter for computing H_0 (receive)	r_2	<u>21.299</u>	$41.92 \theta f h_{r_e}$
Frequency gain function	H_0	<u>.4 db</u>	Pages 9-3 and 9-4
Height of horizon ray crossover above line connecting horizons	h_1	<u>.3742km</u>	$sD_s \theta / (1+s)^2$
Scattering efficiency correction	F_0	<u>-0.076 db</u>	$1.086(n_s/h_0)(h_0-h_1-h_{L_t}-h_{L_r})$
Atmospheric absorption factor	A_a	<u>0.85 db</u>	Section 3 and Figure 3.6
Reference value of long term median transmission loss for troposcatter	L_{brs}	<u>194.1 db</u>	$30 \log f - 20 \log d + F(\theta d) + H_0 - F_0 + A_a$
Reference value of long term median transmission loss for diffraction	L_{bd}	<u>271.8 db</u>	From diffraction worksheet
Resultant reference value of long term median transmission loss	L_{cr}	<u>194.1 db</u>	Figure 9.9 (page 9-21)
Effective distance	d_e	<u>192.3 km</u>	Page 10-8
Type climate		<u>4 #</u>	Pages 10-6 and 10-7
Correction factor	$V(0.5, d_e)$	<u>5.7 db</u>	Section III.7
Predicted median long term transmission loss	$L_m(0.5)$	<u>188.4 db</u>	$L_{cr} - V(0.5, d_e)$

Figure B-3 (Cont'd)

CONTINUATION TROPOSCATTER TRANSMISSION LOSS WORKSHEET - 4			
<u>DEFINITION</u>	<u>SYMBOL</u>	<u>VALUE</u>	<u>REFERENCE/EQUATION</u>
Long term variability for 99.99% of all hours	Y(0.9999)	<u>-33.8 db</u>	Section III.7
Transmission loss not exceeded for 99.99% of all hours	$L_n(q)$	<u>222.2 db</u>	$L_n(0.5) - Y(0.9999)$
COMMENTS:			
LINK T-1609 TKL-02/PSL-03			

ROUGH EARTH DIFFRACTION WORKSHEET (REFERENCE: NBS TECH NOTE 101)		TEST ENGINEER'S SIGNATURE	
DCS LINK NO. T-1609	STATIONS UNDER TEST TAKHLI (TKL-02) TO PHITSANULOKE (PSL-03)		
DEFINITION	SYMBOL	VALUE	REFERENCE/EQUATION
Path distance	d	<u>170.22</u> km	170.216878
Distance from transmit antenna to horizon	d_{Lt}	<u>29.29</u> km	
Distance from receive antenna to horizon	d_{Lr}	<u>10.46</u> km	
Height of transmit antenna above sea level	h_{ts}	<u>.2786</u> km	
Height of receive antenna above sea level	h_{rs}	<u>.0680</u> km	
Height of transmit obstacle above sea level	h_{Lt}	<u>.1853</u> km	
Height of receive obstacle above sea level	h_{Lr}	<u>.0613</u> km	
Effective height of transmit antenna above ground	h_{te}	<u>.2149</u> km	Page 6-4
Effective height of receive antenna above ground	h_{re}	<u>.0244</u> km	Page 6-4
Surface refractivity reduced to sea level	N_0	<u>362</u>	Figure 4.1 (page 4 - 3)
Average value of N at the earth surface	N_a	<u>360</u>	Equation 4.3
Effective earth radius	a	<u>3770</u> km	Equation 4.4 or Figure 4.2
Horizon elevation angle at transmit antenna	θ_{et}	<u>-.00468</u> rad	$(h_{Lt}-h_{ts})/d_{Lt} - d_{Lt}/2a$
Horizon elevation angle at receive antenna	θ_{er}	<u>-.00116</u> rad	$(h_{Lr}-h_{rs})/d_{Lr} - d_{Lr}/2a$
Angular distance	θ	<u>.01156</u> rad	$d/a + \theta_{et} + \theta_{er}$, valid for θd less than $\frac{1}{2}$
Angle between line joining antennas and transmit horizon ray	α_{oo}	<u>.00527</u> rad	$d/2a + \theta_{et} + (h_{ts}-h_{rs})/d$

Figure B-4

CONTINUATION: ROUGH EARTH DIFFRACTION WORKSHEET - 2			
DEFINITION	SYMBOL	VALUE	REFERENCE/EQUATION
Angle between line joining antennas and receive horizon ray	β_{00}	$\frac{.00629}{\text{rad}}$	$d/2a + \theta_{er} + (h_{rs} - h_{ts})/d$
Distance angle assuming straight rays for radius a	α_{00}	$\frac{.01156}{\text{rad}}$	$\alpha_{00} + \beta_{00}$
Angular elevation of transmit horizon ray at transmit horizon	θ_{ot}	$\frac{-.00168}{\text{rad}}$	$\theta_{ot} + d_{Lt}/a$
Angular elevation of receive horizon ray at receive horizon	θ_{or}	$\frac{-.00011}{\text{rad}}$	$\theta_{or} + d_{Lr}/a$
Distance transmit horizon to horizon ray crossover	d_{st}	$\frac{63.3}{\text{km}}$	$d \beta_{00}/\theta_{00} - d_{Lt}$
Distance receive horizon to horizon ray crossover	d_{sr}	$\frac{67.1}{\text{km}}$	$d \alpha_{00}/\theta_{00} - d_{Lr}$
Distance between horizon obstacles	D_s	$\frac{130.5}{\text{km}}$	$d_{st} + d_{sr}$ or $d - d_{Lt} - d_{Lr}$
Correction angle for exponential atmosphere (transmit)	$\Delta\alpha_0$	NA rad	Pages 6-6 and 6-7
Correction angle for exponential atmosphere (receive)	$\Delta\beta_0$	NA rad	Page 6-6 and 6-7
Corrected α_{00}	α_0	$\frac{.00527}{\text{rad}}$	$\alpha_{00} + \Delta\alpha_0$
Corrected β_{00}	β_0	$\frac{.00629}{\text{rad}}$	$\beta_{00} + \Delta\beta_0$
Angular distance	θ	$\frac{.01156}{\text{rad}}$	$\alpha_0 + \beta_0$, valid for all cases
Radius of terrain between transmit antenna and horizon	a_1	$\frac{1996}{\text{km}}$	$d_{Lt}^2/(2h_{te})$
Radius of terrain between receive antenna and horizon	a_2	$\frac{2242}{\text{km}}$	$d_{Lr}^2/(2h_{re})$

Figure B-4 (Cont'd)

CONTINUATION: ROUGH EARTH DIFFRACTION WORKSHEET - 3			
DEFINITION	SYMBOL	VALUE	REFERENCE/EQUATION
Radius of terrain between transmit horizon and horizon ray crossover	a_t	10650 km	$D_{sd_{st}}/(\theta_{d_{st}})$
Radius of terrain between receive horizon and horizon ray crossover	a_r	11967 km	$D_{sd_{sr}}/(\theta_{d_{sr}})$
Carrier frequency	f	1802.5 MHz	
Polarization	p	H (&V)	
Dielectric constant	ϵ	25	Figure 8.1 (page 8-6)
Conductivity	σ	.02 mhos/m	Figure 8.1 (page 8-6)
Diffraction parameter	$K(8497)$.0003	Figure 8.1 (page 8-6)
Diffraction parameter	C_{01}	1.62068183	$(8497/a_t)^{\frac{1}{3}}$
Diffraction parameter	C_{02}	1.55910019	$(8497/a_r)^{\frac{1}{3}}$
Diffraction parameter	C_{0t}	0.92749288	$(8497/a_t)^{\frac{1}{3}}$
Diffraction parameter	C_{0r}	0.89213664	$(8497/a_r)^{\frac{1}{3}}$
Diffraction parameter	K_1	.000486205	$C_{01}K(8497)$
Diffraction parameter	K_r	.00046773	$C_{02}K(8497)$
Diffraction parameter	K_t	.000278248	$C_{0t}K(8497)$
Diffraction parameter	K_r	.000267641	$C_{0r}K(8497)$
Diffraction parameter	b^0	90	Figure 8.2 (page 8-7)
Diffraction parameter	B_1	1.602	Figure 8.3 (page 8-8)
Diffraction parameter	B_2	1.6025	Figure 8.3 (page 8-8)
Diffraction parameter	B_t	1.604	Figure 8.3 (page 8-8)
Diffraction parameter	B_r	1.604	Figure 8.3 (page 8-8)
Diffraction parameter	$C_1(K_1)$	20 db	Figure 8.4 (page 8-9)

Figure B-4 (Cont'd)

CONTINUATION: ROUGH EARTH DIFFRACTION WORKSHEET - 4			
DEFINITION	SYMBOL	VALUE	REFERENCE/EQUATION
Diffraction parameter	$C_1(K_2)$	20 db	Figure 8.4 (page 8-9)
Diffraction parameter	B_{01}	51.21	$f^{\frac{1}{2}} C_{01}^2 B_1$
Diffraction parameter	B_{02}	47.41	$f^{\frac{1}{2}} C_{02}^2 B_2$
Diffraction parameter	B_{0t}	16.79	$f^{\frac{1}{2}} C_{0t}^2 B_t$
Diffraction parameter	B_{0r}	15.54	$f^{\frac{1}{2}} C_{0r}^2 B_r$
Diffraction parameter	x_1	1499.94 km	$B_{01} d_{1t}$
Diffraction parameter	x_2	495.87 km	$B_{02} d_{2r}$
Diffraction parameter	x_0	4101.35 km	$B_{0t} d_{st} + B_{0r} d_{sr} + x_1 + x_2$
Diffraction parameter	$\bar{C}(K_{1,2})$	20 db	$[x_1 C_1(K_1) + x_2 C_1(K_2)] / (x_1 + x_2)$
Diffraction parameter	$G(x_0)$	199.74 db	$0.05751 x_0 - 10 \log x_0$
Diffraction parameter	$F(x_1)$	55 db	Figures 8.5 and 8.6
Diffraction parameter	$F(x_2)$	-4 db	Figures 8.5 and 8.6
Atmospheric absorption	A_a	0.85 db	Section 3 and Figure 3.6
Free space loss	L_{bf}	142.19 db	$20 \log d + 20 \log f + 32.45$
Reference value of long term median transmission loss for diffraction	L_{bd}	271.8 db	$L_{bf} + G(x_0) - F(x_1) - F(x_2) - \bar{C}(K_{1,2}) + A_a$
Reference value of long term median transmission loss for troposcatter	L_{brs}	194.1 db	From troposcatter worksheet
Resultant reference value of long term median transmission loss	L_{cr}	194.1 db	Figure 9.9 (page 9-21)
Effective distance	d_e	192.3 km	Page 10-8
Type climate		4 #	Pages 10-6 and 10-7
Correction factor	$V(0.5, d_e)$	5.7 db	Section III.7

CONTINUATION: ROUGH EARTH DIFFRACTION WORKSHEET - 5			
<u>DEFINITION</u>	<u>SYMBOL</u>	<u>VALUE</u>	<u>REFERENCE/EQUATION</u>
Predicted long term median transmission loss	$L_n(0.5)$	188.4 db	$L_{cr} - v(0.5, d_e)$
Long term variability from 99.99% of all hours	$Y(0.9999)$	-33.8 db	Section 10 and III.7
Transmission loss not exceeded for 99.99% of all hours	$L_n(q)$	222.2 db	$L_n(0.5) - Y(0.9999)$
COMMENTS:			

FORWARD SCATTER MULTIPATH COUPLING LOSS WORKSHEET (REFERENCE NBS TECH NOTE 101)		TEST ENGINEER'S SIGNATURE	
DCS LINK NO.	STATIONS UNDER TEST		
T-1609	TAKHLI (TKL-02)	To	PHITSANULOKE (PSL-03)
DEFINITION	SYMBOL	VALUE	REFERENCE/EQUATION
Antenna diameter (transmit)	D_t	40 ft	
Antenna diameter (receive)	D_r	40 ft	
Carrier frequency	f	1802.5 MHz	
Half-power semi-beamwidth (transmit)	δ_t	.00868 rad	$626/D_t f$
Half-power semi-beamwidth (receive)	δ_r	.00868 rad	$626/D_r f$
Corrected α_{00}	α_0	.00527 rad	From troposcatter transmission loss worksheet
Corrected β_{00}	β_0	.00629 rad	From troposcatter transmission loss worksheet
Function of h_0 and N_0	η_0	.25873	From troposcatter transmission loss worksheet
Parameter equal to one half η_0	ν	.12937	$\eta_0/2$
Path asymmetry factor	s	.8378	α_0/β_0
Antenna asymmetry factor	μ	1	δ_r/δ_t
Product of path and antenna asymmetry factors	$s\mu$.8378	
Ratio used to determine \hat{n}	n	.72465	$\alpha_0/\delta_t, s\mu \geq 1$ or $\beta_0/\delta_r, s\mu \leq 1$
Contraction factor	$f(\nu)$	1.0301	$[1.36 + 0.116\nu] [1 + 0.36 \exp(-0.56\nu)]^{-1}$
Coupling loss parameter	\hat{n}	0.70434	$(n + 0.03\nu)/f(\nu)$
Multipath coupling loss	L_{MP}	2.5 db	Figure 9.8 (page 9-20) For $s\mu < 1$, read Figure 9.8 for $1/s\mu$
COMMENTS:			

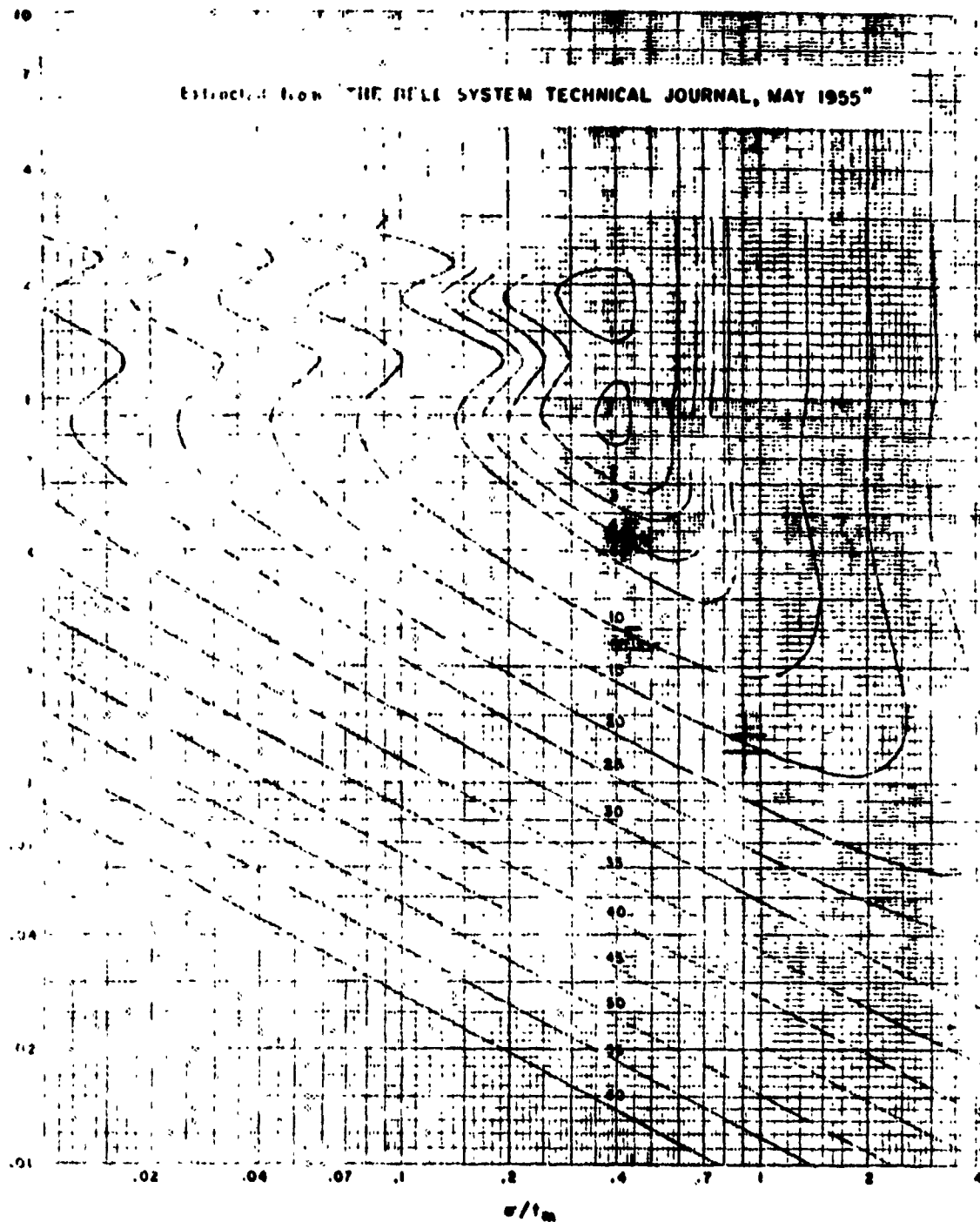
ECHO DISTORTION WORKSHEET			TEST ENGINEER'S SIGNATURE	
REFERENCE: THE BELL SYSTEM TECHNICAL JOURNAL				
DCS LINK NO.	STATIONS UNDER TEST			
T-1609	TAKHLI (TKL-02) TO PHITSANULOKE (PSL-02)			
DEFINITION	SYMBOL	VALUE		REFERENCE/EQUATION
		TRANSMIT STATION	RECEIVE STATION	
VSWR at point A		<u>1.13</u>	<u>1.19</u>	Manufacturer's specs or measurement
Return loss A	L_a	<u>24.3 dB</u>	<u>21.1 dB</u>	$20 \log \left \frac{VSWR+1}{VSWR-1} \right $
VSWR at point B		<u>1.2</u>	<u>1.2</u>	Manufacturer's specs or measurement
Return loss B	L_b	<u>20.8 dB</u>	<u>20.8 dB</u>	$20 \log \left \frac{VSWR+1}{VSWR-1} \right $
Transmission distance	D	<u>49 m</u>	<u>53 m</u>	
Attenuation constant	α	<u>.04593 dB/m</u>	<u>.07874 dB/m</u>	Manufacturer's data
Transmission loss A to B	L_t	<u>2.8 dB</u>	<u>4.7 dB</u>	αD
Velocity of propagation	v	<u>243 m/μs</u>	<u>243 m/μs</u>	Manufacturer's data
Echo delay	T	<u>.40 μs</u>	<u>.44 μs</u>	$2D/v$
RF signal-to-RF echo power ratio	S/E	<u>50.7 dB</u>	<u>51.3 dB</u>	$L_a + L_b + 2L_t$
Number of VF channels	n	<u>72</u>	<u>72</u>	
Top baseband frequency	f_m	<u>.300 MHz</u>	<u>.300 MHz</u>	
Per channel deviation (RMS)	d_{rms}	<u>.142 MHz</u>	<u>.142 MHz</u>	Manufacturer's standard or measurements
Baseband white noise power	P_n	<u>5.72 dBm0</u>	<u>5.72 dBm0</u>	
White noise bandwidth	B_n	<u>288 MHz</u>	<u>288 MHz</u>	
System deviation (RMS)	σ	<u>.2745 MHz</u>	<u>.2745 MHz</u>	$d_{rms} \log^{-1}(0.05P_n)$
Deviation ratio	σ/f_m	<u>.9150</u>	<u>.9150</u>	
Top baseband frequency times echo delay	$f_m T$	<u>.12</u>	<u>.132</u>	
Interference ratio	K	<u>16 dB</u>	<u>15 dB</u>	Figure 1

FIGURE B-6

CONTINUATION ECHO DISTORTION WORKSHEET - 2				
DEFINITION	SYMBOL	VALUE		REFERENCE/EQUATION
		TRANSMIT STATION	RECEIVE STATION	
Signal improvement	I_p	3 dB	3 dB	3 dB for CCIR emphasis
Signal-to-noise ratio due to echo	NPR	69.7 dB	69.3 dB	$S/E + K + I_p$
Signal-to-noise ratio	S/N	95.1 dB	94.7 dB	$NPR - P_n + 10 \log B_n + 25.1$
Sum of echo noise	N_e	0.22 μ WCO	0.24 μ WCO	$\text{Log}^{-1}[0.1 (88.5 - S/N)]$
Sum of echo noise		0.46 μ WCO		Sum of noise powers due to echoes at both stations
COMMENTS				

FIGURE B-6 (Cont'd)

Extracted from "THE BELL SYSTEM TECHNICAL JOURNAL, MAY 1955"



CONTOURS OF CONSTANT INTERFERENCE IN THE TOP CHANNEL OF A MULTI-CHANNEL FM SYSTEM

MULTIPATH DISTORTION WORKSHEET

TEST ENGINEERS SIGNATURE

NAME OF THE SYSTEM TECHNICAL JOURNAL

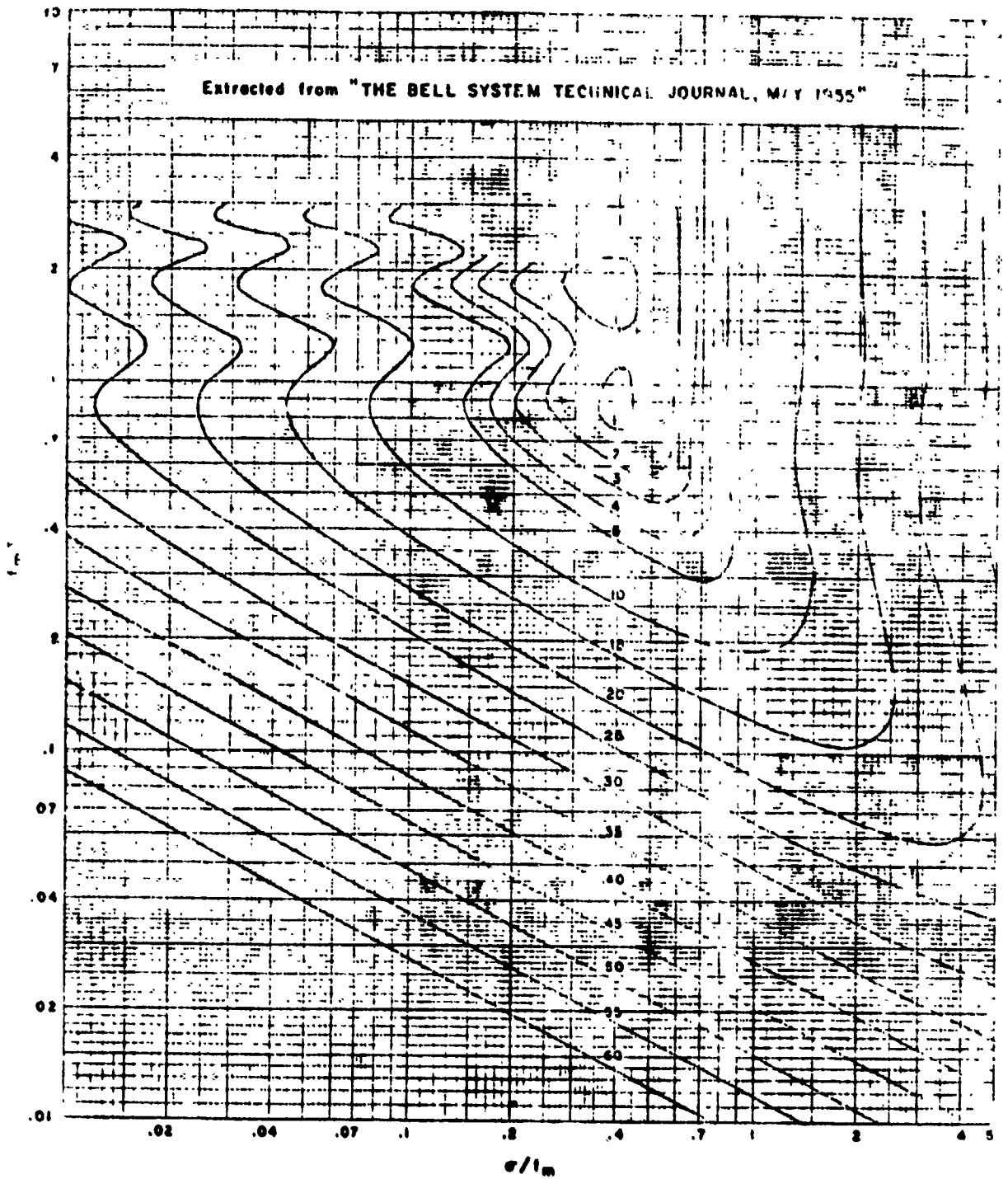
STATIONS UNDER TEST
 TAPLEY (TKI 02)

TO PHITSANULOKE (PSI-03)

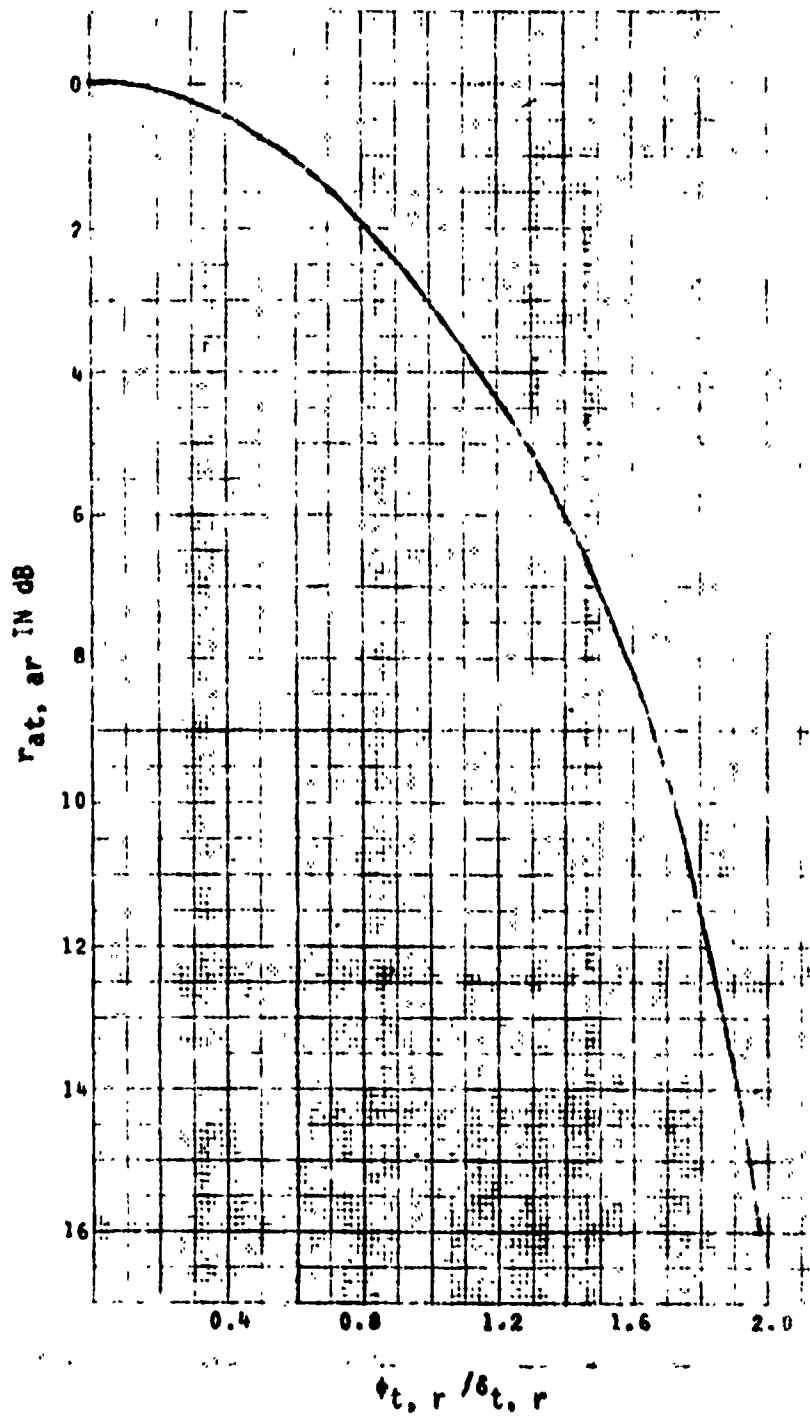
DEFINITION	SYMBOL	VALUE	REFERENCE/EQUATION
Distance	d	170.2 _{km}	170 216875
Antenna gain	α_0	.00527 _{rad}	From propagation of radio waves
Antenna gain	β_0	.00629 _{rad}	From propagation of radio waves worksheet
Frequency	f	1362.5 _{MHz}	Mean
Antenna diameter	D_L	40 _{ft}	
Antenna diameter	D_r	40 _{ft}	
Left semi-beamwidth	δ_L	.00868 _{rad}	$626/D_L f$
Right semi-beamwidth	δ_r	.00868 _{rad}	$626/D_r f$
Number of channels	n	72	
Channel frequency	f_{ch}	.300 _{MHz}	
Channel deviation (RMS)	d_{rms}	.142 _{MHz}	Manufacturer's standard
Channel loading	P_n	5.72 _{dbm0}	$-1 + 4 \log (2/3 n)$
Channel bandwidth	B_n	.288 _{MHz}	
Channel deviation (RMS)	σ	.2745 _{MHz}	$d_{rms} \log^{-1} (0.05 P_n)$
Carrier to noise ratio	c/n_0	9150	
Carrier to noise signal-to-noise ratio	S/I	61.7 _{db}	From Figure 2-8
Correction for multiple echos	Δ	9 _{db}	
Carrier to noise improvement	I_d	6 _{db}	3 db for dual, 6 db for quad
Carrier to noise improvement	I_e	3 _{db}	Approximately 3 db for CCIR Emphasis

CONTINUATION MULTIPATH DISTORTION WORKSHEET - 2			
DEFINITION	SYMBOL	VALUE	REFERENCE/EQUATION
Link signal-to-noise ratio due to multipath propagation	NPR	61.7 db	$10 \log \frac{P_s}{P_n}$
Channel signal-to-noise ratio due to multipath propagation	S/N	75.7 db	$NPR - P_n + 10 \log B_n + 2$
Link channel multipath noise	N_{mp}	19.2 pWCO	$\text{Log}^{-1} 0.1(88.5 - S/N)$
COMMENTS:			
LINK I-1609 TKL-02/PSL-03			

Figure 8 -7 (Cont'd)



CONTOURS OF CONSTANT INTERFERENCE IN THE TOP CHANNEL OF A MULTI-CHANNEL FM SYSTEM



ANTENNA GAIN REDUCTION VERSUS RATIO OF ANGLE FROM BEAM CENTER TO HALF POWER SEMI-BEAMWIDTH

MULTIPATH DISTORTION WORKSHEET

CONTINUATION: MULTIPATH DISTORTION WORKSHEET

r_e (dB)	$\rho-1$	ρ^2-1	ϕ_t (rad)	ϕ_t/ϕ_t	r_{at} (dB)	r_r (rad)	r_r/r_r	r_{ar} (dB)	r_t (dB)	I (μ s)	k (dB)	S/I (dB)
2	0.068	0.141										
4	0.141	0.301										
6	0.218	0.484										
8	0.301	0.693										
10	0.389	0.931										
12	0.484	1.202										
14	0.585	1.512										
16	0.693	1.865										
18	0.808	2.268										
20	0.931	2.728										
22	1.062	3.252										
24	1.202	3.850										
26	1.352	4.532										
28	1.512	5.310										
30	1.683	6.197										

$\rho = \log^{-1}(r_e/70)$
 $r_t = r_e + r_{at} + r_{ar}$

Figure B-8

LINK NOISE PERFORMANCE WORKSHEET		TEST ENGINEER'S SIGNATURE	
DCS LINK NO. T-1609	STATIONS UNDER TEST TAKHLI (TKL-02)	TO PHITSANULOKE (PSL-03)	
DEFINITION	SYMBOL	VALUE	REFERENCE/EQUATION
Median basic transmission loss	$L_n(0.5)$	188.4 dB	From transmission loss worksheet
Transmitter power	P_t	63 dBm	$10 \log P_t$ (milliwatts)
Antenna diameter (transmit)	D_t	40 ft	
Antenna diameter (receive)	D_r	40 ft	
Carrier frequency	f	1802.50 MHz	Mean
Free space antenna gain (transmit) relative to isotropic radiator	G_t	44.7 dB	Manufacturer's specifications or $20 \log D_t + 20 \log f - 52.5$ dB
Free space antenna gain (receive) relative to isotropic radiator	G_r	44.7 dB	Manufacturer's specifications or $20 \log D_r + 20 \log f - 52.5$ dB
Forward scatter multipath coupling loss	L_{gp}	2.5 dB	From coupling loss worksheet
Path antenna gain	G_p	86.8 dB	$G_t + G_r - L_{gp}$
Total transmission line and associated losses	L_t	7.5 dB	Manufacturer's specifications and/or measurements
Median receive carrier power	P_{rc}	-46.1 dBm	$P_t + G_p - L_n(0.5) - L_t$
Receiver noise figure	F	10.5 dB	Manufacturer's specifications or measurements
Receiver IF bandwidth	B	8 MHz	Manufacturer's specifications or measurements
Receiver noise power	P_{rn}	-94.5 dBm	$10 \log B + F - 114$
Median carrier-to-noise ratio	C/N	48.4 dB	$P_{rc} - P_{rn}$
Number of VF channels	n	72	
Top baseband frequency	f_n	300 kHz	
RMS per channel deviation	d_{rms}	142 kHz	Without pre-emphasis
Pre-emphasis improvement for top channel	I_p	3 dB	

Figure B-9

CONTINUATION — LINK NOISE PERFORMANCE WORKSHEET			
DEFINITION	SYMBOL	VALUE	REFERENCE/EQUATION
FM improvement for top channel	I_{fm}	30.6 dB	$20 \log d_{rms} - 20 \log f_m + 10 \log B + I_p + 25.1 \text{ dB}$
Unweighted median channel signal-to-thermal noise ratio for top channel	$S/N(t)$	79.0 dB	$C/N + I_{fm}$
C-message weighted thermal noise power	$N(t)$	8.8 μwCO	$\text{Log}^{-1} 0.1 [88.5 - S/N(t)]$
Order of diversity		4	
Median diversity improvement	I_d	6 dB	
Combined weighted thermal noise power	$N(tc)$	2.2 μwCO	
Equipment noise power ratio	NPR	50 dB	manufacturer's specification
White noise loading	P_n	5.72 dBmO	$-1 + 4 \log (2/3 n)$
White noise bandwidth	B_n	288 kHz	
Equivalent channel signal-to-intermodulation noise ratio	$S/N(i)$	64.0 dB	$\text{NPR} - P_n + 10 \log B_n - 4.9 \text{ dB}$
C-message weighted intermodulation noise power	$N(i)$	283.9 μwCO	$\text{Log}^{-1} 0.1 [88.5 - S/N(i)]$
C-message weighted noise power due to feeder echo	$N(fe)$.46 μwCO	From feeder echo worksheet
C-message weighted noise power due to multipath propagation	$N(mp)$	19.2 μwCO	From path intermodulation worksheet
Total median weighted noise power	$N(\text{total})$	305.76 μwCO	$N(tc) + N(i) + N(fe) + N(mp)$
DCA median noise allocation	$N(\text{DCA})$	203.9 μwCO	30.8 dBrnC0
Design margin		6.0 dB	$10 \log [N(\text{DCA})/N(\text{total})]$

Figure B-9 (Cont'd)

SMOOTH EARTH DIFFRACTION WORKSHEET		TEST ENGINEERS SIGNATURE	
DCS LINK NO.	STATIONS UNDER TEST		
	_____ TO _____		
DEFINITION	SYMBOL	VALUE	REFERENCE/EQUATION
Path distance	d	_____ km	
Height of transmit antenna above sea level	h_{ts}	_____ km	
Height of receive antenna above sea level	h_{rs}	_____ km	
Surface refractivity reduced to sea level	N_0	_____	Figure 4.1 (page 4-3)
Average value of N at the earth surface	N_s	_____	Page 4-1
Effective earth radius	a	_____ km	Equation 4.4 or Figure 4.2
Effective height of transmit antenna above ground	h_{te}	_____ km	Page 6-4
Effective height of receive antenna above ground	h_{re}	_____ km	Page 6-4
Distance from transmit antenna to horizon	d_{Lt}	_____ km	$\sqrt{h_{te}/2a}$
Distance from receive antenna to horizon	d_{Lr}	_____ km	$\sqrt{h_{re}/2a}$
Carrier frequency	f	_____ MHz	
Polarization	p	_____	
Dielectric constant		_____	Figure 8.1 (page 8-6)
Conductivity		_____ mho/m	Figure 8.1 (page 8-6)
Diffraction parameter	K(8497)	_____	Figure 8.1 (page 8-6)
Diffraction parameter	C_0	_____	(8497/a)
Diffraction parameter	K(a)	_____	$C_0 K(8497)$
Diffraction parameter	b°	_____ °	Figure 8.2 (page 8-7)
Diffraction parameter	B(K, b°)	_____	Figure 8.3 (page 8-8)

CONTINUATION: SMOOTH EARTH DIFFRACTION WORKSHEET - 2			
DEFINITION	SYMBOL	VALUE	REFERENCE/EQUATION
Diffraction parameter	B_0	_____	$f C_0 G(K, b^0)$
Diffraction parameter	$C(K, b^0)$	_____ db	Figure 8.4 (page 8-6)
Diffraction parameter	X_0	_____ km	dB_0
Diffraction parameter	X_1	_____ km	$d_{Lt} B_0$
Diffraction parameter	X_2	_____ km	$d_{Lr} B_0$
Diffraction parameter	$G(X_0)$	_____ db	Figures 8.5 and 8.6
Diffraction parameter	$F(X_1)$	_____ db	Figures 8.5 and 8.6
Diffraction parameter	$F(X_2)$	_____ db	Figures 8.5 and 8.6
Atmospheric absorption	A_a	_____ db	Section 3 and Figure 3.6
Free space loss	L_{bf}	_____ db	$20 \log d + 20 \log f + 32.45$
Reference value of long term median transmission loss for diffraction	L_{bd}	_____ db	$L_{bf} + G(X_0) - F(X_1) - F(X_2) - C(K, b^0) + A_a$
Reference value of long term median transmission loss for troposcatter	L_{ts}	_____ db	From troposcatter worksheet
Resultant reference value of long term median transmission loss	L_{cr}	_____ db	Figure 9.9 (page 9-21)
Effective distance	d_e	_____ km	Page 10-8
Type climate		_____ #	Page 10-6 and 10-7
Correction factor	$V(0.5, d_e)$	_____ db	Figure 10.13 (page 10-26)
Predicted long term median transmission loss	$L_n(0.5)$	_____ db	$L_{cr} - V(0.5, d_e)$
Long term variability for 99.99% of all hours	$Y(0.9999)$	_____ db	Section 10 and III.7
Transmission loss not exceeded for 99.99% of all hours	$L_n(q)$	_____ db	$L_n(0.5) - Y(0.9999)$

KNIFE-EDGE DIFFRACTION WORKSHEET (REFERENCE NBS TECH NOTE 101)		TEST ENGINEERS SIGNATURE	
DCS LINK NO	STATIONS UNDER TEST		
	_____ TO _____		
DEFINITION	SYMBOL	VALUE	REFERENCE/EQUATION
Path distance	d	_____ km	
Distance from transmit antenna to knife-edge	d_{Lt}	_____ km	
Distance from receive antenna to knife-edge	d_{Lr}	_____ km	
Height of transmit antenna above sea level	h_{ts}	_____ km	
Height of receive antenna above sea level	h_{rs}	_____ km	
Height of knife-edge above sea level	h_{ke}	_____ km	
Surface refractivity reduced to sea level	N_0	_____	Figure 4.1 (page 4-3)
Average value of " " at the earth surface	N_s	_____	Page 4-1
Effective earth radius	a	_____ km	Equation 4.4 or Figure 4.2
Horizon elevation angle at transmit antenna	θ_{et}	_____ rad	$(h_{ke} - h_{ts})/d_{Lt} - d_{Lt}/2a$
Horizon elevation angle at receive antenna	θ_{er}	_____ rad	$(h_{ke} - h_{rs})/d_{Lr} - d_{Lr}/2a$
Knife-edge angle	θ	_____ rad	$d/a + \theta_{et} + \theta_{er}$
Carrier frequency	f	_____ MHz	
Knife-edge parameter	v	_____	$\pm 2.5830\sqrt{fd_{Lt}d_{Lr}/d}$
Diffraction loss over single isolated knife-edge, no ground reflections	$(v, 0)$	_____	Figure 7.1 (page 7-11) $12.953 + 20 \log v$ for $v > 3$
Residual height gain function (transmit)	$G(\bar{h}_1)$	_____	Pages 7-3 and 7-6
Residual height gain function (receive)	$G(\bar{h}_2)$	_____	Pages 7-3 and 7-6
Crest radius	r	_____ km	Page 7-4
Index of curvature	ρ	_____	$0.676r\bar{f}^{\frac{1}{2}}[d/(d_{Lt}d_{Lr})]^{\frac{1}{2}}$

Figure B-11

KNIFE-EDGE DIFFRACTION WORKSHEET (REFERENCE NBS TECH NOTE 101)		TEST ENGINEER'S SIGNATURE	
DCS LINK NO	STATIONS UNDER TEST		
	TO _____		
DEFINITION	SYMBOL	VALUE	REFERENCE/EQUATION
Path distance	d	_____ km	
Distance from transmit antenna to knife-edge	d_{Lt}	_____ km	
Distance from receive antenna to knife-edge	d_{Lr}	_____ km	
Height of transmit antenna above sea level	h_{ts}	_____ km	
Height of receive antenna above sea level	h_{rs}	_____ km	
Height of knife-edge above sea level	h_{ke}	_____ km	
Surface refractivity reduced to sea level	N_0	_____	Figure 4.1 (page 4-3)
Average value of N at the earth surface	N_s	_____	Page 4-1
Effective earth radius	a	_____ km	Equation 4.4 or Figure 4.2
Horizon elevation angle at transmit antenna	θ_{et}	_____ rad	$(h_{ke} - h_{ts})/d_{Lt} - d_{Lt}/2a$
Horizon elevation angle at receive antenna	θ_{er}	_____ rad	$(h_{ke} - h_{rs})/d_{Lr} - d_{Lr}/2a$
Knife edge angle	θ	_____ rad	$d/a + \theta_{et} + \theta_{er}$
Carrier frequency	f	_____ MHz	
Knife-edge parameter	v	_____	$\pm 2.5830\sqrt{fd_{Lr}d_{Lt}/d}$
Diffraction loss over single isolated knife-edge, no ground reflections	$A(v,0)$	_____	Figure 7.1 (page 7-11) $12.953 + 20 \log v$ for $v > 3$
Residual height gain function (transmit)	$G(\bar{h}_1)$	_____	Pages 7-3 and 7-6
Residual height gain function (receive)	$G(\bar{h}_2)$	_____	Pages 7-3 and 7-6
Crest radius	r	_____ km	Page 7-4
Index of curvature	ρ	_____	$0.676r \bar{r}^2 [d/(d_{Lt}d_{Lr})]^2$

Figure B-11(Cont'd)

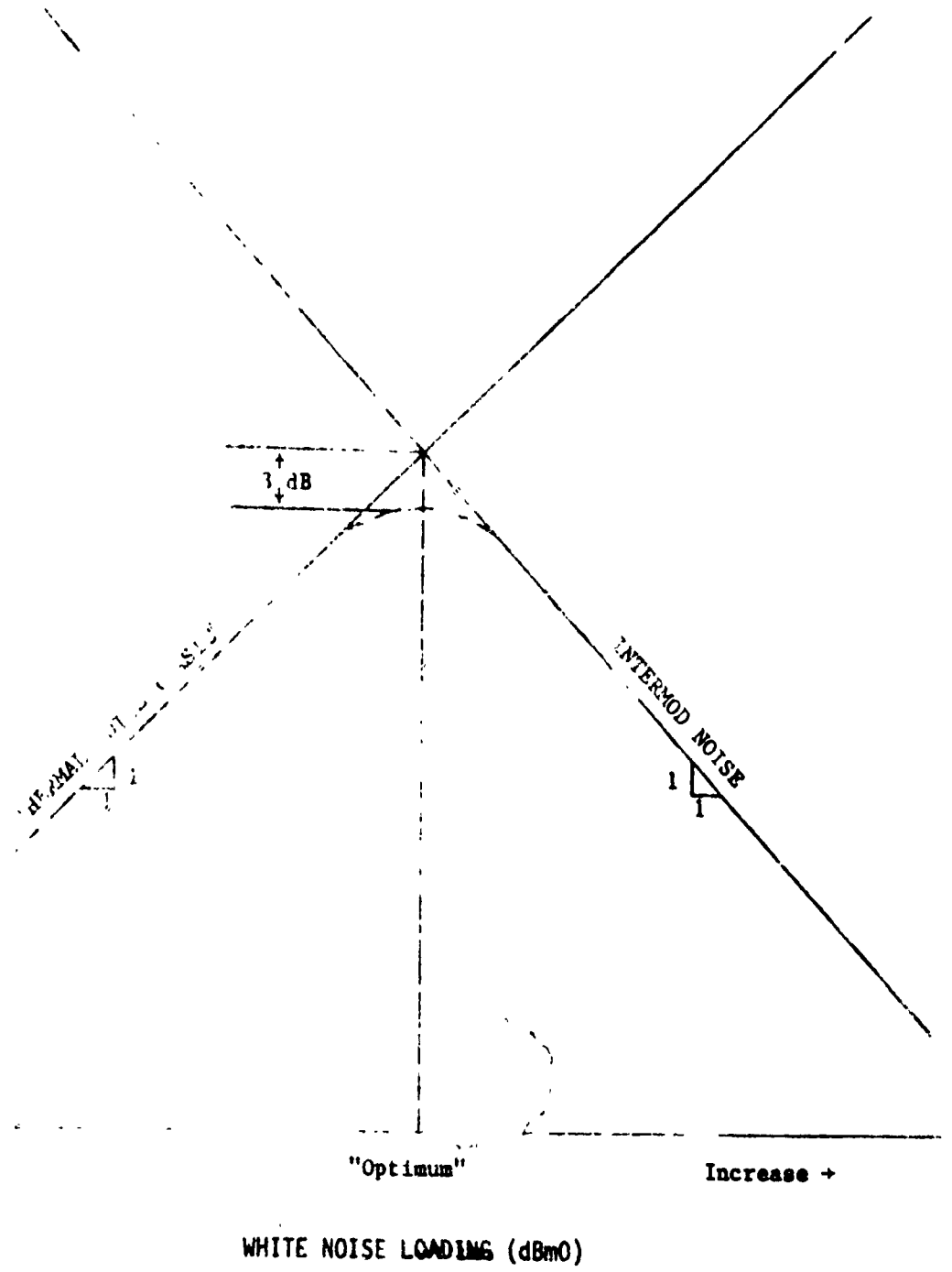


Figure B-12

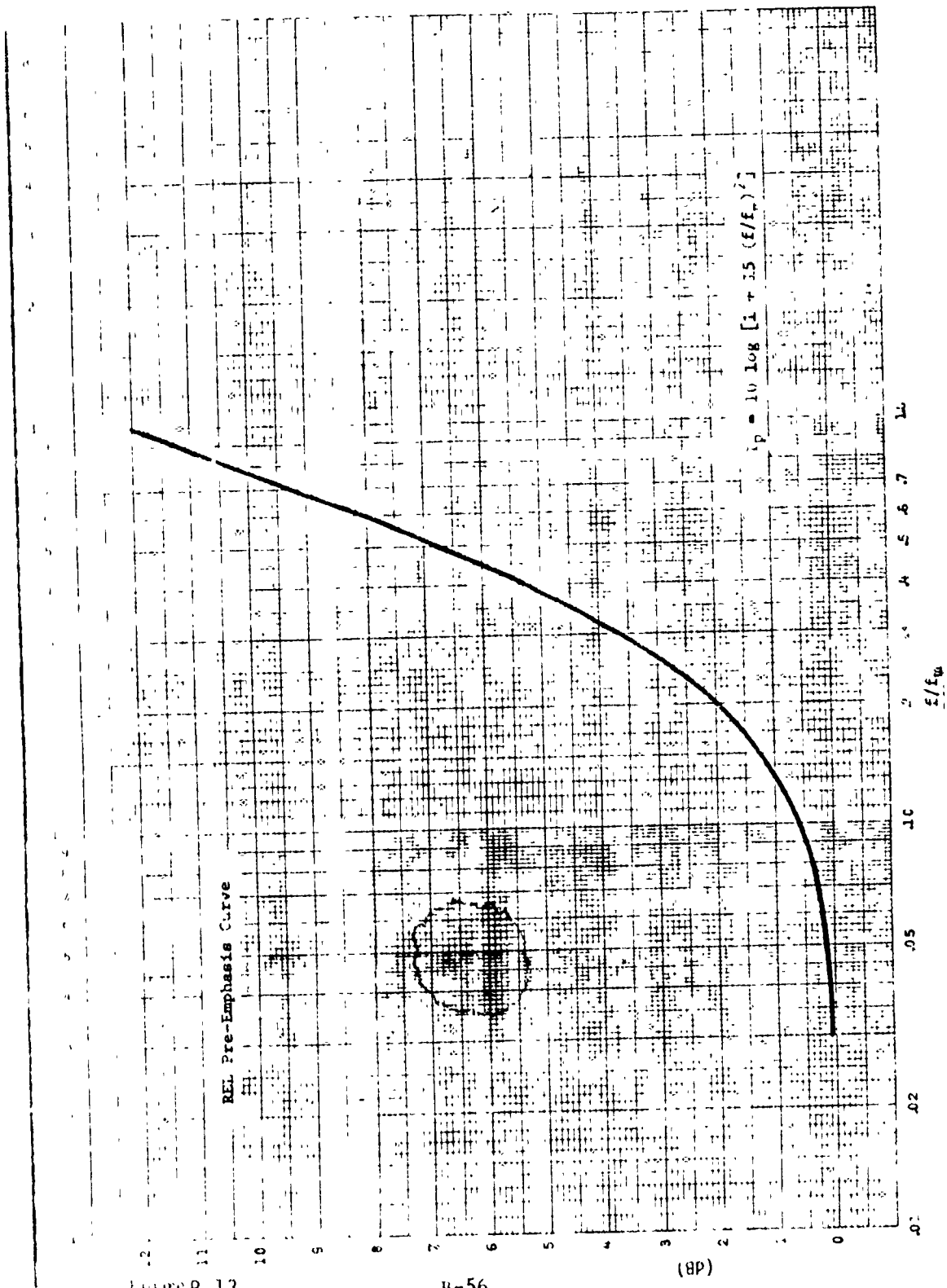


Figure B-13

B-56

(BP)

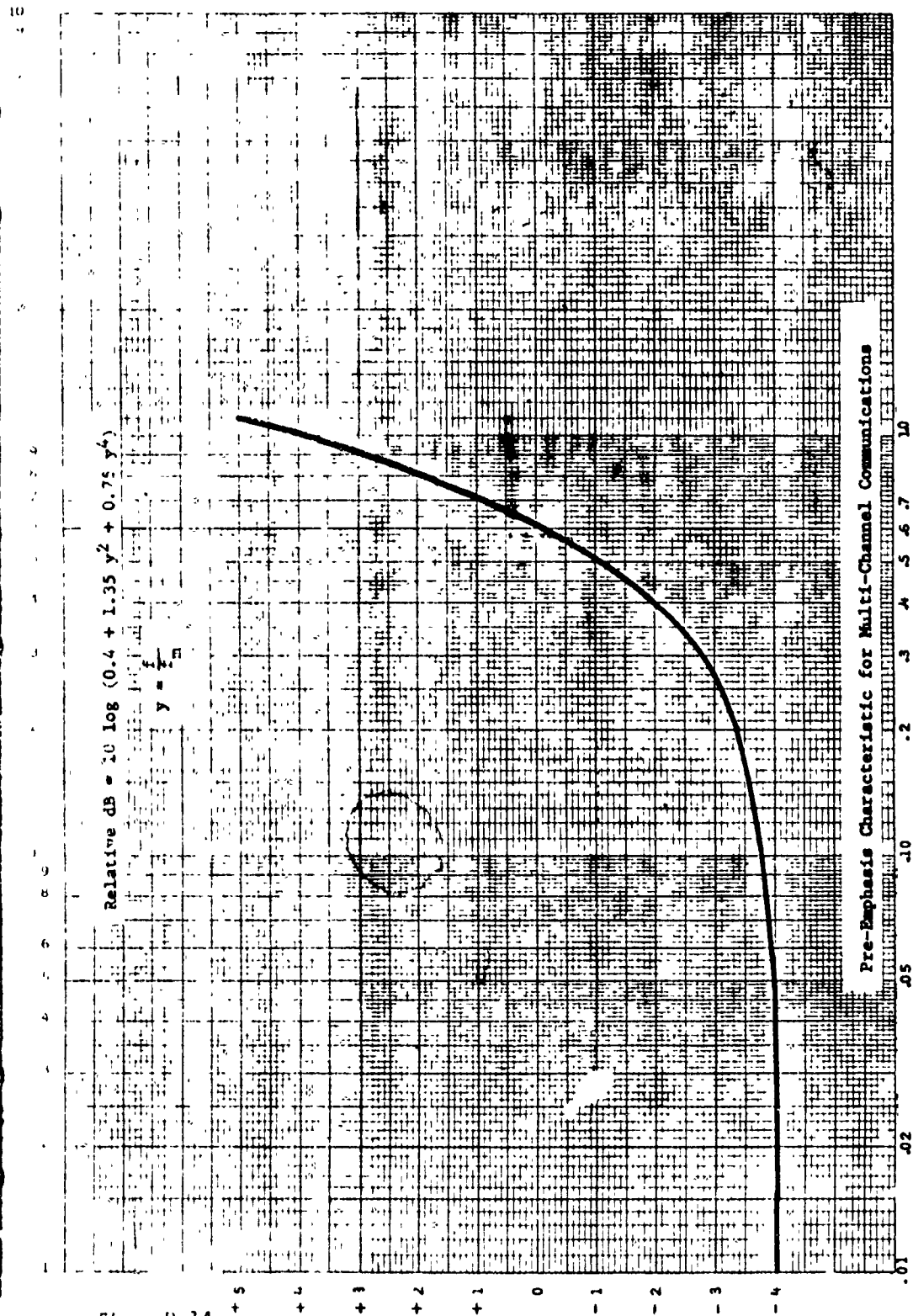


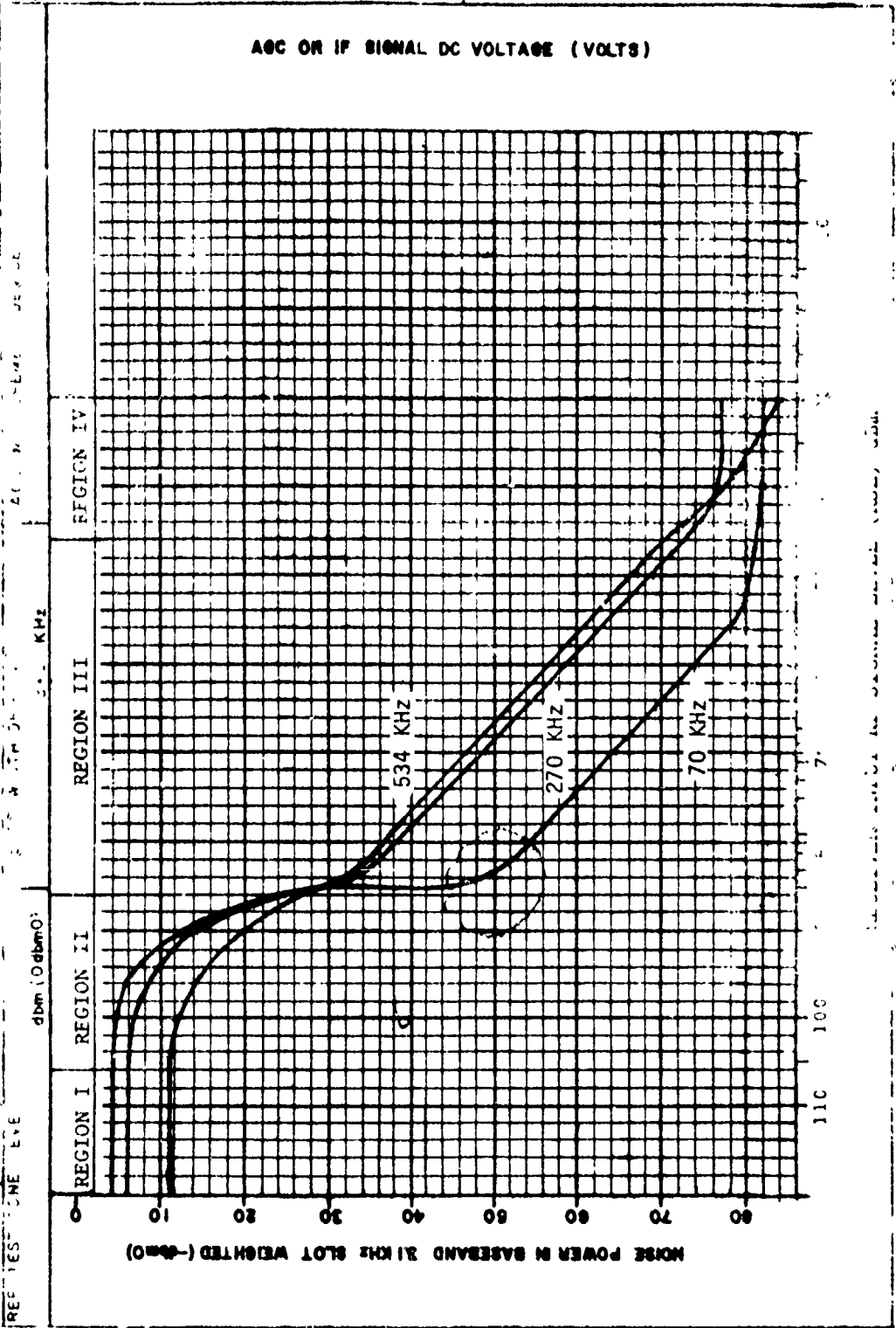
Figure B-14

B-57





RECEIVED NOISE CURRENT (dBm/Hz)



FM RECEIVER NOISE QUIETING, AGC or IF SIGNAL, AND IF LIMITING DATA										PAGE ___ OF ___ PAGES		DATE	
DATA SHEET T34-2												day mo yr	
DCS LINK NO.			STATION UNDER TEST			REF TEST TONE		TEST ENGINEER SIGNATURE					
RECEIVER TYPE			FSV. SLOT WIDTH		70 KHz SLOT		270 KHz SLOT		534 KHz SLOT				
REL			3.1 KHz										
RECEIVER NO.		RSL AT 20db QUIETING			dbm		dbm		dbm				
		RSL AT RECEIVER THRESHOLD			dbm		dbm		dbm				
RSL	AGC/IF SIGNAL VOLTS DC		IF LIMITER OUTPUT RMS VOLTS	POST DET. COMBINED DC CONTROL VOLTS	NOISE POWER IN BASEBAND SLOT - SLOT FREQUENCY								
	AGC	IF			70 KHz		270 KHz		534 KHz				
dbm					MEAS CORR. to dbm	31KHz	dbmO	MEAS CORR. to dbm	31KHz	dbmO	MEAS CORR. to dbm	31KHz	dbmO
-110							-4.0			-6.0			-11.0
-105							-4.0			-6.0			-11.0
-100							-4.5			-7.0			-11.5
-95							-6.0			-9.0			-12.0
-90							-13			-140			-22.0
-85							-30			-32			-22.0
-83							-51			-35			-23.0
-81							-53			-37			-23.0
-79							-55			-39			-23.0
-77							-57			-41			-23.0
-75							-59			-44			-23.0
-70							-64			-49			-23.0
-65							-69			-54			-23.0
-60							-74			-59			-23.0
-55							-79			-64			-23.0
-80							-80.5			-69			-23.0
-45							-81.5			-74			-23.0
-40							-82			-76.5			-23.0
-35							-82			-77			-23.0
-30							-82			-77			-23.0
-25													
-20													

Figure B-16

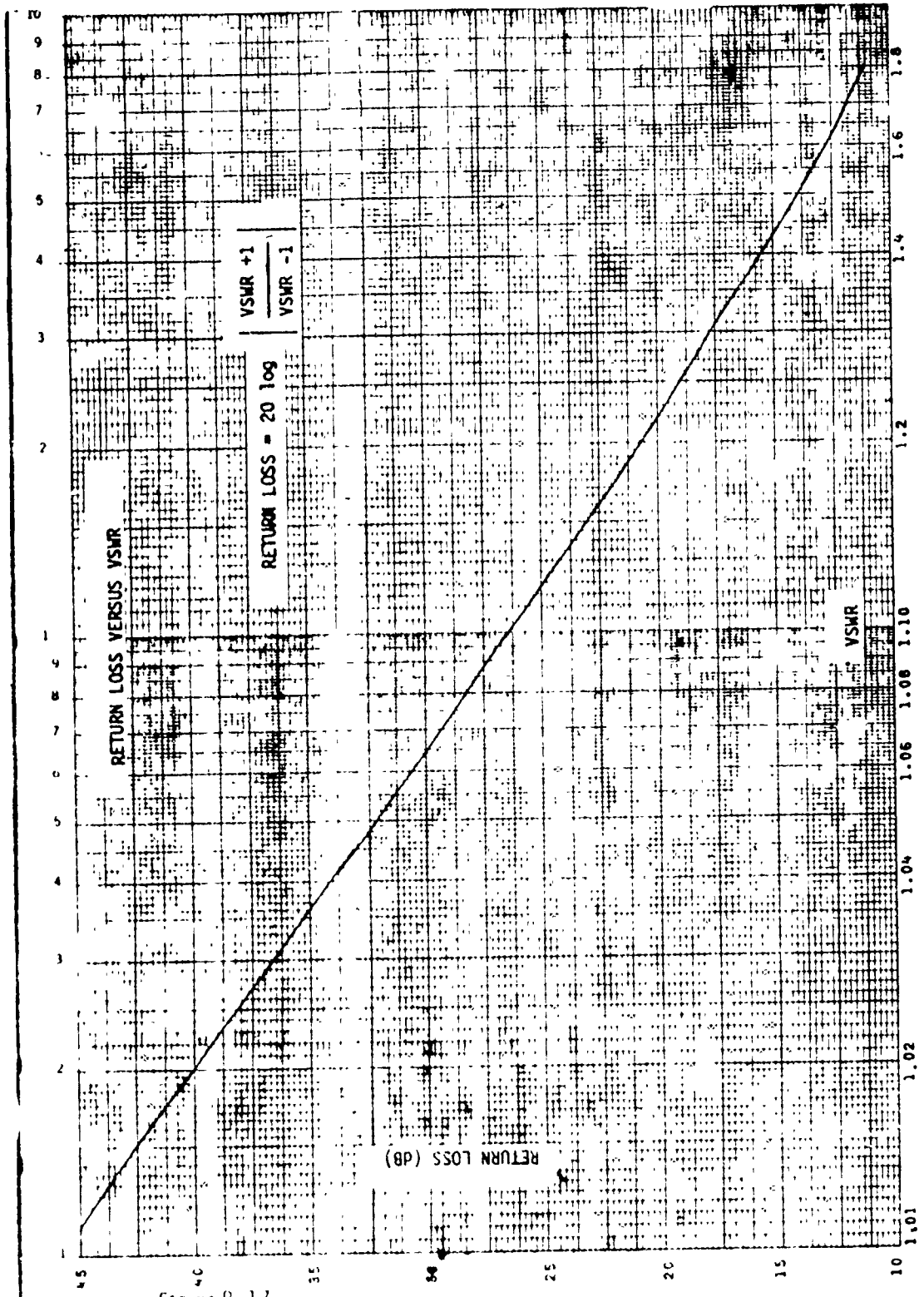
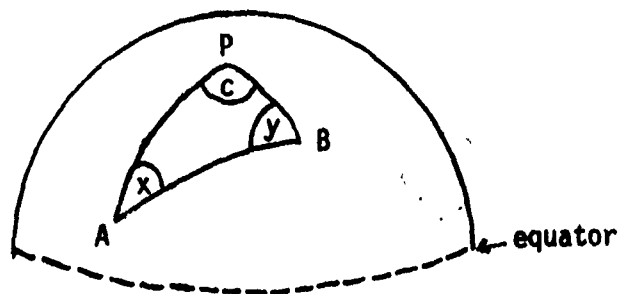


Figure B-17

B-6)

Great Circle Calculations (Tropo)

A. To determine the distance between stations A and B.



B = Place of greater latitude, i.e., nearer the pole.

L_A = Latitude of station A

L_B = Latitude of station B

C = Difference of longitude between stations A and B.

$$\tan \frac{Y-X}{2} = \cot \left(\frac{C}{2} \right) \left[\frac{\sin \frac{L_B - L_A}{2}}{\cos \frac{L_B + L_A}{2}} \right]$$

$$\tan \frac{Y+X}{2} = \cot \left(\frac{C}{2} \right) \left[\frac{\cos \frac{L_B - L_A}{2}}{\sin \frac{L_B + L_A}{2}} \right]$$

Taking the arc tan of the above two equations, $\frac{Y-X}{2}$

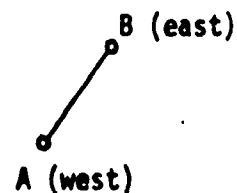
and $\frac{Y+X}{2}$ can be obtained.

OMP 762-1

The distance Z (in degrees) along the great circle between A and B is given by:

$$\tan \frac{Z}{2} = \tan \left(\frac{L_B - L_A}{2} \right) \left[\frac{\left(\sin \frac{Y + X}{2} \right)}{\left(\sin \frac{Y - X}{2} \right)} \right]$$

Z (in degrees) X 111.18 = kilometers
X 69.05 = statute miles
X 60.00 = nautical miles

Path Distance Less Than 75 Miles or 120 Km

$\Delta\lambda$ = Difference between longitudes of stations
A and B.

$\Delta\lambda_{sec}$ = Converted difference into seconds.

$\Delta\theta$ = Difference between latitudes of stations
A and B.

$\Delta\theta_{sec}$ = Converted difference into seconds.

$$B_m = \left(\begin{array}{l} \text{Latitude of the station} \\ \text{closer to the equator} \end{array} \right) + \frac{\Delta\theta}{2}$$

1) Calculate

$$\cot(w) = \frac{(\Delta\lambda_{sec})(B_m/A_m) * (\cos \theta_m)}{\Delta\theta_{sec}}$$

obtain (w)

$$2) D_{meters} = \frac{(\Delta\lambda_{sec})(\cos \theta_m)}{(A_m) * (\cos w)}$$

* B_m/A_m and A_m from tables, for tabulated latitude
nearest to θ_m .

CCP 702-1

Latitude degrees	B_m/A_m	Latitude degrees	B_m/A_m	Latitude degrees	B_m/A_m
00	1.00681343	25	1.00559707	50	1.00281541
01	1.00681343	26	1.00550446	51	1.00269766
02	1.00680648	27	1.00540954	52	1.00258222
03	1.00679488	28	1.00531231	53	1.00246911
04	1.00678098	29	1.00521278	54	1.00235371
05	1.00676243	30	1.00511094	55	1.00224293
06	1.00673925	31	1.00500680	56	1.00213216
07	1.00671375	32	1.00490036	57	1.00202141
08	1.00668362	33	1.00479392	58	1.00191297
09	1.00664885	34	1.00468288	59	1.00180686
10	1.00660944	35	1.00457184	60	1.00170306
11	1.00656772	36	1.00446082	61	1.00160158
12	1.00652137	37	1.00434749	62	1.00150241
13	1.00647038	38	1.00423187	63	1.00140556
14	1.00641708	39	1.00411626	64	1.00130872
15	1.00635915	40	1.00399835	65	1.00121650
16	1.00629659	41	1.00388277	66	1.00112660
17	1.00623171	42	1.00376258	67	1.00104131
18	1.00616452	43	1.00364471	68	1.00095603
19	1.00609271	44	1.00352686	69	1.00087537
20	1.00601858	45	1.00340671	70	1.00079701
21	1.00593982	46	1.00328888	71	1.00072097
22	1.00585875	47	1.00316876	72	1.00064954
23	1.00577538	48	1.00305097		
24	1.00568738	49	1.00293318		

Latitude degrees	A _m	Latitude degrees	A _m	Latitude degrees	CCP 702-1 A _m
00	.03233903	25	.03231945	50	.03227468
01	.03233896	26	.03231797	51	.03227283
02	.03233888	27	.03231640	52	.03227097
03	.03233873	28	.03231484	53	.03226911
04	.03233844	29	.03231328	54	.03226725
05	.03233814	30	.03231164	55	.03226547
06	.03233784	31	.03230993	56	.03226369
07	.03233739	32	.03230822	57	.03226190
08	.03233687	33	.03230651	58	.03226020
09	.03233635	34	.03230480	59	.03225849
10	.03233568	35	.03230301	60	.03225678
11	.03233501	36	.03230115	61	.03225515
12	.03233427	37	.03229937	62	.03225359
13	.03233345	38	.03229751	63	.03225203
14	.03233263	39	.03229565	64	.03225047
15	.03233166	40	.03229371	65	.03224898
16	.03233069	41	.03229186	66	.03224750
17	.03232965	42	.03228985	67	.03224616
18	.03232853	43	.03228806	68	.03224475
19	.03232742	44	.03228613	69	.03224349
20	.03232623	45	.03228420	70	.03224222
21	.03232496	46	.03228234	71	.03224104
22	.03232362	47	.03228041	72	.03223985
23	.03232228	48	.03227847		
24	.03232087	49	.03227662		

DATA ANALYSIS

SECTION I - INSTRUCTIONS

C-1 ANALYSIS OF THE DATA

This section is intended to provide insight into the meaning of data recorded during a technical evaluation. Each individual test performed provides information as to system quality and certain faults that may exist in the radio or multiplex subsystem. Analysis of the test results collectively, however, can result in expeditious fault isolation and correction, eliminating unnecessary and time consuming trial and error procedures. Every test performed has a definite relationship to one or more of the other tests in the sequence. This section will examine the individual tests performed by the TEP Teams and their relationships to other tests. The test results will be examined as possible trouble shooting aids based on engineering information and past experience.

C-2 IDLE CHANNEL NOISE RECORDINGS

Idle channel noise (ICN) is probably the key parameter in system analysis. The ICN readings usually provide the first indication that a problem exists in a system. The ICN is determined by noise from all subsystems as shown below:

ICN = Radio equipment intrinsic noise + thermal noise +
equipment intermodulation + feeder echo distortion +
path intermodulation + multiplex noise

- a. The ICN recordings made by TEP show the noise on the system under normal traffic loading conditions. Normally, the ICN will be greater than the basic noise ratio (BNR) (converted to the same units as ICN) but less than the noise power ratio (NPR), which is taken at system design loading. However, it is possible for ICN to exceed the value measured for NPR if the radio noise is low and the multiplex noise is predominate. This is sometimes the case on line of sight (LOS) links. Another case where the ICN may exceed the NPR value is where the RSL is considerably lower during the ICN recording than during the NPR tests such as on tropo paths where radio thermal noise is usually greater than multiplex noise due to the lower receive signal levels (RSL). As a general rule, as long as the baseband loading is less than that for which the radio was designed, it can be assumed that the RSL and ICN should vary in direct relationship, if the multiplex does not provide significant noise. However, since the multiplex will have a certain relatively constant noise, this will limit improvements in ICN below a certain level. Above this multiplex noise limit the RSL and ICN will normally vary inversely. If the baseband is overloaded, the idle channel noise should be considerably higher than normal.
- b. It should be pointed out that although ICN is a valuable parameter in system analysis, it does not provide a great deal

of information as to the cause of a problem. The first step in fault isolation when ICN is high is to determine if the problem can be attributed to white noise problems or a fading RSL. Beyond this point, other noise data is needed for effective isolation of the problem. A check for white noise can be made with a speaker or headset. Noise spikes and tones can be identified easily and checked with a frequency selective voltmeter. White noise can arise in a channel from thermal sources or from intermodulation products of complex signals. If there are no noise spikes evident from the above checks, further tests will be required to isolate the white noise problem.

- c. An RSL problem can be identified by a check of the AGC voltage, provided suitable site records of AGC vs RSL exist on which to derive a "Normal" median. If an RSL problem does exist that cannot be attributed to a fading condition, the waveguide assembly, circulator, and/or antenna alignment would require further investigation.
- j. If, however, the problem cannot be traced to white noise or low RSLs; NPR/BNR tests, baseband level checks, quieting data, and deviation checks will be required to isolate the problem.

C-3

NPR/BNR DATA

- a. The NPR and BNR data provides a great deal of information about the transmitter and receiver noise composition. Link BNRs are generally a measure of transmitter and receiver intrinsic

noise and thermal noise with the latter usually being the predominate factor on tropo systems. Link NPRs include the same factors governing loopback NPRs plus path intermodulation noise due to multipath effects, however, the path contributions are almost negligible on line of site links.

- b. NPR/BNR measurements are extremely valuable as fault isolation tools. For instance, if a problem is indicated by a high ICN reading, loopback NPR/BNR tests can be performed to isolate the problem (if thermal or intermod) to a particular in station transmitter or receiver. The slot in which a low NPR or BNR reading is observed is also an excellent indicator as to the source of a problem. Considering that the BNR is acceptable and the low slot NPR is bad, the problem is usually a result of "Static Distortion." "Static Distortion" occurs while the signal is in the form of amplitude variations (i.e. before the modulation or after demodulation). Intermodulation products can be attributed to any of the following factors:

- (1) System deviation is improperly adjusted.
- (2) Microphonic tubes/components.
- (3) Defective coupling capacitors in limiter.
- (4) Gassy electron tubes.
- (5) Non-linearities in the transmitter or receiver circuits.
- (6) Excessive power supply ripple.
- (7) Non-linear discriminator response.

(8) Non-linearities in the transmit or receive baseband amplifiers.

c. If the bad NPRs are measured in the high slot, the intermodulation is usually due to "Dynamic Distortion." "Dynamic Distortion" occurs when the signal is carried as frequency modulation, as in RF amplifiers, waveguide, receiver IF, etc.

Some of the causes of high slot distortion are as follows:

- (1) RF interference.
- (2) Impedance mismatches.
- (3) Waveguide defects.
- (4) Antenna defects.
- (5) Non-linearities in the IF amplifiers.
- (6) Propagation time and phase characteristics of RF

filters.

VSWR tests would provide further information if bad high slot NPRs are noted.

d. If the RSL and white noise problems have been eliminated as causes of high ICN, loopback NPR/BNR tests should then be performed (if possible) and the results compared with equipment standards. The RSL should approximate the median operating RSL. If both the NPR and BNR results are poor, thermal noise masking is indicated and the noise figure of the receiver involved should be checked. If the noise figure meets specifications, transmitter deviation should then be checked.

- e. If the BNRs are satisfactory, while the NPRs are bad, an intermodulation problem is indicated. If possible, an IF loopback should be performed to isolate the problem to the IF or RF circuitry. If the IF loopback is satisfactory, a problem in the exciters, power amplifiers, RF amplifiers, or mixers is indicated. As discussed previously, the particular noise slots will provide a key to the location of the problem.
- f. If the loopback NPR/BNR tests prove to be good at both ends of the link, the problem must lie in the multiplex, waveguide/antenna system or the path (least likely to affect LOS). If this is the case, a link NPR/BNR test should be performed. If the link NPR is not acceptable, waveguide/antenna problems or path intermodulation is indicated and VSWR tests will be required. Once again the individual noise slots will provide the best information about the problem.
- g. The usual problem encountered during an evaluation is that of NPRs not meeting specifications in any slot. If this is the case, the most likely cause is a non-linear modulator (klystron). The usual action for correction of this problem is adjustment of the klystron tuning screw and possibly the discriminator linearity adjustment. One other step to assure NPR optimization is to assure that the deviation is properly set. If none of these procedures correct the problem, replacement of the klystron is indicated.

- h. An important consideration in NPR/BNR measurements is the median RSL during the measurement period. Since the receiver thermal noise (thus BNR) is a function of RSL, it is important that the RSL be recorded on the NPR/BNR data sheet. If this is done, the BNRs can be compared to the quieting data at the same RSL. The BNRs should compare within 1 dB or so (if link BNR is used) of the quieting data at an equivalent RSL. This provides an effective check on the data. To do this, BNR has to first be converted to S/N. The following formula is used for this conversion:

$$S/N = \text{BNR} + 10 \log \left(\frac{\text{Baseband Bandwidth}}{\text{Channel Bandwidth}} \right) - \text{Noise Loading Factor}$$

where:

Channel Bandwidth = 3.1 kHz

Baseband Bandwidth is determined by Channel Capacity

$$\left. \begin{aligned} \text{Noise Loading Factor} &= \begin{cases} \left[-1 + 4 \log N \right] & N < 240 \\ \left[-15 + 10 \log N \right] & N \geq 240 \end{cases} \\ &= -10 + 10 \log N \text{ for DCA} \\ &\quad \text{loading all channels} \end{aligned} \right\} \text{CCIR}$$

N = number of channels

In most cases the S/N calculated from the link BNR will be slightly lower than the S/N obtained from the quieting curves (at equivalent RSLs) due to the fact that transmitter and path thermal noise is included. However, the receiver thermal noise

is usually predominate for tropo systems and the difference should normally be one dB or less. In no case, will the S/N calculated from the BNR be greater than that obtained from the quieting curves unless a noisy generator was used to obtain the quieting data.

- i. The link NPR shows the noise performance of the radios and the path (on tropo) under capacity loading conditions. If the same RSL is used when measuring link NPR as was used when evaluating the link BNR and quieting data, the link NPR should reflect considerably more noise (per slot) than either the link BNR or quieting data. This is assuming no thermal noise problems exist. A difference of between 3 to 15 dB can be expected. If the difference is not within this range, a thermal or inter-modulation noise problem is usually indicated. In no case can the NPR be greater than the BNR.
- j. Since the end product of noise generated anywhere in a system is noise in a channel, it is desirable to convert NPR to per-channel noise. This is accomplished in the same manner as BNR is converted to S/N. In the equation NPR is substituted for BNR. The value obtained in this manner indicates the amount of noise which the subsystem evaluated will add to a channel when the system is fully loaded.
- k. In summary, the NPR/BNR data measured during an evaluation is an extremely important trouble shooting tool. By performing in

station RF and IF loopbacks and link tests, a problem can be isolated to a certain portion (transmitter, receiver, etc.) of the system. Furthermore, examination of the different slots provides more information as to location of the abnormality. When the BNR is examined in conjunction with the measured quieting data, an effective check of the test results can be accomplished. One point derived from this discussion is the importance of accurate median RSL recordings during the measurement period. The RSL recordings need to be clearly marked at the beginning and ending of the measurement period. The RSL and median baseband loading level recorded during this test period should be annotated on the NPR/BNR data sheets. This will provide the data analysts with a summary of all the information required so that reference to the strip charts will normally not be necessary.

C-4

NOISE POWER RATIO (NPR) TESTING

- a. Noise Power Ratio (NPR) testing is a special test technique employing White Noise loading of amplifiers, transmitters, and transmission systems to determine or verify equipment or system performance. The most common application of NPR testing normally encountered in the DCS and other communications systems is in the testing of broadband transmission facilities such as microwave, and tropospheric scatter links. The techniques may be applied to a complete baseband of a transmission system or to

groups or supergroup slots in testing of multiplex equipment performance. It is also possible to test overall system performance from audio breakout to audio breakout by use of special white noise generators designed to load individual channels of a frequency division multiplex (FDM) system. It should be noted that NPR testing is generally not applicable to testing of PCM transmission systems. The following discussions will be limited to application in testing of broadband microwave and tropospheric scatter systems from baseband to baseband since this is the most commonly encountered application.

- b. NPR testing developed out of a need to test equipment and transmission system performance under actual operating conditions. When a transmission system is designed, the design is based on providing a particular noise performance under maximum loading conditions. Obviously it becomes impractical or impossible to test the noise performance under normal operating conditions because the instantaneous loading is continually changing and there is no practical method of controlling the channel activity to insure all channels are in use and all levels are correct during the test period. This problem has been overcome by the use of what is termed white noise as a test signal to simulate a fully loaded system. White noise is noise that covers a selected bandwidth and has the same level at all frequencies across the frequency spectrum of interest. The noise is said

to have a flat or gaussian distribution. It has been found that white noise statistically has the same characteristics as a complex signal composed of a multiple number of either voice or data signals. Figure C-1 shows the difference between the peak and RMS values of power for a complex signal and a sine wave signal. The peak to average (P/A) value in dB for a sine wave is readily calculated as 3 dB ($20 \log 1.414$), calculating the P/A of a complex waveform is exceedingly difficult and becomes more of a statistical study. As may be seen from the figure, there are many peaks occurring at various amplitudes. The important point in determining the P/A of a complex signal is in defining what percentage of time a certain level is exceeded rather than the number of peaks, or what the maximum peak level is. In this respect it has been determined that for a P/A of 13 dB, that this level is not exceeded more than approximately .001% of the time for both white noise and complex signals composed of either multiple voice or data channels. This is further illustrated in Figure C-2. As may be seen, the P/A of voice signals varies from approximately 19 dB for one channel down to about 13 dB when the number of voice signals exceed approximately 60 channels. Data signals, however, start at 3 dB for a single tone (sine wave) increasing to about 13 dB at a loading of about 18 tones. White noise then can be used to simulate multichannel baseband signals for testing purposes.

CCP 702-1

- c. When white noise is used to simulate a baseband signal, the white noise signal should occupy the same frequency spectrum as the bandwidth of the baseband signal, and be at the design level for a fully loaded system. Figure C-3 shows a white noise signal and the formulas used to calculate the level required for testing. The Noise Loading Ratio (NLR) is the level in dBm0 or dB referenced to the 0 TLP or Single Channel Test Tone (SCTT) used in the system design. (NOTE: This SCTT corresponds to 0 dBm0 and is not the same as a test tone used to test channels etc., which is at a level of -10 dBm0). The first two formulas are based on the International Consulting Committee on Radio (CCIR) recommendations. The first formula for N-240 takes into account the more severe P/A for lower numbers of channels. The third formula represents the so called "Military Loading" and reflects higher average value of signal levels in channels of military communications systems. This can be misleading since many systems and equipment in use by the military were actually designed to CCIR standards. Two examples in Japan are the Japan Tropo System and 484N Kanto Plains Microwave System. The newer IJCS-PAC Microwave Systems in Taiwan and Okinawa, on the other hand, were designed for military loading. The important thing in using the white noise signal is that the bandwidth and level must be accurately specified for meaningful results.
- d. References to NPR in various technical publications give such

definitions or descriptions as:

(1) Signal to noise ratio (S/N) in dB in a particular channel or slot of the baseband of an amplifier, transmission equipment or transmission path for some specified white noise loading condition.

(2) NPR is an indication or measurement of intermodulation noise for some specified loading condition.

Both of the above properly describe NPR but fall far short of providing an easily understood explanation of what NPR is and how NPR test results may be used and interpreted. To obtain maximum benefit from NPR testing and analysis of the results, a good working knowledge of dB's and other logarithmic units, and the method of performing NPR tests is required. A description of NPR testing is contained in Supplement 1, DCAC 310-70-57, and is briefly discussed in the following paragraph.

- e. Figure C-4 shows a typical setup for white noise testing a transmission system or components of a system to determine its NPR performance capability. The transmission system could be a complete RF link or simply an in-house RF loopback of microwave transmitters and receivers. In any case, the point of interface would be at the baseband inputs and outputs. As shown in the diagram, the output of a white noise generator is connected to the system or device under test through the appropriate high pass and low pass filter combination to band limit the spectrum

of white noise to that of the normal baseband signals. The level of noise is then adjusted to the desired baseband level in accordance with the appropriate NLR formula. At the receive side, the white noise level in a selected slot is measured and becomes the reference level in determining the NPR. Next, a band reject filter is connected into the circuit at the same frequency as the slot measured and another measurement made. The noise measured now should be due to intermodulation noise and inherent basic or thermal noise only. (The band reject filter is deliberately designed to have a 3.1 kHz bandwidth and the receiver bandpass filter is 1 kHz wide to prevent white noise from "slopping" into the slot and causing erroneous reading). The NPR is now simply the difference in dB between the two readings. For example, if the two readings were -16 dBm0 and -71 dBm0, the NPR is the difference, or 55. It is normal practice to perform this measurement at three slots (preferably high, mid and low) in the baseband and at different levels of white noise loading, ranging from -10 dBm0 to +16 dBm0. The results are then drawn on a graph for further analysis.

- f. Another measurement that is used in analysis of the NPR is called the Basic Noise Ratio (BNR) or Basic Intrinsic Noise Ratio (BINR). Figure C-5 shows simply how BNR is measured. The slot is first measured under loaded conditions and the

white noise present becomes the reference. The white noise is then completely removed so that only basic noise (BN) is left (no intermodulation noise because there is no signal i.e. white noise to cause intermodulation) and the level is measured. The difference in levels in dB is then the BNR. For example, the white noise measures -16 dBm0 and the BNR measures -76 dBm0. The BNR is 60 dB, the difference between -76 and -16 dBm0. There are some NPR test sets that give measurements in terms of signal to noise ratio (S/N) in dB for a voice channel instead of NPR. One can be calculated from the other, however, confusion can result in performing measurements if the measurements are read in NPR when actually the reading represents an S/N.

- g. The question is sometimes raised as to what the effect of the bandwidth of the noise slot measured has on the test results. This involves what is termed Bandwidth Ratio (BWR) and is illustrated in Figure C-4. BWR in dB is simply 10 times the ratio of the 2 bandwidths involved. It is easily understood that if a slot that is Y cycles wide admits a certain amount of noise then a slot 2Y cycles wide will admit twice as much noise power, or 3 dB more power ($10 \log 2 = 3 \text{ dB}$). It is important then in determining S/N of channels to know what the bandwidth is but in performing NPR tests it is not important. Figure C-7

demonstrates this fact very simply. The figure assumes a 1 kHz slot for taking measurements. If the bandwidth is widened to 2 kHz, twice as much noise is measured and the levels are 3 dB higher than those measured with the 1 kHz slot. The NPR, however, remains the same because it is the difference between the two levels. The S/N of a channel, however, is another matter because the reference is the 0 TLP, SCTT or 0 dBm0 point and the S/N's are therefore 76 and 73 dB respectively - a 3 dB difference due to the difference in the bandwidth of the noise slot measured.

Figure C-8 shows actual NPR test results obtained on an active microwave system, and Figure C-9 shows the curves plotted from the NPR results. Figure C-10 lists some of the information that can be determined from an analysis of NPR data and curves. These are also listed below:

- (1) Expected channel (or slot) S/N for various loading conditions.
- (2) Optimum loading point.
- (3) Amount of basic noise versus intermodulation noise.
- (4) System and/or microwave equipment performance.
- (5) Identification of possible microwave equipment malfunction or maladjustment.

h. The above are discussed in the paragraphs below, with examples

where applicable.

- (1) The expected S/N in a channel or slot can be readily calculated from the NPR measured by the formula:

$$S/N = NPR + BWR - NLR$$

Where S/N is the S/N for a certain bandwidth which is used to calculate the BWR based on the slot or channel bandwidth and the white noise bandwidth, the S/N is flat weighted and conversion factors must be used to determine the expected S/N for weighting such as "C" message etc. Since white noise simulates actual signal conditions in the baseband, actual S/N under operating conditions can be determined by considering the actual baseband level (BBL) to be the same as the white noise level used for the NPR test. Figure C-11 shows how the above formula is derived. The point of reference is the SCTT or TLP. NLR is calculated in reference to the SCTT which produces a white noise level equal to BWR dB below the NLR. The difference of the basic noise (BN) and intermodulation (IM) noise from the white noise in the slot then equates to the slot NPR in dB. The S/N is the level of the BN and IM noise below the SCTT. The diagram shows that the difference between the SCTT and the white noise in the slot is BWR - NLR. The S/N then is NPR + difference between SCTT and white noise in the slot, or

$$S/N = NPR + BWR - NLR.$$

Figure C-12 gives a summary of the expected S/N for 3.2 kHz

channels in the baseband of the actual system during operation. It should be noted that the best S/N's occur at the lower levels of BBL and get increasingly worse as the BBL increases due to the increase in intermodulation distortion. The apparent improvement in S/N at -5 dBm0 as opposed to -10 dBm0 loading for the 2438 kHz slot is probably attributed to instrumentation or operator error in making the readings. It should be realized that these S/N values apply only to the baseband signal and not to the receive channel output because the multiplex will add noise to the multiplexed channel. If it is assumed (or known) that the multiplex contributes little noise, the value obtained can be used as a fair representation of the expected channel output noise at the frequencies tested.

- (2) The optimum loading point for a transmission system can also be determined from examination of the NPR test data and knowing the range of the baseband levels encountered during normal operation. Levels and adjustment of amplifier gains, frequency deviation, etc., are generally specified in the technical manual, but in many cases military systems are found to deviate from these specifications. Commercial systems, however, are often "optimized" to provide for the best S/N ratio. Figure C-13 is used to illustrate how the system could be optimized by utilizing the NPR test results. Assume that the normal BBL is at the -10 NLR level (+7.8 dBm0). The expected S/N at this

level is 69.2 dB. If the BBL entering the system is increased by 10 dB it will have the same effect as increasing the BBL to the 0 NLR point where the expected S/N is 65.8 dB. By increasing the BBL or deviation we have effectively increased the SCTT by 10 dB, therefore, the expected S/N is now 75.8 dB, or an increase in S/N of 6.6 dB. Note, however, that if the normal level was at 0 NLR, and deviation was increased by 10 dB we would degrade our S/N by 21.8 dB (65.8 - 44). By the same token, if the normal level of BBL was at the + 10 NLR point and deviation or BBL were reduced by 10 dB, we could realize a 21.8 dB increase in S/N. However, if the level was normally at the 0 NLR we would degrade the S/N by 6.6 dB. The optimum point occurs at the point of maximum NPR. Naturally the output of the receiver requires adjustment if the transmit deviation or BBL is changed to provide the proper levels to the receive multiplex equipment. As a matter of note, the optimum point for loading (best NPR) may not necessarily occur at the 0 NLR point.

- (3) The amount of basic noise and intermodulation noise can be readily calculated from the BNR and NPR data. Section III provides details on how to calculate the values. Basically the BNR and NPR values are used to calculate the levels in pW0 representing the BN and BN + IM levels. The level of IM is simply the difference between the two. Figure C-14 shows a tabulation for the 70 kHz slot data. It is interesting to note

CCP 702-1

that as the NLR increases, the intermodulation noise increases at a non-linear rate, the rate of increase being greater as the NLR increases.

Probably the most important item that a microwave repairman is interested in, is: Does the equipment or system meet some NPR (and sometimes BNR) specification in the technical manual? If this is all that is desired, normally it can be satisfied by performing the NPR test at the 0 NLR point only. If NPR only is desired, it is not necessary to check the BNR, but it should be clear that if the BNR is lower than the required NPR, it is impossible to ever get the desired NPR. Whether to perform NPR checks at other than the 0 NLR point depends upon what type information is desired from the analysis or in the case of the military, what the official guidance is. In any case, performing NPR checks at loadings from 0 dBm0 to +16 dBm0 can serve as a useful purpose to evaluate the overall system performance.

- (4) One important factor that is not readily apparent in the testing of microwave and tropo systems is the Received Signal Level (RSL) that is used during the test. This is very important since, for all practical purposes, it determines the basic noise, which in turn places a limit on the maximum NPR that can be obtained. Figure C-15 shows a typical quieting curve for a microwave receiver (a tropo receiver is similar, but normally the useable portion of the curve extends to lower RSL's). In

testing of equipment, it is normal practice to adjust signal levels so that operation occurs on the section of the curve that is controlled by the thermal noise of the receiver, i.e., that portion in Figure C-15 from -40 to -30 dBm. As a rule of thumb, this will normally be about 45 dB above the FM Improvement Threshold, which in this case occurs at about -35 dBm of RSL. In testing system performance on a link basis, the normal signal level is used, or if the equipment is tested on a local loopback, the normal RSL is simulated in adjustment of the equipment used to feed the transmitter output back into the receiver. Referring again to Figure C-15, assume NPR tests are run at RSL's of -35 and -65 dBm and that the IM component is 150 pW0 in each case and the white noise level is -11.2 dBm0, in the same 3.2 kHz slot. The BN at -35 dBm of RSL is about -85 dBm0 which corresponds to 5 dBm0 or 3 pW0. At -65 dBm the BN is approximately -60 dBm0 which corresponds to 30 dBm0 or 1000 pW0. The total noise at -35 dBm and -60 dBm is then 153 pW0 and 1153 pW0 respectively, or roughly -68 dBm0 and -59.4 dBm0. The NPR's then will be 56.8 dB and 48.2 dB for the -35 and -60 dBm RSL's, a difference of 8.6 dB. The importance of using the correct RSL can readily be seen from the above example.

- (5) The shape of the "classical" NPR curve is that of a boomerang hanging from its elbow; the two sides rising at 45 degree angles (equal dB scale for NLR and NPR) and flattening out at

CCP 702-1

some peak value near the design loading level. This type of curve is not always encountered in practice and may not be typical for some equipment. The actual shape of the NPR curve depends upon the distributions of the BN compared to the IM noise at various NLR levels as shown in Figures C-16 through C-20. The NPR curves on the left sides of the figures are calculated from the assumed noise distributions that are plotted on the right hand side of the figures. All of the calculations have been based on an assumed white noise signal of 60 to 2540 kHz at +17.8 dBm0 (600 channel military loading). Noise is measured in a 1 kHz slot, therefore, the BNR is 34 dB. The BNR is 65 dB except for Figure C-19 where it is also figured at 45 and 55 dB. White noise at 0 NLR is -16 dBm0 per 3.2 kHz slot. Figure C-16 shows an NPR slot using the BN only. As may be seen, the curve is a straight line, the slope of which is 45 degrees. Figure C-17 is a family of curves showing the expected NPR's for the noise distributions shown. In these cases, the curves will never peak or begin to drop down again, but will flatten out at some value and remain at a constant value of NPR. This will occur when the IM noise is approximately 20 dB greater than the BN. At this difference in level, the sum of BN plus IM is equal to IM for all practical purposes and since it increases at the same rate as the white noise loading (NLR), the curve is flat. Figure C-18 shows a family of curves of the NPR slots for the

noise distributions shown. In this case the IM noise at the 0 NLR point is the same as in Figure C-17, but the rate change is 2 dB per dB change of NLR versus 1 dB as in Figure C-17. The curves will in this case reach some maximum value and then begin to decrease. The peak NPR will occur when the IM and BN noise are equal, and the slope of the left and right sides of the curves will be roughly 45 degrees. Curve 1 of Figure C-18 is the "classical" NPR curve and only occurs when the IM and BN noise are equal at the 0 NLR and the IM increases at a 2 dB rate for each dB of increase in NLR. Figure C-19 shows a family of NPR curves where the BN and IM noise are equal at the 0 NLR but at -71, -81 and -91 dBm. Note that the curves all have the same shape and the peak occurs at the 0 NLR but at different values of NPR. Figure C-20 is interesting and shows a type of curve that is often encountered with certain tropospheric scatter equipment. The noise distributions assume the noise rising linearly at a 2 dB rate and then "breaking" at the 0 NLR point and increasing at a 5 dB rate after that. The curves in all cases show that the slope of the NPR curve is steeper on the right sides due to the 5 dB rate of change of the IM noise. If the IM noise changed at a greater rate (say 10 dB), the curves would be steeper yet. The point of maximum NPR does not occur at the same NLR point. The actual shape of the NPR curve obtained in testing is due to the distribution of the noise

components and rate change of the IM at different levels of white noise loading. As such in a normally operating system it is a function of the equipment design.

- (6) NPR testing is a valuable tool in determining or verifying performance of systems or equipment because it is a very simple test to perform and the results would generally reflect any malfunction or improper operation in the system or equipment. On the other hand, since almost any problem can affect NPR test results (make them poor) it is sometimes difficult to determine where the problem is. Guidelines can be given for analysis of NPR test results, however, only though experience will the technician be cognizant of the types of problems that are normally encountered on operational systems. These problems generally follow a pattern, and analysis and repair is not exceptionally difficult. As has previously been mentioned, it is impossible to meet NPR requirements if the BNR does not exceed the required NPR. Depending on the distribution of the IM noise, the BNR should normally be at least 3 dB greater at the design loading level than the required NPR, although this is not necessary for all conditions. Where BNR requirements are specified, they will normally be 4 or 6 dB greater than the NPR specified. When BNR requirements are met and NPR requirements are not, the causes can be grouped under two general classifications, i.e., static and dynamic distortion problems.

Dynamic distortion problems generally cause problems in the higher frequencies of the baseband, whereas static distortion affects the lower frequencies. Some examples of problem areas that can cause dynamic and static type distortion are listed below:

a. Dynamic Distortion

- (1) RF interference.
- (2) Impedance mismatches (particularly in the antenna and waveguide system resulting in poor VSWR).
- (3) Defects in waveguides (dents, water, corrosion, misaligned connecting flanges)
- (4) Antenna defects
- (5) Propagation time and phase characteristics of RF filters.
- (6) Multipath reflections causing severe time displacement between main signal and reflected signal.

b. Static Distortion

- (1) System deviation adjustments.
- (2) Improper or missing terminations.
- (3) Microphonic noise.
- (4) Defective coupling capacitors in limiters.
- (5) Gassy electron tubes (in older equipment).
- (6) Linearity adjustments in transmitters and receivers.
- (7) Defective power supplies.

(7) Dynamic and static distortion does not only affect high and low frequencies in the baseband, they also affect all frequencies, however, their affects are more pronounced at the high and low ends respectively. The choice of what corrective actions to take, as mentioned previously, depends upon whether the problems seem to be primarily static or dynamic and from past experience with the particular equipment being tested a determination as to the appropriate course of action can be selected. When NPR results show unsatisfactory for an unfamiliar radio system, probably the best starting point in finding the problem is to insure that the equipment is properly aligned and then repeating the NPR tests. System alignment includes such tests and adjustments as transmitter deviation, klystron sensitivity (where applicable) klystron and discriminator linearity and phase delay characteristics of the IF amplifiers, noise figure and receiver sensitivity tests, etc. In cases where such tests are beyond the scope of local on-site maintenance, corrective actions may be limited to random substitution of basic modules and minor adjustments. In event poor NPR's are not correctable on site, extensive testing may be required by specialized teams, with sophisticated test equipment.

The following are possible pitfalls that could give bad or false results during NPR testing.

a. Improper grounding of test equipment - insure that all test equipment is properly grounded to a common ground and

isolated from any "hot" AC grounds.

b. Excessively long test leads (coaxial cable) causing stray noise pick up.

c. Connected meters (e.g. wideband dB meter used to check NLR) introducing noise when left connected during test.

d. Not using the maximum possible output level of the NPR test set with maximum padding to get the desired NLR. This will improve the S/N (signal here means the white noise) of the output signal.

e. RFI from signal generators, local transmitters or other outside sources.

f. Using the improper (low) RSL - this will affect the BNR.

g. Insure that when measuring NPR, the test set indicates NPR and not S/N. Some test sets indicate S/N instead of NPR and therefore, the reading must be converted to obtain NPR.

$$S/N = NPR + BWR - NLR$$

$$\text{or } NPR = S/N + NLR - BWR$$

h. Improper level or bandwidth of white noise - how many channels? What are baseband limits? CCIR or military loading?

i. Reduction of white noise when "slotting" the white noise signal for low capacity systems. If "slotting" causes a drop in level, the output must be readjusted to the desired level.

j. Lack of knowledge of the proper testing technique.

As can be seen from the preceeding paragraphs, constructive

CCP 702-1

information may be derived from NPR testing and analysis. The results, however, may sometimes be misinterpreted and wrong or misleading conclusions are reached. Take as an example, a transmission system consisting of a single microwave link with multiplex terminals on both ends. Assume that the link NPR results are satisfactory. Does it then follow that the system performance from multiplex (MUX) input to MUX output is also satisfactory? Absolutely not; the MUX was not included in this test and therefore, it could be completely inoperative or have extreme intermodulation problems. Paragraph C-4h.(1) discusses the calculation of S/N from NPR test results, but also notes that this only applies to the equipment tested or that portion of the system tested. Care should be exercised in estimating S/N performance based on NPR tests. Consider another case where the RF transmitters and receivers are locally tested in an RF loopback configuration. Are the NPR test results applicable on a link basis? Not necessarily; there could be serious problems in the waveguide or antenna system that may cause serious intermodulation problems at the higher end of the baseband spectrum. Even though these two examples point out that NPR tests do not give a complete picture of system noise performance, they can be used to provide a good estimate of what can be expected. If system noise performance (i.e. ICN) does not correlate closely to NPR results, RSL and BPL, other problems are indicated and

further investigation may be necessary.

C-5

BASEBAND FREQUENCY RESPONSE

- a. Link baseband frequency response tests are used to determine the frequency response characteristics from the transmitter modulator input to the receiver demodulator output. Response data can be compared to the manufacturer's specifications to determine if any abnormalities exist for this portion tested. Since circuitry from the transmit to the receive baseband amplifier is included, other tests may be required to detect the faulty unit, if abnormalities exist. The NPR/BNR slot data will provide some help in isolating the fault as discussed in Paragraph C-4. One of the most common problems is improper voltage output from the discriminator which can be verified from a plot of the discriminator characteristics.
- b. Baseband frequency response is also useful in pin pointing problems with the pre-emphasis or de-emphasis network. For instance, suppose the pre-emphasis in the transmitter circuits is functioning, but the receiver de-emphasis is not. If this is the case, the baseband frequency response would have a sharp upward slope as frequency increases. A sharp downward slope would result if the de-emphasis is functioning but the pre-emphasis is not. In most cases the pre-emphasis and de-emphasis networks are not adjustable and require either component or complete circuit replacement to correct any problems.

FREQUENCY DEVIATION

The amount of frequency deviation of the RF carrier determines the amount of amplitude detected by the discriminator at the distant receiver. If deviation is set too high, the receive baseband levels will be hot (above specifications); if deviation is set low, receive baseband levels will be cold. The amount of deviation is determined by equipment design, bandwidth requirements, and channel loading which are geared to provide the best possible signal to noise ratio. The most common procedure used by TED, is the first carrier dropout method. This method is discussed in Appendix B, B-4. If the carrier has not completely dropped out when the proper frequency and level is inserted into the modulator, the modulator sensitivity may have to be adjusted if determined necessary. The power remaining in the carrier could present distortion and non-linearity within the modulator. In the event the carrier cannot be made to dropout, the klystron (in LOS systems) will most likely need replacement; however, if there are amplifiers, multipliers or power output stages, any of these may be defective which would affect the dropout. On the AN/FRC-109, the baseband transmit amplifier unit has been found to cause a number of problems with deviation. Additionally, faulty tubes, transistors, or circuit components may produce noise that causes a distorted output with modulation appearing

at points other than those desired. If a deviation problem is noted, each stage should to be examined individually to isolate and correct the problem.

C-7

RECEIVER NOISE FIGURE

- a. The thermal noise contribution of a device can be expressed in terms of a noise figure. Noise figure is defined as the amount of noise added by a device as compared to an ideal device. The noise figure depends on the temperature and bandwidth of the device being tested (temperature is usually assumed to be 290° k) and in wideband system, the noise figure of the receiver is the limiting factor in noise performance. The noise figure of multi-stage amplifiers is usually determined by the first stage. Thus, if a receiver has an RF amplifier, it is this device which primarily governs the receiver noise figure. If there is no RF amplifier, the mixer stage usually determines the noise figure and on LOS systems such as the AN/FRC-109, a high noise figure would most probably be an indication of mixer problems (or possibly, but usually not likely an IF problem). The measured noise figure must be compared to the manufacturer's specified noise figure for the equipment in order to determine if a problem exists. A deviation of 1.0 dB should be allowed for measurement error and system degradation.
- b. When considering a troposcatter system, the noise figure is usually given as an overall noise figure for the receiver. This

is a measure of the noise figure from the input terminals of the receiver through the last stage that would contribute to the noise reading (the IF stage in most cases). The overall noise figure is equated to:

$$F = F_1 + \frac{F_2 - 1}{G_1} + \frac{F_3 - 1}{G_1 G_2} + \dots + \frac{F_n - 1}{G_1 G_2 \dots G_{n-1}}$$

where:

F = the equivalent noise figure

F₁ = the noise figure of the first stage

F₂ = the noise figure of the second stage

G₁ = Gain of the first stage

G₂ = Gain of the second stage

F_n = the noise figure of the Nth stage

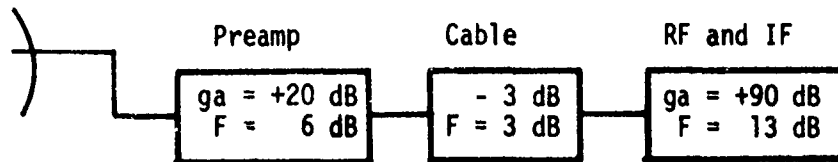
G_n = the gain of the Nth stage

Before using the above equation noise figures and gains expressed in dB have to be converted to power gains as follows:

$$F = \text{Antilog} \frac{F_{dB}}{10}$$

$$G = \text{Antilog} \frac{G_{dB}}{10}$$

As an example, assume a receiver with the following characteristics:



$$G_{\text{preamp}} = \text{Antilog} \frac{20}{10} = 100$$

$$F_{\text{preamp}} = \text{Antilog} \frac{6}{10} = 4$$

$$F_{\text{cable}} = \text{Antilog} \frac{3}{10} = 2$$

$$G_{\text{cable}} = \text{Antilog} \frac{-3}{10} = .5$$

$$G_{\text{rf and IF}} = \text{Antilog} \frac{90}{10} = 1 \times 10^9$$

$$F_{\text{rf and IF}} = 20$$

therefore:

$$\begin{aligned} F &= F_1 + \frac{F_2 - 1}{G_1} + \frac{F_3 - 1}{G_1 G_2} \\ &= 4 + \frac{2 - 1}{100} + \frac{20 - 1}{100 \times .5} = 4.39 \end{aligned}$$

$$F_{\text{dB}} = 10 \log F$$

$$F_{\text{dB}} = 10 \log 4.39$$

$$F_{\text{dB}} = 6.42 \text{ dB}$$

Therefore, the overall noise figure for the example is 6.42 dB. This verifies that the major contributor to the noise figure is the first stage of the subsystem. In this case, the RF amp.

- c. In some cases it is not possible to measure the receiver noise figure and this can be attributed to the waveguide configuration which does not allow room for the noise source to be connected; or there may be a severe impedance mismatch between the test

CCP 702-1

equipment and receiver (as is the case with the AN/FRC-84). In the latter case an extremely high noise figure is usually indicative of an impedance problem.

d. In the event the noise figure cannot be measured, it may be approximated from the quieting and IF data. Using the quieting data the noise figure may be calculated in the following manner:

(1) Select an RSL on the linear portion of the quieting curve and note the corresponding S/N. (It is advisable to use the high slot data)

(2) Assuming that the pre-emphasis is functioning properly, use the value of pre-emphasis boost that is specified by the manufacturer or that was calculated.

(3) The noise figure can now be approximated by the following formula:

$$NF = 174 + RSL + 20 \log \frac{D_p + I_p}{f_m} - 10 \log 2b - S/N$$

where:

NF = noise figure (dB)

S/N = signal-to-thermal noise ratio (dB)

RSL = receive signal level (dBm)

D_p = per channel peak deviation at zero pre-emphasis (kHz)

f_m = slot frequency (kHz)

I_p = pre-emphasis boost for the slot involved

e. Another useful method that can be used in case some of the above

data (such as I_p) is not available is the threshold method. The noise figure can be approximated by using the following formula:

$$NF = T_{FM} + 164 - 10 \log B_w$$

where:

NF = noise figure (dB)

T_{FM} = measured FM threshold (dBm)

B_w = measured IF bandwidth (Hz)

- f. Either of the two methods above will provide an approximate noise figure. The value obtained in this manner can then be compared to the manufacturer's noise figure specification for the equipment to determine if a problem does exist. If a high noise figure is found, the circuitry involved must be considered. The manufacturer's specification is usually for the first receiver stage. As already discussed, some systems have RF amplifiers while others do not. As an example, the noise figure is measured from the input of the receiver through the IF stages on the AN/FRC-109 and if a bad reading is encountered, either the mixer or the IF is causing the problem. On tropo systems utilizing an RF amplifier, this would also have to be included as a probable cause for a bad noise figure reading.
- g. In summary, the noise figure is a figure of merit of a receiver performance. The manufacturer's specification refers to the noise contribution of the first stage, however, if the receiver

noise figure is bad, all stages involved in the measurement should be considered as a possible cause. If noise figure measurements cannot be accomplished, an approximation of the receiver noise figure can be arrived at through the relationship between noise figure, threshold, and IF bandwidth.

C-8

QUIETING CURVES

- a. The receiver quieting curves provide a great deal of information about receiver performance. The 20 dB quieting point generally provides information on the receiver sensitivity. The receiver FM threshold which can be directly extrapolated from the curves, provides a cursory examination of the noise figure and IF bandwidth performance. The most important aspect, however, is the thermal noise contribution of the receiver which can be determined from the quieting curves.
- b. FM threshold is one of the more important parameters obtained from the quieting curves. This is accomplished by drawing a tangent to the high noise slot curve as shown in Figure C-21. The point where the tangent deviates from the curve by 1 dB is the FM threshold point. A second method is to find the RSL corresponding to the 20 dB quieting point, and increasing this value by 4 dB. This value is to be compared to the specified or calculated value of the receiver FM threshold. Any deviation of more than 1 dB should be investigated. Since the calculated or specified value of FM threshold is based on ideal IF

bandwidth and noise figure, an expected value should be calculated and compared to the measured value. This is accomplished by using the formula shown below and replacing the ideal values with the actual measured values.

$$\text{Expected FM Threshold} = -164 + 10 \log B_W + NF$$

where:

B_W = measured IF bandwidth (Hz)

NF = measured noise figure

The value obtained in this manner will provide a general idea of what to expect if the IF bandwidth or noise figure is other than that specified for the system.

- c. If FM threshold is found to be greater than the calculated value, indications are that a higher noise figure, a larger IF bandwidth or a combination of both exists. A decrease in threshold level from the norm would reflect reverse conditions. In most cases it has been found that variations in the IF bandwidth account for major changes noted in the threshold point. The change in IF bandwidth referred to is the logarithmic change, i.e.,

$$\text{Change in Threshold (dB)} = 10 \log \frac{\text{Measured IF Bandwidth}}{\text{Predicted IF Bandwidth}}$$

As an example, assume a receiver has a predicted NF value of 9 dB and the value measured is 10 dB. In this case the threshold must be adjusted upward by 1 dB. Further, assume a

predicted IF bandwidth of 20 MHz and a measured value of 18 MHz. The predicted threshold will also have to be adjusted by the following factor:

$$\begin{aligned} \text{Change in threshold (dB)} &= 10 \log \frac{\text{Measured IF Bandwidth}}{\text{Predicted IF Bandwidth}} \\ &= 10 \log \frac{(18 \times 10^6)}{(20 \times 10^6)} \\ &= -0.46 \text{ dB} \end{aligned}$$

Due to the change in IF bandwidth, the threshold will have to be adjusted downward by 0.46 dB. If the predicted threshold (based on the ideal values) is -81 dBm, then the expected value (based on measured values) would be

$$\begin{aligned} \text{Expected RSL at Threshold} &= -81 + 1 - 0.46 \\ &= -80.46 \text{ dBm} \end{aligned}$$

- d. It should be noted that system loading, deviation, and proper operation of the pre-emphasis and de-emphasis circuits only affect the value of S/N above threshold and not the RSL at threshold. Therefore, only IF bandwidth, noise figure, and possible errors introduced by the signal generator used to perform the measurements need be considered as problem areas if the threshold does not occur at the required RSL.
- e. A second parameter derived from the quieting curves is the 20 dB quieting point. The 20 dB quieting is a measure of FM receiver sensitivity. This is one of the best ways of checking receiver sensitivity because it is easily obtained from the quieting

curves and directly reflects receiver performance from input to output terminals.

- f. Sensitivity of a receiver as measured by the 20 dB method is determined mainly by three parameters: (1) noise figure, (2) IF bandwidth, and (3) effectiveness of limiters. The effectiveness of the limiters can be considered to have been optimized in equipment design and to be uniform from one receiver to another of the same type. Therefore, it can be eliminated in considering the 20 dB quieting point. Figure C-22 shows the empirical relationship between 20 dB quieting, noise figure and receiver noise bandwidth. It is based primarily on experimental data obtained on REL receivers. Because of the many factors influencing the value of the 20 dB quieting, the curves of Figure C-22 should not be regarded as an absolute or mathematical relationship. The approximate accuracy is believed to be ± 2 dB when applied to high quality receivers, however, identical receivers should measure relative to each other ± 1 dB. The curves can be used to provide the technicians and engineers with an approximation of where the 20 dB quieting point should occur during normal quieting measurements. If the measured 20 dB quieting point deviates by 4 dB or more from the approximation, an investigation should be made to determine the reason for departure from the norm.
- g. The 20 dB quieting point is obtained from the quieting curves

by finding the point on the curve where the S/N has increased by 20 dB from the noise saturated portion of the curve. The RSL at this point is the value that should be recorded for the 20 dB quieting point. The high slot should be used for determining the RSL at 20 dB quieting. The value obtained in this manner should be compared to the approximated value from the curves of Figure C-22 to determine if possible IF, noise figure, or limiter problems exist. If a problem does exist, each individual source will have to be investigated.

- h. The third parameter obtained from the quieting curves is the thermal noise contribution of the receivers at the median operating RSL. The thermal noise in a particular noise slot can be obtained by finding the median RSL recorded during the link NPR tests on the quieting curves. The noise corresponding to this RSL is the receiver thermal and intrinsic noise contribution for that particular noise slot. The particular slot noise should compare closely with the link BNR for this given slot (after the BNR has been converted to dBm0). The link BNR should show slightly more noise (per slot) than the quieting data since it includes small amounts of transmitter and multipath noise. However, the receiver noise will usually be predominate and the additional items may only add a couple tenths of a dB if everything is functioning correctly. In no case will the BNR noise be less than the noise quieting data unless a noisy signal

generator was used to perform the quieting curves (one dB of tolerance should be allowed for measurement accuracy). If the BNR noise exceeds 2 dB, a check should be made on the accuracy of the median RSL recorded during the NPR/BNR tests. If the RSL is correct, it is most likely that the difference is due to excessive noise generated by the transmitter (especially on links). Probably the greatest value of the quieting curves is a confirmation of a thermal noise problem indicated by poor BNR readings. If this situation occurs and the quieting curves show that no excessive thermal noise is present, the receiver circuitry may be eliminated as the cause of the problem.

c. 9

IF FREQUENCY RESPONSE

- a. Since the IF bandwidth is usually the determining factor of receiver noise bandwidth, it is important that the measurement be as accurate as possible. The FM threshold of a receiver is controlled by the IF bandwidth (the smaller the IF bandwidth the lower the FM threshold). If the threshold measured from the quieting curves does not meet the equipment specification, the IF data should be examined to determine if it is the major cause of problem. Moreover, if the IF bandwidth is too narrow, intermodulation noise will tend to increase due to sideband distortion.

Some items that should be closely examined in the IF data are as follows:

(1) The 3 dB IF bandwidth should be as close as possible to that specified by the Equipment Technical Manual.

(2) The 3 dB points should be equispaced from the IF center frequency.

(3) No spurious oscillations should be noted.

(4) Response ripple should be at a minimum.

If the above statements prove to be true for the data, the IF strip should not be a cause of any problems.

b. When performing measurements, several factors must be observed to assure that the data is accurate. These are:

(1) Close checks should be made for impedance mismatch to prevent distortion.

(2) Insure that test points are properly terminated when performing the test.

(3) Use the minimum sweep necessary for an adequate display. This should prevent spurious inputs to the IF and provide a convenient display on the oscilloscope.

(4) Assure that the AGC voltage is not varying.

C-10

DISCRIMINATOR DATA

Probably the most important information obtained from the discriminator data is the range of linearity. If the curves are not linear between the IF 3 dB points, distortion could result and an increase in intermodulation noise may be noticed. No single component in the receiver affects baseband response

and intermodulation more than the discriminator. The most important factors that should be observed from the discriminator curves are as follows:

a. The discriminator curve should be linear at least over the range of the IF 3 dB bandwidth. (Figure C-23 and C-24).

b. The zero voltage crossover point for the discriminator curve should be at the IF center frequency. The exact effects if not centered will depend on equipment design and when this condition exists, the equipment manual should be consulted. If the above factors are verified by the data, intermodulation distortion and baseband frequency response will be normal (unless other problems exist).

C-11

DC CONTROL VOLTAGE

DC control voltage is a very important measurement on tropo systems utilizing maximal ratio combining. This voltage, derived from individual receiver noise characteristics, assures that proper combining action is taking place. A curve similar to the one shown in Figure C-25 should be expected although the voltage levels will vary for different types of equipment.

Two important factors should be observed from the curves:

a. The DC control voltage at a particular RSL should be nearly the same for all receivers (of the same type). This assures proper combiner balance.

b. The RSL at which the curve levels (control voltage

becomes constant as RSL increases) should be approximately the same for all receivers and should occur at a relatively high (more positive) RSL. The maximal ratio combiner begins to function as an equal gain combiner when the DC control voltage becomes constant. It is for this reason that the DC control voltage will vary to as high an RSL as possible. For most receivers the DC voltage becomes constant between an RSL of -45 dBm and -60 dBm.

If the above two conditions are met, proper combining should take place providing there are no problems within the combiner circuitry.

G-12

ANALYSIS OF AUDIO TEST RESULTS

If the radio subsystem has been cleared as a source of problems, the audio series tests should provide further information as to an appropriate solution. In most cases the effects of out of specification data is evident. However, each of the tests will be discussed briefly with emphasis placed on a few of the tests whose results may require clarification and/or interpretation. Comments for each test should be provided on the cover sheet (G-1), where applicable, and should include comparison results of the test data to the manufacturer's and/or MIL-STD specifications.

Frequency response, delay distortion, and impulse noise tests must be performed on identical channels at both ends of

the link, in order to obtain a more meaningful correlation of these parameters within the system.

C-13

1 KHZ TEST TONE LEVEL

- a. This test is used to measure and evaluate the voice frequency channel signal level characteristics through the radio, multiplex and in-station equipment. If the measurements are not within the specified equipment tolerance, corrective action should be taken during the preliminary evaluation. To insure the final data is accurate. Test tone levels that exceed the prescribed level throughout the system may result in overloading of the baseband such that additional intermodulation products are created. In some cases the hot levels will also cause adjacent channel crosstalk and degradation of the subscriber service.
- b. In some equipment, provisions have not been incorporated for adjusting the group and supergroup levels. In this case, only the channel and baseband levels can be adjusted to the proper level. If these adjustments do not correct the level disparity at the group and supergroup test points, trouble shooting of the individual circuits may be necessary to isolate the problem. In most cases, this particular situation would be indicative that changes in component values have occurred.

C-14

IDLE CHANNEL NOISE

- a. This test measures and evaluates the degree of interference and

noise introduced into a VF channel. This parameter and its affect on system performance as related to the radio equipment and path have been discussed previously. Additional noise contributions and isolation procedures are discussed below.

- b. Some major contributors to a high noise level in the channels are; in-station wiring, carrier leak, improper or ineffective grounding systems and unbalanced power distribution systems. In the event the measured ICN departs from the predicted value by more than 2 or 3 dB, it will be necessary to investigate any or all of the contributing factors to isolate and correct the problem.
- c. The first stage in isolation is to measure the ICN at the multiplex to eliminate any noise being induced by station equipment. Once this has been accomplished, the noise should be measured from the multiplex line jacks to the primary patch panel. This will provide an indication of the noise level being introduced by in-house wiring. Additional measurements can be performed from the primary patch panel toward the subscriber if the outside cable plant is suspected of introducing excessive noise into the radio system.
- d. When a difference of 2 dB or more exists between ICN measurements obtained using flat as opposed to C-message weighting, alternating currents (AC) or interference is generally indicated. The AC usually results from improper grounding or induction while the interference can most probably be attributed to

carrier leak, extraneous signals such as broadcast stations, mixing of signals which results in unwanted components falling into the VF spectrum. The first step in isolating these interfering components is by sweeping the VF channel bandwidth with a wave analyzer. In some cases audio detection will be useful in determining the type of signal being introduced into the systems.

- c. The data recorded during test T-4 should also be compared to the ICN's recorded under test T-1. This comparison will provide a correlation of the median ICN to the predicted value and an average of all channel measurements should approximate the recorded median.

C-15

CHANNEL IMPULSE NOISE

- a. The purpose of the channel impulse noise test is to measure and evaluate the degree of interference being introduced into a VF channel by random impulse noise hits. Impulse noise can be introduced into a VF channel at any point in a system. It can be generated in the equipment itself, induced from power lines or generated in the environment and radiated into the station. Excessive impulse noise can have a detrimental effect on teletype and data circuits. If excessive impulse noise is measured during the evaluation, isolation procedures should be initiated. On tandem hop links, the circuit exhibiting the impulse noise should be terminated at the transmit end and

impulse noise tests performed on successive links until the problem has been isolated to a particular link. Once the problem link has been identified, the transmit end on that link should be terminated and impulse noise measurements performed at the receive end of the link on that particular channel. Once this has been accomplished, measurements should be performed at the group, supergroup, or baseband of the equipment in an effort to isolate the problem to the multiplex or radio path.

- b. The above isolation procedures are helpful only in isolating the source of the impulse noise and verifying whether the radio, multiplex and path are the cause of the problem. Once these have been eliminated as a potential source, it may be necessary to perform additional in-house tests to determine the specific cause of the impulse noise. The isolation process must consider all those factors listed in Paragraph C-14 above to include verification that the instrumentation is not being affected by the test connections.
- c. After the in-station equipment has been corrected to minimize the impulse noise, over the path impulse noise should be recorded on a long term basis during test T-1. Information from these recordings should be analyzed in relation to the RSL and baseband loading to determine if normal traffic loading is influencing the level of impulse noise. A close examination of the baseband loading and RSL, time correlated to the impulse noise

recording will provide an indication if intermodulation products are influencing the impulse noise during normal traffic loading.

C-16

CHANNEL INTELLIGIBLE CROSSTALK

- a. The purpose of this test is to measure the total amount of crosstalk within a voice channel from all sources and assess its impact on normal communications. Whenever crosstalk is measured in a VF channel or emanating within station equipment, the test results must be analyzed and compared to the manufacturer's specifications and the MIL-STD.
- b. Intelligible crosstalk may be caused by an impedance mismatch in the circuit or capacitive and inductive coupling between disturbing and disturbed channel. These conditions can occur at any point in a communications system, particularly in the distribution frames, wiring and cabling, crosstalk can also result from improper filtering within the multiplex and mal-adjusted channel levels.
- c. One of the first steps during the preliminary evaluation of a system or station is to isolate where the crosstalk is entering the network. To accomplish this, measurements may have to be performed between the various test points (TP-1 through TP-12). Once isolated to high levels, improper filtering, wiring or cabling, the team chief can then determine the course of action necessary to correct any levels that failed to meet specifications.

CCP 702-1

- d. To obtain accurate crosstalk measurements, considerable attention to details is required. Particular care must be exercised to insure the adequacy of the grounds, effectiveness of the shielding, and correctness of terminations in order to avoid ground loops and to insure that the measured data is accurate.

C-17

VOICE CHANNEL FREQUENCY RESPONSE

- a. The VF frequency response test, also referred to as an insertion loss and amplitude versus frequency distortion test, may be performed on any VF transmission path. Its purpose is to measure the amount of attenuation incurred by the path at various frequencies within the audio spectrum. This test basically measures the level of a received test signal at each of the VF frequencies of interest. The loss at each frequency is then compared to the loss at 1 kHz to determine the frequency response of the channel under test.
- b. The results of the frequency response tests are used to determine if the VF channel equipment is operating properly. In the event the circuit under test has equalizers or ringing equipment installed, the test must be performed ahead of these units. A separate test can be used to determine if the equalizers are operating properly.
- c. Figure C-26 shows the data from a typical frequency response test. The figures entered in the channel columns represent the deviation of the test signal at the indicated frequencies

from the 1 kHz test tone reference. The test results are then compared to the equipment specifications to ascertain if the systems are meeting the minimum manufacturer's specifications. The analysis should also include a comparison of the measured data to the applicable MIL-STD. The accepted standards are listed as ranges of permissible losses over a specified frequency range. This is shown in Figure C-27.

C-18

VOICE CHANNEL ENVELOPE DELAY DISTORTION

- a. The purpose of this test is to determine the relative transmit time of the frequencies between 250 Hz to 3400 Hz. This is accomplished by determining which frequency in the audio spectrum arrives first, and comparing the arrival time of other selected frequencies to that of the fastest one. In this way, while the absolute delay (the actual transmit time from send to receive) is not determined, the time differential across the receive audio path is measured.
- b. The results of the delay measurements are to determine whether the multiplex equipment on the path is operating properly and to ascertain if external equalizers are necessary to meet circuit parameters. When delay equalizers are installed, the test must be performed before or after the equalizers to determine whether the equalizers are properly adjusted.
- c. The envelope delay data sheet shown in Figure C-28 reflects the results of a typical evaluation for this parameter. The data

from this worksheet has been transcribed in Figure C-29 to graphically depict the test results. The worksheet shown in Figure C-28 is normally used when the measurements are made in the manual mode. This form is not necessary when using the automatic sweep feature of the delay measuring set, however, if the manual mode is used, the data must be plotted on the form shown in Figure C-29.

- d. The left column in Figure C-28 represents the frequencies at which each measurement was performed. The next column represents the relative delay in microseconds compared to the reference frequency of 1800 Hz. In some cases it may be desirable to enter in the worksheet (Figure C-28) the actual readings taken from the delay measuring set in one column of the worksheet and entering the computed relative delay in an adjacent column. This is shown in Figure C-28 for clarification and the readings in the last column have been subtracted from the first column to obtain the relative delay.
- e. Comparison of the measurements to the applicable standards is easily seen when plotted on a graph as shown in Figure C-29. On this graph, the measurements from Figure C-28 have been plotted along with the standard which readily shows whether the measured channel was or was not within the prescribed standards.

C-15

VOICE CHANNEL PHASE JITTER

- a. This test is used to measure the incremental changes in the

phase of a single frequency transmitted on a VF path. Since phase jitter has little impact on voice communications, minimum attention has been given to this parameter during earlier evaluations. Today, with the increasing use of high speed data circuits, phase jitter has become one of the primary indicators of measuring system performance. As transmission speeds increase, data pulses become narrower with extremely short time intervals between pulses. As this happens, it is possible that the jitter would be seen as a pulse by the receiving equipment and result in message errors. This situation is highly undesirable and could have serious consequences considering the importance of the transmitted message.

- b. Phase jitter on data transmissions systems can be defined as an unwanted change in the phase or frequency of the transmitted signal due to modulation products from another system or source. The modulation process that causes phase jitter may be either phase or frequency modulation depending on the source which is generally in the terminal equipment and not generated on the line. In multiplex units, phase jitter results from incidental phase modulation of the oscillators used for translation of the signals within the channel to a different part of the spectrum for transmission. This incidental modulation is caused by noise and line related ripple on office batteries and on power and bias supplies, and within timing

circuits of FDM systems. This modulation is transferred to the multiplex signal during frequency translations and generally, the greater the number of translations, the greater the phase jitter. Therefore, the signals transmitted over channels in the higher supergroups have the most phase jitter.

- c. Measurements have indicated that for long haul, multi-link systems, the most serious components of incidental phase modulation are power line related, both as harmonics of the line frequency as well as fractions of the line frequencies. Phase jitter most commonly occurs at rates related to power line frequency (60 Hz) and its harmonics and submultiplex, the telephone ringing frequency and the interaction between the two sources. If excessive phase jitter is measured during an evaluation, the sources discussed above should be investigated.
- d. Additional tutorial information of this parameter and its relationship to transmission systems is contained in Appendix F, Section IX of this document.

C-20

CHANNEL HARMONIC DISTORTION

- a. The purpose of the harmonic distortion test is to determine whether any appreciable non-linearities exist within the equipment during the evaluation. The non-linear operation of amplifiers, filters, channel modulators, group modulators, etc., can all contribute harmonic distortion and result in degraded service.

- b. Should the harmonic distortion measured during an evaluation exceed the equipment specifications, an investigation should be accomplished to determine what component(s) is causing the problem. From past experience, it has been found that the primary cause for high harmonic distortion was attributed to the channel modulators and demodulators. In any case high levels of harmonic distortion could influence the idle channel noise readings taken during test T-8.
- c. Analysis of the test data must include a comparison of the measured results with the equipment specifications and the applicable MIL-STD. Moreover, a conclusion must be drawn as to the capability of the equipment to meet specifications and, whenever possible, a concise description of the problem along with recommended corrective action should be documented.

C-21

VOICE FREQUENCY TRANSLATION

- a. This test will determine whether there is a frequency error present in any of the carrier frequency oscillators of the multiplex equipment. If a carrier oscillator is off frequency, the received signal will also be shifted in frequency. Small errors of a few hertz are not noticeable on normal voice circuits but digital transmissions are extremely sensitive to any frequency errors.
- b. The send frequency and received frequency are compared and the difference is stated as the frequency translation or change in

audio frequency. This amount in hertz is compared to the "maximum allowable change in audio frequency" criteria for the circuit. Should the measurement exceed the applicable MIL-STD, it will be necessary to measure and adjust the master oscillator frequency on all multiplex equipment on the link/system.

C-22

STRIP CHART RECORDINGS (T-1)

- a. The strip chart recordings provide the most valuable data on which to base a "dynamic" analysis of system performance. The time correlated recordings will show the performance of a system under actual operating conditions. For this reason they are an important trouble shooting aid to the teams during the evaluation. The chart recordings provide real time data to the test teams which can be used, when properly analyzed, to solve problems on the system in an expeditious manner. The recordings, however, must include appropriate remarks when a discontinuity or anomaly is noted in the data. These notations must be entered at the time of occurrence, otherwise, it may be impossible to determine the cause of the anomaly.
- b. As stated in the previous paragraph, the strip charts are a valuable aid in determining a system's operating performance. Therefore, care must be exercised to insure that all required data is entered on the strip charts. As a minimum, the charts are to be conspicuously marked with the link number, station name, date, time (ZULU), and calibration for each parameter

being recorded. The calibration should be verified on a daily basis and new calibration chart prepared whenever necessary.

- c. Preliminary analysis of the recordings must be on a real time basis if maximum benefits are to be realized from the data. In this respect, all charts are to contain a time, date and the initials of the individuals annotating the charts at least every eight hours, preferably every four hours. Due to the minor speed differences between recorders, coordination of the time marks must be accomplished between the stations being evaluated.
- d. The method of analyzing the strip chart data may vary from team to team, however, pertinent data on the link performance must be included in the reports. To achieve this objective, it must be kept in mind that the required recordings are: (1) receive signal level, (2) idle channel noise, (3) baseband loading, (4) phase jitter and hits, (5) test tone stability. If it is not possible to record these parameters simultaneously, the order of priorities should follow that above. Since combined RSL recordings cannot be accomplished in most cases, the RSL of both receivers on an LOS system and at least three receivers on a tropo system will be recorded simultaneously on both ends of the link. The minimum continuous recording period for all parameters is 72 hours, additional recordings may be performed when deemed necessary by the team chief.
- e. The first step in the reduction of the strip chart data is to

scale the charts into 20 minute intervals. This is considered the minimum number of intervals for 72 hours of recordings when operating the recorder at 5 mm/min. On tropo systems and some LOS systems it may be necessary to operate the recorders at a higher speed such as 25 mm/min in order to obtain accurate medians of the recorded parameters. In this case the minimum interval will be 5 minute medians. It is essential that the recorders at both ends of the link be operated at the same speed if any reasonable correlation is to be obtained without considerable effort in the analysis process.

- f. Several methods are available for determining the median value of the recorded data, however, within limitations, the two most accurate methods are: (1) The placing of a string or straight edge along the data so that equal excursions with respect to the interval period appear above and below the recording being evaluated. The position of the string is considered the median value of the data. (2) Taking a series of equally spaced instantaneous values (the number depending on the time periods) of the data within a time period (20 minutes, hourly, etc.) and finding the median of these values. The accuracy of both methods are approximately the same.
- g. The next step in the data reduction is to find the median for an entire run. (A run in this case is defined as 20 minutes for LOS and 5 minutes for tropo). The best way to accomplish

this, is to plot a histogram of the run medians. The median that is found to have the most occurrences during the run should be recorded as the run median. Figure C-30, represents RSL medians for LOS link while Figure C-31 shows a histogram plotted from this data. It can be seen from the histogram that the median is -28.8 dBm.

- h. The final step is finding the median for the entire evaluation period. One method of doing this, which would provide a very accurate median of the data during the evaluation is to plot a histogram for all individual medians for each run. The median during the evaluation would be the value that occurs most frequently on the histogram. This is the preferred method during the TEP testing, however, some engineers take a median of all run medians. This method is less accurate than the preferred method because of the restricted number of data points that are obtained using the individual run median method.
- i. The methods described above can also be used in arriving at the median of other recorded parameters. As previously stated, the strip chart recordings can provide considerable information on the performance of a system and application to trouble-shooting techniques. This is only valid if the recordings are properly conducted and the data is fully analyzed. The analysis must not only be accomplished on a single station basis, but also on a system basis if maximum benefits are to be realized from the test data.

- j. During the recording period, it is essential that the test teams analyze the recorded data on a near real time basis to detect anomalies that would influence the test data. There are many factors which can and will result in questionable test results. A few of the influencing factors are listed in the following paragraphs; however, it must be realized that these are only examples and are not a comprehensive listing.
- (1) The idle channel noise recordings can be influenced by improperly operating power supplies, carrier leak, crosstalk, interference, etc. Should the recorded value depart from the expected level, it will be necessary to inspect the power system for excessive ripple by observing the channel spectrum with a wave analyzer to detect any extraneous signals that may be interfering with the recordings.
 - (2) Impulse noise recordings can be influenced by switching equipment, ringing tones, radar pulses and etc; these should be investigated on a case by case basis and whenever possible the cause identified and eliminated.
 - (3) Baseband level recordings which exceed the calculated value, based on actual traffic loading, are primarily influenced by hot levels in the baseband. When this situation arises, a sweep of the baseband will be necessary to identify the interfering signals. The sweep should not only cover the traffic spectrum but must extend below baseband to determine if the problem is

being introduced by out of band orderwires and signaling equipment.

- (4) Deficiencies in the receive signal level will be readily apparent from the chart recordings. Extremely deep fades on microwave links should be investigated to determine the cause of the fading. The investigation should include, but not be limited to, an examination of the path profile for adequate beam clearance and, when necessary, physical inspection of the path for obstructions that are not apparent from the path profile. On tropo systems with maximal ratio combiners, the strip chart recordings will provide a method of ascertaining that the combiners are functioning properly. When the combiners are functioning properly, the ICN will be a function of the best received signal, therefore, improper combining can be detected by plotting the voice channel noise versus the receive signal level of each receiver.
- k. Results of all the recordings are to be plotted on the appropriate TEP Forms with the medians clearly identified as shown in Figure C-31 through C-33. As can be seen from these figures, the data is plotted for each parameter as a function of time. As an example, the plot of run median RSL, as shown in Figure C-31, graphically displays the distribution of all the run medians obtained for the recorded period. Figure C-30 contains the stroke data and also shows the respective percentages of

CCP 702-1

time that the receive signal level exceeded the various median levels. To calculate these percentages, first summate all the number of tick marks at each median level, then add all these sub-totals. Begin from the highest median level noted during this period and divide this sub-total by the total number of run medians. Example:

$$\% \text{ at } -26 \text{ dBm} = 1/113 \times 100\% = 0.9\%$$

To obtain the percentage of time this parameter exceeded that of the next level summate the previous sub-total(s) with the sub-total at this level and perform the calculations as follows:

$$\% \text{ at } -26.5 \text{ dBm} = 3/113 \times 100\% = 2.7\%$$

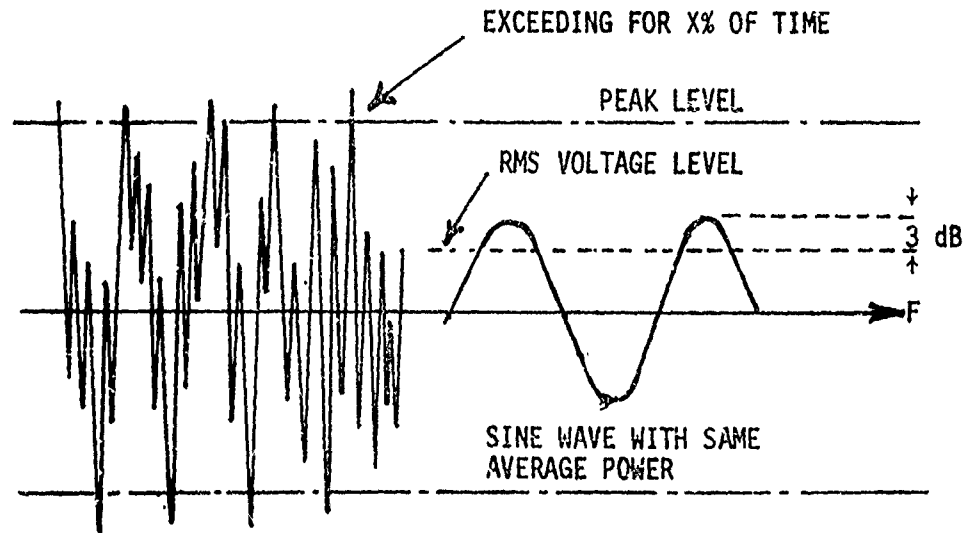
Repeat the above procedure until the percentage for the second to the last median run level is reached. Graphically plot the median run levels with respect to the calculated percentages as shown in Figure C-31 through C-33. Plots for other recorded parameters such as idle channel noise, baseband loading, and test tone stability could be arrived at using similar techniques.

C-23

SUMMARY This section has presented the basic tools for final analysis of the data collected during an evaluation. It should be evident that each test can be utilized to formulate a picture of system performance. Since many of the test results are directly related to other test results, a series of systematic testing can be used to isolate problems in the system. As an example, it was shown that the quieting curves were a function of

the entire receiver, however, when the curves were evaluated with respect to noise figure, and IF test data, problems could be isolated to a particular receiver stage. Each major test that was covered in this section was intended to place emphasis on the analysis of the test data and the methods normally used to isolate problem areas.

ILLUSTRATION OF PEAK / RMS MEASUREMENT



COMPLEX SIGNAL

Figure C-1

PEAK TO AVERAGE VALUES

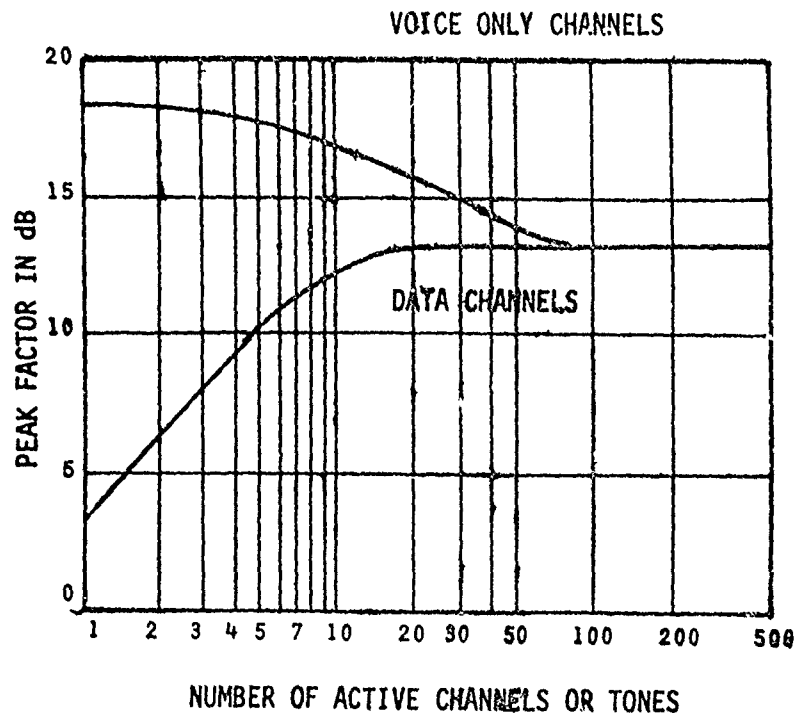


Figure C-2

C-65

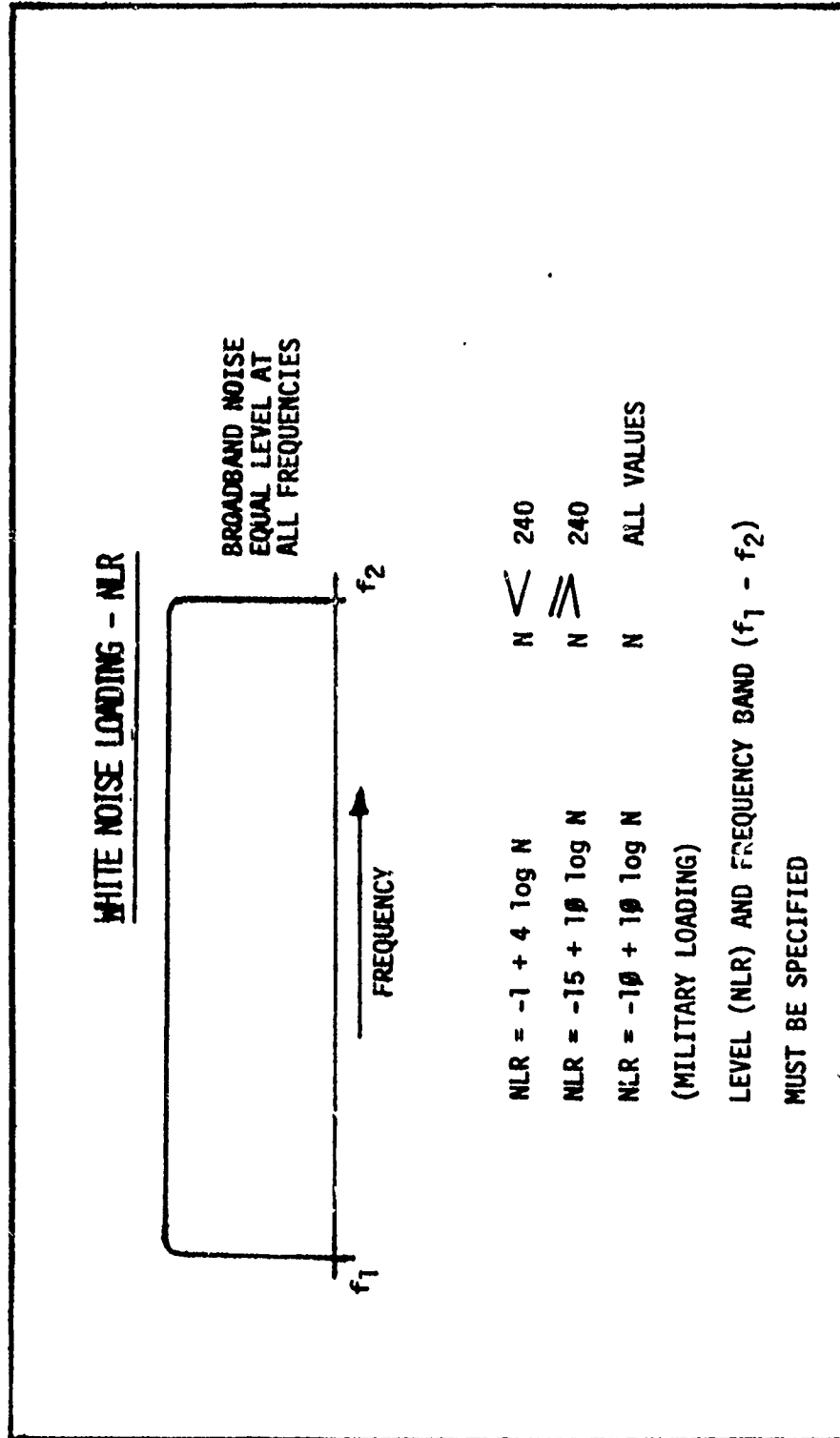


Figure C-3

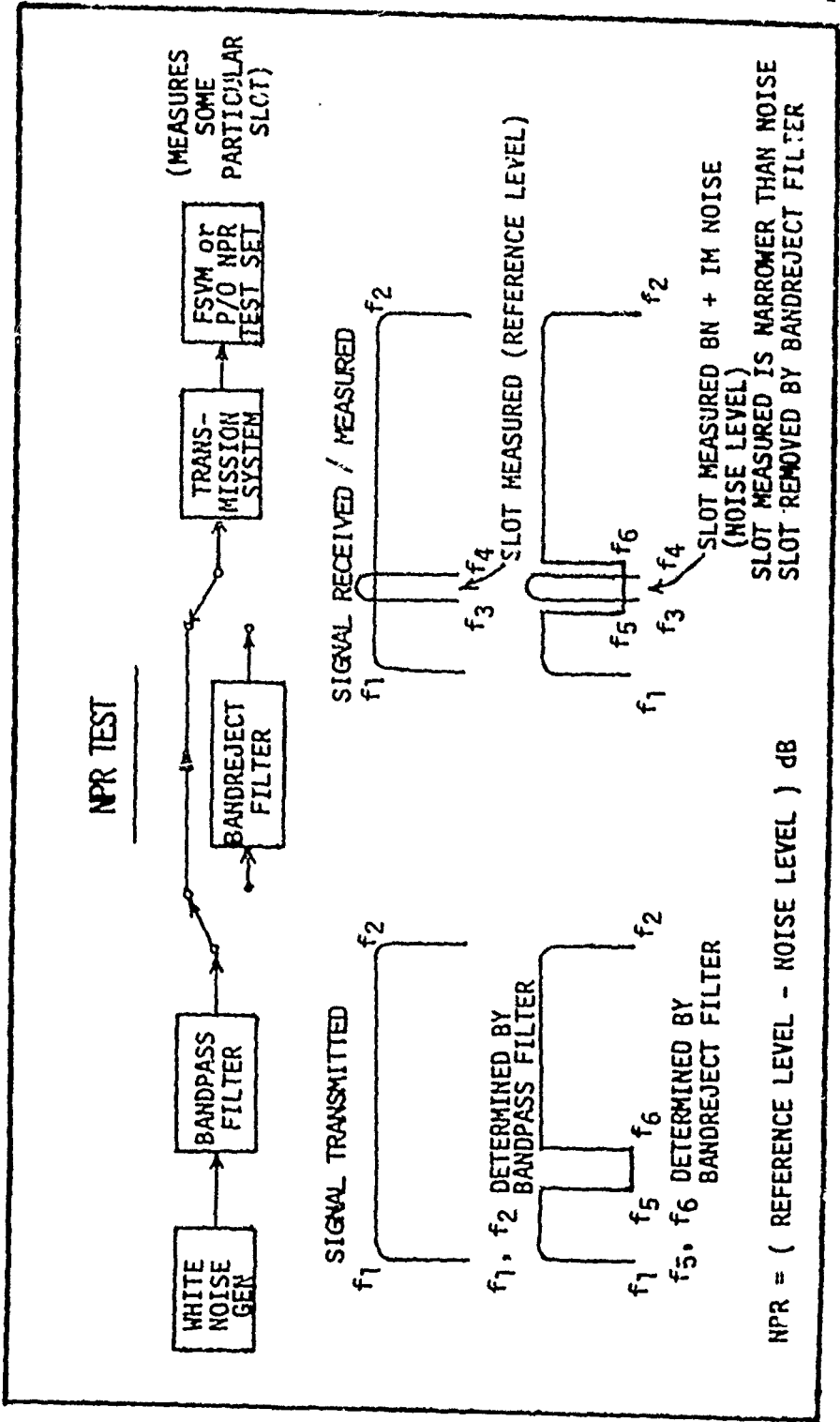
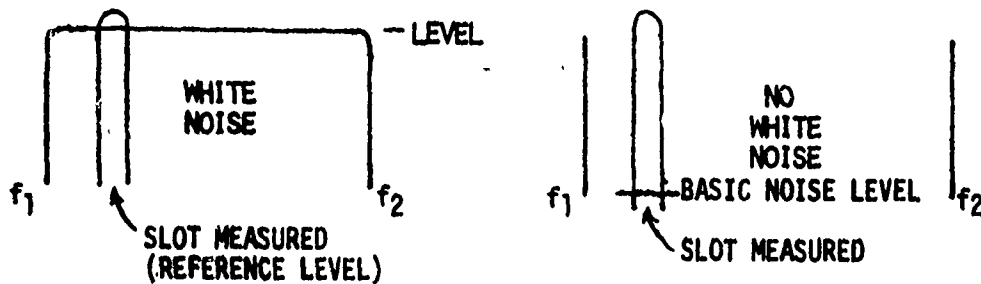


Figure C-4

BASIC NOISE RATIO - BNR

(ALSO CALLED BASIC INTRINSIC NOISE RATIO)

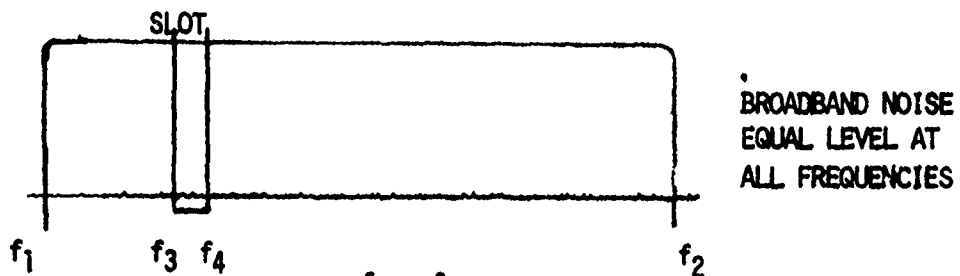
RATIO OF NOISE IN A TEST CHANNEL WITH ALL CHANNELS
LOADED TO THE NOISE PRESENT WITH NO LOADING



$$BNR = (\text{REFERENCE LEVEL} - \text{BASIC NOISE LEVEL}) \text{ dB}$$

Figure C-5

BANDWIDTH RATIO - BWR



$$BWR = 10 \log \frac{f_2 - f_1}{f_4 - f_3}$$

$$NLR = +17.8 \text{ dBm} \quad f_1 = 60 \text{ kHz}, \quad f_2 = 2540 \text{ kHz}$$

SLOT = 3.2 kHz WIDE

$$BWR = 10 \log \frac{2540 - 60}{3.2}$$

$$= 28.89 \text{ or } 29 \text{ dB}$$

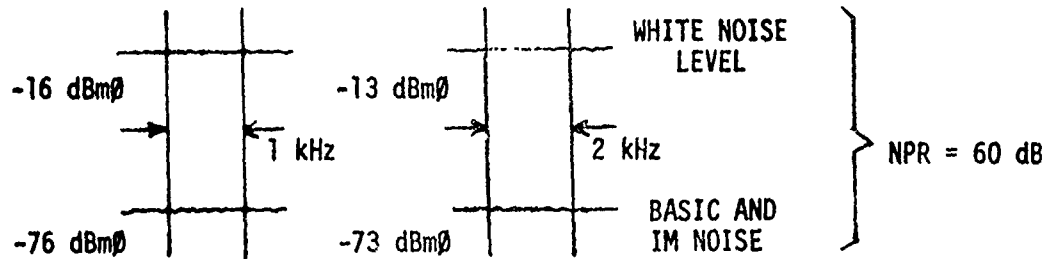
LEVEL IN 3.2 kHz SLOT IS +17.8 dBm - 29 dB or -11.2 dBm

Figure C-6

SLOT BANDWIDTH, NPR AND S/N

NLR +17.8 dBm \emptyset , 6 \emptyset TO 254 \emptyset kHz WHITE NOISE

NPR



S/N

\emptyset - (BASIC AND IM NOISE LEVEL)

$$1 \text{ kHz SLOT} = \emptyset - (-76) = 76 \text{ dB}$$

$$2 \text{ kHz SLOT} = \emptyset - (-73) = 73 \text{ dB}$$

Figure C-7

NPR TEST RESULTS

SITE "X" RECEIVING SITE "Y"

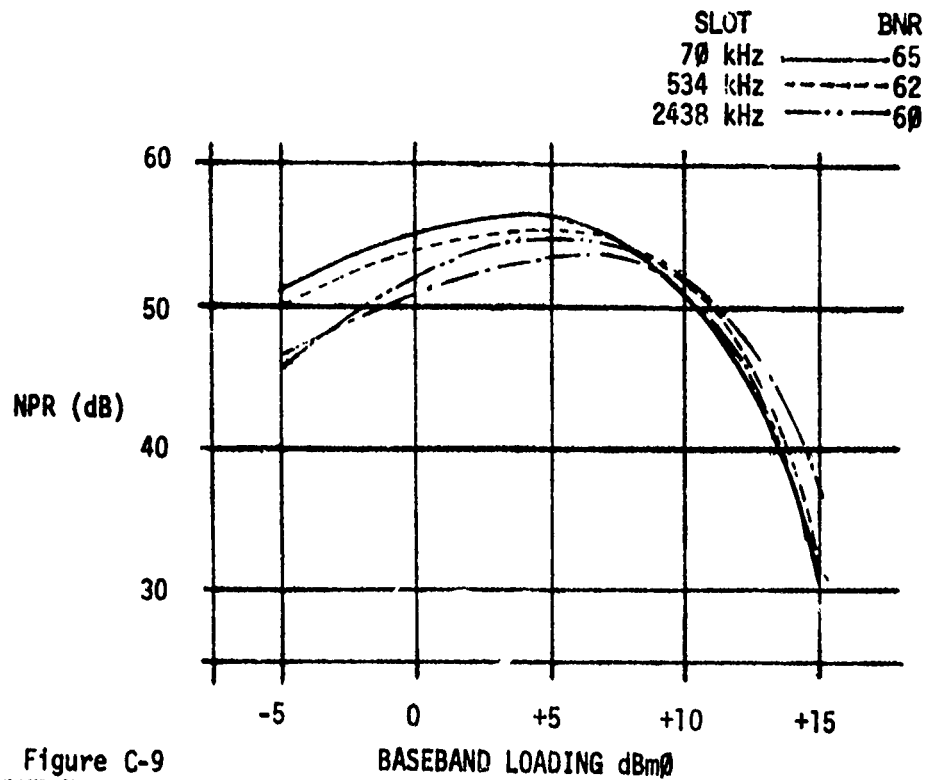
6 $\emptyset\emptyset$ CHANNEL MILITARY LOADING (NLR = +17.8 dB)

WHITE NOISE 6 \emptyset TO 254 \emptyset kHz BAND

SLOT	BNR	NLR				
		-10	-5	0	+5	+10
70 kHz	65	51	55	56	51	32
53.4 kHz	62	54	53	55	52	31
1 $\emptyset\emptyset$ 2 kHz	6 \emptyset	47	51	53	51	32
2438 kHz	58	46	52	55	52	37

(\emptyset NLR = +17.8 dBm \emptyset)

Figure C-8

NPR CURVESNPR CURVE ANALYSIS

1. EXPECTED CHANNEL (OR SLOT) S/N FOR VARIOUS LOADING CONDITIONS
2. OPTIMUM LOADING POINT
3. AMOUNT OF BASIC NOISE VERSUS IM NOISE
4. SYSTEM AND/OR MICROWAVE EQUIPMENT PERFORMANCE
5. IDENTIFICATION OF POSSIBLE MICROWAVE EQUIPMENT MALFUNCTION OR MALADJUSTMENT

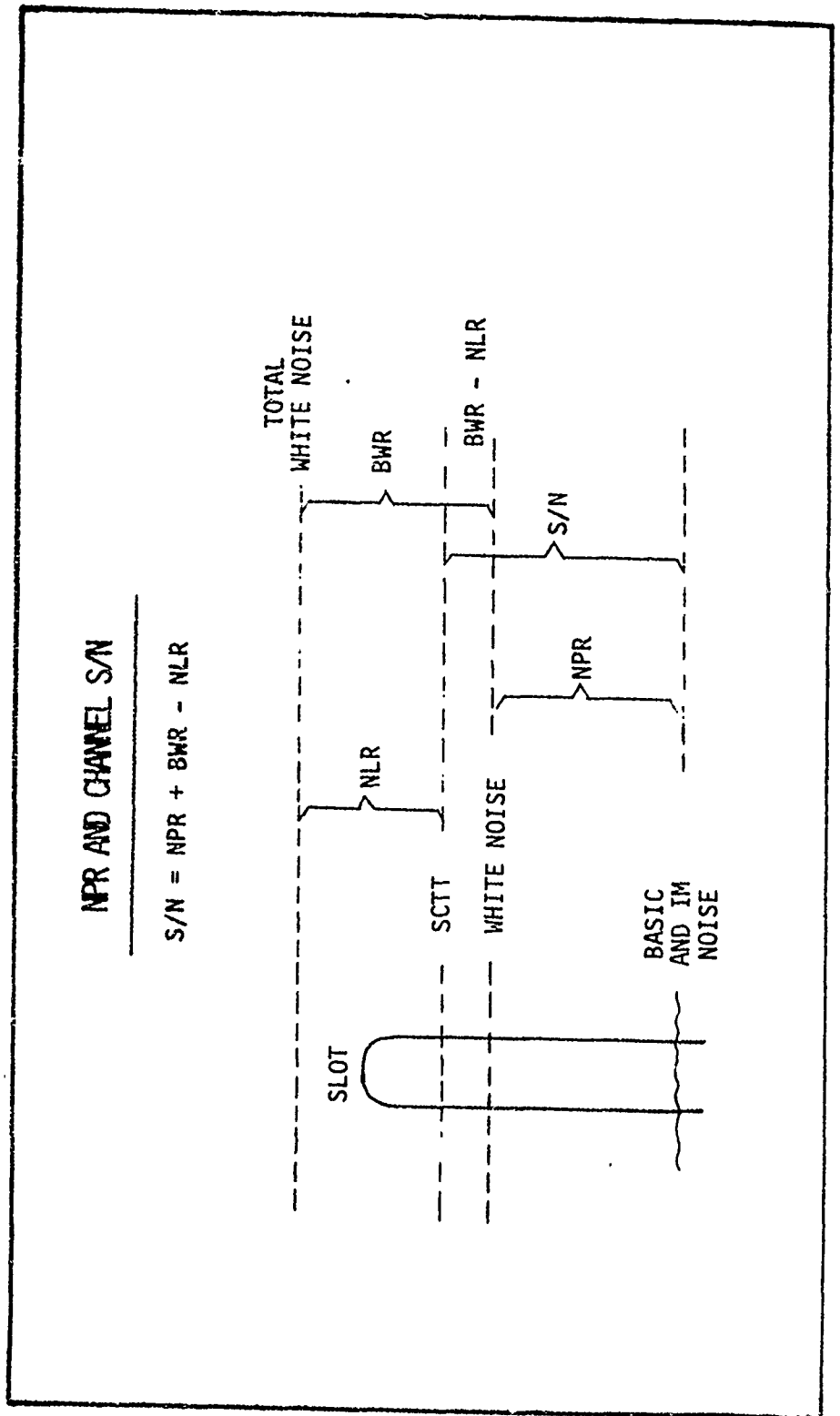


Figure C-11

CHANNEL S/N FOR VARIOUS NLR OR
BASEBAND LEVELS (DBL)

φ NLR = +17.8 dBmφ, 3.2 KHZ CHANNEL, 6φ TO 254φ KHZ WHITE NOISE

NLR OR BBL

SLOT	-10		-5		0		+5		+10	
	NPR	S/N	NPR	S/N	NPR	S/N	NPR	S/N	NPR	S/N
70 KHZ	51	72.2	55	71.2	56	67.2	51	57.2	32	33.2
534 KHZ	54	75.2	53	69.2	55	66.2	52	58.2	31	32.2
1002 KHZ	47	68.2	51	67.2	53	64.2	51	57.2	32	33.2
2438 KHZ	46	67.2	52	68.2	55	66.2	52	58.2	37	38.2

e.g. 70 KHZ AT -5 NLR NPR = 55
BWR = 29 (10 log $\frac{2480}{3.2}$)

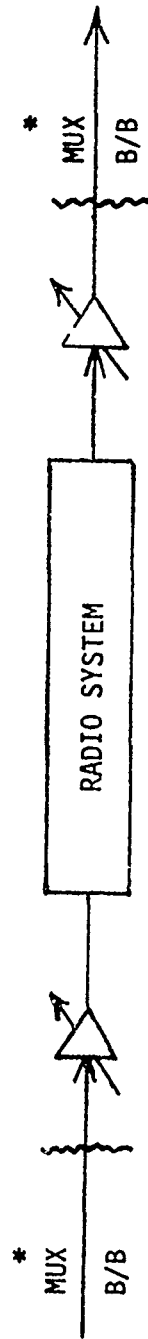
S/N = 55 + 29 - 12.8 = 71.2 dB
NLR = 17.8 - 5

Figure C-12

OPTIMUM LOADING POINT - SYSTEM OPTIMIZATION DEVIATION

* NLR/BBL	dBm \emptyset	NPR	NORM (S/N)	+1 \emptyset	-1 \emptyset
+1 \emptyset dB	+27.8	32.8	34	44	24
+ 5 dB	+22.8	31.5	57.7	67.8	47.7
\emptyset dB	+17.8	54.6	65.8	75.8	55.8
- 5 dB	+12.8	52.5	68.7	78.7	58.7
-1 \emptyset dB	+ 7.8	48	69.2	79.2	59.2

S/N



e.g. NORMAL BBL -1 \emptyset dB (+7.8 dBm \emptyset) S/N = 69.2 dB, INCREASE DEVIATION 1 \emptyset dB, S/N (NORMAL 65.8 dB) BUT TLP INCREASED 1 \emptyset dB S/N 75.8 dB.

Figure C -13

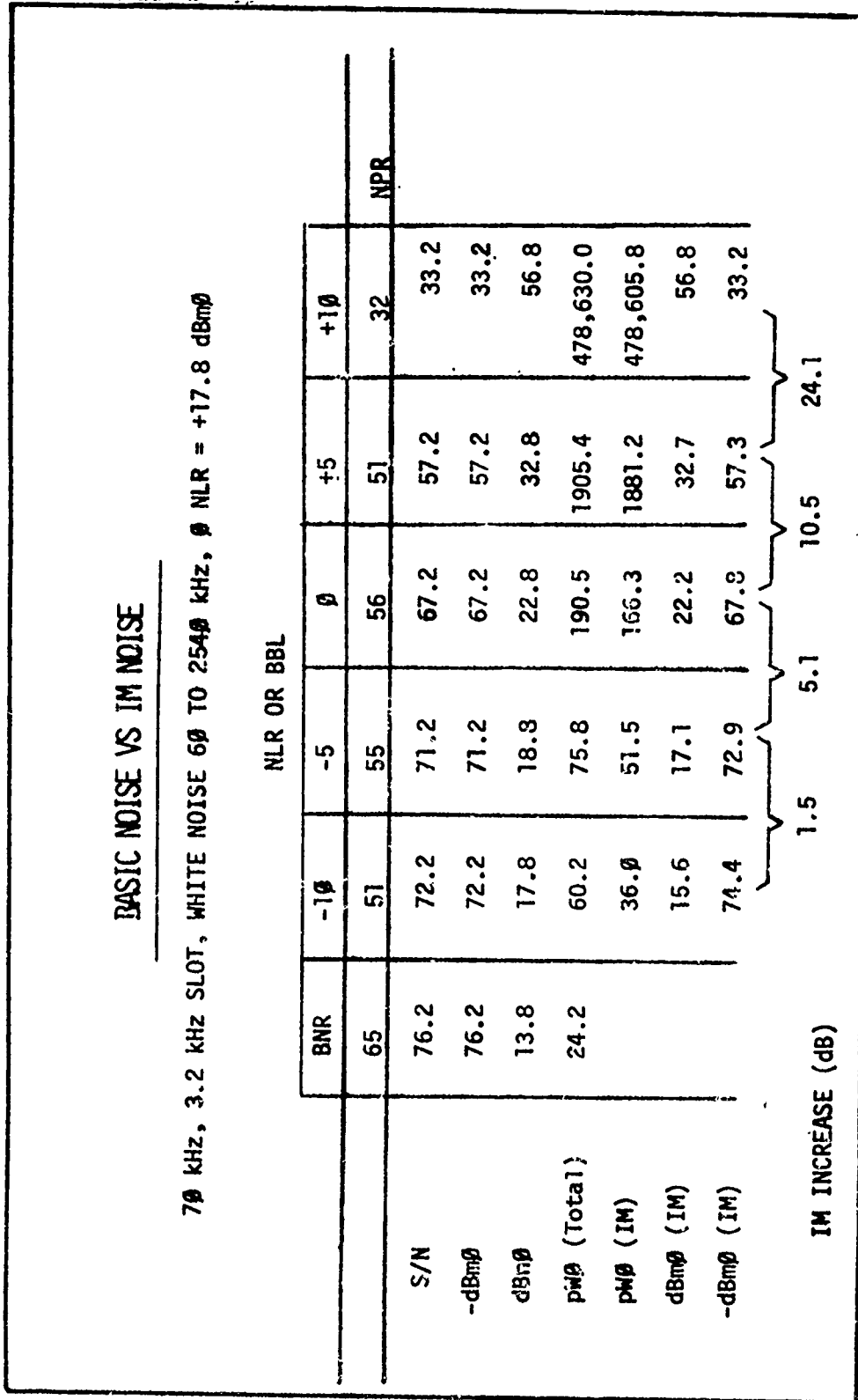


Figure C-14

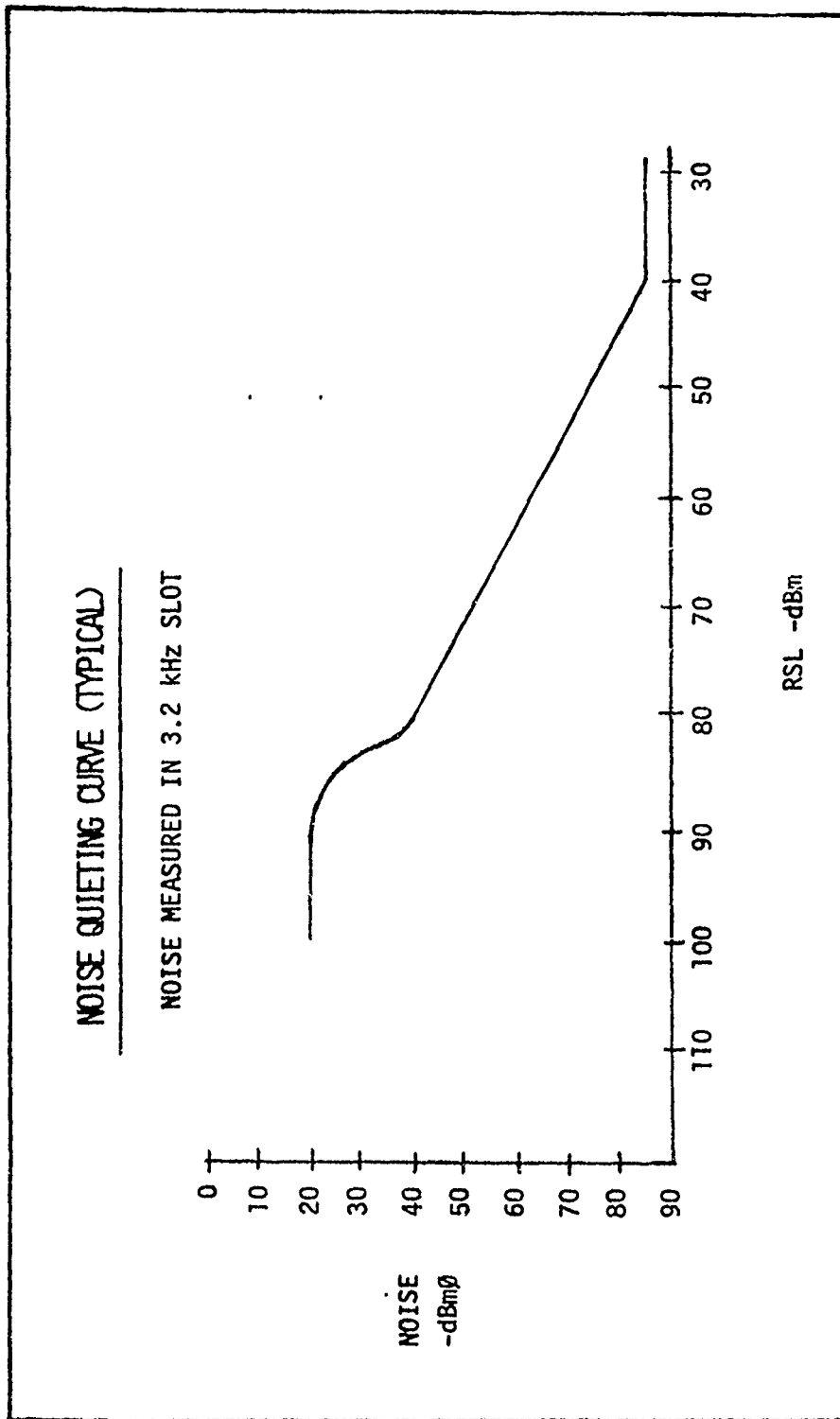


Figure C-15

CCP 702-1

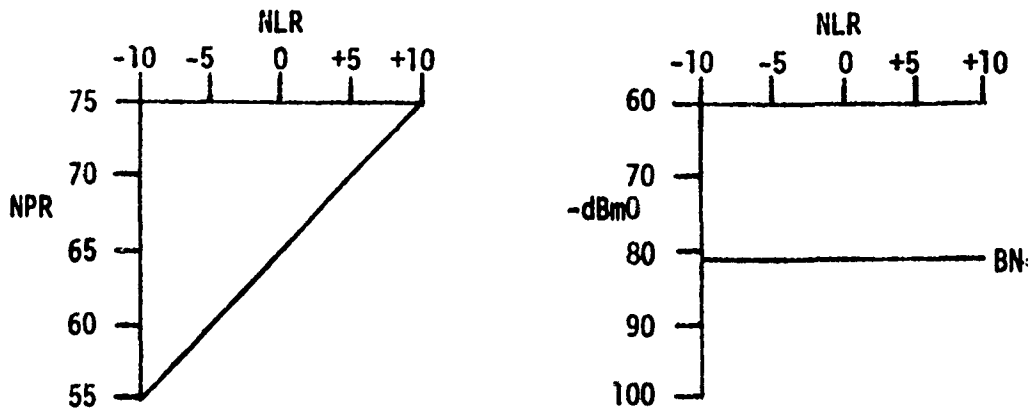


Figure C-16

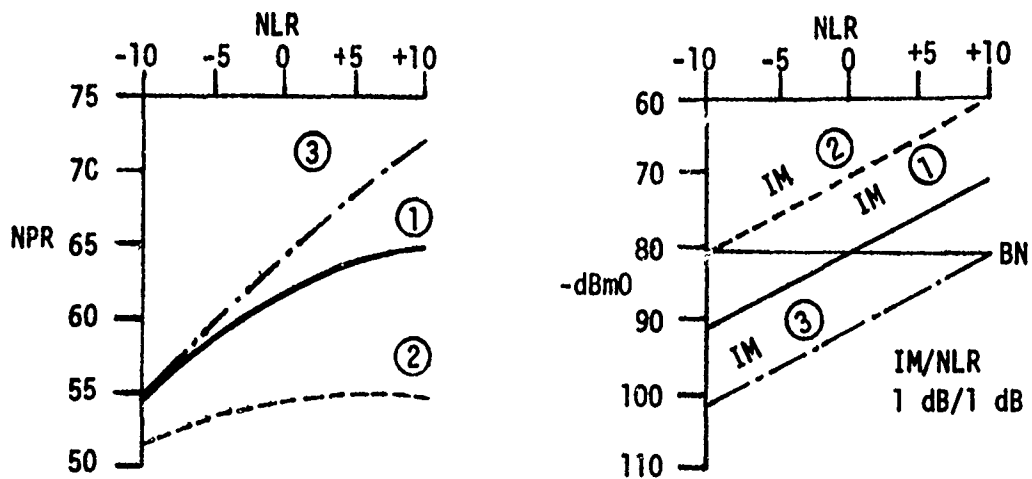


Figure C-17

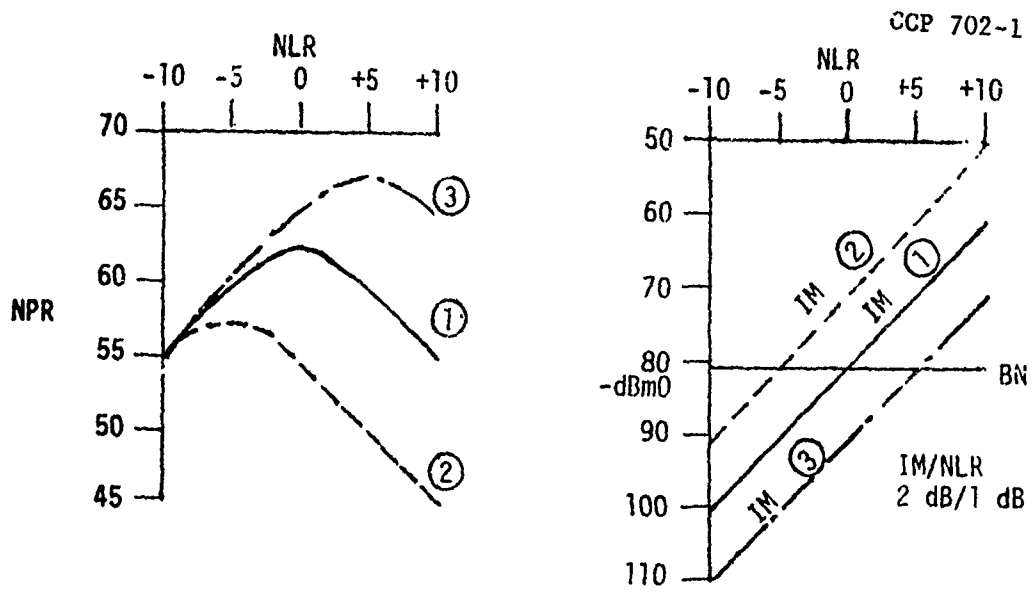


Figure G-18

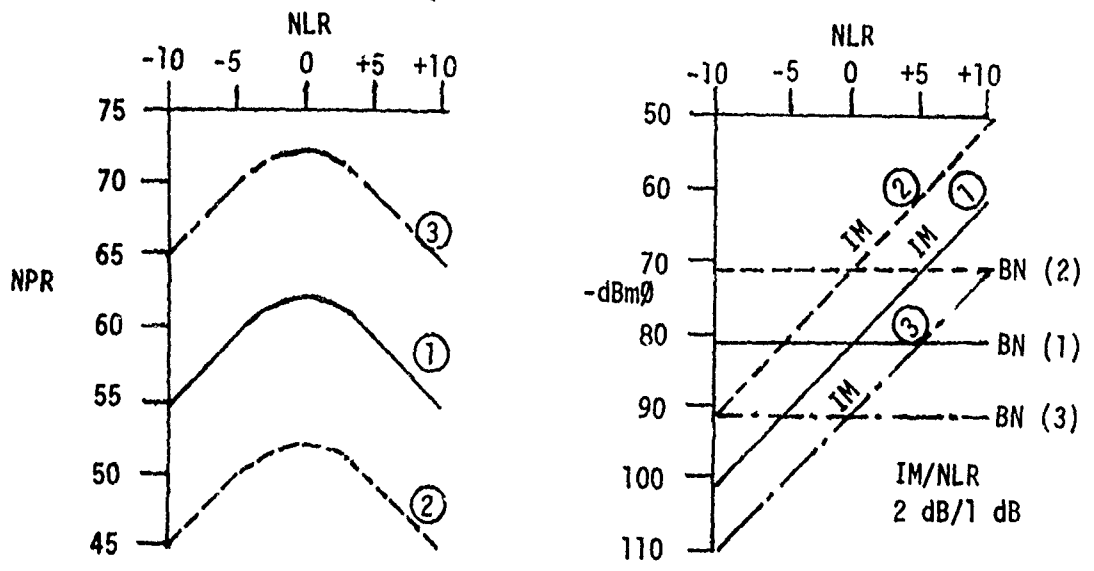


Figure C-19

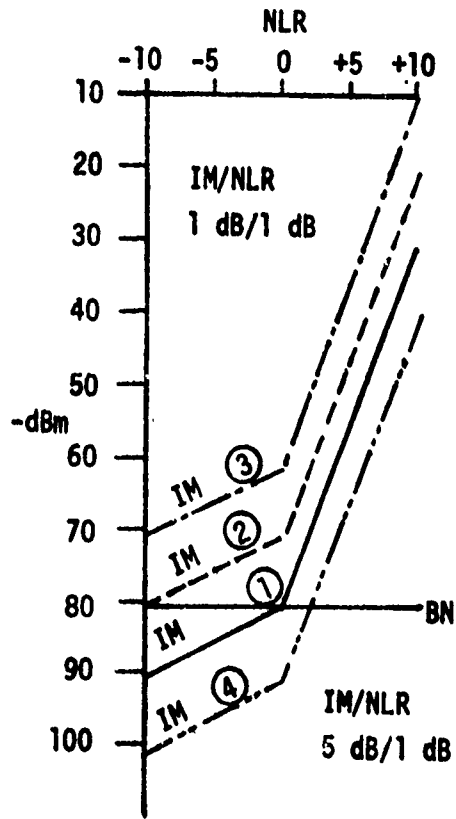
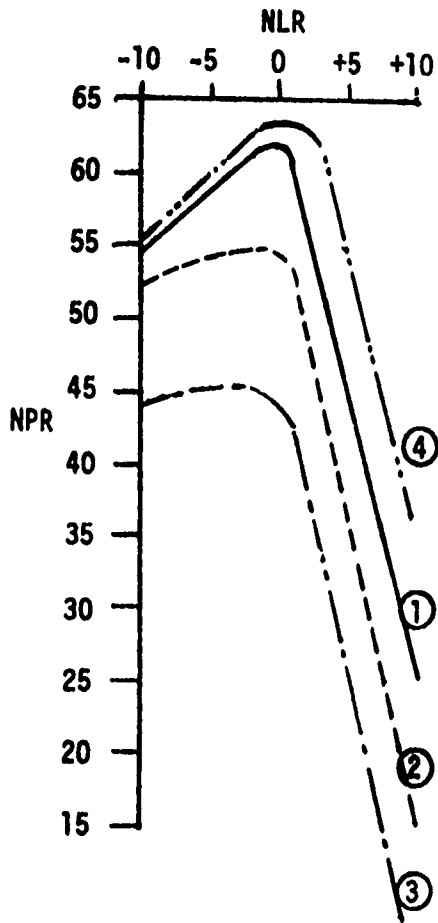


Figure C-20

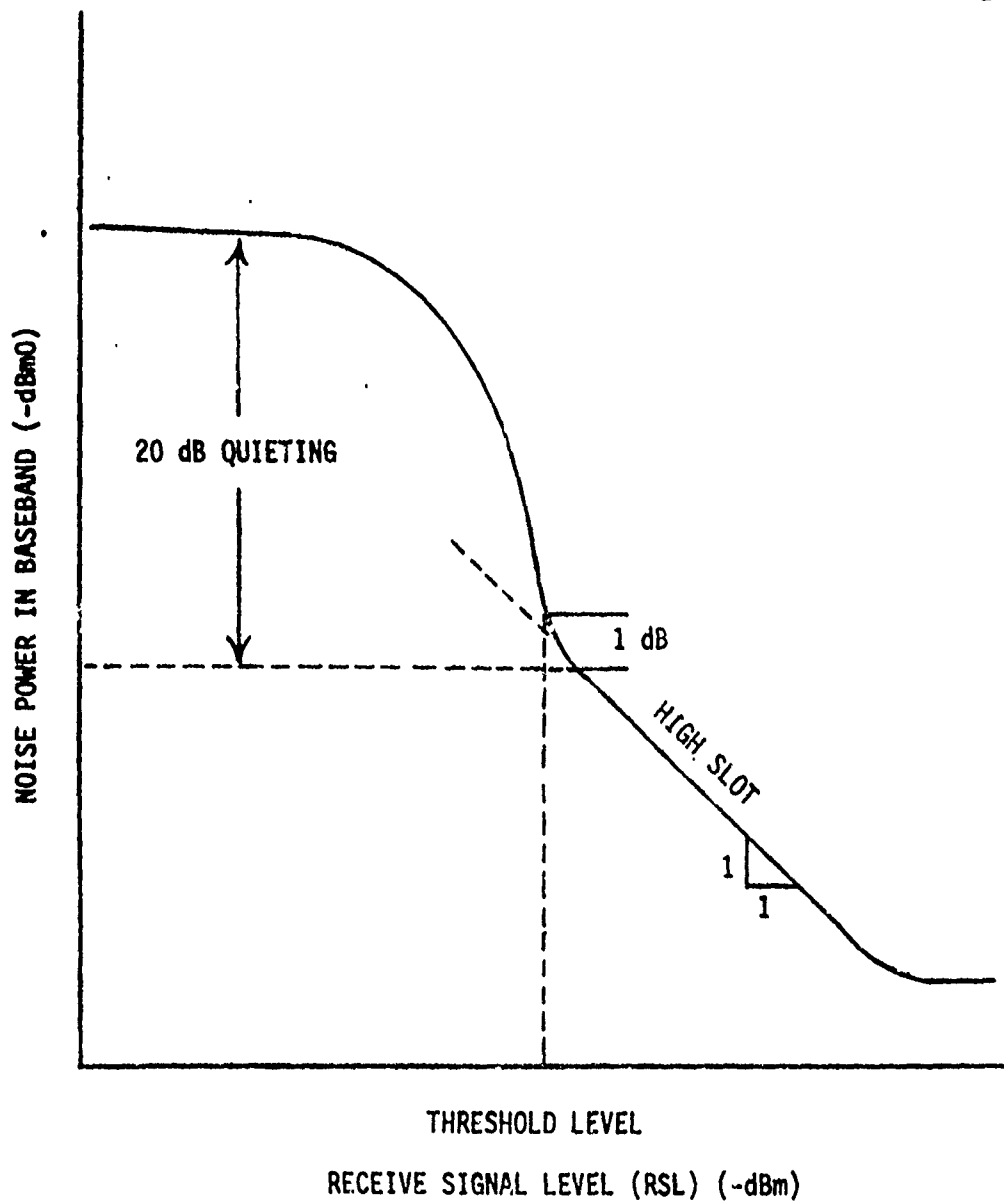


Figure C-21

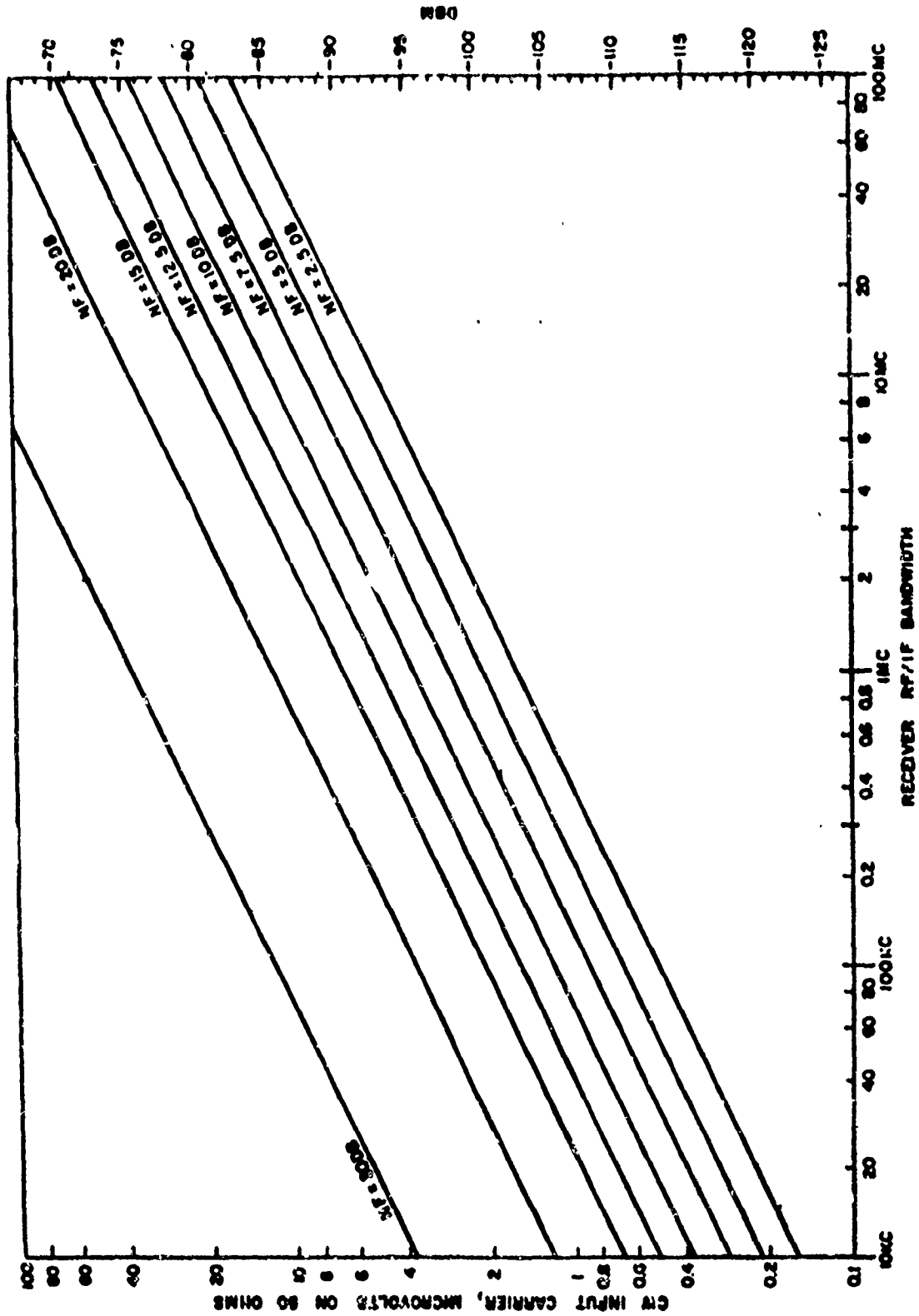
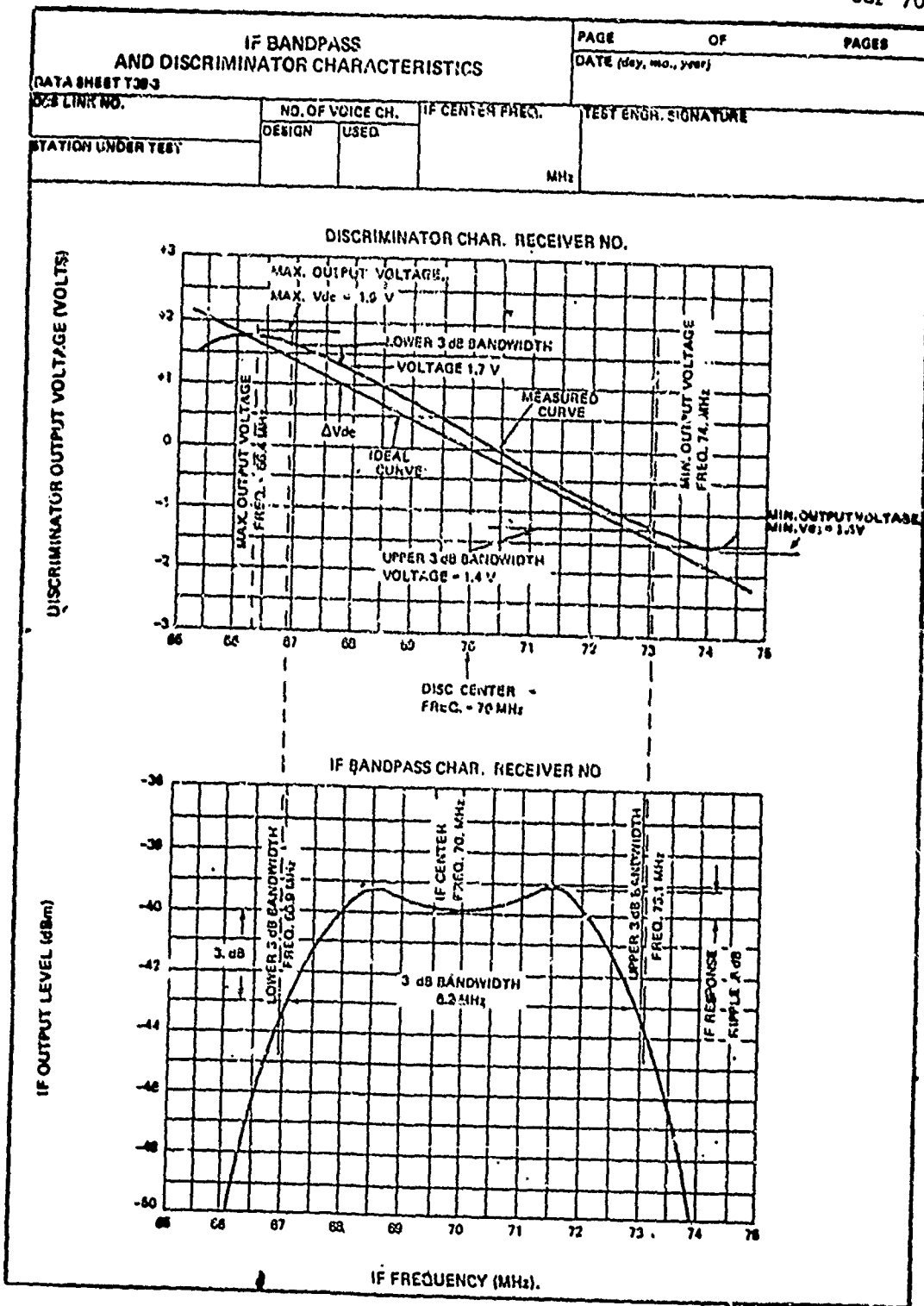


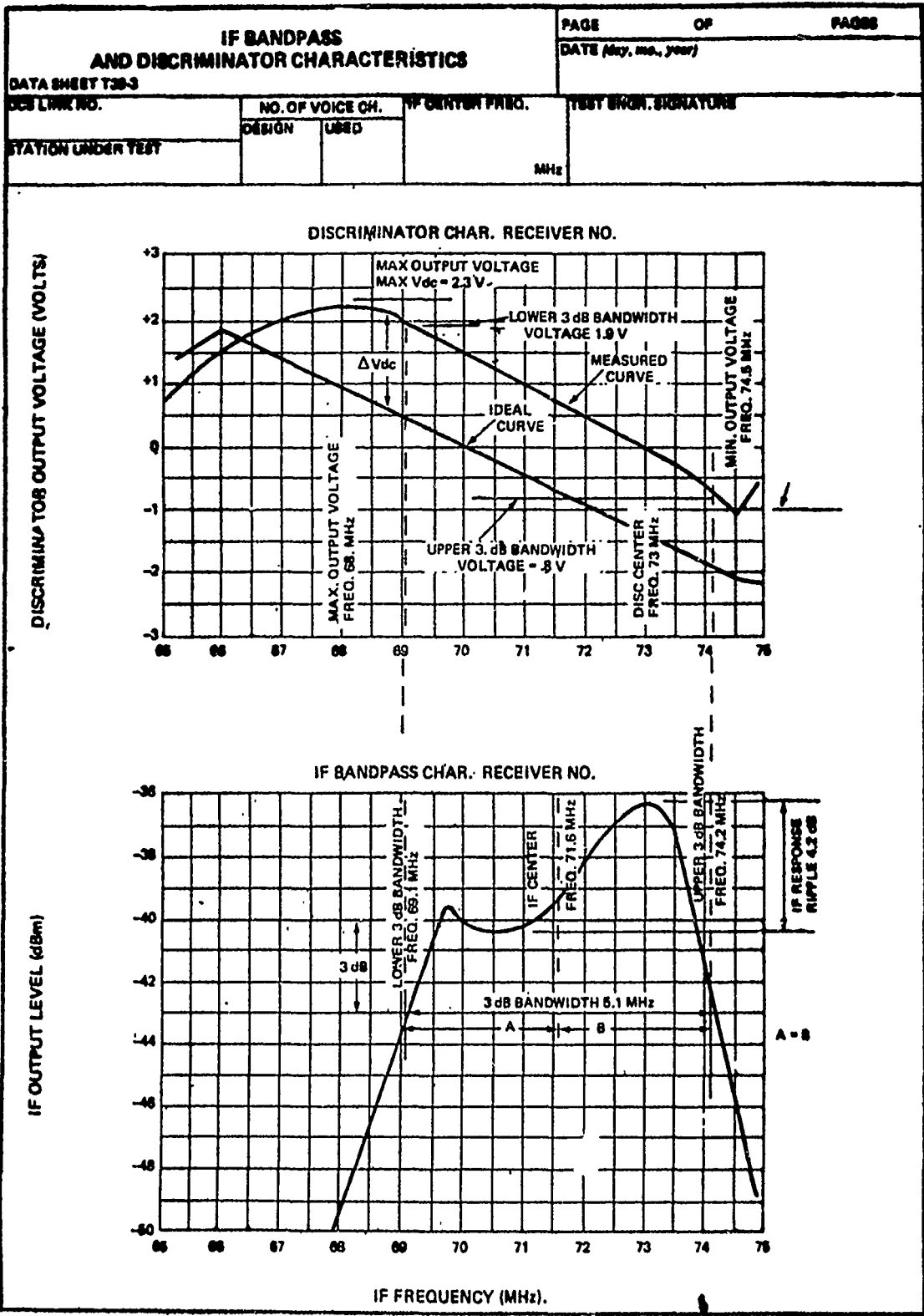
Figure C-22

Receiver Input Required for 20-dB Quieting as a Function of RF/IF Bandwidth



IF BANDPASS AND FM DISCRIMINATOR RESPONSE OF PROPERLY ALIGNED RECEIVER

Figure C-23



EXAMPLE OF IMPROPERLY ALIGNED IF BANDPASS AND FM DISCRIMINATOR RESPONSE

Figure C-24

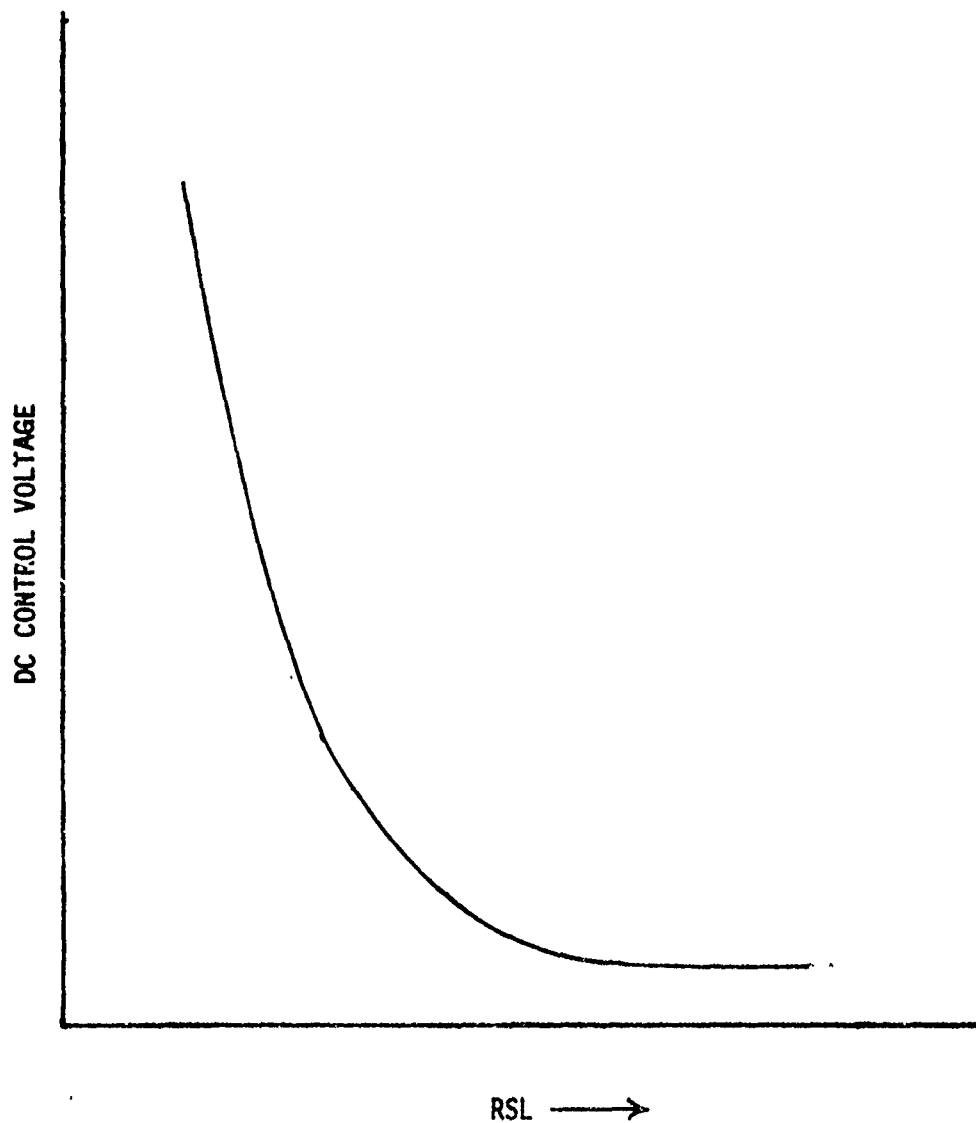


Figure C-25

CCP 702-1

CHANNEL FREQUENCY RESPONSE, MANUAL SWEEP				PAGE _____ OF _____ PAGES			
DATA SHEET T102				DATE (day, mo., year)			
DCS LINK NO.		STATION UNDER TEST		TEST ENG. SIGNATURE			
TEST POINTS							
DISTANT STATION (XMIT)				LOCAL STATION (RCV)			
TP- 3				TP- 10			
CHANNEL	SG	2					
	GP	3					
	CH	2					
FREQ	dBm0		TEST TONE LEVEL (dBm)				
100	-9.8	-6.8					
200	-5.8	-2.8					
300	-3.8	-0.8					
400	-3.2	-0.2					
500	-3.0	0					
600	-3.1	-0.1					
800	-3.1	-0.1					
1000	-3.0	0					
1200	-2.8	+0.2					
1400	-2.6	+0.4					
1600	-2.6	+0.4					
1800	-2.6	+0.4					
2000	-2.6	+0.4					
2200	-2.6	+0.4					
2400	-2.6	+0.4					
2600	-2.6	+0.4					
2800	-2.6	+0.4					
3000	-2.8	+0.2					
3200	-3.3	-0.3					
3400	-4.1	-1.1					
3600	-6.0	-3.0					

Figure C-26

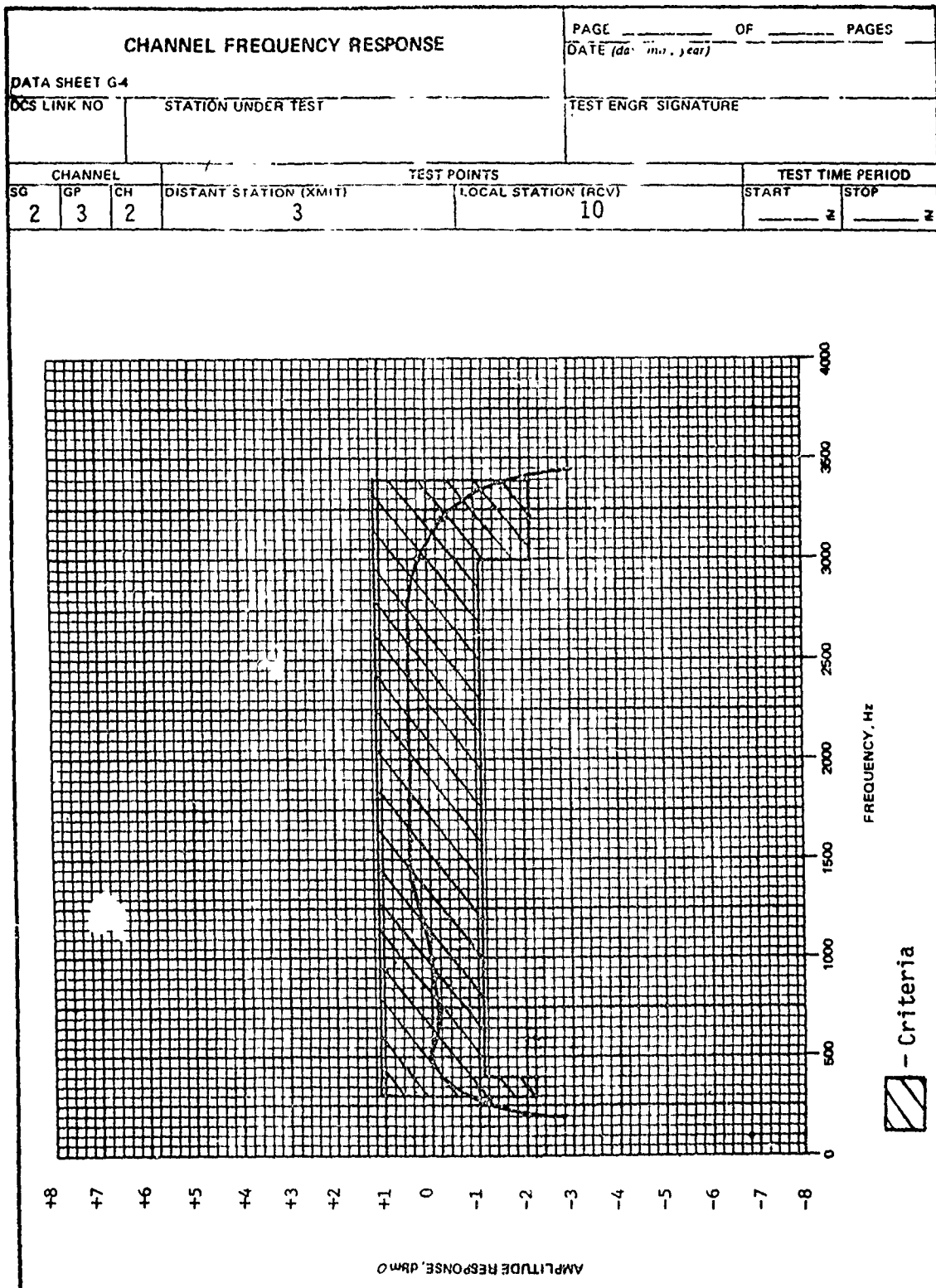


Figure C-27

VOICE CHANNEL DELAY DISTORTION (Manual Sweep - Raw Data)				PAGE _____ OF _____ PAGES	
DATA SHEET T12-2				DATE (Mo., No., Year)	
DESIGN NO.		TEST METHOD USED		TEST ENG SIGNATURE	
TEST POINTS					
DISTANT STATION (XMIT)		LOCAL STATION (RCV)			
3		10			
CHANNEL	SO	2			
	OP	4			
	CH	2			
FREQ	MEASURED RELATIVE DELAY (Microseconds)				
100	3400	2400			
200	2970	1970			
300	2340	1340			
400	1960	960			
500	1725	725			
600	1540	540			
800	1400	400			
1000	1188	180			
1200	1105	105			
1400	1050	50			
1600	1015	15			
1800	1000	0			
2000	1000	0			
2200	1023	23			
2400	1060	60			
2600	1117	117			
2800	1200	200			
3000	1330	330			
3200	1550	550			
3400	2000	1000			
3600	3107	2107			

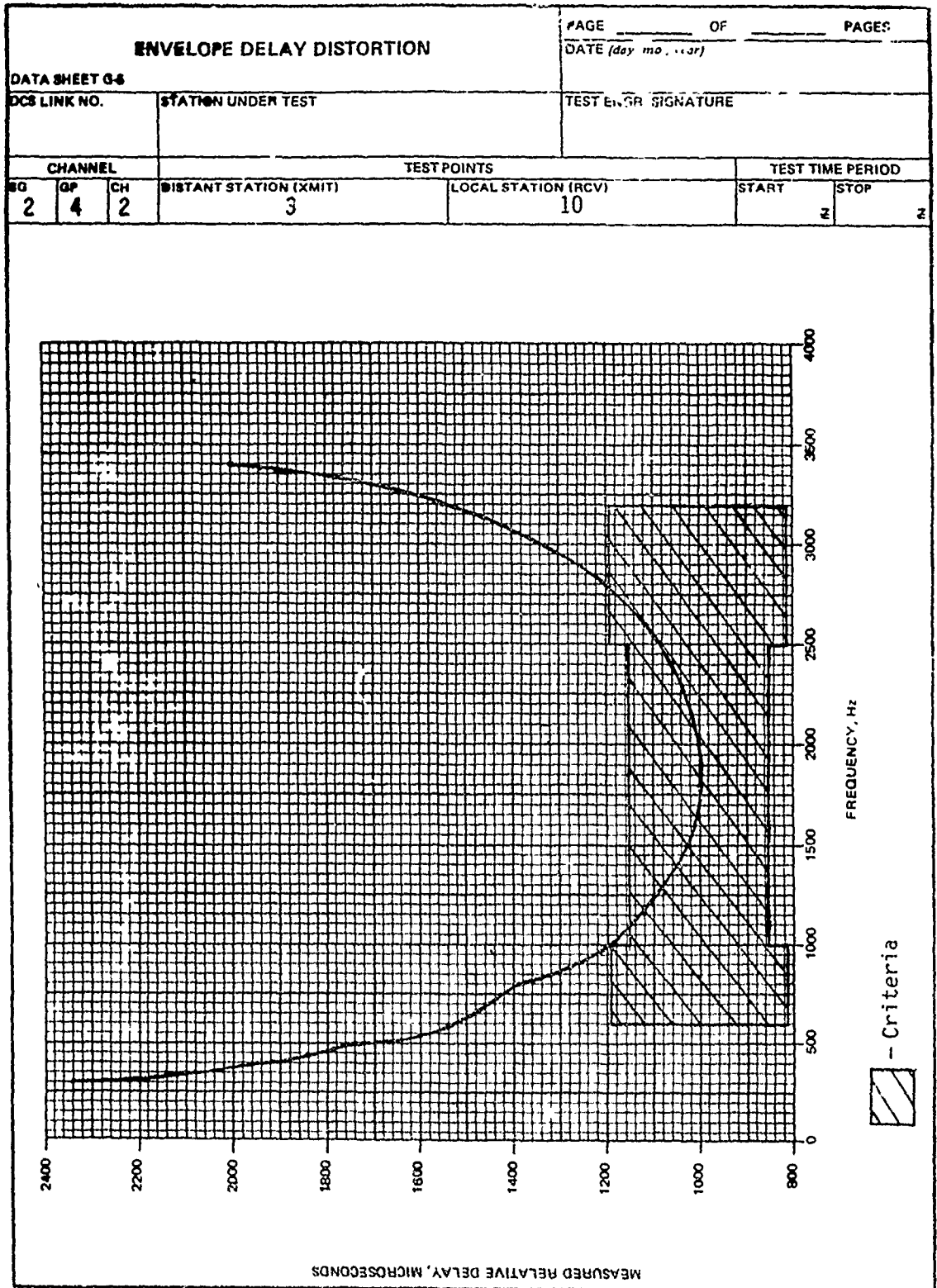


Figure C-29

STROKE CHART FOR RSL RECORDING

Levels		Subtotal	Cumulative	Percentage of time (%)
-26	1	1	1	.9
-26.5	11	2	3	2.7
-27	111	3	6	5.3
-27.5	///	5	11	9.7
-28	/// //	10	21	18.6
-28.5	/// // 1	16	37	32.7
-29	/// // // // //	30	67	59.3
-29.5	/// // // // //	22	89	78.8
-30	/// // 111	13	102	90.3
-30.5	/// 1	6	108	95.6
-31	111	3	111	98.2
-31.5	1	1	112	99.1
-32	1	1		
-32.5				
-33				
TOTAL			113	

Figure C-30

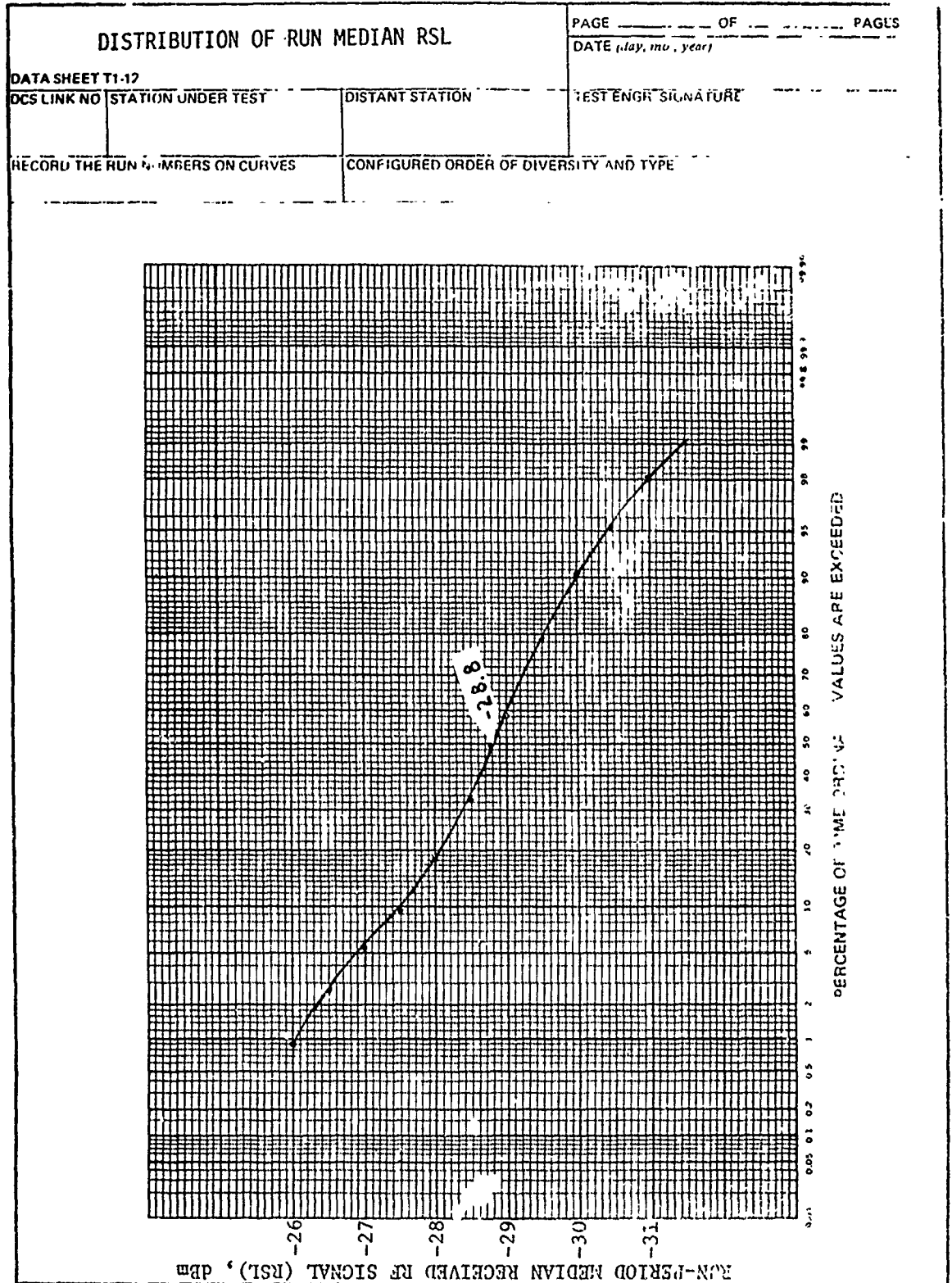


Figure G-31

<p>DISTRIBUTION OF RUN MEDIAN BASEBAND LOADING</p>		<p>PAGE _____ OF _____ PAGES</p>
<p>DATA SHEET T1-14</p>		<p>DATE (day, mo., year)</p>
<p>DCS LINK NO. _____</p>	<p>STATION UNDER TEST _____</p>	<p>TEST ENGR. SIGNATURE _____</p>
<p>RUN NUMBERS</p>		
<p>FROM: _____</p>		
<p>THRU: _____</p>		

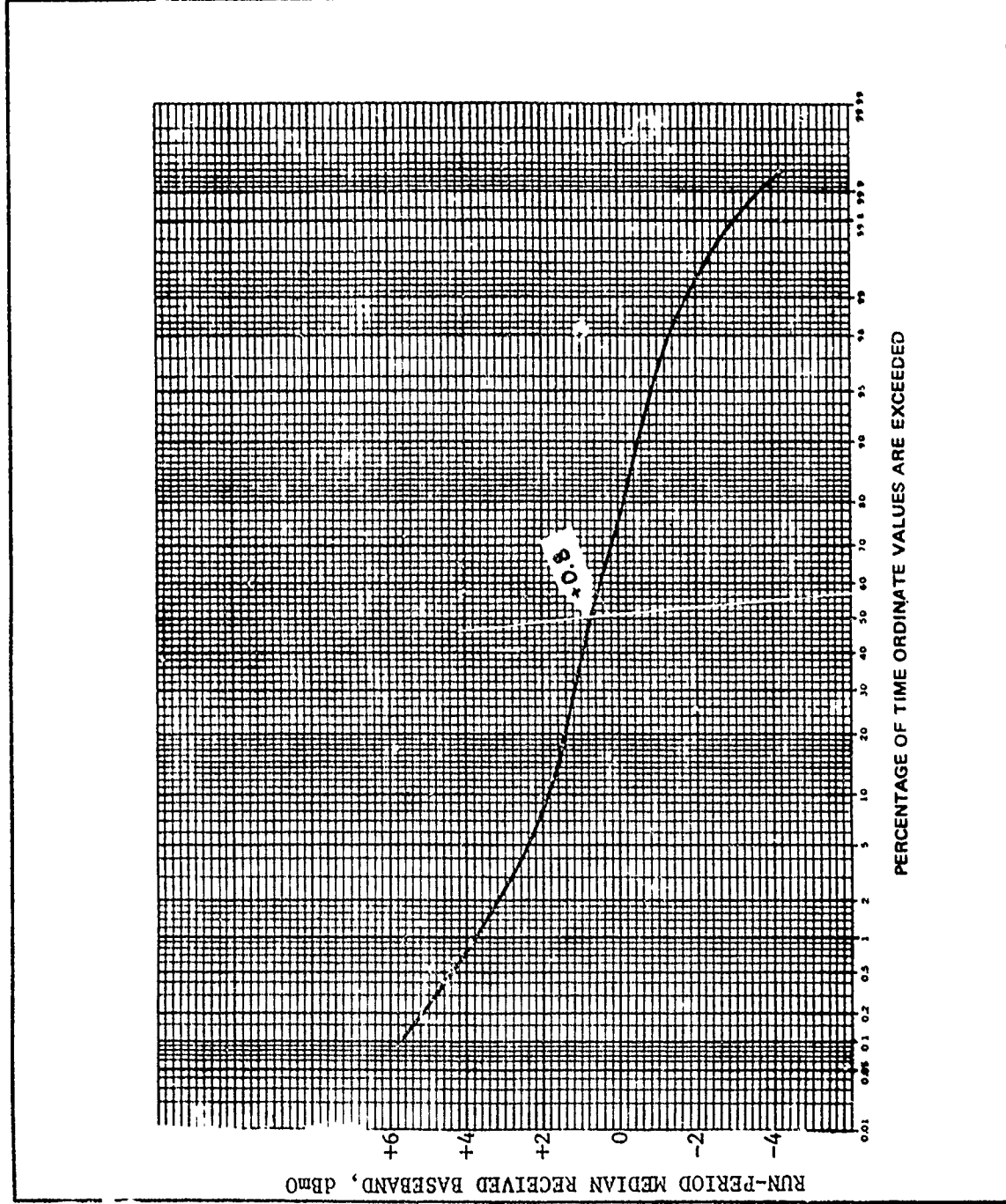


Figure C-32

DISTRIBUTION OF RUN MEDIAN IDLE CHANNEL NOISE (ICN)		PAGE _____ OF _____ PAGES		
		DATE (day, mo., year)		
DATA SHEET T1 14	DCS LINK NO.	STATION UNDER TEST	RUN NUMBERS FROM: _____ THRU: _____	TEST ENGR. SIGNATURE

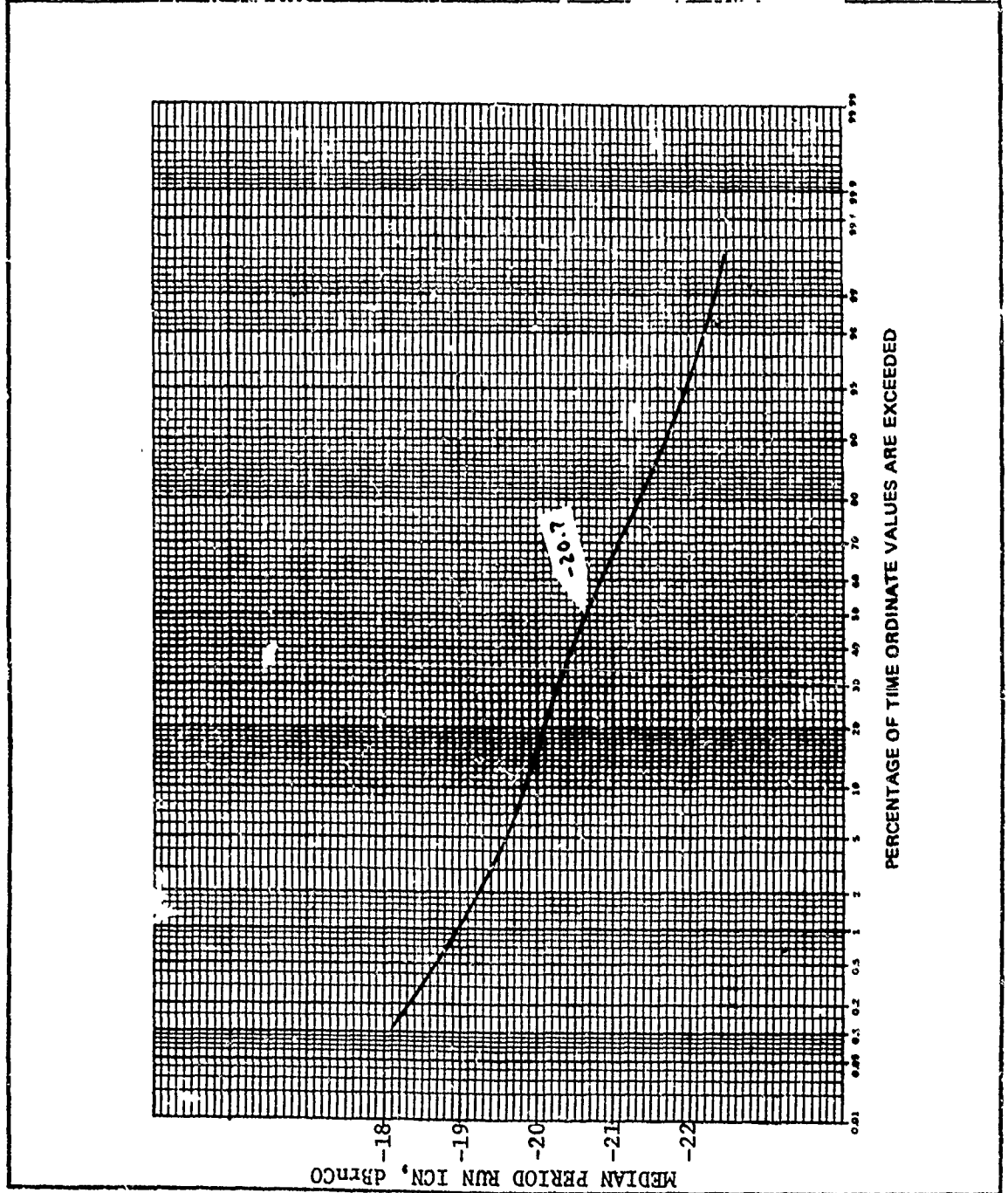


Figure C-33

Data Analysis

Section III - Noise Calculations

C-24

NOISE ANALYSIS

The following is an analysis of Basic Noise Ratio (BNR) and Noise Power Ratio (NPR) in determining actual levels of Basic and Intermodulation noise components. BNR is a S/N in dB of a white noise signal in a slot of certain bandwidth to the level of basic noise present when noise modulation is completely removed and, therefore, no intermodulation noise can be present. NPR is a S/N in dB of a white noise signal in a slot of certain bandwidth to the level of basic noise plus intermodulation noise present when a corresponding slot of white noise is removed from the white noise signal used to load or modulate the system or equipment being tested.

a. To determine the actual levels of basic and intermodulation noise present under various loading conditions, the following factors must be known:

- (1) Level of Noise Load Ratio (NLR) white noise signal used for test.
- (2) Bandwidth of white noise signal.
- (3) Measured BNR.
- (4) Measured NPR.
- (5) Bandwidth of slot desired for analysis. (Note, the bandwidth of the slot used in measuring the BNR or NPR is not required).

b. To determine the actual levels of basic and intermodulation noise the following procedures are used.

- (1) The Bandwidth Ratio (BWR) is calculated based on the bandwidths of the white noise signal and the desired slot for analysis purposes.

CCP 702-1

(2) The level of the basic noise plus intermodulation is calculated in the following manner.

(a) To determine the level of basic noise (BN) in $\text{pW}\emptyset$, convert the BNR to S/N, S/N to $\text{dBm}\emptyset$, $\text{dBm}\emptyset$ to $\text{dBBrn}\emptyset$ and finally converting $\text{dBBrn}\emptyset$ to $\text{pW}\emptyset$.

(b) To determine the level of basic noise plus intermodulation noise in $\text{pW}\emptyset$ the conversion would be the same as in b(1) above.

(c) To determine the level of intermodulation noise in $\text{pW}\emptyset$, subtract the level in $\text{pW}\emptyset$ obtained in b(1) from that in b(2) above.

(d) The level of intermodulation noise in $\text{dBBrn}\emptyset$ or other units can be determined by converting the level of $\text{pW}\emptyset$ to any desired unit.

C-25 NOISE CALCULATION EXAMPLE

White noise NLR = +17.8 $\text{dBm}\emptyset$, bandwidth 60 to 2540 kHz. BNR = 65, NPR = 56. What are the levels of basic and intermodulation noise in $\text{dBBrn}\emptyset$ and $\text{dBm}\emptyset$ in a 3.2 kHz slot?

a. From the above information the BWR = 29 dB $(10 \log \frac{2540 - 60}{3.2})$

b. Basic noise is calculated as follows:

$$\begin{aligned} \text{S/N} &= \text{BNR} + \text{BWR} - \text{NLR} \\ &= 65 + 29 - 17.8 \\ &= 76.2 \text{ dB} \end{aligned}$$

$$\text{dBm}\emptyset = -76.2 \text{ dBm}\emptyset$$

$$\text{dBBrn}\emptyset = -76.2 + 90 = 13.8 \text{ dBBrn}\emptyset$$

$$\text{pW}\emptyset = 24.0 \text{ pW}\emptyset$$

c. Basic plus intermodulation noise is calculated as follows:

$$S/N = NPR + BWR - NLR$$

$$= 56 + 29 - 17.8$$

$$= 67.2 \text{ dB}$$

$$\text{dBm0} = -67.2 \text{ dB}$$

$$\text{dBrn0} = -67.2 + 90 = 22.8 \text{ dBrn0}$$

$$\text{pW0} = 190.6 \text{ pW0}$$

d. Level of intermodulation noise is calculated as follows:

$$\text{pW0} = 190.6 - 24.0 = 166.6 \text{ pW0}$$

$$\text{dBrn0} = 22.2 \text{ dBrn0}$$

$$\text{or } -\text{dBm0} = 22.2 - 90 = -67.8 \text{ dBm0}$$

C-26 Calculated NPR curves based on assumed noise distributions.

a. White noise +17.8 dBm0 (\emptyset NLR) 60 to 2540 kHz

b. 1 kHz slot used for measurements.

c. BWR - 34 dB, BNR - 65 dB

$$\text{White noise level 1 kHz slot } (\emptyset\text{dBm}) = -16 \text{ dBm0}$$

$$\text{Basic noise 1 kHz slot} = -81 \text{ dBm0}$$

NPR calculated from BN above - no IM noise

NLR	-10	-5	0	+5	+10
NOISE	-26	-21	-16	-11	-6
BN	-81	-81	-81	-81	-81
NPR	55	60	65	70	75

NPR calculated from BN and IM noise varying at 1 dB per 1 dB change of NLR, at levels of -81 dBm0, -71 dBm0 and +91 dBm0 at \emptyset NLR.

CCP 702-1

NLR	-10	-5	0	+5	+10
NOISE	-26	-21	-16	-11	-6
BN	-81	-81	-81	-81	-81
IM 1	-91	-86	-81	-75	-71
IM 2	-81	-76	-71	-66	-61
IM 3	-101	-96	-91	-86	-81
BN+IM 1	-80.6	-79.8	-78	-74.8	-70.6
BN+IM 2	-78	-74.8	-70.6	-65.85	-60.9
BN+IM 3	-80.9	-80.85	-80.6	-79.8	-78
NPR 1	54.5	58.8	62	63.8	64.6
NPR 2	52	53.8	54.6	54.85	54.9
NPR 3	54.9	59.85	64.6	68.8	72

NPR calculated from BN and IM noise varying at 2 dB per 1 dB change of NLR at levels of -81 dBm0, -71 dBm0, and -91 dBm0 at 0 NLR.

NLR	-10	-7.5	-5	-2.5	0	+2.5	+5	+7.5	+10
NOISE	-26	-23.5	-21	-18.5	-16	-13.5	-11	-8.5	-6
BN	-81	-81	-81	-81	-81	-81	-81	-81	-81
IM 1	-101		-91	-86	-81	-76	-71		-61
IM 2	-91	-86	-81	-76	-71	-66	-61	-56	-51
IM 3	-111	-106	-101	-96	-91	-86	-81	-76	-71
BN+IM 1	-80.9		-80.6	-79.8	-78	-74.8	-70.6		0.9
BN+IM 2	-80.6	-79.8	-78	-74.8	-70.6	-65.8	-60.9	-56	-51
BN+IM 3	-81	-81	-80.9	-80.8	-80.6	-79.8	-78	-74.8	-70.6
NPR 1	54.9		59.6	61.3	62	61.3	59.6		54.9

NPR 2	54.6	56.3	57	56.3	54.3	52.3	47.9	47.5	45
NPR 3	55	57.5	59.9	62.3	64.6	66.3	67	66.3	64.6

NPR calculated from BN and IM noise varying at 1 dB per 1 dB change of NLR up to \emptyset NLR and 5 dB per 1 dB change above \emptyset NLR. Break point at -81 dBm0, -71 dBm0, -61 dBm0 and -91 dBm0.

NLR	-10	-7.5	-5	-2.5	0	+2.5	+5	+7.5	+10
NOISE	-26	-23.5	-21	-18.5	-16	-13.5	-11	-8.5	-5
BN	-81	-81	-81	-81	-81	-81	-81	-81	-81
IM 1	-91	-88.5	-86	-83.5	-81	-68.5	-56	-43.5	-31
IM 2	-81	-78.5	-76	-73.5	-71	-58.5	-46	-33.5	-21
IM 3	-71	-68.5	-66	-63.5	-61	-48.5	-36	-23.5	-11
IM 4	-101	-98.5	-96	-93.5	-91	-78.5	-66	-53.5	-41
BN+IM 1	-80.6	-80.3	-79.4	-79.2	-78	-68.3	-55.9	-43.5	-31
BN+IM 2	-78	-76.7	-74.8	-72.8	-70.6	-58.5	-46	-33.5	-21
BN+IM 3	-70.6	-68.2	-65.8	-61.4	-59.9	-48.5	-36	-23.5	-11
BN+IM 4	-80.9	-80.9	-80.4	-80.75	-80.6	-76.7	-68.8	-53.5	-41
NPR 1	54.6	56.8	58.8	60.7	62	54.8	44.9	35	25
NPR 2	52	53.2	54.25	54.3	54.6	45	35	25	15
NPR 3	44.6	44.7	44.8	44.9	44.9	35	25	15	5
NPR 4	54.9	57.4	59.9	62.25	64.6	63.2	54.85	45	35

NPR calculated from IM varying at 2 dB change in NLR and equal to BN at \emptyset NLR for BN at levels of -81 dBm0, -71 dBm0 and -91 dBm0. Curves are the same shape as curve 1 of number 3 above with peaks occurring at 62, 52 and 72 on the NPR graph.

Data Analysis

Section IV - Minimum Noise Capability

The MNC is derived from the BNR measured over the link, and added to the multiplex contribution. To do this, it is necessary to convert the BNR's to their respective powers, average, and add the value of their average power to the multiplex contribution. The sum of this operation is then reconverted to dBm, corrected to dBm0 and then overlaid on the composite noise contribution quieting curve. From a typical NPR/BNR data sheet we find that at minimum loading condition the BNR value when converted to dBm units is -82.5 dBm.

Average BNR: So as not to duplicate previous manual conversion routines here, we will go right to the solution:

$$\text{BNR}_{\text{avg}} = -82.5 \text{ dBm} (5.6402945^{-9} \text{ watts})$$

For this example, we will assume the multiplex noise contribution to be 1.26^{-14} watts. The nominal multiplex noise contribution obtained from that listed in Appendix E of this document. Adding the multiplex contribution to the BNR_{avg} causes only a minute increase in the total noise power. We then end up with a fully quieted minimum noise capability (in a nonloaded condition) of:

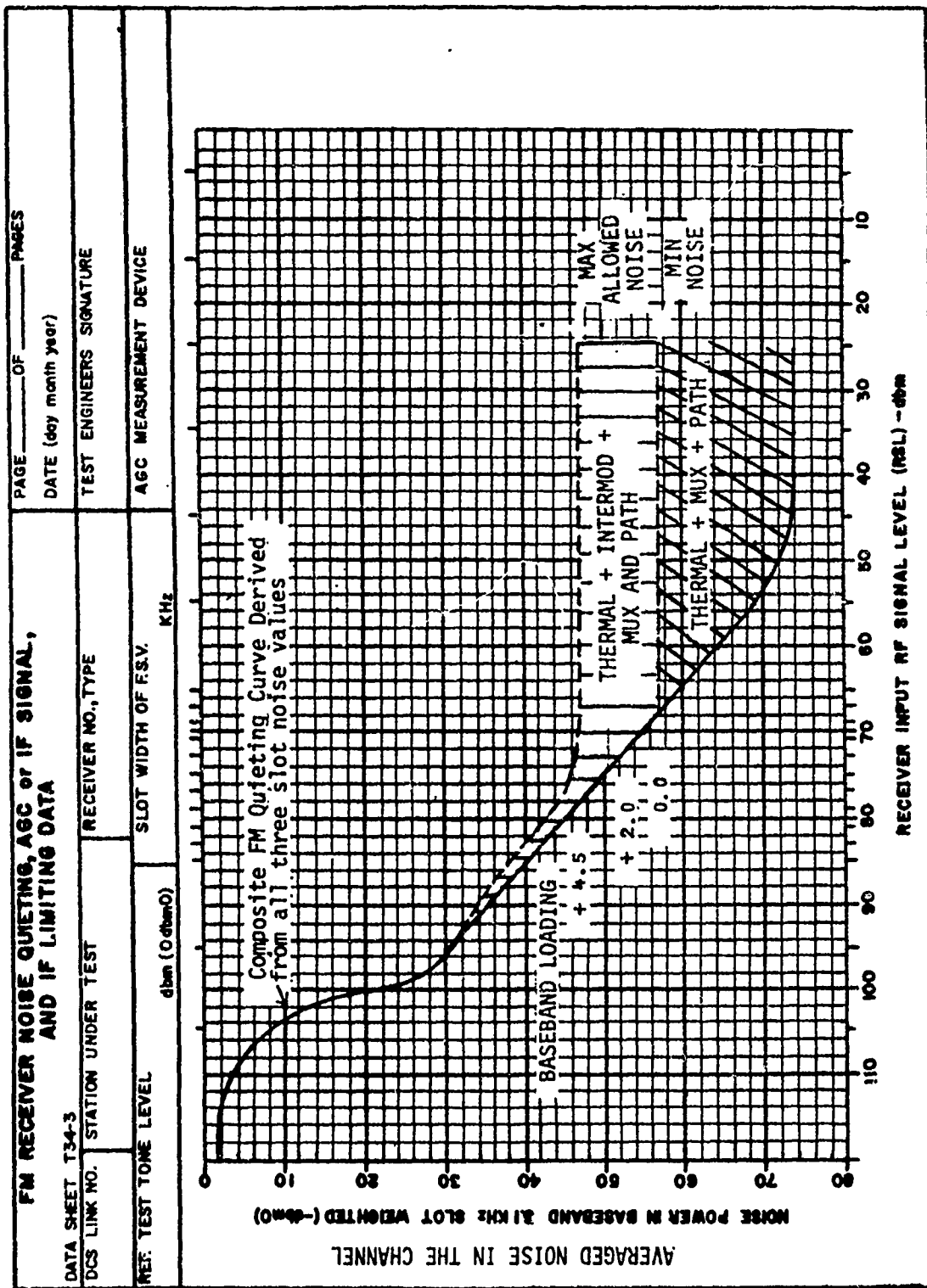
$$\begin{aligned} \text{MNC} &= -82.5 - (-25) \\ &= -57.5 \text{ dBm0 (as measured across the baseband/averaged)} \end{aligned}$$

NOTE: -25 dBm = 0 dBm0 at the baseband

This value can now be plotted across the composite noise quieting curve as shown in Figure C-34. This brings us to a

CCP 702-1

problem which has plagued the user's of 3 kHz flat idle channel noise weighting. The power supply ripple content has a direct bearing on precisely what level of noise signal will be measured in the channel output. We will not debate the effects of the ripple signal on other analog signals present in the channel, but will provide an approximation table for determining the effects of ripple, and how it will effect the output of the channel. The Ripple Correction Graph, is provided as Figure C-35 to this appendix. The correction factor derived from this table should be added algebraically to the computed noise figures.



Composite Noise Contribution Quieting Curve

Figure C-34

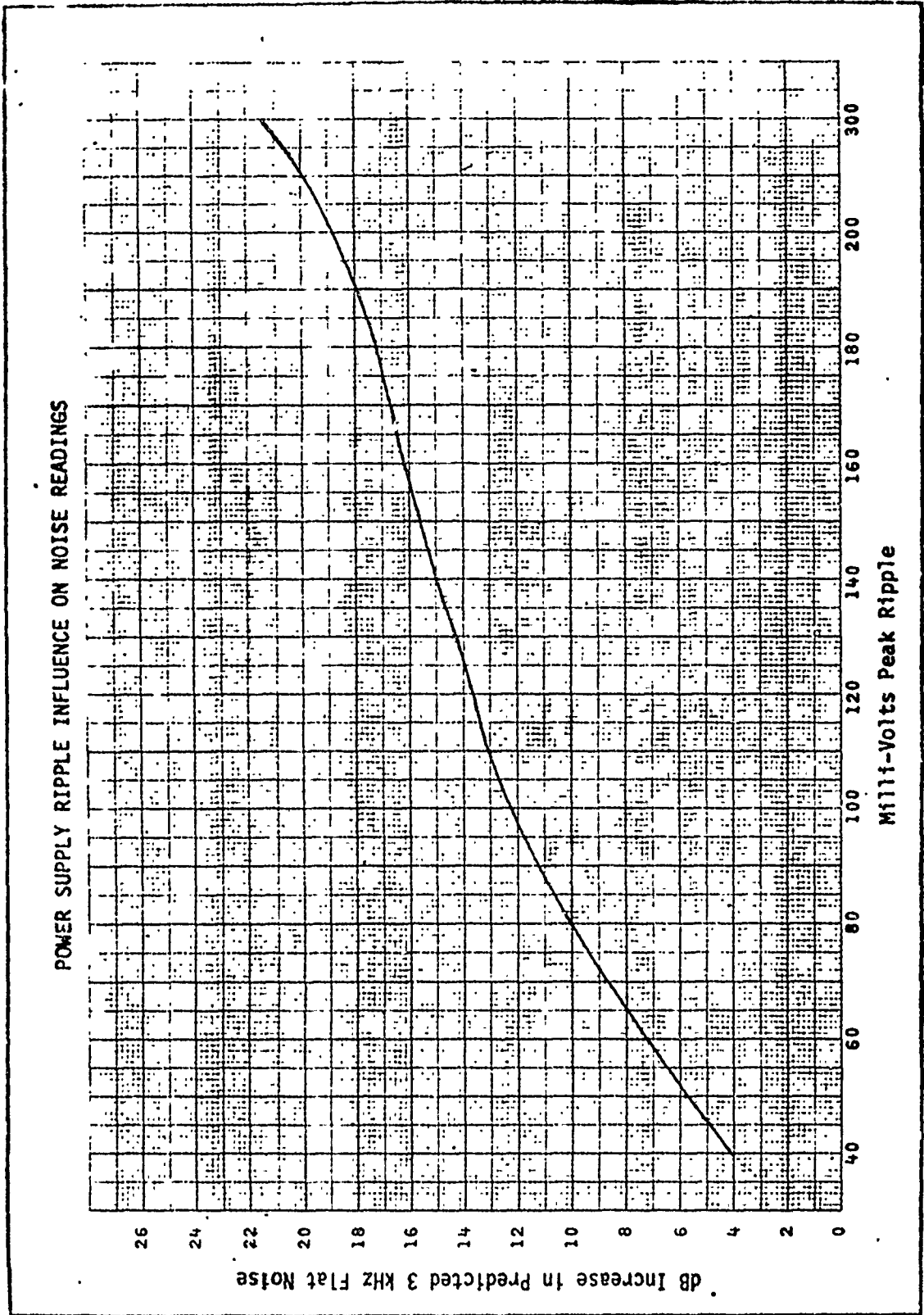


Figure C-35

APPENDIX C

Data Analysis

Section V - Fault Isolation

C-27 FACTORS TO BE CONSIDERED

a. There are basically four or five key tests that can influence the test data for the majority of the tests accomplished by the TEP Teams. During the course of the evaluation, unsatisfactory or questionable results from one of the key tests will necessitate performing additional diagnostic routines to determine the specific cause of the departure from expected values. The method used in isolating a problem will vary from team to team depending on the nature of the problem and methodology used during the isolation process. Regardless of the technique used, each team must develop a systematic and routine method to be used to identify, isolate and correct problems noted during the evaluation.

b. The following factors and sequences are provided as a guide during the process of isolating an anomaly during the evaluation.

(1) Receive Signal Level

- (a) Path Loss
- (b) Antenna Orientation
- (c) Transmission Line Loss
- (d) Transmit Power

(2) Receiver Quieting Characteristics

- (a) Demodulated Baseband Level
- (b) Receiver Noise Figure
- (c) Receiver IF Bandwidth & Insertion Loss

CCP 702-1

- (d) Demphasis Characteristics
 - (e) Radio Interference (Internal & External)
 - (f) Receiver AGC Voltage and Gain
 - (g) IF Amplifier Gain and Linearity
 - (h) Receiver Limiting Action
 - (i) Mixer Noise Figure
- (3) Radio Equipment Noise Power Ratio (NPR)
- (a) Symmetry of Receiver and Transmitter Bandwidth
 - (b) Modulator Linearity
 - (c) Demodulator Linearity
 - (d) Discriminator Characteristics
 - (e) Receiver and Transmit Frequency
 - (f) Receiver Limiter Action
 - (g) Amplifier Distortion
 - (h) Mixer Characteristics
- (4) Link Noise Power Ratio (NPR)
- (a) Combination of: (1), (2), and (3)
 - (b) Waveguide Echoes
 - (c) Transmission Multipath
 - (d) Radio Interference
 - (e) Spurious Emissions
- (5) Baseband Response
- (a) Impedance Mismatches
 - (b) Baseband Filter Response

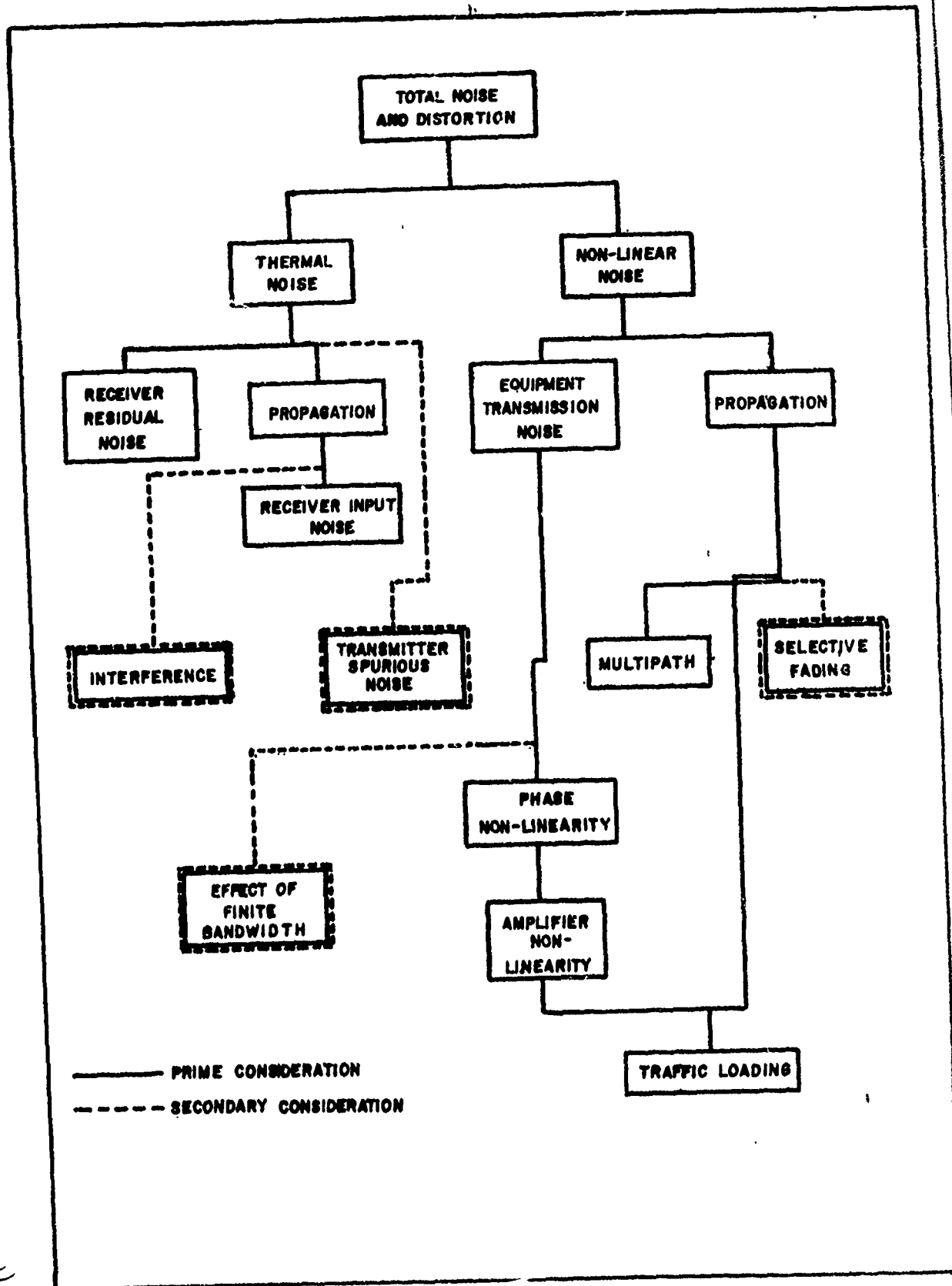


Figure C-36

- (c) Amplifier Gain and Tracking
- (d) Composite Levels
- (6) Idle Channel Noise
 - (a) Receive Signal Level , (1) through (5)
 - (b) Channel Modems
 - (c) Group Modems
 - (d) Improper Levels
 - (e) Capacitive and Inductive Coupling
 - (f) Distortion
 - (g) Ground Loops
 - (h) Ripple Voltage from Power Units
 - (i) Carrier Leak
 - (j) Switching Equipment
 - (k) Improper Combiner Operation

c. The list of potential problems that may be encountered is seemingly endless and the above contains only a few of those items that would be readily apparent. The team chiefs are encouraged to expand and modify the list, to include a logical priority, and submission of their recommendations for updating this appendix.

d. Figure C-36 reflects the primary and secondary factors to be considered when the test data departs from the expected value.

Final Analysis of the Test Data

Section I - Instruction

D-1 GENERAL

- a. The post mission analysis consists simply of arranging the data taken during an evaluation in a manner that permits a logical summary of the overall link performance. This procedure will provide a review of the measured data on which the team chief can base his cover letter. Furthermore, it will place emphasis once again on the "weak" spots in the system that will require further maintenance actions.
- b. Figure D-1 provides a comparison of the measured individual receiver RSLs to the predicted and the expected. The predicted RSL is that RSL obtained during the path calculations. The expected RSL is a value calculated as in the path calculations only with the actual measured distant end transmit power considered. It should be remembered that when frequency diversity is utilized a given receiver's RSL is affected only by the output power of the transmitter of the same frequency; with space diversity a given receiver's RSL is affected by the output power of each transmitter; and if space and polarization diversity is used, a given receiver's RSL is affected almost entirely by the output power of the transmitter with the same polarity. These factors should be considered when calculating the expected RSL.

- c. Figure D-2 compares the measured quieting curve data with the predicted and the expected results. Part I of this figure lists the RSL (on the linear portion of the curve) on which the analysis will be made. The predicted values are those values calculated and obtained as outlined in Appendix B of this document. The expected value is calculated in the same manner except that the values actually measured for noise figure are used in the calculations.
- d. Figure D-3 provides a comparison of results obtained from BNR data to the quieting data. The median RSL is that RSL measured during the period that the BNR data was recorded. Part II of this figure is a summary of all of the BNR data converted to dBm0 by the method discussed in Appendix C of this document. Part III of the figure summarizes the single receiver thermal noise obtained from the quieting curves at the same median RSL measured when collecting the loopback BNR data.
- e. Figure D-4 is basically the same as Figure D-3 except in this case the link BNR is compared to the thermal noise obtained from the quieting curves.
- f. Figure D-5 is a summary of the thermal noise data after combining. Part I of this figure presents the combined thermal noise calculated in the path calculations. Part II gives the median RSL for the test period. The expected combined thermal noise is based on the link BNR data (or quieting data) and the

predicted combiner action at the given RSL. With equal signal to noise ratios in all receivers, the improvement due to the combiner is theoretically; 3 dB for dual diversity and 6 dB for quad diversity. Part III of Figure D-5 presents the measured combined thermal noise based on BNR data measured through the combiner. Part IV is the combined thermal noise adjusted by the amount of thermal noise at the median RSL from the thermal noise at the test period RSL.

- g. Figure D-6 is a summary of the measured loopback intermodulation noise compared to the value calculated in the path calculations. The measured intermodulation data is based on CCIR white noise loading.
- h. Figure D-7 is a summary of the link combined intermodulation noise. Part I of this figure is based on data measured with the system CCIR white noise loaded. Part II is based on data measured with the system loaded with the median baseband loading for the evaluation period.
- i. Figure D-8 summarizes the multiplex noise measurements under idle and loaded conditions. Part I compares the measured and predicted idle multiplex noise. The predicted value is obtained from the manufacturer's specifications. Part II compares the measured and predicted noise in a loopback configuration. One value is listed for the multiplex fully loaded and one value for the multiplex under present loading conditions. Part III

compares the multiplex noise measured over the link to the predicted value. The multiplex noise is measured under fully loaded conditions and loaded for the present multiplex configuration.

- j. The ultimate objective of the evaluation is a summary of the total idle channel noise. The predicted value is obtained directly from the path calculations. The predicted value is compared to the median ICN from the strip chart recordings and the measured ICN calculated from the measured multiplex and radio noise. This last value is the sum of radio combined thermal noise (at the median RSL), the median radio intermod noise with present loading and the link multiplex noise with present loading. This value is to be used only for correlation with the measured idle channel noise. (Actual median).
- k. When these procedures are completed, the team chief should be able to arrive at a conclusion as to the systems noise performance. Any problems that might have been overlooked during the evaluation should become evident. From these data forms the team chief should be able to easily complete the evaluation cover letter.

RECEIVE SIGNAL LEVEL

1. Distant Station Output Power

a. Predicted (T.O. specification) _____ dBm

b. Measured:

Tx #1 _____ dBm _____ dBm

2. Receive Signal Level

a. Predicted (from Path Calculations) _____ dBm

b. Expected (Based on calculations using measured power from distant station transmitter)

Rx #1 _____ dBm Rx #2 _____ dBm Rx #3 _____ dBm Rx #4 _____ dBm

c. Measured (Median from Strip Chart Data):

Rx #1 _____ dBm Rx #2 _____ dBm Rx #3 _____ dBm Rx #4 _____ dBm

RADIO THERMAL NOISE

1. RSL (on linear portion of curve) used to perform the analysis _____ dBm
2. Receiver front end noise at the RSL above (based on calculations performed prior to mission)
 - a. Low Slot _____ dBm
 - b. Mid Slot _____ dBm
 - c. High Slot _____ dBm

3. Expected receiver front end noise (calculated with measure NF considered) (dBm)

	<u>LOW SLOT</u>	<u>MID SLOT</u>	<u>HIGH SLOT</u>
Rcvr #1	_____	_____	_____
Rcvr #2	_____	_____	_____
Rcvr #3	_____	_____	_____
Rcvr #4	_____	_____	_____

4. Receiver front end noise (measured from quieting curves) (dBm)

	<u>LOW SLOT</u>	<u>MID SLOT</u>	<u>HIGH SLOT</u>
Rcvr #1	_____	_____	_____
Rcvr #2	_____	_____	_____
Rcvr #3	_____	_____	_____
Rcvr #4	_____	_____	_____

5. Receiver fully quieted noise (from path calculations) _____ dBm

6. Receiver fully quieted noise (from quieting curves)

HIGH SLOT

Rcvr #1

Rcvr #2

Rcvr #3

Rcvr #4

LOOPBACK BNR VERSUS QUIETING DATA

1. Median RSL (during period BNR data was measured) _____ dBm

2. Single receiver loopback thermal noise (based on BNR converted to dBm0)

	<u>LOW SLOT</u>	<u>MID SLOT</u>	<u>HIGH SLOT</u>
Tx #1 to Rx #1	_____	_____	_____
Tx #1 to Rx #2	_____	_____	_____
Tx #1 to Rx #3	_____	_____	_____
Tx #1 to Rx #4	_____	_____	_____
Tx #2 to Rx #1	_____	_____	_____
Tx #2 to Rx #2	_____	_____	_____
Tx #2 to Rx #3	_____	_____	_____
Tx #2 to Rx #4	_____	_____	_____

3. Single receiver thermal noise from quieting curves (at RSL stated above) (dBm0)

	<u>LOW SLOT</u>	<u>MID SLOT</u>	<u>HIGH SLOT</u>
Rcvr #1	_____	_____	_____
Rcvr #2	_____	_____	_____
Rcvr #3	_____	_____	_____
Rcvr #4	_____	_____	_____

LINK BNR VERSUS QUIETING DATA

1. Median RSL (during the period link BNR was measured) _____ dBm

2. Single receiver link thermal noise (based on link BNR converted to S/N) (dBm0)

	<u>LOW SLOT</u>	<u>MID SLOT</u>	<u>HIGH SLOT</u>
Dist Tx # ___ to Local Rx # ___	_____	_____	_____
Dist Tx # ___ to Local Rx # ___	_____	_____	_____
Dist Tx # ___ to Local Rx # ___	_____	_____	_____
Dist Tx # ___ to Local Rx # ___	_____	_____	_____

3. Single receiver thermal noise from quieting curve data (at RSL stated above) (dBm0)

	<u>LOW SLOT</u>	<u>MID SLOT</u>	<u>HIGH SLOT</u>
Rcvr #1	_____	_____	_____
Rcvr #2	_____	_____	_____
Rcvr #3	_____	_____	_____
Rcvr #4	_____	_____	_____

COMBINED THERMAL NOISE

1. Receiver thermal noise after combining (from path calculations) _____ dBm
2. RSL (during test period) _____ dBm
3. Expected combined thermal noise (based on single receiver thermal noise and predicted combiner action using above RSL)
 - a. Low Slot _____ dBm
 - b. Mid Slot _____ dBm
 - c. High Slot _____ dBm
4. Measured combined thermal noise (based on BNR converted to S/N)
 - a. Low Slot _____ dBm
 - b. Mid Slot _____ dBm
 - c. High Slot _____ dBm
5. Measured combined thermal noise (extrapolated to the median evaluation period RSL)
 - a. Low Slot _____ dBm
 - b. Mid Slot _____ dBm
 - c. High Slot _____ dBm

LOOPBACK RADIO INTERMODULATION NOISE

CCP 702-1

- 1. CCIR loading _____ dBm0
- 2. Loopback intermodulation noise (predicted from path calculations) _____ dBm0
- 3. Loopback intermodulation noise (measured, based on CCIR loading) (dBm0)

	<u>LOW SLOT</u>	<u>MID SLOT</u>	<u>HIGH SLOT</u>
Tx #1 to Rx #1	_____	_____	_____
Tx #1 to Rx #2	_____	_____	_____
Tx #1 to Rx #3	_____	_____	_____
Tx #1 to Rx #4	_____	_____	_____
Tx #2 to Rx #1	_____	_____	_____
Tx #2 to Rx #2	_____	_____	_____
Tx #2 to Rx #3	_____	_____	_____
Tx #2 to Rx #4	_____	_____	_____

Figure D-6

LINK COMBINED INTERMODULATION NOISE

1. Link combined intermodulation noise (based on link NPR and CCIR loading) (dBm0)

	<u>LOW SLOT</u>	<u>MID SLOT</u>	<u>HIGH SLOT</u>
Dist Tx #1	_____	_____	_____
Dist Tx #2	_____	_____	_____

2. Link combined intermodulation noise (based on link NPR and median loading) (dBm0)

	<u>LOW SLOT</u>	<u>MID SLOT</u>	<u>HIGH SLOT</u>
Dist Tx #1	_____	_____	_____
Dist Tx #2	_____	_____	_____

MULTIPLEX NOISE

CCP 702-1

1. Loopback idle multiplex noise

Predicted (manufactures's specs) _____ / _____ dBrn0/dBrnCO

Measured _____ / _____ dBrn0/dBrnCO

2. Loopback loaded multiplex noise

Predicted (path calculations) _____ / _____ dBrn0/dBrnCO

Measured (fully loaded) _____ / _____ dBrn0/dBrnCO

3. Link multiplex noise

Predicted _____ / _____ dBrn0/dBrnCO

Measured, thermal only _____ / _____ dBrn0/dBrnCO

Measured, present loading _____ / _____ dBrn0/dBrnCO

Measured, fully loaded _____ / _____ dBrn0/dBrnCO

Figure D-8

APPENDIX D

Final Analysis of the Test Data

Section III - Notes on Tests & Forms

D-2 NOTES

This appendix relates only to certain forms which have been shown by past experience to be ambiguous.

- a. T-3 IN SERVICE CUSTOMER LEVELS: Currently this test is only performed on continuous traffic channels such as tone packs, etc. Selected voice channels can be measured to observe peak levels after it has been determined that the channel is in use by using the bridging jacks.
- b. T-4 1 kHz TEST TONE LEVELS: When filling out form T 4-2, it is important to retrieve the proper data from station diagrams. TP 2, 3, 10 and 11 present no identification difficulties. In identifying TP 4, 5, 8 and 9, several points may offer GP and SGP appearances.

REMEMBER THAT:

TP 4: Input of GP Modulator

TP 5: Input of SGP Modulator

TP 8: Output of SGP Demodulator

TP 9: Output of GP Demodulator

Do not be confused by associated filters, injection units, or amplifiers prior to the modulators and demodulators.

In some cases the test points do not appear on a jack field. Instead, they may be bridging test points isolated from the point of interest. These test points may require FSVM settings other than the design input impedance of the Mod/Demod units and yield levels difference from those

CCP 702-1

at the input or output. Always reference these levels to the manufacturer's specifications. As an example:

TP 4: Manufacturer's specifications 135 Ω -35 dBm

This is the 0 dBm0 level. However, the monitor point will give a -60 dBm with the FSVM in 75 Ω terminate.

Use the manufacturer's specifications in the appropriate blocks. If the -10 dBm0 tone is measured at -70 dBm at the monitor point, place -45 dBm on the data sheet. If the -10 dBm0 tone reads -69.5 dBm at the monitor point; place -44.5 dBm on the data form.

TLP dBm0 line is for the manufacturer's specification at the 0 dBm0 level.

TLP dBm line must reflect 0 dBm0 plus standard test tone for the test (usually -10 dBm0). Thus, if TLP dBm0 was -25 dBm and standard test tone is -10 dBm0, TLP dBm would be -35 dBm.

The -dBm column is where the measured tone level is recorded. The dev. column is the difference \pm between the - dBm value and the TLP dBm value.

c. T-8 IDLE CHANNEL NOISE: When filling out T 8-2, the TLP [Reference Test Tone Signal Power (ST)] is the 0 dBm0 level from T 4-2.

Relative Test Signal Power (ST) is -10 (0 dBm0 + -10)

S_m is the measured received level of the channel. If performed the same day as T-4, the data need not be reverified.

d. T-9 IDLE CHANNEL IMPULSE NOISE: When completing T 9-2, ST, S'T, and S_m are the same as T 8-2.

Present method for TED is take ICN data in voice band (C-Message).

The high count setting is never less than 72 dBrnC0 (DCA specification 15 or less counts exceeding 72 dBrnC0).

Data channels should be tested in flat weighting.

e. T-15 VOICE CHANNEL FREQUENCY TRANSLATION: Current TED practice is to utilize the square wave method outlined in AFCS 100-61 series manuals for voice channel testing.

If "No frequency translation is observed", so state on cover sheet. It is not necessary to fillout form.

f. T-19 DATA ERROR RATE: A "run" is defined as a period between printer readouts. Since combined RSL cannot be obtained (with a pre-detection combiner) BER vs % time is plotted instead.

g. T-23 LINK NPR VS BASEBAND LOADING: When filling out form T 23-1, observe the following. (Numbers are keyed to example inclosed, Figure D-9)

1. Manufacturer's specification 0 dBm0 of point where voice generator is connected.

2. Manufacturer's specification 0 dBm0 of point where noise receiver is connected.

3. DCA loading $-10 + 10 \log N$

NOTE: If the system was designed for CCIR loading, place this data on the cover sheet as additional data.

4. 1. + 3.

5. 2. + 3.

6, 7, 9 - 12. Values taken from Marconi equipment. 9 - 11 are those

values listed in DCAC 310-70-57, Suppl 1, for a specific channel capacity.

8. 3.1 kHz

13 - 20. Measured data at DCA loading.

NOTE: If the system was designed for CCIR loading place NPR/BNR data on cover sheet in tabular form as additional data.

21. Measured 0 dBmO receive. (i.e. distant end loads transmit test point with white noise to the level of item 1. The level is measured with an RMS voltmeter at the receive end. The measured value goes in item 21.

22. This is the median RSL of the receiver during the test. On Tropo, this is best taken from the chart recordings. On LOS, a panel meter or dc voltage from which RSL can be obtained will be adequate if chart recordings are not available.

23. Measured deviation at time of test.

24. Engineered. specified deviation for the link.

25 - 26. Mark appropriate blocks to identify the path on which data is taken.

NOTE: For items 13 - 20, NPR is read to nearest 1/2 and BNR to the nearest dB.

26. On some systems it has been found that the NPR's were so poor at design loading that the noise test set had to be re-referenced. Whenever necessary, reference the instrument so that the actual NPR's can be read rather than through extrapolation.

h. T-24 BASEBAND LEVEL VS FREQUENCY RESPONSE: Transmitter and receiver

baseband levels (BB level in ____ dBm, BB level out ____ dBm) are manufacturer's specified levels at the point test equipment is attached to collect the data. Reference is taken at 100 kHz, whatever the receive level is for 100 kHz becomes 0 dBm0 for the purposes of plotting the graph and all data in the dBm0 column are referenced to 100 kHz receive levels.

NOTE: For systems less than 120 channels use 70 kHz as reference.

i. T-25 SPURIOUS FREQUENCY SIGNALS: Test conditions I, III & IV are observed.

Performing condition II depends upon the number of channels and terminations available.

V, VI & VII depend upon radio configuration and availability of turn-around mixer.

If "No spurious emissions are observed", so state on cover sheet.

j. T-34 QUIETING CURVES: When filling out T 34-2, the Reference Test Tone Level is measured by having the distant end send 0 dBm0 using the F in or F_p used for measuring deviation.

The RSL is measured in 5 dB steps except around calculated threshold.

Example: If calculated threshold is -79 dBm data is taken at 85, 83, 80, 79, 78, 77, 75 to get a more accurate plot in the area of interest. The threshold taken from the graph should also be calculated from the raw test data to insure that the data has been accurately plotted.

RADIO LINK NPR V₆ BASEBAND LOADING					PAGE _____ OF _____ PAGES															
DATA SHEET T23-1					DATE (Day Month Year) _____															
LINK NO.		STATION UNDER TEST		DISTANT STATION		TEST ENGINEER SIGNATURE														
BASEBAND TEST POINT LEVELS			DCA BASEBAND LOADING LEVEL			RECEIVER														
TRANSMITTER		RECEIVER		CALCULATED		XMIT TEST POINT		RCVR TEST POINT		A		B		A+B						
1 dbm		2 dbm		3 dbm		4 dbm		5 dbm						25						
BASEBAND LIMIT FILTERS			SLOT BANDWIDTH			SLOT FREQUENCIES USED FOR TEST						XMIT								
HIGH PASS		LOW PASS					LOWER		CENTER		UPPER		EXTRA		A		B		A+B	
6 KHz		7 KHz		8 KHz			9 KHz		10 KHz		11 KHz		12 KHz						26	
RECEIVE BASEBAND LEVEL				NOISE POWER RATIO				BASIC NOISE RATIO												
(Meas) 21 dbm				LOWER		CENTER		UPPER		EXTRA		LOWER		CENTER		UPPER		EXTRA		
				13 db		14 db		15 db		16 db		17 db		18 db		19 db		20 db		
RECEIVE SIGNAL LEVEL				TRANSMITTER DEVIATION				STANDARD DEVIATION (SPECIFICATION)												
22 dbm				23 KHz RMS				24 KHz RMS												
— NPR/BNR MEASUREMENTS —																				
NOISE LEVEL		LOWER SLOT			CENTER SLOT			UPPER SLOT			EXTRA									
dbm0		ATTEN.	NPR	BNR	ATTEN.	NPR	BNR	ATTEN.	NPR	BNR	ATTEN.	NPR	BNR							
-10																				
-8																				
-6																				
-4																				
-2																				
0																				
2																				
4																				
6																				
8																				
10																				
12																				
14																				
16																				
18																				
20																				
22																				
24																				
26																				

Figure D-9

TABLE E-1

MULTIPLEX EQUIPMENT-PACIFIC

AN/FCC-55	AN/FCC-7	AN/TCC-13
MX-106	AN/FCC-1	AN/FCC-21
AN/TCC-13	AN/UCC-4	AN/FCC-17
AN/FCC-18	AN/TCC-7	AN/FCC-55
AN/TCC-50	TCS-600 (AN/FCC-18)	AN/FCC-67
AN/FCC-67	AN/TCC-20	
AN/FCC-3A		

TABLE E-2

MULTIPLEX EQUIPMENT-CONUS

AN/FCC-55	MX-103	45BX2
AN/FCC-18	MX-106	

TABLE E-3

MULTIPLEX EQUIPMENT-EUROPE

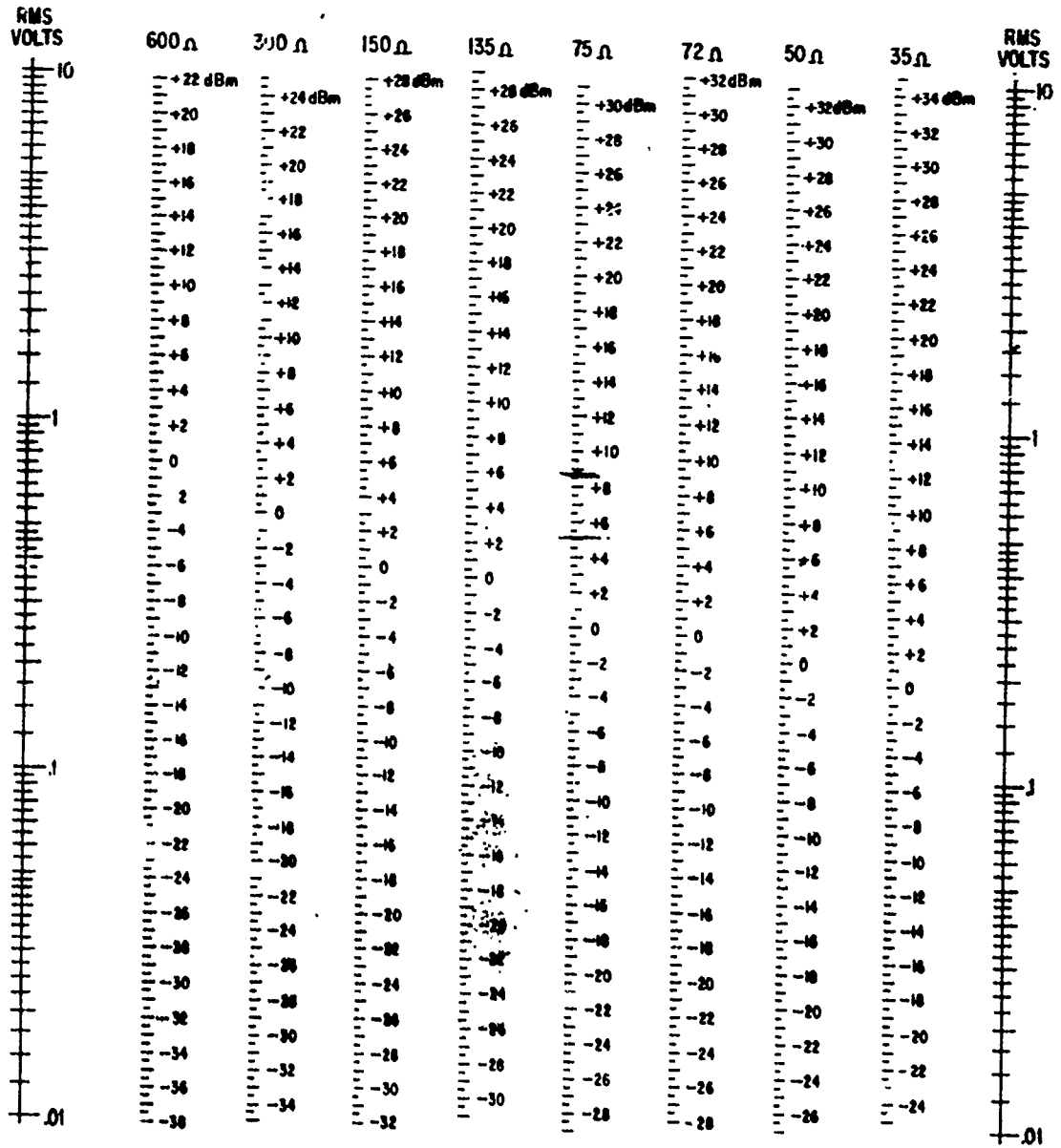
AN/UCC-18 (TCS-600)	Siemens VZ-12
AN/UCC-4	Siemens VZ-60

NOMINAL MULTIFLEX NOISE CONTRIBUTION

TYPE MULTIFLEX	CONTRIBUTION IN PICOWATTS		NOMINAL
	MINIMUM	MAXIMUM	
*AN/FCC-55	126	252	189
*AN/FCC-17	126	252	182
*AN/FCC-18	600	1590	730
*AN/FCC-32	300	560	430
*AN/FCC-58	425	910	667
*AN/MCC-12	140	252	180
*AN/TCC-13	126	252	189
*AN/UCC-2	126	252	183
*AN/UCC-4	126	252	182
A.T.E	420	1950	790
K-Type	110	190	140
L-Type	115	125	117
MX-106	200	500	350
RS-1 (NKC)	250	1100	450
VZ-12/V60-120FU	270	800	357
45BX	150	380	265

*NOTE: FCC/MCC/UCC family of equipment is capable of providing channel to channel noise contributions of less than 100 picowatts, when peak power supply ripple content is less than 40 milli-volts peak

TABLE E-5
 IMPEDANCE OF LOAD



IMPEDANCE OF LOAD

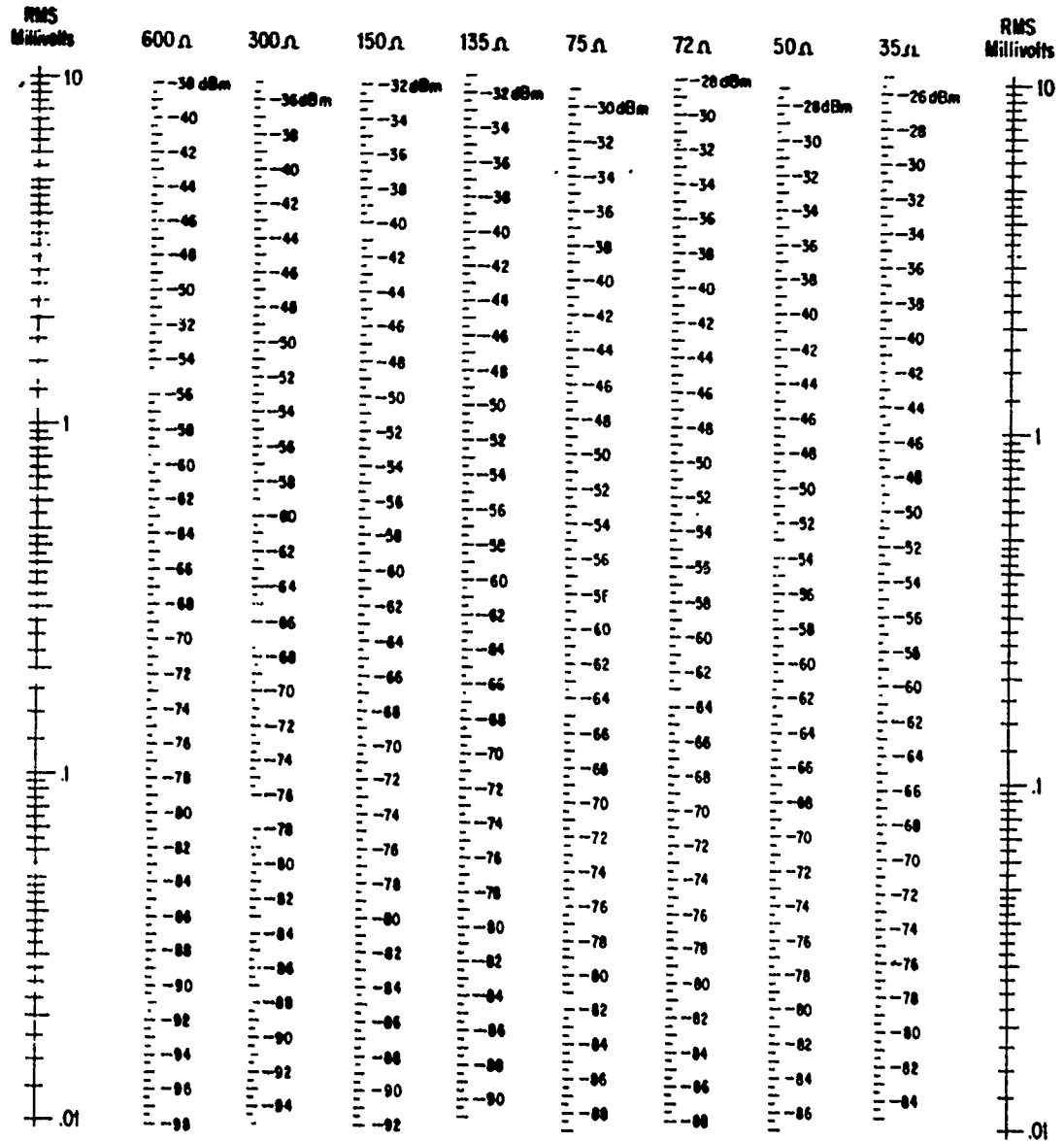


TABLE E-6

MULTIPLEX TRANSLATION

This table provides a ready reference source for determining the channel, group, supergroup and baseband frequency as the signal is translated within the multiplex equipment. The translated pilot frequencies are also included and are typical of the majority of equipment that will be encountered.

Frequencies of 1-Kc Channel Test Tones in the Group, Supergroup, and Line Frequency Bands

		TRANSLATED TEST TONE FREQUENCY, KC													
G R O U P	C H A N	GR BAND	SGR BAND	SGR IN THE LINE FREQUENCY BAND											
				*1	1	2	3	4	5	6	7	8	9	10	
				1	1	107	313	251	299	313	803	1051	1299	1547	1795
	2	103	317	247	295	317	799	1047	1295	1543	1791	2039	2287	2535	
	3	99	321	243	291	321	795	1043	1291	1539	1787	2035	2283	2531	
	4	95	325	239	287	325	791	1039	1287	1535	1783	2031	2279	2527	
	5	91	329	235	283	329	787	1035	1283	1531	1779	2027	2275	2523	
	6	87	333	231	279	333	783	1031	1279	1527	1775	2023	2271	2519	
	7	83	337	227	275	337	779	1027	1275	1523	1771	2019	2267	2515	
	8	79	341	223	271	341	775	1023	1271	1519	1767	2015	2263	2511	
	9	75	345	219	267	345	771	1019	1267	1515	1763	2011	2259	2507	

*Not a standard frequency allocation for Multiplexer Set AN/UCC-4(V)

Frequencies of 1-Kc Channel Test Tones in the Group,
Supergroup, and Line Frequency Bands (Cont)

		TRANSLATED TEST TONE FREQUENCY, KC													
G R O U P	C H A N	GR BAND	SGR BAND	SGR IN THE LINE FREQUENCY BAND											
				*1	1	2	3	4	5	6	7	8	9	10	
	10	71	349	215	263	349	767	1015	1263	1511	1759	2007	2255	2503	
	11	67	353	211	259	353	763	1011	1259	1507	1755	2003	2251	2499	
	12	63	357	207	255	357	759	1007	1255	1503	1751	1999	2247	2495	
2	1	107	361	203	251	361	755	1003	1251	1499	1747	1995	2243	2491	
	2	103	365	199	247	365	751	999	1247	1495	1743	1991	2239	2487	
	3	99	369	195	243	369	747	995	1243	1491	1739	1987	2235	2483	
	4	95	373	191	239	373	743	991	1239	1487	1735	1983	2231	2479	
	5	91	377	187	235	377	739	987	1235	1483	1731	1979	2227	2475	
	6	87	381	183	231	381	735	983	1231	1479	1727	1975	2223	2471	
	7	83	385	179	227	385	731	979	1227	1475	1723	1971	2219	2467	
	8	79	389	175	223	389	727	975	1223	1471	1719	1967	2215	2463	
	9	75	393	171	219	393	723	971	1219	1467	1715	1963	2211	2459	
	10	71	397	167	215	397	719	967	1215	1463	1711	1959	2207	2455	
	11	67	401	163	211	401	715	963	1211	1459	1707	1955	2203	2451	
	12	63	405	159	207	405	711	959	1207	1455	1703	1951	2199	2447	
3	1	107	409	155	203	409	707	955	1203	1451	1699	1947	2195	2443	
	2	103	413	151	199	413	703	951	1199	1447	1695	1943	2191	2439	
	3	99	417	147	195	417	699	947	1195	1443	1691	1939	2187	2435	

*Not a standard frequency allocation for Multiplexer Set AN/UCC-4(V).

Frequencies of 1-Kc Channel Test Tones in the Group, Supergroup, and Line Frequency Bands (Cont)

		TRANSLATED TEST TONE FREQUENCY, KC												
G R O U P	C H A N	GR BAND	SGR BAND	SGR IN THE LINE FREQUENCY BAND										
				*1	1	2	3	4	5	6	7	8	9	10
					4	95	421	143	191	421	695	943	1191	1439
	5	91	425	139	187	425	691	939	1187	1435	1683	1931	2179	2427
	6	87	429	135	183	429	687	935	1183	1431	1679	1927	2175	2423
	7	83	433	131	179	433	683	931	1179	1427	1675	1923	2171	2419
	8	79	437	127	175	437	679	927	1175	1423	1671	1919	2167	2415
	9	75	441	123	171	441	675	923	1171	1419	1667	1915	2163	2411
	10	71	445	119	167	445	671	919	1167	1415	1663	1911	2159	2407
	11	67	449	115	163	449	667	915	1163	1411	1659	1907	2155	2403
	12	63	453	111	159	453	663	911	1159	1407	1655	1903	2151	2399
4	1	107	457	107	155	457	659	907	1155	1403	1651	1899	2147	2395
	2	103	461	103	151	461	655	903	1151	1399	1647	1895	2143	2391
	3	99	465	99	147	465	651	899	1147	1395	1643	1891	2139	2387
	4	95	469	95	143	469	647	895	1143	1391	1639	1887	2135	2383
	5	91	473	91	139	473	643	891	1139	1387	1635	1883	2131	2379
	6	87	477	87	135	477	639	887	1135	1383	1631	1879	2127	2375
	7	83	481	83	131	481	635	883	1131	1379	1627	1875	2123	2371
	8	79	485	79	127	485	631	879	1127	1375	1623	1871	2119	2367
	9	75	489	75	123	489	627	875	1123	1371	1619	1867	2115	2363

*Not a standard frequency allocation for Multiplexer Set AN/UCC-4(V).

Table E-6 (Continued)

Frequencies of 1-Kc Channel Test Tones in the Group,
Supergroup, and Line Frequency Bands (Cont)

		TRANSLATED TEST TONE FREQUENCY, KC													
G R O U P	C H A N	GR BAND	SGR BAND	SGR IN THE LINE FREQUENCY BAND											
				*1	1	2	3	4	5	6	7	8	9	10	
	10	71	493	71	119	493	623	871	1119	1367	1615	1863	2111	2359	
	11	67	497	67	115	497	619	867	1115	1363	1611	1859	2107	2355	
	12	63	501	63	111	501	615	863	1111	1359	1607	1855	2103	2351	
5	1	107	505	59	107	505	611	859	1107	1355	1603	1851	2099	2347	
	2	103	509	55	103	509	607	855	1103	1351	1599	1847	2095	2343	
	3	99	513	51	99	513	603	851	1099	1347	1595	1843	2091	2339	
	4	95	517	47	95	517	599	847	1095	1343	1591	1839	2087	2335	
	5	91	521	43	91	521	595	843	1091	1339	1587	1835	2083	2331	
	6	87	525	39	87	525	591	839	1087	1335	1583	1831	2079	2327	
	7	83	529	35	83	529	587	835	1083	1331	1579	1827	2075	2323	
	8	79	533	31	79	533	583	831	1079	1327	1575	1823	2071	2319	
	9	75	537	27	75	537	579	827	1075	1323	1571	1819	2067	2315	
	10	71	541	23	71	541	575	823	1071	1319	1567	1815	2063	2311	
	11	67	545	19	67	545	571	819	1067	1315	1563	1811	2059	2307	
	12	63	549	15	63	549	567	815	1063	1311	1559	1807	2055	2303	

*Not a standard frequency allocation for Multiplexer Set AN/UCC-4(V).

Table E-6 (Continued)

**Frequencies of Group Pilots in the Supergroup
and Line Frequency Bands**

		TRANSLATED GROUP PILOT FREQUENCY, KC				
		GR 1	GR 2	GR 3	GR 4	GR 5
312-552 KC SGR BAND		315.92	363.92	411.92	459.92	507.92
SGR IN THE LINE FREQ BAND	*1	248.08	200.08	152.08	104.08	56.08
	1	296.08	248.08	200.08	152.08	104.08
	2	315.92	363.92	411.92	459.92	507.92
	3	800.08	752.08	704.08	656.08	608.08
	4	1048.08	1000.08	952.08	904.08	856.08
	5	1296.08	1248.08	1200.08	1152.08	1104.08
	6	1544.08	1496.08	1448.08	1400.08	1352.08
	7	1792.08	1744.08	1696.08	1648.08	1600.08
	8	2040.08	1992.08	1944.08	1896.08	1848.08
	9	2288.08	2240.08	2192.08	2144.08	2096.08
10	2536.08	2488.08	2440.08	2392.08	2344.08	

*Not a standard frequency allocation for Multiplexer Set AN/UCC-4(V).

TABLE E-7
DCS TECHNICAL SCHEDULES

Item Number	User-to-User Circuit	Circuit Parameter Code
	<u>Voice</u>	
1	Nonsecure voice circuit.	V1
	<u>Facsimile</u>	
2	Includes facsimile transmission which can be accommodated over a voice-grade channel with no special conditioning. If the required facsimile (including telephoto) service involves special conditioning of the voice channel, the specific circuit parameters will be developed based on the characteristics of the equipment to be used in the circuit.	V1
	<u>Telegraph and Data</u>	
3	Less than 46 bauds. Includes 60-WPM teletypewriter and other dc keying service below 46 bauds.	N1
4	46 through 75 bauds. Includes 75-WPM and 100-WPM teletypewriter service and other dc keying service from 46 through 75 bauds.	N2 *
5	76 through 150 bauds. Includes 100-baud teletypewriter and other dc keying service from 76 through 150 bauds.	N3
6	300 through 600 bauds. Includes data transmission and other service operating at 300 through 600 bauds.	D2
7	066-063 IBM (10 to 40 cards per minute).	V1

Item Number	User-to-User Circuit	Circuit Parameter Code
8	1,200 bauds. Includes data card transmission and other service operating at 1,200 bauds.	D2
9	2,400 bauds. Includes all types of alternate voice/data service including secure voice operating at 2,400 bauds.	S1
10	2,400 bauds. Limited to data service only.	D1
11	50,000 bits/sec (within 50 kHz) secure voice. This is a special schedule pertaining to encrypted voice baseband transmission over long-distance carrier facilities.	Z1
<u>Voice-Frequency Telegraph</u> <u>(VFTG) Systems</u> (Terminal-to-Terminal DCS Facilities)		
13	Voice-frequency tone group, type 1. Up to 16 teletypewriter channels provided over a voice-frequency circuit between carrier terminals.	D2
14	Voice-frequency tone group, type 2. Up to 26 teletypewriter channels provided over a voice-frequency circuit between carrier terminals.	D1
(Circuit parameters the same as D1 apply except that the maximum change in audio frequency is plus or minus 2 Hz instead of plus or minus 5 Hz).		
<u>Automatic Switched Networks</u> <u>AUTOVON</u> (Access Lines)		
15	Voice grade.	V2

Item Number	User-to-User Circuits	Circuit Parameter Code
16	Special grade, such as 4-wire AUTOVON switch access (2,400 bits/sec). (Trunks, Interswitch)	V2
17	Voice grade.	V2
18	Special grade (no regenerators at either end).	S3
19	Special grade (regenerators at both ends).	S1
20	Special grade (regenerators at one end).	S2
<u>AUTODIN</u> (Access Lines)		
21	1,200 or 2,400 bits/sec.	D1
22	1,200 bits/sec multiplexed. Includes service where user and AUTODIN switching center provide modems which are frequency-division multiplexed to provide a number of channels on a single VF channel. This VF channel may be multiplexed with any compatible combination of 75-, 150-, 300-, or 600-baud modems not to exceed 1,200-bauds total. VF bridging at transmission nodal points is employed to serve noncollocated users. See N2 and N3 for schedule pertaining to 75- to 150-baud dc-keyed access lines. (Trunks)	D2
23	2,400 bits/sec dedicated circuit from one AUTODIN switch to another.	D1

Item Number	User-to-User Circuits	Circuit Parameter Code
	<u>AUTOSEVOCOM</u> (Access Lines)	
24	Secure voice terminal (2,400 bits/sec) to VOCOM switch.	S1
25	Secure voice terminal (2,400 bits/sec) to 4-wire JOSS or 5-D switchboard, part of AUTOSEVOCOM.	S1
26	Secure voice terminal (50 kilobit) to special 758 switch, cordless switchboard, or VOCOM switch:	S1
	over metallic facilities without regenerators; over long-distance carrier facilities.	Z2 Z4
27	Secure voice terminal (50 kilobit) to AN/FTC-31:	
	over metallic facilities without regenerators; over long-distance carrier facilities.	Z1 Z4
	(Trunks)	
28	50 kilobit, over metallic facilities without regenerators.	Z3
29	50 kilobit, over long-distance carrier facilities.	Z4
30	2,400 bits/sec (VOCOM switch to either VOCOM switch or special 758 switch).	S1

TABLE E-8
DCS CIRCUIT PARAMETERS AND SCHEDULES

Characteristics	Unit of Measure	S1	S2	S3	V1	V2	D1	D2	N (1-3)
a. Loss-frequency (kHz)	db								
0.3 - 2.7	db							-2 to +6	
0.3 - 3.0	db	-2 to +6	-1.5 to +4.5	-1 to +3		-3 to +8	-2 to +6	-3 to +12	
0.4 - 2.8	db				-8 to +20				
0.5 - 2.8	db	-1 to +3	-0.5 to +2	-0.5 to +1.5			-1 to +3		
0.6 - 2.4	db			-7 to +12					
1.0 - 2.4	db							-1 to +3	
0.7 - 2.3	db					-1 to +3			
b. Maximum envelope delay distortion (kHz)	micro-sec								
0.5 - 2.8		3000	1500	600			3000		
0.6 - 2.6		1500	750	300			1500		
1.0 - 2.4								1000	
1.0 - 2.6		500	250	100			500	1750	

Characteristics	Unit of Measure	S1	S2	S3	V1	V2	D1	D2	N (1-3)
c. Maximum net loss variation	db	±4	±3	±2	±4	±2	±4	±4	
d. Maximum change in audio frequency	Hz	±5	(Note 1) ±5	(Note 1) ±5	±5	±5	±5	±5	
e. Minimum longitudinal balance	db	40	40	40	40	40	40	40	
f. Maximum total peak telegraph distortion	%								20
g. Maximum mark or space bias distortion	%								(Note-4) 12
h. Maximum allowable channel noise	dbmco								
0-50 miles		31	31	31	31	31	31	31	
51-100		34	34	34	34	34	34	34	
101-400		37	37	37	37	37	37	37	
401-1,000		41	41	41	41	41	41	41	
1,001-1,500		43	43	43	43	43	43	43	

Characteristics	Unit of Measure	S1	S2	S3	V1	V2	D1	D2	N (1-3)
1,501-2,500		45	45	45	45	45	45	45	
2,501-4,000		47	47	47	47	47	47	47	
4,001-8,000		50	50	50	50	50	50	50	
8,001-16,000		53	53	53	53	53	53	53	
1. Maximum single tone interference below circuit noise in each mileage category	db	3	3	3	3	3	3	3	
j. Impulse noise ref level 71 dbrnc0 or 72 dbrnc0 voice band wtg	Max counts in 15 min above ref level	15	15	15			15	15	
(Note 5) k. Terminal impedance 600 ohms	% tolerance	±10	±10	±10	±10	±10	±10	±10	
l. Composite data transmission level	dbm0	-13	-13	-13	-13	-13	-13	-13	
m. Phase jitter (peak to peak)	degrees	15	15	15			15	15	

C

C

C

Characteristics	Unit of Measure	S1	S2	S3	V1	V2	D1	D2	N (1-3)
(Note 6) n. Harmonic distortion	dbm0	-40	-40	-40	-40	-40	-40	-40	

NOTES:

1. Circuits within COMUS ± 3 Hz.
2. For government-owned circuits: 5%.
3. D1 and D2 allowable channel noise for government-owned circuits 47 dbm0 for all distances shown above.
4. Consider a satellite channel as equivalent to a 2,000-mile landline channel in determining circuit length.
5. For leased circuits measured at 100 Hz; for government-owned circuits measured across the frequency band of interest.
6. Applies to the measurement of any of the harmonics of a test frequency of 700 Hz introduced at a level of -10 dbm0.

SCHEDULES Z1, Z2, AND Z3

Characteristic	Unit of Measure	Schedules			
		Z1	Z2		Z3
			Subscriber to Switch	Switch to Subscriber	
a. Lineup loss (Note 1) (kHz)	db				
0.01		+15		+15	
0.1		+13		+13	
1.0		+12	0	+12	0
10.0		+20		+20	
50.0		+30		+30	
0.01-50.0			-2 to +2		-2 to +2
1.0-40.0			-1 to +1		-1 to +1
b. Delay characteristic	Microsecond	±10	±10	±10	±10
c. Maximum loss variation (Note 2)	db	±4	±4	±4	±4
d. Noise characteristic (Note 3)	db $\frac{S+N}{N}$	20	20	20	20
e. Impulse noise	Max peaks per second exceeding 12 db below peak signal level	1	1	1	1
f. Supervisory signal inputs		Note 4	Note 5	Note 5	Note 5

NOTES:

1. These are maximum values. Shorter circuits will have less and will generally correspond to the slope characteristic shown.
2. Referred to lineup losses.
3. Signal plus noise of pseudorandom signal at normal transmission level measured at the user terminal with a true rms voltmeter and with the line terminated in 135 ohms. Noise is measured with same meter at the user terminal with signal removed and input terminated.
4. Schedule Z1.

Ringing tone: 1,000 Hz (Range -6.5 to +5.0 dbm)
 On hook: 2,600 Hz at -21 dbm
 Voice: -17.5 dbm at 0.05 volt (rms)

5. Schedules Z2 and Z3.

CCP 702-1

Ring tone:	1,000 Hz (Range -6.5 to +5.0 dbm)
On-hook:	2,600 Hz at -21 dbm
Dial pulsing:	2,600 Hz burst at -9 dbm
On-hook return:	2,600 Hz at -9 dbm for nominal 260 ms (range 220 to 320 ms) followed by 2,600 Hz at -21 dbm.
Voice:	-17.5 dbm at 0.05 volt (rms)

SCHEDULE Z4

Characteristic	Measure	
	Unit	Typical Value
		4-Wire Carrier, Full-Duplex Operation, Subscriber to Subscriber or Switch to Switch
Nominal data signal amplitude (input/output)	Volts, peak to peak (PP)	1
Impedance (balanced input/output)	Ohms	135
Data rate at baseband (NRZ)	Kilobits/second	50
Jitter from terminal equipment (max)	% Isochronous distortion (= PP jitter)	20
Jitter to terminal equipment (max)	% Isochronous distortion (= PP jitter) (Assumes 0-20% jitter from terminal equipment)	33
Error rate objective	Error rate/time	*
On-hook signal from terminal equipment	Hz	2,600 at -21 dbm
Ring signal to terminal equipment	Hz	1,000 at -6.5 dbm
Dial signal from terminal equipment	Tone burst	2,600 Hz bursts at -9 dbm, 10 PPS, 61% break
On-hook signal following off-hook from terminal equipment	Hz	2,600 Hz at -9 dbm for approx 260 milliseconds
Forwarding switching time (approx)	Milliseconds	400 (following end of last dialed digit)

*The burst rate shall not exceed one error burst per minute averaged over a 1-hour test period. One error burst is not to exceed 350 bits averaged over a 1-hour test period. The average number of bits per burst is equal to the total of bit errors divided by the number of bursts.

TYPICAL BLOCK & LEVEL DIAGRAM AN/FCC-55

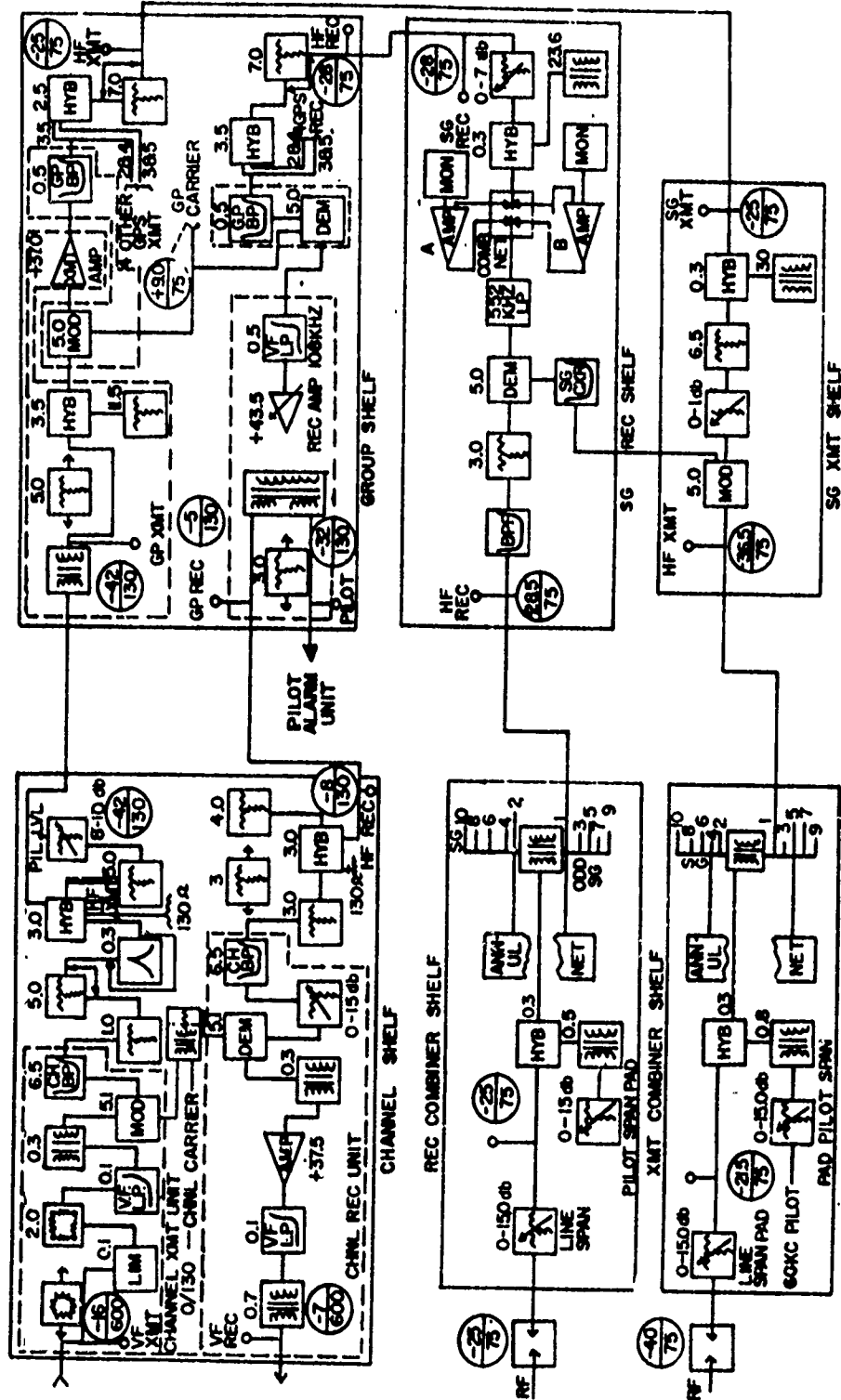


Figure E-1

TYPICAL BLOCK AND LEVEL DRAWING, AN/UCC-4

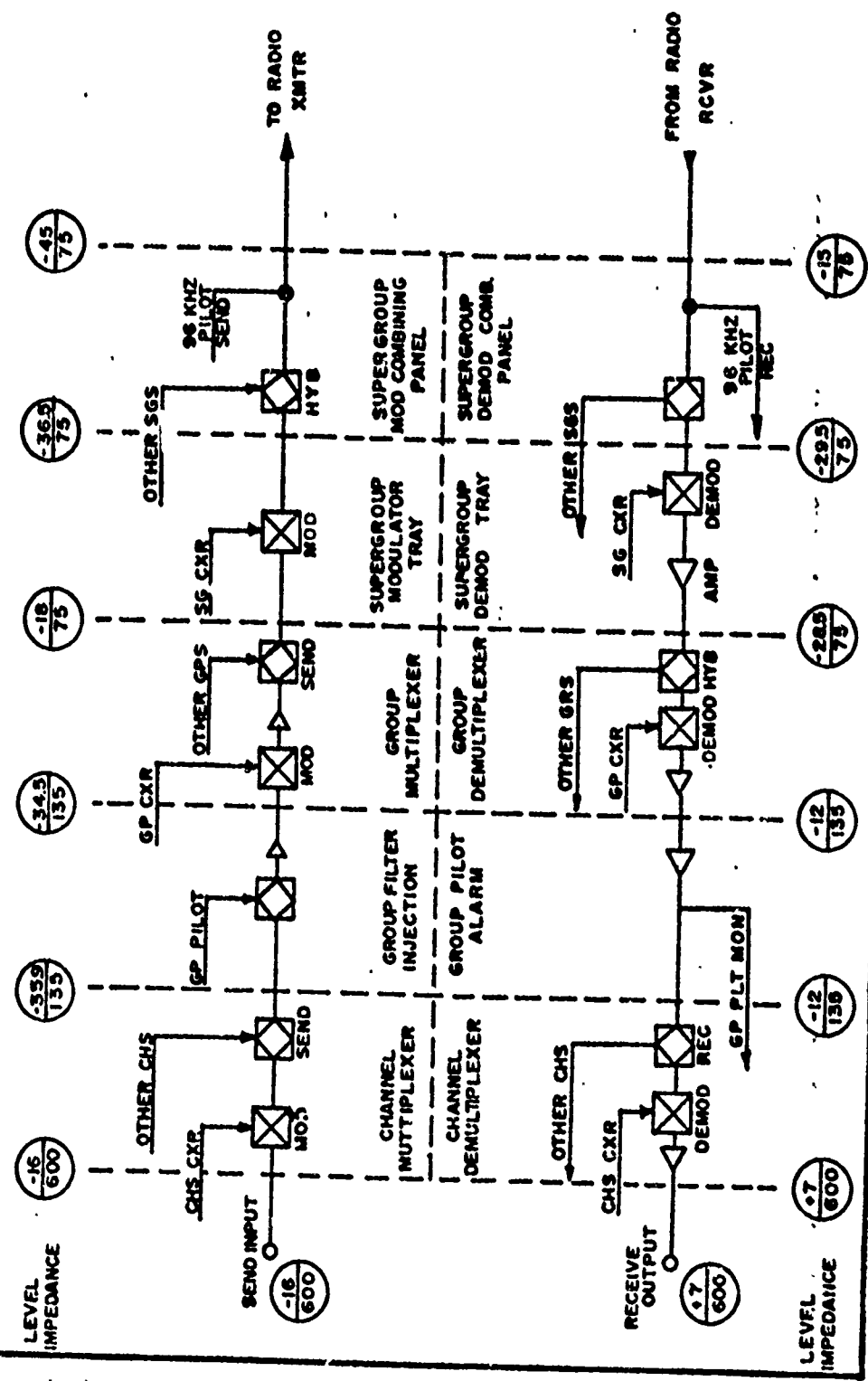


Figure E-3

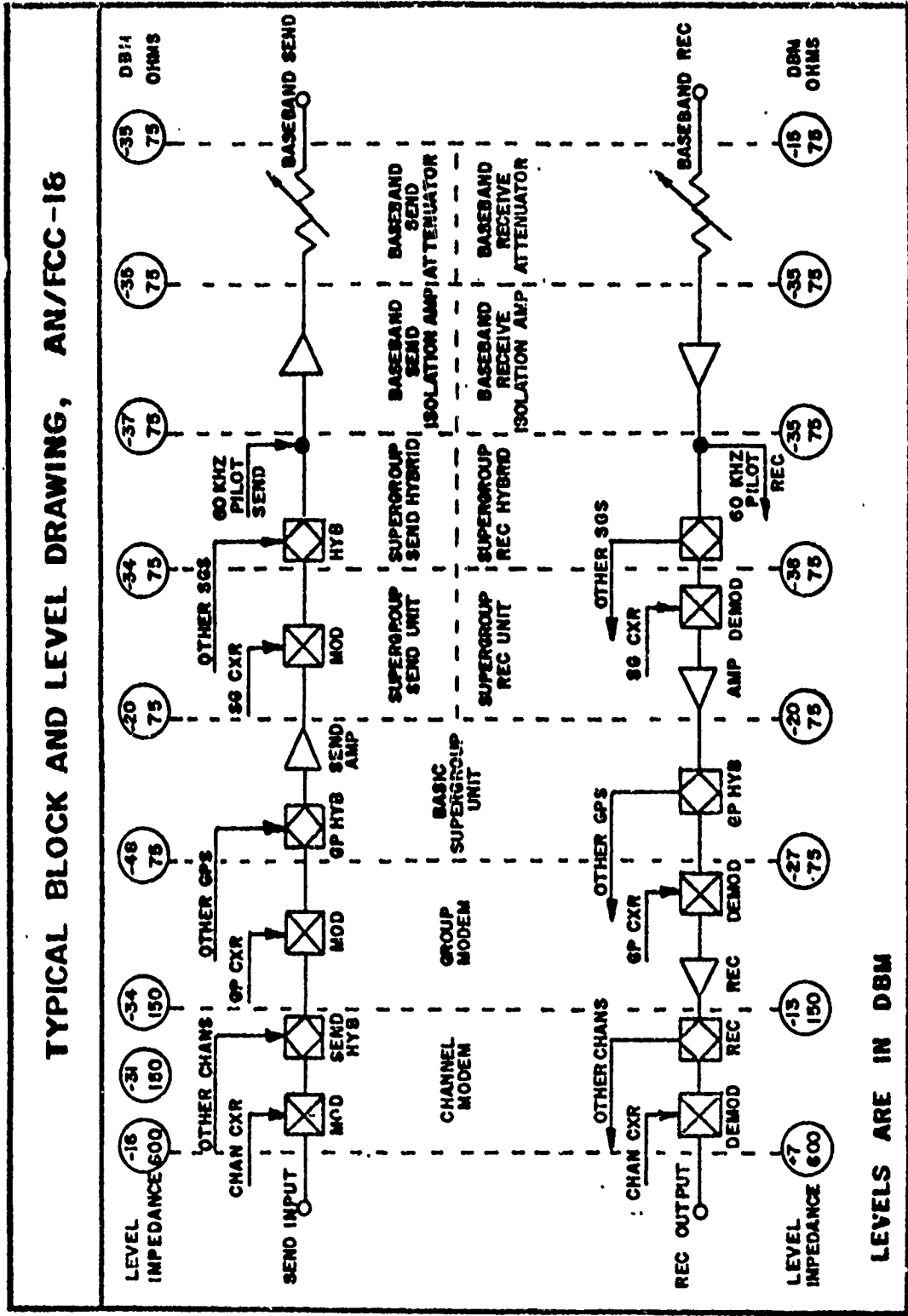
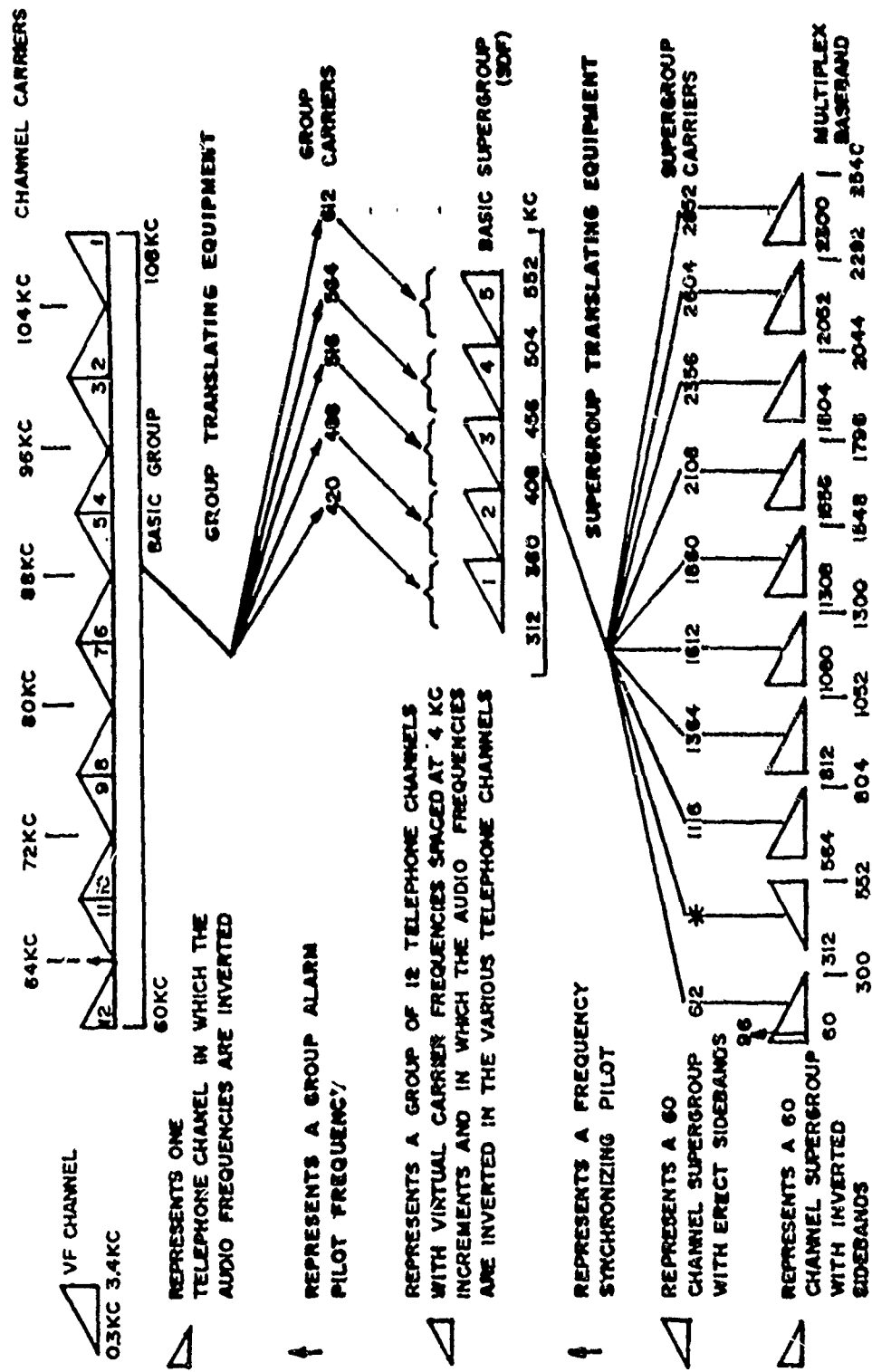


Figure E-4

FREQUENCY ALLOCATIONS AND MODULATION PLAN FOR THE AN/FCC-17 FAMILY OF MULTIPLEXERS



REPRESENTS ONE TELEPHONE CHANNEL IN WHICH THE AUDIO FREQUENCIES ARE INVERTED

REPRESENTS A GROUP ALARM PILOT FREQUENCY

REPRESENTS A GROUP OF 12 TELEPHONE CHANNELS WITH VIRTUAL CARRIER FREQUENCIES SPACED AT 4 KC INCREMENTS AND IN WHICH THE AUDIO FREQUENCIES ARE INVERTED IN THE VARIOUS TELEPHONE CHANNELS

REPRESENTS A FREQUENCY SYNCHRONIZING PILOT

REPRESENTS A 60 CHANNEL SUPERGROUP WITH ERECT SIDEBANDS

REPRESENTS A 60 CHANNEL SUPERGROUP WITH INVERTED SIDEBANDS

* NO MODULATION

Figure E-5

BLOCK & LEVEL DIAGRAM AN / FCC-17

NOTE:
WHEN DC VOLTAGE IS RE-
QUIRED FOR LAMP POWER,
CONNECT TO EXTERNAL DC
POWER SOURCE.

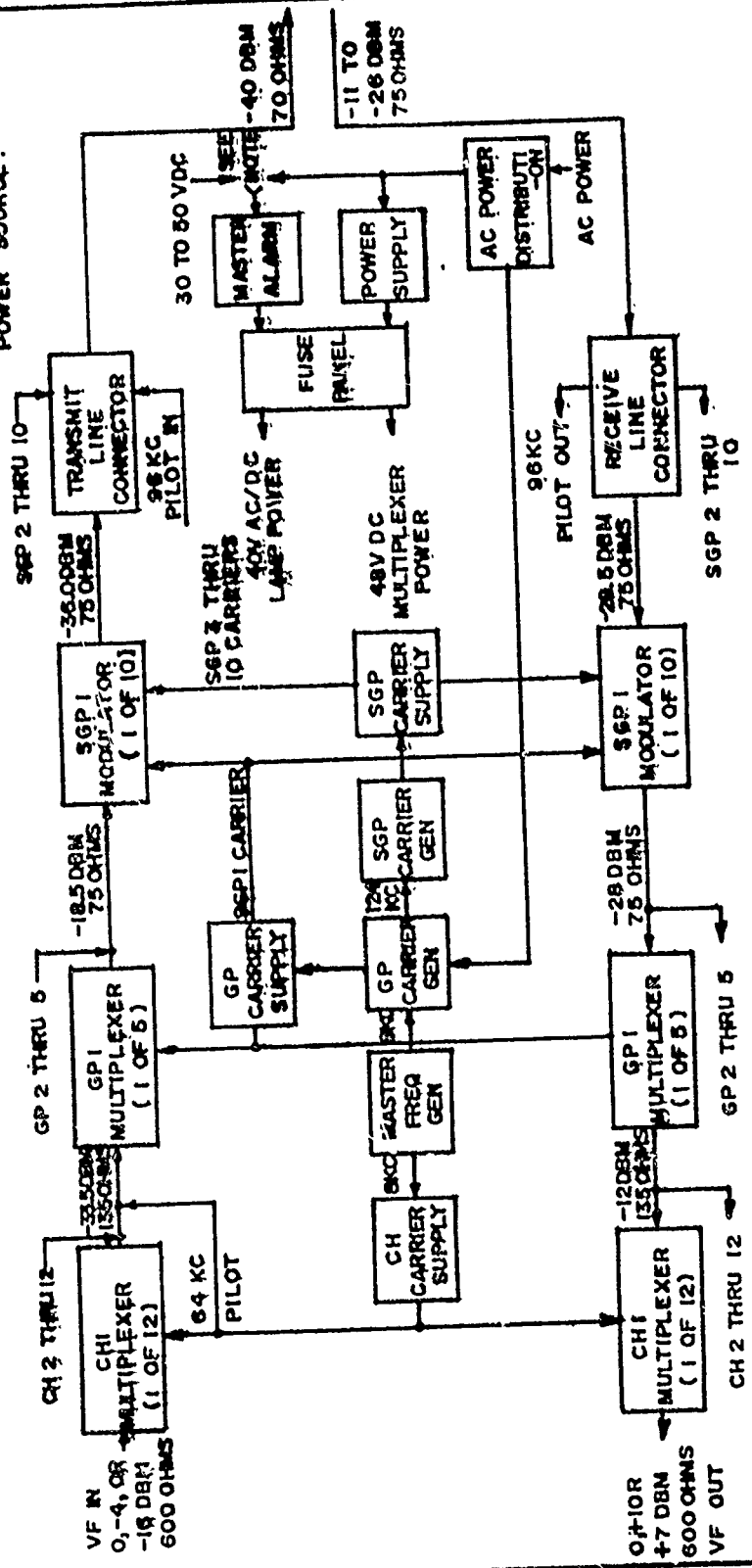
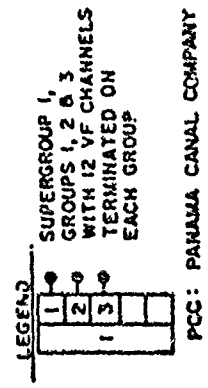
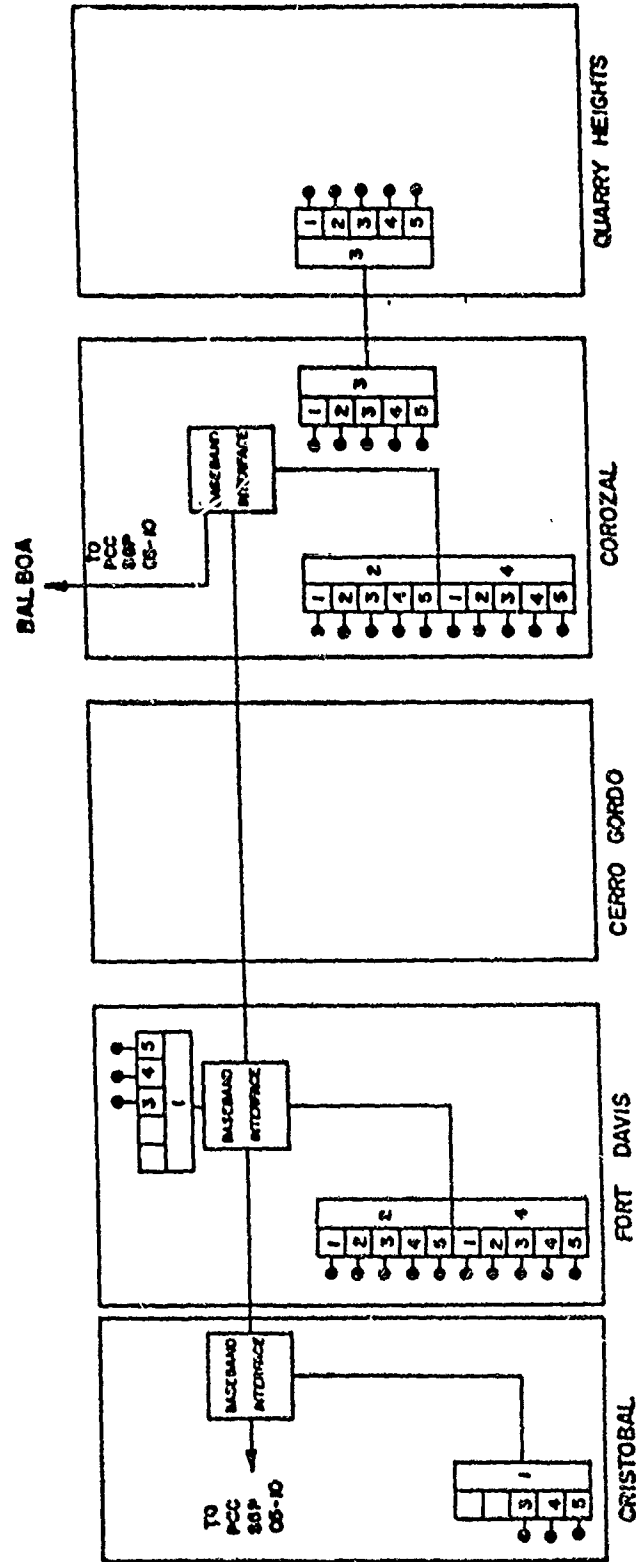


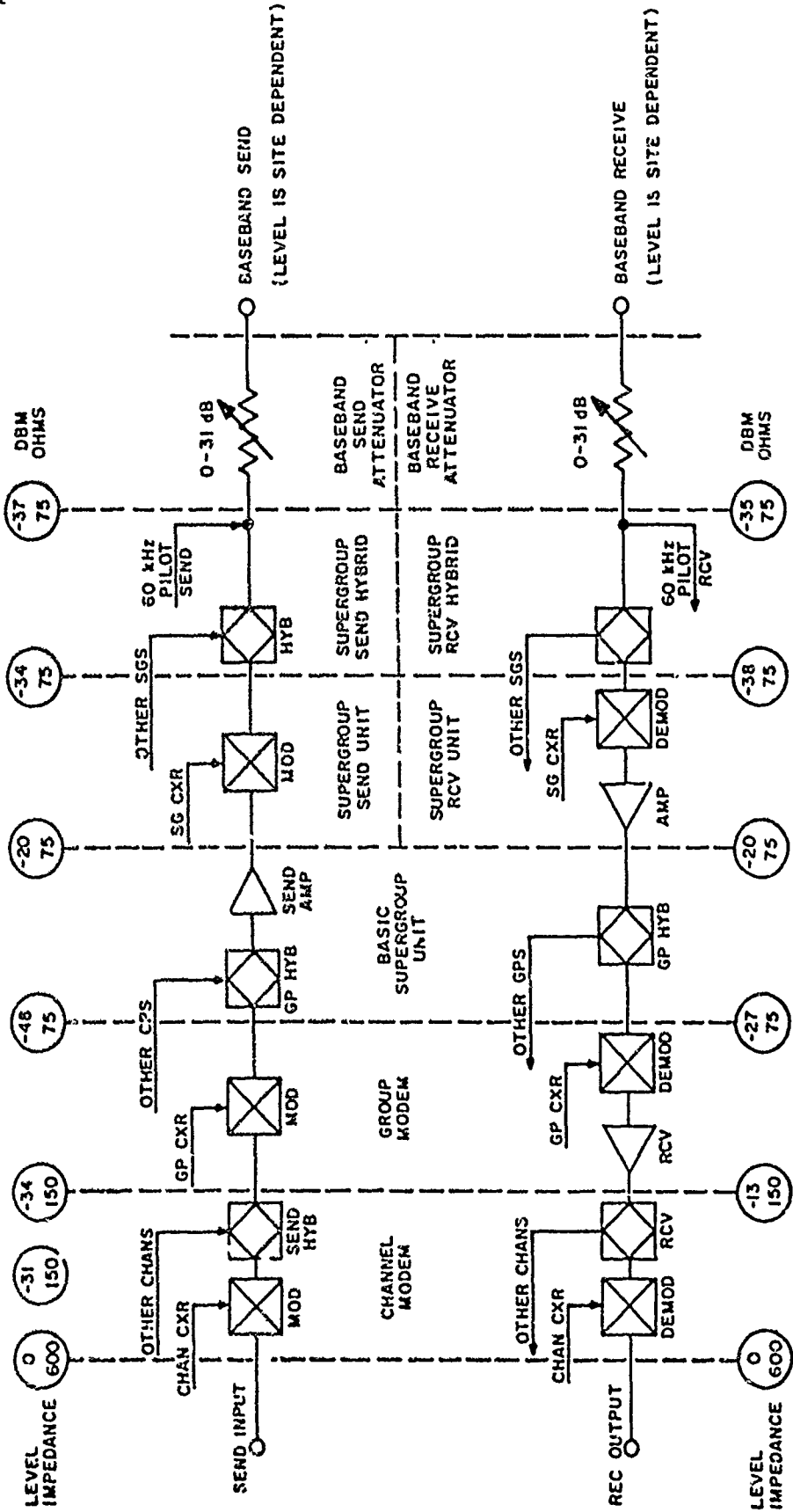
Figure E-6



TRANS-ISTHMIAN MICROWAVE SYSTEM (TIMS)
MULTIPLY PLAN

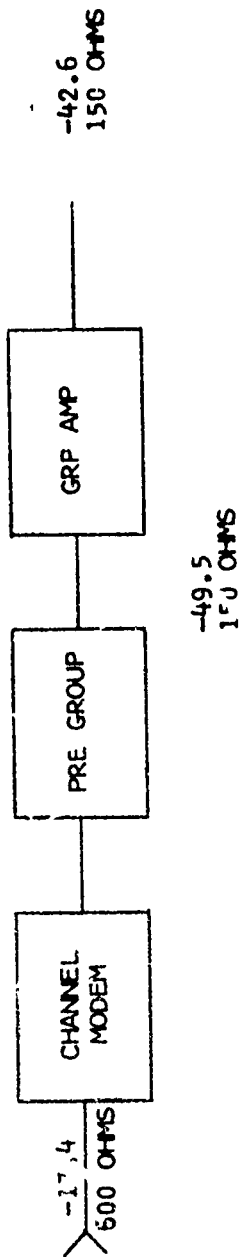
Figure E-7

TRANS - ISTHMIAN MICROWAVE SYSTEM TYPICAL BLOCK AND LEVEL DRAWING, AN/FCC-18



LEVELS ARE IN DBM

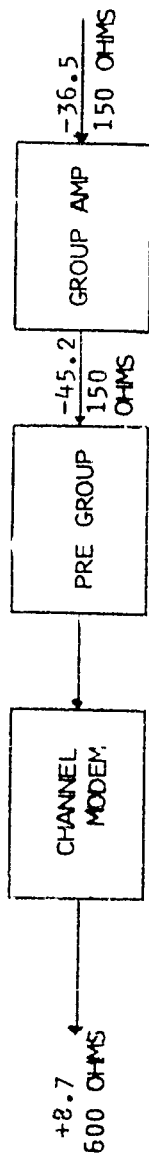
Figure



E-29

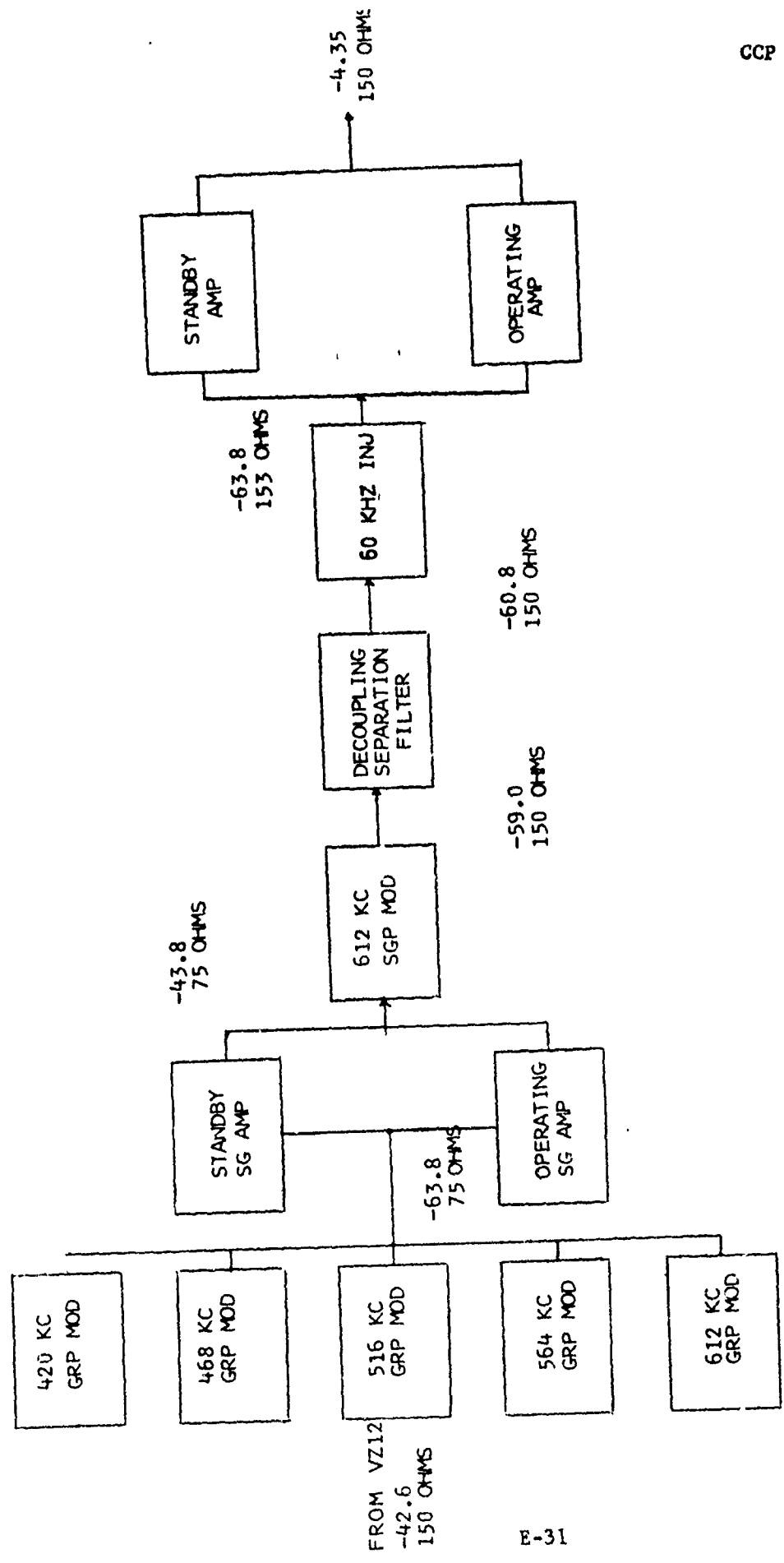
S I E M E N S V Z 1 2 T R A N S M I T

Figure E-9

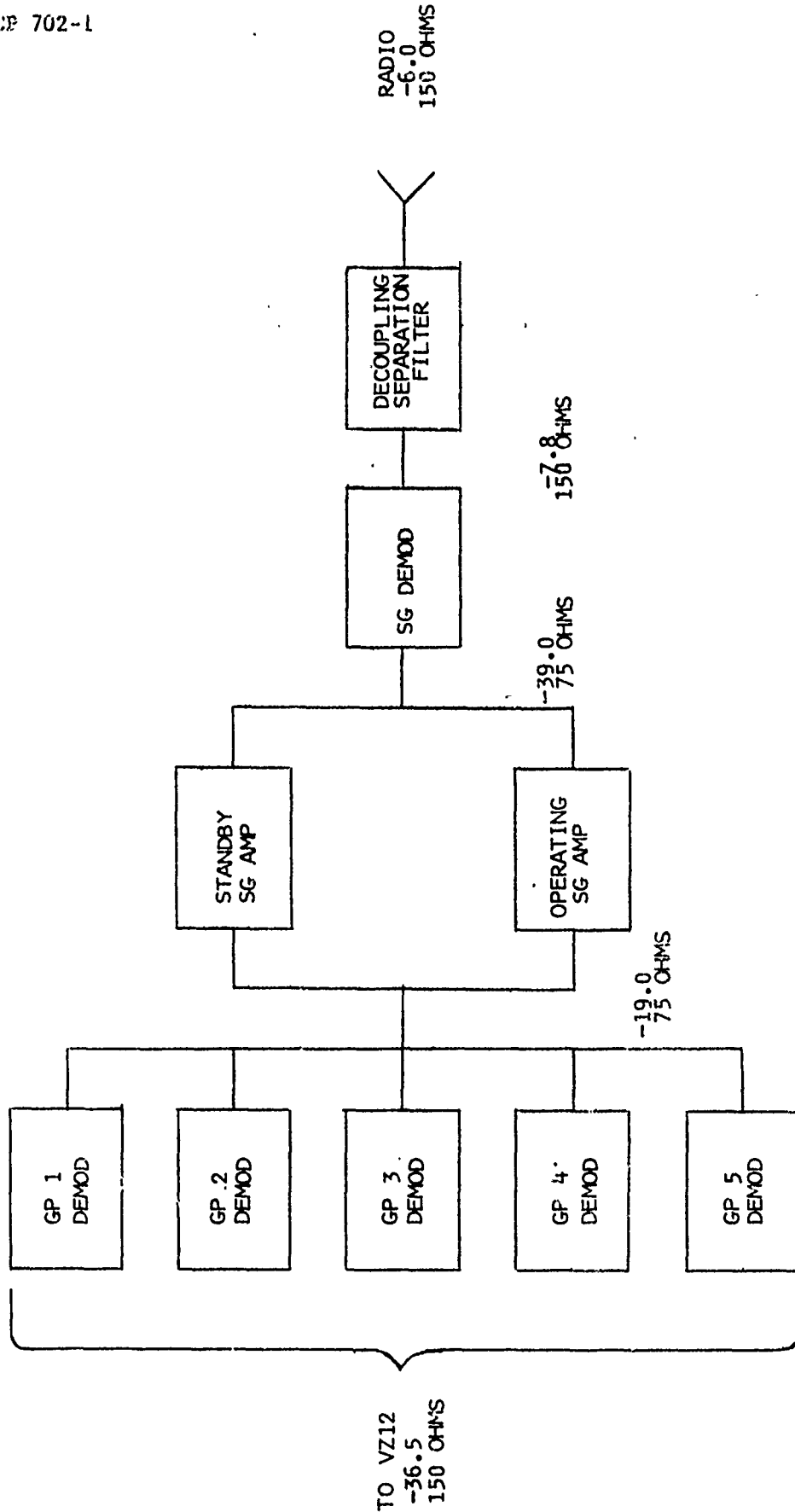


S I E M E N S V Z 1 2 R E C E I V E

Figure E-10



SIEMENS VZ60 TRANSMIT
Figure E-11



S I E M E N S V Z 6 0 R E C E I V E

Figure E-12

TABLE E-9
Manufacturer's Multiplex Specifications

TEST	MIL-STD	MX-106	UCC-4	FCC-18	FCC-55
Voice channel longitudinal balance (T-7)	At least 40 dB below reference signal level	At least 55 dB	40 dB minimum		
Idle channel noise (T-8)	Idle (Design Objective) Type I 75 pmp0/13.75 dBa0 Type II 245 pmp0/18.9 dBa0	10 dBa0 FIA weighted	Less than 15 dBa0	± 5 dBa0 FIA weighted	21 dBmCO (15 dBa0 FIA weighted)
Idle channel impulse noise (T-9)	Shall not exceed 15 counts over any 15 consecutive minutes above a level of 71 dBmCO				
Voice channel frequency response (T-10/11)	Loss in dB referenced to 1 kHz 300- 3400 Hz Type I -0.7, +1.9 ±0.7 Type II -1.1, +2.2 ±1.1	400 - 3000 Hz, ±1 dB 300 - 3400 Hz, +1 dB, -2.0 dB	600 - 2400 Hz, ±1.0 dB 400 - 3000 Hz, -1.0, +2.0 dB 300 - 3400 Hz, -1.0, +3.5 dB	300 - 400 Hz, +0.7, -2.8 dB 400 - 600 Hz, +0.7, -1.4 dB 600 - 2400 Hz, ±0.7 dB 2400 - 3000 Hz, +0.7, -1.4 dB 3000 - 3450 Hz, +0.7, -2.8 dB	In band signaling 250 - 3400, +0.5, -3.0 dB Out of band 300 - 3550 Hz, +0.6, -3.0 dB
Voice channel envelope delay distortion	Delay in microseconds (µsec) 600- 3200 Hz Type I 127 37 Type II 187 147	S6 2 & 4 to 10 1000 - 2500 Hz, < 117 µsec 600 - 3200 Hz, < 187 µsec S6 1 & 3 1000 - 2500 Hz, < 130 µsec 600 - 3200 Hz, < 200 µsec	S6 2 & 4 to 10 1000 - 2500 Hz, < 117 µsec 600 - 3200 Hz, < 187 µsec S6 1 & 3 1000 - 2500 Hz, < 130 µsec 600 - 3200 Hz, < 200 µsec	900 - 2700 Hz, < 300 µsec 120 - 2500, < 150 µsec Without equalizers	Any channel, S6 1 & 3 except SG 1, GP 1, CH 1, and SG 3, GP 5, CH 11 and 12 600 - 3200 Hz, < 200 µsec 1000 - 2500 Hz, < 130 µsec

TABLE E-9 (Continued)

Voice channel harmonic distortion (T-14)	Total should be at least 40 dB below reference (Design Objective)	Total -40 dBm0 (±1) for 1 kHz tone at 0 dBm0.	2nd & 3rd harmonic of 1 kHz > -40 dBm0	Harmonic of any test frequency > 40 dB	Total 1% maximum
Voice channel frequency translation (T-15)	±1 Hz		±0.1 Hz	< 1 Hz	
Voice channel phase jitter (T-16/17)	Total peak to peak jitter shall not exceed 15 degrees (Design Objective)				
Voice channel crosstalk (T-18)	Near and far end crosstalk shall be at least 55 dB below signal level	Less than 18 dBm0 at 1 kHz, 0 dBm0 test tone	Intelligible Near end > -50 dBm0 Far end > -70 dBm0	> 60 dB	
Data error rate (T-19)	1 error in 10 ⁵ bits at 1200 b/s (Design Objective)				
Loaded noise			Loaded channel noise -5 dBm0 white noise per channel 20 dBm0 (max) (400 pWp0)	Less than 23 dBa (FIA weighted) back to back terminals	27 dBm0 at +17 dBm0

FORM 3-5 (C) (used)

MANUFACTURER'S MULTIFLEX SPECIFICATIONS

TEST	MIL-STD	TEST	
VOICE CHANNEL LONGITUDINAL BALANCE (T-7)	AT LEAST 40 DB BELOW REFERENCE SIGNAL LEVEL	DMA	
IDLE CHANNEL NOISE (T-8)	IDLE (DESIGN OBJECTIVE) TYPE I 75pWp0/13.75 dBa0 TYPE II 245pWp0/18.9 dBa0	21 dBm0/125.9pWp0	
IDLE CHANNEL IMPULSE NOISE (T-9)	SHALL NOT EXCEED 15 COUNTS OVER ANY 15 CONSECUTIVE MINUTES ABOVE A LEVEL OF 71 dBm0CO	DMA	
VOICE CHANNEL FREQUENCY RESPONSE (T-10/11)	LOSS IN DB REFERENCED TO 1 kHz 300-400 400-3000Hz 3400Hz 3000Hz TYPE I -0.7+1.9 ±0.7 TYPE II -1.1+2.2 ±1.1	LOSS IN DB REFERENCED TO 800 Hz 300-400Hz +3.4dB 400-600Hz 1.8dB 600-2.4kHz 0.9dB 2.4-3.0Hz 1.8dB 3.0-3.4Hz 3.4dB	
VOICE CHANNEL ENVELOPE DELAY DISTORTION (T-12/13)	DELAY IN MICROSECONDS (μSEC) 600-1000-3200Hz 1000-2500Hz TYPE I 127 87 TYPE II 187 147	DMA	

TABLE E-9 (Continued)

TEST	MIL-STD	VZ12-V60 FU		
VOICE CHANNEL HARMONIC DISTORTION (T-14)	TOTAL SHOULD BE AT LEAST 40dB BELOW REFERENCE (DESIGN OBJECTIVE)	DNA		
VOICE CHANNEL FREQUENCY TRANSLATION (T-15)	±1 Hz	DNA		
VOICE CHANNEL PHASE JITTER (T-16/17)	TOTAL PEAK TO PEAK JITTER SHALL NOT EXCEED 15 DEGREES (DESIGN OBJECTIVES)	DNA		
VOICE CHANNEL CROSS-TALK (T-18)	NEAR AND FAR END CROSSTALK SHALL BE AT LEAST 55 dB BELOW SIGNAL LEVEL	INTELLIGIBLE CROSSTALK 73.8 dB DOWN CROSSTALK BETWEEN GO AND RETURN DIRECTIONS OF THE SAME CHANNEL 52.1 dB		
DATA ERROR RATE (T-19)	1 ERROR IN 10 ⁵ BITS AT 1200 b/s (DESIGN OBJECTIVE)	DNA		
LOADED NOISE		DNA		

TABLE E-10

RADIO EQUIPMENT-PACIFIC

AN/FRC-109	AN/TRC-120	AN/MRC-98
AN/FRC-109(76C)	AN/FRC-104	AN/FRC-39A
AN/FRC-154	AN/MSC-46	AN/TRC-90
MW-508D	NEC M-288-2A	AN/FRC-80
MW-608D	AN/TRC-24	TR-450
AN/TRC-29	LRC-3	NUS-7300
AN/TRC-38	AN/TRC-132	

TABLE E-11

RADIO EQUIPMENT-CONUS

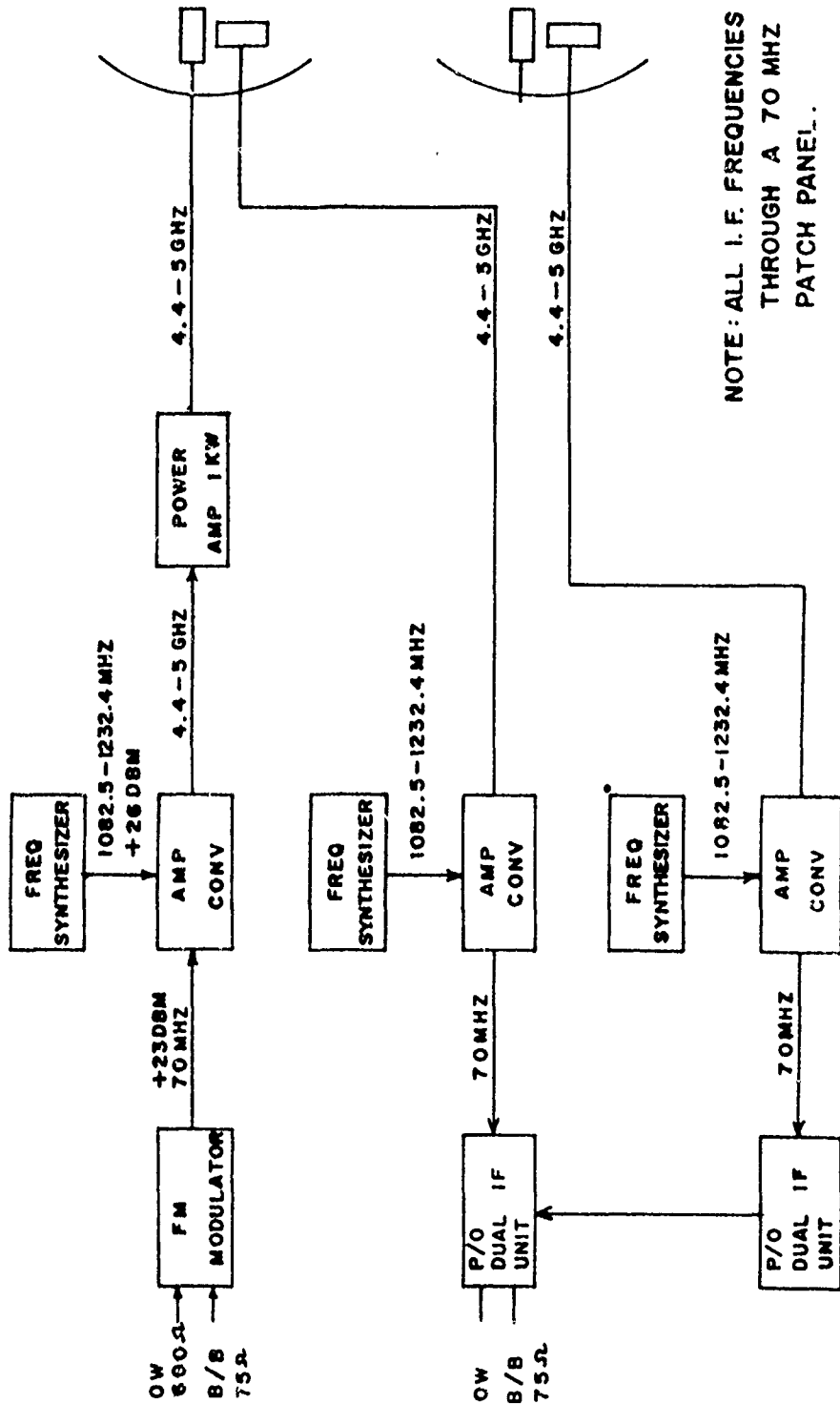
AN/FRC-109	JM-68	MW-508
AN/FRC-109(76C)	MW-502	78F2
AN/FRC-159(V)		

TABLE E-12

RADIO EQUIPMENT-EUROPE

AN/GRC-66	REL-2600
AN/FRC-80	AN/FRC-109
Siemens FM/8000	

TYPICAL BLOCK AND LEVEL DRAWING - AN/TRC-90B



NOTE: ALL I.F. FREQUENCIES GO THROUGH A 70 MHZ PATCH PANEL.

TYPICAL BLOCK AND LEVEL DRAWING - AN/ TRC - 90

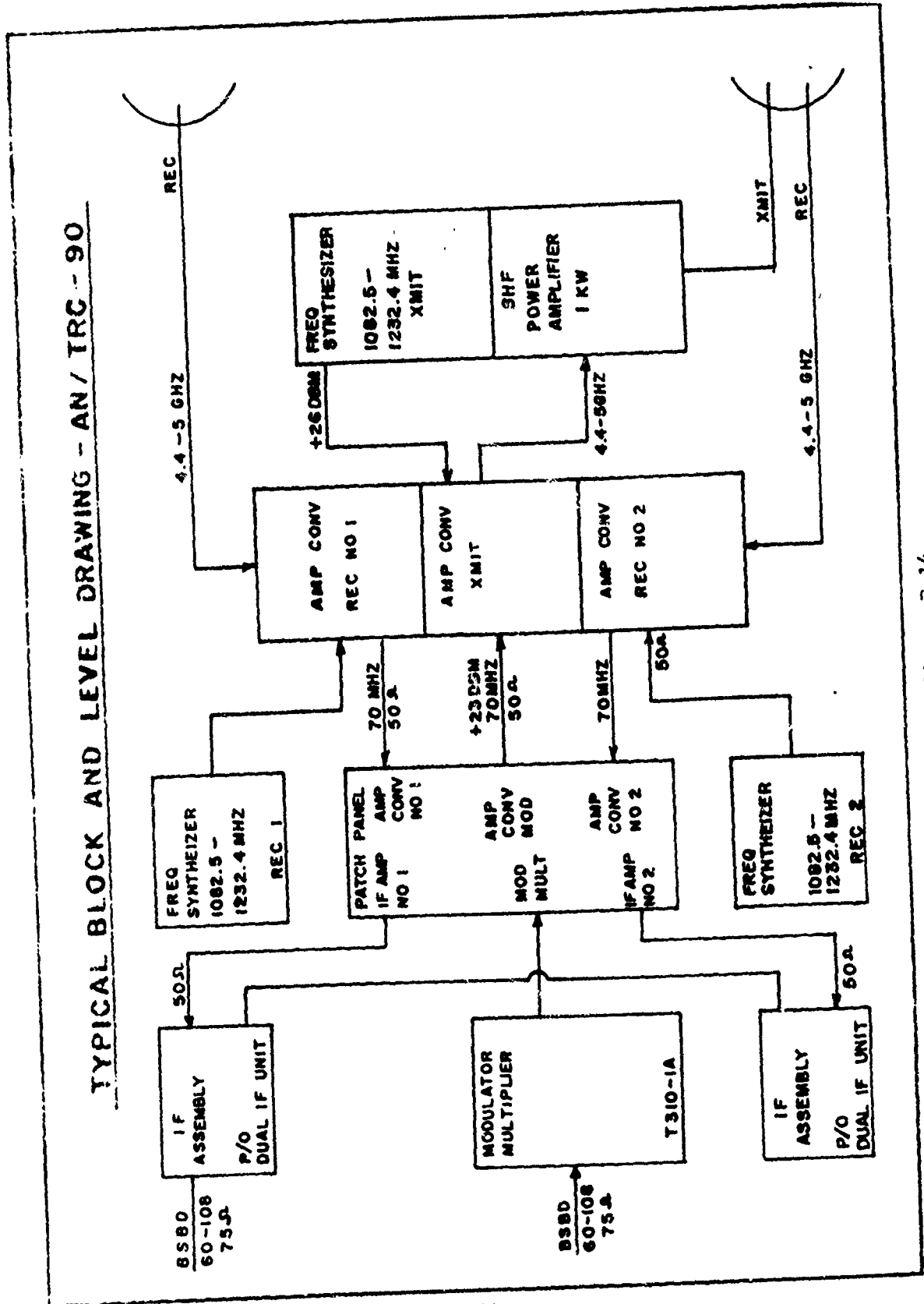


Figure E-14

TYPICAL BLOCK AND LEVEL DRAWING - LRC-3

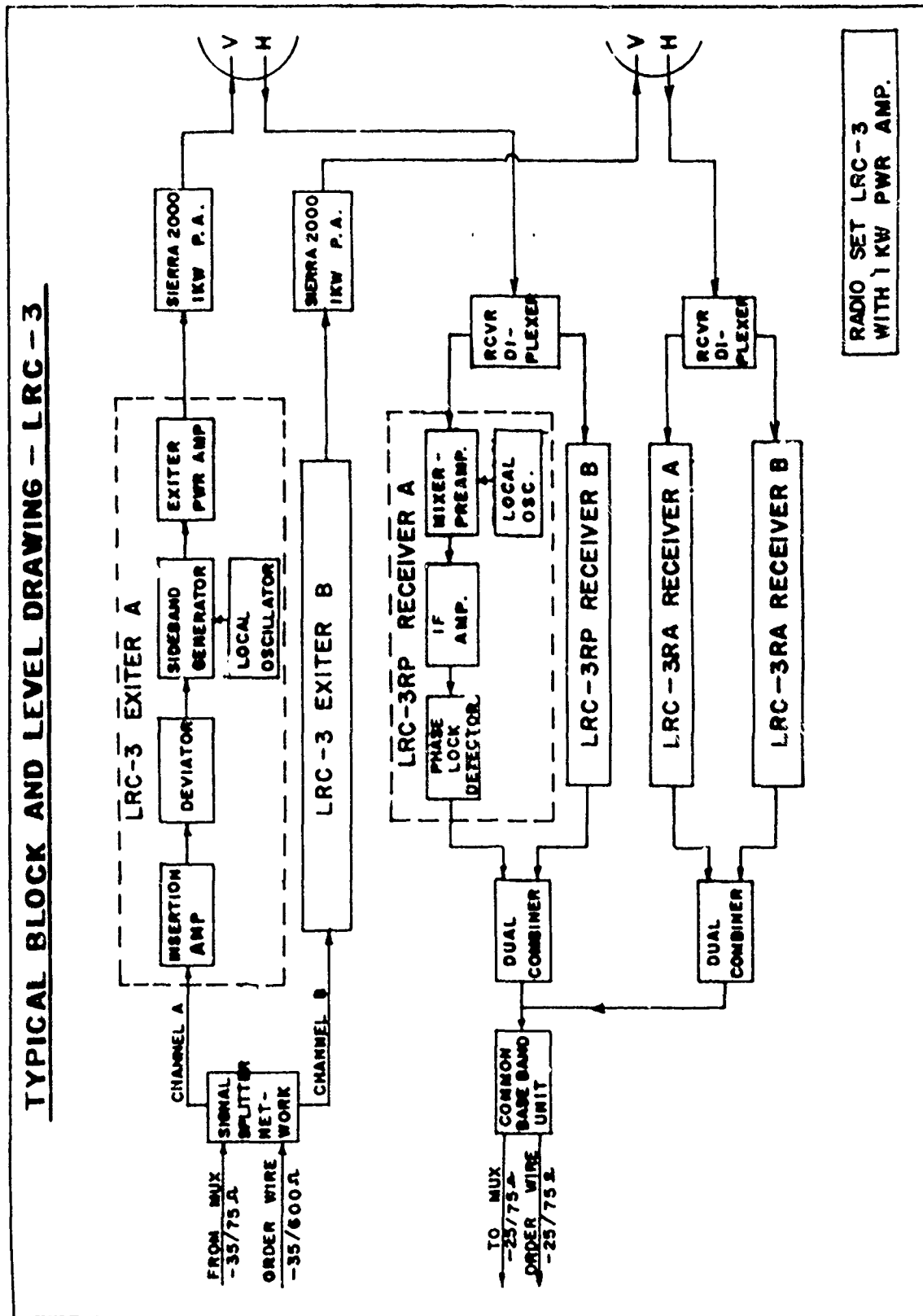


Figure E-15

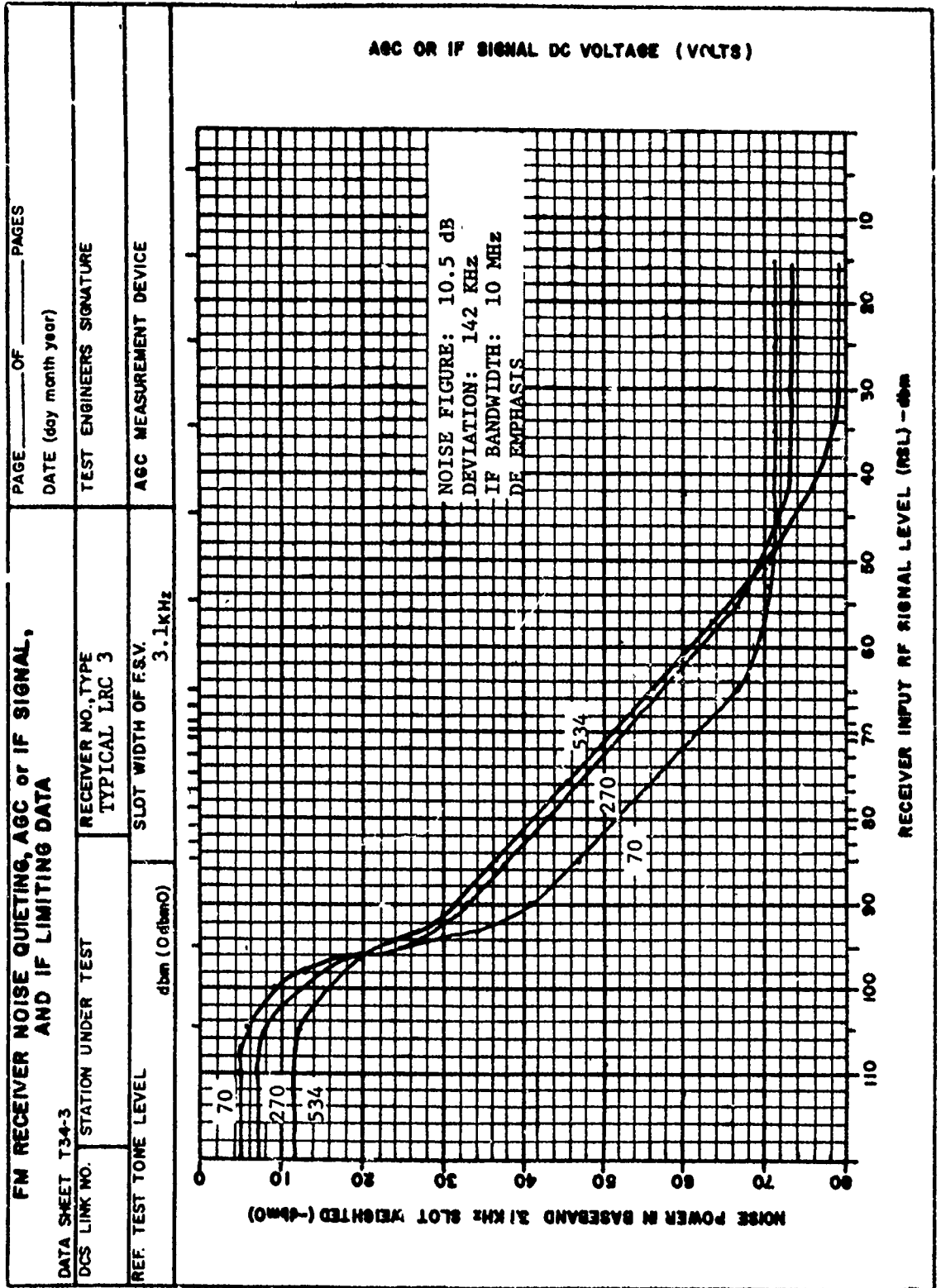


Figure E-16

CCP 702-1

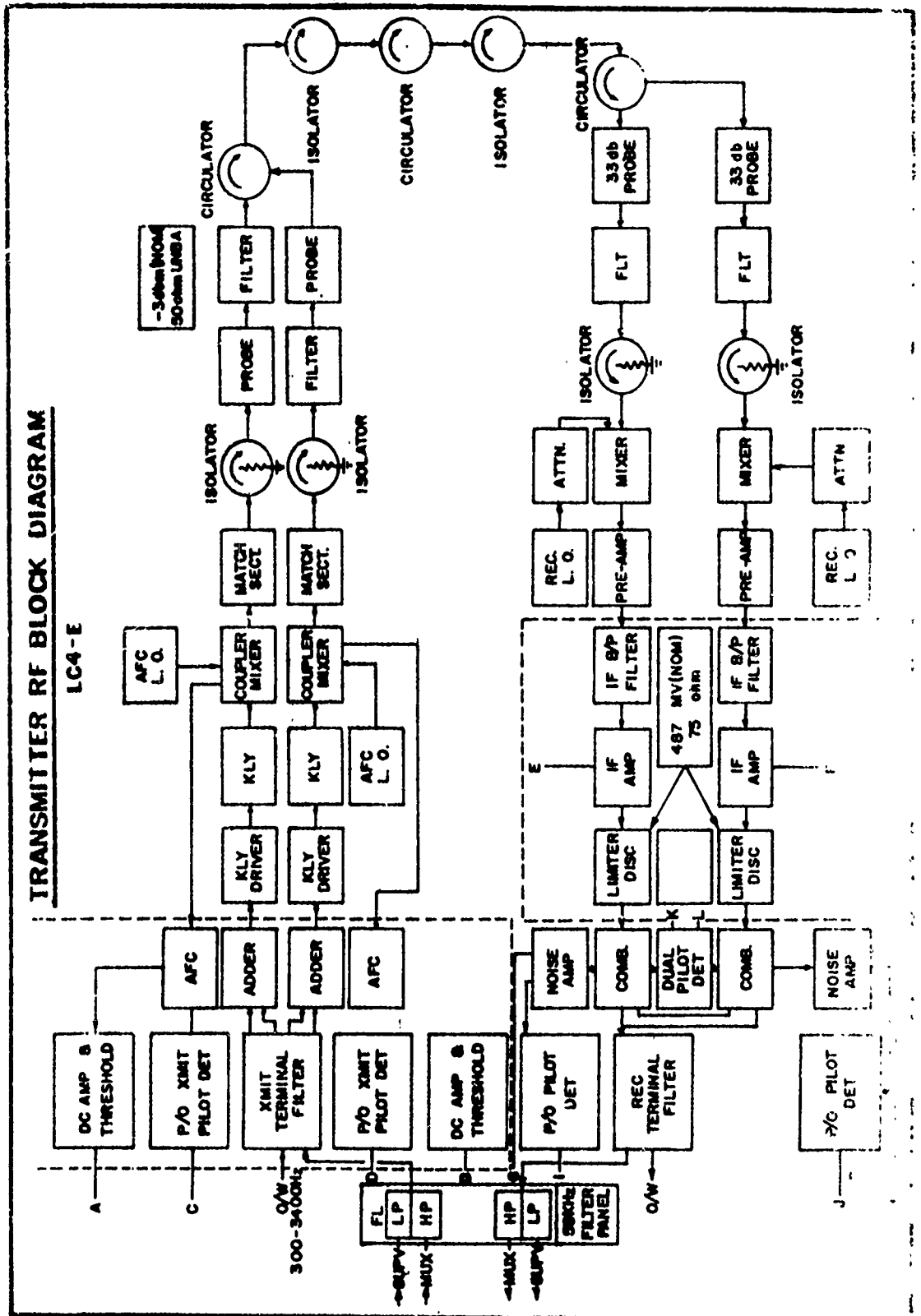
FIGURE E-17

TYPICAL NPR CURVE, LRC-3

TO BE PUBLISHED

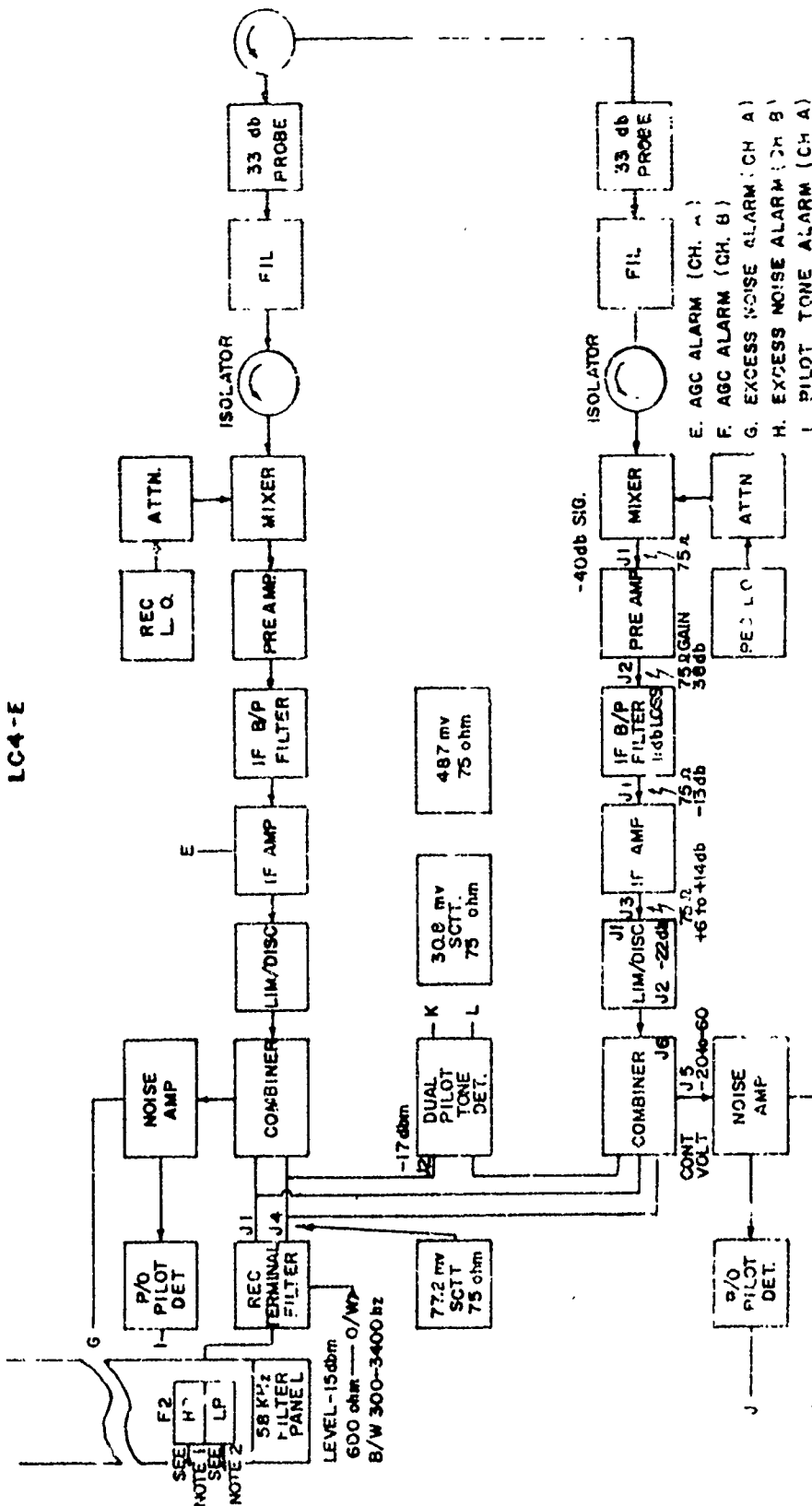
TRANSMITTER RF BLOCK DIAGRAM

LC4-E



RECEIVER RF BLOCK DIAGRAM

LC4-E



NOTE 1 MUX LEVEL -15dbm B/W 60-1052 FOR 240 CH
 NOTE 2 SUPERVISORY SYSTEM -1.5 dbm, 600 ohm B/W IS 4-55 MHz
 NOTE 3 AGC OFF 80 db GAIN. AGC ON 60 db GAIN TP-1.

Figure E-10

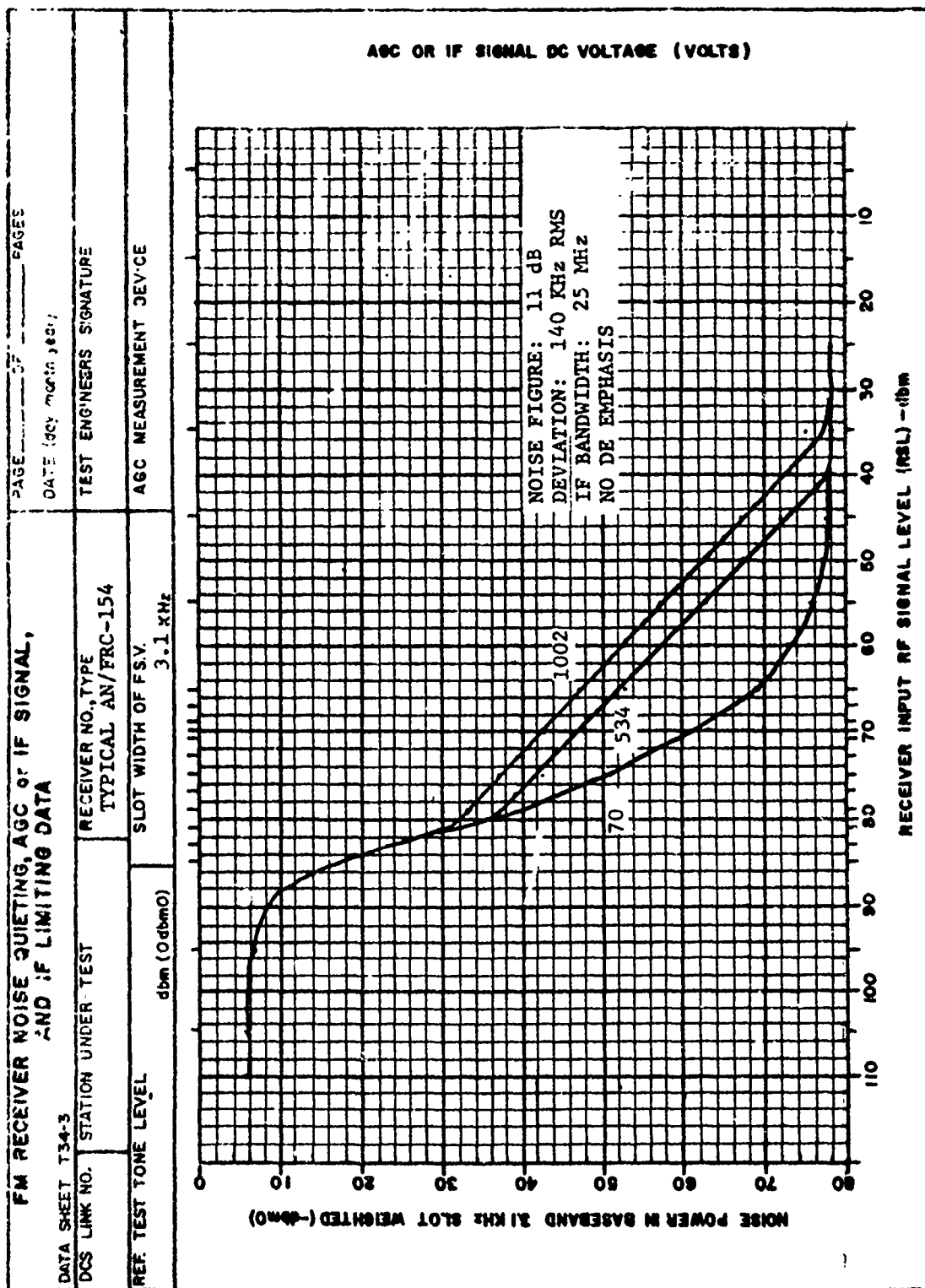


Figure E-20

NPR VS BASEBAND LOADING

PAGE _____ OF _____
 DATE _____

TEST REPORT NO.

TEST STATION

TEST ENGINEER SIGNATURE

UNIT UNDER TEST

MODEL NO. 154

LOWER

KHz

CENTER

KHz

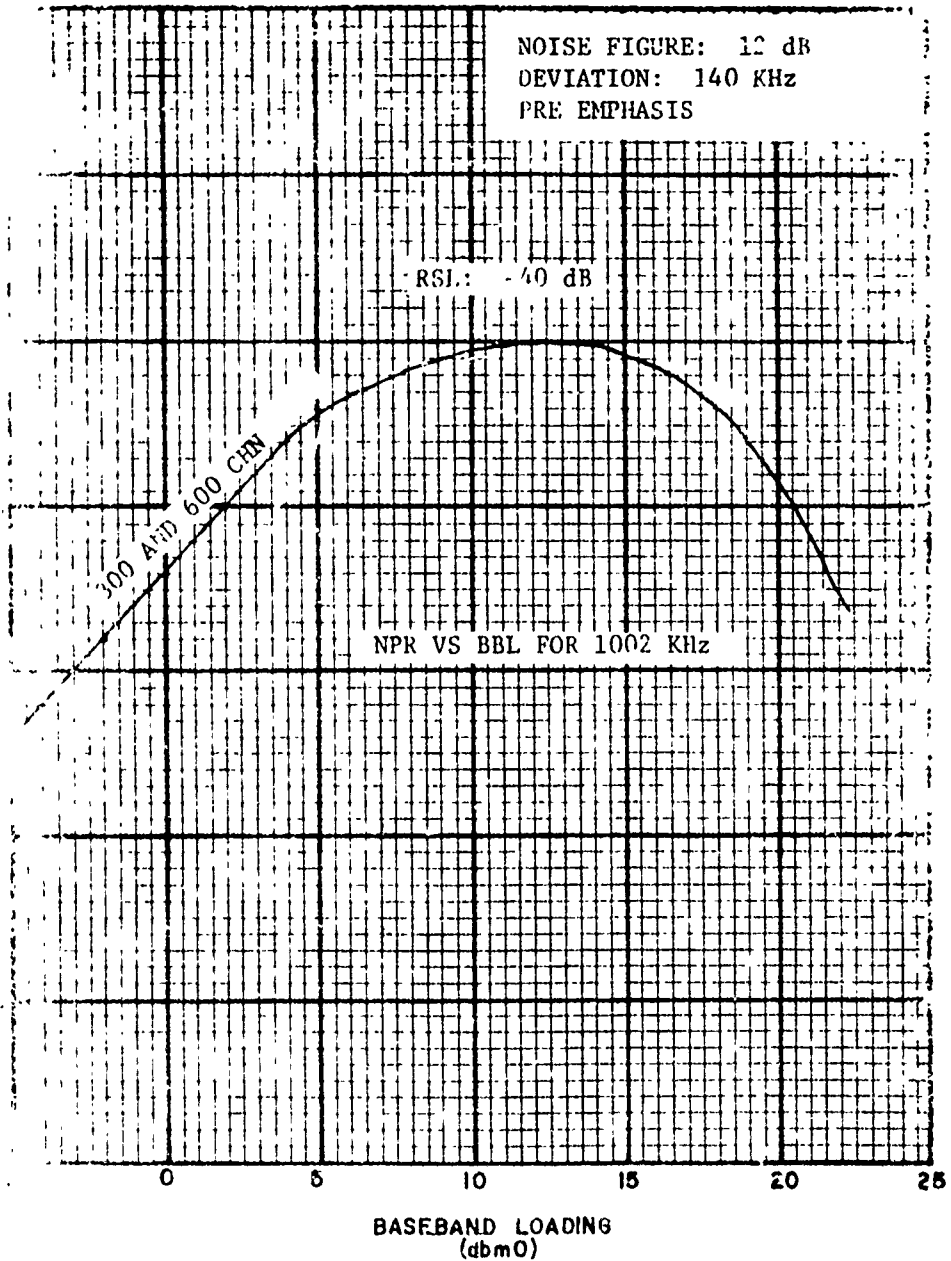
UPPER

KHz

REMARKS

TRANSMITTER

ON A MINIMUM NPR OF 55 DB AT +13.8 DBM OF LOADING



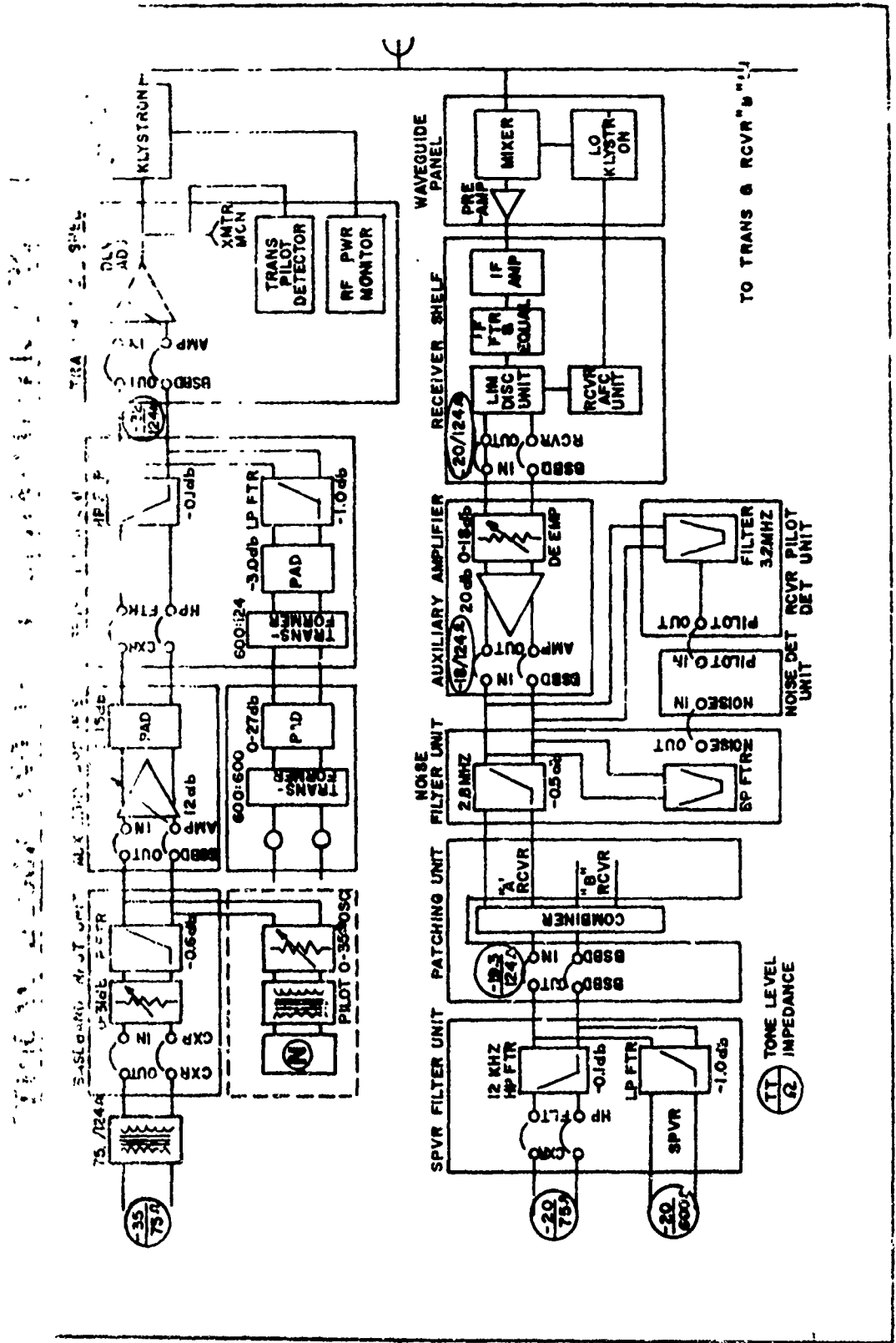


Figure E-22

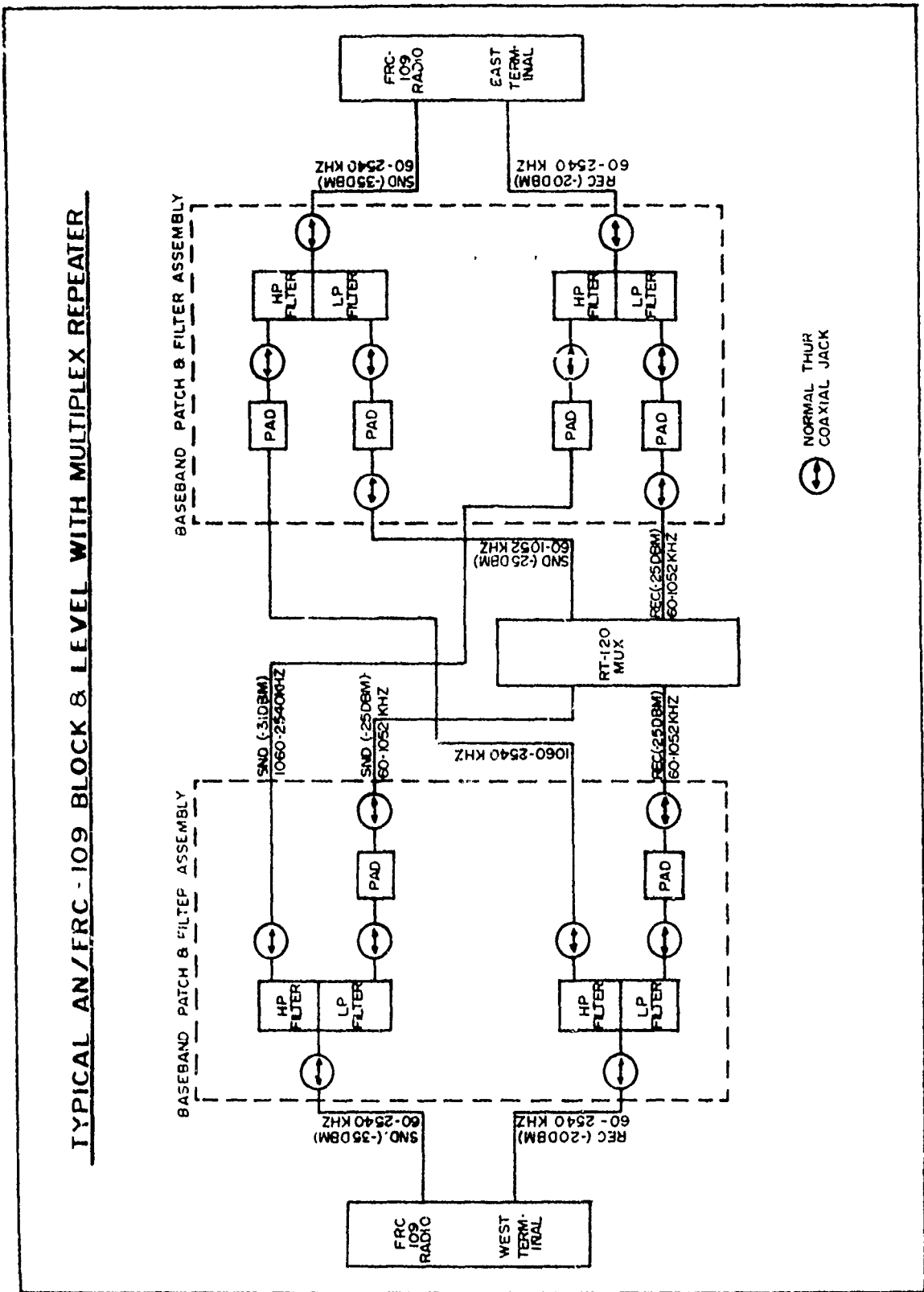


Figure E-23

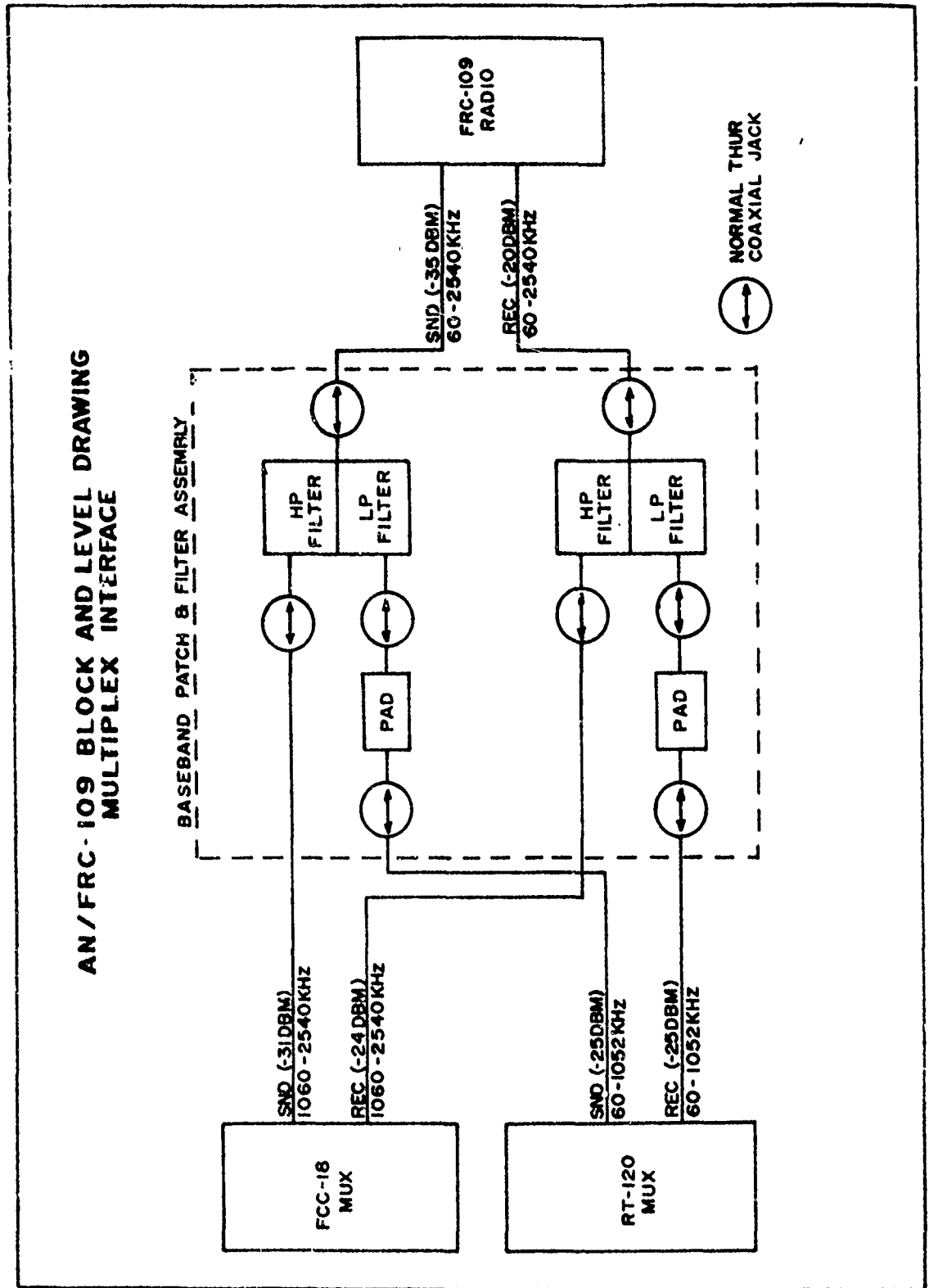


Figure E-24

TYPICAL AGC AND FM QUIETING CURVE AN/FRC-109

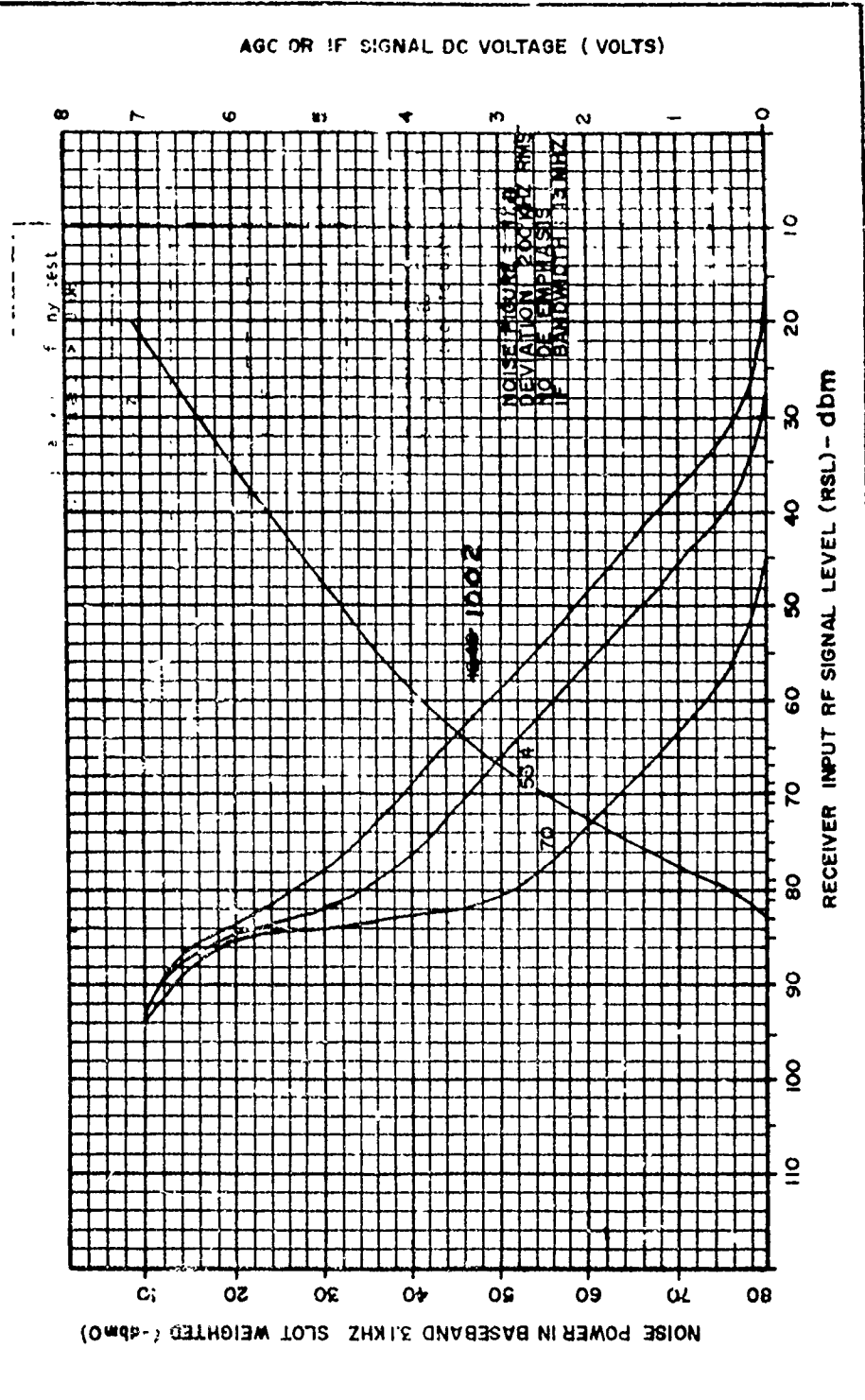


Figure E-25

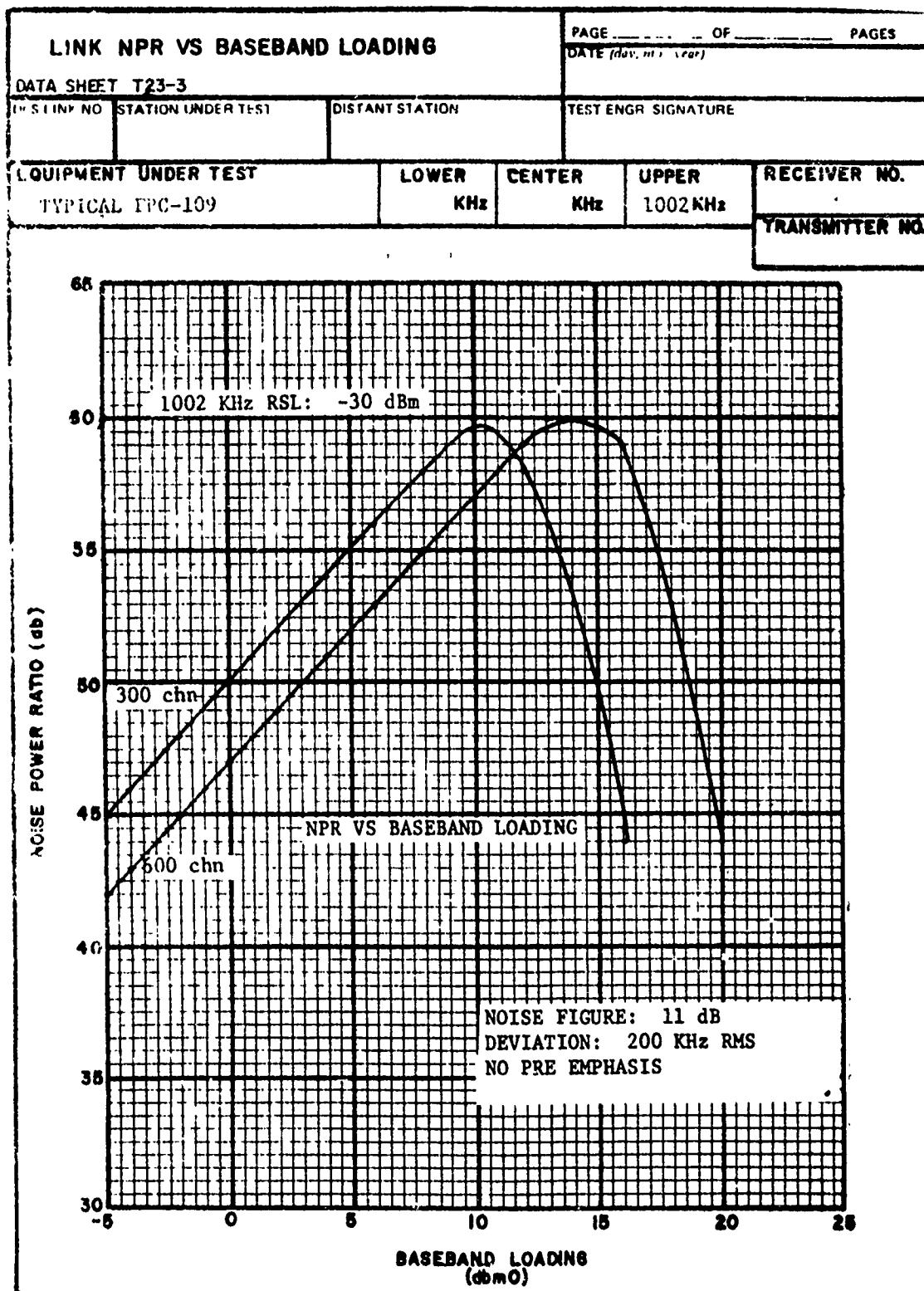


Figure B-26

SYSTEM BLOCK DIAGRAM AN/FRC -8D(V) 1

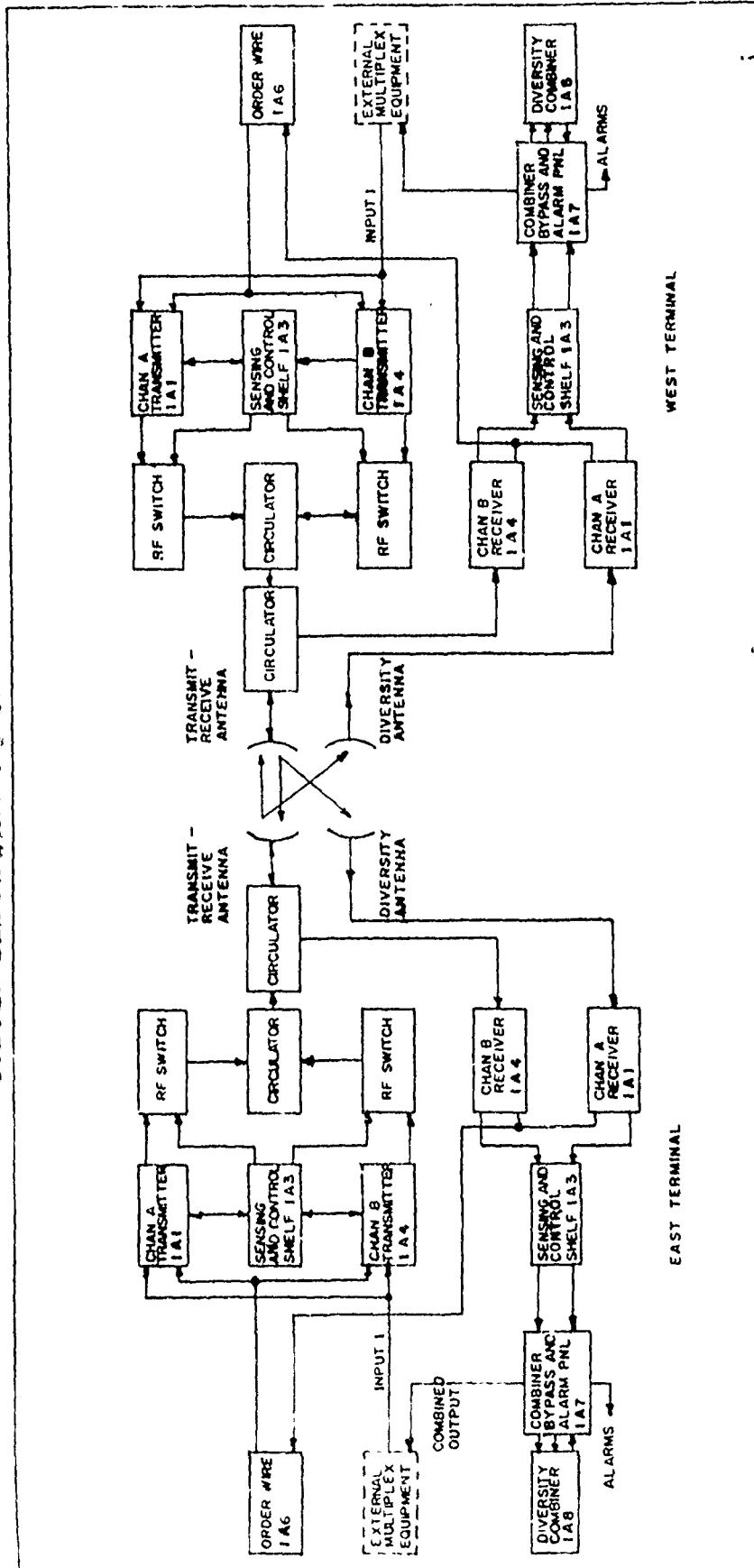


Figure E-27

SYSTEM BLOCK DIAGRAM AM/FRC - 80 (V) 2-3

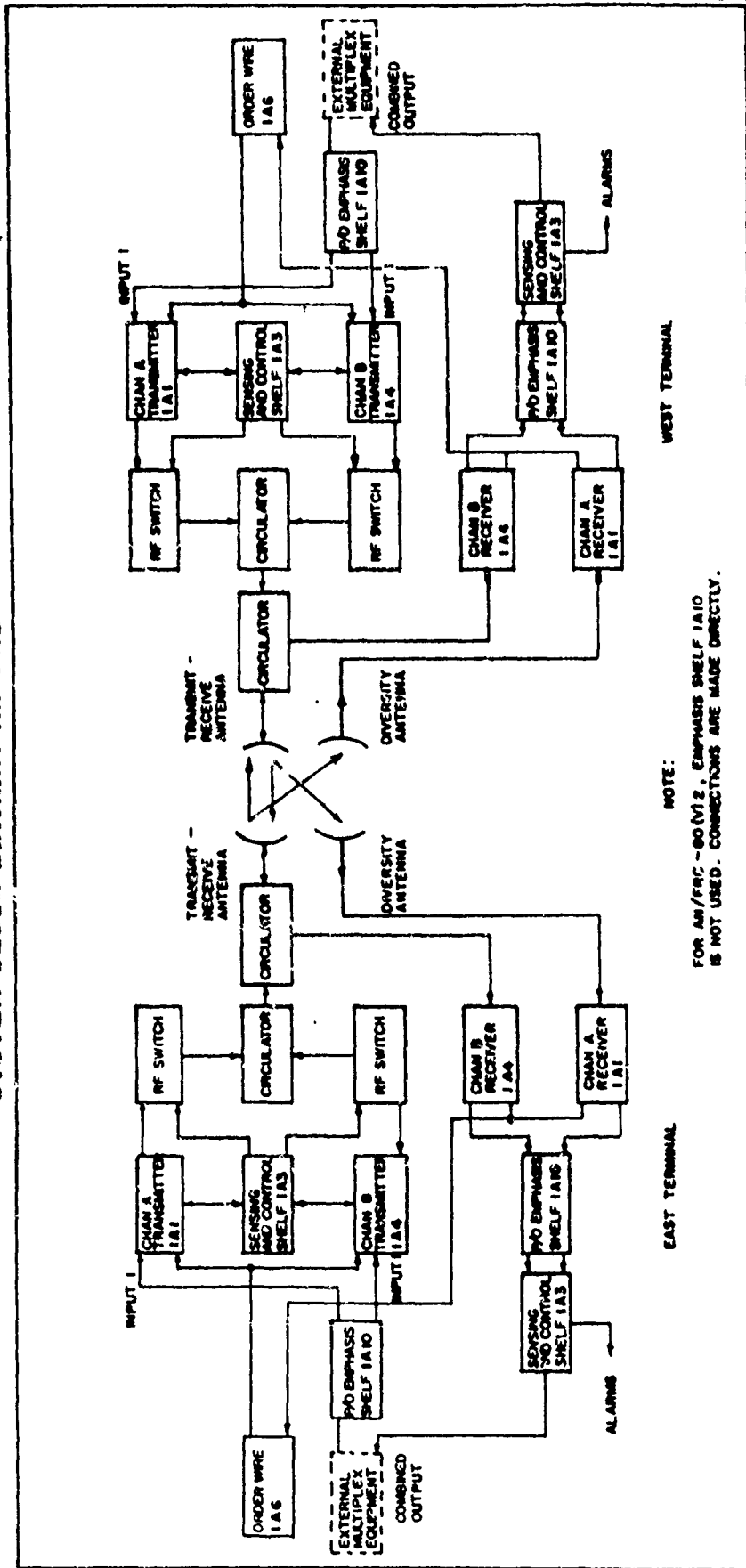


Figure E-28

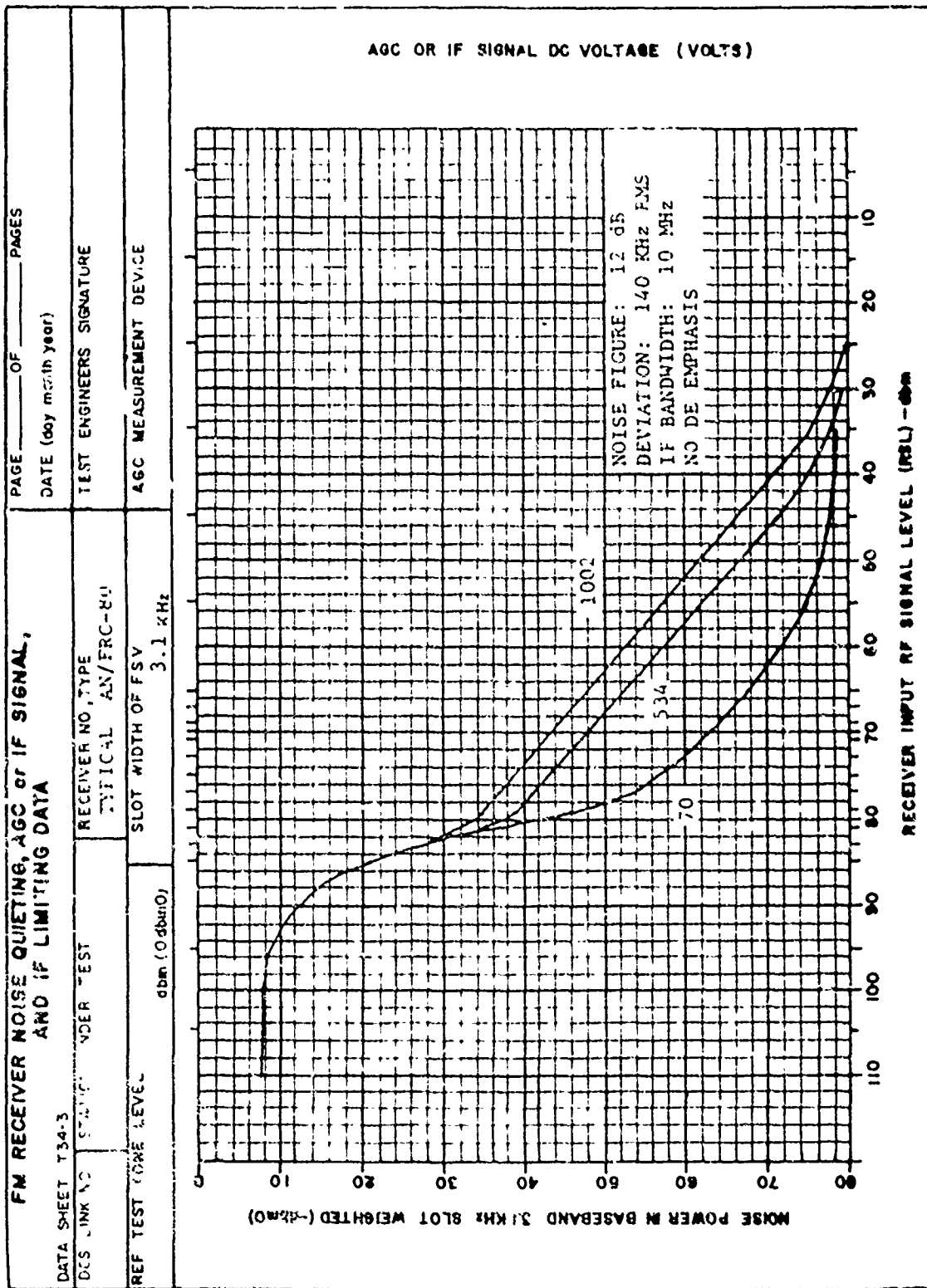


Figure E-29

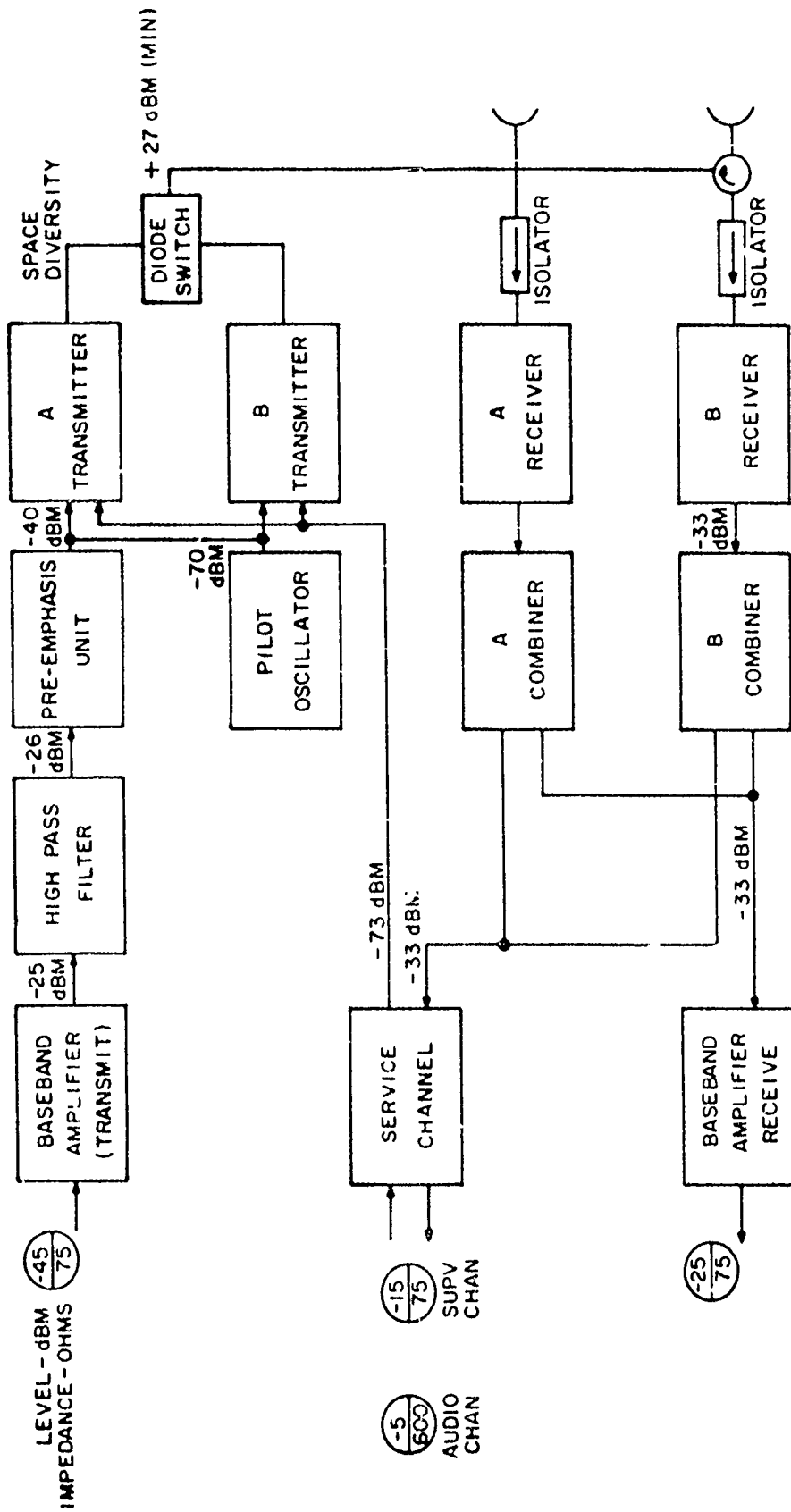
FIGURE E-30

TYPICAL NPR CURVE, AN/FRC-80

TO BE PUBLISHED

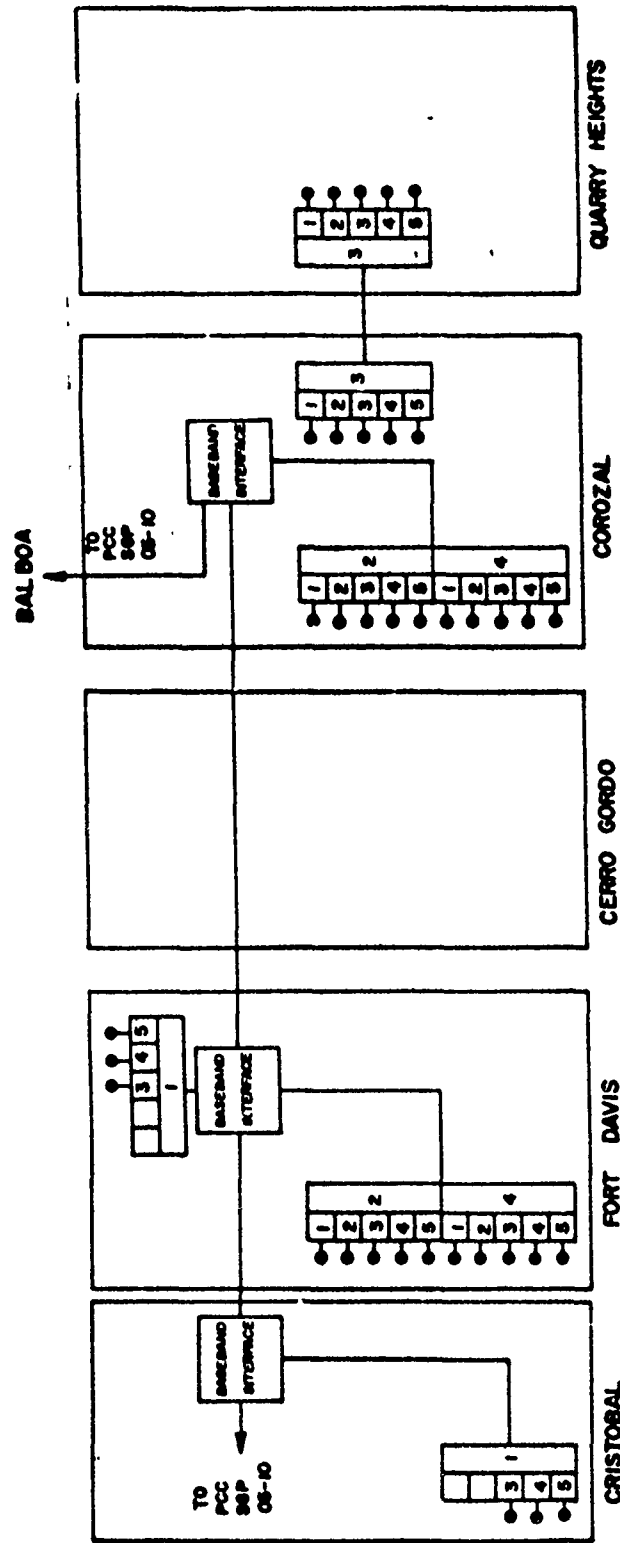
Figure E-30

E-55



AN/FRC-159 (V) RADIO
SIMPLIFIED BLOCK DIAGRAM

Figure E-31



LEGEND

1	2	3
4	5	
1		

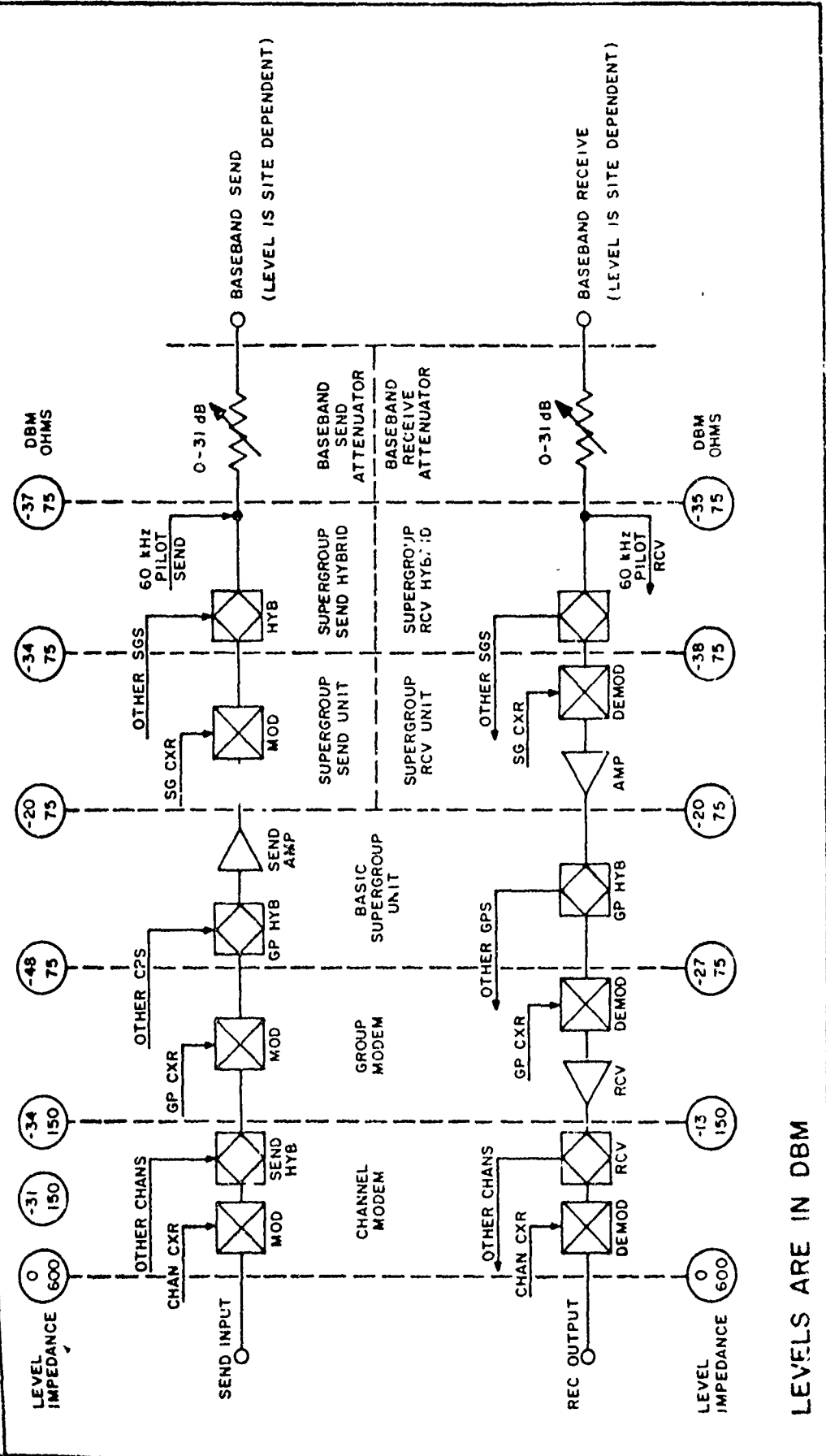
SUPERGROUP 1,
 GROUPS 1, 2 & 3
 WITH 12 V/F CHANNELS
 TERMINATED ON
 EACH GROUP

PCC: PANAMA CANAL COMPANY

TRANS-ISTHMIAN MICROWAVE SYSTEM (TIMS)

Figure E-32

TRANS - ISTHMIAN MICROWAVE SYSTEM TYPICAL BLOCK AND LEVEL DRAWING, AN/FCC-18



LEVELS ARE IN DBM

Figure E-33

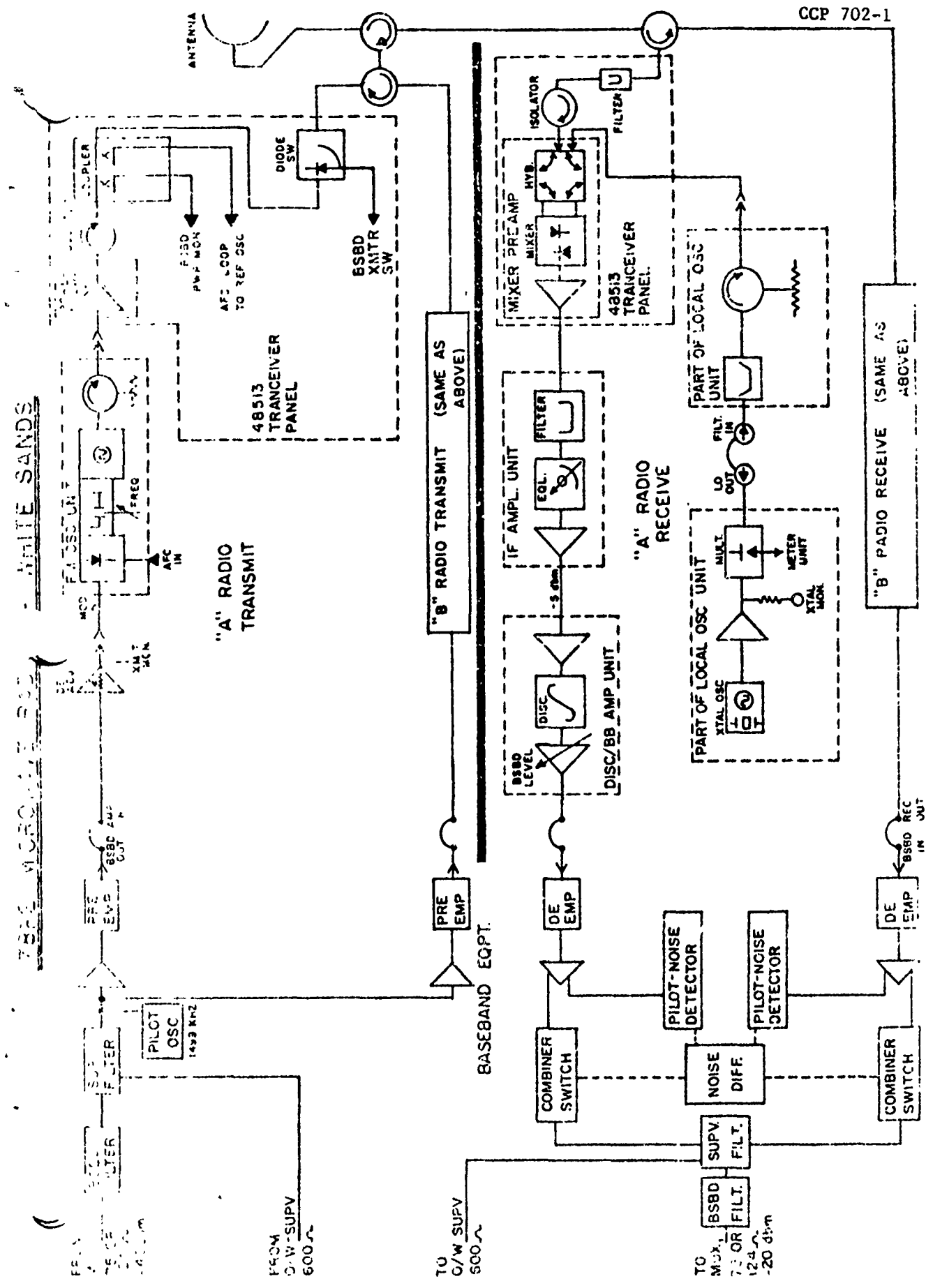
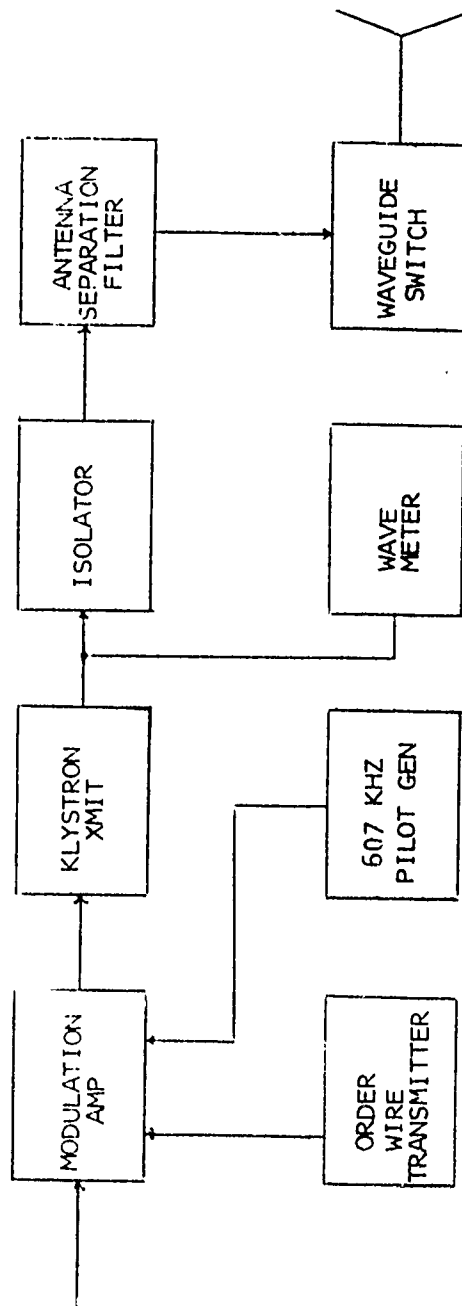
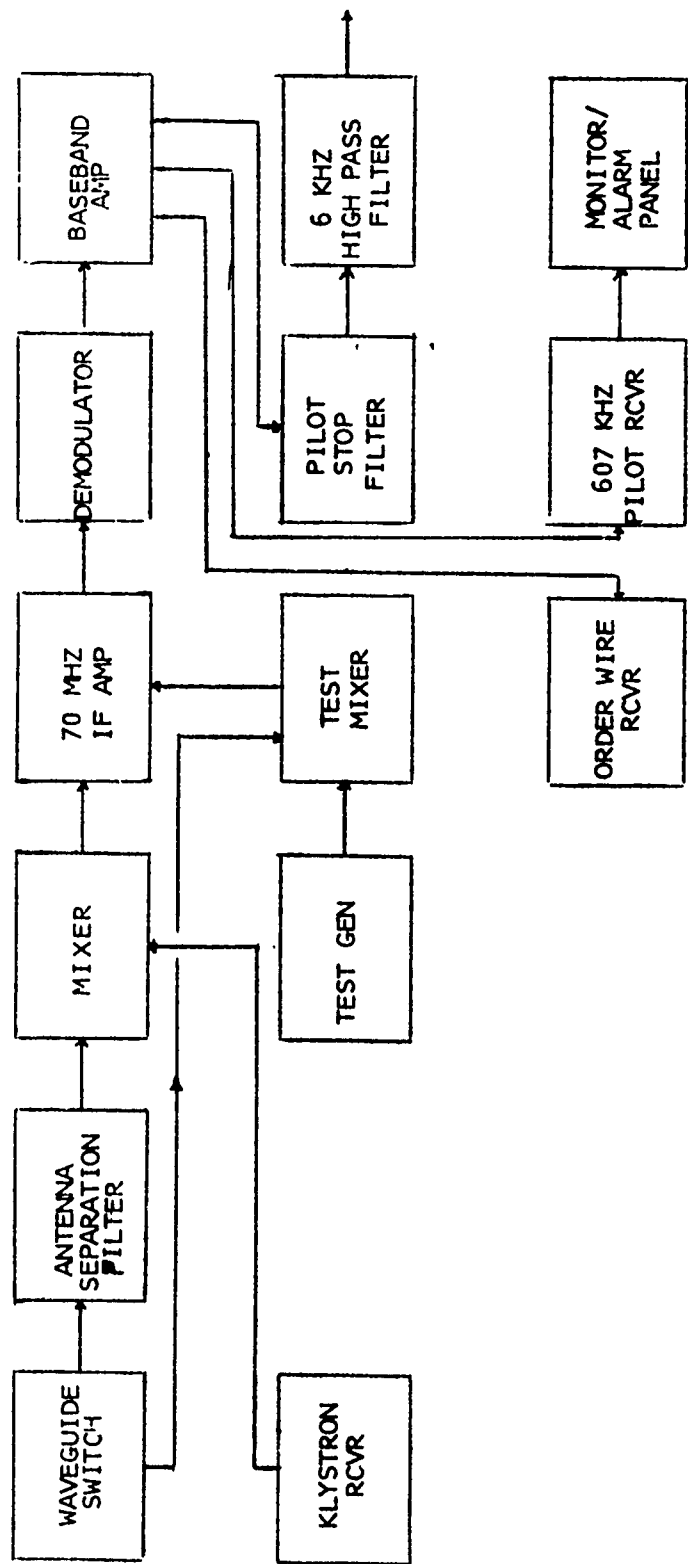


Figure E-34



SIEMENS FM / 8000 TRANSMITTER

Figure B-35



S I E M E N S F M / 8 0 0 0 R E C E I V E R

Figure E-36

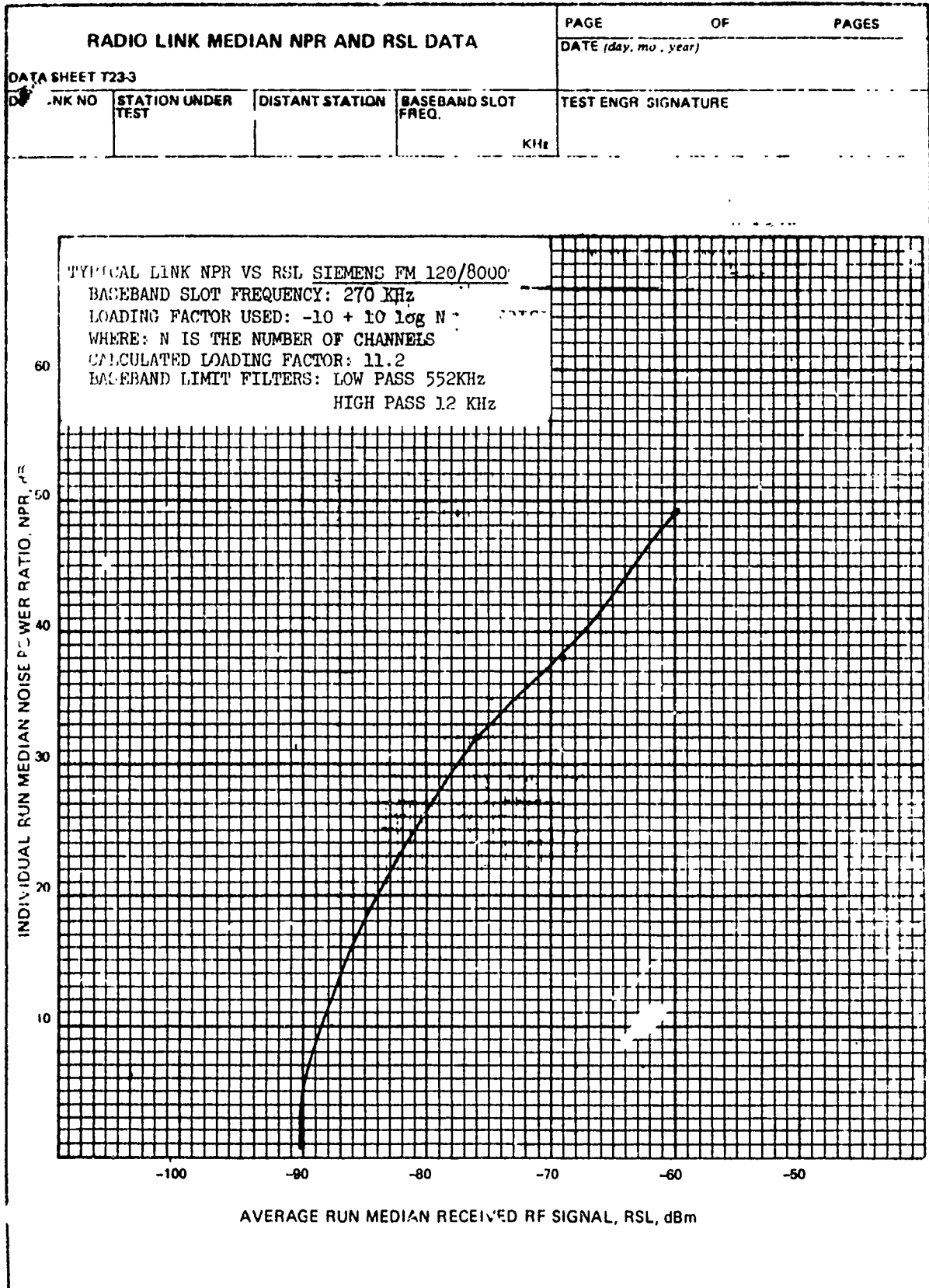


Figure E-37

EQUIPMENT NR VS BASEBAND LOADING

DESIGN SHEET 122

DESIGN SIGNATURE

LINE	NOTED
1	70 KHZ
2	270 KHZ
3	534 KHZ

SCALES
 X RELATIVE TO THE NORMAL COMULATIVE POWER Pm DB
 Y ABSOLUTE POWER Pm DBm
 Z RF ACTIVE TO THE REF TEST TONE SIG POWER, DBm
 Y and Z SCALES SHOWN ARE FOR 132 CHS AND 1000 CHS LDG
 RSL 40 DBm

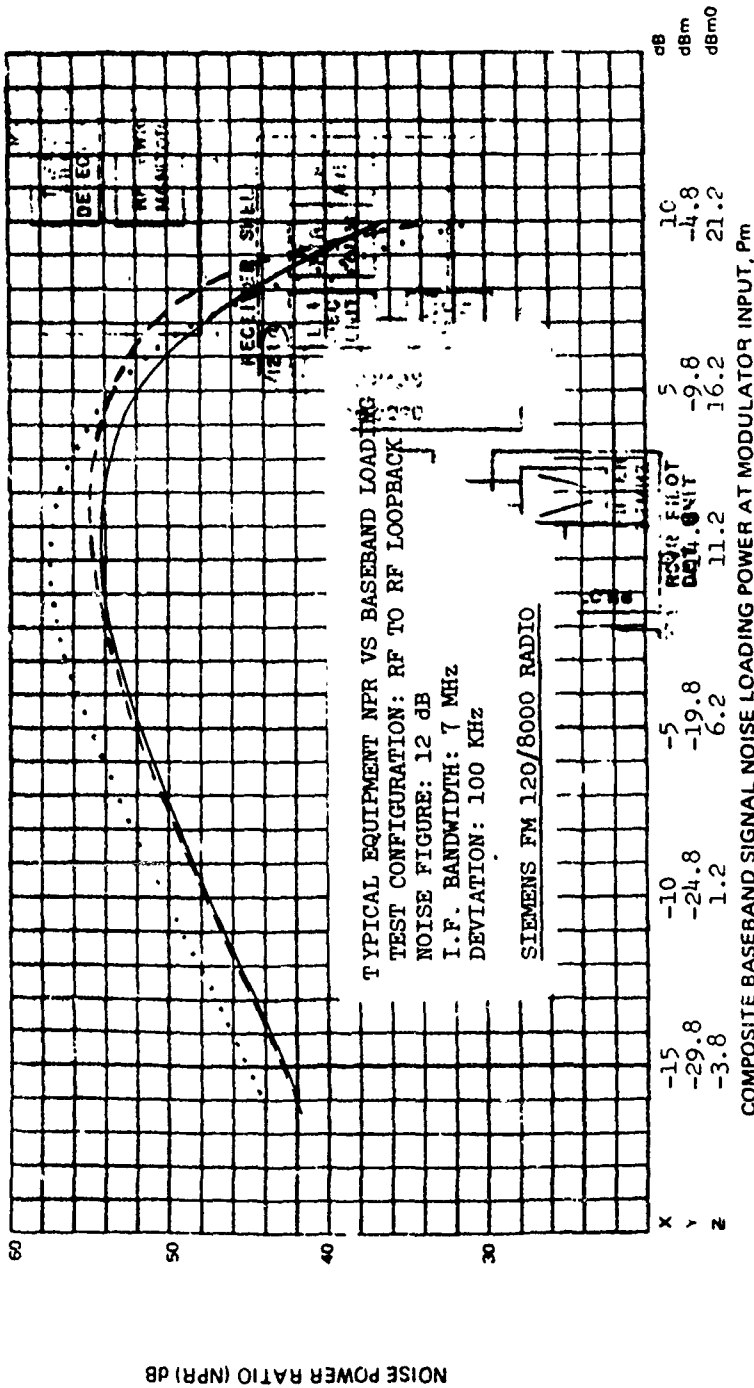
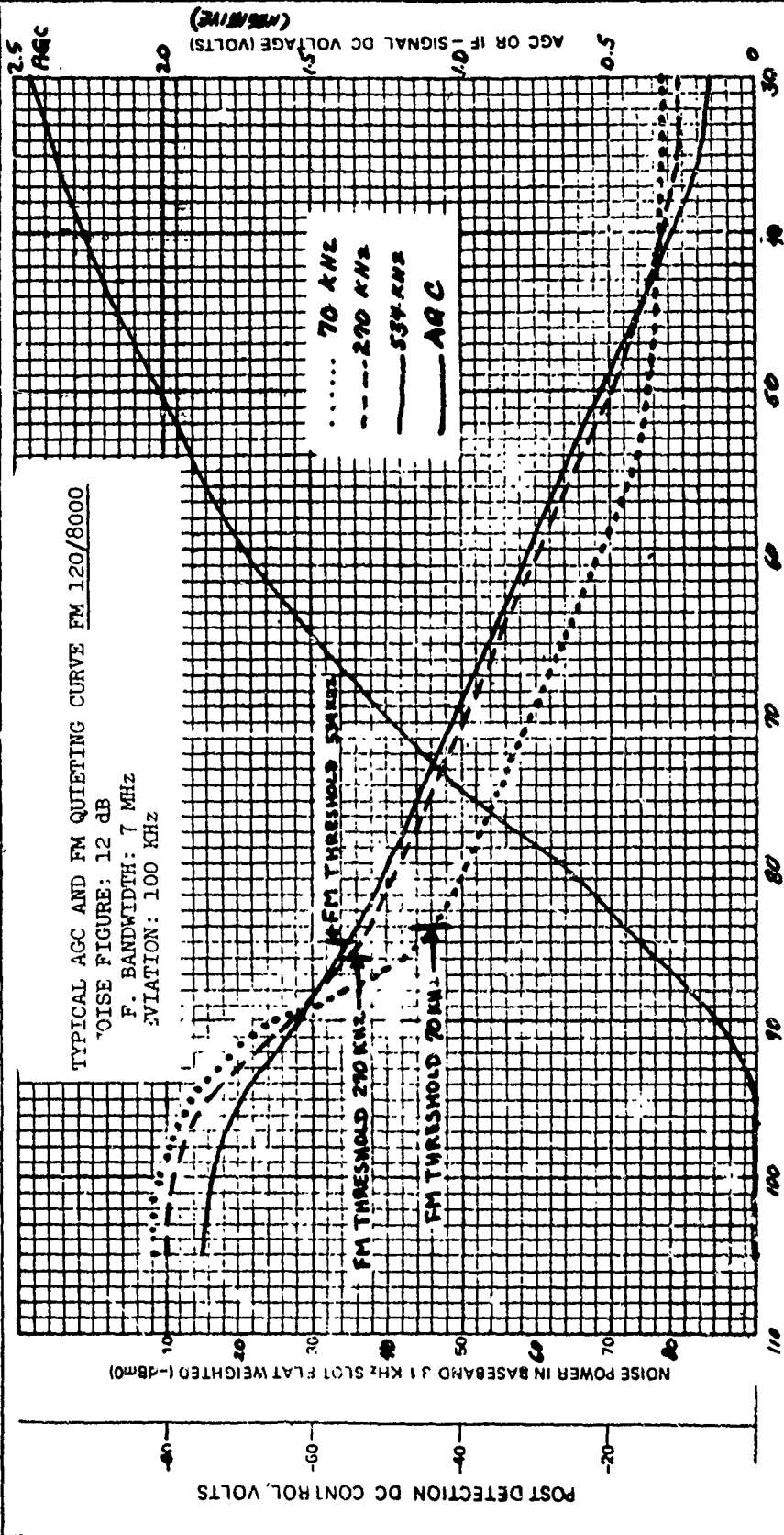


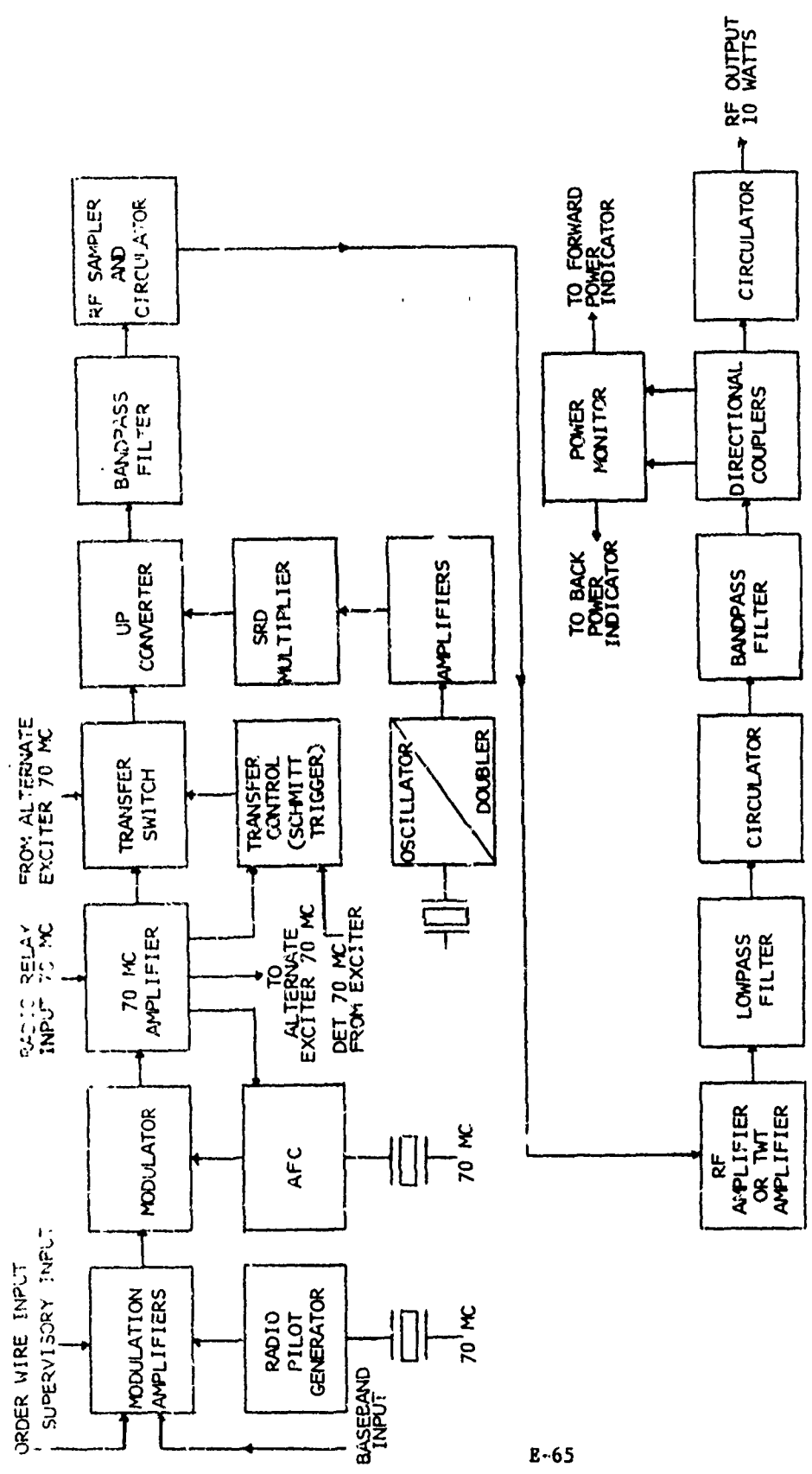
Figure E-38

DATA SHEET T34-3 DCS LINK NO. STATION UNDER TEST REF. TEST TONE LEVEL		FM RECEIVER NOISE QUIETING, AGC OR IF SIGNAL, AND IF LIMITED DATA		PAGE _____ OF _____ PAGES DATE (day month year) _____
(RECEIVER NAME, Model and Manufacturer)		TESTING SIGNATURE		SLOT WIDTH CORRECTION TO 31 KHz dB
dBm (0dBm)		KHz		SLOT WIDTH OF F.S. VOLTMETER



RECEIVER INPUT RF SIGNAL LEVEL (RSL), - dBm

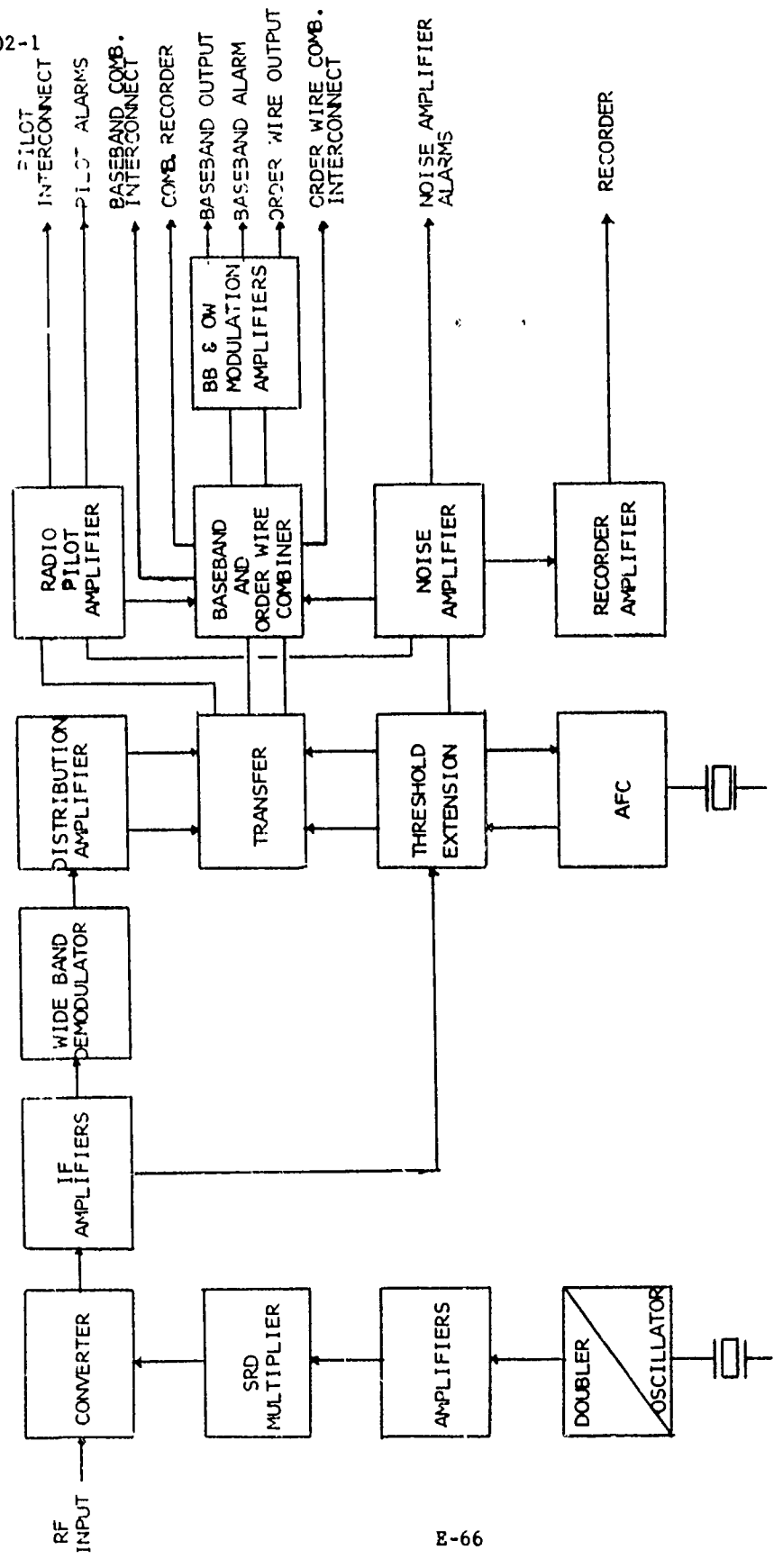
Figure E-39



2600-SERIES EXCITER, SIMPLIFIED BLOCK DIAGRAM

Figure E-40

CCP 702-1



B-66

2600 - SERIES RECEIVER, SIMPLIFIED BLOCK DIAGRAM

Figure B-41

THRESHOLD LEVEL, THRESHOLD EXTENSION, AND NPR CURVES

PAGE _____ OF _____ PAGES
DATE 3/1/57

DATA SHEET T227
RECEIVER NO. _____ TRANSMITTER NO. _____ FREQ. MOD. NO. _____ STATION UNDER TEST DCE. A.K.A. NO. _____ TEST ENG. S. C. NO. _____

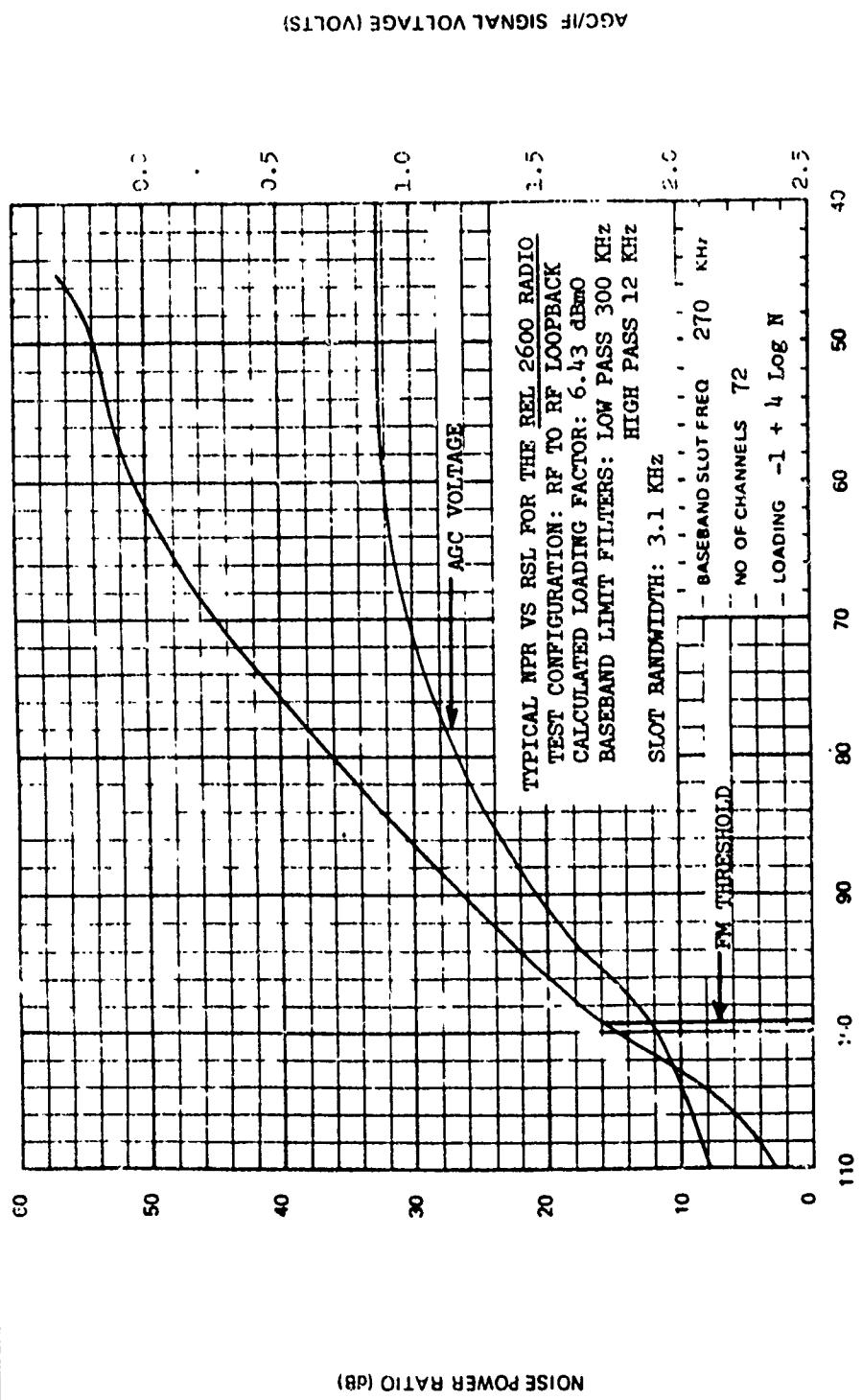
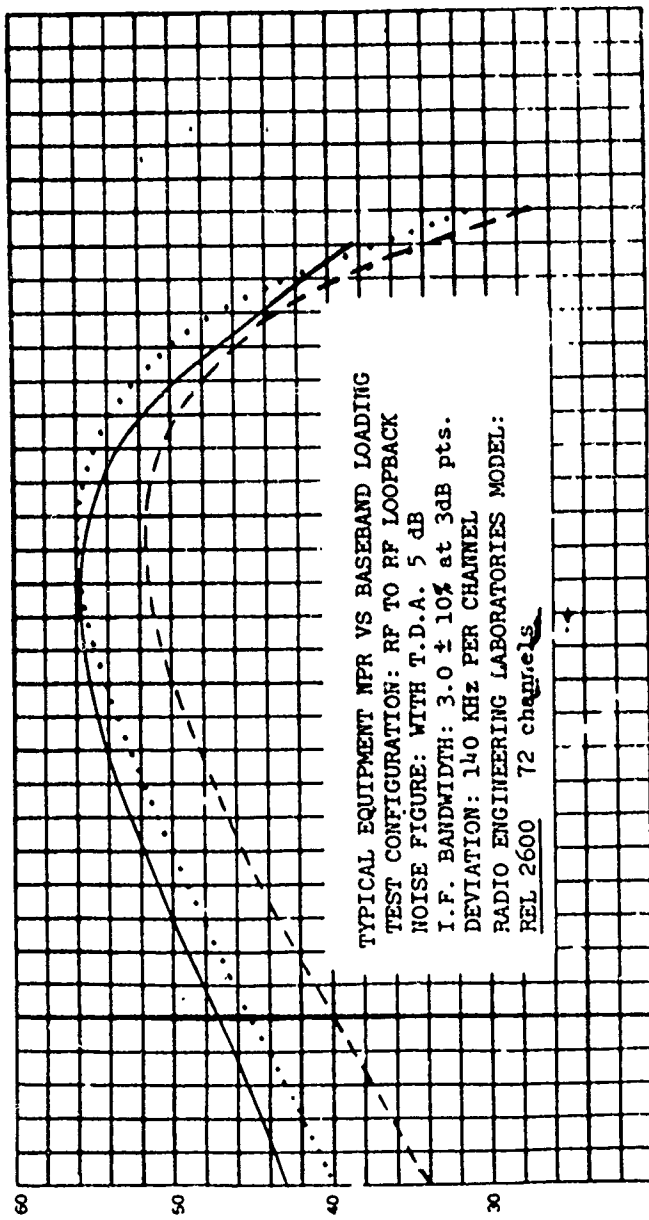


Figure E-42

EQUIPMENT NPR VS BASEBAND LOADING		FILE	CP
DATA SHEET 1222	TEST VOLTAGE	DATE	DESIGN
DGS LINK NO	TRANS NO	TEST ENG SIGNATURE	

SCALES
 X RELATIVE TO THE NORMAL CUMULATIVE POWER Pm, dB
 Y ABSOLUTE POWER Pm, dBm
 Z RELATIVE TO THE REF TEST TONE SIG POWER, dBm0
 Y and Z SCALES SHOWN ARE FOR -12 CHS AND -14 LOG 12 LOG
 RSL, -50 dBm

C	SLOT FREQ
.....	40 KHZ
----	185 KHZ
----	270 KHZ



TYPICAL EQUIPMENT NPR VS BASEBAND LOADING
 TEST CONFIGURATION: RP TO RF LOOPBACK
 NOISE FIGURE: WITH T.D.A. 5 dB
 I.F. BANDWIDTH: 3.0 ± 10% at 3dB pts.
 DEVIATION: 140 KHZ PER CHANNEL
 RADIO ENGINEERING LABORATORIES MODEL:
 REL 2600 72 channels

X	-15	-10	-5	0	5	10
Y	-43.6	-43.6	-36.6	-36.6	-28.6	-28.6
Z	-2.6	-2.6	1.4	1.4	10.4	10.4

COMPOSITE BASEBAND SIGNAL NOISE LOADING POWER AT MODULATOR INPUT, Pm

Figure Panel 3

PAGES

OF

REF. NO. SIGNATURE

FM RECEIVER NOISE QUANTIFYING, AGC OR IF SIGNAL, AND IF LISTENING DATA

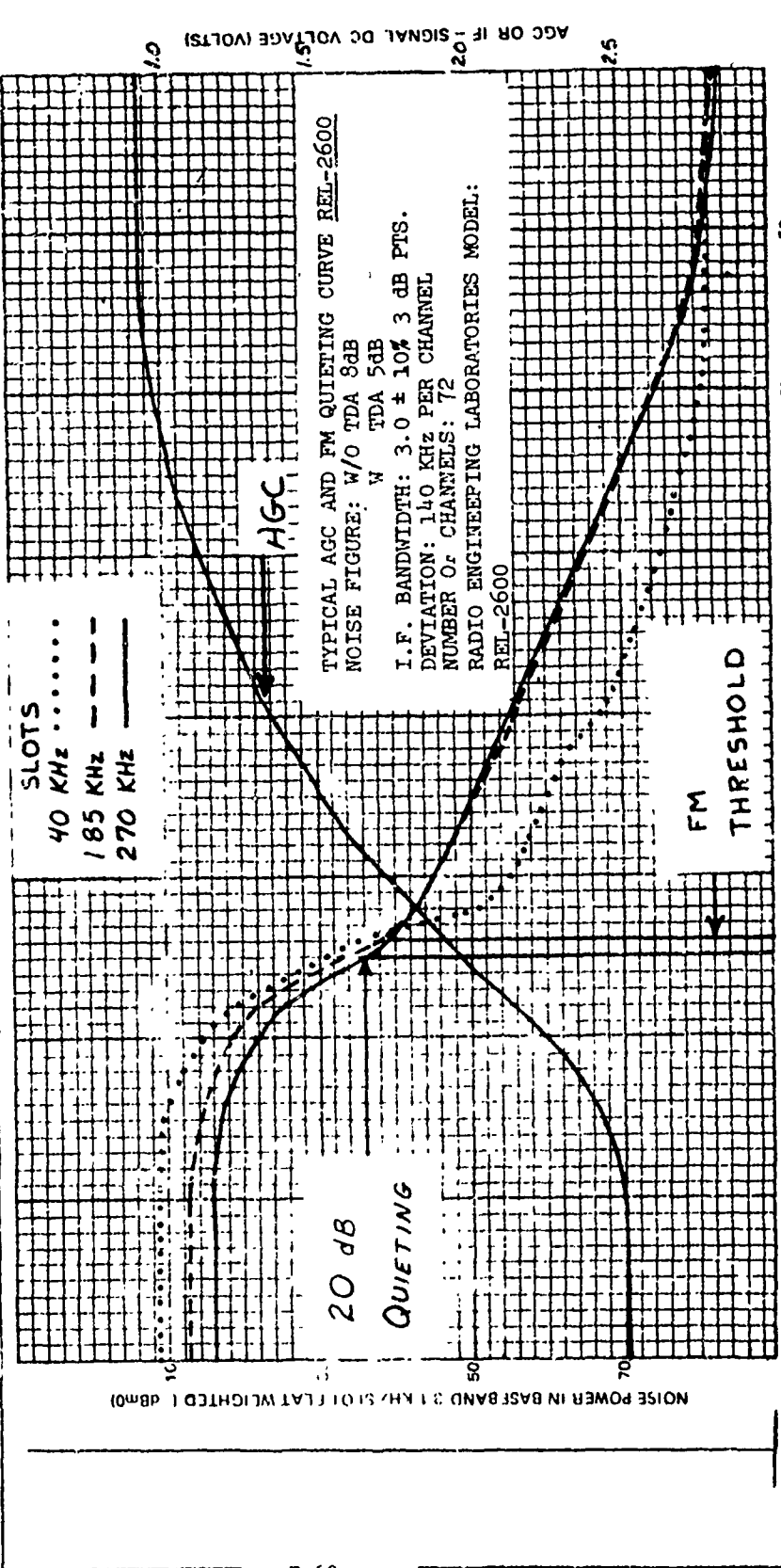
DATA SHEET NO. 2

DCS LINK NO. STATION UNDER TEST

FACE OF

REF. NO. SIGNATURE

REF. TEST TONE LEVEL (dBm) (0dBm=0) SLOT WIDTH OF FS VOLTMETER (KHZ) SLOT WIDTH CORRECTION TO 3 KHZ (dB)

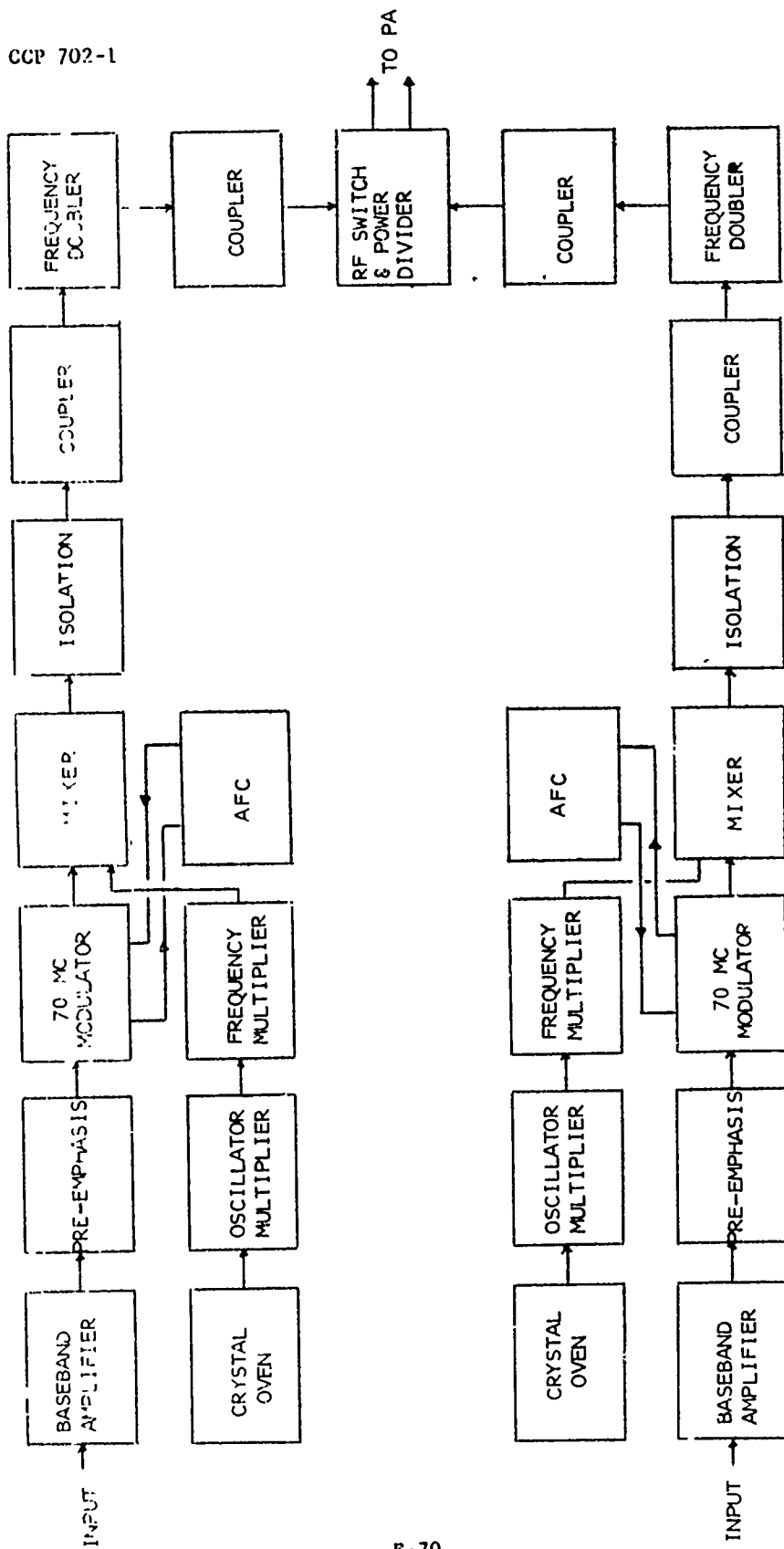


TYPICAL AGC AND FM QUIETING CURVE REL-2600
 NOISE FIGURE: W/O TDA 8dB
 W TDA 5dB
 I.F. BANDWIDTH: $3.0 \pm 10\%$ 3 dB PTS.
 DEVIATION: 140 KHZ PER CHANNEL
 NUMBER OF CHANNELS: 72
 RADIO ENGINEERING LABORATORIES MODEL:
 REL-2600

RECEIVER INPUT RF SIGNAL LEVEL (R.S.L.), - dBm

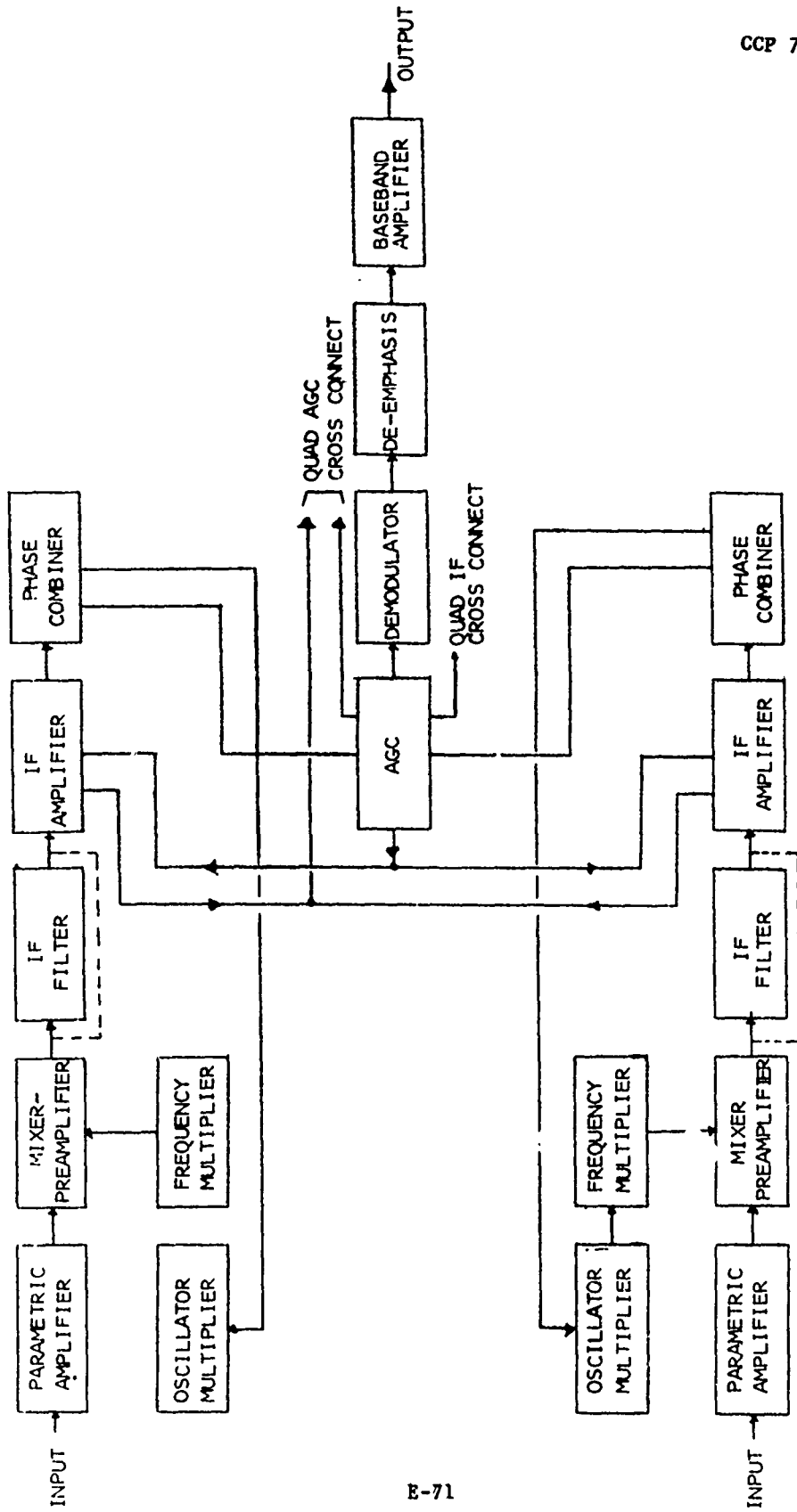
Figure E-44

CCP 702-1



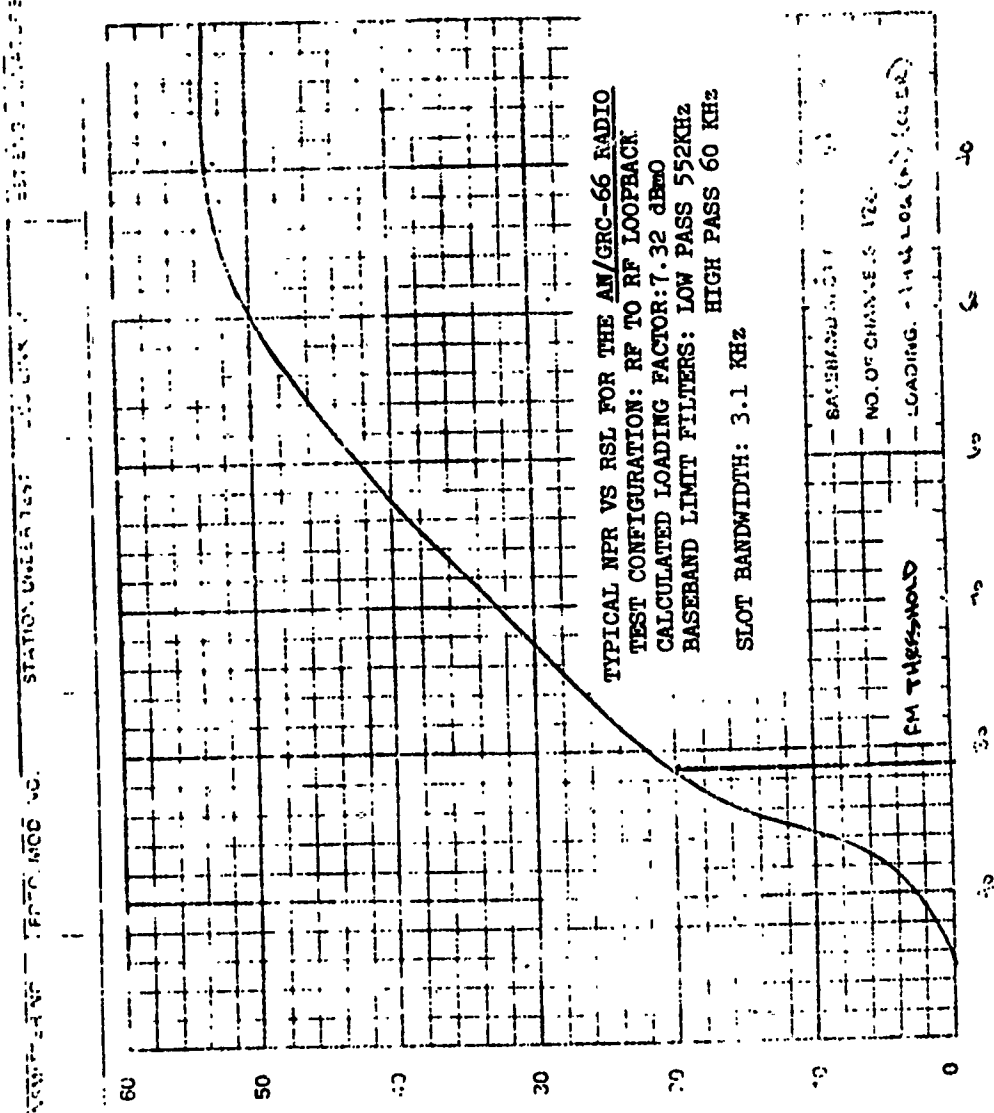
A N / G R C - 6 6 T R A N S M I T T E R

Figure E-45



AN/GRC-66 SIMPLIFIED BLOCK DIAGRAM, RECEIVER
Figure E-46

THRESHOLD LEVEL, THRESHOLD EXTENSION,
AND NPR CURVES



NOISE POWER RATIO (dB)

RF POWER INPUT RE SIGNAL (RSL) (dBm)

Figure 1

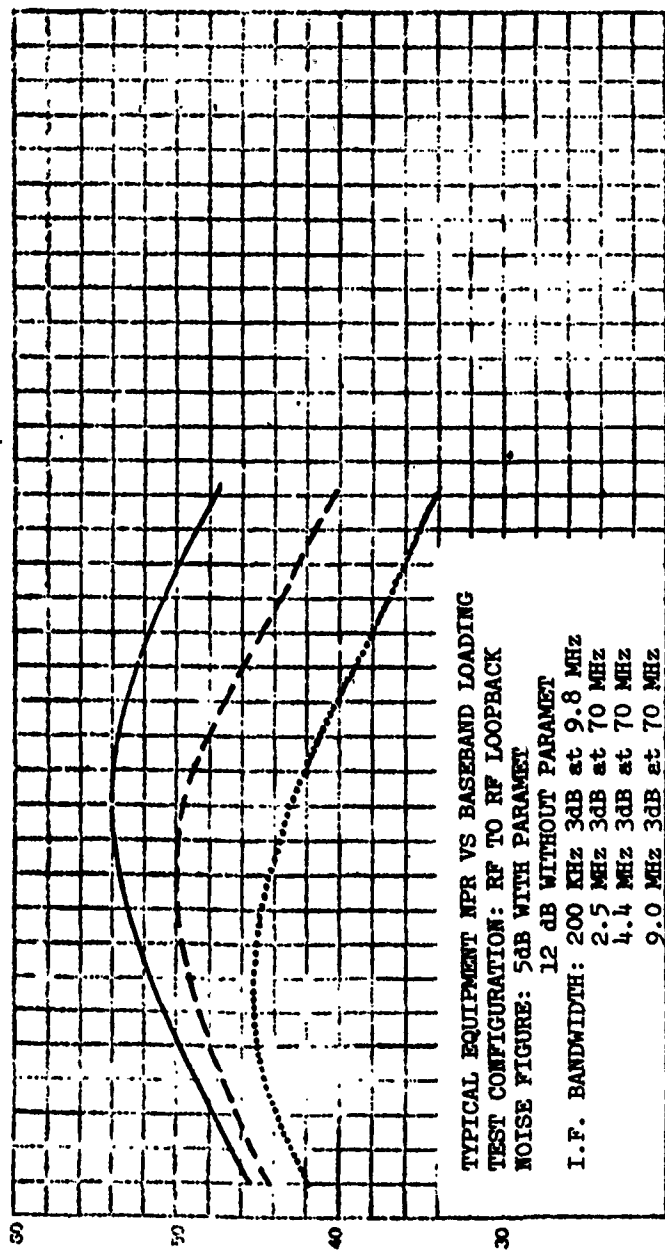
EQUIPMENT NPR VS BASEBAND LOADING

EQUIPMENT UNDER TEST: ITT FEDERAL LABORATORIES
AV/GRC-66

TEST DATE: 8-19-67

CURVE	SLOT FREQ (KHz)
.....	70
-----	210
-----	574

SCALES: X - RELATIVE TO THE "NORMAL" CUMULATIVE POWER Pm, dB
 Y - ABSOLUTE POWER Pm, dBm
 Z - RELATIVE TO THE REF. TEST TONE SIG. (0dB), dBm
 Y and Z SCALES SHOWN ARE FOR 120 C.S. AND 1.5 LOG 120 LOG.



TYPICAL EQUIPMENT NPR VS BASEBAND LOADING
 TEST CONFIGURATION: RF TO RF LOOPBACK
 NOISE FIGURE: 5dB WITH PARAMET
 12 dB WITHOUT PARAMET
 I.F. BANDWIDTH: 200 KHz 3dB at 9.8 MHz
 2.5 MHz 3dB at 70 MHz
 4.4 MHz 3dB at 70 MHz
 9.0 MHz 3dB at 70 MHz

Figure E-46

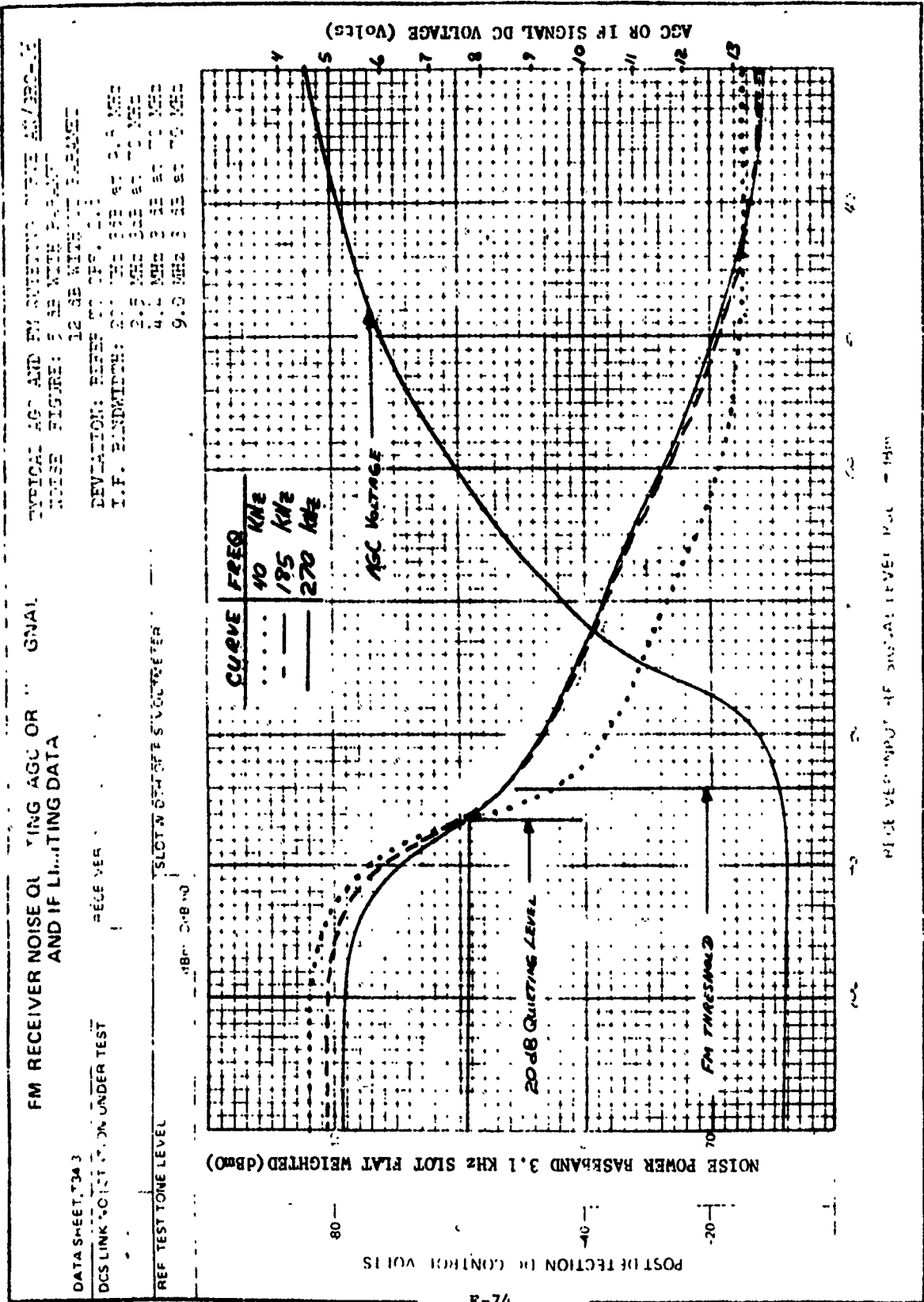


Figure E-49

MANUFACTURER'S RADIO SPECIFICATIONS

TEST	MIL-STD	FRC-80	FRC-109	FRC-154	LRC-3	AM/GRC-147
Link Noise Power Ratio (NPR) (T-23)	55 dB	At CCIR loading NPR at least 53 dB for 120 CH NPR at least 57 dB for 240 CH NPR at least 55 dB for 300 or 600 CH	300 CH at +10 dBmO 70 kHz 56.5 dB 534 kHz 53.5 dB 1248 kHz 50.5 dB 600 CH at +13 dBmO w/o emphasis 70 kHz 57.5 dB 1248 kHz 54.5 dB 2438 kHz 52.5 dB	At DCA loading NPR at least 55 dB for all slots, for 240 CH and 600 CH systems	RF loopback for a -40 dBm (RSL) phase lock receivers, NPR > 50 dB L/D receivers, NPR > 55	For 12 CH (12-60 kHz) at +3.3 dBm on noise generator input-BX-7 should be at least 40 dB for the 3 slots
Link Baseband Frequency Response (T-24)	± 0.5 dB over frequency range ± 1.0 dB between 0.3 and 12 kHz	From 250 through 1500 or 2540 kHz ± 0.5 dB of the level of each adjacent frequency	20 MHz bandwidth: ± 0.5 dB, 20 Hz to 8.5 MHz 15 MHz bandwidth: ± 0.5 dB, 20 Hz to 7.5 MHz 9 MHz bandwidth: ± 0.5 dB, 20 Hz to 5.5 MHz	60 to 2540 KHz, ± 0.5 dB	± 0.5 dB, 12.3 kHz to 552 kHz	
Spiral Suppression (T-25)	Baseband: -70 dBmO RF: -50 dBm between $f_0 \pm 5$ MHz to $f_0 \pm (5\% \text{ of } f_0)$	DNA	No available standard	DNA	Greater than 60 dB down	Greater than 80 dB down

TABLE E-13

TEST	MIL-STD	FRC-80	FRC-109	FRC-154	LRC-3	AV/GRC-147									
Transmitter Frequency Stability (T-27)	1 part in 10 ⁶ or 0.0001%	Within ±0.005% of assigned frequency	±0.02% or better over temperature range from -30 to +55°C, or input voltage variation of ±10%	Within ±0.01% of assigned frequency	±0.002%	±0.007%									
VSMR (T-30)	<table border="1"> <tr> <td>ANT</td> <td>LOS</td> <td>TROPO</td> </tr> <tr> <td>1.08:1</td> <td>1.11:1</td> <td>1.11:1</td> </tr> <tr> <td>EQ</td> <td>1.05:1</td> <td>1.05:1</td> </tr> </table>	ANT	LOS	TROPO	1.08:1	1.11:1	1.11:1	EQ	1.05:1	1.05:1	1.1:1 or better at equipment	At (trans) (rec) output flange 1.1:1 or better	At (trans) (rec) filters 1.1:1 or better	No available standard	Not exceed 1.2:1 taken toward
ANT	LOS	TROPO													
1.08:1	1.11:1	1.11:1													
EQ	1.05:1	1.05:1													
Transmitter Output Power (T-30)	Manufacturer's specs	At least +30 dBm	+27.5 dBm or higher	1.0 watt normal, 750 mw (min)	Exciter equipment configuration have power out of 5 watts (min), except LRC-3EL which has 5 mw (min)	1.0 watt minimum									
Receiver FM Threshold (T-34)	Manufacturer's specs	-80 dBm	-81 dBm (30 dB S/N) 300 CH hot st -79 dBm (30 dB S/N) 600 CH diversity	-79 dBm (240 CH S/N 38 dB min) (600 CH S/N 30 dB)	Tropo Rec (Phase Lock Detector) 24 -97.5 dBm 60 -94.5 dBm 120 -92.5 dBm LOS Rec Limiter Discriminator	12 CH FDM -85 dBm or lower (21 dB S/N) 12/24 & 48/96 CH PCM -85 dBm or lower									
Receiver Noise Figure (T-36)	<table border="1"> <tr> <td>≤ 12 dB (LOS)</td> </tr> <tr> <td>≤ 5 dB (Tropo)</td> </tr> </table>	≤ 12 dB (LOS)	≤ 5 dB (Tropo)	Should not exceed 12 dB	76A, 76B, & 76C: 12 dB 76D & 76E: 14 dB	11 dB	10.5 dB or less	Less than 12 dB							
≤ 12 dB (LOS)															
≤ 5 dB (Tropo)															

TABLE E-13 (Continued)

TEST	MIL-STD	FRC-80	FRC-109	FRC-154	LRC-3	AN/GRC-147
Receiver IF Bandpass Characteristics (T-39)		3 dB points 300 -600 CH 240 CH 120 CH	600 CH 15 MHz, 0.1 dB points 20 MHz, 3 dB points 300 CH 9 MHz, 0.1 dB points 13 MHz, 3 dB points	25 to 28 MHz	L/D (min), 65 to 75 MHz, at -1 dB points Phase lock, 63 to 77 MHz (min) at 1 dB points	65 to 75 MHz at 3 dB points
Receiver FM Discriminator Linearity (T-39)	< 1% over $i.4 (\Delta F_c + F_m)$ ΔF_c = peak carrier deviation, F_m = top B-B frequency	1% 60 - 80 MHz	$\leq 3\% \pm 6$ MHz $\pm 1\%$, 65 to 75 MHz (28418-05 unit 61 MHz to 79 MHz) $\pm 2\%$, 62 to 78 MHz			
IF Frequency at Zero Discriminator Output (MHz)		70	70 MHz ± 300 kHz w/AFC	70	70	FDM-70

TABLE E-13 (Continued)

DESIGN OBJECTIVES

TEST	MIL-STD
Radio Equipment Noise Power Ratio (NPR) (T-22)	55 dB
Transmitter - Modulator Frequency Deviation (T-29)	Manufacturer's specs (min capability ± 7 MHz)
RF Exciter & Power Amplifier Bandwidth (T-31)	0.1 dB RF BW is 2.8 ($\Delta F_C + F_m$) ΔF_C = peak carrier deviation, F_m = top B-B frequency
Receiver LO Frequency Accuracy (T-37)	0.0001% or 1 part in 10^6
Frequency Division Multiplex (T-40)	
a) Noise Power Ratio (NPR)	31 pWp0 or -72.5 dBm0
b) Basic Noise Ratio (BNR)	10 pWp0 or -77.5 dBm0
Radio and Frequency Division Multiplex (T-41)	
a) Radio Pilot	-10 dBm0
b) MUX Pilot	-16 dBm0
c) Group Pilot	-20 dBm0
d) Alarm Activation Limits	Manufacturer's specs

TABLE E-13 (Continued)

MANUFACTURER'S RADIO SPECIFICATIONS

TEST	MIL-STD	FM 120/6000	REL-2600	AN/GRG-66						
LINK NOISE POWER RATIO (NPR) (T-23)	55 db	DNA	DNA	1 MHz DEVIATION LOWEST NPR 52dB 1.5 MHz DEVIATION LOWEST NPR 47 dB						
LINK BASEBAND FREQUENCY RESPONSE (T-24)	+ 0.5 dB over frequency range - 1.0 dB between 0.3 and 12 kHz	DNA	DNA	DNA						
SPURIOUS SUPPRESSION (T-25)	Baseband: -70dBmO RF: -50 dBm between $f_0 \pm 5$ MHz to $f_0 \pm (5\% \text{ of } f_0)$	DNA	80 dB below carrier	-80 dB MAXIMUM						
TRANSMITTER FREQUENCY STABILITY (T-27)	1 part in 10^6 or 0.0001%	DNA	DNA	DNA						
VSWR (T-30)	<table border="1" style="width: 100%; border-collapse: collapse;"> <tr> <td style="text-align: center;">LOS</td> <td style="text-align: center;">TROPO</td> </tr> <tr> <td style="text-align: center;">AWT 1.08:1</td> <td style="text-align: center;">1.11:1</td> </tr> <tr> <td style="text-align: center;">EQ 1.05:1</td> <td style="text-align: center;">1.05:1</td> </tr> </table>	LOS	TROPO	AWT 1.08:1	1.11:1	EQ 1.05:1	1.05:1			1.5:1
LOS	TROPO									
AWT 1.08:1	1.11:1									
EQ 1.05:1	1.05:1									

TABLE E-13 (Continued)

TEST	MIL-STD	FM 110/5000	REMARKS	REQUIREMENTS
TRANSMITTER OUTPUT POWER (T-30)	MANUFACTURER'S SPECS	GREATER THAN 0.5 W 2 W NOMINAL	EXCEPT OUT 10 W P.A. OF 1000 W	1 W NOMINAL 1000 W INTO A 50-Ω WAVEGUIDE
RECEIVER FM THRESHOLD (T-34)	MANUFACTURER'S SPECS	-78.73	WITH TDA -95.27 dBm WITHOUT TDA -89.0 dBm	CH'S COEFFIC dBm 120 W/P & TE -92.76 120 W/P W/C TE -89.76 120 W/O P W/TE -85.76 120 W/O P W/C TE -82.76 60 W/P & TE -95.37 60 W/P W/O TE -92.87 60 W/O P W/TE -88.87 60 W/O P W/O TE -85.87 12 W/P W/O TE -88.32 2 W/P & TE -109.29 LOS 120 W/O P W/C TE -82.76 60 W/O P W/C TE -85.87 2 W/O P W/C TE -99.29
RECEIVER NOISE FIGURE (T-36)	12 dB (LOS) 5 dB (TROPO)	12 dB	WITH TDA 5 dB WITHOUT TDA 8 dB	5 dB WITH PARAMET 12 dB WITHOUT PARAMET
RECEIVER IF BANDPASS CHARACTERISTICS (T-39)		7 MHz	3.0 ± 10% 3 dB PFS.	200 KHz 3dB AT 9.8MHz 2.5 MHz 3dB AT 70 MHz 4.4 MHz 3dB AT 70 MHz 9.0 MHz 3dB AT 70 MHz
RECEIVER FM DISCRIMINATOR LINEARITY (T-39)	< 1% OVER 1.4(Δ F _c +F _m) ▲ F _c = PEAK CARRIER DEVIATION, F _m = TOP B-B FREQUENCY	DNA	DNA	SENSITIVITY 5.1 V PER MHz CHANNEL

TABLE E-13 (Continued)

CASE	TEST CASE	TEST POINT	TEST SIGNAL	TEST RESULT
IF FREQUENCY AT ZERC DISCRIMINATOR OUTPUT (MHz)		70 MHz	70 MHz	70 MHz OR 9.2 MHz

TABLE E-13 (Continued)

MISCELLANEOUS DATA

SECTION 1. FORMULAS AND EQUATIONS

Earth Curvature

$$h' = \frac{d_1 d_2}{12.75 K_e}$$

$$h (K_e = 0) = 0$$

$$h (K_e = 4/3) = \frac{d_1 d_2}{17}$$

$$h (K_e = 2/3) = \frac{d_1 d_2}{8.5}$$

h = meters

d = kilometers

Reflection Point Relations

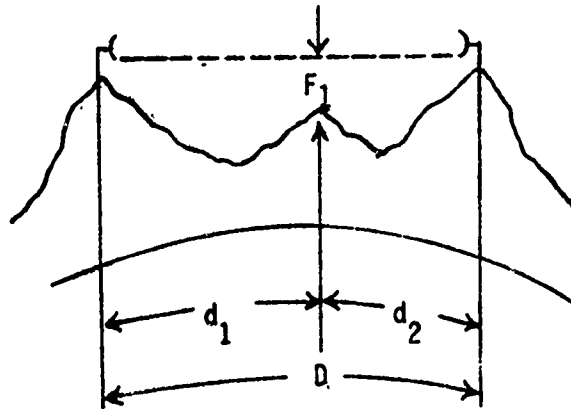
$$\text{For } K_e = 4/3; \quad \frac{h_1}{d_1} - \frac{d_1}{17} = \frac{h_2}{d_2} - \frac{d_2}{17}$$

$$\text{For } K_e = 2/3; \quad \frac{h_1}{d_1} - \frac{d_1}{8.5} = \frac{h_2}{d_2} - \frac{d_2}{8.5}$$

First Fresnel Zones Clearance

$$F_1 = 17.3 \frac{d_1 d_2}{F_{\text{GHz}} D}$$

F_1 in meters, d 's and D in kilometers



FM Threshold

$$T_{\text{FM}} = -164 \text{ dBm} + 10 \log (B_w) + \text{NF}$$

where: B_w = IF Bandwidth (Hz)

NF = Noise Figure (dB)

Noise Units Correlation

$$\text{dBrnC0} = 10 \log \text{pWp0} + 1.0$$

$$= \text{dBa0} + 6.0$$

$$= 88.5 - S/N_{\text{flat}}$$

$$S/N_{\text{flat}} = 88.5 - \text{dBrnC0}$$

$$S/N_{\text{flat}} = 90 - \text{dBrn0}$$

$$S/N_{\text{flat}} = 82.5 - \text{dBa0}$$

$$S/N_{\text{flat}} = 87.5 - \text{dBrn0}_{(\text{pWp})}$$

$$\text{pWCO} = \log^{-1} \left(\frac{X}{10} \right) \quad X \text{ is in dBrnC0 units}$$

$$\text{pWp0} = \log^{-1} \left(\frac{X}{10} \right) \quad X \text{ is in dBrn0}_{(\text{pWp})} \text{ units}$$

$$\text{pW0} = \log^{-1} \left(\frac{X}{10} \right) \quad X \text{ is in dBrn0 units}$$

CCP 702-1

Noise Power Ratio (NPR)

$$S/N = NPR - .NL + .BWR$$

where NL = Noise Loading (dBm0)

CCIR Criteria:

$$NL = -15 + 10 \log N \quad N > 240 \text{ channels}$$

$$NL = -1 + 4 \log N \quad N \leq 240 \text{ channels}$$

Military:

$$NL = -10 + 10 \log N$$

where BWR = Bandwidth Ratio

Channel Capacity	BWR = $\log \left(\frac{f_m - f_o}{b} \right)$
60	18.9
120	22.0
240	25.1
300	26.0
600	29.0

Thermal Noise (Receiver Quieting)

$$S/N = RSL + 136 - NF + 20 \log \frac{D_p}{f_m} + I_p$$

where RSL = Receive Signal Level (dBm)

NF = Receiver Noise Figure (dB)

D_p = Peak Per Channel Deviation (kHz)

f_m = Channel Baseband Frequency of Interest (kHz)

I_p = Pre-Emphasis Improvement

CCP 702-1

VSWR

$$L_R = \text{Return Loss} = 20 \log \left| \frac{\text{VSWR} + 1}{\text{VSWR} - 1} \right|$$

$$\text{VSWR} = \frac{1 + \log^{-1} \left(\frac{L_R}{20} \right)}{-1 + \log^{-1} \left(\frac{L_R}{20} \right)}$$

Useful Conversions

- 1 Nautical mile = 6076.1 ft
- 1 Nautical mile = 1.1508 Statute mile
- 1 Statute mile = 0.8690 Nautical mile
- 1 Statute mile = 1.609 Kilometers
- 1 Kilometer = 0.6214 Statute mile
- 1 Foot = 30.48 Centimeters
- 1 Meter = 3.281 Feet

APPENDIX F
MISCELLANEOUS DATA

CCP 702-1

SECTION II. SYMBOLS AND DEFINITIONS

b	Channel bandwidth, Hz
B _w	IF bandwidth in Hz
D _p	The per channel peak deviation at zero pre-emphasis
D' _p	Per channel peak deviation for the modulating frequency with the effects of pre-emphasis included $= D_p \text{ Antilog } \frac{I'_p}{20}$
D _{RMS}	RMS per channel deviation (equipment specifications)
D' _{RMS}	Per channel RMS frequency deviation for any frequency in the baseband having pre-emphasis
D _s	Peak system deviation in kHz
f	The baseband frequency of interest
f _{max}	Maximum baseband frequency
f ₀	Lowest baseband frequency
f _p	Modulating (pivot) frequency
f _r	Circuit resonant frequency = 1.25 f _{max}
f _t	Test tone frequency required for first carrier dropout
I _p	Pre-emphasis improvement for the frequency of interest
k	Boltzmann's constant = $1.38 \times 10^{-23} \frac{\text{watts} \cdot \text{sec}}{\text{°Kelvin}}$
K	A numerical factor depending upon allowable distortion
L _n (dBm0)	Required test tone level for first carrier dropout
M	Modulation index
N	Number of channels

CCP 702-1

NF Noise figure

R_1 f_0/f_{max} = Lowest baseband frequency divided by the maximum baseband frequency

R_2 f_{max}/f_{max} = Maximum baseband frequency divided by the maximum baseband frequency = 1

RSL Receive Signal Level (dBm)

S/N Signal to noise ratio (dB)

τ Pre-emphasis circuit time constant

T 290 degrees (Kelvin)

T_{FM} FM threshold (dBm)

dBa (FIA) weighted circuit noise in dBa measured on a line by a noise measuring set with FIA weighting

NOTE: 1 milliwatt of a 1 kHz modulating tone reads +85 dBa, but the same white noise power (300-3400 Hz) will read +82.5 dBa due to frequency weighting.

dBa0 Circuit noise power in dBa referred to or measured at a point of zero relative transmission level (0 TLP)

NOTE: It is preferred to convert circuit noise readings from dBa to dBa0 as this makes it unnecessary to know or state the relative transmission level at point of actual measurement

dBm Power in dB relative to 1 milliwatt

dBm0 dBm referred to or measured at a point of zero transmission level

~~dBm~~ (dBm psophometrically weighted) Unit of noise power in dBm measured with psophometric weighting. Conversion as follows:

$$\text{dBm (psoph)} = \text{dBm} - 2.5 \text{ (for flat noise 300 - 3400 Hz)}$$

~~dBm0p~~ Circuit noise in dBm0 measured on a line with a noise measuring set having psophometric weighting

dB_{rn} (Decibels above reference noise) Weighted circuit noise power in dB reference 1 pW (-90 dBm) which is 0 dB_{rn}. Type of weighting indicated in parenthesis.

- NOTE: a. With "C" message weighting, a 1 milliwatt 1 kHz tone will read +90 dB_{rn}, but the same power with white noise randomly distributed over a 3 kHz band (300 - 3400 Hz) will read +88.5 dB_{rn}
- b. With "144" weighting a 1 milliwatt 1 kHz tone will read +90 dB_{rn}, but a 3 kHz band of white noise will read +82.5 dB_{rn} due to the different frequency weighting
- c. With "FIA" weighting a 1 milliwatt 1 kHz will read +85 dB_{rn}, but with a 3 kHz band of white noise will read +82.5 dB_{rn} due to the different frequency weighting

dB_{rn} (144-line) Weighted circuit noise power in dB_{rn}, measured on a line by a noise measuring set with 144 line weighting

dB_{rn} or dB_{rn}C (C-message) Weighted circuit noise power in dB_{rn}, measured on a line by a noise measuring set with C message weighting

dB_{rn}C0 Noise measured in dB_{rn}C referred to zero transmission level point. (0 TLP)

pW (Picowatt equal to 10^{-12} watt or -90 dBm) A unit of absolute power used for both weighted and unweighted noise

$$10 \log_{10} \text{pW} = \text{dBm} - 90$$

pWp (pW psophometrically weighted) Noise power measured in picowatts via a CCIF psophometric filter.

MISCELLANEOUS DATA

SECTION III. STATION GROUND MEASUREMENT

T-49 RESISTANCE OF STATION GROUND

1. GENERAL

The purpose of this test is to determine by means of a Null Balance Earth Tester the resistance of the station ground. An adequate station ground and ground distribution system provides a common electrical reference point for all equipment in an area and eliminates any difference of potential between pieces of equipment and between equipment and the earth. The acceptable standard for this test is 5Ω or less. The test method is the fall-of-potential earth resistance test.

2. TEST EQUIPMENT REQUIRED

Megyer Null-Balance Earth Tester 63220, Accessory Kit 63579, Sledge Hammer (for driving ground rods).

3. TEST PROCEDURE

With the aid of site drawings, locate the connection of the station ground to the earth electrode. After this electrode has been located, the test instrument should be connected as shown in Figure 1. The Null Balance Earth Tester should be located as close to the earth electrode as possible. Terminals P₁ and C₁ on the test instrument are connected to the earth electrode under test. (This configuration removes the resistance of the test lead from the measured value). The first reference rod "C₂" should be placed as far from the earth electrode as practical; this distance will probably be limited by the geography of the surroundings. The distance should be a minimum of 100' from the

CCP 702-1

earth electrode. Table A is a useful guide to P2 and C2 placement when a grid ground is to be tested.

<u>DIAGONAL DIMENSION</u>	<u>DISTANCE E-P2</u>	<u>DISTANCE E-C2</u>
4	62	100
6	78	125
8	87	140
10	99	100
12	105	170
14	118	120
16	124	200
18	130	210
20	136	220
40	198	320
60	242	390
80	279	450
100	310	500
120	341	550
140	366	590
160	397	640
180	422	680
200	440	710

The potential-reference rod "P2" is driven in at a point on a straight line between the earth electrode and "C2" and at a distance from the

earth electrode that is 62% of the distance from the earth electrode to reference rod "C2". The leads should be connected to the rods and instrument. On the instrument set the range switch to x0.01 and the digital readout of the balancing resistor dials to 999. Turn the generator crank slowly and note the galvanometer deflection. If the deflection is positive (+), increase range factor to x0.1 or higher till the deflection becomes negative (-). When the deflection is (-) decrease value of the balancing resistor, digit by digit, starting with the left knob, then the center and finally the right knob, until the galvanometer is nulled. The generator must be cranked while all adjustments on the balancing resistor are made. The cranking speed of the generator should be a minimum of 160 rpm for maximum sensitivity. To avoid the effects of stray currents in the soil, it may be necessary to increase the cranking speed to 200 rpm or more.

Resistance Under Test = Dial reading x range factor

4. DATA RECORDING

- a. Complete the top of Data Sheet G-1 (Test Cover Page).
- b. Make comments as necessary on Data Sheet G-1, including historic data where available (stating resistance, date, and source of information; and a listing of applicable drawings).
- c. Complete the data requirements of Data Sheet T49-1 as follows:

1.0 STATION GROUND

- 1.1 Enter the measured resistance of the earth electrode.
- 1.2 Enter the distance E-C2; indicate feet or meters.
- 1.3 Enter the distance E-P2; indicate feet or meters.
- 1.4 Describe the station ground commenting on the soil type, soil condition, condition of the earth electrode assembly, marking, type of connections, station ground distribution box, provision for watering, etc.
- 1.5 Enter the size of the station ground conductor (i.e. - 1000 MCM, 4/0 AWG, 2 AWG, 3" x 1/2" Cu Bar, 2" x 10 GA Cu Strap, braid, etc.)
- 1.6 Enter the type of chemical treatment used (i.e. None, Magnesium Sulphate, Copper Sulphate, Sodium Nitrate, Calcium Chloride, Sodium Chloride, Iron Sulphate, Potassium Nitrate, Ammonium Nitrate, activated charcoal, coke, etc.)

2.0 INTERIOR GROUND DISTRIBUTION

- 2.1 Describe the interior ground distribution commenting on condition, marking, insulation, connectors, branching, etc.
- 2.2 Enter the size of the interior ground feeder (i.e. - 750 MCM, 4/0 AWG, 2 AWG, etc.)
- 2.3 Enter the size of the rack ground feeder (i.e. - 2 AWG, 6 AWG, etc.)

3.0 EXTERIOR GROUND DISTRIBUTION

- 3.1 Describe the exterior ground distribution commenting on condition, marking, method of connection and bonding, list of major items connected.

- 3.2 Enter the size of the exterior ground feeder (i.e. - 500 MCM, 2/0 AWG, 2 AWG, etc.)
- 3.3 Enter the size of the exterior ground distribution conductor (i.e. 2/0 AWG, 2 MGS, etc.)

STATION GROUND		PAGE _____ OF _____ PAGES
DATA SHEET: T49-1		TEST DATE
DCS LINK	STATION UNDER TEST	TEST ENGR.
1.0 STATION GROUND		
1.1 RE = _____ Ω	1.2 DISTANCE E-C2	1.3 DISTANCE E-P2
1.4 GENERAL DESCRIPTION OF STATION GROUND		
1.5 STATION GROUND CONDUCTOR		1.6 CHEMICAL TREATMENT
2.0 INTERIOR GROUND DISTRIBUTION		
2.1 GENERAL DESCRIPTION OF INTERIOR GROUND DISTRIBUTION		
2.2 INTERIOR GROUND FEEDER CONDUCTOR		2.3 RACK GROUND FEEDER CONDUCTOR
3.0 EXTERIOR GROUND DISTRIBUTION		
3.1 GENERAL DESCRIPTION OF EXTERIOR GROUND DISTRIBUTION		
3.2 EXTERIOR GROUND FEEDER CONDUCTOR		3.3 EXTERIOR GROUND DISTRIBUTION CONDUCTOR

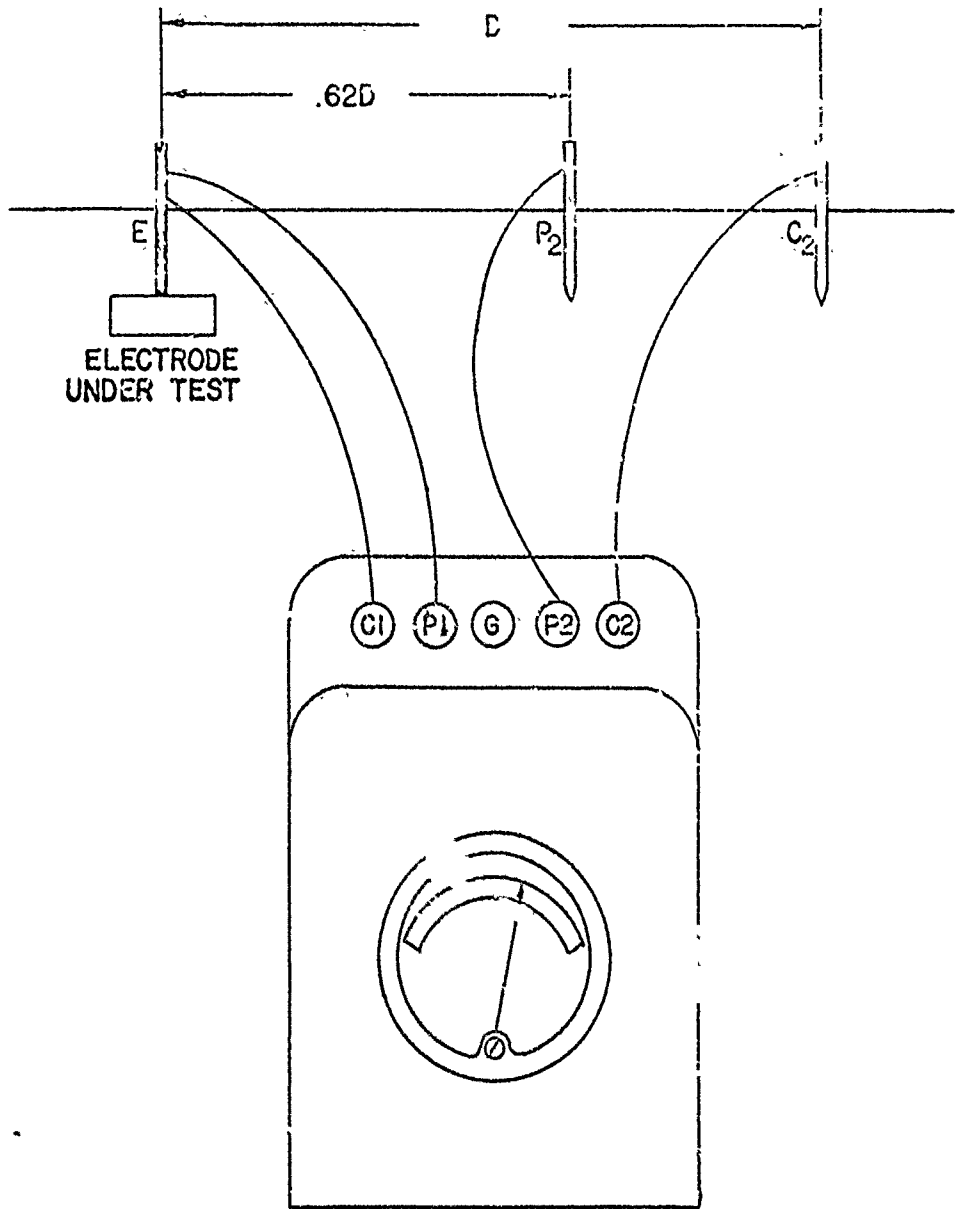


FIGURE 1

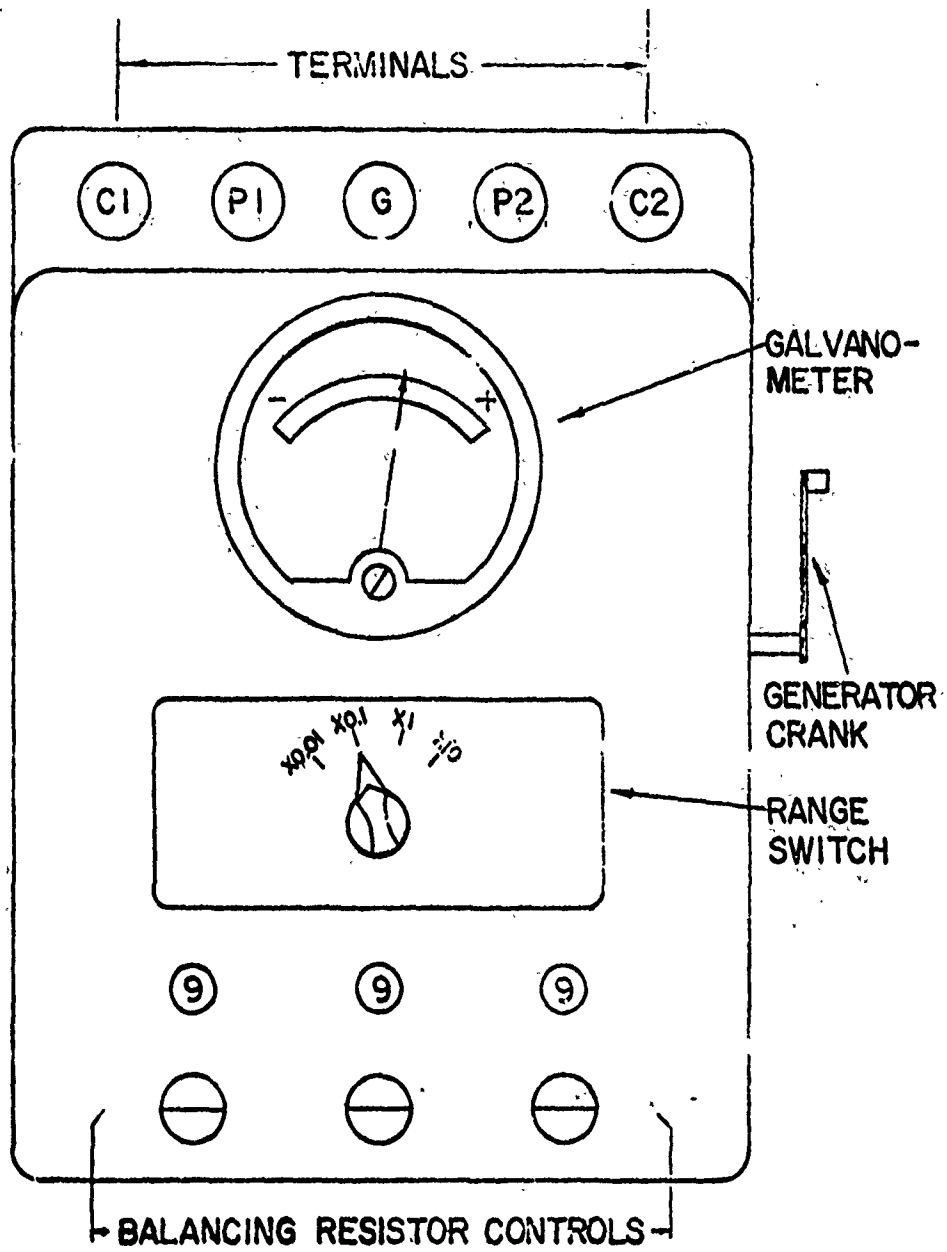


FIGURE 2

JANUARY 1968

INTRODUCTION

The ultimate sensitivity of a detection system is set by the noise presented to the system with the signal. In addition, any detection system adds additional noise in its detection and amplification process. Since the noise contribution of the detection system is usually the larger of these two, and since the level of input noise is generally beyond our control, our approach is to study, measure, and attempt to minimize the noise contribution of the detection system.

BASIC CONSIDERATIONS

A microwave input termination has a certain amount of available noise power which it can deliver to a matched system. For definitions, let's first consider lower frequencies where we can work with lumped constants.

A resistance R at temperature T generates across its open-circuited terminals a voltage resulting from the random motion of free electrons, thermally agitated. This "noise voltage" e_n is infinitely broadbanded and can be defined by the equation.

$$e_n^2/B = 4kTR \text{ (volts)}^2/\text{unit frequency bandwidth}$$

where

- k = Boltzmann's constant, 1.374×10^{-23} joules/°K
- T = absolute temperature, °K
- R = resistance (or resistive component of impedance)
- B = bandwidth

Generally our noise considerations will be concerned with a finite bandwidth, and we may use the more familiar notation of the equation.

$$e_n^2 = 4kTRB \tag{1}$$

If the resistance R is connected to a matched load resistance ($R_L = R$), maximum transfer of the noise power will occur. Noise power P_n dissipated in the load resistance R_L due to the noise voltage generated in the original resistance R will have the value

$$P_n = kTB \tag{2}$$

Equation (2) defines the available noise power from the original resistance. The actual noise power dissipated in the load resistance could be affected by any loss in the connecting leads, a less than perfect match to the original resistance and the noise power generated within the load resistance itself.

In systems operating at frequencies where voltages and resistances cannot be clearly defined, equation (2) becomes the usable expression, containing terms that can be measured.

In certain low noise applications, a deliberate (and carefully determined) mismatch is created between the input termination and the detection device. This technique couples less than the available termination noise power (kTB) into the detection device. However, this system consideration is beyond the scope of this article.

In a microwave receiver, the "input termination" is an antenna coupled to the atmosphere; in an IF strip, the input termination is generally a mixer of some sort. In either case, the termination has an available noise power given by $P_n = kTB$. If there were a perfect amplifier or receiver which added no noise in the amplification process (and if it were perfectly matched to its input termination) its output noise power would be $kTBG$, where G is the power gain of the system.

A figure of merit for an actual microwave receiver or IF amplifier is the ratio of actual output noise power when $T = 290^\circ$ to the theoretical minimum. Noise Figure, F, is this figure of merit referred to room temperature. ($T = 290^\circ\text{K}$.)

Thus

$$F = \frac{N_1}{kT_0BG} \tag{3}$$

where N_1 is the measured noise power output of the system when $T_0 = 290^\circ$. The perfect amplifier would of course have a noise figure of 1, (0 db).

Of the total noise power output of a system ($N_1 = kT_0BGF$) we know that a specific portion is the result of amplified input noise (kT_0BG). The amount of noise power added by the receiver (N_r) is the difference, or

$$\begin{aligned} N_r &= N_1 - kT_0BG \\ &= (F - 1) kT_0BG \end{aligned} \tag{4}$$

NOISE FIGURE MEASUREMENTS WITH A SIGNAL GENERATOR

Noise Figure ($F = N_1/kT_0BG$) can be calculated from measurements taken by a stable, well-attenuated signal generator and suitable power meter. We can measure T , which is the temperature of the input termination in $^{\circ}K$; N_1 can be measured with a power meter at the system output.

To determine accurately the gain bandwidth product (BG), it is necessary to plot the response of the system and graphically integrate the curve...a time-consuming process. Approximations can be made on the basis of the 3 db bandwidth, which shortens the process. After measuring the 3 db points, there are graphs that may be entered to get an approximation of the effective noise bandwidth. Gain, of course, may be easily measured with a proper signal generator and power meter.

From this data, noise figure may be calculated. Often, however, this is only a first step, because the primary objective is to minimize noise figure by repositioning components, by substituting crystals or tubes, or tuning filter networks. Clearly, the many-step process represented by the Signal Generator-Power Meter method has limited value in such a situation, since a new measurement must be made at each readjustment.

THE NOISE SOURCE AS A BROADBAND SIGNAL GENERATOR

If a known level of broadband noise can be introduced at the input of a device under test, a differential power measurement at the output would indicate a gain bandwidth product of the device.

A gas discharge noise source operates as an input termination at a very high temperature, and has an available noise power much higher than the normal termination. The effective thermal agitation of an argon tube noise source, for example, represents an equivalent temperature of approximately 10,000 $^{\circ}K$ compared with room temperature of 290 $^{\circ}K$.

Available excess power from the fired noise source can be expressed in the same terms as the input termination,

$$P_{ns} = k(T_2 - T_0)B$$

where T_2 is the equivalent absolute temperature of the noise source.

Since a measurement of the device output both with and without the additional noise power input will give an indication of gain-bandwidth product, it is possible

to compute noise figure with no further measurements, since all independent variables of equation (3) are known.

Using the system of figure 1, consisting of an input termination, an excess noise source, a receiver under test and an output power detector, it is possible to measure N_1 with the excess noise source "cold" and to measure N_2 with the excess source fired. N_1 is graphically illustrated in figure 2(a), and consists of the amplified input termination noise plus the noise generated within the receiver. N_2 , illustrated in figure 2(b), consists of N_1 plus the amplified excess noise power viewed at the receiver output.

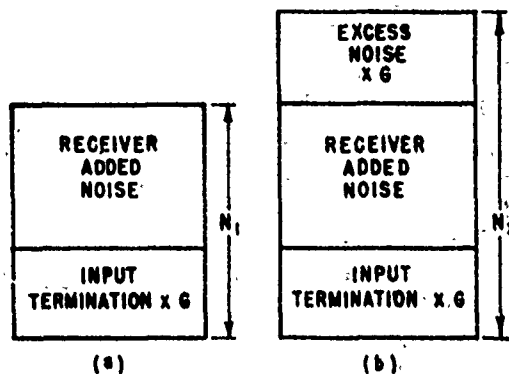


Figure 2. Representation of total noise power output of the system in figure 1 when the Excess Noise Source is "cold" (N_1), and when the Excess Noise Source is "fired" (N_2).

Taking the ratio of these measured powers we have:

$$\frac{N_2}{N_1} = \frac{\left(\frac{\text{input}}{\text{termination}} \right) \times G + (\text{receiver}) + \left(\frac{\text{excess}}{\text{noise}} \right) \times G}{\left(\frac{\text{input}}{\text{termination}} \right) \times G + (\text{receiver})}$$

Substituting from previous equations, and assuming measurement conditions of $T = T_0 = 290^{\circ}K$,

$$\frac{N_2}{N_1} = \frac{kT_0BG + (F-1)kT_0BG + k(T_2-T_0)BG}{kT_0BG + (F-1)kT_0BG}$$

$$= \frac{FT_0 + (T_2-T_0)}{FT_0}$$

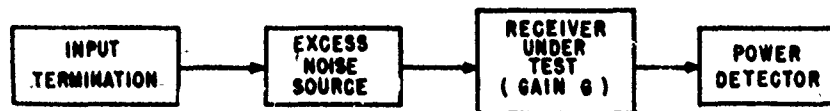


Figure 1. A typical noise figure measuring system.

Appl. Note 57

and, finally

$$F = \frac{(T_2 - T_0)}{T_0} \times \frac{1}{\left(\frac{N_2}{N_1} - 1\right)}$$

Converting to logarithmic notation,

$$F_{db} = 10 \log \frac{(T_2 - T_0)}{T_0} - 10 \log \left(\frac{N_2}{N_1} - 1\right) \quad (5)$$

In equation (5) the ratio $(T_2 - T_0)/T_0$ is a measure of the relative excess noise power available from a noise source and is specified by the manufacturer. In the case of argon gas tubes, this ratio is 33.1; $10 \log (T_2 - T_0)/T_0$ is 15.2 db. When using such a tube equation (5) simplifies to,

$$F_{db} = 15.2 - 10 \log (N_2/N_1 - 1)$$

NOISE FIGURE MEASUREMENT WITH AN EXCESS NOISE SOURCE

Equation (5) opens the door to several measurement techniques utilizing the excess noise source. We shall consider the "twice-power" and "Y-Factor" manual techniques and an automatic approach to noise figure measurements.

A. Twice-Power Method of Manual Noise Figure Measurement

In actually measuring the "N₁" and "N₂" of equation (5), if N₂ was set to be twice N₁ then equation (5) reduces to:

$$F_{db} = 10 \log \frac{(T_2 - T_0)}{T_0} - 10 \log (1) \\ = 10 \log (T_2 - T_0)/T_0$$

With the proper equipment, the condition of N₂ = 2 N₁ can be established by varying the relative excess noise power of the noise source. With the equipment of figure 3, the procedure would be:

- 1) Set a convenient reference on the power detector with the excess noise source "cold" and the 3 db pad out. This is N₁.
- 2) Insert the 3-db pad and fire the excess noise source.

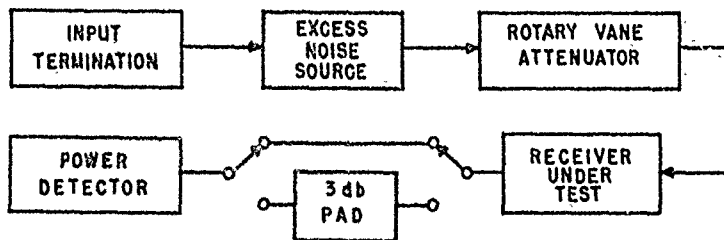


Figure 3. The "twice-power" method of manual noise figure measurement.

- 3) Vary the rotary vane attenuator until the original power detector reference point is reached. This creates a condition of N₂ = 2 N₁.

Figure 4 illustrates this condition, in which the output noise power contributed by the excess noise source exactly equals the sum of the amplified input termination noise plus the receiver noise contribution. Since this excess noise ratio was adjusted with the attenuator to be equal to input termination noise plus receiver noise (thereby causing N₂ = 2 N₁), from equation (5) it can be seen that the attenuated excess noise ratio is equal to the noise figure of the receiver. In the case of an argon source, it can be read as 15.2 db minus the attenuator setting (in db).

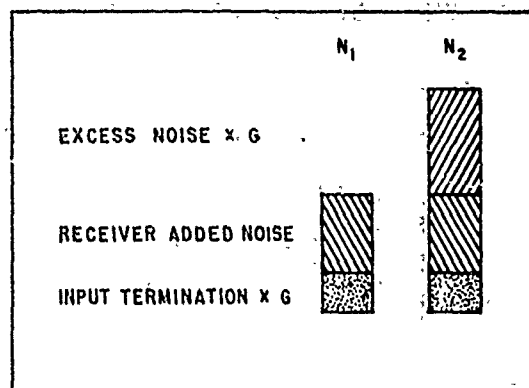


Figure 4. Representation of total noise power output for the "twice-power" method of manual noise figure measurement.

While the attenuator reduces the amount of excess noise injected into the system, it has no effect on input termination noise power if the termination and attenuator are at the same temperature, since, regardless of the amount of attenuation, when the excess noise source is cold the receiver input is still looking at a matched input at temperature T.

B. "Y-Factor" Method of Noise Figure Measurement

A method closely resembling the "Twice-Power" method involves the determination of the numerical ratio N₂/N₁ (which is called Y-Factor) and the calculation of noise figure by substitution in equation (5).

In practice, the Y-Factor method generally makes use of an IF attenuator with a power indicator set to a convenient reference. The IF attenuator change in going from source OF1 to source ON then yields the Y-Factor, which is then entered in the equation. Graphs are also available for specific values of relative excess noise, with co-ordinates calibrated in "Y-Factor" and noise figure. (See figure 5.)

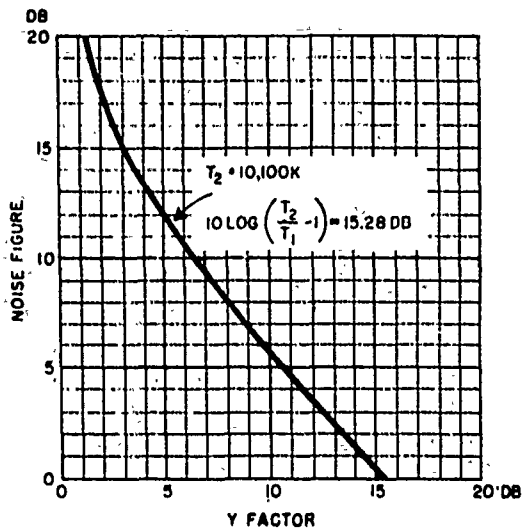


Figure 5. A "Y-Factor" chart for determining noise figure with a 15.28 db excess noise source.

C. Automatic Noise Figure Measurements

While manual measurements yield valid results, they still represent a tedious process...and are often not easily accomplished by unskilled personnel. And since there is not a continuous indication of noise figure, the work of reducing noise figure is considerably slowed by the necessity of a new measurement after each circuit change.

To fill the need for a direct-reading, continuously indicating noise figure meter, at least three automatic systems have been devised. All depend on the periodic insertion of known excess noise into the system. This results in a pulse train of 2 pulse levels, N_2 and N_1 . The pulse train typically is amplified in an IF strip and then separated into two distinct levels by selective gating. These levels, together with the amount of excess noise insertion, contain the information needed to directly indicate the noise figure on a meter face.

The three automatic systems differ in their method of indication. One approach uses a special ratio-resolving meter movement which responds to the ratio of the two signal levels in a manner similar to a wattmeter movement. Such a meter movement is quite expensive,

however, and in general has not achieved wide acceptance in this country.

Another method uses AGC in its IF amplifier to hold constant the value $(N_2 + N_1)/2$ and measures $N_2 - N_1$. This contains the necessary information to measure noise figure, and is especially useful in very high noise figure cases, where N_1 is close in value to N_2 . In such cases, the difference of the levels is more definitive than their ratio.

A third approach actually measures the ratio N_2/N_1 and displays this ratio on a meter face calibrated by the equation:

$$F_{db} = 15.2 - 10 \log (N_2/N_1 - 1)$$

Such an instrument is shown in simplified block diagram form in figure 6.

In operation, the gating source pulses the noise source at a rate of 500 cps; N_1 and N_2 pulses arrive at the IF amplifier. Noise sources have a finite noise build-up time, so the IF amplifier is gated to pass only the final amplitudes of N_1 and N_2 to the square law detector. The detected N_2 pulse is switched to an AGC integrator, where a voltage for gain control of the IF amplifier is derived. The time constant of this circuit is made long enough to control the IF amplifier gain even when the N_1 pulse is passing through it. Since the AGC action keeps the detected N_2 pulse at a constant level, a measurement of the detected N_1 pulse is, in effect, a measurement of the pulse ratio. The N_1 pulse is measured by switching it to the meter integrator and meter.

Convenient internal calibration of the meter is accomplished by artificially creating readings of "+∞" and "-∞". By pulsing the noise source during both the N_2 and N_1 time periods, we obtain a condition of $N_2 = N_1$. In the formula $F_{db} = 15.2 - 10 \log (N_2/N_1 - 1)$ this condition results in a noise figure of +∞. The artificial condition of $F = -∞$ would correspond to an " N_1 " value of "0". This can be created by gating "off" the IF amplifier during the " N_1 " time period. If the metering circuit is designed to be a linear indicator of the power of " N_1 " (square law detector) and the meter minimum position is calibrated as -∞ and the full scale deflection as +∞, all other points on the meter face can be calculated by the formula $F_{db} = 15.2 - 10 \log (N_2/N_1 - 1)$. For example, an " N_1/N_2 " ratio of 1/2 would bring about a mid-scale reading. From the formula this mid-scale reading is calculated to be 15.2. In a similar fashion the balance of the scale is calibrated.

Figure 7 is an actual meter face from an automatic noise figure meter. In addition to calibration for 15.2 db excess noise sources, it is calibrated for 5.2 db temperature-limited diode sources. The linear current scale is used in adjusting noise source excitation current.

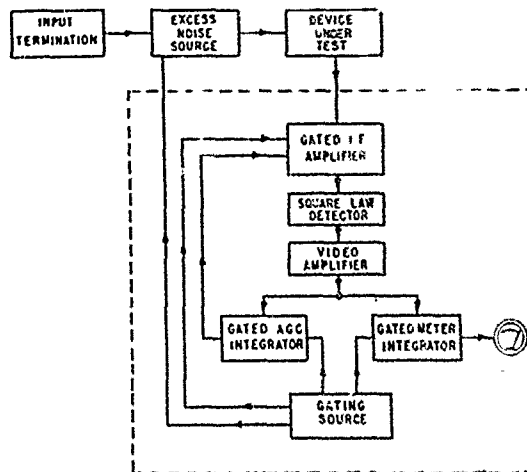


Figure 6. Simplified block diagram of automatic noise figure measurement system.

NETWORKS IN CASCADE

The effects of the noise contribution of networks in cascade can be seen in figure 8. This illustration shows the input termination and three networks, each with gain G and noise figure F. The power graphs assume that each network is active with gain greater than 1. However, the analysis will be equally valid for passive networks with gain less than 1.

The input termination supplies a noise power kTB which is amplified by the three networks and appears at the output as $kTB G_1 G_2 G_3$.

The noise contribution of network 1 (by equation 4) is $(F_1 - 1) kTB G_1$. When further amplified by networks

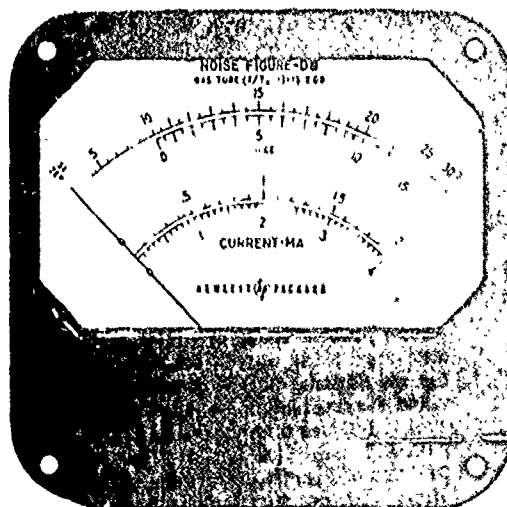


Figure 7. Meter face from an automatic noise figure meter.

2 and 3, the noise power appears at the output as $(F_1 - 1) kTB G_1 G_2 G_3$. Similarly, the output noise contributed by network 2 is $(F_2 - 1) kTB G_2 G_3$; and from network 3, $(F_3 - 1) kTB G_3$. The system noise figure (F_s) is the ratio of actual noise power output to noise power output contributed by the input termination.

$$F_s = \frac{\text{Total noise output}}{kTB G_1 G_2 G_3}$$

$$= \frac{kTB G_1 G_2 G_3 + (F_1 - 1) kTB G_1 G_2 G_3}{kTB G_1 G_2 G_3}$$

$$+ \frac{(F_2 - 1) kTB G_2 G_3 + (F_3 - 1) kTB G_3}{kTB G_1 G_2 G_3}$$

$$= F_1 + \frac{(F_2 - 1)}{G_1} + \frac{(F_3 - 1)}{G_1 G_2}$$

The general equation for the noise figure of networks in cascade is then

$$F_s = F_1 + \frac{(F_2 - 1)}{G_1} + \frac{(F_3 - 1)}{G_1 G_2} + \dots + \frac{(F_n - 1)}{G_1 G_2 \dots G_{(n-1)}}$$

It can be seen that overall noise figure of any cascaded amplifying system depends primarily on noise figure of the first stage. The effects of subsequent stages is reduced by the gain up to that point. The use of a passive stage with gain less than 1, on the other hand increases the importance of the subsequent stage's noise figure.

ACCURACY CONSIDERATIONS

Up to this point we have deliberately ignored several possible sources of error. Actual measurement techniques must consider the possibility of system errors caused by mismatch, temperature, and image and spurious responses. The instrument accuracy of the noise source and noise figure meter should also be considered.

A. Temperature

In the derivation of equation (5),

$$F_{db} = 10 \log \frac{(T_2 - T_0)}{T_0} - 10 \log \left(\frac{N_2}{N_1} - 1 \right)$$

the ambient temperature was assumed to be 290, hence T_0 cancelled out of all terms except the figure "10 log $(T_2 - T_0)/(T_0)$ ". T_2 is the equivalent fired temperature of the noise source. In specifying the relative excess noise power of a noise source, the manufacturer knows the value of T_2 and rates the tube in terms of the standard temperature, 290°K (62.6°F). A variation of 20° from the assumed 290°, for example, would cause an error of about 0.3 db in measured noise figure.

B. Mismatch

Noise power obeys all power transfer laws. But since it is random in phase, mismatches cause ambiguous errors rather than known amounts of power loss. In the automatic noise figure meter measuring the ratio of N_2/N_1 , a mismatch affecting both pulses does not affect accuracy, since the ratio remains unchanged.

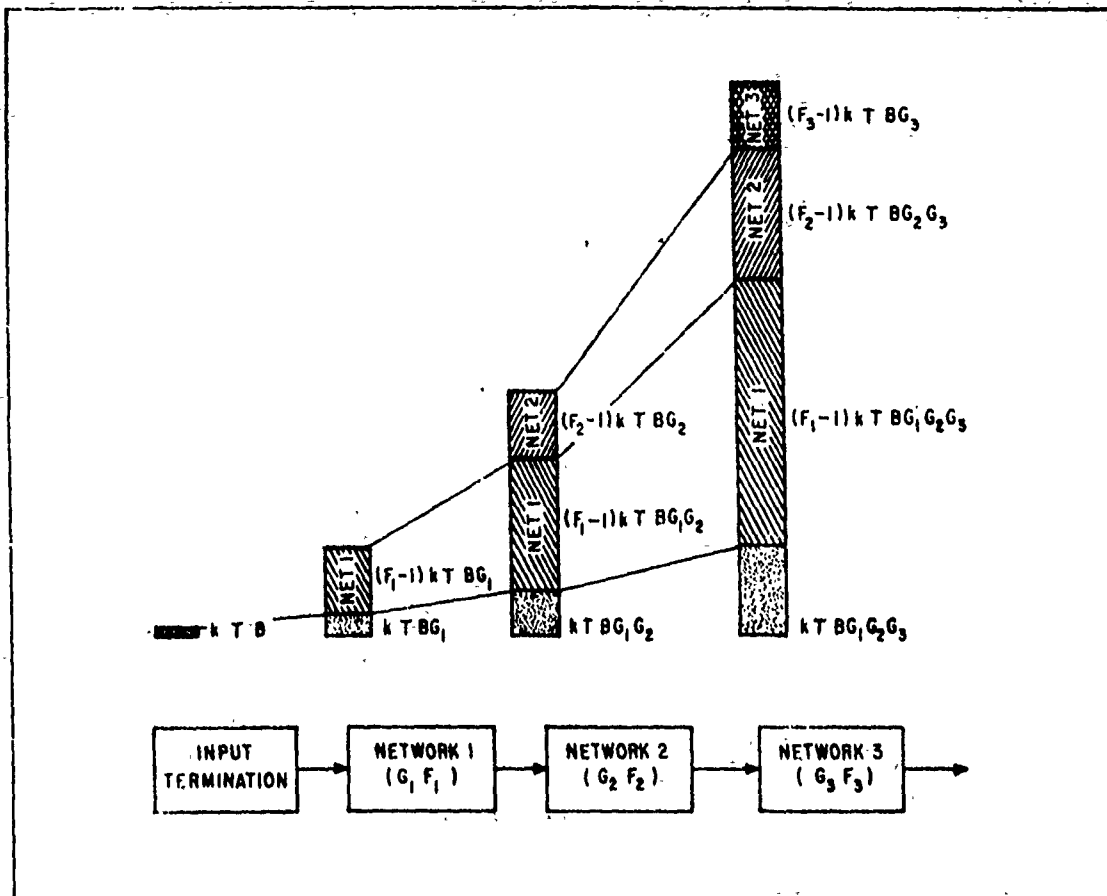


Figure 8. The effects of noise contribution of networks in cascade.

The critical matching situation, then, involves the excess noise source. Noise sources are rated in available excess noise power; thus mismatches will cause an ambiguous amount of excess noise power to be coupled to the system. Figure 9 shows the effect of several possible conditions of mismatch.

Note that the possible error is maximum at low noise figures where the greatest accuracy is usually desired. The importance of well-matched noise sources over the entire frequency range of interest is apparent. Hewlett-Packard waveguide sources are rated as 1.2 maximum, and typically are better than 1.1. Diode sources are 1.3 or better over most of their rated band.

C. Image and Spurious Response

In using a broadband excess noise source, an automatic noise figure meter measures the true noise figure of the total pass band of the device under test. If, in its operation, the device does not utilize the full pass band for signal information (as would be the case of a radar receiver with an image response) its operating noise figure will be higher than the measured

noise figure. This apparent noise figure can be calculated by the equation:

$$\text{Operating } F_{\text{db}} = F_{\text{db}}(\text{reading}) + 10 \log (B_t/B_u),$$

where B_t is the total bandpass of the device, and B_u is the operational bandpass.

This equation is a convenient simplification that assumes constant gain in the device under test.

D. Excess Noise Source Accuracy

At the present time, accuracy of pulse type gaseous discharge noise source tubes is specified ± 0.5 db, for the National Bureau of Standards has not yet provided a certification for pulse-operated tubes. However, NBS does offer certification for cw operation at 9.0, 9.8, and 11.2 gc to ± 0.1 db. The Red Bank Division of Bendix Corporation, Eatontown, N.J., also offers cw certification, with some additional uncertainty over that of NBS.

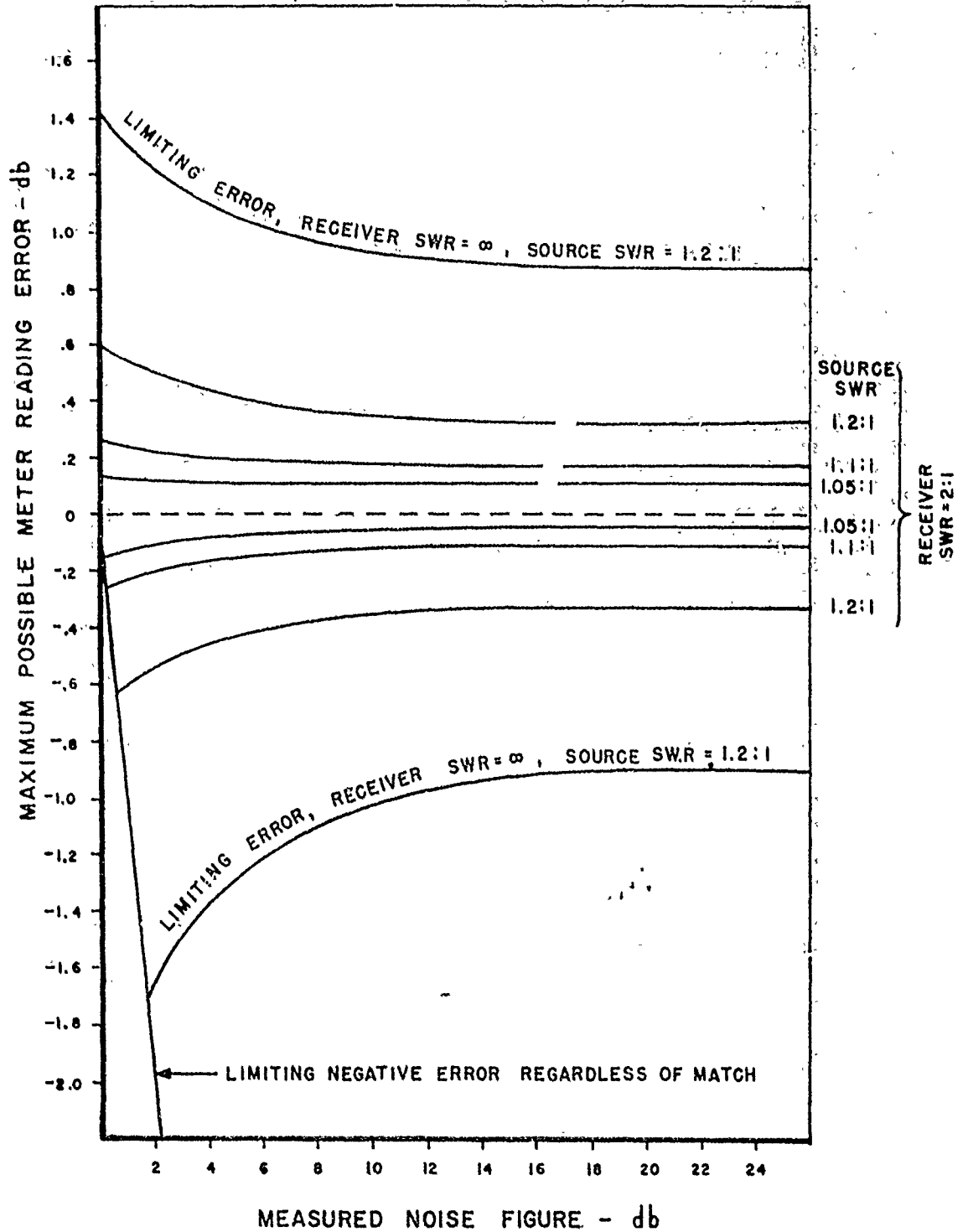


Figure 9. Typical error effects for several possible conditions of mismatch between noise source and receiver.

Temperature-limited diode sources can be made to much closer specifications, but are limited to the vhf region and below.

Correction of the excess noise ratio of a noise source is sometimes necessary to take into account conditions of temperature varying from the standard 290°K (see page 6). This is especially true of diode sources where the heat of the temperature-limited diode tends to raise the ambient temperature of the output resistor.

E. Noise Figure Meter Accuracy

The automatic noise figure meters manufactured by the Hewlett-Packard Company are specified accurate within $\pm 1/2$ db over most of their range, ± 1 db over the remainder. This accuracy specification includes the effects of meter tracking, variation from square law, and aging effects. With the current specifications of noise sources, and the possible errors caused by mismatch and temperature, such meter accuracy would seem to be consistent with overall system accuracy.

For measuring low-noise devices, a modified noise figure meter which provides increased resolution and accuracy is available on special order. The modification expands a 4-db portion of the scale (up to 6 db) over the full range of the meter scale. Noise figure meter accuracy in the expanded mode of operation is ± 0.2 db; either expanded or normal operation can be selected.

NOISE FIGURE INSTRUMENTATION

Hewlett-Packard has the following equipment presently available for making automatic noise figure measurements.

Model 340B Noise Figure Meter. When used with an Ⓢ noise source, automatically measures and continuously displays the noise figure of IF or rf amplifiers tuned to 30 or 60 mc and of radar or microwave receivers with intermediate frequencies of 30 and 60 mc. (Collectively, Ⓢ noise sources cover frequencies from 10 mc to 18 gc.)

Model 342A Noise Figure Meter. Is similar to Ⓢ Model 340B except that it operates on five frequencies

between 30 and 200 mc. Four of these frequencies are 60, 70, 105 and 200 mc; the fifth is the basic 342A tuned amplifier frequency of 30 mc.

Model DY-344A Noise Figure Meter. Provides continuous noise figure measurement on operating radars. Usable with radar receivers in any rf range for which noise sources are available, the 344A permits optimizing the noise figure during operation. High sensitivity permits decoupling the noise source up to 20 db from the main transmitter line to minimize degradation of the system.

Model 343VHF Noise Source. Specifically for IF and rf amplifier noise measurement, a temperature-limited diode source with broadband noise output from 10 to 600 mc.

Model 345B IF Noise Source. Operates at either 30 or 60 mc, as selected by a switch (other frequencies between 10 and 60 mc on special order). Another selector permits matching 50, 100, 200 and 400 ohm impedances.

Model 347A Waveguide Noise Sources. Argon gas discharge tubes mounted in waveguide sections. For all frequencies from 2.6 through 18.0 gc, providing uniform noise throughout range; maximum swr of 1.2.

Model 349A UHF Noise Source. Argon discharge tube for automatic noise figure readings on scatter communications receivers, L-band radars, parametric amplifiers, or other devices 400 to 4,000 mc. The source can also be furnished with a neon discharge tube.

For detailed information and specifications on any of these noise figure devices, please contact your nearby Hewlett-Packard field engineer.

ADDITIONAL INFORMATION

Two issues of the Ⓢ laboratory publication, the Hewlett-Packard Journal, also contain information on noise figure and the operation of the Ⓢ noise figure devices. A limited number of copies are on hand, and are yours for the asking. For a copy of each issue (Vol. 9, No. 5 and Vol. 10, No. 6-7), simply contact your local Hewlett-Packard field engineer.

Microwave System Engineering Using Large Passive Reflectors*

MERVIN L. NORTON†, MEMBER, IRE

Summary This paper will provide the microwave engineer with the basic techniques of microwave system engineering using large passive reflectors and will outline the many advantages of their use. Small passive reflectors of the "periscope type" have been used for many years on microwave systems. Large passive reflectors have also been used but to a much lesser degree. Large passives may be used at intermediate points on long (200 miles or more) microwave links in lieu of active repeaters. Most microwave engineers have little knowledge of system engineering using these reflectors. This paper describes their use in both the "near" and "far fields" in line-of-sight systems and describes how they may be used on non-line-of-sight systems (tropospheric scatter and diffraction systems). Formulas are developed and graphs provided which will enable the microwave engineer to determine the path loss of multihop passive reflector systems. Large passive reflectors should be considered as another tool which can be used by the microwave engineer for planning and engineering communications systems. When used effectively with line-of-sight, diffraction and tropospheric scatter modes of propagation, communication systems may be engineered more economically, with more reliability and with a decrease in the operating and maintenance problems.

INTRODUCTION

FOR MANY YEARS microwave systems have used passive reflectors of the "periscope type" operating in the "near-field" of the antenna (Fig. 1 a). These small passive reflectors may introduce a slight gain or loss in the microwave system. The use of these reflectors in the "near field" has been adequately described.¹⁻⁴ Passive reflectors may be used in microwave systems in both the "near field" and the "far field." Even as early as 1945 while microwave systems were still in their infancy, pioneering experimentation and testing of passive reflectors in both the "near field" and "far field" was being conducted by the U. S. Army Signal Research and Development Laboratory, Fort Monmouth, N. J., (formerly the Signal Corps Engineering Laboratories).⁵ Large reflectors may be used in this manner to extend the distance

* Received April 12, 1962. The views of the author do not necessarily reflect the position of the Department of the Army or the Signal Corps.

† U. S. Army Electronics Research and Development Laboratory, Fort Monmouth, N. J.

¹ L. G. Fobes, "Multichannel radio communications within the army," IRE TRANS. ON MILITARY ELECTRONICS, vol. MIL-4, pp. 611-612; October, 1960.

² W. C. Jakes, Jr., "A theoretical study of an antenna reflector problem," Proc. IRE, vol. 41, pp. 272-274, February, 1953.

³ D. R. Crosby, "Theoretical gain of flat microwave reflectors," 1954 IRE CONVENTION RECORD, pt. 1, pp. 71-76.

⁴ R. E. Greenquist and A. J. Orlando, "An analysis of passive reflector antenna systems," Proc. IRE, vol. 42, pp. 1173-1178, July, 1954.

⁵ J. Drexler, "An experimental study of a microwave periscope," Proc. IRE (Correspondence), vol. 42, p. 1022, June, 1954.

⁶ I. Takasu, "The Passive Antenna of Reflect Plane," Japan Telecomm. Rev., Nippon Telegraph and Telephone Public Corp., Autumn, 1959.

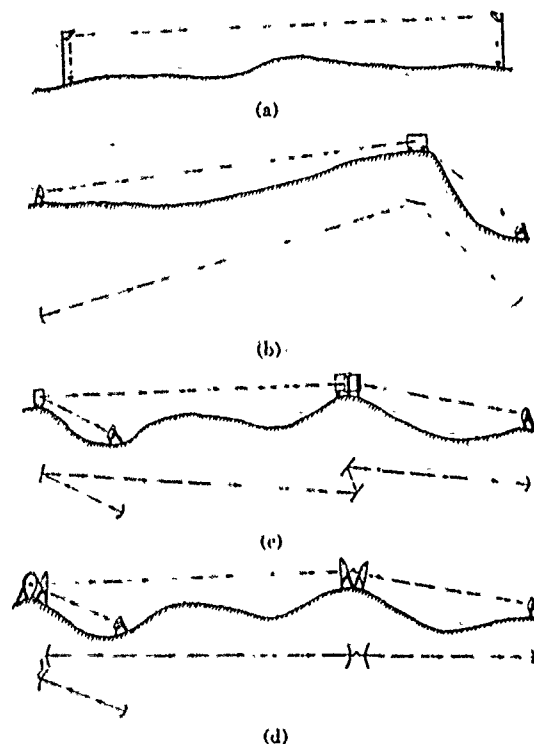


Fig. 1. Types of passive antenna systems. (a) Periscope type. (b) Two hop system using single passive reflector. (c) Three hop system using angle and double passive reflectors. (d) Three hop system using back-to-back antennas.

between two active microwave terminals or in lieu of active microwave repeaters. A few articles have been published⁶⁻¹² the use of large passive reflectors operating in the "far field."

Most microwave engineers have very little knowledge of system engineering using large passive reflectors even though these reflectors have been widely used in hundreds of different locations primarily in mountainous areas. It is commonly believed that large passive reflectors are

⁷ H. Mugniski and T. F. Koch, "Passive repeater bands microwave beam," Electronics, vol. 26, p. 134; February, 1953.

⁸ R. F. H. Yang, "Passive repeater using double flat reflectors," 1957 IRE NATIONAL CONVENTION RECORD, pt. 1, pp. 36-41.

⁹ F. Cappuccini and F. Casparini, "Passive repeater using double flat reflectors," Proc. IRE, vol. 46, pp. 784-785; April, 1958.

¹⁰ R. Aschden, "Passive relay by microwave mirror," TSP et TV, vol. 33, pp. 5-7; January, 1958.

¹¹ R. Aschden, "Passive TV relay and its practical possibilities," TSP et TV, vol. 33, pp. 329-330; November, 1957.

¹² ITT, "Reference Data for Radio Engineers," Stratford Press, New York, N. Y., 4th ed., p. 757; 1957.

practical only if they are used on microwave systems where the reflector is located near one end of the path. They are more efficient if located near one end of the microwave path; however, they may also be used on paths of 200 or more miles (Fig. 1(b) and 1(c)) including diffraction and tropospheric scatter paths. The use of tropospheric scatter type equipment (high power transmitters and very sensitive receivers) greatly increases the versatility of large passive reflectors. Two antennas connected back-to-back by a short transmission line may also be used as a passive repeater (Fig. 1(d)). However, they are more expensive and less efficient.

Formulas are developed and graphs are provided which will enable the microwave engineer to determine the path loss of multihop passive reflector systems using reflectors in both the "near" and "far" fields. This paper augments that information previously published and will attempt to acquaint the microwave engineer with the basic techniques of microwave system engineering using large passive reflectors and to outline many advantages of their use.

NEAR FIELD--FAR FIELD

In order to calculate the loss of a microwave system using large passive reflectors it must be determined whether the reflectors are in the "near field" or "far field" of the terminal antenna. An antenna is normally considered a point source and transmits a spherical wave. If this wave front varies from a plane wave by a small amount Δr (Fig. 2(a)) then the wave front may be considered as a plane wave. The most commonly accepted definition of the "far field" is that space in the field of an antenna where, over a given area, the spherical wave varies from a plane wave by less than $\lambda/16$ (Fig. 2(b)).¹³ If this variation is more than $\lambda/16$ the given area is normally considered to be in the "near field." Therefore the radius r of the "near field" is

$$r = \frac{2D^2}{\lambda} \text{ or } \frac{2a^2}{\lambda} \quad (1)$$

where antenna diameter D or reflector side a and λ are in the same units. Expressing r , D and a in feet and converting λ to megacycles we have

$$r = \frac{D^2}{492} \text{ or } \frac{a^2}{492} \quad (2)$$

The radius of the "near field" for different antenna and passive reflector sizes is plotted in Fig. 3.

Two different methods are described in this paper for determining the systems loss when passive reflectors are used. These methods may be referred to as the "far field" and "near field" methods.

¹³ S. Silver, "Microwave Antenna Theory and Design," M.I.T. Rad. Lab. Ser., McGraw-Hill Book Co., Inc., New York, N. Y., vol. 12, pp. 196-199; 1949.

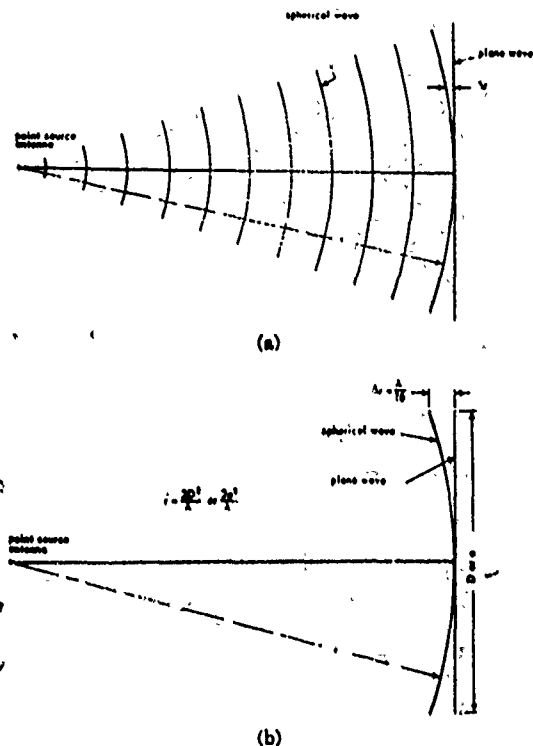


Fig. 2--Determination of the "near field."

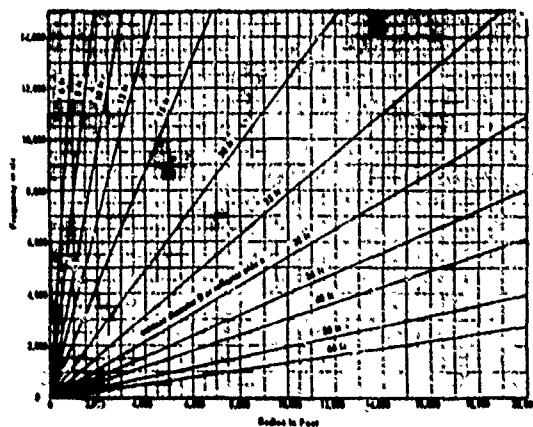


Fig. 3--Radius of the "near field."

TWO HOP SYSTEM USING A PASSIVE REFLECTOR IN THE "FAR FIELD"

Consider a passive reflector of projected area a^2 located in the "far field" of the terminal antennas (Figs. 1(b) and 4). A passive reflector has the gain of two back-to-back aperture antennas. The gain G_r of an aperture antenna is

$$G_r = \frac{4\pi a^2}{\lambda^2} \quad (3)$$



Fig. 4--Determination of passive reflector projected area.

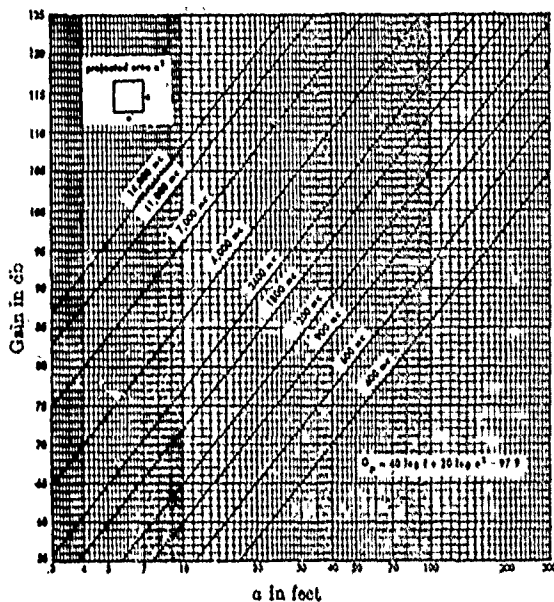


Fig. 5--Gain of a passive reflector in the "far field."

Therefore, the gain G_r of a 100 per cent efficient passive reflector is

$$G_r = \left(\frac{4\pi a^2}{\lambda^2} \right)^2, \quad (4)$$

and the gain G_r of a 95 per cent efficient passive reflector is

$$G_r = 0.95 \left(\frac{4\pi a^2}{\lambda^2} \right)^2, \quad (5)$$

which expressed in decibels and converting λ to frequency is

$$G_r = 40 \log f + 20 \log a^2 - 97.9, \quad (6)$$

where

$$\begin{aligned} f &= \text{megacycles,} \\ a^2 &= \text{projected area in square feet.} \end{aligned}$$

The gain of a passive reflector in the "far field" is plotted in Fig. 5. The projected area is the effective area of the reflector in a plane normal to the direction of transmission

as shown in Fig. 4. Projected area a^2 is

$$a^2 = A^2 \sin^2 \theta, \quad (7)$$

where

$$\begin{aligned} A^2 &= \text{the actual area,} \\ \theta &= \text{deflection angle.} \end{aligned}$$

Basic transmission loss L_t is the ratio of transmitted power P_t to received power P_r ,

$$L_t = \frac{P_t}{P_r}, \quad (8)$$

which assuming isotropic antennas is

$$L_t = \left(\frac{4\pi d}{\lambda} \right)^2, \quad (9)$$

which expressed in decibels and converting λ to frequency becomes the familiar free space loss formula

$$L_t = 36.6 + 20 \log f + 20 \log d, \quad (10)$$

where

$$\begin{aligned} f &= \text{megacycles,} \\ d &= \text{miles.} \end{aligned}$$

Free space losses are plotted in Fig. 6 and the gains of parabolic antennas are plotted in Fig. 7.

By combining the passive reflector gain G_r with two space losses L_t ((10) with (10)) we can determine the total loss L_p on a two hop system using a passive reflector in the "far field"

$$L_p = 171.1 + 20 \log d_1 + 20 \log d_2 - 20 \log a^2, \quad (11)$$

where

$$\begin{aligned} d_1 &= \text{distance from Terminal A to passive reflector in miles,} \\ d_2 &= \text{distance from Terminal B to passive reflector in miles,} \\ a^2 &= \text{projected area of passive reflector in square feet.} \end{aligned}$$

It should be noted that for a two hop microwave system using a passive reflector in the "far field" the total space loss between isotropic antennas is independent of frequency.

Space losses L_p of two hop systems using passive reflectors in the "far field" are plotted in Fig. 8.

THREE HOP SYSTEM USING PASSIVE REFLECTORS IN THE "FAR FIELD"

Consider two passive reflectors of projected area a_1^2 and a_2^2 located in the "far field" of each other and of the terminal antennas (Fig. 1(c)). By combining the passive reflector gains G_r with three space losses L_t ((8) with (10)) we can determine the total loss L_p on a three hop system using two passive reflectors in the "far field"

$$\begin{aligned} L_p &= 305.5 + 20 \log d_1 + 20 \log d_2 + 20 \log d_3 \\ &\quad - 20 \log a_1^2 - 20 \log a_2^2 - 20 \log f, \quad (12) \end{aligned}$$

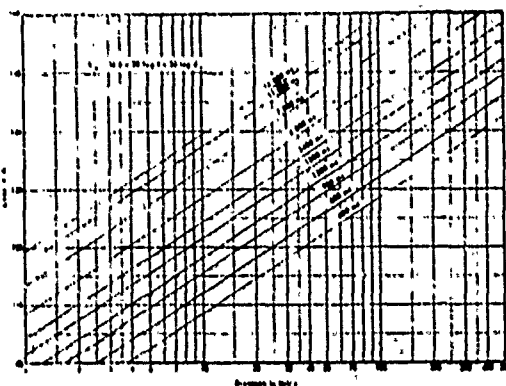


Fig. 6—Free space loss.

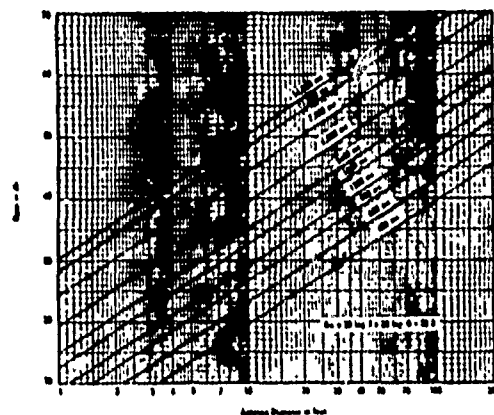


Fig. 7—Gain of parabolic antenna.

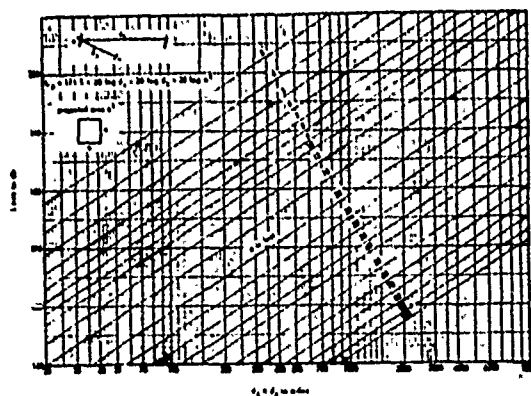


Fig. 8—Space loss on a two hop passive reflector system.

where

- d_1 = distance from Terminal A to Passive Reflector 1 in miles,
- d_2 = distance from Passive Reflector 1 to Passive Reflector 2 in miles,
- d_3 = distance from Passive Reflector 2 to Terminal B in miles,
- a_1^2 = projected area of Passive Reflector 1 in square feet,
- a_2^2 = projected area of Passive Reflector 2 in square feet.

It should be noted that for a three hop microwave system using two passive reflectors in the "far field" the total space loss between isotropic antennas is dependent on frequency with the loss inversely proportional to the square of the frequency. Therefore the higher the frequency, the less the total space loss between isotropic terminal antennas on a three hop system.

USE OF PASSIVE REFLECTORS IN THE "NEAR FIELD"

There is very little difference in the use of large passive reflectors in the "near field" and the use of the more common "periscope type." The only difference is in the size of antennas and reflectors and the spacing between them. As can be seen from Fig. 3 the radius of the "near field" can be quite large. A 7000 Mc, 60-foot antenna has a "near field" radius of approximately 10 miles. Passive reflector efficiencies are plotted in Fig. 9. These reflector efficiencies are the gains and losses of the antenna-reflector combination as compared to the antenna alone.

Consider a 7000 Mc, 30-foot antenna with a passive reflector of projected area of 1200 square feet (approximately 35-foot projected square) located one mile away. From Fig. 9, l is approximately 0.8, $1/k$ is approximately 0.5 and there is no additional loss. Therefore the system has the same loss as if the terminal antenna was in the passive reflector location. In effect we have moved the terminal antenna one mile with no additional loss.

USE OF DOUBLE PASSIVE REFLECTORS IN THE "NEAR FIELD"

Single passive reflectors as previously described can be efficiently used when the deflection angle at a repeater site is greater than approximately 40° or 50° . When the required deflection angle is less than 40° or 50° double passive reflectors will normally be more efficient. The efficiency of double passive reflectors as compared with a single passive reflector is a function of the wave length, projected area of the two reflectors and spacing. The use of double passive reflectors has been adequately described.⁴ Double passives have a gain or loss over the gain of a single passive of projected area equal to the projected area of the smaller of the double passives. These gains or losses are plotted in Fig. 10.

The most efficient arrangement of double passives is two reflectors with equal projected areas located close to each

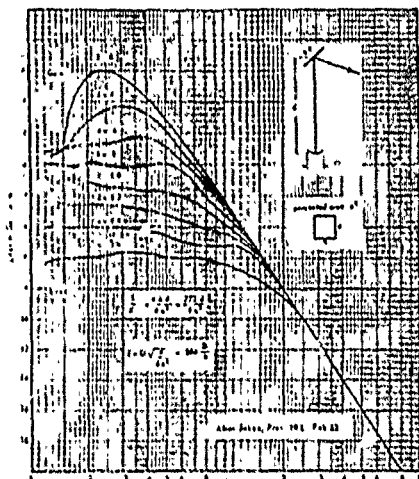


Fig. 9- Efficiency of passive reflectors in the "near field."

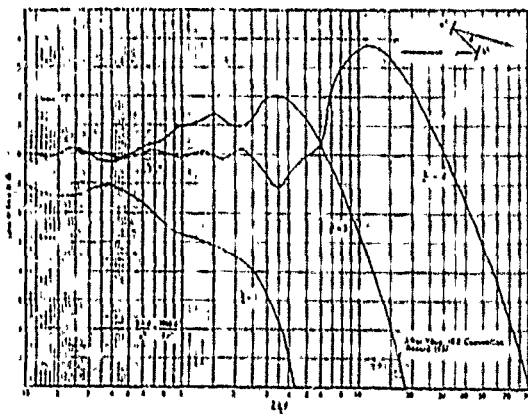


Fig. 10 Efficiency of double passive reflectors.

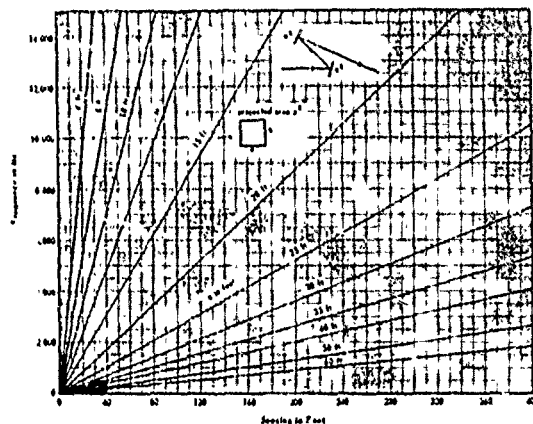


Fig. 11—Maximum spacing of double passive reflectors for loss < 1 db.

other The additional loss can be kept below 1 db (Fig. 10), if

$$\frac{2\lambda d}{a^2} \leq 0.13, \tag{13}$$

where

- λ = wave length,
- d = spacing between reflectors,
- a^2 = projected area of reflector.

The maximum reflector spacings in which the additional loss can be kept below 1 db are plotted in Fig. 11. As can be seen on the higher frequencies the spacing can be several hundred feet.

INSTALLATION CONSIDERATIONS

The same installation practices used for large parabolic antennas should be used for large passive reflectors. In order for the path loss equations used in this paper to be accurate the passive reflectors must be installed using good microwave system engineering practices. First fresnel zone clearance should be maintained on all paths. If first fresnel zone clearance is not maintained then the additional loss due to grazing, diffraction or tropospheric scattering must be considered.

There are additional considerations required when double passive reflectors are utilized. Consider double passive reflector installations as shown in Fig. 12. That portion of the wave front that is reflected by each reflector must clear the other reflector by several wavelengths. From the experience gained from the installation of many double passive reflectors it has been determined the clearance should be at least 15 wavelengths which is only approximately 2 feet at 7000 Mc.

Double passive reflectors may be arranged in a symmetrical or asymmetrical configuration as shown in Fig. 12. The minimum spacing between reflectors is determined by symmetry and the required 15 wavelengths clearance. The smaller the deflection angle the greater the required spacing between reflectors. Consider two installations requiring 50° and 24° deflection angles. At 7000 Mc the minimum spacings are 67 feet and 146 feet (Fig. 12(a) and (b)). Although an asymmetrical configuration requires much less space (Fig. 12(c)) wider reflectors are required in order to maintain the desired projected width. In Fig. 12 all reflectors have a projected width of 30 feet.

An interference problem may develop when the required deflection angle is zero or very small. The direct wave may be propagated to the distant terminal due to diffraction, scattering, ducting or other means. This direct wave may be out of phase with the wave from the passive reflector and cause fading or cancellation. To prevent this type of problem will require careful investigation of the possible field strengths of the direct wave. If interference seems probable one possible solution is the use of two cross

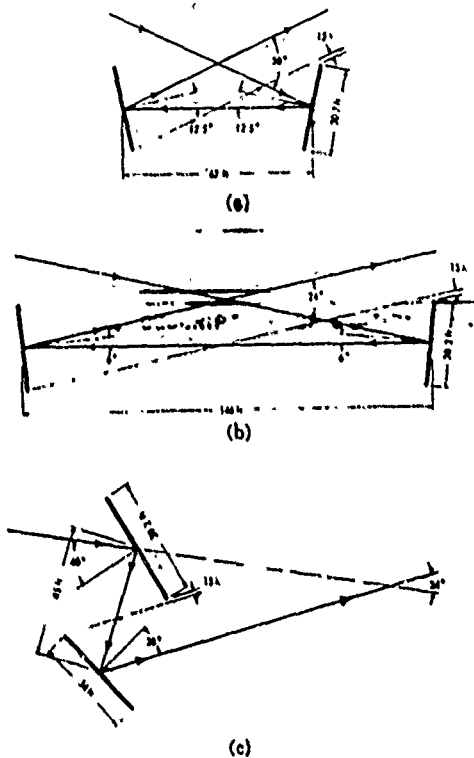


Fig. 12—Installation of double passive reflectors.

polarised back-to-back parabolic reflector antennas. This will minimise the interference between the direct and reflected waves. However, the parabolic reflectors may be more economical than either tropospheric scatter or line-of-sight active repeater systems. If back-to-back parabolic reflector antennas are used they will have to have a diameter 50 per cent greater than the width of passive reflectors (assuming square projected area) in order to have the same gain (see Figs. 5 and 7).

SYSTEM PLANNING

If a requirement exists between two non-line-of-sight locations in which there are one or two intermediate points which are in line-of-sight of each other and the terminal locations, then the use of a two or three hop passive reflector system will normally provide less loss than tropospheric scatter and may be more economical than either tropospheric scatter or a line-of-sight system. Plotted in Fig. 13 are the terminal-to-terminal losses of a typical 100 mile line-of-sight, passive reflector and tropospheric scatter systems with 30-foot parabolic terminal antennas. The tropospheric scatter losses include "antenna-to-medium" coupling loss.

For example a 100-mile tropospheric scatter system with 0° take off angles will have a terminal-to-terminal loss of

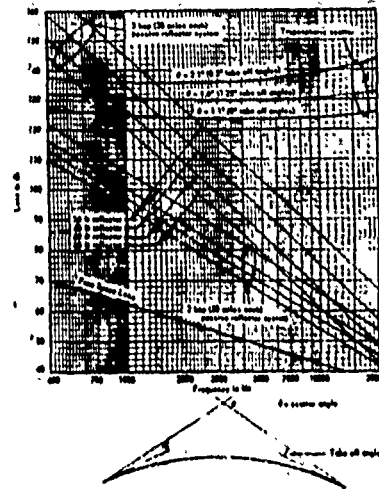


Fig. 13—Comparison of terminal to terminal loss of a typical 100 mile line-of-sight, tropospheric scatter and passive reflector systems, each with 30 foot parabolic terminal antennas.

from 123 to 127 db. In contrast a 7000-Mc three-hop system with 30-foot passive reflectors will have a terminal-to-terminal loss of 95 db and a two hop system with a 30-foot passive reflectors will have a terminal-to-terminal loss of only 72 db. This is an improvement of 29 db for a three hop system and 51 db for a two hop system. These improvements would be much greater if there were positive take off angles on the tropospheric scatter system or if larger reflectors were used on the passive reflector systems. Since the path loss on a passive reflector system is proportional to the product of the path distances, any reduction in this product by proper site selection will also reduce the path loss and give an additional improvement over a tropospheric scatter system.

A 120-channel military microwave system using active repeaters is routed as shown in Fig. 14. These active repeaters could be eliminated by increasing the 6-foot terminal antennas on the A-B link to a diameter of 20 feet, increasing the 4-foot terminal antennas on the B-C link to a diameter at 30 feet, and installing 30 foot square (projected area) double passive reflectors at relays 1, 2 and 3. The receive signal levels would be approximately 30 db above the receiver threshold. The use of tropospheric scatter would be extremely difficult and costly. The scatter angle between Terminal A and Terminal B is 1.9° and between Terminal B and Terminal C is 3.8°. These two links would require 60 foot or larger antennas in space diversity with transmitter powers of 1 kw or greater on the A-B link and 10 kw or greater on the B-C link.

A military tropospheric scatter system efficiently uses large passive reflectors in the "near field" (Fig. 15). Double 52.5 foot (projected area) reflectors are located 1.4 miles from the 33-foot terminal antenna. The scatter

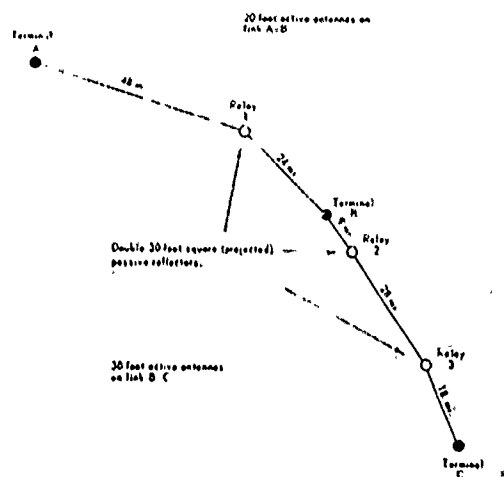


Fig. 14—Military microwave system which could efficiently use large passive reflectors.

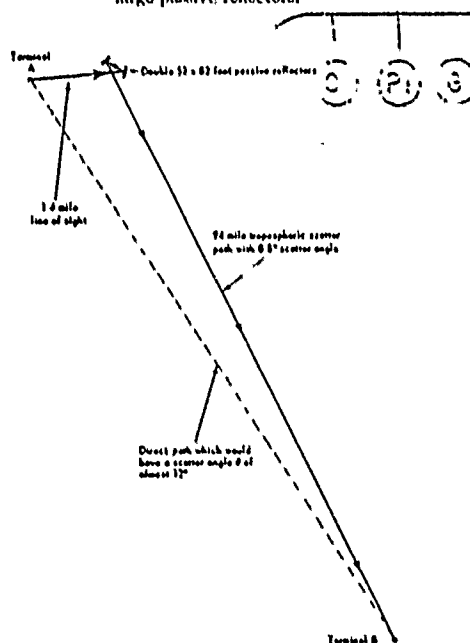


Fig. 15—Military tropospheric scatter system which uses large passive reflectors.

path from the passive reflectors to the distant terminal is 91 miles with a scatter angle of 0.8° . Communication between the two terminals via tropospheric scatter without the passive reflectors would be impossible since the scatter angle between the two terminals would be almost 12° . From Figs. 9 and 10 it can be determined that the additional loss introduced by the passive reflectors is approximately 4 db more than the loss from the passive reflectors to the distant terminal. The transmitter power used on this link is only 100 w at 1800 Mc.

ECONOMIC CONSIDERATIONS

There are many factors involved in the planning and designing of microwave systems. Economic considerations may determine if a communication requirement will be met by a line-of-sight active repeater system, line-of-sight passive repeater system, tropospheric scatter system or diffraction system.

An active microwave repeater requires buildings, primary and emergency power, microwave equipment, access roads, frequent maintenance, and in some cases, full time operating personnel. In contrast passive repeaters may be installed in a normally inaccessible location. There are no requirements for buildings, power, microwave equipment, access roads or operational personnel. The passive reflector and all installation materials may be delivered by any means, even by helicopter. When passive reflectors are used in lieu of active repeaters normally an antenna of higher gain will be required at the terminal sites. A completely new active repeater site costs approximately \$260,000.¹⁴ In contrast a passive repeater using double passive reflectors and high gain antennas at the terminals (30-foot terminal antennas and 30-foot double passive reflectors) will only cost approximately \$80,000.

Tropospheric scatter systems normally require high power transmitters, very sensitive receivers in dual, quadruple and in some cases octuple diversity. The cost of tropospheric scatter terminals in the typical 100-mile system previously mentioned would normally be much greater than that of the passive reflector system due to the higher system losses. In many cases the use of passive reflector systems can provide the same grade of service much more economically.

In addition to the reduction in the initial cost of microwave systems using large passive reflectors there is also a great reduction in operational cost. Elimination of active repeaters or a reduction in the power requirements and complexity of the terminals results in a reduction in the number of operating and maintenance personnel, reduces the quantity of spare parts, reduces the cost for commercial and emergency power and reduces site operation and maintenance cost.

RELIABILITY

There are many factors which determine the reliability of a communication system. Reliability is proportional to the complexity and quantity of the electronic equipment and to the quantity and quality of operating personnel. The use of large passive reflectors will in many instances reduce both the quantity and complexity of the electronic equipment and reduce the quantity of operating personnel. These reductions will cause a corresponding increase in the reliability of the communication system.

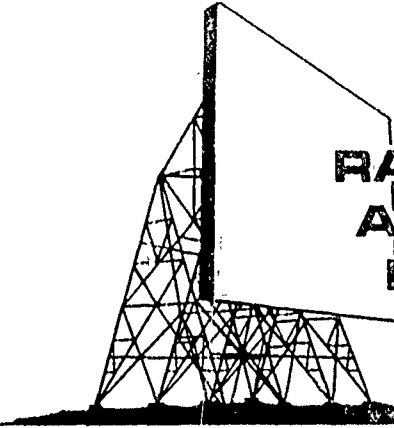
¹⁴ R. D. Chipp and T. Cosgrove, "Economic analysis of communication systems," presented at 7th NAT'L COMMUNICATIONS SYMP., Utica, N. Y.; October 2-4, 1961.

CONCLUSIONS

Large passive reflectors are extremely practical. They can be used to replace active repeaters on line-of-sight microwave systems and can also be used on diffraction and tropospheric scatter systems. By the use of high power transmitters and very sensitive receivers long, two or more hop systems may be effectively utilized. The space loss on a two hop system is *independent* of frequency and on a three or more hop system is *dependent* on frequency with *less* loss at the *higher* frequencies. By the use of frequencies of several gigacycles with their higher gain antennas, the system losses can be quite low. Large terminal antennas and passive reflectors may be sited and installed using the same engineering and installation practices normally used for tropospheric scatter systems.

Large passive reflectors are also economical. When used to replace active microwave repeaters or to extend a tropospheric scatter or diffraction system considerable savings in initial and operating cost can be realized. The reliability of communication systems using large passive reflectors will be considerably higher due to a reduction of the quantity and/or complexity of the electronic equipment.

Large passive reflectors should be considered as another tool which can be used by the microwave engineer for planning and engineering communication systems. When used effectively with line-of-sight, diffraction and the tropospheric scatter modes of propagation, communication systems may be engineered more economically, with more reliability and with a decrease in the operating and maintenance problems.



RADIATION PATTERNS AND THE PASSIVE REPEATER

by THOMAS J. WORRING
Chief Engineer
Microflect Co. Inc.

© COPYRIGHT 1971 BY MICROFLECT CO. INC.

One problem facing the microwave transmission engineer today is that of interference calculations. This paper deals with the interference calculations as they relate to passive repeaters. Very little practical information has been available to describe or calculate radiation patterns for passive repeaters. Accordingly, those making interference studies on systems employing passive repeaters used what they considered a conservative approach. One such method is to treat the passive repeater as a comparable active station. Most felt their conservative assumptions were unsatisfactory. Perhaps at times the assumptions were not conservative and at other times excessively conservative. The need for methods of evaluating the radiation from passive repeaters has become apparent. The problem is to make the methods practical and general and yet retain an accuracy consistent with radiation pattern data used for the other microwave system components.

Accordingly, Microflect set about to determine a practical method of developing the theoretical pattern for a given passive repeater. The theory was explored. Comparisons were made with past and very recent plots made from measurements obtained during alignment of actual passive repeater installations. Some examples of these plots are depicted in Figures 1, 2, and 3.

Typically, the mechanical limitations of rotating the passive repeaters prevented measurements about the main-beam axis beyond about $\pm 2^\circ$. However, correlation between the theoretical and measured plots offered encouragement for future use of the method for plotting the theoretical pattern. It is in this range that the information is most significant. This deviation from the main axis ($\pm 2^\circ$ of adjustment) may typically allow a reading at about the 5th minor lobe peak, which is approximately 24.7 dB down from the main lobe. From the measured plots one could probably safely extrapolate that the theoretical pattern plot (examples shown in Fig.'s No. 4 & No. 5) will have good accuracy to a level 30 dB down from the main lobe peak and that satisfactory accuracy may often be obtained at levels 40-45 dB down from the main lobe peak. It may also seem a logical assumption that the reflected and diffracted signal level will not be higher than the 40-45 dB level down from the main beam for the large angles to the side and behind the reflector surface.

EXTREME ISOLATION POSSIBLE WITH PASSIVE REPEATER

When a passive repeater is not properly aligned, as when it is first installed and not peaked, it has been observed that the signal level may be about 70 dB below a receiver median design level. In these instances the assumption that the level is no higher than 40-45 dB down for wide angles is obviously conservative. On some 6 GHz and 11 GHz systems Microflect has helped to align, the following conditions were present to indicate that the off-angle radiation from the passive may be 70 dB below the receiver design median signal.

- a. Receiver Design Median Signal Level = -38 dBm
- b. F.M. Improvement Threshold Level = -81 dBm
- c. Transmitter fully deviated for a 600 voice channel system with a single 1 kHz tone.

It can be shown that full transmitter deviation can provide about a 28 dB advantage below the -81 dBm FMIT, so that the tone will be discernable at about 109 dBm. (This technique has proven useful for aligning radio paths.) With a median design level of -38 dBm and a signal level of -109 dBm there is over 70 dB isolation from off-angle radiation for these specific cases.

It should be noted that the passive repeater major lobe and the first few minor lobes can be more narrow than just the half power beam width of an active repeater antenna.

PLOTTING THE PATTERNS

There are two convenient forms of plotting the radiation pattern of a passive repeater. These are the polar decibel plot and the rectangular decibel plot. Figure 4 is an example of a polar decibel plot. Figure 5 is an example of a rectangular decibel plot. The information for these plots are shown in Table I. Note that unless the angular scale (angle θ and/or turns of actual adjusting mechanism) is carefully observed on the rectangular decibel plot, an impression that the passive repeater radiation pattern is very broad may

be derived from the general appearances of the plot. As this impression can be misleading it is a recommended practice that the rectangular plot be accompanied by a corresponding polar plot. The polar plot provides a better visualization of the spatial distribution of the pattern.

To make a pattern plot one could use the following procedure:

- (1) Review the information shown on Fig. 6 to assess what parameters are required as "input" for the problem or the "given" portion of the problem. At this time also consider the effects of the qualifications of the method with respect to the particular pattern required.
- (2) With the given data, complete Table II as illustrated in the Example of Table I.
- (3) Complete the rectangular decibel plot from the "blank" form of the pattern shown as Fig. 7. This plot is complete by affixing the proper scale for " θ " on the lower edge of the graph. The use of this standard form eliminates the need to plot various shape curves, as only the scale of the angle, θ , changes with different plots. This scale can be placed on the plot by using the "evaluation of $\sin \theta$ in terms of the parameter u " as completed on Table II.
- (4) Make a polar plot from the completion of Table II. This plot is conveniently made from the tabulation of the minor lobe peak values, as the plot represents the envelope of the radiation pattern.

Because the data does not cover the full 360° one has to extrapolate or assume that the levels are no higher than the last plotted point from the tabulated data. Thus, the curve is completed by approximating this level thru the values of " θ " for which the decibel levels are not calculated.

An examination of Figures 1, 2, & 3 shows a scale in "turns" of the adjusting mechanism horizontally and the scale of θ slanted and scaled in minutes or arc with the designation being θ Min. The light lines of the pattern indicate the calculated theoretical pattern and the dark heavy lines the measured pattern.

In order to illustrate how these scales (turns and θ Min.) may be affixed to the standard rectangular plot the following example uses the data of Table I and Fig. 5. The installation drawings of a Microflect $24' \times 30'$ passive indicate that ten turns of an adjusting handle will rotate the unit (panels) about a vertical axis 20.2 minutes, or one turn corresponds to 2.02 minutes of rotation. In the plane of the incident and reflected beam axes, one minute of passive rotation causes an angle, θ , of two minutes. Thus, the relationship is derived that one turn of the adjusting handle corresponds to θ Min. = 4.04.

From Table I the relationship, $\sin \theta = (0.00239)(u)$, is shown derived. By choosing a convenient multiplying factor of $u=10$, one finds the corresponding value of $\sin \theta = 0.0239$; and for values of θ less than 10° , $\sin \theta$ approximately equals θ in radians. Thus $\theta = 0.0239$ radians or about 1.37° . (θ can also be evaluated by using a table of natural trigonometric functions). The value of θ Min. = $(1.37)(60) = 82.2$ Min. By drawing a vertical line at the point of $u=10$ and intersecting this with a scale placed with the beginning at the " $\theta = 0$ " point and meeting the vertical line at the value of 82.2, a scale in θ Min. can readily be marked on the standard plot. (An engineer's and/or a metric scale is handy for a variety of values). See Fig. 8.

From previous remarks 10 turns corresponded to 40.4 minutes for this specific example. If on the θ Min. scale the 40.4 minute point is projected vertically to a horizontal line, a scale in turns can be constructed.

In applying the foregoing methods of radiation pattern plotting it must be remembered that " θ " cannot be evaluated for the entire 360° by using " $20 \text{ Log } u$ " as the envelope. Large deviations from the major lobe axis are not consistent with the original assumptions made for the mathematical development of the formulas needed to make these plots. It should also be noted that the quantitative accuracy of the plot decreases with angular deviation from the major lobe axis.

To return to more exacting methods of applying the complete mathematical relationships for diffraction phenomena would greatly increase the difficulty of evaluating the radiation pattern for any commercially available microwave aperture device, either parabolas or flat reflectors. Each set of patterns evaluated could represent an effort beyond practical or economical engineering methods.

The methods of determination shown here are known to be reliably accurate to at least the fifth minor lobe, and probably are reasonably accurate for most interference studies to a level 30-40 dB down from the major lobe. Beyond these ranges some comparisons could be made with complete radiation patterns obtained on antenna ranges to make a rough extrapolation for the remainder of the pattern.

In summation, we have found the foregoing methods of plotting far field radiation patterns agrees closely with measurements on actual installations. The correlation of measured plots compared to theoretical plots are such that we have placed radiation patterns for our standard passive repeaters and tower-mounted reflectors "on file" with the Federal Communications Commission in Washington and the Department of Communications in Ottawa.

TABULATION OF DATA FOR PLOT OF PASSIVE REPEATER RADIATION PATTERN

PASSIVE SIZE	24' x 30'	PLANE OF PATTERN CUT	HORIZONTAL
INCLUDED ANGLE BETWEEN INCIDENT AND REFLECTED BEAMS			90°
FREQUENCY (GHZ)	= 6.175	WAVELENGTH (FT.)	= $\frac{0.9836}{6.175}$ = 0.1593'

EVALUATION OF "SIN Θ" IN TERMS OF PARAMETER "U"

$$U = (a) \left(\frac{\pi}{\lambda} \right) (\sin \theta) = [(30)(\cos 45^\circ)] (3.1416/0.1593)(\sin \theta) = 418.4 \sin \theta \text{ or}$$

$$\sin \theta = (0.00239)(U)$$

EVALUATION OF ANGLE "Θ" FOR 3dB, 10dB, and 40dB POINTS

- 3dB POINTS (U ≈ 1.39) θ = 0.19° (HALF POWER BEAM WIDTH = 2θ)
- 10dB POINTS (U ≈ 2.32) θ = 0.32° (COMMON REFERENCE FOR STRUCTURAL RIGIDITY)
- 40dB POINTS (U ≈ 3.11) θ = 0.43° (POINTS VERY NEAR 1st NULL POINT)

TABULATION OF MINOR LOBE PEAK VALUES

MINOR LOBE	U	20 Log U	θ Degrees	MINOR LOBE	U	20 Log U	θ Degrees
1	4.5	13.3	0.62	21	67.5	36.6	9.29
2	7.7	17.8	1.05	22	70.7	37.0	9.73
3	10.9	20.8	1.49	23	73.8	37.4	10.16
4	14.1	23.0	1.93	24	77.0	37.7	10.61
5	17.2	24.7	2.36	25	80.1	38.1	11.04
6	20.4	26.2	2.80	26	83.3	38.4	11.49
7	23.6	27.4	3.23	27	86.4	38.7	11.92
8	26.7	28.5	3.66	28	89.5	39.0	12.36
9	29.9	29.5	4.10	29	92.7	39.3	12.81
10	33.0	30.4	4.53	30	95.8	39.6	13.24
11	36.1	31.2	4.95	31	99.0	39.9	13.69
12	39.3	31.9	5.39	32	102.1	40.2	14.13
13	42.4	32.5	5.82	33	105.2	40.4	14.57
14	45.6	33.2	6.26	34	108.4	40.7	15.02
15	48.7	33.8	6.69	35	111.5	41.0	15.46
16	51.8	34.3	7.11	36	114.7	41.2	15.92
17	55.0	34.8	7.56	37	117.8	41.4	16.36
18	58.1	35.3	7.99	38	121.0	41.7	16.82
19	61.3	35.7	8.43	39	124.1	41.9	17.26
20	64.4	36.2	8.86	40	127.2	42.1	17.71

TABLE 1
EXAMPLE OF DATA TABULATED FOR RADIATION PATTERN PLOTS

TABULATION OF DATA FOR PLOT OF PASSIVE REPEATER RADIATION PATTERN

PASSIVE SIZE

PLANE OF PATTERN CUT

INCLUDED ANGLE BETWEEN INCIDENT AND REFLECTED BEAMS

FREQUENCY (GHZ) =

WAVELENGTH (FT.) =

EVALUATION OF "SIN θ " IN TERMS OF PARAMETER "u"EVALUATION OF ANGLE " θ " FOR 3dB, 10dB, and 40dB POINTS3dB POINTS (u \approx 1.39) θ = (HALF POWER BEAM WIDTH = 2θ)10dB POINTS (u \approx 2.32) θ = (COMMON REFERENCE FOR STRUCTURAL RIGIDITY)40dB POINTS (u \approx 3.11) θ = (POINTS VERY NEAR 1st NULL POINT)

TABULATION OF MINOR LOBE PEAK VALUES

MINOR LOBE	u	20 Log u	θ Degrees	MINOR LOBE	u	20 Log u	θ Degrees
1	4.5	13.3		21	67.5	36.6	
2	7.7	17.8		22	70.7	37.0	
3	10.9	20.8		23	73.8	37.4	
4	14.1	23.0		24	77.0	37.7	
5	17.2	24.7		25	80.1	38.1	
6	20.4	26.2		26	83.3	38.4	
7	23.6	27.4		27	86.4	38.7	
8	26.7	28.5		28	89.5	39.0	
9	29.9	29.5		29	92.7	39.3	
10	33.0	30.4		30	95.8	39.6	
11	36.1	31.2		31	99.0	39.9	
12	39.3	31.9		32	102.1	40.2	
13	42.4	32.5		33	105.2	40.4	
14	45.6	33.2		34	108.4	40.7	
15	48.7	33.8		35	111.5	41.0	
16	51.8	34.3		36	114.7	41.2	
17	55.0	34.8		37	117.8	41.4	
18	58.1	35.3		38	121.0	41.7	
19	61.3	35.7		39	124.1	41.9	
20	64.4	36.2		40	127.2	42.1	

TABLE II
EXAMPLE OF "BLANK" TABULAR FORM FOR RADIATION PATTERN DATA

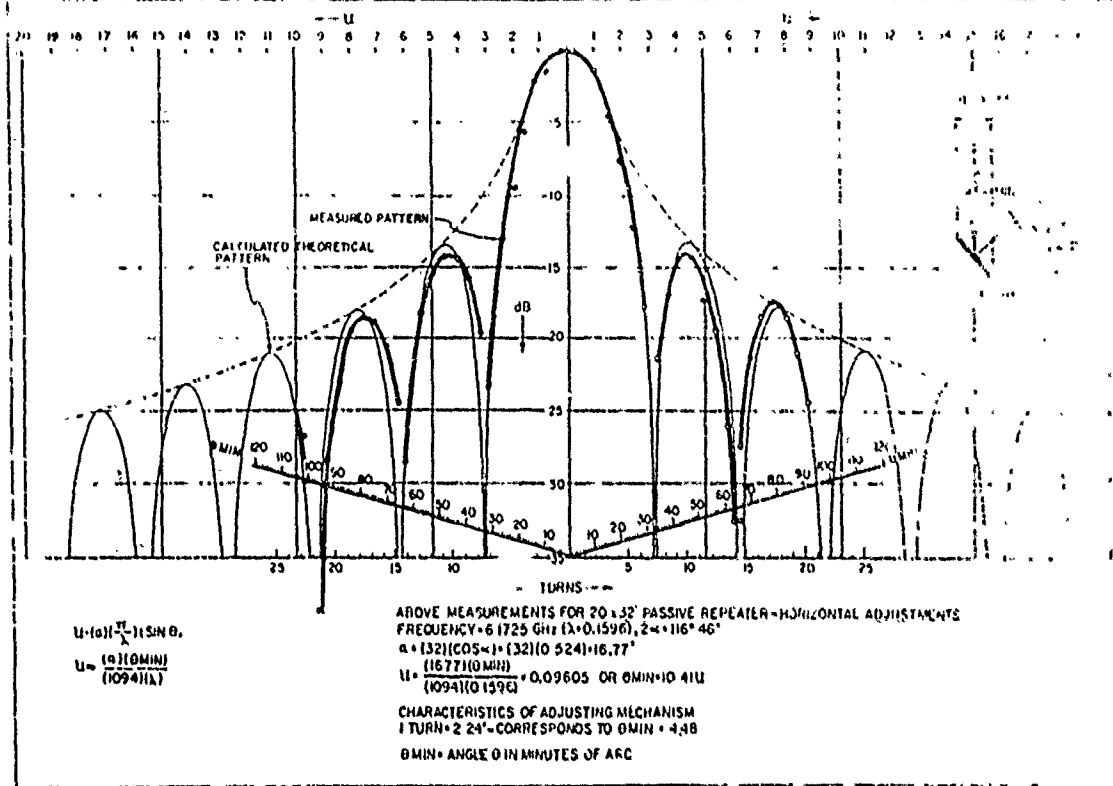


FIGURE 1

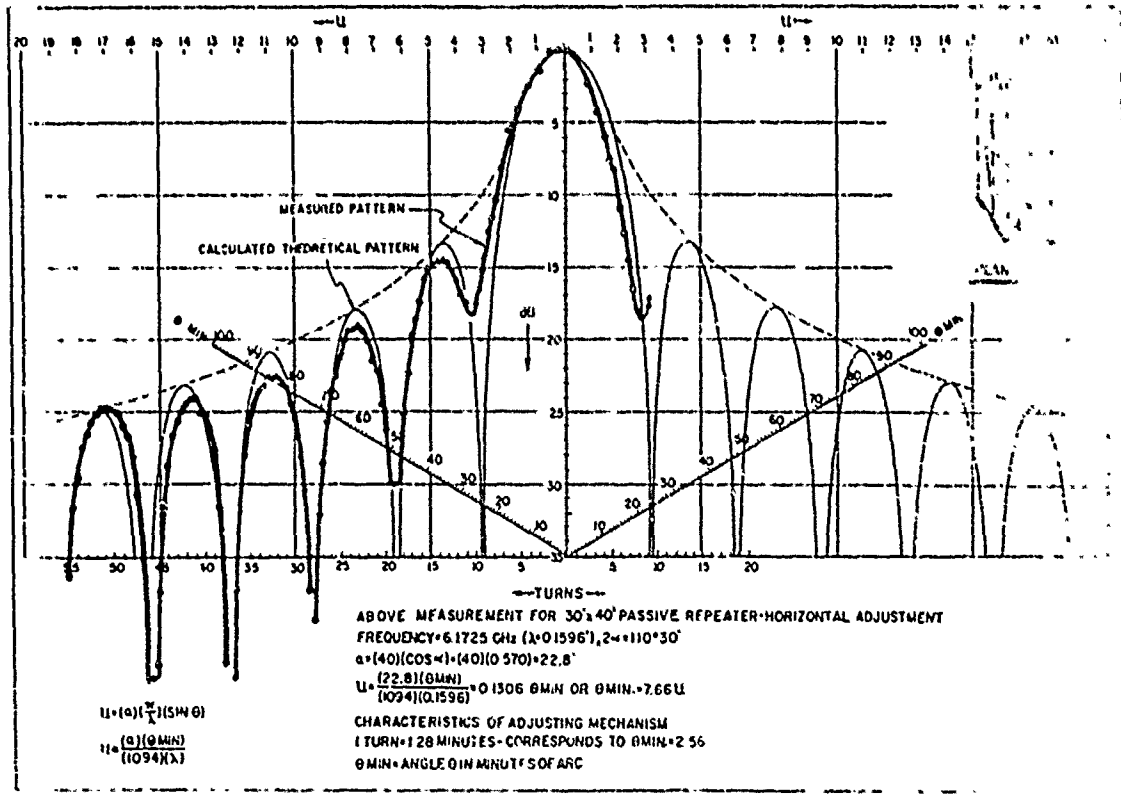


FIGURE 2

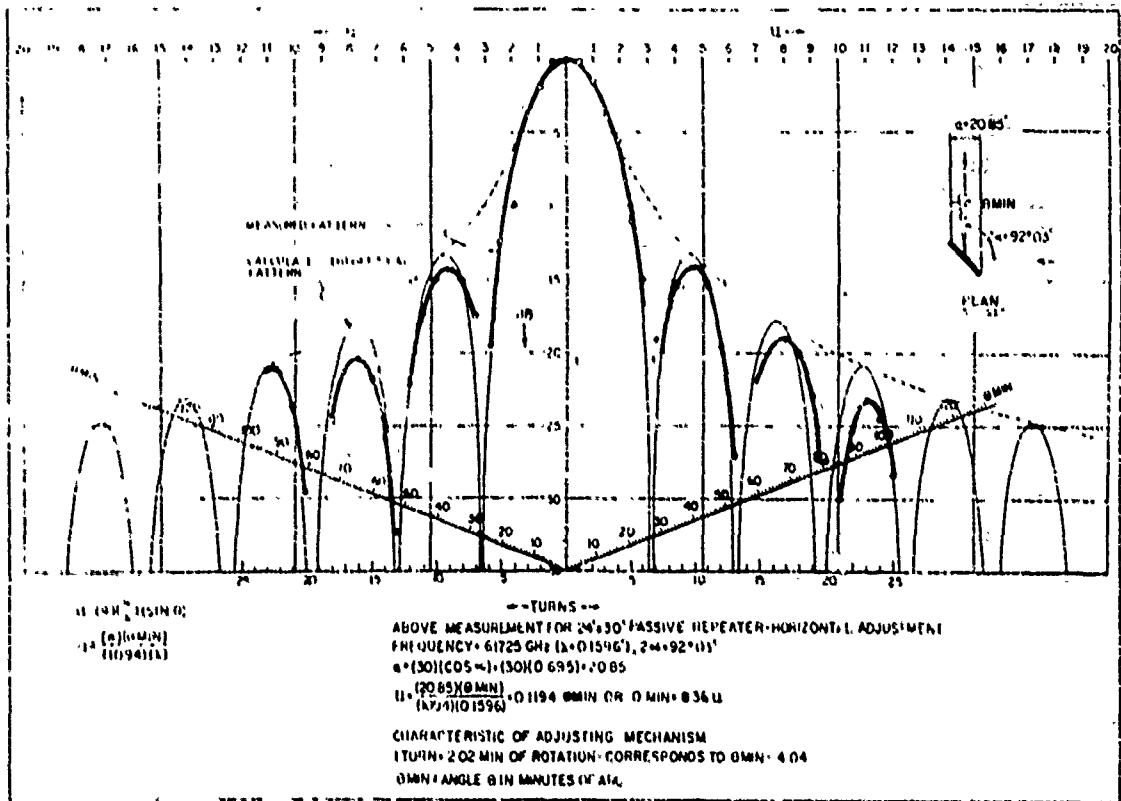


FIGURE 3

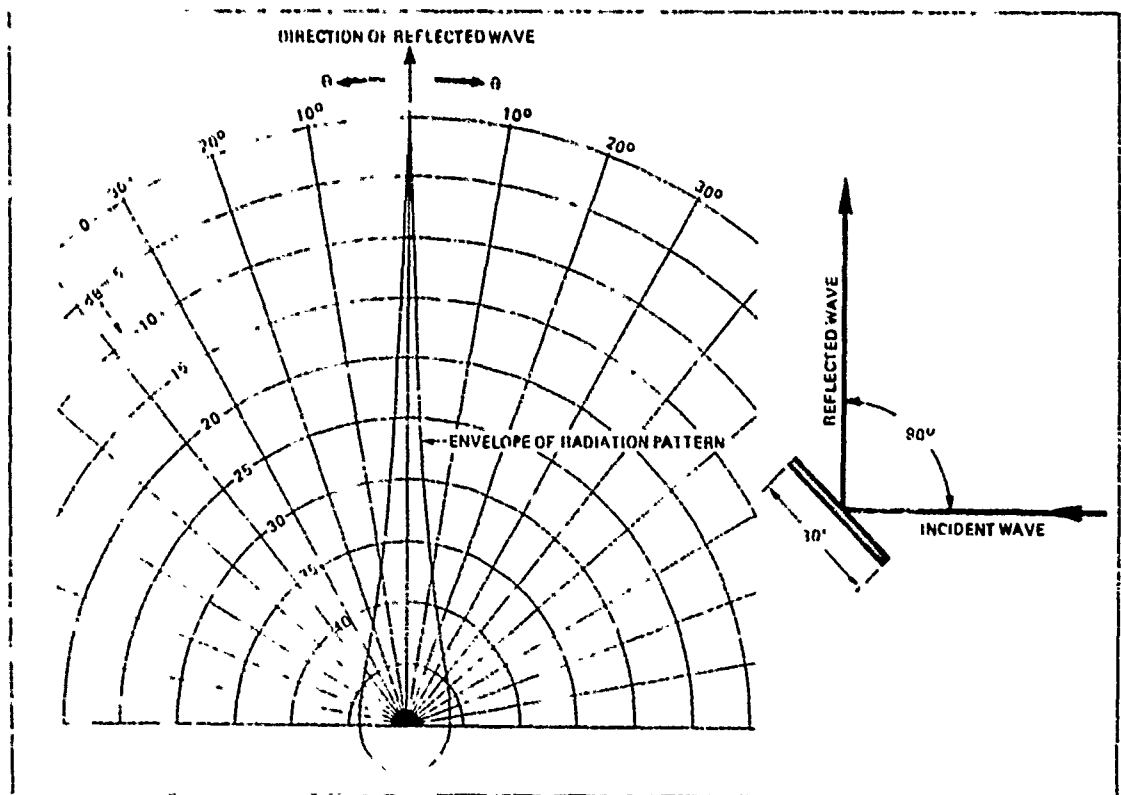


FIGURE 4

EXAMPLE OF POLAR DECIBEL PLOT OF 24x30' PASSIVE REPEATER
 (f = 6.175 GHz)

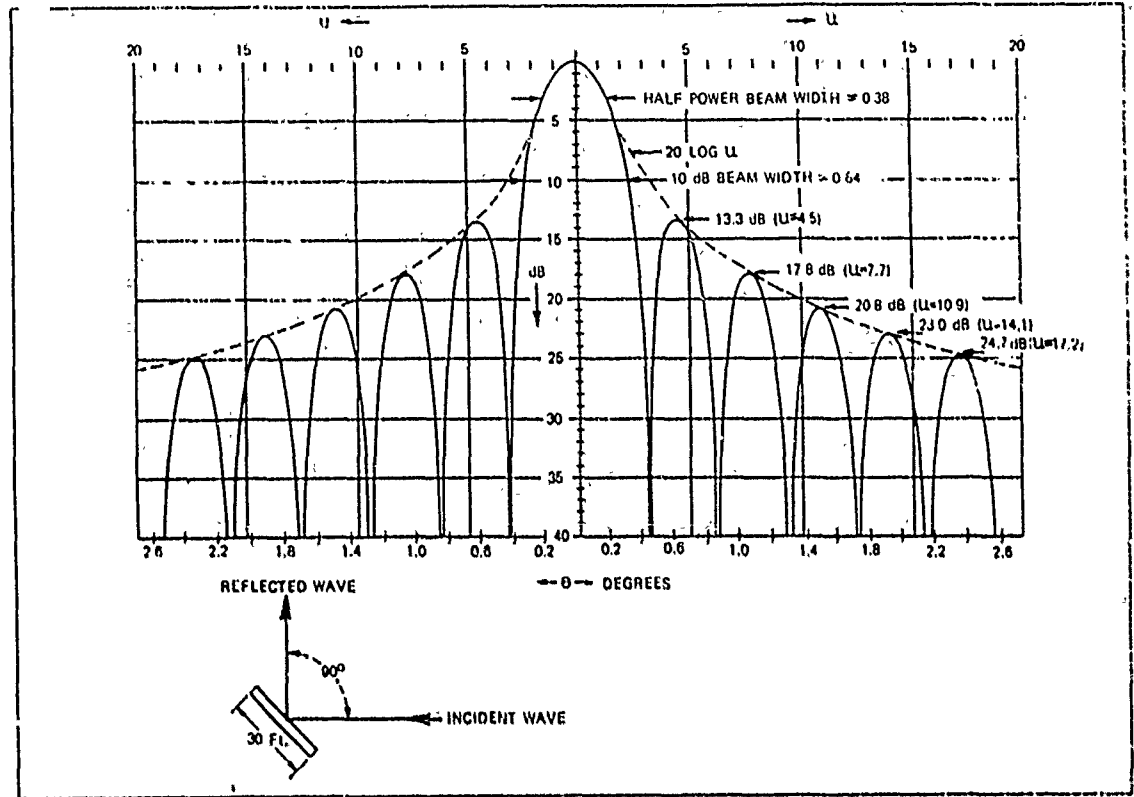


FIGURE 5
EXAMPLE OF RECTANGULAR DECIBEL PLOT OF 24'x30' PASSIVE REPEATER
(f=6,175 GHz)

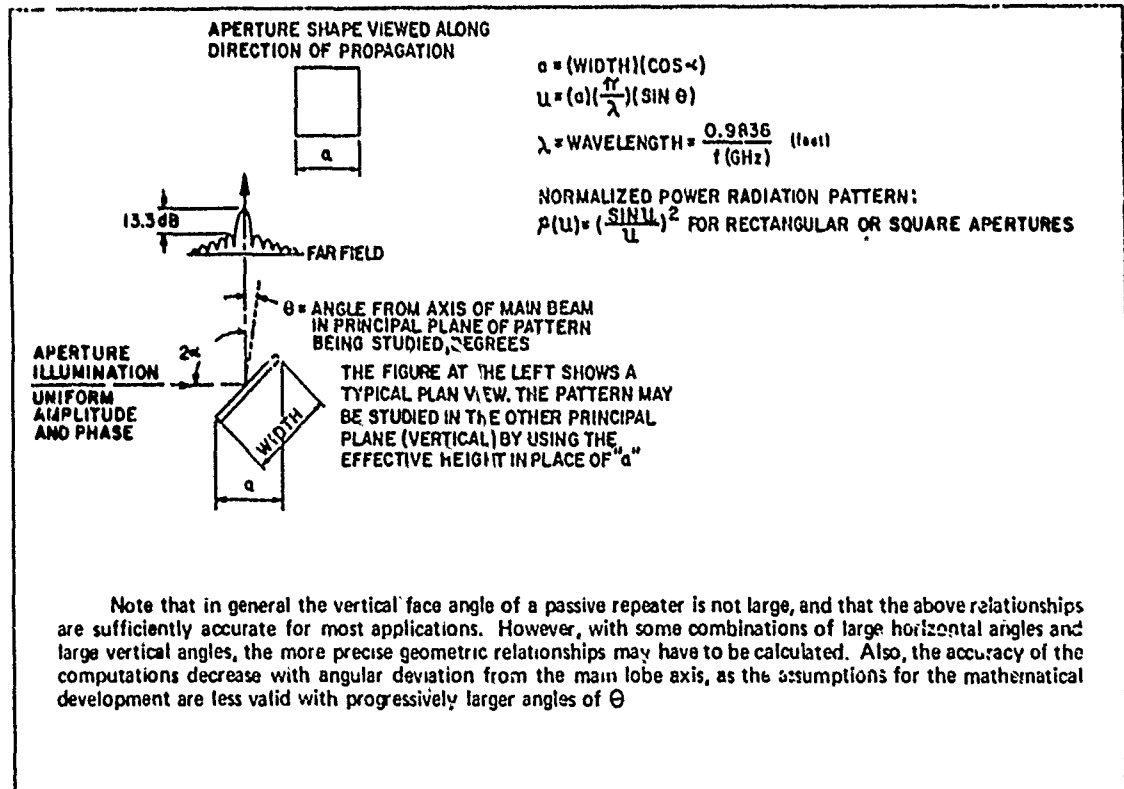


FIGURE 6
GENERAL PATTERN PLOT FORMULAS

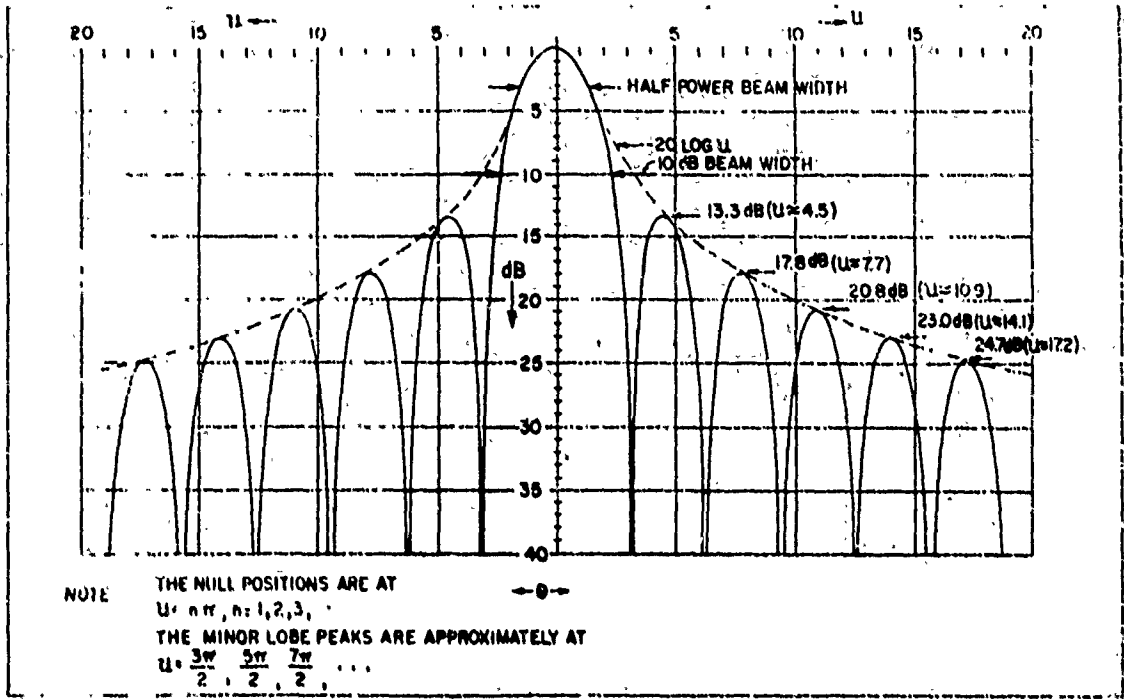


FIGURE 7
 EXAMPLE OF "BLANK" FORM OF RECTANGULAR DECIBEL PLOT

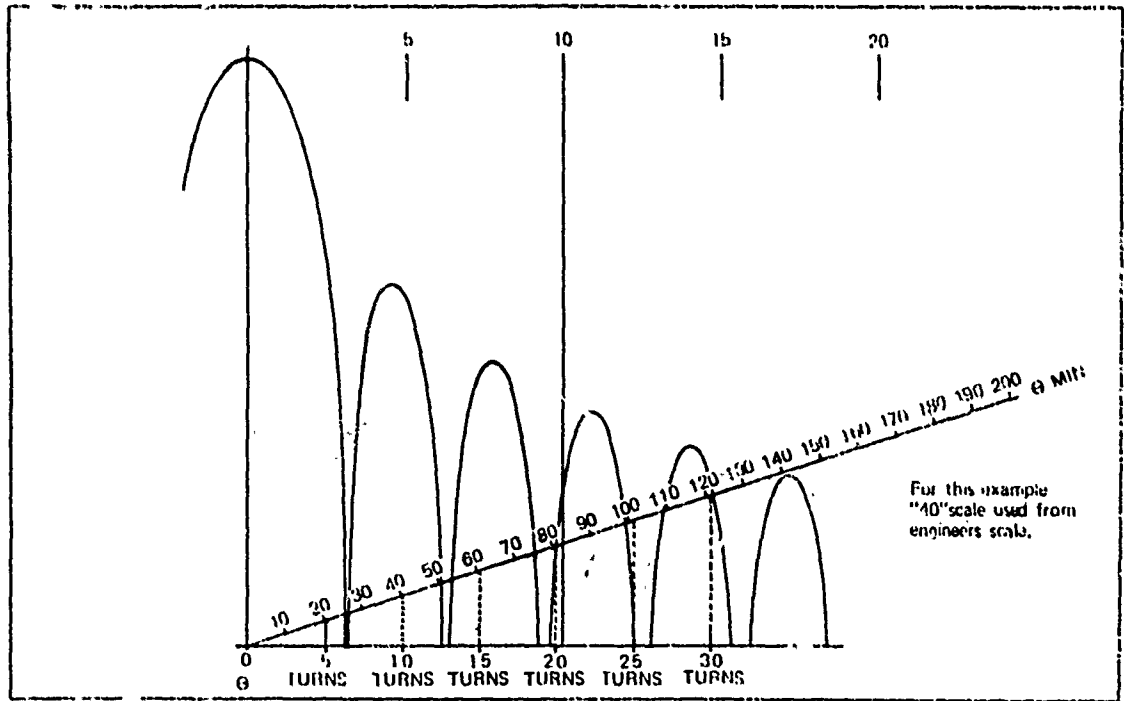
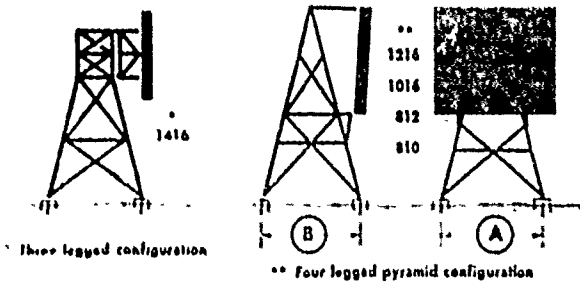
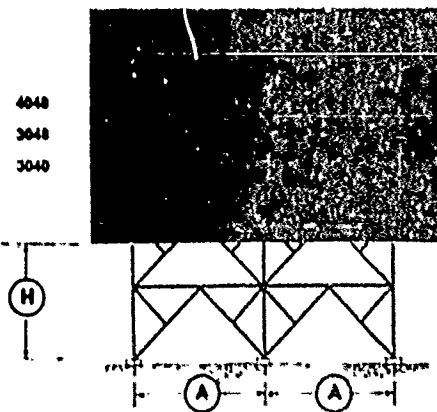
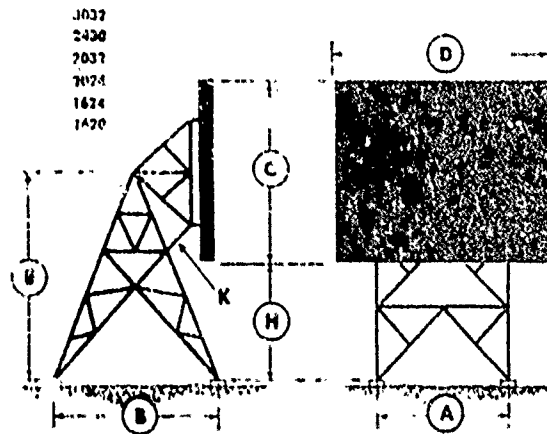


FIGURE 8
 EXAMPLE OF MARKING SCALE ON STANDARD RECTANGULAR PLOT





H							
Model	No. of Frames	A Ft./In.	B Ft./In.	C Feet	D Feet	F Ft./In.	Ice Load Tons
3048-8	3	14-0	19-2	30	48	23-0	33.0
3040-8	3	14-0	19-2	30	40	23-0	27.4
3032-8	2	18-3	19-2	30	32	23-0	21.9
2430-8	2	18-0	16-8	24	30	20-0	16.1
2032-8	2	16-0	15-0	20	32	18-0	12.7
2024-8	2	16-0	15-0	20	24	18-0	10.3
1624-8	2	12-0	13-4	16	24	16-0	8.1
1620-8	2	12-0	13-4	16	20	16-0	6.7
1416-8	*	11-0	9-4	14	16	15-0	4.7
1216-8	**	10-0	10-0	12	16	14-3	4.0
1016-8	**	10-0	10-0	10	16	13-5	3.3
812-8	**	8-0	8-0	8	12	10-9	2.0
810-8	**	8-0	8-0	8	10	10-9	2.0

H							
Model	No. of Frames	A Ft./In.	B Ft./In.	C Feet	D Feet	E Ft./In.	Ice Load Tons
4060-15	4	15-0	29-2	40	60	35-0	50.0
4048-15	3	15-0	29-2	40	48	33-0	40.0
3048-15	3	14-0	25-0	30	48	30-0	33.0
3040-15	3	14-0	25-0	30	40	30-0	27.4
3032-15	2	18-3	25-0	30	32	30-0	21.9
2430-15	2	18-0	22-4	24	30	27-0	16.1
2032-15	2	16-0	20-10	20	32	25-0	12.7
2024-15	2	16-0	20-10	20	24	25-0	10.3
1624-15	2	12-0	19-2	16	24	23-0	8.1
1620-15	2	12-0	19-2	16	20	23-0	6.7
1416-15	*	14-0	12-11	14	16	22-0	4.7
1216-15	**	10-0	10-0	12	16	21-0	4.0
1016-15	**	10-0	10-0	10	16	20-0	3.3
812-15	**	8-0	8-0	8	12	19-0	2.0
810-15	**	8-0	8-0	8	10	19-0	2.0

* Three legged configuration

** Four legged pyramid configuration

See price list for weights, cubas, unit and crated prices
4060 & 4048 are 15 ft. ground clearance models only.



MICROFLECT CO., Inc.

3575 25TH STREET, S.E. - SALEM, ORE. - 503/363-9267

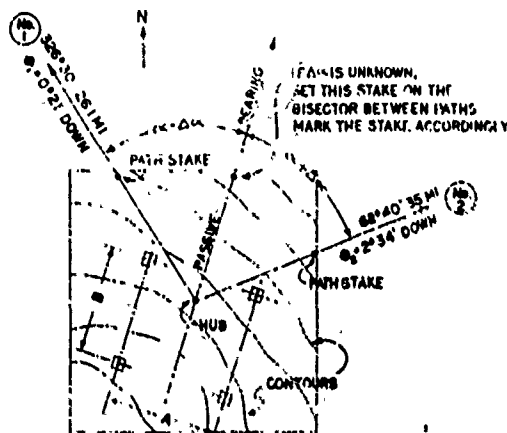
Ordering Information

The following items of information should be supplied when ordering a Microflex passive repeater:

- (1) Size
- (2) Ground clearance, 8' or 15'
- (3) Face angle of the passive, θ_3
- (4) Site information, one of the following:
 - (a) Level site, or if not level
 - (b) The relative elevations of the four piers, or . . .
 - (c) A four foot contour site topography

The face angle and the horizontal correction angle will be calculated by Microflex from receipt of (1) the horizontal included angle between paths, $2\theta_2$, and (2) the vertical path angles θ_1 and θ_2 as shown on the sketch to the right. If four stakes shown in the sketch should be set by the customer from which the foundation can be located by the contractor, for a complete description of the method used to determine the face angle and the horizontal correction angle, refer to Microflex's Manual 1A1, available on request.

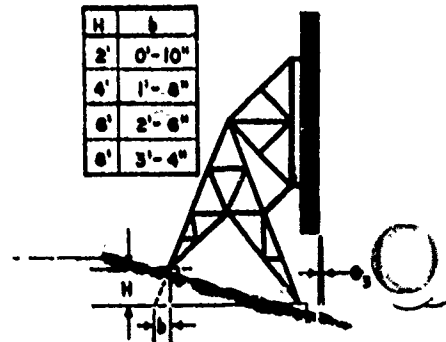
The sketch below shows the stepped footing arrangement which is available, at no extra cost, to eliminate the cost of leveling a site. From your site information, Microflex's engineers will select the optimum footing arrangement to keep the installation costs to a minimum.



Foundations

Foundations represent about half the cost of a passive repeater installation. Since ground conditions vary considerably, Microflex has available, for each size passive, a foundation design for four different soil conditions:

- (1) Sand, gravel, and loam. Hand excavation
- (2) Weathered broken rock. Excavation with some drilling and shooting.
- (3) Solid rock suitable for drilling and grouting rebar into the rock.
- (4) Ground incapable of supplying uplift strength or a site where concrete is easily available and excavation is inconvenient or expensive. Concrete foundations are supplied for this condition with the weight of the concrete resisting all uplift.



MICROFLECT COMPANY CAPABILITIES

ENGINEERING Experienced Engineers and Draftsmen assure the customer well designed standard products as well as custom designed structures for unusual requirements.

Some Microflex engineers have had many years of experience in the application of passive repeaters in microwave systems, they are able to help their customers with passive repeater application problems.

MANUFACTURING Microflex's new plant in Salem, Oregon has been designed for the efficient production of passive repeaters and towers. Modern equipment and trained personnel assure the customer of well built products and dependable delivery dates.

FIELD INSTALLATION Microflex's experienced crews have installed microwave structures throughout the U.S. including Alaska and Hawaii. By utilizing helicopters, custom built vehicles, and modern portable power tools, they are able to do first class work in even the most remote areas.

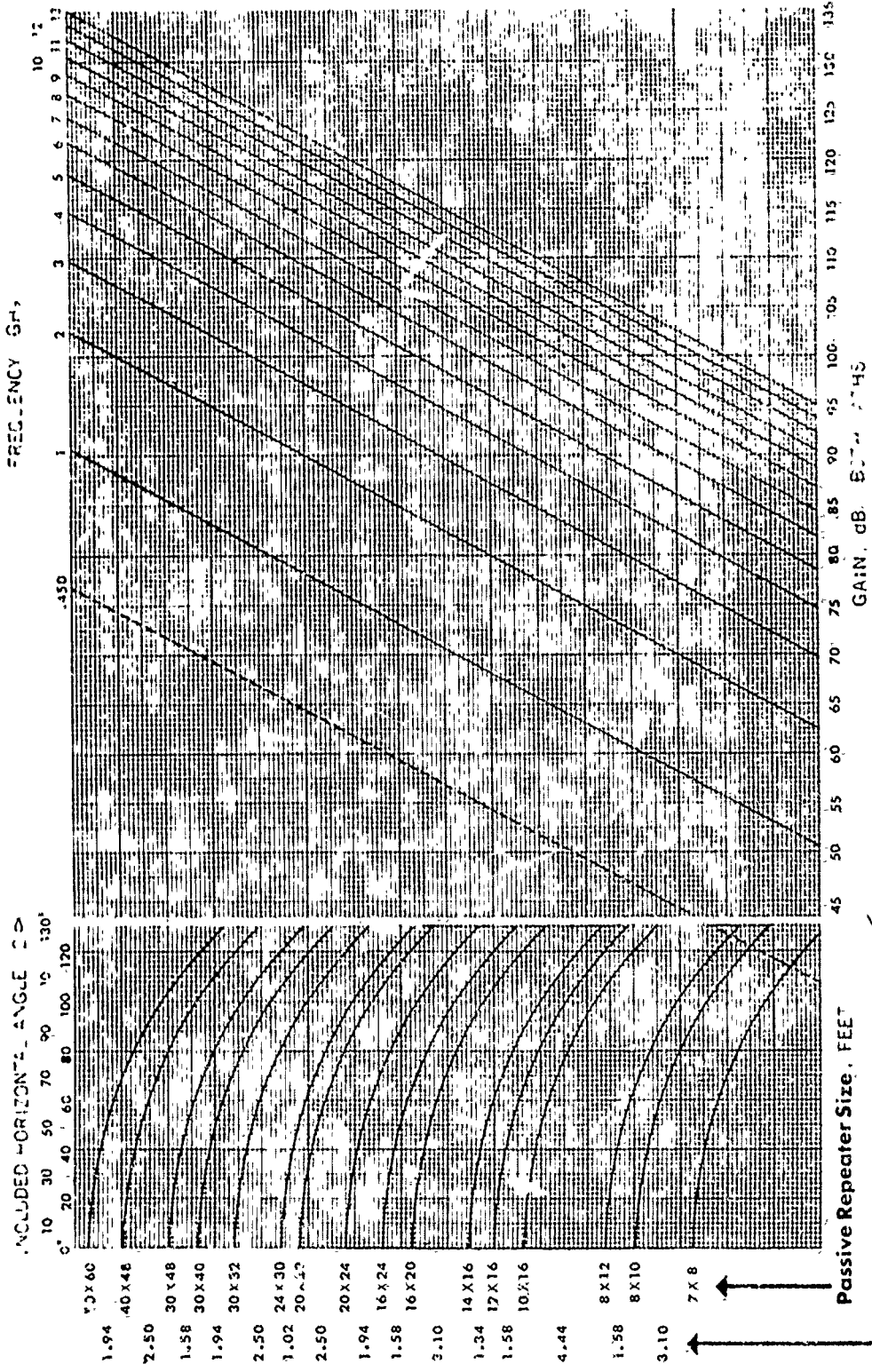
PRODUCTS In addition to the passive repeater sizes listed in this brochure, Microflex produces flat passive repeaters, 6'x8', 8'x10', 8'x12', 10'x16', 12'x16', and 14'x16', complete with supporting structure or adaptable for mounting on walls of buildings, smokestacks, roofs, water towers, or guyed and self-supporting microwave towers. Special corrosion protection has been developed by Microflex for the severely corrosive atmospheres associated with smokestacks where passive repeaters are installed on a smokestack.

Microflex also fabricates a wide range of small self-supporting towers, roof mounts, stub towers, and many other specialized structures designed to accommodate any manufacturer's antennas in the required combination of sizes and layouts. Submit your antenna mounting problems to us and we will be glad to offer a proposal.

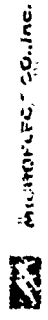
In Summary Microflex has the engineering, fabrication, and field installation capability to handle your structural microwave requirements in a first-class manner.

F-44

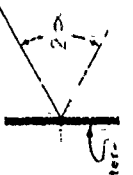
Order or Specify ... "MICROFLECTORS"



PASSIVE REPEATER SIZE SELECTOR



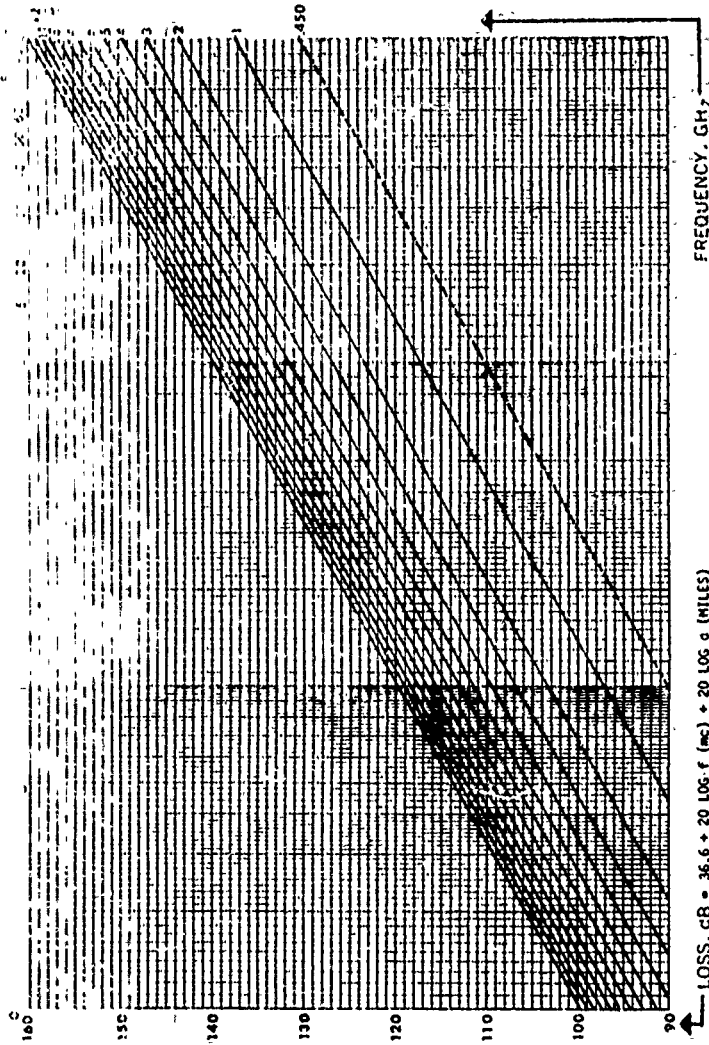
GAIN FOR BOTH PATHS = $20 \log \frac{4\pi A^2 \cos \alpha}{\lambda^2}$
 A = PASSIVE REPEATER AREA, SQ. FT.
 α = HORIZONTAL ANGLE, DEGREE
 λ = WAVELENGTH, FEET



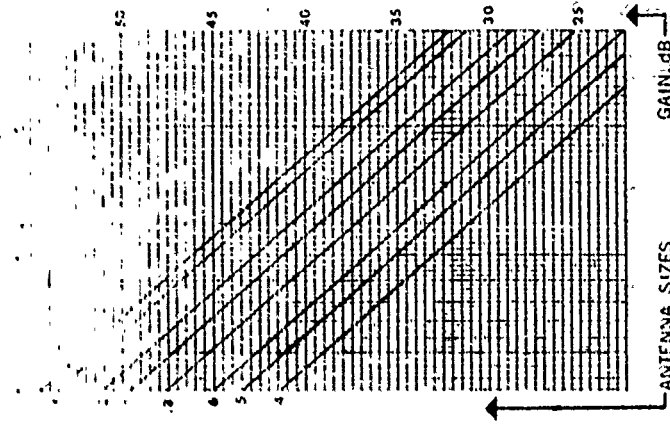
INCREMENTAL GAIN BETWEEN PASSIVE REPEATER SIZES, DB

Passive Repeater

Free Space Loss Between Isotropic Radiators



Passive Repeater Gain



$$\text{GAIN} \approx 10 \log \frac{5 d^2}{\lambda^2}$$

PASSIVE REPEATER



$$A^2 = 1.4 \times 10^{-10} \lambda^2$$

PASSEIVE REPEATER

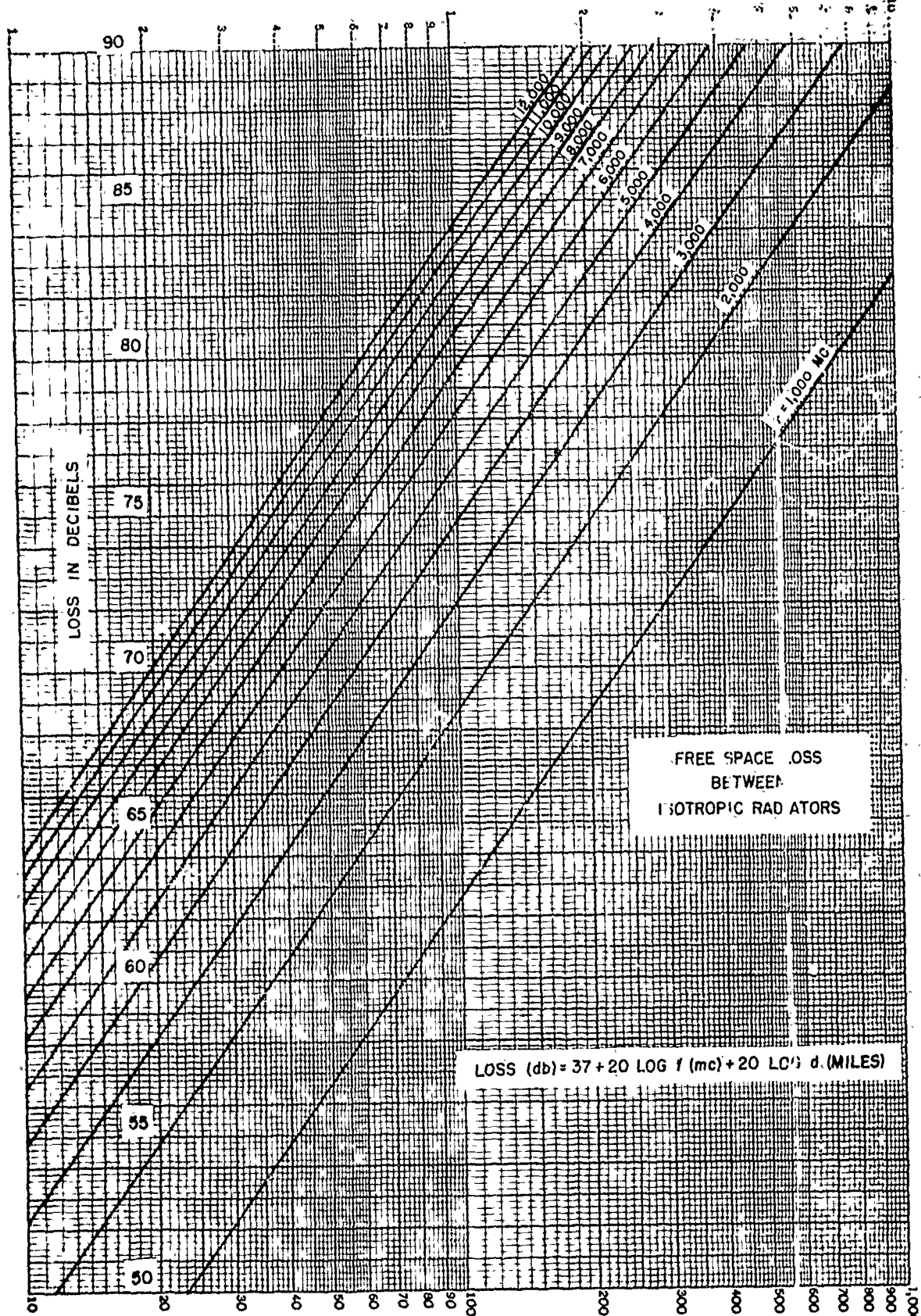
Relative Efficiency of Passive Repeater - Antenna Combinations

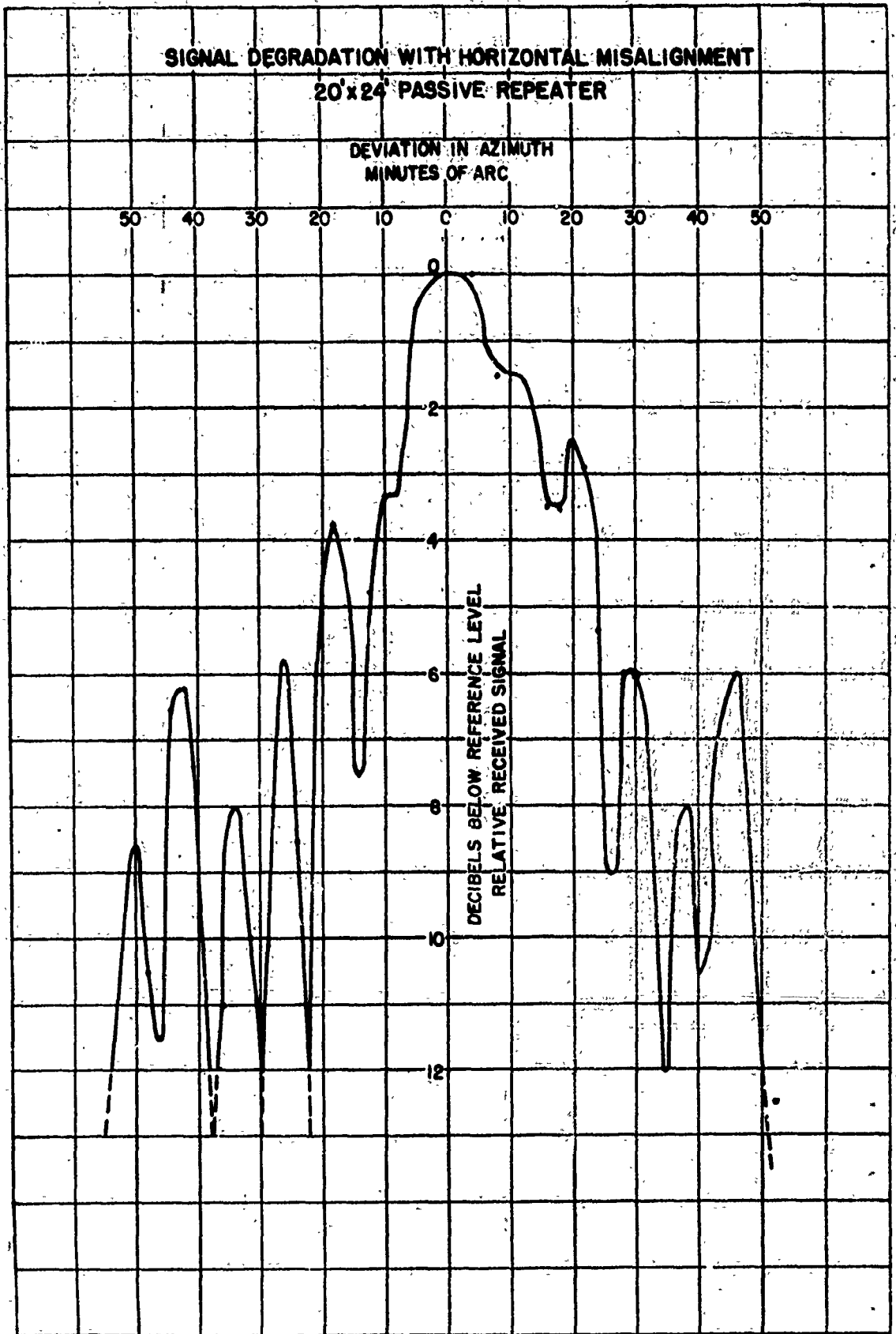
ρ	0.1	0.125	0.15	0.175	0.2	0.25	0.3	0.35	0.4	0.5	0.6	0.7	0.8	0.9	1.0	1.1	1.2	1.3	1.4	1.5	1.6		
0.002	+3.0	-12.2	+0.5	+4.0	+5.5	+2.0	+5.7	+5.1	+4.4	+3.0	+1.6	+0.6	-0.2	-1.5	-2.3	-5.6	-6.3	-10.3	-10.3	-10.3	-10.3	-10.3	-10.3
0.2	-0.2	-5.7	-0.5	+2.6	+4.2	+5.3	+5.2	+4.6	+4.1	+2.8	+1.5	+0.5	-0.5	-1.6	-2.4	-5.9	-6.3	-10.3	-10.3	-10.3	-10.3	-10.3	-10.3
0.4	-0.4	+0.4	+0.8	+1.4	+2.3	+3.5	+3.9	+3.6	+3.2	+2.2	+1.1	+0.2	-0.8	-1.8	-2.4	-6.9	-8.4	-10.3	-10.3	-10.3	-10.3	-10.3	-10.3
0.6	+0.7	+0.9	+1.1	+1.4	+1.8	+2.0	+1.9	+1.3	+0.5	+0.1	-0.5	-1.1	-1.8	-2.5	-3.1	-6.0	-8.5	-10.4	-10.4	-10.4	-10.4	-10.4	-10.4
0.8	+0.4	+0.2	+0.3	+0.2	+0.4	+0.2	-0.1	-0.2	-0.1	-0.5	-1.1	-1.7	-2.0	-2.6	-3.1	-6.1	-8.5	-10.5	-10.5	-10.5	-10.5	-10.5	-10.5
1.0	-0.7	-0.9	-0.9	-0.2	-1.0	-1.2	-1.5	-1.6	-1.5	-1.2	-0.5	-0.1	-0.5	-1.1	-1.8	-3.1	-4.6	-6.1	-10.1	-10.1	-10.1	-10.1	-10.1
1.2	-1.9	-2.1	-2.2	-1.3	-2.1	-2.4	-2.5	-2.6	-2.5	-1.9	-1.1	-0.5	-0.1	-0.5	-1.1	-3.1	-4.6	-6.1	-10.1	-10.1	-10.1	-10.1	-10.1
1.4	-5.7	-3.8	-3.8	-3.7	-3.1	-2.1	-1.1	-0.2	-0.2	-0.2	-0.2	-0.2	-0.2	-0.2	-0.2	-4.7	-6.1	-7.1	-10.5	-10.5	-10.5	-10.5	-10.5
1.6	-5.6	-5.7	-5.6	-5.6	-5.6	-5.6	-5.6	-5.6	-5.6	-5.6	-5.6	-5.6	-5.6	-5.6	-5.6	-5.6	-5.6	-5.6	-5.6	-5.6	-5.6	-5.6	-5.6

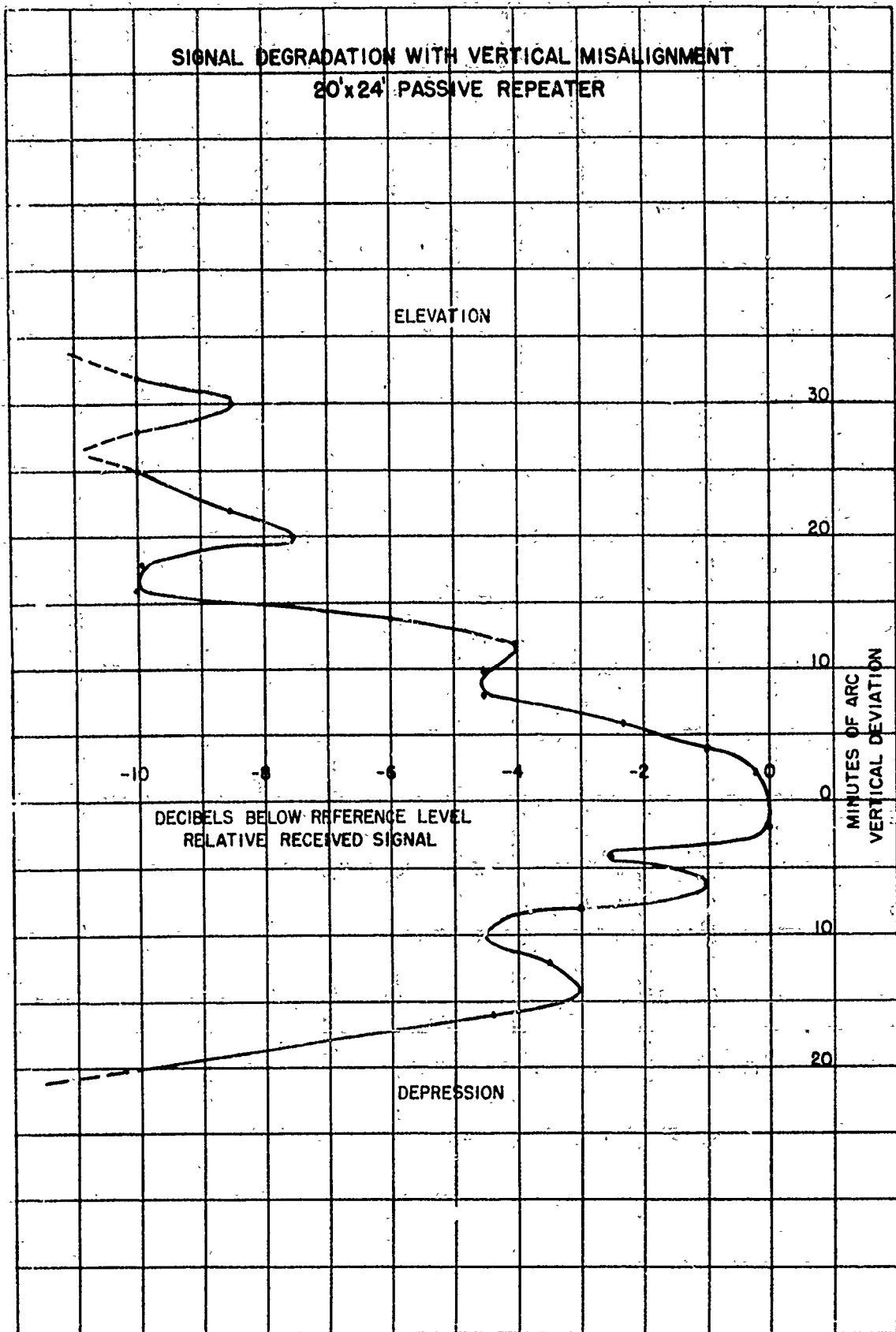
$$\frac{1}{k} = \frac{\pi \lambda d^2}{4 \lambda^2}$$

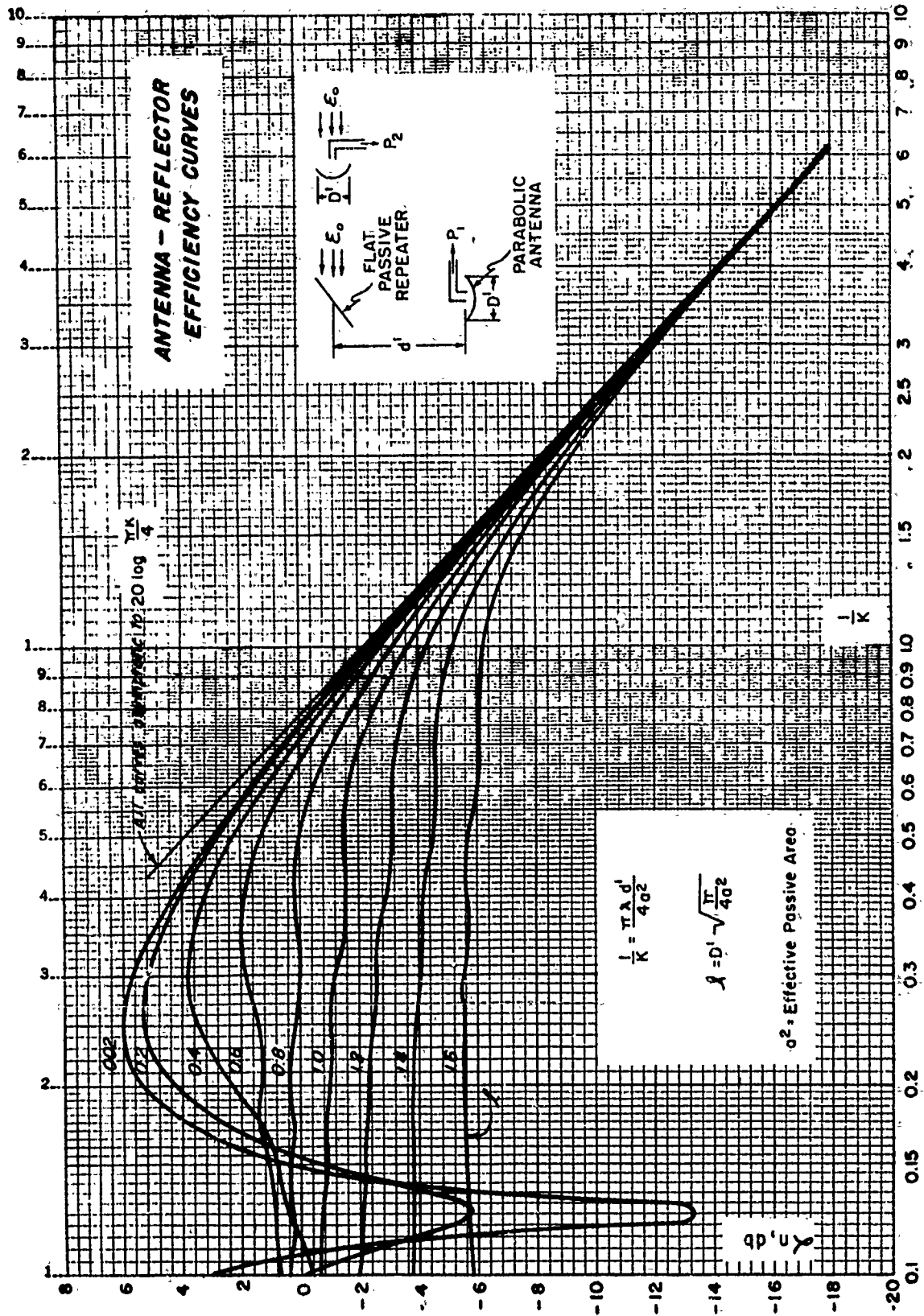
$$\rho = 0.1 \sqrt{\frac{\pi}{4 \lambda^2}}$$

λ^2 = Effective Passive Area









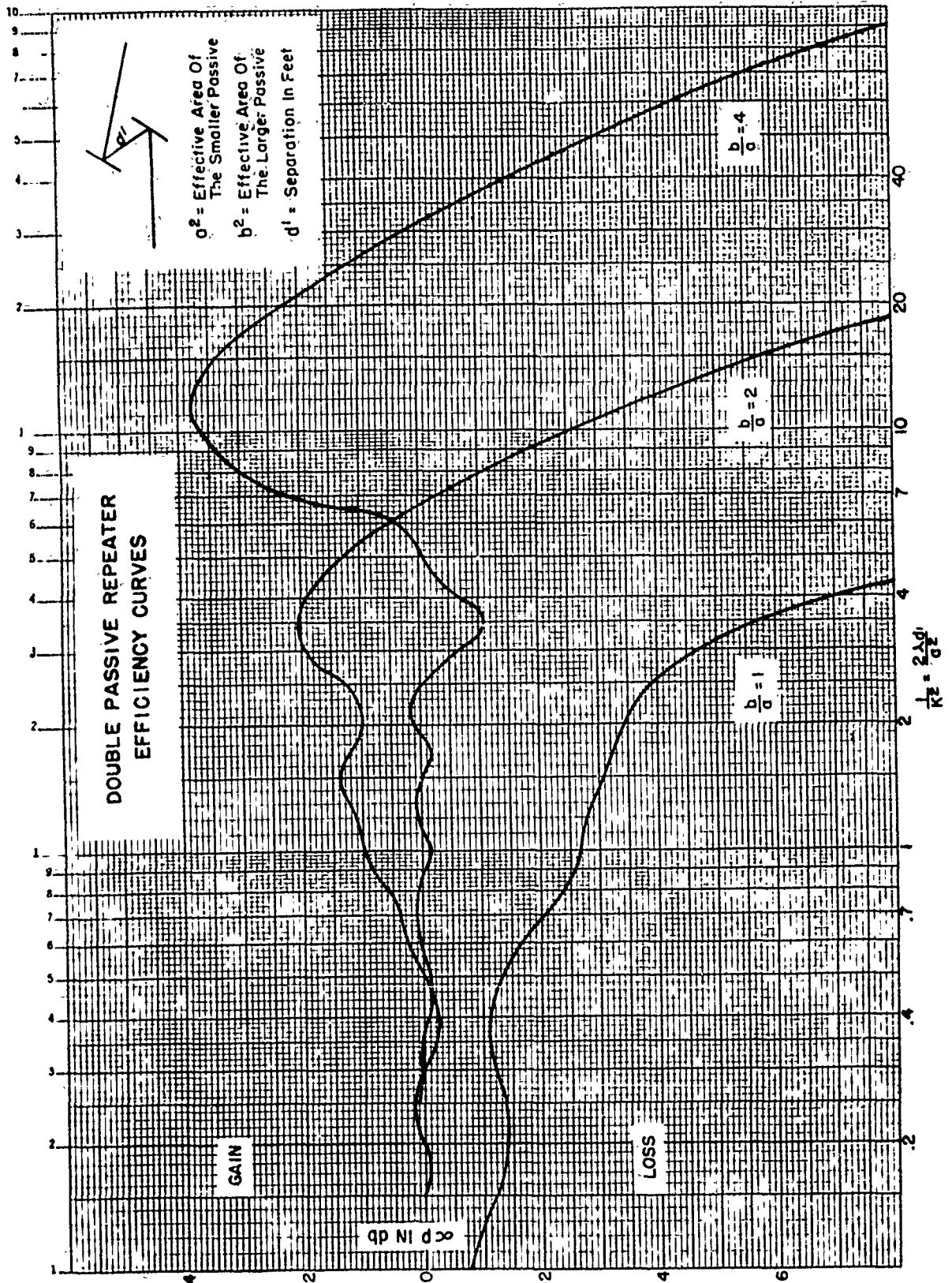


Figure 44

THE APPLICATION OF PASSIVE REPEATERS

In a typical passive repeater application problem, the microwave engineer is faced with a situation in which the frequency of the system has been selected, the terminal stations are located, and direct communication between the terminal stations is impossible because of an intervening obstruction of some sort. The problem becomes one of selecting the most suitable site for a passive repeater, or of finding two sites if a double passive repeater application is indicated.

The parameters which may be varied to find the most economical installation are, (1) The size of the terminal parabolic antennas, (2) the length of the shortest path, (3) the included horizontal angle, and (4) the size of the passive repeater. Usually the most economical combination will result by using large parabolic antennas and minimizing the shortest path length and the included horizontal angle.

The efficiency of any microwave system using passive repeaters is directly related to the product of the path distances. Halve the product of the path distances and the size of the passive may be cut in half. In effect this means that the closer the passive repeater to either of the terminal stations, the smaller the passive repeater may be.

The gain of a parabolic antenna, over an isotropic radiator, may be given by the following equation:

$$\text{gain, db} = 10 \text{ Log } \frac{5 (D')^2}{\lambda^2}$$

where D' is the nominal diameter of the antenna in feet and λ is the wavelength in feet.

Parabolic Antenna Gain, db

<u>Dish diameter</u> <u>in feet</u>	<u>Frequency</u>		
	2,000 mc	6,000 mc	11,000 mc
4'	25.2	34.7	40.0
6'	28.7	38.3	43.5
8'	31.2	40.7	46.0
10'	33.1	42.7	48.0

The attenuation of microwave energy, in free space, is the result of the spreading out of the microwave beam and not from any intrinsic loss of energy as the signal travels through space. The gain of a passive repeater results from the interception of a part of the energy transmitted from the antenna and the concentration of this energy into a narrow beam which is redirected toward the receiving antenna. The "gain" of a passive repeater is thus divided into two equal parts; that which pertains to the incoming beam and the part which pertains to the reflected beam. For simplification, the gain of a passive repeater, in this text, will include both the

incoming and the reflected beams and is given by the following equation:

$$\text{gain, db} = 20 \text{ Log } \frac{4\pi A \cos \alpha}{\lambda^2}$$

where "A cos α " is the effective area of the passive in square feet, λ is the wavelength in feet, and α is half the included horizontal angle.

The gain of a passive is thus seen to increase with an increase in area and frequency, and with a decrease in the horizontal included angle. The most effective use of a given passive repeater area will be made with the passive located directly behind and above either of the terminal stations.

The attenuation or loss of microwave energy in free space is commonly given by the following two equations which have a different form but will give the same results:

1. loss, db = 36.6 + 20 Log f (MC) + 20 Log d (mi)
2. loss, db = 20 Log $\frac{4\pi d_1}{\lambda}$ (where d_1 is in feet)

The above equations give the attenuation between isotropic radiators and are plotted on figures 39 and 40.

The passive repeater gain equation is plotted in figure 38 for all 14 standard passive repeater sizes and all frequencies from 2 Kmc to 11 Kmc. To illustrate the use of the curves, suppose it was required to find the gain of a 16'x20' passive repeater at 6 Kmc if the included horizontal angle were 90 degrees. Enter the chart at the lower left hand side at 45 degrees and proceed upwards to the curve marked 16'x20'. From this point follow straight across to the line marked 6 Kmc. Read straight down a gain of 100.4 db. The horizontal included angle is assumed to be equal, or very nearly so, to the true angle between the incoming and reflected beams.

The effective area of a passive repeater is the projected area in the direction of transmission. To find the effective area of a passive, multiply the actual area by the cosine of one half the horizontal included angle and also by the cosine of one half the vertical included angle. Usually the vertical angle is small and is neglected.

The maximum included horizontal angle, beyond which it is impractical to go, is 140 degrees. Beyond this point the effective area of the passive is small and the installation becomes uneconomical. Several Microflect passives are in service with horizontal angles in excess of 120 degrees with the maximum to date 137 degrees. Beyond 140 degrees a double passive repeater installation is indicated.

CCP 702-1

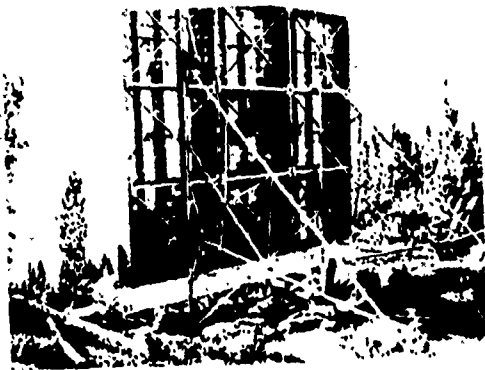


Figure 45. First Microflect 24'x 30' installed in 1956. No maintenance or readjustment has been necessary.



Figure 46. 8'x 14' and 10'x 16' passives getting final inspect before being crated and shipped.

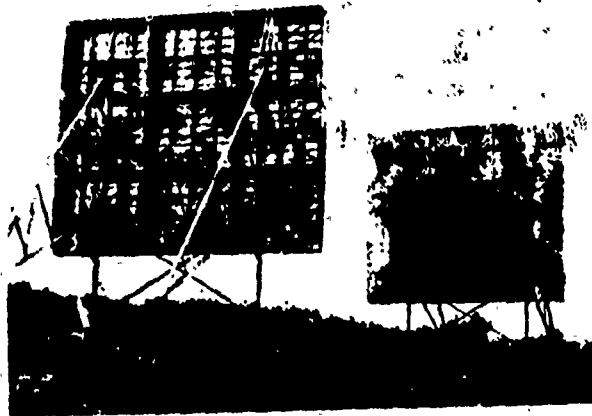


Figure 47. Double 24'x 30' passives installed and optically aligned by the transit method required no further adjustment. Note reflection of one passive in the face of the other.



Figure 48. Final optimizing of a 16'x 20' passive.

A minimum spacing between two passive repeaters or between a passive repeater and the illuminating antenna, must be observed when applying the gain equation for a passive repeater. In general, when the gain of the passive repeater is within ten db of the space loss, the "near field" method should be used to figure the net path performance. Example problems will explain this more fully.

DOUBLE PASSIVE REPEATERS

Double passive repeaters are used when the transfer angle is less than 50 degrees, or where no site exists from which one passive could "see" both terminal stations. The transfer angle is the angle through which it is required to bend the microwave beam and it is also the compliment of the horizontal included angle.

The calculations for a double passive repeater installation are straightforward as subsequent examples will show. Several pairs of Microflect passive repeaters are presently working in double passive systems.

When the spacing between the two passives is decreased to the point that the space loss in the path between the two is less than, or within seven db of the gain of the larger of the two passives, then the close-coupling effect of the passives must be considered. A paper discussing this effect was presented to the IRE national convention in 1957 by Richard F. H. Yang. A recent application of two large passive repeaters spaced 80' apart has been evaluated and found to agree with the results predicted by calculations based upon Mr. Yang's paper. Sample problems have been included to illustrate the necessary calculations.

References

- (1) Richard F. H. Yang, "Passive Repeater Using Double Flat Reflectors". I.R.E. National Convention paper, 1957.
- (2) P. W. Austin and C. W. Lund, "An 11,000 mc Passive Repeater Application", A.I.E.E. Conference Paper 60-1073, 1960.

When this paper was written, the author included information and expressed opinions believed to be correct and reliable. Because of the constant advance of technical knowledge, the widely differing conditions of possible specific application, and the possibility of misapplication, any application of the contents of this paper must be at the sole discretion and responsibility of the user.

SAMPLE PROBLEMS

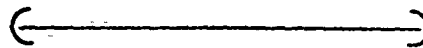
The following sample problems are included to illustrate the general principles involved in the theoretical and practical application of passive repeaters. The calculations will involve the path from the transmitting antenna to the receiving antenna. No attempt will be made to evaluate the waveguide and filter losses, receiver threshold levels, transmitter output, signal to noise ratios and so forth, as these items vary from system to system. Some manufacturers, as a safety factor, add 1 db loss to each dish, path, and passive repeater in the system. This allows some cushion above the guaranteed system performance.

Symbols

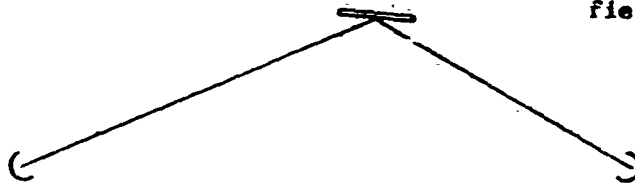
- d total gain or loss in db for a microwave path including the gain of the terminal parabolic antennas.
- d_1, d_2, d_3 path attenuation in db.
- G_t, G_r gain of the transmitting and receiving antennas. This may be the combined gain of a dish and reflector combination where a vertical dish illuminates a curved or flat tower-mounted reflector.
- G_a gain of the smaller of two passives in a double passive arrangement, or the gain of the passive in a single passive arrangement.
- G_b gain of the larger of the two passives in a double passive arrangement.
- d_h gain or loss of a passive repeater in the near field of an antenna compared with the gain of the antenna alone in the position of the passive.
- d_p gain or loss when the smaller of two passives replaces both passives in a double passive arrangement.
- λ wavelength in feet = $985/f(\text{mc})$
- a^2 effective area in square feet of the passive repeater or of the smaller of the two in a double passive arrangement.
- b^2 effective area in square feet of the larger of two passives.
- A Actual passive repeater area in square feet
- D' parabolic antenna diameter in feet.

The following equations give the net gain or loss, in db units, of the particular microwave path including the gain of the terminal parabolic antennas.

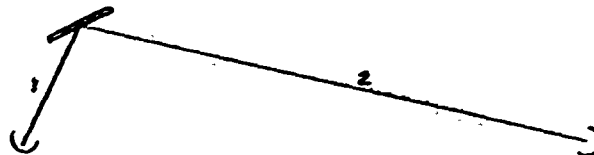
(1) $\alpha = G_t + \alpha_1 + G_r$ Simple path, no passive



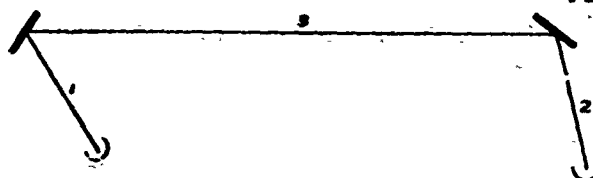
(2) $\alpha = G_t + \alpha_1 + G_a + \alpha_2 + G_r$ Single passive, far field



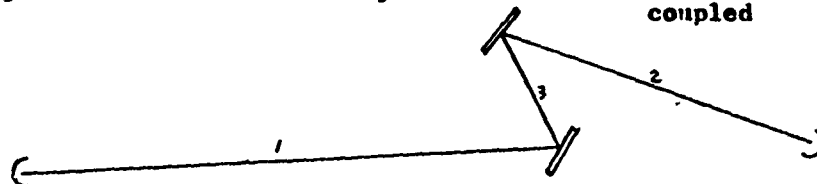
(3) $\alpha = G_t + \alpha_n + \alpha_2 + G_r$ Single passive, near field



(4) $\alpha = G_t + \alpha_1 + G_a + \alpha_3 + G_b + \alpha_2 + G_r$ Double passives, far field



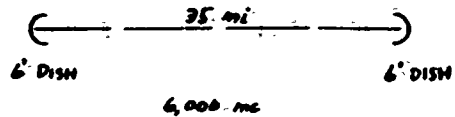
(5) $\alpha = G_t + \alpha_1 + G_a + \alpha_p + \alpha_2 + G_r$ Double passives, close coupled



Note that equation (3) is the same as equation (2) with α_n replacing the terms $\alpha_1 + G_a$. Likewise, equation (5) is the same as equation (4) with α_p replacing the terms $\alpha_3 + G_b$.

CCP 702-1

Example 1, Find the net path gain for the system shown to the right.



$$\left[\mathcal{L} = G_t + d_1 + G_r \right]$$

$$G_t = G_r = 10 \text{ Log} \frac{5 D^2}{\lambda^2} = 10 \text{ Log} \frac{(5 \times 6)^2}{(985/4000)^2} = 10 \text{ Log} 6,680$$

$$= 10 (3.83) = +38.3 \text{ db} \leftarrow$$

$$-d_1 = 37 + 20 \text{ Log} D(\text{mi}) + 20 \text{ Log} f(\text{mc})$$

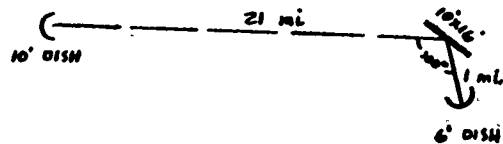
$$= 37 + 20 \text{ Log} 35 + 20 \text{ Log} 4,000$$

$$= 37 + 20(1.545) + 20(3.70) = 143.5 \text{ db}$$

$$d_1 = -143.5 \text{ db} \leftarrow$$

$$\mathcal{L} = +38.3 - 143.5 + 38.3 = -66.9 \text{ db} \leftarrow$$

Example 2, Find the net path gain for the system shown to the right with a frequency of 2,000 mc.



$$\left[\mathcal{L} = G_t + d_1 + G_a + d_2 + G_r \right]$$

$$G_t = +28.7 \text{ db}, \quad G_r = +33.1 \text{ db} \text{ from the table on page 34.}$$

$$d_1 = -103 \text{ db}, \quad d_2 = -129.5 \text{ db} \text{ from the curves on page 29.}$$

$$G_a = 20 \text{ Log} \frac{4\pi A \cos \alpha}{\lambda^2} = \frac{(4\pi \times 160 \cos 50^\circ)}{(985/2000)^2} = 20 \text{ Log} 5,340 = +74.6 \text{ db} \leftarrow$$

$$\mathcal{L} = +28.7 - 103 + 74.6 - 129.5 + 33.1 = -96.1 \text{ db} \leftarrow$$

Example 3, Assume the same path as in example 2 with a system frequency of 6,000 mc instead of 2,000 mc. Find net path gain.

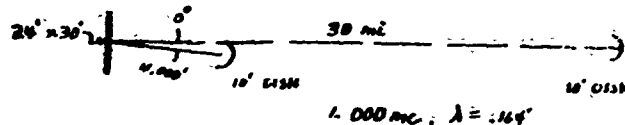
$$G_t = +38.3 \text{ db}, \quad G_r = +42.7 \text{ db} \text{ from page 34.}$$

$$d_1 = -113 \text{ db}, \quad d_2 = -139 \text{ db} \text{ from page 29.}$$

$$G_a = +93.8 \text{ db} \text{ from the curves on page 27 showing the gain of passive repeaters.}$$

$$\mathcal{L} = +38.3 - 113 + 93.8 - 139 + 42.7 = -77.2 \text{ db} \leftarrow$$

Example 4, Find the net gain for the system to the right.



First, determine whether or not the passive is in the near field with respect to the antenna.

$$\frac{1}{K} = \frac{\pi \lambda d_1}{4 a^2} = \frac{\pi (0.164)(4000)}{(4)(720)} = 0.717 < 2.5$$

inspection of the curves on page 32 will show

that values for $1/K$ of less than 2.5 indicate that the passive is in the near field with respect to the antenna. Use equation 3.

$$\left[\alpha = G_t + \alpha_n + \alpha_z + G_r \right]$$

$$G_t = G_r = +42.7 \text{ db}, \quad \alpha_z = -142.3 \text{ db}$$

$$\alpha = D \sqrt{\frac{\pi}{(4K a^2)}} = 10 \sqrt{\frac{\pi}{(4)(720)}} = 0.93$$

for a value of 0.33 for "1" and 0.717 for "1/K" read

on the graph on page 32 for α_n a value of + 0.2 db.

$$\alpha = +42.7 + 0.2 - 142.3 + 42.7 = -56.7 \text{ db} \leftarrow$$

Example 5, Same as example 4 except with the short leg increased to 2.5 mi which would make the long leg 31.75 miles.

$$\frac{1}{K} = \frac{\pi \lambda d_1}{4 a^2} = \frac{\pi (0.164)(2.5)(5280)}{(4)(720)} = 2.36 < 2.5$$

This is practically on the boarderline between the near and the far zones. The problem will be solved both ways for comparison.

Near field method: $\alpha = 0.33$ AS BEFORE. FROM CHART, $\alpha_n = -9.4 \text{ db}$

$$\alpha_z = -142.7 \text{ db for 31.75 MILES.}$$

$$\left[\alpha = G_t + \alpha_n + \alpha_z + G_r \right]$$

$$\alpha = +42.7 - 9.4 - 142.7 + 42.7 = -66.7 \text{ db} \leftarrow$$

Far field methods:

$$\left[\alpha = G_t + \alpha_1 + G_a + \alpha_2 + G_r \right]$$

$$\alpha_1 = -120.8 \text{ db for a 2.5 mile path}$$

$$G_a = 20 \text{ Log } \frac{4\pi A \cos \alpha}{\lambda^2} = 20 \text{ Log } \frac{(4\pi)(720)}{(0.164)^2} = 20 \text{ Log } 336,000$$

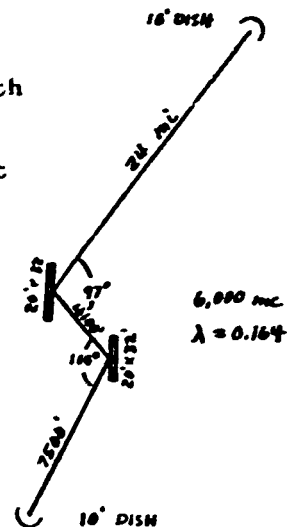
$$G_a = 20(5.527) = +110.8 \text{ db}$$

CCP 702-1

$$\alpha = +42.7 - 142.7 + 110.8 - 120.8 + 42.7 = \underline{-67.3 \text{ db}}$$

The path losses are the same by both methods as they should be, within the accuracy of the charts and graphs used for the solutions.

EXAMPLE 6, Find the net gain for the system shown to the right. Check to determine whether the two passives are in the near field with respect to each other and also check to see if the smaller terminal log puts the passive in the near field with respect to the dish.



$$G_t = G_r = +42.7 \text{ db for } 10' \text{ dishes}$$

$$7500' \text{ PATH, } \alpha_1 = -116 \text{ db}$$

$$24' \text{ PATH, } \alpha_2 = -140.3 \text{ db}$$

$$4100' \text{ PATH, } \alpha_3 = -118.8 \text{ db}$$

$$G_a = 20 \text{ Log } \frac{4\pi A \cos \alpha}{\lambda^2} = \frac{(4\pi)(640 \cos 52^\circ)}{(0.164)^2}$$

$$G_a = 20 \text{ Log } 185,000 = +105.4 \text{ db}$$

$$G_b = 20 \text{ Log } \frac{(4\pi)(640 \cos 48^\circ)}{(0.164)^2}$$

$$G_b = 20 \text{ Log } 199,000 = +106 \text{ db}$$

Consider the 7,500' path:

$$\frac{1}{K} = \frac{\pi \lambda d_i}{4 a^2} = \frac{\pi (0.164)(7500)}{(4)(640 \cos 52^\circ)} = 2.46 \approx 2.5$$

$$\text{FROM THE CHART, } \alpha_n = -10 \text{ db}$$

$$G_1 - \alpha_1 = +105.4 - 116 = -10.6 \text{ db}$$

Thus the first passive is on the border between the near and the far field and the loss is the same, within the accuracy of the charts, for both methods.

Consider the two passives:

$$a^2 = 640 \cos 52^\circ = 394, \quad a = 19.9 \quad \frac{b}{a} = 1.04$$

$$b^2 = 640 \cos 48^\circ = 424, \quad b = 20.0$$

$$\frac{1}{K^2} = \frac{\pi \lambda d_i}{a^2} = \frac{(\pi)(0.164)(4100)}{394} = 3.41$$

$$\text{FROM THE CURVES ON PAGE 33, } \alpha_p = -5.6 \text{ db}$$

$$G_b - \alpha_3 = +106 - 110.8 = -4.8 \text{ db}$$

This indicates that the two passives are slightly less effective when the calculations are based on the near field method when compared with the far field method.

$$\text{net path, far field} \quad \Delta = G_t + d_1 + G_a + d_3 + G_b + d_2 + G_r$$

$$\Delta = +42.7 - 116.0 + 105.4 - 110.8 + 106 - 140.3 + 42.7 = \underline{-70.3 \text{ db}}$$

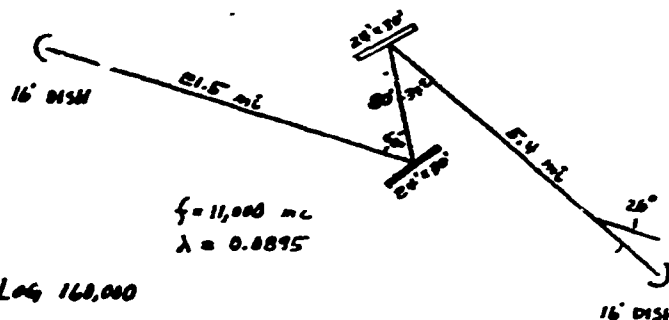
net path, near field for both the first leg and the two passives

$$\Delta = G_t + d_n + d_p + d_2 + G_r$$

$$\Delta = +42.7 - 10.0 - 5.6 - 140.3 + 42.7 = \underline{-70.5 \text{ db}}$$

Thus, in borderline cases, both methods give the same results.

Example 7, Find the net path gain for the close-coupled system shown to the right.



$$G_t = G_r = 10 \text{ Log} \frac{5(D')^2}{\lambda^2}$$

$$= 10 \text{ Log} \frac{5(16)^2}{(0.0095)^2} = 10 \text{ Log} 160,000$$

$$G_t = G_r = \underline{+52 \text{ db}}$$

$$d_1 = -132.6 \text{ db for } 5.4 \text{ mi path}$$

$$d_2 = -144.5 \text{ db for } 21.5 \text{ mi path}$$

Check to see if the 5.4 mile path is short enough to put the first passive in the near field of the antenna.

$$\frac{1}{K} = \frac{\pi \lambda d_1}{4 R^2} = \frac{\pi (0.0095)(5.4)(5280)}{(4)(720 \cos 17^\circ)} = 2.92 > 2.5 \text{ so use the}$$

far field scheme for the dish and the passive. The two passives, only 80' apart are clearly close-coupled.

$$a^2 = 720 \cos 30^\circ = 624, \quad a = 25$$

$$b^2 = 720 \cos 17^\circ = 689, \quad b = 26.2$$

$$\frac{b}{a} = 1.05$$

$$\frac{1}{K^2} = \frac{2 \lambda d_1}{a^2} = \frac{(2)(0.0095)(80)}{624} = 0.023$$

$$\text{FROM PAGE 33, } d_p = 0$$

$$\text{FROM PAGE 27, } G_a = +120.5 \text{ db}$$

CCP 702-1

For very small values of $1/K^2$, $d_p = 0$ db regardless of the size of the larger passive.

$$\left[\alpha = G_t + \alpha_1 + G_a + d_p + \alpha_2 + G_r \right]$$

$$\alpha = +52 - 132.6 + 120.5 + 0 - 144.5 + 52 = \underline{-52.6 \text{ db}}$$

Example 8, Assume one was unaware of the close-coupling effect of two passives. Solve problem 7, incorrectly by the far field method.

FROM PAGE 27, $G_b = +121.3 \text{ db}$

FROM PAGE 28, $\alpha_3 = -81.6 \text{ db}$

$$\left[\alpha = G_t + \alpha_1 + G_a + \alpha_3 + G_b + \alpha_2 + G_r \right]$$

$$\alpha = +52 - 132.6 + 120.5 - 81.6 + 121.3 - 144.5 + 52 = \underline{-12.9 \text{ db}}$$

Ignoring the coupling effect would thus result in an error of 40 db and would doubtless result in failure of the path.

Example 9, Prove that the curve on figure 43, page 32, gives the same results as the far field method when $1/K$ is greater than 2.5.

If this is true then $\alpha_n = \alpha_1 + G_a$

$$\alpha_n = 20 \text{ Log } \frac{\pi K}{4} = 20 \text{ Log } \frac{\pi 4 a^2}{\pi 4 \lambda d_1} = 20 \text{ Log } \frac{a^2}{\lambda d_1} \longleftarrow \alpha_n$$

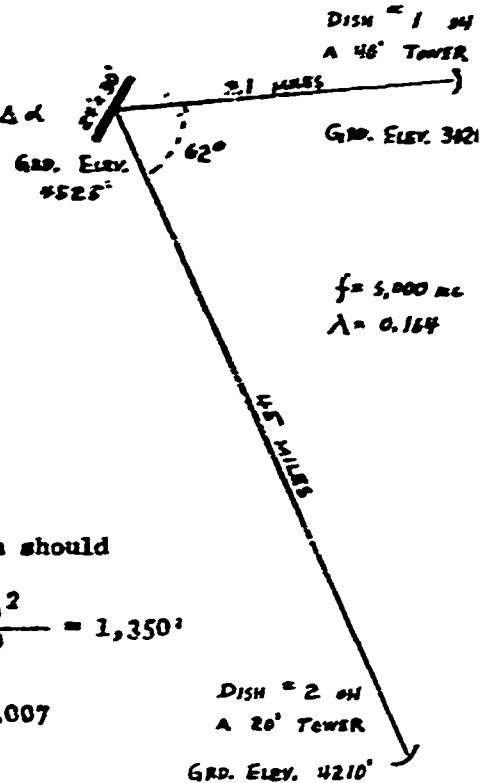
$$\alpha_1 = -20 \text{ Log } \frac{4 \pi d_1}{\lambda}$$

$$G_a = 20 \text{ Log } \frac{4 \pi a^2}{\lambda^2}$$

$$\alpha_1 + G_a = 20 \text{ Log } \frac{\frac{4 \pi a^2}{\lambda^2}}{\frac{4 \pi d_1}{\lambda}} = 20 \text{ Log } \frac{a^2}{\lambda d_1} \longleftarrow$$

Example 10. For the system to the right, determine-

1. Face angle, θ_1
2. Horizontal correction angle, $\Delta \alpha$
3. Effective passive area
4. Vertical and horizontal beamwidth in degrees.



Elev. of P.R. center, $4525' + 18' = 4543'$

Elev. of dish #1, $3020' + 40' = 3060'$

Elev. of dish #2, $4210' + 20' = 4230'$

$$\theta_1 = \tan^{-1} \frac{4543 - 3060}{(2.1)(5280)} = 0.134$$

$\theta_1 = 7^{\circ}38'$ downward from the passive

A correction for the curvature of the earth should be applied to paths over a few miles long.

Path #2, Curvature correction, $\frac{(4.5)^2(5280)^2}{41,800,600} = 1,350'$

$$\theta_2 = \tan^{-1} \frac{4543 - (4230 - 1350)}{45(5280)} = \frac{1663}{238,000} = 0.007$$

$\theta_2 = 0^{\circ}24'$ downward

Calculations based on the equations shown on page 17 are made on the calculation sheet on the next page for the face angle and the horizontal correction angle. The calculations indicate a face angle of $4^{\circ}41'$ downward and a correction angle of $0^{\circ}08'$ towards path #2 which is the path with the least vertical angle. The horizontal correction always rotates the bearing of the passive in the direction of the path with the least vertical angle, regardless of whether the angle is upward or downward from the passive.

$$\text{Effective Area} = A \cos \alpha \cos \theta, \quad \theta = 7^{\circ}38' - 0^{\circ}24' = 7^{\circ}14'$$

$$= (24 \times 30)(\cos 31^{\circ})(\cos 7^{\circ}14')$$

$$= 612 \text{ square feet.}$$

For beamwidth calculations: effective width = $30 \cos 31^{\circ} = 25.7'$

$$\text{effective height} = 24 \cos 7^{\circ}14' = 23.8'$$

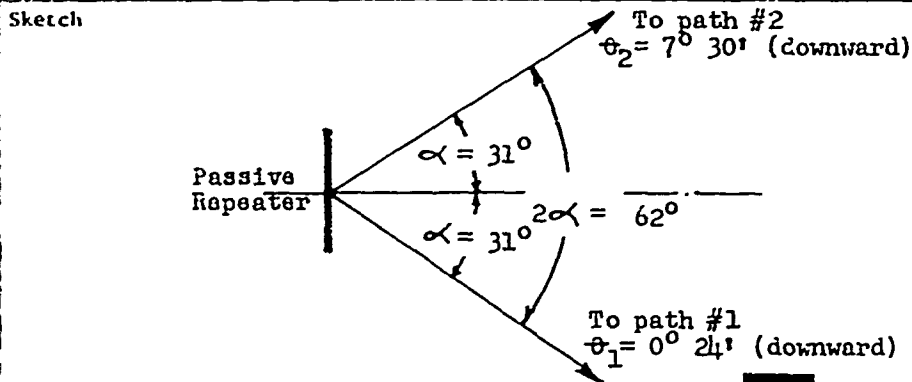
$$\text{Horizontal beamwidth} = \theta_h = \frac{58.7 \lambda}{25.7} = \frac{(58.7)(0.164)}{25.7} = 0.374 \text{ degrees}$$

$$\text{Vertical beamwidth, } \theta_v = \frac{(58.7)(0.164)}{23.8} = 0.404 \text{ degrees.}$$

PASSIVE REPEATER BEARING CALCULATION SHEET (Sample calculation)

Passive Site	Any	SITE Hilltop	Location
1	Horizontal included angle between paths:		$2\alpha = 62^\circ$ degrees
2	One-half the horizontal included angle		$\alpha = 31^\circ$ degrees
3	Vertical angle from horizontal to path 1: $\theta_1 = 0^\circ 24'$		degrees <input type="checkbox"/> Up <input checked="" type="checkbox"/> Down
4	Vertical angle from horizontal to path 2: $\theta_2 = 7^\circ 30'$		degrees <input checked="" type="checkbox"/> Up <input type="checkbox"/> Down
5	$\cos \theta_1$	= 0.99998	8 $\cos \theta_1$ = 0.99998
6	$\cos \theta_2$	= 0.99114	9 $\cos \theta_2$ = 0.99114
7	$\cos \theta_1 + \cos \theta_2$	= 1.99112	10 $\cos \theta_1 - \cos \theta_2$ = 0.00884
11	$\sin \theta_1$	= 0.00698	14 $\tan \alpha$ = 0.60086
12	$\sin \theta_2$	= 0.13053	15 $\cos \alpha$ = 0.85717
13	$\sin \theta_1 + \sin \theta_2$	= 0.13751	
16	$\tan \Delta\alpha = \tan \alpha \frac{\cos \theta_1 - \cos \theta_2}{\cos \theta_1 + \cos \theta_2} = \frac{(14) (0.60086) (10) (0.00884)}{(7) (1.99112)} = 0.00257$		
17	$\Delta\alpha = 0^\circ 09'$ degrees toward θ_1		
18	$\cos \Delta\alpha = 1.0000$		
19	$\tan \theta_3 = \frac{\cos \Delta\alpha \sin \theta_1 + \sin \theta_2}{\cos \alpha \cos \theta_1 + \cos \theta_2} = \frac{(18) (1.0000) (11) (0.13751)}{(12) (0.85717) (7) (1.99112)} = 0.08057$		
20	$\theta_3 = 4^\circ 36'$	degrees	(when $\tan \theta_3$ is negative) <input type="checkbox"/> Up (when $\tan \theta_3$ is positive) <input checked="" type="checkbox"/> Down

Sign Convention: Cosines and tangents are positive. Sines are positive when the angle slopes downward from the passive repeater, and negative when the angle slopes upward from the passive repeater. Note that $\Delta\alpha$ always rotates the passive bearing towards the path with the least vertical angle. Slide rule accuracy sufficient.



Reference: Microflect Passive Repeater Engineering Manual



MICROFLECT CO., Inc.
3175 26th STREET SALEM ORE 97307

Customer

Computations by W. Branch

Date 8-22-67

PASSIVE REPEATER BEARING CALCULATION SHEET

Passive Size	SITE	Location
--------------	------	----------

1 Horizontal included angle between paths: $2\alpha =$ degrees

2 One-half the horizontal included angle $\alpha =$ degrees

3 Vertical angle from horizontal to path 1: $\theta_1 =$ degrees Up Down

4 Vertical angle from horizontal to path 2: $\theta_2 =$ degrees Up Down

5 $\cos \theta_1 =$ 8 $\cos \theta_1 =$

6 $\cos \theta_2 =$ 9 $\cos \theta_2 =$

7 $\cos \theta_1 + \cos \theta_2 =$ 10 $\cos \theta_1 - \cos \theta_2 =$

11 $\sin \theta_1 =$ 14 $\tan \alpha =$

12 $\sin \theta_2 =$ 15 $\cos \alpha =$

13 $\sin \theta_1 + \sin \theta_2 =$

16 $\tan \Delta\alpha = \tan \alpha \cdot \frac{\cos \theta_1 - \cos \theta_2}{\cos \theta_1 + \cos \theta_2} = \frac{\overset{(14)}{\quad} \overset{(10)}{\quad}}{\overset{(7)}{\quad}} =$

17 $\Delta\alpha =$ degrees toward


18 $\cos \Delta\alpha =$

19 $\tan \theta_3 = \frac{\cos \Delta\alpha \sin \theta_1 + \sin \theta_2}{\cos \alpha \cos \theta_1 + \cos \theta_2} = \frac{\overset{(18)}{\quad} \overset{(13)}{\quad}}{\overset{(15)}{\quad} \overset{(7)}{\quad}} =$

20 $\theta_3 =$ degrees
 (when $\tan \theta_3$ is negative) → Up Down
 (when $\tan \theta_3$ is positive) → Up Down

Sign Convention: Cosines and tangents are positive. Sines are positive when the angle slopes downward from the passive repeater, and negative when the angle slopes upward from the passive repeater. Note that $\Delta\alpha$ always rotates the passive bearing towards the path with the least vertical angle. Slide rule accuracy sufficient.

Sketch

Reference: Microflect Passive Repeater Engineering Manual  **MICROFLECT CO., Inc.**
3273 234 STREET - GALENA, ILL. - 508/243 9147

Customer	Computations by	Date
----------	-----------------	------

PASSIVE REPEATER BEARING CALCULATION SHEET			
Passive Size	SITE	Location	
1	Horizontal included angle between paths:	$2\alpha =$	degrees
2	One-half the horizontal included angle	$\alpha =$	degrees
3	Vertical angle from horizontal to path 1: $\theta_1 =$	degrees	Up Down
4	Vertical angle from horizontal to path 2: $\theta_2 =$	degrees	Up Down
5	$\cos \theta_1 =$	8	$\cos \theta_1 =$
6	$\cos \theta_2 =$	9	$\cos \theta_2 =$
7	$\cos \theta_1 + \cos \theta_2 =$	10	$\cos \theta_1 - \cos \theta_2 =$
11	$\sin \theta_1 =$	14	$\tan \alpha =$
12	$\sin \theta_2 =$	15	$\cos \alpha =$
13	$\sin \theta_1 + \sin \theta_2 =$		
16	$\tan \Delta\alpha = \tan \alpha \frac{\cos \theta_1 - \cos \theta_2}{\cos \theta_1 + \cos \theta_2} = \frac{(\text{14})}{(\text{7})} \left(\frac{(\text{10})}{(\text{7})} \right) =$		
17	$\Delta\alpha =$ degrees toward		
18	$\cos \Delta\alpha =$		
19	$\tan \theta_3 = \frac{\cos \Delta\alpha \sin \theta_1 + \sin \theta_2}{\cos \alpha \cos \theta_1 + \cos \theta_2} = \frac{(\text{18})}{(\text{15})} \left(\frac{(\text{13})}{(\text{7})} \right) =$		
20	$\theta_3 =$	degrees	(when $\tan \theta_3$ is negative) → Up (when $\tan \theta_3$ is positive) → Down
<p>Sign Convention: Cosines and tangents are positive. Sines are positive when the angle slopes downward from the passive repeater, and negative when the angle slopes upward from the passive repeater. Note that $\Delta\alpha$ always rotates the passive bearing towards the path with the least vertical angle. Slide rule accuracy sufficient.</p>			
<p>Sketch</p>			
<p>Reference: Microflect. Passive Repeater Engineering Manual</p>			
Customer		Computations by	Date





MICROFLECT CO., Inc.
3675 23rd STREET - SAGINAW, MICH. - 48607-2967

DATE _____
ENGINEER _____

MICROWAVE PATH DATA CALCULATION SHEET

CUSTOMER _____		FREQUENCY _____	
PROJECT NO. _____		EQUIPMENT _____	
SYSTEM _____		LOADING _____ dbm0 (_____ CHANNELS OF _____)	
1	SITE		
2	LATITUDE		
3	LONGITUDE		
4	ELEVATION	Ft.	
5	TOWER HEIGHT	Ft.	
6	TOWER TYPE		
7	AZIMUTH FROM TRUE NORTH.		
8	PATH LENGTH	Mi.	
9	PATH ATTENUATION	dB	
10	RIGID WAVEGUIDE	Ft.	
11	FLEXIBLE WAVEGUIDE	Ft.	
12	WAVEGUIDE LOSS	dB	
13	CONNECTOR LOSS	dB	
14	CIRCULATOR OR HYBRID LOSS	dB	
15	RADOME LOSS, TYPE *	dB	
16	NEAR FIELD LOSS	dB	
17	CLOSE COUPLING LOSS (DOUBLE PASS.)	dB	
18	TOTAL FIXED LOSSES	dB	
19	TOTAL LOSSES	dB	
20	PARABOLA HEIGHT	Ft.	
21	PARABOLA DIAMETER	Ft.	
22	MICROFLECTOR HEIGHT	Ft.	
23	MICROFLECTOR SIZE, TYPE	Ft.	
24	PARABOLA-MICROFLECTOR SEP.	Ft.	
25	NEAR FIELD GAIN	dB	
26	ANTENNA SYSTEM GAIN	dB	
27	TOTAL GAINS	dB	
28	NET PATH LOSS	dB	
29	TRANSMITTER POWER	dBm	
30	MED. RECEIVED POWER (± 2 dB)	dBm	
31	RECEIVER NOISE THRESHOLD	dBm	
32	THEORETICAL RF C/N RATIO	dB	
33	FM IMP. THRESHOLD (_____ dBa)	dBm	
34	FADE MARGIN (To FM Imp. Thresh.)	dB	
35	RELIABILITY SPACING †	%	
36	POLARIZATION †		
37	PROFILE NUMBER		

NOTES _____

U - Unheated
 H - Heated
 F - Feed Heater
 † { F - Frequency Diversity
 S - Space Diversity
 N - Non-Diversity
 Q - Space And Frequency Diversity
 V - Vertical
 H - Horizontal
 (Reliability Figures Are For Rayleigh Distributed Fading Only)



MICROFLECT CO., Inc.
2470 21st STREET SALINA, OKLA. - 74150-7207

DATE _____
 ENGINEER _____

MICROWAVE PATH DATA CALCULATION SHEET	
CUSTOMER _____	
PROJECT NO. _____	FREQUENCY _____
SYSTEM _____	EQUIPMENT _____
LOADING: _____ dbm (_____ CHANNELS OF _____)	
1	SITE
2	LATITUDE
3	LONGITUDE
4	ELEVATION Ft.
5	TOWER HEIGHT Ft.
6	TOWER TYPE
7	AZIMUTH FROM TRUE NORTH.
8	PATH LENGTH Mi.
9	PATH ATTENUATION dB
10	RIGID WAVEGUIDE Ft.
11	FLEXIBLE WAVEGUIDE Ft.
12	WAVEGUIDE LOSS dB
13	CONNECTOR LOSS dB
14	CIRCULATOR OR HYBRID LOSS dB
15	RADOME LOSS, TYPE * dB
16	NEAR FIELD LOSS dB
17	CLOSE COUPLING LOSS (DOUBLE PASS.) dB
18	TOTAL FIXED LOSSES dB
19	TOTAL LOSSES dB
20	PARABOLA HEIGHT Ft.
21	PARABOLA DIAMETER Ft.
22	MICROFLECTOR HEIGHT Ft.
23	MICROFLECTOR SIZE, TYPE Ft.
24	PARABOLA-MICROFLECTOR SEP. Ft.
25	NEAR FIELD GAIN dB
26	ANTENNA SYSTEM GAIN dB
27	TOTAL GAINS dB
28	NET PATH LOSS dB
29	TRANSMITTER POWER dBm
30	MED. RECEIVED POWER (± 2 dB) dBm
31	RECEIVER NOISE THRESHOLD dBm
32	THEORETICAL RF C/N RATIO dB
33	FM IMP. THRESHOLD (dBa) dBm
34	FADE MARGIN (To FM Imp.Thresh.) dB
35	RELIABILITY SPACING † %
36	POLARIZATION †
37	PROFILE NUMBER

U - Unheated Feed Heater
 H - Heated Feed Heater
 F - Frequency Diversity
 S - Space Diversity
 N - Non-Diversity
 Q - Space And Frequency Diversity
 V - Vertical
 H - Horizontal
 (Reliability Figures Are For Rayleigh Distributed Fading Only)

NOTES _____

NATIONAL BUREAU OF STANDARDS

Technical Note 101

ISSUED May 7, 1965

REVISED May 1, 1966

REVISED January 1, 1967

TRANSMISSION LOSS PREDICTIONS FOR TROPOSPHERIC COMMUNICATION CIRCUITS

VOLUME I

P. L. Rice, A. G. Longley, K. A. Norton, and A. P. Barsis
Institute for Telecommunication Sciences and Aeronomy*
Environmental Science Services Administration
Boulder, Colorado

NBS Technical Notes are designed to supplement the Bureau's regular publications program. They provide a means for making available scientific data that are of transient or limited interest. Technical Notes may be listed or referred to in the open literature.

*Formerly the Central Radio Propagation Laboratory of the National Bureau of Standards.
ESSA will use the NBS publication series until establishment of their ESSA counterparts.

FOREWORD

A short history of the development of the prediction methods in this Technical Note will permit the reader to compare them with earlier procedures. Some of these methods were first reported by Norton, Rice and Vogler [1955]. Further development of forward scatter predictions and a better understanding of the refractive index structure of the atmosphere led to changes reported in an early unpublished NBS report and in NBS Technical Note 15 [Rice, Longley and Norton, 1959]. The methods of Technical Note 15 served as a basis for part of another unpublished NBS report which was incorporated in Air Force Technical Order T. O. 312-10-1 in 1961. A preliminary draft of the current technical note was submitted as a U. S. Study Group V contribution to the CCIR in 1962.

Technical Note 101 uses the metric system throughout. For most computations both a graphical method and formulas suitable for a digital computer are presented. These include simple and comprehensive formulas for computing diffraction over smooth earth and over irregular terrain, as well as methods for estimating diffraction over an isolated rounded obstacle. New empirical graphs are included for estimating long-term variability for several climatic regions, based on data that have been made available.

For paths in a continental temperate climate, these predictions are practically the same as those published in 1961. The reader will find that a number of graphs have been simplified and that many of the calculations are more readily adaptable to computer programming. The new material on time availability and service probability in several climatic regions should prove valuable for areas other than the U. S. A.

Changes in this revision concern mainly sections 2 and 10 of volume 1, annexes I, II and V of volume 2, and certain changes in notation and symbols. The latter changes make the notation more consistent with statistical practice.

Section 10, Long-Term Power Fading contains additional material on the effects of atmospheric stratification.

For convenience in using volume 2, those symbols which are found only in an annex are listed and explained at the end of the appropriate annex. Section 12 of volume 1 lists and explains only those symbols used in volume 1.

Note. This Technical Note consists of two volumes as indicated in the Table of Contents.

TABLE OF CONTENTS

Volume 1

	PAGE NO.
1. INTRODUCTION	1-1
2. THE CONCEPTS OF SYSTEM LOSS, TRANSMISSION LOSS, PATH ANTENNA GAIN, AND PATH ANTENNA POWER GAIN	2-1
2.1 System Loss and Transmission Loss	2-1
2.2 Antenna Directive Gain and Power Gain	2-3
2.3 Polarization Coupling Loss and Multipath Coupling Loss	2-5
2.4 Path Loss, Basic Transmission Loss, Path Antenna Gain, and Attenuation Relative to Free Space	2-7
3. ATMOSPHERIC ABSORPTION	3-1
3.1 Absorption by Water Vapor and Oxygen	3-1
3.2 Sky-Noise Temperature	3-3
3.3 Attenuation by Rain	3-4
3.4 Attenuation in Clouds	3-6
4. DETERMINATION OF AN EFFECTIVE EARTH'S RADIUS	4-1
5. TRANSMISSION LOSS PREDICTION METHODS FOR WITHIN-THE-HORIZON PATHS	5-1
5.1 Line-of-Sight Propagation Over Irregular Terrain	5-1
5.2 Line-of-Sight Propagation Over a Smooth or Uniformly Rough Spherical Earth	5-3
5.2.1 A curve-fit to terrain	5-8
5.2.2 The terrain roughness factor, σ_h	5-9
5.3 Some Effects of Cluttered Terrain	5-10
5.4 Examples of Line-of-Sight Predictions	5-11
6. DETERMINATION OF ANGULAR DISTANCE FOR TRANSHORIZON PATHS	6-1
6.1 Plotting a Great Circle Path	6-1
6.2 Plotting a Terrain Profile and Determining the Location of Radio Horizon Obstacles	6-3
6.3 Calculation of Effective Antenna Heights for Transhorizon Paths	6-4
6.4 Calculation of the Angular Distance, θ	6-5
7. DIFFRACTION OVER A SINGLE ISOLATED OBSTACLE	7-1
7.1 Single Knife Edge, No Ground Reflections	7-1
7.2 Single Knife Edge with Ground Reflections	7-3
7.3 Isolated Rounded Obstacle, No Ground Reflections	7-4
7.4 Isolated Rounded Obstacle with Ground Reflections	7-6
7.5 An Example of Transmission Loss Prediction for a Rounded Isolated Obstacle	7-7

	<u>PAGE NO.</u>
8. DIFFRACTION OVER SMOOTH EARTH AND OVER IRREGULAR TERRAIN	8-1
8.1 Diffraction Attenuation Over a Smooth Earth	8-1
8.2 Diffraction Over Irregular Terrain	8-3
8.2.1 Diffraction over paths where $d_{st} \approx d_{sr}$	8-4
8.2.2 For horizontal polarization	8-4
8.3 Single-Horizon Paths, Obstacle not Isolated	8-5
9. FORWARD SCATTER	9-1
9.1 The Attenuation Function, $F(\theta)$	9-2
9.2 The Frequency Gain Function, H_o	9-3
9.3 The Scattering Efficiency Correction, F_o	9-5
9.4 Expected Values of Forward Scatter Multipath Coupling Loss	9-6
9.5 Combination of Diffraction and Scatter Transmission Loss	9-7
9.6 An Example of Transmission Loss Predictions for a Transhorizon Path.	9-8
10. LONG-TERM POWER FADING	10-1
10.1 Effects of Atmospheric Stratification	10-4
10.2 Climatic Regions	10-6
10.3 The Effective Distance, d_e	10-8
10.4 The Functions $V(0.5, d_e)$ and $Y(q, d_e)$	10-9
10.5 Continental Temperate Climate	10-10
10.6 Maritime Temperate Climate	10-12
10.7 Other Climates	10-13
10.8 Variability for Knife-Edge Diffraction Paths	10-13
11. REFERENCES	11-1
12. LIST OF SYMBOLS AND ABBREVIATIONS	12-1

TABLE OF CONTENTS

Volume 2

	<u>PAGE NO.</u>
ANNEX I: AVAILABLE DATA, STANDARD CURVES, AND A SIMPLE PREDICTION MODEL	I-1
I.1 Available Data as a Function of Path Length	I-1
I.2 Standard Point-to-Point Transmission Loss Curves	I-2
I.3 Preliminary Reference Values of Attenuation Relative to Free Space A_{cr}	I-25
I.3.1 Introduction	I-29
I.3.2 The Terrain Roughness Factor Δh	I-29
I.3.3 The Diffraction Attenuation, A_d	I-30
I.3.4 The Forward Scatter Attenuation, A_g	I-31
I.3.5 Radio Line-of-Sight Paths	I-32
I.3.6 Ranges of the Prediction Parameters	I-34
I.3.7 Sample Calculations	I-35
ANNEX II: AVAILABLE POWER, FIELD STRENGTH, AND MULTIPATH COUPLING LOSS	II-1
II.1 Available Power from the Receiving Antenna	II-1
II.2 Propagation Loss and Field Strength	II-4
II.3 Beam Orientation, Polarization, and Multipath Coupling Loss	II-9
II.3.1 Representation of Complex Vector Fields	II-9
II.3.2 Principal and Cross-Polarization Components	II-12
II.3.3 Unit Complex Polarization Vectors	II-14
II.3.4 Power Flux Densities	II-19
II.3.5 Polarization Efficiency	II-19
II.3.6 Multipath Coupling Loss	II-20
II.3.7 Idealized Theoretical Antenna Patterns	II-23
II.3.8 Conclusions	II-31
II.4 List of Special Symbols Used in Annex II	II-34
ANNEX III: SUPPLEMENTARY INFORMATION AND FORMULAS USEFUL FOR PROGRAMMING	III-1
III.1 Line-of-Sight	III-2
III.2 Diffraction Over a Single Isolated Obstacle	III-15
III.3 Diffraction Over a Single Isolated Obstacle with Ground Reflections	III-17
III.4 Parameters K and b^* for Smooth Earth Diffraction	III-23
III.5 Forward Scatter	III-24
III.6 Transmission Loss with Antenna Beams Elevated or Directed Out of the Great Circle Plane	III-37

	<u>PAGE NO.</u>
III 7 Long-Term Power Fading	III-44
III 7.1 Diurnal and seasonal variability in a continental temperate climate	III-45
III 7.2 Two mix distributions	III-54
III 8 List of Special Symbols Used in Annex III	III-73
ANNEX I FORWARD SCATTER	IV-1
IV 1 General Discussion	IV-1
IV 2 Models for Forward Scattering	IV-2
IV 3 List of Special Symbols Used in Annex IV	IV-11
ANNEX V PHASE INTERFERENCE FADING AND SERVICE PROBABILITY	V-1
V 1 The Two Components of Fading	V-3
V 2 The Nakagami-Rice Distribution	V-5
V 3 Noise-Limited Service	V-13
V 4 Interference-Limited Service	V-15
V 5 The Joint Effect of Several Sources of Interference Present Simultaneously	V-19
V 6 The System Equation for Noise-Limited Service	V-20
V 7 The Time Availability of Interference-Limited Service	V-22
V 8 The Estimation or Prediction Error	V-23
V 9 The Calculation of Service Probability Q for a Given Time Availability q	V-25
V 10 Optimum Use of the Radio Frequency Spectrum	V-31
V 11 List of Special Symbols Used in Annex V	V-35

TRANSMISSION LOSS PREDICTIONS FOR
TROPOSPHERIC COMMUNICATION CIRCUITS

P. L. Rice, A. G. Loogley, K. A. Norton, and A. P. Harsis

1. INTRODUCTION

This report presents comprehensive methods of calculation which have been found useful either for explaining or for predicting cumulative distributions of transmission loss for a wide range of radio frequencies over almost any type of terrain and in several climatic regions. Such quantitative estimates of propagation characteristics help to determine how well proposed radio systems will meet requirements for satisfactory service, free from harmful interference. Thus they should provide an important step toward more efficient use of the radio frequency spectrum.

The need for comprehensive and accurate calculation methods is clearly demonstrated when measured transmission loss data for a large number of radio paths are shown as a function of path length. In figures I.1 to I.4 of annex I, long-term median values of attenuation relative to free space for more than 750 radio paths are plotted versus distance. The extremely wide scatter of these data is due mainly to path-to-path differences in terrain profiles and effective antenna heights. Values recorded for a long period of time over a single path show comparable ranges, sometimes exceeding 100 decibels. Such tremendous path-to-path and time variations must be carefully considered, particularly in cases of possible interference between co-channel or adjacent-channel systems. Included in annex I is a method for obtaining preliminary reference values of transmission loss for a wide range of prediction parameters.

The detailed point-to-point methods described here depend on propagation path geometry, atmospheric refractivity near the surface of the earth, and specified characteristics of antenna directivity. They have been tested against measurements in the radio frequency range 40 to 10,000 MHz (megahertz = megacycles per second). Estimates of attenuation due to absorption and scattering of radio energy by various constituents of the atmosphere are included in order to extend the application of these methods to frequencies up to 100 GHz.

Calculations of long-term median reference values of transmission loss are based on current radio propagation theory. A large sample of radio data was used to develop the empirical predictions of regional, seasonal, and diurnal changes in long-term medians. Estimates of long-term fading relative to observed medians are given for several climatic regions and periods of time, including some regions where few observations are available.

Calculations of transmission loss for paths within the radio horizon are based on geometric-optics ray theory. For paths with a common horizon, Fresnel-Kirchoff knife-edge diffraction theory is applied and extended to predict diffraction attenuation over isolated topographic obstacles. For double horizon paths that extend only slightly beyond the horizon, a modification of the Van der Pol-Bremmer method for computing field intensity in the far diffraction region is

and for longer paths, extending well beyond radio horizon, predictions are based on free space theory. Radio data were used to estimate the efficiency of scattering at various heights in the atmosphere. Where some doubt exists as to which propagation mechanism predominates, transmission loss is calculated by two methods and the results are compared.

Annex I, showing how to compute transmission loss for a line-of-sight path, an isolated ground obstacle, and a long transhorizon path are given following sections 5, 7 and 9 respectively. Section 12 provides a list of symbols and abbreviations used in the text. Special symbols used only in an annex are defined at the end of the appropriate annex.

Annex I includes a set of "standard" curves of basic transmission loss and curves showing attenuation below free space for earth space communications, prepared using the methods described in the report. Such curves, and the medians of data shown on figures I.1 to I.4, may serve for general qualitative analysis, but clearly do not take account of particular terrain profiles or climatic effects that may be encountered over a given path.

Annex II supplements the discussion of transmission loss and directive antenna gains given in section 2. This annex contains a discussion of antenna beam orientation, polarization, and multipath coupling loss.

Annex III contains information required for unusual paths, including exact formulas for computing line-of-sight transmission loss with ground reflections, as well as modifications of the formulas for antenna beams which are elevated, or directed out of the great circle plane. Analytic expressions suitable for use on a digital computer are also included.

Annex IV reviews tropospheric propagation theory with particular attention to the mechanisms of forward scatter from atmospheric turbulence, from layers, or from small randomly oriented surfaces. References to some of the work in this field are included.

Annex V presents a discussion of "phase interference fading" as contrasted to "long-term power fading", provides a method for computing the probability of obtaining adequate reception in the presence of noise and/or interfering signals, and includes a brief summary of ways to achieve optimum use of the radio frequency spectrum.

Previous NBS Technical Notes in this series, numbered 95 to 103, describe tropospheric propagation phenomena and siting problems [Kirby, Rice, and Maloney, 1961], meteorological phenomena and their influence on tropospheric propagation [Dutton, 1961, Dutton and Thayer, 1961], synoptic radio meteorology [Bean, Horn, and Riggs, 1962], techniques for measuring the refractive index of the atmosphere [McGavin, 1962], determination of system parameters [Florman and Tary, 1962], performance predictions for communication links [Barsis, Norton, Rice, and Elder, 1961], and equipment characteristics [Borghausen, et al., 1963].

2. THE CONCEPTS OF SYSTEM LOSS, TRANSMISSION LOSS, PATH ANTENNA GAIN, AND PATH ANTENNA POWER GAIN

Definitions have been given in CCIR Recommendation 341 for system loss, L_s , transmission loss, L_t , propagation loss, L_p , basic transmission loss, L_b , path antenna gain, G_p , and path antenna power gain G_{pp} . This section restates some of the definitions, introduces a definition of "path loss", L_o , illustrates the use of these terms and concepts, and describes methods of measurement [Norton, 1953, 1959, Wait 1959]. The notation used here differs slightly from that used in Recommendation 341 and in Report 112 [CCIR 1963 a, b]. For the frequency range considered in this report system loss, transmission loss, and propagation loss can be considered equal with negligible error in almost all cases, because antenna gains and antenna circuit resistances are essentially those encountered in free space.

2.1 System Loss and Transmission Loss

The system loss of a radio circuit consisting of a transmitting antenna, receiving antenna, and the intervening propagation medium is defined as the dimensionless ratio, w_t'/w_a' , where w_t' is the radio frequency power input to the terminals of the transmitting antenna and w_a' is the resultant radio frequency signal power available at the terminals of the receiving antenna. The system loss is usually expressed in decibels:

$$L_s = 10 \log (w_t'/w_a') = W_t' - W_a' \text{ db} \quad (2.1)$$

Throughout this report logarithms are to the base 10 unless otherwise stated.

The inclusion of ground and dielectric losses and antenna circuit losses in L_s provides a quantity which can be directly and accurately measured. In propagation studies, however, it is convenient to deal with related quantities such as transmission loss and basic transmission loss which can be derived only from theoretical estimates of radiated power and available power for various hypothetical situations.

In this report, capital letters are often used to denote the ratios, expressed in db, dbu, or dbw, of the corresponding quantities designated with lower-case type. For instance, in (2.1), $W_t' = 10 \log w_t'$ in dbw corresponds to w_t' in watts.

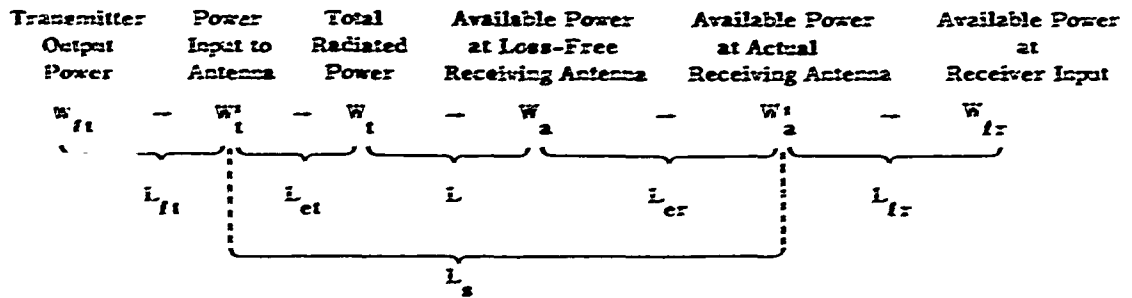
Transmission loss is defined as the dimensionless ratio w_t/w_a , where w_t is the total power radiated from the transmitting antenna in a given band of radio frequencies, and w_a is the resultant radio frequency signal power which would be available from an equivalent loss-free antenna. The transmission loss is usually expressed in decibels:

$$L = 10 \log (w_t/w_a) = W_t - W_a = L_s - L_{et} - L_{er} \text{ db} \quad (2.2)$$

$$L_{et} = 10 \log f_{et}, \quad L_{er} = 10 \log f_{er} \quad (2.3)$$

where $1/L_{ct}$ and $1/L_{er}$ as defined in annex II are power radiation and reception efficiencies for the transmitting and receiving antennas, respectively. With the frequencies and antenna heights usually considered for tropospheric communication circuits, these efficiencies are nearly unity and the difference between L_s and L is negligible. With antennas a fraction of a wavelength above ground, as they usually are at lower frequencies, and especially when horizontal polarisation is used, L_{ct} and L_{er} are not negligible, but are influenced substantially by the presence of the ground and other nearby portions of the antenna environment.

From transmitter output to receiver input, the following symbols are used:



It should be noted that L_{ft} and L_{fr} are conceptually different. Since W_{ft} and W'_t represent the power observed at the transmitter and at the transmitting antenna, respectively, L_{ft} includes both transmission line and mismatch losses. Since W'_a and W_{fr} represent available power at the receiving antenna and at the receiver, mismatch losses must be accounted for separately, since L_{fr} includes only the transmission line loss between the antenna and the receiver. Available power and effective loss factors are discussed in annex II.

2.2 Antenna Directive Gain and Power Gain

A transmitting antenna has a directive gain $g_t(\hat{r})$ in the direction of a unit vector \hat{r} if:

- (1) it radiates a total of w_t watts through the surface of any large sphere with the antenna at its center, and
- (2) it radiates $g_t w_t / (4\pi)$ watts per steradian in the direction \hat{r} .

The same antenna has a power gain $g_t'(\hat{r})$ in the direction \hat{r} if:

- (1) the power input to the antenna terminals is $w_t' = l_{et} w_t$, and
- (2) it radiates $g_t' w_t' / (4\pi)$ watts per steradian in the direction \hat{r} .

The antenna power gain g_t' is smaller than the directive gain g_t simply as a result of the loss factor l_{et} . It follows that

$$G_t(\hat{r}) = G_t'(\hat{r}) \div L_{et} \quad (2.4a)$$

expressed in decibels above the gain of an isotropic radiator. Note that the antenna power gain $G_t'(\hat{r})$ is less than the antenna directive gain $G_t(\hat{r})$ by the amount L_{et} dB, where the power radiation efficiency $1/l_{et}$ is independent of the direction \hat{r} .

The gain of an antenna is the same whether it is used for transmitting or receiving. For a receiving antenna, the directive gain $G_r(\hat{r})$ and power gain $G_r'(\hat{r})$ are related by

$$G_r(\hat{r}) = G_r'(\hat{r}) + L_{er}. \quad (2.4b)$$

The remainder of this report will deal with directive gains, since the power gains may be determined simply by subtracting L_{et} or L_{er} . The maximum value of a directive gain $G(\hat{r})$ is designated simply as G . As noted in Annex II, it is sometimes useful to divide the directive gain into principal and cross-polarization components.

An idealized antenna in free space with a half-power semi-beamwidth δ expressed in radians, and with a circular beam cross-section, may be assumed to radiate x percent of its power isotropically through an area equal to $\pi\delta^2$ on the surface of a large sphere of unit radius, and to radiate $(100-x)$ percent of its power isotropically through the remainder of the sphere. In this case the power radiated in the direction of the main beam is equal to $xw_t/(100\pi\delta^2)$ watts per steradian and the maximum gain g is, by definition, equal to $4\pi x/(100\pi\delta^2)$. One may assume a beam solid angle efficiency $x = 56$ percent for parabolic reflectors with 10 db tapered illumination, and obtain $g = 2.24/\delta^2$. The maximum free space gain G in decibels relative to an isotropic radiator is then

$$G = 10 \log g = 3.50 - 20 \log \delta \text{ db}. \quad (2.5)$$

If azimuthal and vertical beamwidths $2\delta_w$ and $2\delta_z$ are different:

$$\delta = \sqrt{\delta_w \delta_z} \quad (2.6)$$

The above analysis is useful in connection with measured antenna radiation patterns.

For antennas such as horns or parabolic reflectors which have a clearly definable physical aperture, the concept of antenna aperture efficiency is useful. For example, the free space maximum gain of a parabolic dish with a 56 percent aperture efficiency and a diameter D is the ratio of 56 percent of its area to the effective absorbing area of an isotropic radiator:

$$G = 10 \log \left[\frac{0.56 \pi D^2 / 4}{\lambda^2 / 4\pi} \right] = 20 \log D + 20 \log f - 42.10 \text{ db} \quad (2.7)$$

where D and λ are in meters and f is the radio frequency in megahertz, MHz. Equations (2.5) and (2.7) are useful for determining the gains of actual antennas only when their beam solid angle efficiencies or aperture efficiencies are known, and these can be determined accurately only by measurement.

With a dipole feed, for instance, and $10 < D/\lambda < 25$, experiments have shown the following empirical formula to be superior to (2.7):

$$G = 23.3 \log D + 23.3 \log f - 55.1 \text{ db} \quad (2.8)$$

where D is expressed in meters and f in MHz.

Cozzens [1962] has published a nomograph for determining paraboloidal maximum gain as a function of feed pattern and angular aperture. Discussions of a variety of commonly used antennas are given in recent books [Jasik, 1961; Thourel, 1960].

Much more is known about amplitude, phase, and polarization response of available antennas in the directions of maximum radiation or reception than in other directions. Most of the theoretical and developmental work has concentrated on minimizing the transmission loss between antennas and on studies of the response of an arbitrary antenna to a standard plane wave. An increasing amount of attention, however, is being devoted to maximizing the transmission loss between antennas in order to reject unwanted signals. For this purpose it is important to be able to specify, sometimes in statistical terms, the directivity, phase, and polarization response of an antenna in every direction from which multipath components of each unwanted signal may be expected. A large part of annex II is devoted to this subject.

For the frequencies of interest in this report, antenna radiation resistances r_v at any radio frequency ν hertz are usually assumed independent of their environment, or else the immediate environment is considered part of the antenna, as in the case of an antenna mounted on an airplane or space vehicle.

2.3 Polarization Coupling Loss and Multipath Coupling Loss

It is sometimes necessary to minimize the response of a receiving antenna to unwanted signals from a single source by way of different paths. This requires attention to the amplitudes, polarizations, and relative phases of a number of waves arriving from different directions. In any theoretical model, the phases of principal and cross-polarization components of each wave, as well as the relative phase response of the receiving antenna to each component, must be considered. Complex voltages are added at the antenna terminals to make proper allowance for this amplitude and phase information.

In annex II it is shown how complex vectors \bar{e} and \bar{e}_r may be used to represent transmitting and receiving antenna radiation and reception patterns which will contain amplitude, polarization, and phase information [Kales, 1951] for a given free-space wavelength, λ . A bar is used under the symbol for a complex vector $\bar{e} = \bar{e}_p + i \bar{e}_c$, where $i = \sqrt{-1}$ and \bar{e}_p , \bar{e}_c are real vectors which may be associated with principal and cross-polarized components of a uniform elliptically polarized plane wave.

Calculating the power transfer between two antennas in free space, complex polarization vectors $\hat{p}(\vec{r})$ and $\hat{p}_r(-\vec{r})$ are determined for each antenna as if it were the transmitter and the other were the receiver. Each antenna must be in the far field or radiation field of the other. The sense of polarization of the field \bar{e} is right-handed or left-handed depending on whether the axial ratio of the polarization ellipse, a_x , is positive or negative:

$$a_x = e_c / e_p. \quad (2.9)$$

The polarization is circular if $|e_p| = |e_c|$ and linear if $e_c = 0$, where $\bar{e}_p = \bar{e} \hat{e}_p$ is in the principal polarization direction defined by the unit vector \hat{e}_p . The polarization coupling loss in free space is

$$L_{cp} = -10 \log |\bar{p} \cdot \bar{p}_r|^2 \text{ db}, \quad (2.10)$$

In terms of the axial ratios a_x and a_{xr} defined by (II. 48) and (II. 50) and the acute angle ψ_p between principal polarization vectors \bar{e}_p and \bar{e}_{pr} , the corresponding polarization efficiency may be written as

$$|\bar{p} \cdot \bar{p}_r|^2 = \frac{\cos^2 \psi_p (a_x a_{xr} + 1)^2 + \sin^2 \psi_p (a_x + a_{xr})^2}{(a_x^2 + 1)(a_{xr}^2 + 1)}. \quad (2.11)$$

This is the same as (II. 62). Annex II explains how these definitions and relationships are extended to the general case where antennas are not in free space.

There is a maximum transfer of power between two antennas if the polarization ellipse of the receiving antenna has the same sense, eccentricity, and principal polarization direction as the polarization ellipse of the incident radio wave. The receiving antenna is completely "blind" to the incident wave if the sense of polarization is opposite.

the eccentricity is the same, and the principal polarization direction is orthogonal to that of the incident wave. In theory this situation would result in the complete rejection of an unwanted signal propagating in a direction $-\hat{r}$. Small values of $g_r(-\hat{r})$ could at the same time discriminate against unwanted signals coming from other directions.

When more than one plane wave is incident upon a receiving antenna from a single source, there may be a "multipath coupling loss" which includes beam orientation, polarization coupling, and phase mismatch losses. A statistical average of phase incoherence effects, such as that described in subsection 9.4, is called "antenna-to-medium coupling loss." Multipath coupling loss is the same as the "loss in path antenna gain," L_{gp} , defined in the next subsection. Precise expressions for L_{gp} may also be derived from the relationships in annex II.

2.4 Path Loss, Basic Transmission Loss, Path Antenna Gain, and Attenuation Relative to Free Space

Recorded values of transmission loss are often normalized to "path loss" by adding the sum of the maximum free space gains of the antennas, $G_t + G_r$, to the transmission loss, L . Path loss is defined as

$$L_p = L + G_t + G_r \quad \text{db.} \quad (2.12)$$

Basic transmission loss, L_b , is the system loss for a situation where the actual antennas are replaced at the same locations by hypothetical antennas which are:

- (1) Isotropic, so that $G_t(\hat{r}) = 0$ db and $G_r(-\hat{r}) = 0$ db for all important propagation directions, \hat{r} .
- (2) Loss-free, so that $L_{et} = 0$ db and $L_{er} = 0$ db.
- (3) Free of polarization and multipath coupling loss, so that $L_{cp} = 0$ db.

If the maximum antenna gains are realized, $L_o = L_b$.

Corresponding to this same situation, the path antenna gain, G_p , is defined as the change in the transmission loss if hypothetical loss-free isotropic antennas with no multipath coupling loss were used at the same locations as the actual antennas. Assumptions used in estimating G_p should always be carefully stated.

Replace both antennas by loss-free isotropic antennas at the same locations, with no coupling loss between them and having the same radiation resistances as the actual antennas, and let W_{ab} represent the resulting available power at the terminals of the hypothetical isotropic receiving antenna. Then the basic transmission loss L_b , the path antenna gain G_p , and the path antenna power gain G_{pp} , are given by

$$L_b = W_t - W_{ab} = L + G_p \quad \text{db} \quad (2.13)$$

$$G_p = W_a - W_{ab} = L_b - L \quad \text{db} \quad (2.14a)$$

$$G_{pp} = W_a^i - W_{ab} = L_b - L_s \quad \text{db} \quad (2.14b)$$

where W_t , W_a , W_a^i and L_s are defined in section 2.1.

In free space, for instance:

$$W_a = W_t + G_t(\hat{r}) + G_r(-\hat{r}) - L_{cp} + 20 \log \left(\frac{\lambda}{4\pi r} \right) \quad \text{dbw} \quad (2.15a)$$

$$W_{ab} = W_t + 20 \log \left(\frac{\lambda}{4\pi r} \right) \quad \text{dbw.} \quad (2.15b)$$

A special symbol, L_{bf} , is used to denote the corresponding basic transmission loss in free space:

$$L_{bf} = 20 \log \left(\frac{4\pi r}{\lambda} \right) = 32.45 + 20 \log f + 20 \log r \quad \text{db} \quad (2.16)$$

where the antenna separation r is expressed in kilometers and the free space wavelength λ equals $0.2997925/f$ kilometers for a radio frequency f in megahertz.

When low gain antennas are used, as on aircraft, the frequency dependence in (2.16) indicates that the service range for UHF equipment can be made equal to that in the VHF band only by using additional power in direct proportion to the square of the frequency. Fixed point-to-point communications links usually employ high-gain antennas at each terminal, and for a given antenna size more gain is realized at UHF than at VHF, thus more than compensating for the additional free space loss at UHF indicated in (2.16).

Comparing (2.13), (2.14), and (2.15), it is seen that the path antenna gain in free space, G_{pf} , is

$$G_{pf} = G_t(\bar{r}) + G_r(-\bar{r}) - L_{cp} \text{ db.} \quad (2.17)$$

For most wanted propagation paths, this is well approximated by $G_t + G_r$, the sum of the maximum antenna gains. For unwanted propagation paths it is often desirable to minimize G_{pf} . This can be achieved not only by making $G_t(\bar{r})$ and $G_r(-\bar{r})$ small, but also by using different polarizations for receiving and transmitting antennas so as to maximize L_{cp} .

In free space the transmission loss is

$$L = L_{bf} - G_{pf} \text{ db.} \quad (2.18)$$

The concepts of basic transmission loss and path antenna gain are also useful for normalizing the results of propagation studies for paths which are not in free space. Defining an "equivalent free-space transmission loss", L_f , as

$$L_f = L_{bf} - G_p, \quad (2.19)$$

note that G_p in (2.19) is not equal to $G_t + G_r$ unless this is true for the actual propagation path. It is often convenient to investigate the "attenuation relative to free space", A , or the basic transmission loss relative to that in free space, defined here as

$$A = L_b - L_{bf} = L - L_f \text{ db.} \quad (2.20)$$

This definition, with (2.19), makes A independent of the path antenna gain, G_p . Where terrain has little effect on line-of-sight propagation, it is sometimes desirable to study A rather than the transmission loss, L .

Although G_p varies with time, it is customary to suppress this variation [Hartman, 1963] and to estimate G_p as the difference between long-term median values of L_b and

Multipath coupling loss, or the "loss in path antenna gain", L_{gp} , is defined as the difference between path loss L_o and basic transmission loss L_b :

$$L_{sp} = L_o - L_b = C \quad G_r - G_p \quad \epsilon_s. \quad (2.21)$$

The loss in path antenna gain will therefore, in general, include components of beam orientation loss and polarization coupling loss as well as any aperture-to-medium coupling loss that may result from scattering by the troposphere, by rough or irregular terrain, or by terrain clutter such as vegetation, buildings, bridges, or power lines.

The relationships between transmission loss, propagation loss and field strength are discussed in annex II.

2. ATMOSPHERIC ABSORPTION

At frequencies above 2 GHz attenuation of radio waves due to absorption or scattering by constituents of the atmosphere, and by particles in the atmosphere, may seriously affect microwave relay links, communication via satellites, and radio and radar astronomy. At frequencies below 1 GHz the total radio wave absorption by oxygen and water vapor for propagation paths of 1000 kilometers or less will not exceed 2 decibels. Absorption by rainfall begins to be barely noticeable at frequencies from 2 to 3 GHz, but may be quite appreciable at higher frequencies.

For frequencies up to 100 GHz, and for both optical and transmission paths, this section provides estimates of the long-term median attenuation A_a of radio waves by oxygen and water vapor, the attenuation A_r due to rainfall, and the order of magnitude of absorption by clouds of a given water content. The estimates are based on work reported by Artman and Gordon [1954], Bean and Abbott [1957], Bussey [1950], Crawford and Hogg [1956], Gann and East [1954], Hathaway and Evans [1959], Hogg and Mumford [1960], Hogg and Semplek [1961], Lane and Sutton [1952], Laws and Parsons [1943], Perlet and Voge [1953], Straiton and Tolbert [1960], Tolbert and Straiton [1957], and Van Vleet [1947a, b; 1951].

3.1 Absorption by Water Vapor and Oxygen

Water vapor absorption has a resonant peak at a frequency of 22.23 GHz, and oxygen absorption peaks at a number of frequencies from 53 to 66 GHz and at 120 GHz. Figure 3.1, derived from a critical appraisal of the above references, shows the differential absorption γ_{oo} and γ_{wo} in decibels per kilometer for both oxygen and water vapor, as determined for standard conditions of temperature and pressure and for a surface value of absolute humidity equal to 10 grams per cubic meter. These values are consistent with those prepared for the Xth Plenary Assembly of the CCIR by U.S. Study Group IV [1963d] except that the water vapor density is there taken to be 7.5 g/m^3 . For the range of absolute humidity likely to occur in the atmosphere, the water vapor absorption in db/km is approximately proportional to the water vapor density.

The total atmospheric absorption A_a decibels for a path of length r_0 kilometers is commonly expressed in one of two ways, either as the integral of the differential absorption $\gamma(r)$ dr:

$$A_a = \int_0^{r_0} \gamma(r) \text{ dr} \quad \text{db} \quad (3.1)$$

or in terms of an absorption coefficient $\Gamma(r)$ expressed in reciprocal kilometers:

$$A_a = -10 \log \exp \left[- \int_0^{r_0} \Gamma(r) \text{ dr} \right] = 4.343 \int_0^{r_0} \Gamma(r) \text{ dr} \quad \text{db}. \quad (3.2)$$

The argument of the logarithm in (3.2) is the amount of radio wave energy that is not absorbed in traversing the path.

The total gaseous absorption A_a over a line-of-sight path of length r_0 kilometers is

$$A_a = \int_0^{r_0} dt [\gamma_o(h) + \gamma_w(h)] \quad (3.3)$$

where h is the height above sea level at a distance r from the lower terminal, measured along a ray path between terminals. For radar returns, the total absorption is $2A_a$ db.

Considering oxygen absorption and water vapor absorption separately, (3.3) may be written

$$A_a = \gamma_{o0} r_{eo} + \gamma_{w0} r_{ew} \quad (3.4)$$

where r_{eo} and r_{ew} are effective distances obtained by integrating γ_o/γ_{o0} and γ_w/γ_{w0} over the ray path.

The effective distances r_{eo} and r_{ew} are plotted versus r_0 and frequency for elevation angles $\theta_0 = 0, 0.01, 0.02, 0.05, 0.1, 0.2, 0.5, 1,$ and $\pi/2$ radians in figures 3.2-3.4. Figure 3.5 shows the relationship between r_0 and the sea level arc distance, d , for these values of θ_0 .

A_a may be estimated from figures 1.21 to 1.26 of annex 1, where attenuation relative to free space, A , is plotted versus r_0 , θ_0 , and r_0 , ignoring effects of diffraction by terrain.

For nonoptical paths, the ray from each antenna to its horizon makes an angle θ_{cr} with the horizontal at the horizon, as illustrated in figure 6.1 of section 6. The horizon rays intersect at distances d_1 and d_2 from the transmitting and receiving terminals. The total absorption A_a is the sum of values A_{a1} and A_{a2} .

$$A_a = A_{a1} + A_{a2} \quad (3.5)$$

where $A_{a1} = A_a(f, \theta_{cr}, d_1)$ and $A_{a2} = A_a(f, \theta_{cr}, d_2)$.

For propagation over a smooth earth, $\theta_{cr} = \theta_{cr} = 0$, and $A_a = 2A_a(f, 0, d/2)$. For transmission paths and the frequency range 0.1 - 10 GHz, figure 3.6 shows A_a plotted versus distance over a smooth earth between 10 meter antenna heights.

3.2 Sky-Noise Temperature

The ionized atmosphere is a source of radio noise, with the same properties as a radiator that it has as an absorber. The effective sky-noise temperature T_s may be determined by integrating the gas temperature T multiplied by the differential fraction of re-radiated power that is not absorbed in passing through the atmosphere to the antenna:

$$T_s (K) = \int_0^{\infty} T(z) \Gamma(z) \exp \left[- \int_0^z \Gamma(z') dz' \right] dz \quad (3.6)$$

where the absorption coefficient $\Gamma(z)$ in reciprocal kilometers is defined by (3.2). For ionospheric absorption:

$$\Gamma(z) = (2.93 - 6.54) \text{ km}^{-1} \quad \text{for } h < 12 \text{ km.}$$

and

$$\Gamma(z) = 210 \text{ km}^{-1} \quad \text{for } h \geq 12 \text{ km.}$$

Figure 3.7 shows the sky-noise temperature due to oxygen and water vapor for various angles of elevation and for frequencies between 0.1 and 100 GHz.

In estimating antenna temperatures, the antenna pattern and radiation from the earth's surface must also be considered.

3.3 Attenuation by Rain

The attenuation of radio waves by suspended water droplets as in rain often exceeds the combined oxygen and water vapor absorption. Water droplets of size of 1 mm will scatter radio waves in all directions whether the drops are small compared to the wavelength or comparable to the wavelength. In the latter case, raindrops trap and absorb some of the radio wave energy. Accordingly, rain attenuation is much more serious at millimeter wavelengths than at centimeter wavelengths.

In practice it has been convenient to express rain attenuation as a function of the precipitation rate R_r which depends on both the liquid water content and the fall velocity of the drops, the latter in turn depending on the size of the drops. There is little evidence that rain with a known rate of fall has a unique drop-size distribution, and the problem of estimating the attenuation of radio waves by the various forms of precipitation is quite difficult.

Total absorption A_r due to rainfall over a path of length r can be estimated by integrating the differential rain absorption $\gamma_r(r) dr$ along the path between two inter-visible antennas, or along horizon rays in the case of transhorizon propagation:

$$A_r = \int_0^r \gamma_r(r) dr \text{ decibels.} \tag{3.7}$$

Fitting an arbitrary mathematical function empirically to theoretical results given by Hathaway and Evans [1959] and Ryde and Ryde [1945], the rate of absorption by rain γ_r can be expressed in terms of the rainfall rate R_r in millimeters per hour as

$$\gamma_r = K R_r^a \text{ db/km} \tag{3.8}$$

for frequencies above 2 GHz. The functions $K(f_G)$ and $a(f_G)$ are plotted in figures 3.8 and 3.9, where f_G is the radio frequency in GHz,

$$K = [3(f_G - 2)^2 - 2(f_G - 2)] \times 10^{-2} \tag{3.8a}$$

$$a = [1.14 - 0.07(f_G - 2)^{1/2}] + 0.055 f_G^{-1} + \exp(-0.05 f_G^2) \tag{3.8b}$$

An examination of the variation of rainfall rate with height suggests a relation of the form

$$R_r / h = \exp(-0.2 h) \tag{3.9}$$

where R_{rs} is the surface rainfall rate. Then

$$A_r = \gamma_{rs} r_{er} db, \quad (3.11)$$

$$\gamma_{rs} = KR_{rs}^{\alpha} db/km, \quad r_{er} = \int_0^r dr \exp(-0.2 \alpha b^2) km \quad (3.12)$$

where γ_{rs} is the surface value of the rate of absorption by rain, and r_{er} is an "effective rainbearing distance". Figures 3.10-3.13 show r_{er} versus r_0 for several values of θ_0 and α . The curves shown were computed using (3.12).

A "standard" long-term cumulative distribution of rain absorption is estimated, using some statistics from Ohio analyzed by Bussey [1950], who relates the cumulative distribution of instantaneous path average rainfall rates for 25, 50, and 100-kilometer paths, respectively, with the cumulative distributions for a single rain gauge of half-hour, one-hour, and two-hour mean rainfall rates, recorded for a year. The total annual rainfall in Ohio is about 110 centimeters.

Rainfall statistics vary considerably from region to region, sometimes from year to year, and often with the direction of a path (with or across prevailing winds). For instance, in North America, east-west systems seem particularly vulnerable, as they lie along the path of frequent heavy showers.

For very long paths, the cumulative distribution of instantaneous path average rainfall rates, \bar{R}_r , depends on how R_r varies with elevation above the surface and upon the correlation of rainfall with distance along the path. Figure 3.14 provides estimates of the instantaneous path average rainfall rate \bar{R}_r exceeded for 0.01, 0.1, 1, and 5 percent of the year as a function of r_{er} and normalized to a total annual rainfall of 100 cm. To obtain A_r from (3.11), replace R_{rs} in (3.12) with \bar{R}_r from figure 3.14, multiplied by the ratio of the total annual rainfall and 100 cm. These estimates are an extrapolation of the results given by Bussey [1950] and are intended to allow for the average variation of R_r with height, as given by (3.17) and allowed for in the definition of r_{er} , and for the correlation of surface rainfall rate R_{rs} with distance along the surface, as analyzed by Bussey.

3.4 Attenuation in Clouds

Cloud droplets are regarded here as those water or ice particles having radii smaller than 100 microns or 0.01 cm. Although a rigorous approach to the problem of attenuation by clouds must consider drop-size distribution, it is more practical to speak of the water content of clouds rather than the drop-size distribution. Reliable measurements of both parameters are scarce, but it is possible to make reasonable estimates of the water content, M , of a cloud from a knowledge of the vertical extent of the cloud and the gradients of pressure, temperature, and mixing ratio, which is the ratio of the mass of water vapor to the mass of dry air in which it is mixed. The absorption within a cloud can be written as

$$A_c = K_1 M \Delta z \quad (3.13)$$

where A_c is the total absorption attenuation within the cloud, K_1 is an attenuation coefficient, values for which are given in table 3.1, and M is the liquid water content of the cloud, measured in grams per cubic meter. The amount of precipitable water, M , in a given pressure layer can be obtained by evaluating the average mixing ratio in the layer, multiplying by the pressure difference, and dividing by the gravity. Using this method of obtaining M and the values of K_1 from table 3.1, it is possible to get a fairly reliable estimate of the absorption of radio energy by a cloud.

Several important facts are demonstrated by table 3.1. The increase in attenuation with increasing frequency is clearly shown. The values change by about an order of magnitude from 10 to 30 GHz. Cloud attenuation can be safely neglected below 6 GHz. The data presented here also show that attenuation increases with decreasing temperature. These relations are a reflection of the dependence of the refractive index on both wavelength and temperature. The different dielectric properties of water and ice are illustrated by the difference in attenuation. Ice clouds give attenuations about two orders of magnitude smaller than water clouds of the same water content.

TABLE 3.1

One-Way Attenuation Coefficient, K_1 , in db/km/gm/m³

Temperature (°C)		Frequency, GHz,			
		33	24	17	9.4
Water	20	0.647	0.311	0.128	0.0483
	10	0.681	0.406	0.179	0.0630
Cloud	0	0.99	0.532	0.267	0.0858
	-8	1.25	0.684	0.34	0.112
				(extrapolated)	(extrapolated)
Ice	0	6.74×10^{-3}	6.35×10^{-3}	4.36×10^{-3}	2.46×10^{-3}
Cloud	-10	2.93×10^{-3}	2.11×10^{-3}	1.46×10^{-3}	8.19×10^{-4}
	-20	2.0×10^{-3}	1.45×10^{-3}	1.0×10^{-3}	5.63×10^{-4}

SURFACE VALUES γ_{00} AND γ_{90} OF ABSORPTION
OF OXYGEN AND WATER VAPOR
PRESSURE 760mmHg
TEMPERATURE 20°C
WATER VAPOR HEIGHT 100mm

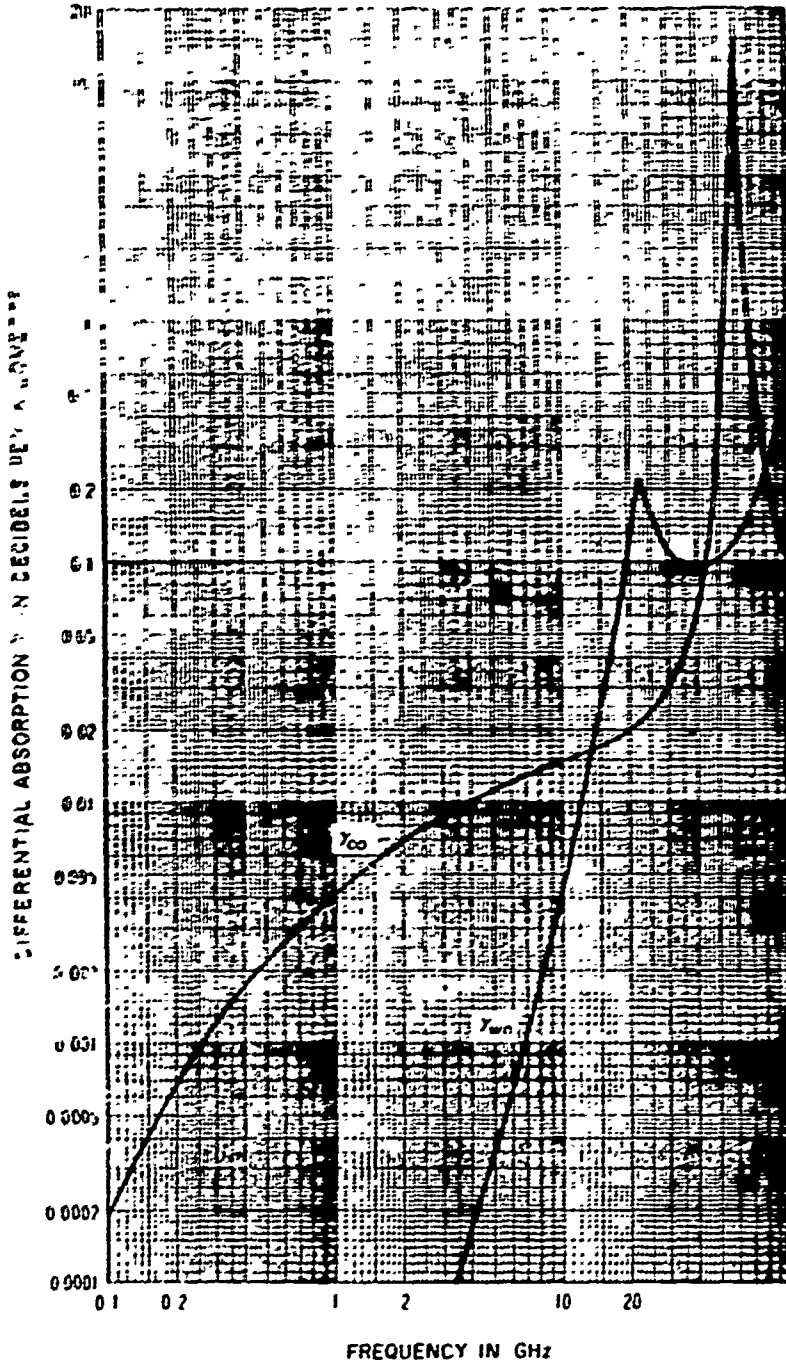


Figure 3.1

EFFECTIVE DISTANCES r_{eo} AND r_{ew} FOR ABSORPTION BY OXYGEN AND WATER VAPOR
 $\beta_0 = 0, 0.001, 0.02$

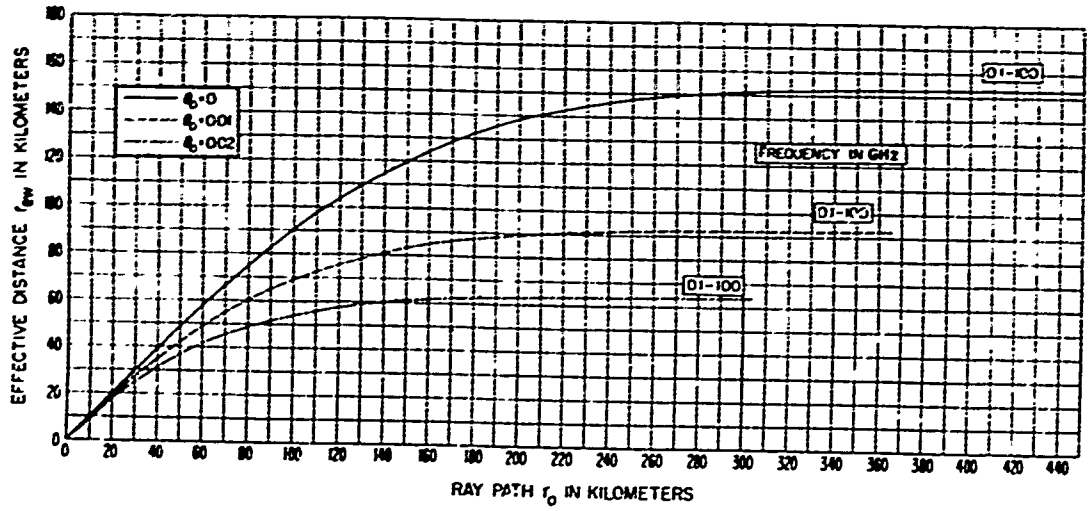
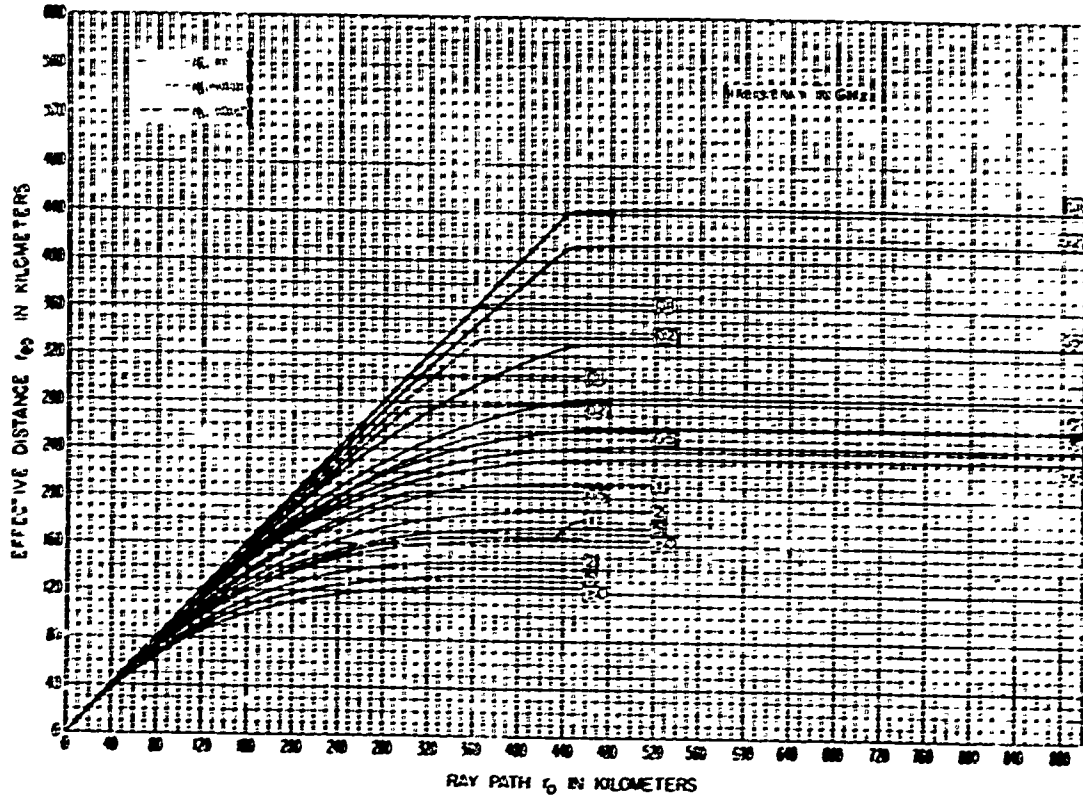


Figure 3.2

EFFECTIVE DISTANCES r_{eo} AND r_{ew} FOR ABSORPTION BY OXYGEN AND WATER VAPOR
 $\theta_0 = 0.05, 0.1, 0.2$

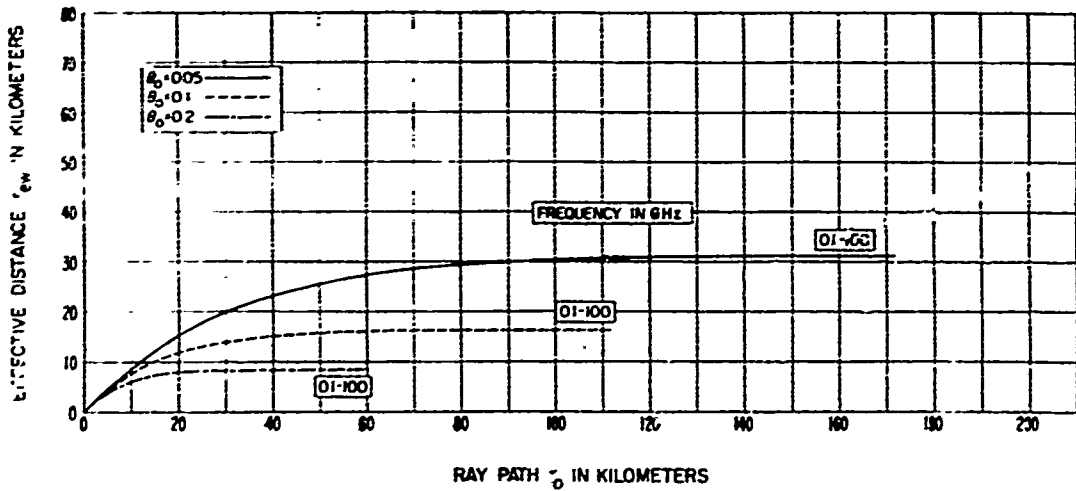
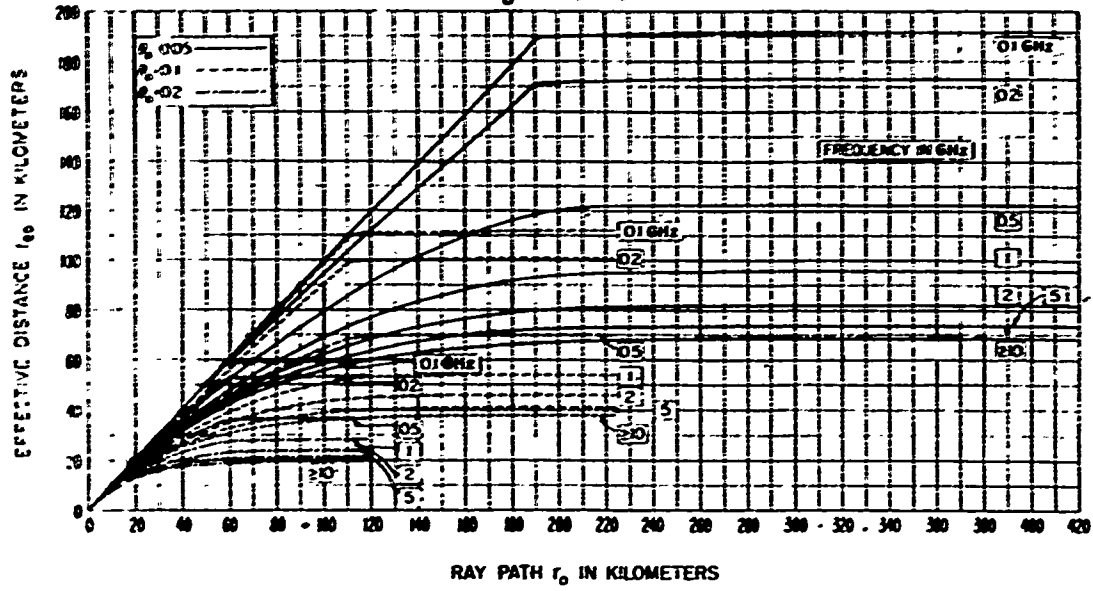


Figure 3.3

EFFECTIVE DISTANCES r_{eo} AND r_{ew} FOR ABSORPTION BY OXYGEN AND WATER VAPOR
 $\theta_0 = 0.5, 1, \pi/2$

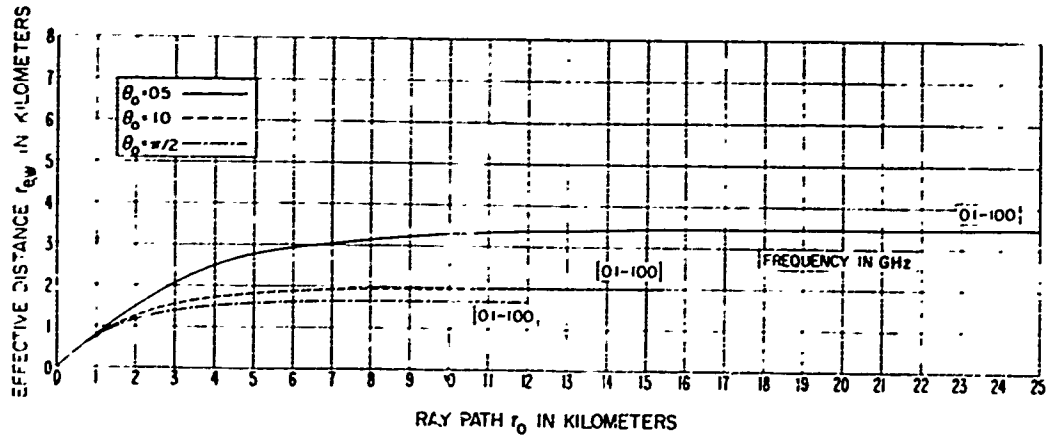
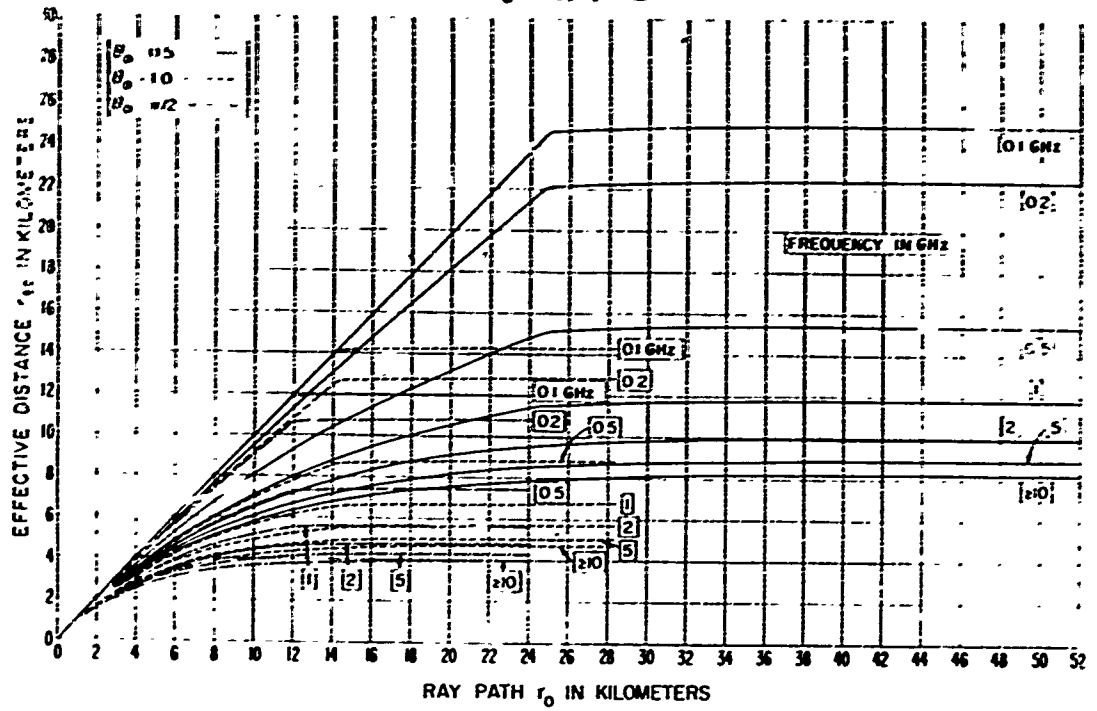
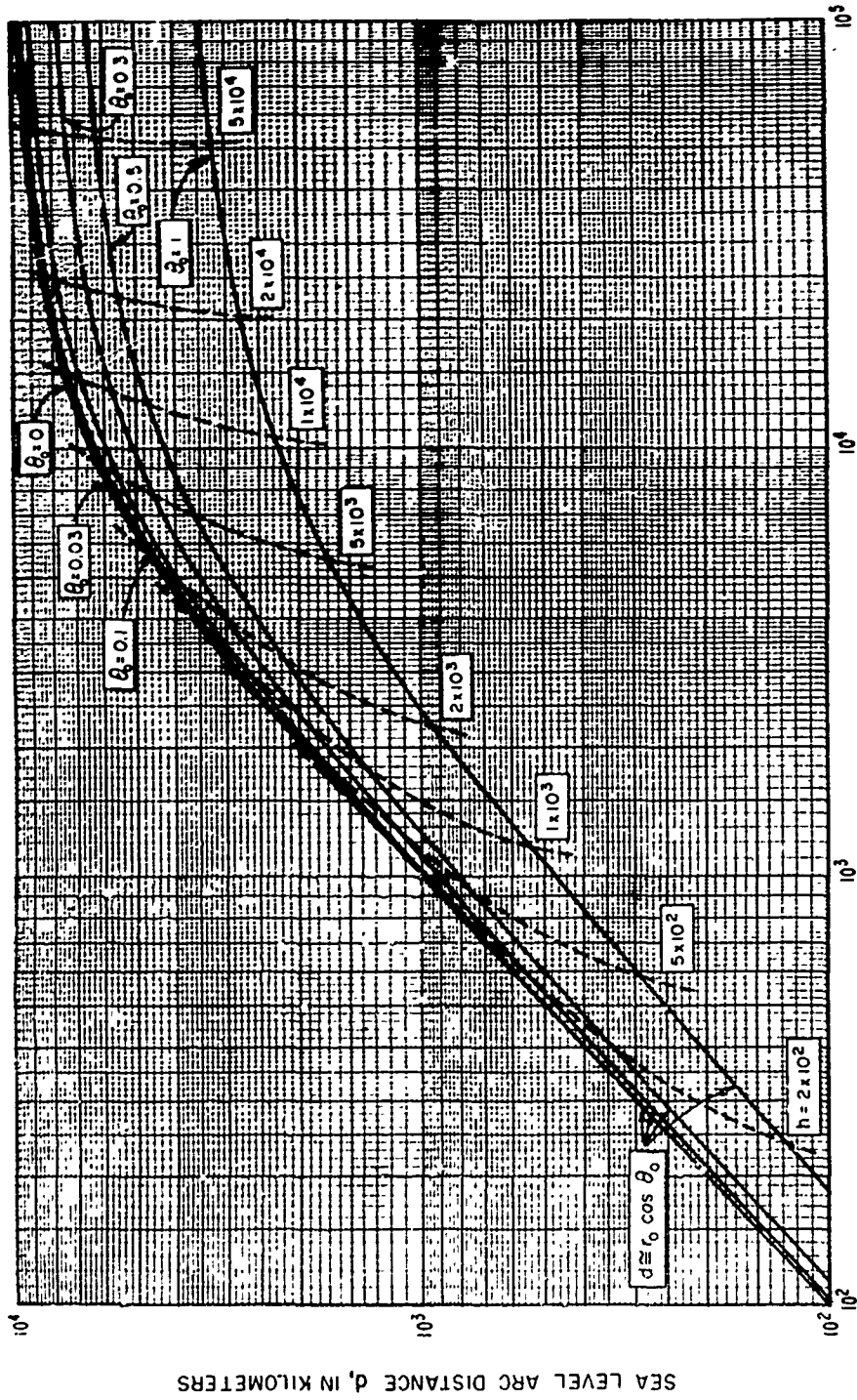


Figure 3.4

RAY PATH LENGTH, r_0 , VERSUS SEA LEVEL ARC DISTANCE, d
 $\theta_0 = 0, 0.03, 0.1, 0.3, 0.5, 1$



RAY PATH r_0 IN KILOMETERS

Figure 3.5

ESTIMATE OF MEDIAN OXYGEN AND WATER VAPOR ABSORPTION
FROM AUGUST DATA, WASHINGTON, D. C.

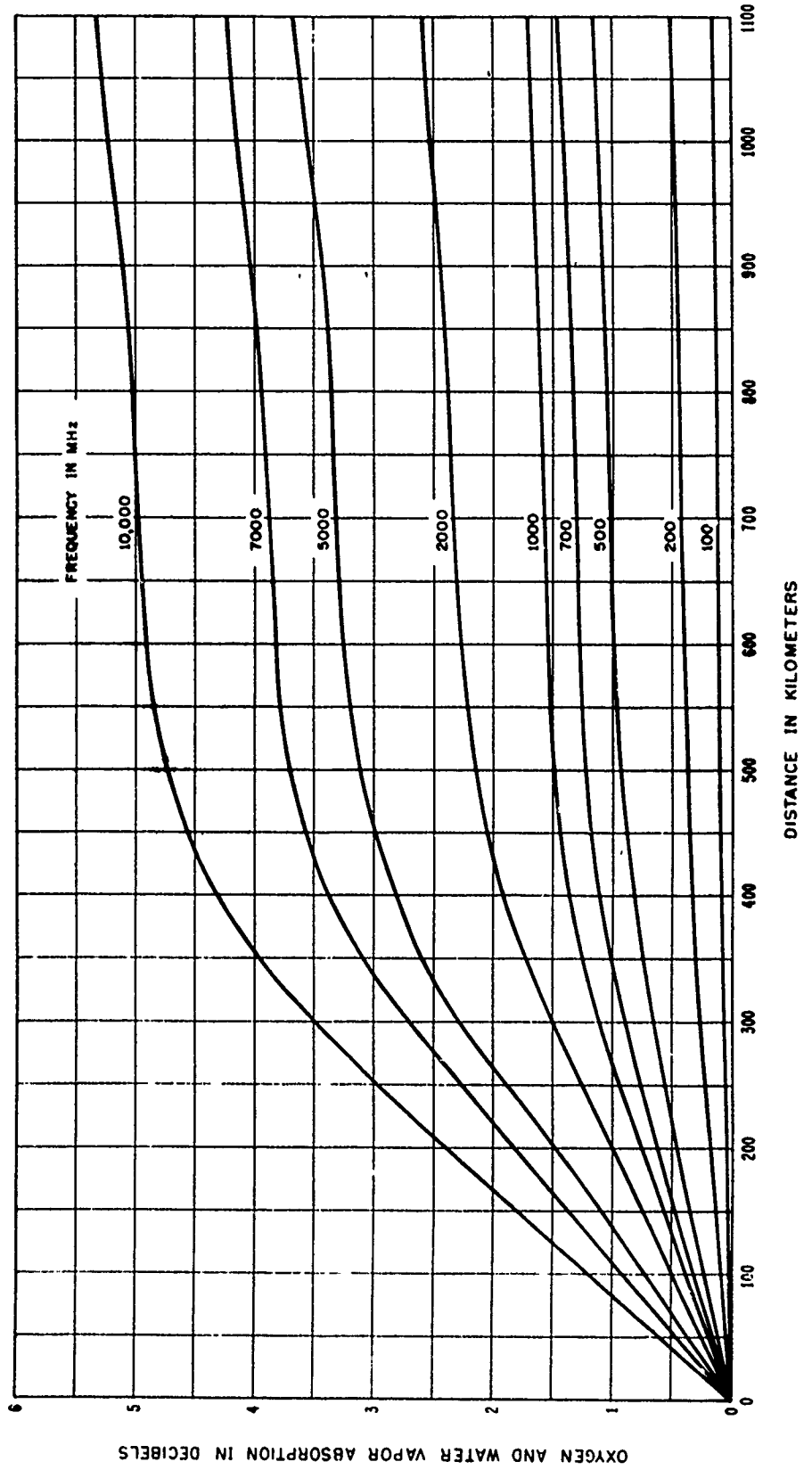


Figure 3.6

SKY NOISE TEMPERATURE DUE TO RERADIATION BY OXYGEN AND WATER VAPOR

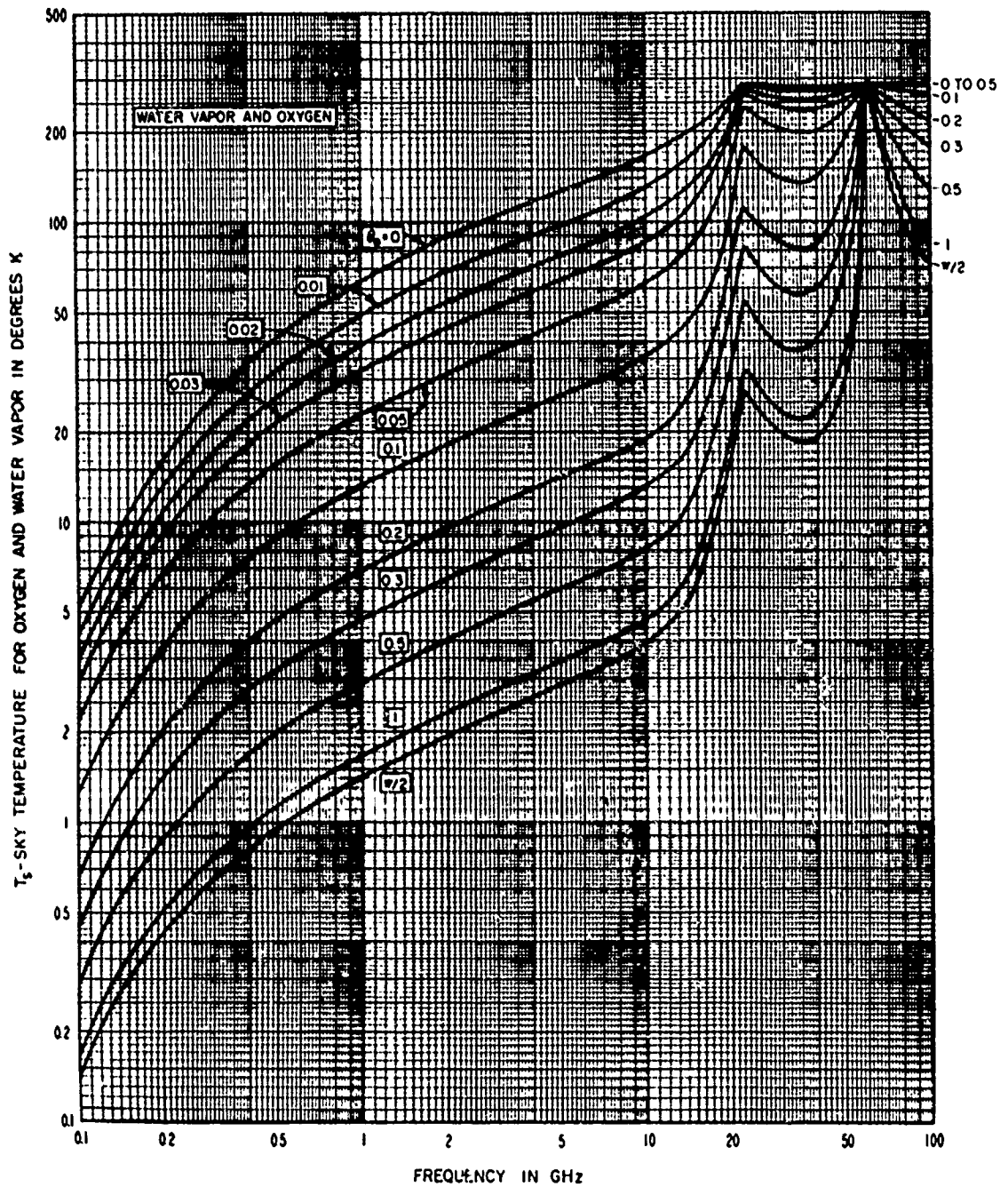


Figure 37

RAINFALL ABSORPTION COEFFICIENT K vs FREQUENCY

$\gamma = KR_r^2$ db/km, WHERE R_r IS THE RAINFALL RATE IN MILLIMETERS/HOUR

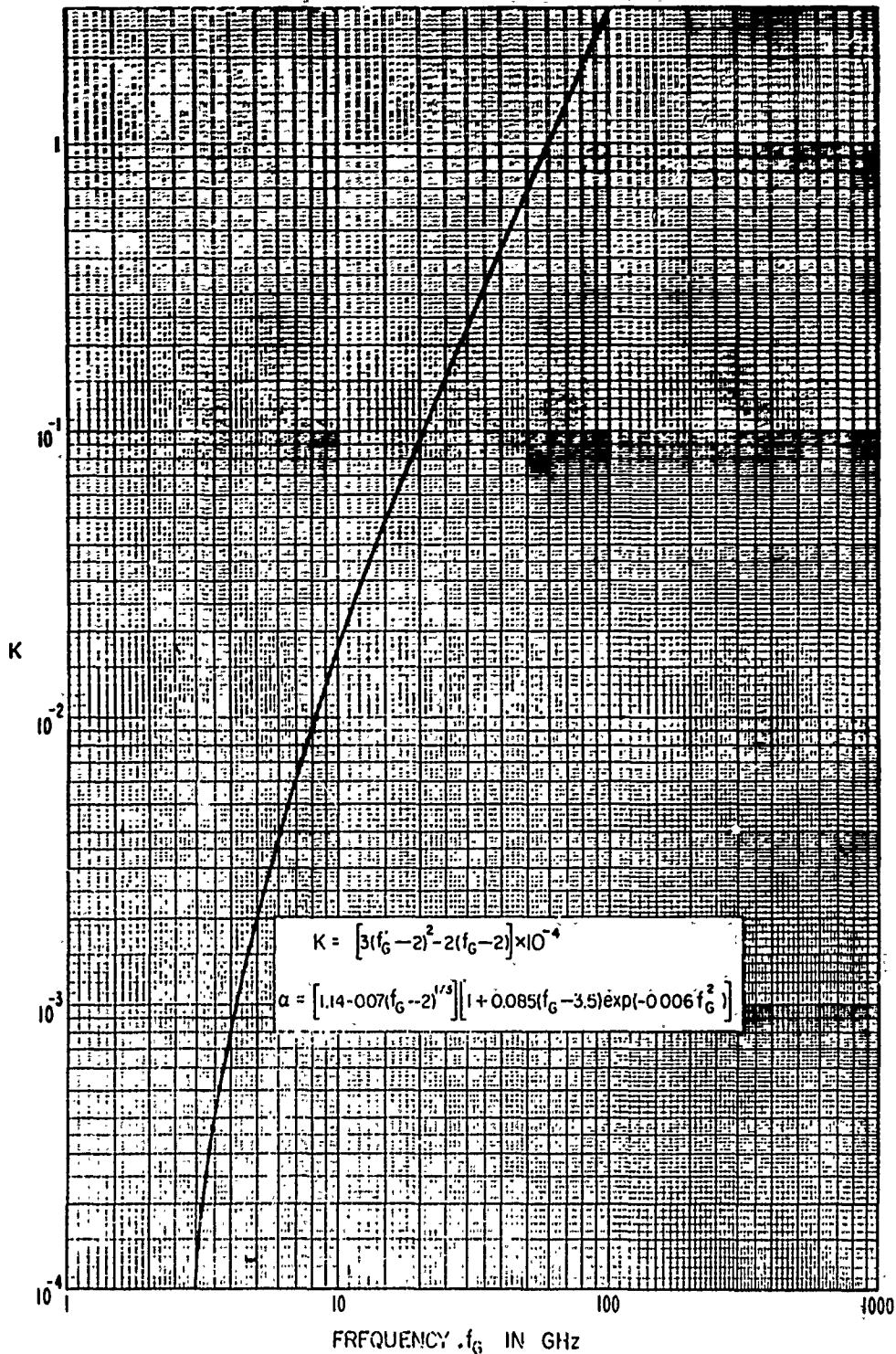


Figure 3.8

RAINFALL ABSORPTION EXPONENT α VS FREQUENCY

$\gamma = KR^2$ db/km, WHERE R , IS THE
RAINFALL RATE IN MILLIMETERS/HOUR

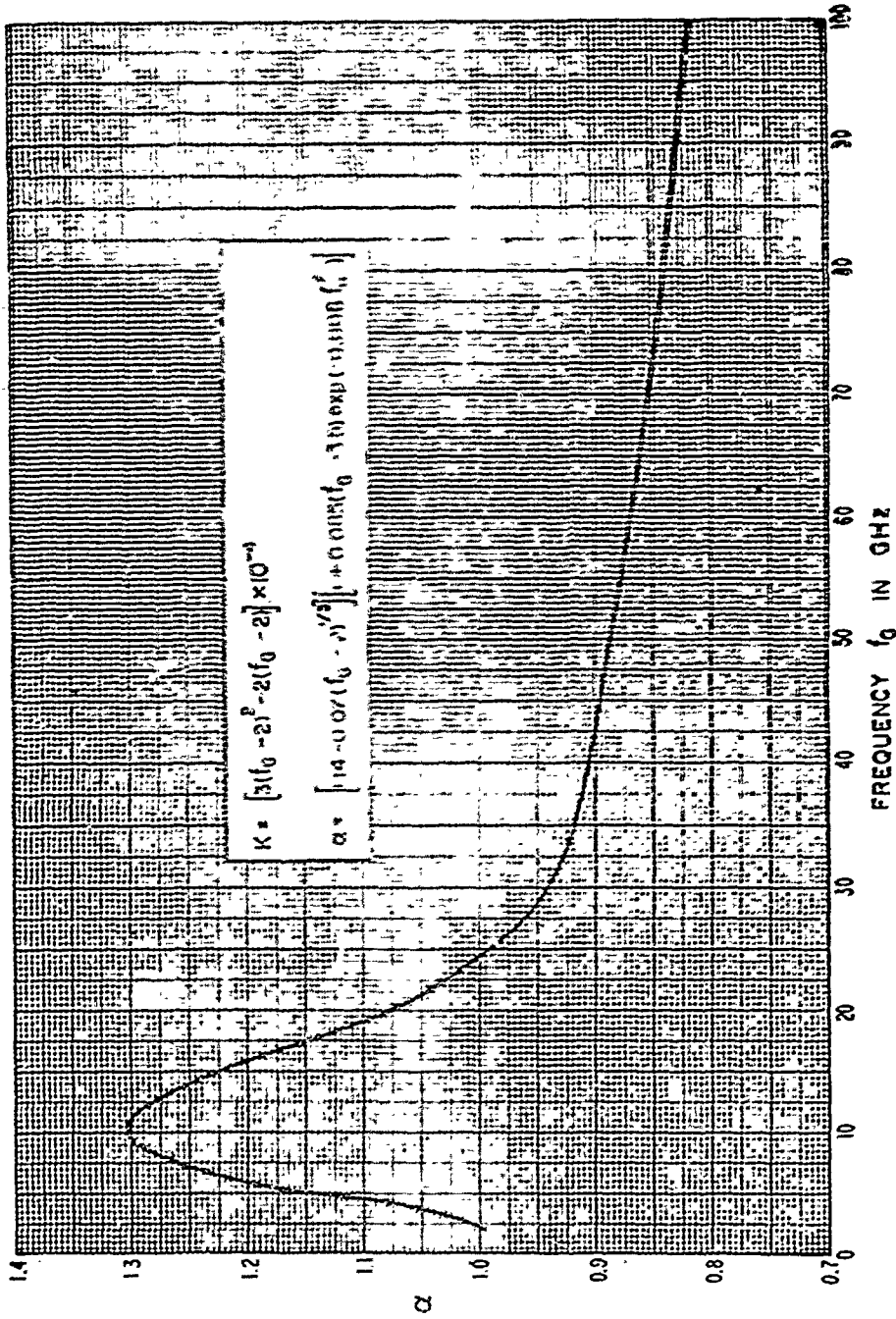


Figure 3.9

EFFECTIVE DISTANCE r_e FOR RAIN ABSORPTION
 $\theta_0 = 0.001, 0.002$

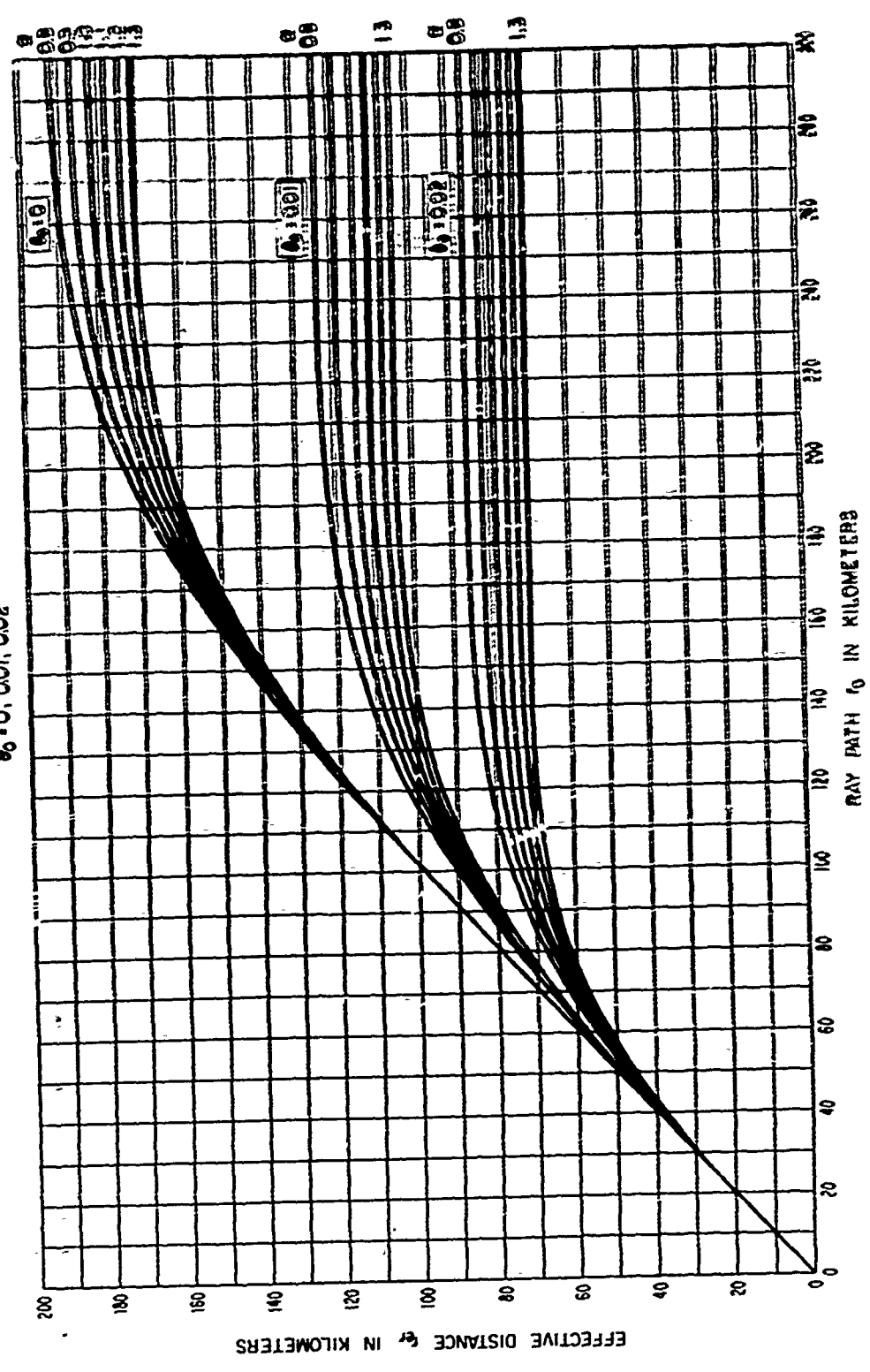
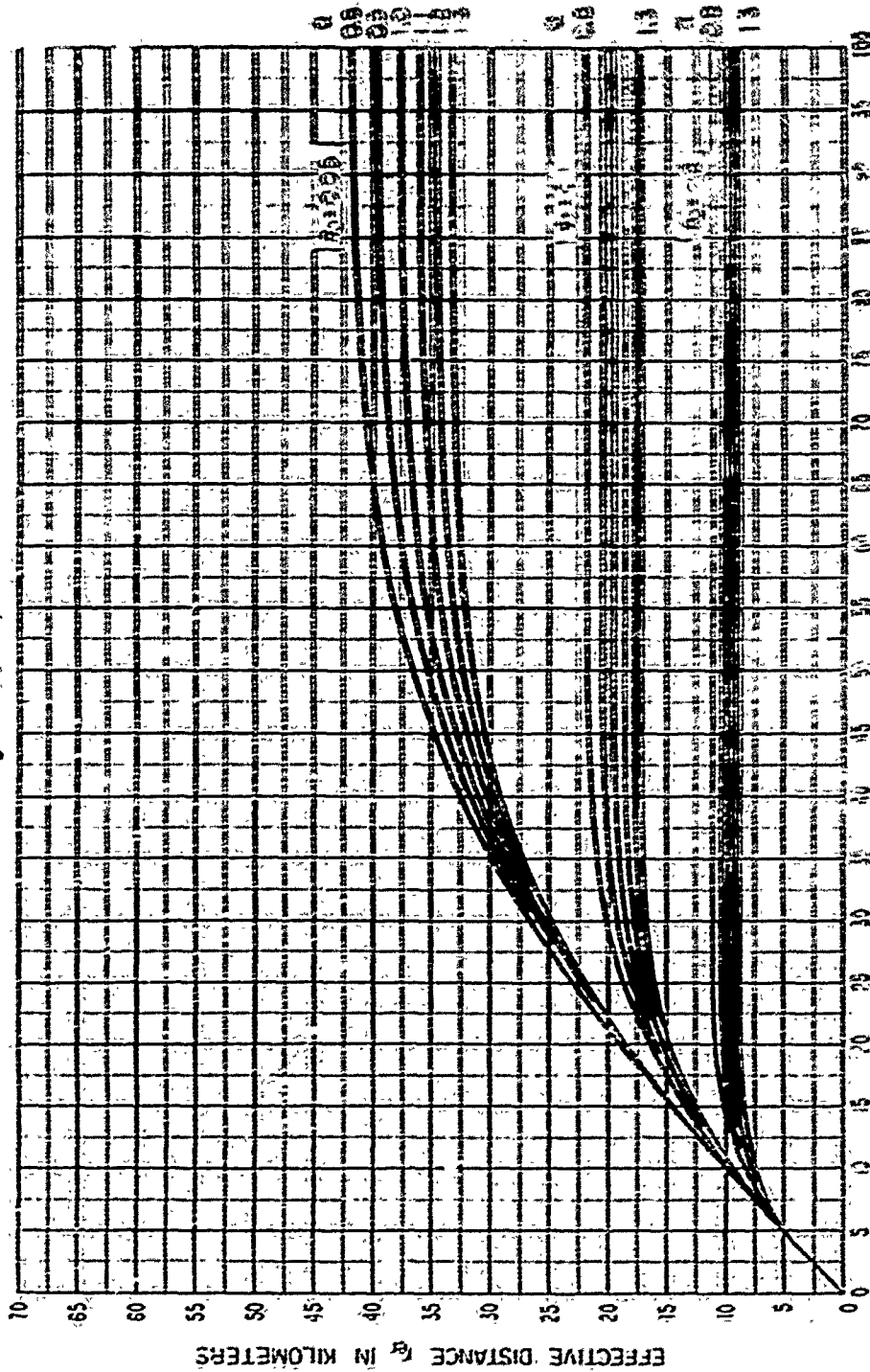


Figure 3.10

EFFECTIVE DISTANCE r_e FOR RAIN ABSORPTION
 $\theta_0 = 0.05, 0.1, 0.2$



RAY PATH L_0 IN KILOMETERS

Figure 3.11

EFFECTIVE DISTANCE ρ_r FOR RAIN ABSORPTION
 $\rho_0 = 0.5$ AND 1

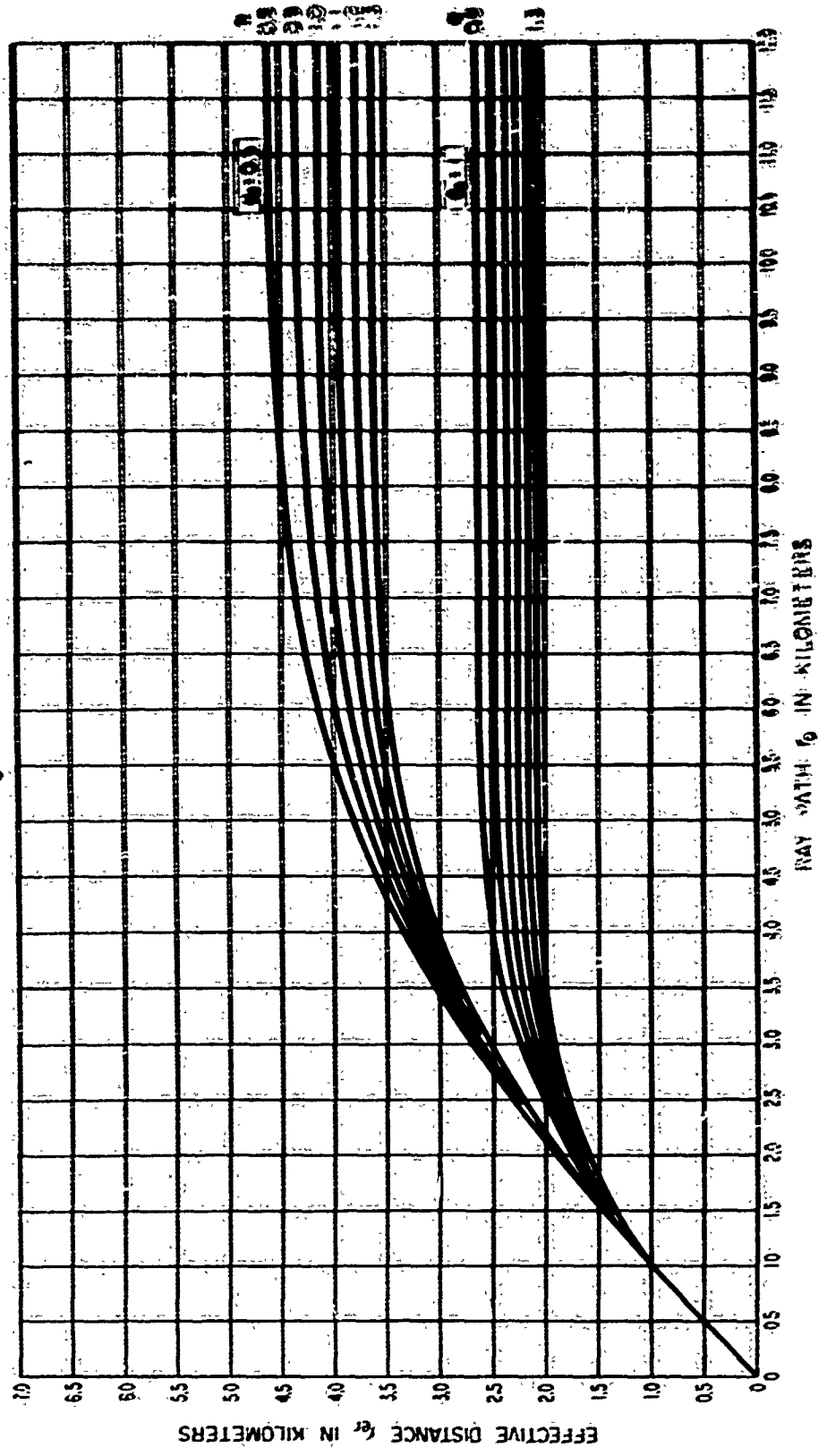
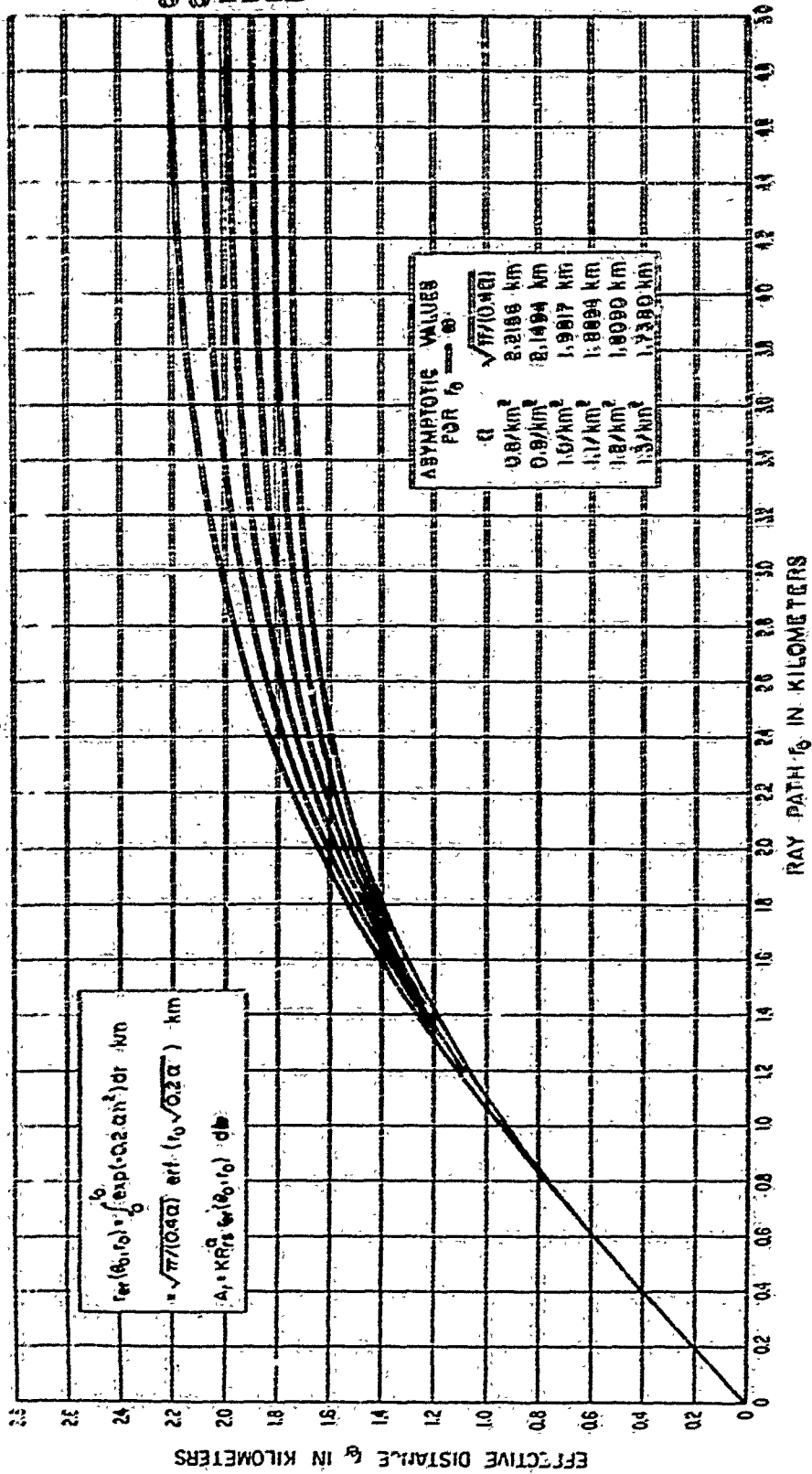


Figure 3-12

EFFECTIVE DISTANCE d_e FOR RAIN ABSORPTION ON
 $60 \pm 77/2$



$$d_e(r_0, \sigma) = \int_0^{r_0} \exp(-0.22 \sigma^2 r) dr \text{ km}$$

$$= \sqrt{77(0.401)} \operatorname{erf}(\sigma \sqrt{0.22} r_0) \text{ km}$$

$$A_1 = KR^2 \sigma(r_0, \sigma) \text{ dB}$$

Figure 3.13

14-MH AVERAGE RAINFALL RATE, R_1 , VS EFFECTIVE RAINBEARING DISTANCE, r_{er}
(TOTAL ANNUAL RAINFALL, 1000mm)

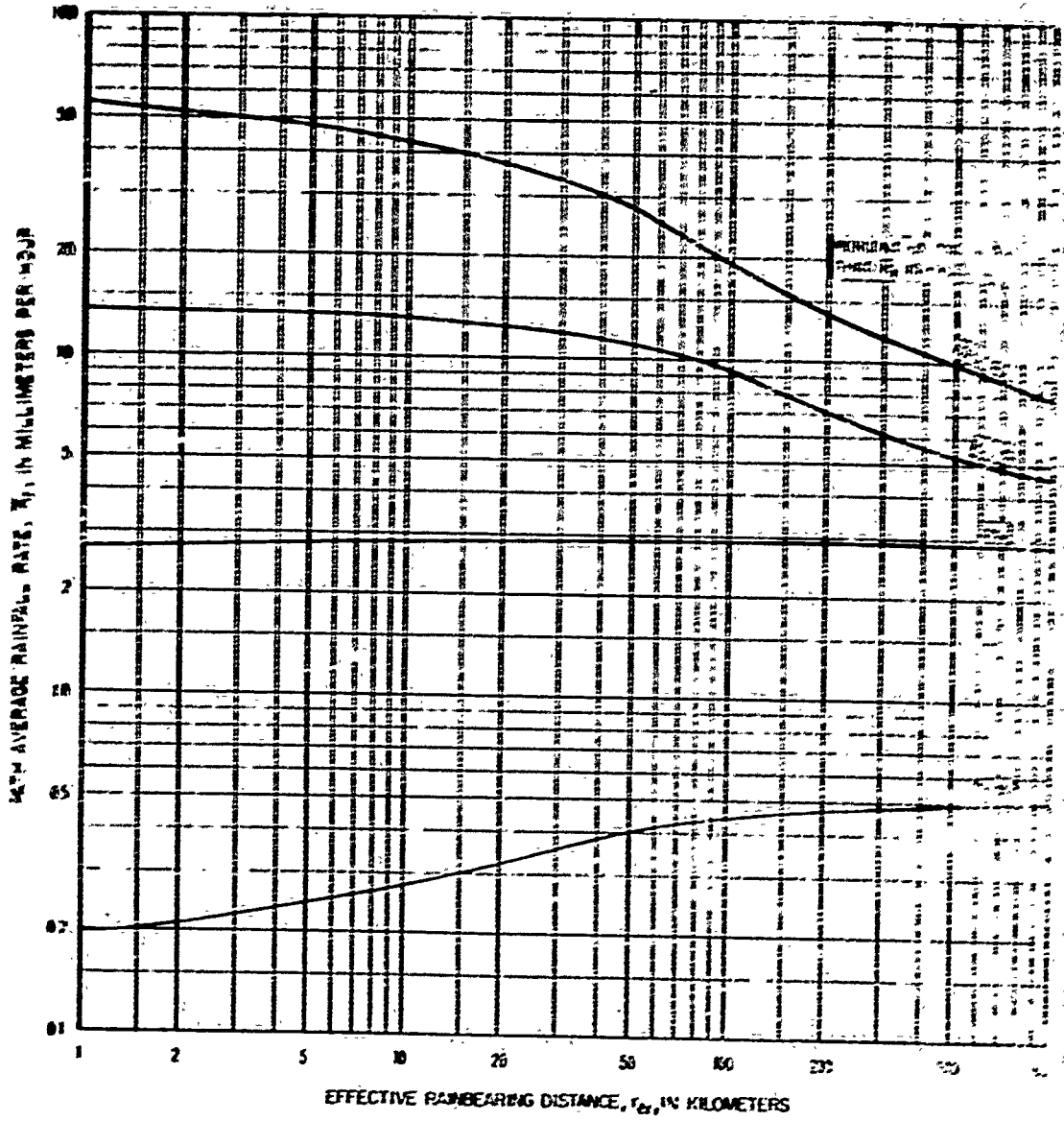


Figure 3.14

4. DETERMINATION OF AN EFFECTIVE EARTH'S RADIUS

The bending of a radio ray as it passes through the atmosphere is largely determined by the gradient of the refractive index near the earth's surface. In order to represent radio rays as straight lines, at least within the first kilometer above the surface, an "effective earth's radius" is defined as a function of the refractivity gradient, ΔN , or of the surface refractivity value N_s .

$$N_s = (n_s - 1) \times 10^6 \quad (4.1)$$

where n_s is the atmospheric refractive index at the surface of the earth.

In the United States the following empirical relationship has been established between the mean N_s and the mean refractivity gradient ΔN in the first kilometer above the surface:

$$\Delta N/\text{km} = -7.32 \exp(0.005577 N_s) \quad (4.2)$$

Similar values have been established in West Germany and in the United Kingdom [CCIR 1963].

In this paper values of N_s are used to characterize average atmospheric conditions during periods of minimum field strength. In the northern temperate zone, field strengths and values of N_s reach minimum values during winter afternoons. Throughout the world, regional changes in expected values of transmission loss depend on minimum monthly mean values of a related quantity, N_0 , which represents surface refractivity reduced to sea level:

$$N_s = N_0 \exp(-0.1057 h_s) \quad (4.3)$$

where h_s is the elevation of the surface above mean sea level, in kilometers, and the refractivity N_0 is read from the map shown in figure 4.1 and taken from Bean, Horn, and Ozanich [1960].

Most of the refraction of a radio ray takes place at low elevations, so it is appropriate to determine N_0 and h_s for locations corresponding to the lowest elevation of the radio rays most important to the geometry of a propagation path. As a practical matter for within-the-horizon paths, h_s is defined as the ground elevation immediately below the lower antenna terminal, and N_0 is determined at the same location. For beyond-the-horizon paths, h_s and N_0 are determined at the radio horizons along the great circle path between the antennas, and N_s is the average of the two values calculated from (4.3). An exception to this latter rule occurs if an antenna is more than 150 meters below its radio horizon; in such a case, h_s and N_0 should be determined at the antenna location.

The effective earth's radius, a , is given by the following expression:

$$a = a_0 [1 - 0.04665 \exp(0.005577 N_s)]^{-1} \quad (4.4)$$

where a_0 is the actual radius of the earth, and is taken to be 6370 kilometers. Figure 4.2 shows the effective earth's radius, a , plotted versus N_s . The total bending of a radio ray which is elevated more than 0.785 radians (45°) above the horizon and which passes all the way through the earth's atmosphere is less than half a milliradian. For studies of earth-satellite communication ray bending is important at low angles. At higher angles it may often be neglected and the actual earth's radius is then used in geometrical calculations.

Large values of ΔN and N_s are often associated with atmospheric ducting, which is usually important for part of the time over most paths, especially in maritime climates. The average occurrence of strong layer reflections, superrefraction, ducting, and other focusing and defocusing effects of the atmosphere is taken into account in the empirical time variability functions to be discussed in section 10. Additional material on ducting will be found in papers by Anderson and Gossard [1953a, b], Bean [1959], Booker [1946], Booker and Walkinshaw [1946], Clemow and Bruce-Clayton [1963], Dutton [1961], Fok, Vainshtein, and Belkina [1958], Friend [1945], Hay and Urwin [1952], Ikegami [1959], Kitchen, Joy, and Richards [1958], Nomura and Takaku [1955], Onoe and Nishikori [1957], Pekeris [1947], Schönemann [1957], and Urwin [1953].

MONTHLY MEAN SURFACE REFLECTIVITY VALUES BETWEEN 10°N AND 10°S

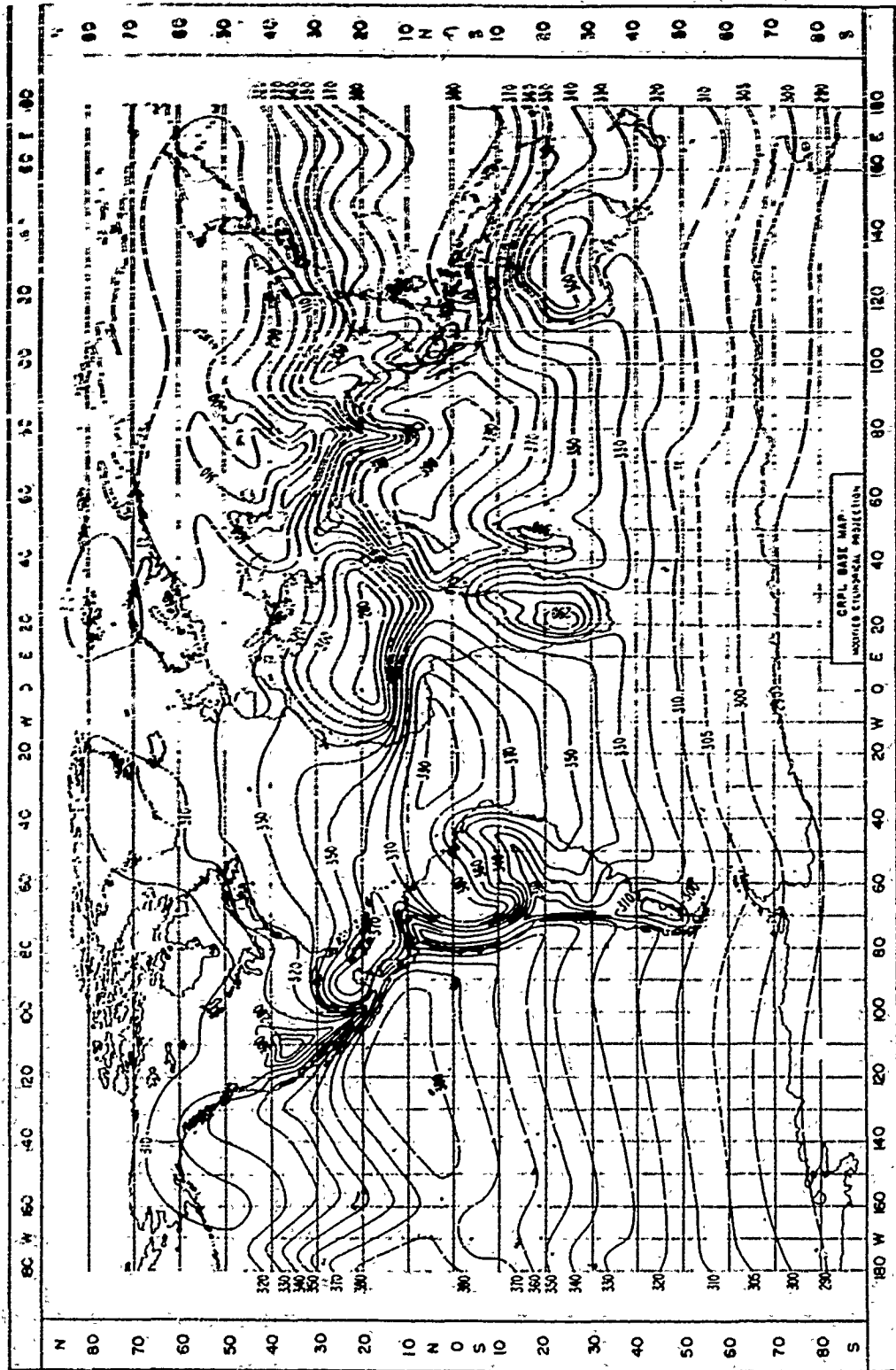


Figure 41

EFFECTIVE EARTH'S RADIUS, a , VERSUS SURFACE REFRACTIVITY, N_s

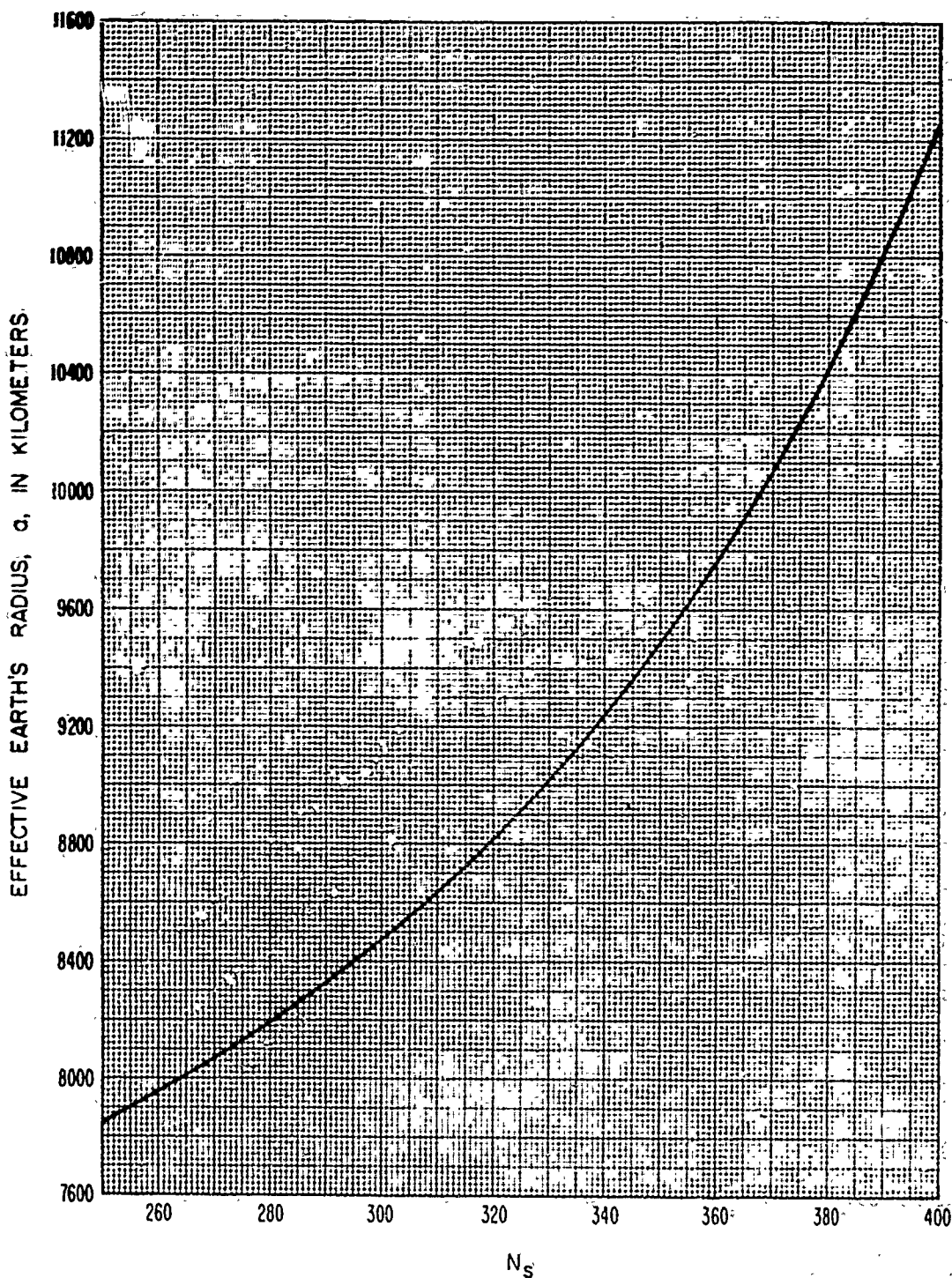


Figure 4.2

5. TRANSMISSION LOSS PREDICTION METHODS FOR WITHIN-THE-HORIZON PATHS

Ground wave propagation over a smooth spherical earth of uniform ground conductivity and dielectric constant, and with a homogeneous atmosphere, has been studied extensively. Some of the results were presented in CCIR Atlases [1955, 1959]. Recent work by Bachynski [1959, 1960, 1963], Wait [1963], Furutsu [1963], and others considers irregularities of electrical ground constants and of terrain. A distinction is made here between the roughness of terrain which determines the proportion between specular and diffuse reflection of radio waves, and large scale irregularities whose average effect is accounted for by fitting a straight line or curve to the terrain.

A comprehensive discussion of the scattering of electromagnetic waves from rough surfaces is given in a recent book by Beckmann and Spizzichino [1963]. Studies of reflection from irregular terrain as well as absorption, diffraction, and scattering by trees, hills, and man-made obstacles have been made by Beckmann [1957], Biot [1957 a, b], Kalinin [1957, 1958], Kühn [1958], McGavin and Maloney [1959], McPetrie and Ford [1946], McPetrie and Saxton [1942], Saxton and Lane [1955], Sherwood and Ginzton [1955], and many other workers. Examples of studies of reflection from an ocean surface may be found in papers by Beard, Katz and Spetner [1956], and Beard [1961].

A semi-empirical method for predicting transmission loss for within-the-horizon paths is given in annex I.

Reflections from hillsides or obstacles off the great circle path between two antennas sometimes contribute a significant amount to the received signal. Discrimination against such off-path reflections may reduce multipath fading problems, or in other cases antenna beams may be directed away from the great circle path in order to increase the signal level by taking advantage of off-path reflection or knife-edge diffraction. For short periods of time, over some paths, atmospheric focusing or defocusing will lead to somewhat smaller or much greater values of line-of-sight attenuation than the long-term median values predicted for the average path by the methods of this section.

If two antennas are intervisible over the effective earth defined in section 4, ray optics may be used to estimate the attenuation A relative to free space, provided that the great circle path terrain visible to both antennas will support a substantial amount of reflection and that it is reasonable to fit a straight line or a convex curve of radius a to this portion of the terrain.

5.1 Line-of-Sight Propagation Over Irregular Terrain

Where ray optics formulas, described in section 5.2, are not applicable a satisfactory estimate of line-of-sight transmission loss may sometimes be made by one of the following methods:

1. If a slight change in the position of either antenna results in a situation where ray optics formulas may be used, then A may be estimated by extrapolation or interpolation.
2. Instead of a single curve fit to terrain as in 5.2 the method may, in some cases, be extended to multiple curve fits and multiple reflections from these curves.
3. If terrain is so irregular it cannot be reasonably well approximated by a single curve, the line-of-sight knife-edge formulas of section 7 may be applicable.
4. Interpolation between curves in an atlas, or standard propagation curves such as those given in appendix I, may provide a satisfactory estimate. A useful set of calculations for $\theta = 0$ is given by Domb and Pryce [1947].
5. Empirical curves drawn through data appropriate for the problem of interest may be useful. For example, the dashed curves of figures I.1-I.3 show how values of attenuation relative to free space vary with distance and frequency for a large sample of recordings of television signals over random paths. The data shown in figures I.1-I.4 correspond to a more careful selection of receiving locations and to a greater variety of terrain and climatic conditions.

5.2 Line-of-Sight Propagation Over a Smooth or Uniformly Rough Spherical Earth

The simplest ray optics formulas assume that the field at a receiving antenna is made up to two components, one associated with a direct ray having a path length r_0 , and the other associated with a ray reflected from a point on the surface, with equal grazing angles ψ . The reflected ray has a path length $r_1 + r_2$. The field arriving at the receiver via the direct ray differs from the field arriving via the reflected ray by a phase angle which is a function of the path length difference, $\Delta r = r_1 + r_2 - r_0$, illustrated in figure 5.1. The reflected ray field is also modified by an effective reflection coefficient R_e and associated phase lag $(\pi - c)$, which depend on the conductivity, permittivity, roughness, and curvature of the reflecting surface, as well as upon the ratio of the products of antenna gain patterns in the directions of direct and reflected ray paths.

Let g_{o1} and g_{o2} represent the directive gain for each antenna in the direction of the other, assuming antenna polarizations to be matched. Similar factors g_{r1} and g_{r2} are defined for each antenna in the direction of the point of ground reflection. The effective reflection coefficient R_e is then

$$R_e = DR \left(\frac{g_{r1} g_{r2}}{g_{o1} g_{o2}} \right)^{1/2} \exp \left(\frac{-0.6 \sigma_h \sin \psi}{\lambda} \right) \quad (5.1)$$

where the divergence factor D allows for the divergence of energy reflected from a curved surface, and may be approximated as

$$D = \left[1 + \frac{2d_1 d_2}{a d \tan \psi} \right]^{-1/2} \quad (5.2)$$

A more exact expression for the divergence factor, D , based on geometric optics was derived by Riblet and Barker [1948]. The term R represents the magnitude of the theoretical coefficient, $R \exp[-i(\pi - c)]$, for reflection of a plane wave from a smooth plane surface of a given conductivity and dielectric constant. In most cases c may be set equal to zero and R is very nearly unity. A notable exception for vertical polarization over sea water is discussed in annex III. Values of R and c vs ψ are shown on figures III.1 to III.8 for both vertical and horizontal polarization over good, average, and poor ground, and over sea water.

The grazing angle ψ and the other geometrical parameters d , d_1 , d_2 , and a are shown on figure 5.1. The terrain roughness factor, σ_h , defined in section 5.2.2, and the radio wave length, λ , are expressed in the same units. The exponent $(\sigma_h \sin \psi)/\lambda$ is Rayleigh's criterion of roughness.

If the product $DR \exp(-0.6 \sigma_h \sin \psi / \lambda)$ is less than $\sqrt{\sin \psi}$, and is less than 0.5, ground reflection may be assumed to be entirely diffuse and R_e is then expressed as

$$R_e = \left[\frac{g_{r1} g_{r2}}{g_{o1} g_{o2}} \sin \psi \right]^{1/2} \quad (5.3)$$

where terrain factors D , R and σ_h are ignored. The factor $g_{r1} g_{r2} / g_{o1} g_{o2}$ in (5.3) makes R_e approach zero when narrow-beam antennas are used to discriminate against ground reflections.

For a single ground reflection, the attenuation relative to free space may be obtained from the general formula

$$A = -10 \log \left\{ g_{o1} g_{o2} \left[1 + R_e^2 - 2 R_e \cos \left(\frac{2\pi \Delta r}{\lambda} - c \right) \right] \right\} + G_p + A_a \quad \text{db} \quad (5.4)$$

where the path antenna gain G_p may not be equal to the sum of the maximum antenna gains. Losses A_a due to atmospheric absorption, given by (3.4), may be important at frequencies above 1 GHz. The basic transmission loss L_b is

$$L_b = 32.45 + 20 \log f + 20 \log r + A. \quad (5.5)$$

Over a smooth perfectly-conducting surface, $R_e = 1$ and $c = 0$. Assuming also that free space antenna gains are realized so that $G_p = 10 \log(g_{o1} g_{o2})$, the attenuation relative to free space is

$$A = -6 - 10 \log \sin^2 (\pi \Delta r / \lambda) \quad \text{db.} \quad (5.6)$$

Exact formulas for computing Δr are given in annex III. The appropriate approximations given in (5.9) to (5.13) suffice for most practical applications. If Δr is less than 0.12λ , (5.4) may underestimate the attenuation and one of the methods of section 5.1 should be used.

Section 5.2.1 shows how to define antenna heights h_1' and h_2' above a plane earth, or above a plane tangent to the earth at the point of reflection. The grazing angle ψ is then defined by

$$\tan \psi = h_1' / d_1 = h_2' / d_2 \quad (5.7)$$

where heights and distances are in kilometers and d_1 and d_2 are distances from each antenna to the point of specular reflection:

$$d_1 + d_2 = d, \quad d_1 = d(1 + h'_2/h'_1)^{-1}, \quad d_2 = d(1 + h'_1/h'_2)^{-1}, \quad (5.8a)$$

The distances d_1 and d_2 may be approximated for a spherical earth by substituting antenna heights h_1 and h_2 above the earth for the heights h'_1 and h'_2 in (5.8a). Then these heights may be calculated as

$$h'_1 = h_1 - d_1^2/(2a), \quad h'_2 = h_2 - d_2^2/(2a) \quad (5.8b)$$

for an earth of effective radius a , and substituted in (5.8a) to obtain improved estimates of d_1 and d_2 . Iterating between (5.8a) and (5.8b), any desired degree of accuracy may be obtained.

The path length difference between direct and ground reflected rays is

$$\Delta r = \sqrt{d^2 + (h'_1 + h'_2)^2} - \sqrt{d^2 + (h'_1 - h'_2)^2} \cong 2h'_1 h'_2 / d \quad (5.9)$$

where the approximation in (5.9) is valid for small grazing angles.

Referring to (5.5) the greatest distance, d_0 , for which A is zero, (assuming that $R_0 = 1$ and that free space gains are realized) occurs when $\Delta r = \lambda/6$. From (5.9) $\Delta r \cong 2h'_1 h'_2 / d$; therefore:

$$d_0 = 12 h'_1 h'_2 / \lambda. \quad (5.10a)$$

This equation may be solved graphically, or by iteration, choosing a series of values for d_0 , solving (5.8) for h'_1 , h'_2 , and testing the equality in (5.10a).

For the special case of equal antenna heights over a spherical earth of radius a , the distance d_0 may be obtained as follows:

$$\Delta r = \lambda/6 = \frac{2}{d_0} \left[h - d_0^2/(8a) \right]^2 = 2h^2/d_0 - h d_0/(2a) + d_0^3/(32a^2) \quad (5.10b)$$

where

$$d_1 = d_2 = d/2, \quad h_1 = h_2 = h, \quad \text{and} \quad h' = h - d_0^2/(8a).$$

For this special case where $h_1 = h_2$ over a smooth spherical earth of radius a , the angle ψ may be defined as

$$\tan \psi = 2h/d - d/(4a) \quad (5.11a)$$

and

$$\Delta r = d(\sec \psi - 1) = d \left[\sqrt{1 + \tan^2 \psi} - 1 \right]. \quad (5.11b)$$

Let θ_h represent the angle of elevation of the direct ray r_0 relative to the horizontal at the lower antenna, h_1 , assume that $h_1 \ll h_2$, $h_1 \ll 9a\psi^2/2$, and that the grazing angle, ψ , is small; then, over a spherical earth of effective radius a ,

$$\Delta r \cong 2h_1 \sin \psi \cong h_1 \left[\sqrt{\theta_h^2 + 4h_1/(3a) + \theta_h} \right] \quad (5.12)$$

whether θ_h is positive or negative. For $\theta_h = 0$, $d_1 \cong 2h_1/(3\psi)$.

Two very useful approximations for Δr are

$$\Delta r \cong 2\psi^2 d_1 d_2 / d \cong 2h_1 \sin \psi \text{ kilometers} \quad (5.13)$$

and the corresponding expressions for the path length difference in electrical radians and in electrical degrees are

$$2\pi\Delta r/\lambda = 41.917 f h_1^2 h_2^2 / d = 41.917 f \psi^2 d_1 d_2 / d \cong 42 f h_1 \sin \psi \text{ radians} \quad (5.14a)$$

$$360\Delta r/\lambda = 2401.7 f h_1^2 h_2^2 / d = 2401.7 f \psi^2 d_1 d_2 / d \cong 2402 f h_1 \sin \psi \text{ degrees} \quad (5.14b)$$

where f is the radio frequency in MHz and all heights and distances are in kilometers. The last approximation in (5.13) should be used only if h_1 is small and less than $h_2/20$, as it involves neglecting $d_1^2/(2a)$ relative to h_1 in (5.8) and assuming that $d_2 \cong d$.

As noted following (5.5), ray optics formulas are limited to grazing angles such that $\Delta r > 0.06\lambda$. With this criterion, and assuming $R_e = 1$, the attenuation A is 15 dB for the corresponding minimum grazing angle

$$\psi_m \cong \sqrt{0.03 \lambda d / (d_1 d_2)} \text{ radians}$$

where antennas are barely intervisible. A comparison with the CCIR Atlas of smooth-earth diffraction curves shows that the attenuation relative to free space varies from 10 to 20 decibels for a zero angular distance ($\theta = 0$, $\psi = 0$) except for extremely low antennas.

Figure 5.1a shows how rays will bend above an earth of actual radius $a_0 = 6370$ kilometers, while figure 5.1b shows the same rays drawn as straight lines above an earth of effective radius a . Antenna heights above sea level, h_{ts} and h_{rs} , are usually slightly greater than the effective antenna heights h'_1 and h'_2 , defined in 5.2.1. This difference arises from two circumstances: the smooth curve may be a curve-fit to the terrain instead of representing sea level, and straight rays above an effective earth overestimate the ray bending at high elevations. This latter correction is insignificant unless d is large.

5.2.1 A Curve-Fit to Terrain

A smooth curve is fitted to terrain visible from both antennas. It is used to define antenna heights h_1^t and h_2^r , as well as to determine a single reflection point where the angle of incidence of a ray r_1 is equal to the angle of reflection of a ray r_2 in figure 5.1. This curve is also required to obtain the deviation, σ_h , of terrain heights used in computing R_e in (5.1). Experience has shown that both h_1^t and h_2^r should exceed 0.16λ for the following formulas to be applicable. One of the prediction methods listed in subsection 5.1 may be used where these formulas do not apply.

First, a straight line is fitted by least squares to equidistant heights $h_i(x_i)$ above sea level, and $x_1^2/(2a)$ is then subtracted to allow for the sea level curvature $1/a$ illustrated in figure 6.4. The following equation describes a straight line $h(x)$ fitted to 21 equidistant values of $h_i(x_i)$ for terrain between $x_i = x_0$ and $x_i = x_{20}$ kilometers from the transmitting antenna. The points x_0 and x_{20} are chosen to exclude terrain adjacent to either antenna which is not visible from the other:

$$h(x) = \bar{h} + m(x - \bar{x}) \quad (5.15a)$$

$$\bar{h} = \frac{1}{21} \sum_{i=0}^{20} h_i, \quad \bar{x} = \frac{x_0 + x_{20}}{2}, \quad m = \frac{2 \sum_{i=0}^{20} h_i(i-10)}{77(x_{20} - x_0)} \quad (5.15b)$$

Smooth modified terrain values given by

$$y(x) = h(x) - x^2/(2a) \quad (5.16)$$

will then define a curve of radius a which is extrapolated to include all values of x from $x = 0$ to $x = d$, the positions of the antennas.

The heights of the antennas above this curve are

$$h_1^t = h_{ts} - h(0), \quad h_2^r = h_{rs} - h(d) \quad (5.17)$$

If h_1^t or h_2^r is greater than one kilometer, a correction term, Δh , defined by (6.12) and shown on figure 6.7 is used to reduce the value given by (5.17).

Where terrain is so irregular that it cannot be reasonably well approximated by a single curve, σ_h is large and $R_e = 0$, not because the terrain is very rough, but because it is irregular. In such a situation, method 3 of section 5.1 may be useful.

5.2.2 The terrain roughness factor, σ_h

The terrain roughness factor σ_h in (5.1) is the root-mean-square deviation of modified terrain elevations, y_1 , relative to the smooth curve defined by (5.16), within the limits of the first Fresnel zone in the horizontal reflecting plane. The outline of a first Fresnel zone ellipse is determined by the condition that

$$r_{11} + r_{21} = r_1 + r_2 + \lambda/2$$

where $r_{11} + r_{21}$ is the length of a ray path corresponding to reflection from a point on the edge of the Fresnel zone, and $r_1 + r_2$ is the length of the reflected ray for which angles of incidence and reflection are equal. Norton and Omberg [1947] give general formulas for determining a first Fresnel zone ellipse in the reflecting plane. Formulas are given in annex III for calculating distances x_a and x_b from the transmitter to the two points where the first Fresnel ellipse cuts the great circle plane.

A particularly interesting application of some of the smooth-earth formulas given in this section is the work of Lewin [1962] and others in the design of space-diversity configurations to overcome phase interference fading over line-of-sight paths. Diffraction theory may be used to establish an optimum antenna height for protection against long-term power fading, choosing for instance the minimum height at which the attenuation below free space is 20 db for a horizontally uniform atmosphere with the maximum positive gradient of refractivity expected to be encountered. Then the formulas of this section will determine the optimum diversity spacing required to provide for at least one path a similar 20 db protection against multipath from direct and ground-reflected components throughout the entire range of refractivity gradients expected. In general, the refractive index gradient will vary over wider ranges on over-water paths [Ikegami, 1964].

5.3 Some Effects of Cluttered Terrain

The effects of refraction, diffraction, and absorption by trees, hills, and man-made obstacles are often important, especially if a receiving installation is low or is surrounded by obstacles. Absorption of radio energy is probably the least important of these three factors except in cases where the only path for radio energy is directly through some building material or where a radio path extends for a long distance through trees.

Studies made at 3000 MHz indicate that stone buildings and groups of trees so dense that the sky cannot be seen through them should be regarded as opaque objects around which diffraction takes place [McPetrie and Ford, 1946]. At 3000 MHz the loss through a 23-centimeter thick dry brick wall was 12 db and increased to 46 db when the wall was thoroughly soaked with water. A loss of 1.5 db through a dry sash window, and 3 db through a wet one were usual values.

The only objects encountered which showed a loss of less than 10 db at 3000 MHz were thin screens of leafless branches, the trunk of a single tree at a distance exceeding 30 meters, wood-framed windows, tile or slate roofs, and the sides of light wooden huts. Field strengths obtained when a thick belt of leafless trees is between transmitter and receiver are within about 6 db of those computed assuming Fresnel diffraction over an obstacle slightly lower than the trees. Loss through a thin screen of small trees will rarely exceed 6 db if the transmitting antenna can be seen through their trunks. If sky can be seen through the trees, 15 db is the greatest expected loss.

The following empirical relationship for the rate of attenuation in woods has been given by Saxton and Lane [1955]:

$$A_w = d(0.244 \log f - 0.442) \text{ decibels, } (f > 100 \text{ MHz}) \quad (5.18)$$

where A_w is the absorption in decibels through d meters of trees in full leaf at a frequency f megahertz.

The situation with a high and a low antenna in which the low antenna is located a small distance from and at a lower height than a thick stand of trees is quite different from the situation in which both antennas may be located in the woods. Recent studies at approximately 500 MHz show the depression of signal strengths below smooth earth values as a function of clearing depth, defined as the distance from the lower antenna to the edge of the woods [Head, 1960]. The following empirical relation is established:

$$\Delta_c = 52 - 12 \log d_c \text{ decibels} \quad (5.19)$$

where Δ_c is the depression of the field strength level below smooth earth values and d_c is the clearing depth in meters.

5.4 Sample Calculation of Line-of-Sight Predictions

Attenuation relative to free space is predicted for a short line-of-sight path shown in figure 5.2. Measurements at a frequency of 100 MHz were made using vertical polarization. The transmitting and receiving antennas are 4 meters and 9 meters, respectively, above ground.

A straight line is fitted by least squares to the terrain visible from both antennas. Terrain near the transmitter is excluded because it is shadowed by high foreground terrain. Twenty-one equidistant points $x_i = x_0, x_1, \dots, x_{20}$ are chosen as shown on figure 5.2a and the corresponding terrain heights, h_i , are read. From (5.15) the average terrain height \bar{h} is 1531.8 m, the average distance \bar{x} is 13.0 km, and the slope m is -6.0 meters per kilometer. The equation for the straight line is then

$$h(x) = 1531.8 - 6(x-13) \text{ m} = 1.5318 - 6(x-13) \cdot 10^{-3} \text{ km.}$$

An effective earth's radius, a , is obtained using figure 4.1 and equations (4.3) and (4.4). For this area in Colorado N_s is 280 and $a = 8200$ km. From (5.16) the adjustment to allow for the sea level curvature is

$$y(x) = h(x) - x^2 / (16,400) \text{ km.}$$

Figure 5.2b shows the curve $y(x)$ vs x and terrain which has been modified to allow for the sea level curvature.

At the transmitter, $x = 0$ and $h(x = 0)$ is 1609.5 m. At the receiver, $x = d = 19.75$ km and $h(x = 19.75)$ is 1491.4 m. From (5.17) the antenna heights above the smooth reflecting plane are then:

$$h_1^t = h_{ts} - h(0) = 1647.1 - 1609.5 = 37.6 \text{ m} = 0.0376 \text{ km,}$$

$$h_2^r = h_{rs} - h(d) = 1524.0 - 1491.4 = 32.6 \text{ m} = 0.0326 \text{ km,}$$

where $h_{ts} = 1647.1$ m and $h_{rs} = 1524.0$ m are the heights above sea level at the transmitter and receiver respectively. At 100 MHz ($\lambda = 3$ m), the criterion that both h_1^t and h_2^r must exceed 0.16λ is met. Neither h_1^t nor h_2^r exceeds one kilometer, so no correction factor Δh is required. From (5.6) and (5.7) the distances d_1 and d_2 from each antenna to the point of specular reflection are

$$d_1 = d(1 + h_2^t/h_1^t)^{-1} = 10.58 \text{ km, } d_2 = d(1 + h_1^t/h_2^t)^{-1} = 9.17 \text{ km,}$$

and the grazing angle ψ is

$$\tan \psi = h_1^t/d_1 = h_2^r/d_2 = 0.003554$$

$$\psi = 0.003554 \text{ radians.}$$

From (5.4) the path length difference, Δr , between direct and reflected rays is

$$\Delta r = \left[d^2 + (h_1' + h_2')^2 \right]^{\frac{1}{2}} - \left[d^2 + (h_1' - h_2')^2 \right]^{\frac{1}{2}} = 1.2413 \times 10^{-4} \text{ km.}$$

The approximation

$$\Delta r \approx 2h_1'h_2'/d = 1.2413 \times 10^{-4} \text{ km} = 0.124 \text{ m} \approx 0.04\lambda$$

is also valid in this case. Note that Δr is less than 0.12λ and optical methods including a divergence factor may underestimate the attenuation.

One should note that important reflections might occur from the high ground near the transmitter. In this case the reflecting plane would correspond to the foreground terrain giving $h_1' = 4 \text{ m}$, $h_2' = 50 \text{ m}$, $d_1 = 1.53 \text{ km}$, $d_2 = 18.22 \text{ km}$ and $\Delta r = 0.02 \text{ m}$ which is much less than 0.16λ . Optical methods would not be applicable here.

The attenuation relative to free space may be estimated using one of the methods described in subsection 5.1. Of these, methods 4 and 5 would apply in this case. Choosing heights $h_1 = 4 \text{ m}$, $h_2 = 25 \text{ m}$, as heights above foreground terrain, the theoretical smooth earth curves in the CCIR Atlas [1959] show the predicted field to be about 36 db below the free space value. The "standard" propagation curves, annex I, figure I.7, drawn for 100 MHz and $h_1 = h_2 = 30 \text{ meters}$ show the median basic transmission loss to be about 15 dB below the free space loss. Greater attenuation would be expected with lower antennas over irregular terrain. Method 5 using the empirical curve through data recorded at random locations, annex I, figure I.1 shows the attenuation to be about 20 dB below free space. These data were recorded with an average transmitter height of about 250 m, and a receiver height of 10 m.

For the very low antennas used on this Colorado path one would expect the losses to exceed the values shown on figures I.7 and I.1, and also to exceed the theoretical smooth earth value of $A \approx 36 \text{ db}$ obtained from the CCIR Atlas. Spot measurements yield a value of about 40 db.

If a prediction were desired for transmission over the same path at 300 MHz, $\lambda = 1 \text{ m}$, then $\Delta r = 0.124 \text{ m}$ is slightly greater than 0.12λ and optical methods could be used. Using the value $\Delta r = 0.124 \text{ m}$ the path length difference in electrical radians $2\pi\Delta r/\lambda = 0.7805$ radians. As a check, this quantity may be computed using (5.14a):

$$\begin{aligned} 2\pi\Delta r/\lambda &= 41.917 fh_1'h_2'/d = 0.7805 \text{ radians} \\ &= 44.7 \text{ degrees.} \end{aligned}$$

Equation (5.4) shows the attenuation relative to free space assuming a single ground reflection from the smooth curve $y(x)$, figure 5.2b. Assuming that free space gains are realized so that $G_p = 10 \log g_{01} g_{02}$ the equation may be written

$$A = -10 \log \left[1 + R_e^2 - 2R_e \cos \left(\frac{2\pi \Delta r}{\lambda} - c \right) \right]$$

where R_e is the effective reflection coefficient defined by (5.1):

$$R_e = DR \left(\frac{g_{r1} g_{r2}}{g_{o1} g_{o2}} \right)^{\frac{1}{2}} \exp \left(\frac{-0.6 \sigma_h \sin \psi}{\lambda} \right).$$

With $f = 300$ MHz, and $\tan \psi = 0.003554$, figure III.3, annex III shows the theoretical reflection coefficient $R = 0.97$ and the phase shift $c = 0$ for vertical polarization over average ground. The angle between the direct and the reflected ray is small so the ratio of gains in (5.1) may be considered to be unity. The divergence factor D and effective reflection coefficient R_e are

$$D = \left(1 + \frac{2d_1 d_2}{ad \tan \psi} \right)^{-\frac{1}{2}} = 0.865$$

$$R_e = 0.839 \exp \left(\frac{-0.6 \sigma_h \sin \psi}{\lambda} \right).$$

The terrain roughness factor, σ_h , is the root-mean-square deviation of modified terrain elevations relative to the curve $y(x)$ within the limits of the first Fresnel zone in the horizontal reflecting plane. The first Fresnel ellipse cuts the great circle plane at two points x_a and x_b kilometers from the transmitter. The distances x_a and x_b may be computed using equations (III.18) or (III.19) to (III.21) of annex III,

$$B = 0.135, \quad x_0 = 10.02, \quad x_1 = 9.12$$

$$x_a = x_0 - x_1 = 0.90 \text{ km}, \quad x_b = x_0 + x_1 = 19.14 \text{ km}$$

The first Fresnel zone cuts the great circle plane at points 0.9 and 19.14 km from the transmitter with an intervening distance of 18.24 km. Equidistant points are chosen at $x = 1, 2, \dots, 19$ and corresponding modified terrain heights and values of $y(x)$ are obtained. With height differences in kilometers:

$$\sigma_h^2 = \sum_{j=1}^{19} (y_j - h_j)^2 / 19, \quad \sigma_h = 0.008222.$$

The effective reflection coefficient is then

$$R_e = 0.839 \exp - 0.01753 = 0.824$$

which is greater than 0.5 and greater than $\sqrt{\sin \psi}$. The predicted attenuation relative to free space A is then

$$-10 \log \left[1 + R_c^2 - 2R_c \cos \frac{2\pi \Delta r}{\lambda} - c \right] = -10 \log [1.6793 - 1.6484 \cos 0.7805] \approx 3 \text{ db.}$$

Due to diffraction effects over irregular terrain, the attenuation A is often observed to be much greater than the values corresponding to the ray theory calculations illustrated in this example. Ray theory is most useful to identify the location and depth of nulls in an interference pattern in the region visible to two antennas. Figure 5.3 shows an interference pattern from an aircraft at 10,000 ft., transmitting on 328.2 MHz. Measured values compared with theoretical curves based on ray theory are shown on the figure.

GEOMETRY FOR WITHIN-THE-HORIZON PATHS

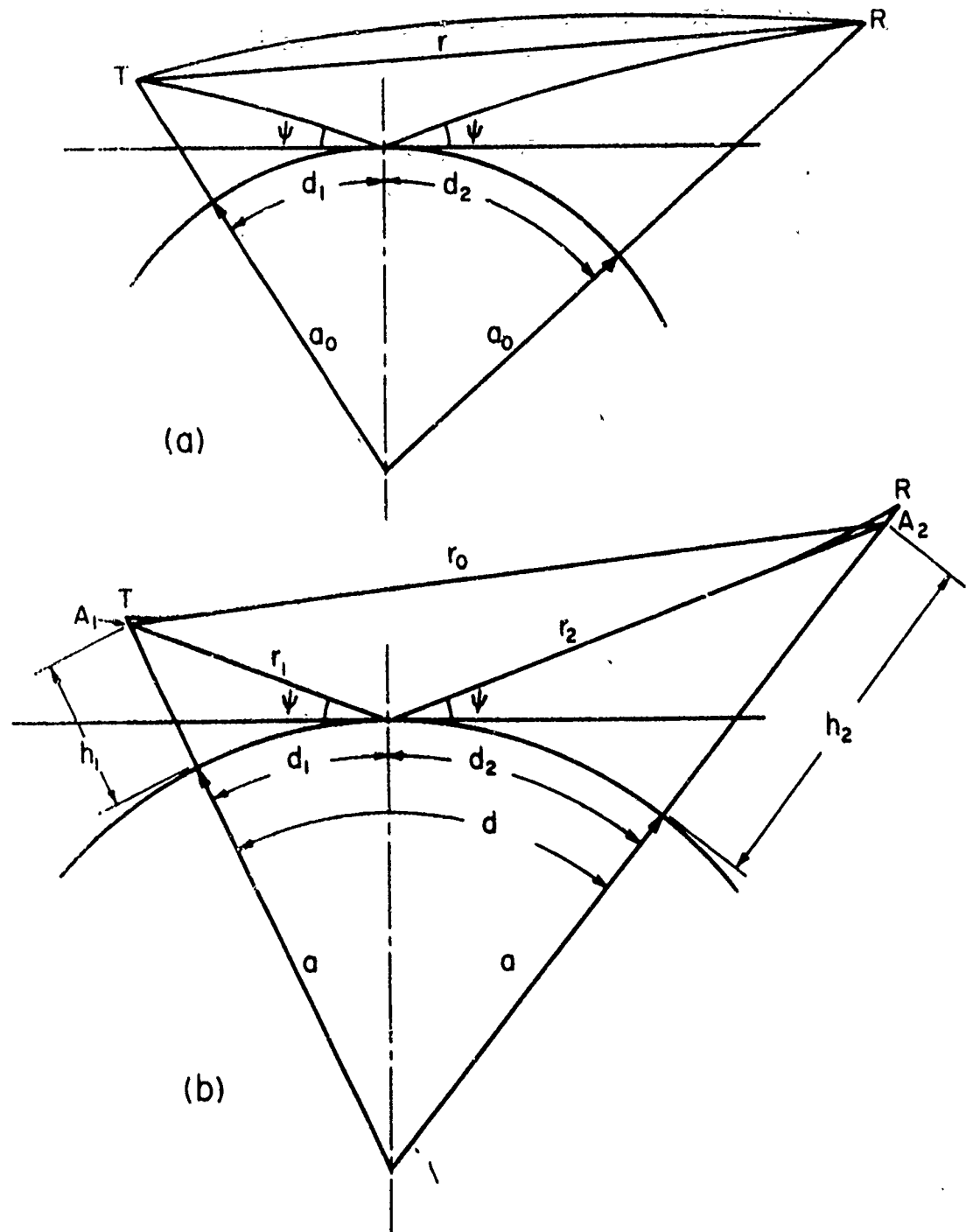


Figure 5.1

A LINE-OF-SIGHT PATH NEAR BOULDER, COLORADO
 $f=100$ AND 300 MHz, $h_{tg}=4$ m, $h_{rg}=9$ m

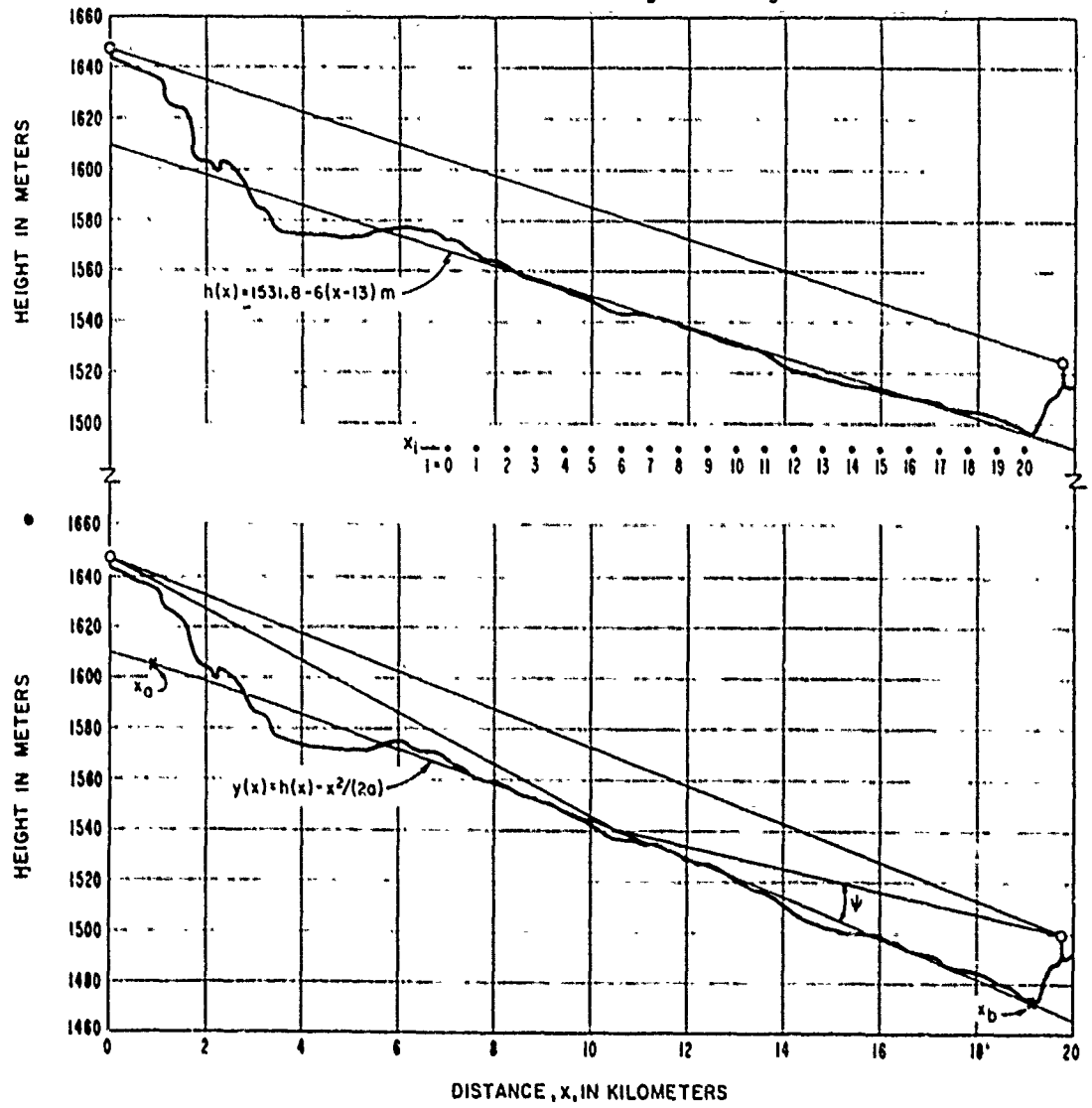


Figure 5.2

**OBSERVED INPUT VOLTAGE VARIATION AT GROUND STATION RECEIVER
FROM AN AIRCRAFT AT 10,000 FEET TRANSMITTING ON 328.2 MHz**
 TRANSMITTER POWER: 6 WATTS; TRANSMITTING AND RECEIVING ANTENNA GAIN: 2.15 db (RELATIVE TO AN ISOTROPIC)
 GROUND ANTENNA HEIGHT: 75 FEET; TRANSMISSION OVER WATER; 6 db COMMUNICATIONS SYSTEM LOSS ASSUMED FOR THEORETICAL CURVES

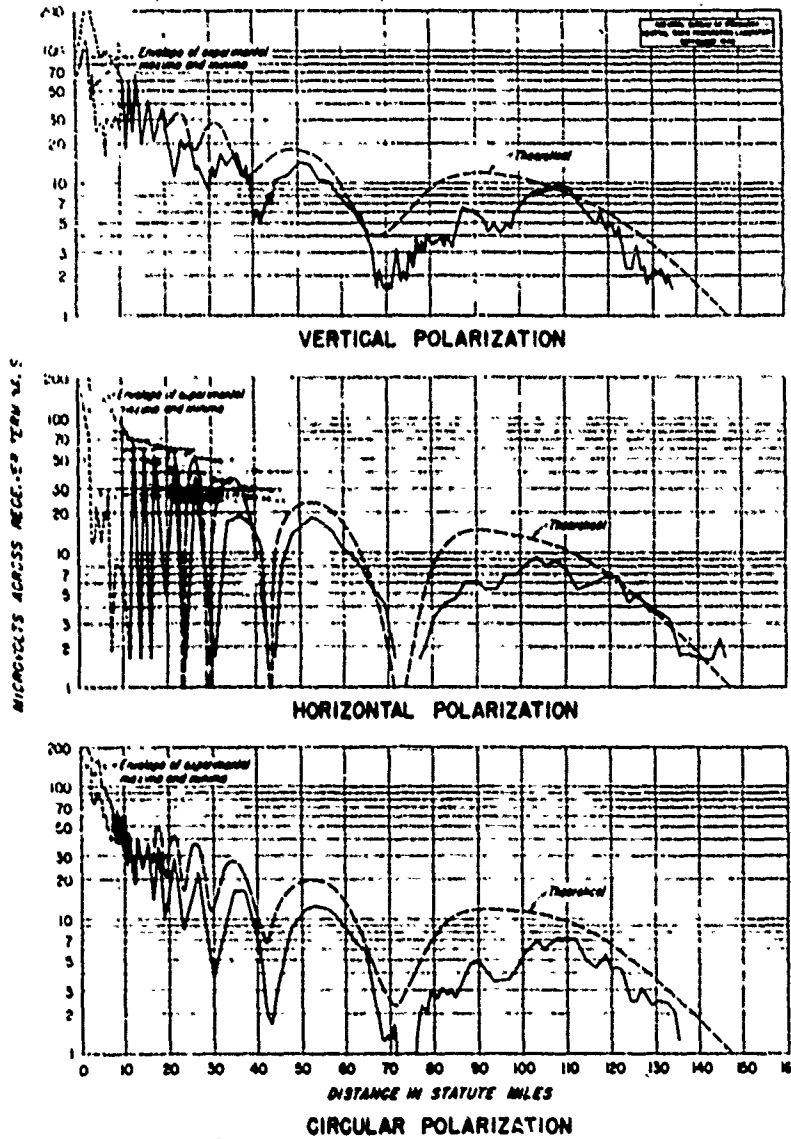


Figure 5.3

6. DETERMINATION OF ANGULAR DISTANCE FOR TRANSHORIZON PATHS

The angular distance, θ , is the angle between radio horizon rays in the great circle plane defined by the antenna locations. This important parameter is used in diffraction theory as well as in forward scatter theory. Angular distance depends upon the terrain profile, as illustrated in figure 6.1, and upon the bending of radio rays in the atmosphere. Figure 6.1 assumes a linear dependence on height of the atmospheric refractive index, n , which implies a nearly constant rate of ray refraction. If heights to be considered are less than one kilometer above the earth's surface, the assumption of a constant effective earth's radius, a , makes an adequate allowance for ray bending. Atmospheric refractivity $N = (n - 1) \times 10^6$ more than one kilometer above the earth's surface, however, is assumed to decay exponentially with height [Bean and Thayer, 1959]. This requires corrections to the effective earth's radius formulas, as indicated in subsection 6.4.

To calculate θ , one must first plot the great circle path and determine the radio horizons.

6.1 Plotting a Great Circle Path

For distances less than 70 kilometers, the great circle path can be approximated by a rhumb line, which is a line intersecting all meridians at the same angle. For greater distances, the organization of a map study is illustrated on figure 6.2. Here, a rhumb line is first plotted on an index map to show the boundaries of available detailed topographic sheets. Segments of the actual great circle path are later plotted on these detailed maps.

The spherical triangle used for the computation of points on a great circle path is shown on figure 6.3, where PAB is a spherical triangle, with A and B the antenna terminals, and P the north or south pole. B has a greater latitude than A, and P is in the same hemisphere. The triangle shown is for the northern hemisphere but may readily be inverted to apply to the southern hemisphere. B' is any point along the great circle path from A to B, and the triangle PAB' is the one actually solved. The latitudes of the points are denoted by Φ_A , Φ_B , and $\Phi_{B'}$, while C and C' are the differences in longitude between A and B and A and B', respectively. Z and Z' are the corresponding great circle path lengths. The following formulas are practical for hand computations as well as for automatic digital computers. Equations (6.1) to (6.4) have been taken, in this form, from a well-known reference book [I. T. and T., 1956], where they appear on pages 730-739.

The initial bearings (X from terminal A, and Y from terminal B) are measured from true north, and are calculated as follows:

$$\tan \frac{Y - X}{2} = \cot \frac{C}{2} \left[\frac{\left(\sin \frac{\Phi_B - \Phi_A}{2} \right)}{\left(\cos \frac{\Phi_B + \Phi_A}{2} \right)} \right] \quad (6.1)$$

$$\tan \frac{Y+X}{2} = \cot \frac{C}{2} \left[\left(\cos \frac{\phi_B - \phi_A}{2} \right) / \left(\sin \frac{\phi_B + \phi_A}{2} \right) \right] \quad (6.2)$$

$$\frac{Y+X}{2} + \frac{Y-X}{2} = Y, \quad \text{and} \quad \frac{Y+X}{2} - \frac{Y-X}{2} = X. \quad (6.3)$$

The great circle distance, Z , is given by

$$\tan \frac{Z}{2} = \tan \frac{\phi_B - \phi_A}{2} \left[\left(\sin \frac{Y+X}{2} \right) / \left(\sin \frac{Y-X}{2} \right) \right] \quad (6.4)$$

To convert the angle Z obtained in degrees from (6.4) to units of length, the following is used, based on a mean sea level earth's radius of 6370 km:

$$d_{\text{km}} = 111.18 Z^\circ. \quad (6.5)$$

The following formulas show how to calculate either the latitude or the longitude of a point on the great circle path, when the other coordinate is given. The given coordinates correspond to the edges of detailed maps, and to intermediate points usually about 7.5 minutes apart, so that straight lines between points will adequately approximate a great circle path.

For predominantly east-west paths, calculate the latitude $\phi_{B'}$ for a given longitude difference C' :

$$\cos Y' = \sin X \sin C' \sin \phi_A - \cos X \cos C' \quad (6.6)$$

$$\cos \phi_{B'} = \sin X \cos \phi_A / \sin Y'. \quad (6.7)$$

For predominantly north-south paths, calculate the longitude difference C' for a given latitude $\phi_{B'}$:

$$\sin Y' = \sin X \cos \phi_A / \cos \phi_{B'} \quad (6.8)$$

$$\cot \frac{C'}{2} = \tan \frac{Y' - X}{2} \left[\left(\cos \frac{\phi_{B'} + \phi_A}{2} \right) / \left(\sin \frac{\phi_{B'} - \phi_A}{2} \right) \right]. \quad (6.9)$$

Where the bearing of a path is close to 45 degrees, either method may be used.

6.2 Plotting a Terrain Profile and Determining the Location of Radio Horizon Obstacles

This subsection explains how to determine the sea level arc distance, $d_{Lt,r}$ from an antenna to its radio horizon obstacle, and the height, $h_{Lt,r}$ of this obstacle above mean sea level. The horizon obstacles are represented by the points (d_{Lt}, h_{Lt}) and (d_{Lr}, h_{Lr}) in the great circle plane containing the antennas. These points may be determined by the tops of high buildings, woods, or hills, or may be entirely determined by the bulge of the earth itself. All of the predictions of this paper replace the earth by a cylinder whose elements are perpendicular to the great circle plane and whose cross-section is in general irregular and determined by the antenna and horizon locations in the great circle plane. When the difference in elevations of antenna and horizon greatly exceeds one kilometer, ray tracing is necessary to determine the location of radio horizons accurately [Bean and Thayer, 1959].

Elevations h_i of the terrain are read from topographic maps and tabulated versus their distances x_i from the transmitting antenna. The recorded elevations should include those of successive high and low points along the path. The terrain profile is plotted on linear graph paper by modifying the terrain elevations to include the effect of the average curvature of the radio ray path and of the earth's surface. The modified elevation y_i of any point h_i at a distance x_i from the transmitter along a great circle path is its height above a plane which is horizontal at the transmitting antenna location:

$$y_i = h_i - x_i^2 / (2a) \quad (6.10)$$

where the effective earth's radius, a , in kilometers is calculated using (4.4), or is read from figure 4.2 as a function of N_g . The surface refractivity, N_g , is obtained from (4.3), where N_0 is estimated from the map on figure 4.1.

A plot of y_i versus x_i on linear graph paper is the desired terrain profile. Figure 6.4 shows the profile for a line-of-sight path. The solid curve near the bottom of the figure indicates the shape of a surface of constant elevation ($h = 0$ km). Profiles for a path with one horizon common to both antennas and for a path with two radio horizons are shown in figures 6.5 and 6.6. The vertical scales of these three figures are exaggerated in order to provide a sufficiently detailed representation of terrain irregularities. Plotting terrain elevations vertically instead of radially from the earth's center leads to negligible errors where vertical changes are small relative to distances along the profile.

On a cartesian plot of y_i versus x_i , as illustrated in figures 6.4, 6.5, and 6.6, the ray from each antenna to its horizon is a straight line, provided the difference in antenna and horizon elevations is less than one kilometer. Procedures to be followed where this is not the case are indicated in the next subsection.

6.3 Calculation of Effective Antenna Heights for Transhorizon Paths

If an antenna is located on another structure, or on a steep cliff or mountainside, the height of this structure, cliff, or mountain above the surrounding terrain should be included as part of the antenna height. To obtain the effective height of the transmitting antenna, the average height above sea level \bar{h}_t of the central 80 per cent of the terrain between the transmitter and its horizon is determined. The following formula may be used to compute \bar{h}_t for 31 evenly spaced terrain elevations h_{ti} for $i = 0, 1, 2, \dots, 30$, where h_{t0} is the height above sea level of the ground below the transmitting antenna, and, $h_{t30} = h_{Lt}$:

$$\bar{h}_t = \frac{1}{25} \sum_{i=3}^{27} h_{ti}, \quad h_t = h_{ts} - \bar{h}_t \text{ for } \bar{h}_t < h_{t0}; \quad (6.11a)$$

otherwise

$$h_t = h_{ts} - h_{t0} \quad (6.11b)$$

where h_{ts} is the height of the transmitting antenna above mean sea level. The height h_r is similarly defined.

If h_t or h_r as defined above is less than one kilometer, $h_{te} = h_t$ or $h_{re} = h_r$. For antennas higher than one kilometer, a correction Δh_e , read from figure 6.7, is used to reduce h_t or h_r to the value h_{te} or h_{re} :

$$h_{te} = h_t - \Delta h_e(h_t, N_s), \quad h_{re} = h_r - \Delta h_e(h_r, N_s). \quad (6.12)$$

The correction Δh was obtained by ray tracing methods described by Bean and Thayer [1959]. For a given effective earth's radius, the effective antenna height h_{te} corresponding to a given horizon distance d_{Lt} is smaller than the actual antenna height, h_t . Over a smooth spherical earth with $h_{te} < 1$ km and $h_{re} < 1$ km, the following approximate relationship exists between effective antenna heights and horizon distances:

$$h_{te} = d_{Lt}^2 / (2a), \quad h_{re} = d_{Lr}^2 / (2a) \quad (6.13a)$$

If the straight line distance r between antennas is substantially different from the sea level arc distance d , as in communication between an earth terminal and a satellite, the effective antenna heights must satisfy the exact relation:

$$h_{te} = a[\sec(d_{Lt}/a) - 1], \quad h_{re} = a[\sec(d_{Lr}/a) - 1] \quad (6.13b)$$

6.4 Calculation of the Angular Distance, θ

The angular distance, θ , is the angle between horizon rays in the great circle plane, and is the minimum diffraction angle or scattering angle unless antenna beams are elevated. Calculations for cases where the antenna beams are elevated are given in annex III.

In calculating the angular distance, one first calculates the angles θ_{et} and θ_{er} by which horizon rays are elevated or depressed relative to the horizontal at each antenna, as shown on figure 6.1. In this report, all heights and distances are measured in kilometers, and angles are in radians unless otherwise specified. When the product θd is less than 2,

$$\theta = \theta_{oo} = d/a + \theta_{et} + \theta_{er} \quad (6.14)$$

where a in (6.14) is the effective earth's radius defined in section 4. The horizon ray elevation angles θ_{et} and θ_{er} may be measured with surveying instruments in the field, or determined directly from a terrain profile plot such as that of figure 6.5 or 6.6, but are usually computed using the following equations:

$$\theta_{et} = \frac{h_{Lt} - h_{ts}}{d_{Lt}} - \frac{d_{Lt}}{2a}, \quad \theta_{er} = \frac{h_{Lr} - h_{rs}}{d_{Lr}} - \frac{d_{Lr}}{2a} \quad (6.15)$$

where h_{Lt} , h_{Lr} are heights of horizon obstacles, and h_{ts} , h_{rs} are antenna elevations, all above mean sea level. As a general rule, the location (h_{Lt}, d_{Lt}) or (h_{Lr}, d_{Lr}) of a horizon obstacle is determined from the terrain profile by using (6.15) to test all possible horizon locations. The correct horizon point is the one for which the horizon elevation angle θ_{et} or θ_{er} is a maximum. When the trial values are negative, the maximum is the value nearest zero. For a smooth earth,

$$\theta_{et,er} = -\sqrt{2 h_{te,re}/a} \quad \text{for } h_{te,re} < 1 \text{ km}.$$

At the horizon location, the angular elevation of a horizon ray, θ_{ot} or θ_{or} , is greater than the horizon elevation angle θ_{et} or θ_{er} :

$$\theta_{ot} = \theta_{et} + d_{Lt}/a, \quad \theta_{or} = \theta_{er} + d_{Lr}/a. \quad (6.16)$$

If the earth is smooth, θ_{ot} and θ_{or} are zero, and $\theta \cong D_s/a$, where

$$D_s = d - d_{Lt} - d_{Lr}. \quad (6.17)$$

Figure 6.8, valid only for $\theta_{ot} + \theta_{or} = 0$, is a graph of θ versus D_s for various values of surface refractivity, N_s .

In the general case of irregular terrain, the angles α_{oo} and β_{oo} shown in figure 6.1 are calculated using the following formulas:

$$\alpha_{oo} = \frac{d}{2a} + \theta_{et} + \frac{h_{ts} - h_{rs}}{d} \quad (6.18a)$$

$$\beta_{oo} = \frac{d}{2a} + \theta_{er} + \frac{h_{rs} - h_{ts}}{d} \quad (6.18b)$$

These angles are positive for beyond-horizon paths. To allow for the effects of a non-linear refractivity gradient, α_{oo} and β_{oo} are modified by corrections $\Delta\alpha_o$ and $\Delta\beta_o$ to give the angles α_o and β_o whose sum is the angular distance, θ , and whose ratio defines a path asymmetry factor s :

$$\alpha_o = \alpha_{oo} + \Delta\alpha_o \quad (6.19a)$$

$$\beta_o = \beta_{oo} + \Delta\beta_o \quad (6.19b)$$

$$\theta = \alpha_o + \beta_o, \quad s = \alpha_o / \beta_o \quad (6.19c)$$

The corrections $\Delta\alpha_o$ and $\Delta\beta_o$ are functions of the angles θ_{ot} and θ_{or} , (6.16), and of the distances d_{st} and d_{sr} from each horizon obstacle to the crossover of horizon rays. These distances are approximated as

$$d_{st} = d\beta_{oo}/\theta_{oo} - d_{Lt}, \quad d_{sr} = d\alpha_{oo}/\theta_{oo} - d_{Lr} \quad (6.20)$$

The sum of d_{st} and d_{sr} is the distance D_s between horizon obstacles, defined by (6.17). Over a smooth earth $d_{st} = d_{sr} = D_s/2$.

Figure 6.9, drawn for $N_s = 301$, shows $\Delta\alpha_o$ as a function of θ_{ot} and d_{st} . Similarly, $\Delta\beta_o$ is read from the figure as a function of θ_{or} and d_{sr} . For values of N_s other than 301, the values as read from the figure are multiplied by $C(N_s)$:

$$\Delta\alpha_o(N_s) = C(N_s) \Delta\alpha_o(301), \quad \Delta\beta_o(N_s) = C(N_s) \Delta\beta_o(301) \quad (6.21a)$$

$$C(N_s) = (1.3 N_s^2 - 60 N_s) \times 10^{-5} \quad (6.21b)$$

For instance, $C(250) = 0.66$, $C(301) = 1.0$, $C(350) = 1.38$, and $C(400) = 1.84$. Figure 6.10 shows $C(N_s)$ plotted versus N_s .

For small $\theta_{ot,r}$ no correction $\Delta\alpha_o$ or $\Delta\beta_o$ is required for values of $d_{st,r}$ less than 100 Km. When both $\Delta\alpha_o$ and $\Delta\beta_o$ are negligible:

$$\theta = \theta_{oo} = \alpha_{oo} + \beta_{oo} \quad (6.22)$$

which is the same as (6.14).

If θ_{ot} or θ_{or} is negative, compute

$$d'_{st} = d_{st} - |a\theta_{ot}| \quad \text{or} \quad d'_{sr} = d_{sr} - |a\theta_{or}|, \quad (6.23)$$

substitute d'_{st} for d_{st} or d'_{sr} for d_{sr} , and read figure 6.9, using $\theta_{ot,r} = 0$.

If either θ_{ot} or θ_{or} is greater than 0.1 radian and less than 0.9 radian, determine $\Delta\alpha_o$ or $\Delta\beta_o$ for $\theta_{ot} = 0.1$ radian and add the additional correction term

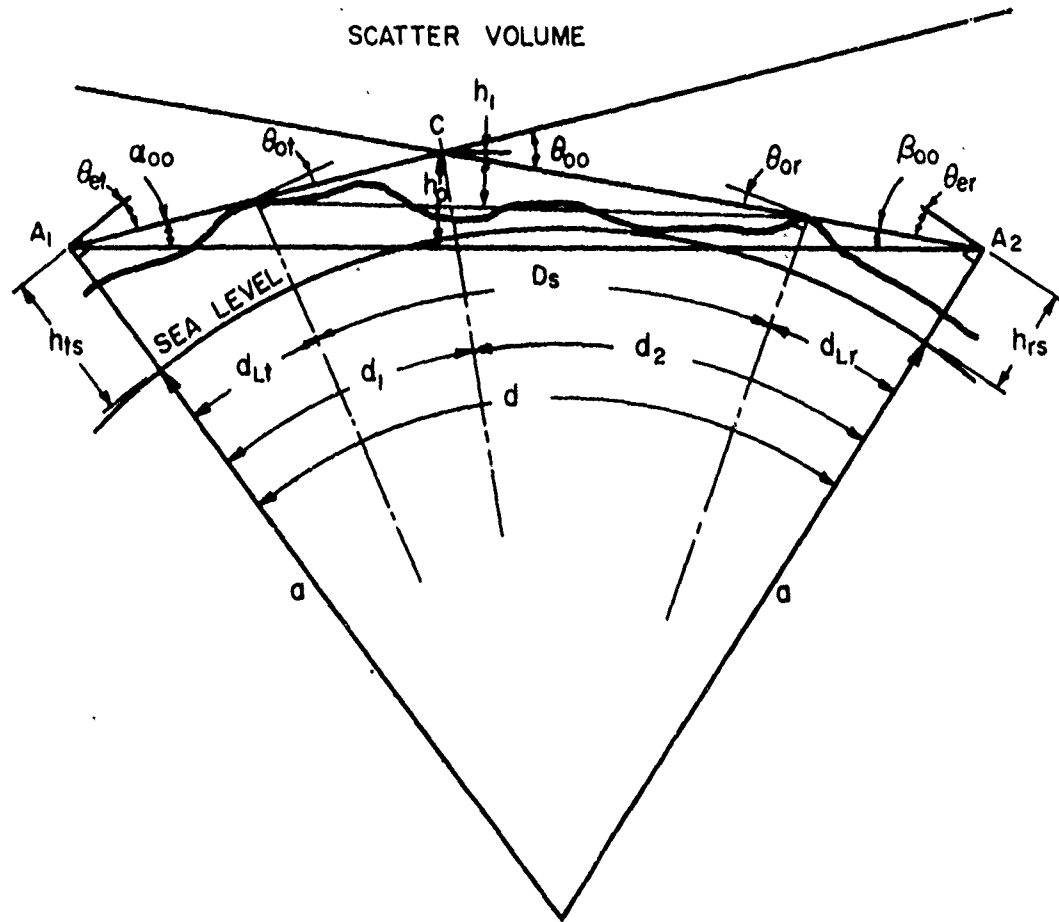
$$N_s (9.97 - \cot\theta_{ot,r}) [1 - \exp(-0.05 d_{st,r})] \times 10^{-6} \text{ radians.}$$

The bending of radio rays elevated more than 0.9 radian above the horizon and passing all the way through the atmosphere is less than 0.0004 radian, and may be neglected.

Other geometrical parameters required for the calculation of expected transmission loss are defined in the sections where they are used.

Many of the graphs in this and subsequent sections assume that $s = \alpha_o/\beta_o \leq 1$, where α_o and β_o are defined by (6.19a) and (6.19b). It is therefore convenient, since the transmission loss is independent of the actual direction of transmission, to denote as the transmitting antenna whichever antenna will make s less than or equal to unity. Alternatively, s may be replaced by $1/s$ and the subscripts t and r may be interchanged in some of the formulas and graphs, as noted in later sections.

PATH GEOMETRY



DISTANCES ARE MEASURED IN KILOMETERS ALONG A GREAT CIRCLE ARC.

$$\theta_{oo} = \frac{D_s}{a} + \theta_{ot} + \theta_{or} = \frac{d}{a} + \theta_{et} + \theta_{er}$$

Figure 6.1

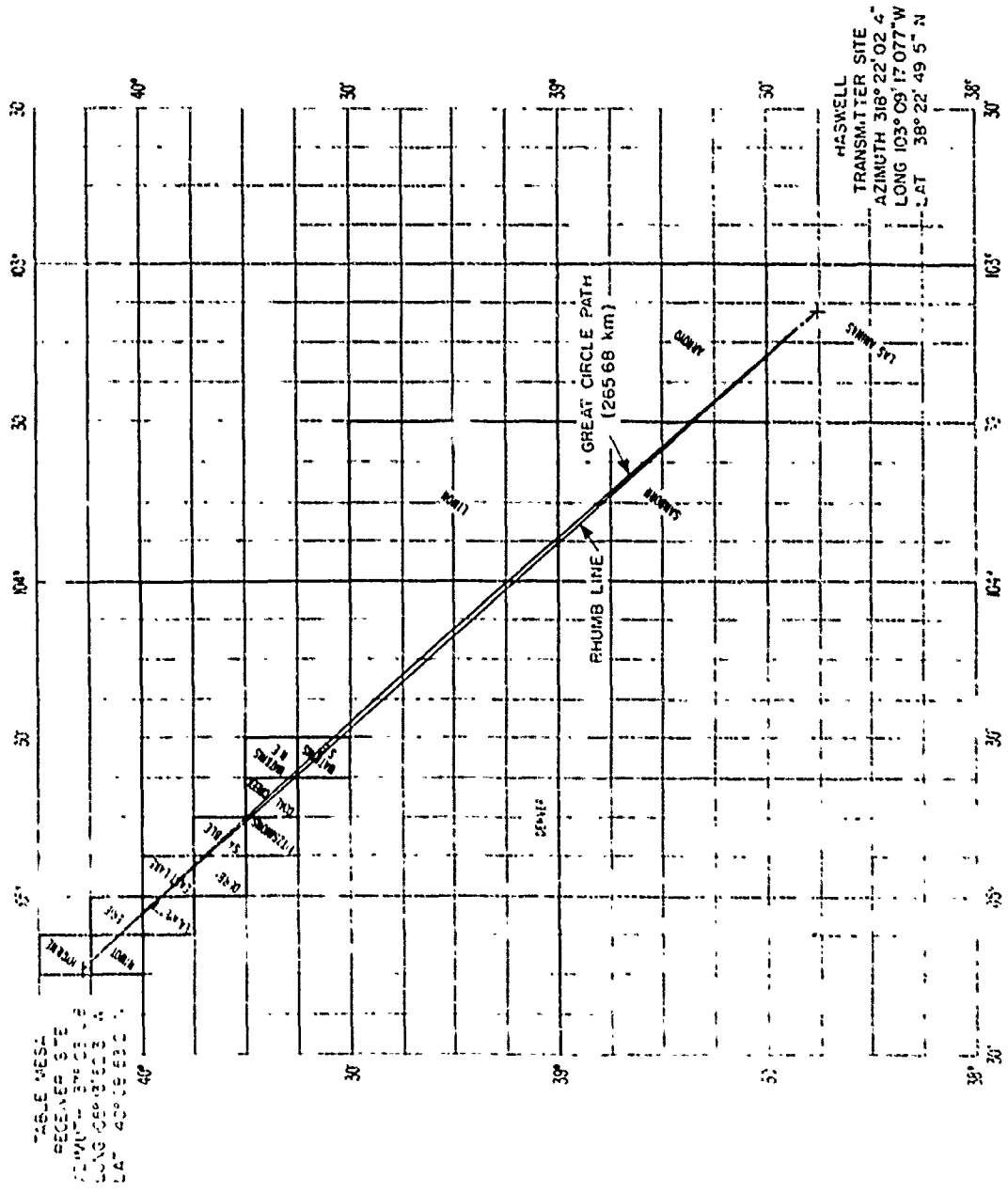
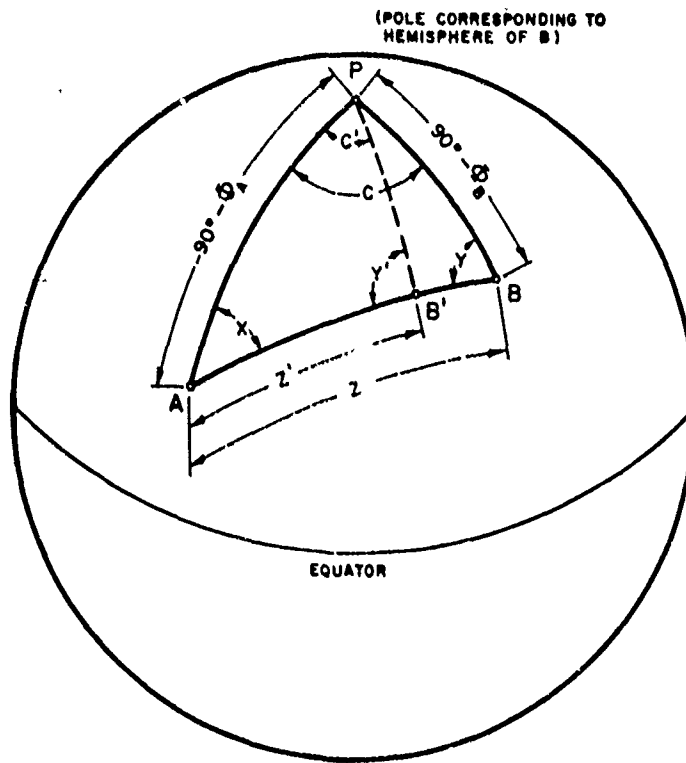


Figure 6.2



SPHERICAL TRIANGLE FOR
GREAT CIRCLE PATH COMPUTATIONS

Figure 6.3

MODIFIED TERRAIN PROFILE FOR A
LINE-OF-SIGHT PATH

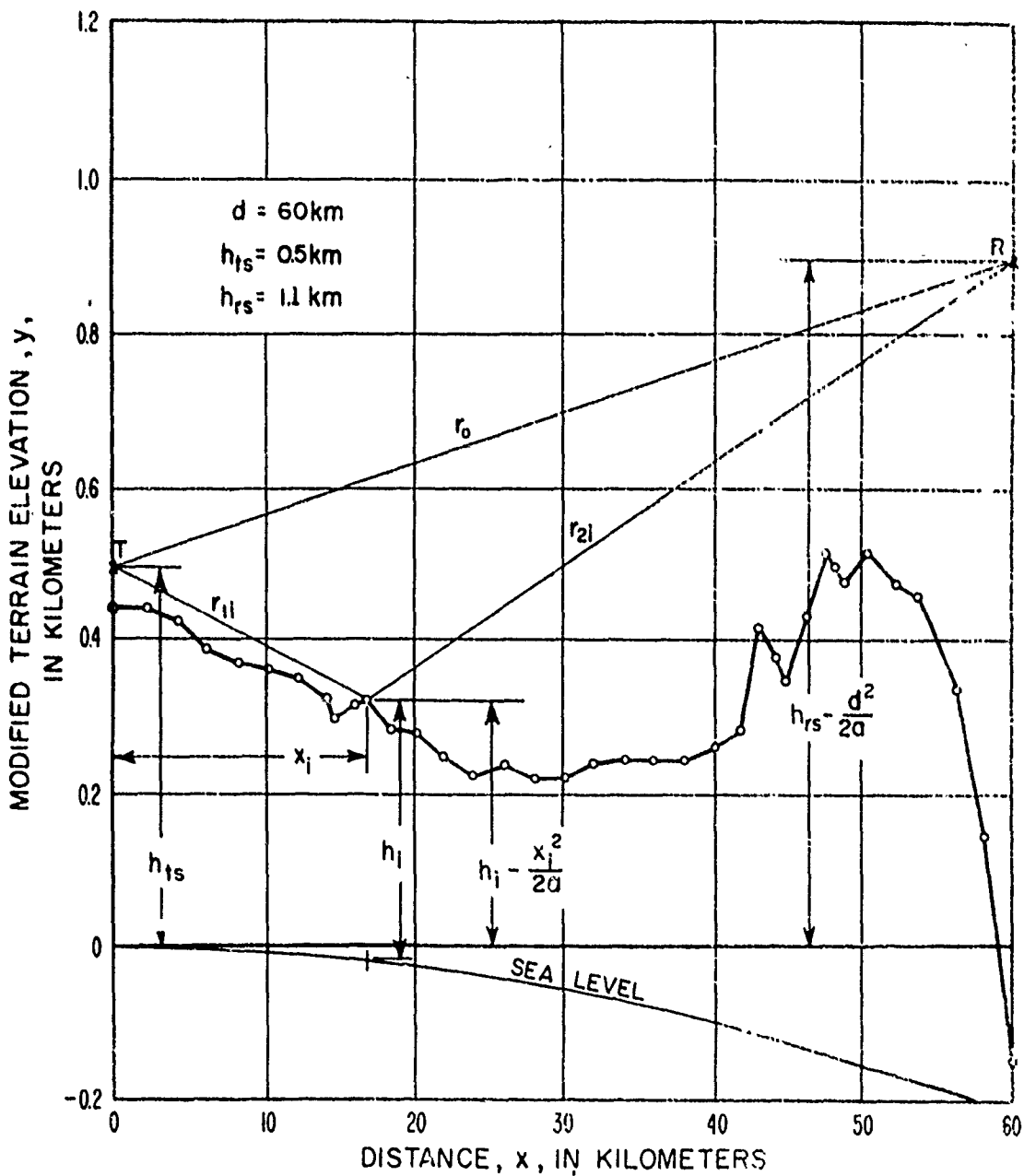


Figure 6.4

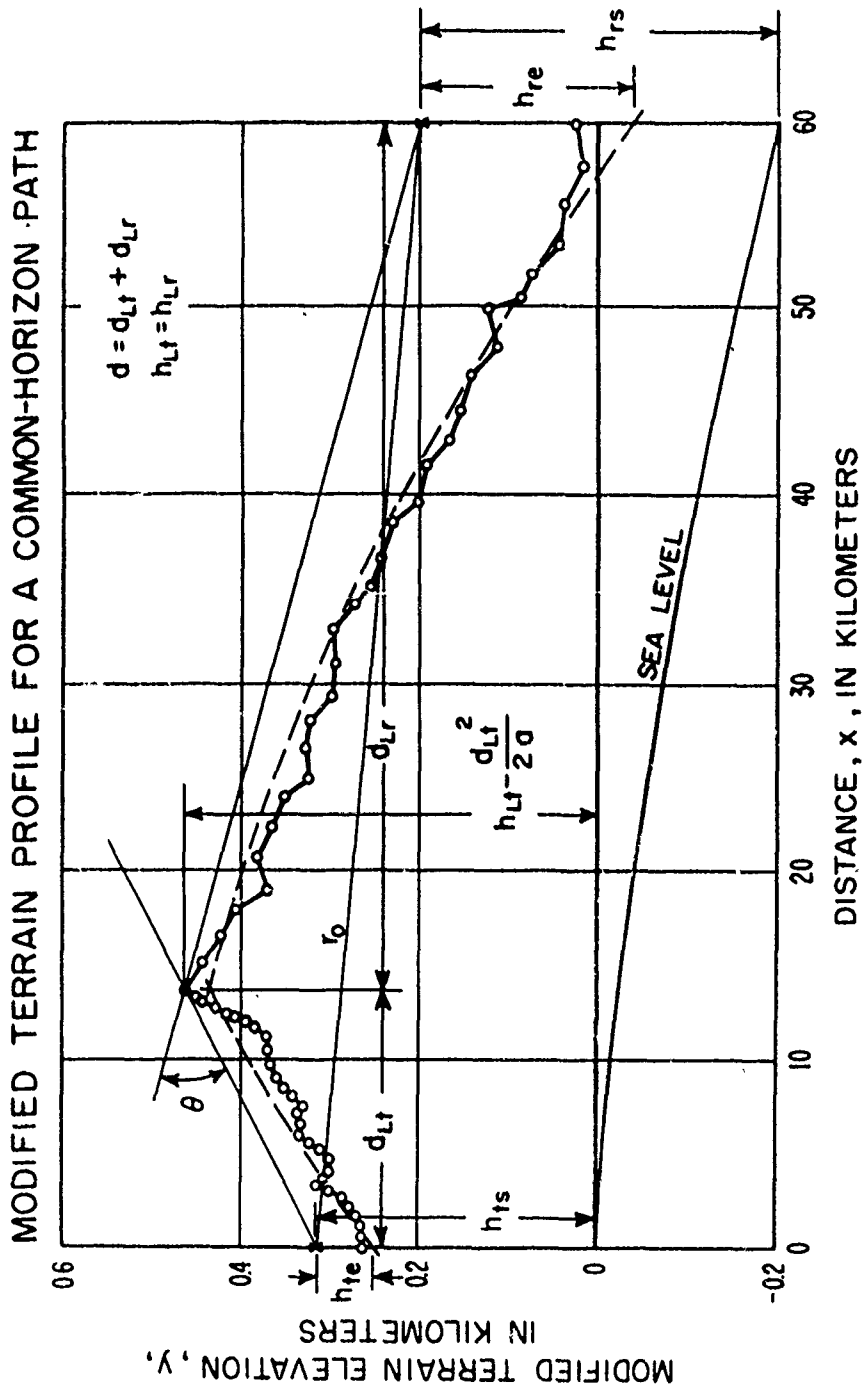


Figure 6.5

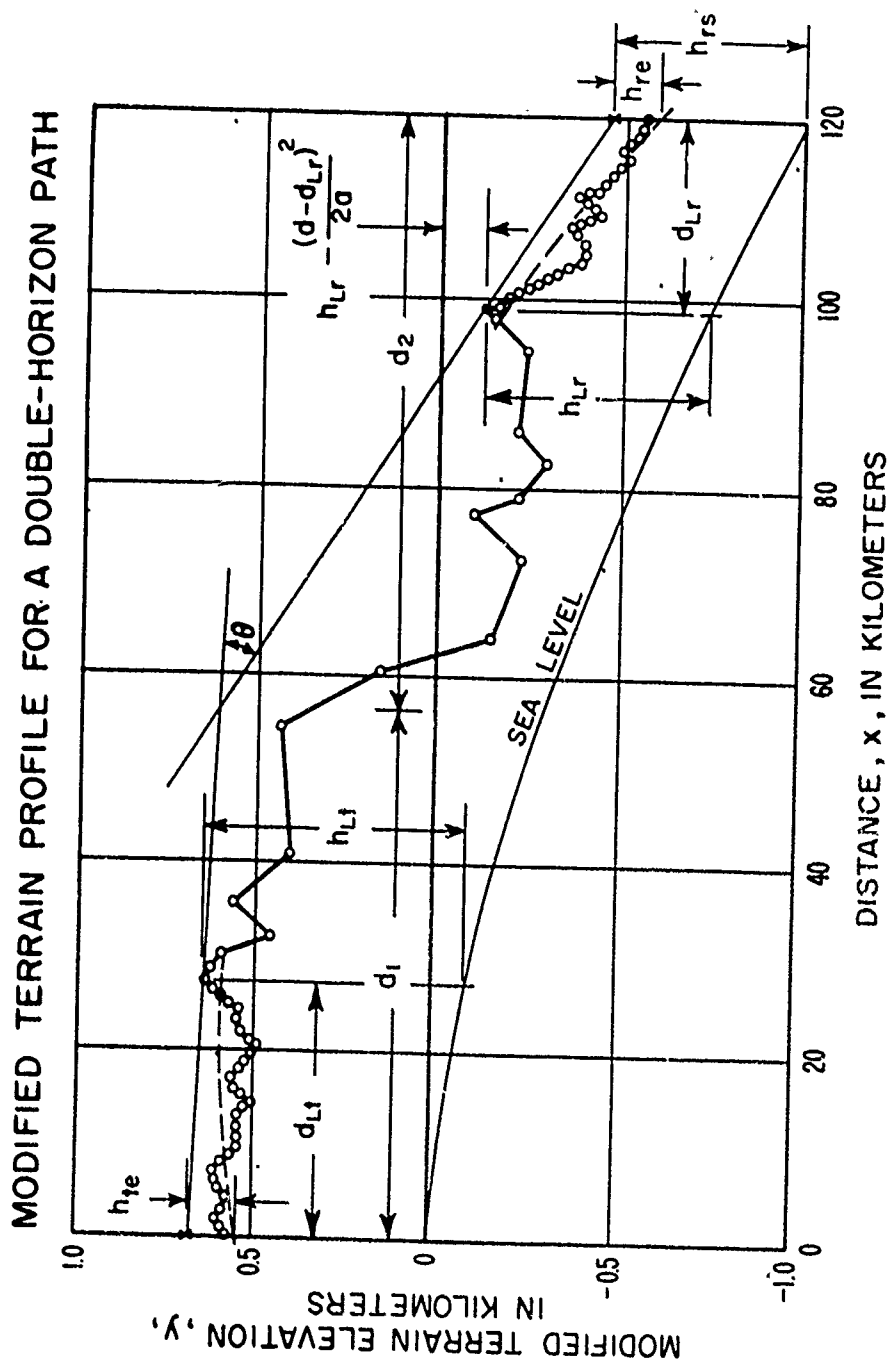


Figure 6.6

REDUCTION OF ANTENNA HEIGHT FOR VERY HIGH ANTENNAS

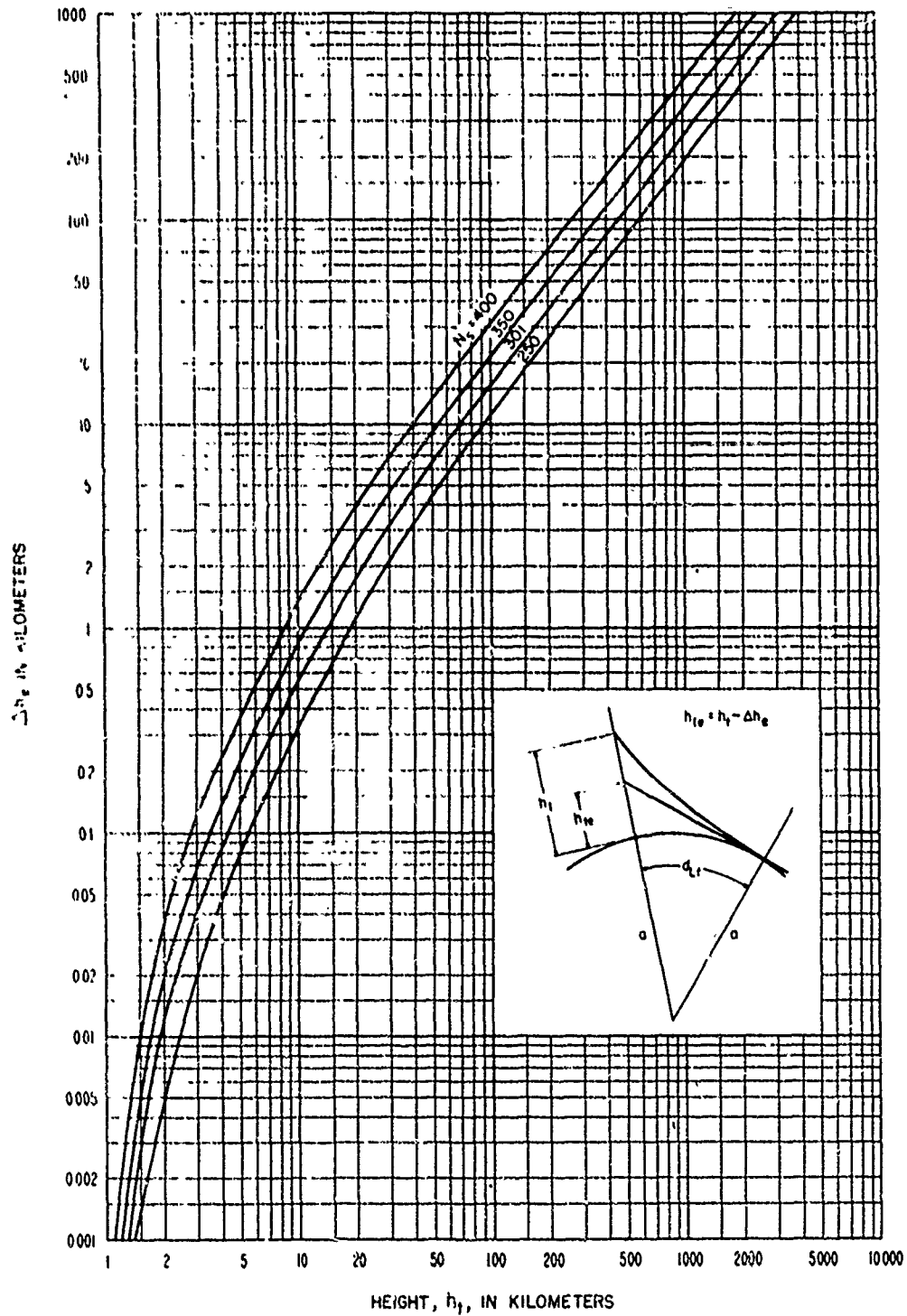
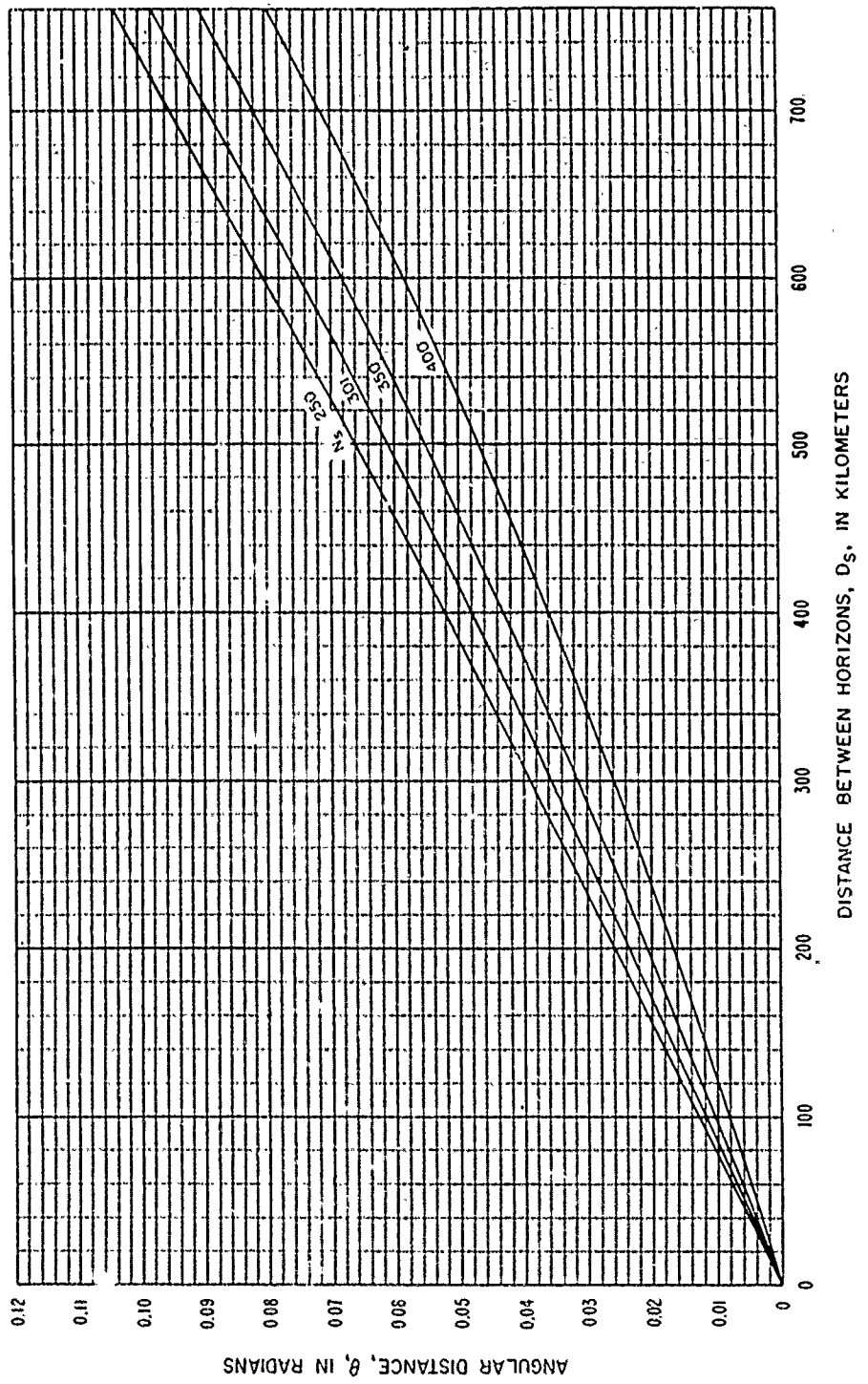


Figure 6.7

ANGULAR DISTANCE, θ , OVER A SMOOTH EARTH
VS DISTANCE BETWEEN HORIZONS, D_s



DISTANCE BETWEEN HORIZONS, D_s , IN KILOMETERS

Figure 68

CORRECTION TERMS $\Delta\alpha_0, \Delta\beta_0$ FOR $N_3 = 301$

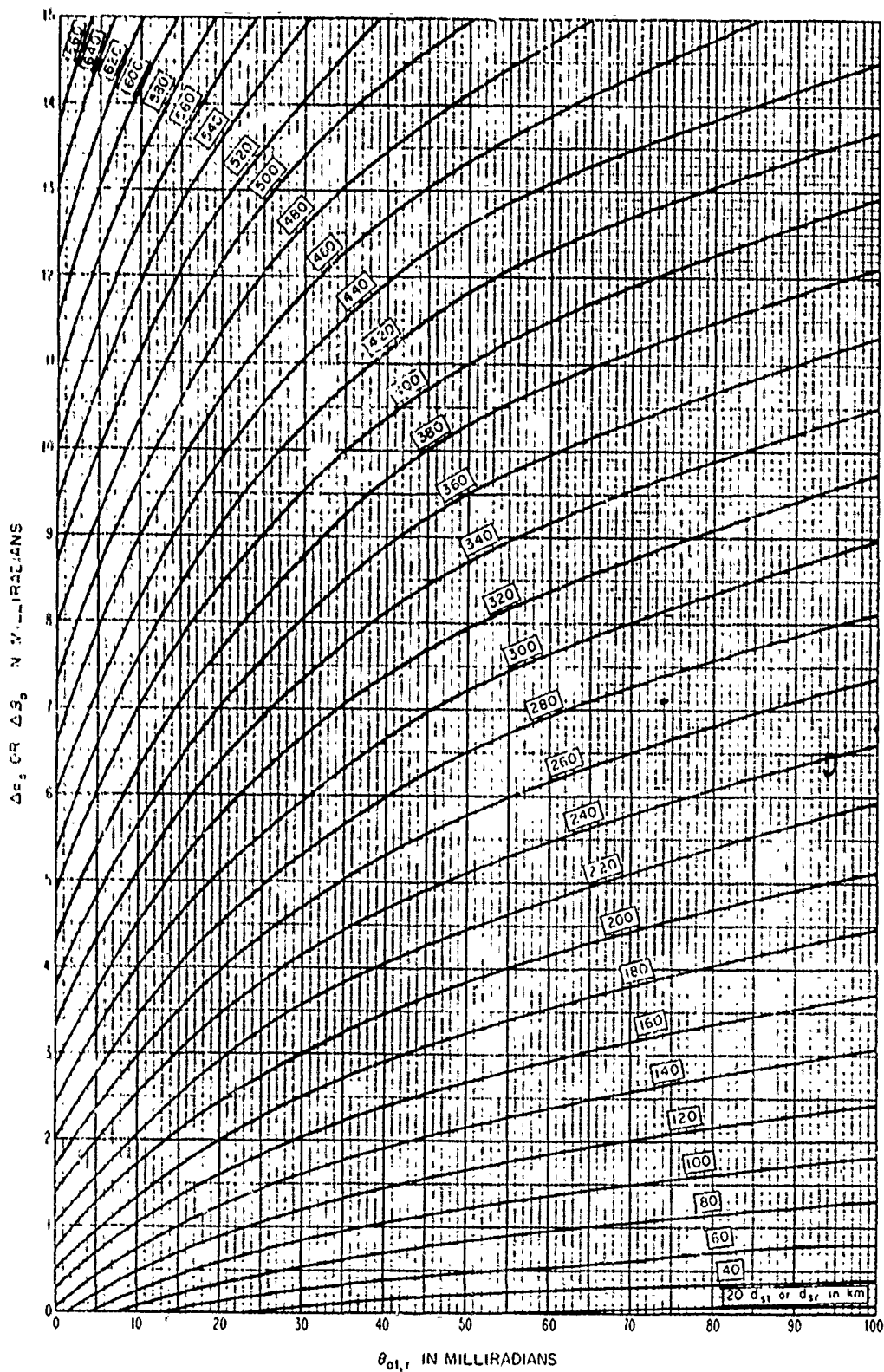


Figure 6.9

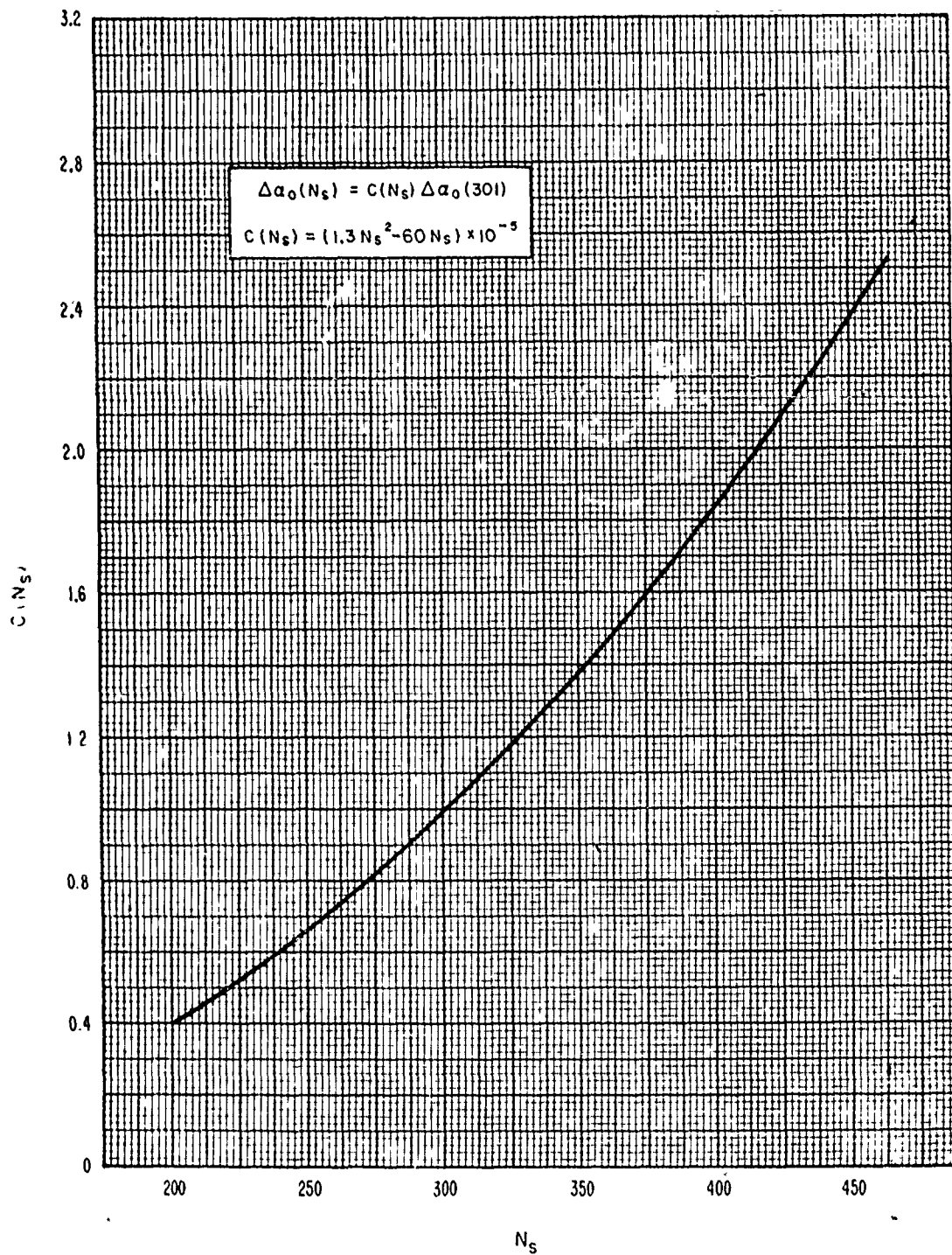
THE COEFFICIENT $C(N_S)$ 

Figure 6.10

7. DIFFRACTION OVER A SINGLE ISOLATED OBSTACLE

A propagation path with a common horizon for both terminals may be considered as having a single diffracting knife edge. In some cases, reflection from terrain may be neglected as discussed in section 7.1; in other cases, ground reflections must be considered as shown in section 7.2 and appendix III. In actual situations, the common horizon may be a mountain ridge or similar obstacle, and such paths are sometimes referred to as "obstacle gain paths", [Barris and Kirby, 1961; Dickson, Egli, Herbstreit and Wickizer, 1953; Furutsu, 1956, 1959, 1963; Kirby, Dougherty and McQuate, 1955; Rider, 1953; Ugai, Aoyagi, and Nakahara, 1963]. A ridge or mountain peak may not provide an ideal knife edge. The theory of "rounded obstacles" is discussed by Bachynski [1960], Dougherty and Maloney [1964], Neugebauer and Bachynski [1960], Rice [1954], Wait [1958, 1959], and Wait and Conda [1959]. Furutsu [1963] and Millington, Hewitt, and Immirzi [1962a] have recently developed tractable expressions for multiple knife-edge diffraction. In some cases, over relatively smooth terrain or over the sea, the common horizon may be the bulge of the earth rather than an isolated ridge. This situation is discussed in section 8.

7.1 Single Knife Edge, No Ground Reflections

A single diffracting knife edge where reflections from terrain may be neglected is illustrated in figure 7.1, where the wedge represents the knife edge. The diffraction loss $A(v, 0)$ is shown on figure 7.1 as a function of the parameter v ; from Schelleng, Burrows, and Ferrell [1933] and is defined as

$$v \cong \pm 2\sqrt{\Delta r/\lambda} = \pm \sqrt{2d \tan \alpha_0 \tan \beta_0}/\lambda \quad (7.1a)$$

or in terms of frequency in MHz:

$$v = \pm 2.583 \theta \sqrt{f d_1 d_2/d} \quad (7.1b)$$

where the distances are all in kilometers and the angles in radians. The distance

$$\Delta r \cong r_1 + r_2 - r_0 = \theta^2 d_1 d_2 / (2d)$$

is discussed in section 5, and the distances d_1 and d_2 from the knife edge to the transmitter and receiver, respectively, are shown on figure 7.1. The radio wavelength, λ , is, in the same units as the total path distance, d . The angles α_0 , β_0 , and θ are defined in section 6. In this case, $h_{Lt} = h_{Lr}$, and since $d_{st} = d_{sr} = 0$, no corrections $\Delta\alpha_0$ or $\Delta\beta_0$ are required. For the line-of-sight situation, shown in figure 7.1 and discussed in section 5.1, the angles α_0 and β_0 are both negative, and the parameter v is negative. For transhorizon paths, α_0 and β_0 are both positive and v is positive.

If v is greater than 3, $A(v, 0)$ may be expressed by:

$$A(v, 0) \approx 12.953 + 20 \log v \text{ db} \quad (7.2)$$

The basic transmission loss, L_{bd} , for a knife-edge diffraction path is given by adding $A(v, 0)$ to the free space loss:

$$L_{bd} = L_{bf} + A(v, 0) \text{ db} \quad (7.3)$$

where L_{bf} is given by (2.16). For frequencies above about 1 GHz, an estimate of the loss due to absorption (3.1), should be added to (7.3) and (7.4).

If the angles α_0 and β_0 are small, the basic transmission loss over a knife-edge diffraction path may be written as:

$$L_{bd} = 30 \log d + 30 \log f + 10 \log \alpha_0 + 10 \log \beta_0 + 53.644 \text{ db} \quad (7.4)$$

which, however, is accurate only if $v > 3$, $d \gg \lambda$, and $(d/\lambda) \tan \alpha_0 \tan \beta_0 > 4$.

For many paths, the diffraction loss is greater than the theoretical loss shown in (7.2), (7.3), and (7.4), because the obstacle is not a true knife edge, and because of other possible terrain effects. For a number of paths studied, the additional loss ranged from 10 to 20 db.

The problem of multiple knife-edge diffraction is not discussed here, but for the double knife-edge case, where diffraction occurs over two ridges, a simple technique may be used. The path is considered as though it were two simple knife-edge paths, (a) transmitter - first ridge - second ridge, and (b) first ridge - second ridge - receiver. The diffraction attenuation $A(v, 0)$ is computed for each of these paths, and the results added to obtain the diffraction attenuation over the whole path. When the parameter v is positive and rather small for both parts of the path, this method gives excellent results. Methods for approximating theoretical values of multiple knife-edge diffraction have been developed by Wilkerson [1964].

7.2 Single Knife-Edge with Ground Reflections

Theoretically, received fields may be increased by as much as 12 db due to enhancement, or deep nulls may occur due to cancellation of the signal by ground reflections. Reflection may occur on either or both sides of the diffracting edge. When the reflecting surface between the diffracting knife-edge and either or both antennas is more than the depth of a first Fresnel zone below the radio ray, and where geometric optics is applicable, the four ray knife-edge theory described in annex III may be used to compute diffraction attenuation. This method is used when details of terrain are known so that reflecting planes may be determined rather accurately. Using the four ray theory, the received field may include three reflected components, with associated reflection coefficients and ray path differences, in addition to the direct ray component.

When an isolated knife edge forms a common horizon for the transmitter and receiver, the diffraction loss may be estimated as:

$$A \approx A(v, 0) - G(\bar{h}_1) - G(\bar{h}_2) \text{ db} \quad (7.5)$$

where

$$\bar{h}_1 = 2.2325 B^2(K, b^*) (f^2/a_1)^{\frac{1}{3}} h_{te} \approx 5.74 (f^2/a_1)^{\frac{1}{3}} h_{te} \quad (7.6a)$$

$$\bar{h}_2 = 2.2325 B^2(K, b^*) (f^2/a_2)^{\frac{1}{3}} h_{re} \approx 5.74 (f^2/a_2)^{\frac{1}{3}} h_{re} \quad (7.6b)$$

$$a_1 = d_{Lt}^2 / (2h_{te}), \quad a_2 = d_{Lr}^2 / (2h_{re}).$$

The parameters b^* , K , and $B(K, b^*)$ are defined in subsection 8.1. The knife-edge attenuation $A(v, 0)$ is shown on figure 7.1, and the function $G(\bar{h})$ introduced by Norton, Rice and Vogler [1955] is shown on figure 7.2. Effective antenna heights h_{te} , h_{re} , and the distances d_{Lt} , d_{Lr} are defined in section 6. In these and other formulas, f is the radio frequency in MHz.

The function $G(\bar{h}_{1,2})$ represents the effects of reflection between the obstacle and the transmitter or receiver, respectively. These terms should be used when more than half of the terrain between an antenna and its horizon cuts a first Fresnel zone ellipse which has the antenna and its horizon as foci and lies in the great circle plane. Definite criteria are not available, but in general, if terrain near the middle distance between a transmitting antenna and its horizon is closer to the ray than $0.5(\lambda d_{Lt})^{\frac{1}{2}}$ kilometers, $G(\bar{h}_1)$ should be used. The same criterion, depending on d_{Lr} , determines when $G(\bar{h}_2)$ should be used. When details of terrain are not known, an allowance for terrain effects, $G(\bar{h}_{1,2})$, should be used if $0.5(\lambda d_{Lt, Lr})^{\frac{1}{2}} > |h_{Lt, Lr} - h_{ts, rs}| / 2$, where all distances and heights are in kilometers.

7.3 Isolated Rounded Obstacle, No Ground Reflections

Dougherty and Maloney [1964] describe the diffraction attenuation relative to free space for an isolated, perfectly conducting, rounded knife edge. The rounded obstacle is considered to be isolated from the surrounding terrain when

$$k h [2/(kr)]^{\frac{1}{3}} \gg 1$$

where $k = 2\pi/\lambda$, r is the radius of curvature of the rounded obstacle, and h is the smaller of the two values $[(d_{Lt}^2 + r^2)^{\frac{1}{2}} - r]$ and $[(d_{Lr}^2 + r^2)^{\frac{1}{2}} - r]$.

The diffraction loss for an isolated rounded obstacle and irregular terrain shown in figure 7.3 is defined as:

$$A(v, \rho) = A(v, 0) + A(0, \rho) + U(v\rho) \quad \text{db} \quad (7.7)$$

where v is the usual dimensionless parameter defined by (7.1) and ρ is a dimensionless index of curvature for the crest radius, r in kilometers, of the rounded knife edge:

$$v\rho = 1.746 \theta(fr)^{\frac{1}{3}} \quad (7.8)$$

$$\rho = 0.676 r^{\frac{1}{3}} f^{\frac{1}{6}} [d/(r_1 r_2)]^{\frac{1}{2}} \quad (7.9)$$

where, f is the radio frequency in MHz, d is the path distance in kilometers, and r_1, r_2 shown in figure 7.3 are the distances in kilometers from the transmitter and receiver, respectively to the rounded obstacle. For all practical applications, $r_1 r_2$ may be replaced by $d_1 d_2$. Where the rounded obstacle is the broad crest of a hill, the radius of curvature, r , for a symmetrical path is:

$$r = D_s / \theta \quad (7.10)$$

where $D_s = d - d_{Lt} - d_{Lr}$ is the distance between transmitter and receiver horizons in kilometers, and θ is the angular distance in radians (6.19). Where the ratio $\alpha_o/\beta_o \neq 1$, the radius of curvature is defined in terms of the harmonic mean of radii a_t and a_r defined in the next section, (8.9), and shown in figure 8.7:

$$r = \frac{2 D_s d_{st} d_{sr}}{6 \left(d_{st}^2 + d_{sr}^2 \right)} \quad (7.11)$$

In (7.7), the term $A(v, 0)$ is the diffraction loss for the ideal knife edge ($r = 0$), and is read from figure 7.1. The term $A(0, \rho)$ is the magnitude of the intercept values ($v = 0$) for various values of ρ and is shown on figure 7.4. The last term $U(v\rho)$ is a function of the product, $v\rho$, and is shown on figure 7.5.

Arbitrary mathematical expressions, given in annex III, have been fitted to the curves of figures 7.1, 7.3, 7.4, and 7.5 for use in programming the method for a digital computer.

The diffraction loss $A(v, \rho)$ as given by (7.7) is applicable for either horizontally or vertically polarized radio waves over irregular terrain provided that the following conditions are met:

- (a) the distances d , d_1 , d_2 , and r are much larger than λ ,
- (b) the extent of the obstacle transverse to the path is at least as great as the width of a first Fresnel zone:

$$\sqrt{\lambda d_{1,2} (1 - d_{1,2}/d)}$$

- (c) the components α_0 and β_0 of the angle θ are less than 0.175 radians, and
- (d) the radius of curvature is large enough so that $(\pi r/\lambda)^{\frac{1}{3}} > 1$.

In applying this method to computation of diffraction loss over irregular terrain, some variance of observed from predicted values is to be expected. One important source of error is in estimating the radius of curvature of the rounded obstacle, because the crests of hills or ridges are rarely smooth. Differences between theoretical and observed values are apt to be greater at UHF than at VHF.

7.4 Isolated Rounded Obstacle with Ground Reflections

If a rounded obstacle has a small radius and is far from the antennas, (7.7) may neglect important effects of diffraction or reflection by terrain features between each antenna and its horizon.

Such terrain foreground effects may be allowed for, on the average, by adding a term, $10 \exp(-2.3\rho)$ to (7.7). The effect of this term ranges from 10 db for $\rho = 0$ to 1 db for $\rho = 1$. When some information is available about foreground terrain, the $G(\bar{h}_{1,2})$ terms discussed in section 7.2 may be used if more than half of the terrain between an antenna and its horizon cuts a first Fresnel zone in the great circle plane:

$$A = A(v, \rho) - G(\bar{h}_1) - G(\bar{h}_2) \quad \text{db} \quad (7.12)$$

where $A(v, \rho)$ is defined by (7.7), \bar{h}_1, \bar{h}_2 by (7.6), and the functions $G(\bar{h}_{1,2})$ are shown on figure 7.2.

When details of terrain are known, and the reflecting surfaces between the rounded obstacle and either or both antennas are more than the depth of a first Fresnel zone below the radio ray, the geometric optics four-ray theory described in annex III may be applicable. In this case, the phase lag of the diffracted field with reference to the free space field must be considered in addition to the ray path differences of the reflected components. The phase lag $\Phi(v, \rho)$ of the diffracted field is defined as

$$\Phi(v, \rho) = 90 v^2 + \phi(v, 0) + \phi(0, \rho) + \phi(v, \rho) \quad \text{degrees} \quad (7.13a)$$

where the functions $\phi(v, 0)$, $\phi(0, \rho)$, and $\phi(v, \rho)$ are shown on figures 7.1, 7.4, and 7.5, respectively. For an ideal knife-edge, $\rho = 0$, the phase lag of the diffracted field is

$$\Phi(v, 0) = 90 v^2 + \phi(v, 0) \quad \text{for } v > 0 \quad (7.13b)$$

and
$$\Phi(v, 0) = \phi(v, 0) \quad \text{for } v \leq 0 \quad (7.13c)$$

7.5 An Example of Transmission Loss Prediction for a Rounded Isolated Obstacle

The path selected to provide an example of knife-edge diffraction calculations is located in eastern Colorado, extending from a location near Beulah, southwest of Pueblo, to Table Mesa north of Boulder. The common horizon is formed by Pikes Peak, with an elevation 4300 meters above mean sea level. For the purpose of these calculations Pikes Peak is considered to be a single rounded knife edge. The complete path profile is shown in figure 7.6. Table 7.1 gives all applicable path and equipment parameters and permits a comparison of calculated and actually measured values.

TABLE 7.1
Path and Equipment Parameters

Carrier Frequency	751 MHz
Total Great Circle Path Distance	223, 3 km
Great Circle Distances from Pikes Peak	
to Transmitter Site	77.3 km
to Receiver Site	146.0 km
Terminal Elevations above Mean Sea Level	
Transmitter Site	1, 905 m
Receiver Site	1, 666 m
Elevation of Pikes Peak	
Above Mean Sea Level	4, 300 m
Above Mean Terminal Elevation	2, 507 m
Transmitting Antenna Height Above Ground	7.3 m
Transmitting Antenna Gain Above Isotropic (4.3 m Dish)	26.7 db
Receiving Antenna Height Above Ground	20.0 m
Receiving Antenna Gain Values Above Isotropic (3 m Dish)	23.6 db
Polarization	Horizontal
Modulation	Continuous Wave
Transmitter Power	445 watts

Calculations are given for single-ray diffraction, neglecting possible specular reflections from foreground terrain.

The minimum monthly surface refractivity N_0 (referred to mean sea level) from figure 4.1 is 300 N-units. From Table 7.1 the terminal elevations are 1905 and 1666 m, respectively. Corresponding surface refractivity values N_s are 245 and 251 N-units (4.3), and the average of these values is $N_s = 248$. In this example, N_s is calculated for the terminals, as the antennas are more than 150 m below their 4300 m radio horizon. Using (4.4) or an extrapolation of figure 4.2, the effective earth radius a for $N_s = 248$ is found to be 7830 km.

CCP 702-1

The angular distance θ in radians and related parameters are calculated using (6.15) and (6.18a, b): $\theta_{et} = 0.008581$, $\theta_{er} = 0.025953$, $u_{oo} = 0.021827$, $\beta_{oo} = 0.041225$. In this example d_{st} and d_{sr} are negligibly small, and the corrections Δu_o and $\Delta \beta_o$ (6.19a, b) can be neglected. Thus, $u_{oo} = u_o$, $\beta_{oo} = \beta_o$, and $\theta = 0.063052$ radians.

The free-space loss and the attenuation relative to free space are computed considering Pikes Peak to be a single isolated rounded obstacle. From a study of large-scale topographic maps, the distance D_g between the radio horizons at the top of the peak is estimated to be 0.040 km. With $f = 751$ MHz, $d_1 = 146.0$ km, and $d_2 = 77.3$ km, we determine:

$$v = 31.73 \text{ (v is positive, as both } u_o \text{ and } \beta_o \text{ are greater than zero)} \quad (7.1b)$$

$$r = 0.6344 \text{ (7.10), } v\rho = 0.858 \text{ (7.8) and } \rho = 0.0271$$

The test described in section 7.3 shows that the assumption of an isolated obstacle is applicable. The components of basic transmission loss are then determined as follows:

$$\text{Free-space Loss } L_{bf} = 137.0 \text{ db} \quad (2.16)$$

$$A(v, \theta) = 43.0 \text{ db} \quad \text{figure 7.1}$$

$$A(\theta, \rho) = 6.0 \text{ db} \quad \text{figure 7.4}$$

$$U(v, \rho) = 5.1 \text{ db} \quad \text{figure 7.5}$$

Totals are: $A(v, \rho) = 54.1$ db, and from (7.3), $L_{bd} = L_{bf} + A(v, \rho) = 191.1$ db.

The average atmospheric absorption term, A_a , from figure 3.6 is 0.7 db. Then the total basic transmission loss value $L_{dr} = 191.8$ db, which is equal to the long-term reference value L_{cr} . This reference value, is strictly applicable only to those hours of the year which are characterized by a surface refractivity of approximately 250 N-units.

The expected behavior of the hourly median basic transmission loss for all hours of the year over this path can be determined using the methods described in section 10. A function $V(0.5, d_e)$ which is used with L_{cr} to compute the long-term median transmission loss for a given climatic region is described in subsection 10.4. A function $Y(q, d_e)$ describes the variability relative to this long-term median that is expected for a fraction of hours q . The total cumulative distribution for this path in a Continental Temperate climate is computed as shown in subsection 10.5.

Since this is a knife-edge diffraction path, it will be necessary to calculate cumulative distributions $Y(q, d_e)$ separately for portions of the path on each side of Pikes Peak and to combine the results as described in subsection 10.8. Effective antenna heights are computed as heights above curves fitted to terrain on each side of Pike's Peak using (5.15) and (5.16). The curves are extrapolated to each antenna and to Pike's Peak. The effective heights are then the heights of the antennas and of the Peak above these curves. From Beulah to Pikes

Peak the terrain near the Peak is excluded because it is partially shadowed. Twenty-one evenly spaced points, x_i , from $d = 3.3$ km to $d = 70$ km were selected and the corresponding terrain heights x_i were read. From (5.15b) $\bar{h} = 2100$ m, $\bar{x} = 36.6$ km, and $m = 25.5$, and the straight line fitted to terrain is

$$h(x) = 2100 + 25.5(x - 36.6) \text{ meters.}$$

At the Beulah antenna, $x = 0$ and $h(x) = 1167$ meters, at Pikes Peak $x = 75.5$ kilometers and $h(x) = 3095$ meters. The effective antenna heights are then 738 and 1205 meters. Using (10.1) to (10.3) the distances $d_{1c} = 262.5$ km, $d_{a1} = 33.2$ km, and the effective distance d_{1e} is 34.0 km.

Similarly on the Table Mesa side much of the terrain is shadowed by the small peak about 122 km and by the elevated area at about 202 km. The curve fit is therefore required for the intervening terrain with $x_0 = 122.5$ km and $x_{20} = 200.5$ km. Using (1) equation for terrain heights between these points (5.15b) gives $\bar{h} = 2025$ m, $\bar{x} = 161.5$ km, and $m = 17.7$. From (5.15a) $h(x = 75.5) = 2827$, $h(x = 223.3) = 1448$ meters. The effective antenna heights are then 1473 and 218 meters (5.17). $d_{1c} = 222.5$, $d_{a1} = 33.2$ km, and the effective distance $d_{1e} = 74.3$ km.

We thus have two paths in tandem where the effective distances are 34.0 and 74.3 km, respectively. Cumulative distributions are obtained using figures 10.13, 10.14, 10.15, and equations (10.4) to (10.7). The frequency factors are $g(0.1, \eta) = 1.33$, $g(0.9, \eta) = 1.26$.

	Table Mesa Side	Beulah Side	
$V(0.5, d_{1e})$	0.2	0	figure 10.14
$Y(0.1, d_{1e}, 100 \text{ MHz})$	4.7	1.2	figure 10.14
$Y(0.9, d_{1e}, 100 \text{ MHz})$	-3.1	-0.6	figure 10.14
$Y(0.1)$	6.3	1.6	(10.6)
$Y(0.9)$	-4.0	-0.77	(10.6)

Using the reference value $L_{CR} = 191.8$ db and the ratios given in (10.7) the predicted cumulative distributions for both portions and for the entire path are tabulated below.

q	$L_b(q)$ in db		
	Table Mesa	Beulah	Entire Path
0.0001	170.6	186.5	170.6
0.001	174.4	187.4	174.4
0.01	179.0	188.6	178.6
0.1	185.3	190.2	184.5
0.5	191.6	191.8	191.6
0.9	195.6	192.6	195.6
0.99	198.9	193.2	198.9
0.999	201.2	193.7	201.2
0.9999	203.2	194.0	203.2

CCP 702-1

The cumulative distribution of predicted basic transmission loss for the entire path was obtained by convoluting the distributions for each part of the path, as described in subsection 10.8. This cumulative distribution is shown graphically in figure 7.7 together with a distribution derived from measurements over this path, reflecting 1056 hours of data obtained in 1960 and 1962.

The confidence limits on figure 7.7 were derived assuming that

$$\sigma_c^2(q) = 16.73 + 0.12 Y^2(q)$$

where the variance $\sigma_c^2(0.5) = 12.73 \text{ db}^2$ given in (V.40) has been increased by 4 db^2 to allow for equipment and reading errors.

KNIFE EDGE DIFFRACTION LOSS, $A(v,0)$

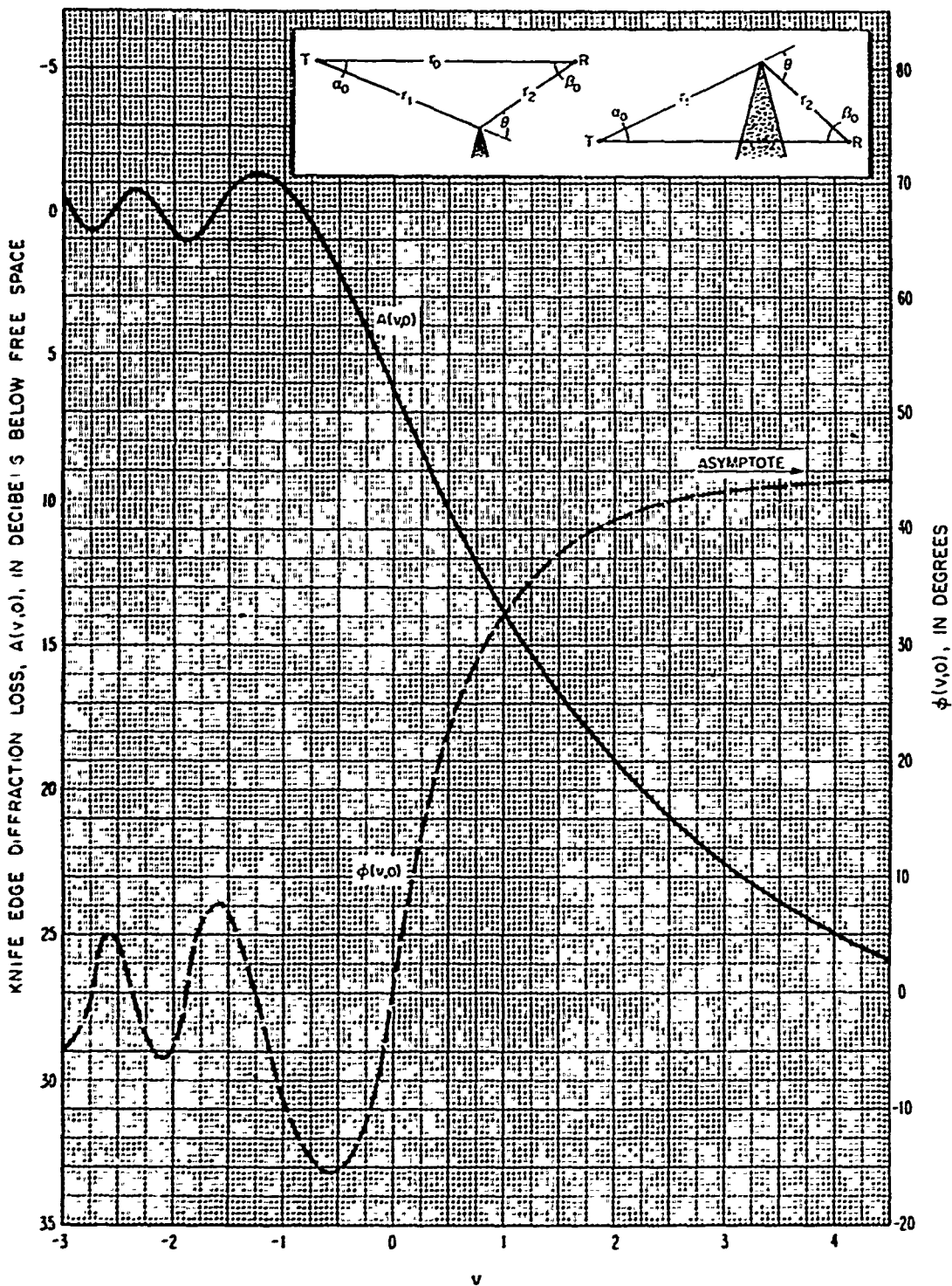


Figure 7.1

7-11

THE RESONANT HEIGHT GAIN CURVE
OSKSO: $b=90^\circ, 180^\circ$

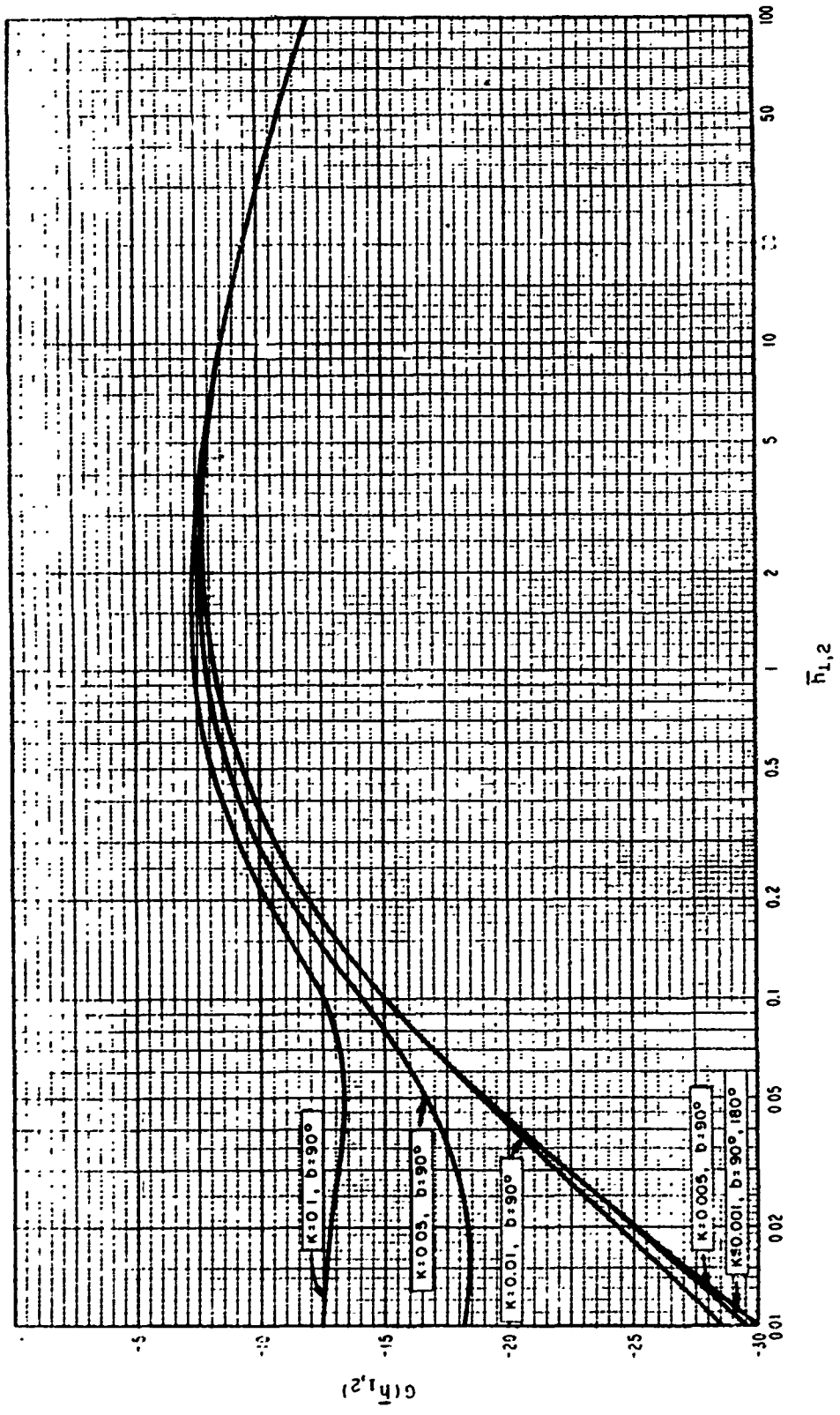


Figure 7.2

DIFFRACTION LOSS, $A(v, \rho)$, FOR A ROUNDED OBSTACLE

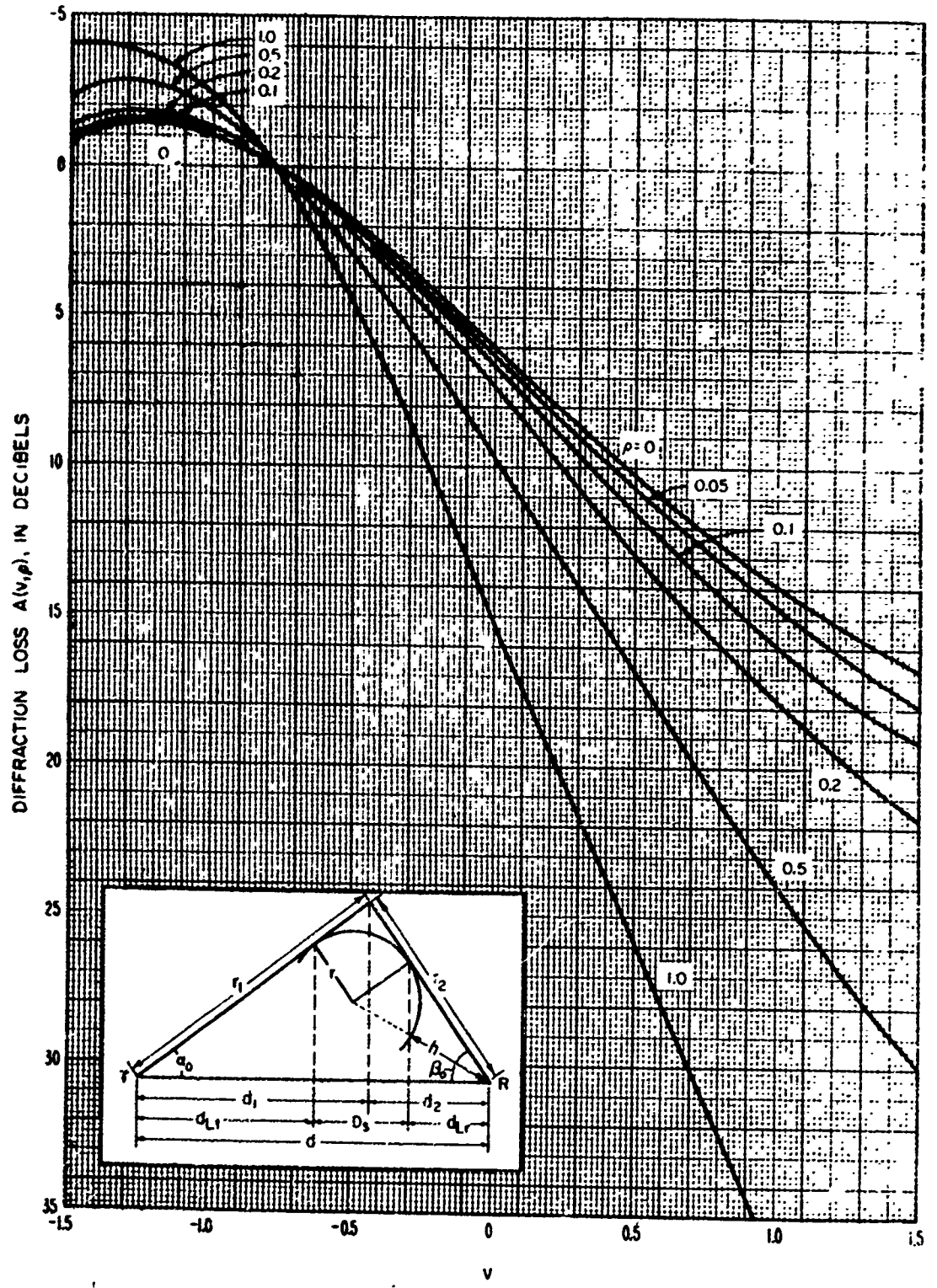
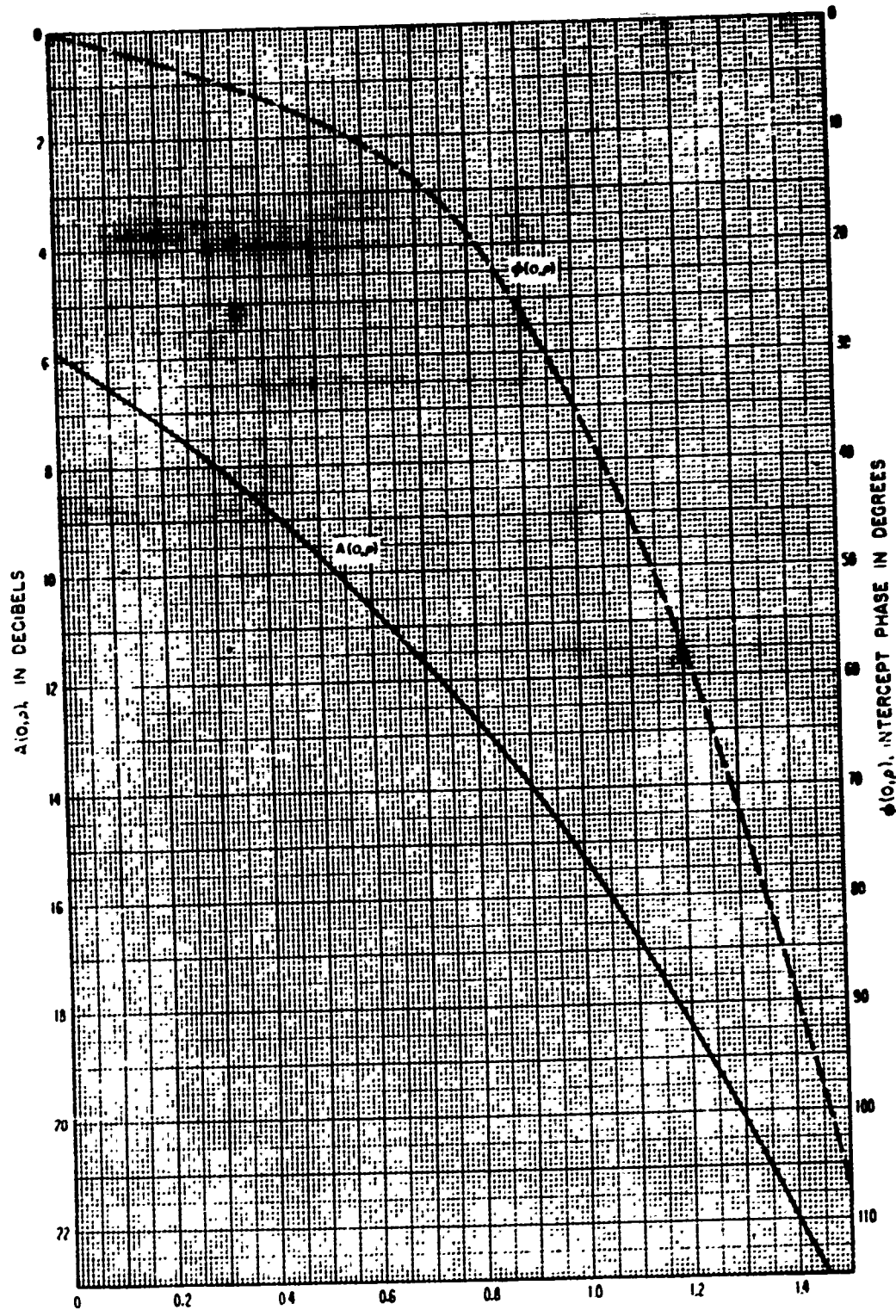


Figure 7.3

7-13

F-157

INTERCEPT MAGNITUDE AND PHASE FOR DIFFRACTION OVER A ROUNDED OBSTACLE



UNIVERSAL DIFFRACTION CURVE FOR A ROUNDED OBSTACLE

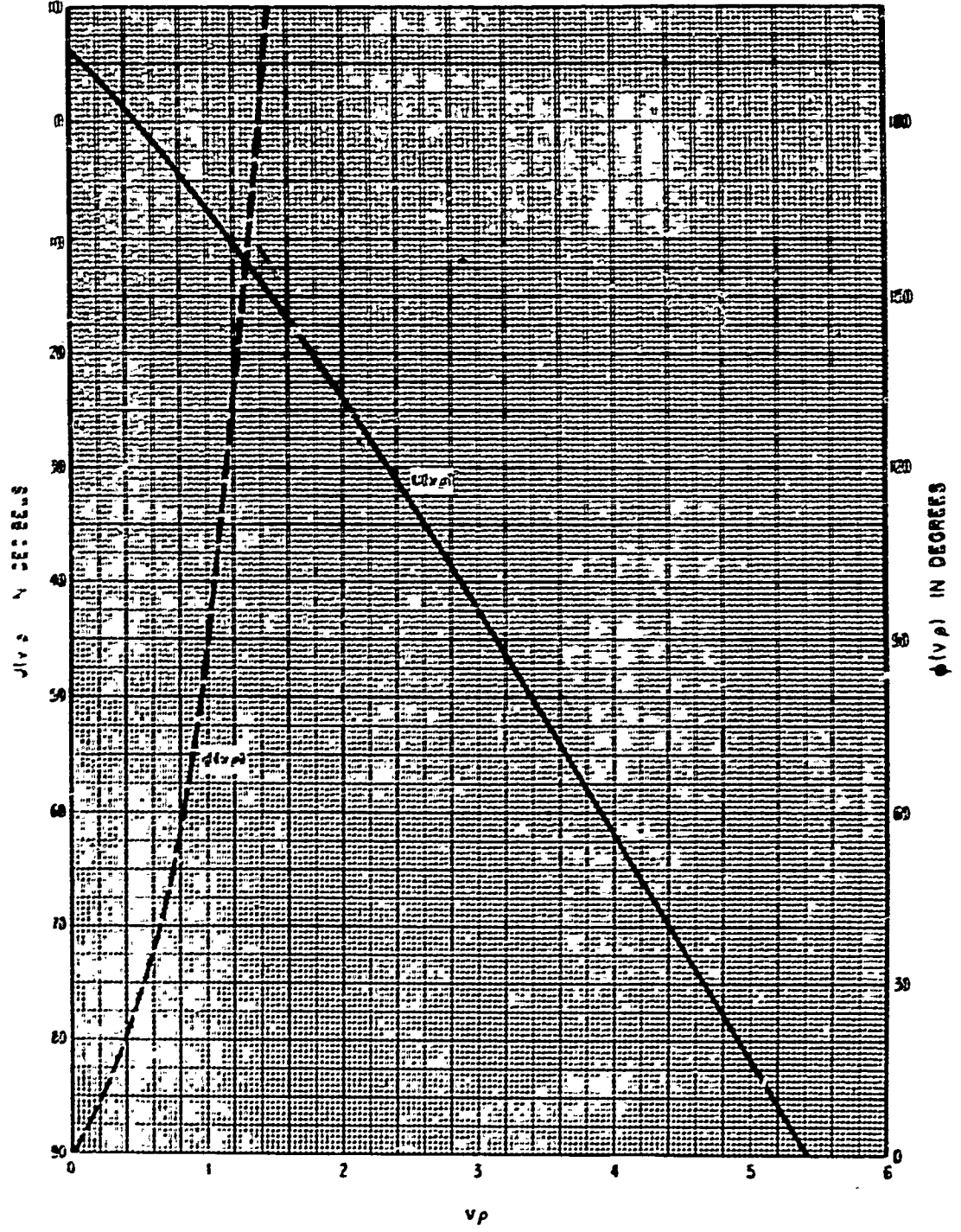


Figure 7.5

TERRAIN PROFILE FOR COLORADO KNIFE-EDGE DIFFRACTION PATH

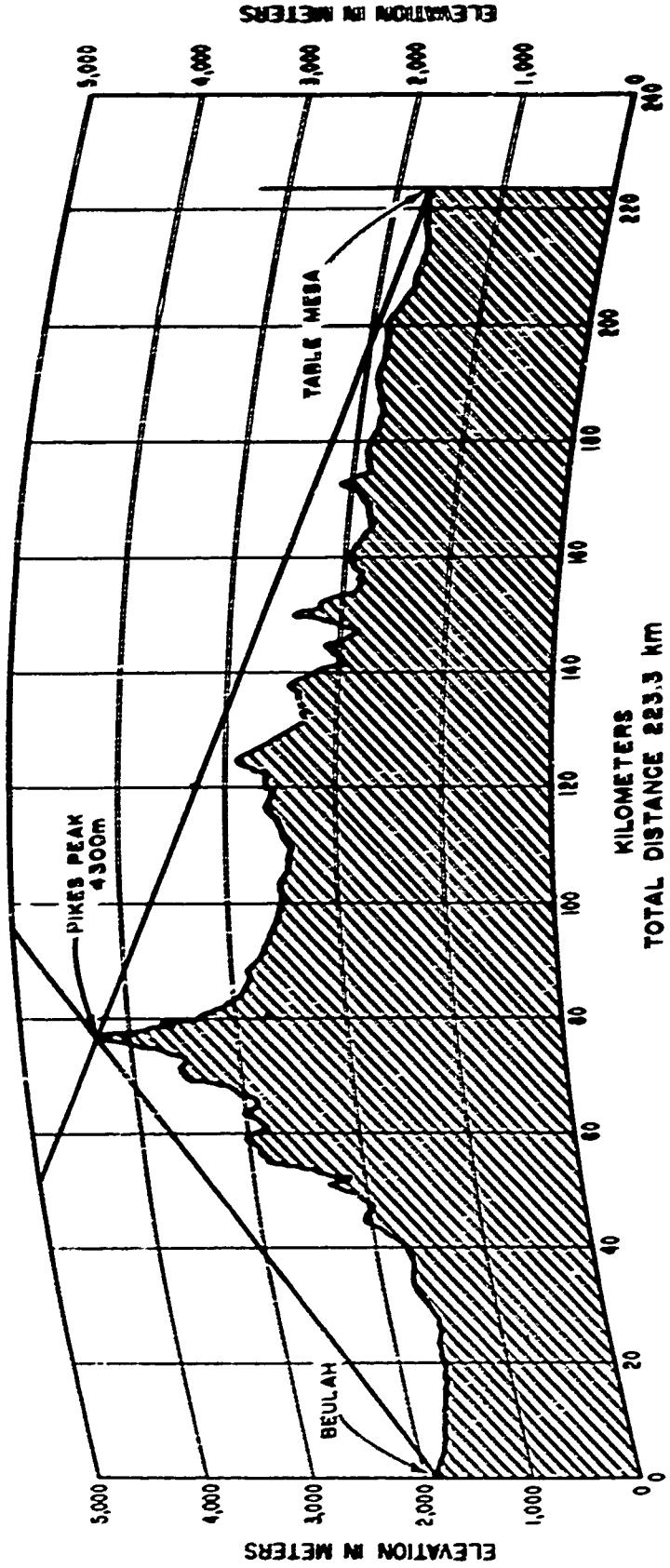


Figure 7.6

CUMULATIVE DISTRIBUTIONS $L_b(g)$ OBSERVED AND PREDICTED VS g
DIFFRACTION PATH OVER PIKES PEAK, COLORADO

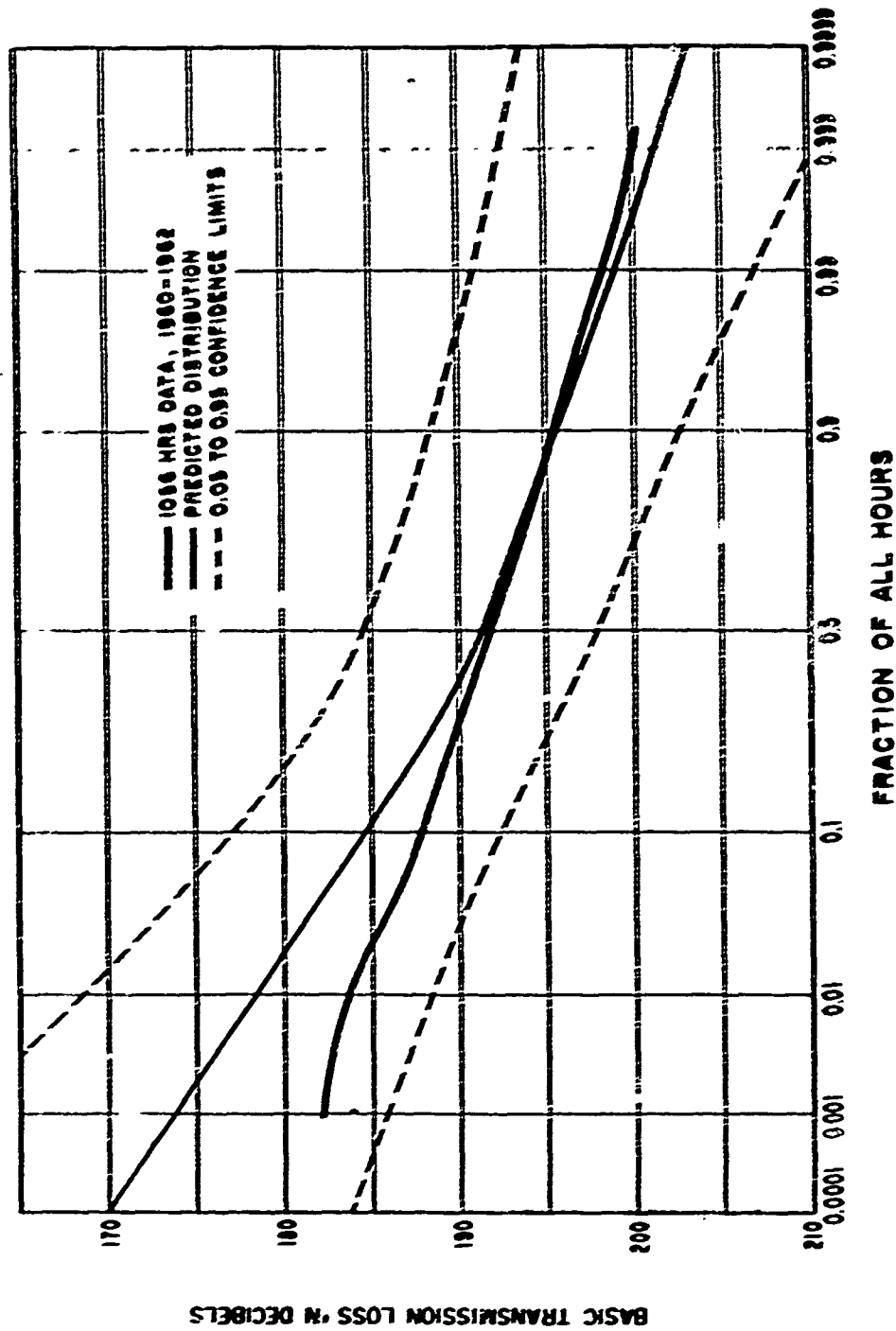


Figure 7.7

N. DIFFRACTION OVER SMOOTH EARTH AND OVER IRREGULAR TERRAIN

Diffraction attenuation over an isolated ridge or hill has been discussed in section 7. The following methods are used to compute attenuation over the bulge of the earth and over irregular terrain. The methods are applicable to the far diffraction region, where the diffracted field intensity may be determined by the first term of the Van der Pol-Brewster residue series [Brewster, 1949]. This region extends from near the radio horizon to well beyond the horizon. A criterion is given to determine the minimum distance for which the method may be used. In some situations the first term of the series provides a valid approximation to the diffracted field even at points slightly within line-of-sight [Vogler, 1964].

A simplified graphical method for determining ground wave attenuation over a spherical homogeneous earth in this far diffraction region was recently developed by Vogler [1964], based on a paper by Norton [1941]. The method described in section 8.1 is applicable to either horizontal or vertical polarization, and takes account of the effective earth's radius, ground constants, and radio frequency. In section 8.2, a modification of the method for computing diffraction attenuation over irregular terrain is described, and section 8.3 considers the special case of a common horizon which is not an isolated obstacle.

For frequencies above 1000 MHz, the attenuation due to gaseous absorption should be added to the diffraction loss. See (3.1) and figure 3.6.

8.1 Diffraction Attenuation Over a Smooth Earth

The attenuation relative to free space may be expressed in terms of a distance dependence, the dependence on antenna heights, and the dependence on electromagnetic ground constants, the earth's radius, and the radio frequency:

$$A = G(x_0) - F(x_1) - F(x_2) - C_1(K, b') \pm A_2 \quad (8.1)$$

where A_2 is the atmospheric absorption, given by (3.5), and

$$x_0 = d B_0, \quad x_1 = d_{Lr} B_0, \quad x_2 = d_{Lr} B_0 \quad (8.1a)$$

$$B_0 = f^{\frac{1}{3}} C_0^2 B(K, b'), \quad C_0 = (8497/a)^{\frac{1}{2}} \quad (8.1b)$$

The basic diffraction transmission loss L_{bd} is

$$L_{bd} = L_{bf} + A \text{ db} \quad (8.2)$$

where the basic transmission loss in free space, L_{bf} , is given by (2.16).

The distances d , d_{Lr} , d_{Lr} , and the effective earth's radius, a , have been defined in sections 4 and 6, and f is the radio frequency in megahertz.

The parameters K and b° depend on polarization of the radio wave and the relative dielectric constant, ϵ , and conductivity, σ , of the ground. Figures 8.1 and 8.2 show curves of K and b° versus frequency for combinations of ϵ and σ corresponding to pure, average, and good ground, and to sea water. Figure 8.1 shows K for $a = 4000$ feet, B for other values of effective earth's radius.

$$E(a) = C_{\theta} K(3+2F^2) \tag{8.3}$$

General formulas for K and b° for both horizontal and vertical polarization are given in section III.4 of annex III.

The parameter $B(K, b^{\circ})$ in (8.2b) is shown as a function of K and b° in figure 8.3. The limiting value $B = 1.607$ for $K = 0$ may be used for most cases of horizontal polarization. The parameter $C_1(K, b^{\circ})$ in (8.1) is shown in figure 8.4.

The function $G(x_0)$ in (8.1) is shown on figures 8.5 and 8.6, and is defined as

$$G(x_0) = 0.0575 x_0 - 10 \log x_0 \tag{8.4}$$

and the functions $F(x_{1,2})$ are plotted in figures 8.5 and 8.6 versus K and b° . For x_0 values of x_1 or x_2 , $F(x)$ is approximately equal to $G(x)$.

Since this method is based on only the first term of the residue series, it is limited to the following distances to insure that A is accurate within approximately 1.5 db:

$$x_0 - x_1(\Delta x_1) - x_2(\Delta x_2) > 335, \quad \text{for } B = 1.607, (K \geq 0.1) \tag{8.5a}$$

$$x_0 - x_1(\Delta x_1) - x_2(\Delta x_2) > 115, \quad \text{for } B = 0.700, (K \geq 10). \tag{8.5b}$$

For values of B lying between these two limits, linear interpolation between the $\Delta(x)$ curves of figure 8.6, and the two minimum values in (8.5) gives a fair approximation of the range of validity of (8.1). Using linear interpolation:

$$x_0 - x_1 \Delta(x_1, B) - x_2 \Delta(x_2, B) > x_{\min} \tag{8.6}$$

$$x_{\min} = 335 - 242.6(1.607 - B) \tag{8.7a}$$

$$\Delta(x, B) = \Delta(x, 1.607) + 1.103(1.607 - B) [\Delta(x, 0.700) - \Delta(x, 1.607)] \tag{8.7b}$$

$\Delta(x, 0.700)$ and $\Delta(x, 1.607)$ are the values read from the upper and lower curves of Δx in figure 8.6.

8.2 Diffraction Over Irregular Terrain

To compute diffraction attenuation over irregular terrain, the single effective earth's radius, a , used in (8.2) is replaced by four different radii as shown in figure 8.7. The radii a_1 and a_2 of the terrain between the antennas and their horizons, and the radii a_t and a_r of the terrain between radio horizons and the crossover point of horizon rays are defined by

$$a_1 = d_{Lr}^2 / (2h_{te}), \quad a_2 = d_{Lr}^2 / (2h_{re}) \quad (8.8)$$

$$a_t = D_s d_{st} / (\theta d_{sr}), \quad a_r = D_r d_{sr} / (\theta d_{st}) \quad (8.9)$$

The distances D_s , d_{st} , d_{sr} , d_{Lr} , d_{Lr} , the effective antenna heights h_{te} and h_{re} , and the angular distance θ are defined in section 6.

These four radii are used in (8.2) and (8.3) to obtain values of $K(a) = K_{1,2,t,r}$ for each of the four radii. Corresponding values $B_{1,2,t,r}$ are then read from figure 8.3 for each value of K .

The diffraction attenuation relative to free space is then:

$$A = G(x_0) - F(x_1) - F(x_2) - \bar{C}_1(K_{1,2}) + A_2 \quad (8.10)$$

where A_2 is the atmospheric absorption defined by (3.1), and is negligible for frequencies less than 1 GHz, and $\bar{C}_1(K_{1,2})$ is the weighted average of $C_1(K_1, b)$ and $C_1(K_2, b)$ read from figure 8.4:

$$\bar{C}_1(K_{1,2}) = [x_1 C_1(K_1) + x_2 C_1(K_2)] / (x_1 + x_2) \quad (8.11)$$

$$x_1 = B_{e1} d_{Lr}, \quad x_2 = B_{e2} d_{Lr} \quad (8.12a)$$

$$x_0 = B_{ot} d_{st} + B_{or} d_{sr} + x_1 + x_2 \quad (8.12b)$$

$$B_{e1} = f^{1/3} C_{e1}^2 B_1, \quad B_{e2} = f^{1/3} C_{e2}^2 B_2 \quad (8.13a)$$

$$B_{ot} = f^{1/3} C_{ot}^2 B_t, \quad B_{or} = f^{1/3} C_{or}^2 B_r \quad (8.13b)$$

This method is applicable to computation of diffraction attenuation over irregular terrain for both vertical and horizontal polarization for transhorizon paths. The method may be somewhat simplified for two special cases: diffraction over paths where $d_{st} \approx d_{sr}$, and for most paths when horizontal polarization is used.

8.2.1 Diffraction over paths where $d_{st} \approx d_{sr}$

For paths where the distances d_{st} and d_{sr} are equal, the parameter x_0 may be defined in terms of D_{str} and the corresponding earth's radius a_s :

$$x_0 = B_{os} D_{str} + x_1 + x_2 \quad (8.14)$$

$$D_{str} = f^2 d_{st} = f^2 d_{sr}, \quad a_s = D_{str} / \theta, \quad C_{os} = (8497/a_s)^2, \quad B_s = B(K_s, b) \quad (8.15a)$$

$$B_{os} = f^3 C_{os}^2 B_s \quad (8.15b)$$

where x_1 and x_2 are defined by (8.12). The diffraction attenuation is then computed using (8.10).

8.2.2 For horizontal polarization

For horizontally polarized radio waves, at frequencies above 100 MHz, and with $K(a) = 0.001$, the parameter $B(K, b)$ approaches a constant value, $B \approx 1.607$, and $C_1(K, b) = 20.03$ db. Assuming $B = 1.607$ and $C_1 = 20.03$, the diffraction attenuation may be computed as follows:

$$A = G(x_0) - F(x_1) - F(x_2) - 20.03 \text{ db} \quad (8.16a)$$

$$x_1 = 669 f^3 d_{L1} / a_1^2, \quad x_2 = 669 f^3 d_{L2} / a_2^2 \quad (8.16b)$$

$$x_0 = 669 f^3 \theta^2 D_{str} + x_1 + x_2 \quad (8.16c)$$

where

$$D_{str} = (d_{st} d_{sr})^{1/2} \left(d_{st}^{-1/2} + d_{sr}^{-1/2} \right) / (d_{st} + d_{sr})^{1/2}$$

The parameter D_{str} is shown in figure 8.8 as a function of d_{st} and d_{sr}

For paths where $d_{st} = d_{sr}$, using horizontal polarization, the parameter x_0 simplifies to

$$x_0 = 669 f^3 (\theta^2 D_s)^{1/2} + x_1 + x_2 \quad (8.16d)$$

8.3 Single-Horizon Paths, Obstacle not Isolated

In some cases, over rather regular terrain or over the sea, a common horizon may be the bulge of the earth rather than an isolated ridge or mountain. For such paths, the path distance, d , is just the sum of d_{Lt} and d_{Lr} , and in this case, the method described in section 8.2 is simplified to one with only two earth's radii instead of four. The parameters x_1 and x_2 are defined by (8.12), and $x_0 = x_1 + x_2$. The diffraction attenuation is then computed using (8.10).

The diffraction loss predicted by this method agrees very well with observed values over a number of paths in the United Kingdom and the United States where the common horizon is not isolated.

For transhorizon paths of short to medium length, when it is not known whether diffraction or scatter is the dominant propagation mechanism, both diffraction and scatter loss should be computed. The next section shows how to compute scatter loss, and how to combine the two computed values when they are nearly equal.

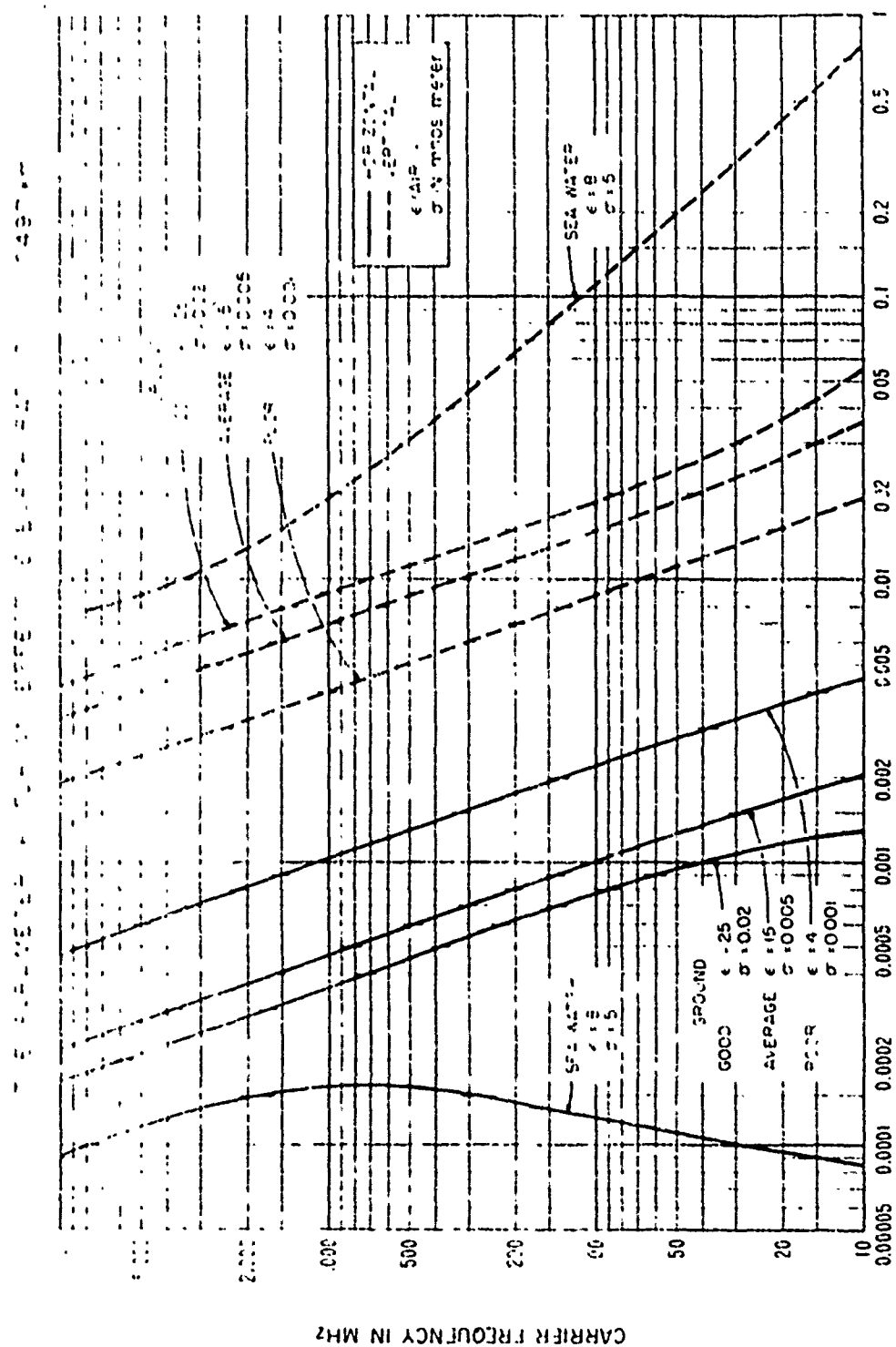


Figure 8:

TIME PARAMETER IN (K, D)

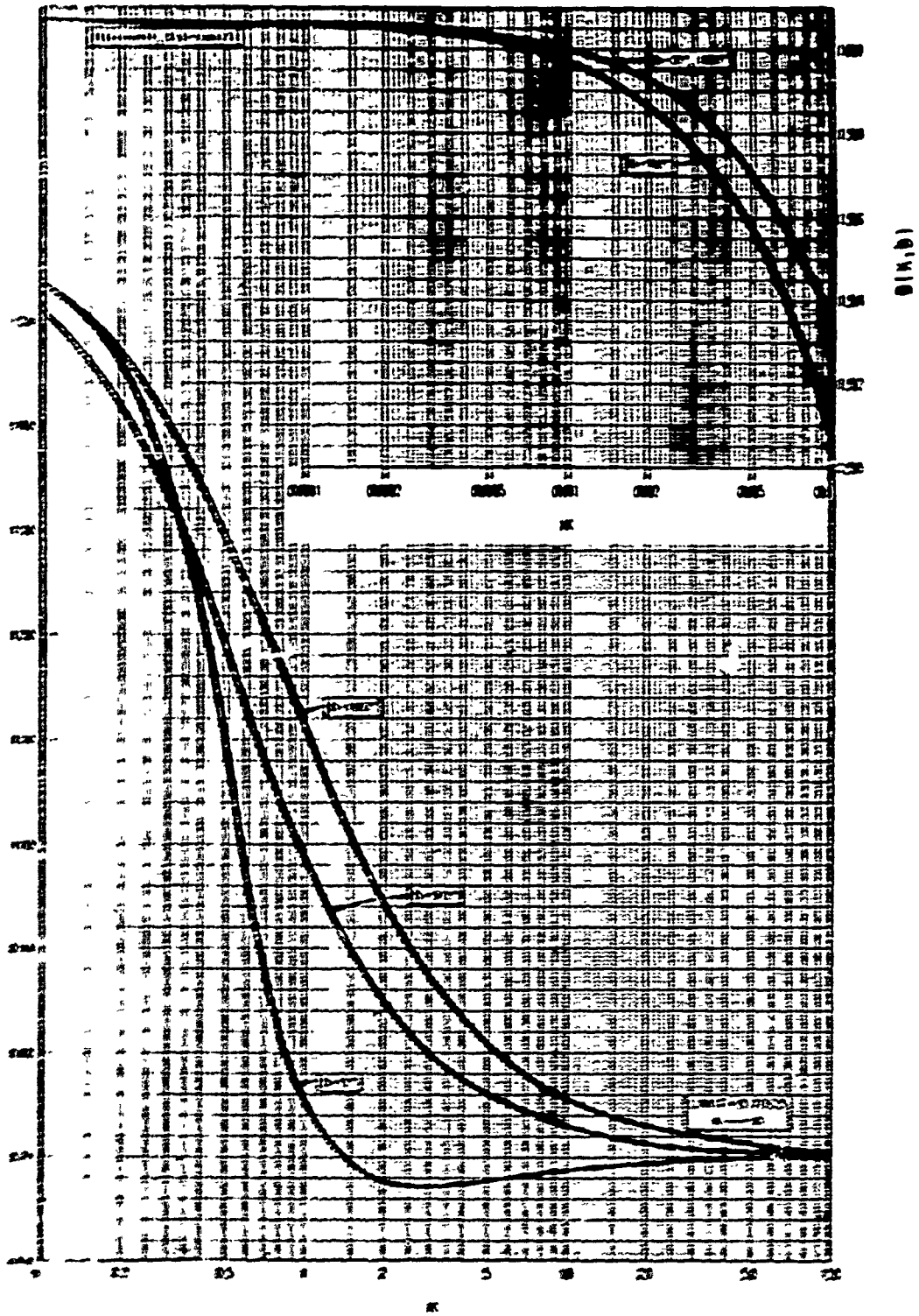


Figure 8.3

THE PARAMETER $G_1(K, b^2)$

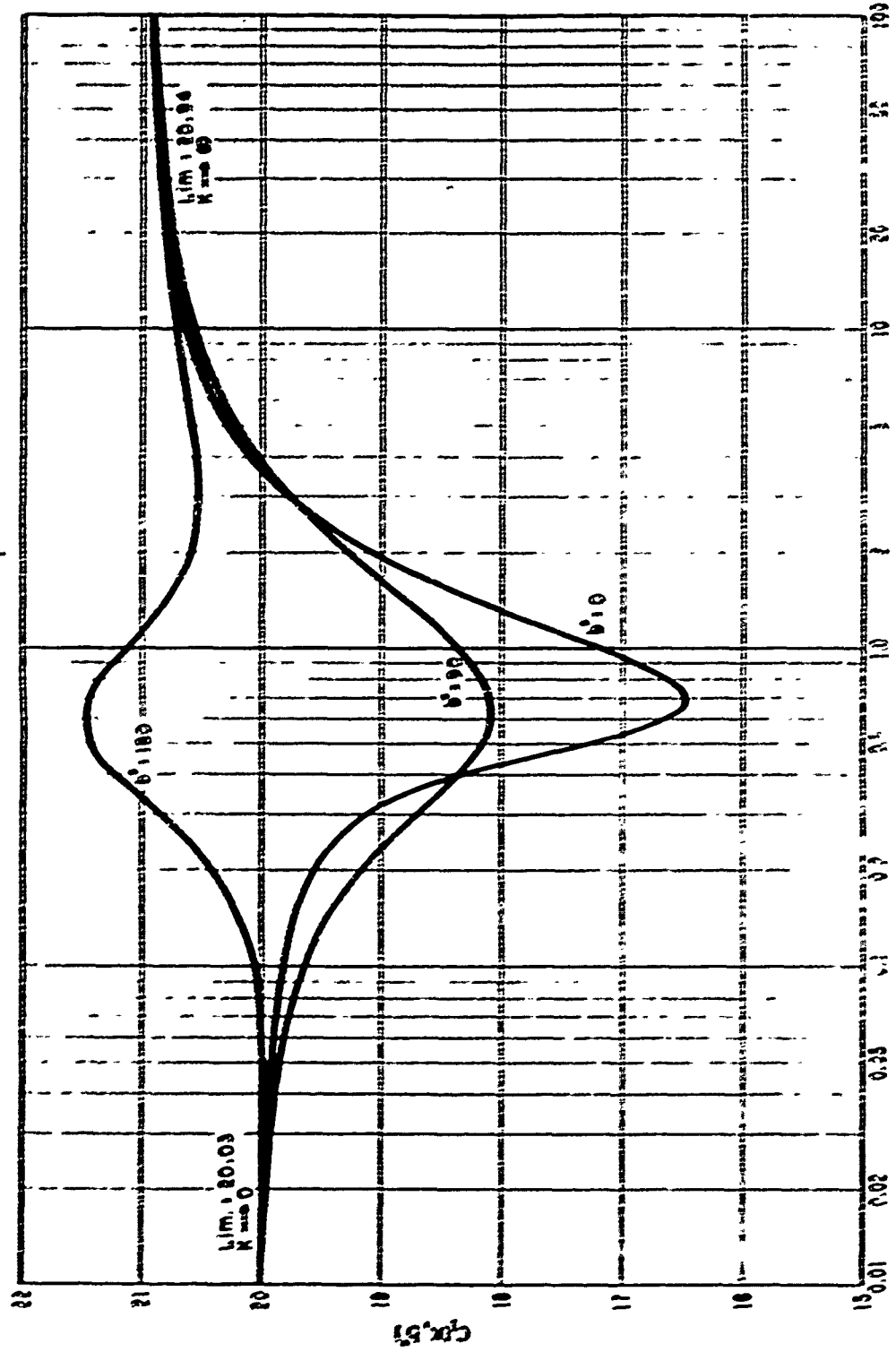


Figure 0.4

THE FUNCTION $F(x_1, x_2)$ FOR $K=0.1$ AND $G(x_1)$
FOR LARGE $x: F(x) \sim G(x)$

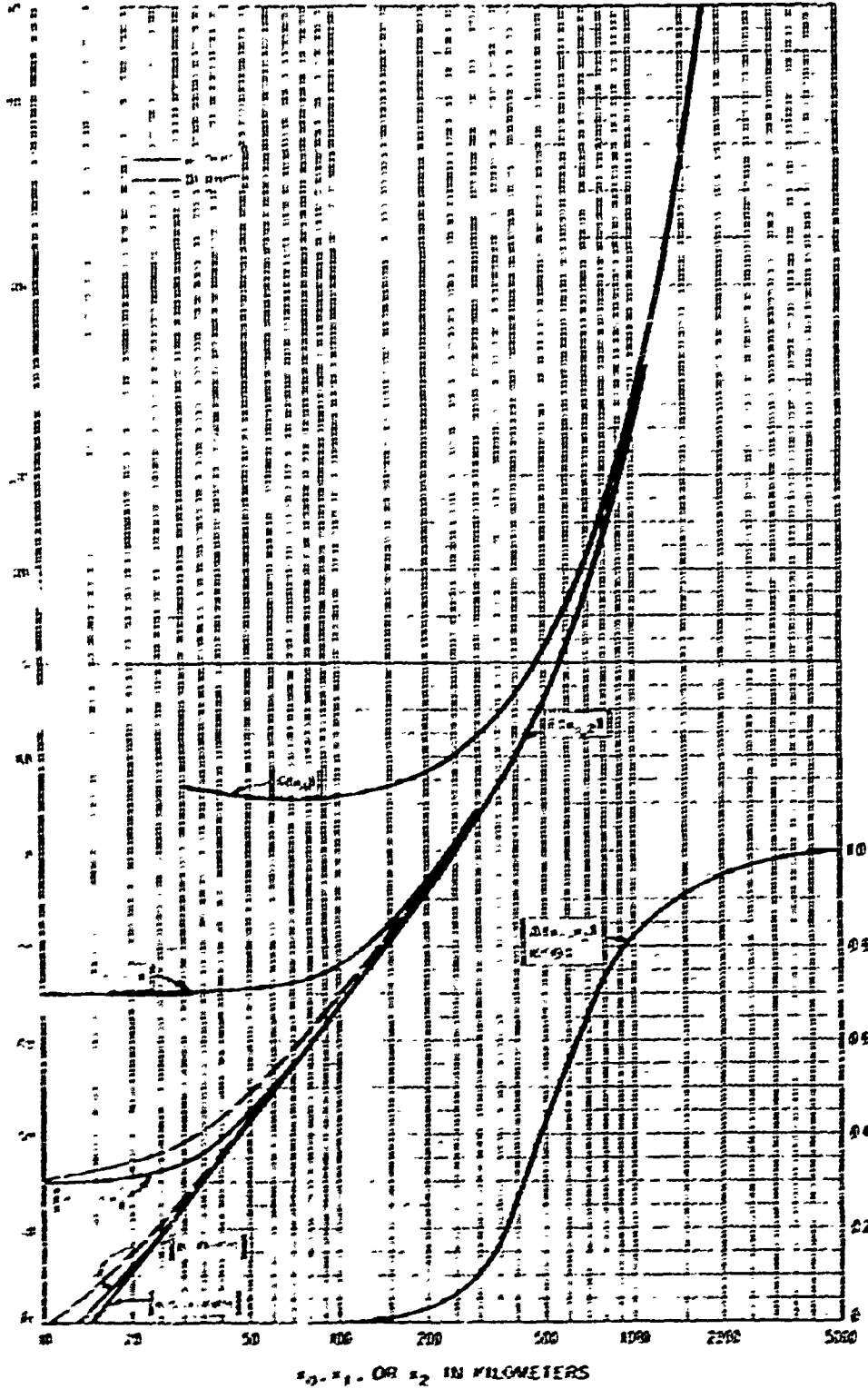


Figure 8 5

THE FUNCTIONS $F(x_1)$, $F(x_2)$ AND $G(x_0)$ FOR THE RANGE $0 \leq x \leq 1$

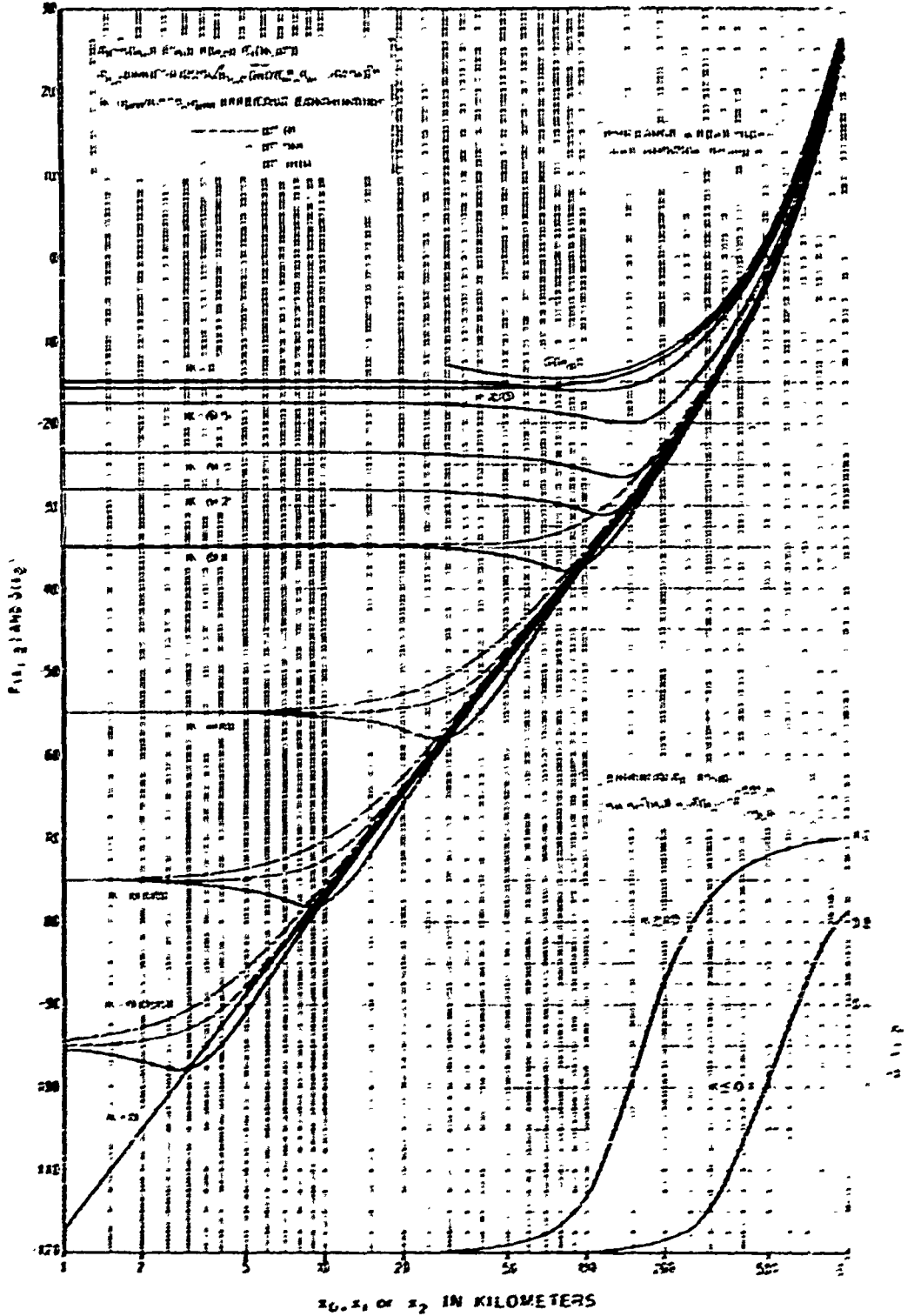


Figure 8.6

GEOMETRY FOR DIFFRACTION OVER IRREGULAR TERRAIN

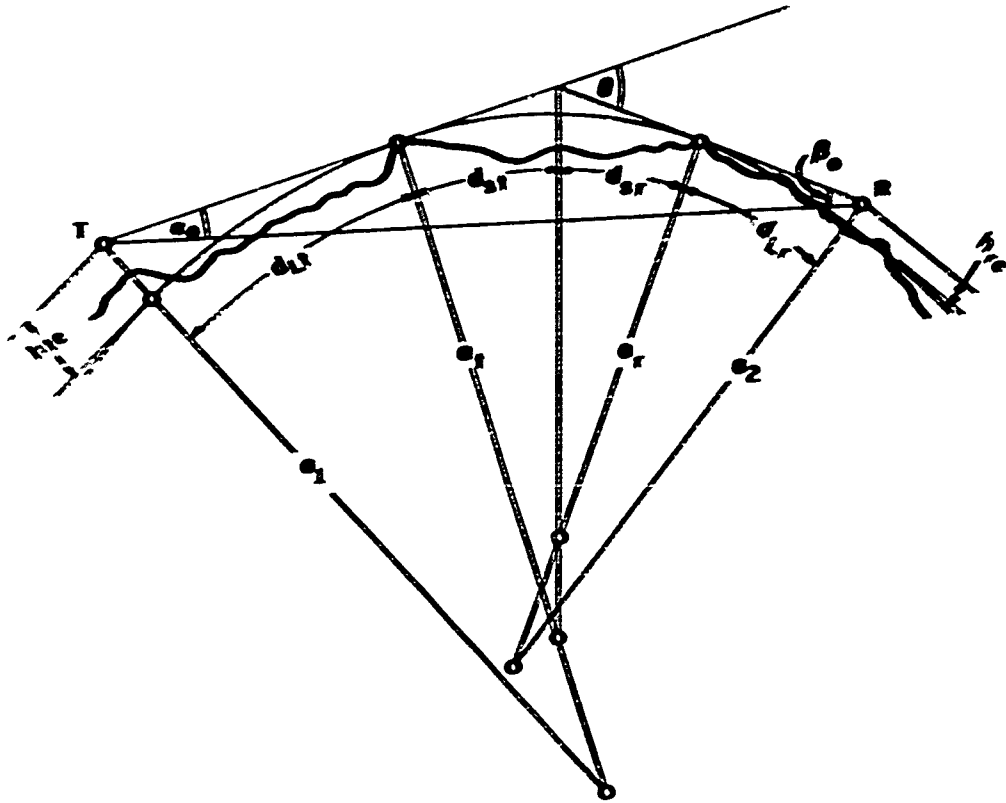


Figure 8.7

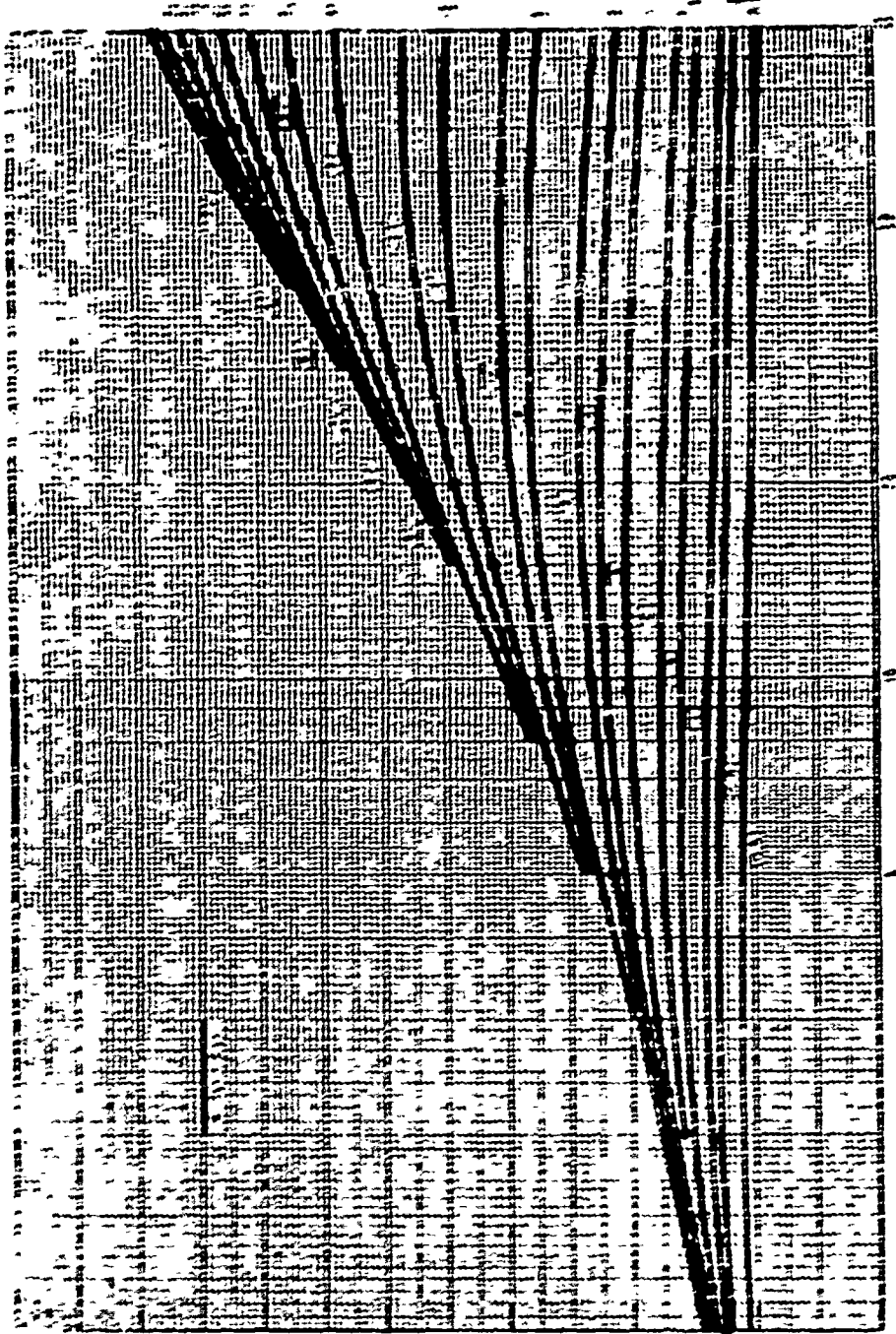


Figure 0.0

Figure 0.0

9 POINT-TO-POINT SCATTER

This section gives methods for calculating reference values of long-term median basic transmission loss over paths that extend well beyond the horizon and for combining different and better transmission loss estimates where this is appropriate. Empirical estimates of the median values and long-term variability of transmission loss for several different systems and periods of time are given in section 10 and annex III.

For long atmospheric paths the propagation mechanism is usually forward scatter, usually during times of day and seasons of the year when diurnal and seasonal layers are present. For other periods of time, as scattering becomes more coherent it is more generally a blind reflection. The examination of transmission loss variation over a particular path during some periods for which detailed information about layer heights, etc., and other data is available can be very illuminating; see for instance Anagnostou and Edlund [1955], and some of the data shown for the "forward scatter" from a turbulent atmosphere and "blind reflection" from patchy elevated layers. The first viewpoint is described in papers by Friis [1947], Booker and Gordon [1950a], Ogawa [1950, 1951, 1952], Kittington [1950], Secor [1952, 1955], Taylor [1957], Truitt [1956, 1957a], Vallis and Wenzel [1955], Vogt [1953, 1955], and Wachen [1957, 1958], while the second viewpoint is emphasized in papers by Bookman [1957, 1960, 1961a, b], deCastel, Meane, and Vogt [1960], Friis, Crawford and Vogt [1957], Scarkey, Turner, Sadler, and Kitchin [1958], and Vogt [1960, 1961]. The general prediction methods described here are for the most part compared with either viewpoint, and agree with long-term median values for all available data. A typical case of forward scatter theories is shown in annex IV.

The reference value, L_{ref} , of long-term median basic transmission loss due to forward scatter is

$$L_{ref} = 30 \log f - 20 \log d + F(\theta) - F_0 + H + A \quad (9.1) \quad (9.2)$$

For most applications the first three terms of (9.1) are sufficient for calculating L_{ref} . f is the radio frequency in MHz, and d is the mean sea level arc distance in kilometers. The attenuation function $F(\theta)$, the scattering efficiency term F_0 , and the frequency correction term H , are discussed in the following subsections. Atmospheric absorption, A , defined by (5.1) and shown on figure 2.5, may be neglected at lower frequencies, but may be more than 1 dB over a long path of 1000 km, and becomes increasingly important with increasing frequency.

For ground-based scatter links the sea level arc distance, d , and the straight line distance, r_0 , between antennas are approximately equal. To estimate transmission loss between the earth and a satellite, where r_0 is much greater than d , a term $20 \log(r_0/d)$

PRECEDING PAGE BLANK-NOT FILMED

should be added to the reference value L_{ref} . Annex III contains a discussion of transmission loss over ground when antennas are elevated above the surface, or directed away from the ground under plane illumination by the surface loss.

The method described in section 4.2.1.1 of Annex III is the basic transmission loss, L_{loss} . The path antenna gain, G_p . Section 4.2.1.2 shows how to estimate the loss in path antenna gain L_{loss} when there is a loss in antenna gain due to scatter. Section 4.2.1.3 shows how to estimate diffraction and scatter losses following Annex III. The scattering of diffraction and the diffraction of scatter losses are approximated.

4.2 The Attenuation Function $F(f, d)$

The attenuation function $F(f, d)$ depends upon the mean impedance densities of the propagation path and upon the surface roughness, σ . The function includes a small empirical adjustment needed available in the frequency range from 100 to 2000 MHz.

For most land-based surface links Figure 9.1 may be used, where $F(f, d)$ is plotted versus the product of the $N_s = 301, 347, 393$ and 450 . The path distance, d , is in kilometers and the surface roughness, σ , in meters. For values of $nd > 10$ the curves of Figure 9.1 are valid for all values of the asymmetry parameter $a = \sigma/\rho_0$. For values of d greater than 10 the curves may be used for values of a from 0.7 to unity. For a greater than 1 use 1/3 in reading the graph.

For highly asymmetrical paths with $nd > 10$, Figures III.11 to III.14 of Annex III are used to obtain $F(f, d)$. Annex III also contains analytical functions fitted to the curves $F(f, d)$ for $nd = 1$ for all values of the product nd for $N_s = 301$. A function is also given to adjust these empirical values for all values of N_s . Using the analytic functions for $F(f, d)$ with $N_s = 301$, the reference median basic transmission loss is

For $nd = 10$:

$$L_{ref} = 135.8 + 50 \log f + 30 \log \sigma + 10 \log d + 0.332 nd \quad (9.2a)$$

For $nd = 50$:

$$L_{ref} = 129.5 + 30 \log f + 37.5 \log \sigma + 17.5 \log d + 0.212 nd \quad (9.2b)$$

Reference values may be computed in a similar manner for other values of N_s .

The approximations in (9.2) do not make any allowance for the frequency gain function. For the usual cases of transmission at frequencies above 400 MHz the approximations in (9.2) are good results. For the higher frequencies an estimate of atmospheric absorption should be added. For lower frequencies, or lower antenna heights, ground-reflected energy tends to cancel the direct ray and the approximation in (9.2) will underestimate the transmission loss.

9.2 The Frequency Gain Function, H_{θ}

It is assumed that if antennas are sufficiently high, reflection of energy by the ground doubles the power incident on scatterers visible to both antennas, and again doubles the power scattered to the receiver. As the frequency is reduced, effective antenna heights h_{te}/λ and h_{re}/λ in wavelengths become smaller, and ground-reflected energy tends to cancel direct-ray energy at the lower part of the antenna pattern, where scattering efficiency is greatest. The frequency gain function H_{θ} in (9.1) is an estimate of the corresponding increase in transmission loss.

This function first decreases rapidly with increasing distance and then approaches a constant value. For $h_{te}/\lambda > 4 \lambda/d$ and $h_{re}/\lambda > 4 \lambda/d$, H_{θ} is negligible. The upper limit of H_{θ} as h_{te} and h_{re} approach zero is $H_{\theta} = 4 + A_{\theta}$ dB, where A_{θ} is the diffraction attenuation over a smooth earth, relative to free space, at $\theta = 0$. For frequencies up to 10 GHz, A_{θ} may be estimated from the CCIR Atlas of Ground Wave Propagation Curves [1955, 1959]. H_{θ} should rarely exceed 25 dB except for very low antennas.

The frequency gain function, H_{θ} , depends on effective antenna heights in terms of wave lengths, path asymmetry, and the parameter η_s shown on figure 9.2 and defined as

$$\eta_s = 0.5676 h_{te} \{ 1 + (0.051 - 2.32 N_s \times 10^{-3} + 5.67 N_s^2 \times 10^{-6}) \exp[-3.8 h_{te}^6 \times 10^{-6}] \} \quad (9.32)$$

$$h_{te} = s d e / (1 + s)^2 \text{ km.} \quad (9.33)$$

The parameters r_1 and r_2 are defined as

$$r_1 = 4r\theta h_{te} / \lambda, \quad r_2 = 4r\theta h_{re} / \lambda \quad (9.34)$$

where θ is the angular distance in radians, and the effective antenna heights h_{te} , h_{re} are in the same units as the radio wave length, λ . In terms of frequency r_1 and r_2 may be written

$$r_1 = 41.92\theta f h_{te}, \quad r_2 = 41.92\theta f h_{re} \quad (9.45)$$

where θ is in radians, f in MHz, and h_{te} , h_{re} are in kilometers.

For the great majority of transhorizon paths, s is within the range $0.7 \leq s \leq 1$. The effect of very small values of s , with $\alpha_0 \ll \beta_0$, may be seen in figures III.15 to III.19, which have been computed for the special case where effective transmitting and receiving antenna heights are equal.

a) From η_s determine distance s equal to H_0 .

Read $H_0(r_1)$ and $H_0(r_2)$ from figure 9.3; then H_0 is

$$H_0 = [H_0(r_1) + H_0(r_2)]/2 + \Delta H_0 \tag{9.5}$$

where

$$\Delta H_0 = 6(0.6 - \log \eta_s) \log s \log q$$

$$s = r_2 / \eta_s \quad q = r_2 / r_1$$

If $\eta_s < 1$ the value of H_0 for $\eta_s = 5$ is used. The correction term ΔH_0 is zero for $\eta_s = 1$, or $q = 1$ and reaches a maximum value, $\Delta H_0 = 3.6$ db, for highly asymmetrical paths when $\eta_s = 1$. The value of ΔH_0 may be computed as shown or read from the nomogram, figure 9.4. A straight line between values of s and q on their respective scales intersects the vertical line marked 0. This point of intersection when connected by a straight line to the appropriate value of η_s intersects the ΔH_0 scale at the desired value.

The following limits should be applied in determining ΔH_0 :

If $s > 10$ or $q > 10$, use $s = 10$ or $q = 10$.

If $s < 0.1$ or $q < 0.1$, use $s = 0.1$ or $q = 0.1$.

If $\Delta H_0 = [H_0(r_1) + H_0(r_2)]/2$, use $H_0 = H_0(r_1) + H_0(r_2)$.

If ΔH_0 would make H_0 negative, use $H_0 = 0$.

b) η_s less than 1:

First obtain H_0 for $\eta_s = 1$ as described above, then read H_0 for $\eta_s = 0$ from figure 9.5. Figure 9.5 shows $H_0(\eta_s = 0)$ for the special case of equal antenna heights. The desired value is found by interpolation:

$$H_0(\eta_s < 1) = H_0(\eta_s = 0) + \eta_s [H_0(\eta_s = 1) - H_0(\eta_s = 0)] \tag{9.6}$$

The case $\eta_s = 0$ corresponds to the assumption of a constant atmospheric refractive index.

A special case, $h_{rc} = h_{rc}$, $r_1 = r_2$ occurs frequently in systems design. For this case H_0 has been plotted versus r in figures III.15 to III.19 for $\eta_s = 1, 2, 3, 4, 5$ and for $s = 0.1, 0.25, 0.5, 0.75$ and 1. For given values of η_s and s , H_0 is read directly from the graphs using linear interpolation. No correction term is required. For $\eta_s < 1$ the value $H_0(\eta_s = 1)$ is read from figure 9.3 with $r_1 = r_2$ and $H_0(\eta_s = 0)$ is read from figure 9.5.

9.3 The Scattering Efficiency Correction, F_o

The correction term F_o in (9.1) allows for the reduction of scattering efficiency at great heights in the atmosphere:

$$F_o = 1.086(\eta_s/h_o)(z_o - h_1 - h_{Lt} - h_{Lr}) \text{ db} \quad (9.7)$$

where η_s and h_o are defined by (9.3) and h_1 is defined as

$$h_1 = sD_s \theta / (1 + s)^2, \quad D_s = d - d_{Lt} - d_{Lr} \quad (9.8)$$

The heights of the horizon obstacles, h_{Lt} , h_{Lr} and the horizon distances d_{Lt} , d_{Lr} are defined in section 6. All heights and distances are expressed in kilometers.

The correction term F_o exceeds 2 decibels only for distances and antenna heights so large that h_o exceeds h_1 by more than 3 kilometers.

9.4 Expected Values of Forward Scatter Multipath Coupling Loss

Methods for calculating expected values of forward scatter multipath coupling loss are given in several papers, by Rice and Daniel [1955], Booker and de Bettencourt [1955], Staras [1957], and Hartman and Wilkerson [1959]. This report uses the most general method available based on the paper by Hartman and Wilkerson [1959].

As explained in section 2, the path antenna gain is

$$G_p = G_t + G_r - L_{gp} \quad \text{db} \quad (9.9)$$

where G_t and G_r are free space antenna gains in decibels relative to an isotropic radiator. The influence of antenna and propagation path characteristics in determining the loss in path antenna gain or multipath coupling loss L_{gp} are interdependent and cannot be considered separately.

This section shows how to estimate only that component of the loss in path antenna gain which is due to phase incoherence of the forward scattered fields. This quantity is readily approximated from figure 9.6 as a function of η_g , defined by (9.3), and the ratio θ/Ω , where $\Omega = 2\delta$ is the effective half-power antenna beamwidth. If the antenna beamwidths are equal, $\Omega_t = \Omega_r$, and if $s = 1$, values of L_{gp} from figure 9.6 are exact. When antenna beamwidths are not equal the loss in gain may be approximated using $\Omega = \sqrt{\Omega_t \Omega_r}$.

The relation between the free-space antenna gain G in decibels relative to an isotropic radiator and the half power beamwidth $\Omega = 2\delta$ was given by (2.5) as:

$$G = 3.50 - 20 \log \delta = 9.52 - 20 \log \Omega \quad \text{db}$$

where δ and Ω are in radians.

Assuming 56% aperture efficiencies for both antennas,

$$\theta/\Omega \approx \theta(\Omega_t \Omega_r)^{-1/2} \approx 0.3350 \exp \{ 0.0576 (G_t + G_r) \} \quad (9.10)$$

where θ is the angular distance in radians and G_t , G_r are the free space gains in decibels.

Section 2 shows that the gain for parabolic dishes with 56% aperture efficiency may be computed as (2.7):

$$G = 20 \log D + 20 \log f - 42.10 \quad \text{db}$$

where D is the diameter of the dish in meters and f is the frequency in MHz.

For dipole-fed parabolic antennas where $10 < D/\lambda < 25$, an empirical correction gives the following equation for the antenna gain (2.8):

$$G = 23.3 \log D + 23.3 \log f - 55.1 \quad \text{db}$$

The general method for calculating L_{gp} requires the following parameters:

$$v = \eta_g/2, \quad \mu = \delta_r/\delta_t \quad (9.11)$$

$$\text{For } su \geq 1, n = \alpha_0/\delta_t. \quad \text{For } su \leq 1, n = \beta_0/\delta_r \quad (9.12a)$$

$$\hat{n} = (n + 0.03v)/f(v) \quad (9.12b)$$

$$f(v) = [1.36 + 0.116v] [1 + 0.36 \exp(-0.56v)]^{-1} \quad (9.13)$$

where η_g , α_0 and β_0 have been defined, δ_t and δ_r are the effective half-power semi-beamwidths of the transmitting and receiving antennas, respectively, and $f(v)$ as defined by (9.13) is shown on figure 9.7.

Figure 9.8 shows L_{gp} versus \hat{n} for various values of the product su . For $su < 1$ read figure 9.8 for $1/(su)$ instead of su .

9.5 Combination of Diffraction and Scatter Transmission Loss

For transmission paths extending only very slightly beyond line-of-sight, diffraction will be the dominant mechanism in most cases and scattering may be neglected. Conversely, for long paths, the diffracted field may be hundreds of decibels weaker than the scattered field, and thus the diffraction mechanism can be neglected. In intermediate cases, both mechanisms have to be considered and the results combined in the following manner:

Figure 9.9 shows a function, $R(0.5)$, which depends on the difference between the diffraction and scatter transmission loss. Calculate this difference ($L_{dr} - L_{sr}$) in decibels, determine $R(0.5)$ from figure 9.9 and then determine the resulting reference value of hourly median transmission loss, L_{cr} , from the relation

$$L_{cr} = L_{dr} - R(0.5). \quad (9.14)$$

If the difference between the diffracted and the scattered transmission loss values exceeds 15 dB, the resulting value of L_{cr} will be equal to L_{dr} if it is smaller than L_{sr} , or to L_{sr} if this is the smaller value. In general, for most paths having an angular distance greater than 0.02 radians the diffraction calculations may be omitted; in this case, $L_{cr} = L_{sr}$.

The angular distance $\theta = 22.251 \text{ mrad} = 0.12558$ radians and the product $\theta d = 0.10$. The value of $\frac{\sin \theta}{\theta} = 0.999$. Then the function $F(\theta d)$ from figure 2.2 or figures III.22 and III.23 is $F(\theta d) = 0.999$ db. From (II.3) the height $h = 4.85 \text{ km}$, and $\tau = 2.74$. From (II.4) and figure 2.3 the parameters $\tau_1 = 0.93$, $H_{10} = 0.85 \text{ db}$, $\tau_2 = 2.34$, and $H_{20} = 1.2$ db. From figure 2.4 and (II.5) $\Delta H = 0.44 \text{ db}$ and $H = 2.90 \text{ db}$. The correction term δ from (II.7) is negligible. Figure 2.6 shows that the allowed ϵ for absorption $\delta = 0.1 \text{ db}$.

The effective earth's radius is determined as described in section 4. From figure 2.2 the effective earth's radius of R_{eff} for each of the appropriate horizon locations. Approximate values are given in (II.3) for appropriate horizon values of R_{eff} , without coverage as $R_{eff} = \dots$. From (II.4) the effective earth's radius is then found as $R_{eff} = \dots$.

The effective earth's radius R_{eff} is determined as described in section 4. From figure 2.2 the effective earth's radius of R_{eff} for each of the appropriate horizon locations. Approximate values are given in (II.3) for appropriate horizon values of R_{eff} , without coverage as $R_{eff} = \dots$. From (II.4) the effective earth's radius is then found as $R_{eff} = \dots$.

The effective earth's radius R_{eff} is determined as described in section 4. From figure 2.2 the effective earth's radius of R_{eff} for each of the appropriate horizon locations. Approximate values are given in (II.3) for appropriate horizon values of R_{eff} , without coverage as $R_{eff} = \dots$. From (II.4) the effective earth's radius is then found as $R_{eff} = \dots$.

Table: Station to Station, Traces

$$d = 252.8 \text{ km}, \quad z = 216.5 \text{ GHz}, \quad R_0 = 6371 \text{ km}, \quad \alpha = 0.0003 \text{ km}^{-1}$$

Parameter	Parameter	Parameter	Reference
R_{10}	252.8 km	252.8 km	Figure 2.23
R_{20}	252.8 km	7.6 km	(II.23) and (II.24)
R_{30}	252.8 km	7.6 km	Figure 2.23
R_{40}	252.8 km	7.6 km	Figure 2.23
R_{50}	252.8 km	7.6 km	(II.23)
R_{60}	252.8 km	7.6 km	(II.23)
R_{70}	252.8 km	7.6 km	(II.23)
R_{80}	252.8 km	7.6 km	(II.23)
R_{90}	252.8 km	7.6 km	Figure 2.4
R_{100}	252.8 km	7.6 km	(II.23)

The angular distance $\theta = 22.251 \text{ mrad} = 0.12558$ radians and the product $\theta d = 0.10$. The value of $\frac{\sin \theta}{\theta} = 0.999$. Then the function $F(\theta d)$ from figure 2.2 or figures III.22 and III.23 is $F(\theta d) = 0.999$ db. From (II.3) the height $h = 4.85 \text{ km}$, and $\tau = 2.74$. From (II.4) and figure 2.3 the parameters $\tau_1 = 0.93$, $H_{10} = 0.85 \text{ db}$, $\tau_2 = 2.34$, and $H_{20} = 1.2$ db. From figure 2.4 and (II.5) $\Delta H = 0.44 \text{ db}$ and $H = 2.90 \text{ db}$. The correction term δ from (II.7) is negligible. Figure 2.6 shows that the allowed ϵ for absorption $\delta = 0.1 \text{ db}$.

The effective earth's radius R_{eff} is determined as described in section 4. From figure 2.2 the effective earth's radius of R_{eff} for each of the appropriate horizon locations. Approximate values are given in (II.3) for appropriate horizon values of R_{eff} , without coverage as $R_{eff} = \dots$. From (II.4) the effective earth's radius is then found as $R_{eff} = \dots$.

$200 \text{ Hz } d = 600,000$

$200 \text{ Hz } d = 600,000$

$W(100) = 1127.0 \text{ Figure 11.1}$

$F_{00} = 0 \text{ (17.7)}$

$F_{00} = 2.00 \text{ (17.9)}$

$A_{00} = 0.00 \text{ Figure 11.2}$

and $F_{00} = 100 \text{ dB}$.

Although this is almost certainly a correct path, the diffraction loss for a transmission path is computed as an example. For the assumed polarization over average ground figures A, B and C above $W(100) = 1127.0$ and $h = 35$. The following diffraction parameters are computed:

				Reference
$d_1 = 5000 \text{ km}$	$d_2 = 3000 \text{ km}$	$d_3 = 1000 \text{ km}$	$d_4 = 2000 \text{ km}$	(17.7) and (17.9)
$C_{00} = 1.155$	$C_{00} = 1.570$	$C_{00} = 0.955$	$C_{00} = 1.155$	(17.7)
$F_{00} = 0.00000$	$F_{00} = 0.00000$	$F_{00} = 0.00000$	$F_{00} = 0.00000$	(17.7)
$B_{00} = 1.0000$	$B_{00} = 1.0000$	$B_{00} = 1.0000$	$B_{00} = 1.0000$	Figure 11.3
$C_{00}(B_{00}) = 20.00$	$C_{00}(B_{00}) = 20.00$	$C_{00}(B_{00}) = 20.00$	$C_{00}(B_{00}) = 20.00$	Figure 11.4
$A_{00} = 300.00$	$A_{00} = 200.00$	$A_{00} = 100.00$	$A_{00} = 200.00$	(17.7) and (17.9)
$B_{00}(A_{00}) = -11.0$	$B_{00}(A_{00}) = -26.5$	$B_{00}(A_{00}) = -11.0$	$B_{00}(A_{00}) = -11.0$	Figure 11.5
$Q_{00}(A_{00}) = 100.00$				(17.9)

Then from (17.10) the attenuation relative to free space $A = 1127.0 - A_{00} = 100 \text{ dB}$. The free space loss (17.14) is $L_{00} = 100 \text{ dB}$ and the long-term average median transmission loss due to diffraction $L_{00} = 254.5 \text{ dB}$. As expected this is much more than the predicted median loss and the long-term reference value $L_{00} - L_{00} = 154.5 \text{ dB}$.

Long-term variability of hourly median median transmission loss over this path can be computed using the methods described in section 20. An "effective" distance d_e is computed using (17.4). The appropriate value of $W(5, d_e)$ is read from Figure 11.12 of annex III and subtracted from L_{00} to obtain the long-term median transmission loss. Variability about the median is then determined as a function $W(5, d_e)$. The effective distance d_e is computed using (17.4), (17.2) and (17.3b). $d_e = 36.6 \text{ km}$, $d_e = 62.0 \text{ km}$ and $d_e = 206.4 \text{ km}$. From Figures 10.14, 10.15, 10.16, 10.17 and 10.18 the following parameters are:

Parameter	Summer	Winter	All times	Reference
$200 \text{ Hz } d_e$	5.0	1.0	1.0	Figure 10.14
$200 \text{ Hz } d_e \times 100 \times 10^{-25}$	2.75	2.75	2.75	Figure 10.14
$200 \text{ Hz } d_e \times 100 \times 10^{-35}$	4.35	4.35	4.35	Figure 10.15
$200 \text{ Hz } d_e$	1.055	1.055	1.055	Figure 10.16
$200 \text{ Hz } d_e$	1.055	1.055	1.055	Figure 10.16
$200 \text{ Hz } d_e$	4.20	4.20	4.20	Figure 10.17
$200 \text{ Hz } d_e$	4.20	4.20	4.20	Figure 10.18

CCP 112-1

Using the reference value $q_{ref} = 100 \text{ dB}$ and the path as given in (10.7) the predicted cumulative distribution function, number and all hours are calculated as follows:

q	Summer	Winter	All Hours
100	100.0	100.0	100.0
99	100.0	100.0	100.0
98	100.0	100.0	100.0
97	100.0	100.0	100.0
96	100.0	100.0	100.0
95	100.0	100.0	100.0
94	100.0	100.0	100.0
93	100.0	100.0	100.0
92	100.0	100.0	100.0
91	100.0	100.0	100.0
90	100.0	100.0	100.0

These cumulative distributions are shown graphically on Figure 9.22 together with distributions derived from measurements over the path. The data represent more than 22,000 hourly median values from measurements over a period of more than 3 years. The arrows on the curves at 95 dB indicate that losses were less than the values plotted while those at 90 dB and 85 dB indicate that the losses were greater than the values plotted.

An example may be included here on the method of averaging distributions described in subsection 10.1.2. The summer and winter distributions of data may be mixed in order to obtain the distribution of hourly median values for all hours. Several levels of transmission loss from 85 to 115 dB are chosen and the value of q is read from Figure 9.22 for each distribution. A weighted average is then obtained at each level to provide the mixed distribution of data corresponding to all hours. The weights are the number of hours of data in each case and the weighted average is $\frac{h}{h_1 + h_2}$ (e.g. $\frac{100}{100 + 100} = 0.5$).

Level	ρ_{winter}	ρ_{summer}	Average ρ (all months)
155	<0.0005	0.397	0.0048
170	0.023	0.109	0.063
175	0.063	0.252	0.143
180	0.262	0.590	0.406
185	0.50	0.863	0.683
190	0.86	0.967	0.913
195	<0.9995	<0.9995	>0.9985

The weighted averages of ρ are plotted on Figure 2.13 at each of these levels of concentration and show very good agreement with the distribution obtained directly from the data.

THE ATTENUATION FUNCTION, $A(f, R)$
AS A FUNCTION OF FREQUENCY f AND RANGE R
(IN DB/DOM)

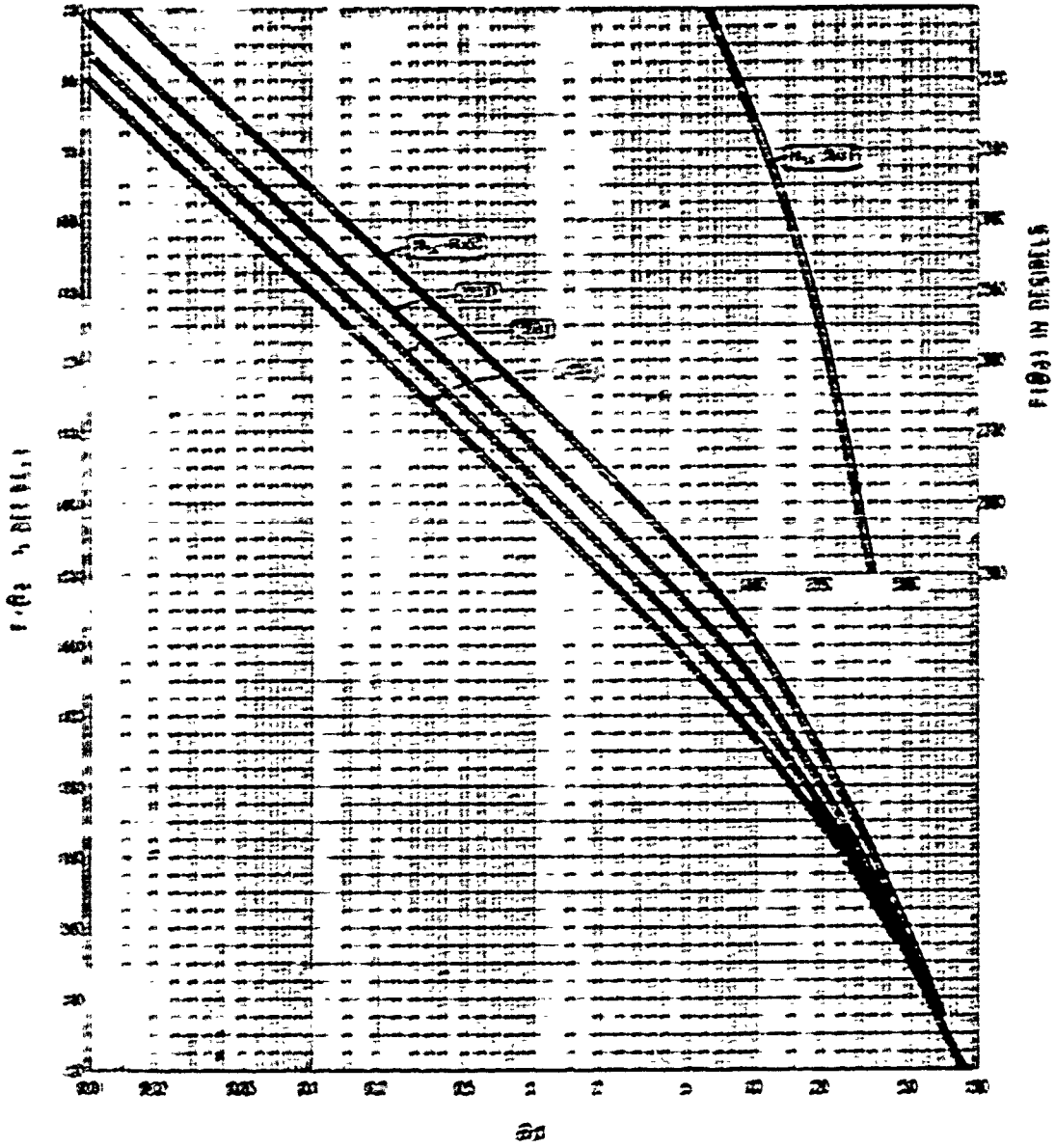


Figure 21

THE PARAMETER $\gamma_3(H_0)$ USED TO COMPUTE H_0

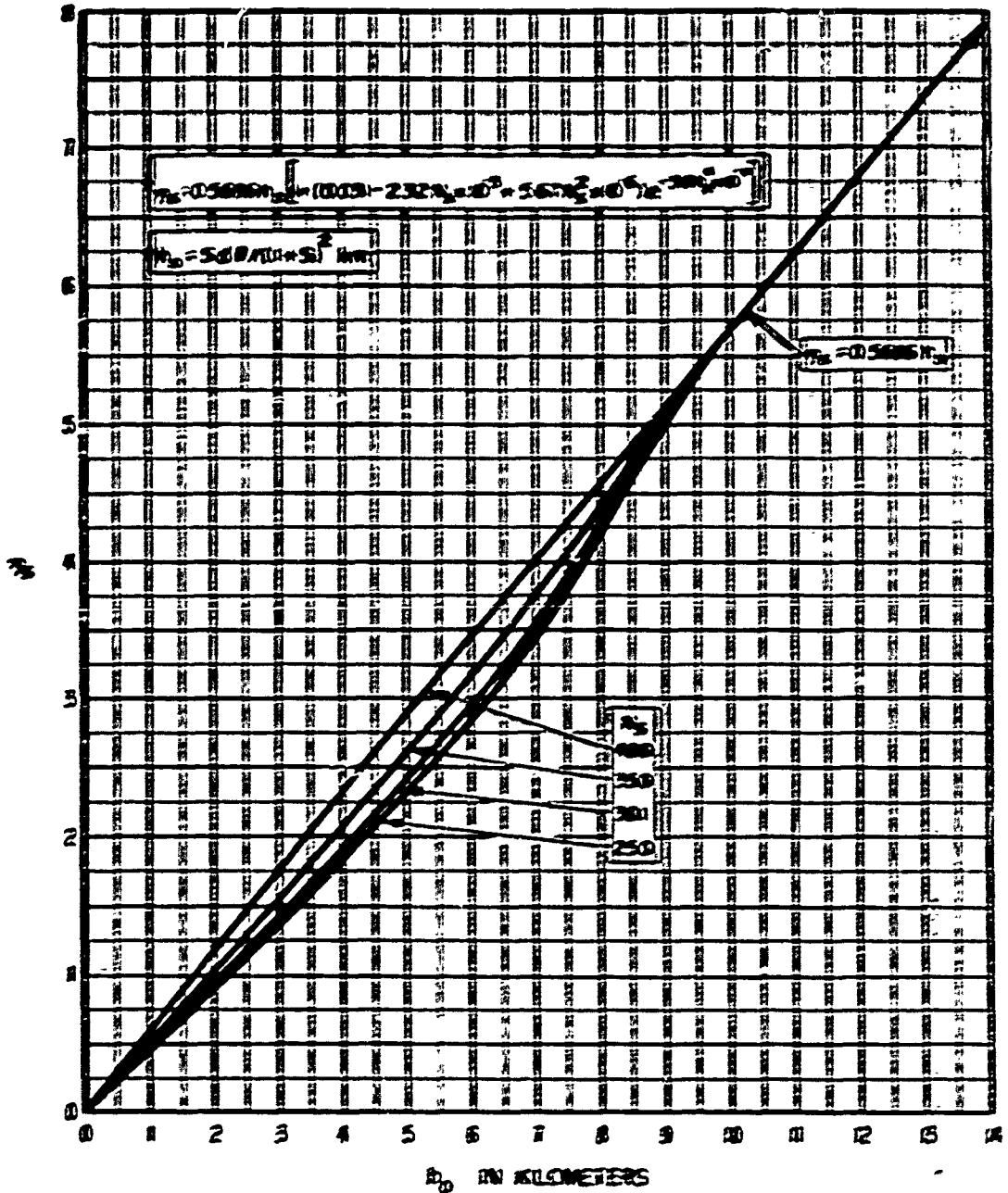


Figure 92

THE FREQUENCY GAIN FUNCTION, M_0

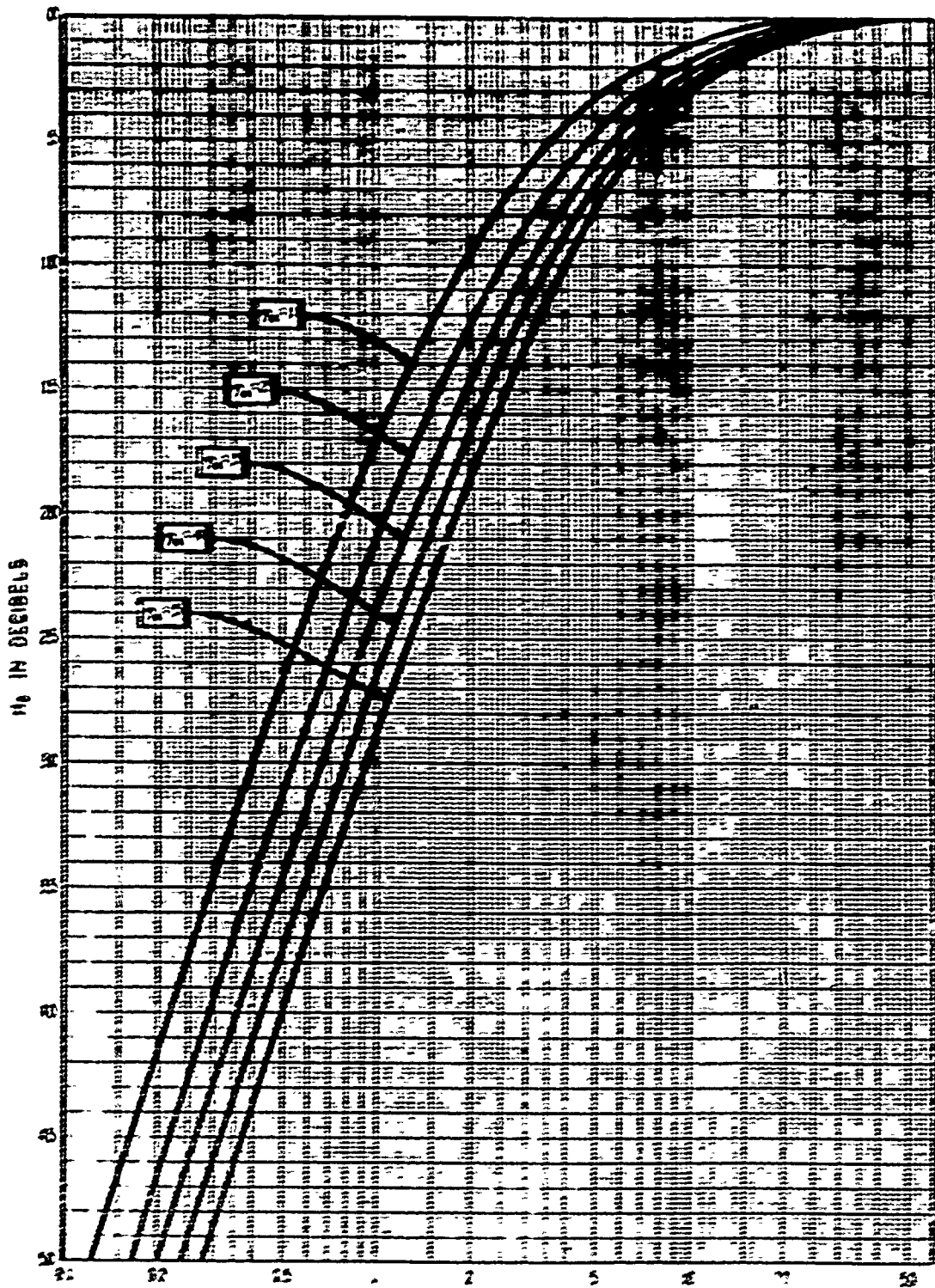
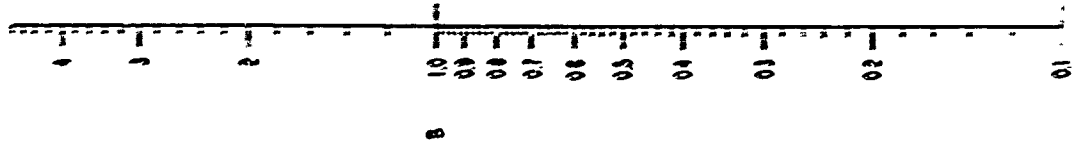


Figure 23

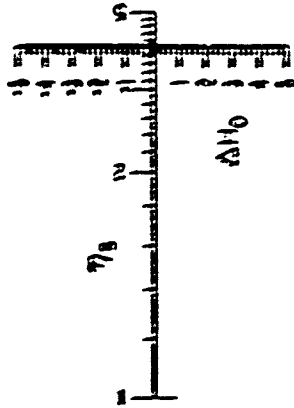
NOMOGRAM TO DETERMINE ΔH_0

$$\Delta H_0 = 6(0.6 - 109 \gamma_s) / 109 + 109 q$$

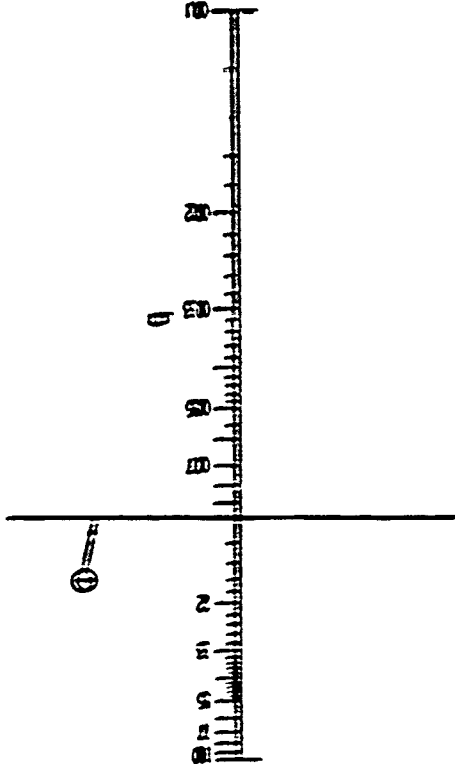
$$q = r_g / (107) , s = \sigma_0 / \beta_0$$



s



ΔH_0



9-15
F-191

Figure 9.4

THE PARAMETER H_0 FOR $\eta_0 = 0$
($\omega = 5-20$)

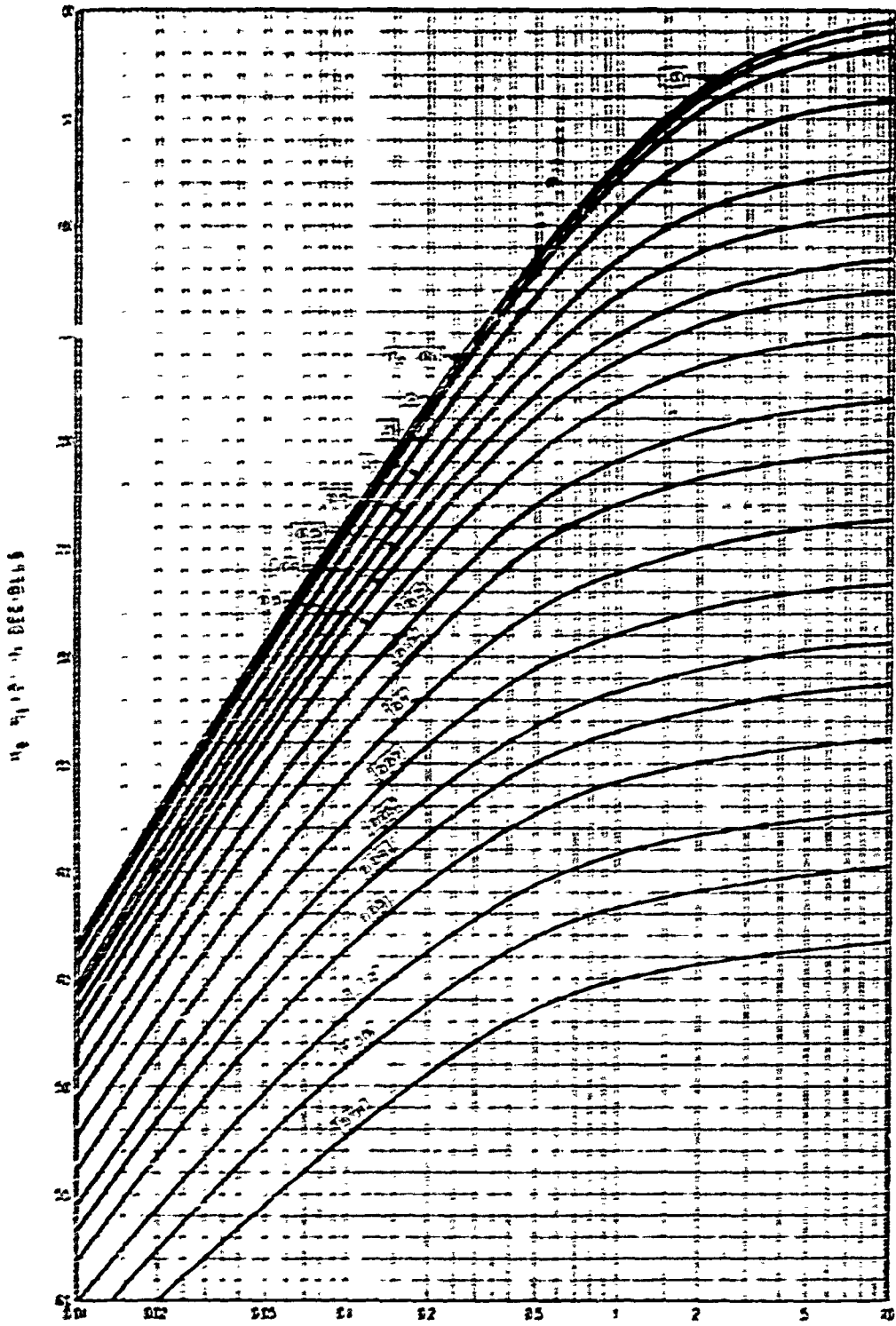
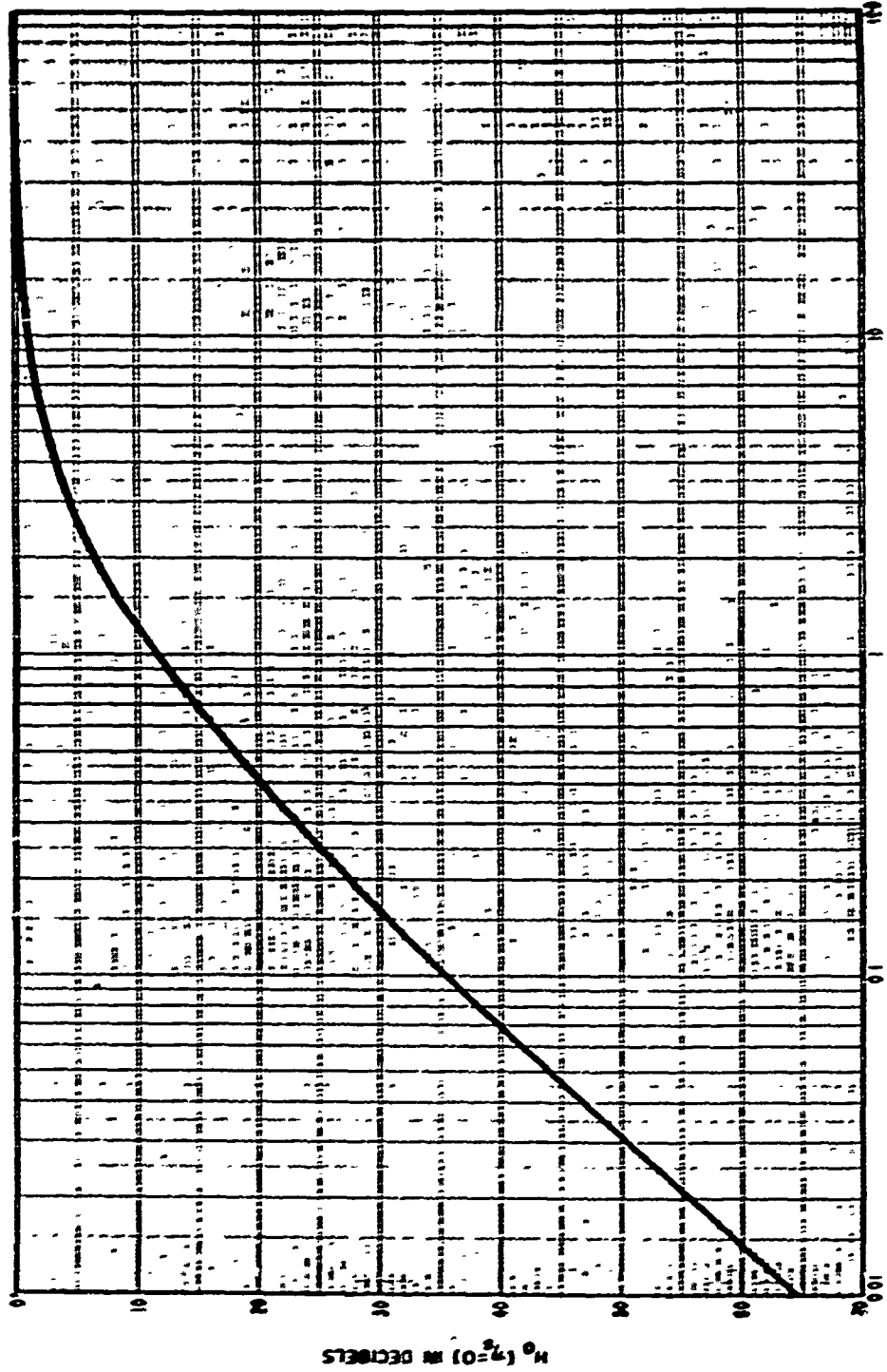


Figure 95a

THE PARAMETER H FOR $\eta_{0.50}$ AND $\eta_{10.50}$



f1 = f2

Figure 95h

LOSS IN ANTENNA GAIN, L_{sp}
 assuming equal free space gains G_t and G_r
 of the terminals of a symmetrical path

$$\Omega_t = \Omega_r, s=1$$

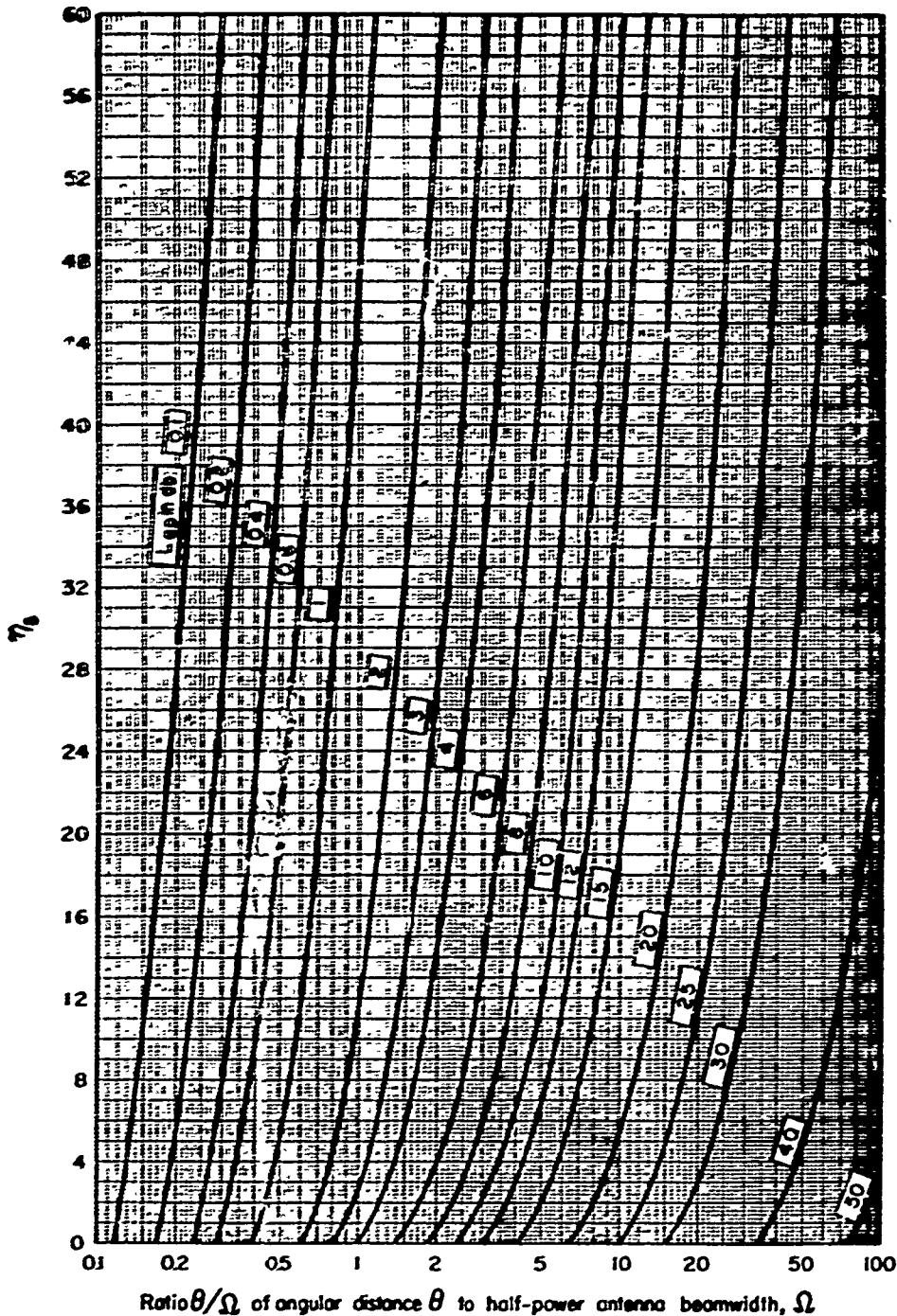


Figure 9.6

THE CONTRACTION FACTOR $f(\nu)$

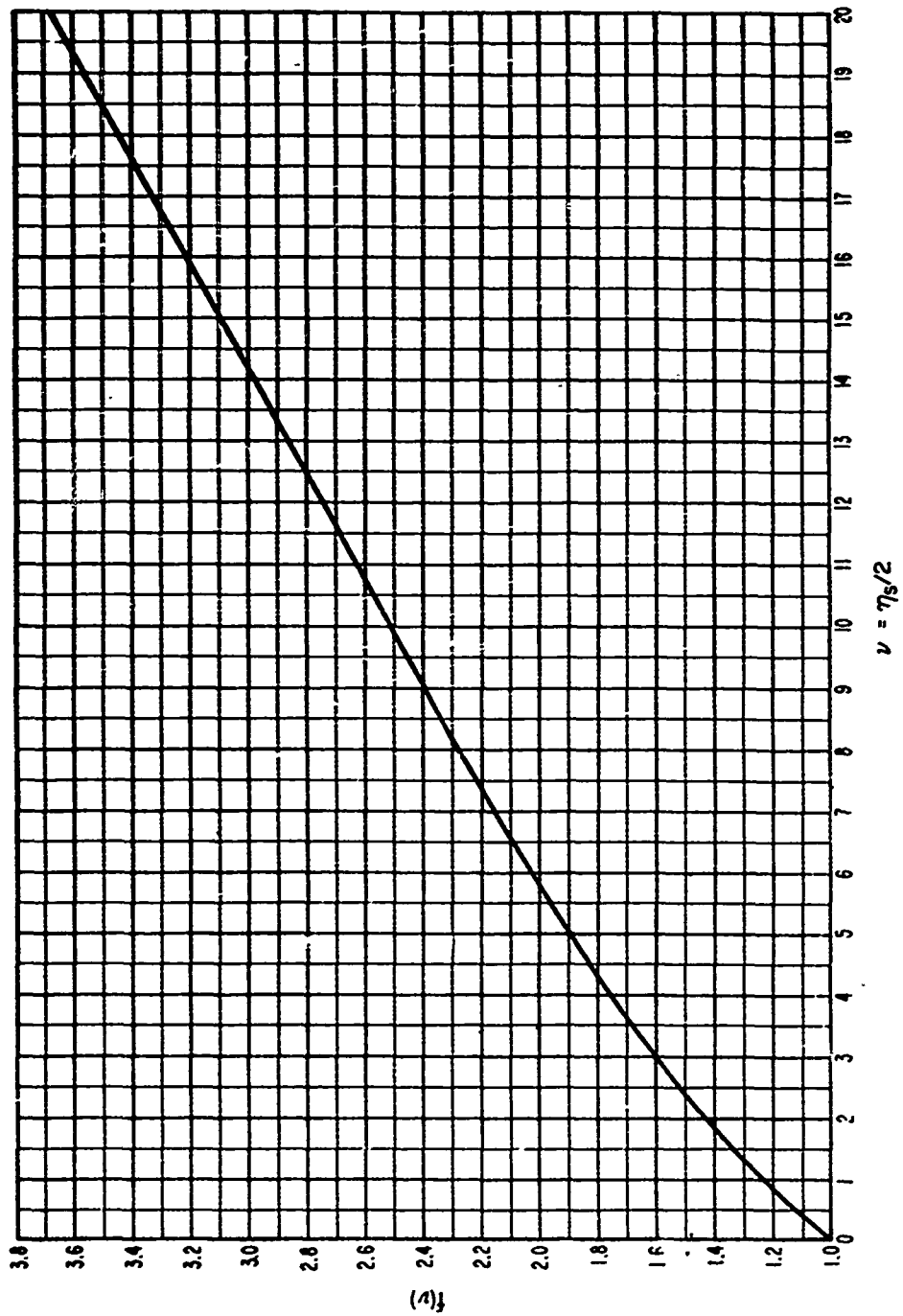


Figure 9.7

LOSS IN PATH ANTENNA GAIN vs \hat{n}

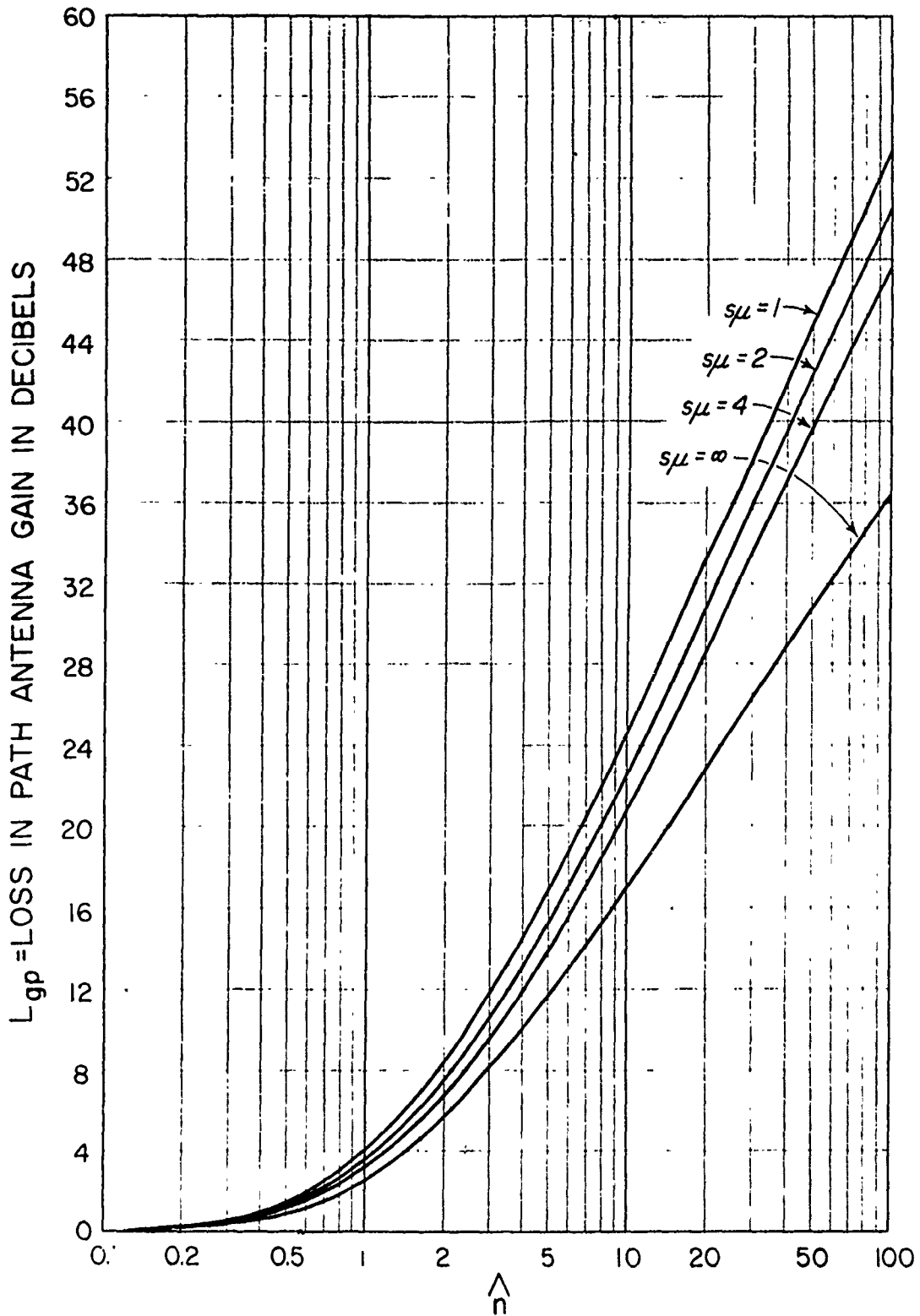


Figure 9.8

THE MEDIAN, $R_{0.5}$, FROM THE CUMULATIVE DISTRIBUTION OF THE
 RESULTANT AMPLITUDE OF A CONSTANT DIFFRACTED FIELD
 PLUS A RAYLEIGH DISTRIBUTED SCATTERED FIELD

$$L_{cr} = L_{dr} - R(0.5)$$

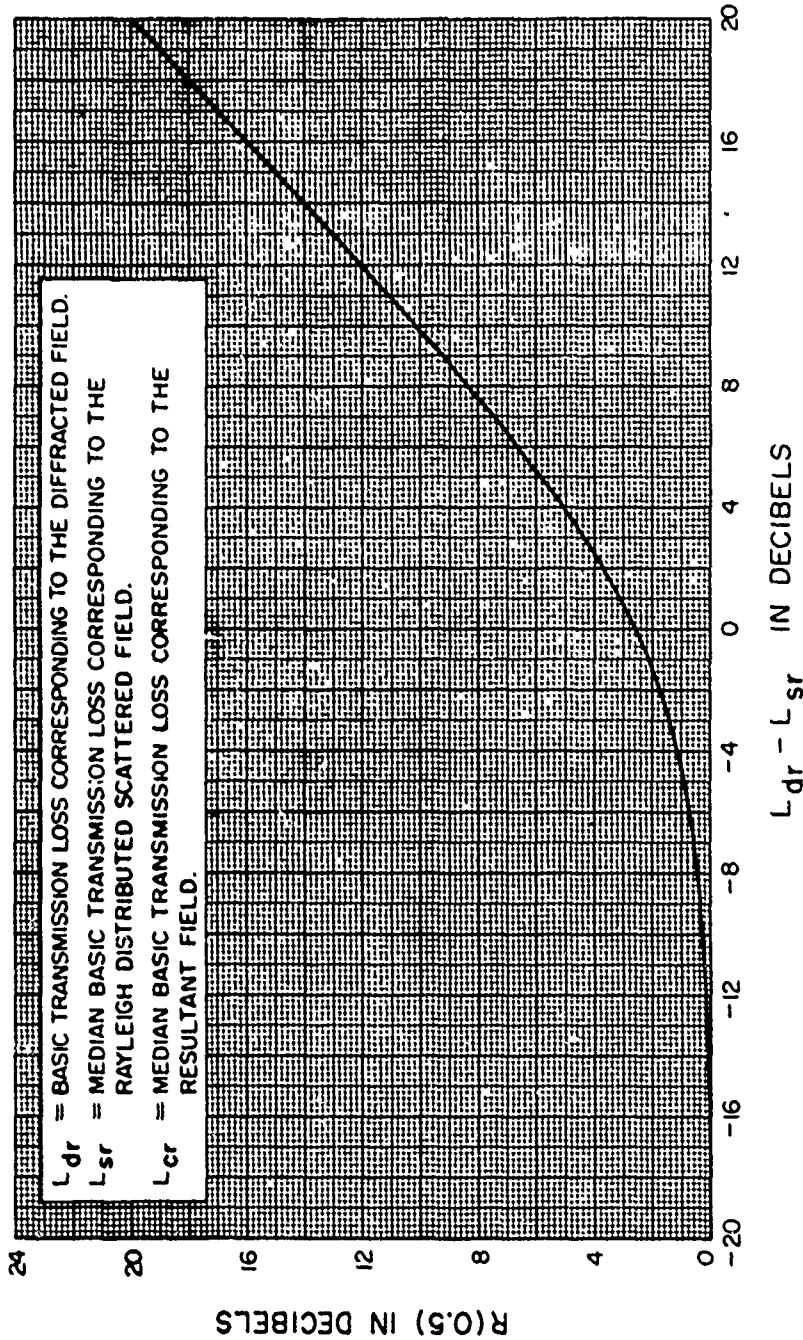


Figure 9.9

PROFILE OF A TRANSHORIZON PATH
DALLAS TO AUSTIN, TEXAS

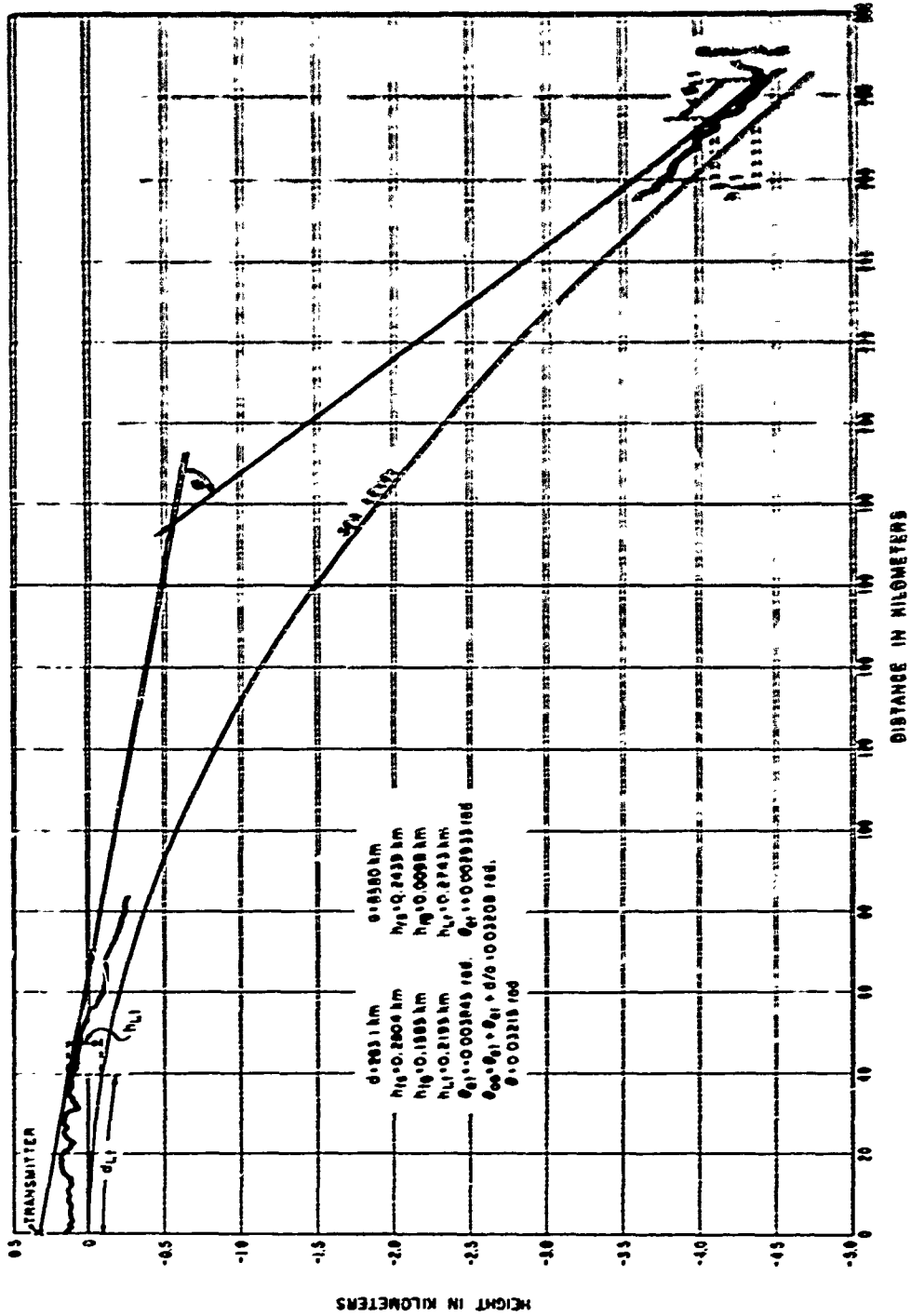


Figure 9.10

**CUMULATIVE DISTRIBUTIONS $L_b(q)$ OBSERVED AND PREDICTED VS q
 SUMMER, WINTER, AND ALL HOURS
 DALLAS TO AUSTIN, TEXAS**

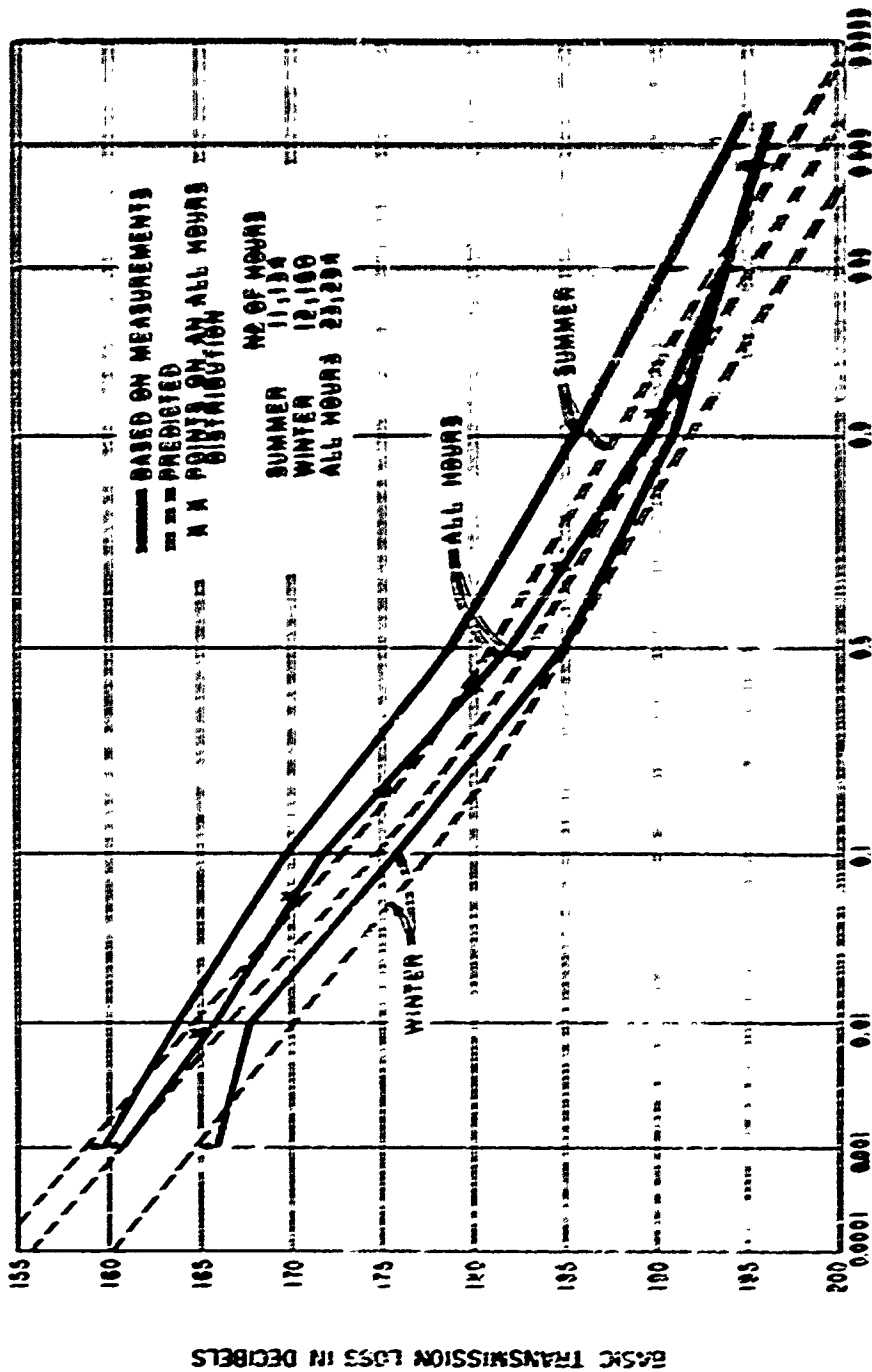


FIGURE 9.11

III. LONG-DURATION POWER FADING

The variability of the propagation of radio transmission in the ionosphere and space-communication systems is due to changes in the refractive index of the ionosphere and to the variability of the propagation mechanism. The variability of the propagation is associated with the variability of the refractive index of the ionosphere, in particular, in the E-layer. The effects of this type of fading are predicted with the variability of the refractive index of the ionosphere. Long-term power fading is associated with the variability of the refractive index of the ionosphere, in particular, in the E-layer, and with the variability of the refractive index of the ionosphere.

An estimate of the long-term power fading is based on the expected average over a given path in a given direction. The possibility that unusually high ionospheric fields may occur for an appreciable fraction of time places restrictions on various operating on the same or adjacent frequencies. The basis for the mainly empirical predictions of long-term variability given here needs to be well understood in order to appreciate their value as well as their limitations.

An increase in atmospheric refraction increases long distance diffraction or forward scatter fields but may lead to multipath fading problems over short paths. Increased turbulence of the atmosphere may result in either an increase or a decrease of radio transmission loss depending on the geometry of a particular path and on the dominance of various propagation mechanisms. Increased scattering losses propagation by reflection from electric layers and sometimes the guiding of energy by ducts or layers. Such scattering usually increases long-distance fields but may be associated with groundwave fadeouts at short distances.

Just beyond radio line-of-sight, fading rate and fading range depend in a very complex manner on the relative importance of various propagation mechanisms. During periods of layering and ducting in the atmosphere, transmission loss shows a tendency to go into deep fades, with durations from less than a minute to more than an hour. Ordinarily a ducted signal fades slowly if at all, and the fades are of relatively short duration and very deep. A tropospheric forward scatter signal, on the other hand, exhibits the rapid and severe fading characteristic of the Rayleigh distribution. An intermediate type of fading results when the scattered power is nearly equal to power introduced by some mechanism such as diffraction, for which the variation in time is usually very slow. Aircraft reflections introduce rapid, intense, and relatively regular fading. Meteor bursts and some types of ionospheric propagation add spikes to a paper chart record.

Space-wave fadeouts [Bean, 1954] may represent power fading due to defocusing of radio energy in some regions of space, (radio holes) accompanied by a focusing effect and

PRECEDING PAGE BLANK-NOT FILM

equal values over all other regions [Dobson, 1952; Grant, 1956], or any corresponding phase shift between fading phenomena. In temperate continental climates, sporadic fading events are likely to occur primarily at night and most frequently during the summer months. They are more frequent at UHF than at VHF, and their occurrence can be correlated with the occurrence of ground-to-surface refractive index profiles [Hines and Salmer, 1942]. Such fading phenomena in geographic areas where layers and ducts occur frequently. A diversity equal diversity does not appear to be helpful in overcoming this type of fading. During periods of uniform refractive index layer rates, prolonged fades are much less common or do not occur. Sometimes these fades do occur are caused by multipath reflections which occur on such a plane and amplitude relationship that a slight change in the layer rate will cause a large change in the resultant field. The latter type can be overcome in most instances by either reducing the ground antennas or by the use of space diversity.

General discussions of the time fading of VHF and UHF radio fields will be found in reports by Huntington [1950], de Groot [1952], Clutter [1953], Cummings [1954], Kocumlik [1954], Tomasi [1954], and Ugoi [1954]. Sturman [1957] discusses some of the theory of the short-term fading of scatter signals. Foxworth [1957] discusses signal distortion due to multipath scatter, while Buchanan [1958] considers related depolarization phenomena.

The observed correlation of radio data with various meteorological parameters is discussed by Bean [1954, 1954], Bean and Cahoon [1957], de Groot and Moore [1957], Longshon and Blumquist [1958], Moore [1958, 1958, 5, 6, 1962], Moler and Holden [1960], and Rytte [1960]. Meteorological parameters such as surface refractivity and the height gradient of refractive index have been found more useful as a basis for predicting seasonal changes than for predicting diurnal or seasonal variations. In this report meteorological information has been used to distinguish between climatic regions, while radio data are dependent on to predict long-term variability about the computed long-term median value in each of these regions.

The basic data used in developing these estimates of long-term power fading were recorded in various parts of the world over more than a thousand propagation paths. Path distances extend from within line-of-sight to about 1000 kilometers, and frequencies range from 40 MHz to 10 GHz.

As more data are collected, particularly in regions where little information is currently available, these estimates should be re-examined and revised. Allowances should sometimes be made for predictable long-term variations in antenna gain, interference due to reflections from aircraft or satellites, and variations in equipment performance. Microwave attenuation due to rainfall, discussed in section 3, should be allowed for in estimating

the variability of transmission loss at frequencies above 3 GHz. The long-term variability of day, night, and winter-spring absorption may be important above 15 GHz.

It is often desirable to specify rather precisely the conditions for which an estimate of power fading characteristics is desired. For instance, the average frequency dependence of long-term variability over a given type of profile depends critically on the relative dominance of various propagation mechanisms, and this in turn depends on climate, season, time of day, and average terrain characteristics. When it becomes possible to describe the actual (unaveraged), stratified, and turbulent atmospheric noise independently, it should also be found possible to "mix" predicted cumulative distributions of transmission loss for a variety of propagation mechanisms.

Three important effects of the atmosphere on radio propagation are considered. The amount of radio ray in flux and the frequency of atmospheric turbulence are usually associated with the surface refractivity, N_s . The frequency and stability of various types of stratification in the atmosphere are often not well correlated with N_s . Though terrain and high winds both tend to increase mixing in the atmosphere and consequently reduce the occurrence of superrefractive layers.

11.3 Effects of Atmospheric Stratification

Ground-based superrefractive layers tend to trap radio energy which is propagated within the layer in a manner similar to that in a waveguide. A "normal" gradient of refractive index exists at the surface of the ground is about -100 N/km , a ground-based superrefractive layer has a gradient from -100 to -200 N/km . Several layers with stronger negative refractive index gradients may show ducts in which radio energy is refracted to such a degree that it follows the curvature of the earth. If a radio wave is elevated above a minimum angle, usually less than half a degree, the energy penetrates and escapes the duct.

If a transmitter radiating energy in a horizontal direction is located in a duct, the theoretical radio horizon distance over a smooth spherical earth would be infinite. On the other hand on a layer with a subrefractive gradient, (positive values of refractive index gradient) the energy is refracted upwards and the corresponding horizon distance may be much less than that with a normal gradient. For example, a transmitting antenna 30 m above a smooth earth would have a radio horizon distance of about 30 km with a "normal" gradient of about -100 N/km , but the horizon distance might be as little as 5 km under subrefractive conditions or as much as 3 to 5 times the normal distance in a ground-based duct. Such changes would result in unusual variations in corresponding values of transmission loss.

The minimum radio frequency that may be trapped by a duct depends on the total thickness and the average refractive index gradient within it. Thicker, stronger ducts will trap frequencies of 100 MHz or less, somewhat smaller and thinner ducts will trap higher frequencies. Frequencies as low as 30 MHz would rarely be trapped. A duct that traps frequencies of about 1000 MHz will guide higher frequencies even more strongly while lower frequencies will exhibit greater attenuation or may not be trapped at all.

It is difficult to predict the fraction of time that high fields due to ducting conditions may be expected to occur. Figures 11.8 to 11.12, which are reproduced from a World Atlas of Atmospheric Radio Refractivity by Bean, Cannon, Samson and Taylor [1956], show the percentage of time ground-based ducts may occur. These maps are based on radiosonde data recorded at about 100 weather stations, normally for a period of 5 years. The months of February, May, August and November were selected as representative of the seasons. Unfortunately few stations recorded profiles more than once a day so no information on diurnal trends is included. These maps show for frequencies of 300, 1000 and 3000 MHz the percentage of observations in each of the four "seasonal" months that trapping of radio waves may be expected to occur. Such maps indicate general or regional conditions but more information would be required for detailed local predictions.

In large areas of the world, primarily over temperate oceans and arctic areas, the incidence of ducting is less than one percent. Strong ground-based ducts are most common in tropical and subtropical regions from 0° to 30° north latitude, especially in western coastal areas and the Persian Gulf. Strong ducting conditions, for frequencies of 3000 MHz and above and centered on the Persian Gulf may occur as much as 75 percent of the time in

August and only 20 percent of the time in February. In contrast to this on the west coast of Africa, about 20° north latitude, dusting conditions occur about 50 percent of the time in February and December and only 20 to 30 percent of the time in the summer months. Strong subsynoptic conditions, with corresponding increased transmissivity loss, may occur more than 5 percent of the time in tropical Africa, the east coast of South America, the eastern Mediterranean, southeastern Asia and northern Australia.

Some of the better-known dusting areas of superoceanic origin listed by Doherty (1941). These include the west coasts of Africa and India, the northern part of the Arabian sea especially around the Persian Gulf in summer, and the northern part of Australia. Dusting during summer months during conditions occur in Atlantic coastal areas of Europe, the eastern Mediterranean, the Pacific Coastal areas of China, and in Japan. These early observations of the occurrence of dusting activities are reflected in the records of world-wide maps, figures 10, 11 and 12. It is apparent that the most intense superoceanic is encountered in tropical climates, in trade wind areas, and in most of the principal deserts of the world.

High fohls due to ground-based dusts are essentially a fine weather phenomenon. In fact, during fine weather, dusting is most noticeable at night. Over the sea dusting is most marked when the warm dry air of an adjacent land-mass extends out over a comparatively cool sea. Areas of divergence, which favor elevated dust formation, appear to be most persistent over ocean areas from 10° to 40° north and south latitudes, especially during winter months. (Doherty and Smith, 1946; Randall, 1942). Elevated dusts are usually less important than ground-based dusts for tropospheric propagation.

III. Climatic Regions

Climatic regions may be defined in several different ways: (1) by geographic areas on a map, (2) by average meteorological conditions, (3) by the predominance of various propagation mechanisms, or (4) by averages of available data. In various so-called "climates," at different times of day or seasons of the year, different propagation mechanisms may be dominant. For example, in a continental temperate climate the characteristics of a received signal over a given path may be quite different in the early morning hours in May than during the afternoon hours in February.

Based on our current knowledge of meteorological conditions and their effects on radio propagation, the International Radio Consultative Committee (CCIR 1953a) has defined several "climates." A large amount of data is available from continental temperate and maritime temperate climates. Other climatic regions, where few data are available, are discussed in annex III. The division into radio climates is somewhat arbitrary, based on present knowledge of radio meteorology, and is not necessarily the same as the division into meteorological climates (Haurwitz and Austin, 1944).

World maps of minimum monthly mean N_{∞} , figure II.1, and of the annual range of monthly mean N_{∞} , figure III.51, may be useful in deciding which climate or climates are applicable in a given region. The boundaries between various climatic regions are not well defined. In some cases it may be necessary to interpolate between the curves for two climates giving additional weight to the one whose occurrence is considered more likely.

Some important characteristics of the climatic regions for which estimates of time variability are shown, are noted below:

1. Continental Temperate characterized by an annual mean N_{∞} of about 320 N-units with an annual range of monthly mean N_{∞} of 20 to 40 N-units. A continental climate in a large land mass shows extremes of temperature in a "temperate" zone, such as 30° to 60° north or south latitude. Pronounced diurnal and seasonal changes in propagation are expected to occur. On the east coast of the United States the annual range of N_{∞} may be as much as 40 to 50 N-units due to contrasting effects of arctic or tropical maritime air masses which may move into the area from the north or from the south.

2. Maritime Temperate Overland characterized by an annual mean N_{∞} of about 400 N-units with a rather small annual range of monthly mean N_{∞} of 20 to 30 N-units. Such climatic regions are usually located from 20° to 50° north or south latitude, near the sea, where prevailing winds, unobstructed by mountains, carry moist maritime air inland. These conditions are typical of the United Kingdom, the west coasts of North America and Europe and the northwestern coastal areas of Africa.

Although the islands of Japan lie within this range of latitude the climate differs in showing a much greater annual range of monthly mean N_{∞} , about 60 N-units, the prevailing winds have traversed a large land mass, and the terrain is rugged. One would therefore not expect to find radio propagation conditions similar to those in the United Kingdom although

the annual mean N_g is 500 to 520 N-units in each direction. Climate 1 is probably more appropriate than climate 2 in this case, but ducting may be important in coastal and over-sea areas of Japan as much as 5 percent of the time in summer.

4. Maritime Temperate Oversea coastal and over-sea areas with the same general characteristics as those for climate 2. The distinction made is that a radio path with both horizons on the sea is considered to be an overseas path, otherwise climate 2 is used. During is rather common for a small fraction of time between the United Kingdom and the European Continent, and along the west coast of the United States and Mexico.

5. Maritime Subtropical Continental characterized by an annual mean N_g of about 500 N-units with an annual range of monthly mean N_g of 20 to 60 N-units. Such climates may be found from about 30° to 40° north and south latitude, usually on land near the sea with definite rainy and dry seasons. Where the land area is dry radio-ducts may be present for a considerable part of the year.

6. Maritime Subtropical Oversea conditions observed in coastal areas with the same range of latitude as climate 5. The curves for this climate were based on an inadequate amount of data and have been deleted. It is suggested that the curves for climates 5 or 4 be used, selecting whichever seems more applicable to each specific case.

7. Desert Sahara characterized by an annual mean N_g of about 280 N-units with year-round semiarid conditions. The annual range of monthly mean N_g may be from 20 to 80 N-units.

8. Equatorial a maritime climate with an annual mean N_g of about 360 N-units and annual range of 0 to 30 N-units. Such climates may be observed from 20°N to 20°S latitude and are characterized by monotonous heavy rains and high average summer temperatures. Typical equatorial climates occur along the Ivory Coast and in the Congo of Africa.

9. Continental Subtropical typified by the Sudan and monsoon climates, with an annual mean N_g of about 320 N-units and an annual range of 60 to 100 N-units. This is a hot climate with seasonal extremes of winter drought and summer rainfall, usually located from 20° to 40°N latitude.

A continental polar climate, for which no curves are shown, may also be defined. Temperatures are low to moderate all year round. The annual mean N_g is about 310 N-units with an annual range of monthly mean N_g of 10 to 40 N-units. Under polar conditions, which may occur in middle latitudes as well as in polar regions, radio propagation would be expected to show somewhat less variability than in a continental temperate climate. Long-term median values of transmission loss are expected to agree with the reference values L_{cr} .

High mountain areas or plateaus in a continental climate are characterized by low values of N_g and year-round semiarid conditions. The central part of Australia with its hot dry desert climate and an annual range of N_g as much as 50 to 70 N-units may be intermediate between climates 1 and 6.

Prediction of long-term median reference values of transmission loss, by the methods of sections 5 to 9, takes advantage of theory in allowing for the effects of path geometry and radio ray refraction in a standard atmosphere. Meteorological information is used to distinguish between climatic regions. Median values of data available in each of these regions are related to the long-term reference value by means of a parameter $V(0.5, d_e)$ which is a function of an "effective distance," d_e , defined below. Long-term fading about the median for each climatic region is plotted in a series of figures as a function of d_e . For regions where a large amount of data is available, curves are presented that show frequency-related effects. (Seasonal and diurnal changes are given in annex III for a continental temperature climate.)

10.3 The Effective Distance, d_e

Empirical estimates of long-term power fading depend on an effective distance, d_e , which has been found superior to other parameters such as path length, angular distance, distance between actual horizons, or distance between theoretical horizons over a smooth earth. The effective distance makes allowance for effective antenna heights and some allowance for frequency.

Define θ_{s_1} as the angular distance where diffraction and forward scatter transmission loss are approximately equal over a smooth earth of effective radius $a = 9100$ kilometers, and define d_{s_1} as $9100 \theta_{s_1}$. Then:

$$d_{s_1} = 65(100/f)^{3/2} \text{ km.} \tag{10.1}$$

The path length, d , is compared with the sum of d_{s_1} and the smooth-earth distances to the radio horizons:

$$d_L = 3\sqrt{2h_{te}} + 3\sqrt{2h_{re}} \text{ km.} \tag{10.2}$$

where the effective antenna heights h_{te} and h_{re} are expressed in meters and the radio frequency f in Mc/s.

It has been observed that the long-term variability of hourly medians is greatest on the average for values of d only slightly greater than the sum of d_{s_1} and d_L . The effective distance d_e is arbitrarily defined as:

$$\text{for } d \leq d_L + d_{s_1}, \quad d_e = 130 d / (d_L + d_{s_1}) \text{ km} \tag{10.3a}$$

$$\text{for } d > d_L + d_{s_1}, \quad d_e = 130 + d - (d_L + d_{s_1}) \text{ km.} \tag{10.3b}$$

10.4 The Functions $V(0.5, d_e)$ and $Y(q, d_e)$

The predicted median long-term transmission loss for a given climatic region $L_m(0.5)$, characterized by a subscript m , is related to the calculated long-term reference value L_{cr} by means of the function $V(0.5, d_e)$

$$L_m(0.5) = L_{cr} - V_m(0.5, d_e) \quad \text{dB} \quad (10.4)$$

where $L_m(0.5)$ is the predicted transmission loss exceeded by half of all hourly medians in a given climatic region. $V_m(0.5, d_e)$ is shown on figure 10.13 for several climates as a function of the effective distance d_e . For the special case of forward scatter during winter afternoons in a temperate continental climate, $V(0.5) = 0$ and $L(0.5) = L_{cr}$. In all other cases, the calculated long-term reference value L_{cr} should be adjusted to the median $L_m(0.5)$ for the particular climatic region or time period considered. The function $F(0.5)$ in the scatter prediction of a long-term reference median contains an empirical adjustment to data. The term $V(0.5, d_e)$ provides a further adjustment to data for all propagation mechanisms and for different climatic regions and periods of time.

In general, the transmission loss not exceeded for a fraction q of hourly medians is

$$L_m(q) = L_m(0.5) - Y_m(q, d_e) \quad \text{dB} \quad (10.5)$$

where $Y_m(q, d_e)$ is the variability of $L_m(q)$ relative to its long-term median value $L_m(0.5)$. For a specified climatic region and a given effective distance, the cumulative distribution of transmission loss may be obtained from (10.5). In a continental temperate climate transmission loss is often nearly log-normally distributed. The standard deviation may be as much as twenty decibels for short transhorizon paths where the mechanisms of diffraction and forward scatter are about equally important. When a propagation path in a maritime temperate climate is over water, a log-normal distribution may be expected from $L(0.5)$ to $L(0.999)$, but considerably higher fields are expected for small fractions of time when pronounced superrefraction and ducting are present.

10.5 Continental Temperate Climate

Data from the U.S.A., West Germany, and France provide the basis for predicting long-term power fading in a continental temperate climate. More than half a million hourly median values of basic transmission loss recorded over some two hundred paths were used in developing these estimates.

Figure 10.14 shows basic estimates $Y(q, 100 \text{ MHz})$ of variability in a continental temperate climate. Curves are drawn for fractions 0.1 and 0.9 of all hours of the day for summer, winter and all year for a "typical" year. In the northern temperate zone, "summer" extends from May through October and "winter" from November through April.

A "frequency factor" $g(q, f)$ shown in figure 10.15 adjusts the predicted variability to allow for frequency-related effects:

$$Y(q) = Y(q, d_e, 100 \text{ MHz}) g(q, f). \quad (10.6)$$

The function $g(q, f)$ shows a marked increase in variability as frequency is increased above 100 MHz to a maximum at 400 to 500 MHz. Variability then decreases until values at 1 or 2 GHz are similar to those expected at 100 MHz. The empirical curves $g(q, f)$ should not be regarded as an estimate of the dependence of long-term variability on frequency, but represent only an average of many effects, some of which are frequency-sensitive. The apparent frequency dependence is a function of the relative dominance of various propagation mechanisms, and this in turn depends on climate, time of day, season, and the particular types of terrain profiles for which data are available. For example, a heavily forested low altitude path will usually show greater variability than that observed over a treeless high altitude prairie, and this effect is frequency sensitive. An allowance for the year-to-year variability is also included in $g(q, f)$. Data summarized by Williamson et al. [1960] show that $L(0.5)$ varies more from year to year than $Y(q)$. Assuming a normal distribution of L within each year and of $L(0.5)$ from year to year, L would be normally distributed with a median equal to $L(0.5)$ for a "typical" year. $Y(q)$ is then increased by a constant factor, which has been included in $g(q, f)$.

Estimates of $Y(0.1)$ and $Y(0.9)$ are obtained from figures 10.14, 10.15 and from equation 10.6. These estimates are used to obtain a predicted cumulative distribution using the following ratios:

$$\begin{aligned} Y(0.0001) &= 3.33 Y(0.1) & Y(0.9999) &= 2.90 Y(0.9) \\ Y(0.001) &= 2.73 Y(0.1) & Y(0.999) &= 2.41 Y(0.9) \\ Y(0.01) &= 2.00 Y(0.1) & Y(0.99) &= 1.82 Y(0.9) \end{aligned} \quad (10.7)$$

For example, assume $f = 100 \text{ MHz}$, $d_e = 112 \text{ km}$, and a predicted reference median basic transmission loss, $L_{\text{bcr}} = 179 \text{ db}$, so that $V(0.5, d_e) = 0.9 \text{ db}$, (figure 10.13), $Y(0.1, d_e, 100 \text{ MHz}) = 8.1 \text{ db}$, and $Y(0.9, d_e, 100 \text{ MHz}) = -5.8 \text{ db}$, (figure 10.14), $g(0.1, f) = g(0.9, f) = 1.05$ (figure 10.15). Then $Y(0.1) = 1.05 Y(0.1, d_e, 100 \text{ MHz}) = 8.5 \text{ db}$, and $Y(0.9) = 1.05 Y(0.9, d_e, 100 \text{ MHz}) = -6.1 \text{ db}$. Using the ratios given above:

$$Y(0.0001) = 28.3, \quad Y(0.001) = 23.2, \quad Y(0.01) = 8.5,$$

$$Y(0.9999) = -17.7, \quad Y(0.999) = -14.7, \quad Y(0.99) = -11.1, \quad Y(0.9) = -6.1.$$

The median value is

$$L_b(0.5) = L_{bcx} - V(0.5) = 178.1 \text{ db}$$

and the predicted distribution of basic transmission loss is;

$$L(0.0001) = 149.8, \quad L(0.001) = 154.9, \quad L(0.01) = 161.1, \quad L(0.1) = 169.6, \quad L(0.5) = 178.1,$$

$$L(0.9) = 184.2, \quad L(0.99) = 189.2, \quad L(0.999) = 192.8 \text{ and } L(0.9999) = 195.8 \text{ db.}$$

These values are plotted as a function of time availability, q , on figure 10.16 and show a complete predicted cumulative distribution of basic transmission loss.

For antennas elevated above the horizon, as in ground-to-air or earth-to-space communication, less variability is expected. This is allowed for by a factor $f(\theta_h)$ discussed in annex III. For transhorizon paths $f(\theta_h)$ is unity and does not affect the distribution. For line-of-sight paths $f(\theta_h)$ is nearly unity unless the angle of elevation exceeds 0.15 radians.

Allowance must sometimes be made for other sources of power fading such as attenuation due to rainfall or interference due to reflections from aircraft that may not be adequately represented in available data. For example, at microwave frequencies the distribution of water vapor, oxygen, rain, snow, clouds and fog is important in predicting long-term power fading. Let Y_1, Y_2, \dots, Y_n represent estimates corresponding to each of these sources of variability, and let ρ_{ij} be the correlation between variations due to sources i and j . Then the total variability is approximated as:

$$Y^2(q) = \sum_{i=1}^m Y_i^2(q) + 2 \sum_{\substack{i, j+1 \\ i < j}}^m Y_i Y_j \rho_{ij} \quad (10.8)$$

where $Y(q)$ is positive for $q < 0.5$, zero for $q = 0.5$, and negative for $q > 0.5$. Section 3 shows how to estimate $Y_a(q)$ and $Y_r(q)$ for atmospheric absorption by oxygen and water vapor, and for rain absorption respectively. Let ρ_{1a} be the correlation between variations Y of available data and variations Y_a due to microwave absorption by oxygen and water vapor. Let ρ_{1r} be the correlation between Y and Y_r . Assuming that $\rho_{1a} = 1$, $\rho_{1r} = 0.5$, and $\rho_{ar} = 0$,

$$Y^2(q) = (Y + Y_a)^2 + Y_r^2 + Y Y_r \quad (10.9)$$

This method was used to allow for the effects of rainfall at frequencies above 5 GHz for fractions 0.99 and 0.9999 of all hours in figures I.6 to I.11 of annex I.

Figures 10.17 to 10.22 show variability, $Y(q)$ about the long-term median value as a function of d_e for period of record data in the following frequency groups; 40-88, 88-108, 108-250, 250-450, 450-1000, and > 1000 MHz. The curves on the figures show predicted values of $Y(q)$ for all hours of the year at the median frequency in each group. These medians are: 47.1, 98.7, 192.8, 417, 700, and 1500 MHz for data recorded in a continental temperate climate. Equation (10.6) and figures 10.14 and 10.15 were used to obtain the curves in figures 10.17 to 10.22.

An analytic function fitted to the curves of $V(0.5, d_e)$ and $Y(q, d_e, 100 \text{ MHz})$ is given in annex III. Diurnal and seasonal variations are also discussed and functions listed to predict variability for several times of day and seasons.

10.6 Maritime Temperate Climate

Studies made in the United Kingdom have shown appreciable differences between propagation over land and over sea, particularly at higher frequencies. Data from maritime temperate regions were therefore classified as overland and oversea, where oversea paths are categorized as having the coastal boundaries within their radio horizons. Paths that extend over a mixture of land and sea are included with the overland paths.

The data were divided into frequency groups as follows:

Bands I and II	(40-100 MHz)
Band III	(150-250 MHz)
Bands IV and V	(450-1000 MHz)

Long-term variability of the data for each path about its long-term median value is shown as a function of effective distance in figures 10.23 to 10.28. Curves were drawn through medians of data for each fraction of time $q = 0.0001, 0.001, 0.01, 0.1, 0.9, 0.99, 0.999, 0.9999$. Figures 10.23 to 10.28 show that it is not practical to use a formula like (10.6) for the maritime temperate climate, because the frequency factor $g(q, f)$ is not independent of d_e , as it is in the case of the continental temperate climate. The importance of tropospheric ducting in a maritime climate is mainly responsible for this difference.

These figures demonstrate greater variability oversea than overland in all frequency groups. The very high fields noted at UHF for small fractions of time are due to persistent layers and ducts that guide the radio energy. In cases of propagation for great distances over water the fields approach free space values for small fractions of time. Curves have been drawn for those distance ranges where data permitted reasonable estimates. Each curve is solid where it is well supported by data, and is dashed for the remainder of its length.

10.7 Other Climates

A limited amount of data available from other climatic regions has been studied, [CCIR 1963f]. Curves showing predicted variability in several climatic regions are shown in annex III, figures III.25 to III.29.

At times it may be necessary to predict radio performance in an area where few if any measurements have been made. In such a case, estimates of variability are based on whatever is known about the meteorological conditions in the area, and their effects on radio propagation, together with results of studies in other climatic regions. If a small amount of radio data is available, this may be compared with predicted cumulative distributions of transmission loss corresponding to somewhat similar meteorological conditions. In this way estimates for relatively unknown areas may be extrapolated from what is known.

10.8 Variability for Knife-Edge Diffraction Paths

The variability of hourly medians for knife-edge diffraction paths can be estimated by considering the path as consisting of two line-of-sight paths in tandem. The diffracting knife-edge then constitutes a common terminal for both line-of-sight paths. The variability of hourly median transmission loss for each of the paths is computed by the methods of this section and characterized by the variability functions

$$V_1(q) = V_1(0.5) + Y_1(q) \text{ db}$$

$$V_2(q) = V_2(0.5) + Y_2(q) \text{ db}$$

During any particular hour, the total variability function V for the diffraction path would be expected to be the sum of V_1 plus V_2 . To obtain the cumulative distribution of all values of V applicable to the total path a convolution of the individual variables V_1 and V_2 may be employed [Davenport and Root, 1958].

Assuming that V_1 and V_2 are statistically independent variables, their convolution is the cumulative distribution of the variable $V = V_1 + V_2$. The cumulative distribution of V may be obtained by selecting n equally-spaced values from the individual distributions of $V_1(q)$ and $V_2(q)$, calculating all possible sums $V_k = V_{1i} + V_{2j}$ and forming the cumulative distribution of all values V_k obtained in this manner.

Another method of convolution that gives good results requires the calculation and ordering of only n , instead of n^2 , values of V . As before $V_1(q)$ and $V_2(q)$ are obtained for n equally spaced percentages. Then one set is randomly ordered compared to the other so that the n sums $V = V_1 + V_2$ are randomly ordered. The cumulative distribution of these sums then provides the desired convolution of V_1 and V_2 . If the distribution of $V_1 - V_2$ is desired this is the convolution of V_1 and $-V_2$.

Computations required to estimate long-term variability over a knife-edge diffraction path are given in the example described in section 7.5.

Percent of Time Trapping Frequency is Less Than 3000 MHz: February

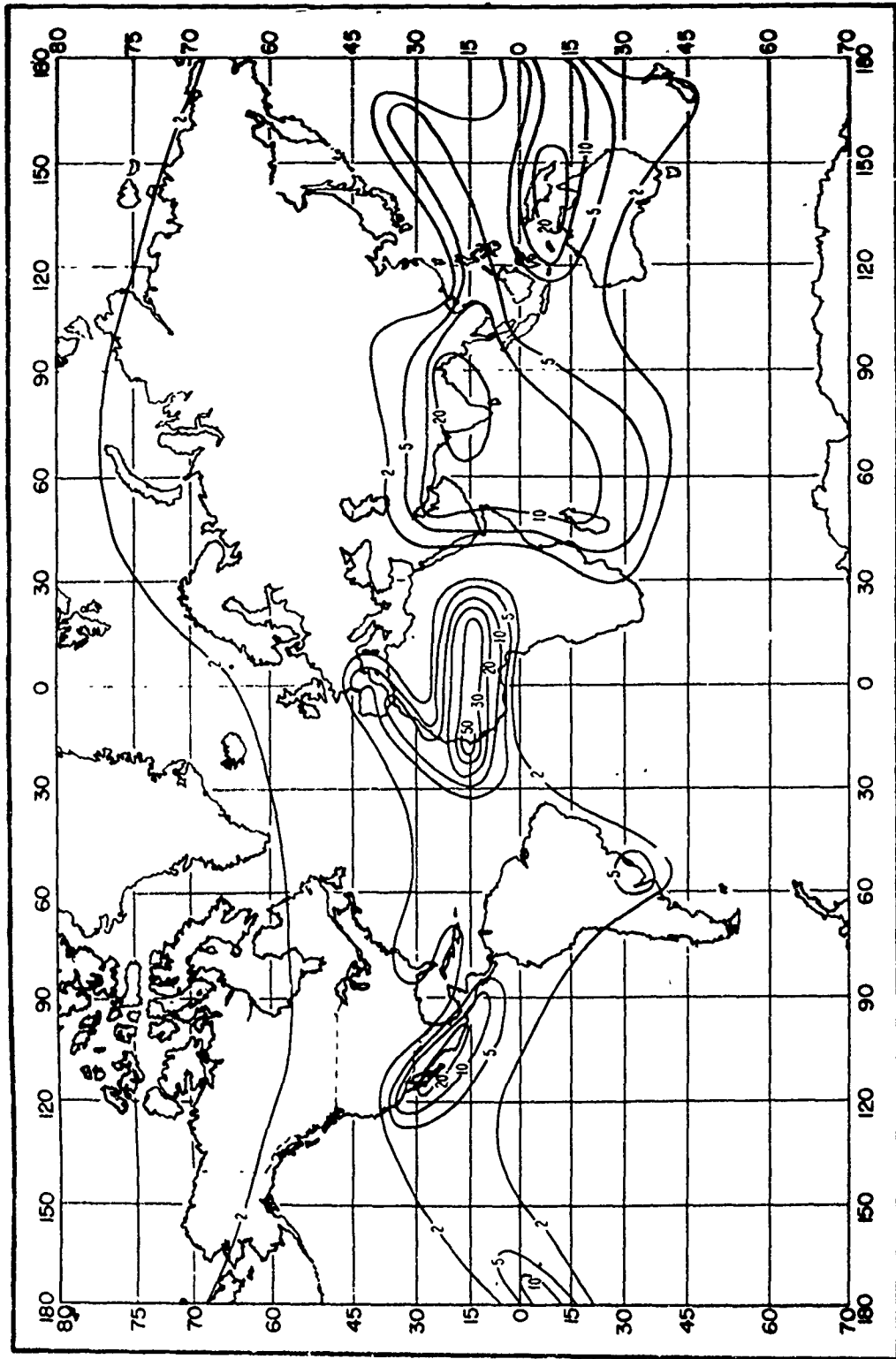


Figure 10'

Percent of Time Trapping Frequency is Less Than 3000 MHz: May

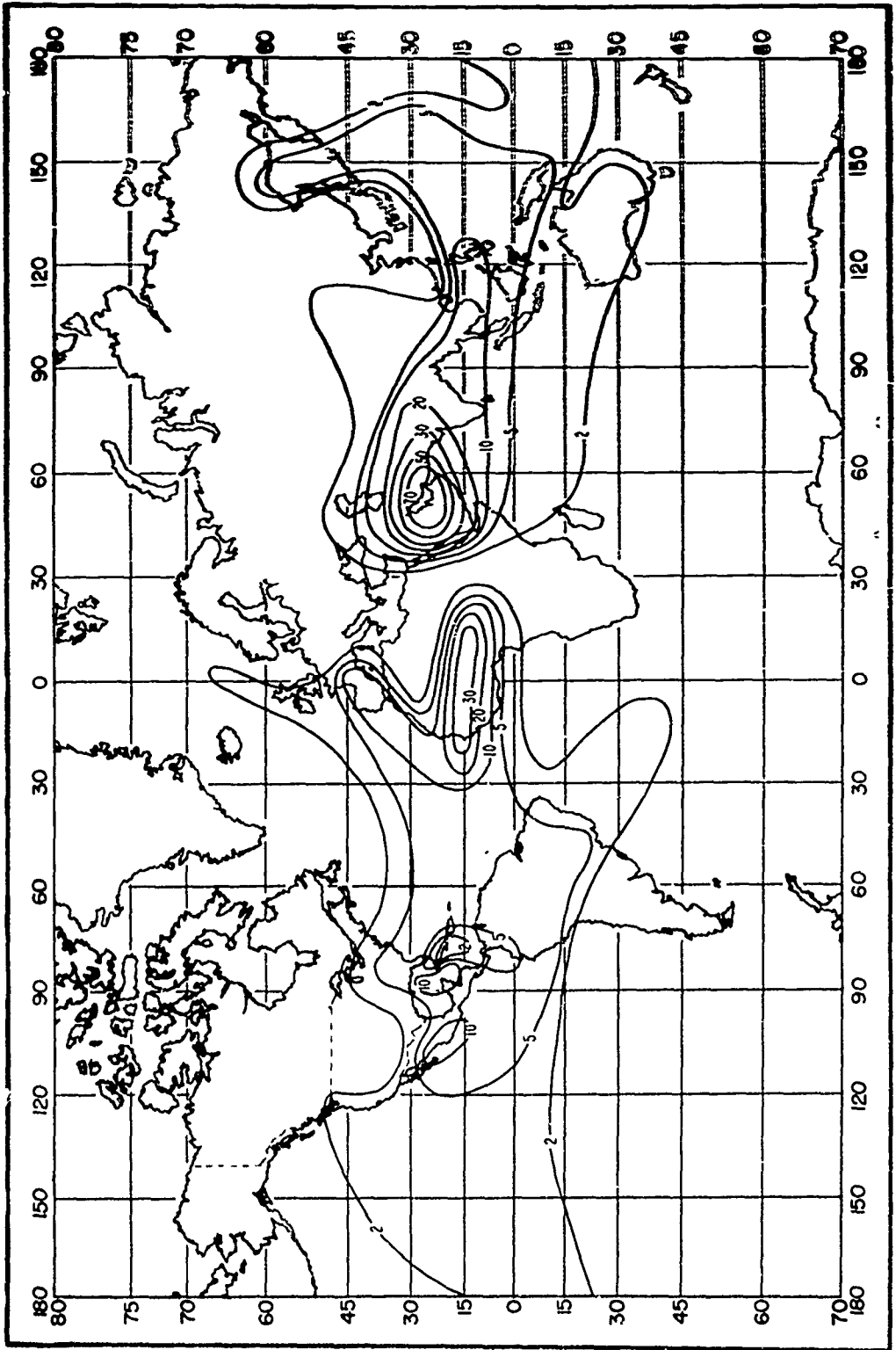


Figure 10.2

Percent of Time Trapping Frequency is Less Than 3000 MHz: August

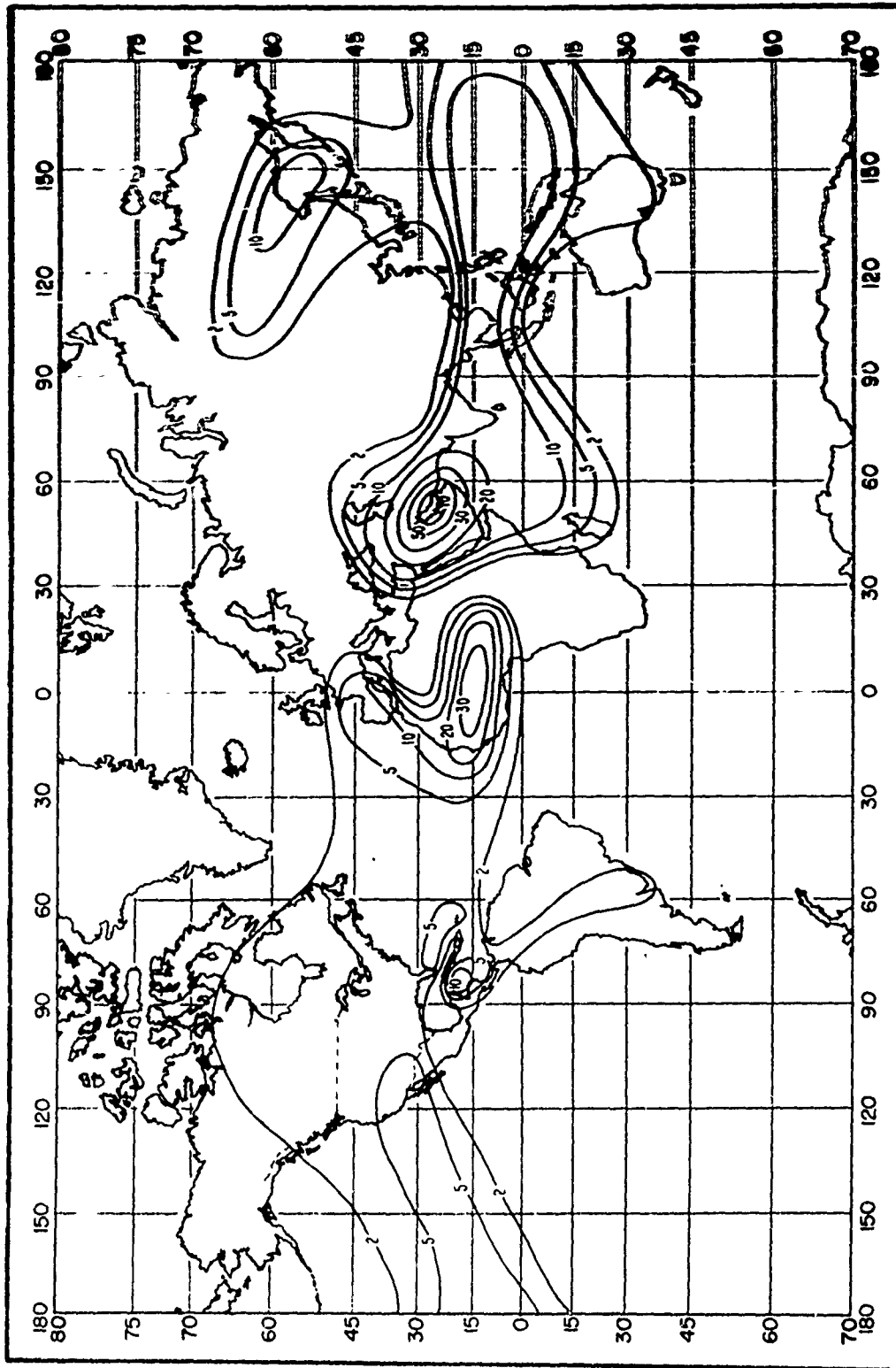


Figure 10.3

Percent of Time Trapping Frequency is Less Than 3000 MHz: November

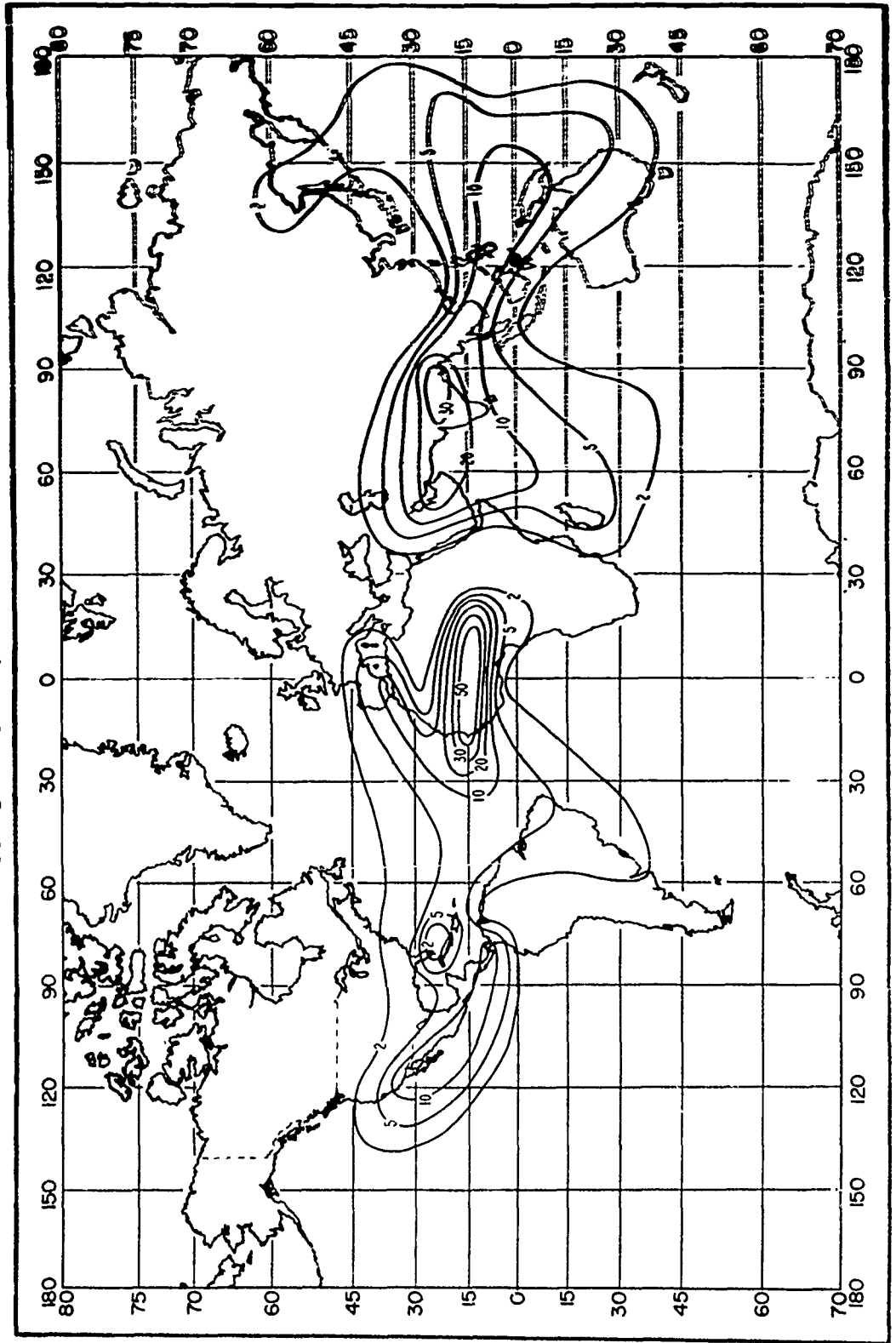


Figure 10.4

Percent of Time Trapping Frequency is Less Than 1000 MHz; February

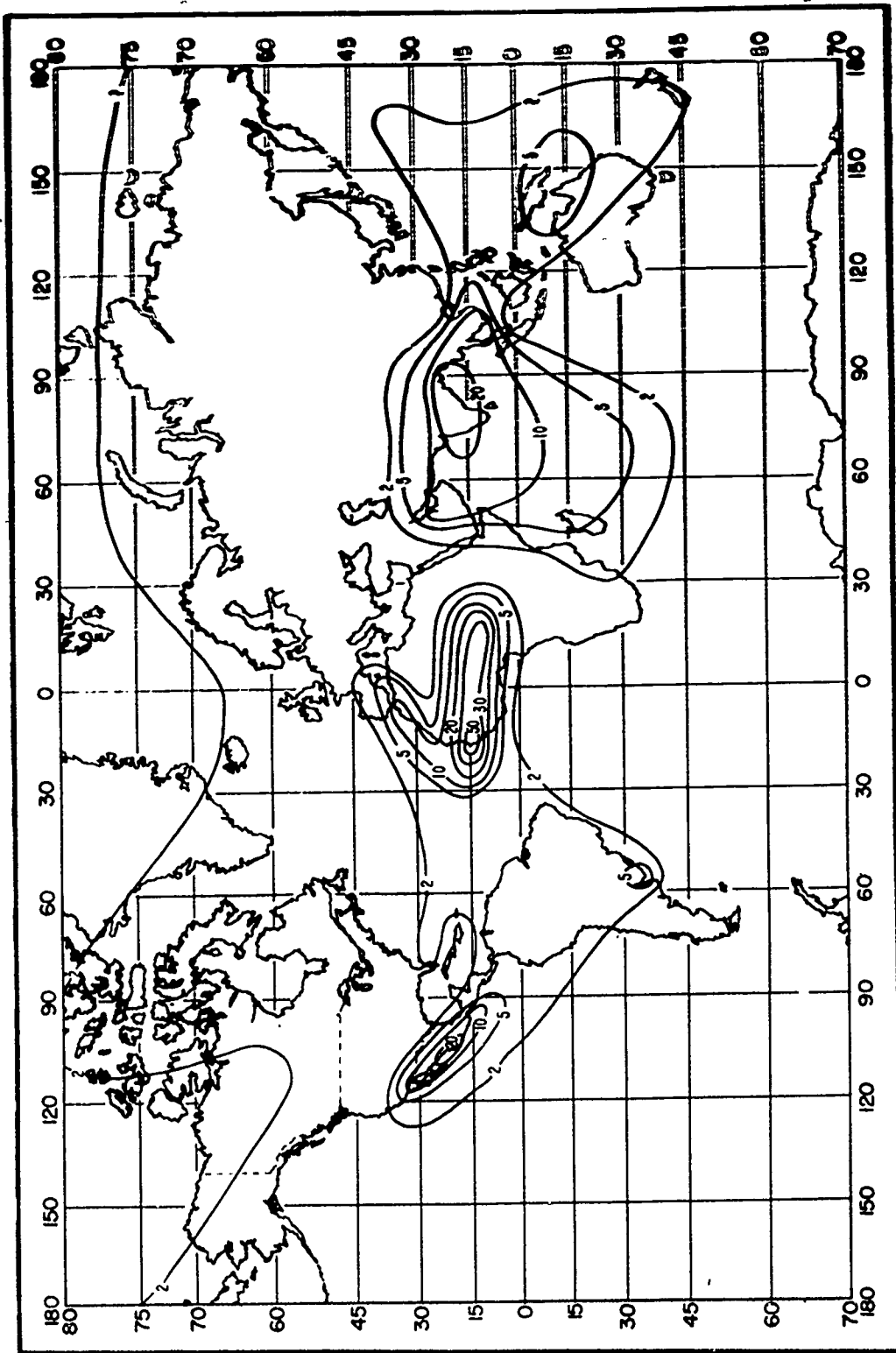
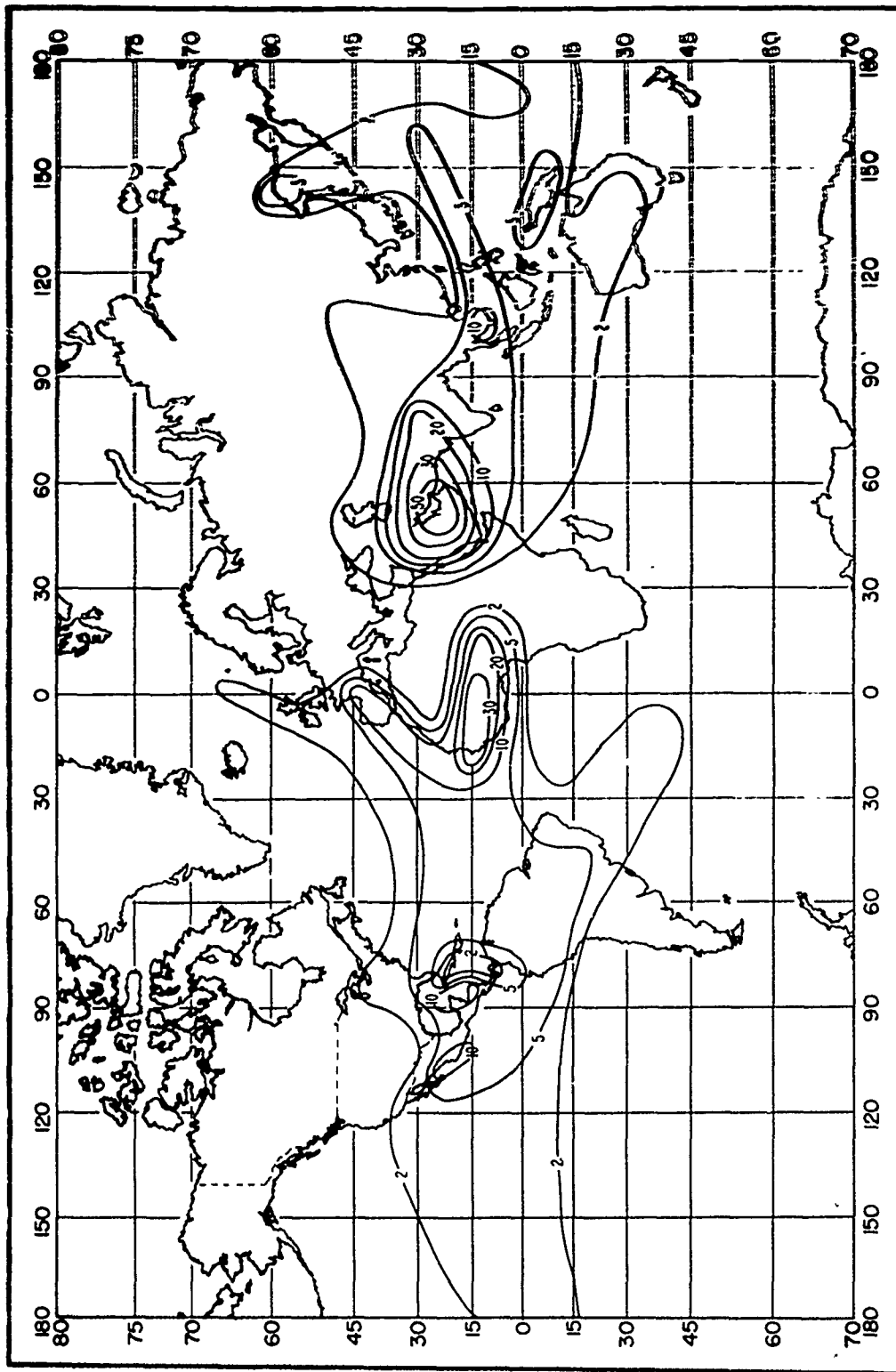


Figure 10.5

Percent of Time Trapping Frequency is Less Than 1000 MHz: May



10-19
F-219

Figure 106

Percent of Time Trapping Frequency is Less Than 1000 MHz: AUGUST

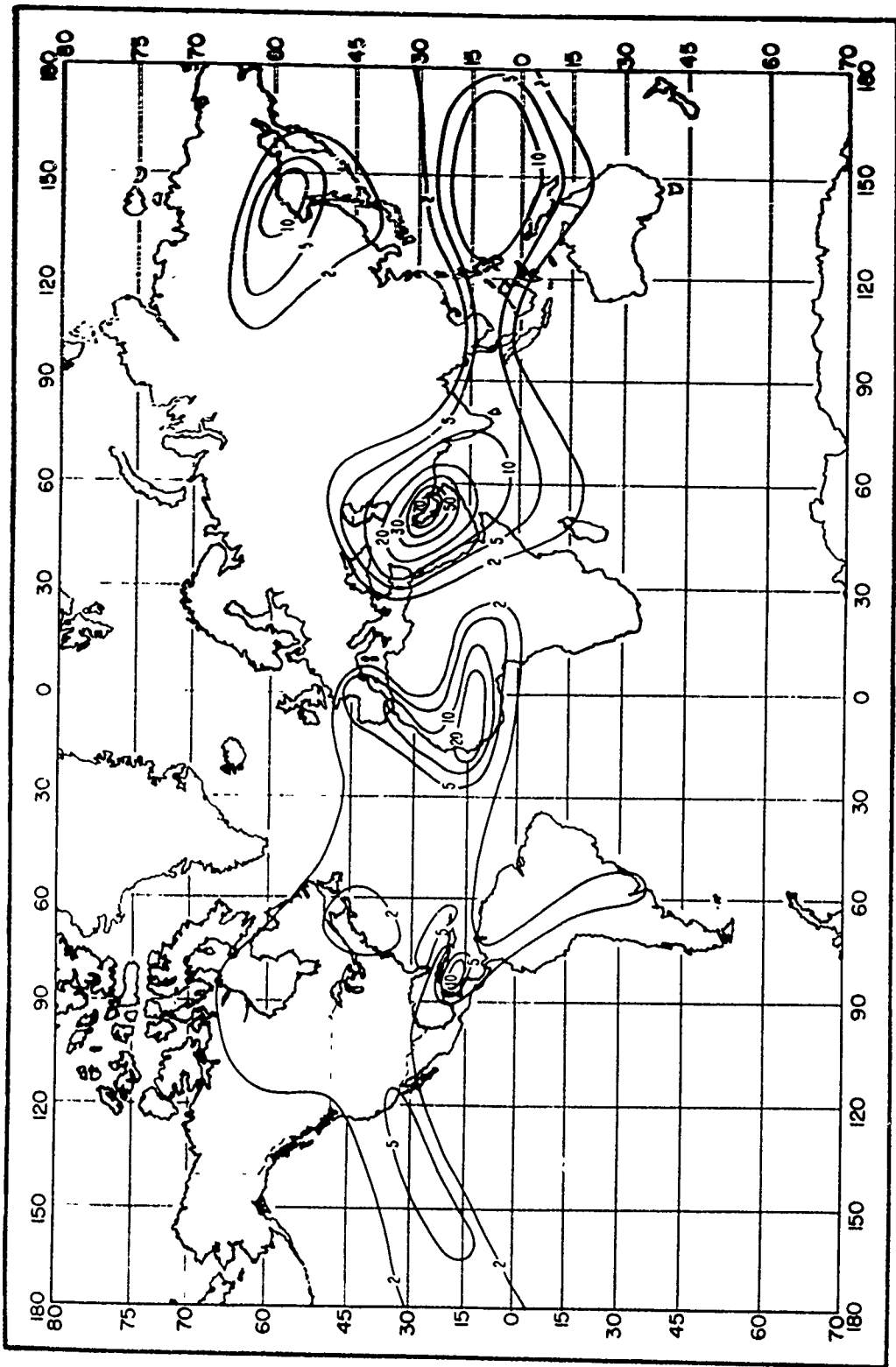


Figure 107

10-20
F-220

Percent of Time Trapping Frequency is Less Than 1000 MHz: November

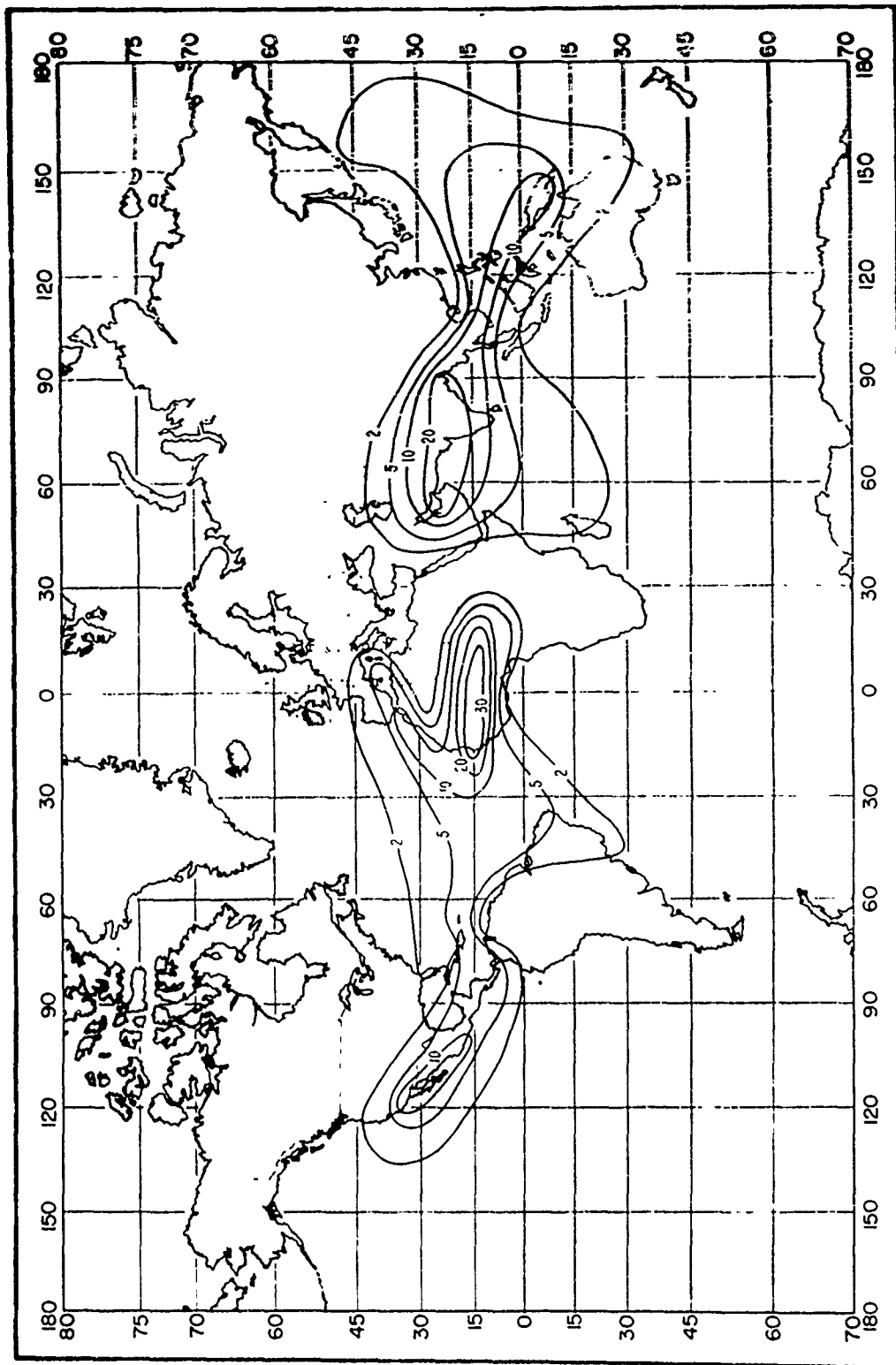


Figure 10 8

Percent of Time Trapping Frequency is Less Than 300 MHz: February

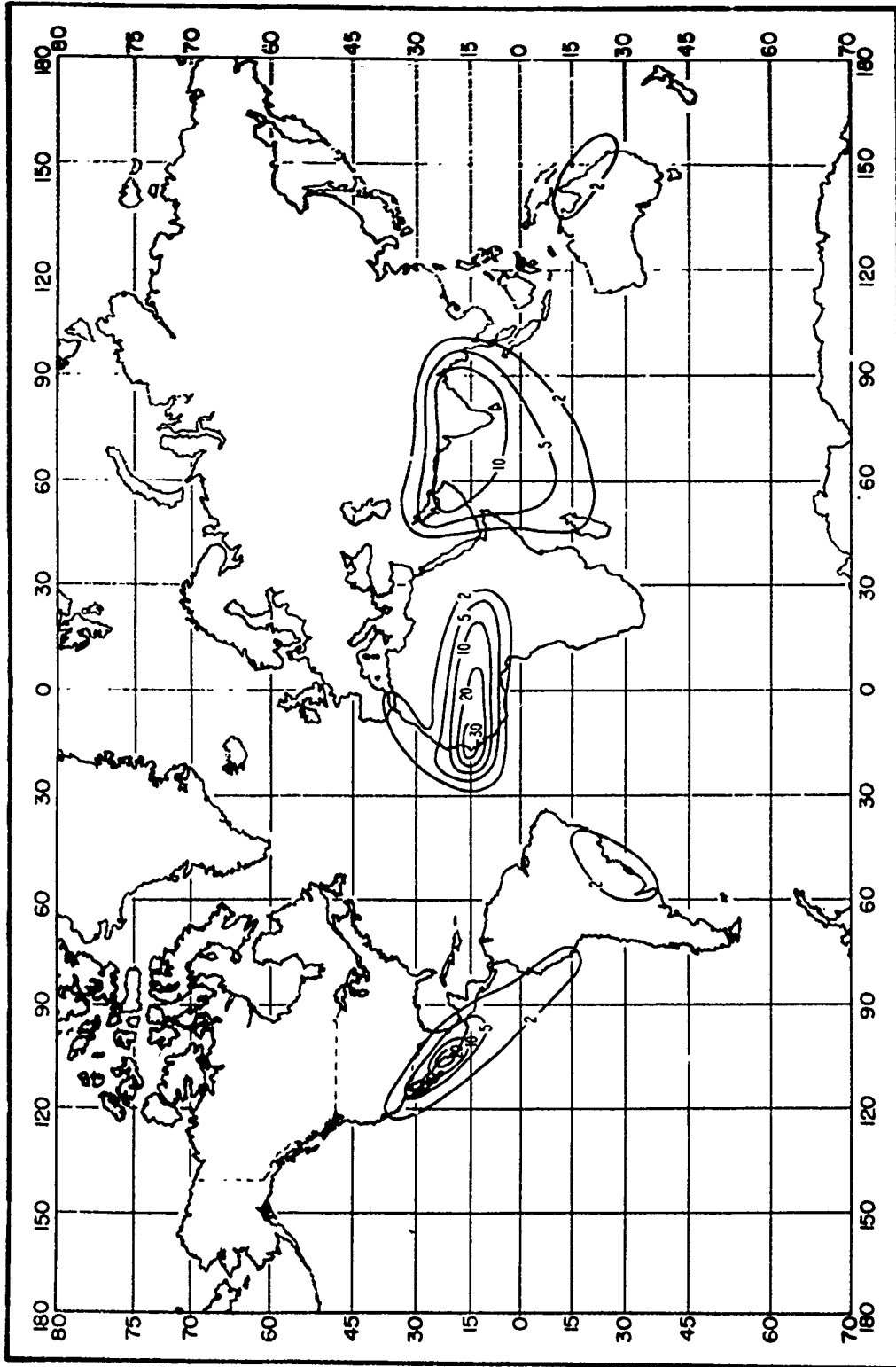


Figure 10.9

Percent of Time Trapping Frequency is Less Than 300 MHz: May

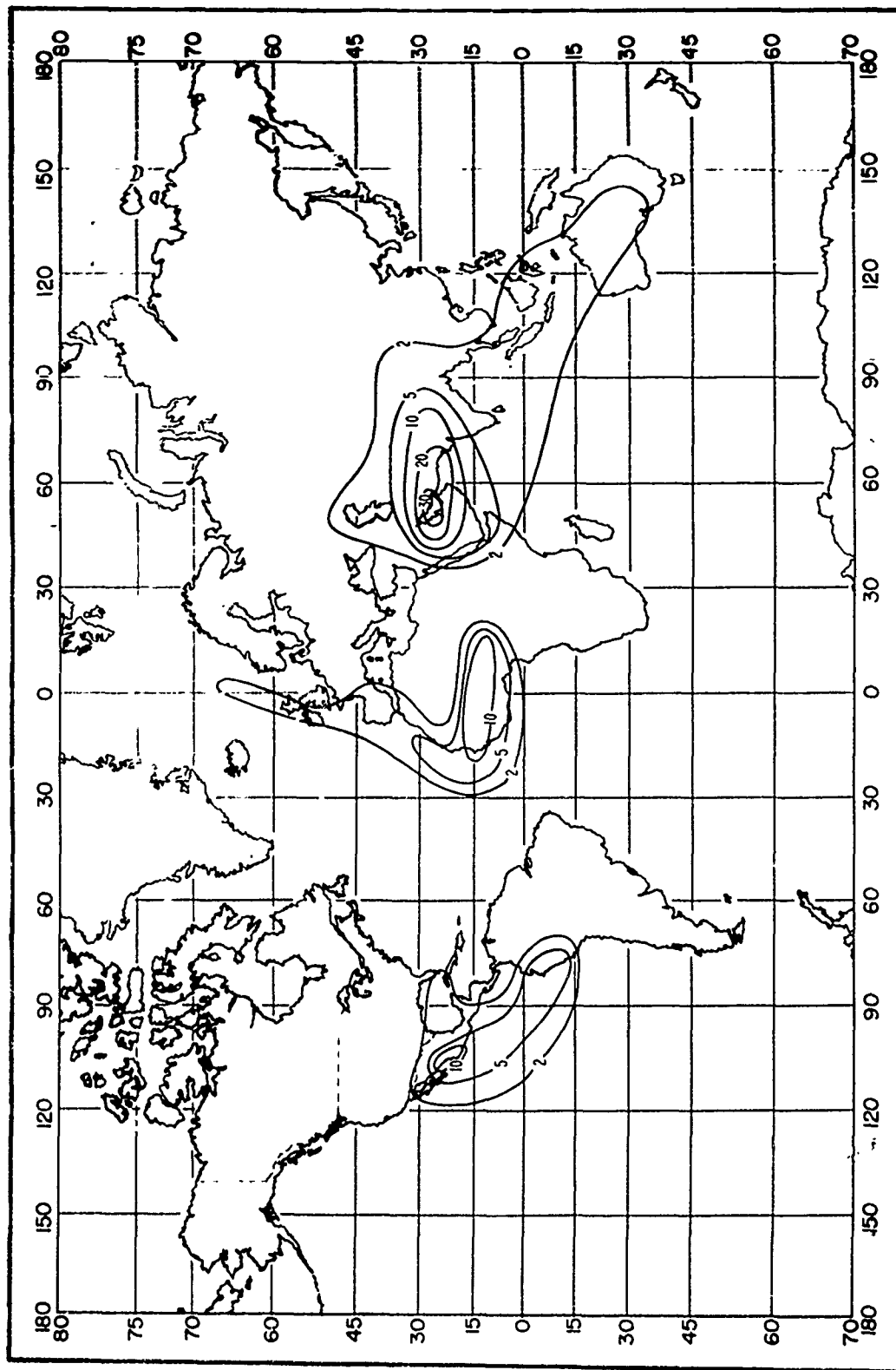


Figure 10.10

Percent of Time Tracing Frequency is Less Than 300 MHz: August

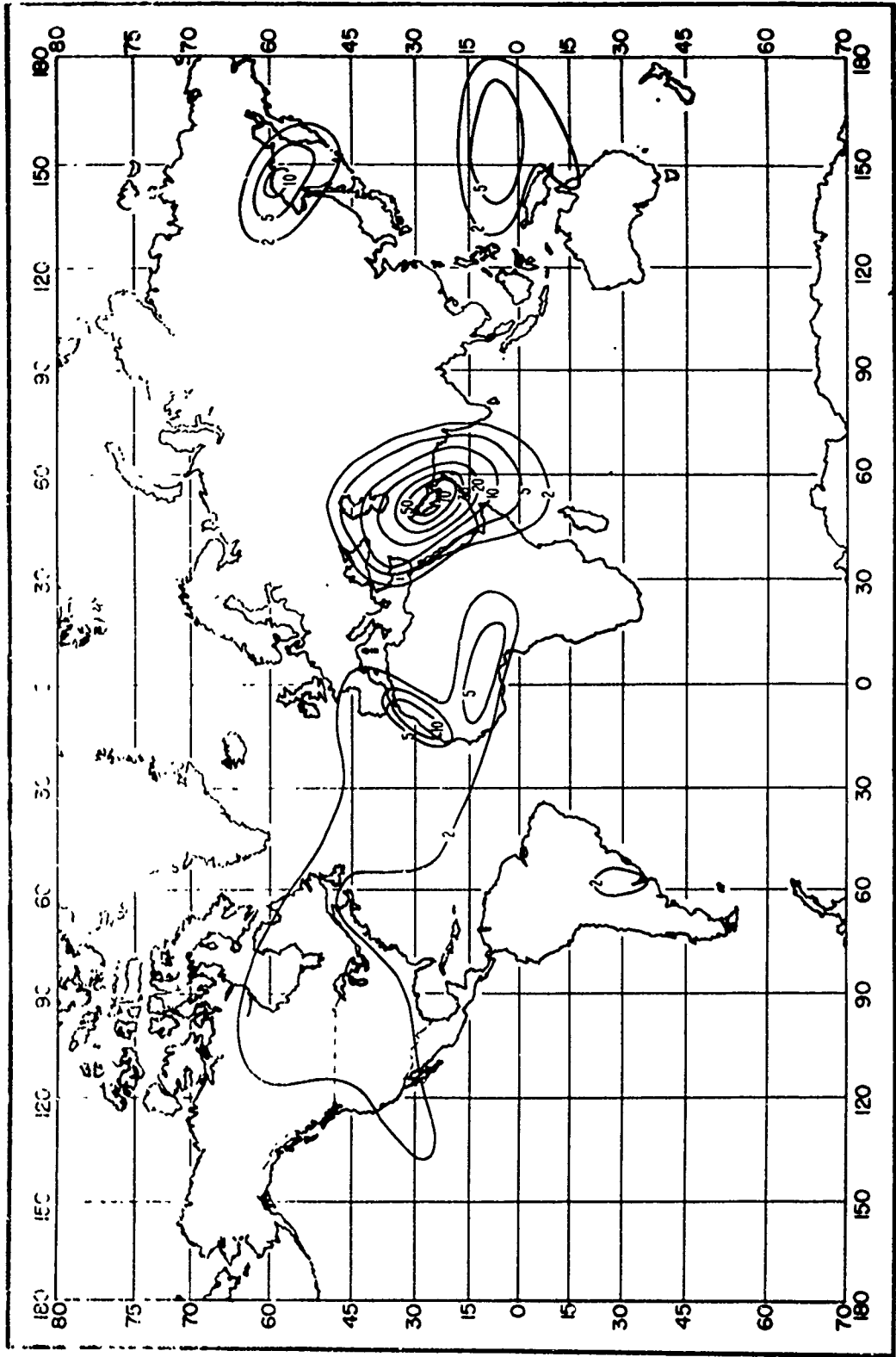


Figure 10.11

Percent of Time Trapping Frequency is Less Than 300 MHz: November

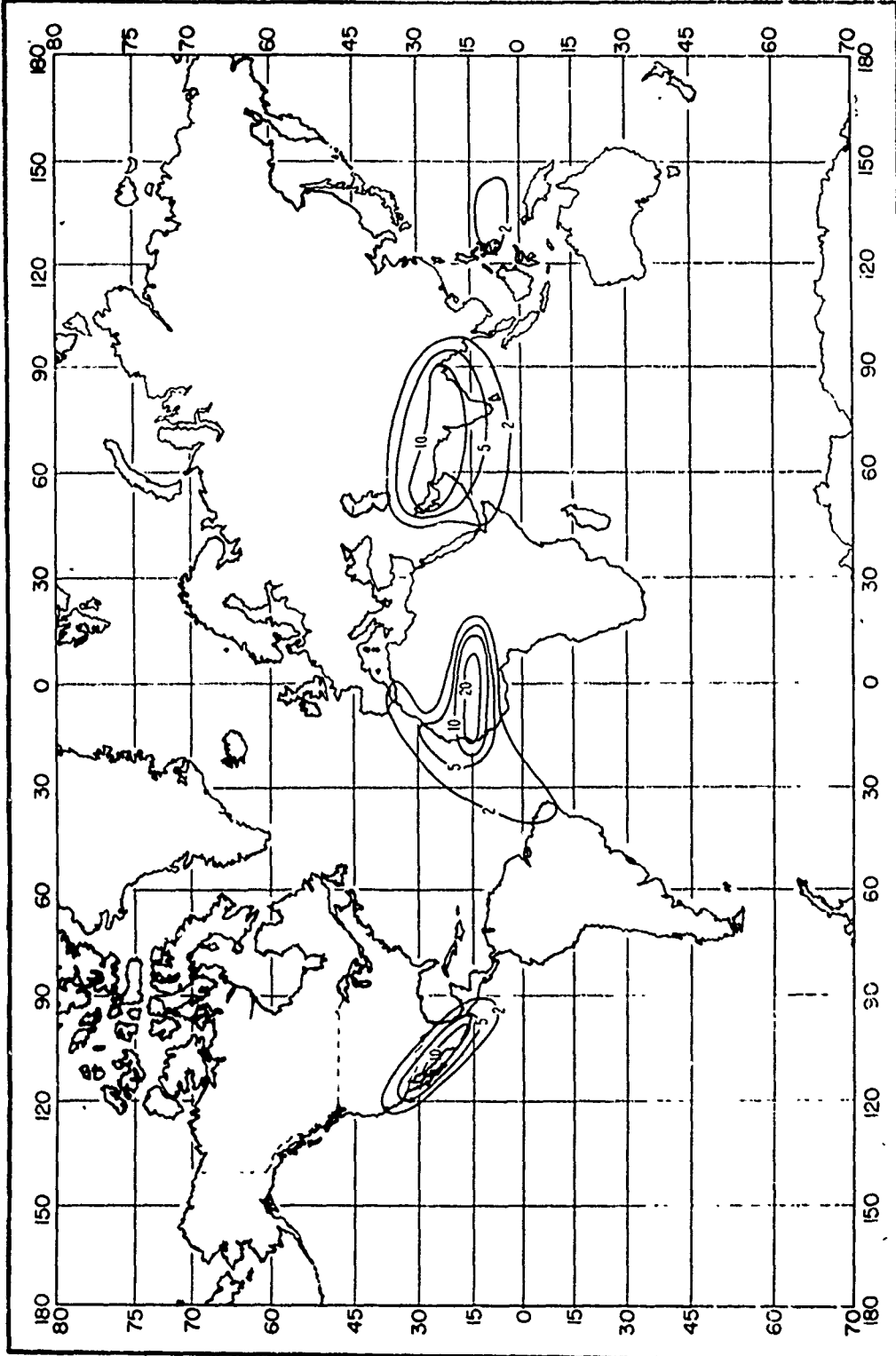


Figure 10.12

10-25
F-225

THE FUNCTION $V(0.5, d_e)$ FOR 8 CLIMATIC REGIONS

$L(0.5) = L_{cr} - V(0.5, d_e)$ db

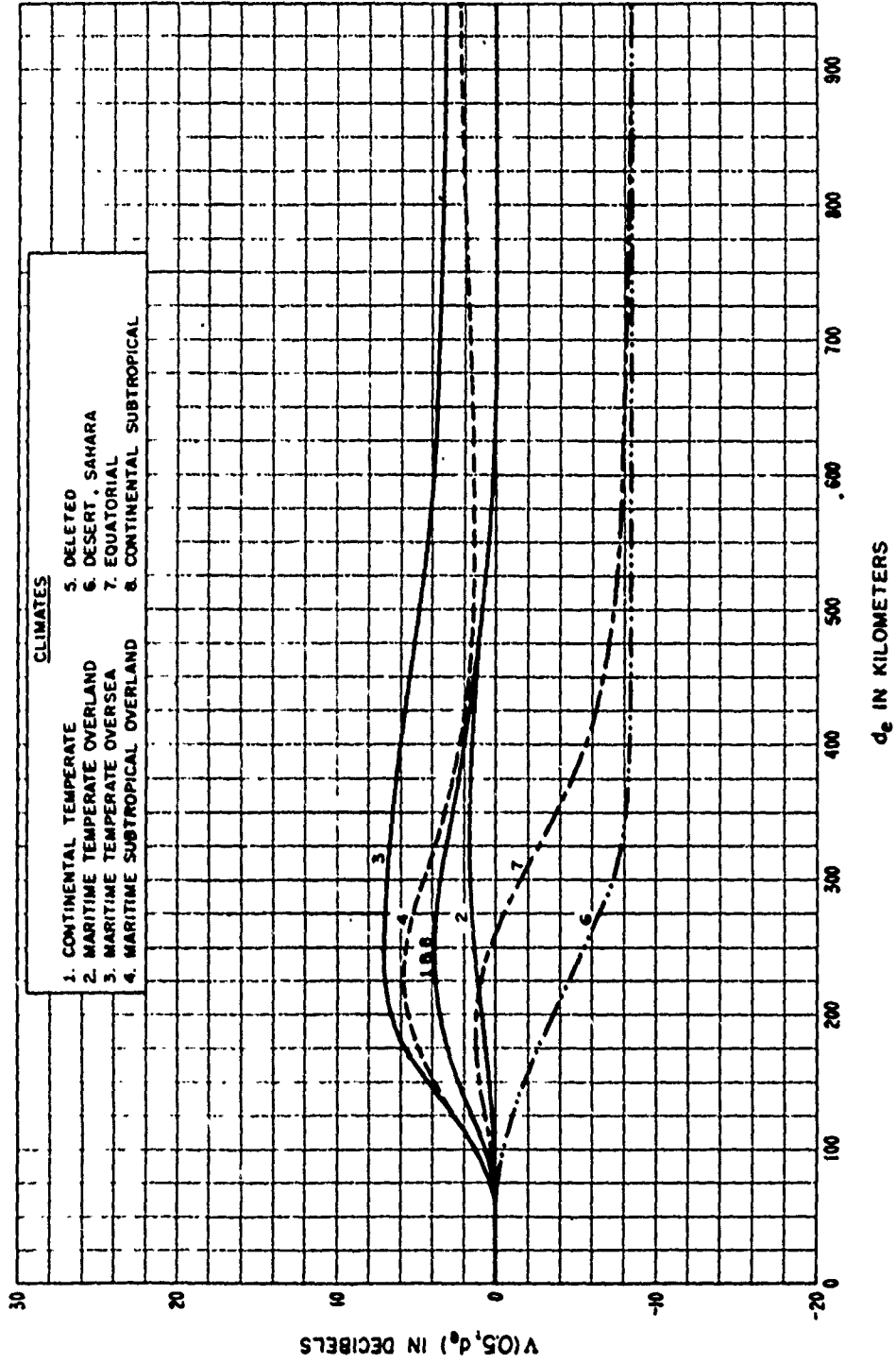


Figure 10.13

LONG - TERM POWER FADING FUNCTION $Y(q, d_e, 100 \text{ MHz})$
CONTINENTAL TEMPERATE CLIMATE

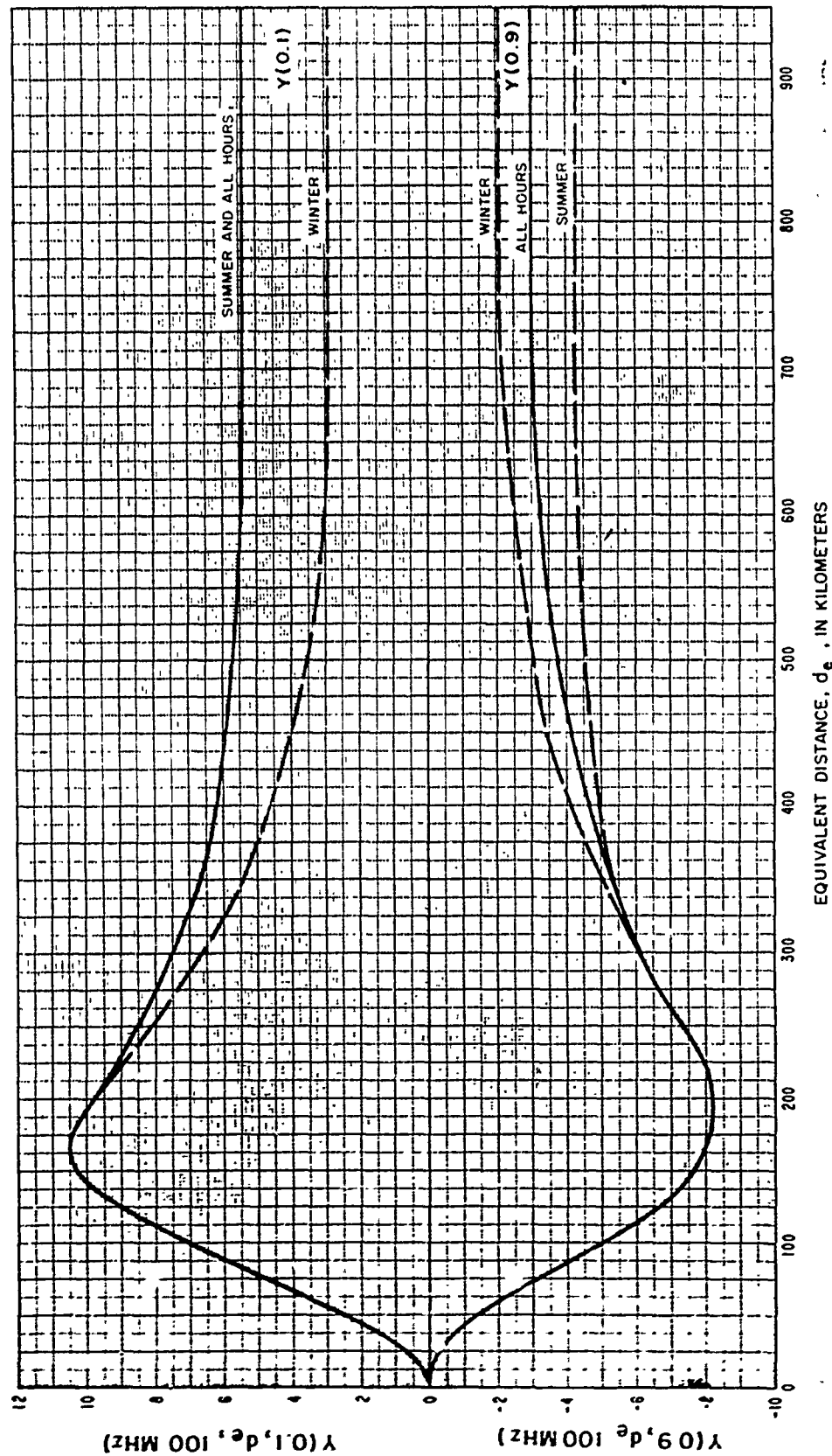


Figure 10.14

POWER FADING ADJUSTMENT FACTOR $g(q,f)$
BASED ON U.S. OVERLAND DATA

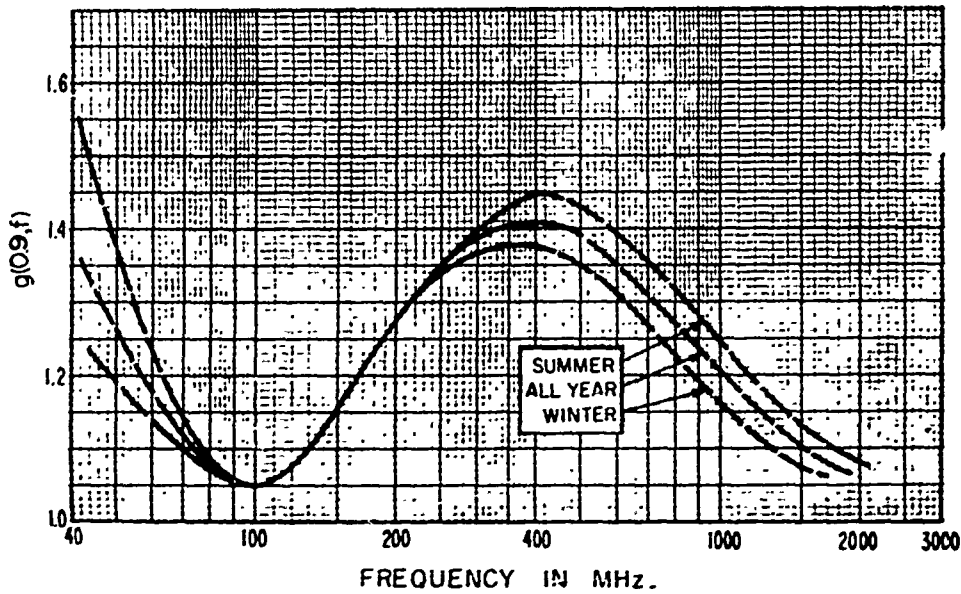
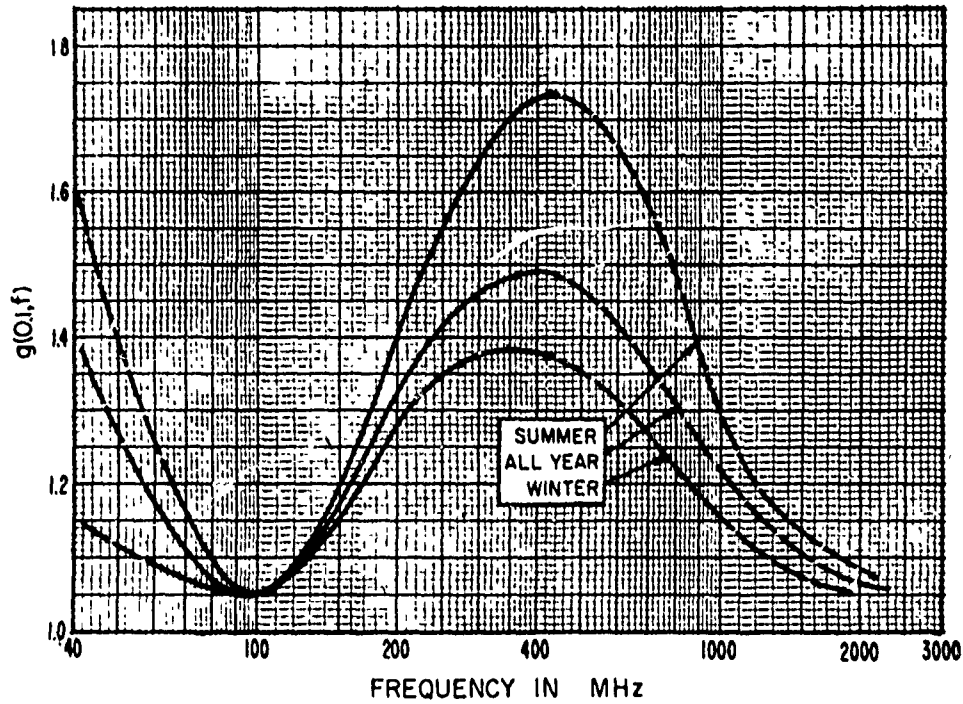


Figure 10.15

EXAMPLE OF A CUMULATIVE DISTRIBUTION $L_b(q)$ VERSUS q

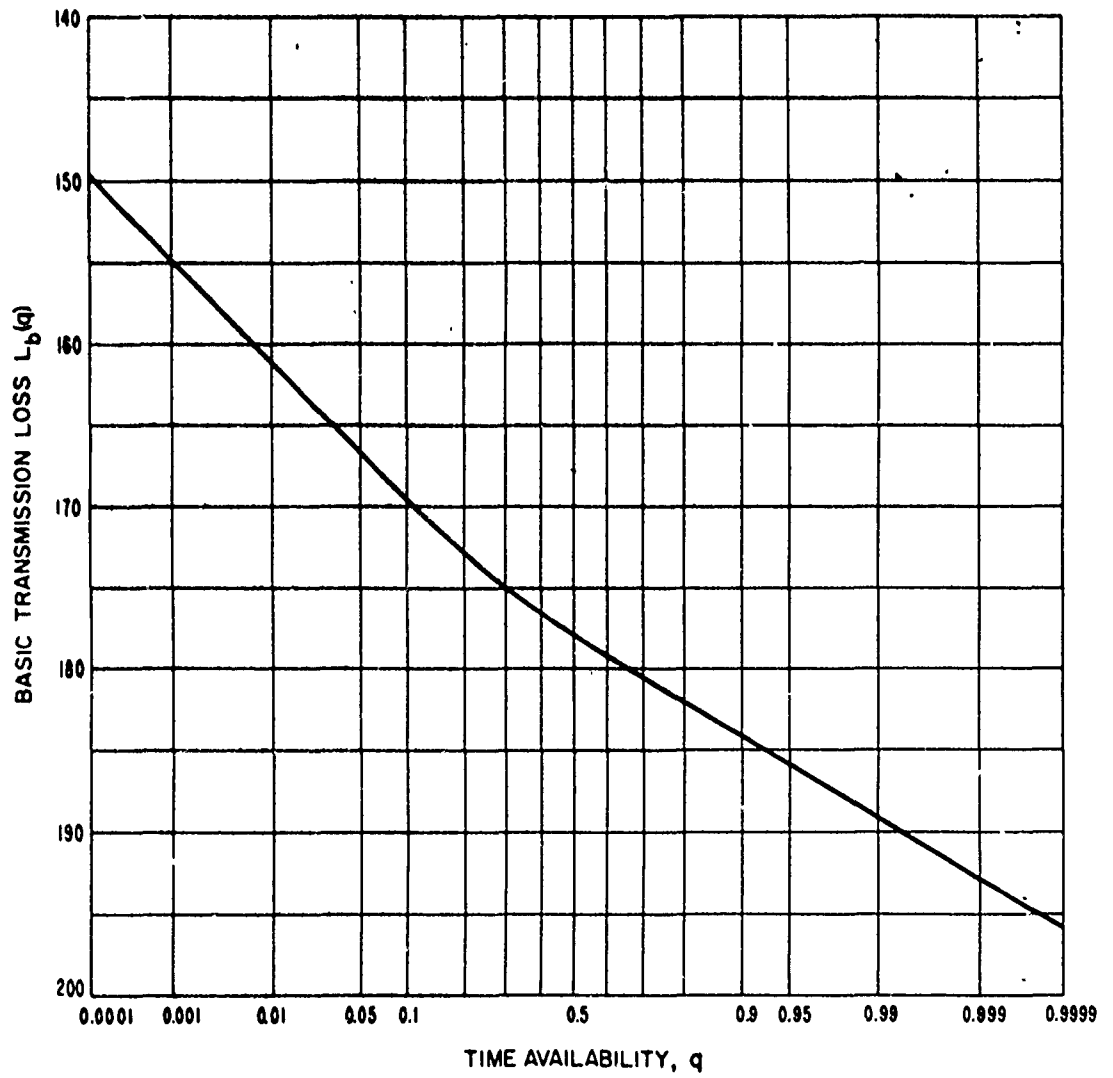


Figure 10.16

LONG-TERM POWER FADING
CONTINENTAL TEMPERATE CLIMATE, 40 - 88 MHz

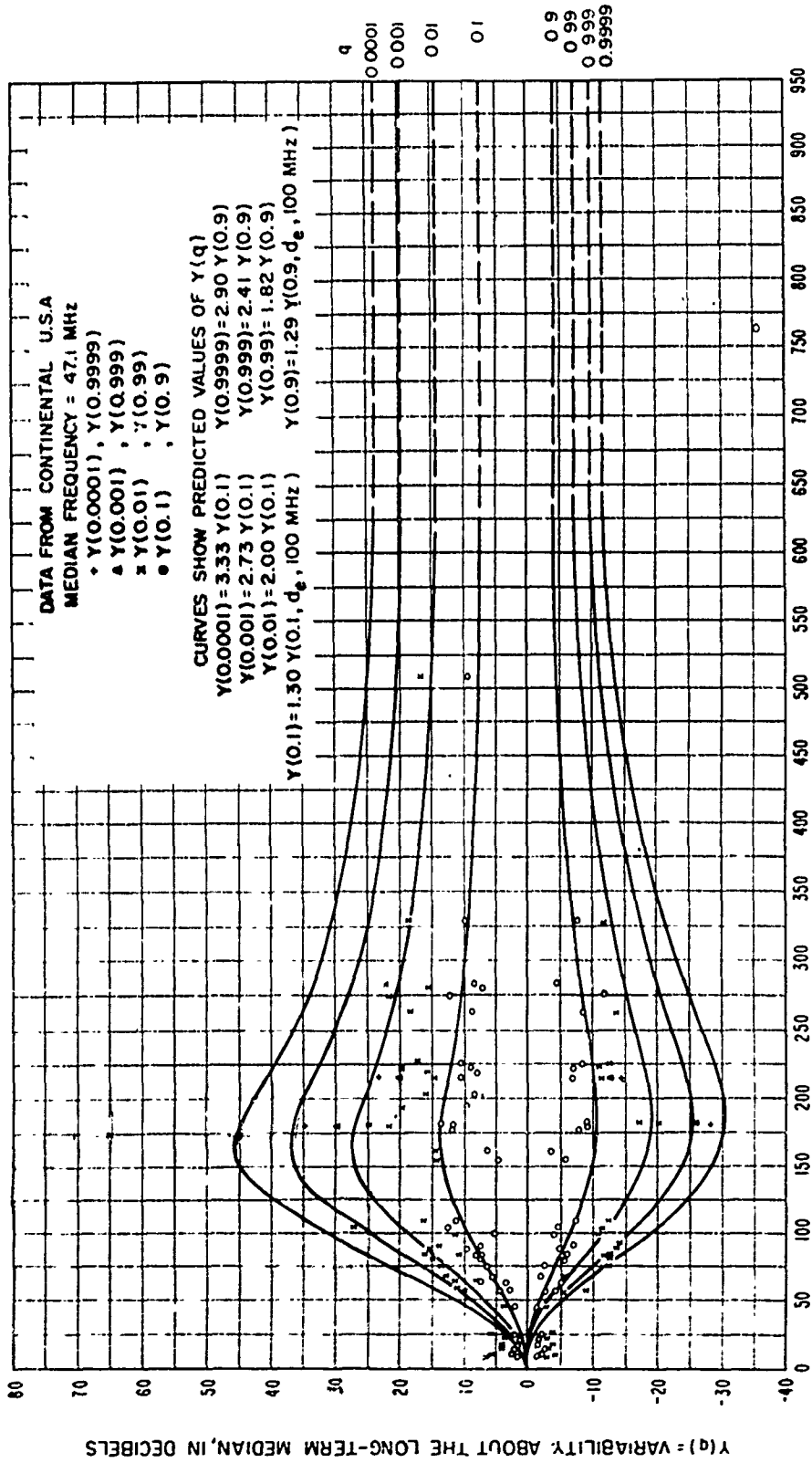


Figure 10.17

LONG-TERM POWER FADING
CONTINENTAL TEMPERATE CLIMATE, 88-108 MHz

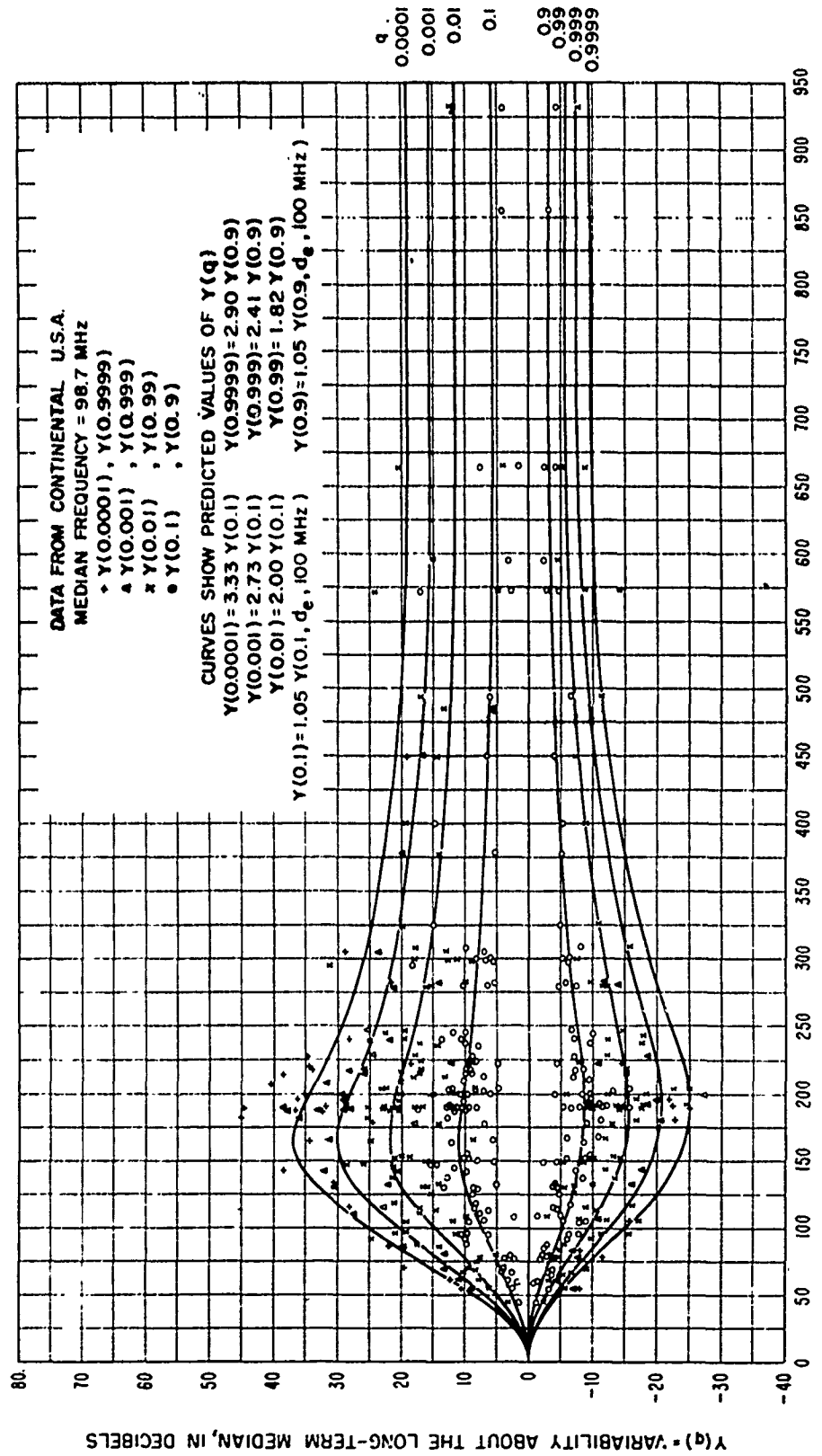


Figure 1018

LONG-TERM POWER FADING
CONTINENTAL TEMPERATE CLIMATE, 108-250 MHz

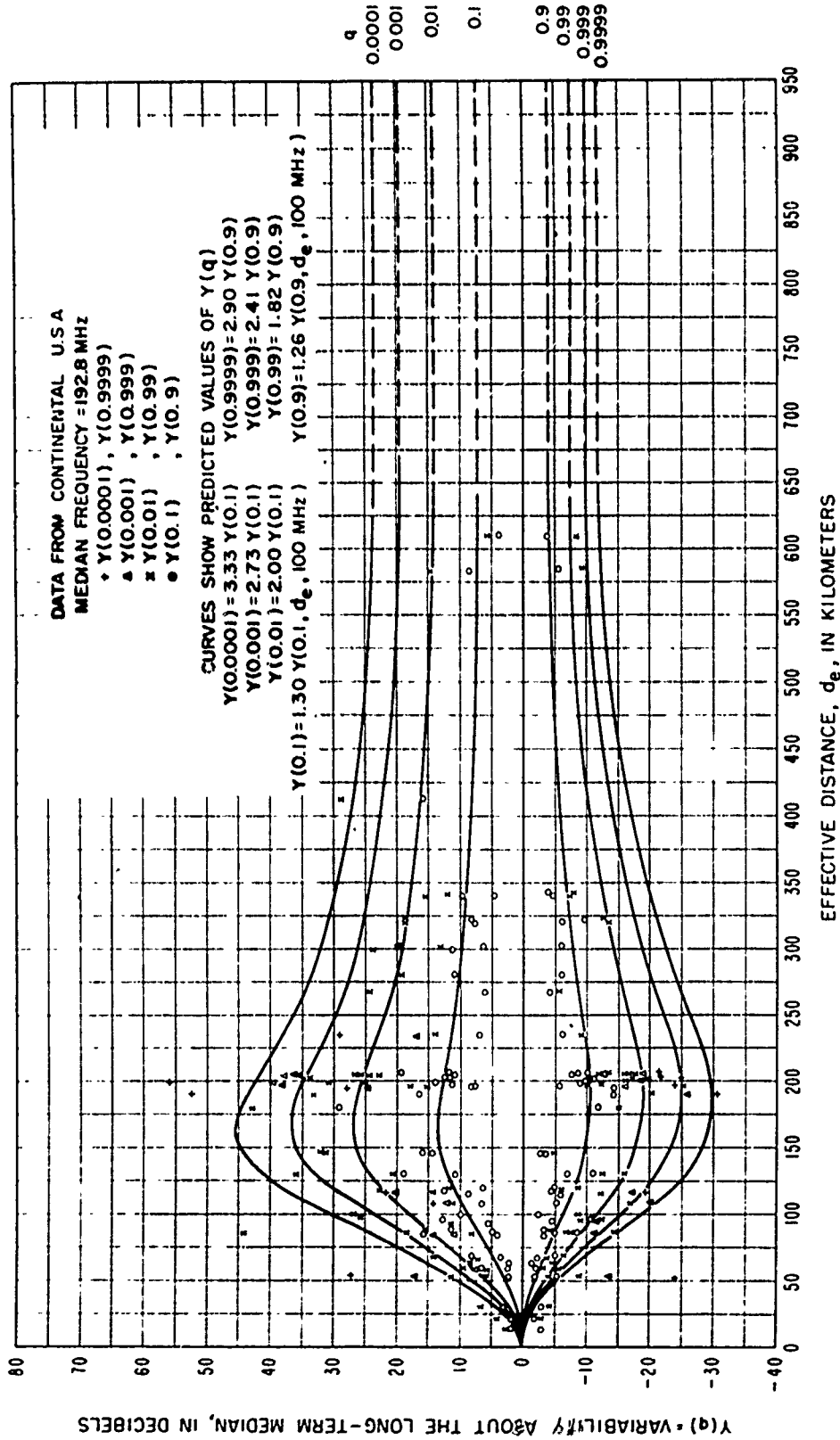


Figure 10.19

LONG-TERM POWER FADING
CONTINENTAL TEMPERATE CLIMATE, 250-450 MHz

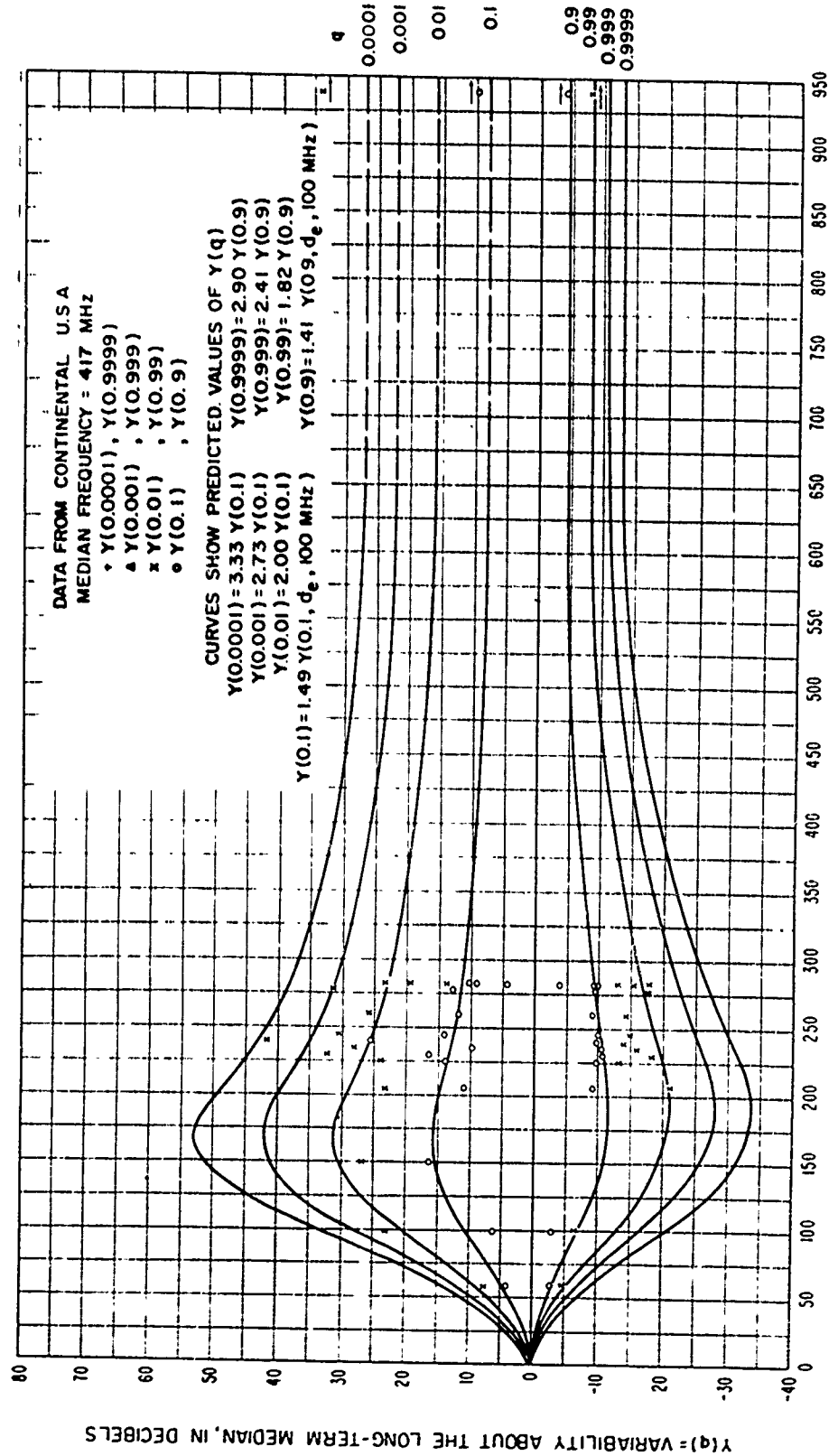


Figure 10.20

LONG-TERM POWER FADING
CONTINENTAL TEMPERATE CLIMATE, 450 - 1000 MHz

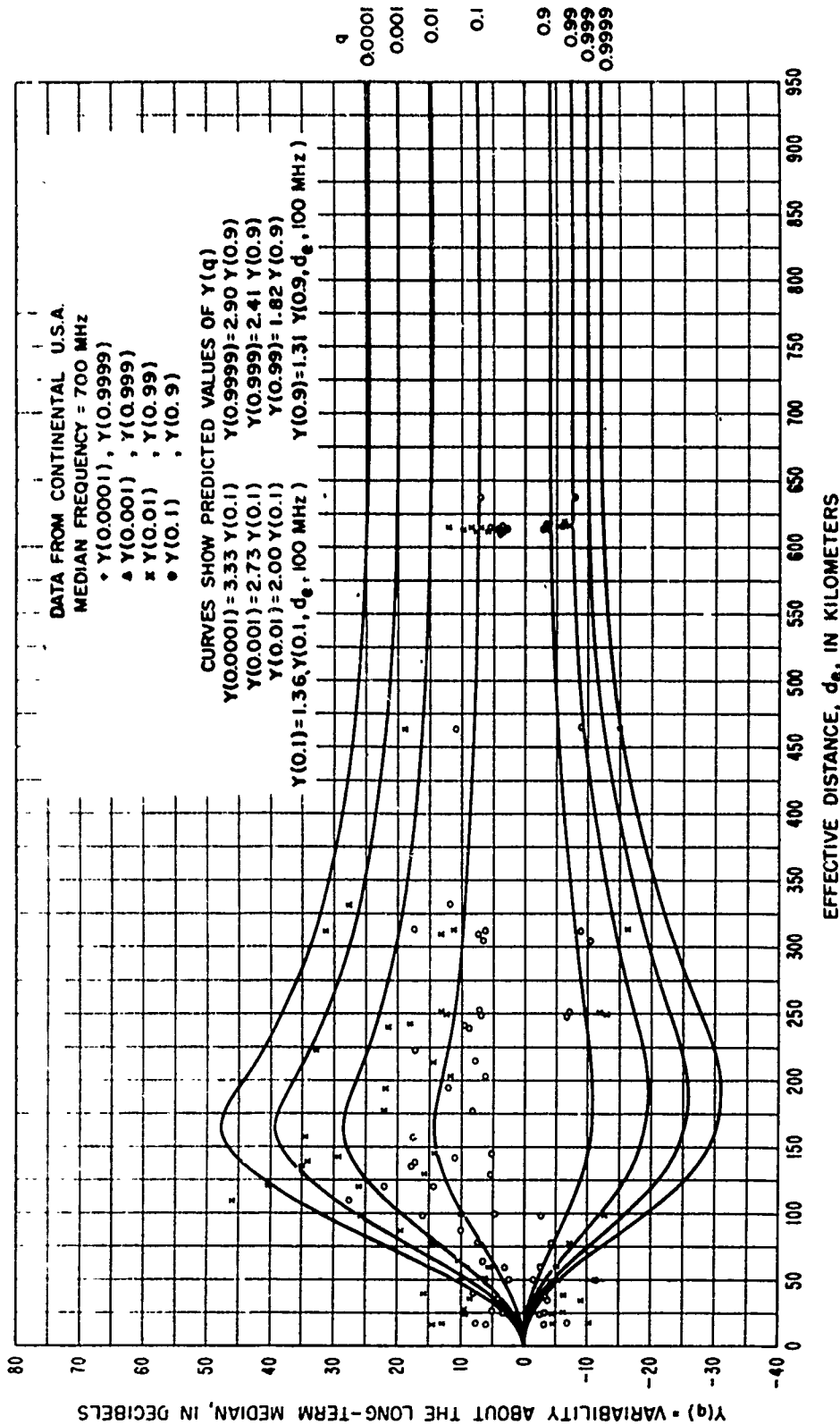


Figure 10.21

LONG-TERM POWER FADING
CONTINENTAL TEMPERATE CLIMATE, FREQ > 1000 MHz

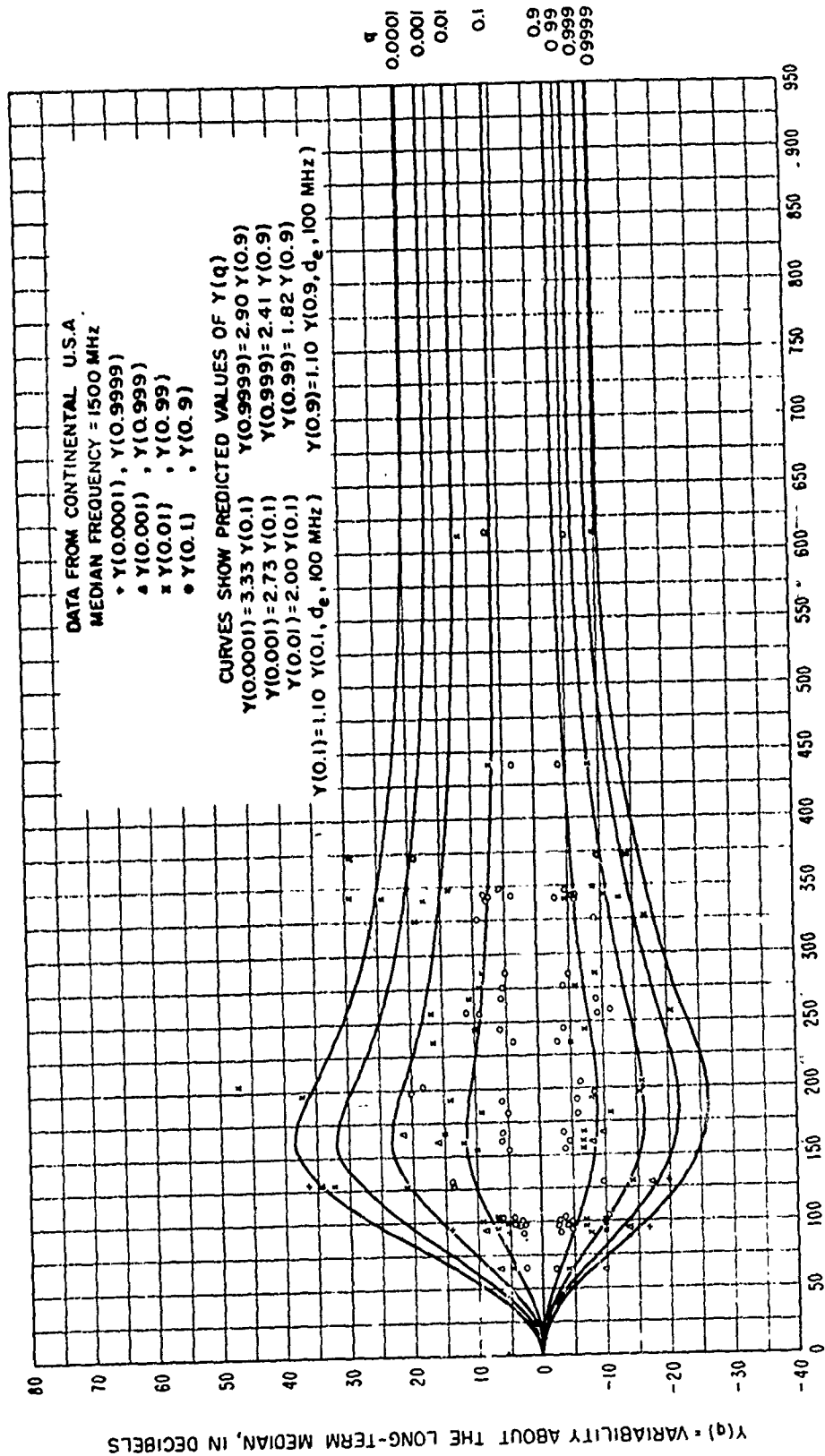


Figure 10.22

LONG-TERM POWER FADING
 MARITIME TEMPERATE CLIMATE OVERLAND, BANDS I AND II (40 - 100 MHz)

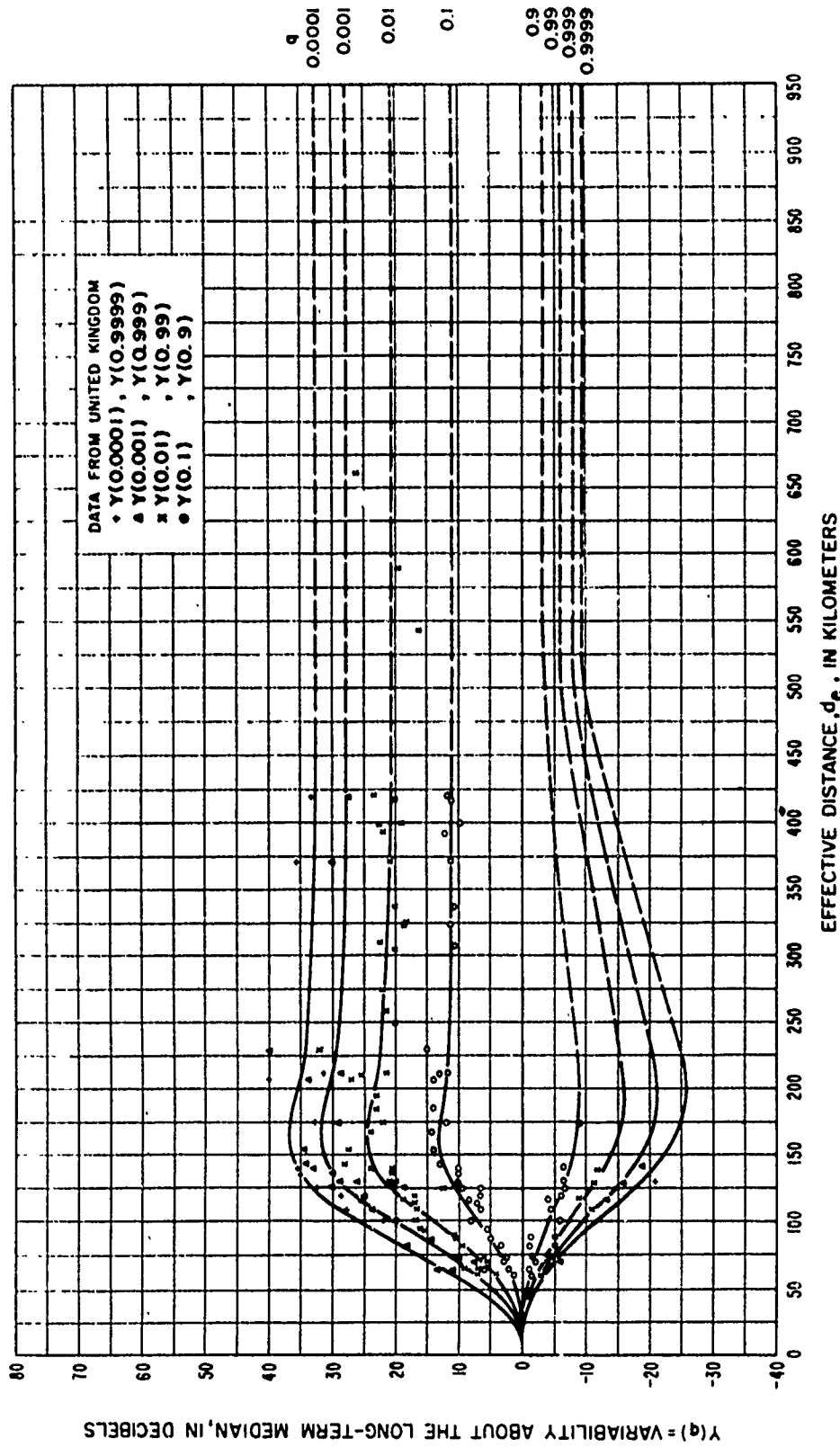


Figure 10.23

LONG-TERM POWER FADING
 MARITIME TEMPERATE CLIMATE OVERSEA, BANDS I AND II (40 - 100 MHz)

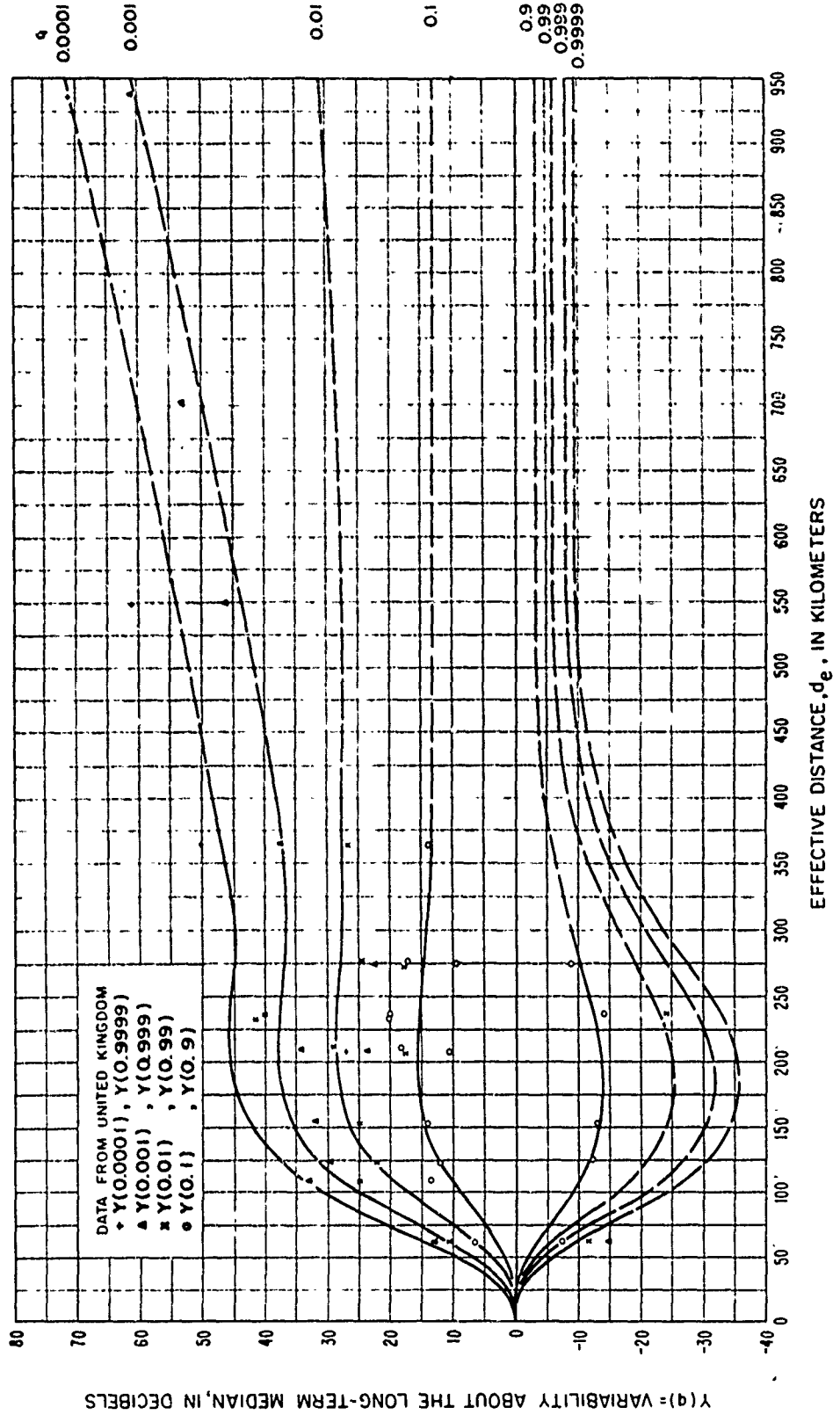


Figure 1024

LONG-TERM POWER FADING
MARITIME TEMPERATE CLIMATE OVERLAND, BAND III (150-250 MHz)

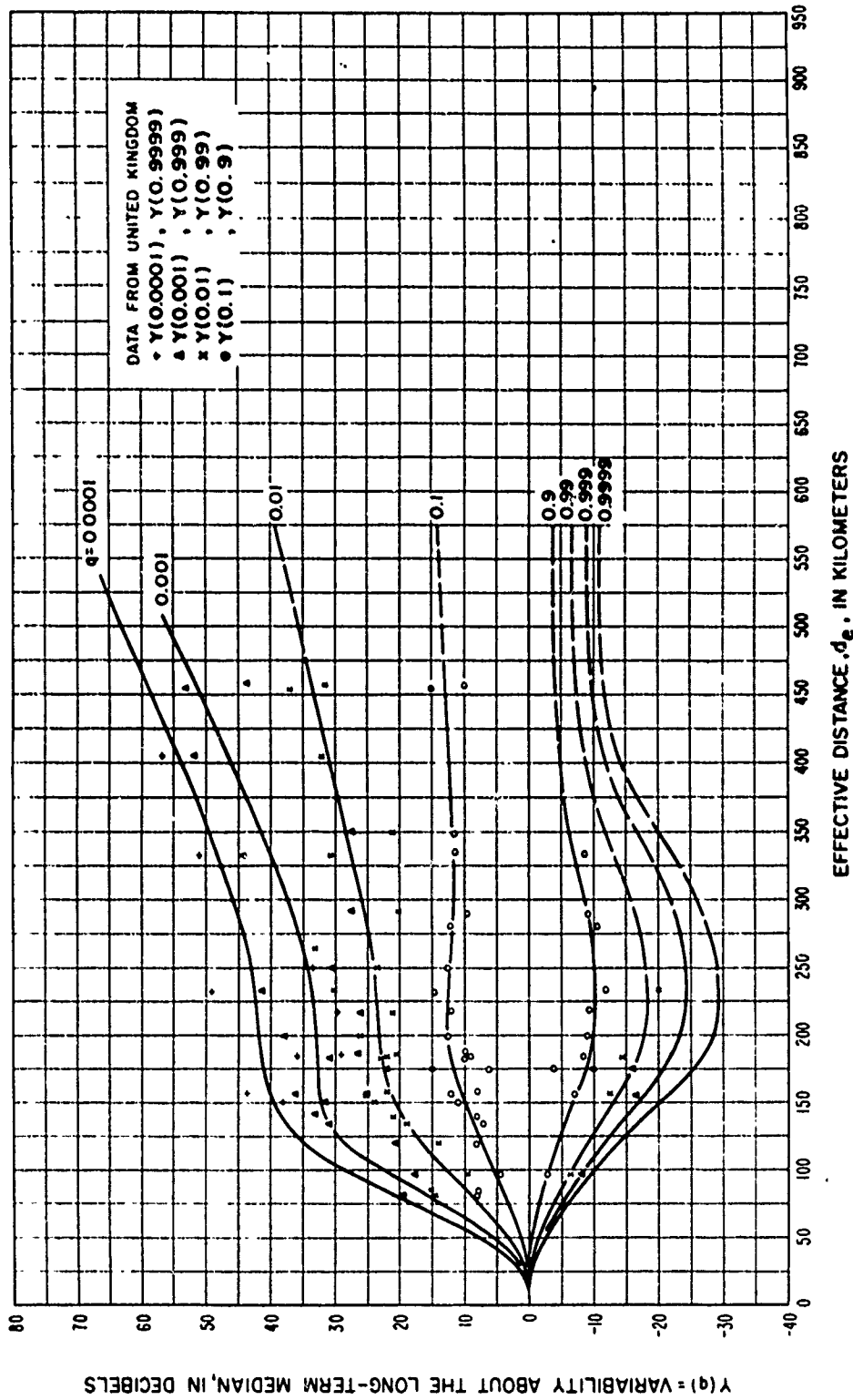


Figure 10.25

LONG-TERM POWER FADING
 MARITIME TEMPERATE CLIMATE OVERSEA . BAND III (150-250 MHz)

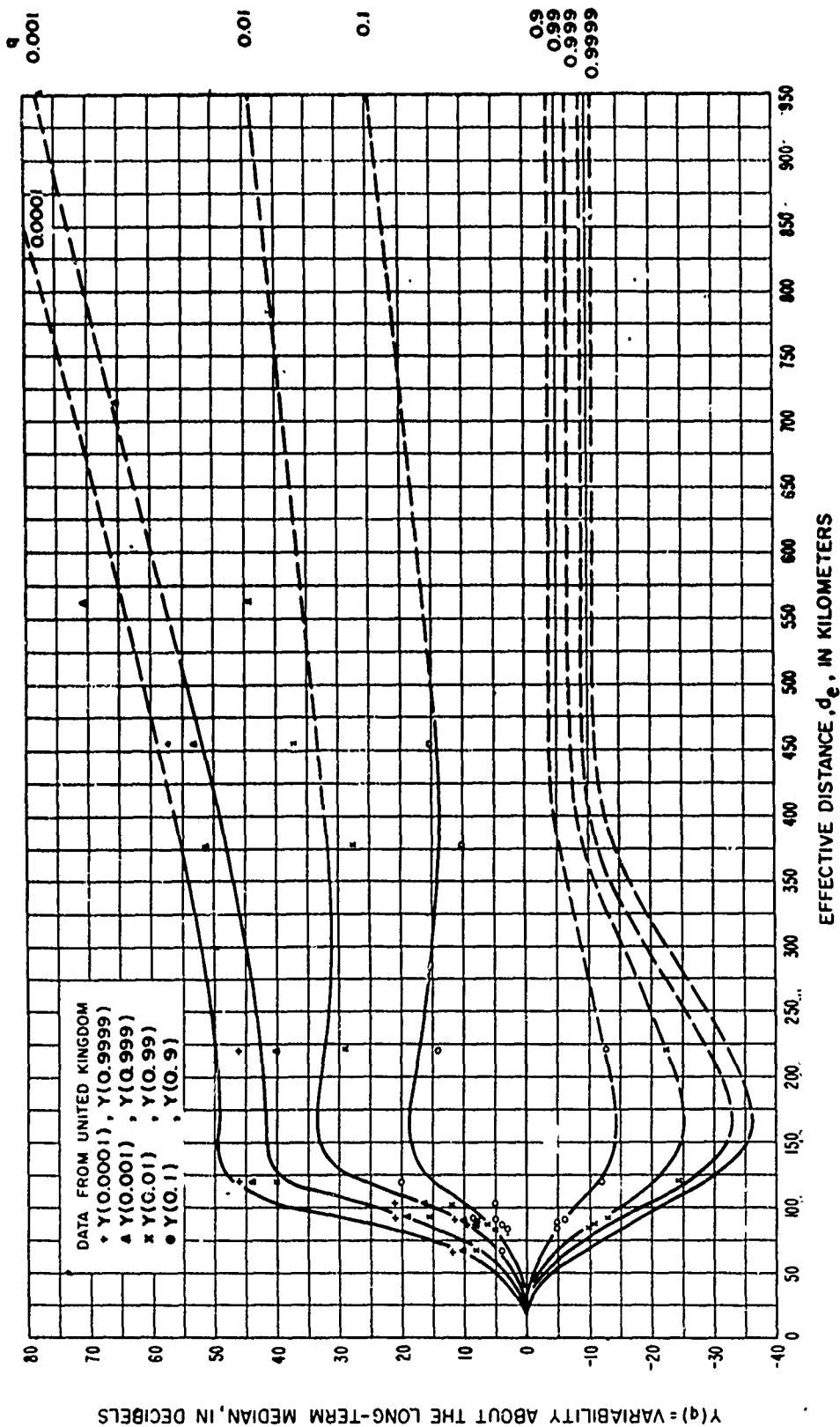


Figure 10.26

LONG-TERM POWER FADING
 MARITIME TEMPERATE CLIMATE OVERLAND, BANDS IV AND V (450-1000 MHz)

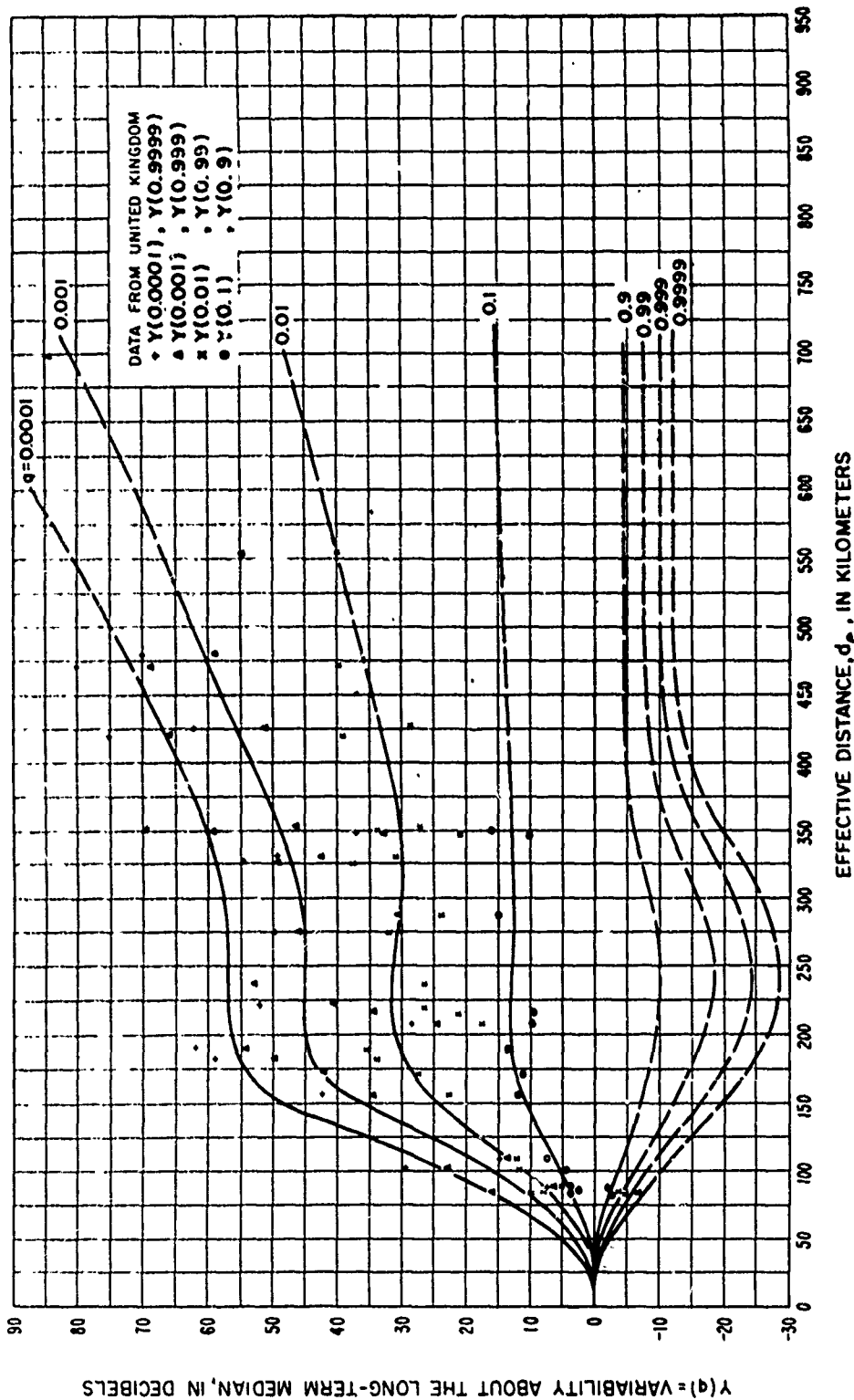


Figure 10.27

LONG-TERM POWER FADING
 MARITIME TEMPERATE CLIMATE OVERSEA, BANDS IV AND V (450-1000 MHz)

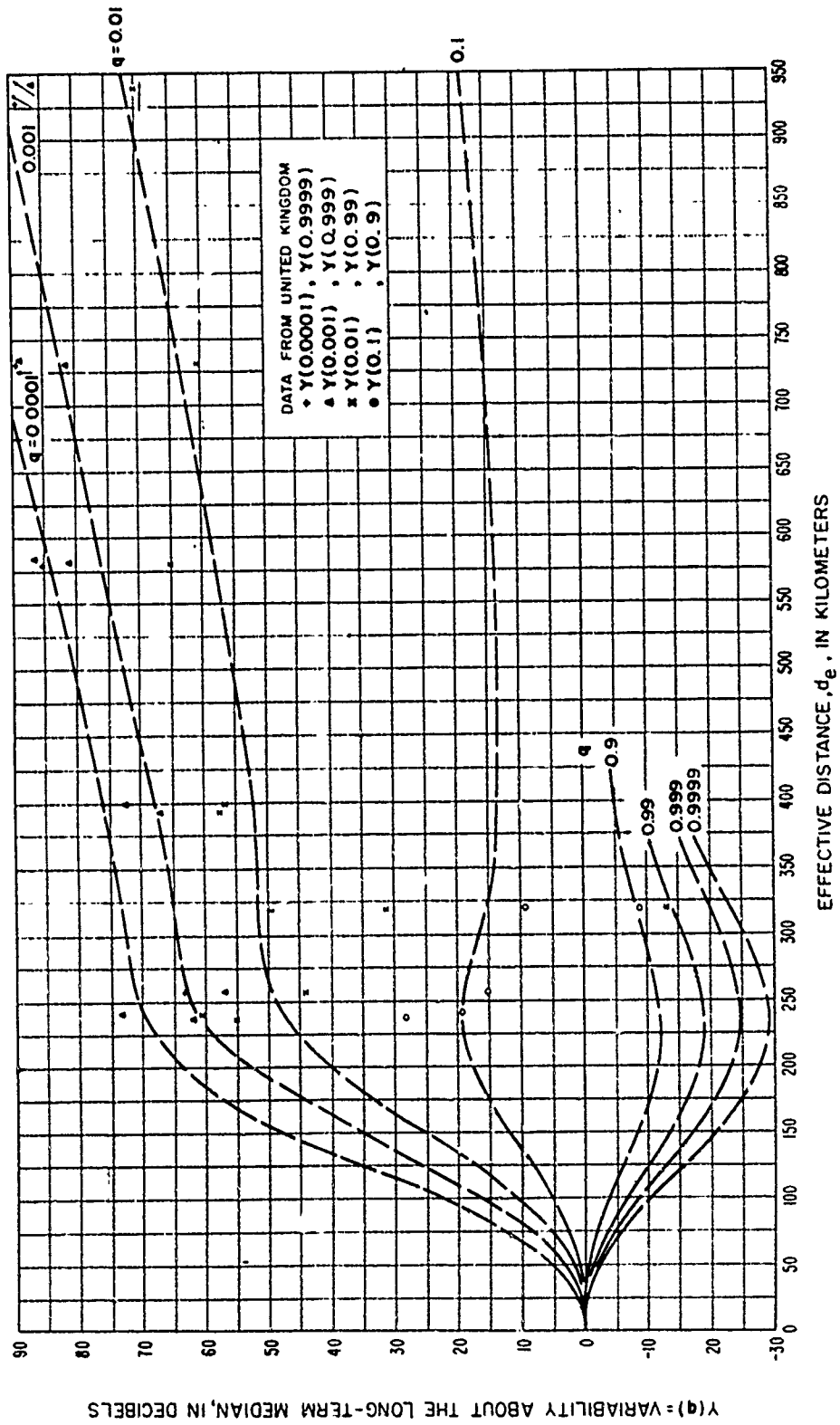


Figure 10.28

11. REFERENCES

The references given below include only selected papers referred to in the text of this report. A comprehensive survey of work in the field of tropospheric propagation, and an extensive bibliography will be found in the following report:

Shkarofsky, I. P. (March 1958), Tropospheric scatter propagation, Res. Rpt. No. 7-200-1, RCA Victor Co., Ltd. Res. Labs, Montreal, Canada.

Four recent bibliographies are:

Abbott, R. L. (Nov. 1960), Bibliography of tropospheric radio wave scattering, NBS Tech. Note No. 80.

Abbott, R. L., and E. R. Westwater (Dec. 1961), Bibliography of microwave thermal emissions by atmospheric gases, Private Communication.

Nupen, Wilhelm (1964), Bibliography on propagation of radio waves through the troposphere, NBS Tech. Note No. 304.

Dougherty, H. T. (Aug. 1964), Bibliography of fading on microwave line-of-sight tropospheric propagation paths and associated subjects, NBS Tech. Note No. 302.

Anderson, L. J., and E. E. Gossard (Oct. 1953a), The effect of the oceanic duct on microwave propagation, Am. Geophys. Union Trans. 34, No. 5, 695-700.

Anderson, L. J., and E. E. Gossard (Jan. 1953b), Prediction of the nocturnal duct and its effect on UHF, Proc. IRE 41, No. 1, 136-139.

Arons, L. D. (Oct. 1956), An analysis of radio-wave scattering in the diffraction region, Cornell University E. E. Report 312.

Artman, J. O., and J. P. Gordon (Dec. 1954), Absorption of microwaves by oxygen in the millimeter wavelength region, Phys. Rev. 96, No. 5, 1237-1245.

Bachynski, M. P. (1959), Microwave propagation over rough surfaces, RCA Review 20, No. 2, 308-335.

Bachynski, M. P. (July-Aug. 1960), Propagation at oblique incidence over cylindrical obstacles, J. Res. NBS 64D (Radio Prop.), No. 4, 311-315.

Bachynski, M. P. (March 1963), Scale model investigations of electromagnetic wave propagation over natural obstacles, RCA Review 24, No. 1, 105-144.

Barghausen, A. F., F. O. Giraud, R. E. McGavin, S. Murahata, and R. W. Wilber (Jan. 1963), Equipment characteristics and their relation to system performance for tropospheric communication circuits, NBS Tech. Note 103.

Barsis, A. P., and M. E. Johnson (Nov. - Dec. 1962), Prolonged space-wave fade-outs in tropospheric propagation, J. Res. NBS 66D (Radio Prop.), No. 6, 681-694.

Barsis, A. P., and R. S. Kirby (Sept. - Oct. 1961), VHF and UHF signal characteristics observed on a long knife-edge diffraction path, J. Res. NBS 65D (Radio Prop.), No. 5, 437-448.

Barsis, A. P., K. A. Norton, P. L. Rice, and P. H. Elder (Aug. 1961), Performance predictions for single tropospheric communication links and for several links in tandem, NBS Tech. Note 102. (See also IRE Transactions on Communication Systems CS-10, No. 1, 2-22, March 1962).

CCP 702-1

- Batchelor, G. K. (1947), Kolmogoroff's theory of locally isotropic turbulence, Proc. Camb. Phil. Soc. 43, 533-559.
- Batchelor, G. K. (1953), The theory of homogeneous turbulence, (Cambridge University Press).
- Bean, B. R. (May, 1954), Prolonged space-wave fadeouts at 1,046 Mc observed in Cheyenne Mountain propagation program, Proc. IRE 42, No. 5, 848-853.
- Bean, B. R. (1956), Some meteorological effects on scattered VHF radio waves, IRE Trans. Comm. Syst., CS4(1), 32-38.
- Bean, B. R. (July-Aug. 1959), Climatology of ground-based radio ducts, J. Res. NBS 63D (Radio Prop.), No. 1, 29-34.
- Bean, B. R. (1961), Concerning the bi-exponential nature of the tropospheric radio refractive index, Beiträge zur Physik der Atmosphäre 34, No. 1/2, 81-91.
- Bean, B. R., and R. L. Abbott (1957), Oxygen and water vapor absorption of radio waves in the atmosphere, Geofisica Pura e Applicata - Milano 37, 127-134.
- Bean, B. R., and B. A. Cahoon (Nov. 1957), The use of surface observations to predict the total atmospheric bending of radio rays at small elevation angles, Proc. IRE 45, No. 11, 1545-1546.
- Bean, B. R., B. A. Cahoon, C. A. Samson, G. D. Thayer (1966), A world atlas of atmospheric radio refractivity, to be published as a Monograph.
- Bean, B. R., J. D. Horn, and A. M. Ozanich, Jr. (Nov. 1960), Climatic charts and data of the radio refractive index for the United States and the world, NBS Monograph No. 22.
- Bean, B. R., J. D. Horn, and L. P. Riggs (Oct. 1962), Synoptic radio meteorology, NBS Tech. Note 98.
- Bean, B. R., and G. D. Thayer (May 1959), Models of the atmospheric radio refractive index, Proc. IRE 47, No. 5, 740-755.
- Beard, C. I. (September 1961, Coherent and incoherent scattering of microwaves from the ocean, IRE Trans. Ant. Prop. AP-9, 470-483.
- Beard, C. I., I. Katz, and L. M. Spetner (April 1956), Phenomenological vector model of microwave reflection from the ocean, IRE Trans. Ant. Prop. AP-4, No. 2, 162-167.
- Beckmann, P. (1957), A new approach to the problem of reflection from a rough surface, Acta, Tech. Ceskosl. Akad. 2, 311-355; see also pp. 323-335, (1959).
- Beckmann, P. (1960), A generalized Rayleigh distribution and its application to tropospheric propagation Electromagnetic Wave Propagation, (Symposium, Liege, 1958), (Academic Press, London, 445-449).
- Beckmann, P. (1961a), The statistical distribution of the amplitude and phase of a multiply scattered field, Inst. Rad. Eng. and Elec., Czechoslovak Akad. Sci., Paper No. 18. See also J. Res. NBS 66D, (Radio Prop.), pp. 231-240, 1962.

- Beckmann, P. (1961b), The depolarization of electromagnetic waves scattered from rough surfaces, *Inst. Rad. Eng. and Elect., Czechoslovak Akad. Sci., Paper No. 19.*
- Beckmann, P. (September 1964), Rayleigh distribution and its generalization, *J. Res. NBS 68D, (Radio Science), No. 9, pp. 927-932.*
- Beckmann, P. and A. Spizzichino (1963), The scattering of Electromagnetic waves from rough surfaces, *International Series of Monographs on Electromagnetic Waves, Vol. 4, (Pergamon Press, New York, N.Y.).*
- Biot, M. A. (Dec. 1957a), Some new aspects of the reflection of electromagnetic waves on a rough surface, *J. Appl. Phys. 28, No. 12, 1455-1463.*
- Biot, M. A. (Nov. 1957b), Reflection on a rough surface from an acoustic point source, *J. Acoust. Soc. Am. 29, No. 11, 1173-1200.*
- Booker, H. G. (1946), Elements of radio meteorology: How weather and climate cause unorthodox radar vision beyond the geometrical horizon, *J. Inst. Elec. Engrs. (London) 93, Pt. III-A, No. 1, 69-78.*
- Booker, H. G., and J. T. de Bettencourt (Mar. 1955), Theory of radio transmission by tropospheric scattering using very narrow beams, *Proc. IRE 43, No. 3, 281-290.*
- Booker, H. G., and W. E. Gordon (Sept. 1950a), Outline of a theory of radio scattering in the troposphere, *J. Geophys. Res. 55, No. 3, 241-246; see also Proc. IRE 38, No. 4, 401, (April, 1950b).*
- Booker, H. G., and W. Walkinshaw (April 1946), The mode theory of tropospheric refraction and its relation to waveguides and diffraction, *Report on Conference on Meteorological Factors in Radio Wave Propagation (The Phys. Soc., and the Royal Met. Soc., London), 80-127.*
- Bray, W. J., F. Hopkins, A. Kitchen, and J. A. Saxton (Jan. 1955), Review of long-distance radio-wave propagation above 30 Mc/s, *Proc. IEE, Paper No. 1782R, Pt. B, 102, 87-95.*
- Bremmer, H. (1949), *Terrestrial radio waves; theory of propagation, (Elsevier Publishing Co., Amsterdam and New York, N.Y.).*
- Bremmer, H. (Sept. 1957), Distortion in tropospheric scatter, *Phillips Telecomm. Rev. 18, No. 3, 137-154.*
- Bremmer, H. (May 1959), On the theory of the fading properties of a fluctuating signal imposed on a constant signal, *NBS Circular 599.*
- Bugnolo, D. S. (July 1958), Multiple scattering of electromagnetic radiation and the transport equation of diffusion, *IRE Trans. Ant. Prop. AP-6, No. 3, 310.*
- Bullington, K. (Jan. 1950), Radio propagation variations at VHF and UHF, *Proc. IRE 38, No. 1, 27-32.*
- Bullington, K. (Oct. 1955), Characteristics of beyond-the-horizon radio transmission, *Proc. IRE 43, No. 10, 1175-1180.*
- Bussey, H. E. (July 1950), Microwave attenuation statistics estimated from rainfall and water vapor statistics, *Proc. IRE 38, No. 7, 781-785.*
- CCIR (1955), *Atlas of ground wave propagation curves for frequencies between 30 Mc/s and 300 Mc/s, ITU, Geneva.*

CCP 702-1

- CCIR (1959), Atlas of ground wave propagation curves for frequencies between 30 and 10,000 Mc/s (Vertical polarization only; prepared by the Radio Research Laboratories, Ministry of Postal Services, Tokyo, Japan, January 1958), ITU, Geneva.
- CCIR (1963a), The concept of transmission loss in studies of radio systems, Documents of the Xth Plenary Assembly, ITU, Geneva, Vol. III, Recommendation 341, 29-31.
- CCIR (1963b), Transmission loss in studies of radio systems, Documents of the Xth Plenary Assembly, ITU, Geneva, Vol. III, Report 112, 84-89.
- CCIR (1963c), Optimum use of the radio spectrum, Documents of the Xth Plenary Assembly, ITU, Geneva, Vol. III, Resolution 1, 111.
- CCIR (1963d), Line frequencies or bands of interest to radioastronomy and related sciences, in the 30 - 300 Gc/s range arising from natural phenomena, Documents of the Xth Plenary Assembly, ITU, Geneva, Vol. IV, Report 223, 304-307.
- CCIR (1963e), Reference atmospheres, Documents of the Xth Plenary Assembly, ITU, Geneva, Vol. II, Report, 231, 74-75.
- CCIR (1963f), Estimation of tropospheric-wave transmission loss, Documents of the Xth Plenary Assembly, ITU, Geneva, Vol. II, Report 244, 191-213.
- CCIR (1963g), Propagation curves for VHF/UHF broadcasting in the African Continent, Documents of the Xth Plenary Assembly, ITU, Geneva, Vol. III, Report 240, 143-181.
- CCIR (1963h), VHF and UHF propagation curves for the frequency range from 40 Mc/s to 1000 Mc/s - Broadcasting and mobile services, Documents of the Xth Plenary Assembly, ITU, Geneva, Vol. III, Recommendation 370, 24-36.
- CCIR (1963i), Communication satellite systems-frequency sharing between communication satellites systems and terrestrial services, Documents of the Xth Plenary Assembly, ITU, Geneva, Vol. IV, Report 209, 221-232.
- CCIR (1963j), Influence of the atmosphere on wave propagation, Documents of the Xth Plenary Assembly, ITU, Geneva, Vol. II, Report 233, 76-120.
- CCIR (1963k), Propagation data required for radio relay systems, Documents of the Xth Plenary Assembly, ITU, Geneva, Vol. II, Report 242, 182-187.
- CCIR (1963l), Fading of signals propagated by the ionosphere, Documents of the Xth Plenary Assembly, ITU, Geneva, Vol. II, Report 266, 327-334.
- CCIR (1963m), Terms and definitions, Documents of the Xth Plenary Assembly, ITU, Geneva, Vol. I, Report 321, 239.
- CCIR (1964), Optimum use of the radio frequency spectrum, Document being prepared for the XIth Plenary Assembly, in accordance with Resolution 1 of the Xth Plenary Assembly, ITU, Geneva, Vol. III, 111.
- Chernov, L. A. (Jan. - June 1955), Correlation of amplitude and phase fluctuations for wave propagation in a medium with random irregularities, Akust. Zh. 1, 89; translation in Soviet Phys. - Acoust. 1, No. 1-2, 94-101.

- Grosskopf, J. (June 1956), On the existing condition of research in the realm of tropospherically scattered radiation, *Nachrtech. Z.* 9, No. 6, 272-279.
- Grosskopf, J. (Nov. 1958), Some remarks on the analysis of fading in the meter and decimeter range, *Nachrtech. Z.* 11, No. 11, 577-586.
- Gunn, K. L. S., and T. W. R. East (Oct. 1954), The microwave properties of precipitation particles, *Quart. J. Roy. Meteorol. Soc. (London)* 80, 522-545.
- Harper, A. E. (1941), Rhombic antenna design, (D. van Nostrand Co., Princeton, N. J.).
- Hartman, W. J. (May 1963), Path antenna gain and comments on "Properties of 400 Mcps long-distance tropospheric circuits," *Proc. IEEE* 51, No. 5, 847-848.
- Hartman, W. J., and R. E. Wilkerson (Nov. - Dec. 1959), Path antenna gain in an exponential atmosphere, *J. Res. NBS* 63D (Radio Prop.), No. 3, 273-286.
- Hathaway, S. D., and H. W. Evans (Jan. 1959), Radio attenuation at 11 kMc and some implications affecting relay system engineering, *Bell Syst. Tech. J.* 38, No. 1, 73-97.
- Haurwitz, B. and J. M. Austin [1944], *Climatology*, McGraw-Hill Co. Inc., New York.
- Hay, H. G., and R. S. Unwin (Dec. 1952), Tropospheric wave propagation in a duct of non-uniform height, *Phys. Soc. London Proc.* 65, No. 396b, 981-989.
- Head, H. T. (June 1960), The influence of trees on television field strengths at ultra-high frequencies, *Proc. IRE* 48, No. 6, 1016-1020.
- Heisenberg, W. (Dec. 1948), On the theory of statistical and isotropic turbulence, *Proc. Roy. Soc. London* A195, 402-406.
- Herbstreit, J. W., and P. L. Rice (Sept. 1959), Survey of Central Radio Propagation Laboratory research in tropospheric propagation, 1948-1956, NBS Tech. Note No. 26.
- Hirai, Masaichi (May 1961a), Multipath properties of tropospheric propagation of very short radio waves beyond the horizon, *Jour. Radio Res. Lab., Japan* 8, No. 37, 147-174.
- Hirai, Masaichi (Sept. 1961b), Diversity effects in spaced-antenna reception of tropospheric scatter waves, *Jour. Radio Res. Lab., Japan* 8, 301-329.
- Hitchcock, R. J., and P. A. C. Morris (July 1961), The HF band: Is a new look required? *Wireless World*, 375-378.
- Hogg, D. C., and W. W. Mumford (March 1960), The effective noise temperature of the sky, *Microwave J.* 3, 80-84.
- Hogg, D. C., and R. A. Semplak (Sept. 1961), The effect of rain and water vapor on sky noise at centimeter wavelengths, *Bell Syst. Tech. J.* 40, No. 5, 1331-1348.
- Ikegami, F. (July 1959), Influence of an atmospheric duct on microwave fading, *IRE Trans. Ant. Prop.* AP7, No. 3, 252-257.
- Ikegami, F. (May-June 1964), Radiometeorological effects in propagation over the sea and islands, *Rev. Elect. Commun. Lab., Tokyo*, Vol. 12, No. 5-6, 312-324.

- duCastel, F. (May 1957a), Different types of fluctuations of tropospheric fields and their physical interpretation, *L'Onde Electrique* 37, No. 362, 501-506.
- duCastel, F. (Nov. 1957b), The use of ultra short waves for long distance telephone links in Africa (Results of Tests in the Cameroons), *L'Onde Electrique* 37, No. 368, 1025-1035.
- duCastel, F. (Nov.-Dec. 1960), Experimental results from transhorizon tropospheric propagation, *Ann des T&Ccomm.* 15, No. 11-12, 255-259.
- duCastel, F., and P. Misme (Nov. 1957), Elements of radio-climatology, *L'Onde Electrique* 37, No. 368, 1015-1052.
- duCastel, F., P. Misme, and J. Voge (March 1958), Reflection of an electromagnetic wave from an atmospheric layer with variable index of refraction, *C. R. Acad., Sci. Fr.* 246, No. 12, 1838-1840.
- duCastel, F., P. Misme, A. Spizzichino, and J. Voge (1962), On the role of the process of reflection in radio wave propagation, *J. Res. NBS* 66D, (Radio Science), No. 3, 273-284.
- Dutton, E. J. (June 1961), On the climatology of ground-based radio ducts and associated fading regions, *NBS Tech. Note* 96.
- Dutton, E. J., and G. D. Thayer (Oct. 1961), Techniques for computing refraction of radio waves in the troposphere, *NBS Tech. Note* 97.
- Fengler, G. (1964), Untersuchungen der elektromagnetischen Wellenausbreitung im 500 MHz-Bereich über Land unter besonderer Berücksichtigung der Meteorologie, *Berichte des Instituts für Radiometeorologie und Maritime Meteorologie an der Universität Hamburg*, Report No. 8.
- Fengler, G., J. Jeske, and G. Stilke, Radiometeorological papers II, *Berichte des Instituts für Radiometeorologie und Maritime Meteorologie an der Universität Hamburg*, Report No. 9.
- Florman, E. F., and J. J. Tary (Jan. 1962), Required signal-to-noise ratios, RF signal power, and bandwidth for multichannel radio communications systems, *NBS Tech. Note* 100.
- Fok, V. A., L. A. Vainshtein, and M. G. Belkira (1958), Radiowave propagation in surface tropospheric ducts, *Radio Eng. Electron. USSR*, 3, No. 12, 1-27.
- Friend, A. W. (June 1945), A summary and interpretation of ultra high frequency wave propagation data collected by the late Ross A. Hull, *Proc. IRE* 33, 358.
- Friis, H. T., A. B. Crawford, and D. C. Hogg (May 1957), A reflection theory for propagation beyond the horizon, *Bell Syst. Tech. J.* 36, No. 3, 627-644.
- Furutsu, K. (1956), On the multiple diffraction of electromagnetic waves by spherical mountains, *J. Radio Res. Labs., Tokyo* 3, 331.
- Furutsu, K. (1959), Wave propagation over an irregular terrain, I, II, III, *J. Radio Res. Labs., Tokyo* 4, 135, 349 (1957), and 6, 71 (1959).
- Furutsu, K. (Jan. - Feb. 1963), On the theory of radio wave propagation over inhomogeneous earth, *J. Res. NBS* 67D (Radio Prop.), No. 1, 39-62.

- Grosskopf, J. (June 1956), On the existing condition of research in the realm of tropospherically scattered radiation, *Nachrtech. Z.* 9, No. 6, 272-279.
- Grosskopf, J. (Nov. 1958), Some remarks on the analysis of fading in the meter and decimeter range, *Nachrtech. Z.* 11, No. 11, 577-586.
- Gunn, K. L. S., and T. W. R. East (Oct. 1954), The microwave properties of precipitation particles, *Quart. J. Roy. Meteorol. Soc. (London)* 80, 522-545.
- Harper, A. E. (1941), Rhombic antenna design, (D. van Nostrand Co., Princeton, N. J.).
- Hartman, W. J. (May 1963), Path antenna gain and comments on "Properties of 400 Mcps long-distance tropospheric circuits," *Proc. IEEE* 51, No. 5, 847-848.
- Hartman, W. J., and R. E. Wilkerson (Nov. - Dec. 1959), Path antenna gain in an exponential atmosphere, *J. Res. NBS* 63D (Radio Prop.), No. 3, 273-286.
- Hathaway, S. D., and H. W. Evans (Jan. 1959), Radio attenuation at 11 kMc and some implications affecting relay system engineering, *Bell Syst. Tech. J.* 38, No. 1, 73-97.
- Haurwitz, B. and J. M. Austin [1944], *Climatology*, McGraw-Hill Co. Inc., New York.
- Hay, H. G., and R. S. Unwin (Dec. 1952), Tropospheric wave propagation in a duct of non-uniform height, *Phys. Soc. London Proc.* 65, No. 396b, 981-989.
- Head, H. T. (June 1960), The influence of trees on television field strengths at ultra-high frequencies, *Proc. IRE* 48, No. 6, 1016-1020.
- Heisenberg, W. (Dec. 1948), On the theory of statistical and isotropic turbulence, *Proc. Roy. Soc. London* A195, 402-406.
- Herbstreit, J. W., and P. L. Rice (Sept. 1959), Survey of Central Radio Propagation Laboratory research in tropospheric propagation, 1948-1956, NBS Tech. Note No. 26.
- Hirai, Masaichi (May 1961a), Multipath properties of tropospheric propagation of very short radio waves beyond the horizon, *Jour. Radio Res. Lab., Japan* 8, No. 37, 147-174.
- Hirai, Masaichi (Sept. 1961b), Diversity effects in spaced-antenna reception of tropospheric scatter waves, *Jour. Radio Res. Lab., Japan* 8, 301-329.
- Hitchcock, R. J., and P. A. C. Morris (July 1961), The HF band: Is a new look required? *Wireless World*, 375, 378.
- Hogg, D. C., and W. W. Mumford (March 1960), The effective noise temperature of the sky, *Microwave J.* 3, 80-84.
- Hogg, D. C., and R. A. Semplak (Sept. 1961), The effect of rain and water vapor on sky noise at centimeter wavelengths, *Bell Syst. Tech. J.* 40, No. 5, 1331-1348.
- Ikegami, F. (July 1959), Influence of an atmospheric duct on microwave fading, *IRE Trans. Ant. Prop.* AP 7, No. 3, 252-257.
- Ikegami, F. (May-June 1964), Radiometeorological effects in propagation over the sea and islands, *Rev. Elect. Commun. Lab., Tokyo*, Vol. 12, No. 5-6, 312-324.

CCP 702-1

- International Telephone and Telegraph Corporation (1956), Reference data for radio engineers, Fourth Edition, (ITT, New York).
- Janes, H. B., and P. I. Wells (Oct. 1955), Some tropospheric scatter propagation measurements near the radio horizon, Proc. IRE 43, No. 10, 1336-1340.
- Jasik, H. (1961), Antenna Engineering Handbook, (McGraw Hill).
- Johnson, M. A. (1958), A review of tropospheric scatter propagation theory and its application to experiment, Proc. IEE 105B, Suppl. 8, 165-176.
- Josephson, B., and A. Blomquist (April 1958), The influence of moisture in the ground, temperature and terrain on ground wave propagation in the VHF band, IRE Trans. Ant. Prop. AP-6, No. 2, 169-172.
- Josephson, B., and G. Carlson (April 1958), Distance dependence, fading characteristics and pulse distortion of 3000 Mc trans-horizon signals, IRE Trans. Ant. Prop. AP-6, No. 2, 173-175.
- Josephson, B., and F. Eklund (April 1958), Some microwave propagation experiences from a just-below-horizon path, IRE Trans. Ant. Prop. AP-6, No. 2, 176-178.
- Jowett, J. K. S. (Jan. 1958), The measurement and prediction of VHF tropospheric field strengths at distances beyond the horizon, Proc. IEE 105B, Supp. 8, 91-96, and 122-126, Paper No. 2500R.
- Joy, W. R. R. (Jan. 1958a), The long-range propagation of radio waves at 10 cm wavelength, Proc. IEE 105B, Supp. 8, 153-157, Paper No. 2522R.
- Joy, W. R. R. (1958b), Radio propagation far beyond the horizon at about 3.2 cm wavelength, Proc. IEE 105B, Supp. 8, 158-164 and 184-188, Paper No. 2528R.
- Kales, M. L. (May 1951), Elliptically polarized waves and antenna, Proc. IRE 39, No. 5, 544-549.
- Kalinin, A. I. (1957), Approximate methods of computing the field strength of ultra short waves with consideration of terrain relief, Radio Eng. 12, No. 4, 13-26, Radiotekhn. i Elektron. 12, No. 4, 13-23.
- Kalinin, Iu. K (1958), Perturbation of plane radio wave by inhomogeneities of the earth's surface, Radiotekhn. and Elektron. 3, 557-561, Translation in Radio Engineering and Electronics 3, No. 4, 143-149.
- Kerr, D. E. (1951), Propagation of short radio waves, MIT Radiation Laboratory Series 13, (Boston Technical Publishers, Inc., Lexington, Mass.).
- Kirby, R. S., H. T. Dougherty, and P. L. McQuate (Oct. 1955), Obstacle gain measurements over Pike's Peak at 60 to 1046 Mc/s, Proc. IRE 43, No. 10, 1467-1472.
- Kirby, R. S., P. L. Rice, and L. J. Maloney (Oct. 1961), Characteristics of point-to-point tropospheric propagation and siting considerations, NBS Tech. Note No. 95.

- Kitchen, F. A., and I. J. Richmond (March 1957), Some characteristics of long distance scatter transmissions (two parts), *British Comm. and Electr.* 4, No. 2, 74-78 (Feb. 1957); 4, No. 3, 146-148, (March 1957).
- Kitchen, F. A., E. G. Richards, and I. J. Richmond (Jan. 1958), Some investigations of metre-wave radio propagation in the transhorizon region, *Proc. IEE* 105B, Supp. 8, 106-116, Paper No. 2509R.
- Kitchen, F. A., W. R. R. Joy, and E. G. Richards (Aug. 1958), Influence of the semi-permanent low-level ocean duct on centimetre wave scatter propagation beyond the horizon, *Nature* 182, No. 4632, 385-386.
- Kolmogoroff, A. N. (1941), Dissipation of energy in locally isotropic turbulence, *Comptes Rendus (Doklady) de l'Académie des Sciences de l'USSR* 32, No. 1, 16-18.
- Krasil'nikov, V. A. (1949), The effect of variations of the coefficient of refraction in the atmosphere upon the propagation of ultra-short waves, *Izvest. Akad. Nauk, S.S.S.R. Sev. Geografi Geofiz.* 13, No. 1, 33-57 (in Russian).
- Kühn, V. (Feb. and May 1958), Propagation investigation of the effect of various types of terrain in frequency bands I, II, and III, *Tech. Comm. Lab. for Commercial Radio and Telev.*, BRF, DDR.
- Lane, J. A., and J. A. Saxton (July 1952), Dielectric dispersion in pure polar liquids at very high radio frequencies, *Proc. Roy. Soc.* A213, 400-408.
- Laws, J. O., and D. A. Parsons (Apr. 1943), The relation of raindrop-size to intensity, *Trans. Amer. Geophys. Union* 24, 452-460.
- Lewin, L. (July 1962), Diversity reception and automatic phase correction, *Proc. IEE* 109, Part B, No. 46, 295-304.
- McGavin, R. E. (May 1962), A survey of the techniques for measuring the radio refractive index, *NBS Tech. Note* 99.
- McGavin, R. E., and L. J. Maloney (Sept. - Oct. 1959), Study at 1046 Mc/s of the reflection coefficient of irregular terrain at grazing angles, *J. Res. NBS* 63D (Radio Prop.), No. 2, 235-248.
- McPetrie, J. S., and J. A. Saxton (Sept. 1942), Diffraction of ultra-short radio waves, *Nature* 150, 292.
- McPetrie, J. S., and L. H. Ford (1946), Some experiments on the propagation over land of radiation of 9.2 cm wavelength, especially on the effect of obstacles, *Proc. IEE* 93, Pt. 3-A, Nos. 1-4, 531-538.
- Megaw, E. C. S. (Dec. 1950), Scattering of electromagnetic waves by atmospheric turbulence, *Nature* 166, 1100-1104.
- Megaw, E. C. S. (April 1954), Interpretation of stellar scintillation, *Quart. J. Roy. Met. Soc.* 80, 248-251.
- Megaw, E. C. S. (Sept. 1957), Fundamental radio scatter propagation theory, *Proc. IEE*, Pt. C 104, No. 6, 441-455, see also Monograph 236R, May 1957.
- Merkulov, V. V. (1957), On the theory of propagation of electromagnetic waves in media with random inhomogeneities in the index of refraction, *Soviet Physics: Tech. Phys.* 2, 958-961, *J. Electro-Tech. Phys.* 27, No. 5, 1051.

- Millington, G. (May 1958), Tropospheric scatter propagation, *Electronic Eng.* 30, No. 363, 248-252.
- Millington, G., R. Hewitt, and F. S. Immirzi (Sept. 1962a), Double knife-edge diffraction in field strength predictions, *Proc. IEE* 109, Part C, No. 16, 419-429. See also IEE Monograph No. 507E (Mar. 1962).
- Millington, G., R. Hewitt, and F. S. Immirzi (Sept. 1962b), The Fresnel surface integral, *Proc. IEE* 109, Part C, 430-437. See also IEE Monograph No. 508E (Mar. 1962).
- Millington, G., and G. A. Isted (July 1950), Ground wave propagation over an inhomogeneous, smooth earth, Part 2: Experimental evidence and practical implications, *Proc. IEE*, Part III 97, No. 48, 209.
- Misme, P. (July 1958), The correlation between the electric field at a great distance and a new radiometeorological parameter, *Trans. IRE Trans. Ant. Prop.* AP-6, No. 3, 289-292.
- Misme, P. (March-April 1960a), The equivalent gradient direct measurements and theoretical calculations, *Ann. des Télécomm.* 15, Nos. 3-4, 92-99.
- Misme, P. (Aug. 1960b), Comments on 'Models of the atmospheric radio refractive index,' *Proc. IRE* 48, No. 8, 1498-1501.
- Misme, P. (Nov.-Dec. 1960c), Some aspects of radiometeorology and radioclimatology, *Ann. des Télécomm.* 15, No. 11-12, 266-273.
- Misme, P. (May-June 1961), The influence of the equivalent gradient and atmospheric stability on transhorizon paths in the Sahara and the Congo, *Ann. des Télécomm.* 16, Nos. 5-6, 110-116.
- Moler, W. F., and D. B. Holden (Jan. - Feb. 1960), Tropospheric scatter propagation and atmospheric circulations, *J. Res. NBS* 64D (Radio Prop.), No. 1, 82-94.
- Nakagami, M. (Oct. 1940), Study on the resultant amplitude of many vibrations whose phases and amplitudes are random, *Nippon Elec. Comm. Eng.* 22, 69-92.
- National Bureau of Standards (1954), *Applied Mathematics Series* 32, Table of the sine and cosine integrals for arguments from 10 - 100.
- National Bureau of Standards (June 1964), *Applied Mathematics Series* 55, Handbook of Mathematical Functions.
- Neugebauer, H. E. J., and M. P. Bachynski (July-Aug. 1960), Diffraction by smooth conical obstacles, *J. Res. NBS* 64D (Radio Prop.), No. 4, 317-329.
- Newton, R. G., and T. F. Rogers (Nov. 1953), Dependence of total microwave atmospheric absorption on propagation path elevation, Air Force Cambridge Report AFCRC Tech. 53-54A.
- Nomura, Y. A., and K. Takaku (Aug. 1955), On the propagation of electromagnetic waves in an inhomogeneous atmosphere, *J. Phys. Soc. Japan* 10, No. 8, 700-714.

- Norton, K. A. (Dec. 1941), The calculation of ground-wave field intensity over a finitely conducting spherical earth. Proc. IRE 29, No. 12, 623-639.
- Norton, K. A. (1950), Addendum to Reference E to the report of Ad Hoc Committee of the F.C.C. for the Evaluation of the Radio Propagation Factors Concerning the TV and FM Broadcasting Services in the Frequency Range Between 50 and 250 Mc/s. (See Norton and Fine reference below.)
- Norton, K. A. (Jan. 1953), Transmission loss in radio propagation, Proc. IRE 41, No. 1, 146-152.
- Norton, K. A. (July-Aug. 1959), System loss in radio wave propagation, J. Res. NBS 63D (Radio Prop.), No. 1, 53-73.
- Norton, K. A. (July 1960), Carrier frequency dependence of the basic transmission loss in tropospheric forward scatter propagation, J. Geophys. Res. 65, No. 7, 2029-2045.
- Norton, K. A. (1962), Efficient use of the radio spectrum, NBS Tech. Note 158.
- Norton, K. A., and E. C. Barrows (1964), Observed vertical wavenumber spectra of refractivity near the ground, to be published.
- Norton, K. A., and H. Fine (Aug. 1, 1949), A study of methods for the efficient allocation of radio frequencies to broadcasting services operating in the range above 50 Mc, Reference E to the Report of Ad Hoc Committee of the F.C.C. for the Evaluation of the Radio Propagation Factors Concerning the TV and FM Broadcasting Services in the Frequency Range Between 50 and 250 Mc/s.
- Norton, K. A., and A. C. Omberg (Jan. 1947), The maximum range of a radar set, Proc. IRE 35, No. 1, 4-24.
- Norton, K. A., P. L. Rice, H. B. James, and A. P. Barsis (Oct. 1955), The rate of fading in propagation through a turbulent atmosphere, Proc. IRE 43, No. 10, 1341-1353.
- Norton, K. A., P. L. Rice, and L. E. Vogler (Oct. 1955), The use of angular distance in estimating transmission loss and fading range for propagation through a turbulent atmosphere over irregular terrain, Proc. IRE 43, No. 10, 1488-1526.
- Norton, K. A., H. Staras, and M. Blum (Feb. 1952), A statistical approach to the problem of multiple radio interference to FM and television service, IRE Trans. Ant. Prop. AP-1, 43-49.
- Norton, K. A., L. E. Vogler, W. V. Mansfield, and P. J. Short (Oct. 1955), The probability distribution of the amplitude of a constant vector plus a Rayleigh-distributed vector, Proc. IRE 43, No. 10, 1354-1361.
- Obukhov, A. M. (1941), On the distribution of energy in the spectrum of turbulent flow, Bull. Acad. Sci. USSR Geol. and Geophys. Ser. 4-5, 453. See also Comptes Rendus (Doklady) L'Academie des Sciences de l'USSR 32, No. 1, 19 (1941).
- Obukhov, A. M. (1953), On the effect of inhomogeneities of the atmosphere on sound and light propagation, Bull. Acad. Sci. USSR, Geol. and Geophys. Ser. 2, 155.

- Onoe, M., M. Hirai, and S. Niwa (April 1958), Results of experiments of long distance over-land propagation of ultra-short waves, *J. Radio Res. Lab. (Tokyo)* 5, No. 20, 79-94.
- Onoe, M., and K. Nishikori (Oct. 1957), Microwave propagation over the sea beyond the line of sight, *Radio Res. Lab. J.* 4, No. 18, 395-406.
- Pearcey, T. (1956), *Table of the Fresnel integral*, (Cambridge Univ. Press, New York, N. Y.).
- Pekeris, C. L. (Feb. 1947), Note on scattering of radiation in an inhomogeneous medium, *Phys. Rev.* 71, No. 3, 268-269.
- Perlat, A., and J. Voge (Dec. 1953), Attenuation of centimeter and millimeter waves by the atmosphere, *Ann. des Télécomm.* 8, No. 12, 395-407.
- Price, W. L. (July 1948), Radio shadow effects produced in the atmosphere by inversions, *Proc. Phys. Soc. London* 61, No. 343, 59-78.
- Randall, D. L. (1964), A summary of tropospheric radio duct meteorology at V.H.F. and UHF as observed on a trip around the world, *World Conference on Radio Meteorology* Boulder, Colorado, September 14-18.
- Rayleigh, Lord (Aug. 1880), On the resultant of a large number of vibrations of the same pitch and of arbitrary phase, *Phil. Mag.* 10, 73-78.
- Riblet, H. J., and C. B. Barker (1948), A general divergence formula, *J. Appl. Phys.* 19, 63.
- Rice, P. L., and F. T. Daniel (Apr. 1955), Radio transmission loss vs. distance and antenna height at 100 Mc, *Trans. IRE Ant. Prop.* AP-3, No. 2, 59-62.
- Rice, P. L., and J. W. Herbstreit (1964), Tropospheric propagation, (to be published in Vol. 20 of *Advances in Electronics*, Academic Press).
- Rice, S. O. (Jan. 1945), Mathematical analysis of random noise, *Bell. System Tech. J.* 24, 46-156.
- Rice, S. O. (1954), Diffraction of plane radio waves by a parabolic cylinder, *Bell System Tech. J.* 33, 417-504.
- Rider, G. C. (1953), Some VHF experiments upon the diffraction effect of hills, *The Marconi Rev.* 16, No. 109, 96-106, 2nd quarter.
- Rowden, R. A., L. F. Tagholm, and J. W. Stark (1958), A survey of tropospheric wave propagation measurements by the BBC, 1946-1957, *Proc. IEE* 105B, Suppl. 8, 84-90 and 122-126, Paper No. 2517R.
- Ryde, J. W. (1946), The attenuation and radar echoes produced at centimetre wavelengths by various meteorological phenomena, *Conference on meteorological factors in radio-wave propagation*, *Phys. Soc. (London)* and *Royal Meteorological Society*, 169-188.
- Ryde, J. W. and D. Ryde (1945), Attenuation of centimeter waves by rain, hail, fog, and clouds, *General Electric Co., Wembley, England.*

- Saxton, J. A. (Sept. 1951), The propagation of metre radio waves beyond the normal horizon, Part 1, Proc. IEE 98, Part III, No. 55, 360-369.
- Saxton, J. A., and J. A. Lane (May 1955), VHF and UHF reception-effects of trees and other obstacles, Wireless World 61, 229-232.
- Saxton, J. A., J. A. Lane, R. W. Meadows, and P. A. Matthews (Feb. 1964), Layer structure of the troposphere, Proc. IEE 111, No. 2, 275-283.
- Schelkunoff, S. A. and H. T. Friis (1952), Antennas, theory and practice, Wiley and Sons, New York City.
- Schelleng, J. C., C. R. Burrows, and E. B. Ferrell (Mar. 1933), Ultra-short wave propagation, Proc. IRE 21, No. 3, 427-463.
- Schünemann, R. (Sept. 1957), Mechanism of ultra short wave propagation over great distances; Hochfreq. u. Elektroak. 66, No. 2, 52-61.
- Sherwood, E. M., and W. L. Ginzton (July 1955), Reflection coefficients of irregular terrain at 10 cm., Proc. IRE 43, No. 7, 877-878.
- Shkarofsky, I. P. (Mar. 1958), Tropospheric scatter propagation, Res. Rpt. No. 7-200-1, RCA Victor Co., Ltd. Res. Labs., Montreal, Canada.
- Siddiqui, M. M. (March-April 1962), Some problems connected with Rayleigh distributions, J. Res. NBS 66D (Radio Propagation), No. 2, pp. 167-174.
- Silverman, R. A. (Apr. 1957), Fading of radio waves scattered by dielectric turbulence, J. Appl. Phys. 28, No. 4, 506-511. Also New York Univ. Inst. of Math. Sci., Electromagnetic Res. Division, Res. Rept. EM 101 (Jan. 1957).
- Staras, H. (Oct. 1952), Scattering of electromagnetic energy in a randomly inhomogeneous atmosphere, J. Appl. Phys. 23, No. 10, 1152-1156.
- Staras, H. (Oct. 1955), Forward scattering of radio waves by anisotropic turbulence, Proc. IRE 43, No. 10, 1374-1380.
- Staras, H. (April 1957), Antenna-to-medium coupling loss, IRE Trans. Ant. Prop. AP-5, No. 2, 228-231.
- Starkey, B. J., W. R. Turner, S. R. Badcoe, and G. F. Kitchen (Jan. 1958), The effects of atmospheric discontinuity layers up to and including the tropopause on beyond-the-horizon propagation phenomena, Proc. IEE 105B, Suppl. 8, 97-105 and 122-126, Paper No. 2486R.
- Stokes, G. G. (1922), Mathematical and physical papers, Vol. III, On the composition and resolution of streams of polarized light from different sources, (Cambridge University Press, London), 233-258.
- Straiton, A. W., and C. W. Tolbert (May 1960), Anomalies in the absorption of radio waves by atmospheric gases, Proc. IRE 48, No. 5, 898-903.
- Sutton, O. G. (1955), Atmospheric turbulence (John Wiley and Co.).
- Tao, K. (Jan. 1957), On the relationship between the scattering of radio waves and the statistical theory of turbulence, J. Radio Res. Lab. (Tokyo) 4, No. 15, 15-24.
- T.A.S.O. (March 1959), Engineering aspects of television allocations, Report of the television allocations study organization.

- Vogler, L. E., and J. L. Noble (Sept. - Oct. 1963), Curves of ground proximity loss for dipole antennas (a digest), J. Res. NBS 67D (Radio Prop.), No. 5, 567-568.
- Vvedenskii, B. A., and A. G. Arenberg (1957), Long distance tropospheric propagation of ultra-short waves, Radio Eng. 12, No. 1, 3-13; Radio Eng. 12, No. 2, 10-25.
- Vvedenskii, B. A., and A. V. Sokolov (1957), Investigation of tropospheric propagation of meter, decimeter, and centimeter radio waves in the USSR, Radio Eng. and Elect. (USSR) 2, No. 11, 84-105.
- Vysokovskii, D. M. (1957a), Calculation of multiple scattering in the diffusion propagation of ultra-short waves in the troposphere, Radio Eng. and Elect. (USSR) 2, No. 6, 183-187.
- Vysokovskii, D. M. (1957b), Geometrical characteristics of the scattering of radio waves by turbulent inhomogeneities in the troposphere, Telecommunications (USSR) 9, 11-20.
- Vysokovskii, D. M. (1958), Diffused propagation of ultra-short waves in the troposphere with high-directivity antennas, Telecommunications (USSR) 5, 488-497.
- Wait, J. R. (1958), On the theory of propagation of electromagnetic waves along a curved surface, Can. J. Phys. 36, No. 1, 9-17.
- Wait, J. R. (1959), Electromagnetic radiation from cylindrical structures (Pergamon Press, New York, N. Y.).
- Wait, J. R. (April 1959), Transmission of Power in Radio Propagation, Electronic and Radio Engineer, Vol. 36, Series No. 4, pp. 146-150.
- Wait, J. R. (1962), Electromagnetic waves in stratified media, International Series of Monographs on Electromagnetic Waves 3, (Pergamon Press, New York, N. Y.).
- Wait, J. R. (Nov. 1963), Oblique propagation of ground waves across a coastline, part I, J. Res. NBS 67D (Radio Prop.), No. 6, 617-624.
- Wait, J. R., and A. M. Conda (Sept. - Oct. 1959), Diffraction of electromagnetic waves by smooth obstacles for grazing angles, J. Res. NBS 63D (Radio Prop.), No. 2, 181-197.
- Wait, J. R., and C. M. Jackson (Nov. 1963), Oblique propagation of ground waves across a coastline, part II, J. Res. NBS 67D (Radio Prop.), No. 6, 625-630.
- Wheelon, A. D. (June 1957), Relation of radio measurements to the spectrum of tropospheric dielectric fluctuations, J. Appl. Phys. 28, 684-693.
- Wheelon, A. D. (Sept. - Oct. 1959), Radio-wave scattering by tropospheric irregularities, J. Res. NBS 63D (Radio Prop.), No. 2, 205-234; also, J. Atmos. and Terr. Phys. 15, Nos 3, 4, 185-205 (Oct. 1959).
- Wilkerson, R. (1964), Multiple knife-edge diffraction, (private communication).
- Williamson, D. A., V. L. Fuller, A. G. Longley, and P. L. Rice (Mar. 1960), A summary of VHF and UHF tropospheric transmission loss data and their long-term variability, NBS Tech. Note 43.

12. LIST OF SYMBOLS AND ABBREVIATIONS

In the following list the English alphabet precedes the Greek alphabet, and lower-case letters precede upper-case letters. As a general rule, upper-case letters have been used for quantities expressed in decibels, for example w_t is transmitter power in watts, and W_t is transmitter power in decibels above one watt. When the upper-case symbol is the decibel equivalent of a lower-case symbol they are usually listed together. Symbols that are used only in an annex are defined at the end of the appropriate annex, in Volume 2.

Sometimes a symbol may be used in quite different contexts, in which case it is listed for each separate context. Subscripts are used to modify the meaning of symbols. The order is:

- | | |
|---|----------------|
| 1. Symbol without a subscript | h |
| 2. Symbol with a subscript, (letter subscripts in alphabetical order followed by number subscripts in numerical order). | h_r
h_1 |
| 3. Symbol as a special function. | $h(x)$ |
| 4. Abbreviations. | ht |

Following each definition an equation number or section number is given to show the term in its proper context. Where applicable, reference is made to a figure.

Throughout the report, logarithms are to the base 10 unless otherwise noted.

- a Effective earth's radius, allowing for average radio ray bending near the surface of the earth, (4.4) figure 4.2.
- a_e An equivalent earth's radius which is the harmonic mean of the radii a_t and a_r , (7.10).
- a_r The radius of a circular arc that is tangent to the receiving antenna horizon ray at the horizon, and that merges smoothly with the corresponding arc through the transmitting antenna horizon, (8.9) figure 8.7.
- a_s Effective earth's radius factor corresponding to D_s , (8.15).
- a_t Radius of a circular arc that is tangent to the transmitting horizon ray at the horizon, and that merges smoothly with the corresponding arc through the receiving antenna horizon, (8.9) figure 8.7.
- a_x The axial ratio of the polarization ellipse of a plane wave, (2.11).
- a_{xr} The axial ratio of the polarization ellipse associated with the receiving pattern (2.11).
- a_o The actual earth's radius, usually taken to be 6370 kilometers, (4.4).
- a_1 Radius of the circular arc that is tangent to the transmitting antenna horizon ray at the horizon, and that passes through a point h_{te} kilometers below the transmitting antenna, (8.8) figure 8.7.
- a_2 Radius of the circular arc that is tangent to the receiving antenna horizon ray at the horizon, and that passes through a point h_{re} kilometers below the receiving antenna, (8.8) figure 8.7.

- A** Attenuation relative to free space, expressed in decibels, defined as the basic transmission loss relative to that in free space, (2.20).
- A_a** The long-term median attenuation of radio waves due to atmospheric absorption by oxygen and water vapor, section 3.
- A_{ar}, A_{at}** For transhorizon paths, $A_a = A_{at} + A_{ar}$, the sum of the absorption from the transmitter to the crossover of horizon rays and the absorption from the crossover of horizon rays to the receiver, section 3.
- A_c** Total absorption attenuation within a cloud, (3.13).
- A_r** Total absorption due to rainfall over a given path, (3.7).
- A_w** Rate of attenuation through woods in full leaf, (5.18).
- A₀** Diffraction attenuation relative to free space at an angular distance $\theta = 0$ over a smooth earth, section 9.2.
- A(v, 0)** Attenuation relative to free space as a function of the parameter v , (7.2) figure 7.1.
- A(v, ρ)** Diffraction attenuation relative to free space for an isolated perfectly conducting rounded obstacle, (7.7), figure 7.3.
- A(0, ρ)** The diffraction loss for $\theta = 0$ over an obstacle of radius r , (7.7) figure 7.4.
- B_a** The parameter $B(K, b)$ corresponding to the effective earth's radius a_e , (8.15).
- B_{1, 2, t, r}** Values of the parameter $B(K, b)$ that correspond to values of $K_{1, 2, t, r}$, (8.13).
- B₀₁, B₀₂**, Defined by (8.2), (8.13) and (8.15) as the product of several factors, combined for convenience in computing diffraction attenuation.
- B_{ot}, B_{or}**
- B'** Any point along the great circle path between antenna terminals A and B, figure 6.3.
- B(K, b^{*})** A parameter plotted in figure 8.3 as a function of K and b^* , (8.2).
- c** Free space velocity of radio waves, $c = 299792.5 \pm 0.3$ km/sec.
- C₁(K₁, b^{*})** A parameter used in calculating diffraction attenuation, (8.1) figure 8.4.
- C₁(K₁, b^{*}), C₁(K₂, b^{*})** The parameter $C_1(K, b^*)$ corresponding to K_1 and K_2 , also written $C_1(K_1)$ and $C_1(K_2)$, (8.11).
- $\bar{C}_1(K_{1, 2})$** The weighted average of values of $C_1(K_1, b^*)$ and $C_1(K_2, b^*)$, (8.11).
- CCIR** International Radio Consultative Committee.
- d** Great circle propagation path distance, measured at sea level along the great circle path determined by two antenna locations, A_1 and A_2 , figure 6.1.
- d_c** Clearing depth in meters, defined as the distance from the edge of woods to the lower antenna along a propagation path, (5.19).
- d_e** Effective propagation path distance, a function of d , f_{mc} , h_{te} , and h_{re} , section 10.1, (10.3).
- d_L** The sum of the horizon distances d_{Lr} and d_{Lt} . In section 10, d_L is defined for a smooth spherical earth of radius 9000 km, (10.2) and (10.3).
- d_{Lr}, d_{Lt}** Great circle distances from the receiving and from the transmitting antennas to the corresponding horizons, figure 6.1.

- d_{sr}, d_{st} Distance between the receiving or transmitting antenna horizon and the crossover of horizon rays as measured at sea level, (6.20).
- d_{sr}^i, d_{st}^i If θ_{or} or θ_{ot} is negative, d_{sr}^i or d_{st}^i is computed (6.23) and substituted for d_{sr} or d_{st} in reading figure 6.9.
- d_{s1} The theoretical distance where diffraction and scatter fields are approximately equal over a smooth earth, (10.1).
- d_o The greatest distance for which the attenuation relative to free space is zero, (5.10).
- d_1, d_2 Distance from the transmitting, or the receiving antenna, to the crossover of horizon rays, measured at sea level, figure 6.1.
- d_1, d_2 Great circle distance from one antenna of a pair to the point of reflection of a reflected ray, figure 5.1.
- dB Decibels = $10 \log_{10}$ (power ratio) or $20 \log_{10}$ (voltage ratio). In this report, all logarithms are to the base 10 unless otherwise stated.
- dBu Decibels above one microvolt per meter.
- dBW Decibels above one watt.
- D Divergence coefficient, a factor used to allow for the divergence of energy due to reflection from a convex surface, (5.2).
- D Diameter of a parabolic reflector in meters, (2.7).
- D_s Great circle distance between transmitting and receiving horizons, (6.17), figure 6.1.
- D_{str} A function of d_{st}, d_{sr} used in computing diffraction loss, (8.16), figure 8.8.
- e_c, e_p The positive to negative amplitude of the cross-polarized vector component \vec{e}_c and of the principal polarization component \vec{e}_p of a complex polarization vector \vec{e} , section 2.3 and annex II.
- \vec{e} A complex vector $\vec{e} = \vec{e}_p + i\vec{e}_c$, section 2.3 and annex II.
- f Radio wave frequency in megahertz (megacycles per second).
- $f(v)$ A function used in computing path antenna gain, defined by (9.13) figure 9.7.
- F_o The correction term F_o allows for the reduction of scattering efficiency at great heights in the atmosphere, (9.1) and (9.7).
- $F(x_1), F(x_2)$ Functions used in computing diffraction attenuation, (8.1) and figures 8.5 and 8.6.
- $F(\theta d)$ The attenuation function used in calculating median basic transmission loss for scatter paths, (9.1) figures 9.1, and III.11 to III.14.
- g_r, g_t, G_r, G_t Maximum free space directive gains for the receiving and transmitting antennas respectively, $G_r = 10 \log g_r$ db, $G_t = 10 \log g_t$ db, section 2.2.
- g_{r1}, g_{r2} Directive gain factors defined for each antenna in the direction of the point of ground reflection, (5.1).
- g_o The maximum value of the operating gain of a receiving system, (V.7).
- g_o The directive gain for one antenna in the direction of the other, section 5.1.
- g_{o1}, g_{o2} The directive gain of the transmitting and receiving antennas, each in the direction of the other, assuming matched antenna polarizations, (5.1).

CCP 702-1

- $g(p, f)$ A frequency factor used to adjust predicted long-term variability to allow for frequency-related effects, (10.6) figure 10.3.
- $g_t(\hat{r}), G_t(\hat{r})$ Free space directive gain of the transmitting antenna in the direction \hat{r} , see also $g'_t(\hat{r}), G'_t(\hat{r}) = 10 \log g_t(\hat{r})$ db, section 2.2.
- g'_t Power gain of a transmitting antenna when the power input to the antenna terminals is w'_t watts, section 2.2.
- $g'_t(\hat{r}), G'_t(\hat{r})$ Power gain of a transmitting antenna in the direction \hat{r} , $G'_t(\hat{r}) = 10 \log g'_t(\hat{r})$ db, section 2.2.
- G The maximum free space directive gain relative to an isotropic radiator (2.5).
- G_p Path antenna gain, the change in transmission loss or propagation loss if hypothetical loss-free isotropic antennas with no orientation, polarization, or multipath coupling loss were used at the same locations as the actual antennas, (2.14).
- G_{pf} Path antenna gain in free space, (2.17).
- G_{pp} Path antenna power gain, (2.14).
- $G(\bar{h})$ Residual height gain function, figure 7.1.
- $G'_r(\hat{r})$ Power gain, in decibels, of a receiving antenna, (2.4).
- $G(\bar{h}_1), G(\bar{h}_2)$ The function $G(\bar{h})$ for the transmitting and receiving antennas, respectively, (7.5).
- $G(\hat{r})$ Directive gain of an antenna in the direction \hat{r} . The maximum value of $G(\hat{r})$ is G , section 2.2.
- $G'_r(\hat{r})$ Directive gain, in decibels, of a receiving antenna in the direction \hat{r} , (2.4).
- $G(x_o)$ A function used in computing diffraction, (8.1) figures 8.5 and 8.6.
- GHz Radio frequency in gigacycles per second.
- h Height above the surface of the ground as used in (3.10), (3.12).
- h Height referred to sea level.
- h_i Equidistant heights of terrain above sea level, (5.15), (6.10).
- h_{Lr}, h_{Lt} Height of the receiver or transmitter horizon obstacle above sea level, (6.15).
- h_o Height of the intersection of horizon rays above a straight line between the antennas, determined using an effective earth's radius, a , (9.3b) and figure 6.1.
- h_r, h_t The height h_r or h_t is defined as the height of the receiving or transmitting antenna above the average height of the central 80% of the terrain between the antenna and its horizon, or above ground, whichever gives the larger value, (6.11).
- h_{re}, h_{te} Effective height of the receiving or transmitting antenna above ground. For h_r, h_t less than one kilometer $h_{re} = h_r, h_{te} = h_t$. For higher antennas a correction Δh is used, (6.12).
- h_{rs}, h_{ts} Height of the receiving antenna or transmitting antenna above sea level, figure 6.1, (6.11), (6.15).
- h_s Elevation of the surface of the ground above mean sea level, (4.3).
- h_{ti} The heights above sea level of evenly spaced terrain elevations between the transmitter and its horizon, (6.11).

- h_1 Height of the crossover of horizon rays above a straight line between the transmitter and receiver horizon obstacles, (9.7) figure 6.1.
- h_1, h_2 Heights of antenna terminals 1 and 2 above the surface of the earth, figure 5.1.
- h'_1, h'_2 Heights of antenna terminals 1 and 2 above a plane tangent to a smooth earth at the bounce point of a reflected ray, (5.8).
- \bar{h} Average height above sea level, (5.15).
- \bar{h}_t Average height of the transmitting antenna above the central 80% of terrain between the transmitter and its horizon, (6.11).
- \bar{h}_1, \bar{h}_2 Normalized heights of the transmitting and receiving antennas, (7.6).
- $h(x)$ A straight line fitted by least squares to equidistant heights above sea level, (5.15).
- $h(0), h(d)$ Height above sea level of a smooth curve fitted to terrain visible to both antennas, and extrapolated to the transmitter at $h(0)$, and the receiver at $h(d)$, (5.17).
- $h_i(x_i)$ A series of equidistant heights above sea level of terrain visible to both antennas, section 5.1.
- H_0 The frequency gain function, discussed in section 9.2.
- $H_0(\eta_s < 1), H_0(\eta_s = 1)$ Value of the frequency gain function, H_0 , where the parameter η_s is less than or equal to one, respectively, (9.6).
- $H_0(\eta_s = 0)$ The frequency gain function when $\eta_s = 0$ which corresponds to the assumption of a constant atmospheric refractive index, figure 9.5.
- Hz Abbreviation for hertz \equiv cycle per second.
- K A frequency-dependent coefficient, (3.8).
- K A parameter used in computing diffraction attenuation, K is a function of the effective earth's radius, carrier frequency, ground constants, and polarization, figure 8.1 and annex III.4.
- K_1 A frequency and temperature-dependent attenuation coefficient for absorption within a cloud, (3.13) and table 3.1.
- K_1, K_2, K_r, K_s, K_t Values of the diffraction parameter K for corresponding earth's radii a_1, a_2, a_r, a_s, a_t , (8.8) to (8.13).
- $K(a), K(8497)$ The diffraction parameter K for an effective earth's radius a , and for $a = 8497$ km.
- $K(f_{\text{GHz}})$ A frequency-dependent coefficient used in computing the rate of absorption by rain, (3.9a) and figure 3.8.
- l_{er}, L_{er} The effective loss factor for a receiving antenna, or the reciprocal of the power receiving efficiency, (2.3), $L_{er} = 10 \log l_{er}$ db.
- l_{et}, L_{et} The effective loss factor for a transmitting antenna, (2.3), $L_{et} = 10 \log l_{et}$ db.
- L Transmission loss expressed in decibels, (2.2).
- L_b Basic transmission loss, (2.13) and (2.14).
- L_{bd} Basic transmission loss for a diffraction path, (7.3), (7.4).
- L_{bf} Basic transmission loss in free space, (2.16).

CCP 702-1

- L_{bm} Hourly median basic transmission loss.
- L_{bsr} Reference value of long-term median basic transmission loss based on forward scatter loss, (9.1).
- L_c Calculated value of transmission loss.
- L_{cp} Polarization coupling loss, (2.10).
- L_{cr} Reference value of hourly median transmission loss when diffraction and scatter losses are combined, (9.14).
- L_{dr} Reference value of hourly median transmission loss due to diffraction, (9.14).
- L_f An "equivalent free-space transmission loss," (2.19).
- L_{gp} Loss in path antenna gain, defined as the difference between the sum of the maximum gains of the transmitting and receiving antennas and the path antenna gain, (2.21).
- L_{lr}, L_{lt} Transmission line and matching network losses at the receiver and transmitter.
- L_o Path loss, defined as transmission loss plus the sum of the maximum free space gains of the antennas, (2.12).
- L_s The system loss expressed in decibels, defined by (2.1). System loss includes ground and dielectric losses and antenna circuit losses.
- L_{sr} Reference value of median forward scatter transmission loss, used with L_{dr} to obtain the reference value L_{cr} , (9.14).
- $L(q), L(0.5)$ Long-term value of transmission loss not exceeded for a fraction q of hourly medians; $L(0.5)$ is the median value of $L(q)$, section 10.
- $L_b(q), L_b(0.5)$ Long-term value of basic transmission loss not exceeded for a fraction q of hourly medians; $L_b(0.5)$ is the median of $L_b(q)$.
- M Liquid water content of a cloud measured in grams per cubic meter, (3.13).
- MHz Radio frequency in megahertz.
- n Refractive index of the atmosphere, section 4.
- n The ratio α_o/δ_t or β_o/δ_r used to compute \hat{n} , (9.12).
- n_s Atmospheric refractive index at the surface of the earth, (4.1).
- \hat{n} A parameter used in calculating path antenna gain, (9.12).
- N Atmospheric refractivity defined as $N = (n-1) \times 10^6$, section 4.
- N_o Surface refractivity reduced to sea level, (4.3).
- N_s The value of N at the surface of the earth, (4.1).
- $\hat{p}(\vec{r}), \hat{p}_r(-\vec{r})$ Complex polarization vectors, section 2.3 and annex II.
- $|\hat{p} \cdot \hat{p}_r|^2$ Polarization efficiency for transfer of energy in free space at a single radio frequency, (2.11) and (II.62).
- q Time availability, the fraction of time a given value of transmission loss is not exceeded, section 10.
- q The ratio $q = r_2/sr_1$ used to compute ΔH_o , (9.5).
- r The length in free space of the direct ray path between antennas, figure 5.1.
- r Radius of curvature, (7.9).

- r_{eo} Effective distance for absorption by oxygen in the atmosphere, (3.4) figures 3.2 to 3.4.
 r_{er} Effective rain-bearing distance, (3.11) and (3.12) figures 3.10 to 3.13.
 r_{ew} Effective distance for absorption by water vapor in the atmosphere, (3.4), figures 3.2 to 3.4.
 r_o Length of a direct ray between antennas over an effective earth of radius a , figure 5.1.
 r_1, r_2 Parameters used in computing the frequency gain function H_o , and defined by (9.4).
 r_1, r_2 Distances whose sum is the path length of a reflected ray, figure 5.1.
 \hat{r}_1, \hat{r}_2 Direction of the most important propagation path from the transmitter to the receiver, or from the receiver to the transmitter.
 r_{11}, r_{21} Straight line distances from transmitting and receiving antennas to a point on the ground a distance x_1 from the transmitting antenna, figure 6.4.
 r. m. s. Abbreviation of root-mean-square.
 R The magnitude of the theoretical coefficient $R \exp[-i(\pi-c)]$ for reflection of a plane wave from a smooth plane surface of a given conductivity and dielectric constant, (5.1).
 R_e An "effective" ground reflection coefficient, (5.1).
 R_r Rainfall rate in millimeters per hour, (3.10).
 R_{rs} Surface rainfall rate, (3.10).
 \overline{R}_r Cumulative distribution of instantaneous path average rainfall rates, figure 3.14.
 $R(0.5)$ A function of $L_{dr} - L_{cr}$, (9.14) figure 9.9.
 s Path asymmetry factor, $s = \alpha_o / \beta_o$, (6.19).
 T_o Reference absolute temperature, $T_o = 288.37$ degrees Kelvin.
 $T(r)$ Temperature in the troposphere in degrees Kelvin.
 $T_s (^{\circ}K)$ Effective sky noise temperature in degrees Kelvin.
 T. A. S. O. Abbreviation of Television Allocations Study Organization.
 $U(vp)$ A parameter used in computing diffraction over a rounded obstacle, (III.26) and figure 7.5.
 v A parameter used in computing diffraction over an isolated obstacle, (7.1).
 $V(0.5, d_e)$ A parameter used with the calculated long-term reference value, L_{cr} , to predict median long-term transmission loss, figure 10.1 equations (10.4) and (III.67).
 $V_n(0.5, d_e)$ The parameter $V(0.5, d_e)$ for a given climatic region characterized by the subscript n , (10.4) figure 10.1.
 w_a, W_a Radio frequency signal power that would be available from an equivalent loss-free receiving antenna, $W_a = 10 \log w_a$ dbw, (2.2).
 w'_a, W'_a Radio frequency signal power available at the terminals of the receiving antenna, $W'_a = 10 \log w'_a$ dbw, (2.1).
 w_t, W_t Total power radiated from the transmitting antenna in a given band of radio frequencies, $W_t = 10 \log w_t$ dbw, (2.2).
 W_{ab} Available power at the terminals of a hypothetical loss-free isotropic receiving antenna, assuming no orientation, polarization, or multipath coupling loss between transmitting and receiving antennas, (2.13).

CCP 702-1

- x A specified value, the discussion preceding (2.14).
- x A variable designating distance from an antenna, figure 6.4
- x_1 The i^{th} distance from the transmitter along a great circle path, figure 6.4.
- x_0, x_1, x_2 Parameters used to compute diffraction loss, (8.2) figures 8.5 and 8.6.
- x_0, x_{20} Points chosen to exclude terrain adjacent to either antenna which is not visible to the other in computing a curve fit, (5.15).
- \bar{x} The average of distances x_0 and x_{20} , (5.15b).
- X, Y Initial bearings from antenna terminals A and B, measured from true north, figure 6.3.
- y_1 Terrain elevations, modified to account for the curvature of the earth, (6.10).
- $y(x)$ Modified terrain elevation, $y(x) = h(x) - x^2/(2a)$, (5.16).
- Y' Bearing from any point B' along the great circle path AB, figure 6.3.
- $Y(q)$ Long-term variability of L_m or of W_m in terms of hourly medians, (10.6) and (V.4)
- $Y(q, 100 \text{ MHz})$ Basic estimate of variability in a continental temperate climate, figure 10.2.
- $Y(q, d_e, 100 \text{ MHz})$ Basic estimate of variability as a function of effective distance, (10.6) figure 10.2.
- Z Great circle path length between antenna terminals A and B, figure 6.3.
- Z' Great circle path distance between an antenna and an arbitrary point B' , figure 6.3.

- α The parameter α is defined in equation (3.9b) and plotted as a function of frequency on figure 3.9.
- α_o, β_o The angles α_{oo}, β_{oo} modified by the corrections $\Delta\alpha_o, \Delta\beta_o$, (6.19).
- α_{oo}, β_{oo} The angles between a transmitter or receiver horizon ray and a line drawn between the antenna locations on an earth of effective radius, a , (6.18) figure 6.1.
- $\alpha(f_{\text{GHz}})$ The function α in (3.9b) as a function of frequency in GHz, figure 3.9.
- γ_{oo} Differential absorption in decibels per kilometer for oxygen under standard conditions of temperature and pressure, (3.4).
- γ_r Rate of absorption by rain, (3.8).
- γ_{rs} Surface value of the rate of absorption by rain, (3.11).
- γ_{wo} Differential absorption in decibels per kilometer for water vapor under standard conditions of temperature and pressure and for a surface value of absolute humidity of 10 g/cc, (3.4).
- $\gamma(r)$ Differential atmospheric absorption in db/km for a path length r , (3.1).
- $\gamma_r(r)$ Differential rain absorption along a path r , (3.7).
- $\gamma_o(h), \gamma_w(h)$ Differential absorption in dB/km for oxygen and water vapor, respectively, as a function of height, h , (3.3).
- $\Gamma(r)$ Absorption coefficient as a function of path distance r , (3.2) and (3.6).
- δ_r, δ_t The effective half-power semi-beamwidth for the receiving and transmitting antennas, respectively, (9.11) and (9.12).
- δ_w, δ_z Azimuthal and vertical semi-beamwidths, (2.6).
- $\Delta\alpha_o, \Delta\beta_o$ Correction terms applied to compute α_o, β_o (6.19) figure 6.9.
- Δ_c Depression of field strength below smooth earth values, (5.19).
- Δh_e A correction term used to compute the effective height for high antennas, (6.12) figure 6.7.
- Δr The path length difference between a direct ray, r_o , and a reflected ray, $\Delta r = r_1 + r_2 - r_o$, (5.4), (5.9) and (7.1).
- $\Delta_{x_1}, \Delta_{x_2}$ Auxiliary functions used to check the magnitude of error in the graphical determination of diffraction attenuation, (8.5) figures 8.5 and 8.6.
- ΔH_o A correction term applied to the frequency gain function, H_o , (9.5) and figure 9.4.
- ΔN The refractivity gradient from the surface value, N_s , to the value of N at a height of one kilometer above the surface, (4.2).
- $\Delta\alpha_o(N_s), \Delta\beta_o(N_s)$ The correction terms $\Delta\alpha_o, \Delta\beta_o$ for values of N_s other than 301, (6.21) figure 6.10.
- $\Delta\alpha_o(301), \Delta\beta_o(301)$ The correction terms $\Delta\alpha_o, \Delta\beta_o$ for $N_s = 301$, (6.21) read from figure 6.9.
- $\Delta h(h_r, N_s), \Delta h(h_t, N_s)$ The correction Δh_e as a function of N_s and of receiver and transmitter heights h_r and h_t , (6.12) figure 6.7.
- η_s A function of h_o and N_s used in computing F_o and H_o , (9.3) and figure 9.2.
- θ The angular distance, θ , is the angle between radio horizon rays in the great circle plane defined by the antenna locations, (6.19).

- θ_{er}, θ_{et} Horizon elevation angles at the receiver and transmitter, respectively, (6.15).
- θ_h Angle of elevation of a direct ray relative to the horizontal at the lower antenna, (5.12).
See θ_b and $f(\theta_h)$.
- θ_o Angle of elevation above the horizontal, figures 3.2 to 3.4.
- θ_{oo} Angle between radio horizon rays, assuming straight rays above an earth of effective radius, a , figure 6.1.
- θ_{or}, θ_{ot} The angular elevation of a horizon ray at the receiver or transmitter horizon, (6.16) figure 6.1.
- λ Free space radio wave length, used for example in (2.7).
- μ The ratio δ_r/δ_t used in (9.12) and figure 9.8.
- ν A parameter that is half the value of η_a , used in computing loss in antenna gain, (9.11), (9.12) and figure 9.7.
- ν Radio frequency in hertz.
- π A constant, $\pi \approx 3.14159264$.
- ρ Correlation coefficient between two random variables.
- ρ Index of curvature for the crest curvature of a rounded obstacle in the great circle path direction, (7.8).
- ρ_{ij} The correlation between variations due to sources i and j , (10.8).
- ρ_{ia} The correlation between variations Y and Y_a , (10.9).
- ρ_{ir} The correlation between variations Y and Y_r , (10.9).
- σ_h The root-mean-square deviation of great circle path terrain elevations relative to a smooth curve fitted to the terrain, (5.1).
- $\sigma_c(p)$ The standard deviation corresponding to the variance $\sigma_c^2(p)$.
- Σ A symbol to represent the summation of terms, as in (5.15) where $\sum_{i=0}^{20} h_i$ means the sum of all values of h_i from $i=0$ to $i=20$.
- $\Phi(v, \rho)$ The total phase lag of the diffracted field over an isolated rounded obstacle with reflections from terrain, (7.13).
- $\Phi(v, 0)$ The total phase lag of the diffracted field over an ideal knife edge with ground reflections, (7.13).
- Φ_A, Φ_B Latitudes of antenna terminals A and B, (6.1) to (6.9) figure 6.3.
- Φ_B' Latitude of an arbitrary point along the great circle path from A to B, (5.7).
- ψ The grazing angle of a ray reflected from a point on the surface of a smooth earth, (5.1) figure 5.1, or grazing angle at a feuillet, annex IV.
- ψ_{in} Minimum grazing angle, section 5.1.
- ψ_p The acute angle between principal polarization vectors \vec{e}_p and \vec{e}_{pr} , (2.11).
- Ω_r, Ω_t The half-power beamwidths of the receiving and transmitting antennas, respectively, (9.10).

NATIONAL BUREAU OF STANDARDS

Technical Note 101

ISSUED May 7, 1965

REVISED May 1, 1966

REVISED January 1, 1967

TRANSMISSION LOSS PREDICTIONS FOR TROPOSPHERIC COMMUNICATION CIRCUITS

VOLUME II

P. L. Rice, A. G. Longley, K. A. Norton, and A. P. Barsis
Institute for Telecommunication Sciences and Aeronomy*
Environmental Science Services Administration
Boulder, Colorado

NBS Technical Notes are designed to supplement the Bureau's regular publications program. They provide a means for making available scientific data that are of transient or limited interest. Technical Notes may be listed or referred to in the open literature.

**Formerly the Central Radio Propagation Laboratory of the National Bureau of Standards.
ESSA will use the NBS publication series until establishment of their ESSA counterparts.*

For sale by the Superintendent of Documents, U. S. Government Printing Office
Washington, D.C. 20402
Price \$1.00

FOREWORD

A short history of the development of the prediction methods in this Technical Note will permit the reader to compare them with earlier procedures. Some of these methods were first reported by Norton, Rice and Vogler [1955]. Further development of forward scatter predictions and a better understanding of the refractive index structure of the atmosphere led to changes reported in an early unpublished NBS report and in NBS Technical Note 15 [Rice, Longley and Norton, 1959]. The methods of Technical Note 15 served as a basis for part of another unpublished NBS report which was incorporated in Air Force Technical Order T. O. 31Z-10-1 in 1961. A preliminary draft of the current technical note was submitted as a U. S. Study Group V contribution to the CCIR in 1962.

Technical Note 101 uses the metric system throughout. For most computations both a graphical method and formulas suitable for a digital computer are presented. These include simple and comprehensive formulas for computing diffraction over smooth earth and over irregular terrain, as well as methods for estimating diffraction over an isolated rounded obstacle. New empirical graphs are included for estimating long-term variability for several climatic regions, based on data that have been made available.

For paths in a continental temperate climate, these predictions are practically the same as those published in 1961. The reader will find a number of graphs have been simplified and that many of the calculations are more readily adaptable to computer programming. The new material on time availability and service probability in several climatic regions should prove valuable for areas other than the U. S. A.

Changes in this revision concern mainly sections 2 and 10 of volume 1 and annexes I, II and V of volume 2, and certain changes in notation and symbols. The latter changes make the notation more consistent with statistical practice.

Section 10, Long-Term Power Fading contains additional material on the effects of atmospheric stratification.

For convenience in using volume 2, those symbols which are found only in an annex are listed and explained at the end of the appropriate annex. Section 12 of volume 1 lists and explains only those symbols used in volume 1.

Note: This Technical Note consists of two volumes as indicated in the Table of Contents.

TABLE OF CONTENTS

Volume 1

	<u>PAGE NO.</u>
1. INTRODUCTION	1-1
2. THE CONCEPTS OF SYSTEM LOSS, TRANSMISSION LOSS, PATH ANTENNA GAIN, AND PATH ANTENNA POWER GAIN	2-1
2.1 System Loss and Transmission Loss.	2-1
2.2 Antenna Directive Gain and Power Gain	2-3
2.3 Polarization Coupling Loss and Multipath Coupling Loss	2-5
2.4 Path Loss, Basic Transmission Loss, Path Antenna Gain, and Attenuation Relative to Free Space	2-7
3. ATMOSPHERIC ABSORPTION.	3-1
3.1 Absorption by Water Vapor and Oxygen	3-1
3.2 Sky-Noise Temperature.	3-3
3.3 Attenuation by Rain	3-4
3.4 Attenuation in Clouds	3-6
4. DETERMINATION OF AN EFFECTIVE EARTH'S RADIUS	4-1
5. TRANSMISSION LOSS PREDICTION METHODS FOR WITHIN-THE-HORIZON PATHS	5-1
5.1 Line-of-Sight Propagation Over Irregular Terrain.	5-1
5.2 Line-of-Sight Propagation Over a Smooth or Uniformly Rough Spherical Earth	5-3
5.2.1 A curve-fit to terrain	5-8
5.2.2 The terrain roughness factor, σ_h	5-9
5.3 Some Effects of Cluttered Terrain	5-10
5.4 Examples of Line-of-Sight Predictions.	5-11
6. DETERMINATION OF ANGULAR DISTANCE FOR TRANSHORIZON PATHS.	6-1
6.1 Plotting a Great Circle Path	6-1
6.2 Plotting a Terrain Profile and Determining the Location of Radio Horizon Obstacles	6-3
6.3 Calculation of Effective Antenna Heights for Transhorizon Paths	6-4
6.4 Calculation of the Angular Distance, θ	6-5
7. DIFFRACTION OVER A SINGLE ISOLATED OBSTACLE.	7-1
7.1 Single Knife Edge, No Ground Reflections	7-1
7.2 Single Knife Edge with Ground Reflections.	7-3
7.3 Isolated Rounded Obstacle, No Ground Reflections	7-4
7.4 Isolated Rounded Obstacle with Ground Reflections	7-6
7.5 An Example of Transmission Loss Prediction for a Rounded Isolated Obstacle.	7-7

	<u>PAGE NO.</u>
8. DIFFRACTION OVER SMOOTH EARTH AND OVER IRREGULAR TERRAIN	8-1
8.1 Diffraction attenuation Over a Smooth Earth	8-1
8.2 Diffraction Over Irregular Terrain	8-3
8.2.1 Diffraction over paths where $d_{st} \neq d_{sr}$	8-4
8.2.2 For horizontal polarization	8-4
8.3 Single-Horizon Paths, Obstacle not Isolated	8-5
9. FORWARD SCATTER.	9-1
9.1 The Attenuation Function, $F(\theta d)$	9-2
9.2 The Frequency Gain Function, H_o	9-3
9.3 The Scattering Efficiency Correction, F_o	9-5
9.4 Expected Values of Forward Scatter Multipath Coupling Loss	9-6
9.5 Combination of Diffraction and Scatter Transmission Loss	9-7
9.6 An Example of Transmission Loss Predictions for a Transhorizon Path	9-8
10. LONG-TERM POWER FADING	10-1
10.1 Effects of Atmospheric Stratification	10-4
10.2 Climatic Regions	10-6
10.3 The Effective Distance, d_e	10-8
10.4 The Functions $V(0.5, d_e)$ and $Y(q, d_e)$	10-9
10.5 Continental Temperate Climate	10-10
10.6 Maritime Temperate Climate	10-12
10.7 Other Climates	10-13
10.8 Variability for Knife-Edge Diffraction Paths	10-13
11. REFERENCES	11-1
12. LIST OF SYMBOLS AND ABBREVIATIONS	12-1

TABLE OF CONTENTS

Volume 2

	<u>PAGE NO.</u>
ANNEX I: AVAILABLE DATA, STANDARD CURVES, AND A SIMPLE PREDICTION MODEL	I-1
I. 1 Available Data as a Function of Path Length.	I-1
I. 2 Standard Point-to-Point Transmission Loss Curves.	I-2
I. 3 Preliminary Reference Values of Attenuation Relative to Free Space A_{cr}	I-29
I. 3.1 Introduction.	I-29
I. 3.2 The Terrain Roughness Factor Δh	I-29
I. 3.3 The Diffraction Attenuation, A_d	I-30
I. 3.4 The Forward Scatter Attenuation, A_s	I-31
I. 3.5 Radio Line-of-Sight Paths	I-32
I. 3.6 Ranges of the Prediction Parameters	I-34
I. 3.7 Sample Calculations	I-35
ANNEX II: AVAILABLE POWER, FIELD STRENGTH, AND MULTIPATH COUPLING LOSS	II-1
II. 1 Available Power from the Receiving Antenna	II-1
II. 2 Propagation Loss and Field Strength.	II-4
II. 3 Beam Orientation, Polarization, and Multipath Coupling Loss	II-9
II. 3.1 Representation of Complex Vector Fields	II-9
II. 3.2 Principal and Cross-Polarization Components	II-12
II. 3.3 Unit Complex Polarization Vectors	II-14
II. 3.4 Power Flux Densities	II-16
II. 3.5 Polarization Efficiency	II-18
II. 3.6 Multipath Coupling Loss.	II-20
II. 3.7 Idealized Theoretical Antenna Patterns.	II-23
II. 3.8 Conclusions	II-31
II. 4 List of Special Symbols Used in Annex II.	II-34
ANNEX III: SUPPLEMENTARY INFORMATION AND FORMULAS USEFUL FOR PROGRAMMING.	III-1
III. 1 Line-of-Sight	III-2
III. 2 Diffraction Over a Single Isolated Obstacle	III-15
III. 3 Diffraction Over a Single Isolated Obstacle with Ground Reflections	III-17
III. 4 Parameters K and b^* for Smooth Earth Diffraction.	III-23
III. 5 Forward Scatter.	III-24
III. 6 Transmission Loss with Antenna Beams Elevated or Directed Out of the Great Circle Plane	III-37

	<u>PAGE NO.</u>
III. 7 Long-Term Power Fading	III-44
III. 7.1 Diurnal and seasonal variability in a continental temperate climate	III-45
III. 7.2 To mix distributions	III-54
III. 8 List of Special Symbols Used in Annex III	III-73
ANNEX IV: FORWARD SCATTER	IV-1
IV. 1 General Discussion	IV-1
IV. 2 Models for Forward Scattering	IV-2
IV. 3 List of Special Symbols Used in Annex IV	IV-11
ANNEX V: PHASE INTERFERENCE FADING AND SERVICE PROBABILITY . .	V-1
V. 1 The Two Components of Fading	V-3
V. 2 The Nakagami-Rice Distribution	V-5
V. 3 Noise-Limited Service	V-13
V. 4 Interference-Limited Service	V-15
V. 5 The Joint Effect of Several Sources of Interference Present Simultaneously	V-19
V. 6 The System Equation for Noise-Limited Service	V-20
V. 7 The Time Availability of Interference-Limited Service	V-22
V. 8 The Estimation of Prediction Error	V-23
V. 9 The Calculation of Service Probability Q for a Given Time Availability q	V-25
V. 10 Optimum Use of the Radio Frequency Spectrum	V-31
V. 11 List of Special Symbols Used in Annex V	V-35

Annex I

AVAILABLE DATA, STANDARD CURVES, AND A SIMPLE PREDICTION MODEL

The simplest way to predict long-term median transmission loss values would be to use a best-fit curve drawn through measured data (represented by their overall median values) plotted as a function of path length. Such a method ignores essentially all of our understanding of the physics of tropospheric propagation, is subject to especially large errors over rough terrain, and such empirical curves represent only the conditions for which data are available.

Curves that may be useful for establishing preliminary allocation plans are presented in section I.2 of this annex. These "standard" curves were prepared for a fixed combination of antenna heights and assume propagation over a smooth earth. The curves are not suitable for use on particular point-to-point paths, since they make no allowance for the wide range of propagation path profiles or atmospheric conditions that may be encountered over particular paths.

A method for computing preliminary reference values of transmission loss is described in section I.3. This method is based on a simple model, may readily be programmed, and is especially useful when little is known of the details of terrain.

I.1 Available Data as a Function of Path Length

Period-of-record median values of attenuation relative to free space are plotted vs. distance in figures I.1 to I.4 for a total of 750 radio paths, separating the frequency ranges 40-150 MHz, 150-600 MHz, 600-1000 MHz, and 1-10 GHz. Major sources of data other than those referenced by Herbstreit and Rice [1959] are either unpublished or are given by Bray, Hopkins, Kitchen, and Saxton [1955], Bullington [1955], du Castel [1957b], Crysdale [1958], Crysdale, Day, Cook, Psutka, and Robillard [1957], Dolukhanov [1957], Grosskopf [1956], Hirai [1961a, b], Josephson and Carlson [1958], Jowett [1958], Joy [1958a, b], Kitcher and Richmond [1957], Kitchen, Richards, and Richmond [1958], Millington and Isted [1950], Newton and Rogers [1953], Onoe, Hirai, and Niwa [1958], Rowden, Tagholm, and Stark [1958], Saxton [1951], Ugai [1961], and Vvedenskii and Sokolov [1957].

Three straight lines were determined for each of the data plots shown in figures I.1 to I.4. Near the transmitting antenna, $A = 0$ on the average. Data for intermediate distances, where the average rate of diffraction attenuation is approximately $0.09 f^{\frac{1}{3}}$ db per kilometer, determine a second straight line. Data for the greater distances, where the level of forward scatter fields is reached, determine the level of a straight line with a slope varying from 1/18 to 1/14 db per kilometer, depending on the frequency.

The dashed curves of figures I.1-I.3 show averages of broadcast signals recorded at 2500 random locations in six different areas of the United States. The data were normalized to 10-meter and 300-meter antenna heights, and to frequencies of 90, 230, and 750 MHz.

For this data sample [TASO 1959], average fields are low mainly because the receiver locations were not carefully selected, as they were for most other paths for which data are shown.

The extremely large variance of long-term median transmission loss values recorded over irregular terrain is due mainly to differences in terrain profiles and effective antenna heights. For a given distance and given antenna heights a wide range of angular distances is possible, particularly over short diffraction and extra-diffraction paths. Angular distance, the angle between radio horizon rays from each antenna in the great circle plane containing the antennas, is a very important parameter for transmission loss calculations, (see section 6). Figure I.5 shows for a number of paths the variability of angular distance relative to its value over a smooth spherical earth as a function of path distance and antenna heights.

Most of the "scatter" of the experimental long-term medians shown in figures I.1 - I.4 is due to path-to-path differences. A small part of this variation is due to the lengths of the recording periods. For all data plotted in the figures the recording period exceeded two weeks, for 630 paths it exceeded one month, and for 90 paths recordings were made for more than a year.

An evaluation of the differences between predicted and measured transmission loss values is discussed briefly in annex V. In evaluating a prediction method by its variance from observed data, it is important to remember that this variance is strongly influenced by the particular data sample available for comparison. Thus it is most important that these data samples be as representative as possible of the wide range of propagation path conditions likely to be encountered in the various types of service and in various parts of the world.

To aid in deciding whether it is worthwhile to use the point-to-point prediction method outlined in sections 4 - 10, instead of simpler methods, figure I.6 shows the cumulative distribution of deviations of predicted from observed long-term median values. The dash-dotted curve shows the cumulative distribution of deviations from the lines drawn in figures I.1 - I.4 for all available data. The solid and dashed curves compare predictions based on these figures with ones using the point-to-point method for the same paths. Note that the detailed point-to-point method could not be used in many cases because of the lack of terrain profiles.

Figure I.6 shows a much greater variance of data from the "empirical" curves of figures I.1 - I.4 for the sample of 750 paths than for the smaller sample of 217 paths for which terrain profiles are available. The wide scatter of data illustrated in figure I.4 for the frequency range 1 - 10 GHz appears to be mainly responsible for this. Figure I.4 appears to show that propagation is much more sensitive to differences in terrain profiles at these higher frequencies, as might be expected. The point-to-point prediction methods, depending on a number of parameters besides distance and frequency, are also empirical, since they are made to agree with available data, but estimates of their reliability over a period of years have not varied a great deal with the size of the sample of data made available for comparison with them.

PERIOD OF RECORD MEDIANS VERSUS DISTANCE
FREQUENCY RANGE 150-600MHz; MEDIAN FREQUENCY 230MHz
183 PATHS

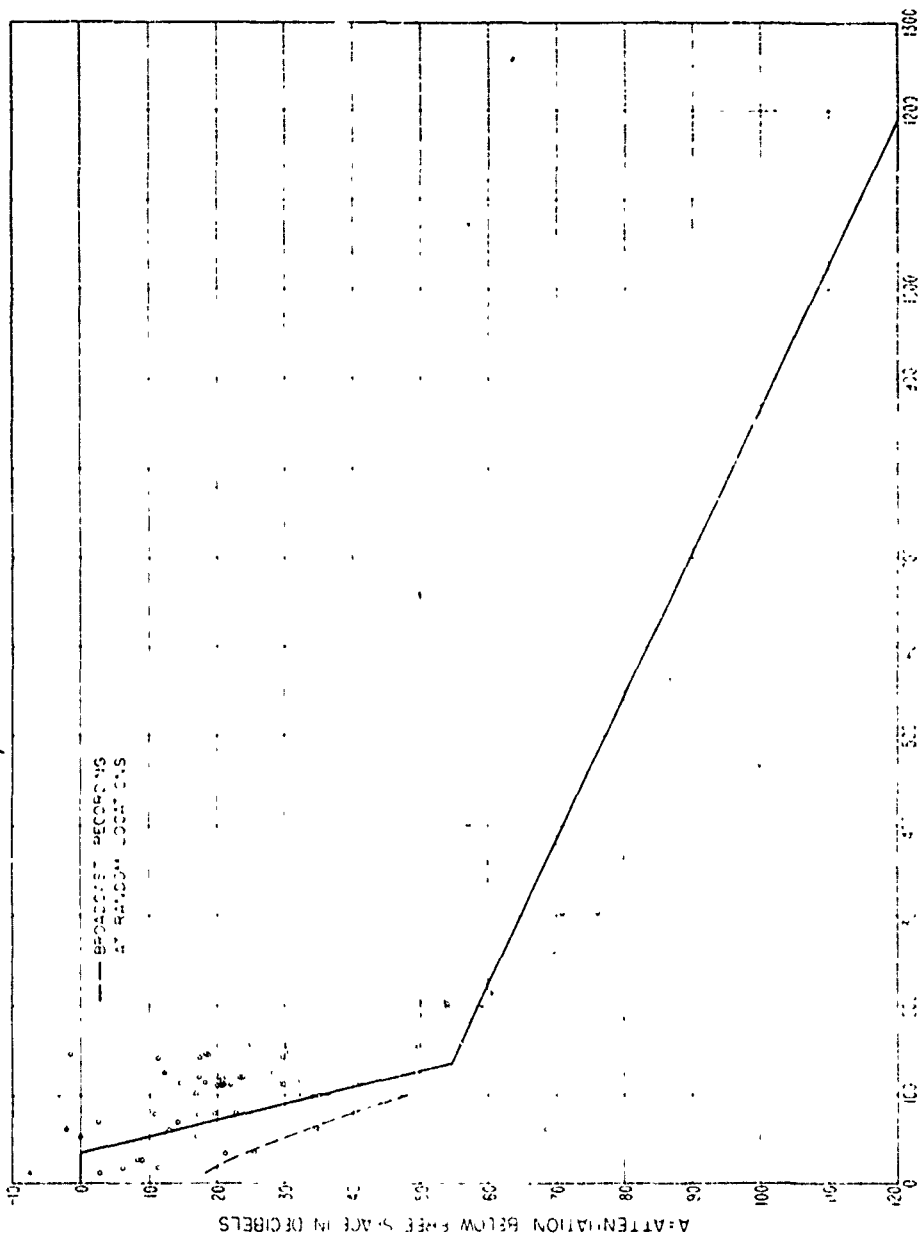


Figure 12

PERIOD OF RECORD MEDIANS VERSUS DISTANCE
FREQUENCY RANGE: 600-1000MHZ; MEDIAN FREQUENCY: 750MHZ
108 PATHS

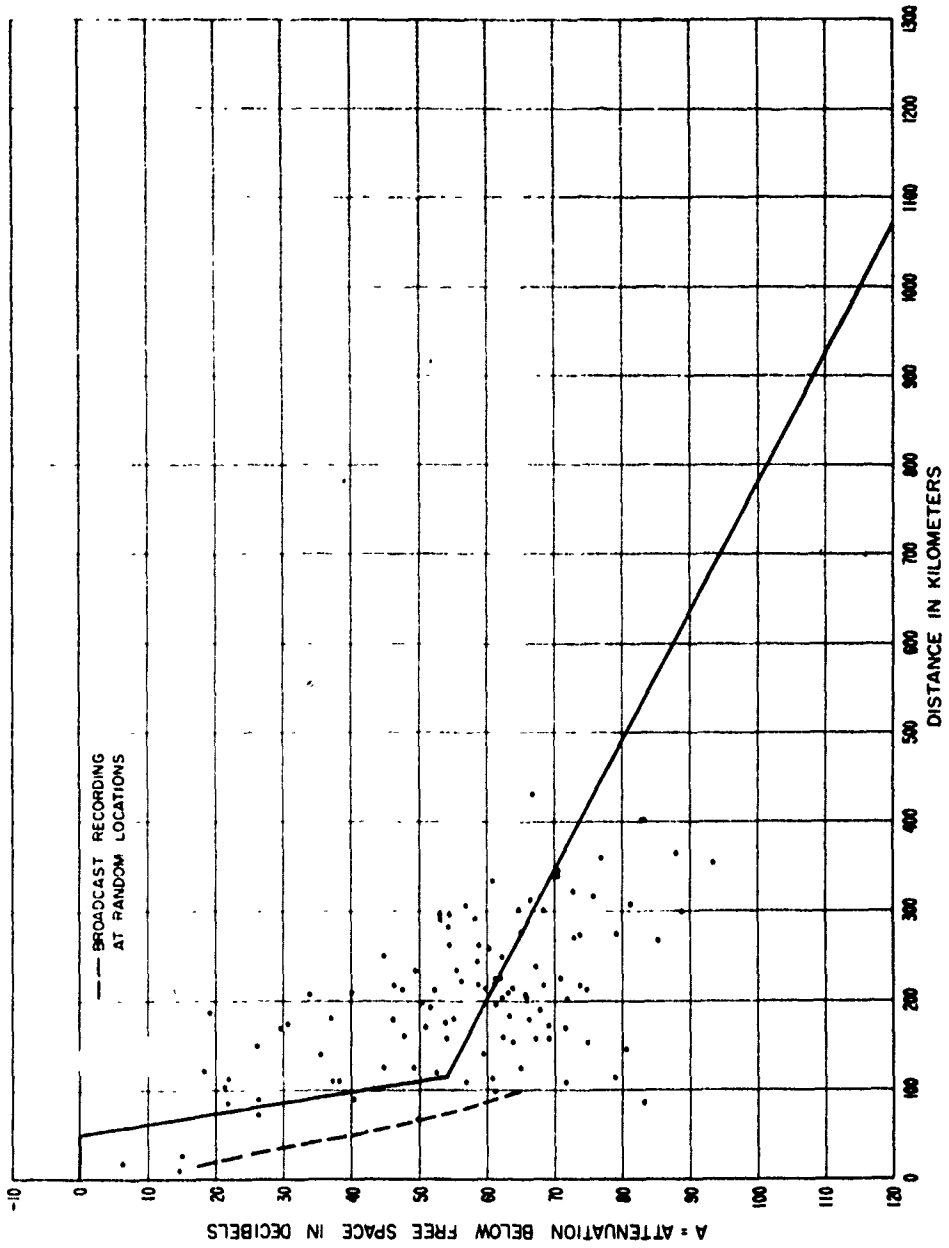


Figure 1.3

PERIOD OF RECORD MEDIANS VERSUS DISTANCE
FREQUENCY RANGE 1000-0.000MHZ, MEDIAN FREQUENCY 3500MHZ
110 PATHS

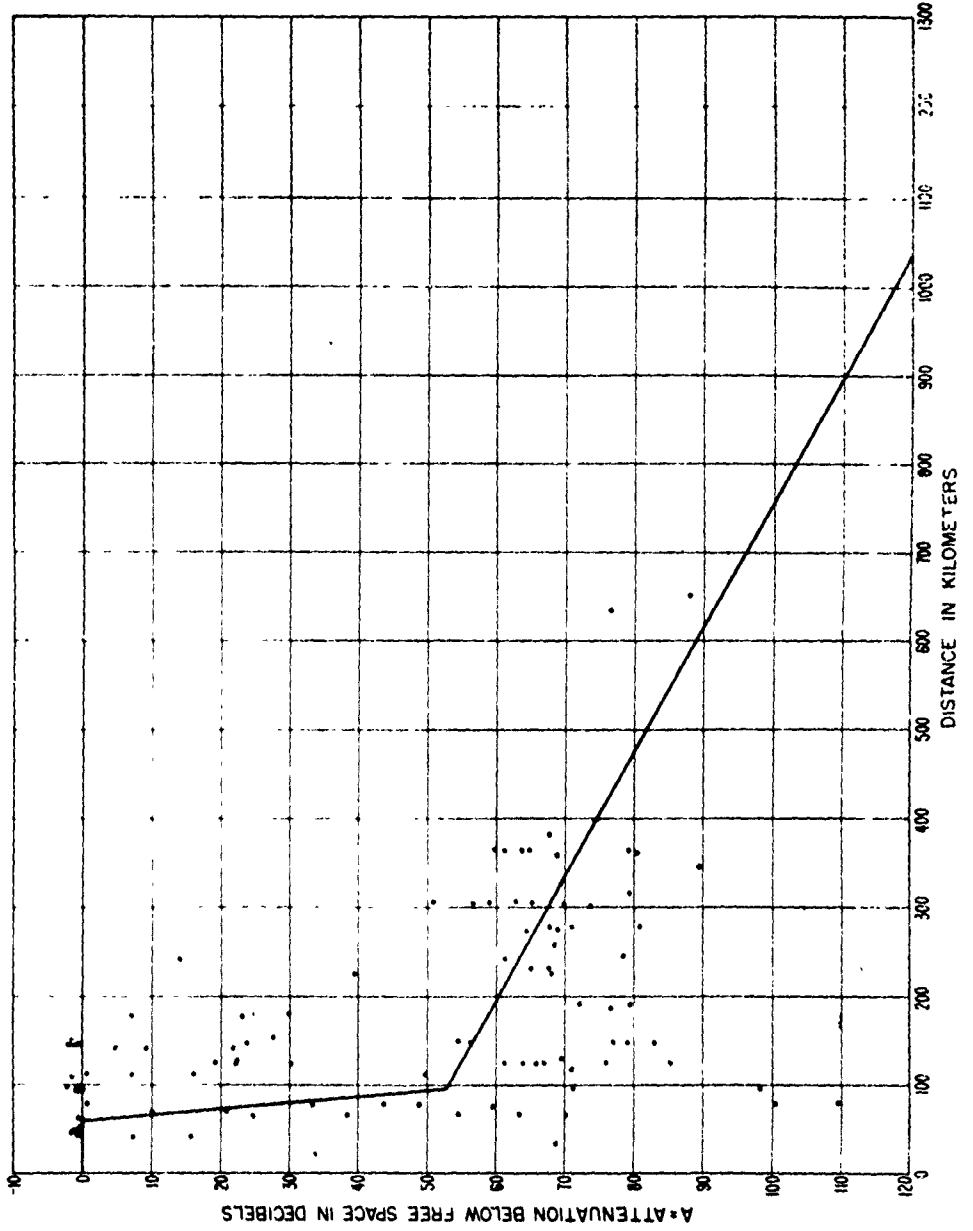


Figure I.4

ANGULAR DISTANCE VERSUS DISTANCE FOR THE 290 PATHS FOR WHICH
TERRAIN PROFILES ARE AVAILABLE

THE CURVES SHOW ANGULAR DISTANCE, θ , AS A FUNCTION OF DISTANCE
OVER A SMOOTH EARTH OF EFFECTIVE RADIUS = 9000 KILOMETERS

THE WIDE SCATTER OF THE DATA ON THIS FIGURE ARISES ALMOST ENTIRELY
FROM DIFFERENCES IN TERRAIN PROFILES, AND ILLUSTRATES THE
IMPORTANCE OF ANGULAR DISTANCE AS A PREDICTION PARAMETER

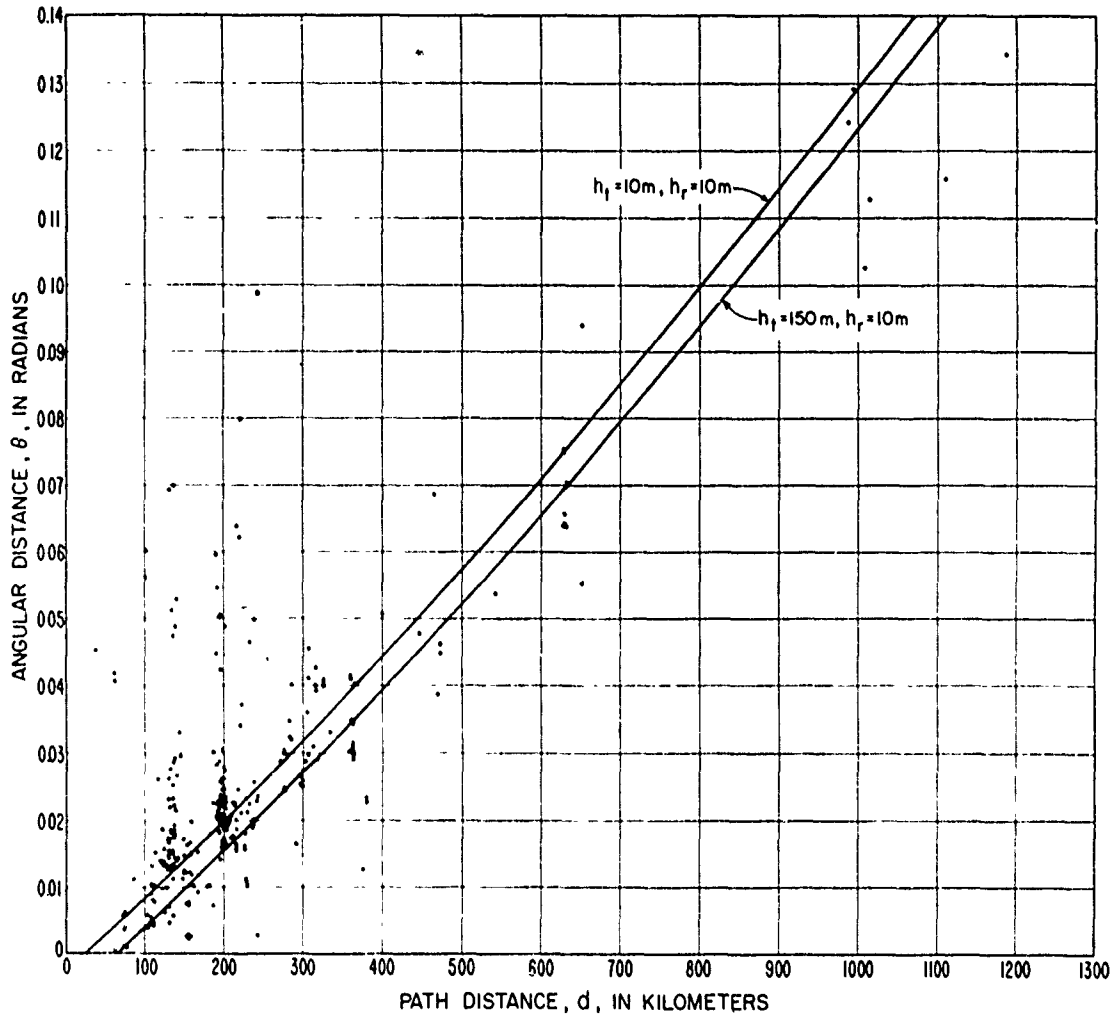


Figure 1.5

CUMULATIVE DISTRIBUTION OF DEVIATIONS OF OBSERVED FROM PREDICTED VALUES OF TRANSMISSION LOSS

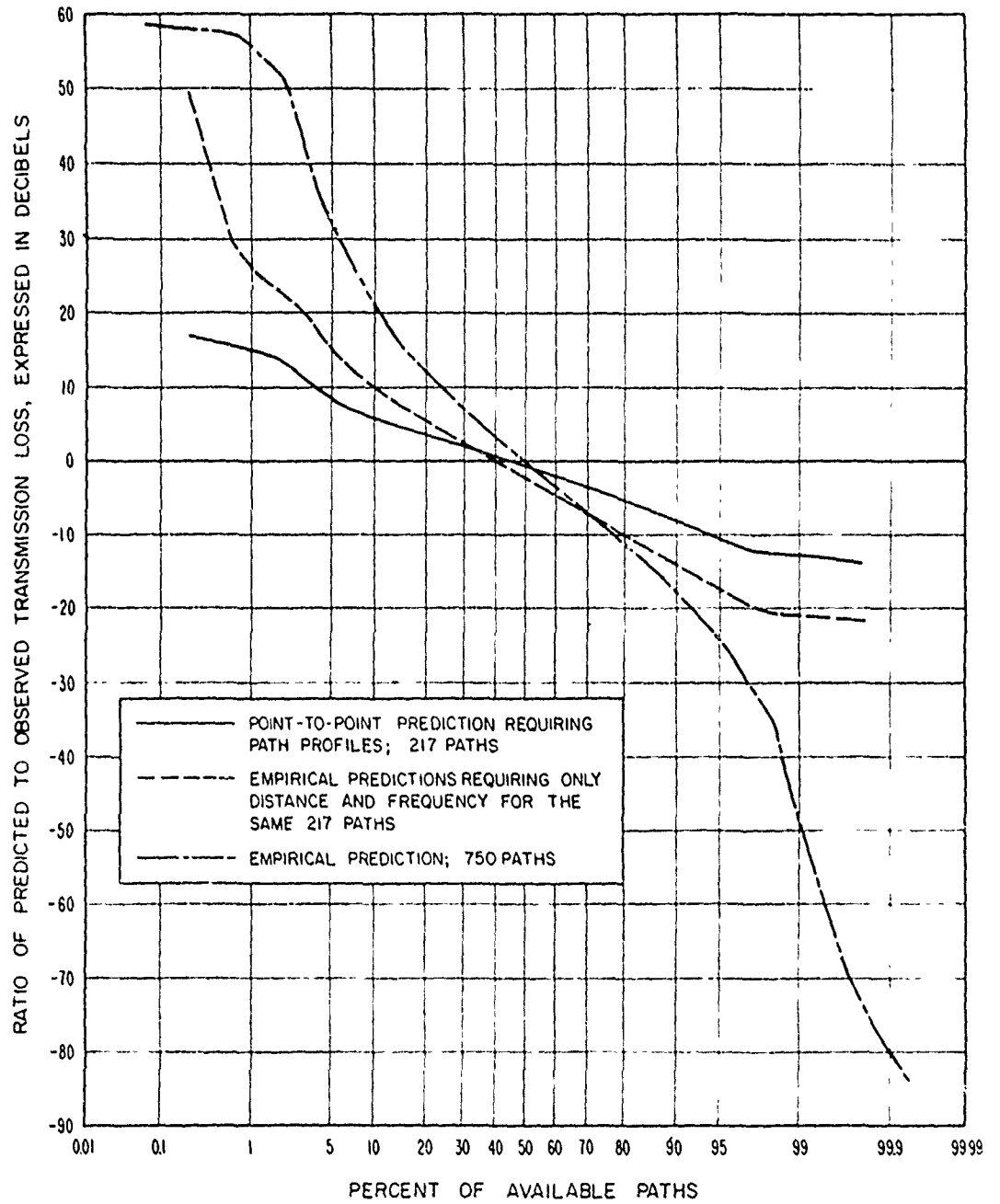


Figure 1.6

STANDARD PROPAGATION CURVES
MEDIUM BASIC TRANSMISSION LOSS
VERSUS DISTANCE AND TIME AT 30 MHz
FREQUENCY 0 GHz $N_{\text{eff}} = 1.0$

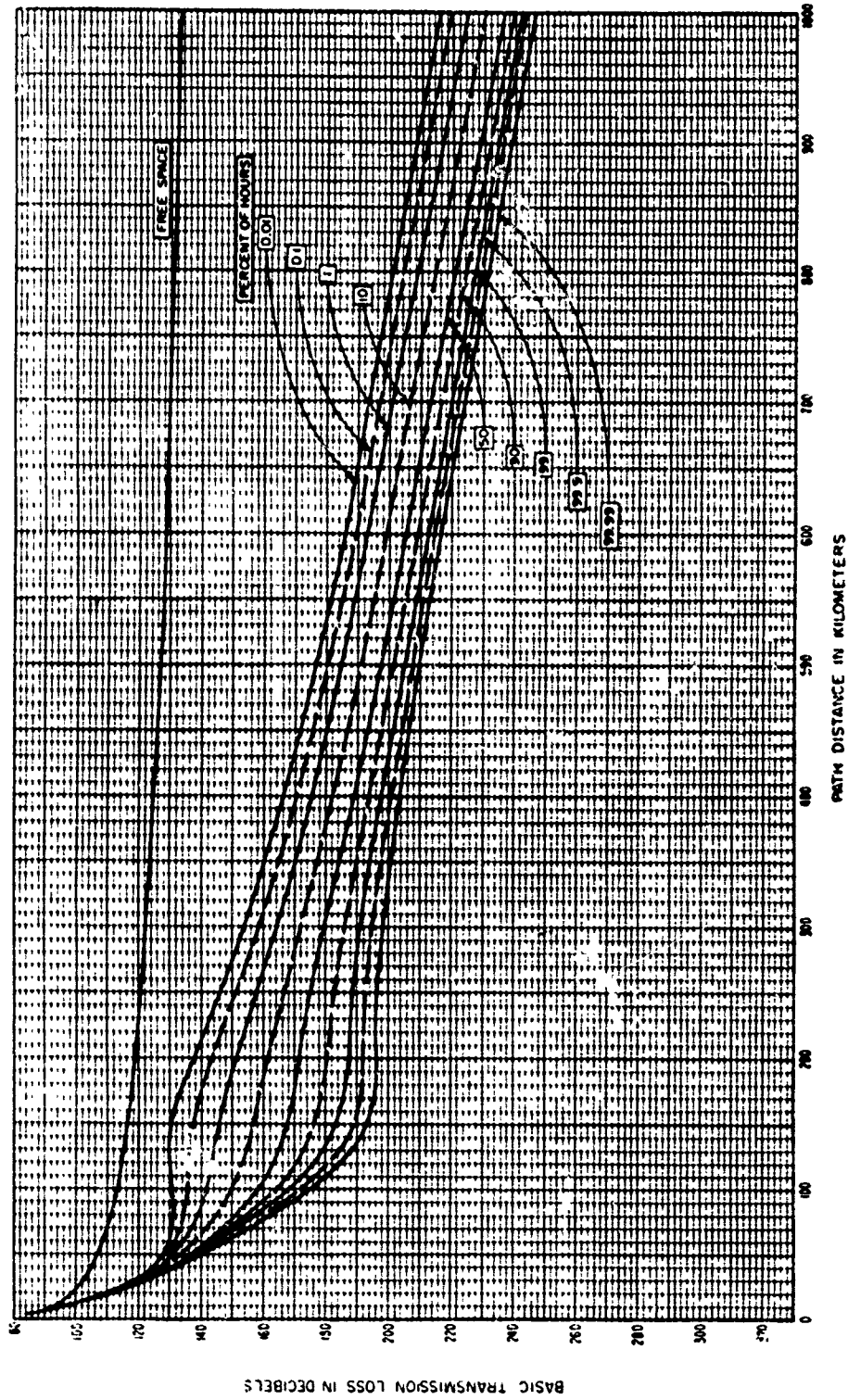


Figure I.7

STANDARD PROPAGATION CURVES
HOURLY MEDIAN BASIC TRANSMISSION LOSS
VERSUS DISTANCE AND TIME OF DAY
FREQUENCY 0.2 GHz $n_{fp} = 1.4$ $n_{fc} = 3.0$

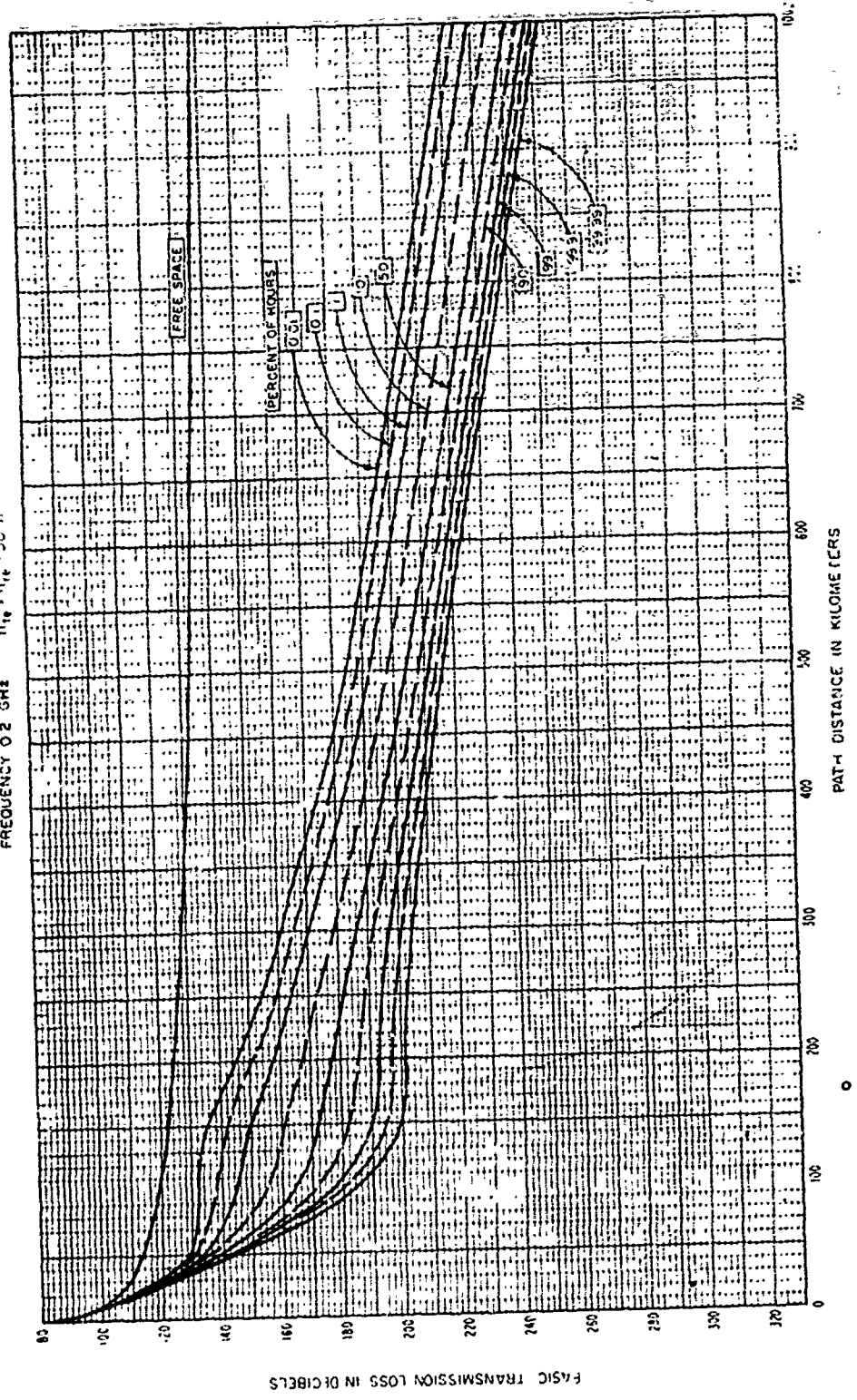


Figure 1.8

STANDARD PROPAGATION CURVES
HOURLY MEDIAN BASIC TRANSMISSION LOSS
VERSUS DISTANCE AND TIME AVERAGE
FREQUENCY 0.5 GHz $h_p = h_a = 30$ m

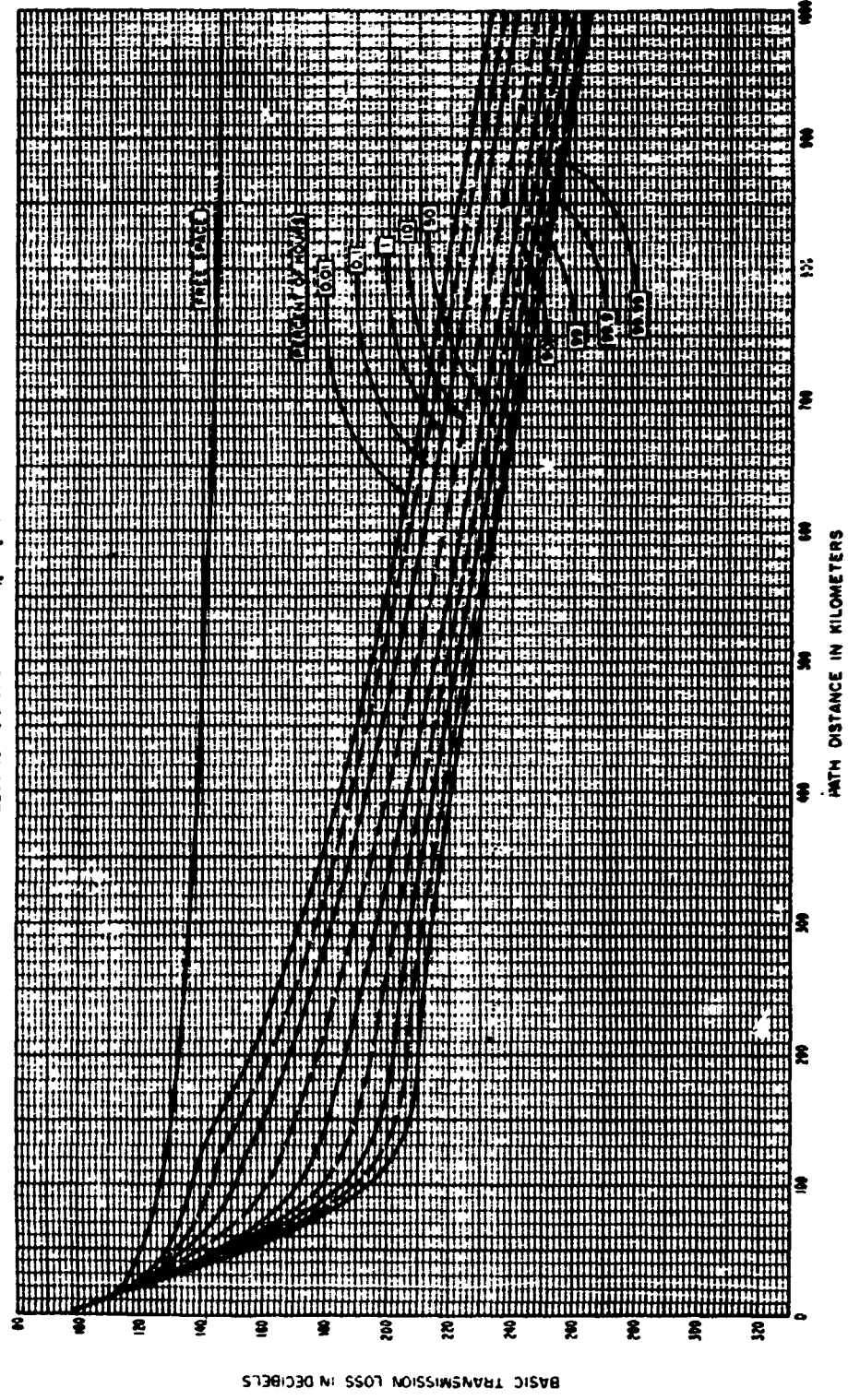


Figure I.9

STANDARD PROPAGATION CURVES
HOURLY MEDIAN BASIC TRANSMISSION LOSS
VERSUS DISTANCE AND TIME AVAILABILITY
FREQUENCY 1 GMZ $h_{10} = h_{10} = 30$ m

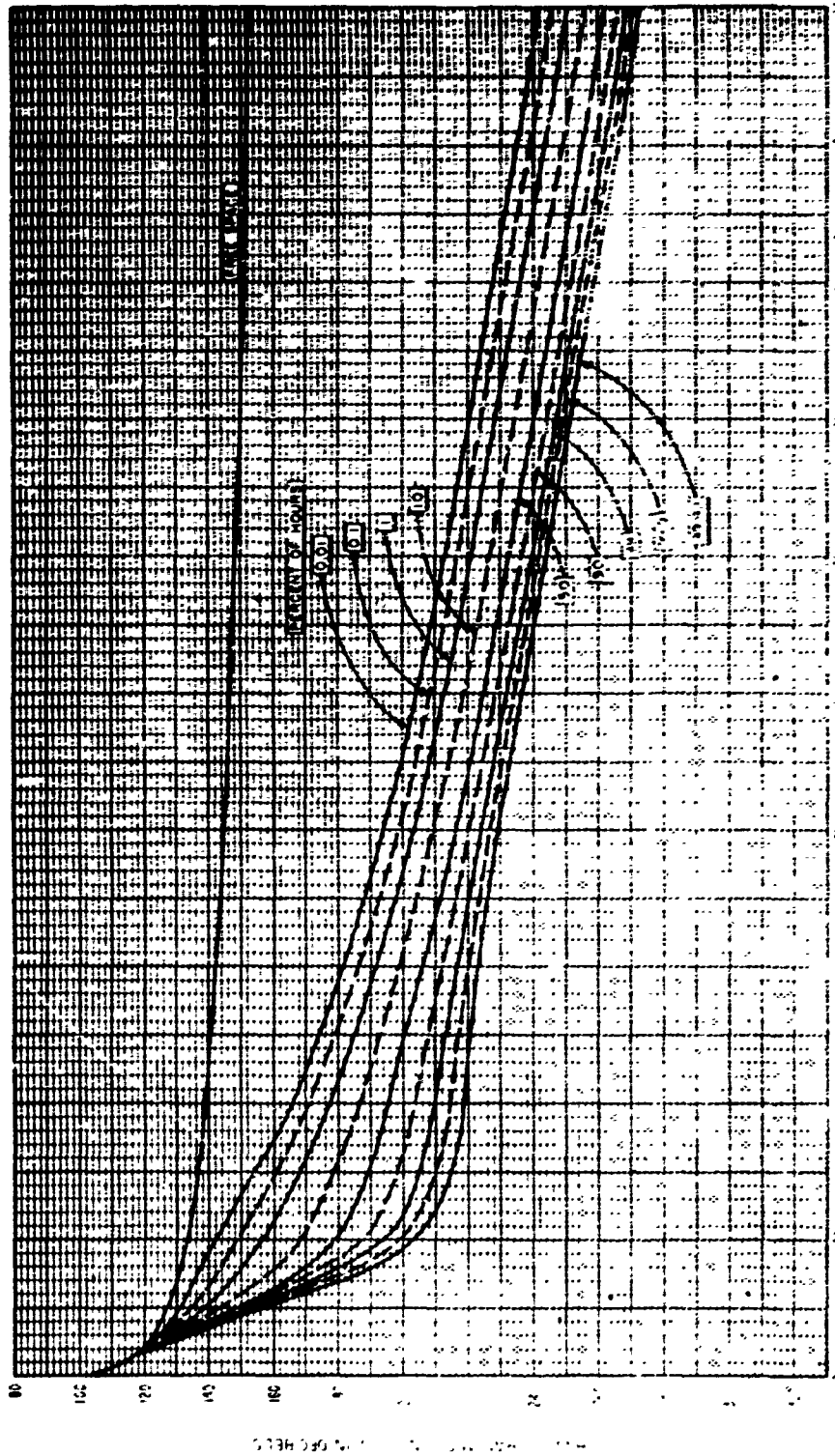


Figure 1.10

STANDARD PROPAGATION CURVES
40-RLY MEDIAN BASIC TRANSMISSION LOSS
VERSUS DISTANCE AND TIME AVAILABLE
FREQUENCY 2 GHz $\gamma_{0.01} = 1.0 \times 10^{-3}$ CM

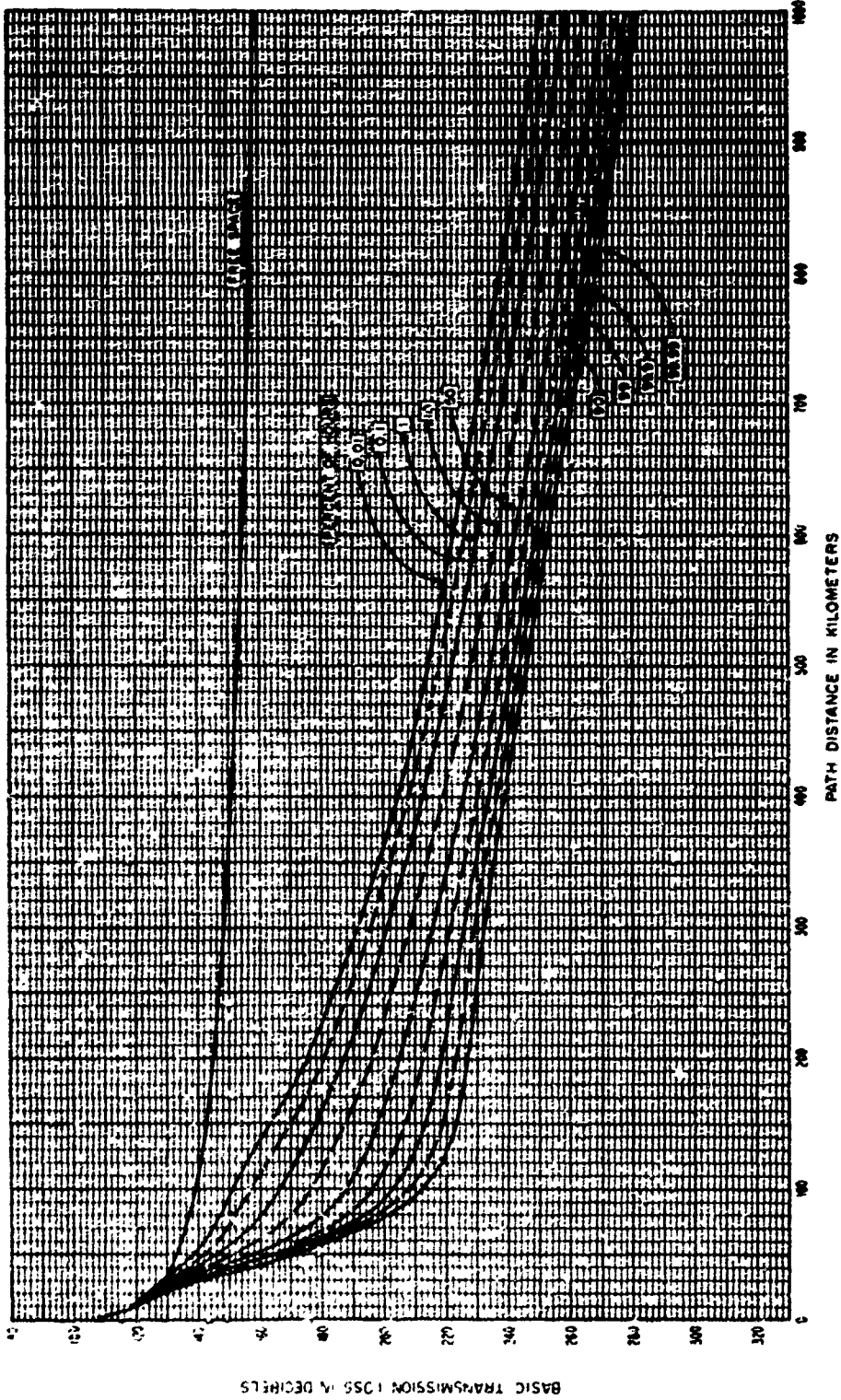
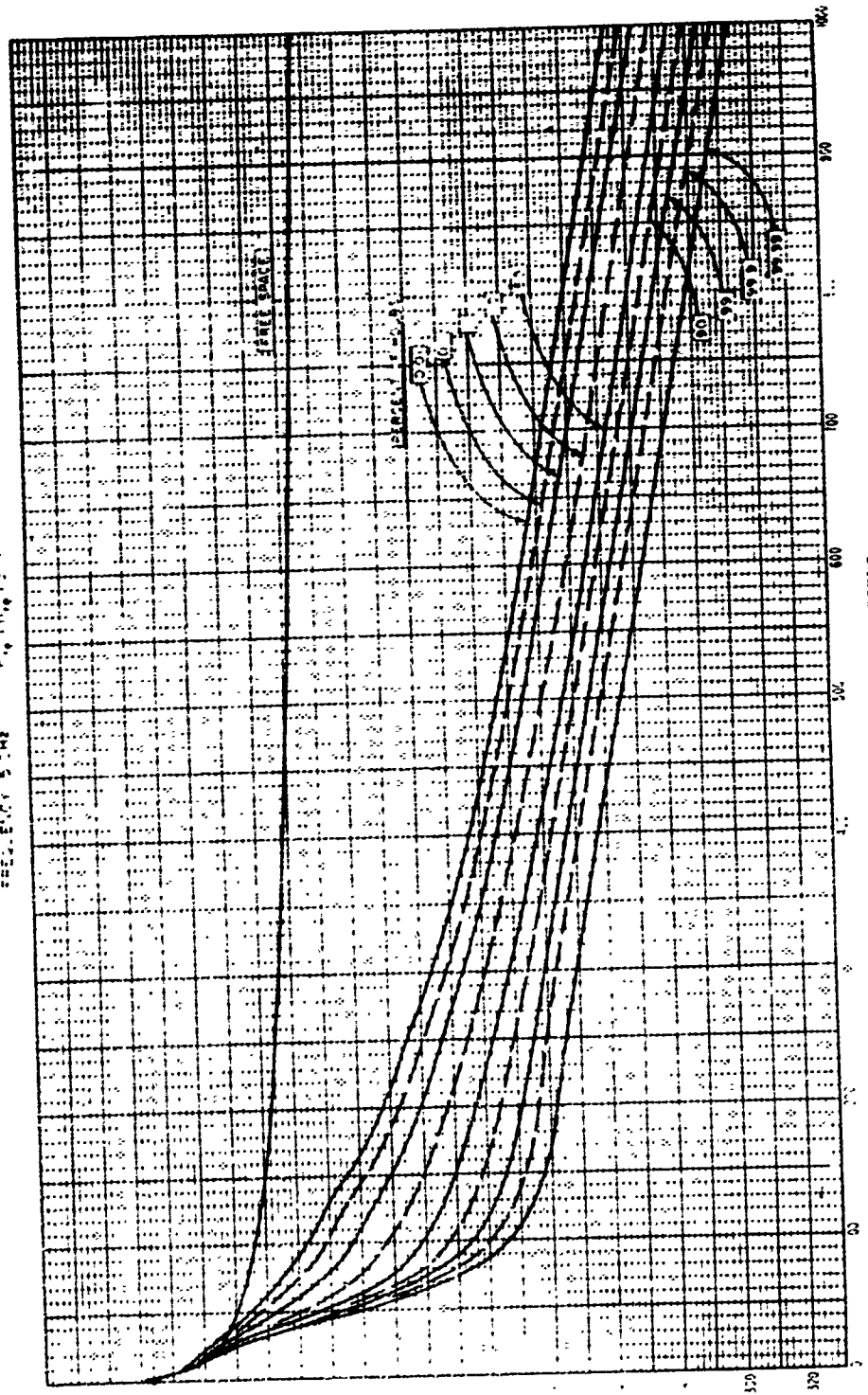


Figure 1.11

STANDARD PROPAGATION CURVES
- LOSS IN DB PER 100 KM TRANSMISSION LOSS
- LOSS IN DB PER 100 KM TRANSMISSION LOSS
- LOSS IN DB PER 100 KM TRANSMISSION LOSS
- LOSS IN DB PER 100 KM TRANSMISSION LOSS



DISTANCE IN KILOMETERS

Figure 1.12

STANDARD PROPAGATION CURVES
HOURLY MEDIAN BASIC TRANSMISSION LOSS
VERSUS DISTANCE AND TIME AVAILABILITY
FREQUENCY 10 GHE $h_{10} = h_{10} = 30m$

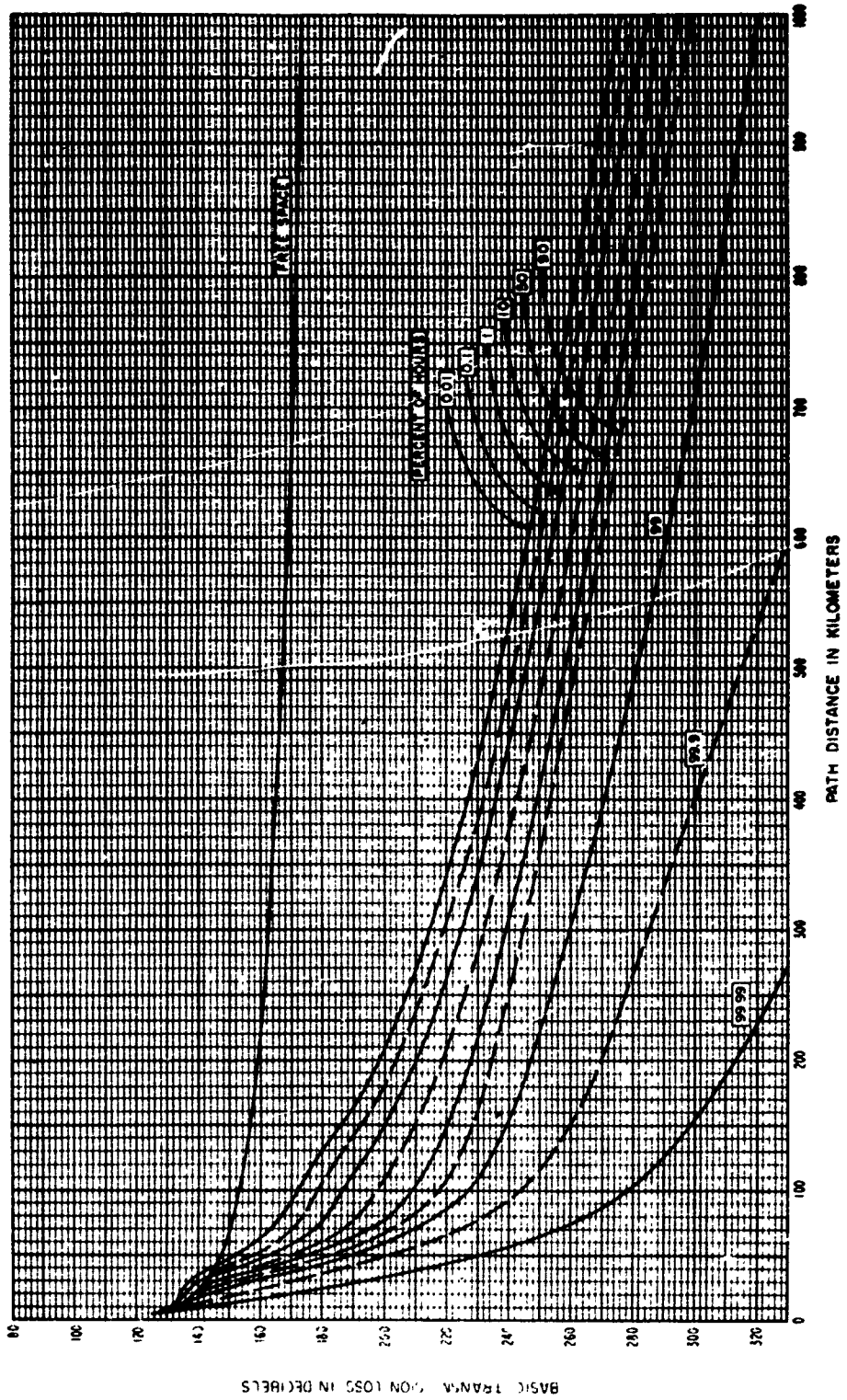
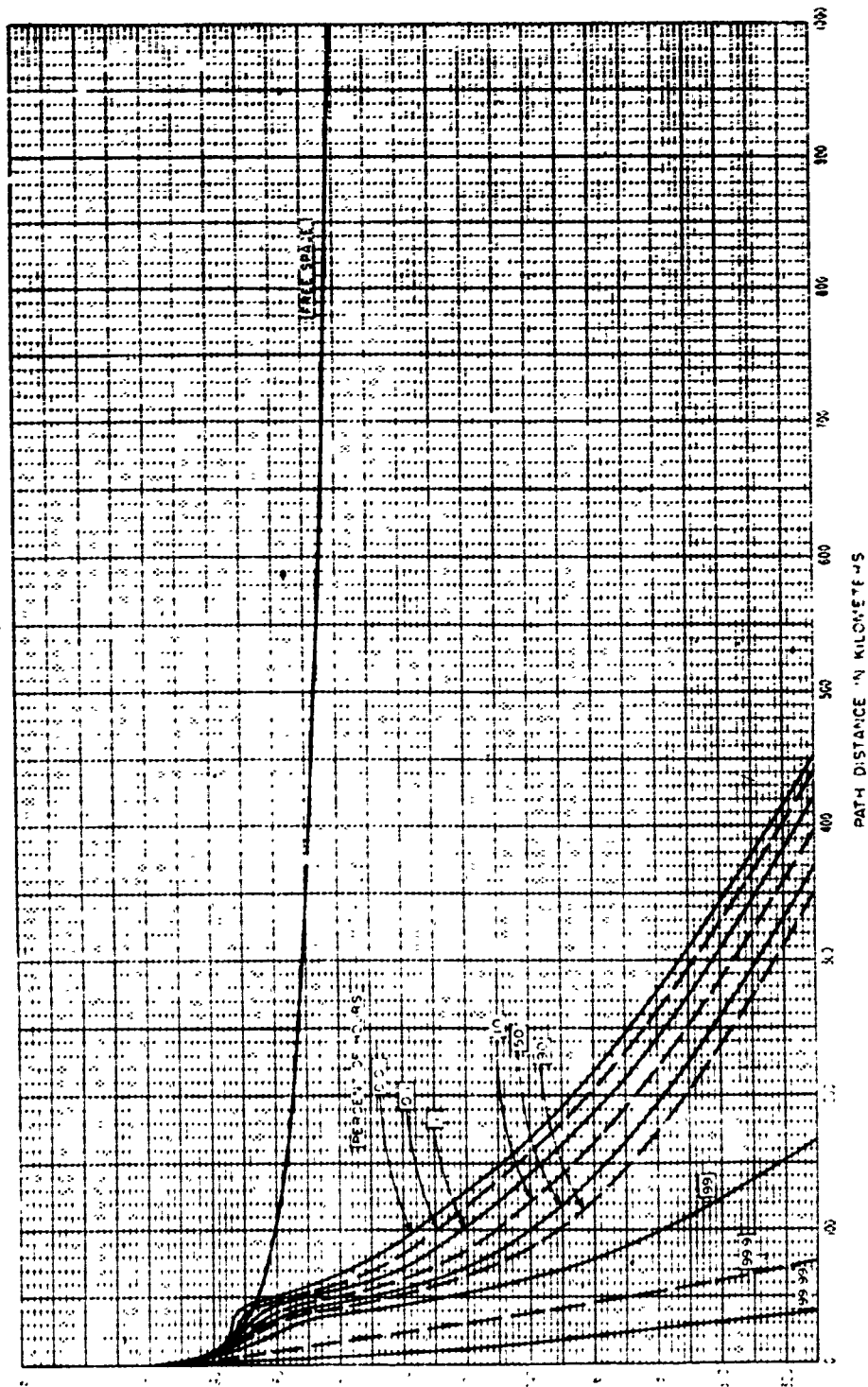


Figure 1.13

STANDARD PROPAGATION CURVES
FOR THE IONOSPHERIC REFRACTION INDEX
FOR THE FREQUENCY RANGE 3000 kHz TO 30 MHz
FOR THE DISTANCE RANGE 0 TO 4000 km



PATH DISTANCE IN KILOMETERS

Figure I.14

STANDARD PROPAGATION CURVES
HOURLY MEDIAN BASIC TRANSMISSION LOSS
VERSUS DISTANCE AND TIME AVAILABILITY
FREQUENCY 32.5 GHz $r_{p0} = 1.30$ m

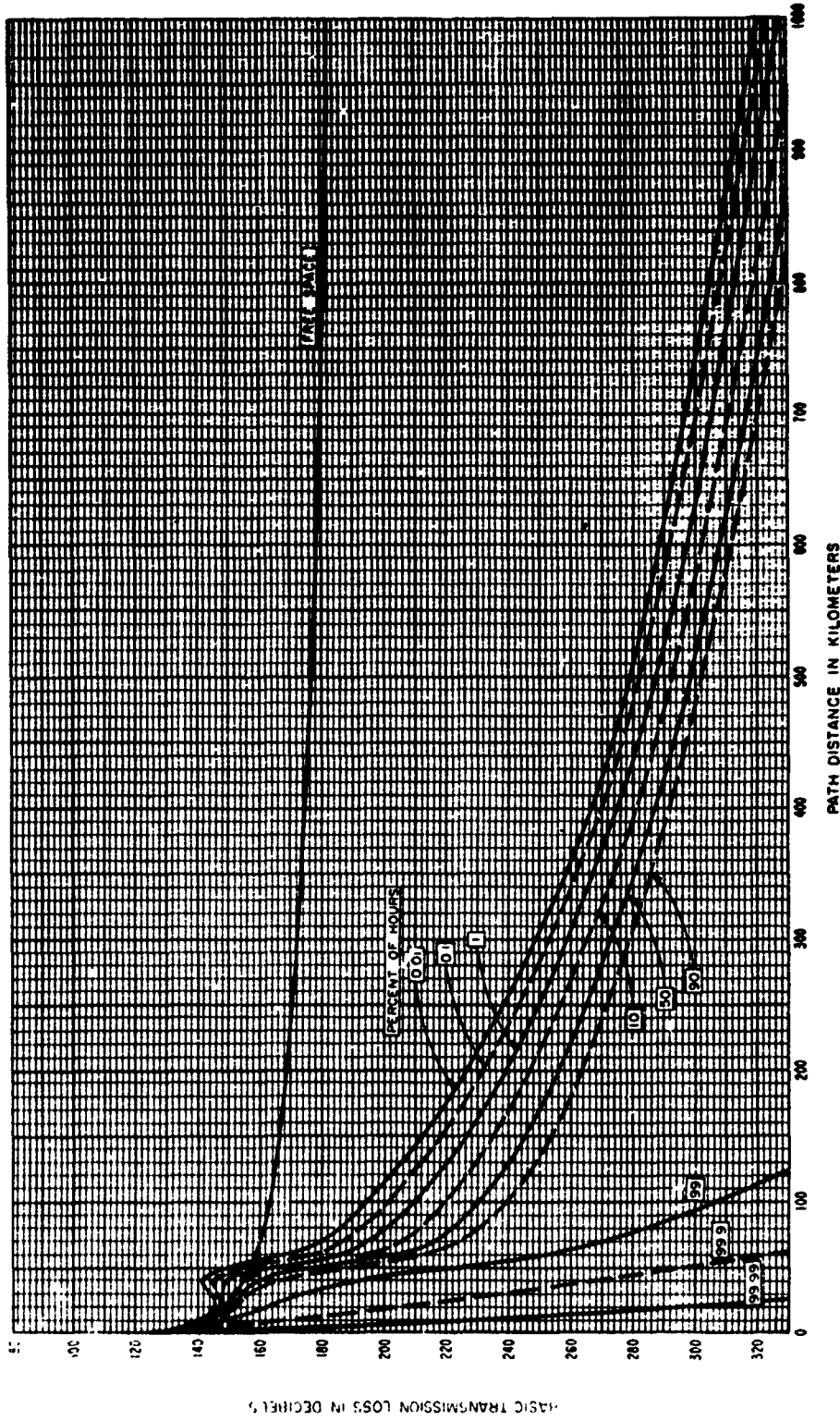
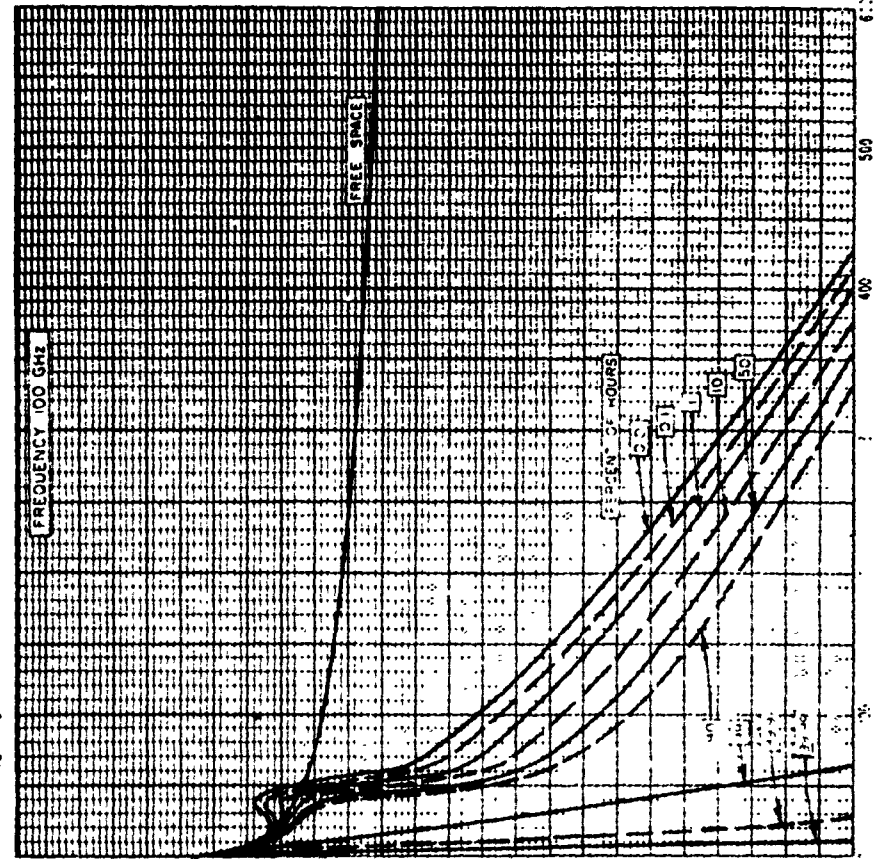


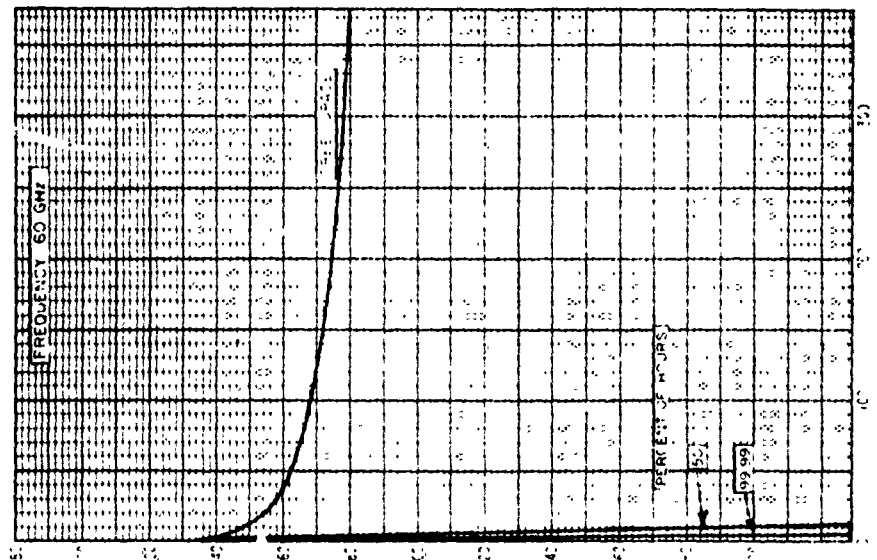
Figure I.15

STANDARD PROPAGATION CURVES
 DENSITY MEDIAN BASIC TRANSMISSION LOSS
 VERSUS DISTANCE AND TIME AVAILABILITY
 $h_{t0} = h_{r0} = 30 \text{ m}$



DISTANCE IN KILOMETERS

Figure 1.17



DISTANCE IN KILOMETERS

Figure 1.16

STANDARD PROPAGATION CURVES
PREDICTED MEDIAN LEVELS OF BASIC TRANSMISSION LOSS
FOR FREQUENCIES FROM 0.1 TO 100 GHz

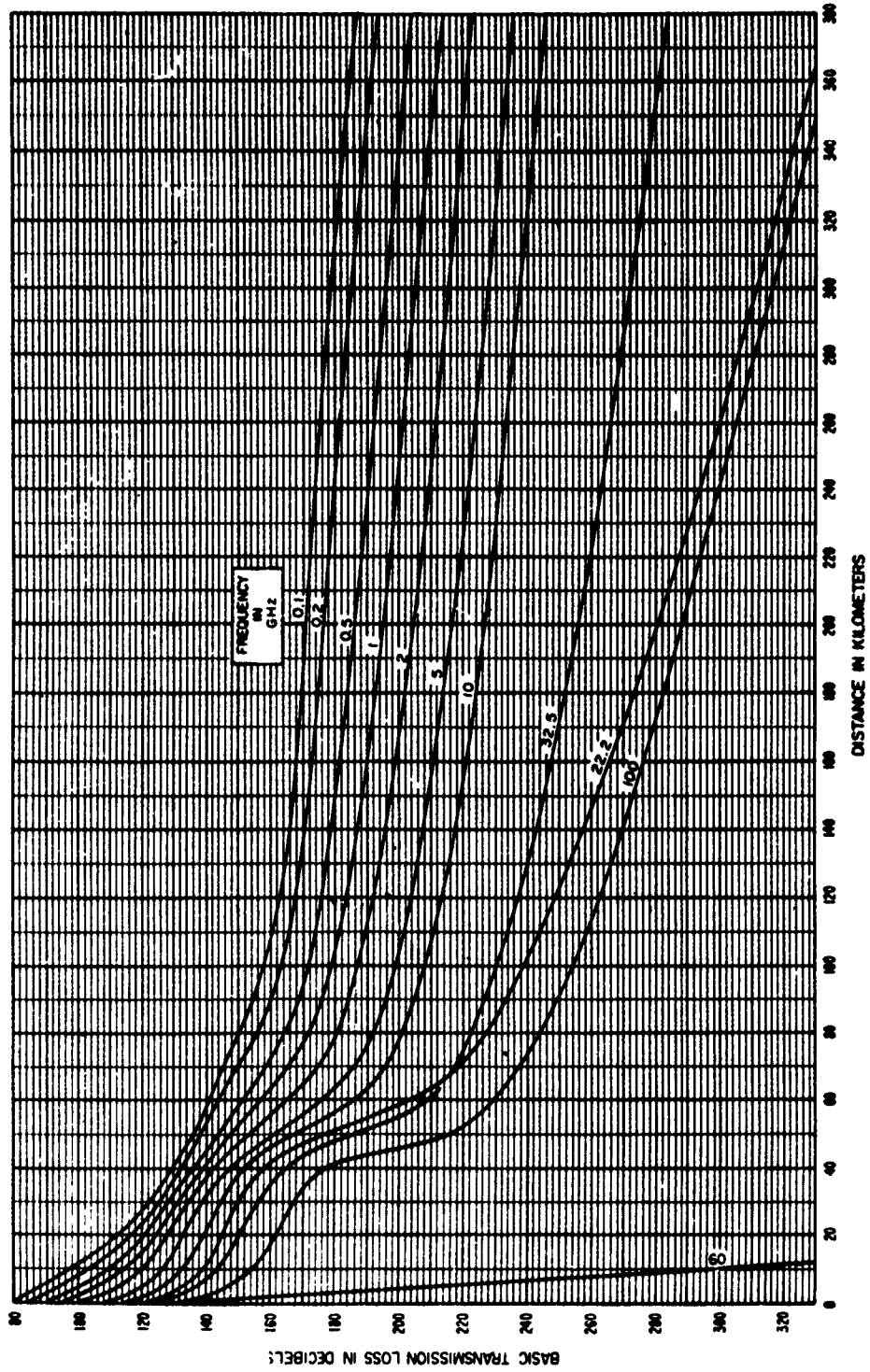


Figure 1.16

STANDARD PROPAGATION CURVES
 BASIC TRANSMISSION LOSS NOT EXCEEDED FOR 99 AND 99.99 PERCENT OF ALL HOURS
 INCLUDING AN ESTIMATE OF ABSORPTION BY RAIN, ASSUMING 100% TOTAL ANNUAL RAINFALL
 THE CURVES ARE DRAWN FOR FREQUENCIES BETWEEN 5 AND 100 GHz

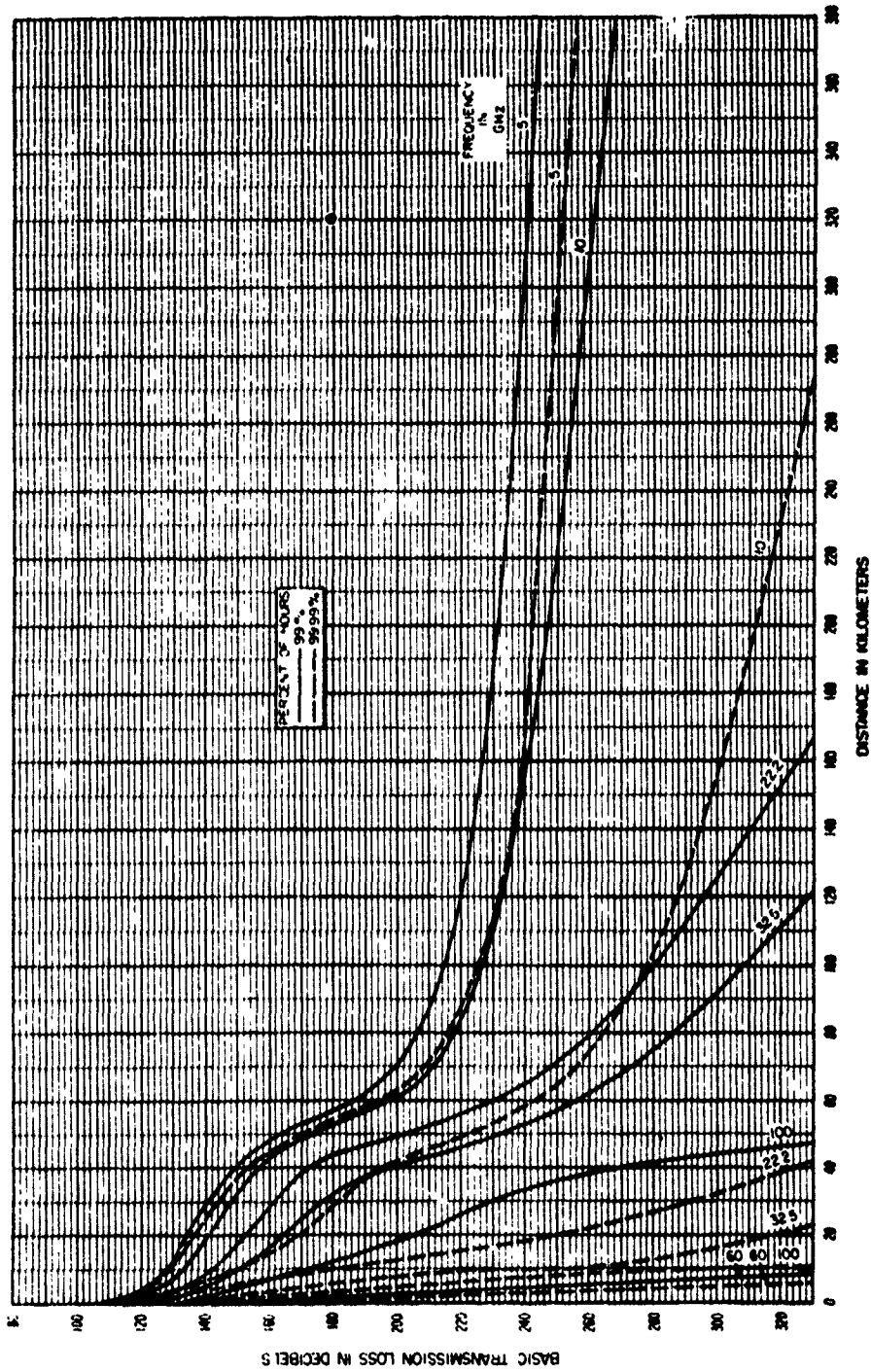


Figure 1.20

STANDARD PROPAGATION CURVES FOR EARTH-SPACE LINKS
 $\theta_0 = 0$ RADIANS
 NO ALLOWANCE HAS BEEN MADE FOR GROUND REFLECTION

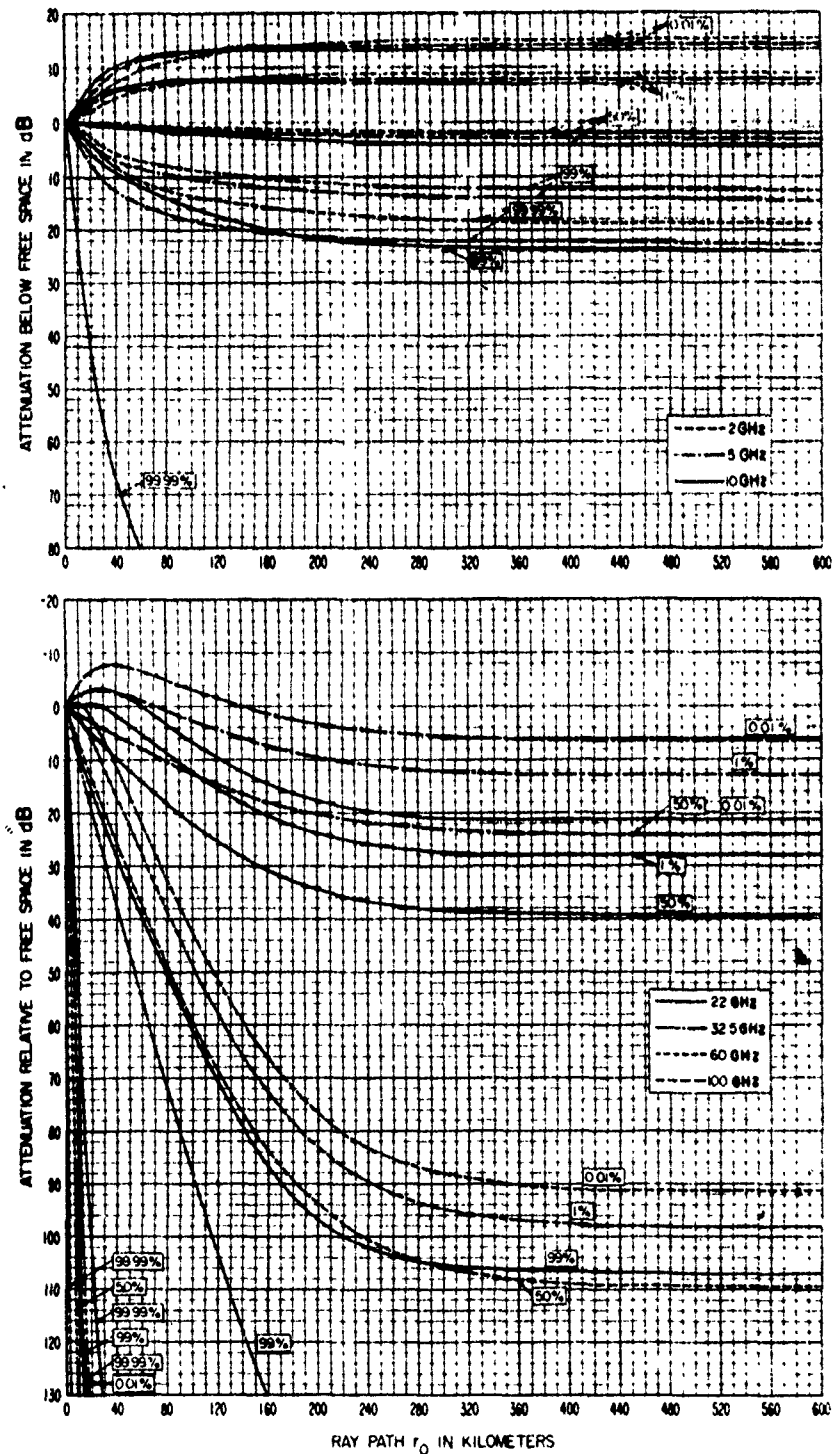


Figure I.21

STANDARD PROPAGATION CURVES FOR EARTH SPACE LINKS
 $\theta_0 = 0.03$ RADIANS
 NO ALLOWANCE HAS BEEN MADE FOR GROUND REFLECTION

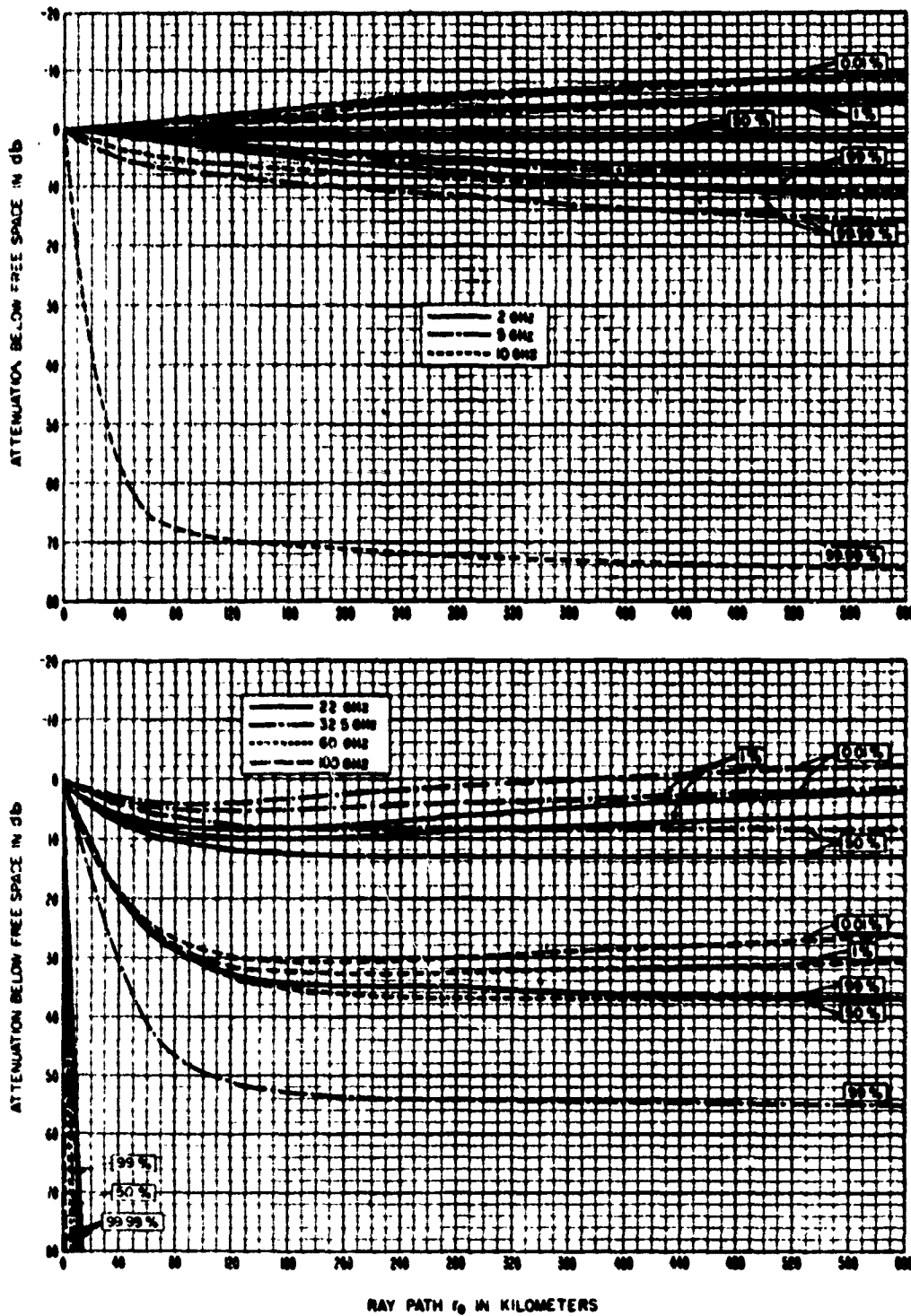


Figure I.22

STANDARD PROPAGATION CURVES FOR EARTH-SPACE LINKS
 $\theta_0 = 0.1$ RADIANS
 NO ALLOWANCE HAS BEEN MADE FOR GROUND REFLECTION

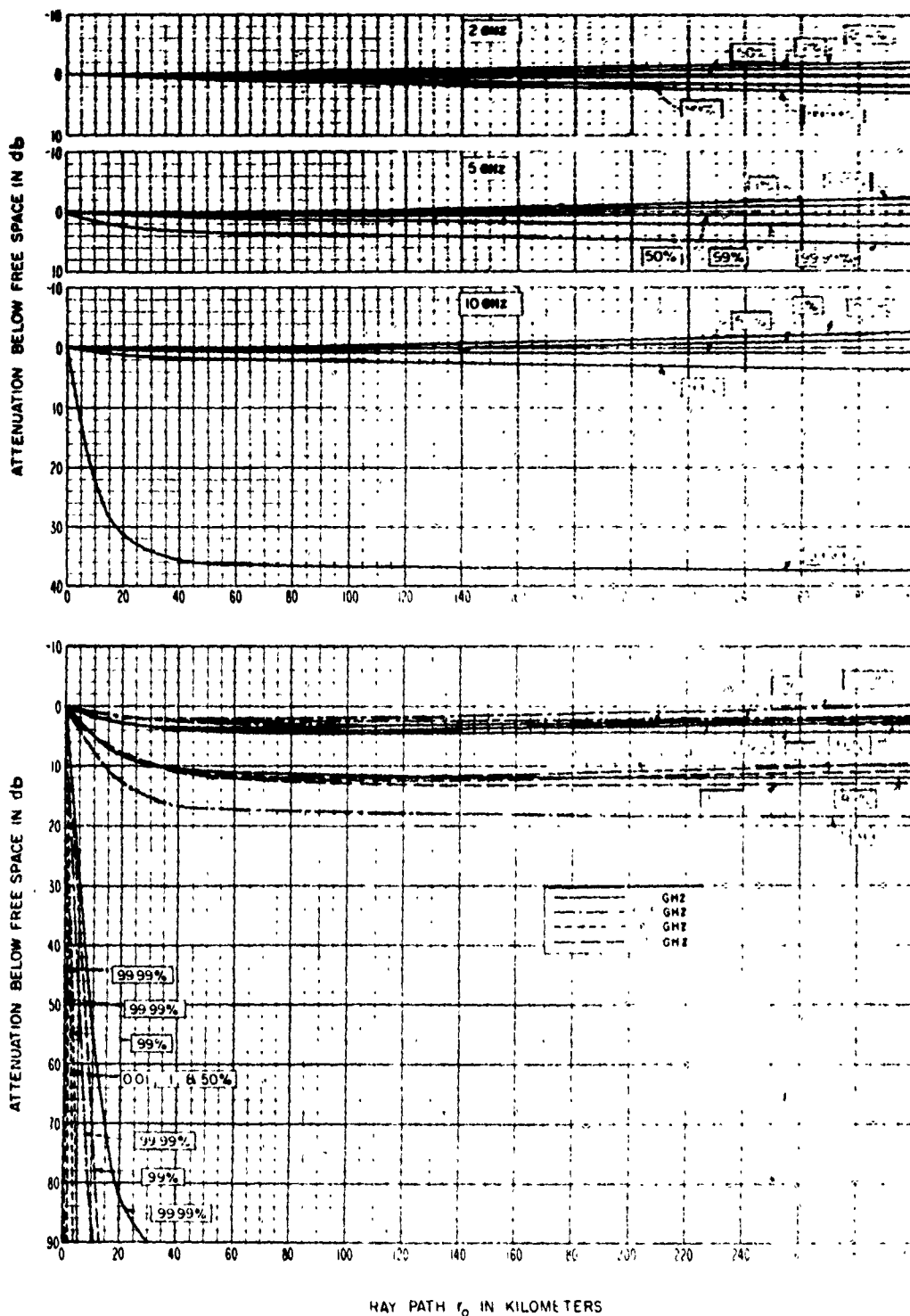


Figure 1.23

STANDARD PROPAGATION CURVES FOR EARTH-SPACE LINKS
 $\epsilon_0 = 0.3$ RADIIAS
 NO ALLOWANCE HAS BEEN MADE FOR GROUND REFLECTION

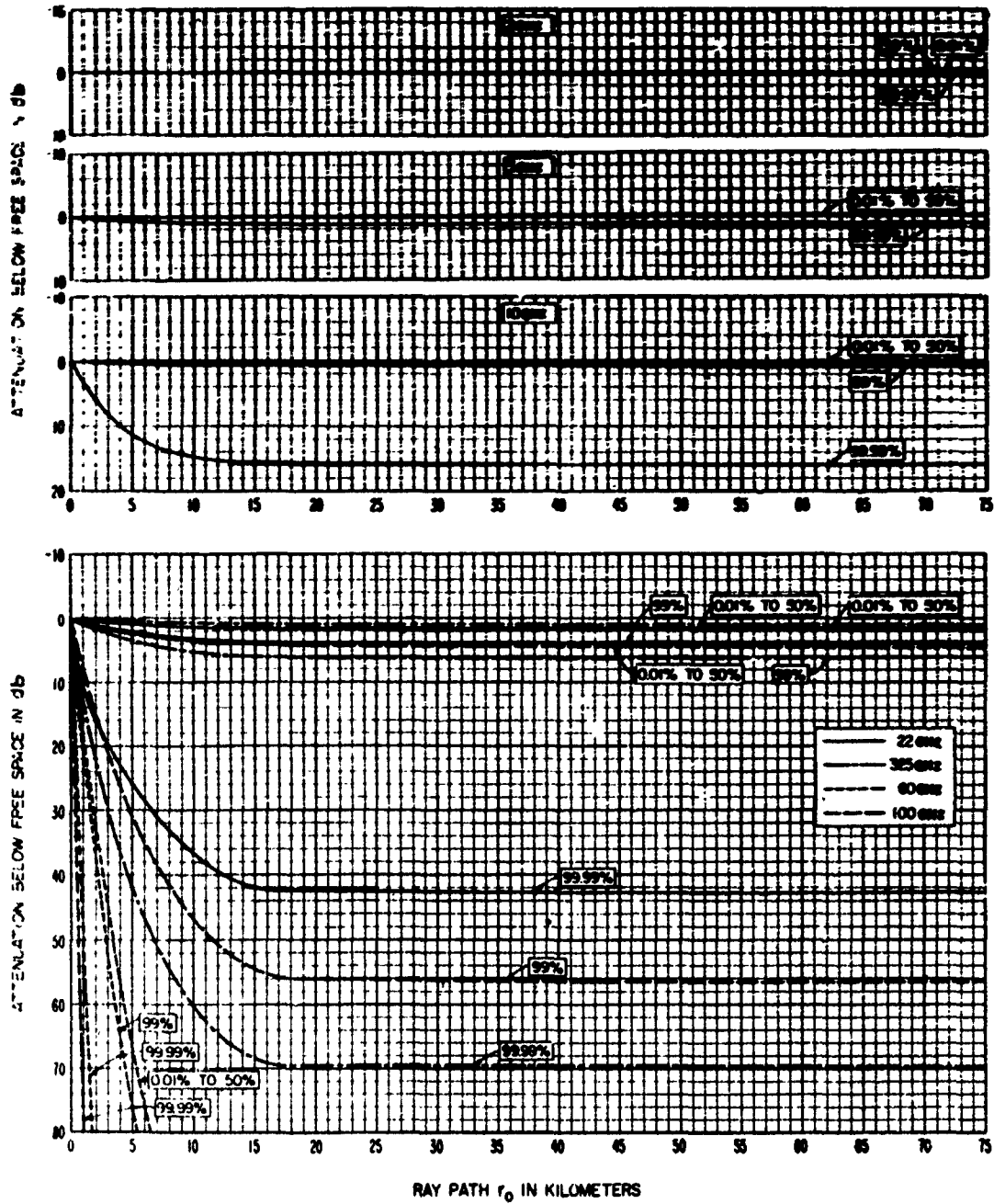


Figure 1.24

STANDARD PROPAGATION CURVES FOR EARTH-SPACE LINKS

$\theta_0 = 10$ RADIAN

NO ALLOWANCE HAS BEEN MADE FOR GROUND REFLECTION

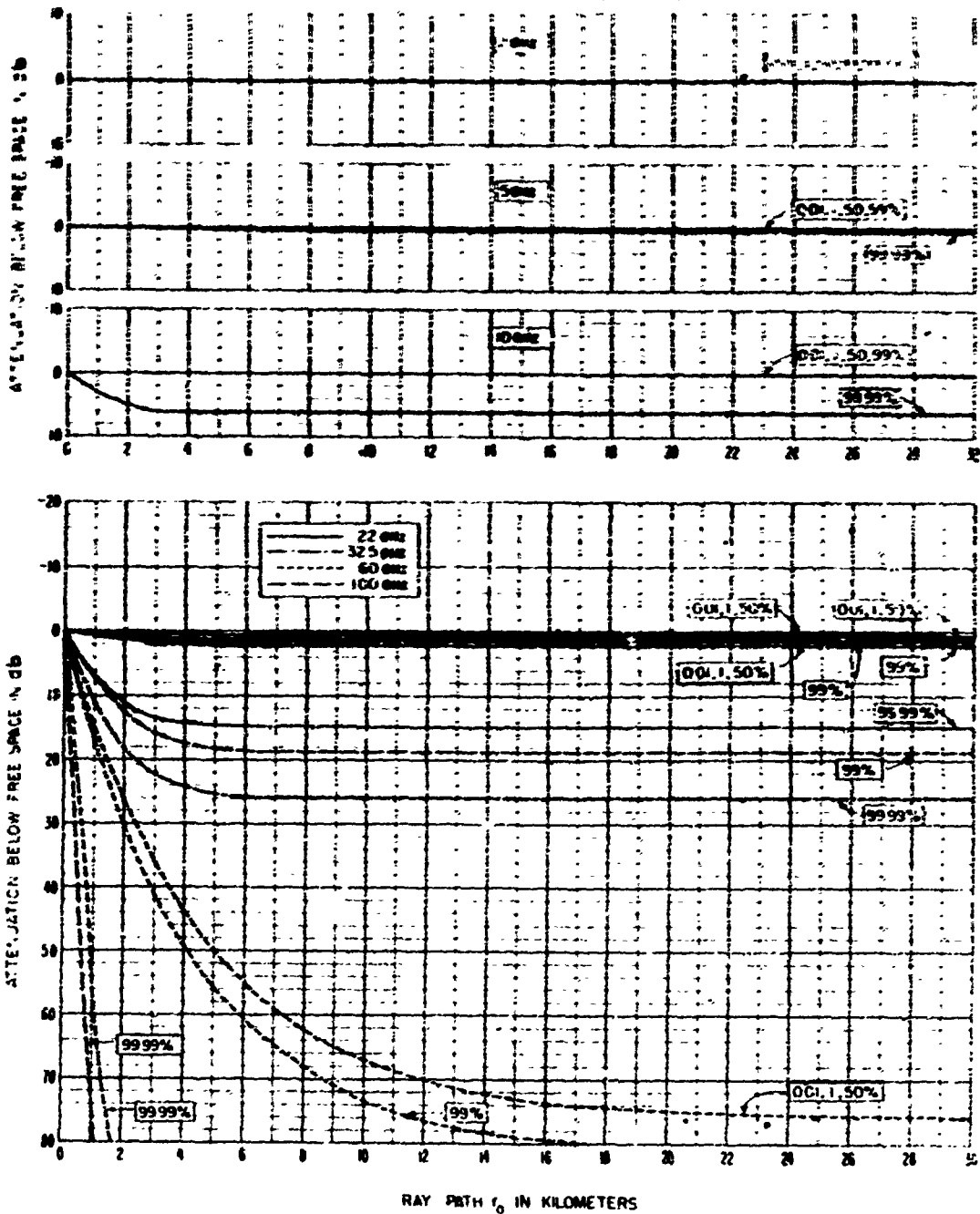


Figure 1.25

STANDARD PROPAGATION CURVES FOR EARTH-SPACE LINKS

$$Q = 1/2$$

NO ALLOWANCE HAS BEEN MADE FOR GROUND REFLECTION

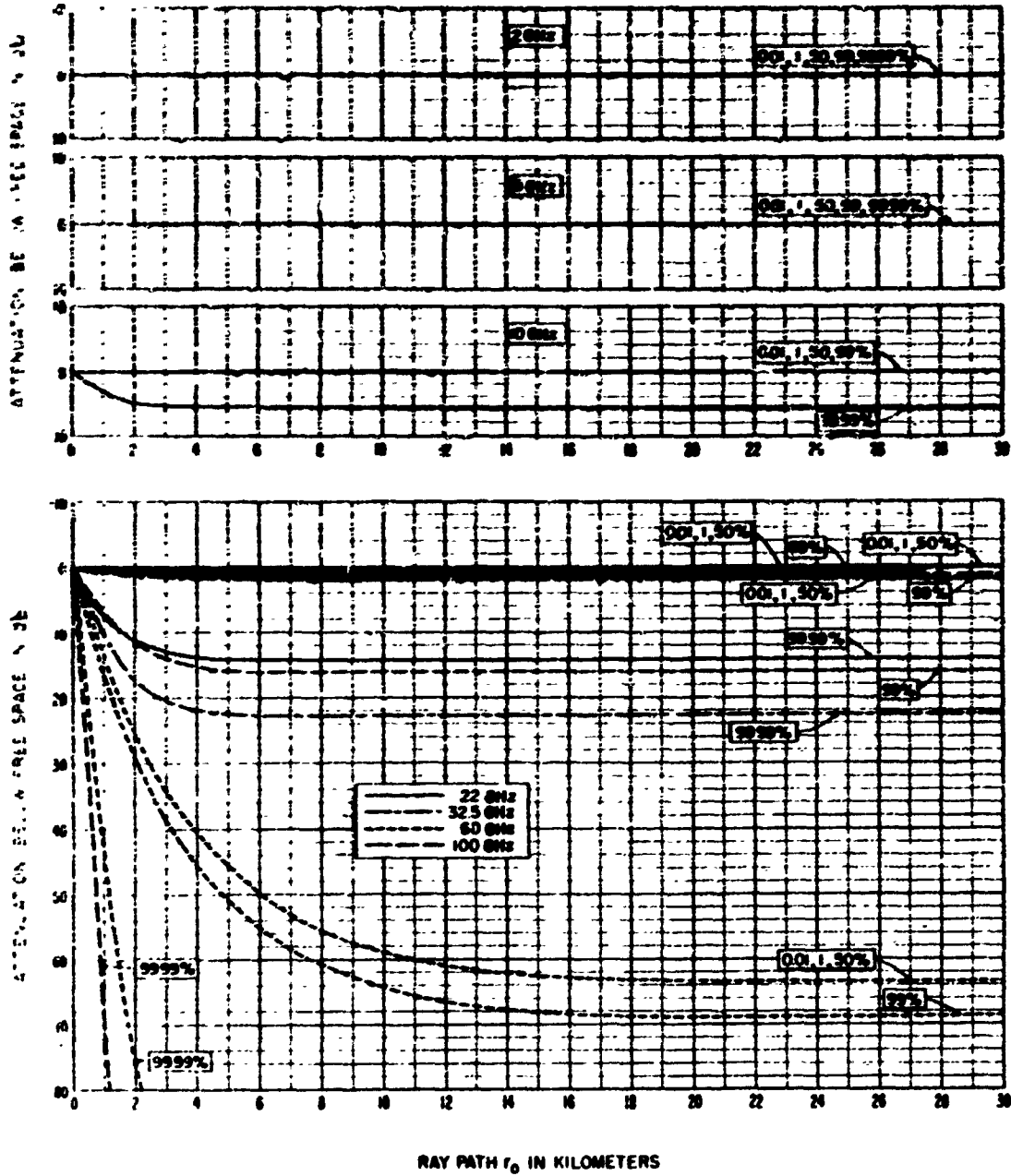


Figure I.26

I.3 Preliminary Reference Values of Attenuation Relative to Free Space, A_{cr}

I.3.1 Introduction

Three main elements of the problem of prediction are the intended application, the characteristics of available data, and the basis of relevant propagation models. The theoretical basis of the model proposed here is simple, and its advantages and limitations are easily demonstrated. Preliminary comparisons with data indicate standard errors of prediction considerably greater than those associated with the specific methods described in volume 1, which are designed for particular applications. However, the method described below is especially useful when little is known of the details of terrain; it may readily be programmed for a digital computer; and it is adequate for most applications where a preliminary calculated reference value A_{cr} of attenuation relative to free space is desired. The minimum prediction parameters required are frequency, path distance, and effective antenna heights. For the other parameters mentioned typical values are suggested for situations where accurate values are not known.

For radio line-of-sight paths the calculated reference value A_{cr} is either a "foreground attenuation" A_f or an extrapolated value of diffraction attenuation A_d , whichever is greater. For transhorizon paths, A_{cr} is either equal to A_d or to a forward scatter attenuation A_s , whichever is smaller.

I.3.2 The Terrain Roughness Factor Δh

Different types of terrain are distinguished according to the value of a terrain roughness factor Δh . This is the interdecile range of terrain heights in meters above and below a straight line fitted to the average slope of the terrain. When terrain profiles are available Δh is obtained by plotting terrain heights above sea level, fitting a straight line by least squares to define the average slope and obtaining a cumulative distribution of deviations of terrain heights from the straight line. Ordinarily Δh will increase with distance to an asymptotic value. This is the value to be used in these computations.

When terrain profiles are not available estimates of Δh may be obtained from the following table:

TABLE I.1

Type of Terrain	Δh (meters)
Water or very smooth terrain	0-1
Smooth terrain	10-20
Slightly rolling terrain	40-60
Hilly terrain	80-150
Rugged mountains	200-500

I. 3.3 The Diffraction Attenuation A_d

If the earth is smooth $A_d = R$ is computed using the method described in section 8 of volume 1. If the terrain is very irregular, the path is considered as though it were two simple knife edges: a) transmitter-first ridge-second ridge, and b) first ridge-second ridge-receiver. The total diffraction attenuation K is then the sum of the losses over each knife-edge.

$$K = A(v_1, 0) + A(v_2, 0) \quad (I.1)$$

These functions are defined by (I. 7) to (I. 12).

The main features of a transhorizon propagation path are the radio horizon obstacles, the radio horizon rays and the path distance d , which is greater than the sum d_L of the distances d_{Lt} and d_{Lr} to the radio horizons of the antennas. The diffraction attenuation A_d depends on d , d_{Lt} , d_{Lr} , the minimum monthly mean surface refractivity N_s , the radio frequency f in MHz, the terrain roughness factor Δh , and the sum θ_e of the elevations θ_{et} and θ_{er} of horizon rays above the horizontal at each antenna. The latter parameters may be measured, or may be calculated using (6. 15) of volume 1.

In general, the diffraction attenuation A_d is a weighted average of K and R plus an allowance A_{bs} for absorption and scattering by oxygen, water vapor, precipitation, and terrain clutter:

$$A_d = (1 - \Lambda) K + \Lambda R + A_{bs} \quad (I.2)$$

where Λ is an empirical weighting factor:

$$\Lambda = \left[1 + 0.045 \left(\frac{\Delta h}{\lambda} \right)^{\frac{1}{2}} \left(\frac{a \theta + d_L}{d} \right)^{\frac{1}{2}} \right]^{-1} \quad (I.3)$$

$$d_L = d_{Lt} + d_{Lr} \quad \text{km} \quad (I.4)$$

$$\theta = \theta_e + d/a \quad \text{radians,} \quad (I.5)$$

$$a = 6370 / [1 - 0.04665 \exp(0.005577 N_s)] \quad (I.6)$$

The angular distance θ is in radians and the wavelength λ is expressed in meters. The parameter $(a\theta + d_L)/d$ in (I.5) is unity for a smooth earth, where $\Delta h/\lambda$ is small and $\Lambda \approx 1$. For very irregular terrain, both $\Delta h/\lambda$ and $(a\theta + d_L)/d$ tend to be large so that $\Lambda \approx 0$.

The following set of formulas used to calculate K and R are consistent with sections 7 and 8, volume 1.

$$v_{1,2} = 1.2915 \theta \left[f d_{Lt,r} (d-d_L) / (d-d_L + d_{Lt,r}) \right]^{\frac{1}{2}} \quad (I.7)$$

$$A(v, 0) = \begin{cases} 6.02 + 9.11 v - 1.27 v^2 & \text{for } 0 < v \leq 2.4 \\ 12.953 + 20 \log v & \text{for } v > 2.4 \end{cases} \quad (I.8)$$

$$R = G(x_0) - F(x_1) - F(x_2) - C_1(K_{1,2}) \quad (I.9)$$

$$x_1 = B_{01} d_{Lt}, \quad x_2 = B_{02} d_{Lr}, \quad x_0 = B_{0s} D_s + x_1 + x_2 \quad (I.10)$$

$$B_{01} = f^{\frac{1}{3}} C_{01}^2 B_1, \quad B_{02} = f^{\frac{1}{3}} C_{02}^2 B_2, \quad B_{0s} = f^{\frac{1}{3}} C_{0s}^2 B_s$$

$$C_{01} = (8497/a_1)^{\frac{1}{3}}, \quad C_{02} = (8497/a_2)^{\frac{1}{3}}, \quad C_{0s} = (8497/a_s)^{\frac{1}{3}} \quad (I.11)$$

$$a_1 = d_{Lt}^2 / (2 h_{te}), \quad a_2 = d_{Lr}^2 / (2 h_{re}), \quad a_s = D_s / \theta \quad (I.12)$$

If the path distance d is less than d_3 as given by (I.13), it is advisable to calculate A_d for larger distances d_3 and d_4 and to extrapolate a straight line through the points (A_{d_3}, d_3) and (A_{d_4}, d_4) back to the desired value (A, d) . The following is suggested for d_3 and d_4 :

$$d_3 = d_L + 0.5 (a^2/f)^{\frac{1}{3}} \text{ km}, \quad d_4 = d_3 + (a^2/f)^{\frac{1}{3}} \text{ km} \quad (I.13)$$

I.3.4 The Forward Scatter Attenuation, A_s

The scatter attenuation A_s for a transhorizon path depends on the parameters d , N_s , f , θ , h_{te} , h_{re} and A_{bs} . If the product θd of the angular distance θ and the distance d is

greater than 0.5, the forward scatter attenuation A_s is calculated for comparison with A_d :

$$A_s = \begin{cases} S + 103.4 + 0.332 \theta d - 10 \log(\theta d) & \text{for } 0.5 < \theta d \leq 10 \\ S + 97.1 + 0.212 \theta d - 2.5 \log(\theta d) & \text{for } 10 \leq \theta d \leq 70 \\ S + 86.8 + 0.157 \theta d + 5 \log(\theta d) & \text{for } \theta d \geq 70 \end{cases} \quad (I.14)$$

$$S = H_o + 10 \log(f \theta^4) - 0.1 (N_s - 301) \exp(-\theta d/40) + A_{bs} \quad (I.15)$$

$$H_o = \left[\frac{1}{h_{te}} + \frac{1}{h_{re}} \right] / \left[\theta f |0.007 - 0.058 \theta| \right] \text{ or}$$

$$H_o = 15 \text{ db, whichever is smaller.} \quad (I.16)$$

The reference attenuation $A_{cr} = A_s$ if $A_s < A_d$.

I.3.5 Radio Line-of-Sight Paths

For line-of-sight paths the attenuation relative to free space increases abruptly as d approaches d_L , so an estimate of d_L is required in order to obtain A_{cr} . For sufficiently high antennas, or a sufficiently smooth earth, (see [I.18]), d_{Lt} and d_{Lr} are expected to equal the smooth earth values d_{Lst} and d_{Lsr} :

$$d_{Lst} = \sqrt{0.002 a h_{te}} \text{ km, } d_{Lsr} = \sqrt{0.002 a h_{re}} \text{ km} \quad (I.17)$$

where a is the effective earth's radius in kilometers and h_{te} , h_{re} are heights in meters above a single reflecting plane which is assumed to represent the dominant effect of the terrain between the antennas or between each antenna and its radio horizon. The effective reflecting plane is usually determined by inspection of the portion of terrain which is visible to both antennas.

For a "typical" or "median" path and a given type of terrain d_{Lt} and d_{Lr} may be estimated as

$$d_{Lt} = d_{Lst} [1 \pm 0.9 \exp(-1.5 \sqrt{h_{te}/h})] \text{ km} \quad (I.18a)$$

$$d_{Lr} = d_{Lsr} [1 \pm 0.9 \exp(-1.5 \sqrt{h_{re}/h})] \text{ km.} \quad (I.18b)$$

If for a median path an antenna is located on a hilltop, the plus sign in the corresponding square bracket in (I.18a) or (I.18b) is used, and if the antenna is behind a hill, the minus sign is used. If $d_L = d_{Lt} + d_{Lr}$ is less than a known line-of-sight path distance d , the estimates (I.18a) and (I.18b) are each increased by the ratio (d/d_L) so that $d_L = d$.

For example, in a broadcasting situation with $h_{te} = 150$ meters, $h_{re} = 10$ meters, and $\Delta h = 50$ meters, (I. 18) using minus signs indicates that $d_{Lt} = 0.97 d_{Lst}$ and $d_{Lr} = 0.63 d_{Lsr}$.

For small grazing angles, (5.6) and (5.9) of volume 1 may be combined to describe line-of-sight propagation over a perfectly-conducting smooth plane earth:

$$A = 20 \log \left[\frac{\lambda d - 10^3}{4\pi h_{te} h_{re}} \right] \text{ db} \quad (\text{I. 19})$$

where d is in kilometers and h_{te} , h_{re} , and the radio wavelength λ are in meters. This formula is not applicable for small values of $\lambda d / (h_{te} h_{re})$, where the median value of A is expected to be zero. It is proposed therefore to add unity to the argument of the logarithm in (I. 19).

The expression (I. 19) is most useful when d is large and nearly equal to d_L . Better agreement with data is obtained if d is replaced by d_L and the constant $10^3 / (4\pi)$ is replaced by $\Delta h / \lambda$, the terrain roughness factor expressed in wavelengths. Accordingly, the foreground attenuation factor A_f can be written as

$$A_f = 20 \log \left[1 + d_L \Delta h / (h_{te} h_{re}) \right] + A_{bs} \text{ db.} \quad (\text{I. 20})$$

The absorption A_{bs} defined following (I. 2) is discussed in sections 3 and 5 of volume 1. For frequencies less than 10,000 MHz the major component of A_{bs} is usually due to terrain clutter such as vegetation, buildings, bridges, and power lines.

For distances small enough so that A_f is greater than the diffraction attenuation extrapolated into the line-of-sight region, the calculated attenuation relative to free space A_{cr} is given by (I. 20) and depends only on h_{te} , h_{re} , Δh , A_{bs} and an estimate of d_L . For long line-of-sight paths, the foreground attenuation given by (I. 20) is less than the extrapolated diffraction attenuation A_d , so $A_{cr} = A_d$.

If d_{Lt} , d_{Lr} , and θ_e are known, these values are used to calculate A_d . Otherwise, (I. 18) may be used to estimate d_{Lt} and d_{Lr} , and θ_e is calculated as the sum of a weighted average of estimates of θ_{et} and θ_{er} for smooth and rough earth. For a smooth earth,

$$\theta_{et, r} = -0.002 h_{te, re} / d_{Lt, r} \text{ radians,}$$

and for extremely irregular terrain it has been found that median values are nearly

$$\theta_{et, r} = (\Delta h / 2) / (d_{Lt, r} \cdot 10^3) \text{ radians.}$$

Using $d_{Lt, r} / d_{Lst, r}$ and $(1 - d_{Lt, r} / d_{Lst, r})$ respectively as weights, the following formula is suggested for estimating $\theta_{et, r}$ when this parameter is unknown:

$$\theta_{ct, r} = \frac{0.0005}{d_{Lst, r}} \left[\left(\frac{d_{Lst, r}}{d_{Lt, r}} - 1 \right) \Delta h - 4 h_{te, re} \right] \text{ radians} \quad (I. 21a)$$

$$\theta_e = \theta_{et} + \theta_{er} \text{ or } \theta_e = -d_L/a, \text{ whichever is larger algebraically.} \quad (I. 21b)$$

As explained following (I. 12), the formulas for A_d require a path distance d greater than d_3 . If a line-of-sight path d is always less than d_L , so A_d is calculated for the distances d_3 and d_4 given by (I. 13) and a straight line through the points (A_3, d_3) and (A_4, d_4) is extrapolated back to the desired value (A, d) . This straight line has the formula

$$A_d = A_e + Md \text{ db} \quad (I. 22)$$

where

$$M = (A_{d_4} - A_{d_3}) / (d_4 - d_3) \text{ db/km} \quad (I. 23)$$

$$A_e = A_{d_4} - Md_4 \text{ db.} \quad (I. 24)$$

The straight line given by (I. 22) intersects the level A_f where the path distance is

$$d_f = (A_f - A_e) / M \text{ km.} \quad (I. 25)$$

$$\text{For } d \leq d_f, \quad A_{cr} = A_f. \quad (I. 26a)$$

$$\text{For } d > d_f, \quad A_{cr} = A_d. \quad (I. 26b)$$

I. 3.6 Ranges of the Prediction Parameters

These estimates of A_{cr} are intended for the following ranges of the basic parameters:

TABLE I. 2

$20 \leq f \leq 40,000 \text{ MHz}$	$1 \leq d \leq 2000 \text{ km}$
$\lambda/2 \leq h_{te, re} \leq 10,000 \text{ m}$	$250 \leq N_s \leq 400$
$-d_L/a \leq \theta_e \leq 0.2 \text{ radians}$	$0 \leq A_{bs} \leq 50 \text{ db}$
$0.1 d_{Lst} \leq d_{Lt} \leq 3 d_{Lst}$	$0.1 d_{Lsr} \leq d_{Lr} \leq 3 d_{Lsr}$
$0 \leq \Delta h \leq 500 \text{ m}$	

I.3.7 Sample Calculations

Table I.3 lists a set of sample calculations referring to the example introduced after Table I.1. Values for the following independent parameters are assumed: $h_{te} = 150$ m, $h_{re} = 10$ m, $\Delta h = 50$ m, $N_s = 301$, $f = 700$ MHz, $d_{Lt} = 49.0$ km, $d_{Lr} = 8.2$ km, $\theta_e = -0.00634$ radians, $A_{bs} = 0$ db. An appropriate equation number is listed in parentheses after each of the calculated parameters in Table I.3. For these calculations the arbitrary distance d_3 was set equal to $d_L + 1$ instead of $d_L + 0.3(a^2/f)^{1/2}$.

TABLE I.3

$d_L = 57.2$ km	(I.4)	$a = 8493$ km	(I.6)
$\Delta h/\lambda = 116.8$		$A_f = 9.3$ db	(I.20)
$d_3 = 58.2$ km		$d_4 = 105.1$ km	(I.13)
$\theta_3 = 0.000514$ rad.		$\theta_4 = 0.00603$ rad.	(I.5)
$v_3 = 0.096$		$v_4 = 1.95$	(I.7)
$v_{13} = 0.0174$		$v_{14} = 1.014$	(I.8)
$v_{23} = 0.0166$		$v_{24} = 0.546$	(I.8)
$v_3 \rho_3 = 0.10$		$v_4 \rho_4 = 1.87$	(I.9)
$\rho_3 = 1.04$		$\rho_4 = 0.96$	(I.9)
$A(v_3, 0) = 6.9$ db		$A(v_4, 0) = 18.9$ db	(I.10)
$A(v_{13}, 0) = 6.2$ db		$A(v_{14}, 0) = 14.0$ db	(I.10)
$A(v_{23}, 0) = 6.2$ db		$A(v_{24}, 0) = 10.6$ db	(I.10)
$A(0, \rho_3) = 16.0$ db		$A(0, \rho_4) = 14.7$ db	(I.11)
$U(v_3, \rho_3) = -.9$ db		$U(v_4, \rho_4) = 14.7$ db	(I.12)
$K_3 = 12.4$ db		$K_4 = 24.6$ db	(I.6)
$R_3 = 18.1$ dB		$R_4 = 55.3$ db	(I.5)
$\frac{a \theta_3 + d_L}{d_3} = 1.058$		$\frac{a \theta_4 + d_L}{d_4} = 1.032$	
$\Lambda_3 = 0.667$		$\Lambda_4 = 0.669$	(I.3b)
$A_{d_3} = 29.5$ db		$A_{d_4} = 58.5$ db	(I.3a)
$d_3 \theta_3 = 0.0299$		$d_4 \theta_4 = 0.634$	
		$H_{04} = 3.8$ db	(I.16)
		$S_4 = -56.5$ db	(I.15)
		$A_{S4} = 49.1$ db	(I.14)
$A_{cr_3} = 29.5$ db		$A_{cr_4} = 49.1$ db	

For this example, $M = 0.619$ db/km, $\Lambda_e = -0.49$ db, and $d_l = 25.5$ km. The corresponding basic transmission loss L_{bcr} and field strength E_{bcr} for distances less than d_f are $98.65 + 20 \log d$ db and $97.62 - 20 \log d$ db, respectively, corresponding to a constant value $A_{cr} = A_f = 9.3$ db. In general:

CCP 702-1

$$L_{\text{bcr}} = 32.45 + 20 \log d + 20 \log f + A_{\text{cr}} \text{ db} \quad (\text{I.27})$$

$$E_{\text{bcr}} = 106.92 - 20 \log d - A_{\text{cr}} \text{ db} \quad (\text{I.28})$$

For the example given above, $L_{\text{bcr}_3} = 154.2 \text{ db}$, $L_{\text{bcr}_4} = 178.9 \text{ db}$, $E_{\text{bcr}_3} = 42.1 \text{ db}$, and $E_{\text{bcr}_4} = 17.4 \text{ db}$.

Annex II

AVAILABLE POWER, FIELD STRENGTH AND MULTIPATH COUPLING LOSS

II.1 Available Power from the Receiving Antenna

The definitions of system loss and transmission loss in volume 1 depend on the concept of available power, the power that would be delivered to the receiving antenna load if its impedance were conjugately matched to the receiving antenna impedance. For a given radio frequency ν in hertz, let z_{lv} , z'_v , and z_v represent the impedances of the load, the actual lossy antenna in its actual environment, and an equivalent loss-free antenna, respectively:

$$z_{lv} = r_{lv} + ix_{lv} \quad (\text{II. 1a})$$

$$z'_v = r'_v + ix'_v \quad (\text{II. 1b})$$

$$z_v = r_v + ix_v \quad (\text{II. 1c})$$

where r and x represent resistance and reactance, respectively. Let w_{lv} represent the power delivered to the receiving antenna load and write w'_{av} and w_{av} , respectively, for the available power at the terminals of the actual receiving antenna and at the terminals of the equivalent loss-free receiving antenna. If v'_v is the actual open-circuit r.m.s. voltage at the antenna terminals, then

$$w_{lv} = \frac{v'^2_v r_{lv}}{|z'_v + z_{lv}|^2} \quad (\text{II. 2})$$

When the load impedance conjugately matches the antenna impedance, so that $z_{lv} = z'^*_v$ or $r_{lv} = r'_v$ and $x_{lv} = -x'_v$, (II. 2) shows that the power w_{lv} delivered to the load is equal to the power w'_{av} available from the actual antenna:

$$w'_{av} = \frac{v'^2_v}{4 r'_v} \quad (\text{II. 3})$$

Note that the available power from an antenna depends only upon the characteristics of the antenna, its open-circuit voltage v'_v , and the resistance r'_v , and is independent of the load

impedance. Comparing (II. 2) and (II. 3), we define a mismatch loss factor

$$l_{mv} = \frac{w_{av}^i}{w_{lv}^i} = \frac{(r_v^i + r_{lv}^i)^2 + (x_v^i + x_{lv}^i)^2}{4 r_v^i r_{lv}^i} \quad (\text{II. 4})$$

such that the power delivered to a load equals w_{av}^i / l_{mv} . When the load impedance conjugately matches the antenna impedance, l_{mv} has its minimum value of unity, and $w_{lv}^i = w_{av}^i$. For any other load impedance, somewhat less than the available power is delivered to the load. The power available from the equivalent loss-free antenna is

$$w_{av} = \frac{v_v^2}{4 r_v} \quad (\text{II. 5})$$

where v_v is the open circuit voltage for the equivalent loss-free antenna.

Comparing (II. 3) and (II. 5), it should be noted that the available power w_{av}^i at the terminals of the actual lossy receiving antenna is less than the available power $w_{av} = l_{erv} w_{av}^i$ for a loss-free antenna at the same location as the actual antenna:

$$l_{erv} = \frac{w_{av}}{w_{av}^i} = \frac{r_v^i v_v^2}{r_v v_v^2} \approx 1. \quad (\text{II. 6})$$

The open circuit voltage v_v^i for the actual lossy antenna will often be the same as the open circuit voltage v_v for the equivalent loss-free antenna, but each receiving antenna circuit must be considered individually.

Similarly, for the transmitting antenna, the ratio of the total power w_{tv}^i delivered to the antenna at a frequency ν is l_{etv} times the total power w_{tv} radiated at the frequency ν :

$$l_{etv} = w_{tv}^i / w_{tv} \quad (\text{II. 7})$$

The concept of available power from a transmitter is not a useful one, and l_{etv} for the transmitting antenna is best defined as the above ratio. However, the magnitude of this ratio can be obtained by calculation or measurement by treating the transmitting antenna as a receiving antenna and then determining l_{etv} to be the ratio of the available received powers from the equivalent loss-free and the actual antennas, respectively.

General discussions of l_{erv} are given by Crichlow et al. [1955] and in a report prepared under CCIR Resolution No. 1 [Geneva 1963c]. The loss factor l_{erv} was successfully

determined in one case by measuring the power w_{tv} radiated from a loss-free target transmitting antenna and calculating the transmission loss between the target transmitting antenna and the receiving antenna. There appears to be no way of directly measuring either l_{erv} or l_{etv} without calculating some quantity such as the radiation resistance or the transmission loss. In the case of reception with a unidirectional rhombic terminated in its characteristic impedance, l_{erv} could theoretically be greater than 2 [Harper, 1941], since nearly half the received power is dissipated in the terminating impedance and some is dissipated in the ground. Measurements were made by Christiansen [1947] on single and multiple wire units and arrays of rhombics. The ratio of power lost in the termination to the input power varied with frequency and was typically less than 3 db.

For the frequency band ν_l to ν_m it is convenient to define the effective loss factors L_{er} and L_{et} as follows:

$$L_{er} = 10 \log \frac{\int_{\nu_l}^{\nu_m} (d w_{av}/d\nu) d\nu}{\int_{\nu_l}^{\nu_m} (d w_{av}'/d\nu) d\nu} \text{ db} \quad (\text{II. 8})$$

$$L_{et} = 10 \log \frac{\int_{\nu_l}^{\nu_m} (d w_{tv}'/d\nu) d\nu}{\int_{\nu_l}^{\nu_m} (d w_{tv}/d\nu) d\nu} \text{ db} \quad (\text{II. 9})$$

The limits ν_l and ν_m on the integrals (II. 8) and (II. 9) are chosen to include essentially all of the wanted signal modulation side bands, but ν_l is chosen to be sufficiently large and ν_m sufficiently small to exclude any appreciable harmonic or other unwanted radiation emanating from the wanted signal transmitting antenna.

II.2 Propagation Loss and Field Strength

This subsection defines terms that are most useful at radio frequencies lower than those where tropospheric propagation effects are dominant.

Repeating the definitions of r and r' used in subsection II.1, and introducing the new parameter r_f :

$r_{t,r}$ = antenna radiation resistance,

$r'_{t,r}$ = resistance component of antenna input impedance,

r_{ft}, r_{fr} = antenna radiation resistance in free space,

where subscripts t and r refer to the transmitting antenna and receiving antenna, respectively. Next define

$$L_{et} = 10 \log (r'_{t}/r_t), \quad L_{er} = 10 \log (r'_{r}/r_r) \quad (\text{II. 10})$$

$$L_{ft} = 10 \log (r'_{t}/r_{ft}), \quad L_{fr} = 10 \log (r'_{r}/r_{fr}) \quad (\text{II. 11})$$

$$L_{rt} = 10 \log (r_t/r_{ft}) = L_{ft} - L_{et} \quad (\text{II. 12})$$

$$L_{rr} = 10 \log (r_r/r_{fr}) = L_{fr} - L_{er} \quad (\text{II. 13})$$

[Actually, (II.8) and (II.9) define L_{et} and L_{er} while (II.10) defined r_t and r_r , given r'_t and r'_r].

Propagation loss first defined by Wait [1959] is defined by the CCIR [1963a] as

$$L_p = L_s - L_{ft} - L_{fr} = L - L_{rt} - L_{rr} \text{ db.} \quad (\text{II. 14})$$

Basic propagation loss is

$$L_{pb} = L_p + G_p. \quad (\text{II. 15})$$

Basic propagation loss in free space is the same as the basic transmission loss in free space, L_{bf} , defined by (II. 74).

The system loss L_s defined by (2.1) is a measurable quantity, while transmission loss L , path loss L_o , basic transmission loss L_p , attenuation relative to free space A , propagation loss L_p , and the field strength E are derived quantities, which in general require a theoretical calculation of L_{et}, L_{er} and/or L_{ft}, L_{fr} as well as a theoretical estimate of the loss in path antenna gain L_{gp} .

The following paragraphs explain why the concepts of effective power, and an equivalent plane wave field strength are not recommended for reporting propagation data.

A half-wave antenna radiating a total of w_t watts produces a free space field intensity equal to

$$s_o = 1.64 w_t / (4\pi r^2) \text{ watts/km}^2 \quad (\text{II. 16})$$

at a distance r kilometers in its equatorial plane, where the directive gain is equal to its maximum value 1.64, or 2.15 db. The field is linearly polarized in the direction of the antenna. In general, the field intensity s_p at a point \vec{r} in free space and associated with the principal polarization for an antenna is

$$s_p(\vec{r}) = w_t g_p(\hat{r}) / (4\pi r^2) \text{ watts/km}^2 \quad (\text{II. 17})$$

as explained in a later subsection. In (II. 17), $\vec{r} = r \hat{r}$ and $g_p(\hat{r})$ is the principal polarization directive gain in the direction \hat{r} . A similar relation holds for the field intensity $s_c(\vec{r})$ associated with the cross-polarized component of the field.

Effective radiated power is associated with a prescribed polarization for a test antenna and is determined by comparing s_o as calculated using a field intensity meter or standard signal source with s_p as measured using the test antenna:

$$\text{Effective Radiated Power} = W_t + 10 \log(s_p / s_o) = W_t + G_{pt}(\hat{r}_1) - 2.15 \text{ dbw} \quad (\text{II. 18})$$

where $G_{pt}(\hat{r}_1)$ is the principal polarization directive gain relative to a half-wave dipole in the direction \hat{r}_1 towards the receiving antenna in free space, and in general is the initial direction of the most important propagation path to the receiver.

These difficulties in definition, together with those which sometimes arise in attempting to separate characteristics of an antenna from those of its environment, make the effective radiated power an inferior parameter, compared with the total radiated power W_t , which can be more readily measured. The following equation, with W_t determined from (II. 18), may be used to convert reported values of Effective Radiated Power to estimates of the transmitter power output W_{lt} when transmission line and mismatch losses L_{lt} and the power radiation efficiency $1/l_{et}$ are known:

$$W_{lt} = W_t + L_{lt} = W_t + L_{et} + L_{lt} \text{ dbw} \quad (\text{II. 19})$$

The electromagnetic field is a complex vector function in space and time, and information about amplitude, polarization, and phase is required to describe it. A real antenna responds to the total field surrounding it, rather than to E , which corresponds to the r. m. s. amplitude of the usual "equivalent" electromagnetic field, defined at a single point and for a specified polarization.

Consider the power averaged over each half cycle as the "instantaneous" available signal power, w_v

$$w_v = v^2/R_v \text{ watts}$$

where v is the r.m.s. signal voltage and R_v is the real part of the impedance of the receiving antenna, expressed in ohms. The signal power w_v available from an actual receiving antenna is a directly measurable quantity.

The field strength and power flux density, on the other hand, cannot be measured directly, and both depend on the environment. In certain idealized situations the relationship of field strength e , and power flux density, s , to the available power may be expressed as

$$s = e^2/z = w_v 4\pi/(g\lambda^2) \text{ watts/m}^2$$

where e is the r.m.s. electric field strength in volts/m, z is the impedance in free space in ohms, λ is the free space wavelength in meters and g is the maximum gain of the receiving antenna.

The common practice of carefully calibrating a field strength measuring system in an idealized environment and then using it in some other environment may lead to appreciable errors, especially when high gain receiving antennas are used.

For converting reported values of E in dbu to estimates of W_{ft} or estimates of the available power W_{fr} at the input to a receiver, the following relationships may be useful:

$$W_{ft} = E + L_{ft} + L_{fr} - G_t + L_{pb} - 20 \log f - 107.22 \text{ dbw} \quad (\text{II. 20})$$

$$W_{fr} = E - L_{fr} - L_{fr} + G_r - L_{gp} - 20 \log f - 107.22 \text{ dbw} \quad (\text{II. 21})$$

$$W_{fr} = W'_a - L_{fr} = W_a - L_{er} - L_{fr} \text{ dbw} \quad (\text{II. 22})$$

In terms of reported values of field strength E_{1kw} in dbu per kilowatt of effective radiated power, estimates of the system loss, L_s , basic propagation loss L_{pb} , or basic transmission loss L_b may be derived from the following equations,

$$L_s = 139.37 + L_{et} + L_{fr} - G_p + G_t - G_{pt}(\hat{r}_1) + 20 \log f - E_{1kw} \text{ db} \quad (\text{II. 23})$$

$$L_{pb} = 139.37 - L_{rt} + G_t - G_{pt}(\hat{r}_1) + 20 \log f - E_{1kw} \text{ db} \quad (\text{II. 24})$$

$$L_b = 139.37 + L_{rr} + G_t - G_{pt}(\hat{r}_1) + 20 \log f - E_{1kw} \text{ db} \quad (\text{II. 25})$$

provided that estimates are available for all of the terms in these equations.

For an antenna whose radiation resistance is unaffected by the proximity of its environment, $L_{rt} = L_{rr} = 0$ db, $L_{ft} = L_{et}$, and $L_{fr} = L_{er}$. In other cases, especially important for frequencies less than 30 MHz with antenna heights commonly used, it is often assumed that $L_{rt} = L_{rr} = 3.01$ db, $L_{ft} = L_{et} + 3.01$ db, and $L_{fr} = L_{er} + 3.01$ db, corresponding to the assumption of short vertical electric dipoles above a perfectly-conducting infinite plane. At low and very low frequencies, L_{et} , L_{er} , L_{ft} , and L_{fr} may be very large. Propagation curves at HF and lower frequencies may be given in terms of L_p or L_{pb} so that it is not necessary to specify L_{et} and L_{er} .

Naturally, it is better to measure L_s directly than to calculate it using (II.23). It may be seen that the careful definition of L_s , L_p , L , or L_o is simpler and more direct than the definition of L_b , L_{pb} , A , or E .

The equivalent free-space field strength E_o in dbu for one kilowatt of effective radiated power is obtained by substituting $W_{ft} = W_t = \text{Effective Radiated Power} = 30$ dbw, $G_{pt}(\hat{r}_1) = G_t = 2.15$ db, $L_{ft} = L_{et} = 0$ db, and $L_{pb} = L_{bf}$ in (II.18) - (II.20), where L_{bf} is given by (2.16):

$$E_o = 106.92 - 20 \log d \quad \text{dbu/kw} \quad (\text{II.26})$$

where r in (2.16) has been replaced by d in (II.26). Thus e_o is 222 millivolts per meter at one kilometer or 138 millivolts per meter at one mile. In free space, the "equivalent inverse distance field strength", E_I , is the same as E_o . If the antenna radiation resistances r_t and r_r are equal to the free space radiation resistances r_{ft} and r_{fr} , then (II.25) provides the following relationship between E_{1kw} and L_b with $G_{pt}(\hat{r}_1) = G_t$:

$$E_{1kw} = 139.37 + 20 \log f - L_b \quad \text{dbu/kw} \quad (\text{II.27})$$

Consider a short vertical electric dipole above a perfectly-conducting infinite plane, with an effective radiated power = 30 dbw, $G_t = 1.76$ db, and $L_{rr} = 3.01$ db. From (II.18) $W_t = 30.39$ dbw, since $G_{pt}(\hat{r}_1) = 1.76$ db. Then from (II.26) the equivalent inverse distance field is

$$E_I = E_o + L_{rt} + L_{rr} = 109.54 - 20 \log d \quad \text{dbu/kw} \quad (\text{II.28})$$

corresponding to $e_I = 300$ mv/m at one kilometer, or $e_I = 186.4$ mv/m at one mile. In this situation, the relationship between E_{1kw} and L_b is given by (II.25) as

$$E_{1kw} = 142.38 + 20 \log f - L_b \quad \text{dbu/kw} \quad (\text{II.29})$$

The foregoing suggests the following general expressions for the equivalent free space field strength E_o and the equivalent inverse distance field E_I :

$$E_o = (W_t - L_{rt} + G_t) - 20 \log d + 74.77 \quad \text{dbu} \quad (\text{II. 30})$$

$$E_I = E_o + L_{rt} + L_{rr} \quad \text{dbu} \quad (\text{II. 31})$$

Note that L_{rt} in (II. 30) is not zero unless the radiation resistance of the transmitting antenna in its actual environment is equal to its free space radiation resistance. The definition of "attenuation relative to free space" given by (2. 20) as the basic transmission loss relative to that in free space, may be restated as

$$A = L_b - L_{bf} = L - L_f = E_I - E_o \quad \text{db} \quad (\text{II. 32})$$

Alternatively, attenuation relative to free space, A_t , might have been defined (as it sometimes is) as basic propagation loss relative to that in free space:

$$A_t = L_{pb} - L_{bf} = A - L_{rt} - L_{rr} = E_o - E \quad \text{db} \quad (\text{II. 33})$$

For frequencies and antenna heights where these definitions differ by as much as 6 db, caution should be used in reporting data. For most paths using frequencies above 50 MHz, $L_{rt} + L_{rr}$ is negligible, but caution should again be used if the loss in path antenna gain L_{gp} is not negligible. It is then important not to confuse the "equivalent" free space loss L_f given by (2. 19) with the loss in free space given by (2. 18).

II.3 MULTIPATH COUPLING LOSS

Ordinarily, to minimize the transmission loss between two antennas, they are oriented to take advantage of maximum directive gains (directivity) and the polarizations are matched. This maximizes the path antenna gain. With a single uniform plane wave incident upon a receiving antenna, there will be a reduction in the power transferred if the antenna beam is not oriented for maximum free space gain. If the polarization of the receiving antenna is matched to that of the incident wave, this loss in path antenna gain is due to "orientation coupling loss", and if there is a polarization mismatch, there will be an additional "polarization coupling loss". In general, more than one plane wave will be incident upon a receiving antenna from a single source because of reflection, diffraction, or scattering by terrain or atmospheric inhomogeneities. Mismatch between the relative phases of these waves and the relative phases of the receiving antenna response in different directions will contribute to a "multipath coupling loss" which will include orientation, polarization, and phase mismatch effects. If multipath propagation involves non-uniform waves whose amplitudes, polarizations, and phases can only be described statistically, the corresponding loss in path antenna gain will include "antenna-to-medium coupling loss", a statistical average of phase incoherence effects.

This part of the annex indicates how multipath coupling loss may be calculated when incident waves are plane and uniform with known phases, and when the directivity, polarization, and phase response of the receiving antenna are known for every direction. It is assumed that the radiation resistance of the receiving antenna is unaffected by its environment, and that the electric and magnetic field vectors of every incident wave are perpendicular to each other and perpendicular to the direction of propagation.

II.3.1 Representation of Complex Vector Fields

Studying the response of a receiving antenna to coherently phased plane waves with several different directions of arrival, it is convenient to locate the receiving antenna at the center of a coordinate system. A radio ray traveling a distance r from a transmitter to the receiver may be refracted or reflected so that its initial and final directions are different: If $-\hat{f}$ is the direction of propagation at the receiver, $\vec{r} = \hat{f}r$ is the vector distance from the receiver to the transmitter if the ray path is a straight line, but not otherwise.

A paper by Kales [1951] shows how the amplitude, phase, and polarization of a uniform, monochromatic, elliptically polarized and locally plane wave may be expressed with the aid of complex vectors. For instance, such a wave may be expressed as the real part of the sum of two linearly polarized complex plane waves $\sqrt{2}\vec{e}_p \exp(i\tau)$ and $i\sqrt{2}\vec{e}_i \exp(i\tau)$. These components are in time phase quadrature and travel in the same direction $-\hat{f}$, where $i = \sqrt{-1}$ and \vec{e}_p and \vec{e}_i are real vectors perpendicular to \hat{f} . The vector $\vec{e}_p + i\vec{e}_i$ is then a complex vector. Field strengths are denoted in volts/km (10^3 microvolts per meter) and field intensities in watts/km² (10^{-3} milliwatts per square meter), since all lengths are in kilometers.

The time-varying phase

$$\tau = k(ct - r) \quad (\text{II. 34})$$

is a function of the free-space wavelength λ , the propagation constant $k = 2\pi/\lambda$, the free-space velocity of radio waves $c = 299792.5 \pm 0.3$ km/sec, the time t at the radio source, and the length of a radio ray between the receiver and the source.

Figure II-1 illustrates three sets of coordinates which are useful in studying the phase and polarization characteristics associated with the radiation pattern or response pattern of an antenna. Let $\vec{r} = fr$ represent the vector distance between the antenna and a distant point, specified either in terms of a right-handed cartesian unit vector coordinate system $\hat{x}_0, \hat{x}_1, \hat{x}_2$ or in terms of polar coordinates r, θ, ϕ :

$$\vec{r} = fr = \hat{x}_0 x_0 + \hat{x}_1 x_1 + \hat{x}_2 x_2, \quad r^2 = x_0^2 + x_1^2 + x_2^2 \quad (\text{II. 35a})$$

$$x_0 = r \cos \theta, \quad x_1 = r \sin \theta \cos \phi, \quad x_2 = r \sin \theta \sin \phi \quad (\text{II. 35b})$$

$$f = f(\theta, \phi) = \hat{x}_0 \cos \theta + (\hat{x}_1 \cos \phi + \hat{x}_2 \sin \phi) \sin \theta. \quad (\text{II. 35c})$$

As a general rule, either of two antennas separated by a distance r is in the far field or radiation field of the other antenna if $r > 2D^2/\lambda$, where D is the largest linear dimension of either antenna.

The amplitude and polarization of electric field vectors \vec{e}_θ and \vec{e}_ϕ , perpendicular to each other and to f , is often calculated or measured to correspond to the right-handed cartesian unit vector coordinate system $f, \hat{\delta}_\theta, \hat{\delta}_\phi$ illustrated in figure II-1. The unit vector $\hat{\delta}_\phi$ is perpendicular to f and \hat{x}_0 , and $\hat{\delta}_\theta$ is perpendicular to $\hat{\delta}_\phi$ and f . In terms of vector cross-products:

$$\hat{\delta}_\phi = (f \times \hat{x}_0) / \sin \theta = \hat{x}_1 \sin \phi - \hat{x}_2 \cos \phi \quad (\text{II. 36a})$$

$$\hat{\delta}_\theta = \hat{\delta}_\phi \times f = (\hat{x}_0 - f \cos \theta) / \sin \theta. \quad (\text{II. 36b})$$

The directive gain g , a scalar, may be expressed as the sum of directive gains g_θ and g_ϕ associated with polarization components $\vec{e}_\theta = \hat{e}_\theta e_\theta$ and $\vec{e}_\phi = \hat{e}_\phi e_\phi$, where the coefficients e_θ and e_ϕ are expressed in volts/km:

$$g = g_\theta + g_\phi. \quad (\text{II. 37})$$

Subscripts t and r are used to refer to the gains g_t and g_r of transmitting and receiving antennas, while g is the ratio of the available mean power flux density and e_0^2/η_0 , where

e_0 as defined by (II.38) is the free space field strength at a distance r in kilometers from an isotropic antenna radiating w_t watts:

$$e_0 = [\eta_0 w_t / (4\pi r^2)]^{1/2} \text{ volts/km.} \quad (\text{II. 38})$$

Here, $\eta_0 = 4\pi c \cdot 10^{-7} = 376.7304 \pm 0.0004$ ohms is the characteristic impedance of free space. The maximum amplitudes of the θ and ϕ components of a radiated or incident field are $|\vec{e}_\theta| \sqrt{Z}$ and $|\vec{e}_\phi| \sqrt{Z}$, where

$$|\vec{e}_\theta| = e_\theta = e_0 g_\theta^{1/2} \text{ volts/km,} \quad |\vec{e}_\phi| = e_\phi = e_0 g_\phi^{1/2} \text{ volts/km,} \quad (\text{II. 39})$$

If phases τ_θ and τ_ϕ are associated with the electric field components \vec{e}_θ and \vec{e}_ϕ , which are in phase quadrature in space but not necessarily in time, the total complex wave at any point \vec{r} is

$$\sqrt{Z} (\vec{e}_r + i\vec{e}_i) \exp(i\tau) = \sqrt{Z} [\vec{e}_\theta \exp(i\tau_\theta) + \vec{e}_\phi \exp(i\tau_\phi)] \exp(i\tau). \quad (\text{II. 40})$$

From this expression and a knowledge of $\vec{e}_{\theta, \phi}$, $\tau_{\theta, \phi}$, we may determine the real and imaginary components \vec{e}_r and \vec{e}_i , which are in phase quadrature in time but not necessarily in space:

$$\vec{e}_r = \hat{e}_r e_r = \vec{e}_\theta \cos \tau_\theta + \vec{e}_\phi \cos \tau_\phi \quad (\text{II. 41a})$$

$$\vec{e}_i = \hat{e}_i e_i = \vec{e}_\theta \sin \tau_\theta + \vec{e}_\phi \sin \tau_\phi. \quad (\text{II. 41b})$$

The next section of this annex introduces components of this wave which are in phase quadrature in both time and space.

II. 3. 2 Principal and Cross-Polarization Components

Principal and cross-polarization components of an incident complex wave $\sqrt{Z} (\vec{e}_r + i\vec{e}_i) \exp(i\tau)$ may be defined in terms of a time-independent phase τ_i which is a function of \vec{r} [Kales, 1951]. If we write

$$\vec{e}_r + i\vec{e}_i = (\vec{e}_1 + i\vec{e}_2) \exp(i\tau_i) \quad (\text{II. 42})$$

and solve for the real and imaginary components of the complex vector $\vec{e}_1 + i\vec{e}_2$, we find that

$$\vec{e}_1 = \hat{\delta}_1 e_1 = \vec{e}_r \cos \tau_i + \vec{e}_i \sin \tau_i \quad (\text{II. 43a})$$

$$\vec{e}_2 = \hat{\delta}_2 e_2 = \vec{e}_i \cos \tau_i - \vec{e}_r \sin \tau_i. \quad (\text{II. 43b})$$

Whichever of these vectors has the greater magnitude is the principal polarization component \vec{e}_p , and the other is the orthogonal cross-polarization component \vec{e}_c :

$$e_1^2 = e_r^2 \cos^2 \tau_i + e_i^2 \sin^2 \tau_i + \vec{e}_r \cdot \vec{e}_i \sin(2\tau_i) \quad (\text{II. 44a})$$

$$e_2^2 = e_r^2 \sin^2 \tau_i + e_i^2 \cos^2 \tau_i - \vec{e}_r \cdot \vec{e}_i \sin(2\tau_i). \quad (\text{II. 44b})$$

The phase angle τ_i is determined from the condition that $\vec{e}_1 \cdot \vec{e}_2 = 0$:

$$\tan(2\tau_i) = 2\vec{e}_r \cdot \vec{e}_i / (e_r^2 - e_i^2). \quad (\text{II. 45})$$

Any incident plane wave, traveling in a direction $-\hat{f}$ is then represented as the real part of the complex wave given by

$$\sqrt{Z} \vec{e} \exp[i(\tau + \tau_i)] = \sqrt{Z} (\vec{e}_p + i\vec{e}_c) \exp[i(\tau + \tau_i)]. \quad (\text{II. 46})$$

The principal and cross-polarization directions $\hat{\delta}_p$ and $\hat{\delta}_c$ are chosen so that their vector product is a unit vector in the direction of propagation:

$$\hat{\delta}_p \times \hat{\delta}_c = -\hat{f}. \quad (\text{II. 47})$$

A bar is used under the symbol for the complex vector $\vec{e} \equiv \vec{e}_p + i\vec{e}_c$ in (II.46) to distinguish it from real vectors such as \vec{e}_θ , \vec{e}_ϕ , \vec{e}_r , \vec{e}_i , \vec{e}_p , and \vec{e}_c . The absolute values of the vector coefficients e_p and e_c may be found using (II.44).

As the time t at the transmitter or the time τ at the receiver increases, the real vector component of (II.46), or "polarization vector",

$$\sqrt{Z} [\vec{e}_p \cos(\tau + \tau_i) - \vec{e}_c \sin(\tau + \tau_i)]$$

describes an ellipse in the plane of the orthogonal unit vectors $\hat{e}_p = \vec{e}_p / e_p$ and $\hat{e}_c = \vec{e}_c / e_c$. Looking in the direction of propagation $-\mathbf{r}(\theta, \phi)$ with e_p and e_c both positive or both negative, we see a clockwise rotation of the polarization vector as τ increases.

Right-handed polarization is defined by the IRE or IEEE and in CCIR Report 321 [1963m] to correspond to a clockwise rotation of a polarization ellipse, looking in the direction of propagation with r fixed and t or τ increasing. This is opposite to the definition used in classical physics.

The "axial ratio" e_c / e_p of the polarization ellipse of an incident plane wave, $\sqrt{Z} \vec{e} \exp[i(\tau + \tau_0)]$ is denoted here as

$$a_x \equiv e_c / e_p \quad (\text{II.48})$$

and may be either positive or negative depending on whether the polarization of the incident wave is right-handed or left-handed. The range of possible values for a_x is -1 to $+1$.

II.3.3 Unit Complex Polarization Vectors

If the receiving antenna were a point source of radio waves, it would produce a plane wave $\sqrt{Z} \underline{e}_r \exp[i(\tau + \tau_r)]$ at a point \bar{r} in free space. The receiving pattern of such an antenna as it responds to an incident plane wave $\sqrt{Z} \underline{e} \exp[i(\tau + \tau_r)]$ traveling in the opposite direction $-\hat{f}$ is proportional to the complex conjugate of $\underline{e}_r \exp(i\tau_r)$ [S. A. Schelkunoff and H. T. Friis, 1952]:

$$[\underline{e}_r \exp(i\tau_r)]^* = (\underline{e}_{pr} - i\underline{e}_{cr}) \exp(-i\tau_r). \quad (\text{II. 49})$$

The axial ratio e_{cr}/e_{pr} of the type of wave that would be radiated by a receiving antenna is defined for propagation in the direction \hat{f} . An incident plane wave, however, is propagating in the direction $-\hat{f}$, and by definition the sense of polarization of an antenna used for reception is opposite to the sense of polarization when the antenna is used as a radiator. The polarization associated with a receiving pattern is right-handed or left-handed depending on whether a_{xr} is positive or negative, where

$$a_{xr} = -e_{cr}/e_{pr}, \quad e_{cr} = -e_{pr} a_{xr}. \quad (\text{II. 50})$$

The amplitudes $|e_{pr}|$ and $|e_{cr}|$ of the principal and cross-polarization field components \underline{e}_{pr} and \underline{e}_{cr} are proportional to the square roots of principal and cross-polarization directive gains g_{pr} and g_{cr} , respectively. It is convenient to define a unit complex polarization vector $\hat{\underline{e}}_r$ which contains all the information about the polarization response associated with a receiving pattern:

$$\hat{\underline{e}}_r = (\hat{\underline{e}}_{pr} + i\hat{\underline{e}}_{cr} a_{xr}) (1 + a_{xr}^2)^{-1/2} \quad (\text{II. 51})$$

$$a_{xr}^2 = g_{cr}/g_{pr}. \quad (\text{II. 52})$$

The directions $\hat{\underline{e}}_{pr}$ and $\hat{\underline{e}}_{cr}$ are chosen so that

$$\hat{\underline{e}}_{pr} \times \hat{\underline{e}}_{cr} = \hat{f}. \quad (\text{II. 53})$$

In a similar fashion, the axial ratio a_x defined by (II. 48) and the orientations $\hat{\underline{e}}_p$ and $\hat{\underline{e}}_c$ of the principal and cross-polarization axes of the polarization ellipse completely describe the state of polarization of an incident wave $\sqrt{Z} \underline{e} \exp[i(\tau + \tau_1)]$, and its direction of propagation $-\hat{f} = \hat{\underline{e}}_p \times \hat{\underline{e}}_c$. The unit complex polarization vector for the incident wave is

$$\hat{p} = \vec{e} / |\vec{e}| = (\epsilon_p + i\epsilon_c a_x)(1 + a_x^2)^{-1/2}. \quad (\text{II. 54})$$

The magnitude of a complex vector $\vec{e} = \vec{e}_p + i\vec{e}_c$ is the square root of the product of \vec{e} and its complex conjugate $\vec{e}_p - i\vec{e}_c$:

$$|\vec{e}| = (\vec{e} \cdot \vec{e}^*)^{1/2} = (e_p^2 + e_c^2)^{1/2} \quad \text{volts/km.} \quad (\text{II. 55})$$

II. 3. 4 Power Flux Densities

The coefficients e_p and e_c of the unit vectors \hat{e}_p and \hat{e}_c are chosen to be r.m.s. values of field strength, expressed in volts/km, and the mean power flux densities s_p and s_c associated with these components are

$$s_p = e_p^2 / \eta_0 \quad \text{watts/km}^2, \quad s_c = e_c^2 / \eta_0 \quad \text{watts/km}^2, \quad (\text{II. 56})$$

The corresponding principal and cross-polarisation directive gains g_p and g_c are

$$g_p = 4\pi r^2 s_p / w_t, \quad g_c = 4\pi r^2 s_c / w_t \quad (\text{II. 57})$$

where w_t is the total power radiated from the transmitting antenna. This is the same relation as that expressed by (II. 39) between the gains g_θ , g_ϕ , and the orthogonal polarisation components \vec{e}_θ and \vec{e}_ϕ .

The total mean power flux density s at any point where \vec{e} is known to be in the radiation field of the transmitting antenna and any reradiating sources is

$$\begin{aligned} s &= |\vec{e}|^2 / \eta_0 = g e_0^2 / \eta_0 = s_p + s_c = (e_p^2 + e_c^2) / \eta_0 \\ &= (e_r^2 + e_i^2) / \eta_0 = (e_\theta^2 + e_\phi^2) / \eta_0 \quad \text{watts/km}^2 \end{aligned} \quad (\text{II. 58a})$$

$$g = g_p + g_c = g_\theta + g_\phi = 4\pi r^2 s / p_t = s \eta_0 / e_0^2 \quad (\text{II. 58b})$$

where e_0 is given by (II. 38). The power flux density s is proportional to the transmitting antenna gain g_t , but in general g is not equal to g_t as there may be a fraction a_p of energy absorbed along a ray path or scattered out of the path. We therefore write

$$g = g_p (1 + a_x^2) = a_p g_{pt} (1 + a_x^2) = a_p g_t. \quad (\text{II. 59})$$

The path absorption factor a_p can also be useful in approximating propagation mechanisms which are more readily described as a sum of modes than by using geometric optics. For instance, in the case of tropospheric ducting a single dominant TEM mode may correspond theoretically to an infinite number of ray paths, and yet be satisfactorily approximated by a single great-circle ray path if a_p is appropriately defined. In such a case, a_p will occasionally be greater than unity rather than less.

Orienting a receiving dipole for maximum reception to determine s_p and for minimum reception to determine s_c will also determine $\hat{\epsilon}_p$ and $\hat{\epsilon}_c$, except in the case of circular polarization, where the direction of $\hat{\epsilon}_p$ in the plane normal to \vec{r} is arbitrary. In the general case where $|a_x| < 1$, either of two opposite directions along the line of principal polarization is equally suitable for $\hat{\epsilon}_p$.

Reception with a dipole will not show the sense of polarization. Right-handed and left-handed circularly polarized receiving antennas will in theory furnish this information, since \vec{e} may also be written to correspond to the difference of right-handed and left-handed circularly polarized waves which are in phase quadrature in time and space:

$$\vec{e} \equiv (\hat{\epsilon}_p + i\hat{\epsilon}_c) \left(\frac{e_p + e_c}{2} \right) - i(\hat{\epsilon}_c - i\hat{\epsilon}_p) \left(\frac{e_p - e_c}{2} \right). \quad (\text{II. 60})$$

The mean power flux densities s_r and s_l associated with right-handed and left-handed polarizations are

$$s_r = (e_p + e_c)^2 / (2\eta_0) \text{ watts/km}^2 \quad (\text{II. 61a})$$

$$s_l = (e_p - e_c)^2 / (2\eta_0) \text{ watts/km}^2 \quad (\text{II. 61b})$$

so the sense of polarization may be determined by whether s_r/s_l is greater than or less than unity. The flux densities s_r and s_l are equal only for linear polarization, where $e_c = 0$.

II.3.5 Polarization Efficiency

The polarization efficiency for a transfer of energy from a single plane wave to the terminals of a receiving antenna at a given radio frequency may be expressed as a function of the unit complex polarization vectors defined by (II.51) and (II.54) and the angle ψ_p between principal polarization directions associated with $\underline{\hat{e}}$ and $\underline{\hat{e}}_r$. This polarization efficiency is

$$|\underline{\hat{p}} \cdot \underline{\hat{p}}_r|^2 = \frac{\cos^2 \psi_p (a_x a_{xr} + 1)^2 + \sin^2 \psi_p (a_x + a_{xr})^2}{(a_x^2 + 1)(a_{xr}^2 + 1)} \quad (\text{II.62})$$

where

$$\underline{\hat{e}}_p \cdot \underline{\hat{e}}_{pr} = -\underline{\hat{e}}_c \cdot \underline{\hat{e}}_{cr} = \cos \psi_p, \quad \underline{\hat{e}}_p \cdot \underline{\hat{e}}_{cr} = \underline{\hat{e}}_{pr} \cdot \underline{\hat{e}}_c = \sin \psi_p. \quad (\text{II.63})$$

As noted in section 2 following (2.11), any receiving antenna is completely "blind" to an incoming plane wave $\sqrt{Z} \underline{\hat{e}} \exp[i(\tau + \tau_i)]$ which has a sense of polarization opposite to that of the receiving antenna if the eccentricities of the polarization ellipses are the same ($|a_x| = |a_{xr}|$) and if the principal polarization direction $\underline{\hat{e}}_p$ of the incident wave is perpendicular to $\underline{\hat{e}}_{pr}$. In such a case, $\cos \psi_p = 0$, $a_x = -a_{xr}$, and (II.62) shows that the polarization efficiency $|\underline{\hat{p}} \cdot \underline{\hat{p}}_r|^2$ is zero. As an interesting special case, reflection of a circularly polarized wave incident normally on a perfectly conducting sheet will change the sense of polarization so that the antenna which radiates such a wave cannot receive the reflected wave. In such a case $a_x = -a_{xr} = \pm 1$, so that $|\underline{\hat{p}} \cdot \underline{\hat{p}}_r|^2 = 0$ for any value of ψ_p .

On the other hand, the polarization efficiency given by (II.62) is unity and a maximum transfer of power will occur if $a_x = a_{xr}$ and $\psi_p = 0$, that is, if the sense, eccentricity, and principal polarization direction of the receiving antenna match the sense, eccentricity, and principal polarization direction of the incident wave.

For transmission in free space, antenna radiation efficiencies, their directive gains, and the polarization coupling efficiency are independent quantities, and all five must be maximized for a maximum transfer of power between the antennas. A reduction in either one of the directive gains $g(-\hat{p})$ and $g_r(\hat{p})$ or a reduction in the polarization efficiency $|\underline{\hat{p}} \cdot \underline{\hat{p}}_r|^2$ will reduce the transfer of power between two antennas.

With each plane wave incident on the receiving antenna there is associated a ray of length r from the transmitter, an initial direction of radiation, and the radiated wave $\underline{\hat{e}}_t \exp[i(\tau + \tau_t)]$ which would be found in free space at this distance and in this direction. When it is practical to separate antenna characteristics from environmental and path characteristics, it is assumed that the antenna phase response τ_t , like τ_r , is a characteristic of the antenna and its environment and that

$$\tau_i = \tau_t + \tau_p$$

(II.64)

where τ_p is a function of the ray path and includes allowances for path length differences and diffraction or reflection phase shifts.

Random phase changes in either antenna, absorption and reradiation by the environment, or random fluctuations of refractive index in the atmosphere will all tend to fill in any sharp nulls in a theoretical free-space radiation pattern \vec{e} or \vec{e}_r . Also, it is not possible to have a complex vector pattern \vec{e}/r which is independent of r in the vicinity of antenna nulls unless the radiation field, proportional to $1/r$, dominates over the induction field, which is approximately proportional to $1/r^2$.

II. 3. 6 Multipath Coupling Loss

Coherently phased multipath components from a single source may arrive at a receiving antenna from directions sufficiently different so that τ_i and τ_r vary significantly. It is then important to be able to add complex signal voltages at the antenna terminals. Let $n = 1, 2, \dots, N$ and assume N discrete plane waves incident on an antenna from a single source. The following expressions represent the complex open-circuit r.m.s. signal voltage v_n corresponding to a radio frequency ν cycles per second, a single incident plane wave $\sqrt{2} \vec{e}_n \exp[i(\tau + \tau_{in})]$, a loss-free receiving antenna with a directivity gain g_{rn} and an effective absorbing area a_{en} , matched antenna and load impedances, and an input resistance r_ν which is the same for the antenna and its load:

$$v_n = (4r_\nu a_{en})^{1/2} (\hat{e}_n \cdot \hat{p}_{rn}) \exp[i(\tau + \tau_{pn} + \tau_{tn} - \tau_{rn})] \text{ volts} \quad (\text{II. 65})$$

$$s_n = |\vec{e}_n|^2 / \eta_0 = w_r a_{pn} g_{tn} / (4\pi r_n^2) \text{ watts/km}^2 \quad (\text{II. 66})$$

$$a_{en} = g_{rn} \lambda^2 / (4\pi) \text{ km}^2 \quad (\text{II. 67})$$

$$\hat{p}_n \cdot \hat{p}_{rn} = [(1 + a_{xn}^2)(1 + a_{xrn}^2)]^{-1/2} \{ (1 + a_{xn} a_{xrn}) \cos \psi_{pn} + i(a_{xn} + a_{xrn}) \sin \psi_{pn} \} \quad (\text{II. 68})$$

If the polarization of the receiving antenna is matched to that of the incident plane wave, then $a_{xn} = a_{xrn}$, $\psi_{pn} = 0$, $\hat{e}_n \cdot \hat{p}_{rn} = 1$, and

$$v_n = [4r_\nu w_r a_{pn} g_{tn} g_{rn} \lambda^2 / (4\pi r_n^2)]^{1/2} \exp[i(\tau + \tau_{pn} + \tau_{tn} - \tau_{rn})] \text{ volts} \quad (\text{II. 69})$$

If the coefficient of the phasor in (II. 69) has the same value for two incident plane waves, but the values of $\tau_{in} - \tau_{rn}$ differ by π radians, the sum of the corresponding complex voltages is zero. This shows that the multipath coupling efficiency can theoretically be zero even when the beam orientation and polarization coupling are maximized. Adjacent lobes in a receiving antenna directivity pattern, for instance, may be 180° out of phase and thus cancel two discrete in-phase plane-wave components.

Equation (II. 3) shows the relation between the total open-circuit r.m.s. voltage

$$v_\nu = \left[\sum_{n=1}^N \sum_{m=1}^N v_n v_m^* \right]^{1/2} \text{ volts} \quad (\text{II. 70})$$

and the power w_a available at the terminals of a loss-free receiving antenna:

$$w_a = v_v^2 / (4r_v) \text{ watts} \quad (\text{II. 71})$$

In writing w_a for w_{av} in (II. 71), the subscript v has been suppressed, as with almost all of the symbols in this annex. Studying (II. 65) - (II. 68), (II. 70), and (II. 71), it is seen that the expression for w_a is symmetrical in the antenna gains g_p , g_{pr} , and $g_t = a_x^2 g_p$, $g_{cr} = a_{xr}^2 g_{pr}$, and that w_a is a linear function of these parameters, though v_v is not. From this follows a theorem of reciprocity, that the transmission loss $L = -10 \log (w_a / w_t)$ is the same if the roles of the transmitting and receiving antennas are reversed.

The basic transmission loss L_b is the system loss that would be expected if the actual antennas were replaced at the same locations by hypothetical antennas which are:

- (a) loss-free, so that $L_{et} = L_{er} = 0$ db. See (2.3).
- (b) isotropic, so that $g_t = g_r = 1$ in every direction important to propagation between the actual antennas.
- (c) free of polarization coupling loss, so that $|\hat{p}_t \cdot \hat{p}_r|^2 = 1$ for every locally plane wave incident at the receiving antenna.
- (d) isotropic in their phase response, so that $\tau_t = \tau_r = 0$ in every direction.

The available power w_{ab} corresponding to propagation between hypothetical isotropic antennas is then

$$w_{ab} = \frac{w_t \lambda^2}{(4\pi)^2} \sum_{n=1}^N \sum_{m=1}^N \frac{(a_{pn} a_{pm})^{1/2} \cos(\tau_{pn} - \tau_{pm})}{r_n r_m} \quad (\text{II. 72})$$

The basic transmission loss L_b corresponding to these assumptions is

$$L_b = -10 \log (w_{ab} / w_t) = W_t - W_{ab} \text{ db} \quad (\text{II. 73})$$

The basic transmission loss in free space, L_{bf} , corresponds to $N = 1$, $a_{p1} = 1$, $\tau_{p1} = 0$, $r_1 = r$:

$$L_{bf} = -10 \log [\lambda / (4\pi r)]^2 = 32.45 + 20 \log f + 20 \log r \text{ db} \quad (\text{II. 74})$$

where f is in megacycles per second and r is in kilometers. Compare with (2.16).

As may be seen from the above relations, only a fraction s_e of the total flux density s_n per unit radiated power w_t contributes to the available received power w_a from N plane waves. While s_n is expressed in watts/km², s_e is expressed in watts/km² for each watt

of the power w_t radiated by a single source:

$$s_e = 4\pi w_t / (\lambda^2 w_t) \quad (\text{II. 75})$$

For each plane wave from a given source, $\vec{e}_n \exp(i\tau_{in})$ or $\vec{e}_{rn} \exp(-i\tau_{rn})$ may sometimes be regarded as a statistical variable chosen at random from a uniform distribution, with all phases from $-\pi$ to π equally likely. Then real power proportional to $|\vec{e}_n \cdot \vec{e}_{rn}^*|^2$ may be added at the antenna terminals, rather than the complex voltages defined by (II. 65)-(II. 68). For this case, the statistical "expected value" $\langle s_e \rangle$ of s_e is

$$\langle s_e \rangle = \sum_{n=1}^N a_{pn} g_{tn} g_{rn} |\hat{p}_n \cdot \hat{p}_{rn}|^2 / (4\pi r_n^2). \quad (\text{II. 76})$$

In terms of s_e , the transmission loss L is

$$L = 21.46 + 20 \log f - 10 \log s_e \quad \text{db.} \quad (\text{II. 77})$$

Substituting $\langle s_e \rangle$ for s_e in (II. 77), we would not in general obtain the statistical expected value $\langle L \rangle$ of L, since $\langle L \rangle$ is an ensemble average of logarithms, which may be quite different from the logarithm of the corresponding ensemble average $\langle s_e \rangle$. For this reason, median values are often a more practical measure of central tendency than "expected" values. With w_t and λ fixed, median values of s_e and L always obey the relation (II. 77), while average values of s_e and L often do not.

The remainder of this annex is concerned with a few artificial problems designed to show how these formulas are used and to demonstrate some of the properties of radiation and response patterns. In general, information is needed about antenna patterns only in the few directions which are important in determining the amplitude and fading of a tropospheric signal. Although section II. 3.7 shows how a complex vector radiation or reception pattern may be derived from an integral over all directions, it is proposed that the power radiation efficiencies and the gains $g_r(\hat{f})$ or $g_t(-\hat{f})$ for actual antennas should be determined by measurements in a few critical directions using standard methods and a minimum of calculations.

II.3.7 Idealized Theoretical Antenna Patterns

Consider a point source of plane waves, represented by complex dipole moments in three mutually perpendicular directions, \hat{x}_0 , \hat{x}_1 , and \hat{x}_2 . These three unit vectors, illustrated in figure II.1, define a right-handed system, and it is assumed that the corresponding elementary dipoles support r.m.s. currents of I_0 , I_1 , and I_2 amperes, respectively. The corresponding peak scalar current dipole moments are $\sqrt{2} I_m l$ ampere-kilometers, where $m = 0, 1, 2$, and the sum of the complex vector dipole moments $\hat{x}_m \sqrt{2} I_m l \exp(i\tau_m)$ may be expressed as follows:

$$\vec{a} = \vec{a}_1 + i\vec{a}_2 \quad (\text{II.78a})$$

$$\vec{a}_1 = \sqrt{2} l (\hat{x}_0 c_0 + \hat{x}_1 c_1 + \hat{x}_2 c_2), \quad \vec{a}_2 = \sqrt{2} l (\hat{x}_0 s_0 + \hat{x}_1 s_1 + \hat{x}_2 s_2) \quad (\text{II.78b})$$

$$I^2 = I_0^2 + I_1^2 + I_2^2, \quad c_m = (I_m/I) \cos \tau_m, \quad s_m = (I_m/I) \sin \tau_m, \quad m = 0, 1, 2. \quad (\text{II.79})$$

Here, τ_0 , τ_1 , and τ_2 represent initial phases of the currents supported by the elementary dipoles. The time phase factor is assumed to be $\exp(ikct)$.

Using the same unit vector coordinate system to represent the vector distance \vec{r} from this idealized point source to a distant point:

$$\vec{r} = \hat{x}_0 x_0 + \hat{x}_1 x_1 + \hat{x}_2 x_2 = fr \quad (\text{II.80})$$

where x_0 , x_1 , and x_2 are given by (II.35b) as functions of r , θ , ϕ . The complex wave at \vec{r} due to any one of the elementary dipoles is polarized in a direction

$$\hat{f} \times (\hat{x}_m \times \hat{f}) = \hat{x}_m - \hat{f} x_m / r \quad (\text{II.81})$$

which is perpendicular to the propagation direction \hat{f} and in the plane of \hat{x}_m and \hat{f} . The total complex wave at \vec{r} may be represented in the form given by (II.41):

$$\begin{aligned} \sqrt{2} \vec{e}(\vec{r}) \exp(i\tau) &= \sqrt{2} (\vec{e}_r + i\vec{e}_i) \exp(i\tau) = \sqrt{2} (\vec{e}_p + i\vec{e}_c) \exp[i(\tau + \tau_t)] \\ &= [\hat{f} \times (\vec{a} \times \hat{f})] [\eta_0 / (2\lambda r)] \exp(i\tau) \end{aligned} \quad (\text{II.82})$$

$$\tau = k(ct - r) + \pi/4 \quad (\text{II.83})$$

$$\sqrt{2} \vec{e}_r = [\vec{a}_1 - \hat{f}(\vec{a}_1 \cdot \hat{f})] \eta_0 / (2\lambda r) \text{ volts/km} \quad (\text{II.84a})$$

$$\sqrt{Z} \vec{e}_i = [\vec{a}_2 - \beta(\vec{a}_2 \cdot \beta)] \eta_0 / (2\lambda r) \text{ volts/km.} \quad (\text{II. 84b})$$

The total mean power flux density $s(\vec{r})$ at \vec{r} is given by (II. 58a):

$$s(\vec{r}) = (\vec{e}_r^2 + \vec{e}_i^2) / \eta_0 = [a_1^2 - (\vec{a}_1 \cdot \beta)^2 + a_2^2 - (\vec{a}_2 \cdot \beta)^2] / \eta_0$$

$$- \frac{\eta_0 (II)^2}{4\lambda^2 r^2} [1 - (I_0^2 x_0^2 + I_1^2 x_1^2 + I_2^2 x_2^2) / (Ir)^2 - 2(c_{01} x_0 x_1 + c_{02} x_0 x_2 + c_{12} x_1 x_2) / r^2]$$
(II. 85)

$$c_{mn} = (I_m I_n / I^2) \cos(\tau_m - \tau_n). \quad (\text{II. 86})$$

The total radiated power w_t is obtained by integrating $s(r)$ over the surface of a sphere of radius r , using the spherical coordinates r, θ, ϕ illustrated in figure II. 1:

$$w_t = \int_0^{2\pi} d\phi \int_0^\pi d\theta r^2 s(\vec{r}) \sin\theta = \frac{2\pi \eta_0 (II)^2}{3\lambda^2} \text{ watts.} \quad (\text{II. 87})$$

From (II. 87) it is seen that the peak scalar dipole moment \sqrt{ZII} used to define \vec{a}_1 and \vec{a}_2 in (II. 78) may be expressed in terms of the total radiated power:

$$\sqrt{ZII} = \lambda \sqrt{3w_t / (\pi \eta_0)} \text{ ampere-kilometers.} \quad (\text{II. 88})$$

The directive gain $g(\hat{r})$ is

$$g(\hat{r}) = 4\pi r^2 s(\vec{r}) / w_t = \frac{3}{2} \left[1 - \left(\frac{I_0}{I}\right)^2 \cos^2\theta - \left(\frac{I_1}{I}\right)^2 \sin^2\theta \cos^2\phi \right. \\ \left. - \left(\frac{I_2}{I}\right)^2 \sin^2\theta \sin^2\phi - (c_{01} \cos\phi + c_{02} \sin\phi) \sin(2\theta) - c_{12} \sin^2\theta \sin(2\phi) \right]. \quad (\text{II. 89})$$

This is the most general expression possible for the directive gain of any combination of elementary electric dipoles centered at a point. Studying (II. 89), it may be shown that no combination of values for $I_0, I_1, I_2, \tau_0, \tau_1, \tau_2$ will provide an isotropic radiator. As defined in this annex, an isotropic antenna radiates or receives waves of any phase and polarization equally in every direction.

For the special case where $I_0 = I_1 = I_2 = 1/\sqrt{3}$, $\tau_0 = \pi/2$, $\tau_1 = 0$, and $\tau_2 = \pi$, (II.89) shows that

$$g(\hat{r}) = 1 + \sin^2 \theta \sin \phi \cos \phi. \quad (\text{II.90})$$

With these specifications, (II.78) shows that $c_0 = 0$, $c_1 = -c_2 = 1/\sqrt{3}$, $s_0 = 1/\sqrt{3}$, $s_1 = s_2 = 0$, and (II.78) with (II.88) shows that

$$\vec{a}_1 = (\hat{x}_1 - \hat{x}_2)b, \quad \vec{a}_2 = \hat{x}_0 b \quad (\text{II.91a})$$

$$b = \lambda \left[w_r / (\pi \eta_0) \right]^{1/2}. \quad (\text{II.91b})$$

Substituting next in (II.84) with the aid of (II.2):

$$\sqrt{2} \vec{e}_r = e_0 (\hat{x}_1 - \hat{x}_2 - \hat{r} b_2), \quad \sqrt{2} \vec{e}_i = e_0 (\hat{x}_0 - \hat{r} \cos \theta) \quad (\text{II.94})$$

$$e_0 = \left[\eta_0 w_t / (4\pi r^2) \right]^{1/2}, \quad b_2 = \sin \theta (\cos \phi - \sin \phi). \quad (\text{II.95})$$

The principal and cross-polarization gains determined using (II.57) and (II.58) are

$$g_p(\hat{r}) = 1 + \sin^2 \theta (\sin \phi \cos \phi - 1/2), \quad g_c(\hat{r}) = 1/2 \sin^2 \theta. \quad (\text{II.94})$$

The subscripts p and c in (II.94) should be reversed whenever $g(0, \phi)$ is less than $\sin^2 \theta$. Minimum and maximum values of g are 1/2 and 3/2 while g_p ranges from 1/3 to 1 and g_c from 0 to 1/2.

The importance of phases to multipath coupling is more readily demonstrated using a somewhat more complicated antenna. The following paragraphs derive an expression for a wave which is approximately plane at a distance r exceeding 200 wavelengths, radiated by an antenna composed of two three-dimensional complex dipoles located at $-5 \lambda \hat{x}_0$ and $+5 \lambda \hat{x}_0$ and thus spaced 10 wavelengths apart. When the radiation pattern has been determined, it will be assumed that this is the receiving antenna. Its response to known plane waves from two given directions will then be calculated.

With the radiated power w_t divided equally between two three-dimensional complex dipoles, \vec{a} is redefined as

$$\vec{a} = (b/\sqrt{2}) \vec{a}_0, \quad \vec{a}_0 = \hat{x}_1 - \hat{x}_2 + i \hat{x}_0. \quad (\text{II.95})$$

Since 5λ is negligible compared to r except in phase factors critically depending on $r_1 - r_2$, the exact expressions

$$\vec{r}_1 = \vec{r} - 5\lambda \hat{x}_0, \quad \vec{r}_2 = \vec{r} + 5\lambda \hat{x}_0 \quad (\text{II. 96})$$

lead to the following approximations and definitions:

$$r_1 = r(1 - \epsilon), \quad r_2 = r(1 + \epsilon), \quad \epsilon = 5(\lambda/r) \cos \theta \quad (\text{II. 97})$$

$$\hat{r}_1 = \hat{r}(1 + \epsilon) - \hat{x}_0 \epsilon \sec \theta, \quad \hat{r}_2 = \hat{r}(1 - \epsilon) + \hat{x}_0 \epsilon \sec \theta \quad (\text{II. 98})$$

$$\hat{r} = \hat{x}_0 \cos \theta + (\hat{x}_1 \cos \phi + \hat{x}_2 \sin \phi) \sin \theta. \quad (\text{II. 99})$$

For distances r exceeding 200 wavelengths, $|\epsilon| < 0.025$ and ϵ^2 is neglected entirely, so that

$$\hat{r}_1 r_1 = \vec{r} - 5\lambda \hat{x}_0, \quad \hat{r}_2 r_2 = \vec{r} + 5\lambda \hat{x}_0. \quad (\text{II. 100})$$

At a point \vec{r} , the complex wave radiated by this antenna is approximately plane and may be represented as

$$\sqrt{Z} (\vec{e}_r + i \vec{e}_i) \exp(i\tau) = \sqrt{Z} [\vec{e}_1 \exp(i\tau_1) + \vec{e}_2 \exp(i\tau_2)] \quad (\text{II. 101})$$

where

$$\tau = k(ct - r) + \pi/4 \quad (\text{II. 102})$$

$$\tau_1 = \tau + \tau_a, \quad \tau_2 = \tau - \tau_a, \quad \tau_a = 10\pi \cos \theta. \quad (\text{II. 103})$$

As in (II. 2), the waves radiated by the two main elements of this antenna are represented in (II. 101) as the product of phasors $\exp(i\tau_1)$ and $\exp(i\tau_2)$ multiplied by the complex vectors $\sqrt{Z} \vec{e}_1$ and $\sqrt{Z} \vec{e}_2$, respectively:

$$\sqrt{Z} \vec{e}_1 = \left[\hat{r}_1 \times (\vec{a} \times \hat{r}_1) \right] \eta_0 / (2\lambda r) = (e_0/2) \left[\vec{a}_0 - \hat{r}_1 (\vec{a}_0 \cdot \hat{r}_1) \right] \quad (\text{II. 104a})$$

$$\sqrt{Z} \vec{e}_2 = \left[\hat{r}_2 \times (\vec{a} \times \hat{r}_2) \right] \eta_0 / (2\lambda r) = (e_0/2) \left[\vec{a}_0 - \hat{r}_2 (\vec{a}_0 \cdot \hat{r}_2) \right] \quad (\text{II. 104b})$$

Evaluating $\vec{a}_0 \cdot \hat{r}_1$, $\vec{a}_0 \cdot \hat{r}_2$, \vec{e}_1 , and \vec{e}_2 with the aid of (II.95), (II.98), (II.99) and (II.104):

$$\vec{a}_0 \cdot \hat{r}_1 = b_2(i + \epsilon) + i \left[\cos \theta - \epsilon (\sec \theta - \cos \theta) \right] \quad (\text{II.105a})$$

$$\vec{a}_0 \cdot \hat{r}_2 = b_2(1 - \epsilon) + i \left[\cos \theta + \epsilon (\sec \theta - \cos \theta) \right] \quad (\text{II.105b})$$

$$\begin{aligned} \vec{e}_1 = (e_0/2) \left\{ \left[\hat{x}_1 - \hat{x}_2 - \hat{r} b_2(1 + 2\epsilon) + \hat{x}_0 b_2 \epsilon \sec \theta \right] \right. \\ \left. + i \left[\hat{x}_0(1 + \epsilon) - \hat{r} \cos \theta + \hat{r} \epsilon (\sec \theta - 2 \cos \theta) \right] \right\} \quad (\text{II.106a}) \end{aligned}$$

$$\begin{aligned} \vec{e}_2 = (e_0/2) \left\{ \left[\hat{x}_1 - \hat{x}_2 - \hat{r} b_2(1 - 2\epsilon) - \hat{x}_0 b_2 \epsilon \sec \theta \right] \right. \\ \left. + i \left[\hat{x}_0(1 - \epsilon) - \hat{r} \cos \theta - \hat{r} \epsilon (\sec \theta - 2 \cos \theta) \right] \right\} . \quad (\text{II.106b}) \end{aligned}$$

Since the sum and difference of $\exp(i\tau_1)$ and $\exp(i\tau_2)$ are $2 \cos \tau_a \exp(i\tau)$ and $2i \sin \tau_a \exp(i\tau)$, respectively, \vec{e}_r and \vec{e}_i as defined by (II.101) are

$$\vec{e}_r = e_0 \left\{ \left[\hat{x}_1 - \hat{x}_2 - \hat{r} b_2 \right] \cos \tau_a - \epsilon \left[\hat{x}_0 + \hat{r} (\sec \theta - 2 \cos \theta) \right] \sin \tau_a \right\} \quad (\text{II.107a})$$

$$\vec{e}_i = e_0 \left\{ \left[\hat{x}_0 - \hat{r} \cos \theta \right] \cos \tau_a - b_2 \left[2\hat{r} - \hat{x}_0 \sec \theta \right] \sin \tau_a \right\} . \quad (\text{II.107b})$$

The complex wave $\sqrt{2}(\vec{e}_r + i\vec{e}_i)$ is a plane wave only when \vec{e}_r and \vec{e}_i are both perpendicular to the direction of propagation, \hat{r} , or when

$$\hat{r} \cdot (\vec{e}_r + i\vec{e}_i) = \sin \tau_a \left[(\cos \theta - \sec \theta) + i \sin \theta (\cos \phi - \sin \phi) \right] = 0 \quad (\text{II.108})$$

which requires that $\epsilon = 0$, $\sin \tau_a = 0$, or $\theta = 0$. If ϵ is negligible, the total mean power flux density in terms of the directive gain $g(\hat{r})$ is given by

$$s(\vec{r}) = (e_r^2 + e_i^2) / \eta_0 = g(\hat{r}) e_0^2 / \eta_0 \quad (\text{II.109})$$

$$g(\hat{r}) = 2(1 + \sin^2 \theta \sin \phi \cos \phi) \cos^2 \tau_a . \quad (\text{II.110})$$

That w_1 is the corresponding total radiated power may be verified by substituting (II.108) and (II.110) in (II.87), with the aid of (II.93) and (II.103).

Now let this antenna be a receiving antenna, and suppose that direct and ground-reflected waves arrive from directions $\hat{r}(\theta, \phi)$ equal to

$$\hat{r}_1(0.32, \pi/4) = 0.9492 \hat{x}_0 + 0.2224(\hat{x}_1 + \hat{x}_2) \quad (\text{II.111a})$$

$$\hat{r}_2(0.28, 0.75) = 0.9611 \hat{x}_0 + 0.1430 \hat{x}_1 + 0.1332 \hat{x}_2 . \quad (\text{II.111b})$$

Note that \hat{r}_1 and \hat{r}_2 in (II.111) are not related to \hat{r}_1 and \hat{r}_2 in (II.98) but are two particular values of \hat{r} . Corresponding values of τ_a , $\cos \tau_a$, and $\sin \tau_a$ are

$$\tau_{a1} = 29.82111 , \quad \cos \tau_{a1} = -0.0240 , \quad \sin \tau_{a1} = -0.9997 \quad (\text{II.112a})$$

$$\tau_{a2} = 30.19245 , \quad \cos \tau_{a2} = 0.3404 , \quad \sin \tau_{a2} = -0.9403 . \quad (\text{II.112b})$$

The incoming waves in the two directions \hat{r}_1 and \hat{r}_2 are assumed to be plane, and the distances r_1 and r_2 to their source are assumed large enough so that $e_1 \sin \tau_{a1}$ and $e_2 \sin \tau_{a2}$ are negligible compared to $\cos \tau_{a1}$ and $\cos \tau_{a2}$, respectively. The plane wave response of the receiving antenna in these directions may be expressed in terms of the complex vectors associated with \hat{r}_1 and \hat{r}_2 :

$$\vec{e}_{r1} + i \vec{e}_{i1} = -0.024 e_0 \left[(\hat{x}_1 - \hat{x}_2) + i(0.099 \hat{x}_0 - 0.211 \hat{x}_1 - 0.211 \hat{x}_2) \right] \quad (\text{II.113a})$$

$$\vec{e}_{r2} + i \vec{e}_{i2} = 0.340 e_0 \left[(-0.013 \hat{x}_0 + 0.998 \hat{x}_1 - 1.002 \hat{x}_2) + i(0.076 \hat{x}_0 - 0.137 \hat{x}_1 - 0.128 \hat{x}_2) \right] . \quad (\text{II.113b})$$

Since $\vec{e}_{r1} \cdot \vec{e}_{r2} = 0$, (II.44) with (II.42) and (II.43) shows that $\tau_{r1} = 0$, so that \vec{e}_{r1} and \vec{e}_{i1} are principal and cross-polarization components of the complex vector receiving pattern:

$$\vec{e}_{pr1} + i \vec{e}_{cr1} = \vec{e}_{r1} + i \vec{e}_{i1} . \quad (\text{II.114a})$$

These same equations show that $\tau_{r2} = -0.005$ and that

$$\vec{e}_{pr2} + i \vec{e}_{cr2} = 0.340 e_0 \left[(-0.013 \hat{x}_0 + 0.999 \hat{x}_1 - 1.001 \hat{x}_2) + i(0.076 \hat{x}_0 - 0.132 \hat{x}_1 - 0.113 \hat{x}_2) \right] \quad (\text{II. 114b})$$

differing only slightly from (II. 113b), since τ_{r2} is almost zero.

The axial ratios of the two polarization ellipses, defined by (II. 50), are

$$a_{xr1} = -0.222, \quad a_{xr2} = -0.143 \quad (\text{II. 115})$$

and the unit complex polarization vectors \hat{p}_{r1} and \hat{p}_{r2} defined by (II. 51) are therefore

$$\hat{p}_{r1} = 0.674(\hat{x}_1 - \hat{x}_2) + i(0.067 \hat{x}_0 - 0.142 \hat{x}_1 - 0.142 \hat{x}_2) \quad (\text{II. 116a})$$

$$\hat{p}_{r2} = (-0.009 \hat{x}_0 + 0.692 \hat{x}_1 - 0.694 \hat{x}_2) + i(0.053 \hat{x}_0 - 0.095 \hat{x}_1 - 0.089 \hat{x}_2) \quad (\text{II. 116b})$$

The antenna gains $g_p(\hat{r}_1)$ and $g_p(\hat{r}_2)$ are given by (II. 110);

$$g_p(\hat{r}_1) = 0.0071, \quad g_p(\hat{r}_2) = 0.241 \quad (\text{II. 117})$$

which shows that the gain $G_p(\hat{r}_1) = 10 \log g_p(\hat{r}_1)$ associated with the direct ray is 29.2 db below that of an isotropic antenna, while the gain $G_p(\hat{r}_2)$ associated with the ground-reflected ray is -6.2 db. It might be expected that only the incident wave propagating in the direction $-\hat{r}_2$ would need to be considered in determining the complex voltage at the receiving antenna terminals. Suppose, however, that the ground-reflected ray has been attenuated considerably more than the direct ray, so that the path attenuation factor a_{p2} is 0.01, while $a_{p1} = 1$. Suppose further that the transmitting antenna gain associated with the ground-reflected ray is 6 db less than that associated with the direct ray. Then the mean incident flux density s_2 associated with the ground-reflected ray will be 26 db less than the flux density s_1 associated with the direct ray.

In order to calculate the complex received voltage v given by (II. 70) then, the following is assumed:

$$r_v = 52 \text{ ohms}, \quad s_1 = 1 \text{ watt/km}^2 (= -30 \text{ dbm/m}^2)$$

$$s_2 = 0.0025 \text{ watts/cm}^2, \quad \lambda = 0.0003 \text{ km} (f = 1000 \text{ MHz})$$

$$a_{x1} = 0.2, \quad a_{x2} = 0.4, \quad \psi_{p1} = \pi/2, \quad \psi_{p2} = 1.5$$

$$\tau_{i1} = \tau_{p1} + \tau_{t1} = 0, \quad \tau_{i2} = \tau_{p2} + \tau_{t2} = \pi, \quad (\text{II. 118})$$

It will be seen that these assumptions imply a more nearly complete polarization coupling loss between the direct wave and the receiving antenna than between the ground-reflected wave and the receiving antenna. The effective absorbing area of the receiving antenna for each wave, as given by (II. 67) is

$$a_{e1} = 1.504 \times 10^{-11} \text{ km}^2, \quad a_{e2} = 1.726 \times 10^{-9} \text{ km}^2. \quad (\text{II. 119})$$

The polarization factors are

$$(\hat{p}_1 \cdot \hat{p}_{r1}) = -0.021 i, \quad (\hat{p}_2 \cdot \hat{p}_{r2}) = 0.062 + 0.236 i \quad (\text{II. 120})$$

and the phase factors are $\exp(i\tau)$ and $\exp[i(\tau + 3.137)]$, respectively. Substituting these values in (II. 65), the complex voltages are

$$v_1 = -1.175(10^{-6}) i \exp(i\tau), \quad v_2 = -(1.887 + 7.071i)(10^{-6}) \exp(i\tau). \quad (\text{II. 121})$$

The real voltage at the antenna terminals, as given by (II. 70) is

$$v_v = (v_1 + v_2)(v_1 + v_2)^* = 8.33 \times 10^{-6} \text{ volts} = 8.33 \text{ microvolts} \quad (\text{II. 122})$$

and the corresponding power w_a available at the terminals of the loss-free receiving antenna is

$$w_a = 0.334 \times 10^{-12} \text{ watts}, \quad W_a = -125 \text{ dbw} = -95 \text{ dbm} \quad (\text{II. 123})$$

as given by (II. 71).

II.3.8 Conclusions

The foregoing exercise demonstrates that:

(1) Even small changes in antenna beam orientation, transmission loss, polarization coupling, and multipath phasing may have a visible effect on the available power at the terminals of a receiving antenna.

(2) If the formulation of the general relationships for a completely polarized wave is programmed for a digital computer, it may be feasible to estimate the complete statistics of a received signal whenever reasonable assumptions can be made about the statistics of the parameters described in this annex.

(3) The measurement of antenna characteristics in a few critical directions will often be sufficient to provide valuable information to be used with the relationships given here. The measurement of Stokes' parameters, for instance, will provide information about a_{xr} , g_r , ψ_p , and both the polarized field intensity s_r and the unpolarized field intensity s_o . These parameters [Stokes, 1922] are

$$s_r + s_o = \text{total mean field intensity} \quad (\text{II. 124})$$

$$Q = s_r \cos(2\beta) \cos(2\psi_p) \quad (\text{II. 125})$$

$$U = s_r \cos(2\beta) \sin(2\psi_p) \quad (\text{II. 126})$$

$$V = s_r \sin(2\beta) \quad (\text{II. 127})$$

where

$$\beta = \tan^{-1} a_{xr} \quad (\text{II. 128})$$

The unpolarized or randomly polarized field intensity s_o is determined from (II. 124) and the identity

$$s_r = (Q^2 + U^2 + V^2)^{1/2} \quad (\text{II. 129})$$

Using standard sources and antenna model ranges, the gain g_r may be determined from

$$g_r = s_r / (e_o^2 / \eta_o), \quad e_o^2 = \eta_o P_t / (4\pi r^2) \quad (\text{II. 130})$$

assuming, if e_o is measured, that any power reception efficiency $1/\epsilon_{er}$ less than unity will affect s_r and e_o^2 alike.

CCP 702-1

Finally, a method for measuring relative phase responses τ_p is also needed. In individual cases, multipath coupling loss may be insufficient to provide adequate unwanted signal rejection. Variations of τ_p may lead to phase interference fading of wanted signals, just as variations of a_p are associated with long-term power fading. Because of the complexity of these phenomena, they are usually described in terms of cumulative distributions of signal amplitudes or fade durations. Fortunately, even crude measurements or simple theories may then suffice to provide statistical information about τ_p .

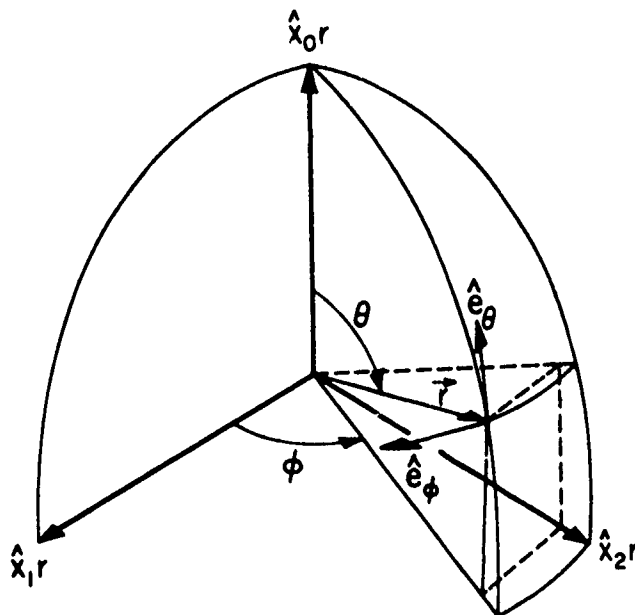
COORDINATE SYSTEMS FOR
STUDYING ANTENNA PATTERNS

Figure II.1

II-33

II.4 List of Special Symbols Used in Annex II

- a_{en}, a_{e1}, a_{e2} The effective absorbing area for the n^{th} discrete plane wave incident on an antenna from a single source, (II.67), and for each of two waves (II.119).
- a_p, a_{pm}, a_{pn} The fraction of energy absorbed along a ray path, or scattered out of it, (II.59), and the fraction of energy, a_p , for the m^{th} and n^{th} multipath components from a single source, where m and n take on integral values from 1 to N , (II.72)
- $a_{x1}, a_{x1'}, a_{x2}$ Axial ratios of the polarization ellipse of the n^{th} , first, and second plane wave from a single source, (II.68) and (II.118).
- $a_{x1n}, a_{x1n'}, a_{x2n}$ Axial ratios of the polarization ellipse associated with the receiving pattern for the n^{th} , first, and second plane wave from a single source, (II.68) and (II.115).
- a_1, a_2 Positive or negative amplitudes of real and imaginary components of a complex vector: $\underline{a} = \underline{a}_1 + ia_2$, $\underline{a}^2 = a_1^2 + a_2^2$, (II.78).
- \hat{a} The real vector $a = a\hat{a}$, where \hat{a} is a unit vector.
- $\underline{a}_1, \underline{a}_2$ Real vectors defining real and imaginary components of a complex vector: $\underline{a} = \underline{a}_1 + ia_2$, (II.78).
- \underline{a} A complex vector: $\underline{a} = \underline{a}_1 + ia_2$, (II.78).
- \underline{a}_0 A complex vector defined in terms of the unit vector system $\hat{x}_0, \hat{x}_1, \hat{x}_2$, (II.95).
- e_{cr} The positive or negative amplitude of the cross-polarized vector component \underline{e}_{cr} of a receiving antenna response pattern, (II.50).
- e_i The positive or negative amplitude of the real vector \underline{e}_i associated with a complex plane wave $\sqrt{2}(\underline{e}_r + ie_i)\exp(i\tau)$, where \underline{e}_r and \underline{e}_i are time-invariant and $\exp(i\tau)$ is a time phasor, (II.41b).
- e_{pr} The positive or negative amplitude of the principal polarization component \underline{e}_p of a receiving antenna response pattern, (II.50).
- e_r The positive or negative amplitude of the real vector component \underline{e}_r associated with a complex plane wave $\sqrt{2}(\underline{e}_r + ie_i)\exp(i\tau)$, where \underline{e}_r and \underline{e}_i are time invariant and $\exp(i\tau)$ is a time phasor, (II.41a).
- e_0 Equivalent free space field strength, (II.38).
- e_1, e_2 The positive or negative real amplitudes of real and imaginary components of the complex polarization vector \underline{e} , (II.43).
- e_θ, e_ϕ The positive amplitudes of real vectors \underline{e}_θ and \underline{e}_ϕ associated with the θ and ϕ components of a complex plane wave, (II.4) figure II.1.
- $\underline{e}_c, \underline{e}_p$ Real vectors associated with cross and principal polarization components of a uniform elliptically polarized plane wave, annex II, section II.3.2.
- \hat{e}_c, \hat{e}_p Directions of cross and principal polarization, chosen so that their vector product $\hat{e}_p \times \hat{e}_c$ is a unit vector in the direction of propagation, (II.47).

$\vec{e}_{cr}, \vec{e}_{pr}$	Cross and principal polarization field components of a receiving antenna response pattern, (II. 49).
$\hat{e}_{cr}, \hat{e}_{pr}$	Directions of cross and principal polarization components of a receiving antenna response pattern, (II. 51), (II. 53).
\vec{e}_i	The real vector associated with the imaginary component of the time-invariant part of a complex plane wave $\sqrt{2} (\vec{e}_r + i\vec{e}_i) \exp(i\tau)$, (II. 41b).
\vec{e}_r	The real vector associated with the real component of the time-invariant part of a complex plane wave $\sqrt{2} (\vec{e}_r + i\vec{e}_i) \exp(i\tau)$, (II. 41a).
\vec{e}_1, \vec{e}_2	Real vector components of a complex polarization vector \vec{e} which has been resolved into components which are orthogonal in both space and time, (II. 43)
$\vec{e}_\theta, \vec{e}_\phi$	Real vectors associated with the θ and ϕ components of a complex plane wave $\sqrt{2} [\vec{e}_\theta \exp(i\tau_\theta) + \vec{e}_\phi \exp(i\tau_\phi)] \exp(i\tau)$, where only the phasor $\exp(i\tau)$ depends on time, (II. 40) figure II.1.
\hat{e}_θ	A unit vector $\hat{e}_\theta \times \hat{r}$ perpendicular to \hat{e}_ϕ and \hat{r} , (II.36b) figure II.1.
\hat{e}_ϕ	A unit vector $(\hat{r} \times \hat{x}_o) / \sin \theta$ perpendicular to \hat{r} and \hat{x}_o , (II. 36a) figure II.1
$\underline{\vec{e}}, \underline{\vec{e}}_r$	A bar is used under the symbol to indicate a complex vector: $\underline{\vec{e}} = \vec{e}_p + i\vec{e}_c$, $\underline{\vec{e}}_r = \vec{e}_{pr} + i\vec{e}_{cr}$, (II. 46).
\vec{e}^*	The complex conjugate of $\underline{\vec{e}}$: $\underline{\vec{e}}^* = \vec{e}_p - i\vec{e}_c$.
$ \underline{\vec{e}} , \underline{\vec{e}}_r $	The magnitudes of the complex vectors $\underline{\vec{e}}$ and $\underline{\vec{e}}_r$, (II. 55).
$ e_c , e_{cr} , e_p , e_{pr} $	The amplitudes of the cross and principal polarization components $\vec{e}_c, \vec{e}_{cr}, \vec{e}_p$, and \vec{e}_{pr} , section II. 3. 3.
E	Field strength in dbu, (II. 20).
E_o	The equivalent free space field strength in dbu, (II. 26).
E_I	The equivalent inverse distance field, (II. 28).
E_{1kw}	Field strength in dBu per kilowatt effective radiated power, (II. 23) -(II. 25).
g	Maximum free space directive gain, or directivity, Section II. 3. 4.
g_c	The cross-polarization component of the directive gain, (II. 57).
g_{cr}	The cross-polarization component of the directive gain of a receiver, (II. 51)
g_p	Principal polarization directive gain, (II. 57).
g_{pr}, g_{pt}	Principal polarization directive gains for the receiving and transmitting antennas, respectively, (II. 59).
g_{rn}, g_{tn}	The directive gains g_r and g_t for the n^{th} of a series of plane waves, (II. 66) and (II. 67).
g_θ, g_ϕ	Directive gains associated with the field components $\vec{e}_\theta, \vec{e}_\phi$, (II. 37).
$g(\hat{r})$	Directive gain in the direction \hat{r} , (II. 89).
$g_c(\hat{r}), g_p(\hat{r})$	Cross polarization and principal polarization directive gains in the direction \hat{r} , (II. 94).
$g_r(\hat{r}_1), g_r(\hat{r}_2)$	Directive gains associated with direct and ground-reflected rays, respectively, (II. 117).

$G_{pt}(\hat{r}_1)$	Principal polarization directive gain of the transmitter in the direction \hat{r}_1 , which is the initial direction of the most important propagation path to the receiver, (II.18) and (II.23) to (II.25).
i	$i = \sqrt{-1}$.
I_m	Current in r. m. s. amperes where $m = 0, 1, 2$, (II.76).
I_0, I_1, I_2	Current in r. m. s. amperes corresponding to three elementary dipoles in three mutually perpendicular directions, (II.76).
k	Propagation constant, $k = 2\pi/\lambda$, (II.34).
l	Used as a subscript to indicate a load, for example, z_{lv} represents the impedance of a load at a radio frequency ν , (II.1).
l_{erv}, L_{erv}	The effective loss factor for a receiving antenna at a frequency ν hertz (II.6), $L_{erv} = 10 \log l_{erv}$ db, (II.8).
l_{etv}, L_{etv}	The effective loss factor for a transmitting antenna at a radio frequency ν hertz, (II.7), $L_{etv} = 10 \log l_{etv}$ db, (II.9).
l_{mv}	A mismatch loss factor defined by (II.4).
L_{fr}, L_{ft}	The decibel ratio of the resistance component of antenna input impedance to the free space antenna radiation resistance for the receiving and transmitting antennas, respectively, (II.11).
L_{rr}, L_{rt}	The ratio of the actual radiation resistance of the receiving or transmitting antenna to its radiation resistance in free space, (II.12), (II.13).
L_p	Propagation loss, (II.14).
L_{pb}	Basic propagation loss, (II.15). Basic propagation loss in free space is the same as basic transmission loss in free space.
\hat{p}, \hat{p}_n	Unit complex polarization vector for the incident wave, (II.54), and (II.68).
\hat{p}_r, \hat{p}_{rn}	Unit complex polarization vector associated with a receiving pattern, (II.51) and with the receiving pattern of the n^{th} incident wave, (II.68).
$\hat{p}_{r1}, \hat{p}_{r2}$	The complex receiving antenna polarization vectors \hat{p}_r for each of two ray paths between transmitter and receiver, (II.116).
r	Resistance of an antenna, (II.1).
r	Magnitude of the vector $\vec{r} = r \hat{r}$ in the direction $\hat{r}(\theta, \phi)$, and a coordinate of the polar coordinate system r, θ, ϕ , section II.3.1.
r_{fr}, r_{ft}	Antenna radiation resistance in free space for the receiving and transmitting antennas, respectively, (II.11), (II.12) and (II.13).
r_{lv}	Resistance of a load, (II.1).
r_r, r_t	Antenna radiation resistance of the receiving and transmitting antennas, respectively, (II.10).
r_r^i, r_t^i	Resistance component of antenna input impedance for the receiving and transmitting antennas, respectively, (II.10).
r_v	Resistance of an equivalent loss-free antenna, (II.1c).
r_v^i	Resistance of an actual antenna in its actual environment, (II.1b).
\vec{r}	The vector distance between two points, $\vec{r} = r \hat{r}$, (II.80).

\hat{p}	A unit vector, (II. 35)
$\hat{p}, \hat{e}_\theta, \hat{e}_\phi$	A cartesian unit vector coordinate system, (II. 35) and (II. 36).
s	Total mean power flux density, (II. 58).
s_c, s_p	Mean power flux densities associated with cross-polarization, and principal polarization components, (II. 56).
s_e	The fraction of the total flux density that contributes to the available power, (II. 75).
s_l, s_r	Mean power flux densities associated with left-handed, and right-handed polarization, respectively, (II. 61).
s_o	Free space field intensity in watts per square kilometer, (II. 16).
$\langle s_e \rangle$	The statistical "expected value of s_e ", (II. 76).
$s_c(\vec{r}), s_p(\vec{r})$	Mean power flux densities associated with the cross and principal polarization components of \vec{e} in the direction \vec{r} , (II. 17).
v_n	Complex open-circuit r. m. s. signal voltage for coherently phased multipath components, (II. 65).
v_v	The open-circuit r. m. s. voltage for an equivalent loss-free antenna at a frequency ν , (II. 5).
v'_v	The actual open-circuit r. m. s. voltage at the antenna terminals at a frequency ν , (II. 2).
w_{ab}	The available power corresponding to propagation between hypothetical isotropic antennas, (II. 72).
w_{av}	Available power at the terminals of an equivalent loss-free receiving antenna at a radio frequency ν , (II. 5).
w'_{av}	Available power at the terminals of the actual receiving antenna at a radio frequency ν , (II. 3).
w_{lv}	Power delivered to the receiving antenna load, at a radio frequency ν , (II. 2).
w_{tv}	Total power radiated at a frequency ν , (II. 7).
w'_{tv}	Total power delivered to the transmitting antenna at a frequency ν , (II. 7).
x_{lv}, x'_v, x_v	Reactance of a load, an actual lossy antenna, and an equivalent loss-free antenna, respectively, (II. 1).
\hat{x}_m	One of three mutually perpendicular directions, $m=0, 1, 2$, section II. 3. 7.
$\hat{x}_0, \hat{x}_1, \hat{x}_2$	Axes of a cartesian unit vector coordinate system, (II. 35) figure II. 1.
z_{lv}	Impedance of a load, (II. 1).
z_v	Impedance of an equivalent loss-free antenna (II. 1).
z'_v	Impedance of an actual lossy antenna, (II. 1).
z'^*_v	The conjugate of z'_v , following (II. 2).

ϵ	A small increment used in (II. 97) and (II. 98).
η_0	Characteristic impedance of free space, $\eta_0 = 4\pi c \cdot 10^{-7}$, (II. 38).
θ	A polar coordinate, (II. 35).
ν	Radio frequency in hertz (cycles per second), section II. 1.
ν_1, ν_{11}	Limits of integration (II. 8), (II. 9).
τ	The time-varying phase $\tau = k(ct - r)$, where c is the free space velocity of radio-waves, t is the time at the radio source, and r is the length of the radio ray, (II. 34).
τ_a	Time element defined by (II. 103).
τ_{a1}, τ_{a2}	The time element τ_a corresponding to direct and ground-reflected waves at the receiving antenna, (II. 112).
τ_i	A time-independent phase which is a function of \bar{r} , (II. 42), (II. 64).
τ_{in}	The time-independent phase for the n^{th} component of an incident wave, section II. 3. 6.
τ_{i1}, τ_{i2}	The time-independent phase for two components of an incident wave, (II. 118).
$\tau_{m1}, \tau_{m0}, \tau_{m1}, \tau_{m2}$	Initial phase of the current supported by one of m elementary dipoles, where $m = 0, 1, 2$, (II. 79).
τ_p	A function of the ray path, including allowances for path length differences and diffraction or reflection phase shifts, (II. 64).
$\tau_{pn}, \tau_{p1}, \tau_{p2}$	The phase function τ_p for the n^{th} , first, and second plane wave incident on an antenna from a single source, (II. 65) and (II. 118).
τ_r	Antenna phase response for the receiving antenna, (II. 49).
$\tau_{rn}, \tau_{r1}, \tau_{r2}$	The antenna phase response, τ_r , for the n^{th} , first, and second plane wave incident on the receiving antenna, (II. 65) and section II. 3. 7.
τ_t	Antenna phase response for a transmitting antenna, (II. 64).
$\tau_{tn}, \tau_{t1}, \tau_{t2}$	The antenna phase response τ_t for the n^{th} , first, and second plane wave, (II. 65) and (II. 118).
τ_θ, τ_ϕ	Phases associated with the electrical field components $\vec{e}_\theta, \vec{e}_\phi$, (II. 40).
ϕ	One of the polar coordinates, r, θ, ϕ , (II. 89) and figure II.
ψ_{p1}, ψ_{p2}	The acute angle, ψ_p , for each of two waves, (II. 118).

Annex III

SUPPLEMENTARY INFORMATION AND FORMULAS USEFUL FOR PROGRAMMING

The material of this annex is organized into the following sections:

1. Line-of-sight
2. Diffraction over a single isolated obstacle
3. Diffraction over a single isolated obstacle with ground reflections
4. Diffraction over irregular terrain
5. Forward scatter
6. Forward scatter with antennas elevated
7. Long-term variability
8. List of special symbols used in annex III

Section 1 lists geometric optics formulas for computing transmission loss over a smooth earth, for determining the magnitude and phase of the reflection coefficient, and for computing a first Fresnel zone along a great circle path. Graphs of the magnitude R and phase c of the reflection coefficient are included. Section 2 gives mathematical expressions that approximate the curves $A(v, 0)$, $A(0, \rho)$ and $U(v\rho)$ for convenience in using a digital computer. Section 3 lists geometric optics formulas used to compute diffraction attenuation when several components of the received field are affected by reflection from the earth's surface. Section 4 defines the parameters K and b for both horizontally and vertically polarized radio waves. Section 5 shows the function $F(\theta d)$ for $N_g = 250, 301, 350, \text{ and } 400$, and for values of s from 0.01 to 1. Curve fits to the function $F(\theta d)$ and equations for computing $H_o(\eta_g = 0)$ are included. Section 6 suggests modifications of the prediction methods for use when antenna beams are elevated or directed out of the great circle plane. Section 7 shows diurnal and seasonal changes in long-term variability. Mathematical expressions used to compute predicted distributions are shown and a method of mixing distributions is described. Section 8 is a list of special symbols used in this annex.

Section I. 3 of annex I explains an easily programmed method for obtaining reference values of attenuation relative to free space A_{CT} for a wide range of applications. These reference values may be converted to estimates of transmission loss exceeded for $100p = 100(1 - q)$ percent of the time by subtracting the quantities $V(0.5)$ and $Y(q)$ defined by (10.4) and (10.5) of volume 1 and discussed also in section 7 of this annex.

III-1

III.1 Line-of-Sight

Simple formulas for line-of-sight propagation which suffice for most applications, are given in section 5 of the report. Formulas for geometry over a smooth earth and for determining the magnitude and phase of the reflection coefficient are given here. These formulas may be used when the great circle path terrain visible to both antennas will support a substantial amount of reflection, and it is reasonable to fit a smooth convex curve of radius a to this portion of the terrain.

Figure 5.1b illustrates the geometry appropriate for reflection of a single ray by a smooth earth of effective radius a . In the figure, ψ is the grazing angle at the geometrical reflection point located at a distance d_1 from an antenna of height h_1 and at a distance d_2 from an antenna of height h_2 . The total path distance $d = d_1 + d_2$ is measured along an arc of radius a . The difference, Δr , between the reflected ray path length $r_1 + r_2$ and the length of the direct ray, r_0 , is calculated to find the phase of a radio field which is the sum of ground-reflected and free space fields. If Δr is less than 0.06λ , these ray optics formulas are not applicable. For almost all cases of interest the angle ψ is small and the straight line distances r_1 , r_2 and r_0 are very nearly equal to the mean sea level arc-distances d_1 , d_2 and d . The geometric optics formulas given below usually require double-precision arithmetic,

$$\tan \psi = \cot(d_1/a) - (1 + h_1/a)^{-1} \csc(d_1/a) \cong \frac{h_1}{d_1} - \frac{d_1}{2a} \quad (\text{III. 1})$$

$$\tan \psi = \cot(d_2/a) - (1 + h_2/a)^{-1} \csc(d_2/a) \cong \frac{h_2}{d_2} - \frac{d_2}{2a} \quad (\text{III. 2})$$

$$r_0 = a \left\{ (h_1/a)^2 + (h_2/a)^2 - 2(h_1/a)(h_2/a) + 2[1 + h_1/a + h_2/a + (h_1/a)(h_2/a)][1 - \cos(d/a)] \right\}^{1/2} \quad (\text{III. 3})$$

$$r_1 = \left[(a \sin \psi)^2 + h_1(2a + h_1) \right]^{1/2} - a \sin \psi \quad (\text{III. 4})$$

$$r_2 = \left[(a \sin \psi)^2 + h_2(2a + h_2) \right]^{1/2} - a \sin \psi \quad (\text{III. 5})$$

$$\Delta r = r_1 + r_2 - r_0 = 4 r_1 r_2 \sin^2 \psi / (r_1 + r_2 + r_0) \quad (\text{III. 6})$$

Equating (III. 1) and (III. 2) and substituting $d - d_1$ for d_2 in (III. 2), the distance d_1 may be determined graphically or by trial and error, and $\tan \psi$ is then calculated using (III. 1).

Using double precision arithmetic, (III.1) through (III.6) give an accurate estimate of the path difference Δr for reflection of a single ray from a smooth earth. This value is then used in (5.4) or (5.5) of section 5 to compute the attenuation relative to free space.

If either h_1 or h_2 greatly exceeds one kilometer, and if it is considered worthwhile to trace rays through the atmosphere in order to determine ψ more accurately, values of d_1 or d_2 , tabulated by Bean and Thayer [1959], may be used. Given h_1 , h_2 , and the surface refractivity, N_s , select trial values for ψ , calculate d_1 and d_2 , and continue until $d_1 + d_2 = d$. Then (III.1) and (III.2) must be solved for new values of h_1 and h_2 if (III.3), (III.4), and (III.5) are used to obtain the path difference, $\Delta r = r_1 + r_2 - r_0$.

The symbols R in (5.1) and c in (5.4) represent the magnitude and the phase angle relative to w , respectively, of the theoretical coefficient $R \exp[-i(w-c)]$ for reflection of a plane wave from a smooth plane surface of a given conductivity σ and relative dielectric constant ϵ . Values of R and c as a function of the grazing angle ψ are shown in figures III.1 to III.8 for vertical and horizontal polarization over good, average, and poor ground, and over sea water. The magnitude R of the smooth plane earth reflection coefficient is designated R_v or R_h for vertical or horizontal polarization respectively, and is read on the left-hand ordinate scale using the solid curves. The phase angle relative to w , is designated c_v or c_h for vertical or horizontal polarization respectively, and is read in radians on the right-hand scale using the dashed curves. As seen from these figures in most cases when the angle ψ is small, R is very nearly unity and c may be set equal to zero. A notable exception occurs in the case of propagation over sea water using vertical polarization.

In preparing figures III.1 to III.8, the following general expressions for the magnitudes R_v and R_h and lags $(w-c_v)$ and $(w-c_h)$ were used. In these equations, ϵ is the ratio of the surface dielectric constant to that of air, σ is the surface conductivity in mhos per meter, f is the radio frequency in megacycles per second, and ψ is the grazing angle in radians.

$$x = 1.80 \times 10^4 \sigma / f, \quad q = x / (2p) \quad (\text{III. 7})$$

$$2p^2 = \left[(\epsilon - \cos^2 \psi)^2 + x^2 \right]^{1/2} + (\epsilon - \cos^2 \psi) \quad (\text{III. 8})$$

$$b_v = \frac{\epsilon^2 + x^2}{p^2 + q^2}, \quad b_h = \frac{1}{p^2 + q^2} \quad (\text{III. 9})$$

$$m_v = \frac{2(p\epsilon + qx)}{p^2 + q^2}, \quad m_h = \frac{2p}{p^2 + q^2} \quad (\text{III. 10})$$

$$R_v^2 = \left[1 + b_v \sin^2 \psi - m_v \sin \psi \right] \left[1 + b_v \sin^2 \psi + m_v \sin \psi \right]^{-1} \quad (\text{III. 11})$$

$$R_h^2 = \left[1 + b_h \sin^2 \psi - m_h \sin \psi \right] \left[1 + b_h \sin^2 \psi + m_h \sin \psi \right]^{-1} \quad (\text{III. 12})$$

$$\pi - c_v = \tan^{-1} \left(\frac{x \sin \psi - q}{\epsilon \sin \psi - p} \right) - \tan^{-1} \left(\frac{x \sin \psi + q}{\epsilon \sin \psi + p} \right) \quad (\text{III. 13})$$

$$\pi - c_h = \tan^{-1} \left(\frac{-q}{\sin \psi - p} \right) - \tan^{-1} \left(\frac{q}{\sin \psi + p} \right) \quad (\text{III. 14})$$

The angle c_v is always positive and less than π , and c_h is always negative with an absolute magnitude less than π . The pseudo Brewster angle, where c_v suddenly changes from near zero to $\pi/2$, and where R_v is a minimum, is $\sin^{-1} \sqrt{1/b_v}$.

For grazing angles less than 0.1 radian, for overland propagation, and for frequencies above 30 Mc/s, excellent approximations to (III.11) and (III.12) are provided by the following formulas:

$$R_v = \exp(-m_v \psi) \quad (\text{III. 15})$$

$$R_h = \exp(-m_h \psi) \quad (\text{III. 16})$$

The assumption of a discrete reflection point with equal angles of incidence and reflection as shown in figure 5.1 is an oversimplification. Actually, reflection occurs from all points of the surface. For irregular terrain, this is taken into account by a terrain roughness factor σ_h , (subsection 5.1), which is the r. m. s. deviation of terrain relative to a smooth curve computed within the limits of a first Fresnel zone in a horizontal plane. The outline of such a Fresnel ellipse is determined by the condition that the length of a ray path, $r_{11} + r_{21}$, corresponding to scattering from a point on the edge of the ellipse is half a wave length longer than the geometrical ray path, $r_1 + r_2$, where the angles of incidence and reflection are equal.

The first Fresnel ellipse cuts the great circle plane at two points, x_a and x_b kilometers from the transmitter. The distances x_a and x_b are defined by the relation

$$\sqrt{r_1^2 \sin^2 \psi + x^2} + \sqrt{r_2^2 \sin^2 \psi + [(r_1 + r_2) \cos \psi - x]^2} = r_1 + r_2 + \lambda/2 \quad (\text{III. 17})$$

The exact solution for x is

$$2x_{a,b}(1+\delta) = [(r_1+r_2)(1+\delta) + (r_1-r_2)] \cos \psi \pm (r_1+r_2 + \lambda/2) \delta \sqrt{1 + 4r_1r_2/[(r_1+r_2)^2 \delta]} \quad (\text{III. 18})$$

where

$$r_1^2 = h_1'^2 + d_1^2, \quad r_2^2 = h_2'^2 + d_2^2, \quad (r_1+r_2)^2 = (h_1'+h_2')^2 + d^2$$

$$\cos \psi = d_1/r_1 = d_2/r_2, \quad \sin \psi = h_1'/r_1 = h_2'/r_2$$

$$\delta = \left[\frac{\lambda^2}{4(r_1+r_2)^2} + \frac{\lambda}{r_1+r_2} \right] / \sin^2 \psi$$

d_1, d_2 are defined by (5.7), and λ is the radio wavelength in kilometers.

As an alternative method, the points x_a and x_b may be computed in terms of path distance, the heights h_1' and h_2' and the radio frequency. In this method, the distance x_0 to the center of the first Fresnel zone is first computed, then the distance x_1 from the center to the margin of the zone is subtracted from x_0 to give x_a , and added to give x_b .

$$x_0 = d/2 \left[1 + B f(h_1'^2 - h_2'^2) \right] \text{ km} \quad (\text{III. 19})$$

where

$$B = \left[0.3d(1 + 2h_1'h_2'/d^2) + f(h_1'+h_2')^2 \right]^{-1} \quad (\text{III. 20})$$

$$x_1 = 0.548 B d^2 \left\{ \left[f h_1'h_2'/d + 0.075(1 + 2h_1'h_2'/d^2) \right] \left[\frac{1 + (h_1'+h_2')^2/d^2}{1 + 2h_1'h_2'/d^2} \right] \right\}^{1/2} \quad (\text{III. 21})$$

$$x_a = x_0 - x_1 \text{ km}, \quad x_b = x_0 + x_1 \text{ km}.$$

CCP 702-1

The method given in (III.19) to (III.21) is applicable whenever $d \gg \lambda$. If in addition, $h_1' h_2' \ll d^2$, the computation of B , and x_1 may be simplified as follows:

$$B = [0.3d + f(h_1' + h_2')^2]^{-1} \quad (\text{III. 22})$$

$$x_1 = 0.548 \beta d^2 \left\{ [f h_1' h_2' / d + 0.075] [1 + (h_1' + h_2')^2 / d^2] \right\}^{1/2} \quad (\text{III. 23})$$

THE COMPLEX REFLECTION COEFFICIENT $R_e^{i(\pi-c)}$

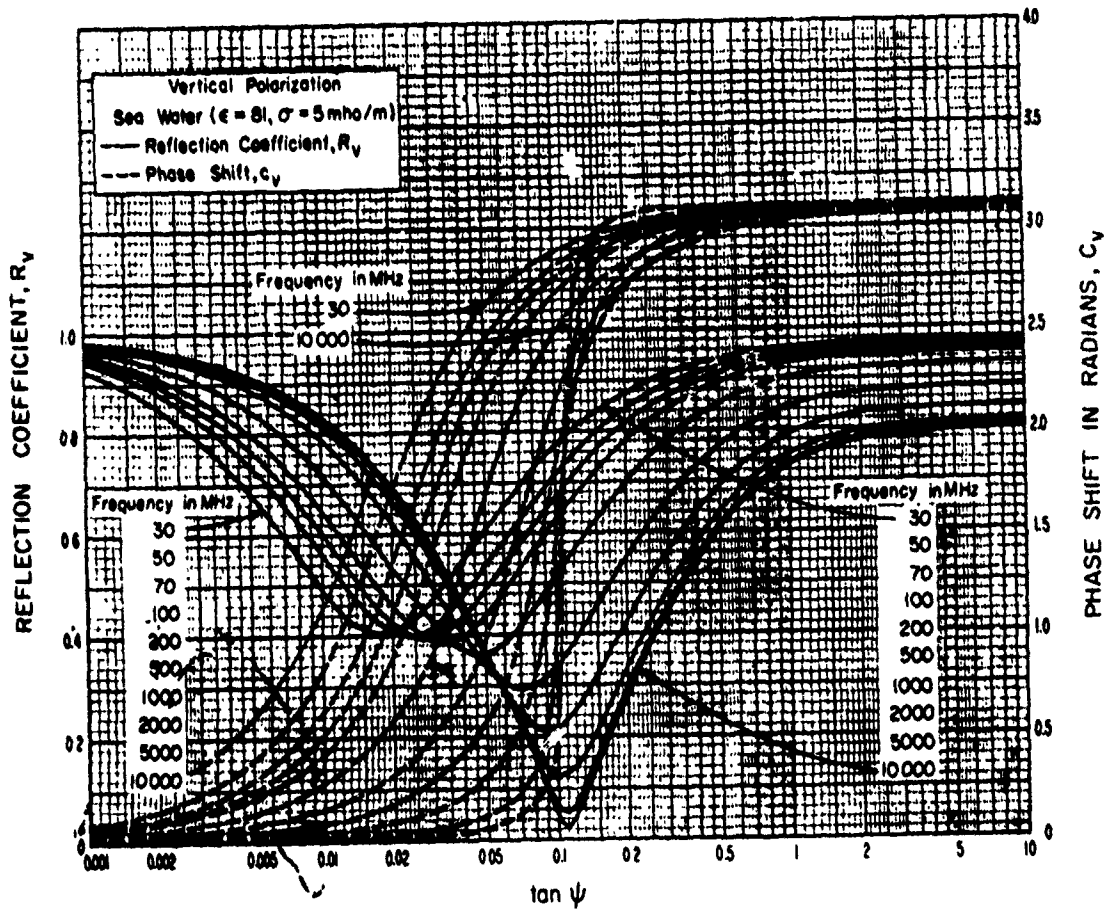


Figure III.1

III-7

THE COMPLEX REFLECTION COEFFICIENT $R_e^{i(\pi-c)}$

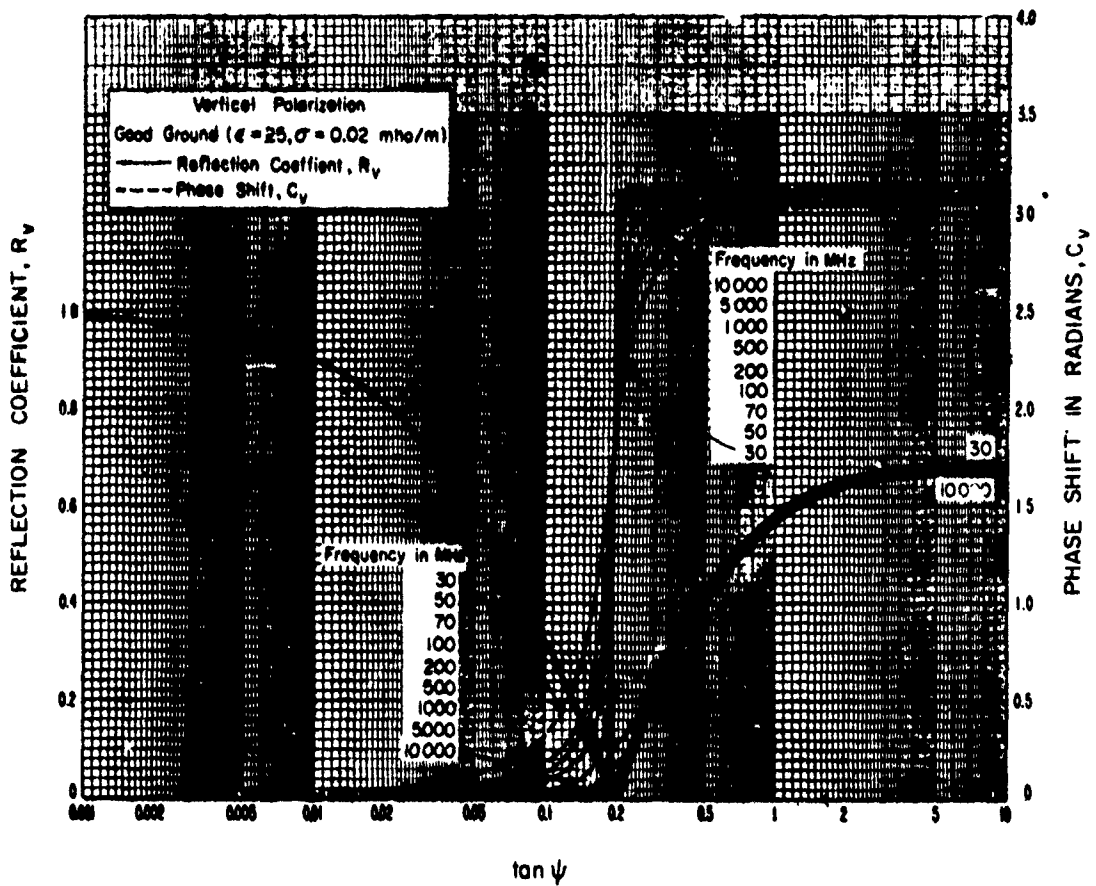


Figure III.2

THE COMPLEX REFLECTION COEFFICIENT $R_e^{(\pi-c)}$

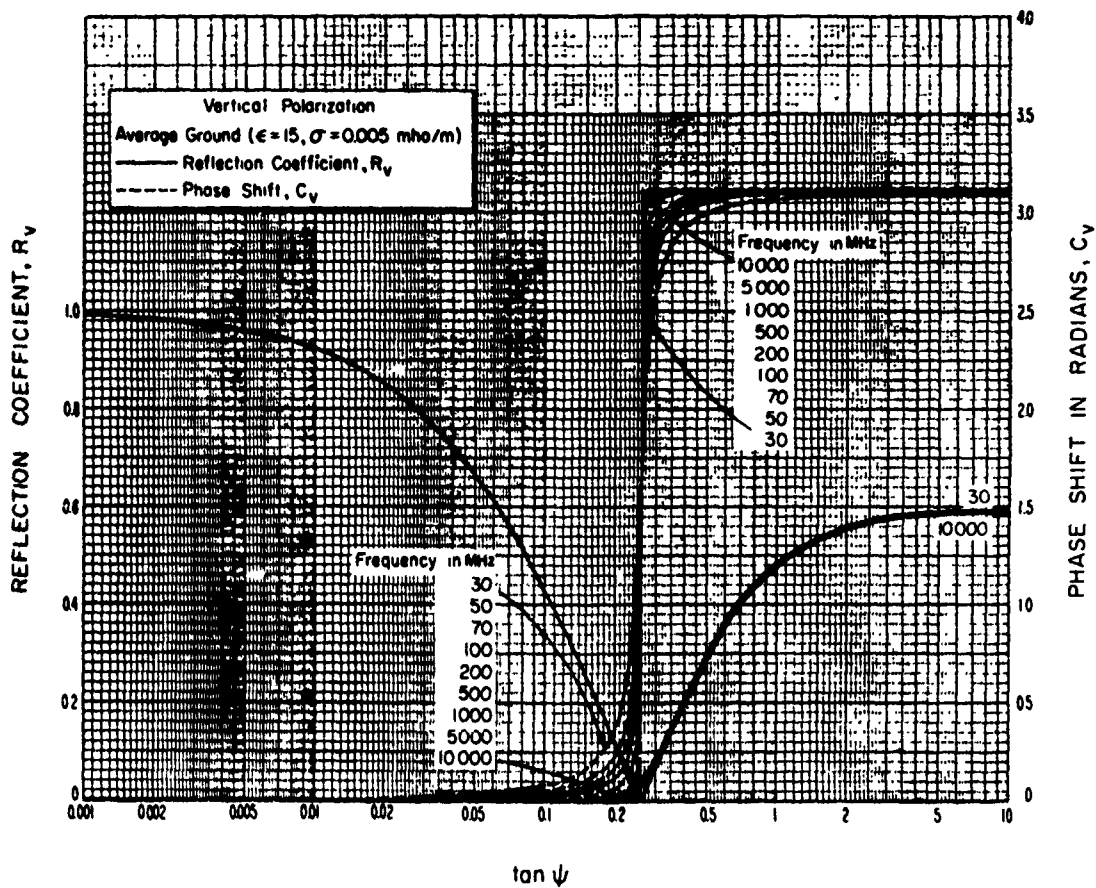


Figure III.3

THE COMPLEX REFLECTION COEFFICIENT $R_v^{(w-c)}$

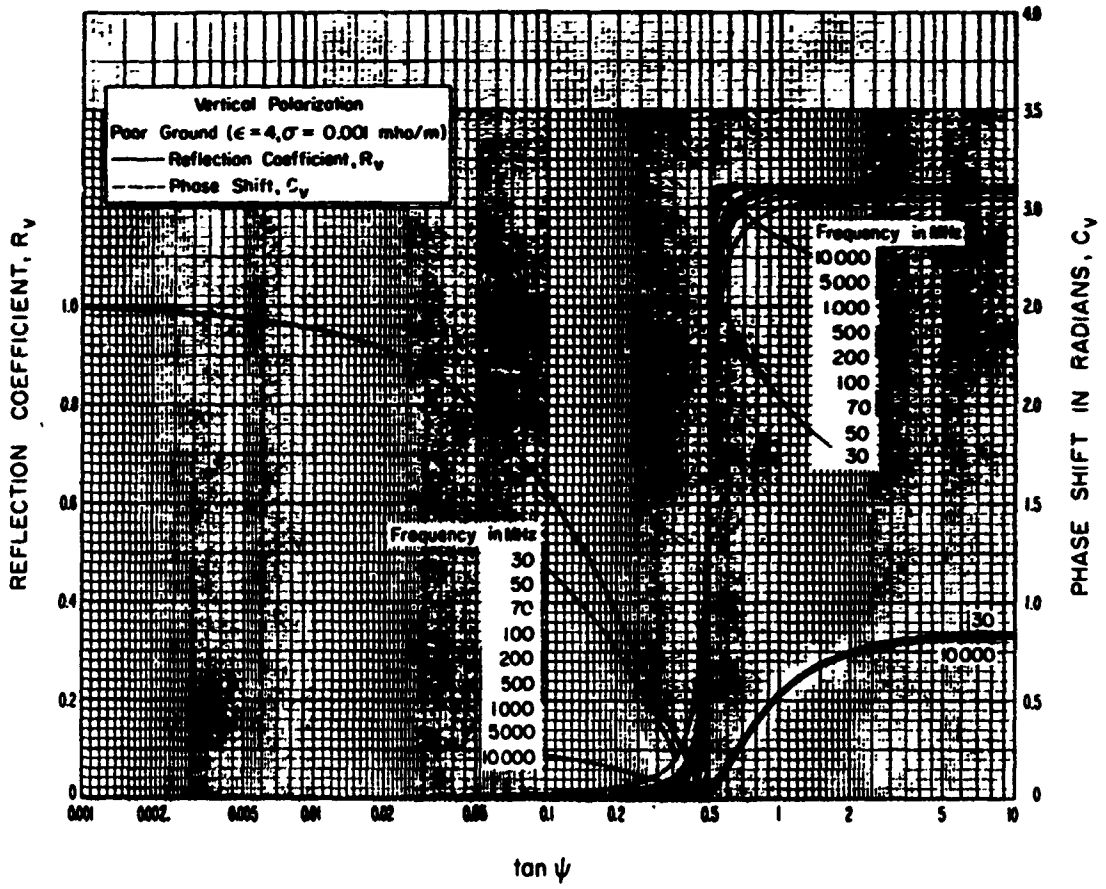


Figure III.4

THE COMPLEX REFLECTION COEFFICIENT $Re^{-i(\pi-c)}$

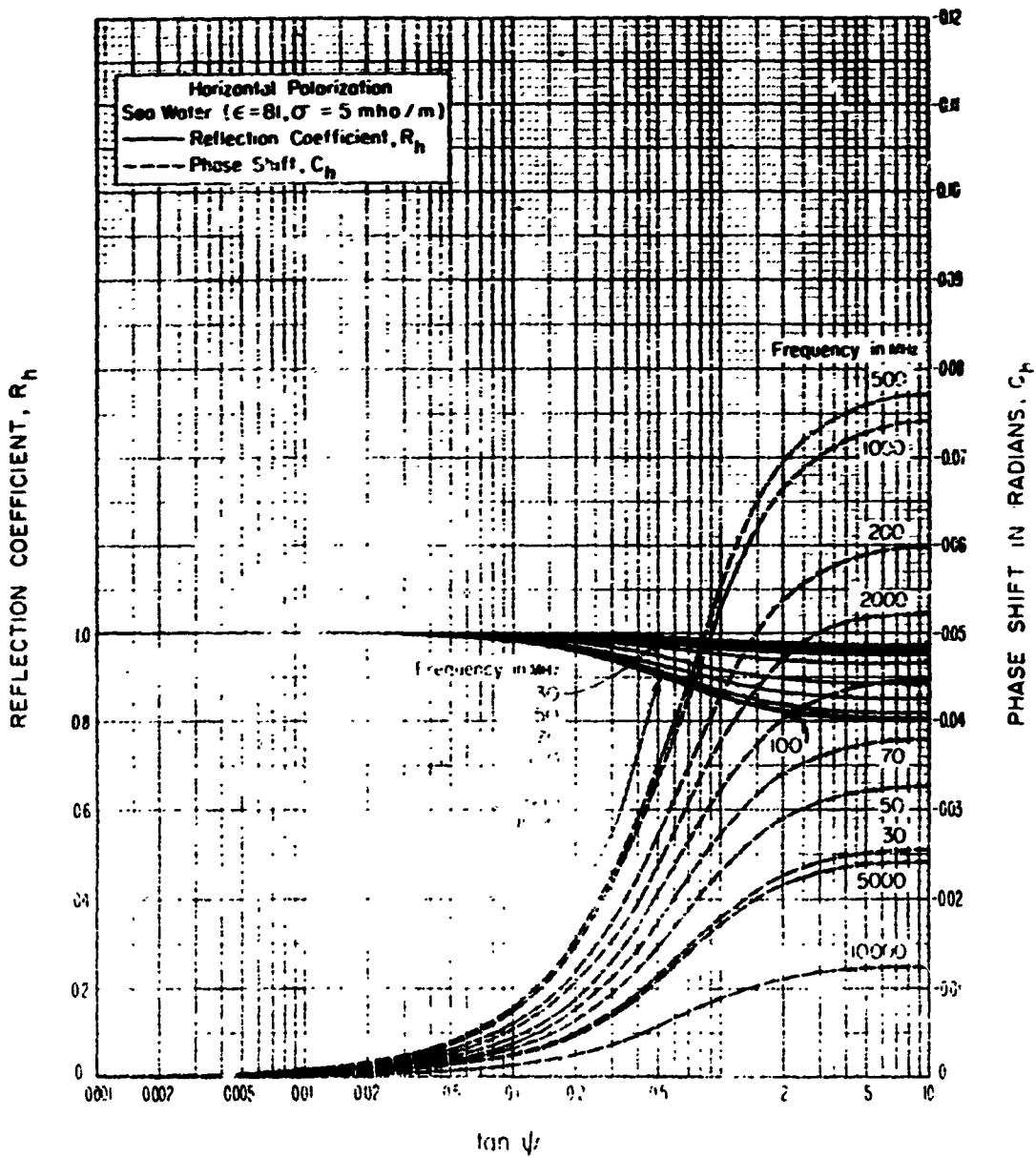


Figure III 5

III-11

THE COMPLEX REFLECTION COEFFICIENT $Re^{-i(\pi-c)}$

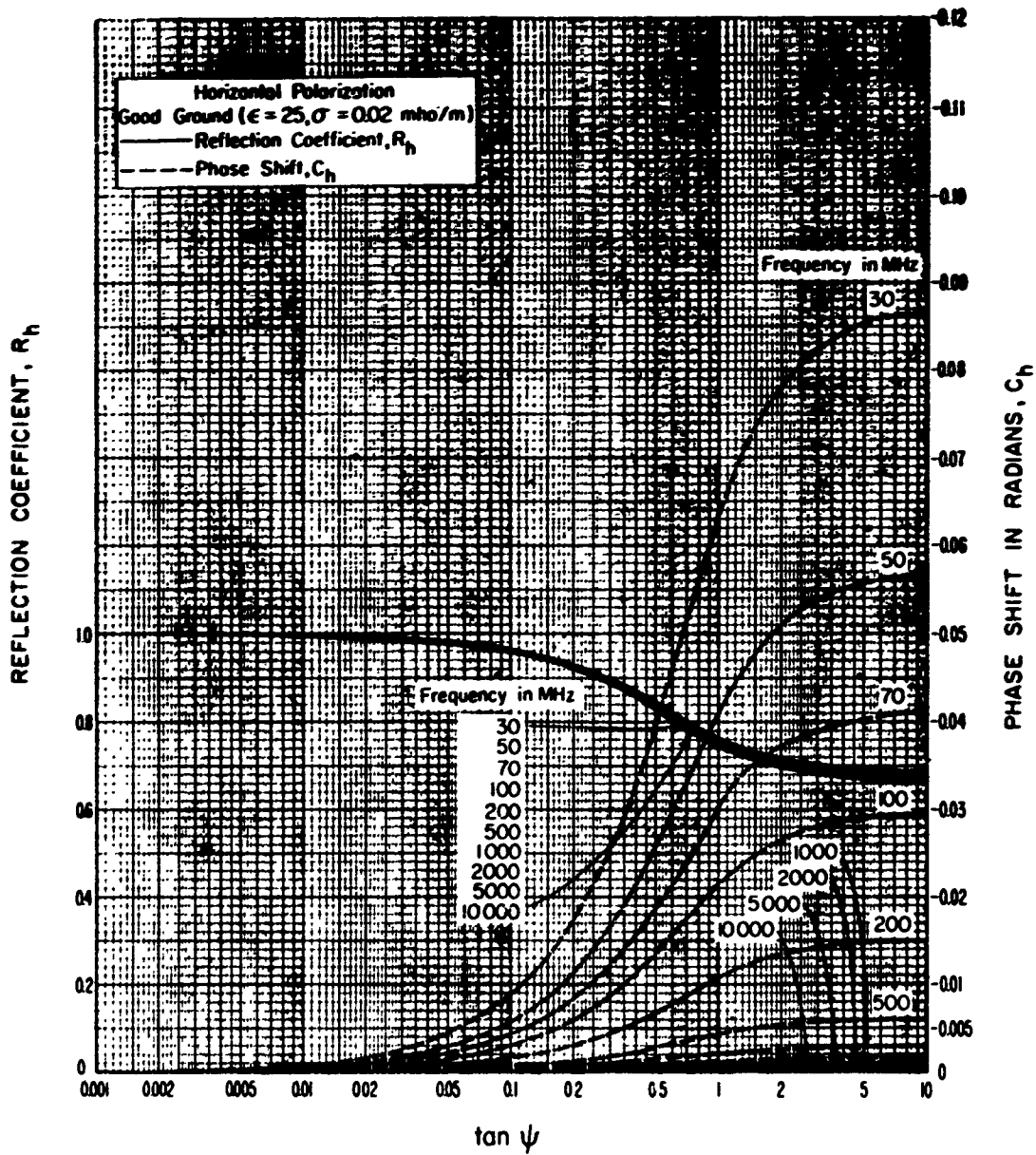


Figure III.6

THE COMPLEX REFLECTION COEFFICIENT $Re^{-i(\pi-c)}$

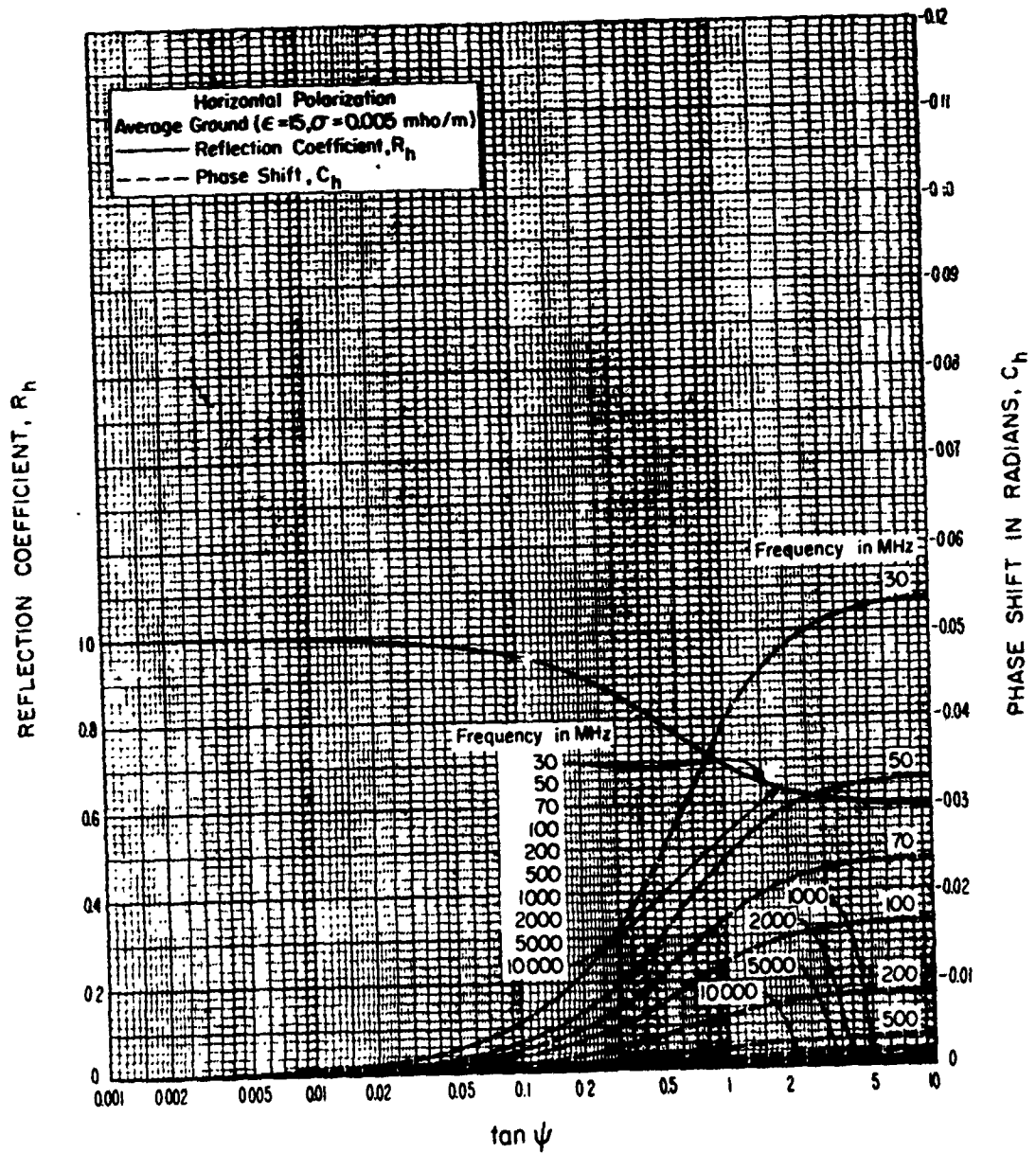


Figure III.7

THE COMPLEX REFLECTION COEFFICIENT $R_0^{-i(\pi-c)}$

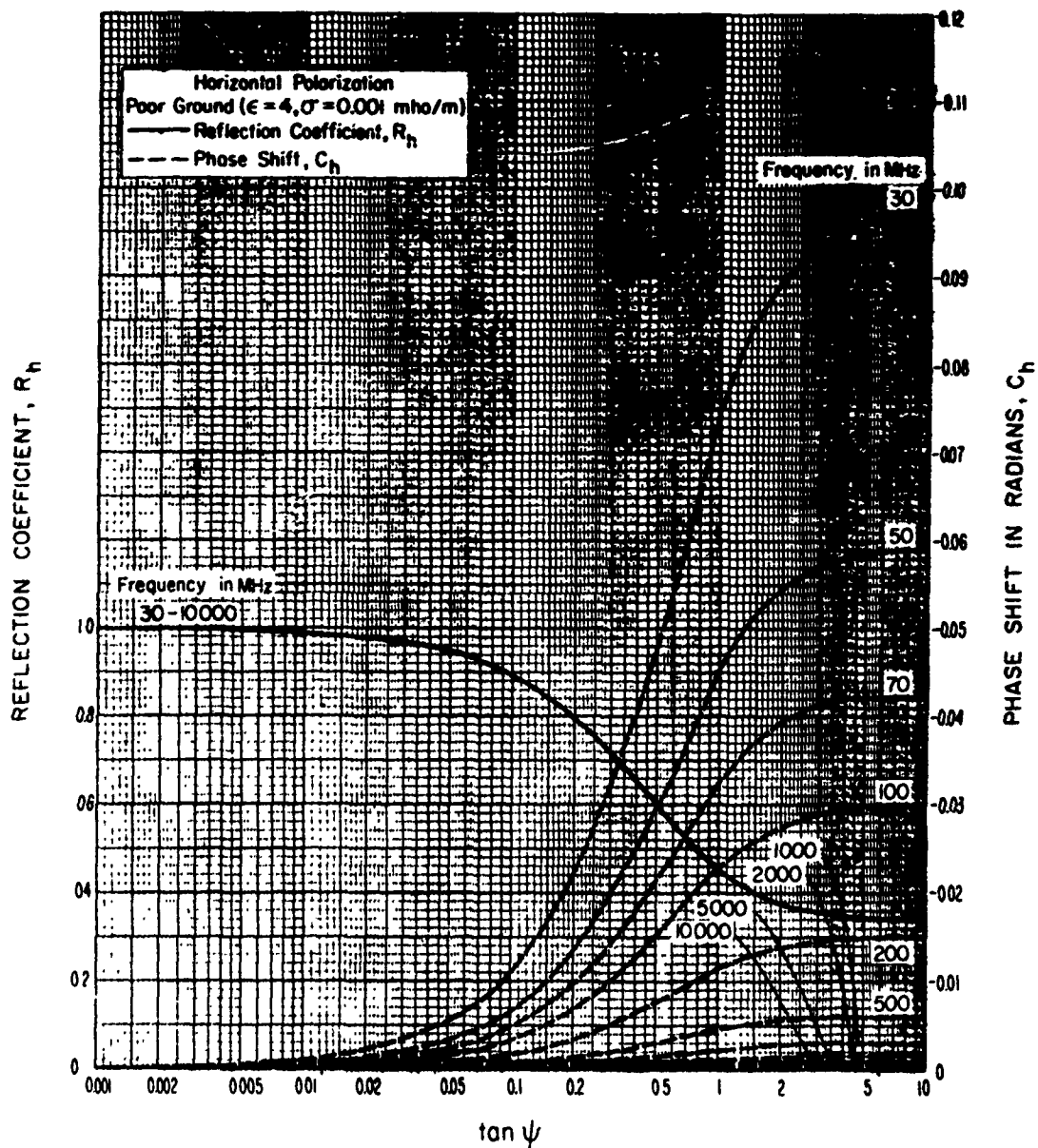


Figure III.8

III.2 Diffraction over a Single Isolated Obstacle.

The theoretical diffraction loss curves on figures 7.1 to 7.4 have been fitted by arbitrary mathematical expressions for convenience in using a digital computer.

The diffraction loss for an isolated rounded obstacle and irregular terrain is given in section 7 as:

$$A(v, \rho) = A(v, 0) + A(0, \rho) + U(v\rho) \text{ db} \quad (7.7)$$

where the parameter v is defined as

$$v = \pm 2\sqrt{\Delta r/\lambda} \cong \pm \sqrt{2d \alpha_0 \beta_0 / \lambda} \quad (7.1a)$$

or

$$v = \pm 2.5830 \sqrt{f d_1 d_2 / d} \quad (7.1b)$$

and ρ an index of curvature of the rounded obstacles is defined as:

$$\rho = 0.676 r^{1/3} f^{-1/6} [d/r_1 r_2]^{1/2} \quad (7.8)$$

For an ideal knife edge, ($\rho = 0$), the diffraction loss is $A(v, 0)$ and is shown on figure 7.1. For values of v from -0.8 to large positive values, this curve may be approximated using the following mathematical expressions:

For $-0.8 \leq v \leq 0$,

$$A(v, 0) = 6.02 + 9.0 v + 1.65 v^2 \text{ db.} \quad (\text{III. 24a})$$

For $0 \leq v \leq 2.4$,

$$A(v, 0) = 6.02 + 9.11 v - 1.27 v^2 \quad (\text{III. 24b})$$

For $v > 2.4$,

$$A(v, 0) = 12.953 + 20 \log v \text{ db.} \quad (\text{III. 24c})$$

The theoretical curve for $A(0, \rho)$ is approximated by:

$$A(0, \rho) = 6.02 + 5.556 \rho + 3.418 \rho^2 + 0.256 \rho^3 \text{ db,} \quad (\text{III. 25})$$

and the curve $U(v\rho)$ is approximated as follows:

CCP 702-1

For $v\rho \leq 3$: $U(v\rho) = 11.45 v\rho + 2.19 (v\rho)^2 - 0.206 (v\rho)^3 - 6.02$ db. (III. 26a)

For $3 < v\rho \leq 5$: $U(v\rho) = 13.47 v\rho + 1.058 (v\rho)^2 - 0.048 (v\rho)^3 - 6.02$ db. (III. 26b)

For $v\rho < 5$: $U(v\rho) = 20 v\rho - 18.2$ db. (III. 26c)

An average allowance for terrain foreground effects may be made by adding a term $10 \exp(-2.3 \rho)$ to $A(0, \rho)$. This term gives a correction which ranges from 10 db for $\rho = 0$ to 1 db for $\rho = 1$.

When reflections from terrain on either or both sides of the obstacle should be considered, the method given in the following section may be used. This method considers the diffraction loss and phase lag over the diffracting obstacle, and the path length differences and reflection coefficients of the reflected waves.

III. 3 Diffraction over a Single Isolated Obstacle with Ground Reflections

Diffraction over an isolated obstacle is discussed in section 7, where ways of approximating the effects of reflection and diffraction from foreground terrain are indicated. Where the effects of reflection are expected to be of great importance, such as in the case of propagation over a large body of water, the following geometric optics method may be used.

Figure III. 9 illustrates four distinct ray paths over a knife edge (which may be rounded), the first ray is not reflected from the ground, the second and third are each reflected once, and the fourth ray is reflected once on each side of the obstacle. Each ray is subject to a diffraction loss $f_j(v, \rho)$ and a phase lag $\phi_j(v, \rho) - 90 v^2$ at the knife edge, where $j = 1, 2, 3, 4$. Both $f_j(v, \rho)$ and $\phi_j(v, \rho)$ depend on the parameters v and ρ given in section III. 2. When the isolated obstacle is an ideal knife edge, the diffraction loss depends only on the parameter v , which may be written:

$$v_j = \pm 2\sqrt{\Delta_j/\lambda} \approx \pm \sqrt{2d \sigma_{oj} \delta_{oj}/\lambda} \quad (\text{III. 27})$$

where Δ_j , by figure III. 9, is

$$\begin{aligned} \Delta_1 &= r_{10} + r_{20} - r_{00}, & \Delta_2 &= r_{11} + r_{12} + r_{20} - r_{02} \\ \Delta_3 &= r_{10} + r_{21} + r_{22} - r_{03}, & \Delta_4 &= r_{11} + r_{12} + r_{21} + r_{22} - r_{04} \end{aligned} \quad (\text{III. 28})$$

Path differences Δ_j used to calculate v_j in (III. 27) are closely approximated by the following formulas:

$$\begin{aligned} \Delta_j &= d_r \theta_j^2, & d_r &= d_1 d_2 / (2d), & \theta_j &= \theta + \theta_{jr} \\ \theta_{1r} &= 0, & \theta_{2r} &= 2d_{11} \psi_1 / d_1, & \theta_{3r} &= 2d_{22} \psi_2 / d_2, & \theta_{4r} &= \theta_{2r} + \theta_{3r} \end{aligned} \quad (\text{III. 29})$$

The total phase lag for an isolated rounded obstacle path relative to a reference free-space path of length $\Delta_j + r_{0j}$ is given by

$$\phi_j(v, \rho) - 90 v_j^2 = \phi(v_j, 0) + \phi(0, \rho_j) + \phi(v_j, \rho_j) \text{ degrees} \quad (\text{III. 30a})$$

where the functions $\phi(v, 0)$, $\phi(0, \rho)$, and $\phi(v, \rho)$ are plotted as dashed curves on figures 7. 1, 7. 4, and 7. 5. For an ideal knife edge, where the radius of curvature of the crest is zero, $\rho = 0$, and (III. 30a) reduces to

$$\text{for } v > 0 \quad \phi_j(v, 0) - 90 v_j^2 = \phi(v_j, 0) \text{ degrees} \quad (\text{III. 30b})$$

$$\text{for } v \leq 0 \quad \phi_j(v, 0) - 90 v_j^2 = \phi(v_j, 0) - 90 v_j^2 \text{ degrees} \quad (\text{III. 30c})$$

The three components of the received field which are affected by reflection from the surface depend also upon effective ground reflection coefficients $R_{e2} \exp[-i(\pi - c_2)]$ and $R_{e3} \exp[-i(\pi - c_3)]$, defined in section 5, and upon ray path differences Δ_{2r} and Δ_{3r} :

$$\begin{aligned} \Delta_{2r} &= r_{11} + r_{12} - r_{10} \approx 2v_1^2 d_{11} d_{12}/d_1 \\ \Delta_{3r} &= r_{21} + r_{22} - r_{20} \approx 2v_2^2 d_{21} d_{22}/d_2 \end{aligned} \quad (\text{III. 31})$$

It may be assumed that $c_2 = c_3 = 0$ so that the reflection coefficients are $-R_{e2}$ and $-R_{e3}$.

Introducing the propagation constant $k = 2\pi/\lambda$ rad/meter = $360/\lambda$ degrees/meter and expressing the ray path differences $k\Delta_{2r}$ and $k\Delta_{3r}$ in electrical degrees, the attenuation relative to free space is then

$$\begin{aligned} A = -20 \log \left\{ \left| f_1 \exp[-i(\theta_1 - 90 v_1^2)] - R_{e2} f_2 \exp[-i(\theta_2 - 90 v_2^2 + k\Delta_{2r})] \right. \right. \\ \left. \left. - R_{e3} f_3 \exp[-i(\theta_3 - 90 v_3^2 + k\Delta_{3r})] + R_{e2} R_{e3} f_4 \exp[-i(\theta_4 - 90 v_4^2 + k\Delta_{2r} + k\Delta_{3r})] \right| \right\} \text{ db} \end{aligned} \quad (\text{III. 32})$$

In the general case of a rounded knife-edge, the magnitudes $f_j = f_j(v, \rho)$ are determined from

$$\log f_j(v, \rho) = -A_j(v, \rho)/20, \quad (\text{III. 33})$$

where $A(v, \rho)$ is defined in (7.7) and shown graphically on figure 7.3. The total phase lag $\theta = \theta_j(v, \rho)$ relative to a reference free space path of length r_{0j} is defined in (7.13a) and (7.14). Components for $A(v, \rho)$ and $\theta(v, \rho)$ are shown graphically in figures 7.1, 7.4 and 7.5. Approximate expressions for the components of $A(v, \rho)$ are given in section III.2.

For the ideal knife-edge, $\rho = 0$, and the f_j and θ_j may be calculated from:

$$\begin{aligned} f_j &= +\frac{1}{2} \sqrt{(1 - C_j - S_j)^2 + (C_j - S_j)^2}, \quad \tan \theta_j = \frac{C_j - S_j}{1 - C_j - S_j} \\ C_j &= \int_0^v \cos\left(\frac{\pi t^2}{2}\right) dt, \quad S_j = \int_0^v \sin\left(\frac{\pi t^2}{2}\right) dt. \end{aligned} \quad (\text{III. 34})$$

Tables [1950], and the NBS AMS 55 Handbook of Mathematical Functions [1964] give complete tables, series expansions, and asymptotic expressions for the Fresnel integrals C_j and S_j . Furthermore, if v is larger than 3:

$$f_j \approx 0.22508/v_j, \quad \theta_j - 90 v_j^2 \approx 45 \text{ degrees} \quad (\text{III. 35})$$

Figure III. 10 is a nomogram which may be used in the determination of $\{(v_j)\}$ and $\Phi(v_j)$ for both positive and negative values of v . This nomogram is based on the representation of Fresnel integrals by the Cornu spiral.

After θ , d , d_1 , d_2 , d_{11} , d_{12} , d_{21} , d_{22} , ψ_1 , and ψ_2 , as shown in figure III. 9 have been determined, the following procedure may be used.

1. Calculate θ_j and Δ_j for $j = 1, 2, 3, 4$, using (III. 29).
2. Calculate v_j , C_j , S_j , f_j , and $\Phi_j - 90 v_j^2$ using (III. 27), (III. 34), (III. 30) and figures in section 7 or equivalent mathematical approximations.
3. Calculate Δ_{2r} and Δ_{3r} from (III. 31).
4. Calculate R_{e2} and R_{e3} from (5. 1), or assume that $R_{e2} = R_{e3} = 1$.
5. Substitute these values in (III. 32).

To check the calculation of each v_j , the approximation given in (III. 27) may be used, with the following formulas for $\alpha_{oj} = d_2 \theta_j / d$ and $\beta_{oj} = d_1 \theta_j / d$:

$$\begin{aligned}
 \alpha_{01} &= d_2 \theta / d & \beta_{01} &= d_1 \theta / d \\
 \alpha_{02} &= \alpha_{01} + 2 d_{11} \psi_1 d_2 / (d_1 d) & \beta_{02} &= \beta_{01} + 2 d_{11} \psi_1 / d \\
 \alpha_{03} &= \alpha_{01} + 2 d_{22} \psi_2 / d & \beta_{03} &= \beta_{01} + 2 d_{22} \psi_2 d_1 / (d_2 d) \\
 \alpha_{04} &= \alpha_{02} + \alpha_{03} - \alpha_{01} & \beta_{04} &= \beta_{02} + \beta_{03} - \beta_{01} \quad (\text{III. 36})
 \end{aligned}$$

A special case will be described for which (III. 29) and (III. 31) may be simplified. Assume that each reflecting surface may be considered a plane. Let h_t and h_{tm} be the heights of the transmitting antenna and the knife edge above the first plane, and let h_{rm} and h_r be the heights of the knife edge and the receiving antenna above the second reflecting plane. Assume that Δ_r is very small for every Δ . In terms of the heights h_t , h_{tm} , h_{rm} , h_r , the parameters θ , d_1 , and d_2 and the parameter $d_r = d_1 d_2 / (2d)$:

$$\begin{aligned}
 \Delta_{2r} &= 2 h_t h_{tm} / d_1, \quad \Delta_{3r} = 2 h_r h_{rm} / d_2 \\
 \Delta_1 &= d_r \theta^2, \quad \Delta_2 = d_r (0 + h_{tm} \Delta_{2r})^2 \\
 \Delta_3 &= d_r (0 + h_{rm} \Delta_{3r})^2, \quad \Delta_4 = d_r (0 + h_{tm} \Delta_{2r} + h_{rm} \Delta_{3r})^2. \quad (\text{III. 37})
 \end{aligned}$$

CCP 702-1

(Page III-20 intentionally omitted)

BEYOND-HORIZON KNIFE-EDGE DIFFRACTION WITH GROUND REFLECTIONS

(KNIFE-EDGE NORMAL TO RAY PATH)

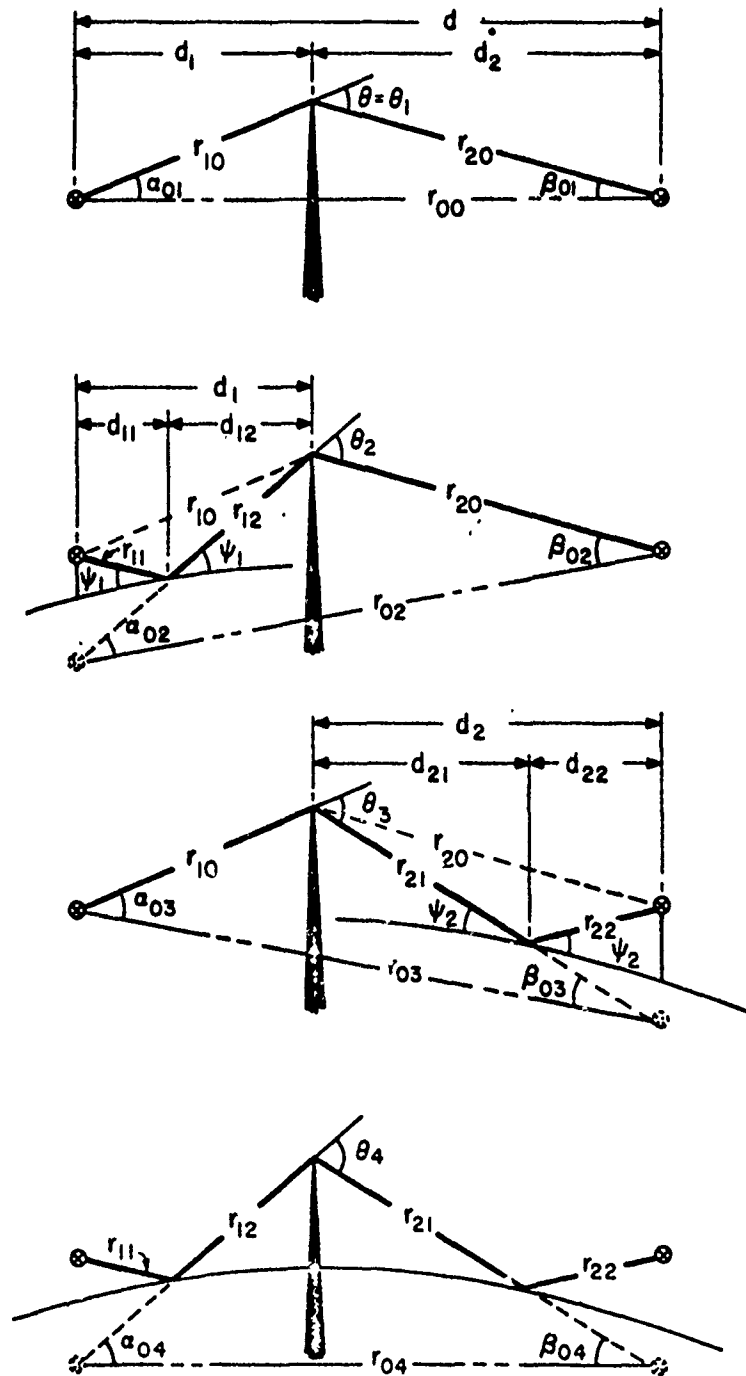


Figure III 9

CORNU'S SPIRAL

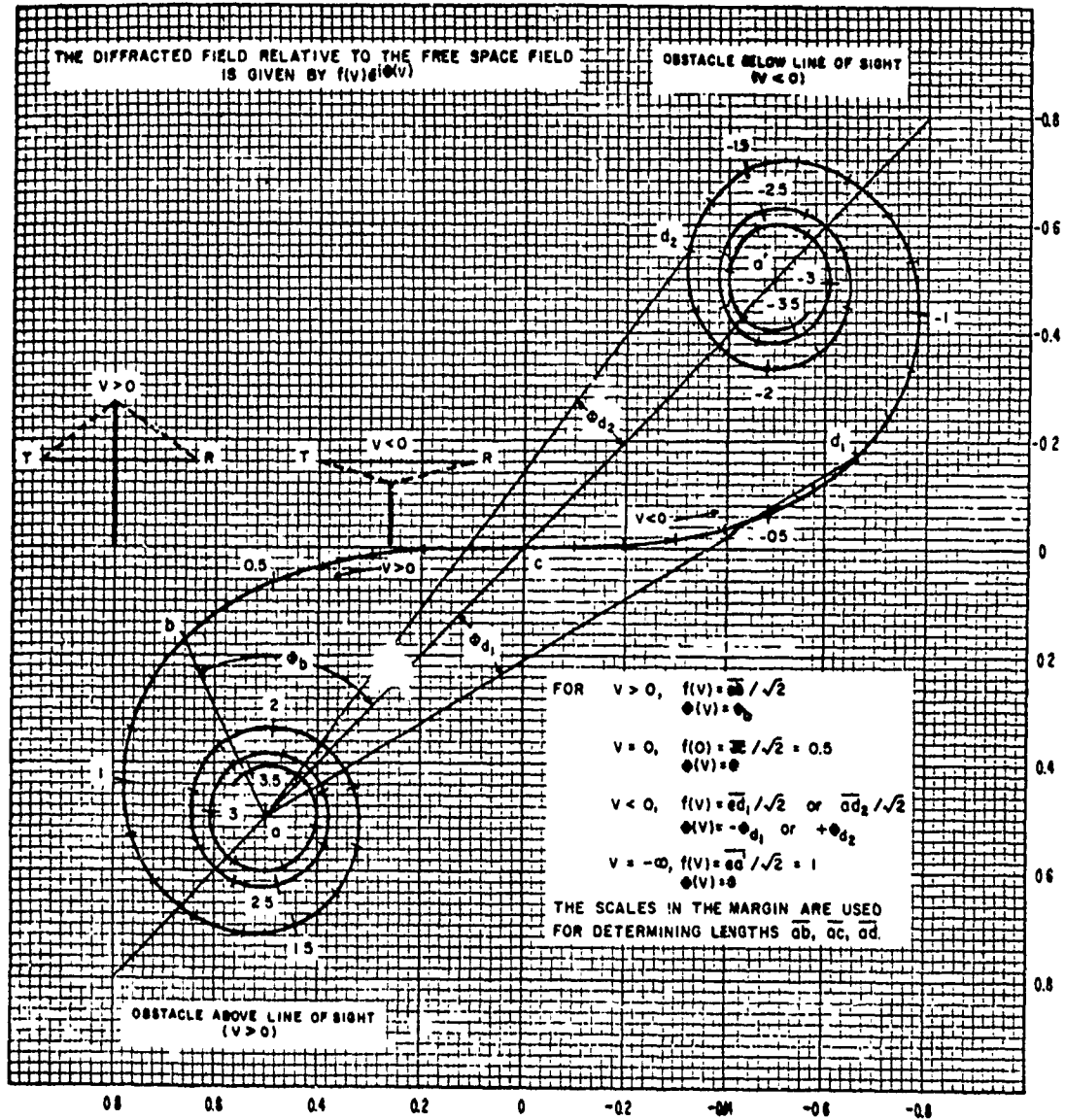


Figure III.10

III.4 Parameters K and b° for Smooth Earth Diffraction

In section 8, the parameters K and b° are shown on figures 8.1 and 8.2 for horizontally and vertically polarized waves for poor, average, and good ground, and for sea water.

Assume a homogeneous ground in which the relative dielectric constant ϵ and conductivity σ of the ground are everywhere constant. K and b° are defined as follows:

For horizontal polarization,

$$K_h = 1.7778 \times 10^{-2} C_o f^{-\frac{1}{3}} [(\epsilon-1)^2 + x^2]^{-\frac{1}{4}} \quad (\text{III. 40a})$$

$$b_h = 180^\circ - \tan^{-1} \left(\frac{\epsilon-1}{x} \right) \text{ degrees} . \quad (\text{III. 40b})$$

For vertical polarization,

$$K_v = (\epsilon^2 + x^2)^{\frac{1}{2}} K_h \quad (\text{III. 41a})$$

$$b_v = 2 \tan^{-1} (\epsilon/x) - \tan^{-1} \left(\frac{\epsilon-1}{x} \right) \text{ degrees} \quad (\text{III. 41b})$$

where x depends on the ground conductivity σ , in mhos per meter, and the radio frequency f , in megacycles per second, and has been defined by (III. 7) as

$$x = 1.8 \times 10^4 \sigma / f$$

C_o is defined in section 8 as

$$C_o = (8497/a)^{\frac{1}{3}}$$

where a is the effective earth's radius in kilometers.

When $\sigma/f \gg (\epsilon/2) \times 10^{-4}$, the parameters K and b° may be written as

$$K_h \approx 1.325 \times 10^{-4} C_o f^{1/6} \sigma^{-1/2} , \quad b_h \approx 180^\circ \quad (\text{III. 42})$$

$$K_v \approx 2.385 C_o \sigma^{1/2} f^{-5/6} , \quad b_v \approx 0^\circ \quad (\text{III. 43})$$

and when $\sigma/f < (\epsilon/2) \times 10^{-4}$, the parameters K and b° may be written as

$$K_h \approx 1.7778 \times 10^{-2} C_o f^{-\frac{1}{3}} (\epsilon-1)^{-\frac{1}{2}} , \quad b_h \approx 90^\circ \quad (\text{III. 44})$$

$$K_v \approx \epsilon K_h , \quad b_v \approx 90^\circ \quad (\text{III. 45})$$

III.5 Forward Scatter

The attenuation function $F(\theta d)$ for $N_s = 250, 301, 350,$ and 400 , shown in figure 9.1, may be used for most land-based scatter links. When a path is highly asymmetrical, the attenuation for a given value of θd is less than it would be for a symmetrical path. Figures III.11 to III.14 show the function $F(\theta d)$ for values of s from 0.01 to 1, and for $N_s = 250, 301, 350$ and 400 . For values of $\theta d \leq 10$, the effect of asymmetry is negligible, but increases with increasing θd , particularly when $s < 0.5$.

For values of s between 0.7 and 1, the function $F(\theta d)$ for $N_s = 301$ may be computed as follows:

$$\text{for } 0.01 \leq \theta d \leq 10, \quad F(\theta d) = 135.82 + 0.33 \theta d + 30 \log(\theta d) \quad (\text{III. 46})$$

$$\text{for } 10 \leq \theta d \leq 70, \quad F(\theta d) = 129.5 + 0.212 \theta d + 37.5 \log(\theta d) \quad (\text{III. 47})$$

$$\text{for } \theta d \geq 70, \quad F(\theta d) = 119.2 + 0.157 \theta d + 45 \log(\theta d). \quad (\text{III. 48})$$

The function $F(\theta d)$ may be obtained for any value of N_s , by modifying the value computed for $N_s = 301$:

$$F(\theta d, N_s) = F(\theta d, N_s = 301) - \left[0.1(N_s - 301) e^{-\theta d/40} \right].$$

The frequency gain function, H_o , for the special case $h_{te} = h_{re}$ frequently used in systems design, is shown as a function of r on figures III.15 to III.19 for $\eta_s = 1, 2, 3, 4, 5$, and for $s = 1, 0.5, 0.25$ and 0.1 . In this case, no correction factor ΔH_o is required.

The function H_o for $\eta_s = 0$, shown on figure 9.5 corresponds to the assumption of a constant atmospheric refractive index. Except for the special case where $h_{te} = h_{re}$ this function may be computed as follows:

$$H_o(\eta_s = 0) = 10 \log \left\{ \frac{2(1 - h_{re}^2/h_{te}^2)}{r_2^2 [h(r_1) - h(r_2)]} \right\} \quad (\text{III. 49})$$

where $r_1 = 4\pi\theta h_{te}/\lambda$, $r_2 = 4\pi\theta h_{re}/\lambda$.

$$h(r_1) = r_1 f(r_1), \quad f(r_1) = \text{Ci}(r_1) \sin r_1 + [\pi/2 - \text{Si}(r_1)] \cos r_1 \quad (\text{III. 50})$$

and

$$h(r_2) = r_2 f(r_2), \quad f(r_2) = \text{Ci}(r_2) \sin r_2 + [\pi/2 - \text{Si}(r_2)] \cos r_2$$

$$\text{Ci}(r) = \int_{\infty}^r \frac{\cos t}{t} dt, \quad \text{Si}(r) = \int_0^r \frac{\sin t}{t} dt. \quad (\text{III. 51})$$

Values of the sine integral $\text{Si}(r)$ and the cosine integral $\text{Ci}(r)$ for arguments from 10 to 100 are tabulated in volume 32 of the U. S. NBS Applied Math Series [1954]. See also [NBS AMS 1964]. The function $h(r)$ is shown graphically in figures III.20 and III.21.

For the special case of equal effective antenna heights, $h_{te} = h_{re}$, equation (III.49) is not applicable. In this case $H_0(\eta_s = 0)$ is computed as:

$$H_0(\eta_s = 0) = 10 \log \left\{ \frac{4}{r^2 [h(r) - r g(r)]} \right\} \quad (\text{III. 52})$$

where

$$g(r) = \text{Ci}(r) \cos r - [\pi/2 - \text{Si}(r)] \sin r \quad (\text{III. 53})$$

When the effective height of one antenna is very much greater than that of the other, the computation may be simplified as follows:

$$\text{For } r_2 \ll r_1, \quad H_0(\eta_s = 0) = 10 \log \left\{ \frac{2}{r_2^2 [1 - h(r_2)]} \right\} \quad (\text{III. 54a})$$

$$\text{For } r_2 \gg r_1, \quad H_0(\eta_s = 0) = 10 \log \left\{ \frac{2}{r_1^2 [1 - h(r_1)]} \right\}. \quad (\text{III. 54b})$$

THE FUNCTION $F(\theta d)$ FOR $N_s = 250$

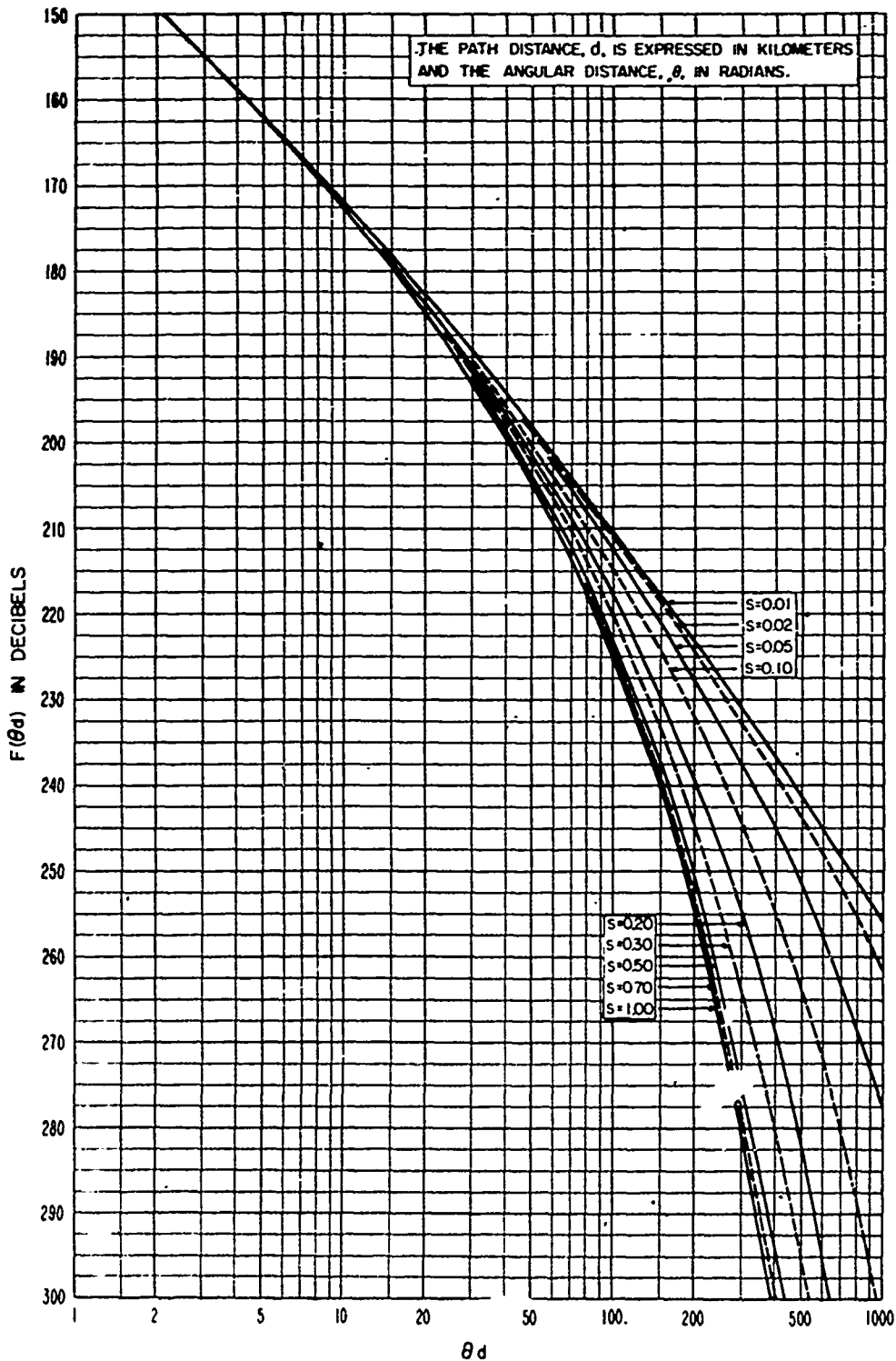


Figure III.11

THE FUNCTION $F(\theta_d)$ FOR $N_s = 301$

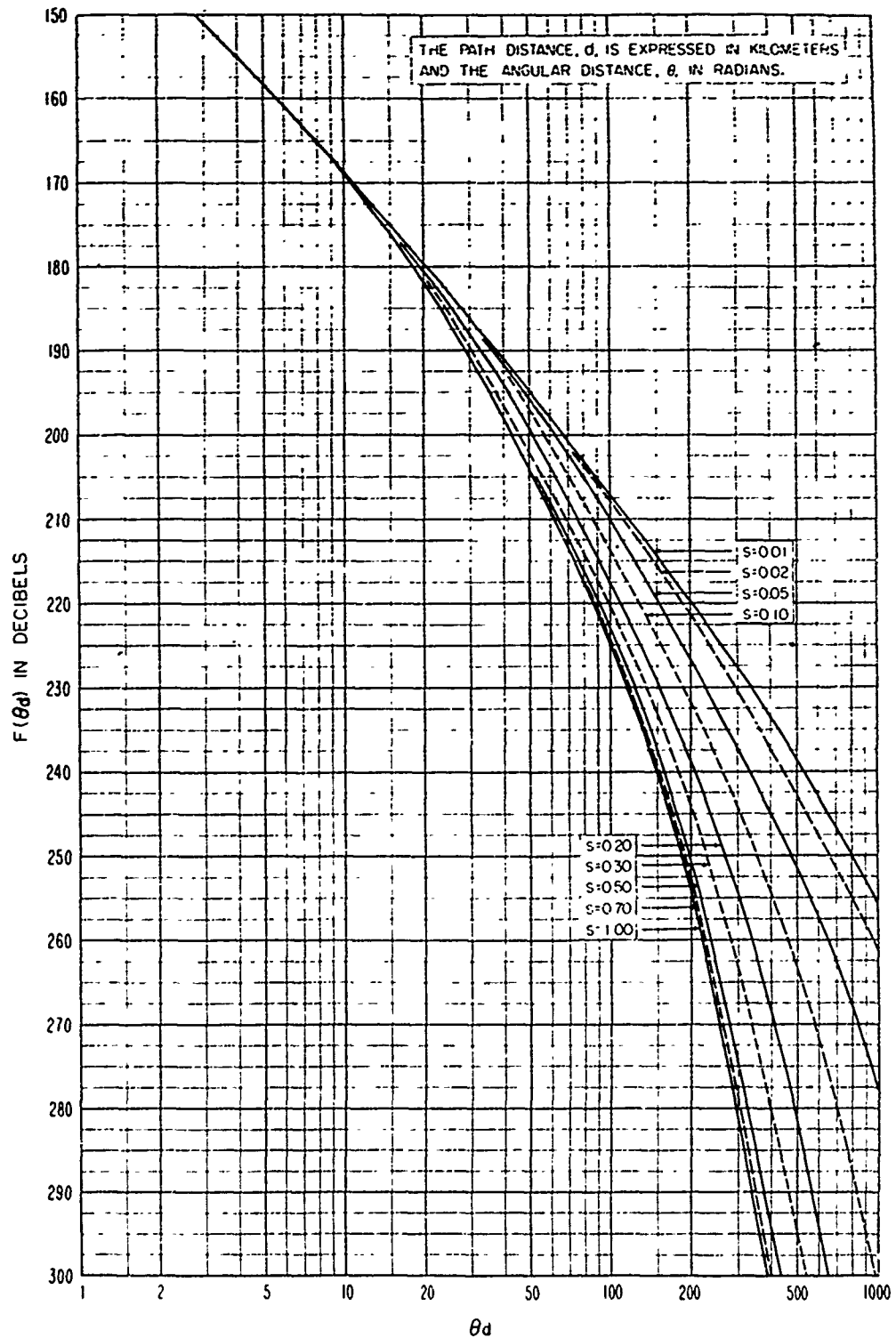


Figure III.12

THE FUNCTION $F(\theta_d)$ FOR $N_s = 350$

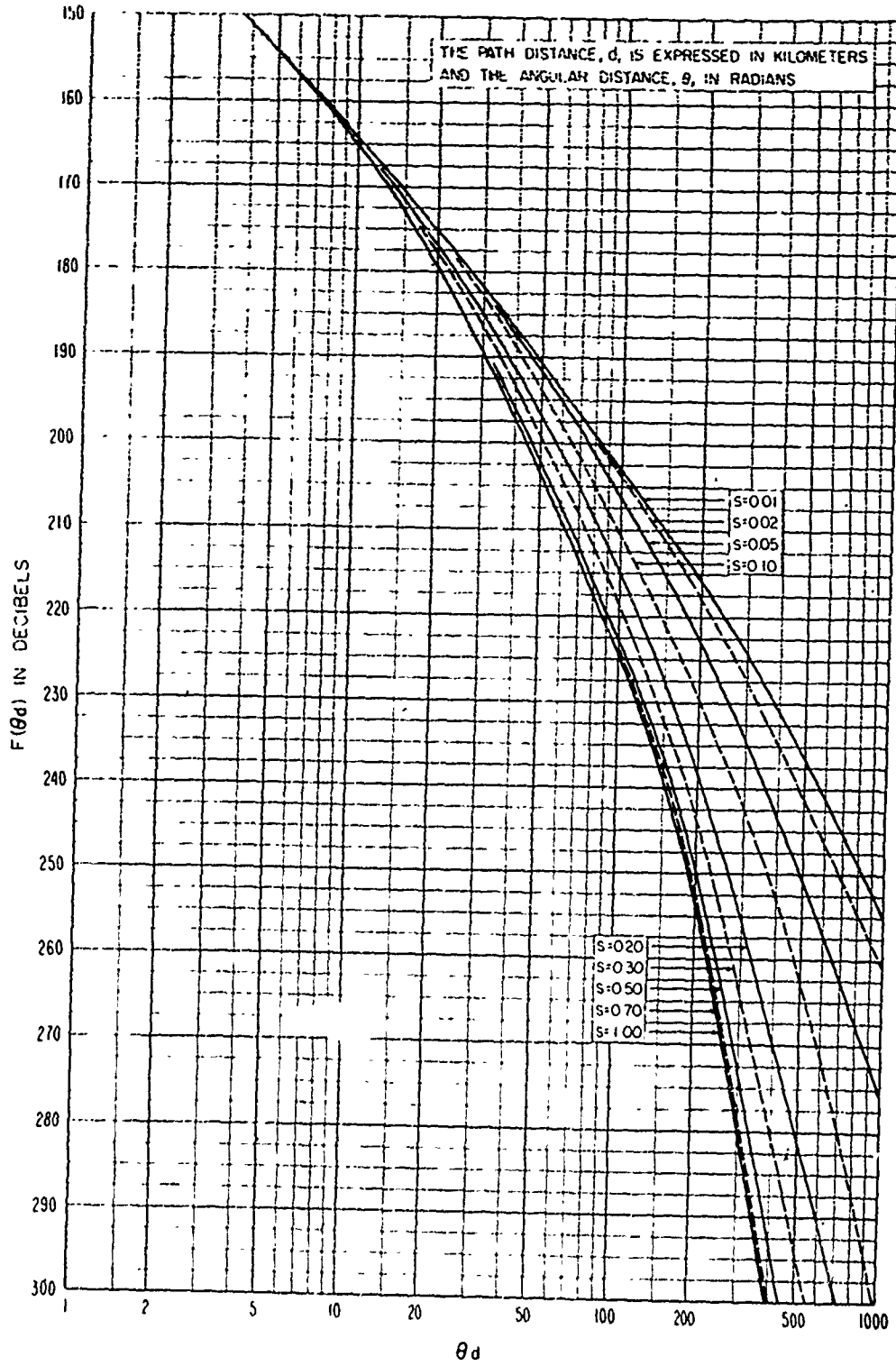


Figure III.13

THE FUNCTION $F(\theta_d)$ FOR $N_s=400$

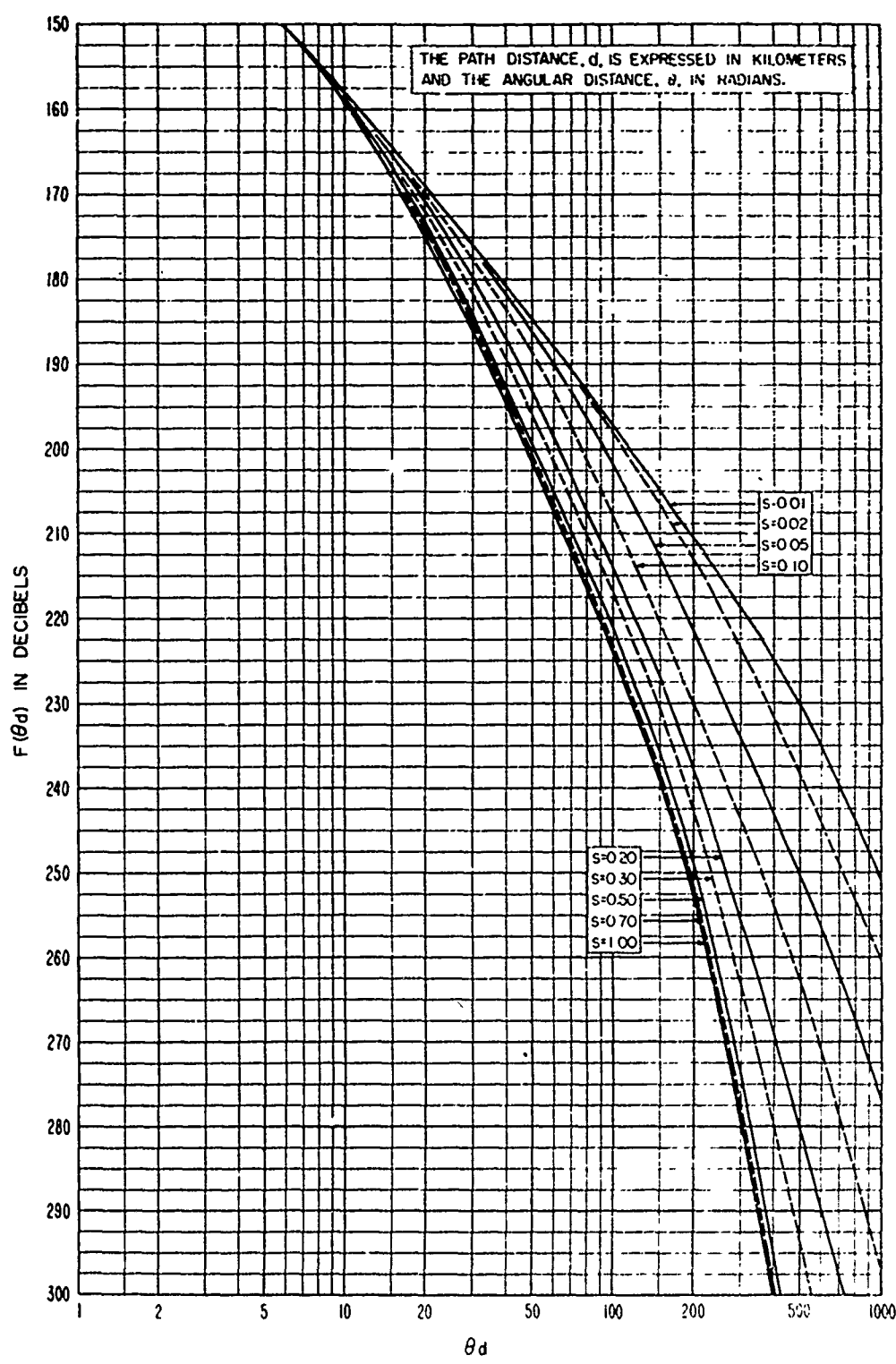


Figure III 14

THE FREQUENCY GAIN FUNCTION, H_0
 $h_{ie} = h_{re}$

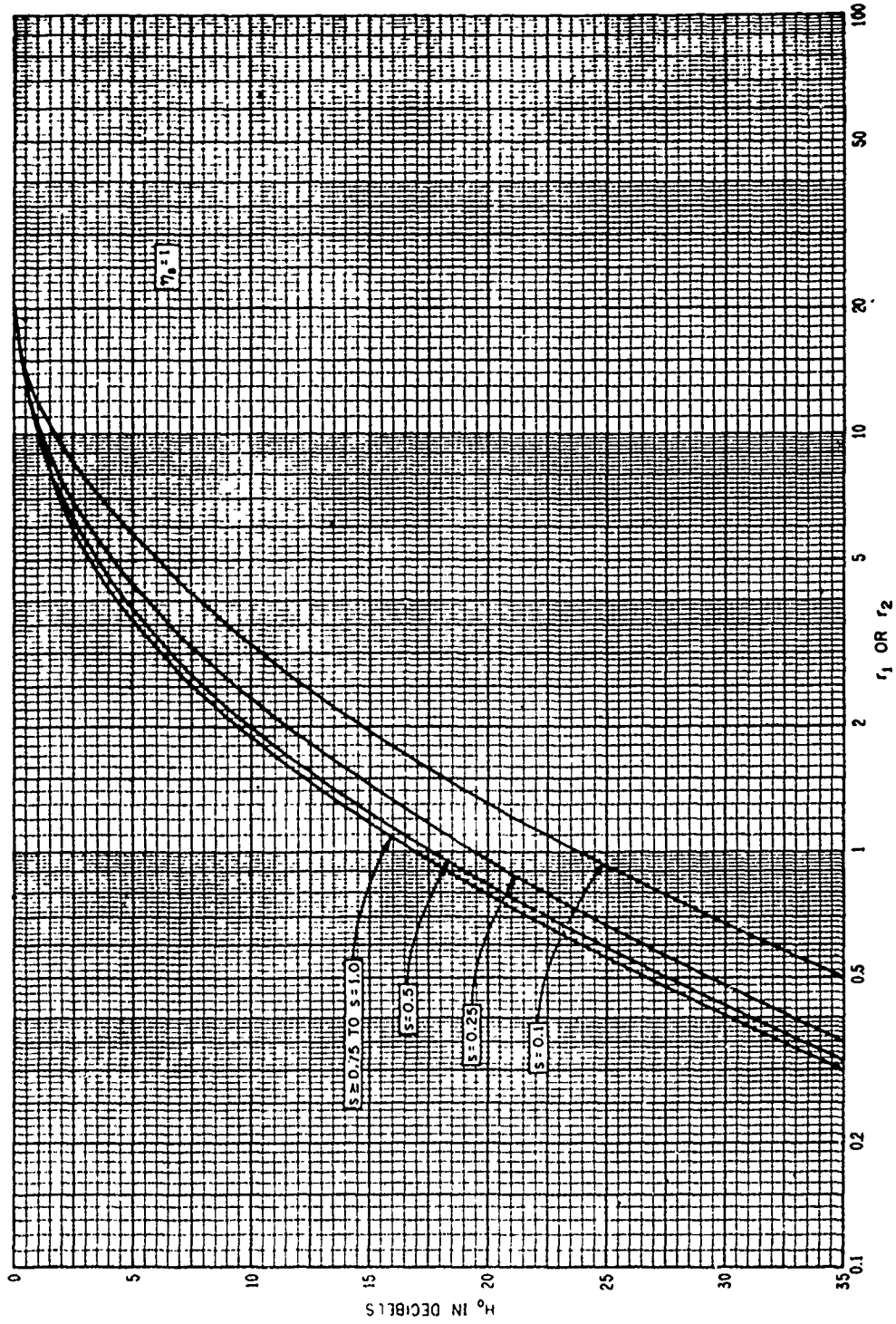


Figure III.15

THE FREQUENCY GAIN FUNCTION, H_0
 $h_{te} = h_{re}$

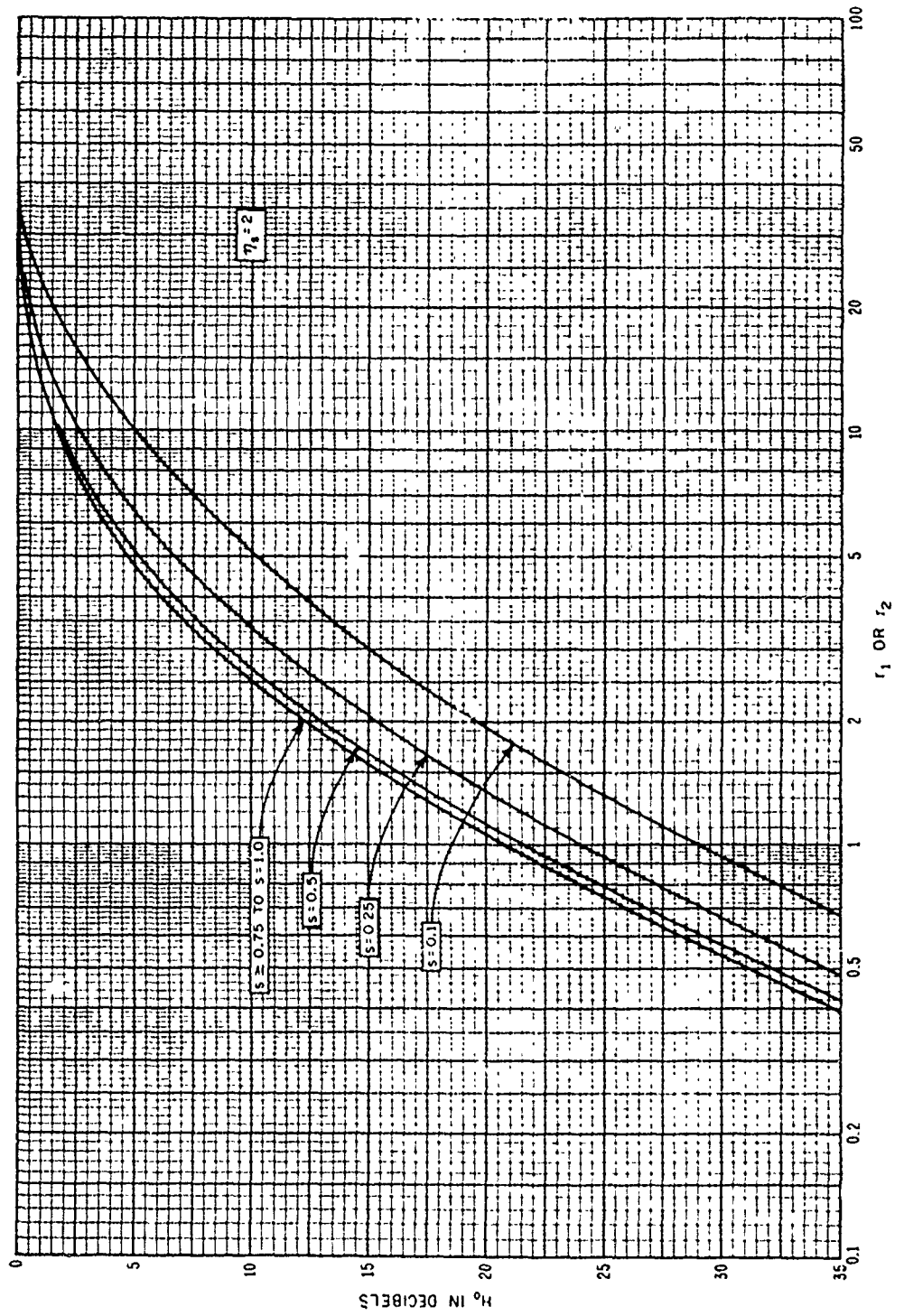


Figure III.16

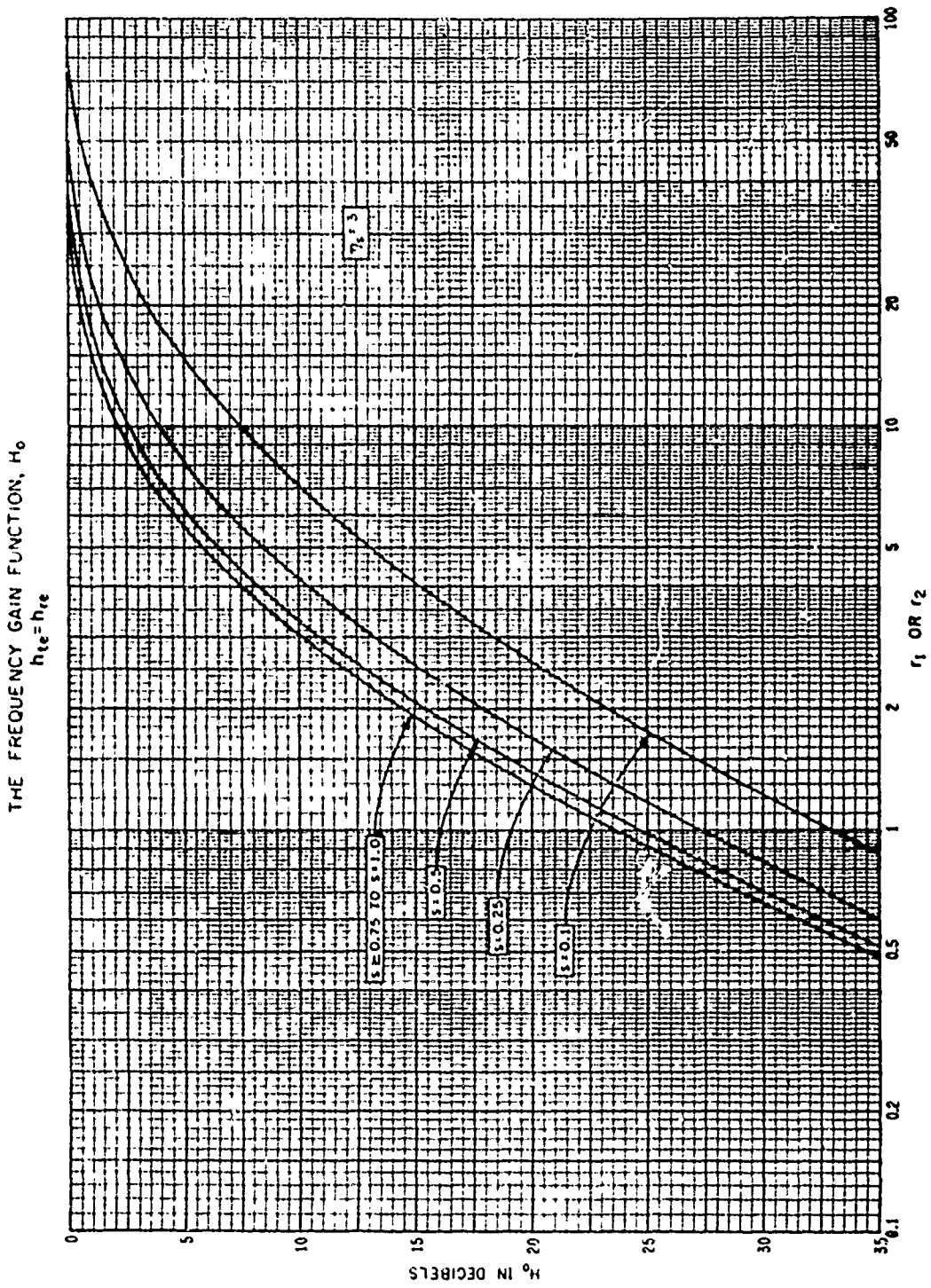


Figure III.17

THE FREQUENCY GAIN FUNCTION, H_o
 $h_{te} = h_{re}$

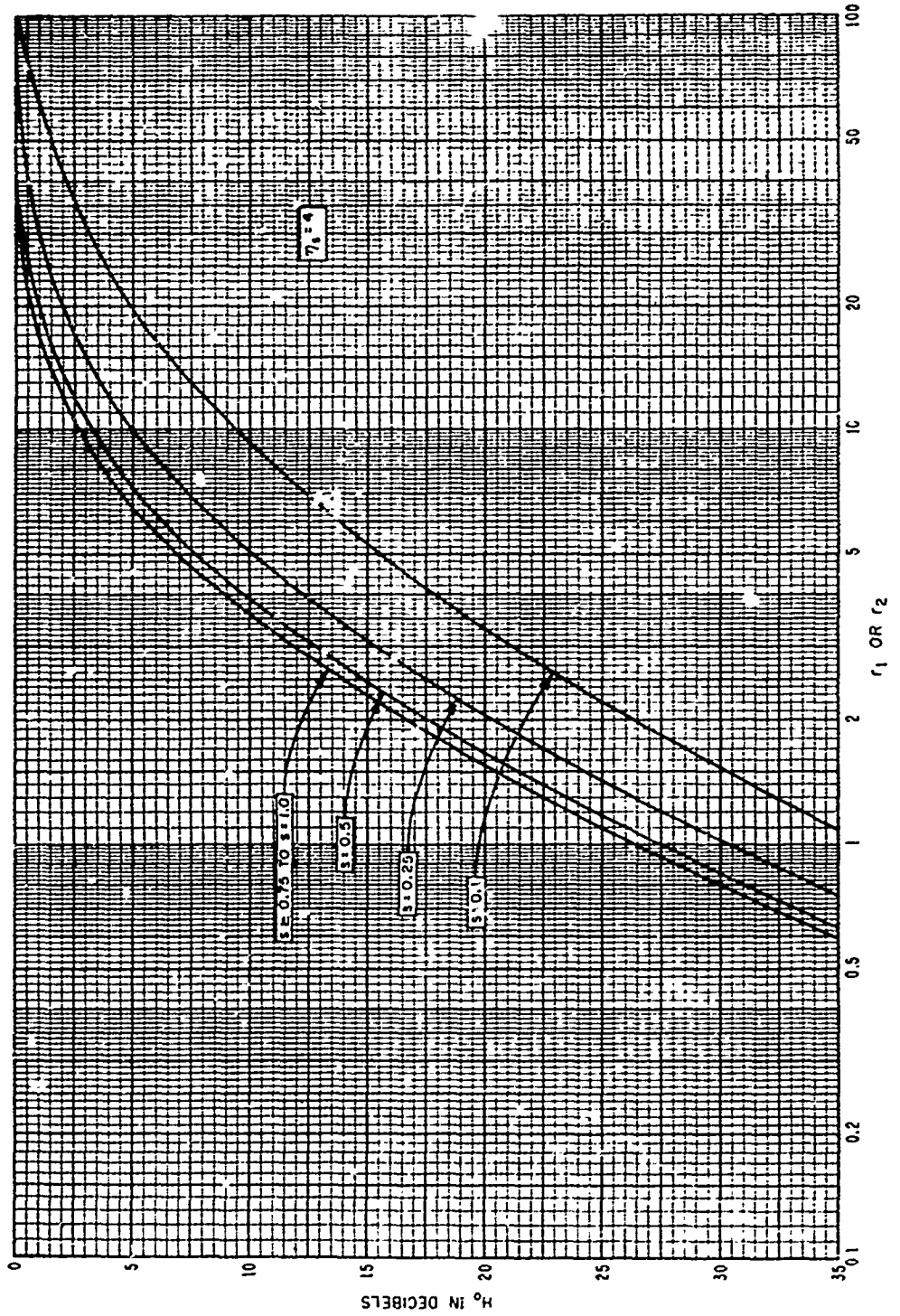


Figure III 18

THE FREQUENCY SCALE FUNCTION, F_{fs}

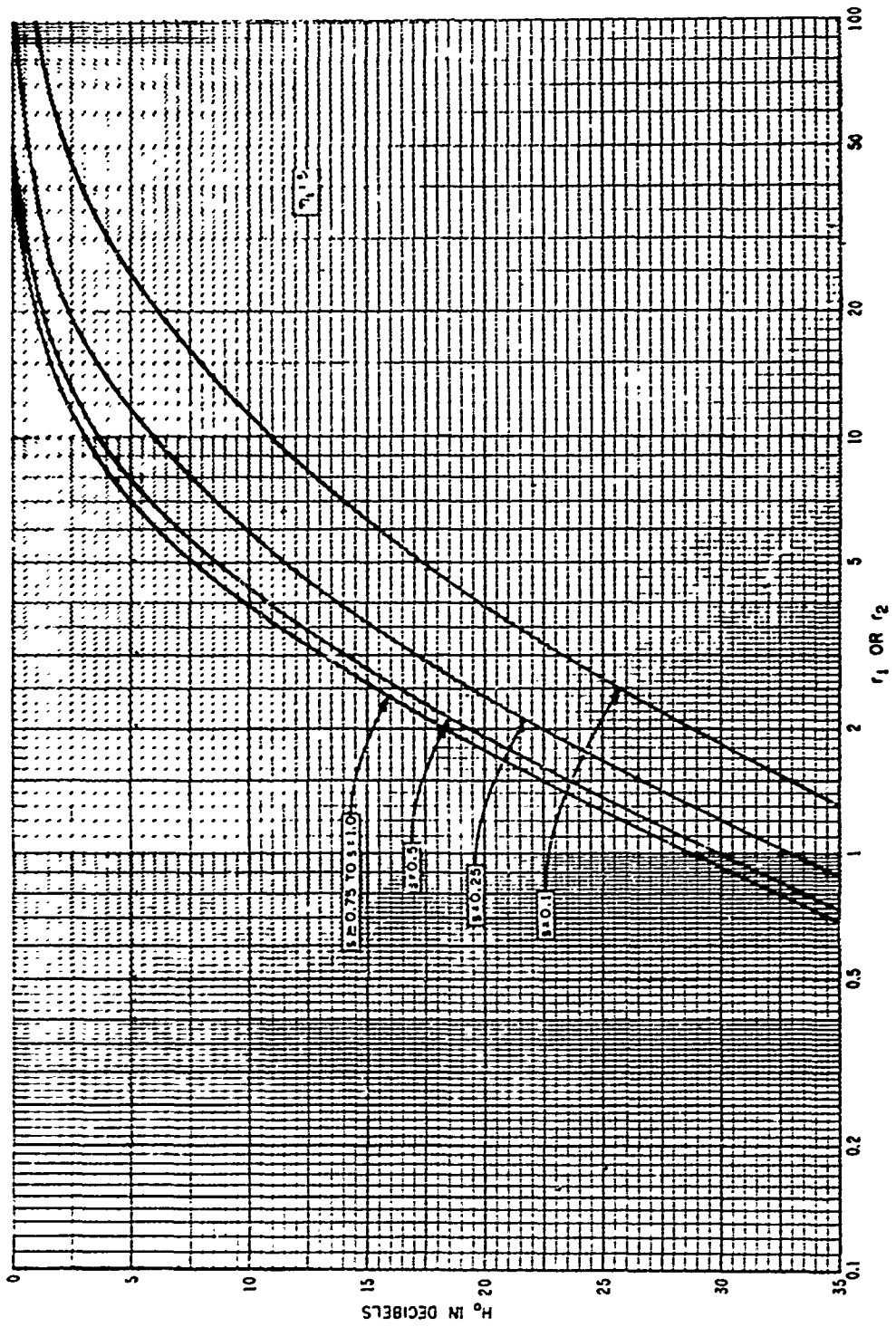


Figure III.19

THE FUNCTION $h(r)$

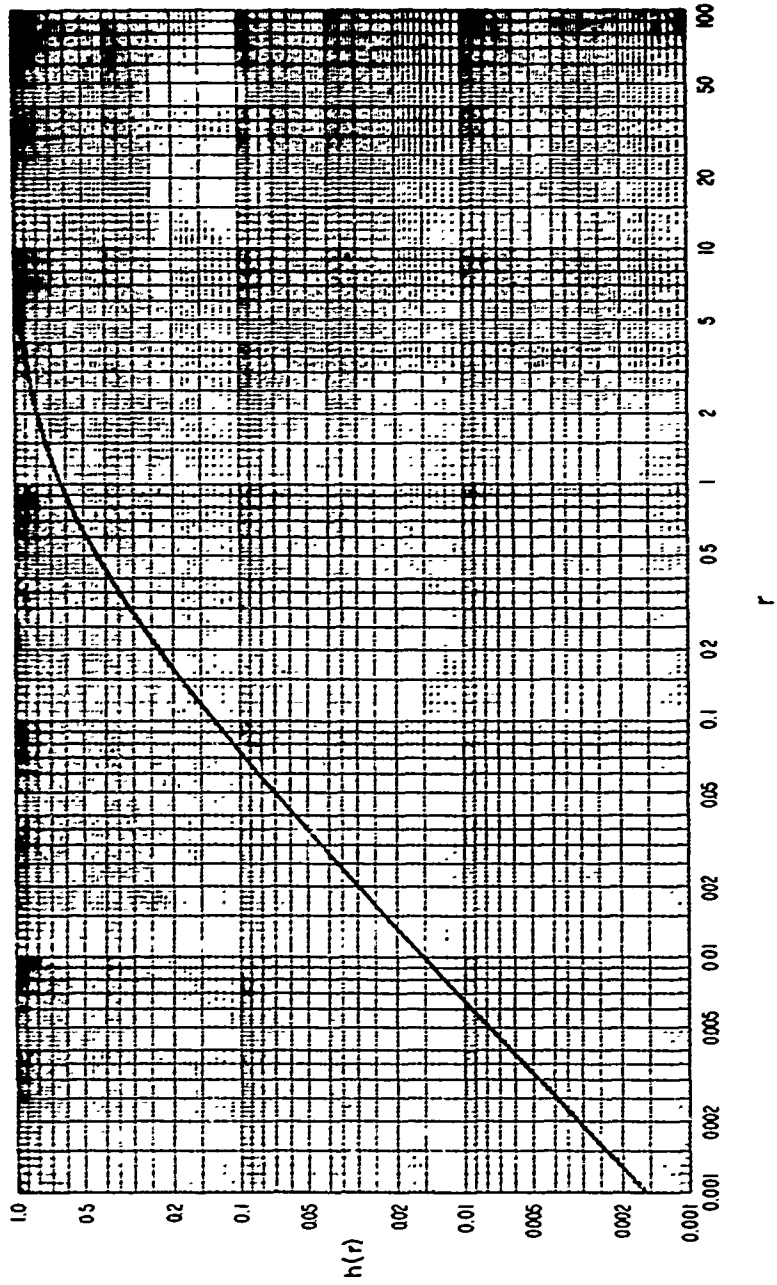


Figure III.20

THE FUNCTION $h(r)$

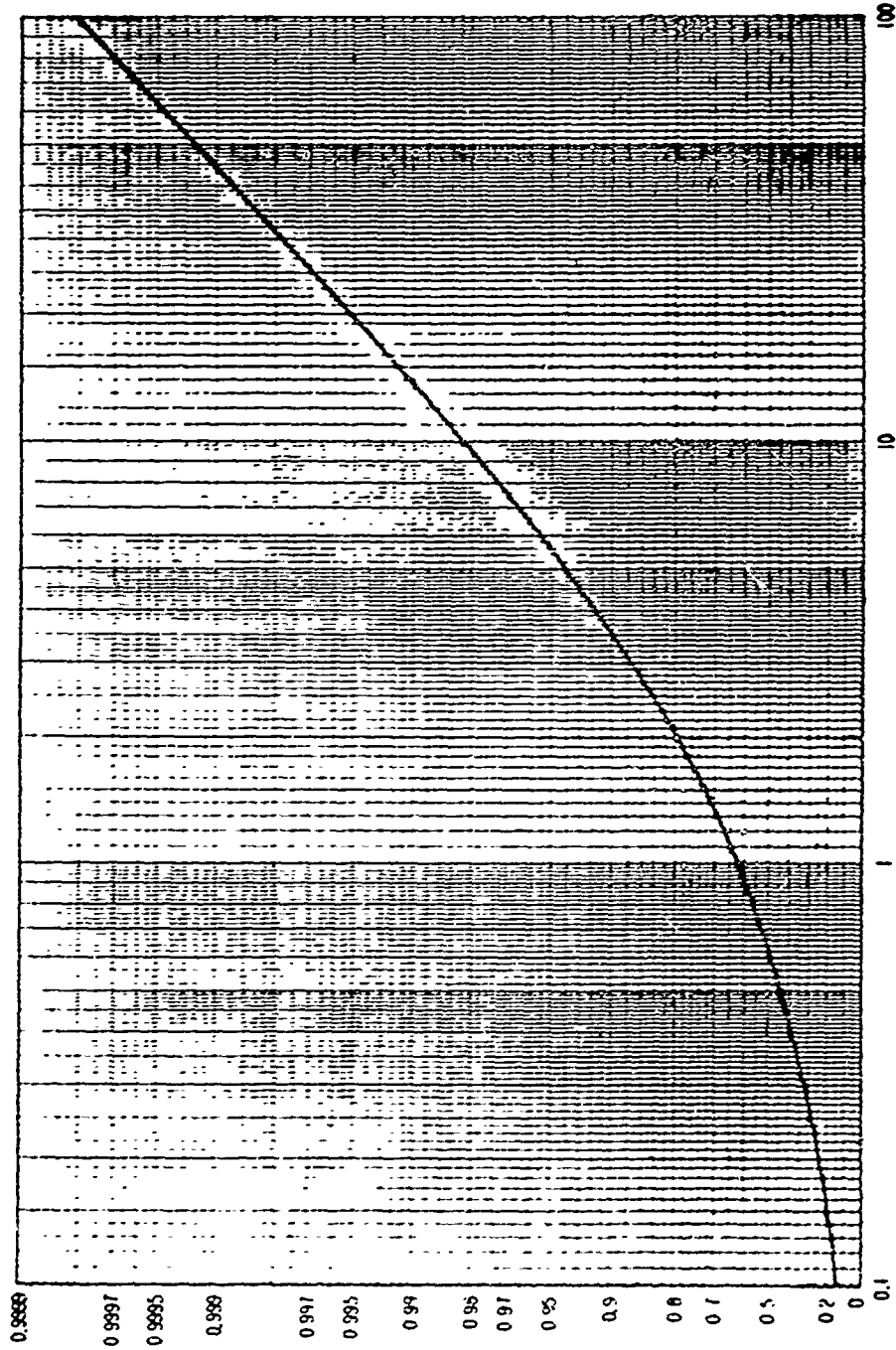


Figure M.21

III.6 Transmission Loss with Antenna Beams Elevated or Directed Out of the Great Circle Plane

The methods of section 9 may be modified to calculate a reference value of long-term median transmission loss when antenna beams are either elevated or directed away from the great circle path between antennas. For many applications, the average transmission loss between antennas with random relative orientation is about 10 db more than the basic transmission loss, which assumes zero db antenna gains.

Figure III.22 shows scattering subvolumes at intersections of antenna main beams and side lobes. A "scatter" theory assumes that the total power available at a receiver is the sum of the powers available from many scattering subvolumes. For high gain antennas, the intersection of main beams defines the only important scattering volume. In general, all power contributions that are within 10 db of the largest one should be added.

For a total radiated power w_t :

$$w_a/w_t = 10^{-0.1 L_{sr}}, \quad w_{ai}/w_t = 10^{-0.1 L_i} \quad (\text{III.55})$$

where L_{sr} is the transmission loss and L_i is the loss associated with the i th power contribution, w_{ai} :

$$L_{sr} = -10 \log(w_a/w_t) = -10 \log \sum_i 10^{-0.1 L_i} \quad (\text{III.56})$$

$$L_i = 30 \log f - 20 \log(d^2/r_o) + F(\theta_{ei}, d) - F_{oi} + H_{oi} + A_a - G_{ti} - G_{ri} + L_{gi} \quad (\text{III.57})$$

In (III.57) f , d , and A_a are defined as in (9.1) and the other terms are related to similar terms in (9.1). If the effective scattering angle θ_{ei} for the i th intersection is equal to the minimum scattering angle θ , then $F(\theta_{ei}, d)$, F_{oi} , H_{oi} are equal to $F(\theta d)$, F_o , and H_o , and $G_{ti} + G_{ri} - L_{gi} = G_p$. Note that a term $20 \log(r_o/d)$ has been added in (III.57) to provide for situations where the straight line distance r_o between antennas is much greater than the sea-level arc distance d . Such differences occur in satellite communication.

Scattering planes, defined by the directions of incident and scattered energy, may or may not coincide with the plane of the great circle path. Each "scattering plane" is determined by the line between antenna locations and the axis of the stronger of the two intersecting beams, making an angle ξ with the great circle plane.

The free space directive gain patterns of the antennas are replaced by equivalent values for ease in computation. For an idealized pencil-beam antenna with a half-power beamwidth 2δ and a circular beam cross-section, the directive gain g is $4/\delta^2$, assuming that all of the power is radiated through the main beam and between the half-power points. An equivalent beam pattern with a square cross-section and a semi-beamwidth δ_0 has a gain of π/δ_0^2 , thus $\delta_0 = \delta\sqrt{\pi/4}$, and the maximum free space gains are

$$G_t = 10 \log g_{t0} = 4.97 - 10 \log \delta_{t\omega} \delta_{tz0} \quad \text{db} \quad (\text{III. 58a})$$

$$G_r = 10 \log g_{r0} = 4.97 - 10 \log \delta_{r\omega} \delta_{rz0} \quad \text{db} \quad (\text{III. 58b})$$

where the subscripts ω and z refer to azimuthal and vertical angles. In most cases, $\delta_{\omega 0}$ and δ_{z0} may be replaced by their geometric mean, $\delta_0 = (\delta_{\omega 0} \delta_{z0})^{1/2}$. The free space directive gain of a main beam may be measured or approximated as $g_0 \approx \pi/(2\delta_{\omega 0} \delta_{z0})$. Gains for side lobes are determined from g_0 and the ratios g_1/g_0 , g_2/g_0 , ..., which may be measured or calculated. The average gain g_b for other directions depends on the fraction of power radiated in those directions. For instance, if half the total power of a transmitter is radiated in these directions, and if the polarization coupling loss, L_{cp} , is 3 db, then

$$G_{bt} - L_{cp} = -6 \text{ db}$$

since the definition of the directive gain, G_{bt} , assumes for every direction the receiving antenna polarization appropriate for maximum power transfer.

Figure III.23 shows an antenna power pattern in several different ways, including a Mercator projection of the surface of a unit sphere.

The plane that determines the "bottom" of a beam is perpendicular to the great circle plane and forms an angle ψ_1 with a horizon plane:

$$\psi_{t1} = \theta_{bt1} - \theta_{et}, \quad \psi_{r1} = \theta_{br1} - \theta_{er} \quad (\text{III. 59})$$

where θ_b is the angle of elevation of the lower half-power point of a beam above the horizontal, and θ_{et} is defined in section 6. If an antenna beam is elevated sufficiently so that ray bending may be neglected, the angles α_e and β_e are denoted α_{e0} and β_{e0} :

$$\alpha_{e0} = (\alpha_{00} + \psi_1) \sec \zeta, \quad \beta_{e0} = (\beta_{00} + \psi_1) \sec \zeta \quad (\text{III. 60})$$

where ζ is the angle away from the great circle plane. The angles α_{00} and β_{00} are defined as in section 6 using the actual radius, $a_0 \approx 6370$ km, instead of an effective radius a .

When ray bending must be considered, the equations for α_e and β_e are

$$\alpha_e = \alpha_{e0} + \tau\left(\theta_{bt}, \frac{d_{Lt} \sec \zeta}{2}, N_s\right) - \tau\left(\theta_{bt}, \frac{d \sec \zeta}{2}, N_s\right) \quad (\text{III.61a})$$

$$\beta_e = \beta_{e0} + \tau\left(\theta_{br}, \frac{d_{Lr} \sec \zeta}{2}, N_s\right) - \tau\left(\theta_{br}, \frac{d \sec \zeta}{2}, N_s\right) \quad (\text{III.61b})$$

where $\tau(\theta_b, d, N_s)$ is the bending of a radio ray which takes off at an angle θ_b above the horizontal and travels d kilometers through an atmosphere characterized by a surface refractivity N_s . The ray bending τ may be determined using methods and tables furnished by Bean and Thayer [1959]. For short distances, d , or large angles, θ_b , τ is negligible. If θ_b is less than 0.1 radians, the effective earth's radius approximation is adequate for determining τ ,

$$\tau\left(\theta_b, \frac{d \sec \zeta}{2}, N_s\right) = \frac{d}{a_0} [1 - a_0/a(N_s)] \quad (\text{III.62})$$

The reference value of long-term median transmission loss L_{sr} is computed using (III.56) where the losses associated with several scattering subvolumes are computed using (III.57). The attenuation function $F(d\theta_{ei})$ is read from figure 9.1 or figures III.11 - III.14 as a function of θ_{ei} .

The generalized scattering efficiency term F_{oi} is

$$F_{oi} = 1.086(\eta_{se}/h_e)(2h_0 - h_1 - h_e - h_{Lt} - h_{Lr}) \quad \text{db} \quad (\text{III.63})$$

where

$$\theta_e = \alpha_e + \beta_e, \quad s_e = \alpha_e/\beta_e, \quad h_e = s_e d \theta_e / (1 + s_e)^2, \quad \eta_{se} = \eta_s(h_e, N_s) \quad (\text{III.64})$$

and the other terms are defined in section 9. In computing the frequency gain function H_{oi} , if $\alpha_e > \alpha_0$ use $r_1 = \infty$, if $\beta_e > \beta_0$ use $r_2 = \infty$, then $H_{oi} = H_0 + 3$ db. If both antennas are elevated above the horizon rays, $H_{oi} = 6$ db. Atmospheric absorption A_a is discussed in section 3. The gains G_{ti} and G_{ri} are the free space directive gains defined by (III.58), and the loss in gain L_{gi} is computed as shown in section 9 replacing η_s , s , δ , and θ by η_{se} , s_e , δ_e , and θ_e .

CCP 702-1

In computing long-term variability of transmission loss for beams elevated above the horizon plane, the estimates of V and Y given in section 10 should be reduced by the factor $f(\theta_h)$ shown in figure III.24, with $\theta_h = \theta_b$:

$$V_e(0.5, d_e) = V(0.5, d_e) f(\theta_h) \quad (\text{III.65a})$$

$$Y_e(q, d_e) = Y(q, d_e) f(\theta_h) \quad (\text{III.65b})$$

The angle θ_h used in (III.65) should be the elevation above the horizontal of the scattering subvolume corresponding to the minimum value of L_i .

SCATTERING SUBVOLUMES IN A SCATTERING PLANE

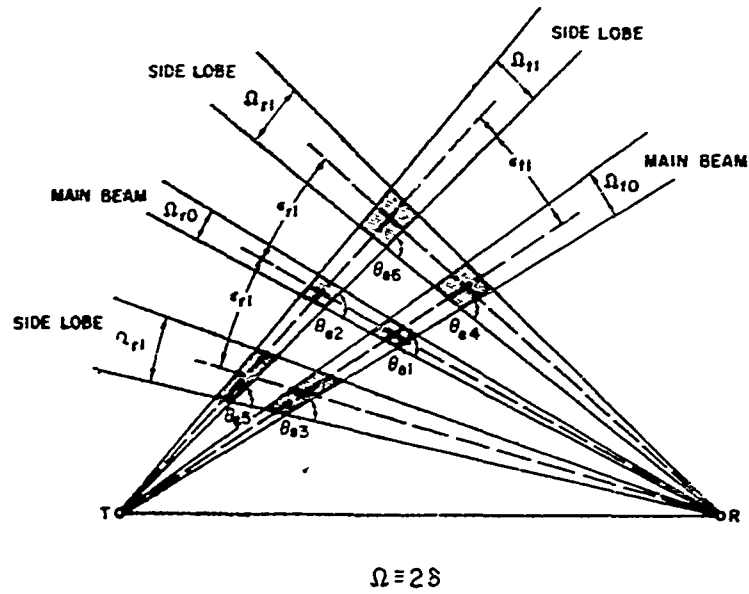


ILLUSTRATION OF A SCATTERING PLANE CONTAINING THE MAIN BEAM OF THE RECEIVING ANTENNA

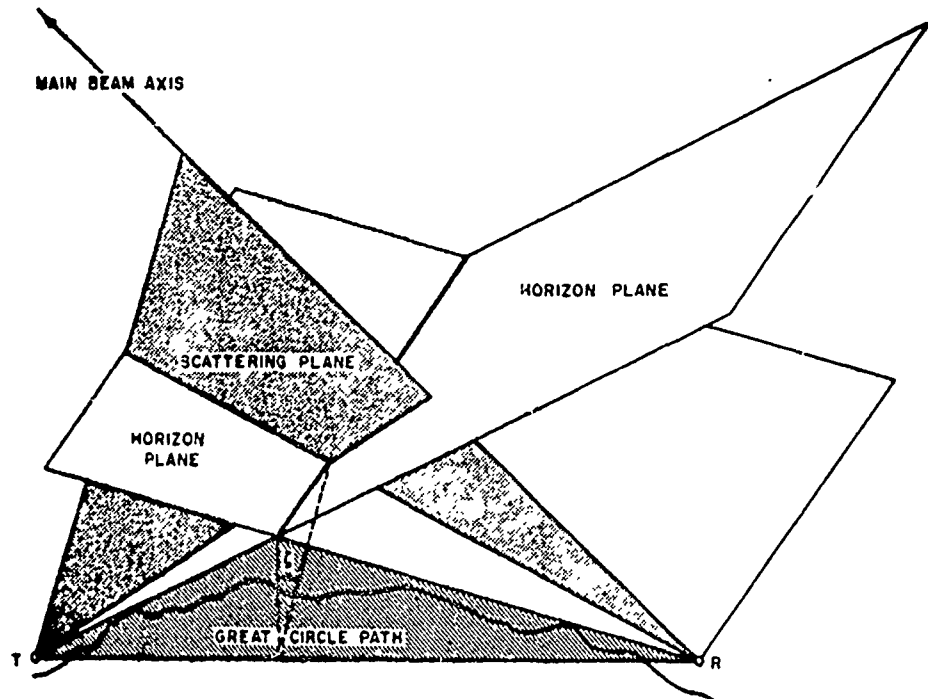
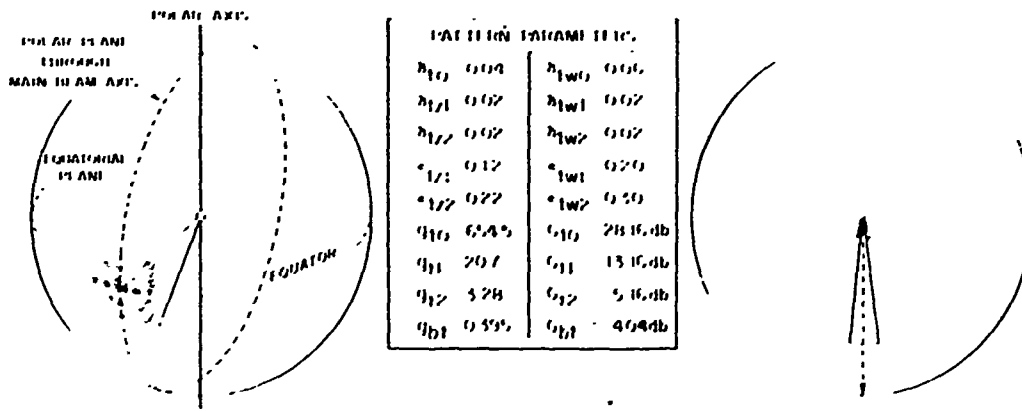


Figure III.22

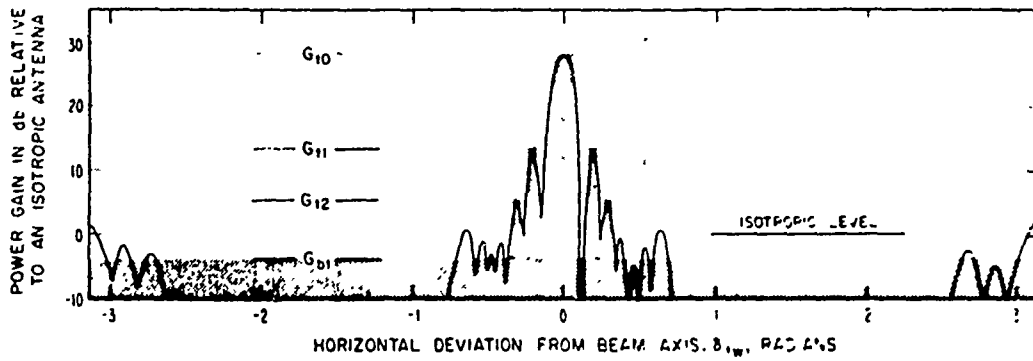
FREE SPACE ANTENNA PATTERN

INTERSECTION OF AN EQUIVALENT ANTENNA POWER PATTERN WITH THE SURFACE OF A UNIT SPHERE

ANTENNA VOLTAGE PATTERN FOR AN DIAGRAM IN THE EQUATORIAL PLANE



CARTESIAN DIAGRAM OF TRANSMITTING ANTENNA POWER PATTERN IN THE EQUATORIAL PLANE



MERCATOR PROJECTION OF THE INTERSECTION OF THE EQUIVALENT TRANSMITTING ANTENNA POWER PATTERN WITH THE SURFACE OF A UNIT SPHERE

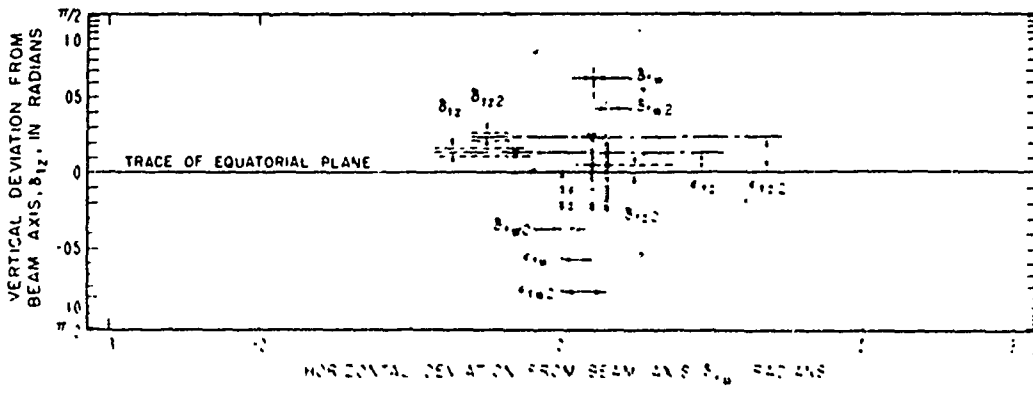
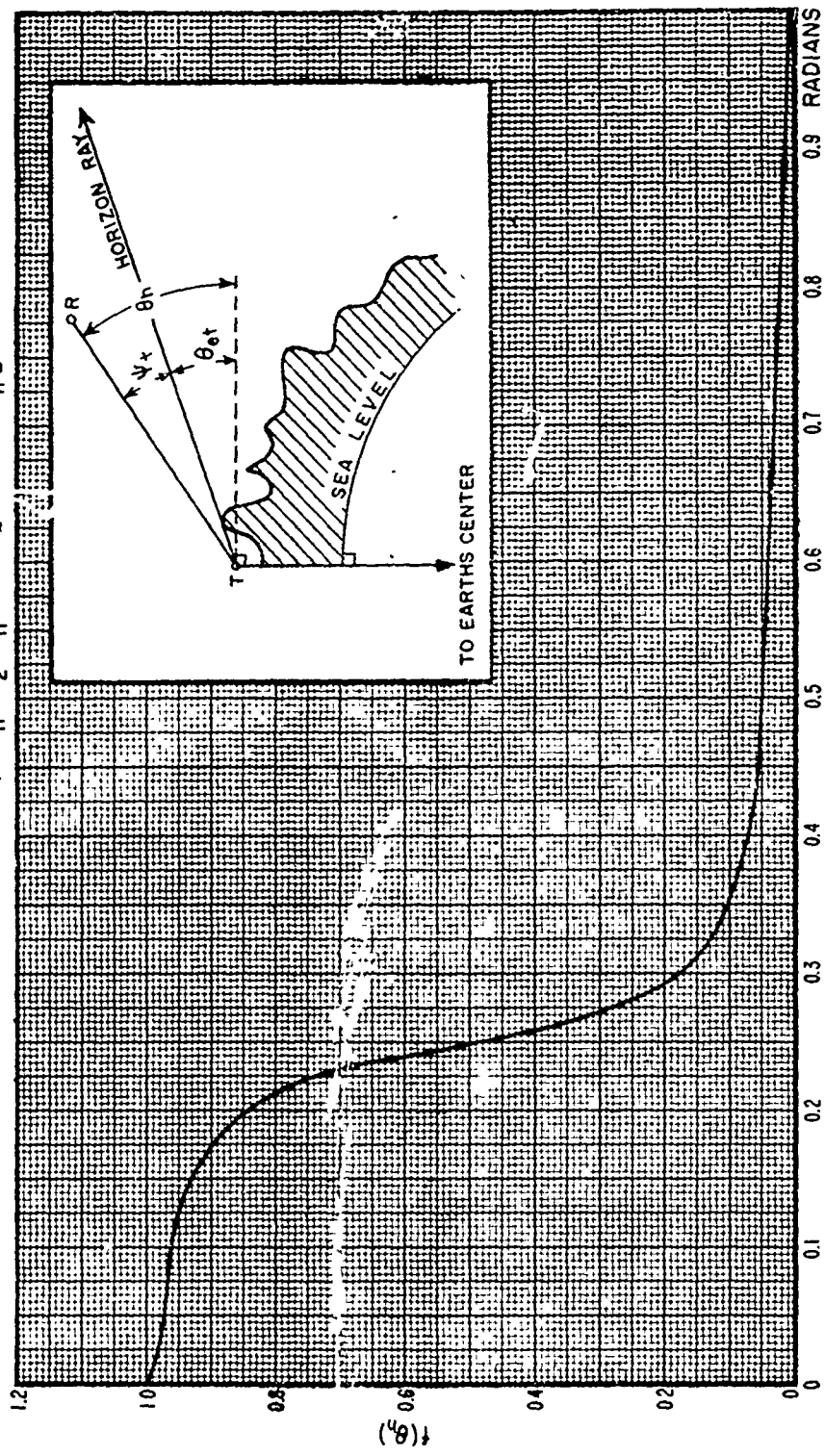


Figure II 23

THE ELEVATION ANGLE CORRECTION $f(\theta_h)$ FOR LINE-OF-SIGHT PATHS

FOR BEYOND-HORIZON PATHS, $f(\theta_h) = 1$
 WITHIN THE HORIZON, $f(\theta_h) = \frac{1}{2} - \frac{1}{\pi} \tan^{-1} [20 \log(4\theta_h)]$



ANGLE OF ELEVATION, θ_h , OF LINE-OF-SIGHT PATH ABOVE HORIZONTAL

Figure III.24

III.7 Long-Term Power Fading

Long-term power fading is discussed in section 10. Figures 10.5 to 10.16 show empirical estimates of all-year variability for (1) continental temperate (2) maritime temperate overland and (3) maritime temperate oversea climates. The curves shown on these figures are based on a large amount of data. Estimates of variability in other climates are based on what is known about meteorological conditions and their effects on radio propagation, but have relatively few measurements to support them.

Figures III.25 to III.29 show curves of variability relative to the long-term median, prepared by the CCIR [1963 f] for the following climatic regions:

- (4) Maritime Subtropical, Overland.
- (5) Maritime Subtropical, Oversea.*
- (6) Desert.
- (7) Equatorial.
- (8) Continental Subtropical.

In some cases, random path differences have undoubtedly been attributed to climatic differences. Available data were normalized to a frequency of 1000 MHz, and the curves correspond to this frequency. They show all-year variability $Y(q, d_e, 1000 \text{ MHz})$ about the long-term median as a function of the effective distance d_e defined by (10.3). Variability estimates for other frequencies are obtained by using the appropriate correction factor $g(f)$ shown in figure III.30:

$$Y(q) = Y(q, d_e, 1000 \text{ MHz}) g(f). \quad (\text{III.66})$$

The empirical curves $g(f)$ are not intended as an estimate of the dependence of long-term variability on frequency, but represent an average of many effects that are frequency-sensitive, as discussed in section 10.

Variability about the long-term median transmission loss $L(0.5)$ is related to the long-term reference median L_{cr} by means of the function $V(0.5, d_e)$ shown on figure 10.1. The predicted long-term median transmission loss is then:

$$L(0.5) = L_{cr} - V(0.5, d_e) \quad (\text{III.67})$$

and the predicted value for any percentage of time is

$$L(q) = L(0.5) - Y(q). \quad (\text{III.68})$$

* Curves for climate 5 have been deleted. They were based on a very small amount of data. For hot, moist tropical areas use climate 4, and for coastal areas where prevailing winds are from the ocean, use climate 3.

III. 7. 1 Diurnal and Seasonal Variability in a Continental Temperate Climate

The curves shown in figures 10.5 to 10.16 and III.25 to III.29 represent variability about the long-term median for all hours of the day throughout the entire year. For certain applications, it is important to know something about the diurnal and seasonal changes that may be expected. Such changes have been studied in the continental United States, where a large amount of data is available. Measurement programs recorded VHF and UHF transmission loss over particular paths for at least a year to determine seasonal variations. Data were recorded over a number of paths for longer periods of time to study year-to-year variability.

As a general rule, transmission loss is less during the warm summer months than in winter, and diurnal trends are usually most pronounced in summer, with maximum transmission loss occurring in the afternoon. The diurnal range in signal level may be about 10 db for paths that extend just beyond the radio horizon, but is much less for very short or very long paths. Variation with season usually shows maximum losses in mid-winter, especially on winter afternoons, and high fields in summer, particularly during morning hours. Transmission loss is often much more variable over a particular path in summer than it is during the winter, especially when ducts and elevated layers are relatively common.

The data were divided into eight "time blocks" defined in table III. 1. The data were assumed to be statistically homogeneous within each of the time blocks. With more and shorter time blocks, diurnal and seasonal trends would be more precisely defined, except that no data would be available in some of the time blocks over many propagation paths. Even with the division of the year into winter and summer and the day into four periods as in table III.1, it is difficult to find sufficient data to describe the statistical characteristics expected of transmission loss in Time Blocks 7 and 8.

Table III. 1
Time Blocks

<u>No.</u>	<u>Months</u>	<u>Hours</u>
1	Nov. - Apr.	0600 - 1300
2	Nov. - Apr.	1300 - 1800
3	Nov. - Apr.	1800 - 2400
4	May - Oct.	0600 - 1300
5	May - Oct.	1300 - 1800
6	May - Oct.	1800 - 2400
7	May - Oct.	0000 - 0600
8	Nov. - Apr.	0000 - 0600

In some applications, it is convenient to combine certain time blocks into groups, for instance, some characteristics of long-term variability are significantly different for the winter group (Time Blocks 1, 2, 3, 8) than for the summer group (Time Blocks 4, 5, 6, 7).

In other climatic regions, if the annual range of monthly average values of N_g is less than 20 N units (figure III. 31), seasonal variations are expected to be negligible. One would also expect less diurnal change, for example, in a maritime temperate climate where changes in temperature during the day are less extreme. In climates where N_g changes considerably throughout the year, the consecutive 4-6 month period when N_g is lowest may be assumed to correspond to "winter", whatever months may be involved.

For the U.S. only, the parameter $V(0.5, d_e)$ for each of the eight time blocks and for "summer" and "winter" is shown in figure III. 32. Curves of the variability $Y(q, d_e, 100 \text{ MHz})$ about the long-term median for each of these times of day and seasons are shown in figures III. 33 to III. 42. These curves are drawn for a frequency of 100 MHz. Figures III. 33 and III. 34 show the range 0.01 to 0.99 of $Y(q, d_e, 100 \text{ MHz})$ for the winter time blocks, 1, 2, 3, 8 and the summer time blocks 4, 5, 6, 7. Each group of data was analysed separately. Some of the differences shown between time blocks 1, 2, 3, and 8 are probably not statistically significant. Marked differences from one time block to another are observed during the summer months.

Figures III. 35 through III. 42 show data coded in the following frequency groups, 88-108, 108-250 and 400 to 1050 MHz as well as curves for $Y(q)$ drawn for 100 MHz. In general these figures show more variability in the two higher frequency groups especially during "summer" (time blocks 4, 5, 6 and 7). Because of the relatively small amount of data no attempt was made to derive a frequency factor $g(q, f)$ for individual time blocks.

The curves for summer, winter, and all hours shown in figures 10. 13 through 10. 22 represent a much larger data sample, since time block information was not available for some paths for which summer or winter distributions were available.

The smooth curves of $V(0.5, d_e)$ and $Y(q, d_e, 100 \text{ MHz})$ versus d_e shown in figures 10. 13, 10. 14, III. 25 to III. 29 and III. 32 to III. 42 may be represented by an analytic function of the general form:

$$\left. \begin{array}{l} V(0.5) \\ Y(0.1) \\ -Y(0.9) \end{array} \right\} = \left[c_1 d_e^{n_1} - f_2(d_e) \right] \exp(-c_3 d_e^{n_3}) + f_2(d_e) \quad \text{III. 69}$$

where

$$f_2(d_e) = f_\infty + (f_m - f_\infty) \exp(-c_2 d_e^{n_2}) \quad \text{III. 70}$$

The terms $c_1, c_2, c_3, n_1, n_2, n_3, f_m$, and f_∞ in (III. 69) and (III. 70) are constants for any given time block and value of q . The parameters f_m and f_∞ are maximum and asymptotic values, respectively. Tables III. 2 to III. 4 list values of the eight parameters required in (III. 69) to obtain $V(0.5, d_e)$, $Y(0.1, d_e, 100 \text{ MHz})$ and $-Y(0.9, d_e, 100 \text{ MHz})$ for the eight time blocks in table III. 1, and for summer, winter, and all hours. The constants given

in Tables III.2 to III.4 for summer, winter and all hours were determined using only radio paths for which time block information is available. They do not yield the curves shown in figures 10.13 and 10.14 of section 10, which represent a much larger data sample.

Tables III.5 to III.7 list values of the eight parameters in (III.59) required to compute $V(0.5)$, $Y(0.1, d_e, f_{\text{MHz}})$ and $Y(0.9, d_e, f_{\text{MHz}})$ for each of the climatic regions discussed in section 10, Volume 1, and section III.7 of this annex.

TABLE III. 2
 Constants for Calculating $V(0.5, d_e)$

Time Block	c_1	$\frac{d_e \text{ in km.}}{c_2}$	c_3	n_1	n_2	n_3	f_m	f_∞
4	1.35^{-6}	5.02^{-18}	1.32^{-7}	2.80	6.74	3.08	5.2	4.0
5	1.05^{-6}	5.02^{-18}	4.14^{-9}	2.70	6.74	3.70	2.4	1.8
6	2.04^{-4}	6.61^{-18}	2.82^{-9}	1.87	6.67	3.76	5.2	4.2
7	8.00^{-4}	3.91^{-16}	1.20^{-5}	1.68	5.94	2.25	7.1	5.6
S*	1.18^{-5}	6.72^{-17}	1.65^{-6}	2.40	6.32	2.61	5.1	4.0
1	2.11^{-4}	3.44^{-17}	1.73^{-4}	1.67	6.52	1.82	1.2	0.9
3	3.47^{-4}	3.76^{-14}	5.42^{-4}	1.60	5.30	1.58	1.3	0.6
8	3.63^{-4}	1.80^{-23}	1.55^{-3}	1.65	8.91	2.36	1.95	0.8
W*	1.40^{-3}	1.79^{-34}	1.05^{-3}	1.27	13.23	2.51	1.05	0.5
A*	1.63^{-4}	1.81^{-25}	8.12^{-6}	1.80	9.59	2.32	3.0	1.9

* Time Blocks "S", "W", and "A" are all hours summer, all hours winter, and all hours all year respectively. See Table III. 1 for definitions of the other time blocks. Small digits represent the exponent of the number, for example $2.33^{-2} = 2.33 \times 10^{-2}$.

GA

G

TABLE III. 3
 Constants for Calculating $X(0.1, d_e, 100 \text{ MHz})$

Time Block	c_1	$\frac{d_e \text{ in km.}}{c_2}$	c_3	n_1	n_2	n_3	f_m	f_∞
4	1.22^{-2}	9.81^{-6}	1.09^{-8}	1.36	2.00	3.58	10.8	5.5
5	2.58^{-4}	3.41^{-6}	2.01^{-11}	2.05	2.25	4.78	8.0	4.0
6	3.84^{-3}	4.22^{-5}	7.76^{-9}	1.57	1.76	3.66	9.6	5.2
7	7.95^{-3}	3.76^{-5}	3.19^{-8}	1.47	1.76	3.40	11.2	5.5
S*	4.47^{-3}	1.66^{-5}	2.06^{-8}	1.55	1.90	3.48	9.98	5.1
1	1.09^{-4}	1.21^{-6}	8.29^{-8}	2.28	2.29	3.26	9.6	2.8
2	1.04^{-5}	4.28^{-8}	3.51^{-8}	2.71	2.91	3.41	9.15	2.8
3	2.02^{-4}	1.45^{-6}	4.27^{-8}	2.15	2.28	3.37	9.4	2.8
8	1.70^{-4}	7.93^{-7}	1.29^{-7}	2.19	2.37	3.18	9.5	3.0
W*	2.46^{-4}	1.74^{-7}	1.27^{-8}	2.11	2.64	3.62	9.37	2.8
A*	5.25^{-4}	1.57^{-6}	4.70^{-7}	1.97	2.31	2.90	10.0	5.4

* Time Blocks "S", "W", and "A" are all hours summer, all hours winter, and all hours all year, respectively. See Table III.1 for definitions of the other time blocks. Small digits represent the exponent of the number, for example $2.33^{-8} = 2.33 \times 10^{-8}$.

TABLE III. 4
 Constants for Calculating - Y(0.9, d₀, 100 MHz)

Time Block	c ₁	$\frac{d_0 \text{ in km.}}{c_2}$	c ₃	n ₁	n ₂	n ₃	f _m	f _∞
4	1.84 ⁻⁴	2.22 ⁻⁶	3.65 ⁻¹⁶	2.09	2.29	6.82	8.0	4.0
5	3.80 ⁻⁴	4.76 ⁻⁶	8.39 ⁻¹⁷	1.92	2.19	7.10	6.6	3.3
6	1.81 ⁻³	5.82 ⁻⁶	6.37 ⁻¹³	1.67	2.15	5.38	8.4	4.1
7	3.19 ⁻³	2.51 ⁻⁶	5.03 ⁻⁹	1.60	2.27	3.69	10.0	4.4
S*	7.42 ⁻⁴	5.55 ⁻⁵	4.37 ⁻⁸	1.84	1.69	3.28	8.25	4.0
1	1.72 ⁻⁴	6.39 ⁻⁸	2.93 ⁻¹⁰	2.10	2.73	4.24	8.2	2.4
2	1.05 ⁻⁵	7.00 ⁻¹³	7.64 ⁻⁹	2.59	4.80	3.68	7.05	2.8
3	3.64 ⁻⁵	3.74 ⁻⁹	3.53 ⁻⁷	2.40	3.28	2.94	7.8	2.2
8	1.64 ⁻⁶	1.43 ⁻⁷	3.14 ⁻⁷	3.08	2.66	3.03	9.6	2.6
W*	3.45 ⁻⁶	1.25 ⁻⁸	7.50 ⁻⁷	2.87	3.07	2.82	7.92	2.45
A*	2.93 ⁻⁴	3.78 ⁻⁸	1.02 ⁻⁷	2.00	2.88	3.15	8.2	3.2

* Time Blocks "S", "W", and "A" are all hours summer, all hours winter, and all hours all year, respectively. See Table III.1 for definitions of other time blocks. Small digits represent the exponent of the number, for example, 4.97⁻⁴ = 4.97 X 10⁻⁴.

TABLE III. 5
 Constants for Calculating $V(0.5, d_0)$ for Several Climatic Regions

Climate	d_0 in km							
	c_1	c_2	c_3	n_1	n_2	n_3	f_m	f_s
1. Continental Temperate	1.59^{-5}	1.56^{-11}	2.77^{-8}	2.32	4.00	3.25	3.9	0
2. Maritime Temperate Overland	1.12^{-4}	1.26^{-20}	1.17^{-11}	1.08	7.30	4.41	1.7	0
3. Maritime Temperate Oversea	1.18^{-4}	3.33^{-13}	3.82^{-9}	2.06	4.60	3.75	7.0	3.2
4. Maritime Subtropical Overland	1.09^{-4}	5.89^{-18}	2.21^{-7}	2.06	6.81	2.97	5.0	4.2
5. Maritime Subtropical Oversea (deleted)								
6. Desert (Sahara) (Computes - $V(0.5)$)	8.85^{-7}	2.76^{-14}	2.25^{-12}	2.80	4.82	4.71	8.4	0.2
7. Equatorial	3.45^{-7}	3.74^{-12}	6.97^{-8}	2.97	4.43	3.14	1.2	-0.4
8. Continental Subtropical	1.59^{-5}	1.56^{-11}	2.77^{-8}	2.32	4.00	3.25	3.9	0

Note - Corresponding curves of $V(0.5, d_0)$ are drawn on figure 10.13, section 10, Volume 1.

TABLE III. 6
 Constants for Calculating $Y(0.1, d_0, f, \text{MHz})$ for Several Climatic Regions

Climatic	Figure	c_1	c_2	c_3	n_1	n_2	n_3	f_{in}	f_c
1. Continental Temperate All hours and Summer Winter	10.14	3.56 ⁻² 3.56 ⁻²	9.85 ⁻⁸ 3.76 ⁻⁸	1.50 ⁻¹¹ 2.05 ⁻¹¹	1.13 1.13	2.80 2.92	4.85 4.78	10.5 10.5	5.4 2.9
2. Maritime Temperate Overland Bands I & II (40-100 MHz) Band III (150-250 MHz) Bands IV & V (450-1000 MHz)	10.23 10.25 10.27	6.96 ⁻³ 3.60 ⁻² 6.28 ⁻⁴	1.57 ⁻⁷ 3.19 ⁻⁸ 3.19 ⁻⁸	1.15 ⁻¹¹ 6.91 ⁻¹⁸ 6.06 ⁻¹²	1.52 1.11 1.92	2.83 2.96 2.96	5.04 7.14 5.05	13.5 12.5 13.0	11.9 11.0 12.5
3. Maritime Temperate Oversea Bands I & II (40-100 MHz) Band III (150-250 MHz) Bands IV & V (450-1000 MHz)	10.24 10.26 10.28	1.37 ⁻² 2.67 ⁻³ 1.82 ⁻²	1.04 ⁻¹¹ 5.88 ⁻¹ 2.40	1.42 ⁻⁵ 8.25 ⁻⁸ 6.92 ⁻¹⁵	1.38 1.79 1.29	4.42 0 0	2.27 3.27 5.78	16.0 18.5 19.0	13.0 16.5 14.0
4. Maritime Subtropical Overland	III.25	4.33 ⁻²	7.13 ⁻¹¹	1.19 ⁻¹²	1.09	3.89	4.93	17.5	13.6
5. Maritime Subtropical Oversea (deleted)									
6. Desert (Sahara)	III.27	6.09 ⁻²	1.36 ⁻⁵	3.18 ⁻¹¹	1.08	1.84	4.60	15.1	6.0
7. Equatorial	III.28	5.22 ⁻³	1.57 ⁻⁴	5.22 ⁻¹⁷	1.39	1.46	6.78	8.5	3.2
8. Continental Subtropical	III.29	1.01 ⁻²	2.26 ⁻⁷	3.90 ⁻⁹	1.46	2.67	3.78	16.0	9.1

Note - Corresponding curves of $Y(0.1, d_0)$ are drawn on the figures listed above.

TABLE III.7
 Constants for Calculating $-Y(0.9, d_e, f_{MHz})$ for Several Climatic Regions

Climatic	Figure	c_1	c_2	c_3	n_1	n_2	n_3	f_m	f_p
1. Continental Temperate All Hours	10.14	9.48 ⁻³	5.70 ⁻¹¹	5.56 ⁻⁶	1.33	3.96	2.44	8.2	3.0
Summer		9.48 ⁻³	1.81 ⁻¹¹	7.00 ⁻⁶	1.33	4.23	2.40	8.2	4.3
Winter		9.48 ⁻³	1.14 ⁻¹¹	7.36 ⁻⁶	1.33	4.22	2.39	8.2	2.1
2. Maritime Temperate Overland Bands I & II (40-100 MHz)	10.23	1.45 ⁻³	1.68 ⁻¹²	8.07 ⁻⁶	1.70	4.61	2.36	9.0	3.5
Band III (150-250 MHz)	10.25	9.32 ⁻⁴	2.66 ⁻¹⁴	1.02 ⁻¹⁶	1.74	5.29	6.82	10.5	3.5
Bands IV & V (450-1000 MHz)	10.27	1.29 ⁻⁴	1.93 ⁻¹⁵	2.81 ⁻⁴	2.14	5.80	1.65	10.0	4.5
3. Maritime Temperate Oversea Bands I & II (40-100 MHz)	10.24	4.52 ⁻²	8.69 ⁻¹⁶	1.28 ⁻³	1.13	5.95	1.14	13.5	3.5
Band III (150-250 MHz)	10.26	1.14 ⁻³	5.76 ⁻⁹	1.29 ⁻⁸	1.90	3.27	3.67	14.5	4.0
Bands IV & V (450-1000 MHz)	10.28	1.25 ⁻³	6.57 ⁻¹⁶	1.49 ⁻⁹	1.72	5.96	3.84	12.0	4.0
4. Maritime Subtropical Overland	III.25	7.24 ⁻³	4.26 ⁻¹⁵	1.12 ⁻⁶	1.35	5.41	2.56	12.7	8.4
5. Maritime Subtropical Oversea (deleted)									
6. Desert (Sahara)	III.27	3.19 ⁻²	5.66 ⁻⁸	7.39 ⁻¹¹	1.14	2.76	4.40	11.4	3.3
7. Equatorial	III.28	6.51 ⁻³	2.53 ⁻⁴	2.61 ⁻¹⁶	1.36	1.36	6.95	8.4	2.7
8. Continental Subtropical	III.29	3.49 ⁻³	1.08 ⁻⁹	9.15 ⁻¹¹	1.55	3.49	4.46	10.1	3.5

Note - These constants will yield positive values, i.e., $-Y(0.9, d_e)$. Corresponding curves of $Y(0.9, d_e)$ are drawn on the figures
 Her 4 above.

III.7.2 To Mix Distributions

When a prediction is required for a period of time not shown on the figures or listed in the tables, it may sometimes be obtained by mixing the known distributions. For example, the distributions for time blocks 5 and 6 would be mixed if one wished to predict a cumulative distribution of transmission loss for summer afternoon and evening hours. In mixing distributions, it is important to average fractions of time rather than levels of transmission loss. Distributions of data for time blocks may also be mixed to provide distributions for other periods of time. For example, data distributions for time blocks 1, 2, 3, and 8 were mixed to provide distributions of data for "winter". When averages are properly weighted, such mixed distributions are practically identical to direct cumulative distributions of the total amount of data available for the longer period.

The cumulative distribution of N observed hourly median values is obtained as follows: (1) the values are arranged in order from smallest to largest, $L_1, L_2, L_3, \dots, L_n, \dots, L_N$, (2) the fraction q of hourly median values less than L_n is computed:

$$q(n) = \frac{n}{N} - \frac{1}{2N};$$

(3) a plot of L_n versus $q(n)$ for values of q from $1/(2N)$ to $1 - 1/(2N)$ is the observed cumulative distribution.

To mix two distributions, the following procedure is used: (1) choose ten to fifteen levels of transmission loss L_1, \dots, L_n , covering the entire range of $L(q)$ for both distributions, (2) at each of these levels, read the value q for each distribution and average these values, (3) plot each selected level of transmission loss at the corresponding average fraction of time to obtain the "mixed" distribution. In this way, any number of distributions may be combined, if each of them represents the same number of hours. If the number of hours is not the same, a weighted average value q should be computed, using as weights the number of hours represented by each distribution.

CLIMATE 4, MARITIME SUBTROPICAL OVERLAND

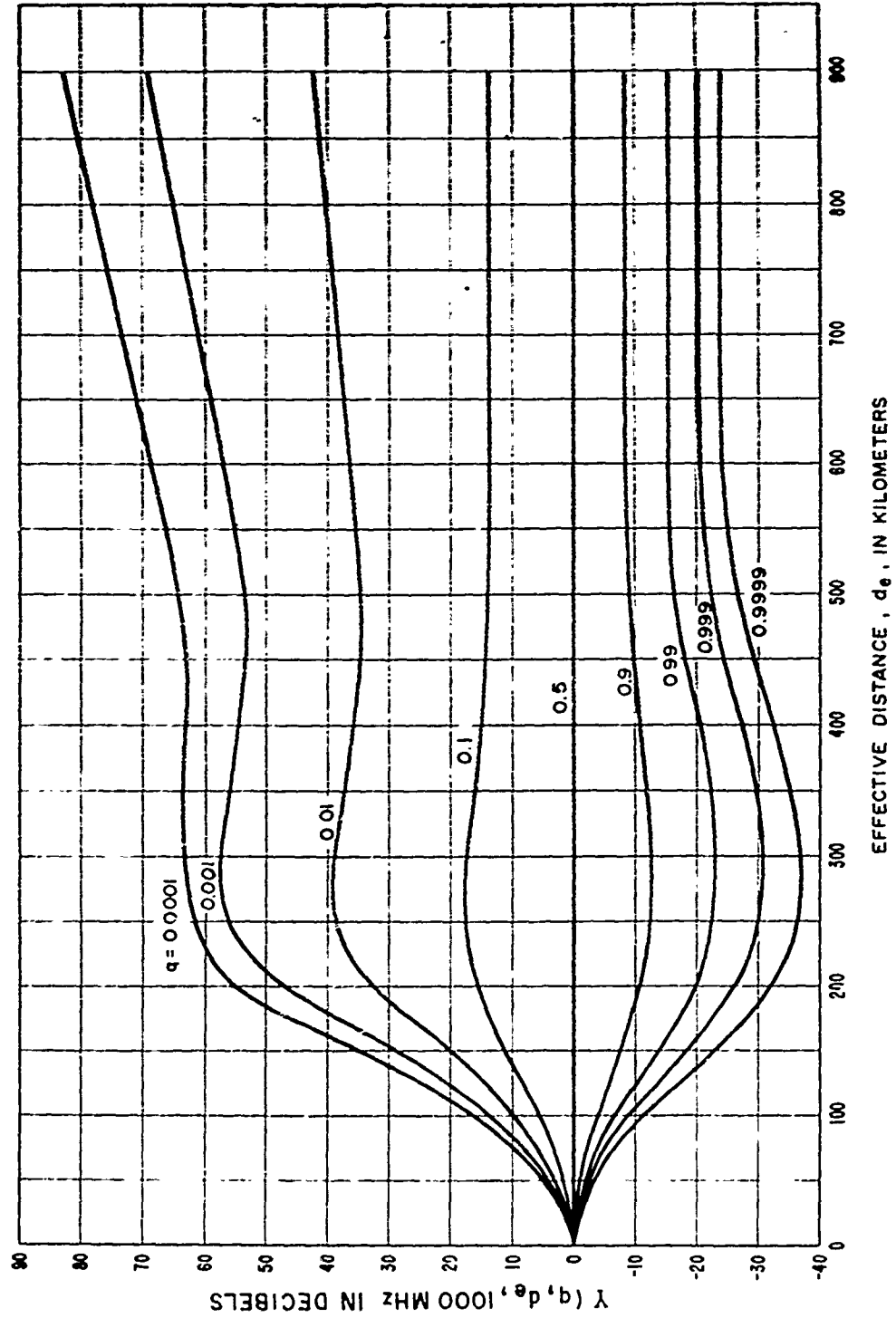


Figure III.25

CCP 702-1

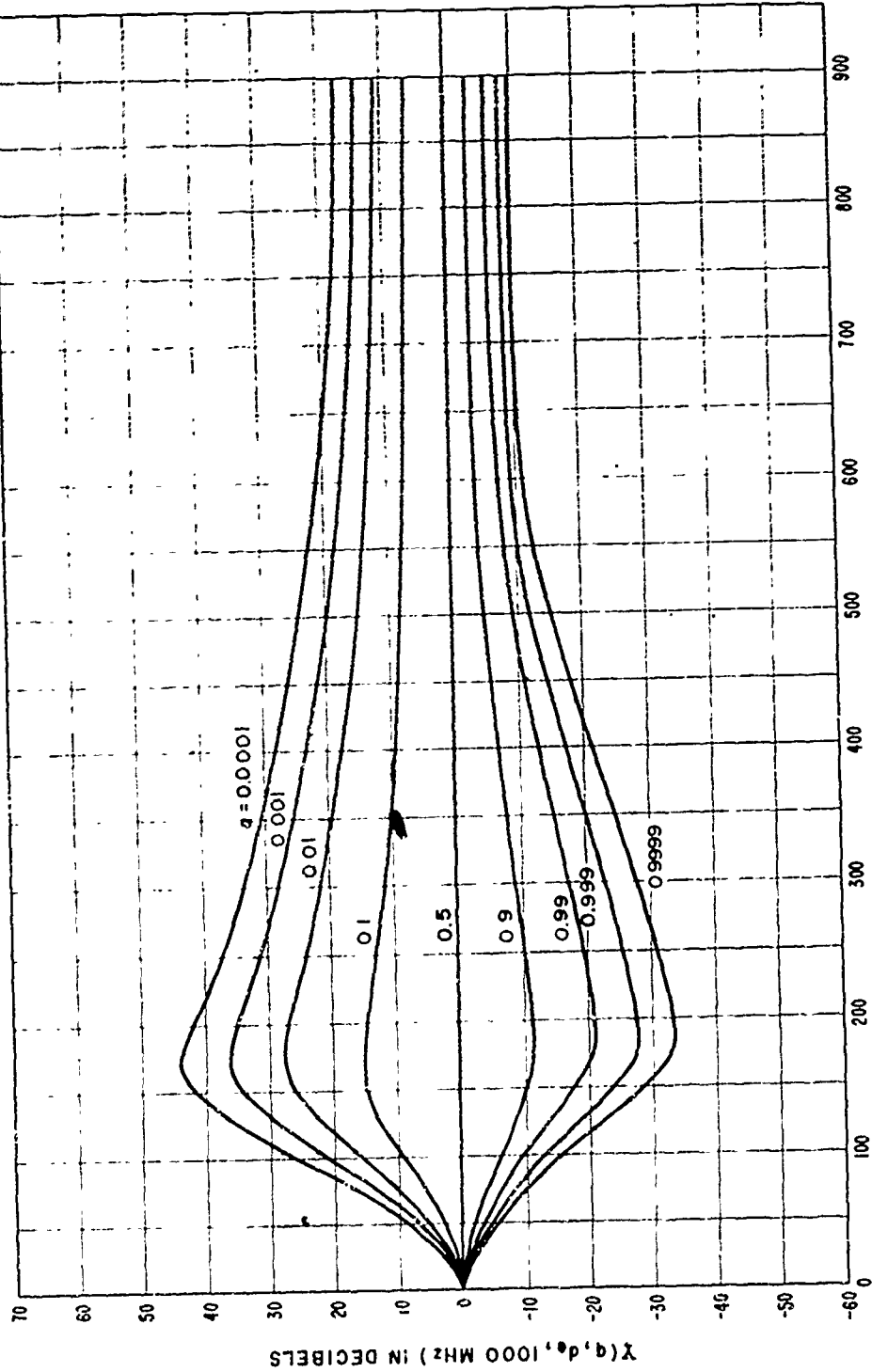
The curves for climate 5, Maritime Subtropical Oversea, have been deleted. These were based on a very small amount of data. Data obtained since the preparation of these curves indicate that the following give good estimates:

Climate 4, Maritime Subtropical Overland, for hot moist tropical areas or climate 3, Maritime Temperate Oversea, for coastal areas where the prevailing winds are from the ocean.

3

G

CLIMATE 6, DESERT, SAHARA



EFFECTIVE DISTANCE, d_e , IN KILOMETERS

Figure III.27

III-57

F-405

G

CLIMATE 7, EQUATORIAL

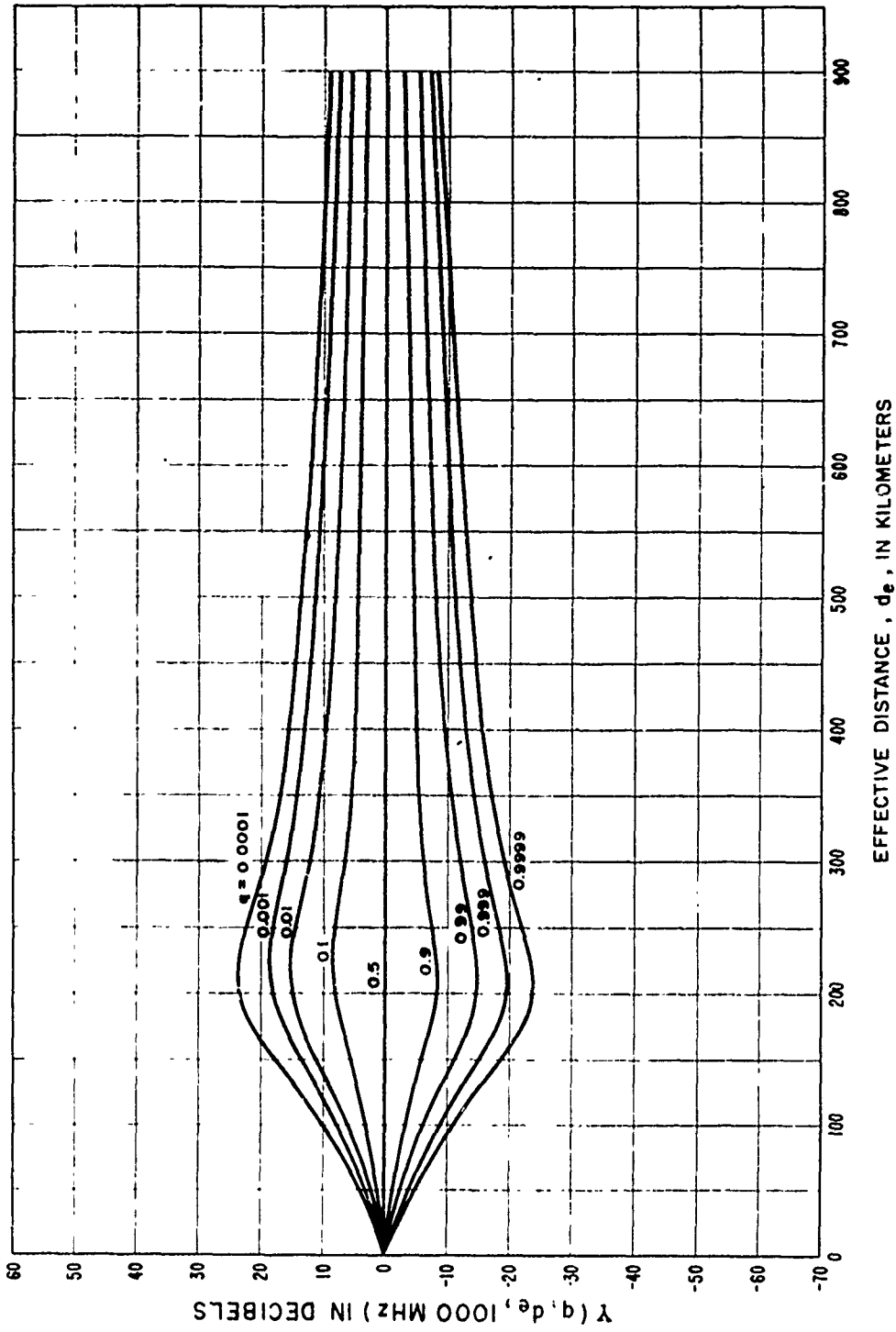
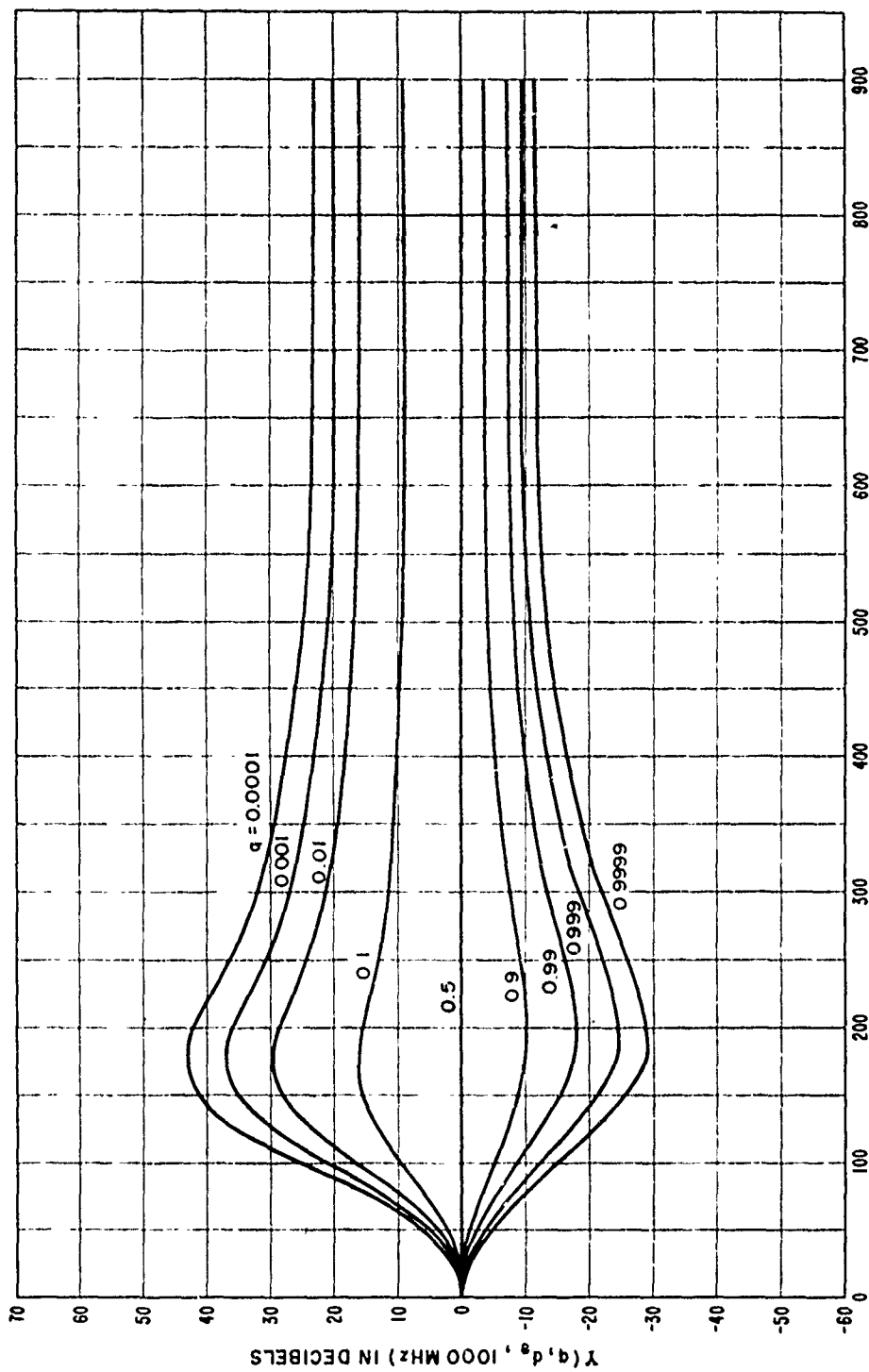


Figure III.28

III-58

F-406

CLIMATE 8, CONTINENTAL SUBTROPICAL



EFFECTIVE DISTANCE, d_e , IN KILOMETERS

Figure III.29

CONTINENTAL SUB-TROPICAL CLIMATE
DESERT CLIMATE

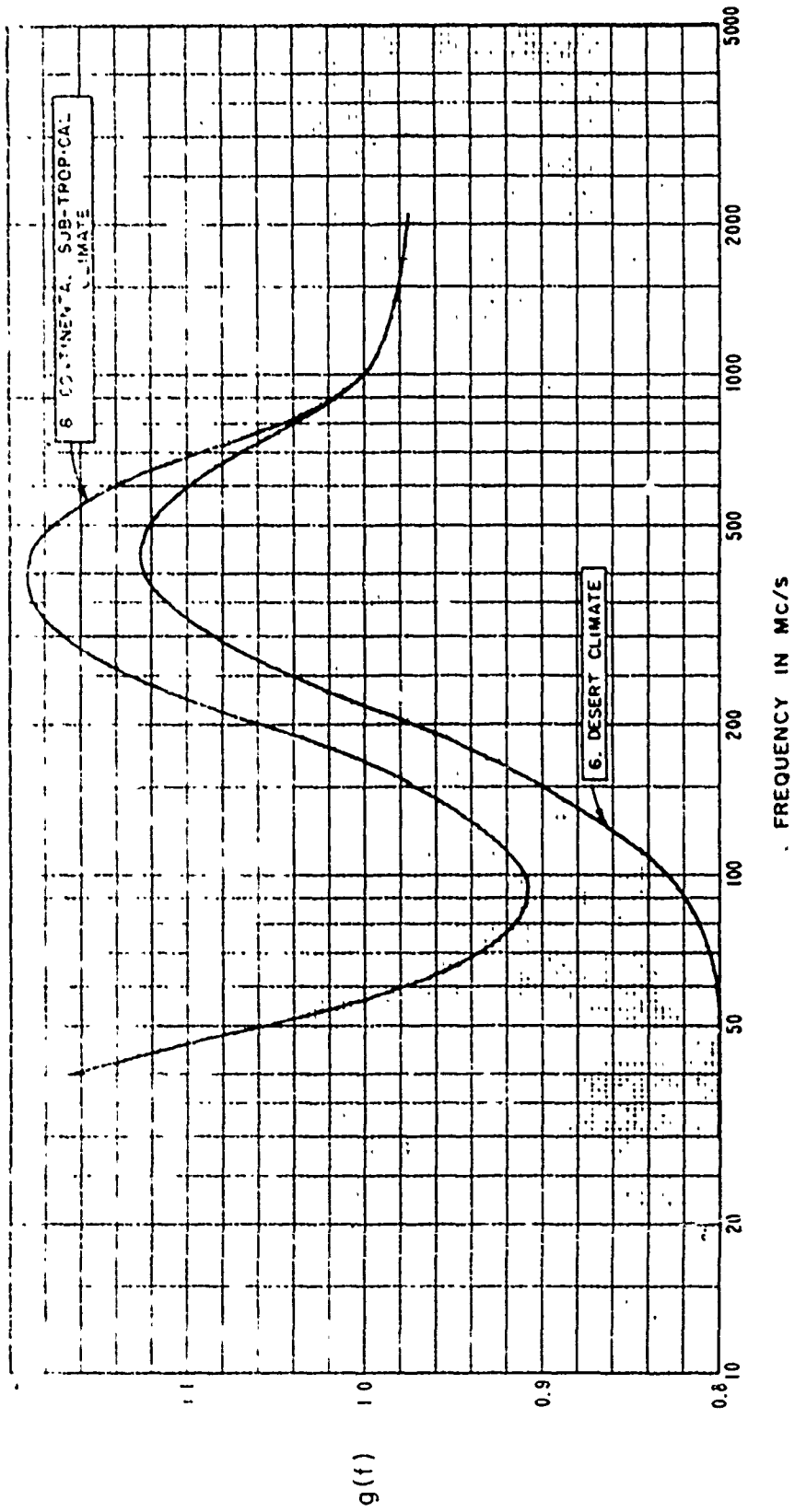
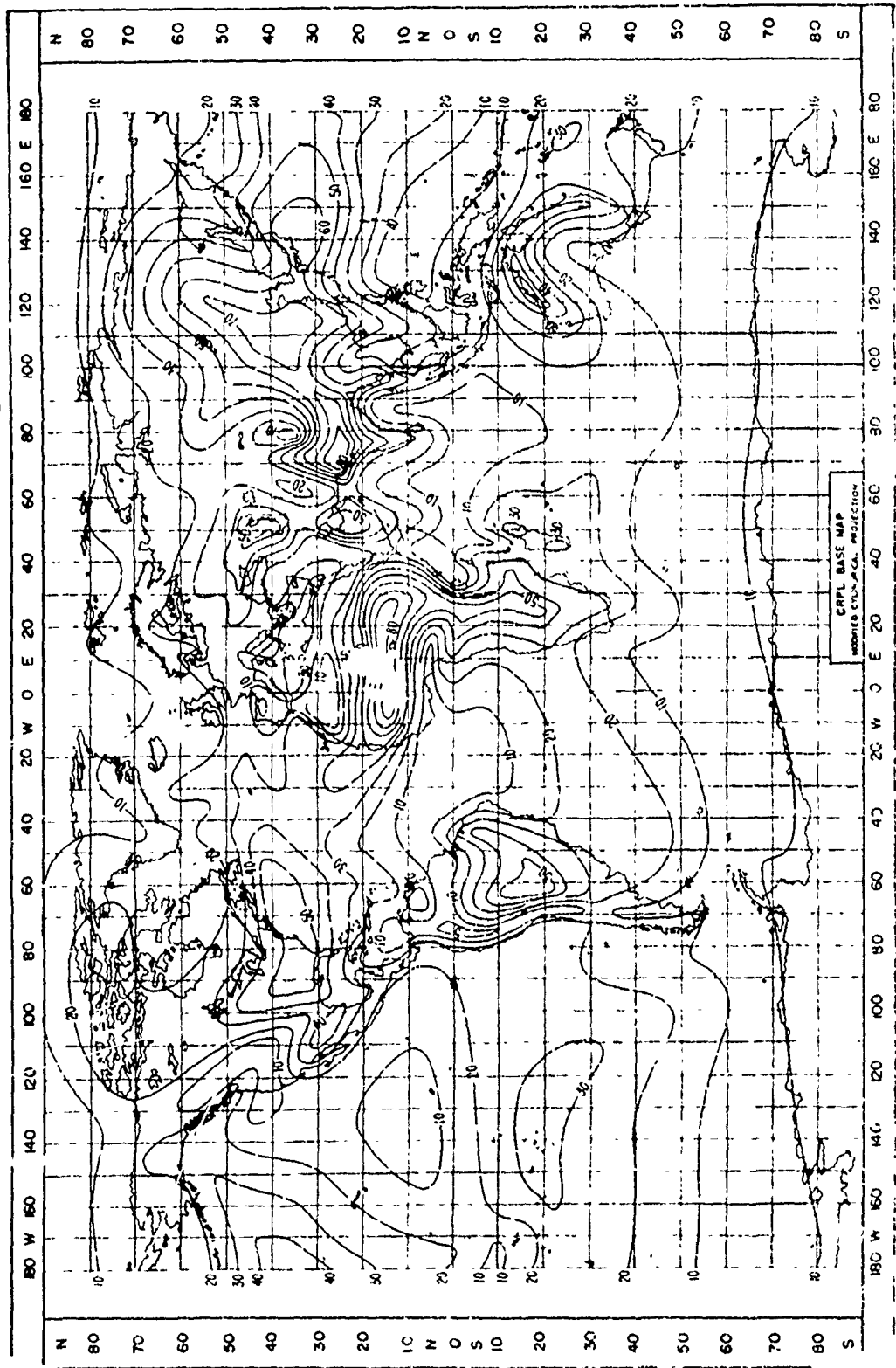


Figure III.30

ANNUAL RANGE OF MONTHLY MEAN N_s



THE FUNCTION $V(0.5, d_e)$ FOR VARIOUS PERIODS OF TIME IN THE U.S.A.

$$L(0.5) = L_{cr} - V(0.5, d_e) \text{ db}$$

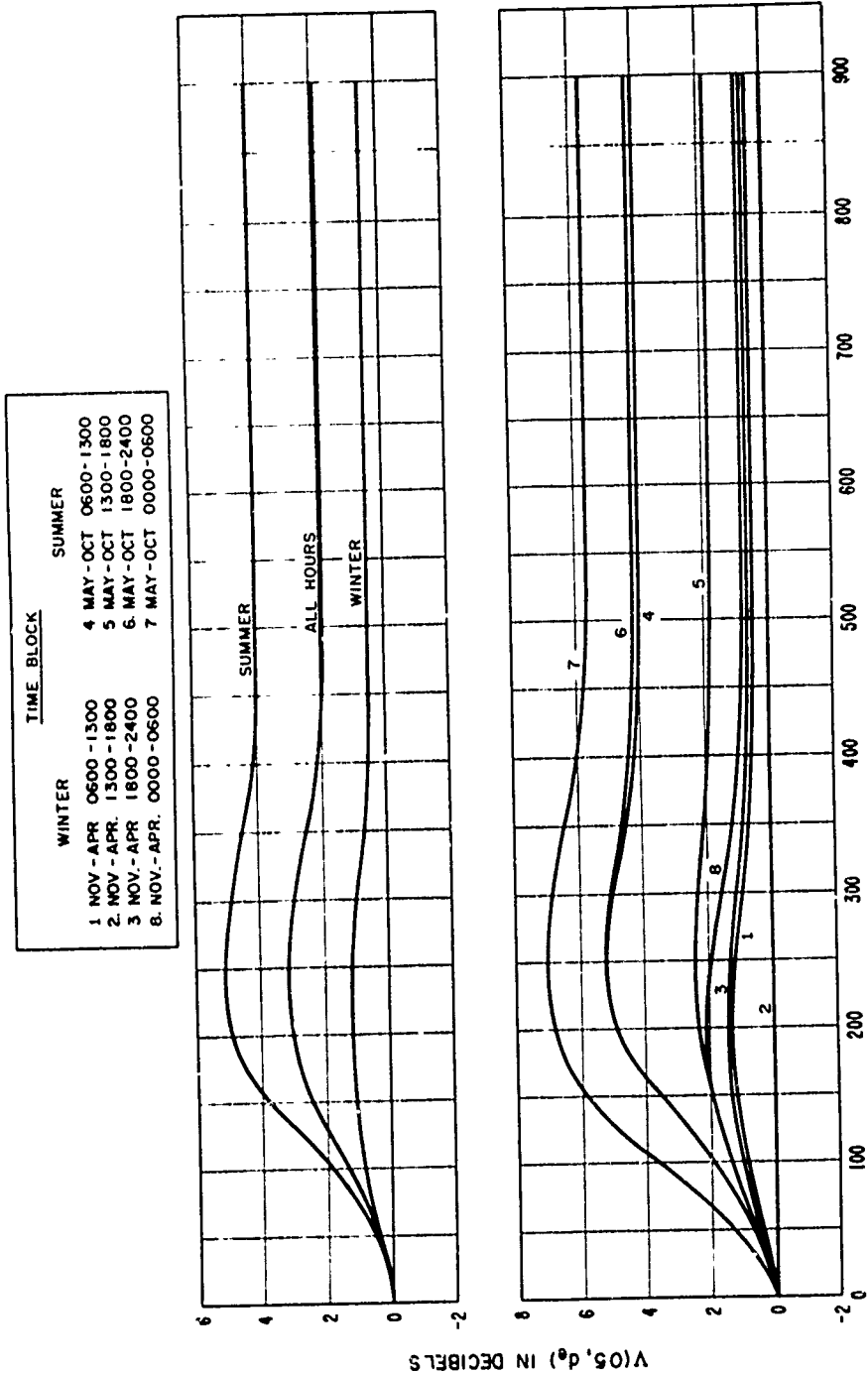


Figure III.32

WINTER TIME BLOCKS, NOV. - APRIL, U. S. A.
CURVES FOR 88 - 108 MHz

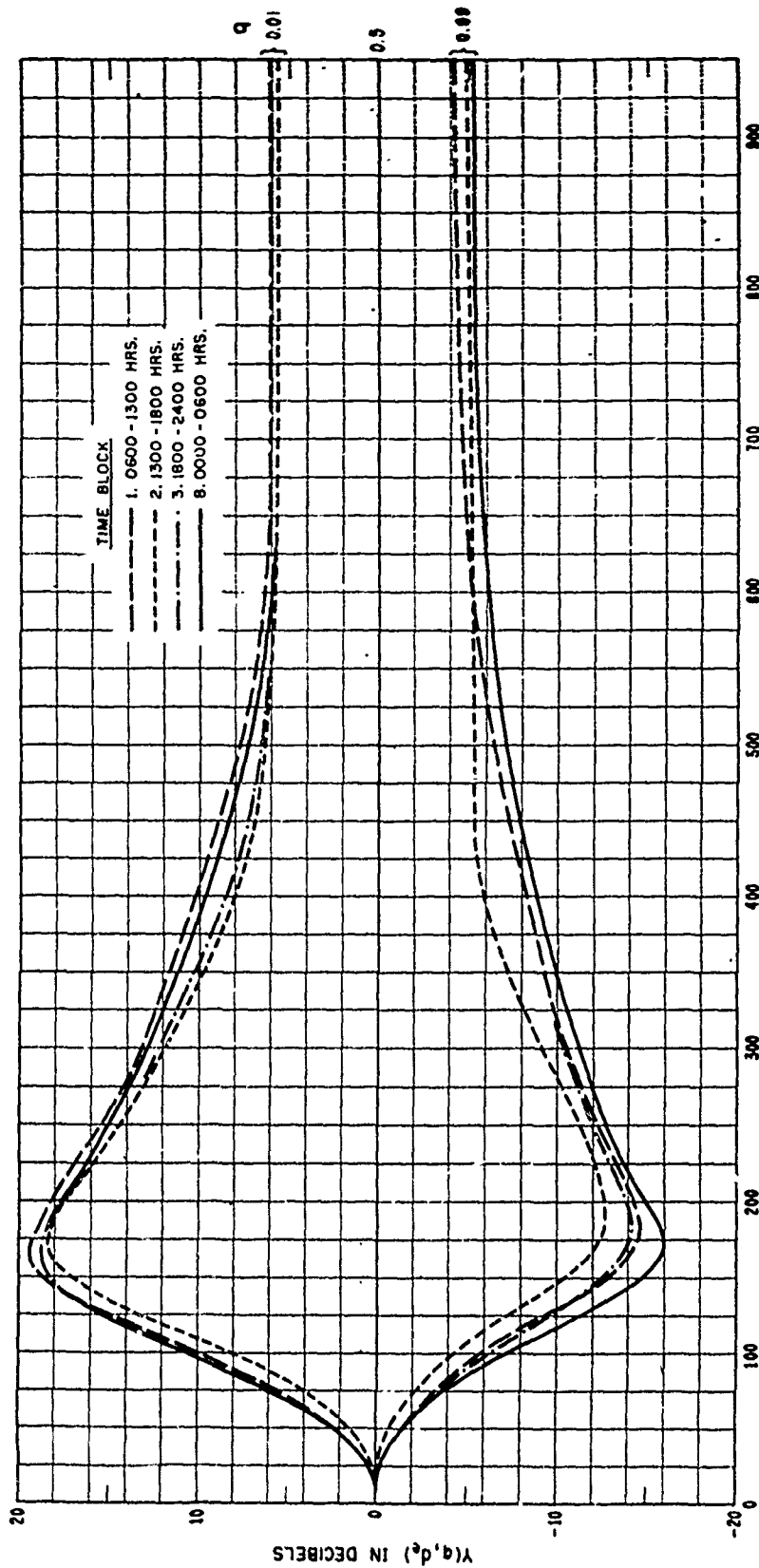


Figure III.33

III-63
F-411

SUMMER TIME BLOCKS, MAY - OCT. U.S.A.
 CURVES FOR 88-108 MHZ

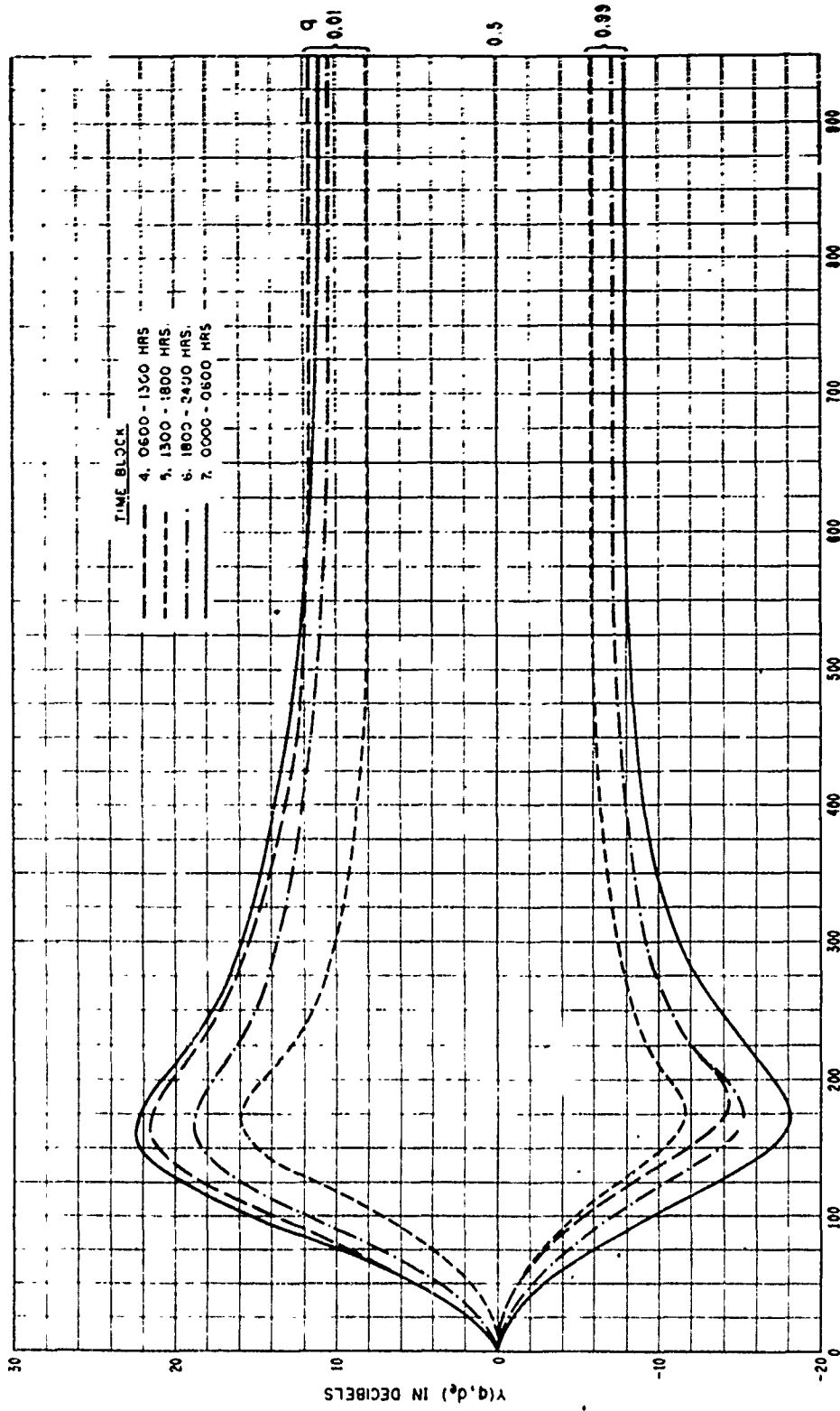
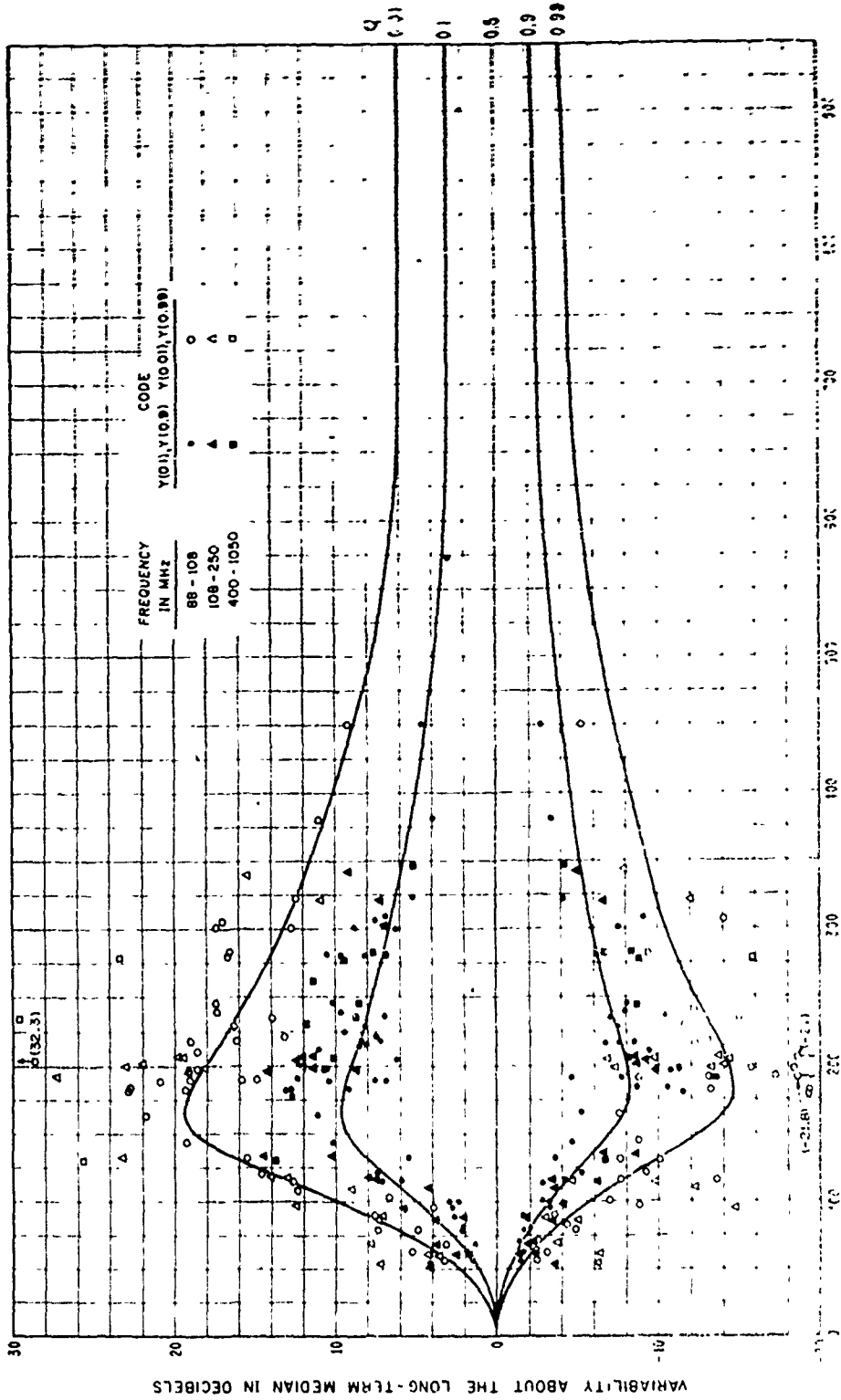


Figure III.34

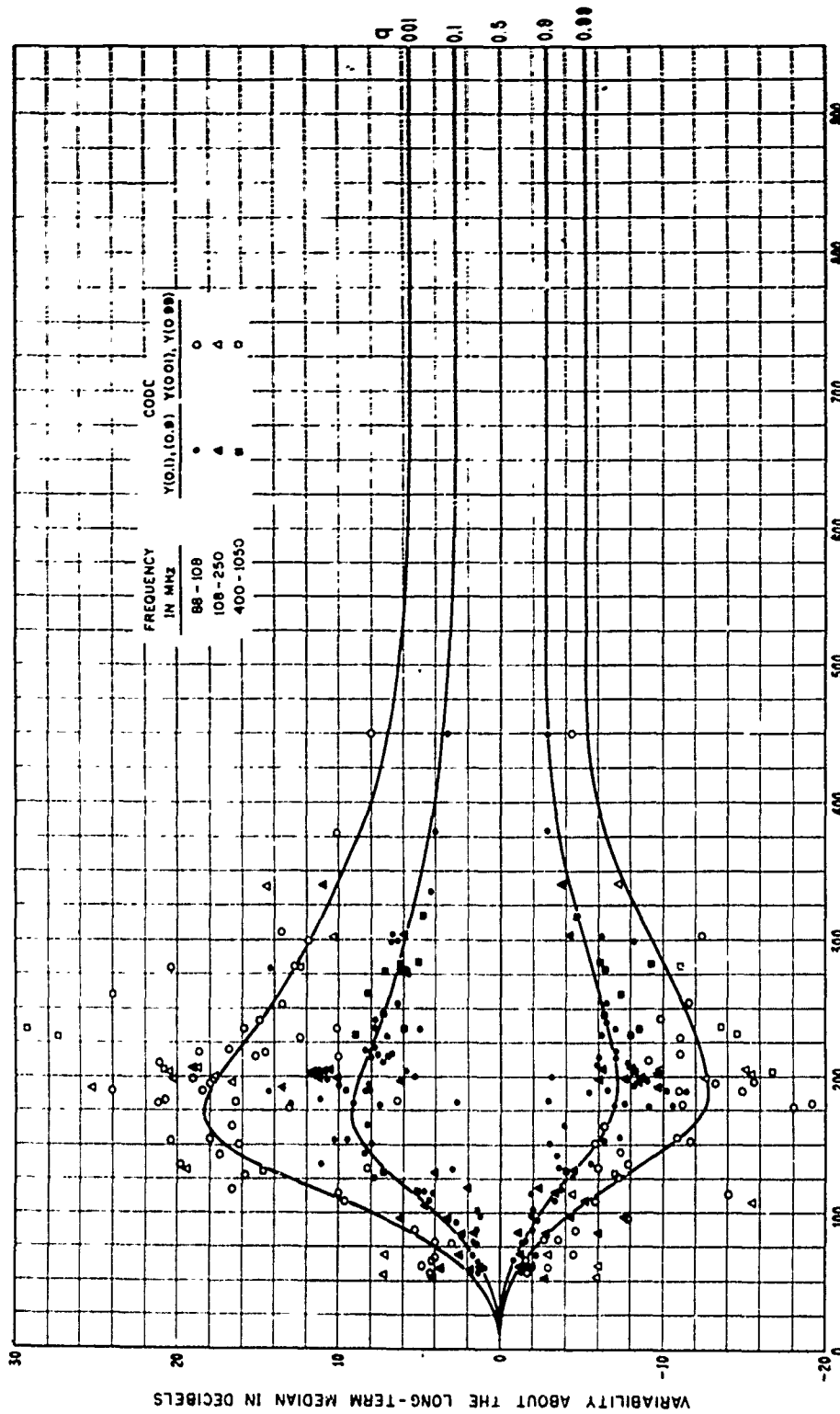
TIME BLOCK 1, NOV. - APRIL, 0600 - 1300 HRS., U.S.A.
CURVES SHOW $Y(q, d_e)$ FOR THE FREQUENCY RANGE 88 - 108 MHz



U.S. GOVERNMENT PRINTING OFFICE: 1965 O 345-111

FIGURE 75

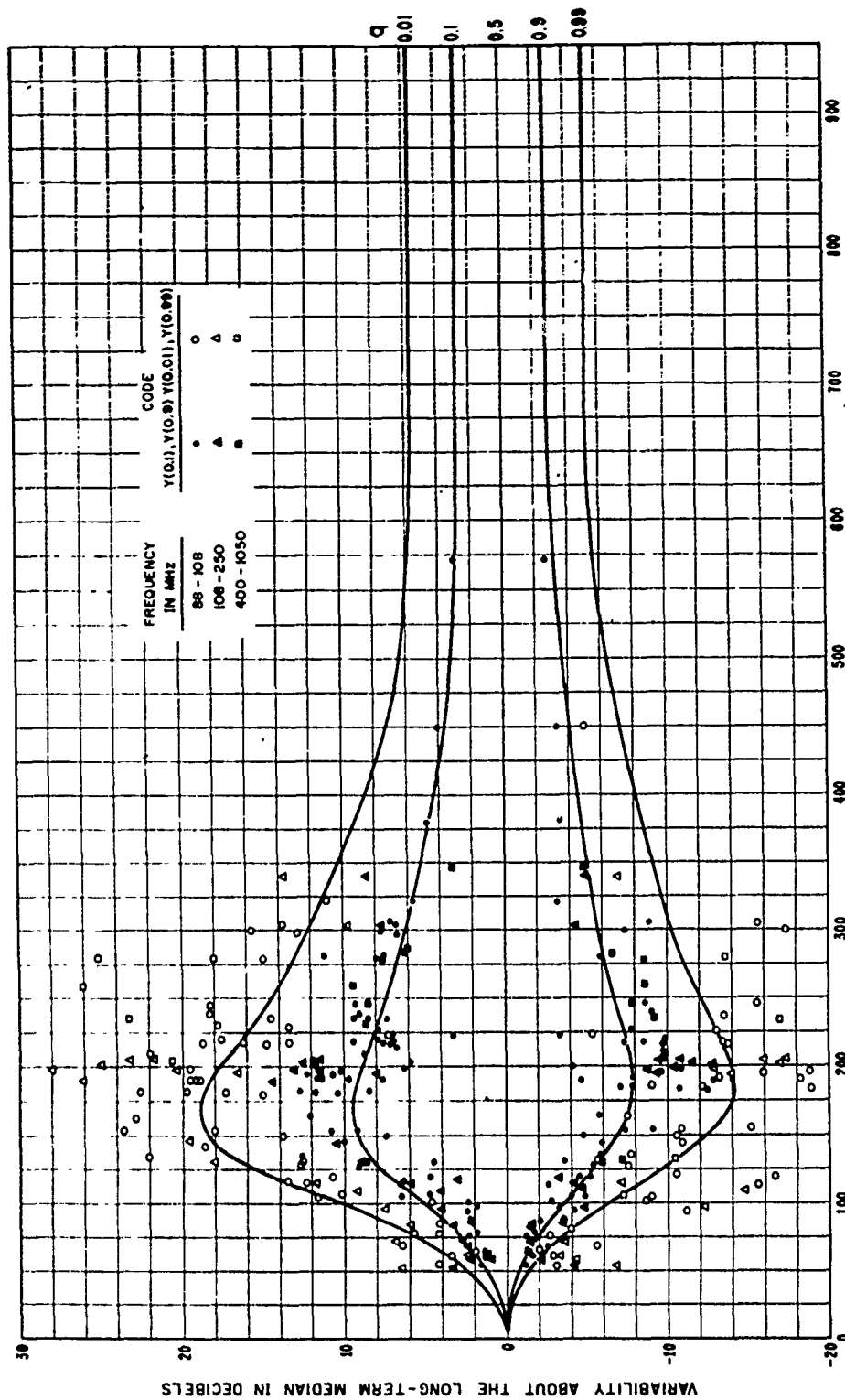
TIME BLOCK 2, NOV. - APRIL, 1300 - 1800 HRS., U. S. A.
 CURVES SHOW $Y(q, d_e)$ FOR THE FREQUENCY RANGE 88 - 108 MHz



EFFECTIVE DISTANCE, d_e , IN KILOMETERS

Figure III.36

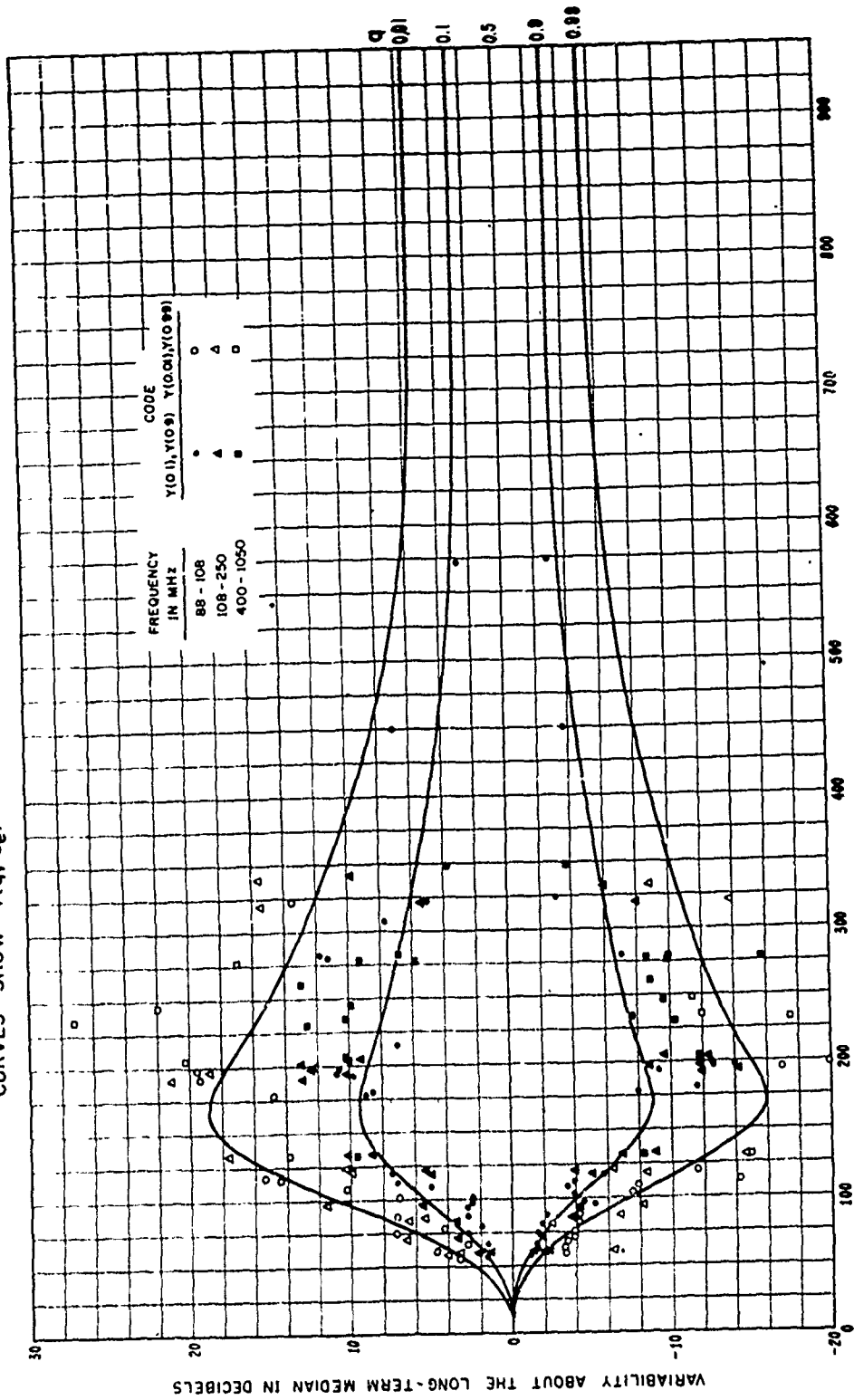
TIME BLOCK 3, NOV. - APRIL, 1800 - 2400 HRS., U. S. A.
 CURVES SHOW $Y(q, d_e)$ FOR THE FREQUENCY RANGE 88 - 108 MHz



EFFECTIVE DISTANCE, d_e , IN KILOMETERS

Figure III.37

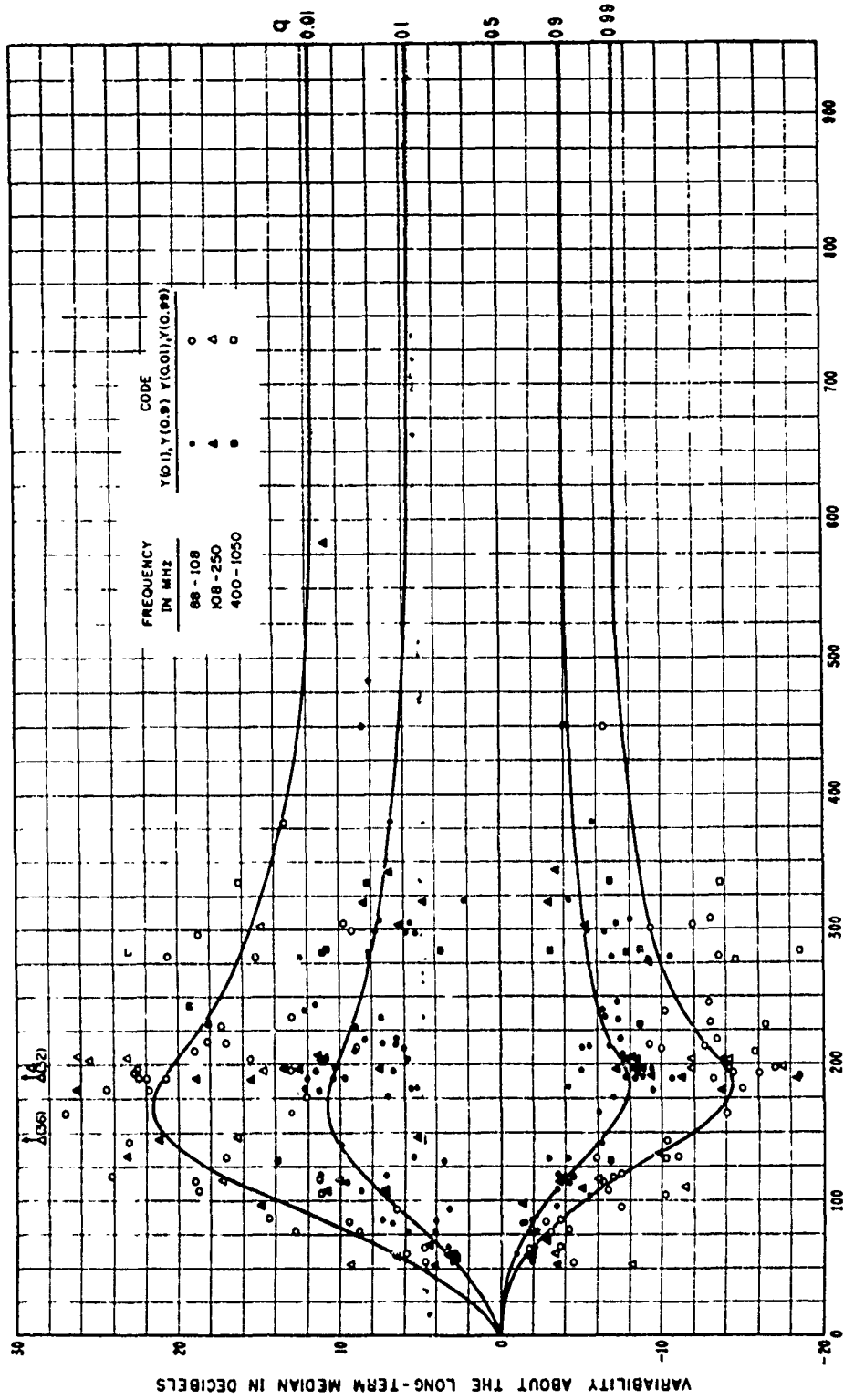
TIME BLOCK 8, NOV. - APRIL, 0000-0600 HRS., U.S.A.
 CURVES SHOW $\gamma(q, d_e)$ FOR THE FREQUENCY RANGE 88 - 108 MHz



EFFECTIVE DISTANCE, d_e , IN KILOMETERS

Figure III.38

TIME BLOCK 4, MAY - OCT., 0600-1300 HRS., U.S.A.
CURVES SHOW $Y(q, d_e)$ FOR THE FREQUENCY RANGE 88-108 MHz

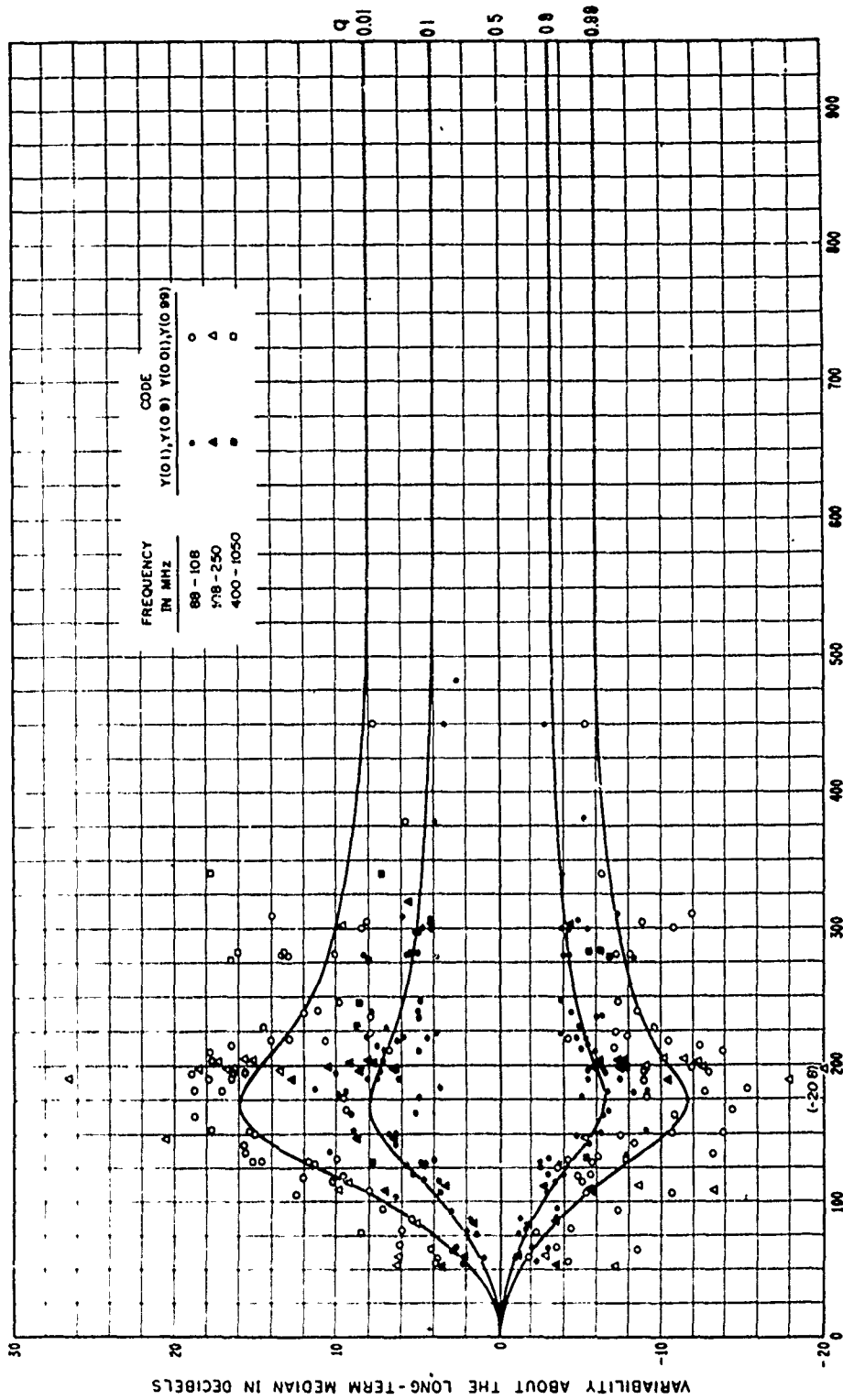


EFFECTIVE DISTANCE, d_e , IN KILOMETERS

Figure III.39

III-69
F-417

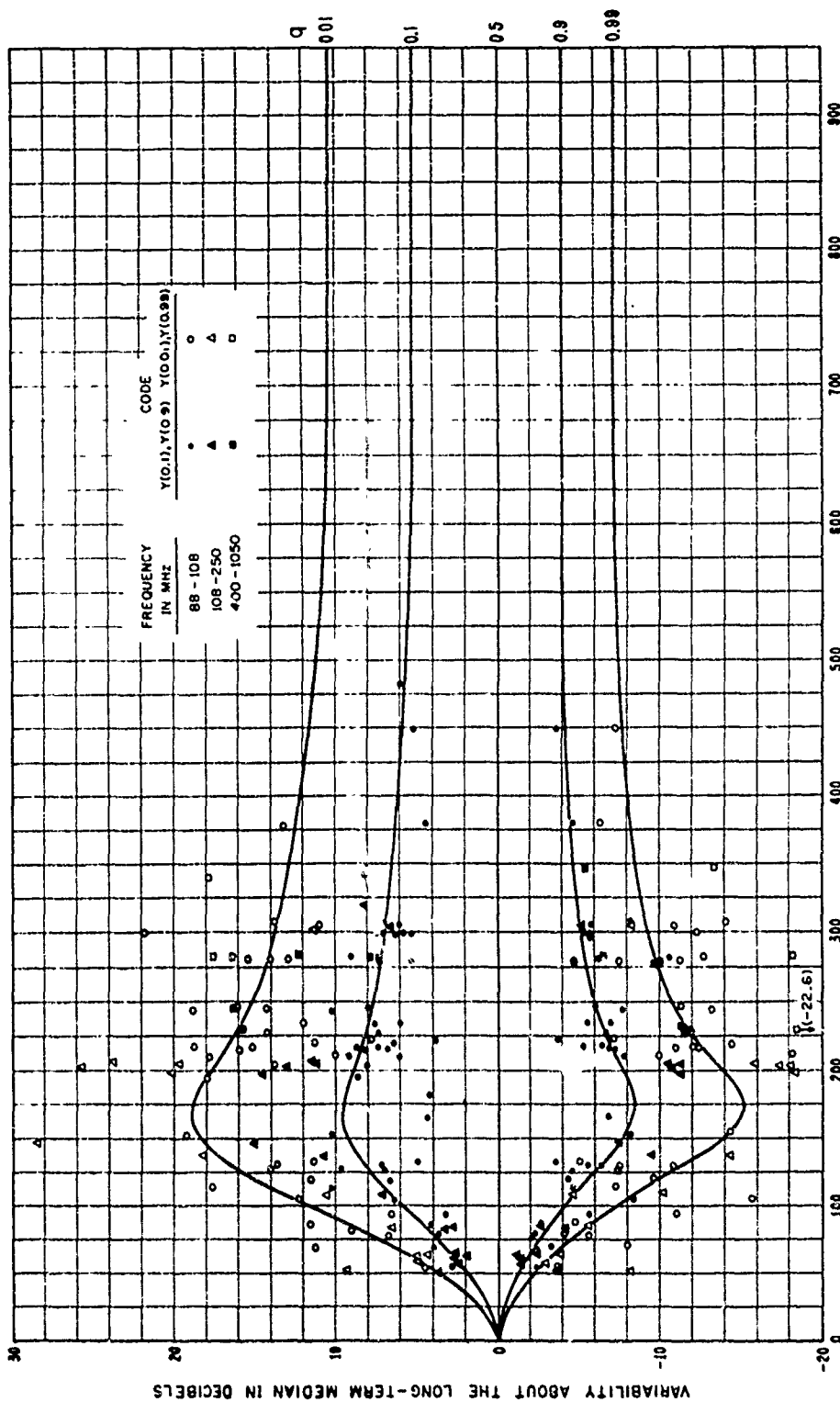
TIME BLOCK 5, MAY - OCT., 1300 - 1800 HRS., U.S.A.
 CURVES SHOW $Y(q, d_e)$ FOR THE FREQUENCY RANGE 88 - 108 MHz



EFFECTIVE DISTANCE, d_e , IN KILOMETERS

Figure III.40

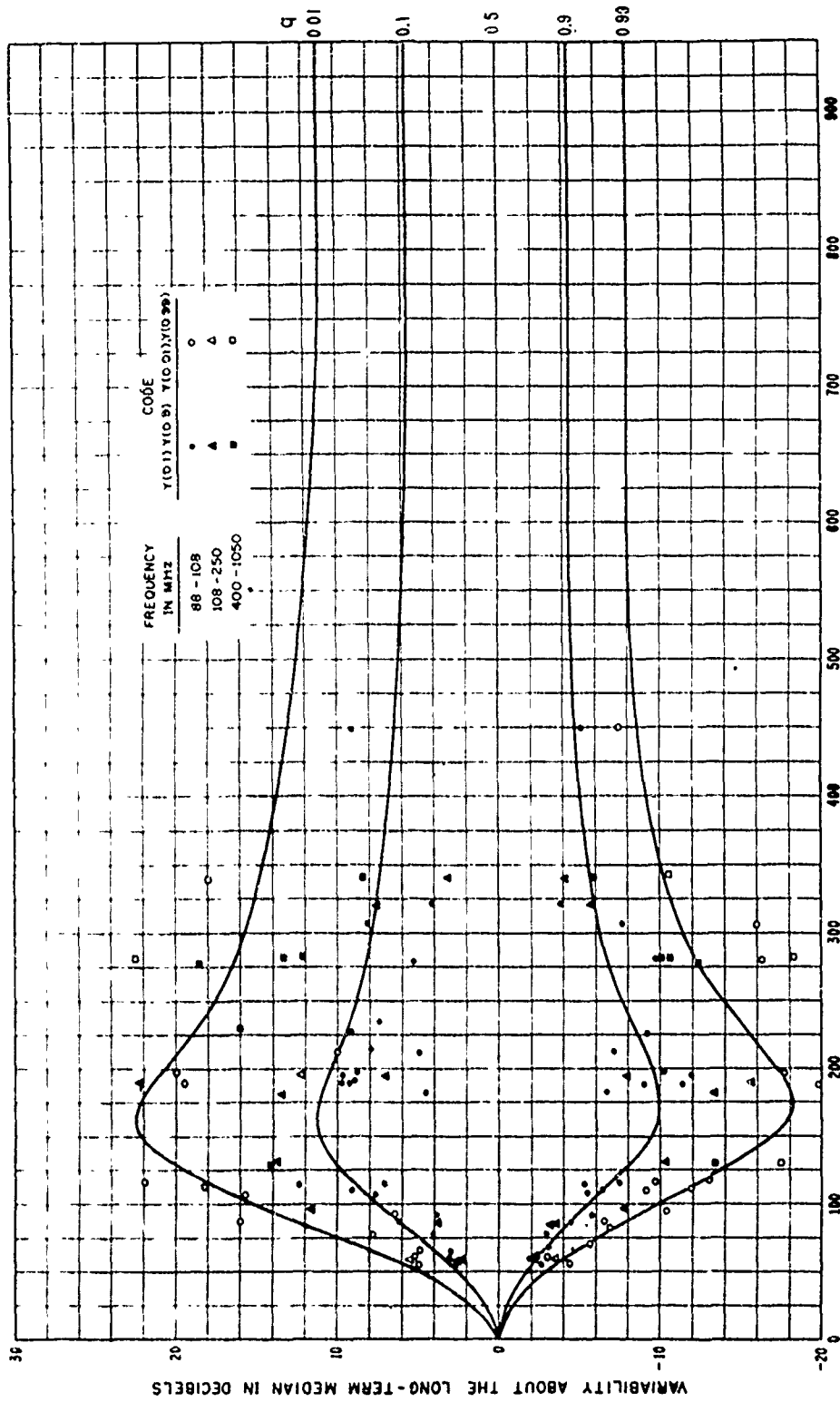
TIME BLOCK 6, MAY - OCT., 1800 - 2400 HRS., U. S. A.
 CURVES SHOW $\gamma(q, d_e)$ FOR THE FREQUENCY RANGE 88 - 108 MHz



EFFECTIVE DISTANCE, d_e , IN KILOMETERS

Figure III.41

TIME BLOCK 7, MAY - OCT., 0000-0600 HRS., U.S.A.
 CURVES SHOW $Y(q, d_e)$ FOR THE FREQUENCY RANGE 88-108 MHz



EFFECTIVE DISTANCE, d_e , IN KILOMETERS

Figure III.42

III.8 List of Special Symbols Used in Annex III

$A(v_j)$	Attenuation relative to free space for each of several rays as a function of the parameter v_j , where $j = 1, 2, 3, 4$, (III. 34).
b	The parameter b , a function of ground constants, carrier frequency, and polarization, expressed in degrees, figure 8.2, and equations (III.40) and (III.41).
b_h	The parameter b for horizontal polarization defined by (III.40).
b_v	The parameter b for vertical polarization, (III.41)
c	A parameter showing the phase change associated with the complex plane wave reflection coefficient $R \exp[-i(\pi-c)]$ corresponding to reflection from an infinite smooth plane surface, (5.4) figures III.1 through III.8.
c_h, c_v	Values of c for horizontal and vertical polarization, respectively, (III.13) and (III.14) figures III.1 through III.8.
C_j	Fresnel integral, (III.33), where $j = 1, 2, 3, 4$.
$Ci(r), Ci(r_1), Ci(r_2)$	Cosine integral as a function of r , (III.51), r_1 and r_2 (III.50).
d_r	Distance used in calculating ground reflections in knife edge diffraction; d_r is defined by (III.29).
$d_{11}, d_{12}, d_{21}, d_{22}$	Distances used in computing diffraction attenuation with ground reflections, (III.31) figure III.9.
f_j	Diffraction loss for each of several distinct rays over an isolated obstacle, where $j = 1, 2, 3, 4$, (III.32-III.35).
f_1, f_2, f_3, f_4	Diffraction loss for each of four distinct rays over an isolated obstacle, (III.32).
$f(r_1), f(r_2)$	Functions of the normalized antenna heights r_1 and r_2 , (III.50).
$f(v_j)$	A function identically equal to f_j for $v = v_j$, (III.33) figure III.10.
$f(\theta_h)$	A factor used to reduce estimates of variability for antenna beams elevated above the horizon plane, (III.65) figure III.22. See θ_h and θ_b
F_{ol}	Scattering efficiency correction term for the i^{th} lobe of an antenna pattern, (III.63).
$F(\theta_{ei}d)$	This function is the same as $F(\theta d)$ with the effective angular distance θ_{ei} substituted for the angular distance, θ , annex III, (III.57).
g_b, g_{bt}	A high gain antenna radiates g_b watts per unit area in every direction not accounted for by the main beam or by one of the side lobes of an antenna. The gain g_b for a transmitting antenna is g_{bt} , section III.6.
$g(f)$	A frequency correction factor shown in figure III.30, (III.66).
G_b, G_{bt}	Decibel equivalent of g_b , $G_b = 10 \log g_b$, and of g_{bt} , annex III section III.6.
G_{ri}, G_{ti}	Gains of the i^{th} lobe of receiving and transmitting antennas, respectively, (III.57).
h_e	A height, using elevated beams, that is equivalent to h_c for horizon rays, (III.63).
h_{rm}, h_{tm}	Height of a knife edge above a reflecting plane on the receiver or transmitter side of the knife edge, (III.37).

$h(r)$	A function of r shown in figures III. 20 and III. 21.
$h(r_1), h(r_2)$	A function of r_1 or r_2 defined by (III. 50) and shown on figures III. 20 and III. 21.
H_{oi}	The frequency gain function for the i^{th} beam intersection in a scattering plane (III. 57).
j	Represents a series of subscripts 1, 2, 3, 4, as used in equations (III. 27) to (III. 35).
K_h	The diffraction parameter K for horizontal polarization, section III. 4.
K_v	The diffraction parameter K for vertical polarization, section III. 4.
L_{gl}	Loss in antenna gain for the i^{th} scattering subvolume, (III. 57).
L_i	Transmission loss associated with the i^{th} power contribution, (III. 55) and (III. 57).
$L_1, L_2, \dots, L_n, \dots, L_N$	A series of hourly median values of transmission loss arranged in order from the smallest to the largest value, section III. 7.
$L(q)$	Transmission loss exceeded a fraction q of the time, (III. 68).
m_h, m_v	Parameters used in computing the magnitudes R_h and R_v of the smooth plane earth reflection coefficient R , (III. 10).
mho.	A unit of conductance, the reciprocal of resistance which is measured in ohms, figures III. 1 to III. 8.
p	A function of the dielectric constant and grazing angle used in computing the plane wave reflection coefficient, (III. 8).
q	A parameter used in calculating a plane wave reflection coefficient, (III. 7) to (III. 14).
$r_{11}, r_{12}, r_{21}, r_{22}$	Distances to and from the bounce point of reflected rays, (III. 28) figure III. 9
R_h	Plane earth reflection coefficient R for horizontal polarization, (III. 12) and figures III. 1 to III. 8.
R_v	Plane earth reflection coefficient R for vertical polarization, (III. 12) figures III. 1 to III. 8.
s_e	Path asymmetry factor for beams elevated above the horizon, $s_e = \alpha_e / \beta_e$, (III. 64).
$Si(r)$	Sine integral as a function of r , (III. 51).
S_j	Fresnel integral, (III. 33).
v_j	The parameter v for each of j paths over an isolated obstacle, (III. 27).
w_{at}	Contribution to the total available power from the i^{th} scattering subvolume, (III. 55) and (IV. 11)
x_a, x_b	Points at which a first Fresnel ellipse cuts the great circle plane, III. 18 to III. 23.
α_e, β_e	The angles between the "bottoms" of transmitting or receiving antenna beams or side lobes and a line joining the antennas, (III. 61).

- α_{ei}, β_{ei} Angles α_e and β_e for the i^{th} lobe of an antenna pattern.
- α_{eo}, β_{eo} When beams are elevated sufficiently that there is no bending of the ray due to atmospheric refraction $\alpha_e = \alpha_{eo}$, $\beta_e = \beta_{eo}$, (III. 60); when ray bending must be considered α_e and β_e are computed using (III. 61).
- α_{oj}, β_{oj} The angles α_o , β_o made by each of j rays, over an isolated obstacle, (III. 36).
- $\alpha_{o1}, \alpha_{o2}, \beta_{o1}, \beta_{o2}$ The angles α_o and β_o for each of four rays over an isolated obstacle, (III. 36).
- δ A parameter used in computing the first Fresnel zone in a reflecting plane, (III. 18).
- δ The effective half-power semi-beamwidth of an antenna, section III. 6.
- δ_e The effective half-power semi-beamwidth of an antenna that is elevated or directed out of the great circle plane, section III. 6.
- δ_o The semi-beamwidth of an equivalent beam pattern with a square cross-section $\delta_o = \delta\sqrt{\pi/4}$, section III. 6.
- $\delta_{rwo}, \delta_{two}$ Azimuthal equivalent semi-beamwidths with square cross-section, (III. 58) figure III. 23.
- $\delta_{rzo}, \delta_{tzo}$ Vertical angle equivalent semi-beamwidths with square cross-section, (III. 58) figure III. 23.
- δ_{wo} Azimuthal equivalent semi-beamwidth with square cross-section, section III. 6.
- δ_{zo} Vertical angle equivalent semi-beamwidth, section III. 6.
- Δ_j The j^{th} value of Δr , where $\Delta r = r_1 + r_2 - r_o$, (III. 27) and (III. 29).
- $\Delta_1, \Delta_2, \Delta_3, \Delta_4$ Ray path differences between a direct ray and a ray path over a single isolated obstacle with ground reflections, (III. 28) figure (III. 9).
- $\Delta_{1r}, \Delta_{2r}, \Delta_{3r}, \Delta_{4r}$ Ray path difference between straight and ground reflected rays on either side of an isolated obstacle, (III. 31), (III. 37).
- ϵ Ratio of the dielectric constant of the earth's surface to the dielectric constant of air, figures 8.1 and 8.2, annex III. 4.
- $\epsilon_{r1}, \epsilon_{t1}$ Angle between the axis of the main beam and the axis of the first side lobe of an antenna pattern, figure III. 22.
- $\epsilon_{tw1}, \epsilon_{tw2}$ Azimuth angles of the first and second lobes of a transmitting antenna relative to the main beam axis, figure III. 23.
- $\epsilon_{tz1}, \epsilon_{tz2}$ Elevation angles of the first and second lobes of a transmitting antenna relative to the main-beam axis, figure III. 23.
- ξ The angle that a scattering plane makes with the great circle plane, (III. 60), (III. 61), and figure III. 22.
- η_{se} A function of h_e and N_s used in computing F_{oi} and H_{oi} for scattering from antenna beams directed above the horizon or away from the great circle plane, (III. 64).
- θ_b Angle of elevation of the lower half power point of an antenna beam above the horizontal, (III. 62). See η_b and $f(\theta_b)$.

- θ_{bt}, θ_{bt} Values of θ_b for the receiving and transmitting antennas, respectively, (III, 61).
 $\theta_{bt1}, \theta_{bt1}$ Values of θ_b for the i^{th} beam intersection, (III, 59).
 θ_e The angle between radio rays elevated above the horizon and/or away from the great circle plane, (III, 64).
 θ_{ei} The angle θ_e at the i^{th} intersection of radio rays elevated above the horizon and/or away from the great circle plane, (III, 57).
 $\theta_{e1}, \theta_{e2}, \dots, \theta_{en}$ The angle θ_e for the first, second, ... n^{th} intersection of radio rays, figure III. 22.
 θ_{hr}, θ_{ht} Angle of elevation of a knife edge relative to the horizontal at the receiving or transmitting antenna, (III, 38).
 θ_j Angle between direct and/or reflected ray over a knife-edge, where $j = 1, 2, 3, 4$ as shown in figure III. 9.
 θ_{jr} Angles defined in (III. 29), where $j = 1, 2, 3, 4$, which are added to θ to determine $\theta_j = \theta + \theta_{jr}$.
 $\theta_{1r}, \theta_{2r}, \theta_{3r}, \theta_{4r}$ Values of θ_{jr} for $j = 1, 2, 3, 4$, (III. 29).
 $\theta_1, \theta_2, \theta_3, \theta_4$ The angle between rays from the transmitting and receiving antennas over an isolated obstacle with ground reflections, figure III. 9.
 σ Surface conductivity in mhos per meter, figures 8.1 and 8.2, section III. 4.
 τ The amount a radio ray bends in the atmosphere, (III. 62).
 $\tau(\theta_b, d, N_s)$ Bending of a radio ray that takes off at an initial angle θ_b and travels d kilometers through an atmosphere characterized by a surface refractivity N_s , (III. 61).
 $\phi(v, 0)$ Component of phase lag due to diffraction over an idealized knife edge, (7.13) figure 7.1, and (III. 30).
 $\phi(v, \rho)$ Component of phase lag due to diffraction over an isolated perfectly-conducting rounded obstacle, (7.13) figure 7.5 and (III. 30).
 $\phi(0, \rho)$ The component of the phase lag of the diffracted field over an isolated perfectly-conducting rounded obstacle for $v = 0$, (7.13) figure 7.4 and (III. 30).
 Φ_j The phase lag of the diffracted field for the j^{th} ray over an isolated perfectly-conducting rounded obstacle (III. 30a), where $j = 1, 2, 3, 4$.
 $\Phi_j(v, \rho)$ The phase lag of the diffracted ray over an isolated rounded obstacle for the j^{th} ray, $\Phi_j(v, \rho) \cong \Phi_j$, (III. 30).
 $\Phi_j(v, 0)$ The phase lag over an ideal knife edge for the j^{th} ray, (III. 30).
 $\Phi_1, \Phi_2, \Phi_3, \Phi_4$ The phase lag $\Phi_j(v, \rho)$ for values of $j = 1, 2, 3, 4$, (III. 32).
 ψ_1, ψ_1 The angle between the plane of the lower half-power point of an antenna beam and the receiver or transmitter horizon plane, (III. 60).
 ψ_r, ψ_t The angle ψ_r or ψ_t for the i^{th} lobe of an antenna pattern, (III. 59).
 ψ_1, ψ_2 Angle of reflection at the ground of a reflected ray that passes over a knife-edge, (III. 36) figure III. 9.

Ω The half-power beamwidth, $\Omega = 26$, (9.10) and figure III.22.

$\Omega_{r0}, \Omega_{r1}, \Omega_{t0}, \Omega_{t1}$ Half-power beamwidths corresponding to $2\theta_0, 2\theta_1$ for the receiving and transmitting antenna patterns, respectively, figure III.22.

Annex IV

FORWARD SCATTER

IV.1 General Discussion

This annex discusses some of the similarities and differences between forward scatter from refractive index turbulence and forward scatter or incoherent reflections from tropospheric layers.

To scatter is to spread at random over a surface or through a space or substance. Scattering which tends to be coherent is more properly called forward scatter, reflection, refraction, focusing, diffraction, or all of these, depending on the circumstances. Modes of scattering as well as mechanisms of propagation bear these names. For example, we may speak of the reflection, refraction, diffraction, focusing, scattering, and absorption of a radio wave by a single spherical hailstone, and all of these modes can be identified in the formal solutions of Maxwell's equations for this problem.

The large volume of beyond-the-horizon radio transmission loss data available in the frequency range 40 to 4000 MHz and corresponding to scattering angles between one and three degrees indicates that the ratio $10^{-A/10}$ corresponding to the transmission loss, A, relative to free space is approximately proportional to the wavelength, λ , or inversely proportional to the radio frequency, f , [Norton, 1960], so that the ratio $10^{-L_b/10}$ corresponding to the forward scatter basic transmission loss is approximately proportional to λ^3 or to f^{-3} . This circumstance is more readily explained in terms of forward scatter from layers [Friis, Crawford, and Hogg, 1957] or in terms of glancing or glinting from brilliant points on randomly disposed "feuillets", [du Castel, Misme, Spizzichino, and Voge, 1962], than in terms of forward scatter from the type of turbulence characterized by the modern Obukhov-Kolmogorov theory [Obukhov, 1941, 1953; Batchelor, 1947, 1953]. There is recent evidence [Norton and Barrows, 1964] that the wavenumber spectrum of refractivity turbulence in a vertical direction has the same form as the more adequately studied spectrum of variations in space in a horizontal direction. Some mechanism other than scatter from refractivity turbulence must be dominant most of the time to explain the observed transmission loss values over a majority of the transhorizon tropospheric paths for which data are available. Scattering from refractivity turbulence and scattering from sharp gradients are mechanisms which coexist at all times in any large scattering volume. Sharp gradients always exist somewhere, and the atmosphere between them is always somewhat turbulent. Power scattered by these mechanisms is occasionally supplemented by diffraction, specular reflection from strong extended layers, and/or ducting.

A tropospheric duct exists, either ground-based or elevated, if a substantial amount of energy is focused toward or defocused away from a receiver as super-refractive gradients of N exceed a critical value called a "ducting gradient." This gradient is about -157 N-units per kilometer at sea level for horizontally launched radio waves. The duct thickness must

exceed about $5062 f^{-3}$ meters with f in MHz [Kerr, 1964] for a duct to completely trap such radio waves. A few useful references in this connection are cited at the end of section 4, Volume 1.

A more or less horizontally homogeneous "kink" in a refractive index profile may indicate the possibility of ducting for very short wavelengths, the presence of a refracting layer for some of the longer waves, and merely a slight and random perturbation of average atmospheric conditions for other frequencies, antenna locations, or antenna beam patterns and elevation angles. The layer that presents a sharp discontinuity for radio frequencies from 30 to 100 MHz ($\lambda = 10$ to 3 meters) may represent a relatively gradual change of refractive index at 300 MHz ($\lambda = 1$ meter) and higher frequencies. A tropospheric layer or "feuillet" requires a sufficiently abrupt change in refractive index, usually associated with fine weather conditions, to reflect a substantial amount of radio energy at the grazing angles and frequencies of interest. These may be horizontal changes, in thermals, for instance, as well as changes of refractivity, N , with height.

Almost specular reflection from tropospheric layers is often observed between 30 MHz and 200 MHz. At higher frequencies, where focusing, defocusing, and ducting are common, and where extensive layers are not sufficiently abrupt or sufficiently numerous to provide strong reflections, a number of small and randomly oriented surfaces come into play. A recent summary of the role of the layer structure of the troposphere in explaining tropospheric propagation [Saxton, Lane, Meadows, and Matthews, 1964] includes an extensive list of references. Also useful are general discussions of tropospheric propagation by Bullington [1955], du Castel [1960], Crawford, Hogg, and Kummer [1959], Fengler [1964], Fengler, Jeske, and Stilke [1964], Kirby, Rice, and Maloney [1961], Johnson [1958], Rice and Herbstreit [1964], Shkarofsky [1958], and Vvedenskii and Arenberg [1957].

There are at least three distinguishing features in most theories of forward scatter from clouds, precipitation, refractive index turbulence, layers, or feuillets. A calculation is first made of the expected or average forward scattering pattern, reradiation pattern, or diffraction pattern of a scatterer or a group of scatterers, usually located in free space, and usually assuming an incident plane wave and a distant receiver. Second, a decision is made that the relative phases of waves scattered from individual raindrops or subvolumes of refractivity turbulence or feuillets are random, so that we may simply add the power contributions from these elements and ignore the phases. This is an essential feature of a random scatter theory. And third, some way is found to relate the actual terrain, atmosphere, and antenna parameters to the theoretical model so that a comparison may be made between data and theory.

IV.2 Models for Forward Scattering

The mechanisms of scattering from refractivity turbulence, reflection from elevated layers, and ducting are much more sensitive to vertical refractivity gradients than to the

horizontal gradients commonly observed. The forward scatter theory used to develop the prediction methods of section 9 assumes that only vertical scales of turbulence or layer thicknesses are important. The radio wave scattered forward by all the scattering sub-volumes visible to both antennas or by all the layers of feuillets visible to both antennas is most affected by a particular range of "eddy sizes", l , or by layers of an average thickness $l/2$. A stack of eddies of size l must satisfy the Bragg condition that reradiation by adjacent eddies shall add in phase. Reflections from the exterior and interior boundaries of a layer will add in phase if the ray traversing the interior of the layer is an odd number of wavelengths longer than the ray reflected from the exterior boundary. Either the mechanism of forward scatter from refractivity turbulence or the mechanism of reflection from layers or feuillets selects a wavenumber direction \hat{k} that satisfies the specular reflection condition corresponding to Snell's law that angles of incidence and reflection, ψ , are equal. Mathematically, these conditions are represented by the following relations:

$$l = \frac{\lambda}{2 \sin(\theta/2)} \cong \frac{\lambda}{\theta}, \quad \hat{k} = \frac{\hat{R}_0 + \hat{R}}{|\hat{R}_0 + \hat{R}|} \quad (\text{IV. 1})$$

where \hat{R}_0 and \hat{R} are unit vectors from the centers of radiation of the transmitting and receiving antenna, respectively, towards an elementary scattering volume, or towards the point of geometrical reflection from a layer. The angle between \hat{R} and \hat{R}_0 is the scattering angle θ illustrated in figure IV-1 and is thus twice the grazing angle ψ for reflection from a layer:

$$\theta = 2\psi = \cos^{-1}(-\hat{R} \cdot \hat{R}_0) \text{ radians.} \quad (\text{IV. 2})$$

The plane wave Fresnel reflection coefficient q_0 for an infinitely extended plane boundary between homogeneous media with refractive indices n_1 and n_2 and for horizontal polarization [Wait, 1962] is

$$q_0 = \frac{\sin \psi - \left[2(n_1 - n_2) + (n_1 - n_2)^2 + \sin^2 \psi \right]}{\sin \psi + \left[2(n_1 - n_2) + (n_1 - n_2)^2 + \sin^2 \psi \right]} \quad (\text{IV. 3})$$

The following approximation, valid for $(n_1 - n_2)^2 < \sin^2 \psi < 1$ is also good for vertical polarization:

$$q_0 \cong \frac{n_2 - n_1}{2\psi^2} \exp \left[- (n_2 - n_1)^2 / (2\psi^2) \right] \cong \frac{n_2 - n_1}{2\psi^2} = \frac{2(n_2 - n_1)}{\theta^2} \quad (\text{IV. 4})$$

A differential amplitude reflection coefficient dq for a tropospheric layer is next defined as proportional to the difference between two gradients of refractive index, m and m_0 , where m is the average refractive index gradient dn/dz across the layer, and m_0 is the average refractive index gradient for the region in which the layer is embedded. Let the layer extend in depth from $z = 0$ to $z = z_0$ in the wavenumber direction \hat{k} defined by (IV. 1), and write the differential reflection coefficient as

$$dq = dz(m - m_0)/(2\psi^2). \quad (\text{IV. 5})$$

A phasor $\exp[-iz(4\pi\psi/\lambda)]$ is associated with dq , and the power reflection coefficient q^2 for a tropospheric layer of thickness z_0 is approximated as

$$q^2 = \left| \int_{z=0}^{z=z_0} dq \exp[-iz(4\pi\psi/\lambda)] \right|^2 = (4\pi)^2 \lambda^2 \psi^{-6} M \quad (\text{IV. 6a})$$

$$M = (m - m_0)^2 [1 - \cos(4\pi\psi z_0/\lambda)] / (4\pi)^4. \quad (\text{IV. 6b})$$

If M is assumed continuous at $z = 0$ and $z = z_0$, somewhat smaller values of q^2 and m will result [Wait, 1962].

Fris, Crawford, and Hogg [1957] point out that the power received by reflection from a finite layer can be approximated as the diffracted power through an absorbing screen with the dimensions of the layer projection normal to the direction of propagation. They then consider layers of large, small, and medium size compared to

$$2x = 2(\lambda R_0 R/d)^{1/2}, \quad d \approx R_0 + R \quad (\text{IV. 7})$$

which is the width of a first Fresnel zone. Let b represent the dimensions of a layer or feuillet in any direction perpendicular to \hat{k} . Since \hat{k} is usually nearly vertical, b is usually a horizontal dimension. Adopting a notation which conforms to that used elsewhere in this report, the available power w_a at a receiver at a distance d from a transmitting antenna radiating w_t watts is

$$w_a = \frac{4w_t \epsilon_t \epsilon_r \lambda^2 q^2}{(4\pi d)^2} [C^2(u) + S^2(u)] [C^2(v) + S^2(v)] \quad (\text{IV. 8})$$

in terms of Fresnel integrals given by (III. 33), where

$$u = b\sqrt{z}/x, \quad v = b\psi\sqrt{z}/x \quad (\text{IV. 9})$$

and g_t and g_r are antenna directive gains. For large u and v ,

$$C^2(u) = S^2(u) = C^2(v) = S^2(v) = 1/4,$$

and for small u and v , $C^2(u) = u^2$, $C^2(v) = v^2$, and $S^2(u) = S^2(v) = 0$.

For large layers, where $b \gg 2x$:

$$w_a = w_t g_t g_r \lambda^4 \psi^{-6} d^{-2} M. \quad (\text{IV. 10a})$$

For intermediate layers, where $b \approx 2x$:

$$w_a = w_t g_t g_r \lambda^3 \psi^{-4} (RR_0 d)^{-1} b^2 M. \quad (\text{IV. 10b})$$

For small layers, where $b \ll 2x$:

$$w_a = w_t g_t g_r \lambda^2 \psi^{-4} (RR_0)^{-2} b^4 M. \quad (\text{IV. 10c})$$

Forward scatter from layers depends on the statistics of sharp refractive index gradients in the directions \hat{k} defined by (IV. 1). The determination of these statistics from radio and meteorological measurements is only gradually becoming practical. A study of likely statistical averages of the meteorological parameters M , $b^2 M$, and $b^4 M$ indicates that these expected values should depend only slightly on the wavelength λ and the grazing angle ψ , as was assumed by Friis, et al. [1957]. The expected value of

$$\{1 - \cos(4\pi \psi z_0 / \lambda)\}$$

can vary only between 0 and 2 and is not likely to be either 0 or 2 for any reasonable assumptions about the statistics of z_0 .

Available long-term median radio transmission loss data usually show the frequency law given by (IV. 10b) for medium-size layers. Long-term cumulative distributions of short-term available power ratios on spaced frequencies rarely show a wavelength law outside the range from λ^2 to λ^4 [Crawford, Hogg, and Kummer, 1959; Norton 1960]. An unreported analysis of 8978 hours of matched simultaneous recordings at 159.5, 599, and 2120 MHz over a 310-km path in Japan shows that this wavelength exponent for transmission loss w_a/w_t is within the range from 2 to 4 ninety-eight percent of the time. This corresponds to a wavelength exponent range from 0 to 2 or a frequency exponent range from 0 to -2 for attenuation relative to free space values, and to corresponding ranges λ^2 to λ^4 or f^{-2} to f^{-4} for values of basic transmission loss, L_b .

Figures IV. 1(a) and IV. 1(b) illustrate forward scattering from a single small layer and from refractivity turbulence in a single small scattering subvolume of the volume V of space visible to two antennas. Figures IV. 1(c) and IV. 1(d) illustrate models for the addition of power contributions from large parallel layers, and from scattering or reflection subvolumes, respectively. Contributions from diffraction or ducting are ignored, as well as returns from well-developed layers for which a geometrical reflection point is not visible to both antennas. Combinations of these mechanisms, though sometimes important, are also not considered here.

For each of the cases shown in figure IV. 1, coherently scattered or reflected power w_{ai} from the neighborhood of a point \vec{R}_{oi} is conveniently associated with a scattering subvolume $d^3R_o = dv = v_i(\vec{R}_{oi})$, so that the total available forward scattered power at a receiver is

$$w_a = \sum_{i=1}^{N_v} w_{ai} = \sum_{i=1}^{N_v} v_i w_{vi} \approx \int_V d^3R_o w_v(\vec{R}_o, \vec{R}) \text{ watts} \quad (\text{IV. 11})$$

where

$$w_{vi} = w_{ai}/v_i = w_v(\vec{R}_o, \vec{R}) \quad (\text{IV. 12})$$

is the available power per unit scattering volume for the i^{th} scattering subvolume, feuillet, or layer, and it is assumed that only N_v such contributions to w_a are important.

Each of the power contributions w_{ai} is governed by the bistatic radar equation. Omitting the subscript i , this equation may be written as

$$w_a = \left(\frac{w_t g_t}{4\pi R_o^2} \right) \left(\frac{a_s c_p}{4\pi R^2} \right) \left(\frac{\lambda^2 g_r}{4\pi} \right) \text{ watts,} \quad (\text{IV. 13})$$

where $a_s c_p$ is the effective scattering cross-section of a single scatterer or group of scatterers, including the polarization efficiency c_p of the power transfer from transmitter to receiver. The first set of parentheses in (IV. 13) represents the field strength in watts per square kilometer at the point \vec{R}_o , the second factor enclosed in parentheses shows what fraction of this field strength is available at the receiver, and $\lambda^2 g_r / (4\pi)$ is the absorbing area of the receiving antenna.

The key to an understanding of scattering from spacecraft, aircraft, rain, hail, snow, refractivity turbulence, or inhomogeneities such as layers or feuillets is the scattering cross-section $a_s c_p$ defined by (IV. 13) or the corresponding scattering cross-section per unit volume a_v , defined from (IV. 12) and (IV. 13) as

$$a_v = (4\pi)^3 (R_o R)^2 w_v / (w_t \epsilon_t \epsilon_x \lambda^2) \text{ per km.} \quad (\text{IV. 14})$$

This quantity is usually estimated by isolating a small volume of scatterers in free space at large vector distances \bar{R}_o and \bar{R} , respectively, from the transmitter and receiver. If both antennas are at the same place, (IV. 13) becomes the monostatic radar equation, corresponding to backscatter instead of to forward scatter.

The scattering cross-sections per unit volume for large, medium, and small layers, assuming a density of N_l layers per unit volume, may be obtained by substituting (IV. 10a) to (IV. 10c) in (IV. 14):

For large layers, where $b \gg 2x$:

$$a_{v1} = x^4 \psi^{-6} M N_l = \lambda^2 \psi^{-6} (R_o R/d)^2 M N_l. \quad (\text{IV. 15})$$

For intermediate layers, where $b \approx 2x$:

$$a_{v2} = x^2 \psi^{-4} b^2 M N_l = \lambda \psi^{-4} (R_o R/d) b^2 M N_l. \quad (\text{IV. 16})$$

For small layers, where $b \ll 2x$:

$$a_{v3} = \psi^{-4} b^2 M N_l = \lambda^0 \psi^{-4} b^2 M N_l. \quad (\text{IV. 17})$$

The modern Obukhov-Kolmogorov theory of homogeneous turbulence in a horizontal direction, when extended to apply to the wavenumber spectrum of instantaneous variations of refractive index in a vertical direction, predicts a $\lambda^{-1/3}$ or $f^{1/3}$ law for the variation with wavelength λ or carrier frequency f of either a_v or attenuation relative to free space, or a $\lambda^{5/3}$ or $f^{-5/3}$ law for variations of the transmission loss w_a/w_t . Theoretical studies of multiple scattering by Beckmann [1961a], Bugnolo [1958], Vysokovskii [1957, 1958], and others suggest that single scattering adequately explains observed phenomena. Descriptions of atmospheric turbulence are given by Batchelor [1947, 1953], de Jager [1952], Heisenberg [1948], Kolmogoroff [1941], Merkulov [1957], Norton [1960], Obukhov [1941, 1953], Rice and Herbstreit [1964], Sutton [1955], Taylor [1922], and Wheelon [1957, 1959].

The observed wavelength exponent for the Japanese transmission loss data previously noted was below 5/3 less than two tenths of one percent of the time, and an examination of other data also leads to the conclusion that forward scatter from Obukhov-Kolmogorov turbulence can rarely explain what is observed with frequencies from 40 to 4000 MHz and scattering angles from one to three degrees.

Early recognition of this fact by Norton, Rice, and Vogler [1955] led to the proposal of a mathematical form for the vertical wavenumber spectrum which would achieve agreement between radio data and the theory of forward scatter from refractivity turbulence [Norton, 1960]. Radio data were used to determine the following empirical form for a_v , upon which the predictions of section 9 are based:

$$a_v = \lambda \psi^{-5} M \quad (\text{IV. 18})$$

$$M = 3 \langle (\Delta n)^2 \rangle / (32 l_0^2) \quad (\text{IV. 19})$$

where

$$\Delta n = n - \langle \Delta n \rangle \quad (\text{IV. 20})$$

is the deviation of refractive index from its expected value $\langle \Delta n \rangle$, and l_0 is a "scale of turbulence" [Rice and Herbstreit, 1964].

Values of the variance $\langle (\Delta n)^2 \rangle$ of refractivity fluctuations and scales of turbulence l_0 obtained from meteorological data lead to good agreement between (IV.18) and radio data when an exponential dependence of M on height is assumed, substituting the corresponding value of w_v in (IV.11). It is not yet clear how the estimates of m , m_0 , z_0 , b , and N_l required by the theory of forward scatter from layers of a given type can be obtained from direct meteorological measurements, nor how these parameters will vary throughout the large volume of space visible to both antennas over a long scatter path. It does seem clear that this needs to be done.

Data from elevated narrow-beam antennas that avoid some of the complex phenomena due to reflection and diffraction by terrain, and which select small scattering volumes, suggest that for scattering angles exceeding ten degrees, reflections from large layers can hardly be dominant over reflection from intermediate and small layers or from refractivity turbulence. Preliminary results indicate that field strengths decrease more slowly at a fixed distance and with scattering angles θ increasing up to fifteen degrees than would be possible with the θ^{-6} dependence of a_v given by (IV.15) added to a probable exponential decay with height of the expected value of the meteorological parameter MN_l for large layers.

The wavelength and angle dependence of forward scatter characterized by the Obukhov-Kolmogorov turbulence theory is nearly the same as that for small layers, given by (IV.17). For scattering from refractivity turbulence:

$$a_{v0} = \lambda^{1/3} \psi^{-11/3} M_0 \quad (\text{IV. 21})$$

$$M_0 = \frac{\Gamma(11/6) \langle (\Delta n)^2 \rangle}{4(2\pi)^{13/3} \Gamma(1/3) l_0^{2/3}} \quad (\text{IV. 22})$$

Although most of the propagation paths which have been studied rarely show this frequency dependence, some occasionally do agree with (IV.21). In general, the radiowave scattering cross-section per unit volume a_v is a weighted average of scattering from all kinds of layers or feuillets and the turbulence between them.

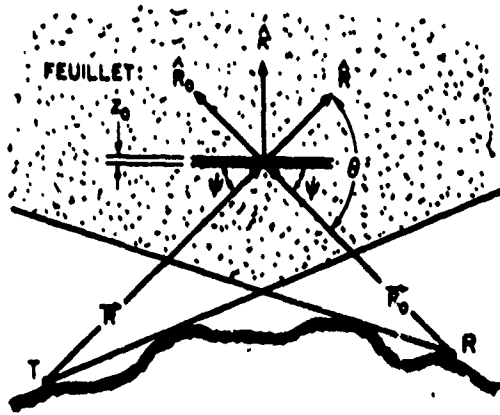
Summarizing the argument:

$$a_v = a_{v0} + a_{v1} + a_{v2} + a_{v3} \approx \lambda \psi^{-5} M \quad (\text{IV.23})$$

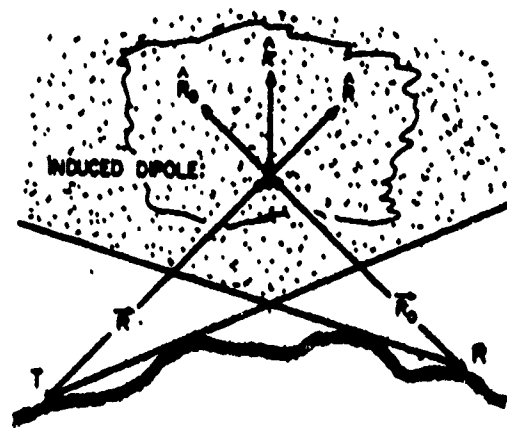
for $10^{-4} < \lambda < 10^{-2}$ km, $0.01 < \psi < 0.03$ radians, where M has been determined from radio data, subject to the assumption that M decreases exponentially with height above the earth's surface. Equation (IV.23) is intended to indicate the present state of the twin arts of formulating theories of tropospheric forward scatter and comparing these theories with available long-term median transmission loss data. A great deal of available data is not forward scatter data, and it is for this reason that estimates of long-term variability as given in section 10 and annex III are almost entirely empirical.

Also, for this reason, estimates of L_{gp} as given in section 9 are restricted to long-term median forward scatter transmission loss. Available measurements of differences in path antenna gain agree within the limits of experimental error with the values predicted by the method of section 9 whenever the dominant propagation mechanism is forward scatter.

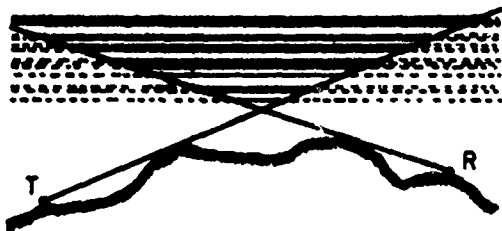
GEOMETRY FOR FORWARD SCATTER



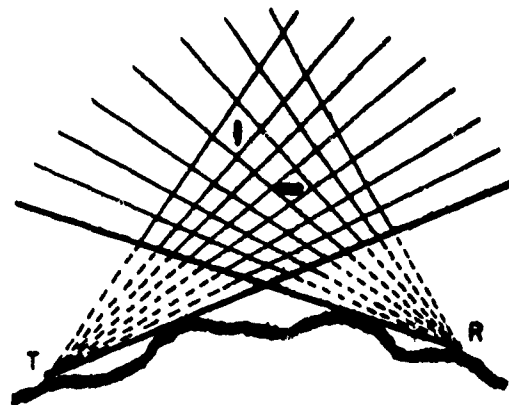
(a)



(b)



(c)



(d)

Figure IX.1

IV. 3 List of Special Symbols Used in Annex IV

a_s	Radiowave scattering cross-section of a single scatterer or group of scatterers, (IV. 13).
a_v	Radiowave scattering cross-section per unit volume, (IV. 14).
a_{v0}	Radiowave scattering cross-section from refractivity turbulence, (IV. 21).
a_{v1}, a_{v2}, a_{v3}	Radiowave scattering cross-sections per unit volume for large, medium, and small layers, (IV. 15) to (IV. 17).
b	The dimensions of an atmospheric layer or feullet in any direction perpendicular to \hat{k} , (IV. 9).
c_p	Polarization efficiency of the power transfer from transmitter to receiver, (IV. 13).
$C(u), C(v)$	Fresnel cosine integrals, (IV. 8).
l	A range of eddy sizes or layers; the radio wave scattered forward is most affected by a particular range of "eddy sizes," l , or by layers of an average thickness $l/2$, that are visible to both antennas, (IV. 1).
l_0	Scale of turbulence, (IV. 19).
m	Average refractive index gradient, dn/dx , across a layer, (IV. 5).
m_0	Average refractive index gradient for the region in which a layer is imbedded, (IV. 5).
M	A term defined by (IV. 6) used in the power reflection coefficient q^2 .
M_0	A term defined by (IV. 22) used in defining a_{v0} , the scattering cross-section from refractivity turbulence.
n_1, n_2	Refractive indices of adjacent layers of homogeneous media, (IV. 3).
N_l	The number of layers per unit volume of a scattering cross-section, (IV. 15) to (IV. 17).
N_v	The number of scattering subvolumes that make an appreciable contribution to the total available power, (IV. 11).
q	The power reflection coefficient, q^2 , for a tropospheric layer is approximated by (IV. 6).
q_0	The plane wave Fresnel reflection coefficient for an infinitely extended plane boundary, (IV. 3).
\bar{R}, \bar{R}_0	Vector distances from transmitter and receiver, respectively, to a point \bar{R}_0 .
\hat{R}, \hat{R}_0	Unit vectors from the centers of radiation of the receiving and transmitting antennas, respectively, (IV. 1).
\bar{R}_{oi}	A point from which power is coherently scattered or reflected, (IV. 11).
$S(u), S(v)$	Fresnel sine integrals, (IV. 8).
u	A parameter defined by (IV. 9).
v	A parameter defined by (IV. 9).
v_i	The i^{th} scattering subvolume, (IV. 11).

CCP 702-1

- w_v Available power per unit scattering volume, (IV. 11).
- w_{vi} Available power per unit scattering volume for the i^{th} scattering subvolume, (IV. 12)
- x Half the width of a first Fresnel zone, (IV. 7).
- z Thickness of a tropospheric layer, (IV. 6).
- z_0 The thickness of a tropospheric layer, (IV. 6).
- Δn The deviation of refractive index from its expected value, (IV. 20).
- $\langle \Delta n \rangle$ The expected value of refractive index, (IV. 20).
- $\langle (\Delta n)^2 \rangle$ The variance of fluctuations in refractive index, (IV. 19).
- \hat{k} A wave number direction defined by (IV. 1).
- ψ The grazing angle for reflection from a layer, (IV. 2).

Annex V

PHASE INTERFERENCE FADING AND SERVICE PROBABILITY

As a general rule, adequate service over a radio path requires protection against noise when propagation conditions are poor, and requires protection against interference from cochannel or adjacent channel signals when propagation conditions are good. Optimum use of the radio spectrum requires systems so designed that the reception of wanted signals is protected to the greatest degree practicable from interference by unwanted radio signals and by noise.

The short-term fading of the instantaneous received power within periods of time ranging from a few minutes up to one hour or more is largely associated with random fluctuations in the relative phasing between component waves. These waves arrive at the receiving antenna after propagation via a multiplicity of propagation paths having electrical lengths that vary from second to second and from minute to minute over a range of a few wavelengths. A small part of this short-term fading and usually all of the long-term variations arise from minute-to-minute changes in the root-sum-square value of the amplitudes of the component waves, i. e., in short-term changes in the mean power available from the receiving antenna. In the analysis of short-term fading, it is convenient to consider the effects of these phase and root-sum-square amplitude changes as being two separate components of the instantaneous fading. Multipath or "phase interference fading" among simultaneously occurring modes of propagation usually determines the statistical character of short-term variability.

Over most transhorizon paths, long-term variability is dominated by "power fading", due to slow changes in average atmospheric refraction, in the intensity of refractive index turbulence, or in the degree of atmospheric stratification. The distinction between phase interference fading and power fading is somewhat arbitrary, but is nevertheless extremely useful. Economic considerations, as contrasted to the requirements for spectrum conservation, indicate that radio receiving systems should be designed so that the minimum practicable transmitter power is required for satisfactory reception of wanted signals in the presence of noise. Fading expected within an hour or other convenient "short" period of time is allowed for by comparing the median wanted signal power w_m available at the receiver with the median wanted signal power w_{mr} which is required for satisfactory reception in the presence of noise. This operating sensitivity w_{mr} assumes a specified type of fading signal and a specified type of noise, but does not allow for other unwanted signals.

In the presence of a specified unwanted signal, but in the absence of other unwanted signals or appreciable noise, the fidelity of information delivered to a receiver output will increase as the ratio r_u of wanted-to-unwanted signal power increases. The degree of fidelity of the received information may be measured in various ways. For example, voice signals are often measured in terms of their intelligibility, television pictures by subjective

observation, and teletype signals by the percentage of correctly interpreted received characters. A specified grade of service provided by a given wanted signal will guarantee a corresponding degree of fidelity of the information delivered to the receiver output. For example, a Grade A teletype service could be defined as one providing 99.99 percent error-free characters, while a Grade B service could be defined as one providing 99.9 percent error-free characters.

The protection ratio r_{ur} required for a given grade of service will depend upon the nature of the wanted and unwanted signals; i.e., their degree of modulation, their location in the spectrum relative to the principal and spurious response bands of the receiving system, and their phase interference fading characteristics. The use of receiving systems having the smallest values of r_{ur} for the kinds of unwanted signals likely to be encountered will permit the same portions of the spectrum to be used simultaneously by the maximum number of users. For instance, FM with feedback achieves a reduction in r_{ur} for a cochannel unwanted signal by occupying a larger portion of the spectrum. But optimum use of the spectrum requires a careful balance between reductions in r_{ur} on the same channel and on adjacent channels, taking account of other system isolation factors such as separation between channels, geographical separation, antenna directivity, and cross-polarization.

Note that the operating sensitivity w_{mr} is a measure of the required magnitude of the median wanted signal power but r_{ur} involves only the ratio of wanted to unwanted signal powers. For optimum use of the spectrum by the maximum number of simultaneous users, the transmitting and receiving systems of the individual links should be designed with the primary objective of ensuring that the various values of r_u exceed r_{ur} for a large percentage of the time during the intended periods of operation. Then sufficiently high transmitter powers should be used so that the median wanted signal power w_m exceeds w_{mr} for a large percentage of the time during the intended period of reception at each receiving location. This approach to frequency assignment problems will be unrealistic in a few cases, such as the cleared channels required for radio astronomy, but these rare exceptions merely serve to test the otherwise general rule [Norton, 1950, 1962 and Norton and Fine 1949] that optimum use of the spectrum can be achieved only when interference from other signals rather than from noise provides the ineluctable limit to satisfactory reception.

This annex discusses the requirements for service of a given grade g , how to estimate the expected time availability q of acceptable service, and, finally, how to calculate the service probability Q for a given time availability.

V.1 Two Components of Fading

Both the wanted and the unwanted signal power available to a receiving system will usually vary from minute to minute in a random or unpredictable fashion. It is convenient to divide the "instantaneous received signal power" $W_r = 10 \log w_r$ into two or three additive components where w_r is defined as the average power for a single cycle of the radio frequency, so as to eliminate the variance of power associated with the time factor $\cos^2(\omega t)$:

$$W_r = W_m + Y_r = W_m(0.5) + Y + Y_r \text{ dbw} \quad (\text{V. 1})$$

W_m is that component of W_r which is not affected by the usually rapid phase interference fading and is most often identified as the short-term median of the available power W_r at the receiving antenna. $W_m(0.5)$ is the median of all such values of W_m , and is most often identified as the long-term median of W_r . In terms of the long-term median transmission loss $L_m(0.5)$ and the total power W_t radiated from the transmitting antenna:

$$W_m(0.5) = W_t - L_m(0.5) \text{ dbw} \quad (\text{V. 2})$$

The characteristics of long-term fading and phase interference fading, respectively, are described in terms of the two fading components Y and Y_r in (V. 1):

$$Y = W_m - W_m(0.5), \quad Y_r = W_r - W_m \quad (\text{V. 3})$$

The long term for which the median power, $W_m(0.5)$, is defined may be as short as one hour or as long as several years but will, in general, consist of the hours within a specified period of time. For most continuously operating services it is convenient to consider $W_m(0.5)$ as the median power over a long period of time, including all hours of the day and all seasons of the year. Observations of long-term variability, summarized in section 10 and in annex III, show that W_m is a very nearly normally distributed random variable characterized by a standard deviation that may range from one decibel within an hour up to ten decibels for periods of the order of several years. These values of standard deviation are representative only of typical beyond-the-horizon propagation paths and vary widely for other propagation conditions.

For periods as short as an hour, the variance of Y_r is generally greater than the variance of W_m . The long-term variability of W_m is identified in section 10 with the variability of hourly medians, expressed in terms of $Y(q)$:

$$Y(q) = W_m(q) - W_m(0.5) = L_m(0.5) - L_m(q) \quad (\text{V. 4})$$

where $W_m(q)$ is the hourly median signal power exceeded for a fraction q of all hours, and $L_m(q)$ is the corresponding transmission loss not exceeded for a fraction q of all hours.

CCP 702-1

Often, data for a path are available in terms of the long-term cumulative distribution of instantaneous power, W_{π} ; that is, we know $W_{\pi}(q)$ versus q , but not $W_m(q)$ versus q . An approximation to the cumulative distribution function $L_o(q)$ versus q is given by

$$L_o(q) \approx L_m(0.5) \pm [Y^2(q) + Y_{\pi}^2(q)]^{\frac{1}{2}} \quad (V.5)$$

The plus sign in (V.5) is used for $q > 50$ percent, and the minus sign for $q < 50$ percent.

CCIR 702-1

V. For studies of the operating sensitivity w_m of a receiver in the presence of a rapidly fading wanted signal, and for studies of the median wanted signal to noise ratio $R_{ur}(g)$ required for a grade g service, it is helpful to consider a particular statistical model which may be used to describe phase interference fading. Minoru Nakagami [1940] describes a model which depends upon the addition of a constant signal and a Rayleigh distributed random signal [Rayleigh 1880; Rice, 1945; Norton, Vogler, Mansfield and Short, 1955; Beckmann, 1961a, 1964]. In this model, the root-sum-square value of the amplitudes of the Rayleigh components is K decibels relative to the amplitude of the constant component. $K = +\infty$ corresponds to a constant received signal. For a Rayleigh distribution, $K = -\infty$ and the probability q that the instantaneous power, w_π , will exceed $w_\pi(q)$ for a given value of the short-term median power, w_m , may be expressed:

$$q[w_\pi > w_\pi(q) | w_m] = \exp\left[-\frac{w_\pi(q) \log_e 2}{w_m}\right], [K = -\infty] \quad (V.6a)$$

Alternatively, the above may be expressed in the following forms:

$$q[Y_\pi > Y_\pi(q)] = \exp[-y_\pi(q) \log_e 2], [K = -\infty] \quad (V.6b)$$

$$Y_\pi(q) = 5.21390 + 10 \log(\log(1/q)), [K = -\infty] \quad (V.6c)$$

Figures V.1-V.3 and table V.1 show how the Nakagami-Rice phase interference fading distribution $Y_\pi(q)$ depends on q , K , and the average \bar{Y}_π and standard deviation σ_{Y_π} of Y_π . It is evident from figure V.1 that the distribution of phase interference fading depends only on K . The utility of this distribution for describing phase interference fading in ionospheric propagation is discussed in CCIR report [1963k] and for tropospheric propagation is demonstrated in papers by Norton, Rice and Vogler [1955], Janes and Wells [1955], and Norton, Rice, Janes and Barsis [1955]. Bremmer [1959] and Beckmann [1961a] discuss a somewhat more general fading model.

For within-the-horizon tropospheric paths, including either short point-to-point terrestrial paths or paths from an earth station to a satellite, K will tend to have a large positive value throughout the day for all seasons of the year. As the length of the terrestrial propagation path is increased, or the elevation angle of a satellite is decreased, so that the path has less than first Fresnel zone clearance, the expected values of K will decrease until, for some hours of the day, K will be less than zero and the phase interference fading for signals propagated over the path at these times will tend to be closely represented

by a Rayleigh distribution. For most beyond-the-horizon paths K will be less than zero most of the time. For knife-edge diffraction paths K is often much greater than zero. When signals arrive at the receiving antenna via ducts or elevated layers, the values of K may be values much greater than zero even for transhorizon propagation paths. For a given beyond-the-horizon path, K will tend to be positively correlated with the median power level W_m ; i.e., large values of K are expected with large values of W_m . For some within-the-horizon paths, K and W_m tend to be negatively correlated.

It is assumed that a particular value of K may be associated with any time availability q , however, few data analyses of this kind are presently available. A program of data analysis is clearly desirable to provide empirical estimates of K versus q for particular climates, seasons, times of day, lengths of recording, frequencies, and propagation path characteristics. It should be noted that K versus q expresses an assumed functional relationship.

An analysis of data for a single day's recording at 1046 MHz over a 364-kilometer path is presented here to illustrate how a relationship between K and q may be established. Figure V.4 shows for a single day the observed interdecile range $W_\pi(0.1) - W_\pi(0.9)$ $L_\pi(0.9) - L_\pi(0.1)$ for each five-minute period plotted against the median transmission loss L_m for the five-minute period. Figure V.1 associates a value of K with each value of $L_\pi(0.9) - L_\pi(0.1)$, and the cumulative distribution of L_m associates a time availability q with each value of L_m . In figure V.4, K appears to increase with increasing L_m for the hours 0000 - 1700, although the usual tendency over long periods is for K to decrease with L_m . The straight line in the figure is drawn through medians for the periods 0000 - 1700 and 1700 - 2400 hours, with linear scales for K and L_m , as shown by the inset for figure V.4. The corresponding curve of K versus q is compared with the data in the main figure.

Figure V.5 shows for $f = 2$ GHz and 30-meter antenna heights over a smooth earth a possible estimate of K versus distance and time availability. These crude and quite speculative estimates are given here only to provide the example in the lower part of figure V.5 which shows how such information with (V.6) may be used to obtain curves of $L_\pi(q)$ versus q . The solid curves in the lower part of figure V.5 show how $L_\pi(q)$ varies with distance for $q = 0.0001, 0.01, 0.5, 0.99$ and 0.9999 , where L_π is the transmission loss associated with the instantaneous power, W_π .

by a Rayleigh distribution. For most beyond-the-horizon paths K will be less than zero most of the time. For knife-edge diffraction paths K is often much greater than zero. When signals arrive at the receiving antenna via ducts or elevated layers, the values of K may be values much greater than zero even for transhorizon propagation paths. For a given beyond-the-horizon path, K will tend to be positively correlated with the median power level W_m ; i.e., large values of K are expected with large values of W_m . For some within-the-horizon paths, K and W_m tend to be negatively correlated.

It is assumed that a particular value of K may be associated with any time availability q , however, few data analyses of this kind are presently available. A program of data analysis is clearly desirable to provide empirical estimates of K versus q for particular climates, seasons, times of day, lengths of recording, frequencies, and propagation path characteristics. It should be noted that K versus q expresses an assumed functional relationship.

An analysis of data for a single day's recording at 1046 MHz over a 364-kilometer path is presented here to illustrate how a relationship between K and q may be established. Figure V.4 shows for a single day the observed interdecile range $W_{\pi}(0.1) - W_{\pi}(0.9)$ $L_{\pi}(0.9) - L_{\pi}(0.1)$ for each five-minute period plotted against the median transmission loss L_m for the five-minute period. Figure V.1 associates a value of K with each value of $L_{\pi}(0.9) - L_{\pi}(0.1)$, and the cumulative distribution of L_m associates a time availability q with each value of L_m . In figure V.4, K appears to increase with increasing L_m for the hours 0000 - 1700, although the usual tendency over long periods is for K to decrease with L_m . The straight line in the figure is drawn through medians for the periods 0000 - 1700 and 1700 - 2400 hours, with linear scales for K and L_m , as shown by the inset for figure V.4. The corresponding curve of K versus q is compared with the data in the main figure

Figure V.5 shows for $f = 2$ GHz and 30-meter antenna heights over a smooth earth a possible estimate of K versus distance and time availability. These crude and quite speculative estimates are given here only to provide the example in the lower part of figure V.5 which shows how such information with (V.6) may be used to obtain curves of $L_{\pi}(q)$ versus q . The solid curves in the lower part of figure V.5 show how $L_{\pi}(q)$ varies with distance for $q = 0.0001, 0.01, 0.5, 0.99$ and 0.9999 , where L_{π} is the transmission loss associated with the instantaneous power, W_{π} .

Table V.1 Characteristics of the Nakagami-Rice
Phase Interference Fading Distribution $Y_r(q)$
 $Y_r > Y_r(q)$ with Probability q ; $Y_r(0.5) = 0$

K	\bar{Y}_r db	ϵ_{Y_r} db	$Y_r(0.005)$	$Y_r(0.01)$	$Y_r(0.02)$	$Y_r(0.05)$	$Y_r(0.1)$	$Y_r(0.9)$	$Y_r(0.95)$	$Y_r(0.98)$	$Y_r(0.99)$	$Y_r(0.995)$	$Y_r(0.1) - Y_r(0.9)$ db
			db	db	db	db	db	db	db	db	db	db	db
40	-0.0002	0.061	0.1568	0.1417	0.1252	0.1004	0.0784	-0.0790	-0.1016	-0.1270	-0.1440	-0.1596	0.1574
35	-0.0007	0.109	0.2768	0.2504	0.2214	0.1778	0.1352	-0.1411	-0.1815	-0.2272	-0.2579	-0.2946	0.2763
30	-0.0022	0.194	0.4862	0.4403	0.3898	0.3136	0.2453	-0.2525	-0.3254	-0.4082	-0.4638	-0.5151	0.4978
25	-0.0069	0.346	0.8460	0.7676	0.6811	0.5496	0.4312	-0.4538	-0.5868	-0.7391	-0.8421	-0.9376	0.8850
20	-0.0217	0.616	1.4486	1.3184	1.1738	0.9524	0.7508	-0.8218	-1.0696	-1.3572	-1.5544	-1.7389	1.5726
18	-0.0343	0.776	1.7840	1.6264	1.4508	1.1846	0.9332	-1.0453	-1.3660	-1.7416	-2.0014	-2.2461	1.9785
16	-0.0543	0.980	2.1856	1.9963	1.7847	1.4573	1.1558	-1.3326	-1.7506	-2.2463	-2.5931	-2.9231	2.4884
14	-0.0859	1.238	2.6605	2.4355	2.1829	1.7896	1.4247	-1.7028	-2.2526	-2.9156	-3.3872	-3.8422	3.1275
12	-0.136	1.569	3.2136	2.9491	2.6507	2.1831	1.7455	-2.1808	-2.9119	-3.8143	-4.4715	-5.1186	3.9263
10	-0.214	1.999	3.8453	3.5384	3.1902	2.6408	2.1218	-2.7975	-3.7820	-5.0372	-5.9833	-6.9452	4.9193
8	-0.334	2.565	4.5493	4.1980	3.7975	3.1602	2.5528	-3.5861	-4.9287	-6.7171	-8.1418	-9.6386	6.1389
6	-0.507	3.279	5.3093	4.9132	4.4591	3.7313	3.0307	-4.5714	-6.4059	-8.9732	-11.0972	-13.4194	7.6021
4	-0.706	4.036	6.0955	5.6559	5.1494	4.3315	3.5366	-5.7101	-8.1216	-11.5185	-14.2546	-17.1017	9.2467
2	-0.866	4.667	6.8613	6.3811	5.8252	4.9219	4.0366	-6.7874	-9.6278	-13.4690	-16.4258	-19.4073	10.8240
0	-0.941	5.094	7.5411	7.0246	6.4248	5.4449	4.4782	-7.5267	-10.5553	-14.5401	-17.5512	-20.5618	12.0049
-2	-0.953	5.340	8.0697	7.5228	6.8861	5.8423	4.8088	-8.0074	-11.0005	-15.0271	-18.0527	-21.0706	12.8162
-4	-0.942	5.465	8.4231	7.8525	7.1873	6.0956	5.0137	-8.0732	-11.1876	-15.2273	-18.2573	-21.2774	13.0869
-6	-0.929	5.525	8.6309	8.0435	7.3588	6.2354	5.1233	-8.1386	-11.2606	-15.3046	-18.3361	-21.3565	13.2619
-8	-0.922	5.551	8.7394	8.1417	7.4451	6.3034	5.1749	-8.1646	-11.2893	-15.3349	-18.3669	-21.3880	13.3396
-10	-0.918	5.562	8.7918	8.1881	7.4857	6.3341	5.1976	-8.1753	-11.3005	-15.3466	-18.3788	-21.4000	13.3729
-12	-0.916	5.567	8.8155	8.2090	7.5031	6.3474	5.2071	-8.1792	-11.3048	-15.3512	-18.3834	-21.4046	13.3863
-14	-0.916	5.569	8.8258	8.2179	7.5106	6.3531	5.2112	-8.1804	-11.3065	-15.3529	-18.3852	-21.4064	13.3916
-16	-0.915	5.570	8.8301	8.2216	7.5136	6.3552	5.2128	-8.1811	-11.3072	-15.3537	-18.3860	-21.4072	13.3929
-18	-0.915	5.570	8.8319	8.2232	7.5149	6.3561	5.2135	-8.1813	-11.3075	-15.3540	-18.3863	-21.4075	13.3948
-20	-0.915	5.570	8.8326	8.2238	7.5154	6.3565	5.2137	-8.1814	-11.3076	-15.3541	-18.3864	-21.4076	13.3951
-∞	-0.915	5.570	8.8331	8.2242	7.5158	6.3567	5.2139	-8.1815	-11.3077	-15.3542	-18.3865	-21.4077	13.3954

THE NAKAGAMI-RICE PROBABILITY DISTRIBUTION OF THE INSTANTANEOUS FADING
ASSOCIATED WITH PHASE INTERFERENCE

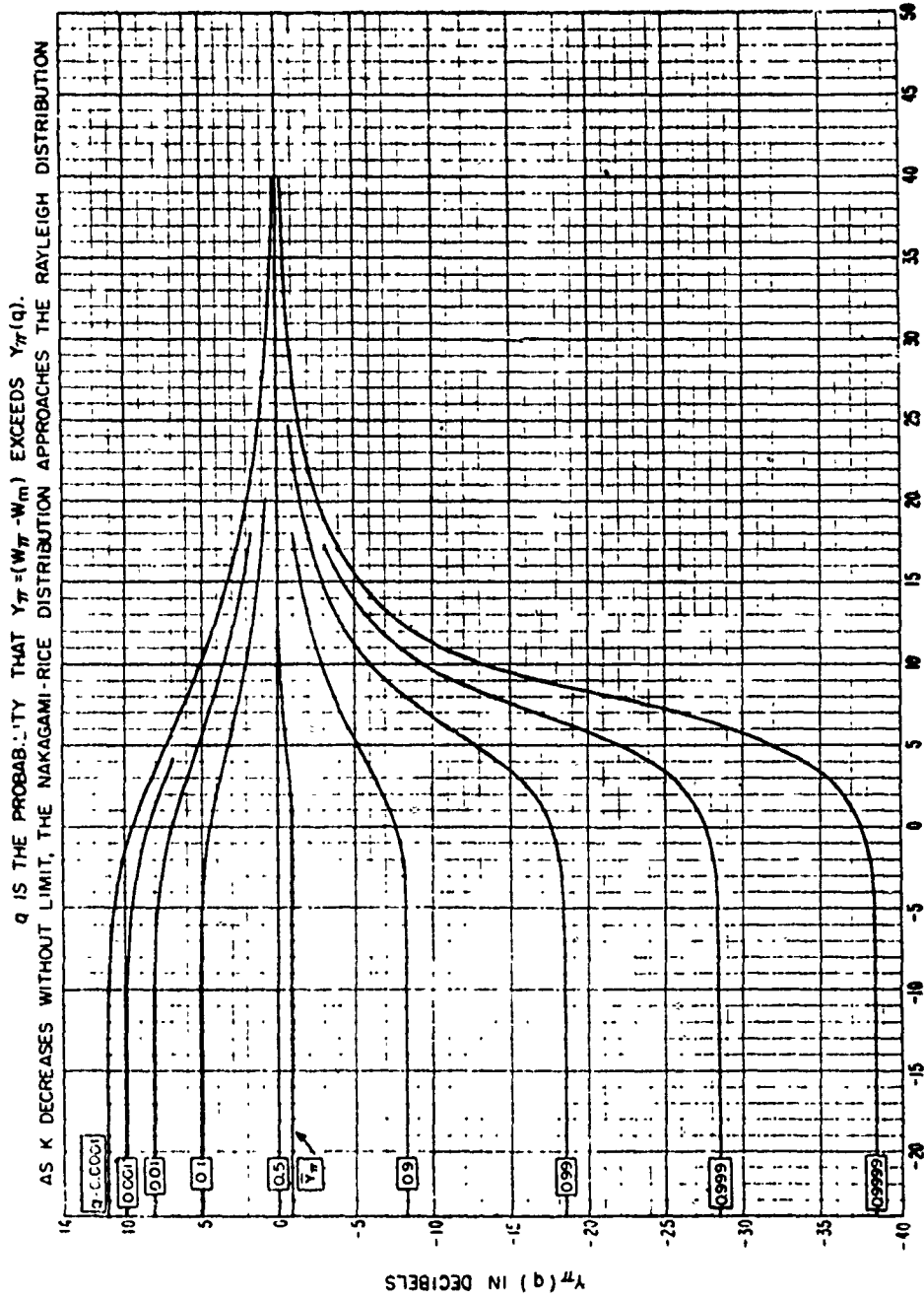
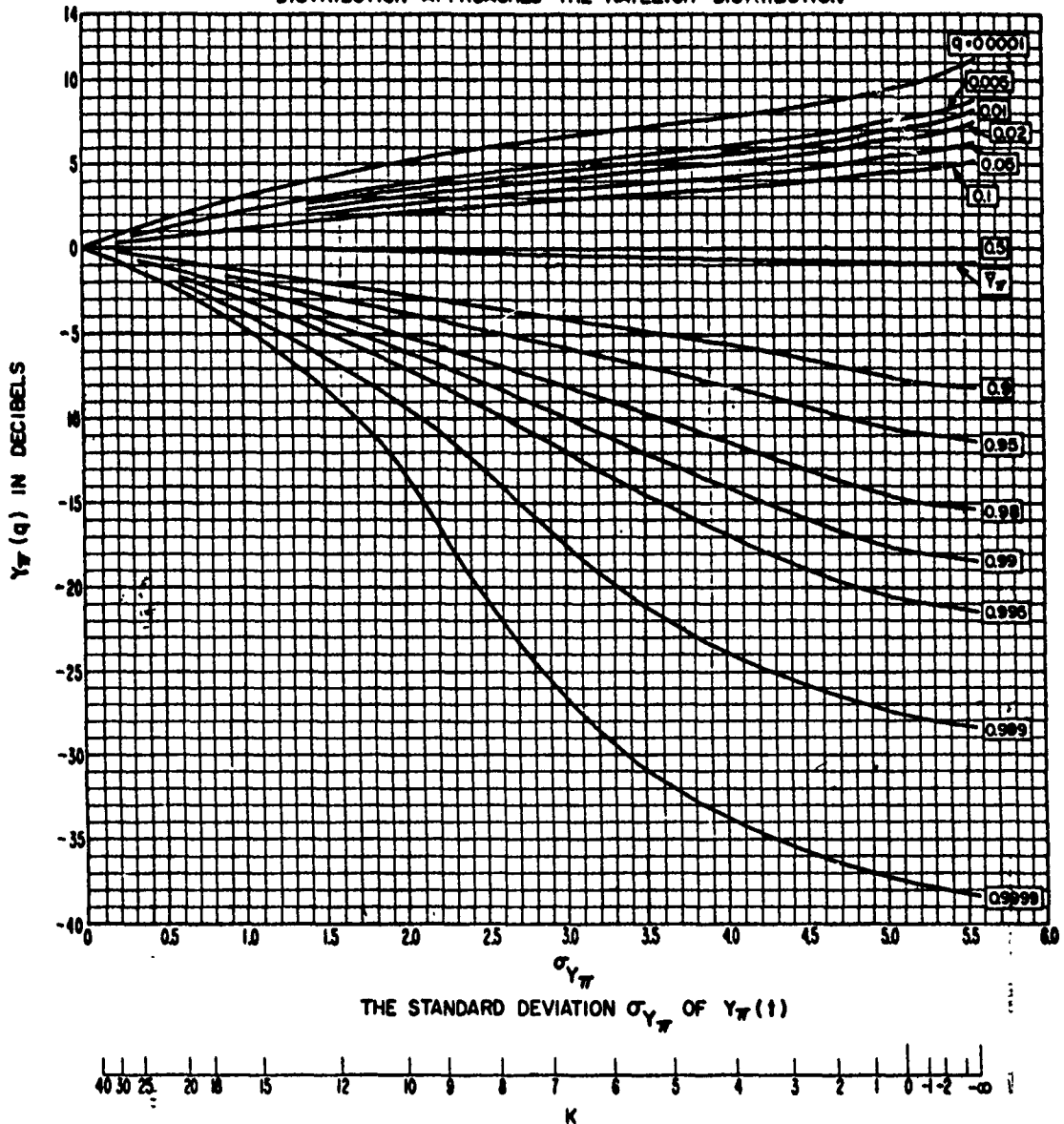


Figure 1

THE NAKAGAMI-RICE PROBABILITY DISTRIBUTION OF THE INSTANTANEOUS FADING ASSOCIATED WITH PHASE INTERFERENCE

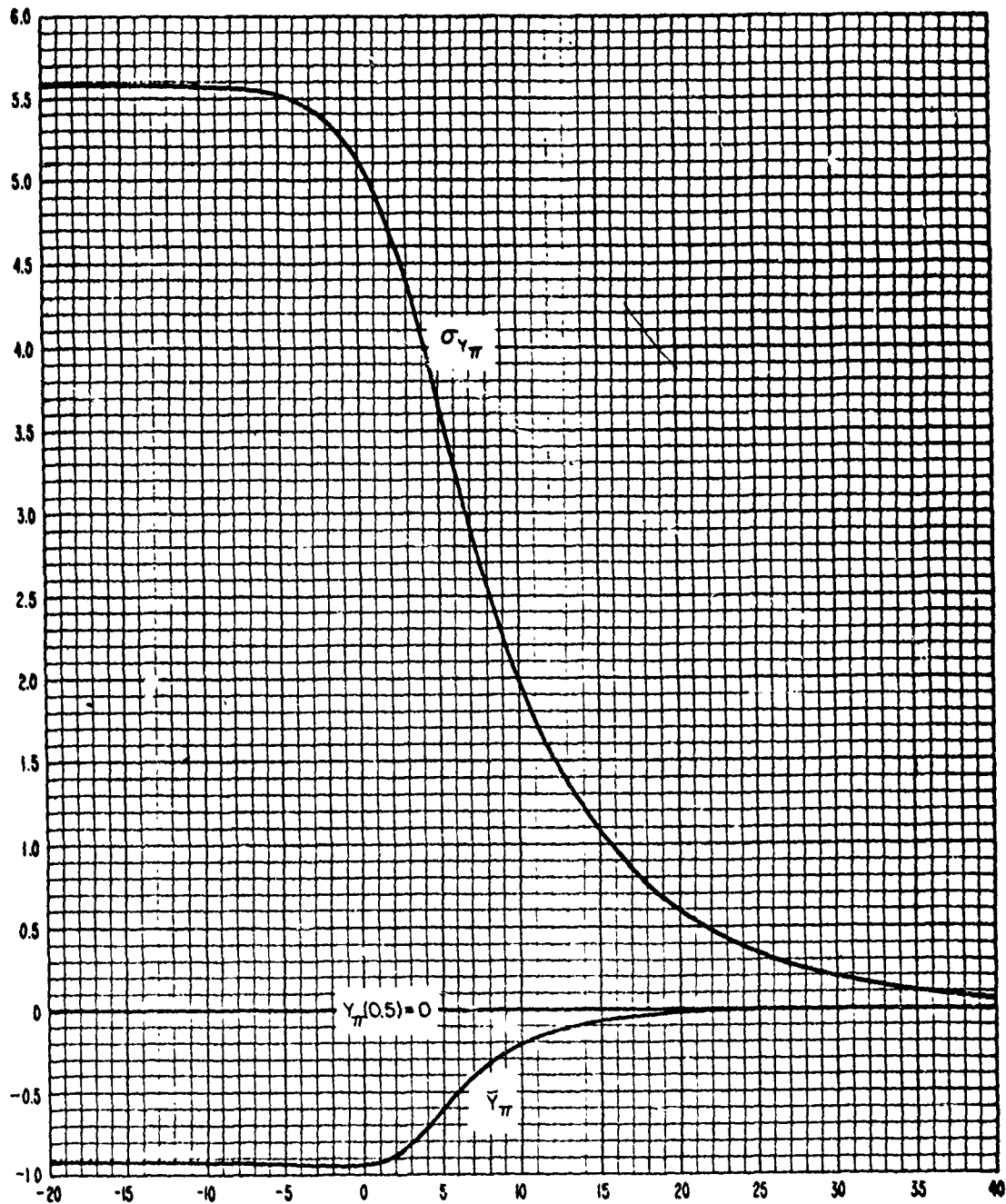
q IS THE PROBABILITY THAT $Y_{\pi} = (W_{\pi} - W_m)$ EXCEEDS $Y_{\pi}(q)$.
 AS K DECREASES WITHOUT LIMIT, THE NAKAGAMI-RICE DISTRIBUTION APPROACHES THE RAYLEIGH DISTRIBUTION



K=RATIO IN DECIBELS BETWEEN THE STEADY COMPONENT OF THE RECEIVED POWER AND THE RAYLEIGH FADING COMPONENT

Figure X.2

STANDARD DEVIATION $\sigma_{Y_{\pi}}$ AND MEAN \bar{Y}_{π} FOR
THE NAKAGAMI-RICE PHASE INTERFERENCE DISTRIBUTION



K=RATIO IN DECIBELS BETWEEN THE STEADY COMPONENT OF
THE RECEIVED POWER AND THE RAYLEIGH FADING COMPONENT

Figure 5.3

CHEYENNE MOUNTAIN, COLORADO TO GARDEN CITY, KANSAS
24 FEBRUARY 1953
1046 MHz d = 364.5 km

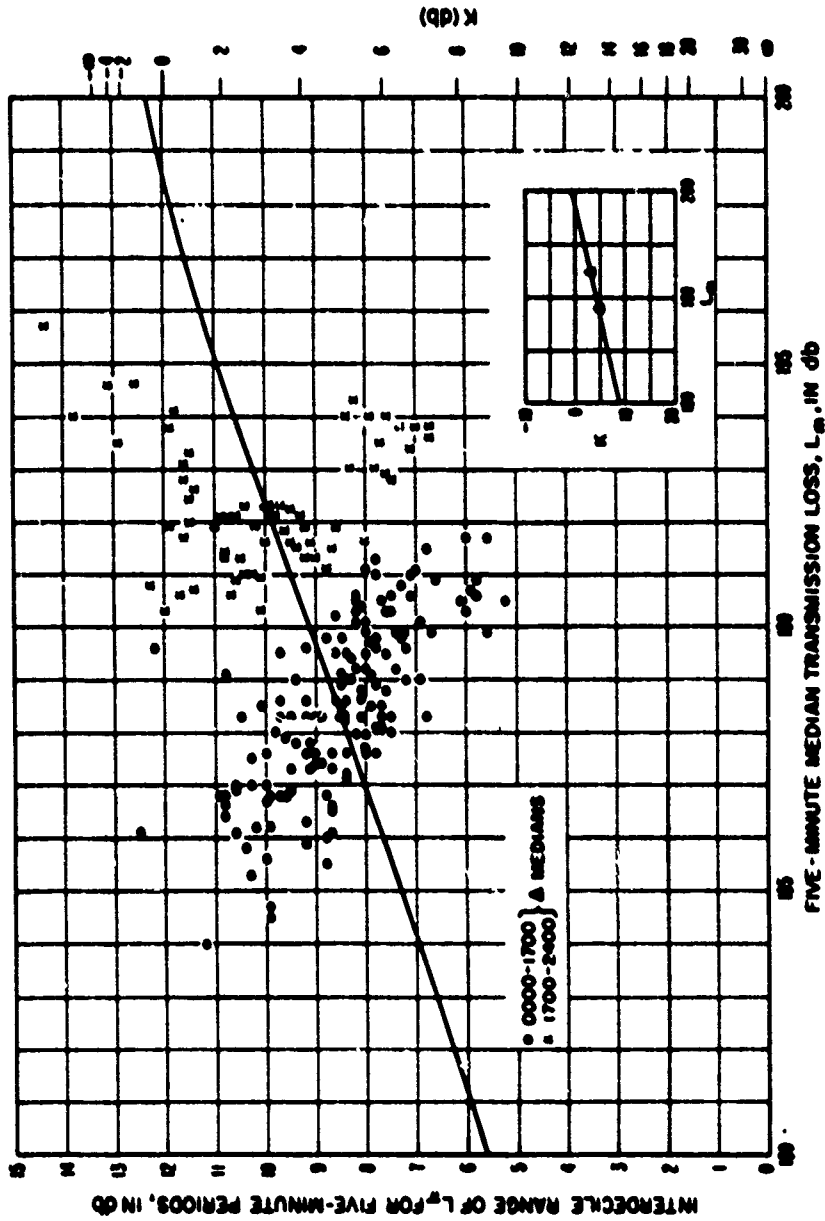
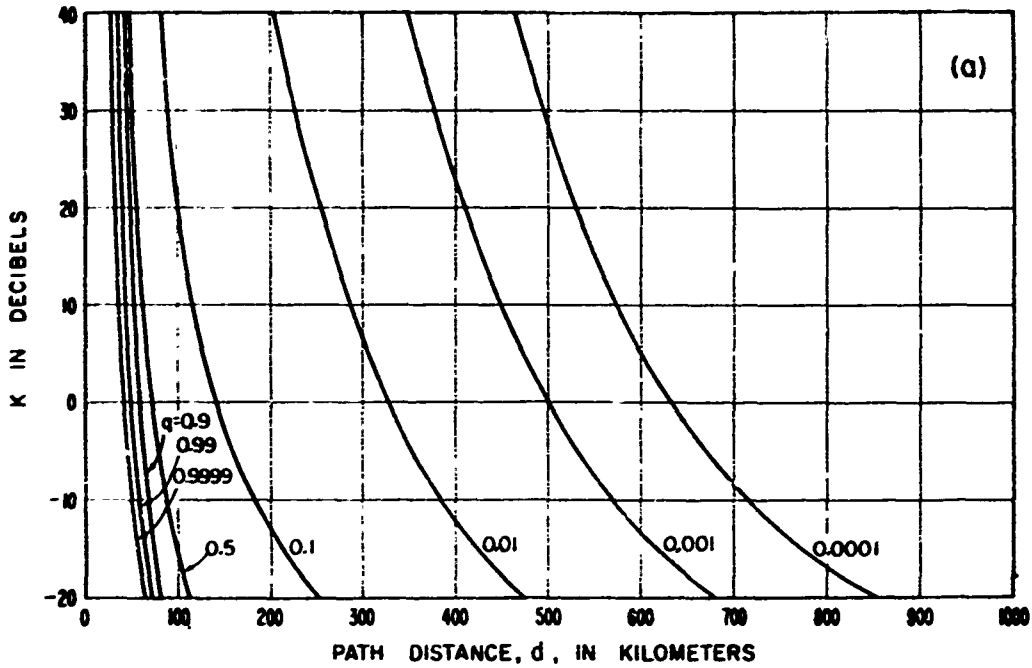


Figure 3.4

TENTATIVE ESTIMATE OF K VERSUS q AND d



CUMULATIVE DISTRIBUTIONS OF INSTANTANEOUS TRANSMISSION LOSS
 FREQUENCY = 2 MHz, $h_{te} = h_{re} = 30$ METERS

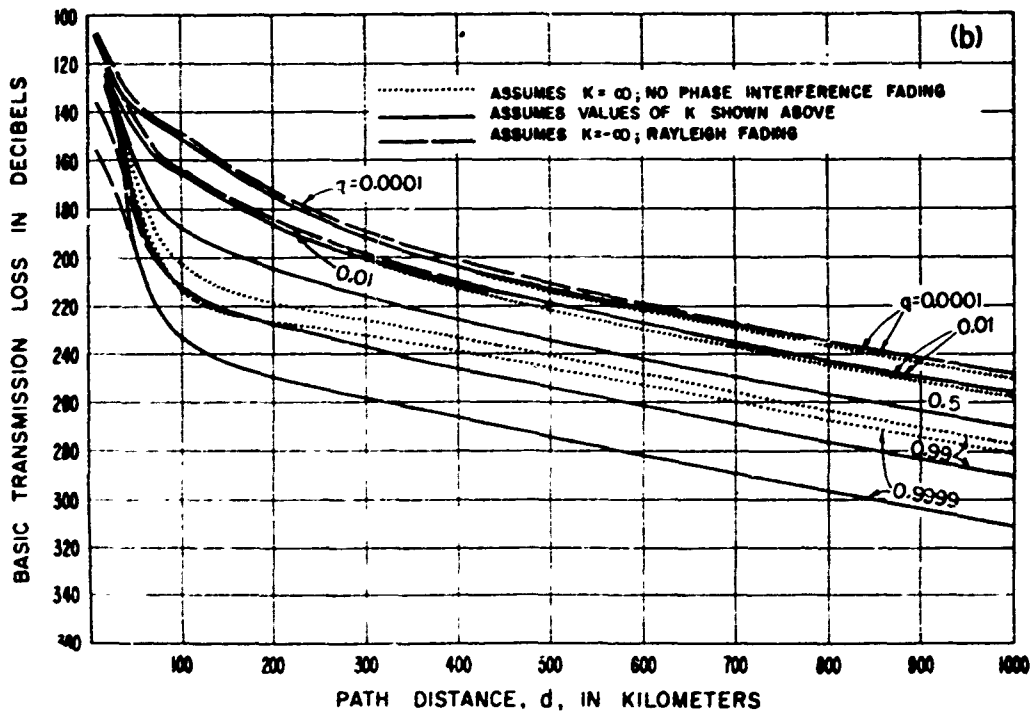


Figure X.5

V.3 Noise-Limited Service

A detailed discussion of the effective noise bandwidth, the operating noise factor, and the operating sensitivity of a receiving system is presented in a recent report, "Optimum Use of the Radio Frequency Spectrum," prepared under Resolution 1 of the CCIR [Geneva, 1963c].

The median value of the total noise power w_{mn} watts in a bandwidth b cycles per second at the output load of the linear portion of a receiving system includes external noise accepted by the antenna as well as noise generated within the receiving system, including both principal and spurious responses of the antenna and transmission line as well as the receiver itself. This total noise power delivered to the pre-detection receiver output may be referred to the terminals of an equivalent loss-free antenna (as if there were only external noise sources) by dividing w_{mn} by g_o , the maximum value of the operating gain of the pre-detection receiving system.

The operating noise factor of the pre-detection receiving system, f_{op} , may be expressed as the ratio of the "equivalent available noise power" w_{mn}/g_o to the Johnson noise power $kT_o b$ that would be available in the band b from a resistance at a reference absolute temperature $T_o = 288.37$ degrees Kelvin, where $k = 1.38054 \times 10^{-23}$ joules per degree is Boltzmann's constant:

$$f_{op} = \frac{w_{mn}/g_o}{k T_o b} \quad (V.7)$$

or in decibels:

$$F_{op} = (W_{mn} - G_o) - (B - 204) \text{ db} . \quad (V.8)$$

The constant 204 in (V.8) is $-10 \log (k T_o)$.

Note that the available power from the antenna as defined in annex II has the desired property of being independent of the receiver input load impedance, making this concept especially useful for the definition and measurement of the operating noise factor f_{op} as defined under CCIR Resolution 1 [Geneva, 1963c].

At frequencies above 100 MHz, where receiver noise rather than external noise usually limits reception, f_{op} is essentially independent of external noise. In general, f_{op} is proportional to the total noise w_{mn} delivered to the pre-detection receiver output and so measures the degree to which the entire system, including the antenna, is able to discriminate against both external noise and receiver noise.

Let W_m represent the median available wanted signal power associated with phase interference fading at the terminals of an equivalent loss-free receiving antenna, and let the "operating threshold" $W_{mr}(g)$ represent the minimum value of W_m which will provide a grade g service in the presence of noise alone. The operating threshold W_{mr} assumes a specified type of wanted signal and a specified type of noise, but does not allow for other unwanted signals. Compared to the total range of their long-term variability, it is assumed that W_m and $W_{mr}(g)$ are hourly median values; i. e., that long-term power fading is negligible over such a short period of time. Let G_{ms} represent the hourly median operating signal gain of a pre-detection receiving system, expressed in db so that $W_m + G_{ms}$ very closely approximates the hourly median value of that component of available wanted signal power delivered to the pre-detection receiver output and associated with phase interference fading. The median wanted signal to median noise ratio available at the pre-detection receiver output is then

$$R_m = [W_m + G_{ms}] - W_{mn} \text{ db} \quad (\text{V. 9a})$$

and the minimum value of R_m which will provide a desired grade of service in the presence of noise alone is

$$R_{mr}(g) = [W_{mr}(g) + G_{ms}] - W_{mn} \text{ db.} \quad (\text{V. 9b})$$

V.4 Interference-Limited Service

Separation of the total fading into a phase interference component Y_{π} and the more slowly varying component Y as described in Section V.1 appears to be desirable for several reasons: (1) variations of Y_{π} associated with phase interference may be expected to occur completely independently for the wanted and unwanted signals, and this facilitates making a more precise determination of the required wanted-to-unwanted signal ratio, $R_{ur}(g)$, (2) the random variable Y_{π} follows the Nakagami-Rice distribution, as illustrated on figure V.1, while variations with time of Y are approximately normally distributed, (3) the variations with time of the median wanted and unwanted signal powers W_m and W_{um} tend to be correlated for most wanted and unwanted propagation paths, and an accurate allowance for this correlation is facilitated by separating the instantaneous fading into the two additive components Y and Y_{π} and (4) most of the contribution to the variance of W_m with time occurs at low fluctuation frequencies ranging from one cycle per year to about one cycle per hour, whereas most of the contribution to the variance of Y_{π} occurs at higher fluctuation frequencies, greater than one cycle per hour. Only the short-term variations of the wanted signal power w_{π} and the unwanted signal power $w_{u\pi}$ associated with phase interference fading are used in determining $r_{ur}(g)$, the ratio of the median wanted signal power w_m to the median unwanted signal power w_{um} required to provide a specified grade of service g . Let $R_{u\pi}$ denote the ratio between the instantaneous wanted signal power $W_m + Y_{\pi}$ and the instantaneous unwanted signal power $W_{um} + Y_{u\pi}$.

$$R_{u\pi} = \frac{W_m + Y_{\pi}}{W_{um} + Y_{u\pi}} = R_u + Z_{\pi} \quad (V.10)$$

where

$$Z_{\pi} = \frac{Y_{\pi}}{W_{um} + Y_{u\pi}} \text{ and } R_u = \frac{W_m}{W_{um}} \quad (V.11)$$

Note that the cumulative distribution function $Y_{\pi}(q, K)$ for Y_{π} will usually be different from the cumulative distribution function $Y_{u\pi}(q, K_u)$ for $Y_{u\pi}$ since the wanted signal propagation path will differ from the propagation path for the unwanted signal. Let $Z_{\pi} > Z_{\pi}^*(q, K, K_u)$ with probability q ; then the approximate cumulative distribution function of Z_{π} is given by:

$$Z_{\pi a}(q, K, K_u) = \pm \sqrt{Y_{\pi}^2(q, K) + Y_{\pi}^2(1-q, K_u)} \quad (V.12)$$

In the above, the plus sign is to be used when $q < 0.5$ and the minus sign when $q > 0.5$; note that $-Z_{\pi a}(1-q, K, K_u) = Z_{\pi a}(q, K, K_u)$. This method of approximation is suggested by two observations: (1) service may be limited for a fraction q of a short period of time either by downfades of the wanted signal corresponding to a level exceeded with a probability q or by

updates of an unwanted signal corresponding to a level exceeded with a probability $1-q$, and (2) the standard deviation of the difference of two uncorrelated random variables Y_{π} and $Y_{u\pi}$ equals the square root of the sum of their variances, and under fairly general conditions $Z_{\pi}^2(q)$ is very nearly equal to $Y_{\pi}^2(q) + Y_{u\pi}^2(1-q)$. Equation (V. 11) is based on the reasonable assumption that Y_{π} and $Y_{u\pi}$ are independent random variables and, for this case, (V. 11) would be exact if Y_{π} and $Y_{u\pi}$ were normally distributed. The departure from normality of the distribution of Y_{π} is greatest in the limiting case of a Rayleigh distribution, and for this special case, the following exact expression is available [Siddiqui, 1962]:

$$Z_{\pi}(q, \infty, \infty) = 10 \log \left(\frac{1}{q} - 1 \right) \quad (V. 13)$$

Table V.2 compares the above exact expression $Z_{\pi}(q, \infty, \infty)$ with the approximate expression $Z_{\pi a}(q, \infty, \infty)$. Note that the two expressions differ by less than 0.2 dB for any value of q and, since this difference may be expected to be even smaller for finite values of K , it appears that (V. 12) should be a satisfactory approximation for most applications and for any values of K and q .

Table V. 2

The Cumulative Distribution Function $Z_{\pi}(q, \infty, \infty)$ for the Special Case of the Ratio of Two Rayleigh-Distributed Variables

q	$Z_{\pi}(q, \infty, \infty)$	$Z_{\pi a}(q, \infty, \infty)$	$Z_{\pi} - Z_{\pi a}$
	db	db	db
0.0001	39.99957	40.0178	-0.01823
0.0002	36.98883	37.0362	-0.04737
0.0005	33.00813	33.0757	-0.06757
0.001	29.99566	30.1099	-0.11424
0.002	26.98101	27.1216	-0.14059
0.005	22.98853	23.1584	-0.16987
0.01	19.95635	20.1420	-0.18565
0.02	16.90196	17.0949	-0.19294
0.05	12.78754	12.9719	-0.18436
0.1	9.54243	9.7016	-0.15917
0.2	6.02060	6.1331	-0.11250
0.5	0	0	0

Let $R_{uro}(g)$ denote the required value of R_u for non-fading wanted and unwanted signals and it follows from (V.10) that the instantaneous ratio for fading signals will exceed $R_{uro}(g)$ with a probability at least equal to q provided that:

$$R_u > R_{ur}(g, q, K, K_u) = R_{uro}(g) - Z_{\pi}(q, K, K_u) \quad (V.14)$$

The use of (V.14) to determine an allowance for phase interference fading will almost always provide a larger allowance than will actually be necessary since (V.14) was derived on the assumption that $R_{uro}(g)$ is constant. For most services, $R_{uro}(g)$ will not have a fixed value for non-fading signals but will instead have either a probability distribution or a grade of service distribution; in such cases $R_{ur}(g)$ should be determined for a given q by a convolution of the distributions of $R_{uro}(g)$ and $-Z_{\pi}$. In still other cases the mean duration of the fading below the level $Z_{\pi}(q, K, K_u)$ will be comparable to the mean duration of the individual message elements and a different allowance should then be made. In some cases it may be practical to determine R_{ur} as a function of $g, q, K,$ and K_u in the laboratory by generating wanted and unwanted signals that vary with time the same as Y_{π} and $Y_{u\pi}$. This latter procedure will be successful only to the extent that the fading signal generators properly simulate natural phase interference fading both as regards their amplitude distributions and their fading duration distributions. As this annex is intended to deal only with general definitions and procedures, functions applicable to particular kinds of wanted and unwanted signals which include an appropriate phase interference fading allowance are not developed here.

The ratio R_u defined as an hourly median value equal to the difference between $W_m(0.5) + Y$ and $W_{um}(0.5) + Y_u$ will also vary with time:

$$R_u = W_m - W_{um} = W_m(0.5) - W_{um}(0.5) + Z \quad (V.15)$$

$$Z = Y - Y_u \quad (V.16)$$

The random variables Y and Y_u tend to be approximately normally distributed with a positive correlation coefficient ρ which will vary considerably with the propagation paths

and the particular time block involved. For the usual period of all hours of the day for several years preliminary analyses of data indicate that ρ will usually exceed 0.4 even for propagation paths in opposite directions from the receiving point. Z will exceed a value $Z_a(q)$ for a fraction of time q where the approximate cumulative distribution function $Z_a(q)$ of Z is given by

$$Z_a(q) = \pm \sqrt{Y^2(q) + Y_u^2(1-q) + 2\rho Y(q) Y_u(1-q)} \quad (V.17)$$

where the plus sign is to be used for $q < 0.5$ and the minus sign for $q > 0.5$ while $Z_a(0.5) = 0$. It follows from (V.15) and (V.17) that R_u will exceed $R_{ur}(g)$ for at least a fraction of time q provided that

$$W_m(0.5) - W_{um}(0.5) > R_{ur}(g) - Z_a(q) \quad (V.18)$$

In some cases it may be considered impractical to determine the function $R_{ur}(g)$ by adding an appropriate phase interference fading allowance to $R_{uro}(g)$; in such cases it may be useful to use the following approximate relation which will ensure that the instantaneous ratio $R_{un} > R_{uro}(g)$ for at least a fraction of time q :

$$W_m(0.5) - W_{um}(0.5) > R_{uro}(g) \pm \sqrt{Z_a^2(q) + Z_n^2(q, K, K_u)} \quad (V.19)$$

In the above, the minus sign is to be used for $q < 0.5$ and the plus sign for $q > 0.5$. Although (V.19), or its equivalent, has often been used in past allocation studies, this usage is deprecated since it does not provide a solution which is as well adapted to the actual nature of the problem as the separation of the fading into its two components Y_n and Y and the separate use of (V.14) and (V.18). Note that (V.19) provides a fading allowance which is too small compared with that estimated using (V.14) and (V.18) separately. The latter formulas are recommended. They make more appropriate allowance for the fact that communications at particular times of the day or for particular seasons of the year are especially difficult.

V.5 The Joint Effect of Several Sources of Interference Present Simultaneously

The effects of interference from unwanted signals and from noise have so far been considered in this report as though each affected the fidelity of reception of the wanted signal independently. Let $w_{mr}(g)$ and $r_{ur}(g)w_{um}$ denote power levels which the wanted median signal power w_m must exceed in order to achieve a specified grade of service when each source of interference is present alone. To the extent that the various sources of interference have a character approximating that of white noise, this same grade of service may be expected from a wanted signal with median level

$$w_m = w_{mr}(g) + \sum r_{ur}(g)w_{um}$$

when these sources are present simultaneously.

An approximate method has been developed [Norton, Staras, and Blum, 1952] for determining for a broadcasting service the distribution with time and receiving location of the ratio

$$w_m / [w_{mr}(g) + \sum r_{ur}(g)w_{um}]$$

Although this approach to the problem of adding the effects of interference will probably always provide a good upper bound to the interference, this assumption that the interference power is additive is often not strictly valid. For example, when intelligible cross-talk from another channel is present in the receiver output circuit, the addition of some white noise will actually reduce the nuisance value of this cross-talk.

Frequently, however, both $w_{mr}(g)$ and w_{um} will be found to vary more or less independently over wide ranges with time and a good approximation to the percentage of time that objectionable interference is present at a particular receiving location may then be obtained [Barsis, et al, 1961] by adding the percentage of time that w_m is less than $w_{mr}(g)$ to the percentages of time that w_m is less than each of the values of $r_{ur}(g)w_{um}$. When this total time of interference is small, say less than 10%, this will represent a satisfactory estimate of the joint influence of several sources of interference which are present simultaneously. Thus, when the fading ranges of the various sources of interference are sufficiently large so that this latter method of analysis is applicable, the various values of $w_{mr}(g)$ and of $r_{ur}(g)w_{um}$ will have comparable magnitudes for negligible percentages of the time so that one may, in effect, assume that the various sources of interference occur essentially independently in time.

Minimum acceptable wanted-to-unwanted signal ratios r_{ur} may sometimes be a function of r_m , the available wanted signal-to-noise ratio. When r_{ur} is within 3 db of r_{mr} , an unwanted signal may be treated the same as external noise, and, in a similar fashion, long-term distributions of available wanted-to-unwanted signal ratios may be determined for each class of unwanted signals for which r_{ur} is nearly the same

V. 6 The System Equation for Noise-Limited Service

Essential elements of a noise-limited communication circuit are summarized in the following system equation. The transmitter output W_{ft} dbw which will provide W_t dbw of total radiated power in the presence of transmission line and matching network losses L_{ft} db, and which will provide a median delivered signal at the pre-detection receiver output which is R_m db above the median noise power W_{mn} delivered to the pre-detection receiver output is given by

$$W_{ft} = L_{ft} + L_m + R_m + (W_{mn} - G_{ms}) \text{ dbw} \quad (\text{V. 20})$$

in the presence of a median transmission loss L_m and a median operating receiving system signal gain G_{ms} . The operating signal gain is the ratio of the power delivered to the pre-detection receiver output to the power available at the terminals of an equivalent loss-free antenna. Let G_o be the maximum of all values of operating signal gain in the receiver pass band, and G_{ms} the median value for all signal frequencies in the pass band. $(W_{mn} - G_{ms})$ in (V. 20) is the equivalent median noise power at the antenna terminals, as defined in section V. 3.

It is appropriate to express the system equation (V. 20) in terms of the operating noise factor F_{op} defined by (V. 8), rather than in terms of W_{mn} or $(W_{mn} - G_{ms})$ in order to separate studies of receiving system characteristics from studies of propagation. For this reason all predicted power levels are referred to the terminals of an equivalent loss-free antenna, and receiving system characteristics such as F_{op} , G_o , G_{ms} , and $B = 10 \log b$ are separated from transmission loss and available power in the formulas.

Rearranging terms of (V. 8), the equivalent median noise power $(W_{mn} - G_{ms})$ delivered to the antenna terminals may be expressed as

$$W_{mn} - G_{ms} = F_{op} + (G_o - G_{ms}) + (B - 204) \quad (\text{V. 21})$$

where G_o and G_{ms} are usually nearly equal. Assuming that L_{ft} , G_o , G_{ms} , and B are constant, it is convenient to combine these parameters into an arbitrary constant K_o :

$$K_o = L_{ft} + G_o - G_{ms} + B - 204 \text{ dbw} \quad (\text{V. 22})$$

and rewrite the system equation as:

$$W_{ft} = K_o + L_m + R_m + F_{op} \text{ dbw} \quad (\text{V. 23})$$

In general, if unwanted signals other than noise may be disregarded, service exists whenever $R_m(q)$ exceeds $R_{mr}(g)$, where $R_m(q)$ is the value of R_m exceeded a fraction q of all hours. With G_{ms} and W_{mn} assumed constant, so that

$$R_m(q) = W_m(q) + G_{ms} - W_{mn} \quad (\text{V. 24})$$

service exists whenever $W_m(q)$ exceeds W_{mr} , or whenever $L_m(q)$ is less than the maximum allowable transmission loss $L_{mo}(g)$. An equivalent statement may be made in terms of the system equation. The transmitter power $W_{ft}(q)$ which will provide for a fraction q of all hours at least the grade g service defined by the required signal-to-noise ratio $R_{mr}(g)$ is

$$W_{ft}(q) = K_o + L_m(q) + F_{op} + R_{mr}(g) \quad (V.25)$$

where $L_m(q)$ is the hourly median transmission loss not exceeded for a fraction q of all hours.

For a fixed transmitter power W_o dbw, the signal-to-noise ratio exceeded q percent of all hours is

$$R_m(q) = W_o - K_o - F_{op} - L_m(q) \quad \text{db} \quad (V.26)$$

for a "median" propagation path for which the service probability, Q , is by definition equal to 0.5.

The maximum allowable transmission loss

$$L_{mo}(g) = W_o - K_o - F_{op} - R_{mr}(g) \quad (V.27)$$

is set equal to the loss $L_m(q, Q)$ exceeded during a fraction $(1 - q)$ of all hours with a probability Q . This value is fixed when P_o , K_o , and $R_{mr}(g)$ have been determined, and for each time availability q there is a corresponding service probability, $Q(q)$. Section V.9 will explain how to calculate $Q(q)$.

When external noise is both variable and not negligible, the long-term variability of F_{op} must be considered, and the following relationships may be used to satisfy the condition

$$R_m(q) > R_{mr}(g) \quad (V.28)$$

$$R_m(q) \cong R_m(0.5) + Y_m(q) \quad (V.29)$$

$$R_m(0.5) \cong W_o - K_o - F_{op}(0.5) - L_m(0.5) \quad (V.30)$$

$$Y_m^2(q) \cong Y^2(q) + Y_n^2(1 - q) - 2\rho_{tn} Y(q) Y_n(1 - q) \quad (V.31)$$

$$Y(q) \cong L_m(0.5) - L_m(q), \quad Y_n(q) \cong F_{op}(q) - F_{op}(0.5) \quad (V.32)$$

where ρ_{tn} is the long-term correlation between W_m and F_{op} . Though ρ_{tn} could theoretically have any value between -1 and 1, it is usually zero.

V.7 The Time Availability of Interference-Limited Service

Let ρ_{tu} denote the long-term correlation between W_m and W_{um} , the power expected to be available at least q percent of all hours at the terminals of an equivalent loss-free receiving antenna from wanted and unwanted stations radiating w_o and w_u watts, respectively:

$$W_m(q) = W_o - L_m(q) \text{ dbw}, \quad W_{um}(q) = W_u - L_{um}(q) \text{ dbw} \quad (V.33)$$

$$W_o = 10 \log w_o \text{ dbw}, \quad W_u = 10 \log w_u \text{ dbw} \quad (V.34)$$

The criterion for service of at least grade g in the presence of a single unwanted signal and in the absence of other unwanted signals or appreciable noise is

$$R_u(q) > R_{ur}(g, q) \quad (V.35)$$

where

$$R_u(q) = R_u(0.5) + Y_R(q) \quad (V.36)$$

$$R_u(0.5) \approx W_m(0.5) - W_{um}(0.5) \quad (V.37)$$

$$Y_R(q) \approx Y_m^2(q) + Y_u^2(1-q) - 2\rho_{tu} Y_m(q) Y_u(1-q) \quad (V.38)$$

$$Y_u(q) = W_{um}(q) - W_{um}(0.5) = L_{um}(0.5) - L_{um}(q) \quad (V.39)$$

If W_m , W_{um} , and F_{op} were exactly normally distributed, (V.31) and (V.38) would be exact; they represent excellent approximations in practice.

V.8 The Estimation of Prediction Errors

Consider the calculation of the power $W_m(q)$ available at the terminals of an equivalent loss-free receiving antenna during a fraction q of all hours. $W_m(q)$ refers to hourly median values expressed in dbw. For a specific propagation path it is calculated in accordance with the methods given in sections 2-10 using a given set of path parameters (d, f, θ, h_{te} , etc.). Denote by $W_{mo}(q)$ observations made over a large number of randomly different propagation paths, which, however, can all be characterized by the same set of prediction parameters. Values of $W_{mo}(q)$ will be very nearly normally distributed with a mean (and median) equal to $W_m(q)$, and a variance denoted by $\sigma_c^2(q)$. This path-to-path variability is illustrated in Fig. V.6 for a hypothetical situation which assumes a random distribution of all parameters which are not taken into account in the prediction method.

The variance σ_c^2 of deviations of observation from prediction depends on available data and the prediction method itself. The most sophisticated of the methods given in this report for predicting transmission loss as a function of carrier frequency, climate, time block, antenna gains, and path geometry have been adjusted to show no bias, on the average, for the data discussed in section 10 and in annex I.

Most of these data are concentrated in the 40-1000 MHz frequency range, and were obtained primarily for transhorizon paths in climates 1, 2, and 3. Normally, one antenna was on the order of 10 meters above ground and the other one was higher, near 200 meters. Even the low receiving antennas were located on high ground or in clear areas well removed from hills and terrain clutter. Few of the data were obtained with narrow-beam antennas. An attempt has been made to estimate cumulative distributions of hourly transmission loss medians for accurately specified time blocks, including estimates of year-to-year variability.

A prediction for some situation that is adequately characterized by the prediction parameters chosen here requires only interpolation between values of these parameters for which data are available. In such a case, $\sigma_c(q)$ represents the standard error of prediction. The mean square error of prediction, referred to a situation for which data are not available, is $\sigma_c^2(q)$ plus the square of the bias of the prediction method relative to the new situation.

Based on an analysis of presently available transhorizon transmission loss data, the variance $\sigma_c^2(q)$ is estimated as

$$\sigma_c^2(q) = 12.73 + 0.12 Y^2(q) \text{ db}^2 \quad (\text{V.40})$$

where $Y(q)$ is defined in section 10. Since $Y(0.5) \equiv 0$, the variance $\sigma_c^2(0.5)$ of the difference between observed and predicted long-term medians is 12.73 db^2 , with a corresponding standard deviation $\sigma_c(0.5) = 3.57 \text{ db}$.

It is occasionally very difficult to estimate the prediction error $\sigma_c(q)$ and the service probability Q . Where only a small amount of data is available there is no adequate way of estimating the bias of a prediction. One may, however, assign weights to the curves of $V(0.5, d_e)$ in figure 10.13 for climates 1-7 based on the amount of supporting data available:

Climate Number	Weight
1	300
2	120
3	60
4	2
5	(deleted)
6	5
7	5

As an example, for $d_e = 600$ km, the average $V(0.5, d_e)$ weighted in accordance with the above is 0.1 db, and the corresponding climate-to-climate variance of $V(0.5)$ is 3.1 db^2 . If a random sampling of these climates is desired the predicted median value $L(0.5)$ is $L_{cr} - V(0.5) = L_{cr} - 0.1$ db, with a standard error of prediction equal to $(12.7 + 3.1)^{\frac{1}{2}} = 4$ db, where 12.7 db^2 is the variance of $V(0.5)$ within any given climate.

If there is doubt as to which of two particular climates i and j should be chosen, the best prediction of $L_b(q)$ might depend on the average of $V_i(0.5, d_e)$ and $V_j(0.5, d_e)$ and the root-mean square of $Y_i(q, d_e)$ and $Y_j(q, d_e)$:

$$L(q) = L_{cr} - 0.5 \left[V_i(0.5, d_e) + V_j(0.5, d_e) \right] - Y_{ij}(q, d_e) \quad \text{db.} \quad (\text{V. 41})$$

$$Y_{ij}(q, d_e) = \left[0.5 Y_i^2(q, d_e) + 0.5 Y_j^2(q, d_e) \right]^{\frac{1}{2}} \quad \text{db} \quad (\text{V. 42})$$

The bias of this prediction may be as large as $\left[0.5 V_i(0.5, d_e) - V_j(0.5, d_e) \right]$ db. The root-mean square prediction error may therefore be estimated as the square root of the sum of the variance, $\sigma_c^2(0.5)$ and the square of the bias, or

$$\left\{ 12.73 + 0.12 Y_{ij}^2(q, d_e) + 0.25 \left[V_i(0.5, d_e) - V_j(0.5, d_e) \right]^2 \right\}^{\frac{1}{2}} \quad \text{db.}$$

According to figure 10.13, $V(0.5, d_e)$ is expected to be the same for climates 1 and 8. This conclusion and the estimate for $Y(q, d_e)$ shown in figure III. 29 for climate 8 are based solely on meteorological data. In order to obtain these estimates, the percentages of time for which surface-based ducts existed in the two regions were matched with the same value of $Y(q, d_e)$ for both climates. In this way, $Y_8(q, d_e)$ was derived from $Y_1(q, d_e)$ by relating q_8 to q_1 for a given Y instead of relating Y_8 to Y_1 for a given q .

V.9 The Calculation of Service Probability Q for a Given Time Availability q

For noise-limited service of at least grade g and time availability q, the service probability Q is the probability that

$$L_{mo}(k) - L_m(q) > 0 \quad (V.43)$$

if external noise is negligible. $L_{mo}(g)$ is defined by (V.27). The criterion for service limited by variable external noise is

$$R_m(q) - R_{mr}(g) > 0 \quad (\text{from equation V.28})$$

For service limited only by interference from a single unwanted signal,

$$R_u(q) - R_{ur}(g, q) > 0 \quad (\text{from equation V.35})$$

Combining (V.22) and (V.27), (V.43) may be rewritten as

$$W_o - L_{ft} - G_o + G_{ms} - B + 204 - F_{op} - R_{mr}(g) - L_m(q) > 0 \quad (V.44)$$

where the terms are defined in (V.8) and section V.6. Assuming that the error of estimation of these terms from system to system is negligible except for the path-to-path variance $\sigma_c^2(q)$ of $L_m(q)$ it is convenient to represent the service probability Q as a function of the standard normal deviate z_{mo} :

$$z_{mo} = \frac{L_{mo} - L_m(q)}{\sigma_c(q)} \quad (V.45)$$

which has a mean of zero and a variance of unity. L_{mo} is identified as the transmission loss exceeded a fraction (1-q) of the time with a probability Q, which is expressed in terms of the error function as

$$Q(z_{mo}) = \frac{1}{2} + \frac{1}{2} \operatorname{erf}(z_{mo}/\sqrt{2}) \quad (V.46)$$

Figure V.7 is a graph of Q versus z_{mo}

For the method described here, the condition

$$0.12 Y(q) z_{mo}(Q) < -\sigma_c(q) \quad (V.47)$$

is sufficient to insure that the service probability Q increases as the time availability q is decreased. A less restrictive condition is

$$Y(q) [L_{mo} - L_m(0.5)] < 106 \text{ db}^2 \quad (V.48)$$

An example is shown in figure V.8, with q versus Q for radiated powers $W_o = 30$ dbw and $W_o = 40$ dbw, and $L_m(q, Q) = W_o + 140$ db. Here,

$$q = 0.5 + 0.5 \operatorname{erf} \left[\frac{L_m(q) - 140}{10\sqrt{2}} \right] \quad (V.49)$$

(corresponding to a normal distribution with a mean $L_m(0.5) = 140$ db and a standard deviation $Y(0.154) = 10$ db. [Note that $L_m(q)$ versus q as estimated by the methods of section 10 is usually not normally distributed].

To obtain the time availability versus service probability curves on figure V.8, $L_m(q)$ was obtained from q , $Y(q)$ from (V.4), $\sigma_c^2(q)$ from (V.49), z_{mo} from (V.45), and Q from figure V.7. This same method of calculation may be used when there are additional sources of prediction error by adding variances to $\sigma_c^2(q)$. Examining possible trade-offs between time availability and service probability shown in figure V.8, note the increase from $q = 0.965$ to $q = 0.991$ for $Q = 0.95$, or the increase from $Q = 0.74$ to $Q = 0.97$ for $q = 0.44$, as the radiated power is increased from one to ten kilowatts.

For the case of service limited by external noise (V.28) to (V.30) may be rewritten as

$$W_o - K_o - F_{op}(0.5) - L_m(0.5) + F_m(q) - R_m(q) > 0 \quad (V.50)$$

One may ignore any error of estimation of W_o , K_o , and $R_m(q)$ as negligible and assume no path-to-path correlation between $F_{op}(0.5)$ and $L_m(0.5)$. The variance $\sigma_{op}^2(q)$ of $F_{op}(0.5) + L_m(0.5) - Y_m(q)$ in (V.50) may then be written as a sum of component variances σ_F^2 and $\sigma_c^2(q)$:

$$\sigma_{op}^2(q) = \sigma_F^2 + 12.73 + 0.12 Y_m^2(q) \text{ db}^2 \quad (V.51)$$

Very little is known about values for the variance σ_F^2 of $F_{op}(0.5)$, but it is probably on the order of 20 db².

The corresponding standard normal deviate z_{op} is:

$$z_{op} = \frac{R_m(q) - R_m(q)}{\sigma_{op}(q)} \quad (V.52)$$

and the service probability $Q(q)$ is given by (V.46) with z_{mo} replaced by z_{op} . The restriction (V.47) still holds with z_{mo} and σ_c replaced by z_{op} and σ_{op} . A less restriction condition equivalent to (V.48) can be stated only if a specific value of σ_F is assumed.

For the case of service limited only by interference from a single unwanted radio signal (V. 35) to (V. 39) may be rewritten as

$$L_{\text{min}}(0.5) - L_{\text{max}}(0.5) + Y_{\text{R}}(\omega) - R_{\text{uc}}(\omega, \omega) > 0 \quad (\text{V. 53})$$

Let ρ_{Iuc} denote the normalized correlation or covariance between path-to-path variations of $W_{\text{min}}(0.5)$ and $W_{\text{max}}(0.5)$. Then assuming a variance of $25.5(1 - \rho_{\text{Iuc}}) + 0.12 Y_{\text{R}}^2(\omega) \text{ dB}^2$ for $R_{\text{uc}}(\omega)$, given by the first three terms of (V. 53) and a variance σ_{uc}^2 for the estimate of $R_{\text{uc}}(\omega, \omega)$, the total variance $\sigma_{\text{uc}}^2(\omega)$ of any estimate of the service criterion given by (V. 53) may be written as

$$\sigma_{\text{uc}}^2(\omega) = 25.5(1 - \rho_{\text{Iuc}}) + 0.12 Y_{\text{R}}^2(\omega) + \sigma_{\text{uc}}^2 \quad (\text{V. 54})$$

where $Y_{\text{R}}^2(\omega)$ is given by (V. 35). The corresponding standard normal deviate z_{uc} is:

$$z_{\text{uc}} = \frac{R_{\text{uc}}(\omega) - R_{\text{uc}}(\omega, \omega)}{\sigma_{\text{uc}}(\omega)} \quad (\text{V. 55})$$

and the service probability $Q(\omega)$ is given by (V. 46) with z_{mo} replaced by z_{uc} . The variance σ_{uc}^2 may range from 10 dB^2 to very much higher values. The restrictions (V. 47) and (V. 48) apply with z_{mo} and σ_c replaced by z_{uc} and σ_{uc} and with 106 dB in (V. 48) replaced by $(212 + \sigma_{\text{uc}}^2) \text{ dB}^2$.

TYPICAL PATH - TO - PATH VARIATION OF INFINITE - TIME DISTRIBUTIONS
FOR A SINGLE SET OF VALUES OF THE PREDICTION PARAMETERS

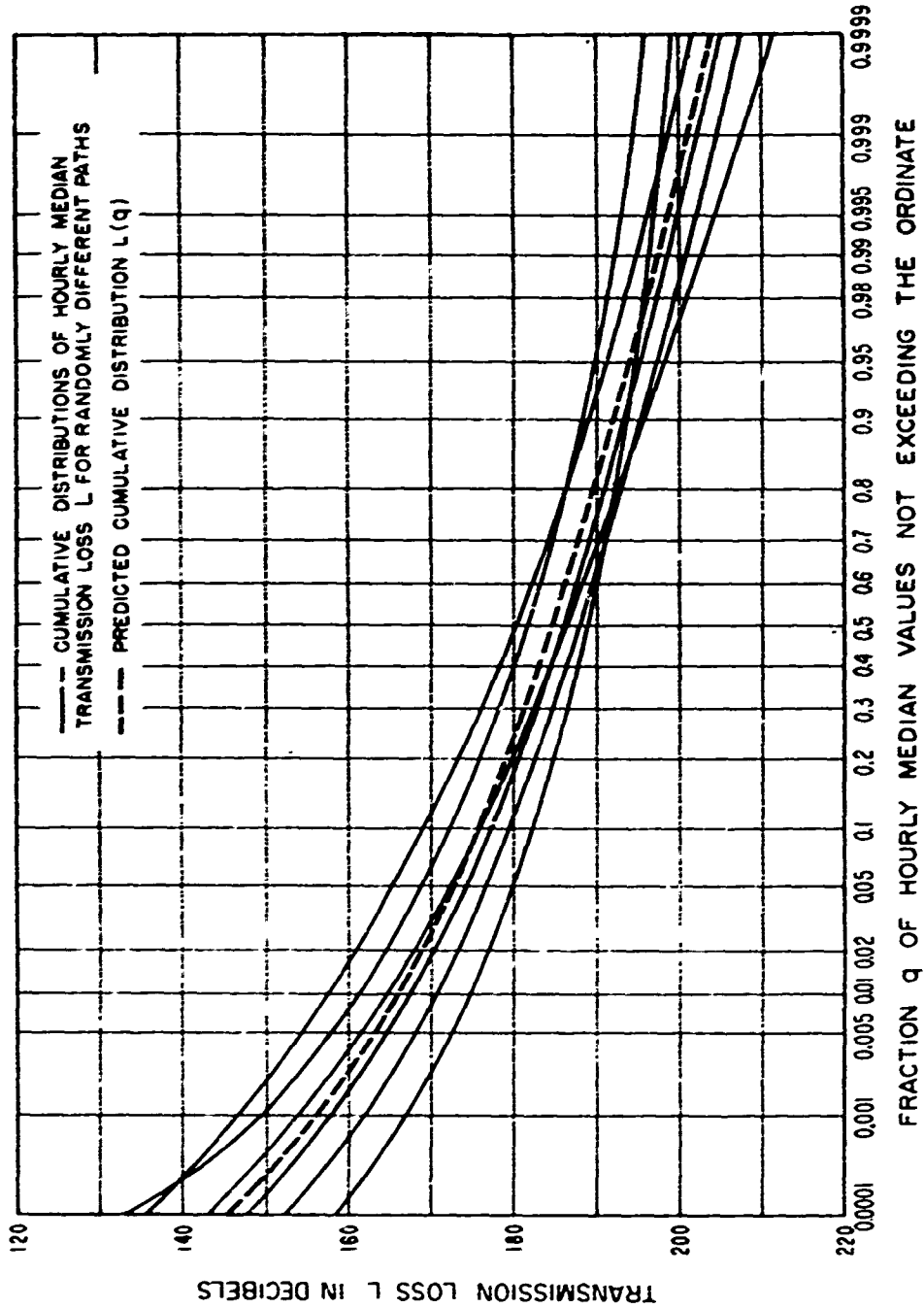
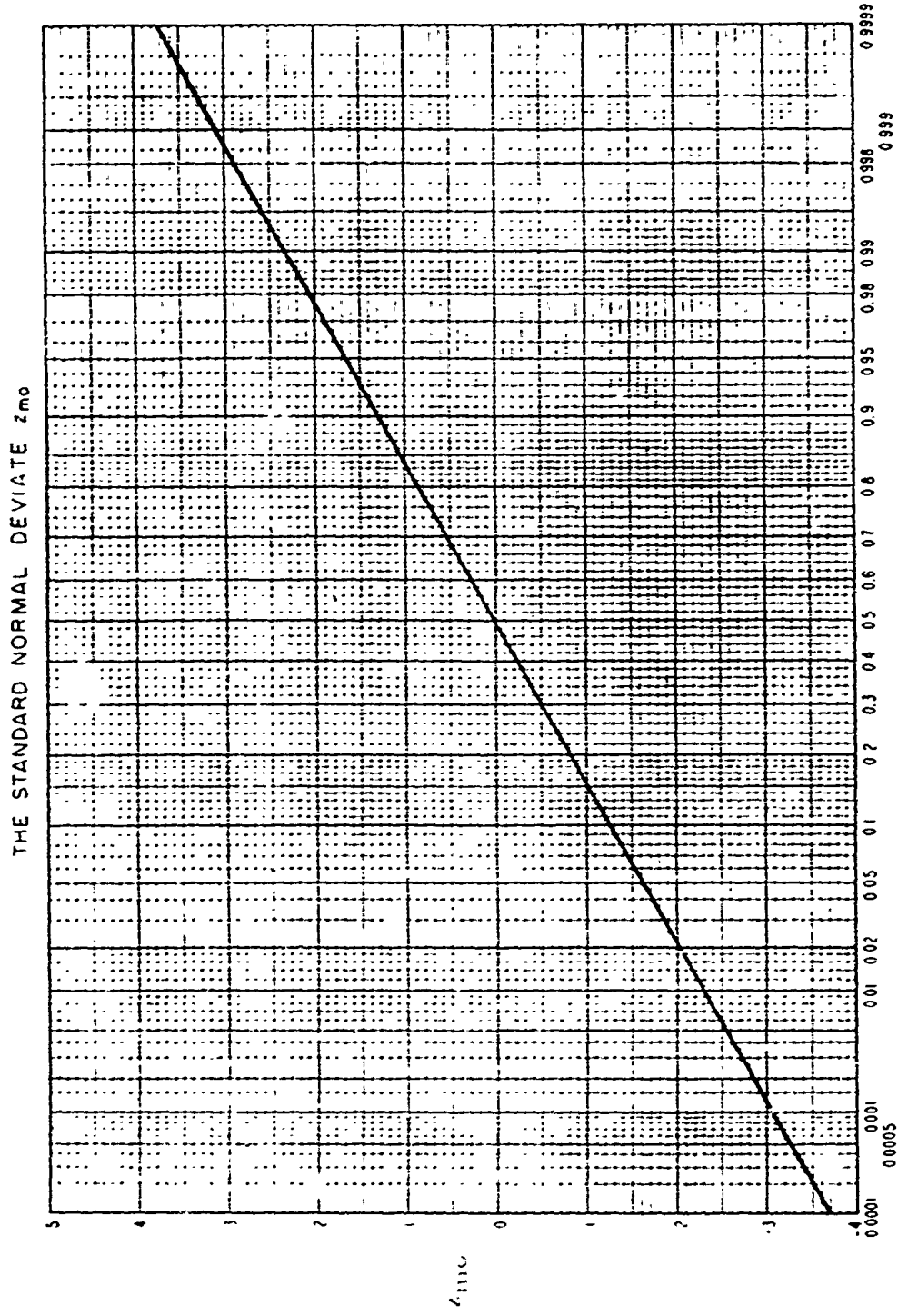
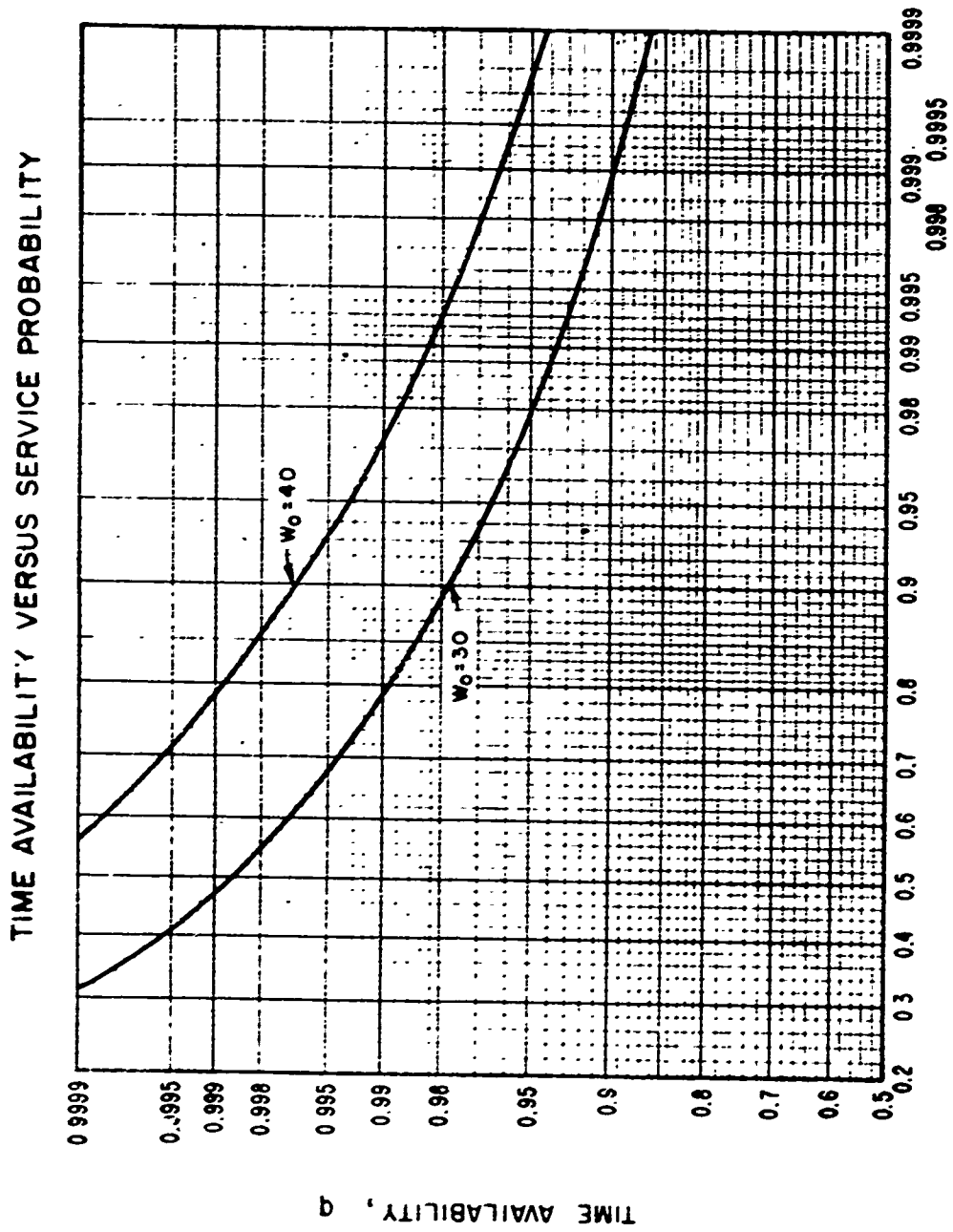


Figure 3.6



SERVICE PROBABILITY, Q

Figure V.7



SERVICE PROBABILITY, Q
Figure V.8

V. 10 Optimum Use of the Radio Frequency Spectrum

The business of the telecommunications engineer is to develop efficient radio systems, and the principal tool for improving efficiency is to adjust the various parameters to their optimum values. For example, it is usually more economical to use lower effective radiated powers from the transmitting systems by reducing the operating sensitivities of the receiving systems. Receiving system sensitivities can be reduced by (a) reducing the level of internally generated noise, (b) using antenna directivity to reduce the effects of external noise, (c) reducing man-made noise levels by using suppressors on noise generators such as ignition systems, relays, power transmission systems, etc., and (d) using space or time diversity and coding. The use of more spectrum in a wide band FM system or in a frequency diversity system can also reduce the receiving system operating sensitivity as well as reduce the acceptance ratios against unwanted signals other than noise.

Unfortunately, unlike other natural resources such as land, minerals, oil, and water, there is currently no valid method for placing a monetary value on each hertz of the radio spectrum. Thus, in the absence of a common unit of exchange, these tradeoffs are often made unrealistically at the present time. It is now generally recognized that the use of large capacity computers is essential for optimizing the assignment of frequencies to various classes of service including the development of optimum channelization schemes. Typical inputs to such computers are:

1. Nominal frequency assignments.
2. Transmitting system locations, including the antenna heights.
3. Transmitting system signatures; i. e., the radiated emission spectrum characteristics including any spurious emission spectrums.
4. Transmitting antenna characteristics.
5. Receiving system locations, including the antenna heights.
6. Spurious emission spectrums of the receiving systems.
7. Operating sensitivities of the receiving systems in their actual environments which thus make appropriate allowance for the effects of both man-made and natural noise.
8. Required values of wanted-to-unwanted phase interference median signal powers for all unwanted signals which could potentially cause harmful interference to the wanted signal; these acceptance ratios include appropriate allowances for reductions in the effects of fading achieved by the use of diversity reception and coding.

9. Long-term median reference values of basic transmission loss and path antenna gain for the wanted path and all of the unwanted signal propagation paths; these path antenna gains include allowances for antenna orientation, polarization, and multipath phase mismatch coupling losses.
10. Distributions with time of the transmission loss for the wanted signal path and all of the unwanted signal paths.
11. Correlations between the transmission losses on the wanted and on each of the unwanted propagation paths.
12. Transmission line and antenna circuit losses.
13. The spurious emission spectrum of any unwanted signals arising from unlicensed sources such as diathermy machines, electronic heaters, welders, garage door openers, etc.
14. Assigned hours of operation of each wanted and each unwanted emission.

The output of the computer indicates simply the identity and nature of the cases of harmful interference encountered. Harmful interference is defined as a failure to achieve the specified grade of service for more than the required fraction of time during the assigned hours of operation. Changing some of the inputs to the computer, an iterative process can be defined which may lead to an assignment plan with no cases of harmful interference.

It is assumed that a given band of radio frequencies has been assigned to the kind of radio service under consideration and that the nature of the services occupying the adjacent frequency bands is also known. Furthermore, it is assumed that the geographical locations of each of the transmitting and receiving antennas are specified in advance, together with the relative values of the radiated powers from each transmitting antenna and the widths and spacings of the radio frequency channels. In the case of a broadcasting service the specification of the intended receiving locations can be in terms of proposed service areas. With this information given, use may be made of the following procedures in order to achieve optimum use of the spectrum by this particular service:

- (a) The system loss for each of the wanted signal propagation paths should be minimized and for each of the unwanted signal propagation paths should be maximized; this may be accomplished by maximizing the path antenna power gains for each of the wanted signal propagation paths, minimizing the path antenna gains for each of the unwanted propagation paths, and in exceptional cases, by appropriate antenna siting. The path antenna gains for the unwanted signal propagation paths may be minimized

by the use of high-gain transmitting and receiving antennas with optimum side lobe suppression and front-to-back ratios and, in some cases, by the use of alternate polarizations for geographically adjacent stations or by appropriate shielding.

(b) The required protection ratios $r_{ur}(g)$ should be minimized by (1) appropriate radio system design, (2) the use of stable transmitting and receiving oscillators, (3) the use of linear transmitting and receiving equipment, (4) the use of wanted and unwanted signal propagation paths having the minimum practicable phase interference fading ranges; from band 6 to band 9 (0.3 to 3000 MHz), minimum phase interference fading may be achieved by the use of the maximum practicable transmitting and receiving antenna heights, and (5) the use of space diversity, time diversity, and coding.

(c) Wanted signal propagation paths should be employed having the minimum practicable long-term power fading ranges. In bands 6 and 9, minimum fading may be achieved by the use of the maximum practicable transmitting and receiving antenna heights.

The above procedures should be carried out with various choices of transmitting and receiving locations, relative transmitter powers, and channel spacings until a plan is developed which provides the required service with a minimum total spectrum usage. After the unwanted signal interference has been suppressed to the maximum practicable extent by the above methods so that, at each receiving location each of the values of r_u exceeds the corresponding protection ratio $r_{ur}(g)$ for a sufficiently large percentage of the time, then the following additional procedures should be adopted in order to essentially eliminate interference from noise:

(d) The system loss on each of the wanted signal propagation paths should be minimized; this may be accomplished by (1) the use of the highest practicable transmitting and receiving antenna heights in bands 8 and 9, and (2) maximizing the path antenna power gains for each of the wanted signal propagation paths. The path antenna power gains of the wanted signal propagation paths may be maximized by using the maximum practicable transmitting and receiving antenna gains and by minimizing the antenna circuit and polarization coupling losses. The minimization of the system loss on each of the wanted signal propagation paths will already have been achieved to a large extent in connection with procedures (a), (b), and (c) above.

(e) In general, receiving systems should be employed which have the lowest practicable values of operating sensitivity $w_{mr}(g)$.

(f) Finally, sufficiently high transmitter powers should be used [keeping the relative powers at the optimum relative values determined by procedures (a), (b), and (c)] so that the wanted signal power w_m will exceed the operating sensitivity $w_{mr}(g)$ for a sufficiently large fraction of the time during the intended period of operation at every receiving location.

Although it might at first seem impracticable, serious consideration should be given to the use of auxiliary channels from wanted receivers to wanted transmitters. The provision of such channels might well be feasible in those cases where two-way transmissions are involved and might lead to important economies in both power and spectrum occupancy [Hitchcock and Morris, 1961].

Ultimately, when optimum use of the spectrum has been achieved, it will not be possible to find a single receiving location at which radio noise rather than either wanted or unwanted signals can be observed for a large percentage of the time throughout the usable portions of the radio spectrum not devoted to the study of radio noise sources, as is the radio astronomy service. Although everyone will agree that the attainment of this ideal goal of interference-free spectrum usage by the maximum number of simultaneous users can be achieved only over a very long period of time because of the large investments in radio systems currently in operation, nevertheless it seems desirable to have a clear statement of the procedures which should be employed in the future in order to move in the direction of meeting this ultimately desirable goal whenever appropriate opportunities arise.

V.II Supplementary List of Symbols for Annex V

b, B	Effective bandwidth, b , of a receiver in cycles per second. $B = 10 \log b$ decibels. (V. 7) and (V. 8).
f_{op}, F_{op}	Operating noise factor of the pre-detection receiving system. $F_{op} = 10 \log f_{op}$ db. (V. 7) and (V. 8)
g	Grade of service. A specified grade of service provided by a given signal with guarantee a corresponding degree of fidelity of the information delivered to the receiver output.
g_o, G_o	The maximum value of the operating gain of a pre-detection receiving system. $G_o = 10 \log g_o$ db. (V. 7) and (V. 8).
g_{ms}, G_{ms}	The hourly median operating signal gain of a pre-detection receiving system. $G_{ms} = 10 \log g_{ms}$ db. (V. 9).
k	Boltzmann's constant. $k = 1.38054 \times 10^{-23}$ joules per degree. (V. 7).
$k T_o$	Johnson's noise power that would be available in the bandwidth b cycles per second at a reference absolute temperature $T_o = 288.37$ degrees Kelvin. (V. 7).
K	The decibel ratio of the amplitude of the constant or power-fading component of a received signal relative to the root-sum-square value of the amplitudes of the Rayleigh components, figure V. 1.
K_o	An arbitrary constant that combines several parameters in the systems equations. (V. 22).
L_{ft}	Transmission line and matching network losses at the transmitter. (V. 20).
L_m	Hourly median transmission loss. (V. 20).
$L_m(q)$	Hourly median transmission loss not exceeded for a fraction q of all hours. o : exceeded $(1-q)$ of all hours. (V. 25).
$L_m(q, Q)$	Hourly median transmission loss exceeded for a fraction $(1-q)$ of all hours with a probability Q , section V. 6.
	Median value of $L_m(q)$, (V. 2).
$L_{mo}(g)$	Maximum allowable hourly median transmission loss for a grade g of service. (V. 27).
$L_o(q)$	Observed values of transmission loss not exceeded a fraction q of the recording period. (V. 5).
$L_{um}(q)$	Hourly median transmission loss of unwanted signal not exceeded for a fraction q of all hours. (V. 33).
$L_{um}(0.5)$	Long-term median value of $L_{um}(q)$. (V. 39).

- L_{π} Transmission loss associated with the "instantaneous" power W_{π} . (V. 6) and figure V. 2.
- $L_{\pi}(q)$ Transmission loss L_{π} not exceeded a fraction q of the time.
- $L_{\pi}(0.9) - L_{\pi}(0.1)$ The interdecile range $L_{\pi}(0.9) - L_{\pi}(0.1)$ of values of transmission loss associated with the "instantaneous" power W_{π} . figure V. 2.
- q Time availability.
- q_1, q_2 Time availability in climates 1 and 2, section V. 8.
- Q Service probability, discussed in section V. 8.
- $Q(q)$ The probability Q of obtaining satisfactory service for a fraction of time q . figure V. 6.
- $Q(z_{mo})$ Service probability Q expressed in terms of the error function of z_{mo} . (V. 46). figure V. 5.
- r_m, R_m Ratio of the hourly median wanted signal power to the hourly median operating noise power, $R_m = 10 \log r_m$ db. (V. 9).
- r_{mr}, R_{mr} A specified value of r_m which must be exceeded for at least a specified fraction of time to provide satisfactory service in the presence of noise alone, $R_{mr} = 10 \log r_{mr}$ db. (V. 9).
- r_u, R_u Ratio of hourly median wanted to unwanted signal power available at the receiver, $R_u = 10 \log r_u$ db. (V. 14).
- r_{ur}, R_{ur} A specified value of r_u which must be exceeded for at least a specified fraction of time to provide satisfactory service in the presence of a single unwanted signal, $R_{ur} = 10 \log r_{ur}$ db. (V. 14).
- $r_{mr}(g), R_{mr}(g)$ The minimum acceptable signal to noise ratio which will provide service of a given grade g in the absence of unwanted signals other than noise, $R_{mr}(g) = 10 \log r_{mr}(g)$ db. (V. 9).
- $r_{ur}(g), R_{ur}(g)$ The protection ratio r_{ur} required to provide a specified grade of service g . $R_{ur}(g) = 10 \log r_{ur}(g)$ db. sections V. 4 and V. 5.
- $R_m(q)$ The value of R_m exceeded at least a fraction q of the time. (V. 24).
- $R_m(0.5)$ The median value of R_m . (V. 29).
- $R_u(q)$ A specified value of R_u exceeded at least a fraction q of the time. (V. 36).
- $R_u(0.5)$ The median value of R_u . (V. 36).
- $R_{ur}(g, q)$ The required ratio R_{ur} to provide service of grade g for at least a fraction q of the time. (V. 35).
- $R_{uro}(g)$ The required ratio R_{ur} for non-fading wanted and unwanted signals. (V. 14).
- $R_{u\pi}$ The ratio between the instantaneous wanted and unwanted signal powers. (V. 10).
- T_o Reference absolute temperature $T_o = 289.37$ degrees kelvin. (V. 7).
- $V(0.5), d_c$ A parameter used to adjust the predicted reference median for various climatic regions or periods of time. section V. 8 and section 10, volume 1

- $V_i(0.5, d_c)$, $V_j(0.5, d_c)$ The parameter $V(0.5, d_c)$ for each of two climates represented by the subscripts i and j , (V.41).
- w_m , W_m The median wanted signal power available at a receiver, $W_m = 10 \log w_m$ dbw, (V.1).
- w_{mn} , W_{mn} The median value of the total noise power is w_{mn} watts, $W_{mn} = 10 \log w_{mn}$ dbw, (V.7) and (V.8).
- w_{mr} , W_{mr} Operating threshold, the median wanted signal power required for satisfactory service in the presence of noise, $W_{mr} = 10 \log w_{mr}$ dbw, (V.9).
- w_o , W_o A fixed value of transmitter output power w_o in watts, $W_o = 10 \log w_o$ dbw, (V.26).
- w_t , W_t Total radiated power in watts and in dbw, section V.6.
- w_u , W_u Power radiated from an unwanted or interfering station, w_u watts, $W_u = 10 \log w_u$ dbw, (V.33).
- w_{um} , W_{um} Median unwanted signal power w_{um} in watts, $W_{um} = 10 \log w_{um}$ dbw, (V.33) and (V.34).
- w_{uz} , W_{uz} Unwanted signal power associated with phase interference fading, w_{uz} in watts, $W_{uz} = 10 \log w_{uz}$ dbw, section V.4.
- w_π , W_π Wanted signal power associated with phase interference fading, w_π is defined as the average power for a single cycle of the radio frequency, $W_\pi = 10 \log w_\pi$ dbw, (V.1).
- W_{ft} Transmitter output power, (V.20).
- $W_{ft}(q)$ Transmitter power that will provide at least grade g service for a fraction q of all hours, (V.25).
- $W_m(q)$ The hourly median wanted signal power exceeded for a fraction q of all hours, (V.24).
- $W_m(0.5)$ Long-term median value of W_m , (V.2).
- $W_{mo}(q)$ Observed values of $W_m(q)$ made over a large number of paths which can be characterized by the same set of prediction parameters, section V.8.
- $W_{mr}(g)$ The operating threshold of a receiving system, defined as the minimum value of W_m required to provide a grade of service g in the presence of noise alone, (V.9).
- $W_{um}(q)$ The hourly median unwanted signal power W_{um} expected to be available at least a fraction q of all hours, (V.33).
- $W_{um}(0.5)$ The median value of $W_{um}(q)$, (V.37).
- $W_\pi(q)$ The "instantaneous" power W_π exceeded for a fraction of time q , (V.6).
- $W_\pi(0.1)$, $W_\pi(0.9)$ The interdecile range $W_\pi(0.1) - W_\pi(0.9)$ of the power $W_\pi(q)$, equivalent to the interdecile range of short term transmission loss shown on figure V.2.
- Y A symbol used to describe long-term fading, (V.1) and (V.3).
- Y_u Long-term fading of an unwanted signal, (V.16).

- Y_{un} Phase interference component of the total fading of an unwanted signal, (V. 10).
 Y_{π} Phase interference fading component for a wanted signal, (V. 10).
 $Y(q)$ Long-term variability Y for a given fraction of hourly medians q , defined by (V. 4).
 $Y(0.5)$ The median value of Y , which by definition is zero.
 $Y_i(q, d_i), Y_j(q, d_j)$ Values of Y for climates i and j , (V. 41) and (V. 42).
 $Y_{ij}(q, d_i, d_j)$ The root-mean-square value of the variability for two climates, (V. 42).
 $Y_{un}(q)$ Long-term variability in the presence of variable external noise, (V. 31).
 $Y_{op}(q)$ Variability of the operating noise factor, F_{op} , (V. 31) and (V. 32).
 $Y_{ur}(q)$ Long-term variability of the wanted to unwanted signal ratio, (V. 38).
 $Y_{un}(q)$ Long-term variability of an unwanted signal, (V. 39).
 $Y_{un}(q)$ The phase interference fading component of the total variability of an unwanted signal, section V. 4.
 $Y_{\pi}(q)$ The phase interference fading component of the total variability of a wanted signal, section V. 4.
 Y_1, Y_8 Values of Y for climates 1 and 8, section V. 9.
 z_{un}, z_{op}, z_{uc} Standard normal deviates defined by (V. 45), (V. 52) and (V. 55).
 Z The decibel ratio of the long-term fading, Y , of a wanted signal and the long-term fading, Y_{un} , of an unwanted signal, (V. 16).
 $Z_{\pi}(q)$ The approximate cumulative distribution function of the variable ratio Z , (V. 17).
 $Z_{\pi}(0.5)$ Median value of the variable ratio, Z , $Z_{\pi}(0.5) = 0$.
 Z_{π} The decibel ratio of the phase interference fading component Y_{π} for a wanted signal and the phase interference fading component Y_{un} for an unwanted signal, (V. 11).
 $Z_{\pi a}(q, K, K_u)$ The approximate cumulative distribution function of Z_{π} , (V. 12).
 ρ_{fu} The normalized correlation or covariance between path-to-path variations of $W_m(0.5)$ and $W_{um}(0.5)$, (V. 54).
 ρ_{tm} The long-term correlation between W_m and F_{op} , (V. 31).
 ρ_{tu} The long-term correlation between W_m and W_{um} , (V. 38).
 σ_{ϵ}^2 The path-to-path variance of deviations of observed from predicted transmission loss, section V. 8.
 $\sigma_{\epsilon}^2(q)$ The path-to-path variance of the difference between observed and predicted values of transmission loss expected for a fraction q of all hours.
 $\sigma_{\epsilon}^2(0.5)$ The path-to-path variance of the difference between observed and predicted long-term median values of transmission loss, (V. 40) and the following paragraph.
 $\sigma_{F_{op}}^2$ The variance of the operating noise factor F_{op} , (V. 51).
 $\sigma_{op}^2(q)$ Total variance of any estimate of the service criterion for service limited only by external noise, (V. 51).

$\sigma_{uc}^2(q)$

Total variance of any estimate of the service criterion for service limited only by interference from a single unwanted source, (V. 54).

 σ_{ur}^2

Variance of the estimate of $R_{ur}(g, q)$, (V. 54).

Taking the mystery out of phase jitter measurement

Early methods of measuring phase jitter have not been entirely successful in predicting data circuit performance. This article reviews phase jitter phenomena and describes measuring techniques which may improve things

Elton Cookson and Charles Volkland

THE RECENT FOCUS of attention on phase jitter has sent many engineers in the telecommunications industry to their technical libraries to "home up." In most cases, the results have been less than satisfying.

Generally, these people have found that phase jitter has a negligible effect on voice transmission, but a potentially disastrous impact on high-speed data transmission. Beyond that, they found some confusion within the industry on the basic mechanisms of jitter, acceptable tolerances, inter-relationships with other parameters, and even basic terminology. Studies are still going on, and standards are still evolving. But now there is general agreement on the "basics" of phase jitter.

The traditional definition of phase jitter is simply uncorrected "angle" modulation. This means that if a pure tone is transmitted over a circuit, and it is frequency or phase modulated in transit, the received tone will acquire associated sidebands. The amplitude of these sidebands (compared to the received tone) is a

ELTON COOKSON and CHARLES VOLKLAND are, respectively, marketing services manager and vice president, marketing, for Telecommunications Technology, Inc. of Sunnyvale, Calif.

measure of the phase jitter imparted to the signal.

While jitter measurements can be made by measuring the carrier (test tone)-to-sideband ratio, the process is cumbersome and there is no convenient way to distinguish between angle modulation and amplitude modulation sidebands. A more convenient measurement technique is to use a zero-crossing detector to check for any disturbance in the periodicity of the received signal, as indicated in Figure 1.

Because zero-crossing detection is the standard technique used in modern phase jitter measuring instruments, the term

"phase jitter" is now used to describe any unwanted variations in the zero crossings of the received signal. Since data modems also look for zero crossings, the zero-crossing technique seems like a straightforward test to identify and measure phase jitter. Unfortunately, it isn't quite that simple. To understand why, it is useful to examine some of the factors that affect zero crossings—and some of the factors that don't.

Signal modulation

When a carrier is modulated by a second tone, sidebands are generated at the carrier frequen-

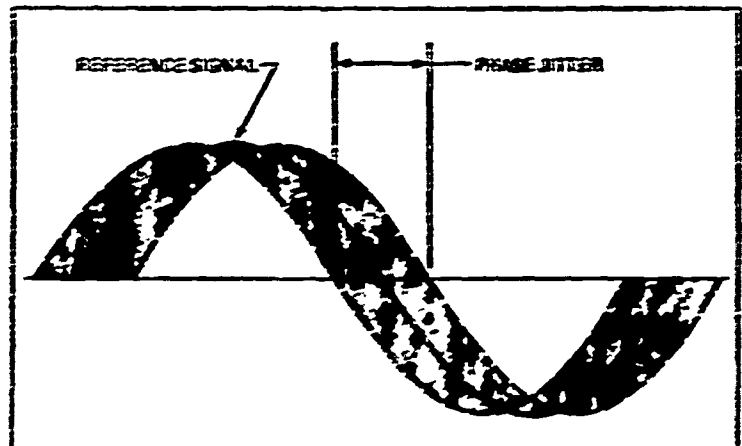


FIG. 1 Phase jitter test sets use signal zero-crossing detection to measure jitter.

or plus and minus the modulating frequency. The effect of these sidebands on the composite composite signal (carrier plus sidebands) depends on the modulation process. Figure 2 shows the vector diagram for amplitude modulation. The upper and lower sideband components rotate synchronously in opposite directions around the carrier vector (which is itself rotating). The resultant of the two sideband vectors is always in phase or 180° out of phase with the carrier vector. Thus, the composite signal amplitude varies, but its phase is not affected by the sidebands. In other words, the periodicity of the carrier's zero crossings is unaffected—and no phase jitter is produced.

As shown in Figure 3, the case of angle modulation is similar, except that the resultant of the sideband vectors is always 90° out of phase with the carrier vector. (We are considering only first-order sidebands here because the modulation index in a jitter situation is usually low.) Since the sideband resultant lies, at any instant, somewhere along the dotted line, the peak phase excursions occur when the two sidebands are directly in phase.

If $\Delta\phi$ is the maximum phase excursion of the composite signal, the signal varies through the total angle $2\Delta\phi$ at the modulating frequency. Thus, $\Delta\phi$ is a measure of the peak total phase jitter, and $2\Delta\phi$ is the peak-to-peak total jitter.

The angle $\Delta\phi$ depends only on the relative magnitudes of the carrier and its sidebands and is independent of the relative frequencies of the carrier and sidebands.

Single-frequency interference

Now suppose that instead of a sideband pair, we are dealing with a single interfering tone. The vector of the interfering tone rotates around the carrier vector at a rate that is equal to the difference in their frequen-

cies. As shown in Figure 4, the composite signal always lies somewhere on the dotted circle. In other words, both the phase and the amplitude of the signal vary. The interfering tone is introducing both angle modulation and amplitude modulation.

If we now limit the received signal to remove the amplitude modulation, we reduce the circle to a straight line. The interfering tone has been effectively split into a pair of coherent sidebands, each having an amplitude one-half that of the interfering tone before limiting. Thus, the composite signal now varies in the same way as the two-sideband case shown in Figure 3. The phase varies at a rate that is equal to the difference between the carrier frequency and the interfering tone. As this frequency difference is increased, the effect

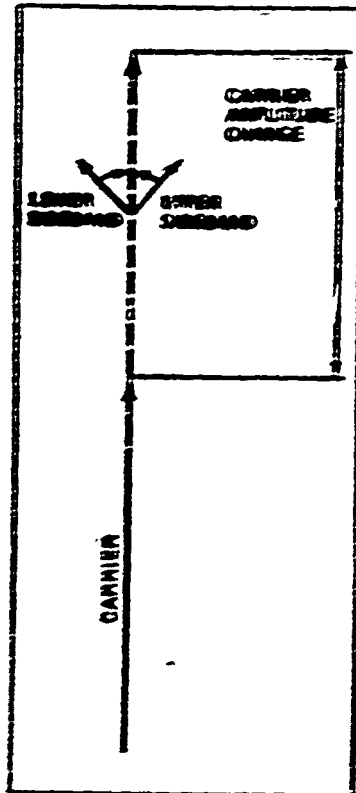


FIG. 2 In amplitude modulation, the resultant of counter-rotating sideband vectors is always in phase or 180° out of phase with carrier vector. This causes amplitude change, but no phase change.

the modulation frequency increases, but $\Delta\phi$ remains constant. After limiting, this carrier-plus-interfering tone can assume the same characteristics as a phase-modulated signal.

The magnitude of the angle $\Delta\phi$ produced by a sideband pair or by a second signal depends on the relative magnitudes of the carrier A_c and the modulating signal A_m . Figure 4 shows that

$$\Delta\phi = 2\arctan \frac{A_m}{A_c}$$

For example, suppose an interfering tone is 20 dB below the carrier. Since this is a ten-to-one voltage ratio, $\tan \Delta\phi = 0.1$, and $\Delta\phi = 5.7^\circ$. In peak-to-peak terms, $2\Delta\phi = 11.4^\circ$. Other differences in level between the carrier and the interfering tone can be calculated the same way. A 30-dB difference in level produces peak-to-peak jitter of 3.5°. If the interfering tone is only 10 dB down, the peak-to-peak jitter is 34.8°.

This "two-tone" generating mechanism has been accepted in the telecommunications industry as a calibration test for phase jitter test sets. Since it is normally performed with the two tones separated by 20 dB, 11.4° peak-to-peak total jitter has come to be something of a "benchmark" in the calibration of jitter test sets.

But exactly the same jitter reading can be produced by two interfering tones, each 26 dB below the carrier with the peak detection technique normally used in phase jitter test sets, two tones at -26 dB (whether they are an angle-modulation sideband pair or are unrelated) produce the same jitter reading as a single tone at -20 dB. Thus, this three-tone arrangement simulates the interfering effect of a pair of genuine angle-modulation sidebands 26 dB below the carrier.

As more tones are added, the situation rapidly becomes more complex. Each tone acts not only

on the carrier, but on all the other tones as well. Carrying this a step farther, if we consider a very large number of tones spread at random frequencies, we have an approximation of white noise. Thus, noise and other types of interference in the band are inescapably tied in with any jitter measurement. In order to make an intelligent measurement, therefore, we must first decide what we want to measure.

Phase jitter background

Most of the early studies of phase jitter were done in connection with frequency-division multiplex systems—primarily L-carrier. Here it was found that the jitter was caused mainly by power supply ripple producing the master frequency generator. As the frequencies were multiplied up in the carrier modulation scheme, the magnitude of this "hum modulation" jitter increased in proportion to the frequency multiplication. The resultant jitter of each carrier was imparted to all signals affected by that carrier. Thus, signals transmitted over channels in the higher super-groups suffered the most.

Regardless of the jitter magnitude, however, the jitter frequency remained constant and independent of the test frequency. And the jitter magnitude was independent of the test tone level. The jitter frequency was the same as the modulating frequency—in this case the 60-Hz power line frequency and its first several harmonics. Another common jitter source was found to be 22-Hz ringing and its first several harmonics. Thus, the jitter from these two sources was concentrated in the band from 20 Hz to 300 Hz.

Since it was recognized that noise also contributes to jitter readings, it seemed desirable to restrict jitter measurements to the band of interest in order to filter out noise contributions

from the rest of the spectrum.

This reasoning led to the establishment of the "Bell Standard" jitter measurement. Input filtering (300 Hz—2800 Hz) limits the spectrum to be tested to approximately 700 Hz each side of the 1000 Hz test tone fre-

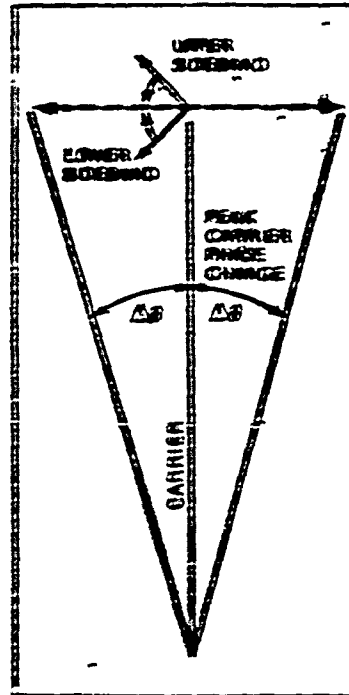


FIG. 3 Bandwidth of carrier-carrying sideband vectors in angle modulation is always 90° out of phase with carrier vector. This causes phase changes, but does not cause a change in amplitude.

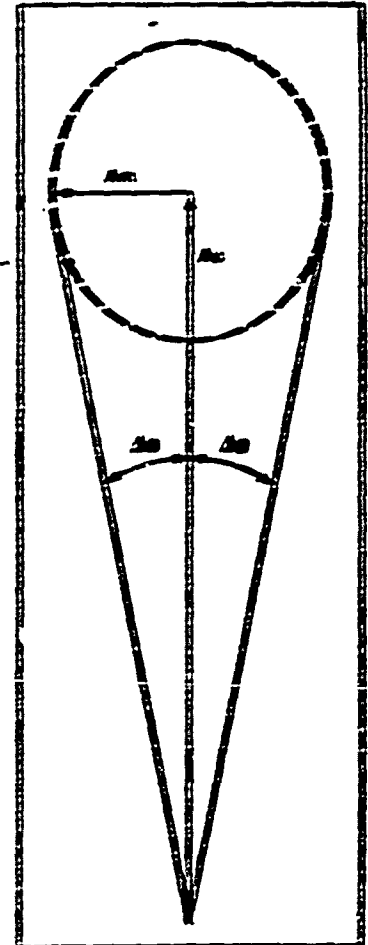


FIG. 4 Interfering line vector A_m creates resultant (dashed circle) which represents both amplitude and angle modulation of carrier vector A_c . $\Delta\theta$ as peak-to-peak phase jitter.

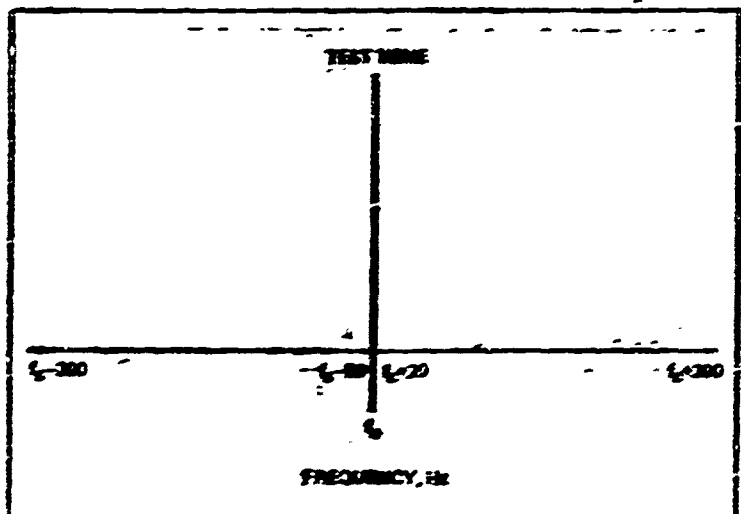


FIG. 5 Band-limited ("Bell-standard") jitter measurement responds to frequency components in the band 70-300 Hz each side of test to

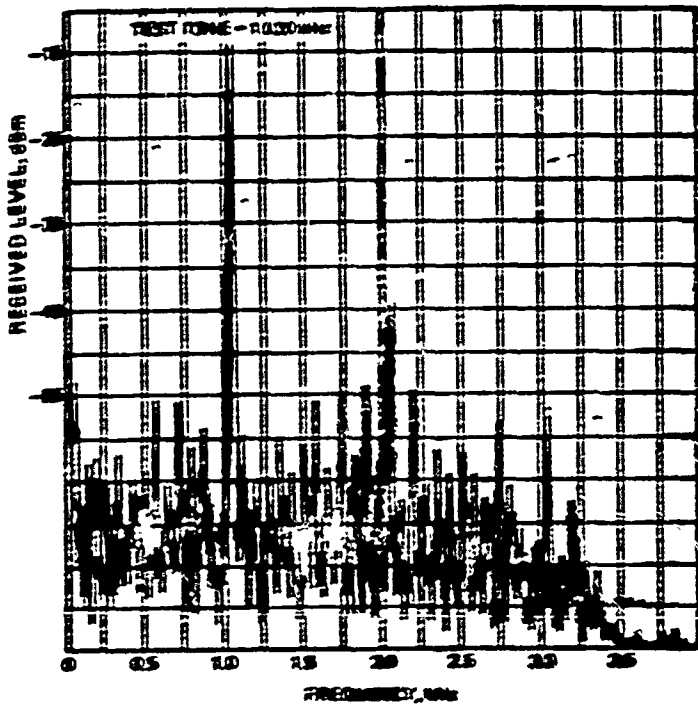


FIG. 6A Spectral analysis of received T-carrier bandwidth shows how distortion components change with test frequency variation. 1920-Hz test frequency results in fairly uniform distribution of distortion products.

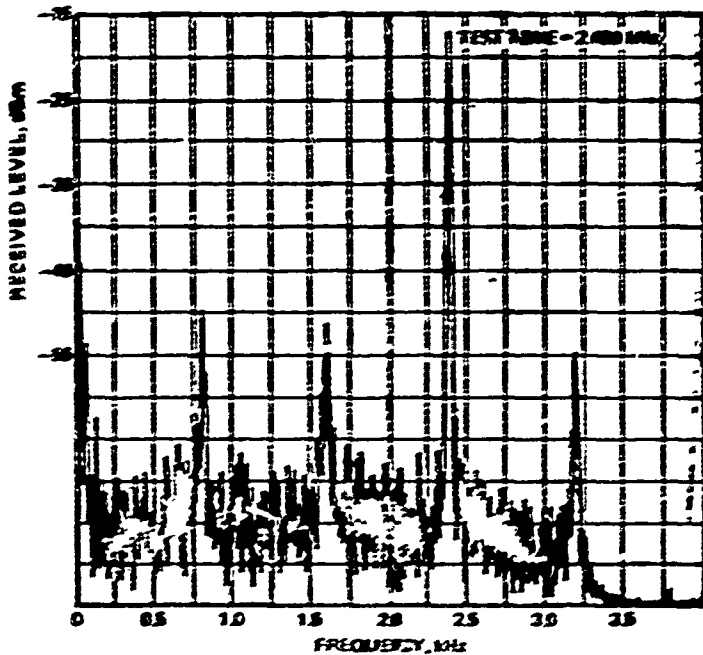


FIG. 6B Slight error in test frequency can bring distortion products sharply into phase.

quency. Filtering the output of the phase detector restricts the phase jitter measurement range to jitter components within 20—300 Hz of the test tone frequency, as shown in Figure 5. (In reference to T-carrier systems, the nominal test tone frequency, f_c , has come to be established as 1920 Hz because 1920 Hz is an exact sub-multiple of the 3000 Hz sampling frequency).

This measurement mode cuts the effective measurement bandwidth to approximately one-fourth the total channel width, centered on the test tone frequency. This reduces, but does not eliminate, the effects of noise and other interference on the jitter measurement. The jitter test set is completely sensitive to noise within the 20—300 Hz band on each side of the test tone. Naturally, it also sees any interfering tones within this band.

At first glance, it seems unlikely that an interfering tone would lie in the jitter-sensitive band, but it should be remembered that such interference can be the result of intermodulation or crosstalk, and can lie anywhere in the voice band.

T-carrier effects

The traditional form modulation jitter does not occur on PCM systems. However, these systems do not escape phase jitter problems. Phase jitter on T-carrier is caused by factors that are unique to digital systems. Distortion in a T-carrier system arises from several sources, including the sampling process, quantizing, compander mistracking, and timing jitter. With the exception of timing jitter, all of these sources contribute to what is sometimes called constant-power distortion. As a result of the sampling process, in combination with harmonic generation, certain distortion products

that would normally fall out of the voice band are "folded over," or reflected back in-band. While these products resemble noise, they are not random.

A small change in the test frequency can make a substantial change in the makeup of the distortion spectrum. Figure 6 shows three received T-carrier spectra using different test frequencies. Spectral analysis indicates that at some test frequencies these distortion products are dispersed throughout the VF spectrum (Figure 6a), while at other test frequencies the distortion products converge or pile up at discrete points throughout the band (Figures 6b and 6c show the results of changing the test frequency by 100 Hz.) But the total power in the distortion products remains constant. Naturally, all these distortion products cause phase jitter in much the same way as noise does.

Unlike phase jitter developed on frequency division multiplex, this T-carrier jitter is frequency dependent, changing in both magnitude and spectral distribution as a function of the test frequency. However, it is independent of the test tone level because the distortion products vary directly with test tone for a constant signal-to-noise ratio.

Careful equipment alignment can reduce the distortion products, and hence the phase jitter, on a T-carrier system. But quantizing noise cannot be eliminated. It arises because the carrier system encoder and transmits a small range of levels as a single discrete level. Thus, the demodulated signal has slight inaccuracies that appear as noise. The result is a phase jitter "floor" which is inherent in PCM system design. This floor is lower for a D2 channel bank than it is for a D1 bank because the D2 uses a smaller quantizing increment.

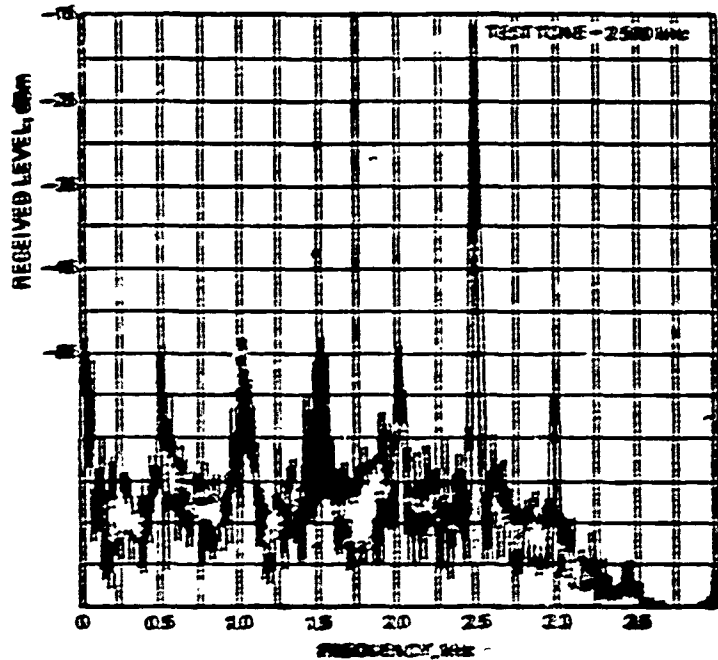


FIG. 6C Like Fig. 6B on page 49, this illustration shows the results of changing the test frequency by 100 Hz.

Timing jitter arises in the PCM repeatered line when the regenerative repeaters introduce slight timing errors in the pulse train.

Thus, when the receiving terminal reconstructs the PCM signal to form pulse-amplitude modulation, some unwanted pulse-position modulation is also present. Since the time displacement of these pulses is the same for any signal frequency, a given displacement has a greater effect on the shorter period of a higher-frequency signal. Thus, the phase jitter caused by timing jitter is directly proportional to signal frequency.

Jitter measurement techniques

Since a phase jitter measurement is simply an examination of zero crossing variations, and there are so many factors that can cause these variations, the practical problem is to develop a useful measurement technique. Unless such a technique provides at least a clue to the jitter

source, it cannot be very useful.

An important characteristic which permits one type of jitter to be distinguished from another type is the frequency distribution of the jitter components. For example, the traditional hum modulation caused by power supply ripple, nearly always produces jitter components that fall within 20-300 Hz of the test tone frequency. By contrast, the other jitter sources we have mentioned produce components that are likely to be distributed across the circuit bandwidth. Thus, valuable clues to the jitter source can be obtained by using both band-limited (or "Bell-standard") measurement and wideband measurement, and comparing and analyzing their similarities or differences.

Band-limited measurements should, of course, be made with a jitter set that has the standard measurement characteristics described earlier. For comparison, an oscilloscope method responds

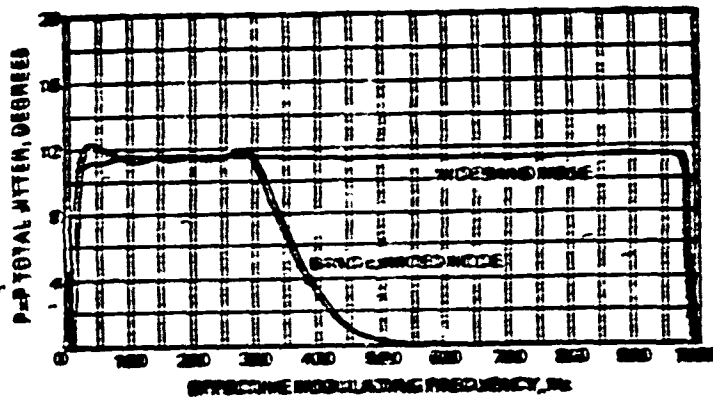


FIG. 7 Comparison of measured phase jitter using band-limited and wideband test modes. Both tests use a 1 kHz primary tone and a second tone attenuated 20 dB and spaced from 1 kHz to 2 kHz. Effective modulation frequencies shown are the frequency differences between the two tones. Modulation frequencies above 1 kHz produce an increase of the wideband value, with "notches" at 1 kHz intervals.

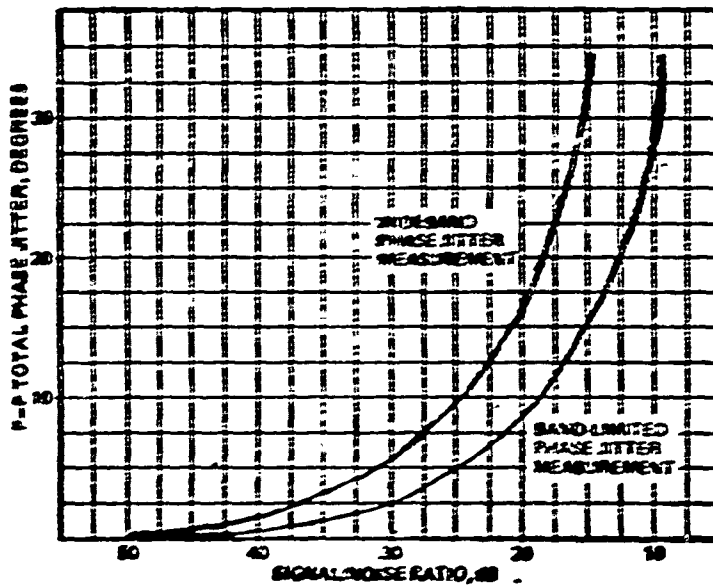


FIG. 8 Comparison of measured jitter as measured with band-limited and wideband modes in the presence of 3.5 kHz band of white noise.

to any frequency components present, and therefore is a wideband measurement. However, the oscilloscope method is somewhat cumbersome, and it lacks precision.

For this reason the techniques presented here are based on the use of a test set which incorporates both band-limited and wideband operating modes, such

as the TTI 1200 Phase Jitter Test Set, manufactured by Telecommunications Technology, Inc., of Sunnyvale, Calif.

Figure 7 shows a comparison of the frequency response of these two operating modes. It is apparent that hum modulation of these two operating modes. It is apparent that hum modulation jitter components falling in the 20-300 Hz band will give the same reading in either mode.

Consequently, approximately equal readings in the two modes point to hum as the likely culprit.

As a double check, the test tone level should be varied while the band-limited jitter reading is observed. If the source is hum modulation, the jitter reading should remain essentially constant.

This occurs because the sidebands vary directly with the test tone level, maintaining a constant carrier-to-sideband ratio. If hum modulation is causing the problem, the power supplies feeding the carrier generators would be suspect. The other likely source of predominant components in the 20-300 Hz band is single-frequency interference. In this case, the jitter reading will vary inversely with changes in test tone level.

Now suppose that the band-limited, wideband comparison reveals a substantially higher wideband reading.* This indicates the presence of significant frequency components more than 300 Hz away from the test frequency. A wideband reading only slightly higher merely indicates that the instrument is only summing the small jitter components that can always be expected across the received bandwidth—and that the primary jitter is still concentrated in the 20-300 Hz band.

If a comparison of the two modes indicates significant components above 300 Hz, it is possible to identify characteristic "signatures" of the different types of noise generated by various carrier equipment. The key

*As Figure 8 shows, a white-noise input to the Phase Jitter Test Set results in a wideband jitter reading approximately twice the band-limited reading. The effective bandwidth involved in the wideband reading is about four times that of the band-limited reading, and it produces four times the noise power. This is a 6-dB increase. Since the instrument responds on a voltage (rather than power) basis, it sees the 6-dB increase as a 2:1 change in phase jitter.

to distinguishing the different types of noise is to vary the test tone level while observing the wideband jitter reading.

If the jitter reading shows an inverse linear relationship to the test tone level, the cause is probably signal-uncorrelated (wide channel) noise. Lowering the test tone level reduces the signal-to-noise ratio and increases the jitter reading in accordance with the curves of Figure 8. This type of noise response is typical of frequency-division multiplex systems such as L-carrier.

If the wideband jitter reading remains constant, or if it varies only slightly with changes in test tone level, the reading is almost certainly associated with signal-correlated noise—noise that is generated only in the presence of a signal. Signal-correlated noise occurs, for example, on T-carrier equipment, where it is the predominant noise generated by the channel. A related effect occurs on other facilities, such as N-carrier, as a result of compander operation.

Since the magnitude of the signal-correlated noise is a function of the signal level, the signal-to-noise ratio remains essentially constant when the test tone level is varied. Thus, the jitter reading typically shows little change for a large variation in test tone level.

For example, it is possible to vary the test tone level as much as 20 dB on a T-carrier channel without changing the signal-to-noise ratio more than 1 dB. Varying the test tone level by 20 dB on an N-carrier channel might result in a 5-dB change in signal-to-noise ratio. When excessive signal-correlated noise is identified, the solution is careful alignment of the carrier facility.

A wideband jitter measurement responds to most noise and distortion products, but is not directly affected by harmonic distortion—because pure harmonics are synchronized with the test tone fundamental and do not disturb its zero crossings. However, the wideband measurement does include secondary effects of harmonics. For example, a harmonic may interact with a 3700-Hz out-of-band signaling frequency on a frequency division carrier channel to produce a 24-B in-band intermodulation product which contributes to the wideband jitter measurement. Likewise, jitter resulting from "constant-power distortion" provides an indirect but positive indication of the relative magnitude of harmonic distortion on T-carrier facilities.

The future of jitter measurements

In this discussion we have avoided any attempt to relate

phase jitter readings to specific data error rates. Undeniably, jitter is a major factor in data errors. But it is not independent. It is closely related to other types of transmission impairments. Furthermore, the modulation technique used in a particular system has a great deal to do with its tolerance to jitter, noise and other impairments.

The ideal situation would be to have a single "figure of merit" which would take into account all types of distortions to predict the error rate at a given transmission rate on a specific data circuit. A number of studies in various parts of the industry are concentrating on finding this magic formula. While it has not yet been found, it is apparent that such a formula cannot rest on the measurement of a single parameter.

Since a wide band jitter measurement responds to a variety of effects such as signal-correlated noise and single-frequency interference, it is a strong candidate for the figure-of-merit role. But regardless of whether it becomes the accepted measurement in that sense, comparisons of band-limited and wide band jitter will continue to provide important clues in tracking down the specific sources of phase jitter. □

Few subjects have stimulated more discussion and less definitive information than has phase jitter during its rise to prominence in the last several years. The reason for the prominence is, of course, that phase jitter causes errors in high speed data transmission. The reason for all the discussion has been that phase jitter test sets are also susceptible to other transmission impairments, with the result that the parameter has become somewhat of a scapegoat for many unidentified transmission problems.

TTI has chosen an unique approach in this product line with the objective of enabling the user to isolate the effects of phase jitter from the effects of other transmission impairments. For a full appreciation of TTI's approach, it is necessary to understand the basic nature of phase jitter and its relationship to other factors that affect transmission performance. For those who are not phase jitter specialists, the following brief review may be helpful.

PHASE JITTER BASICS

Phase jitter is a modulation process. It is customarily defined as uncorrected angle modulation. If we consider a test tone as a carrier, any angle modulation of this carrier will produce side bands. The frequency separation between the side bands and the carrier is equal to the modulating frequency. The amplitude ratio between the angle modulation side bands and the carrier is a measure of phase jitter. Thus, the jitter could be measured, for example, in dB as a S/N ratio.

However, it is a cumbersome process to use a frequency-selective voltmeter or similar instrument to measure the side bands and then to compare their amplitude with that of the carrier. Furthermore, the side bands measured by such a process might well be amplitude-modulation side bands, which produce no phase jitter. Therefore, this method is rarely used. Instead, we choose to measure the effects of the side bands on the carrier.

Figure 1 shows the standard vector diagrams for both amplitude and angle modulation of a reference signal. In each case the two side bands rotate synchronously in opposite directions around the reference vector. The resultant of the two amplitude modulation side band vectors is either in phase or 180° out of phase with the reference

vector and consequently causes only changes in the resultant signal's amplitude, not its phase. For angle modulation, however, the vector resultant is offset from the reference by 90°. Consequently, the resultant signal changes phase, but does not change amplitude. Observed on an oscilloscope the signal appears to jitter or smear along its horizontal axis.

Probably the easiest means for measuring the effect of the angle-modulation side bands is to measure variations in the zero crossings of a reference frequency. For this reason, it is customary in phase jitter test sets to use zero-crossing detector to measure the amount of variation in the zero crossings. Translated into degrees, this variation is a measure of the phase jitter.

Unfortunately, other effects can also produce variations in the zero crossings. One such effect is single-frequency interference. To understand how this comes about consider the

vector diagram of Figure 2. Since there is no offsetting side band vector, the vector of the interfering tone simply rotates about the reference vector. Thus, the resultant signal always lies somewhere on the dashed circle with both its amplitude and the phase varying about that of the reference signal. However, many modern, and virtually all phase jitter test sets, limit the signal to strip out the amplitude modulation. This leaves the resultant signal varying in phase only. The result is virtually indistinguishable from the test angle modulation shown in Figure 1.

If more tones were added, their effects would be superimposed on one another. If a very large number of tones were added at random levels and frequency spacing, their effects would approximate white noise. Thus, it is apparent that noise also affects the zero crossings.

It might be argued that these effects are real, that they will be seen by a data modem, and that therefore the problem of carrying them out is academic. Unfortunately, measuring the

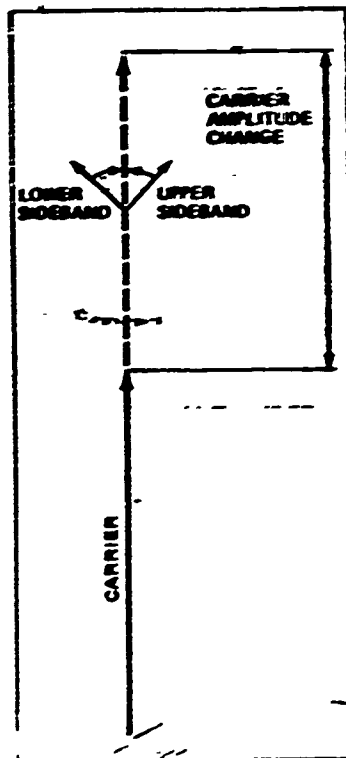


Figure 1A. In amplitude modulation, the resultant of contra-rotating sideband vectors is always in phase or 180° out of phase with carrier vector. This causes amplitude changes, but no phase change.

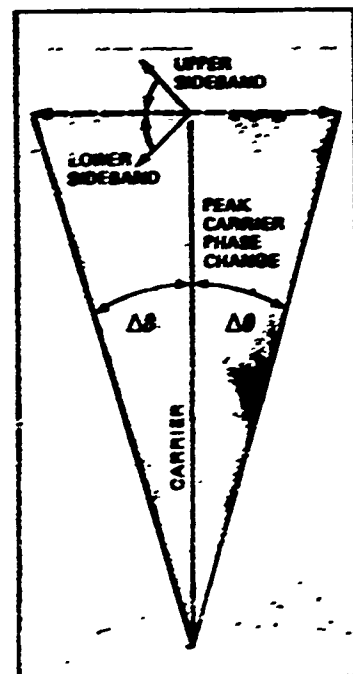


Figure 1B. Resultant of contra-rotating sideband vectors in angle modulation is always 90° out of phase with carrier vector. This causes phase changes, but does not cause a change in amplitude.

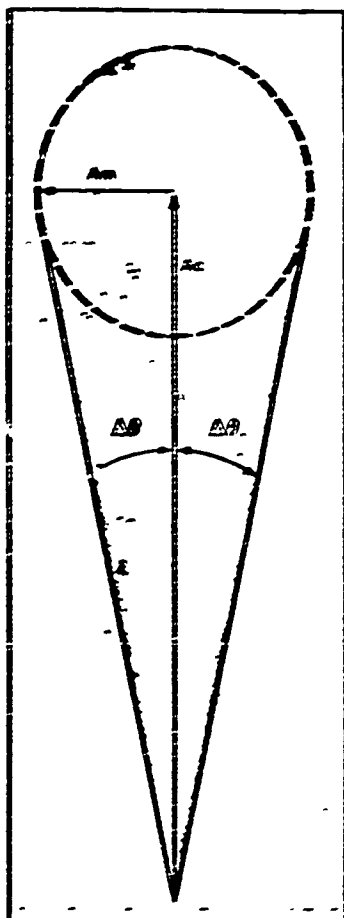


Figure 2. Interfering tone vector A_m creates resultant (dotted circle) which represents both amplitude and angle modulation of carrier vector A_c . $2\Delta\theta$ is peak-to-peak phase jitter.

combined effects of phase jitter, noise, and single-frequency interference is of little value in locating the source of the problem. All of these effects have different causes. A composite measurement will simply indicate that there is a problem without identifying the cause.

CAUSES OF PHASE JITTER

Most of the early problems attributed to phase jitter followed the introduction of high-speed data modems, and were associated with frequency-division multiplex systems—primarily L-carrier. Here it was found that the jitter was caused mainly by power supply ripple modulating the master carrier frequency generator.

As the frequencies were multiplied up in the carrier modulation scheme, the

magnitude of this "hum modulation" jitter increased in direct proportion to the frequency multiplication. The resultant jitter of each carrier was imparted to all signals affected by that carrier. Thus, signals transmitted over channels in the higher supergroups suffered the most.

Regardless of the jitter magnitude, however, the jitter frequency remained constant and independent of the reference signal frequency. And the jitter magnitude was independent of the reference signal level. The jitter frequency was the same as the modulating frequency—in this case the 60-Hz power-line frequency and its first several harmonics. Another common jitter source was found to be 20-Hz ringing and its first several harmonics. Thus, the jitter from these two sources was concentrated in the band from 20 Hz to 300 Hz.

Since it was recognized that noise also contributes to jitter readings, it seemed desirable to restrict jitter measurements to the band of interest in order to filter out noise contributions from the rest of the spectrum.

This reasoning led to the establishment of the "Bell Standard" jitter measurement. Input filtering (300 Hz–1800 Hz) limits the spectrum to be tested to approximately 700 Hz each side of the designated standard 1020 Hz reference signal frequency. Filtering the output of the phase detector restricts the measurement range to jitter components within $\pm (20\text{--}300\text{ Hz})$ of the reference frequency, as shown in Figure 3.

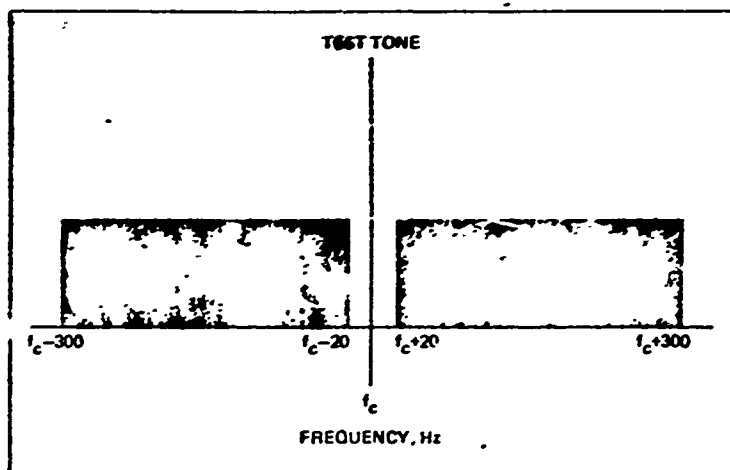


Figure 3. Band-limited ("Bell-standard") jitter measurement responds to frequency components in the band 20-300 Hz each side of test tone.

Thus the effective bandwidth for phase jitter measurements is approximately one-fourth the total channel width, centered on the reference frequency. This reduces, but does not eliminate, the effects of noise and other interference on the jitter measurement. The jitter test set is still completely sensitive to extraneous components within the 20-300 Hz band on each side of the reference signal.

Although phase jitter has been of primary concern in high-speed data transmission, extremely low-frequency jitter has recently begun to cause problems with some specialized data modems. Jitter in the frequency range from 5 to 20 Hz is becoming an increasing problem, particularly in the case of modems which carry bio-medical information over the DDD network. One common source of this low-frequency jitter has been traced to problems in frequency synchronization on N3-type carrier systems. Although the problem is actually due to frequency translation, varying at a 5 to 20 Hz rate, it shows up as low frequency phase jitter.

TRUE PHASE JITTER

As mentioned previously, the "Bell standard" measurement mode minimizes the effects of "noise" on phase jitter measurements by rejecting noise components outside the "jitter spectrum". The measurement is still sensitive to idle-channel noise, single-frequency interference, and signal-correlated noise components within a 600-Hz band surrounding the refer-

CCP 702-1

more signal. Several methods have been proposed for identifying whether a jitter measurement represents "true phase jitter" or is due to the effects of "noise" within this narrow bandwidth. One of these is to observe the effects of change in reference signal level, and another is to combine a phase jitter measurement with a notched noise test.

Varying the Test Tone Level

If it is suspected that noise within the jitter response band is contributing substantially to the jitter reading, some information can be gained by varying the reference signal level. True jitter will be unaffected by a change in reference level (within a normal operating range). This is so because true jitter is a measure of signal-to-side band ratio. This ratio remains constant regardless of the absolute reference level. On the other hand, if the reading includes a substantial contribution from non-signal correlated noise, it will show a significant change with variations in reference level. Since in this case the noise level is independent of reference level, reducing the test tone results in a lower signal-to-noise ratio and an increase in "jitter" reading.

This is a valid technique only if non-signal-correlated noise is involved. It will not distinguish between true phase jitter and the effects of signal-correlated noise. Little attention has been paid to signal-correlated noise until quite recently. However, it is assuming increasing importance as more and more circuits include at least one link of T-carrier or N-carrier. Signal-correlated noise is produced by such factors as compandor action and quantizing noise. It occurs only when a signal is present. Since it is tied directly to signal level, it goes up and down with the reference signal level, maintaining essentially a constant signal-to-noise ratio. Thus the portion of the jitter reading contributed by signal-correlated noise behaves in exactly the same way true jitter behaves as the reference level is varied. Because of the increasing use of T carrier and large number of compandored carrier circuits, varying the reference level is no longer an effective means to identify phase jitter.

Notched Noise Test

The standard test for signal-correlated noise is to make a "notched" noise

test. This is in reality a signal-to-noise measurement. A holding tone is placed on the circuit at the far end and is "notched out" by a very sharp filter at the receiving end. The noise measuring instrument then measures all remaining noise components on the circuit. Most current test procedures specify that the phase jitter test be accompanied by a notched noise test to aid in correlating the contribution of signal-correlated noise to the jitter reading.

With a 2750 Hz or 2800 Hz holding tone this test was a valid, although cumbersome, aid in interpreting a phase jitter reading. Since all harmonics of the holding tone were out of the band of interest, the notched noise measurement did not include any harmonic contribution from the holding tone. The primary contributors were idle-channel noise and signal-correlated noise. The only area of ambiguity concerned the contribution of true phase jitter. If the notch filter was sharp enough, the measurement would include the contribution of the true phase jitter sidebands imparted to the holding test tone. A wider notch would reject those jitter components falling within its stop-band, along with the holding tone. If one assumes that all phase jitter components are rejected by the notch and not included in the measured signal-to-noise ratio, one can refer to a curve of signal-to-noise ratio vs. phase jitter (in degrees) to find the contribution that the noise makes to the jitter reading. By com-

puting this contribution one can get an approximation of the true phase jitter.

However, now that the standard frequency for making notched noise measurements is being moved from 2800 Hz to the millimeter frequency (nominally 1 kHz), this procedure is no longer reliable. With the lower holding tone frequency, the second and third harmonics fall in-band. Since these harmonics are included as "noise" in a notched noise measurement, the signal-to-noise ratio may no longer provide a valid indication of the amount of the jitter reading that is contributed by noise. This point is illustrated by Figure 4 which shows a spectrum analyzer trace of a circuit which has low noise but clearly defined phase jitter. However, there is also reasonably high harmonic content. Hence, the signal-to-noise ratio is significantly decreased due to the harmonic contribution. If one were to translate the signal-to-noise ratio into degrees of phase jitter, the phase jitter reading might logically be attributed to noise effects, where it actually is due to "true" phase jitter. Consequently appreciable harmonic content can cause misinterpretation of the notch noise test results.

This should not be taken as an indictment of the notched noise test. One of the reasons for lowering the test frequency for the notched noise test is to include the contribution of harmonics in the test. This makes it a more valuable test for overall circuit evalua-

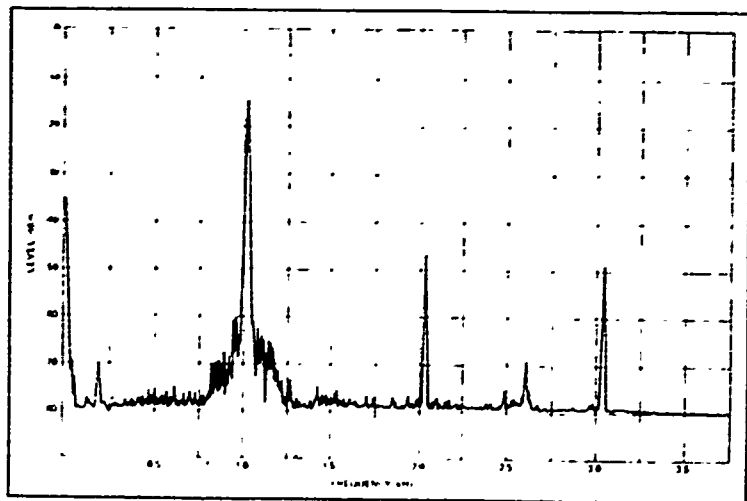


Figure 4. Spectrum analyzer shows both high harmonic content and phase jitter. Since a notched noise measurement would respond to harmonics, indicating a noisy circuit, phase jitter reading might be ignored.

tion, but has the side effect of rendering notched noise information less applicable to the interpretation of a phase jitter test.

WHAT'S THE ANSWER?

Fortunately, there is a way to isolate true phase jitter from the contributions of noise—signal correlated or otherwise. It simply involves the comparison of a standard jitter test to a wideband test which includes the contributions of all noise components but excludes test tone and all harmonics. This wideband test can be made simply by switching out the lowpass filtering of the TTI 1200 series phase jitter test set and measuring the effects of all noise components from 300 Hz to the upper limit of the channel bandwidth, exempting the test tone and its harmonics. Figure 5 shows a comparison of the test set response in these two operating modes. From the curve it is apparent that the wideband response of the instrument is comparable to a notched noise test (with very sharp notches at the test tone frequency and its harmonic frequencies). This measurement "sees" all noise contributions, whether signal correlated or uncorrelated, without recognizing discrete harmonic components. Furthermore, since the detector characteristics and the measurement units,

degrees, are identical to those employed in the standard band-limited phase jitter measurement, the results permit a direct comparison of the two readings.

It may be helpful to consider the two possible extremes involved in this technique. First suppose phase jitter is present, and sufficiently high to override the noise on the channel. In such a case we would expect the reading in the band-limited mode to be approximately the same as that in the wideband mode (both modes are fully responsive to the dominant phase jitter with relatively no contribution from the broad band noise present on the circuit). Now suppose that there is no phase jitter on the channel, but that substantial noise is present. In this case there will be phase jitter readings in both the band-limited and wideband modes. However, the wideband reading is sensitive to a much wider bandwidth. Hence, we would expect the wideband reading to be substantially higher.

These two cases are illustrated by actual spectrum analyzer traces in Figures 6 and 7. In both cases substantial harmonic content is present. However, due to the inherent nature of the phase jitter measurement, this does

not affect either the band-limited or the wideband mode. The channel illustrated by Figure 6 has acceptable noise content but substantial phase jitter. Even without the spectrum analyzer this would be immediately apparent from a comparison of the two readings: 8.5° for the phase jitter reading and 9.0° for the wideband reading. This comparison indicates that the phase jitter reading is truly phase jitter, with relatively little contribution from wideband noise components.

Figure 7 illustrates a channel which has substantial wideband noise and virtually no phase jitter. A rapid comparison of the two readings can be shown to indicate this situation to a relatively unskilled operator. The phase jitter reading is 8.0 degrees, while the wideband reading is 16.0 degrees. The standard phase jitter reading is lower than the wideband reading because it sees a narrower band of noise. Whenever noise throughout the full 3-kHz channel width is the primary contributor to both readings, and little or no phase jitter is present, it can be shown that the standard phase jitter reading will be approximately one-half that of the wideband mode. This is because the effective bandwidth of the standard phase jitter

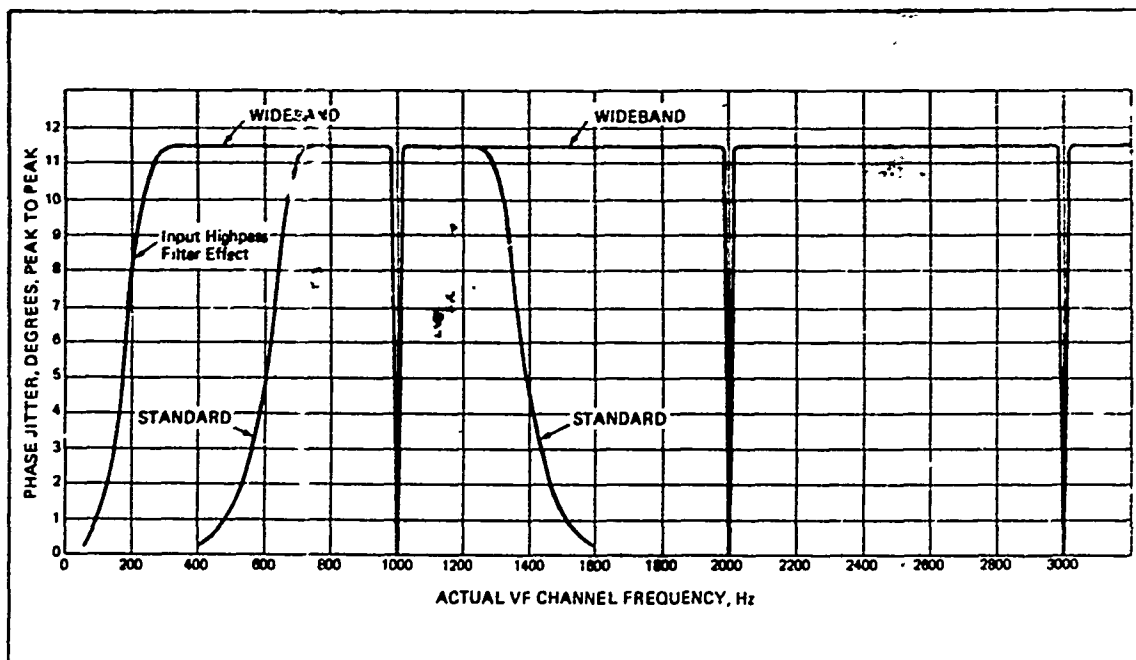


Figure 5. STANDARD measurement mode responds to approximately 700 Hz bandwidth centered about test tone, while WIDEBAND mode provides virtually flat response above 300 Hz with notches at harmonic frequencies. Comparison of readings in the two modes provides the basis for isolating true phase jitter from the effects of noise.

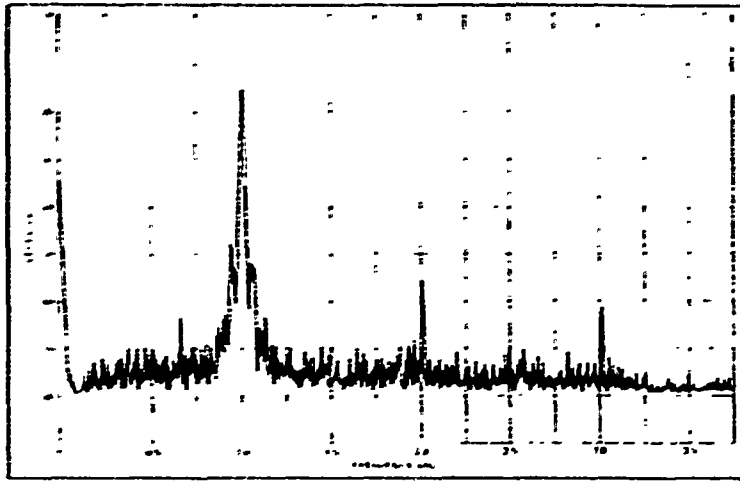


Figure 6. Spectrum analyzer shows high phase jitter and relatively low noise (Test Set does not respond to harmonics). Nearly identical STANDARD and WIDEBAND readings (8.5" and 9.0") indicate true phase jitter.

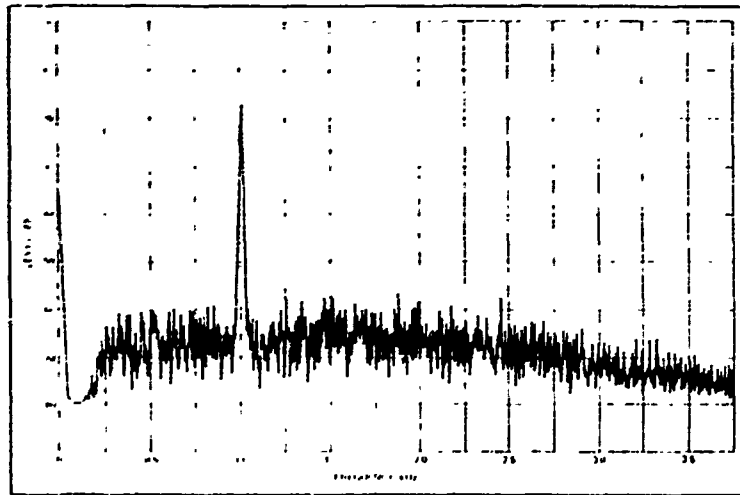


Figure 7. Spectrum analyzer shows wideband noise and no phase jitter. Comparison of STANDARD and WIDEBAND readings (8.0" and 16.0") indicates the "phase jitter" reading is due to noise effects, and not true phase jitter.

mode is essentially one fourth the bandwidth of the wideband mode. Assuming a flat distribution of noise across the channel the standard phase jitter mode will see only one fourth of the noise power seen by the wideband mode. This represents a six dB difference between the two measurement modes. Since the degree readout is a voltage representation, a six dB signal difference shows up as a two to one difference in readings. In the example illustrated by Figure 7, a phase jitter test alone would have indicated a marginal jitter reading. Without the wideband mode comparison, this might have led to unwarranted correc-

tive efforts aimed towards locating a non-existent source of phase jitter. With the wideband mode comparison the problem with the channel is immediately determined to be one of high broad-band noise.

A similar comparison technique can be used to isolate the effects of low frequency jitter (below 20 Hz). For this test we can switch out the sharp 20 Hz highpass filter following the phase jitter detector, leaving all other parameters the same. Figure 8 shows a comparison of the instrument response in the standard phase jitter mode vs. what we choose to call "standard plus

low frequency". Again, a simple comparison technique may be utilized by a relatively unskilled operator. If the two readings are the same, the low frequency components are negligible. However, if the standard plus low frequency reading is higher, it is readily obvious that substantial low frequency components are present.

HARDWARE

TTI's phase jitter measurement technique rests on patented[®] circuitry which measures zero crossing variations digitally. Its post-detection signal contains no vestige of the fundamental reference frequency. Since there are no arbitrarily imposed restraints on the bandwidth that the instrument can see, measurement bandwidth can be selected at will.

The TTI 1200 series phase jitter test sets reflect the use of multi-pole, active, computer-designed filters to provide the sharpest practical cutoff at the band edges. This approach provides clearly defined information for use in interpreting phase jitter readings.

TTI 1200B PHASE JITTER TEST SET

TTI's basic phase jitter set is the 1200B, a second-generation version of the widely known 1200. The 1200B provides the three operating modes described on the previous pages. These three operating modes are designated; "standard," "standard plus low frequency," and "wideband." A comparison of the readings in these three modes permits even a relatively unskilled operator to distinguish between true phase jitter, wideband noise, and low-frequency jitter. Interpretation of the readings merely requires a glance at Table 1, which shows the results to be expected in each of the three cases.

The instrument has been carefully designed throughout to be easily used by even non-technical personnel. At the same time however, it is an accurate and powerful tool for the more skilled operator who may be attempting to trace a particularly "knotty" jitter problem. The test set is designed strictly on a plug-in-and-read basis. The phase lock circuitry automatically locks to the incoming signal frequency. Furthermore, there are no level adjustments to make. The instrument accepts any test tone level from -40 dBm to +10 dBm.

[®] Patent No. 3,737,766

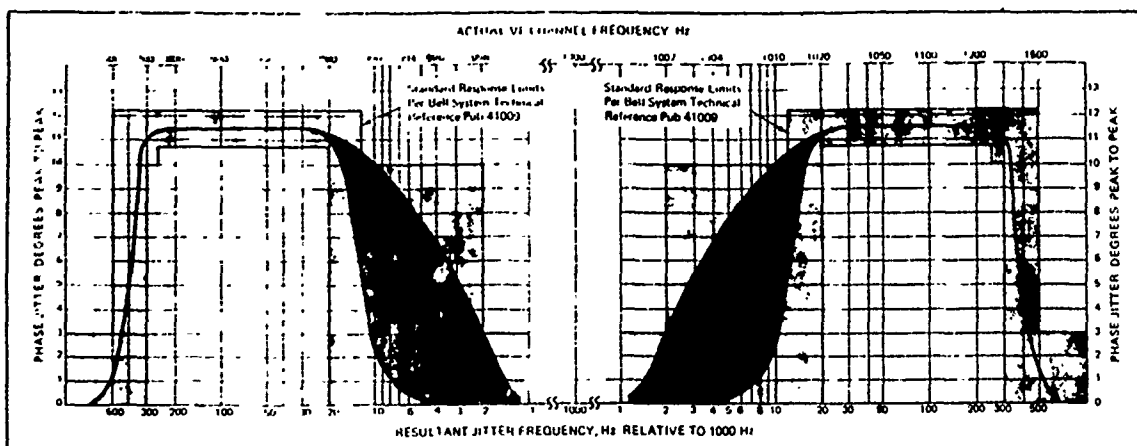


Figure 8. STD + LF measurement mode responds to low-frequency perturbations, as well as standard phase jitter. A higher STD + LF reading verifies the presence of low frequency phase jitter. (The plots have been expanded on each side of the reference tone to show more clearly the low-frequency filter characteristics.)

Table 1. Isolation of transmission impairments by comparison of operating modes.

MEASUREMENT			IMPAIRMENT
STD + L.F.	STANDARD	WIDEBAND	
X	X	2X	Wideband noise.
X	X	X	True Phase Jitter.
>X	X	X	Phase perturbation below 20 Hz
X	X	>2X	Single Frequency Interference.

In the standard mode the instrument accepts a reference signal frequency of 1020 Hz ±40 Hz. Should the reference frequency go outside these limits the display automatically blanks. These same reference frequency limits apply to the "standard plus low frequency" mode. However, in the wideband operating mode the instrument will accept any reference frequency from 500 Hz to 3 kHz.

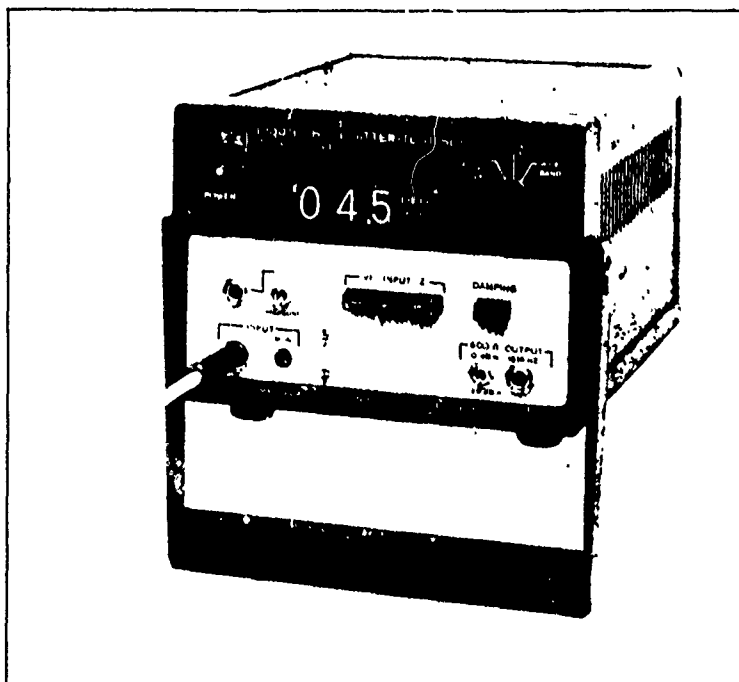


Figure 9. The basic Phase Jitter Test Set is the 1200B which can be equipped with the 1201A Hit Monitor shown in Figure 10.

The digital display provides an unambiguous jitter reading with resolution of 0.1 degree over the entire range of the instrument. For rapidly varying jitter frequencies, a push-button damping switch allows the operator to slow the refresh rate, averaging the fluctuations over a one-second interval.

Input impedance is pushbutton selectable for 600 or 900 ohms, terminating or bridging. An input return loss greater than 30 dB is met throughout the VF band.

A stable 1010 Hz oscillator is incorporated in the 1200B. A convenient front panel jack makes this reference signal source immediately available. The output level is switch selectable for 0 dBm or -29 dBm—normal data transmit levels at a subscriber drop or VF patch bay, respectively.

Terminals on the rear panel provide a convenient analog output which may be connected to an oscilloscope, spectrum analyzer or other display device for detailed analysis of the detected phase jitter signal.

CC-OPS

CCP 702-1

FOR THE COMMANDER:

OFFICIAL:

C.E. McKNIGHT, Jr.
Colonel, GS
Chief of Staff



M.K. Lobar
Colonel, AGC
Adjutant General

DISTRIBUTION:

- 10 - HQDA (DAMO-ZA), WASH DC 20310
- 10 - HQDA (DALO-ZA), WASH DC 20310
- 5 - JCS (J-6), Washington, DC 20310
- 5 - CDR, US Army Forces Command, Ft McPherson, GA 30330
- 5 - CDR, US Army Training and Doctrine Command, Ft Monroe, VA 23651
- 5 - CDR, US Army Materiel Development and Readiness Command,
5001 Eisenhower Ave, Alexandria, VA 22304
- 3 - CDR, US Army Security Agency, Arlington, VA 22212
- 2 - CDR, US Army Electronic Command, Ft Monmouth, NJ 07703
- 3 - CDR, US Army Satellite Communications Agency, Ft Monmouth, NJ
07703
- 2 - CDR, US Army Military District of Washington, Ft Meyer, VA 22211
- 5 - COMDT, US Army Air Defense School, Ft Bliss, TX 79916
- 5 - COMDT, US Army Armor School, Ft Knox, KY 40121
- 5 - COMDT, US Army Aviation School, Ft Rucker, AL 36360
- 5 - COMDT, US Army Command and General Staff College, Ft Leavenworth,
KA 66027
- 5 - COMDT, US Army Communications Electronics School, Ft Monmouth, NJ
07703
- 5 - COMDT, US Army Field Artillery School, Ft Sill, OK 73503
- 5 - COMDT, US Army Infantry School, Ft Benning, GA 31905
- 5 - COMDT, US Army Missile and Munitions Center and School, Redstone
Arsenal, AL 35809
- 5 - COMDT, US Army Ordnance Center and School, Aberdeen Proving
Ground, MD 21005
- 5 - COMDT, US Army Quartermaster School, Ft Lee, VA 23801
- 5 - COMDT, US Army Transportation School, Ft Eustis, VA 23604
- 2 - COMDT, US Military Academy, West Point, NY 10996
- 2 - CDR, US Army Support Command, Hawaii, APO San Francisco 96557
- 6 - Defense Communications Agency, Washington, DC 20305

CCP 702-1

- 2 - DCA-PAC, APO San Francisco 96515
- 2 - DCA-EUR, APO NY 09128
- 2 - CNO, Navy Department, Washington, DC 20350
- 2 - CINCEUR, APO NY 09128
- 2 - CINCSAREUR, APO NY 09403
- 2 - CINCPAC, FPO San Francisco 96610
- 2 - CINCLANT, Norfolk, Va 23501
- 2 - CINCSAC, Offutt AFB, NE 68113
- 2 - CINCPAC, MacDill AFB, FL 33608
- 2 - COMNAVTELCOM, 4401 Massachusetts Ave NW, Washington, DC 20390
- 2 - Superintendent, Naval Academy, Annapolis, MD 21402
- 2 - HQ US Air Force, Washington, DC 20330
- 2 - AFCS, Richards Gebaur AFB, MO 64030
- 2 - USAFA, USAF Academy, CO 80840
- 2 - Third Mobile Communications Group, Tinker AFB, OK 73145
- 198 - CDR, 5th Sig Comd, Worms, Germany, APO NY 09056
- 72 - CDR, 6th Sig Comd, Ft Shafter, HI, APO San Francisco 96558
- 16 - CDR, 7th Sig Comd, Ft Ritchie, MD 21719
- 29 - COMDT, US Army Signal School, Ft Gordon, GA 30905

Vertical text along the left edge of the page, possibly a page number or header.

Small mark or characters at the top left of the page.

Small mark or characters in the upper left quadrant.

Small circular mark or stamp in the upper right quadrant.

Small, illegible text fragment located in the center of the page.

Small, illegible text fragment located in the center of the page, below the first fragment.

Small mark or characters in the lower left quadrant.

Small mark or characters in the lower left quadrant.

Vertical text along the left edge of the page, possibly a page number or header.

APPENDIX B

REGISTERED PROGRAMME LEVELS

SECTION I

INSTRUCTIONS

APPENDIX B

POSTAL PERFORMANCE METRICS

SECTION II

TABLES AND FIGURES

APPENDIX C

DATA ANALYSIS

SECTION 1

INSTRUCTIONS

APPENDIX C

DATA ANALYSIS

SECTION II

FIGURES

APPENDIX C

DATA ANALYSIS

SECTION III

NOISE CALCULATIONS

APPENDIX C

DATA ANALYSIS

SECTION IV

MINIMUM NOISE CAPABILITY

APPENDIX C

DATA ANALYSIS

SECTION V

FAULT ISOLATION

APPENDIX D

FINAL ANALYSIS OF THE TEST DATA

SECTION 1
INSTRUCTIONS

APPENDIX D

FINAL ANALYSIS OF THE TEST DATA

SECTION II

FIGURES

APPENDIX D

SIGNAL ANALYSIS OF THE TEST DATA

SECTION III

NOTES ON TESTS & FORMS

APPENDIX E

TABLES, FIGURES, AND SPECIFICATIONS

SECTION I

MULTIPLEX EQUIPMENT

APPENDIX E

TABLES, FIGURES, AND SPECIFICATIONS

SECTION II

RADIO EQUIPMENT

APPENDIX F

MISCELLANEOUS DATA

SECTION I

FORMULAS AND EQUATIONS

APPENDIX F

MISCELLANEOUS DATA

SECTION II

SYMBOLS AND DEFINITIONS

APPENDIX F

MISCELLANEOUS DATA

SECTION III

STATION GROUND MEASUREMENT

APPENDIX F

MISCELLANEOUS DATA

SECTION IV

NOISE FIGURE PRIMER

(HEWLETT-PACKARD APPLICATION NOTE 57)

APPENDIX F

MISCELLANEOUS DATA

SECTION V

MICROWAVE SYSTEM ENGINEERING
USING LARGE PASSIVE REFLECTORS

EXTRACT FROM IEE
TRANSACTIONS ON COMMUNICATIONS SYSTEMS

APPENDIX F

MISCELLANEOUS DATA

SECTION VI

RADIATION PATTERNS AND THE PASSIVE REPEATER

MICROFLECT COMPANY, SALEM, OREGON

APPENDIX F

MISCELLANEOUS DATA

SECTION VII

NATIONAL BUREAU OF STANDARDS

TECHNICAL NOTE 101

TRANSMISSION LOSS PREDICTIONS FOR TROPOSPHERIC

COMMUNICATION CIRCUITS

VOLUME I

APPENDIX F

MISCELLANEOUS DATA

SECTION VIII

NATIONAL BUREAU OF STANDARDS

TECHNICAL NOTE 101

TRANSMISSION LOSS PREDICTIONS FOR TROPOSPHERIC
COMMUNICATION CIRCUITS

VOLUME II

APPENDIX F

MISCELLANEOUS DATA

SECTION LX

PHASE JITTER MEASUREMENT

TELECOMMUNICATIONS TECHNOLOGY INC. TELEPHONY MAGAZINE, SEPTEMBER 25, 1972